SPRINGER NATURE
Reference

Sanjay Mavinkere Rangappa
Jyotishkumar Parameswaranpillai
Suchart Siengchin
Sabu Thomas
Editors

Handbook of Epoxy/Fiber Composites

Springer

Handbook of Epoxy/Fiber Composites

Sanjay Mavinkere Rangappa •
Jyotishkumar Parameswaranpillai •
Suchart Siengchin • Sabu Thomas
Editors

Handbook of Epoxy/Fiber Composites

With 482 Figures and 100 Tables

Springer

Editors
Sanjay Mavinkere Rangappa
Department of Materials and Production Engineering
The Sirindhorn International Thai German Graduate School of Engineering (TGGS), King Mongkut's University of Technology North Bangkok (KMUTNB)
Bangsue, Bangkok, Thailand

Jyotishkumar Parameswaranpillai
Division of Chemistry
Department of Science
Faculty of Science & Technology
Alliance University
Bengaluru, Karnataka, India

Suchart Siengchin
Department of Materials and Production Engineering
The Sirindhorn International Thai German Graduate School of Engineering (TGGS), King Mongkut's University of Technology North Bangkok (KMUTNB)
Bangsue, Bangkok, Thailand

Sabu Thomas
International and Inter University Centre for Nanoscience and Nanotechnology (IIUCNN)
School of Energy Materials
Mahatma Gandhi University
Kottayam, Kerala, India

ISBN 978-981-19-3602-9 ISBN 978-981-19-3603-6 (eBook)
https://doi.org/10.1007/978-981-19-3603-6

This Springer imprint is published by the registered company Springer Nature Singapore Pte Ltd.
The registered company address is: 152 Beach Road, #21-01/04 Gateway East, Singapore 189721, Singapore

Preface

The objective of this handbook is to summarize many of the recent developments in the field of epoxy fiber composites. Epoxy composites reinforced by carbon fibers, glass fibers, and natural fibers are widely used as an alternative for metals in many advanced applications such as aircraft, automobiles, and construction to reduce the weight and cost of production and fuel efficiency. Recently, many researchers have been interested in hybrid composites containing synthetic and natural fibers. Such a system may be able to show a synergistic effect of both synthetic and natural fibers on the physical and thermo-mechanical properties of the composites. As the title indicates, this handbook focuses on new challenges for the synthesis, characterization, and applications of epoxy/fiber composites. It is very important to mention that, to date, no handbook has been published that deals with epoxy/fiber composites. This handbook comprehensively updated all of the major aspects of epoxy/fiber composites (synthesis, processing, characterization, and application).

This handbook is structured into three parts, each of which covers every important aspect of widely used epoxy/fiber composites (see the Table of Content). Part I deals with state of the art of epoxy/synthetic fiber composites, fundamentals, characteristics, and applications, Part II deals with state of the art of epoxy/natural fiber composites, fundamentals, characteristics, and applications, and Part III deals with state of the art of epoxy/synthetic/natural fiber hybrid composites, fundamentals, characteristics, and applications.

This handbook covers the void of the researchers' need for a one-stop reference book. Leading researchers from industry, academy, government, and private research institutions across the globe have contributed to this book. Academics, researchers, scientists, engineers, and students in epoxy/fiber composites will benefit from this highly application-oriented handbook.

The editors appreciate all the authors' contributions. The editors also express their gratitude to the publisher for their assistance and support.

Bangkok, Thailand — Sanjay Mavinkere Rangappa
Bengaluru, India — Jyotishkumar Parameswaranpillai
Bangkok, Thailand — Suchart Siengchin
Kottayam, India — Sabu Thomas
July 2022 — Editors

Contents

About the Editors

Dr. Sanjay Mavinkere Rangappa is currently a Senior Research Scientist/Associate Professor and also "Advisor within the office of the President for University Promotion and Development towards International goals" at King Mongkut's University of Technology North Bangkok, Bangkok, Thailand. He has received the B.Engg (Mechanical Engineering) in the year 2010; M.Tech (Computational Analysis in Mechanical Sciences) in the year 2013 and Ph.D. (Faculty of Mechanical Engineering Science) from Visvesvaraya Technological University, Belagavi, India, in the year 2018; and Post Doctorate from King Mongkut's University of Technology North Bangkok, Thailand, in the year 2019. He is a Life Member of Indian Society for Technical Education (ISTE) and Associate Member of Institute of Engineers (India). He is also a Board Member of various international journals in the fields of materials science and composites. He is a reviewer for more than 100 international journals (for Nature, Elsevier, Springer, Sage, Taylor & Francis, Wiley, American Society for Testing and Materials, American Society of Agricultural and Biological Engineers, IOP, Hindawi, NC State University USA, ASM International, Emerald Group, Bentham Science Publishers, Universiti Putra, Malaysia), and also a reviewer for book proposals, and international conferences. In addition, he has published more than 180 articles in high-quality international peer-reviewed journals indexed by SCI/Scopus, 9 editorial corners, 60 book chapters, 1 book, 25 books as an Editor (published by lead publishers such as Elsevier, Springer, Taylor & Francis, Wiley), and also presented research papers at national/international conferences. In 2021, his 17 articles have got top-cited article status in various top

journals (*Journal of Cleaner Production*, *Carbohydrate Polymers*, *International Journal of Biological Macromolecules*, *Journal of Natural Fibers*, *Journal of Industrial Textiles*). He is a lead editor of several special issues. Based on Google Scholar, the number of citations amounts to 7500+ and his present H-index is 46 with i10-Index of 126. In addition, one Thailand patent and two Indian patents are granted. He has delivered keynote and invited talks at various international conferences and workshops. His current research areas include natural fiber composites, polymer composites, and advanced material technology. He has received a "Top Peer Reviewer 2019" award, Global Peer Review Awards, Powered by Publons, Web of Science Group. The KMUTNB selected him for the "Outstanding Young Researcher" Award 2020. He is recognized by Stanford University's list of the world's Top 2% of the most-cited scientists in Single Year Citation Impact 2019 and also for the year 2020.

Dr. Jyotishkumar Parameswaranpillai is currently Associate Professor at Alliance University, Bangalore. He received his Ph.D. in Chemistry (Polymer Science and Technology) from Mahatma Gandhi University, Kottayam, India, in the year 2012. He has research experience in various international laboratories such as Leibniz Institute of Polymer Research Dresden (IPF), Germany, Catholic University of Leuven, Belgium, University of Potsdam, Germany, and King Mongkut's University of Technology North Bangkok (KMUTNB), Thailand. He has published around 130 papers in high-quality international peer-reviewed journals on polymer nanocomposites, polymer blends and alloys, and biopolymers. Also, he has published around 70 book chapters and has edited 25 books. He is a frequent invited and keynote speaker and a reviewer for more than 70 international journals, book proposals, and international conferences. He received numerous awards and recognitions including the prestigious INSPIRE Faculty Award 2011, Kerala State Award for the Best Young Scientist 2016, and Best Researcher Award 2019 from King Mongkut's University of Technology North Bangkok. He is named in the world's Top 2% of the most-cited scientists in Single Year Citation Impact 2020, by

Stanford University. His research interests include polymer coatings, shape memory polymers, antimicrobial polymer films, green composites, nanostructured materials, water purification, polymer blends, and high-performance composites.

Prof. Dr.-Ing. habil. Suchart Siengchin is President of King Mongkut's University of Technology North Bangkok (KMUTNB), Thailand. He received his Dipl.-Ing. in Mechanical Engineering from the University of Applied Sciences Giessen/Friedberg, Hessen, Germany; M.Sc. in Polymer Technology from the University of Applied Sciences Aalen, Baden-Wuerttemberg, Germany; M.Sc. in Material Science at the Erlangen-Nürnberg University, Bayern, Germany; Doctor of Philosophy in Engineering (Dr.-Ing.) from the Institute for Composite Materials, University of Kaiserslautern, Rheinland-Pfalz, Germany; and Post-doctoral Research from School of Materials Engineering, Purdue University, USA. In 2016 he completed the Habilitation (Dr.-Ing. habil.) in Mechanical Engineering from Chemnitz University of Technology, Saxony, Germany, and worked as Lecturer for Mechanical and Process Engineering Department at the Sirindhorn International Thai-German Graduate School of Engineering (TGGS), KMUTNB. He has been Full Professor at KMUTNB and became the Vice President for Research and Academic Enhancement in 2012 and elected President of KMUTNB in November 2016. He won the Outstanding Researcher Award in 2010, 2012, and 2013 at KMUTNB and National Outstanding Researcher Award for the year 2021 in engineering and industrial research by National Research Council of Thailand (NRCT). His research interests are in polymer processing and composite material. He is Editor-in-Chief of *Applied Science and Engineering Progress*, International Advisory Board member of *eXPRESS Polymer Letters* and *Journal of Production Systems and Manufacturing Science*, and author of more than 321 peer-reviewed journal articles and edited books and book chapters in more than 139 books. He has participated with presentations in more than 49 international and national conferences with respect to materials science and engineering topics.

Professor. Dr. Sabu Thomas is serving as the Vice Chancellor of Mahatma Gandhi University, Kerala, India. He is also Founder Director and Professor of the International and Interuniversity Centre for Nanoscience and Nanotechnology and Full Professor of Polymer Science and Engineering at the School of Chemical Sciences of Mahatma Gandhi University, Kottayam, Kerala, India. He is an outstanding leader with sustained international acclaims for his work in polymer science and engineering, nano materials, polymer nanocomposites, elastomers, polymer blends, interpenetrating polymer networks, polymer membranes, green composites and nanocomposites, nanomedicine, and green nanotechnology. In collaboration with India's premier tyre company, Apollo Tyres, Professor Thomas's group invented new high performance barrier rubber nanocomposite membranes for inner tubes and inner liners for tyres. He has received a number of national and international awards which include: Fellowship of the Royal Society of Chemistry, London; Distinguished Professorship from Josef Stefan Institute, Slovenia; and MRSI medal, Nano Tech Medal, CRSI medal, Distinguished Faculty Award, and Sukumar Maithy Award for the best polymer researcher in the country. He has been conferred Honoris Causa (DSc) by the University of South Brittany, Lorient, France. He has published over 650 peer-reviewed research papers, reviews, and book chapters. He has co-edited 53 books published by Royal Society, Wiley, Wood head, Elsevier, CRC Press, Springer, Nova, etc. He is the inventor of six patents. He has established a state-of-the-art laboratory at Mahatma Gandhi University in the area of polymer science and engineering and nanoscience and nanotechnology through external funding form DST, CSIR, TWAS, UGC, DBT, DRDO, AICTE, ISRO, DIT, TWAS, KSCSTE, BRNS, UGC-DAE, Du Pont, USA, General Cables, USA, Surface Treat Czech Republic, MRF Tyres, and Apollo Tyres. He has several international collaborative projects with a large number of countries abroad. He has already supervised 75 Ph.D. theses.

Contributors

Prabhat K. Agnihotri Department of Mechanical Engineering, Indian Institute of Technology Ropar, Rupnagar, Punjab, India

Md. Alamgir Department of Mechanical Engineering, RGM College of Engineering and Technology, Nandyal, Andhra Pradesh, India

Ibrahim M. Alarifi Department of Mechanical and Industrial Engineering, College of Engineering, Majmaah University, Al-Majmaah, Saudi Arabia

Engineering and Applied Science Research Center, Majmaah University, Al-Majmaah, Saudi Arabia

José Humberto S. Almeida Jr. Advanced Composites Research Group, School of Mechanical and Aerospace Engineering, Queen's University Belfast, Belfast, UK

Appukuttan Saritha Department of Chemistry, Amrita Vishwa Vidyapeetham, Amritapuri, Kerala, India

Ramazan Asmatulu Department of Mechanical Engineering, Wichita State University, Wichita, KS, USA

V. Suresh Babu Department of Mechanical Engineering, NIT Warangal, Warangal, Telangana, India

Ankur Bajpai School of Engineering, Institute for Materials and Processes, The University of Edinburgh, Edinburgh, UK

Mariana D. Banea Federal Center of Technological Education of Rio de Janeiro (CEFET/RJ), Rio de Janeiro, Brazil

Mattia Bartoli Consorzio Interuniversitario Nazionale per la Scienza e Tecnologia dei Materiali (INSTM), Florence, Italy

Italian Institute of Technology, Torino, Italy

M. Basheer Ahamed Department of Physics, B. S. Abdur Rahman Crescent Institute of Science and Technology, Chennai, Tamil Nadu, India

Harpreet S. Bedi Department of Mechanical Engineering, Indian Institute of Technology Ropar, Rupnagar, Punjab, India

B. Satish Ben Department of Mechanical Engineering, NIT Warangal, Warangal, Telangana, India

Bhargav Department of Mechanical Engineering, NIT Warangal, Warangal, Telangana, India

Swapnil Sureshchandra Bhurat Department of Mechanical Engineering, University of Petroleum and Energy Studies, Dehradun, India

Vasavi Boggarapu Department of Mechanical Engineering, National Institute of Technology, Warangal, India

P. Subash Chandra Bose Department of Mechanical Engineering, National Institute of Technology, Warangal, India

Sandip Budhe Department of Mechanical Engineering, National Institute of Technology, Calicut, Kerala, India

Daniel K. K. Cavalcanti Federal Center of Technological Education of Rio de Janeiro (CEFET/RJ), Rio de Janeiro, Brazil

Vijaya Chalivendra Department of Mechanical Engineering, University of Massachusetts, Dartmouth, MA, USA

Murthy Chavali Division of Chemistry, Department of Science, Faculty of Science & Technology, Alliance University, Bengaluru, Karnataka, India

M. Somaiah Chowdary Department of Mechanical Engineering, National Institute of Technology Warangal, Warangal, Telangana, India

Department of Mechanical Engineering, Prasad V. Potluri Siddhartha Institute of Technology, Kanuru, Andhra Pradesh, India

Anik Das School of Textile Science and Engineering, Tiangong University, Tianjin, China

Key Laboratory of Advanced Textile Composite Materials, Tiangong University, Tianjin, China

B. D. S. Deeraj Department of Chemistry, Indian Institute of Space Science and Technology, Thiruvananthapuram, Kerala, India

Kalim Deshmukh New Technologies – Research Center, University of West Bohemia, Plzeň, Czech Republic

Gang Ding Department of Science and Technology, Tianjin Open University, Tianjin, China

C. D. Midhun Dominic Department of Chemistry, Sacred Heart College (Autonomous), Kochi, Kerala, India

Hossein Ebrahimnezhad-Khaljiri Faculty of Materials Science and Engineering, K. N. Toosi University of Technology, Tehran, Iran

Tarek M. A. A. EL-Bagory Department of Mechanical Design, Faculty of Engineering Materia, Helwan University, Cairo, Egypt

Reza Eslami-Farsani Faculty of Materials Science and Engineering, K. N. Toosi University of Technology, Tehran, Iran

Bejoy Francis Department of Chemistry, St. Berchmans College, Kottayam, Kerala, India

E. A. Franco-Urquiza National Council for Science and Technology (CONACYT–CIDESI), National Center for Aeronautic Technologies (CENTA), Querétaro, Mexico

Mariacristina Gagliardi NEST, Istituto Nanoscienze-CNR and Scuola Normale Superiore, Pisa, Italy

Dheeraj kumar Gara Department of Mechanical Engineering, NIT Warangal, Warangal, Telangana, India

Oluwatoyin Joseph Gbadeyan Composite Research Group, Department of Mechanical Engineering, Durban University of Technology, Durban, South Africa

Jesiya Susan George School of Chemical Sciences, Mahatma Gandhi University, Kottayam, Kerala, India

International and Inter University Centre for Nanoscience and Nanotechnology (IIUCNN), Mahatma Gandhi University, Kottayam, Kerala, India

Mauro Giorcelli Department of Applied Science and Technology, Politecnico di Torino, Turin, Italy

Consorzio Interuniversitario Nazionale per la Scienza e Tecnologia dei Materiali (INSTM), Florence, Italy

Jineesh Ayippadath Gopi Division of Chemistry, Department of Science, Faculty of Science & Technology, Alliance University, Bengaluru, Karnataka, India

Nishar Hameed School of Engineering, Swinburne University of Technology, Hawthorn, VIC, Australia

Naman Jain Department of Mechanical Engineering, Meerut Institute of Engineering and Technology, Meerut, India

Aswathy Jayakumar Department of Mechanical and Process Engineering, King Mongkut's University of Technology North Bangkok, The Sirindhorn International Thai-German Graduate School of Engineering (TGGS), Bangsue, Bangkok, Thailand

Jitha S. Jayan Department of Chemistry, Amrita Vishwa Vidyapeetham, Amritapuri, Kerala, India

Kuruvilla Joseph Department of Chemistry, Indian Institute of Space Science and Technology, Thiruvananthapuram, Kerala, India

Chanchira Jubsilp Department of Chemical Engineering, Faculty of Engineering, Srinakharinwirot University, Nakhon Nayok, Thailand

Yong Chae Jung Institute of Advanced Composite Materials, Korea Institute of Science and Technology (KIST), Jeonbuk, Republic of Korea

Ajay Kumar Kadiyala Irish Composites Centre (IComp), Bernal Institute (Composites), School of Engineering, University of Limerick, Limerick, Ireland

Rakesh Kanakam Department of Mechanical Engineering, National Institute of Technology, Warangal, India

K. Kanny Composite Research Group, Department of Mechanical Engineering, Durban University of Technology, Durban, South Africa

T. K. Gowtham Keerthi Department of Mechanical Engineering, PSG Institute of Technology and Applied Research, Coimbatore, Tamil Nadu, India

Majid Khorami Facultad de Arquitectura y Urbanismo, Universidad UTE, Quito, Ecuador

Young Nam Kim Institute of Advanced Composite Materials, Korea Institute of Science and Technology (KIST), Jeonbuk, Republic of Korea

Department of Chemical and Biomolecular Engineering, Yonsei University, Seoul, Republic of Korea

Senthilkumar Krishnasamy Department of Mechanical Engineering, Francis Xavier Engineering College, Tirunelveli, Tamilnadu, India

M. S. R. Niranjan Kumar Department of Mechanical Engineering, Prasad V. Potluri Siddhartha Institute of Technology, Kanuru, Andhra Pradesh, India

Rajeev Kumar Composite Design and Manufacturing Research Group, School of Engineering, Indian Institute of Technology Mandi, Mandi, Himachal Pradesh, India

Vinod Kushvaha Department of Civil Engineering, Indian Institute of Technology Jammu, Jammu, India

Manish Kumar Lila Department of Mechanical Engineering, Graphic Era Hill University, Dehradun, India

Chao Lu School of Textile Science and Engineering, Tiangong University, Tianjin, China

Key Laboratory of Advanced Textile Composite Materials, Tiangong University, Tianjin, China

Priyanka Madhushri Stanley Black and Decker, Atlanta, GA, USA

Radha Raman Mishra Department of Mechanical Engineering, Birla Institute of Technology and Science, Pilani, India

T. P. Mohan Composite Research Group, Department of Mechanical Engineering, Durban University of Technology, Durban, South Africa

Francisco M. Monticeli Department of Materials and Technology, Fatigue and Aeronautic Materials Research Group, School of Engineering, Sao Paulo State University (UNESP), Guaratingueta, SP, Brazil

Phattarin Mora Department of Chemical Engineering, Faculty of Engineering, Srinakharinwirot University, Nakhon Nayok, Thailand

Moslem Najafi Faculty of Materials Science and Engineering, K. N. Toosi University of Technology, Tehran, Iran

Jorge S. S. Neto Federal Center of Technological Education of Rio de Janeiro (CEFET/RJ), Rio de Janeiro, Brazil

Roberta M. Neves Postgraduate Program in Mining, Metallurgical and Materials Engineering, Federal University of Rio Grande do Sul (UFRGS), Porto Alegre/RS, Brazil

Lin Feng Ng Centre for Advanced Composite Materials (CACM), School of Mechanical Engineering, Faculty of Engineering, Universiti Teknologi Malaysia, Johor Bahru, Johor, Malaysia

C. M. Ó Brádaigh School of Engineering, Institute for Materials and Processes, The University of Edinburgh, Edinburgh, UK

Shakuntala Ojha Department of Mechanical Engineering, Kakatiya Institute of Technology and Science, Warangal, Telangana, India

Heitor Luiz Ornaghi Jr. Postgraduate Program in Mining, Metallurgical and Materials Engineering, Federal University of Rio Grande do Sul (UFRGS), Porto Alegre/RS, Brazil

Suraj P. R. School of Chemical Sciences, Mahatma Gandhi University, Kottayam, Kerala, India

N. H. Padmaraj Department of Aeronautical and Automobile Engineering, Manipal Institute of Technology, Manipal Academy of Higher Education, Manipal, India

Manoj Panchal Department of Mechanical Engineering, RGM College of Engineering and Technology, Nandyal, Andhra Pradesh, India

Jyotishkumar Parameswaranpillai Division of Chemistry, Department of Science, Faculty of Science & Technology, Alliance University, Bengaluru, Karnataka, India

S. K. Khadheer Pasha Department of Physics, VIT-AP University, Guntur, Andhra Pradesh, India

Xiaoyuan Pei School of Textiles Science and Engineering, Tiangong University, Tianjin, China

Composites Research Institute, Tiangong University, Tianjin, China

Saul Piedra Center for Engineering and Industrial Development (CIDESI), National Council for Science and Technology of México (CONACYT), Santiago de Querétaro, Mexico

M. Om Prakash Department of Mechanical Engineering, Kakatiya Institute of Technology and Science, Warangal, Telangana, India

P. Syam Prasad Department of Physics, NIT Warangal, Warangal, Telangana, India

Yufeng Quan Artie McFerrin Department of Chemical Engineering, Texas A&M University, College Station, TX, USA

Sabarish Radoor Department of Mechanical and Process Engineering, King Mongkut's University of Technology North Bangkok, The Sirindhorn International Thai-German Graduate School of Engineering (TGGS), Bangsue, Bangkok, Thailand

Gujjala Raghavendra Department of Mechanical Engineering, National Institute of Technology, Warangal, India

G. Rajeshkumar Department of Mechanical Engineering, PSG Institute of Technology and Applied Research, Coimbatore, Tamil Nadu, India

Sanjay Mavinkere Rangappa Department of Materials and Production Engineering, The Sirindhorn International Thai German Graduate School of Engineering (TGGS), King Mongkut's University of Technology North Bangkok (KMUTNB), Bangsue, Bangkok, Thailand

Manjeet Rani Composite Design and Manufacturing Research Group, School of Engineering, Indian Institute of Technology Mandi, Mandi, Himachal Pradesh, India

Priyanka Rani Department of Physics, B. S. Abdur Rahman Crescent Institute of Science and Technology, Chennai, Tamil Nadu, India

P. Lokanatha Reddy Department of Physics, School of Advanced Sciences, VIT University, Vellore, Tamil Nadu, India

Sarawut Rimdusit Department of Chemical Engineering, Faculty of Engineering, Chulalongkorn University, Bangkok, Thailand

Ali Saeedi Faculty of Mechanical Engineering, Iran University of Science and Technology, Tehran, Iran

Kushairi Mohd Salleh Bioresources and Biorefinery Laboratory, Department of Applied Physics, Faculty of Science and Technology, Universiti Kebangsaan Malaysia, UKM, Bangi, Selangor, Malaysia

S. Arvindh Seshadri Department of Mechanical Engineering, PSG Institute of Technology and Applied Research, Coimbatore, Tamil Nadu, India

Aanchna Sharma Department of Civil Engineering, Indian Institute of Technology Jammu, Jammu, India

Ruiqing Shen Artie McFerrin Department of Chemical Engineering, Texas A&M University, College Station, TX, USA

Suchart Siengchin Department of Mechanical and Process Engineering, King Mongkut's University of Technology North Bangkok, The Sirindhorn International Thai-German Graduate School of Engineering (TGGS), Bangsue, Bangkok, Thailand

Alberto Tagliaferro Department of Applied Science and Technology, Politecnico di Torino, Turin, Italy

Consorzio Interuniversitario Nazionale per la Scienza e Tecnologia dei Materiali (INSTM), Florence, Italy

Youhong Tang Institute for NanoScale Science and Technology, College of Science and Engineering, Flinders University, Adelaide, SA, Australia

Sabu Thomas International and Inter University Centre for Nanoscience and Nanotechnology (IIUCNN), School of Energy Materials, Mahatma Gandhi University, Kottayam, Kerala, India

Sunan Tiptipakorn Department of Chemistry, Faculty of Liberal Arts and Science, Kasetsart University, Nakhon Pathom, Thailand

Mauricio Torres-Arellano Center for Engineering and Industrial Development (CIDESI), National Council for Science and Technology of México (CONACYT), Santiago de Querétaro, Mexico

Akarsh Verma Department of Mechanical Engineering, University of Petroleum and Energy Studies, Dehradun, India

Poornima Vijayan P. Sree Narayana College for Women (Affiliated to University of Kerala), Kollam, Kerala, India

Chunhong Wang School of Textile Science and Engineering, Tiangong University, Tianjin, China

Key Laboratory of Advanced Textile Composite Materials, Tiangong University, Tianjin, China

Lijian Wang School of Textile Science and Engineering, Tiangong University, Tianjin, China

Key Laboratory of Advanced Textile Composite Materials, Tiangong University, Tianjin, China

Qingsheng Wang Artie McFerrin Department of Chemical Engineering, Texas A&M University, College Station, TX, USA

Wenjin Xing Institute for NanoScale Science and Technology, College of Science and Engineering, Flinders University, Adelaide, SA, Australia

Sunny Zafar Composite Design and Manufacturing Research Group, School of Engineering, Indian Institute of Technology Mandi, Mandi, Himachal Pradesh, India

Sarani Zakaria Bioresources and Biorefinery Laboratory, Department of Applied Physics, Faculty of Science and Technology, Universiti Kebangsaan Malaysia, UKM, Bangi, Selangor, Malaysia

Qi Zuo School of Textile Science and Engineering, Tiangong University, Tianjin, China

Key Laboratory of Advanced Textile Composite Materials, Tiangong University, Tianjin, China

Part I

Epoxy/Synthetic Fiber Composites

Introduction to Epoxy/Synthetic Fiber Composites

1

Ankur Bajpai, Ajay Kumar Kadiyala, and C. M. Ó Brádaigh

Contents

Abstract

The adaptability and uniqueness of epoxy resins make them ideal for a variety of industrial applications, including surface coatings, electronic part encapsulation, composite matrices for wind energy blades, automotive, and aerospace. Unmodified epoxy resins are used in a limited number of high-performance

A. Bajpai (✉) · C. M. Ó Brádaigh
School of Engineering, Institute for Materials and Processes, The University of Edinburgh, Edinburgh, UK
e-mail: ankur.bajpai@ed.ac.uk

A. K. Kadiyala
Irish Composites Centre (IComp), Bernal Institute (Composites), School of Engineering, University of Limerick, Limerick, Ireland

S. Mavinkere Rangappa et al. (eds.), *Handbook of Epoxy/Fiber Composites*,
https://doi.org/10.1007/978-981-19-3603-6_1

applications, due to their inherent brittleness and low impact resistance. The drawbacks of epoxies can be solved by modifying them prior to use. Because of their superior mechanical, thermal, and electrical properties, modified epoxy resins are now widely used in the manufacturing of synthetic fiber-reinforced composites and the manufacture of various industrial products. This chapter presents a systematic review of recent literature on the structure of epoxies, as well as their synthesis and various factors influencing final properties. This chapter also aims to cover the recent developments in synthetic fiber-based epoxy composites, such as manufacturing processes and industrial applications.

Keywords

Epoxy · Glass fiber · Carbon fiber · Epoxy composites

Introduction: Epoxy Resins

Composites are defined as a mixture of two or more different materials in micro-scale, possessing synergistic properties compared to those of either component on their own. Composites are generally classified based on two different groups, matrix and reinforcements, as shown in Fig. 1. The matrix level can further be classified into metal, organic (carbon-carbon and polymer matrix composites), and ceramic matrix composites. Based on the type of reinforcement, the composites are further classified as particulate, fiber-reinforced, and structural composites. The combination of fiber and matrix is a widely researched composite material which provides high performance and improved properties. There is a wide range of reinforcing fibers and matrix available, and selection is based on the application as well as the desired properties of the composites. The major function of the matrix is to provide support and protection for the fibers. Fibers mainly act as reinforcements and possess high strength, stiffness, and low-density properties. A strong adhesion between fiber and matrix helps to transfer the load from the matrix to the fibers. In this chapter, we will discuss organic epoxy-based epoxies and various types of synthetic fibers.

For composite applications, epoxies are the most common and widely used polymer matrix. Epoxy resins are forms of thermosetting polymers that have a lot of good properties including adhesion, chemical, mechanical, and thermal properties. Epoxy resins react with a suitable hardener to form insoluble and infusible 3-D

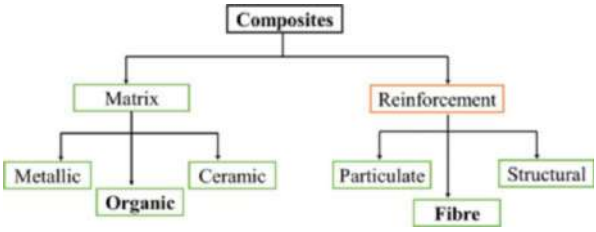

Fig. 1 Broad classification of composites

networks, which can be formed with or without heat. In 1946, the first commercially available epoxy resins were introduced. Pierre Castan of Switzerland and Sylvan Greenlee of the United States were the first to commercialize epoxy resins. Castan developed a bisphenol A-based epoxy resin in 1936 by reacting it with epichlorohydrin and then curing it with phthalic anhydride to create a thermoset composition (Gannon 1986). Figure 2 shows an epoxide ring, which is a three-atom ring consisting of two carbon atoms and an oxygen atom joined with one and two hydrogen atoms, respectively (Mallick 2007). Epoxy resins are formed by molecules containing more than one of these epoxy groups. The resin's functionality is determined by the amount of epoxy groups per molecule. Internally, terminally, on cyclic systems, the groups can be found (Petrie 2005).

A three-dimensional structure can form if this ring is reacted with a suitable hardener.

As depicted in Fig. 3, the ring is arranged in such a way that a one of carbon atom being attacked by a nucleophile or a electrophilic attach of oxygen atom on an electrophile to proceed the reaction.

Epoxy resins were made using epichlorohydrin of olefins and peracids. Diglycidyl ether of bisphenol A (DGEBA) is the key intermediate for epoxy resins, which is a product of bisphenol A and epichlorohydrin. Figure 4 depicts the process of epoxy resin production from bisphenol A. Semi-solid or solid resins may be made by growing the molecular weight of the mixture by applying more

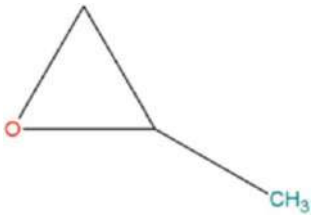

Fig. 2 Chemical structure of epoxy ring

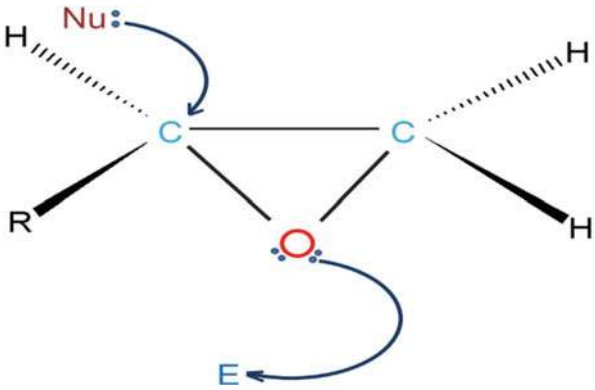

Fig. 3 Mechanisms for an electrophile (E) or a nucleophile (Nu) to open the oxirane ring

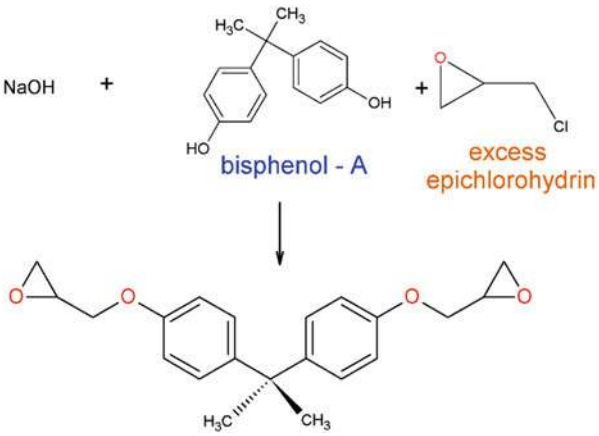

Fig. 4 The synthesis of bisphenol A-based epoxy resins

bisphenol A to liquid DGEBA. These solid resins are used as corrosion-resistant films or as steel coating primers. If the molecular weight of the resin rises, so does its viscosity and functionality. Curing is a chemical process in which the resin is combined with a curing agent (hardener) and/or catalyst to create a three-dimensional network that is tightly cross-linked, resulting in a hard, infusible, and rigid substrate (Petrie 2005). The epoxy resins, hardeners, and/or catalysts used, as well as the curing temperature and period, decide the physical and performance properties of the composites.

Furthermore, the inherent ductility of the resulting unmodified cured epoxy system is calculated by the disparity in cross-link density. Hence, toughenability and effectiveness of the different toughening mechanisms are explored in the epoxies. A thorough knowledge of the physical and chemical properties of unmodified cured epoxy resins is needed to investigate the toughening mechanisms of modified epoxies.

Stepped growth polymerization and chain homopolymerization are the curing reactions of epoxy resins, through one or more curing agents and catalysts, in combination and/or separately (Petrie 2005; Pascault and Williams 2010). Since the curing reaction is essentially a ring-opening operation, all curing reactions are exothermic, resulting in minimal by-products and low shrinkage.

Though the choice of curing agents (or hardeners) or catalysts (accelerators) is largely dictated by manufacturing and final product requirements, epoxy-hardener curing reactions have a significant impact on the type of bond formation inside the structure and extent of cross-linking (Petrie 2005). The primary polyfunctional and secondary amines, as well as acidic anhydrides, are the most common reactive cross-linking agents (hardeners). In most cases, tertiary amines are used as accelerators. Figure 5 shows a three-dimensional cross-connected structure obtained after the hardener has been completely cured with epoxy resin. Anionically or cationically, the epoxy resin can react using one of the two methods:

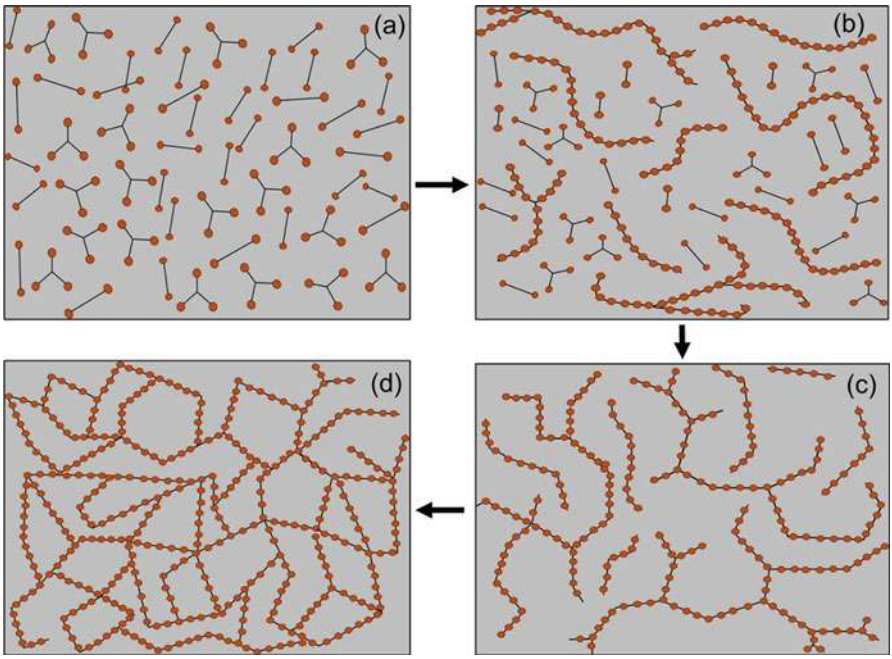

Fig. 5 Thermoset formation is depicted in two dimensions in this diagram. (**a**) Partly polyfunctional monomer. (**b**) Linear and branched materials below gel stage. (**c**) Gelation has started but the cross-linking is still incomplete. (**d**) Cross-linked 3-D network of completely cured epoxy

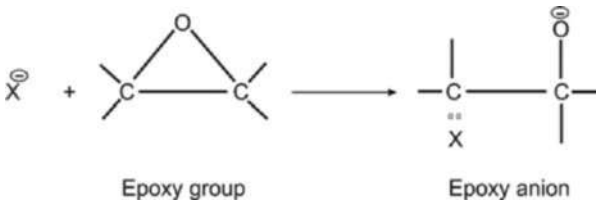

Fig. 6 Anionic formation of the epoxied molecule (Bajpai 2018). (Reused with permission)

Anionic Method

In an anionic process, the epoxy ring is opened from an anion, as illustrated in Fig. 6. Because the generated anion is a free radical, it may undergo further reactions.

Cationic Method

During the cationic process, active hydrogen opens the epoxy group, generating a new chemical bond and a hydroxyl group. This means that the cationic process will take many different paths, three of which are depicted in Fig. 7. The epoxy group can

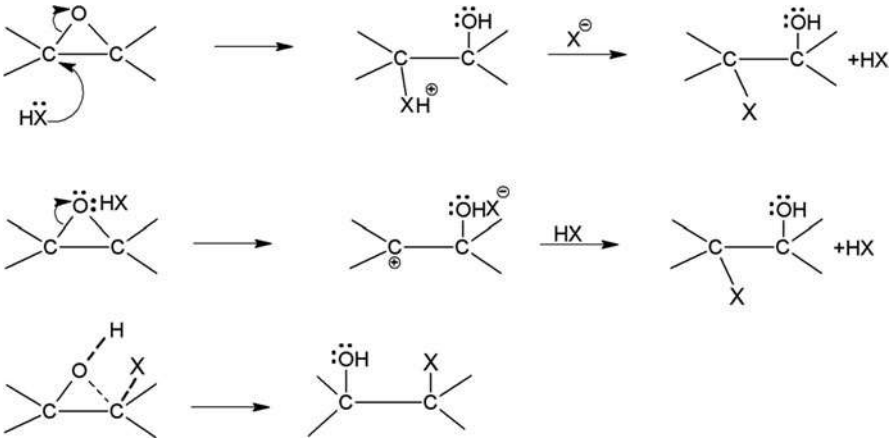

Fig. 7 Cationic formation in epoxy group (Bajpai 2018). (Reused with permission)

react with a wide range of chemical groups, thanks to its two reaction mechanisms. Epoxy resins can be cured using simple curing agents via the cationic route. Curing agents include Lewis bases, amides, primary amines, and secondary amines.

The most important factors to consider when designing a cure cycle are time and temperature. Precision management of the curing cycle is required to generate an epoxy-based composite with desirable mechanical characteristics. Cure rates and reaction pathways are also regulated by temperature. Cross-linking is favored by high-temperature cures, resulting in rigid composites, while chain extension is aided by low-temperature cures, resulting in flexible composites. Gelation is the process of covalent bonds binding throughout a network to produce an endless molecular network.

A thermoset loses its capacity to flow smoothly and is no longer processable above the gel stage, thereby ending its useful life. Gelation, according to Flory's hypothesis (Wall 1954), happens at a certain stage of chemical conversion for a particular system and is reliant on the curing system and reaction environment. Gelation happens when a bulk polymer goes from a liquid to a rubbery form in practice.

Vitrification is the transformation of a polymer into a glassy state. The chemical conversion process is slowed. A reacting system's vitrification point is the point at which further reaction is halted. In the vitrified state, Wisanrakkit et al. (Wisanrakkit and Gillham 1990) demonstrated that sluggish, diffusion-controlled reactions can occur. Vitrification is often conceived of as a progressive process that happens across a major amount of the curing period, rather than a single occurrence (Lange et al. 1999). The cure curve is an isothermal time-temperature-transformation (TTT) created by Gillham (1986). The curve provides the relation of properties of thermo-setting systems to process conditions and is the most widely recognized cure diagram. To detect when the polymer starts to gel and vitrify, he employed Torsional Braid Analysis, and he subsequently utilized the same procedure to cure epoxy resin. The gelation and vitrification procedures are depicted in Fig. 8.

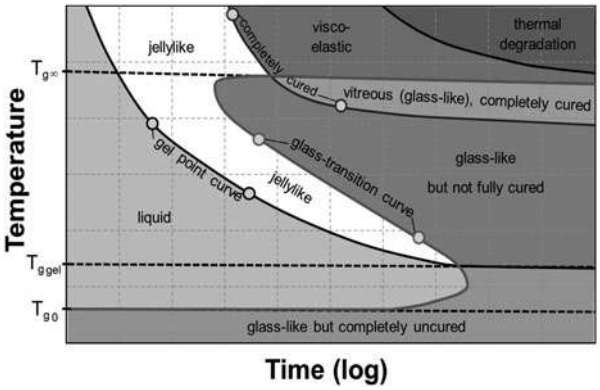

Fig. 8 For a thermosetting (epoxy) system, isothermal cure time-temperature-transformation (TTT) curve (Bajpai 2018). (Reused with permission)

The properties of a cured epoxy/hardener system are influenced by several factors. They are as discussed in the following section. Stoichiometry refers to the precise amount of hardener that should be applied to the epoxy resin for the number of reacting groups in the resin/hardener to be comparable. The stoichiometric ratio is a critical factor in determining the final structure's properties, as it has a big impact on properties like glass transition temperature, elastic modulus, cross-link density, and weight. Several researchers have published on the effect of the stoichiometric ratio of epoxy resins and curing agents on cross-linking degree. Mostovoy et al. (Mostovoy and Ripling 1966) show that at the stoichiometric ratio, ultimate tensile strength reaches its maximum value, while others (Bell 1970; Kim et al. 1978) show that ultimate strength is insensitive to the stoichiometric ratio. The chemical composition of the materials would be altered if the stoichiometric ratio were changed. The viscoelastic properties of thermosetting epoxy resin systems are known to be affected by properties such as hardener chemistry, resin/curing agent ratio, and resin/curing agent molecular ratio (Palmese and McCullough 1992). Anti-plasticization happens when non-stoichiometric hardener variation is performed with epoxy, according to some researchers (Bellenger et al. 1990; Mafi et al. 2009; Boye et al. 1991), resulting in an increase in storage modulus with a decrease in glass transition temperature. From the monomers with a functionality greater than 2, the thermosetting polymers form a cross-connected three-dimensional network. This results in a fundamental property difference between thermoplastics and thermosets. The polymer chain in thermoplastics develops in a linear direction, with all monomers having the functionality of 2. The cross-link density of a thermosetting polymer is influenced by monomer functionality. A monomer with a functionality of 3 will create half as many cross-links as a monomer with a functionality of 4 in its final configuration. A higher cross-link density results in increased dimensional stability, higher T_g, and superior mechanical strength. The cross-link density of the thermosetting polymer is influenced by monomer size. The mobility of the chemical structure influences the glass transition temperature (T_g) as follows:

- Increasing the polarity of the main chain raises the T_g.
- Bulky side groups boost the final healed system's T_g.
- Extending the length of the adjustable side groups reduces the system's T_g.
- T_g is reduced by using flexible main chain elements.

A few residual polymer chains may not have enough chance to bind to reacting sites inside the network, preventing them from cross-linking in rapid or snap cures. Snap cures can often result in greater shrinkage than longer cure periods (Dixon et al. 2003). Longer cure times slow the pace of reaction, allowing unreacted polymer chains to align themselves in the proper place for cross-linking reactions to occur. The kind of cure, such as a longer cure or a speedier cure, should be carefully selected depending on the completed product and the attributes needed.

The maximum "degree of cure" is theoretically characterized as the state in which all reactive sites are reacted during cure before the conversion is stopped. More realistically, a properly cured system is one with ample cross-linking to have the best properties for a specific application. Cross-linking (creation of three-dimensional networks of molecules via reactive constituents) and conversion are the two main types of reactions that occur during the curing process. Because of caging effects, reactive groups in strongly cross-linked networks are often sterically hindered from reacting, resulting in an incomplete reaction between the hardener (e.g., amine or anhydride) and epoxy group (Pearce 1992).

The glass transition temperature is the temperature at which the polymer attains enough thermal energy to slide over one another at a noticeable rate, allowing large-scale viscous flow to occur, limited primarily by each component's inherent resistance to such flow (Bellenger et al. 1987). Figure 9 depicts various experimental methods for determining the glass transition temperature of polymers. Mechanical properties change dramatically in the glass transition region. Young's modulus in a cured epoxy system will drop by a factor of 1000 as the temperature goes up to the glass transition level. As the temperature in the glass transition zone increases, other physical properties of thermoset systems, such as ultimate tensile strength, specific heat capacity (c_p), coefficient of thermal expansion, and refractive index, shift drastically. As a polymer reaches its glass transition temperature, it gains sufficiently thermal energy to bypass two forms of large-scale motion barriers, i.e., inner frictional resistance between individual components is the cause of viscous flow resistance. Their susceptibility to viscous flow is often influenced by the geometrical and topological properties of their atoms. This definition is encapsulated by the hypothesis of chain stiffness. The glass transition happens when chain fragments of up to many statistical (Kuhn) segments have adequate freedom of motion to execute cooperative motions (Bershtein et al. 1985). If the chain stiffness increases, Kuhn segments get larger. The unified forces that hold various molecules and molecular fragments together are known as van

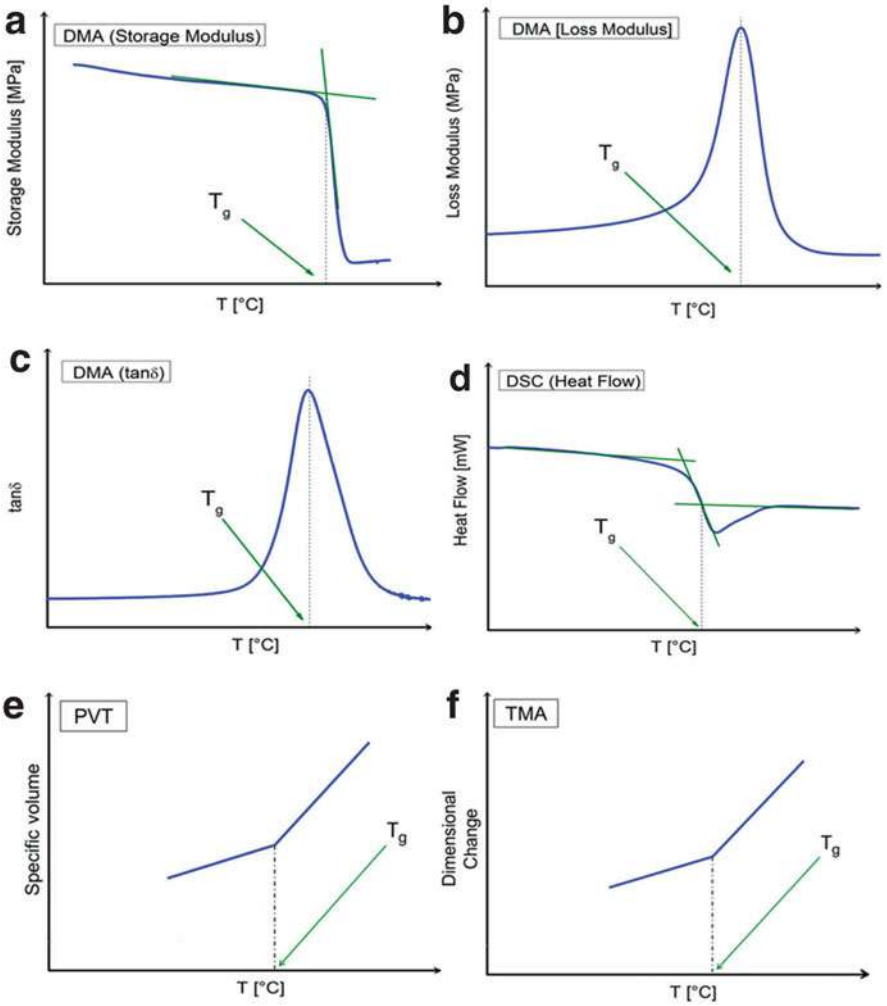

Fig. 9 The following theoretical methods are used to measure T_g: (**a**) sudden dip in storage modulus; (**b**) tip of the loss modulus diagram; (**c**) highest tip of the tanδ curve; (**d**) at the middle point of heat flow dip; and (**e**,**f**) at the point of intersection of linear regions (Bajpai 2018). (Reused with permission)

der Waals forces. The chain fragment and unified forces of amorphous component contribute to the T_g. Cohesive forces may be measured using cohesive energy density and other properties. The cohesive forces increase as polarity increases, causing the T_g to increase (Lee and Sewell 1968).

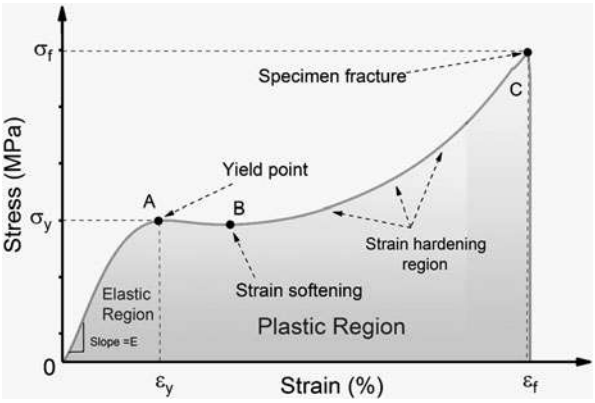

Fig. 10 Different regions of a stress-strain curve for an epoxy system obtained from compression test (Bajpai 2018). (Reused with permission)

(a) Tensile strength: A material's tensile strength is the highest stress that it can endure prior to failing. There are three different kinds of strengths: (i) yield strength (maximum stress a material can withstand before displaying permanent or plastic deformation); (ii) ultimate strength (maximum stress a material can withstand); and (iii) breaking strength (stress under which rupture occurs), as shown in Fig. 10. In the case of polymers, the tensile strength is influenced by the following factors (Halary et al. 2011):
   - Crystallinity: Higher crystallinity in a polymer increases its strength because intermolecular bonding is stronger in the crystalline sections. Consequently, polymer deformation can lead to increased strength and more directed chains.
   - Molecular weight: As the molecular weight of a polymer increases, its tensile strength increases until it reaches a saturation point at a certain molecular weight. The following equation shows the relationship between tensile strength and molecular weight.

$$\sigma = \sigma_{\infty} - \frac{X}{M_w} \tag{1}$$

where σ_{∞} is the tensile strength of the polymer with molecular weight of infinity. X is a constant, and M_w is the molecular weight. The polymer chains are loosely bonded by weak van der Waals forces at lower molecular weights, allowing the chains to travel about freely, resulting in low strength. The chains become long and entangled in large molecular weight polymers, giving the polymer strength.

- Young's modulus (elastic modulus): In the linear elastic field, Young's modulus is the ratio of stress to strain. Elastic modulus is a measure of a material's inherent stiffness.
- Percentage elongation to fracture: This is the percentage change in the material's dimensions before it fractures. It is a ductility metric. In the tensile mode, thermosets have an elongation to fracture value of less than 5%.

- Cross-linking: Polymers can form a 3-D network that restricts motion of polymeric chains, resulting in increased tensile strength.

(b) Toughness: The region under a stress-strain curve, as shown in Fig. 10, determines a material's toughness. The toughness of a material is determined by the amount of energy it absorbs before it ruptures.
(c) Brittleness: A brittle material is one that fractures or breaks without any appreciable plastic (permanent) deformation. Brittleness is the opposite of ductility and is used in this chapter to explain fracture, where sharp cracks run across structures with just slight deformation around the crack tips (Williams 1977).
(d) Ductility: The ability of a material to demonstrate large-scale plastic deformation before failure. Ductility is the opposite of brittleness. Here, ductile failure is described as large-scale plastic deformation around a crack, which frequently results in visible crack tip blunting (Williams 1977).

The yield behavior of unmodified epoxies is studied using compression tests (Yee et al. 2000). Because of their highly cross-linked structure, epoxies are brittle materials that typically fracture before yielding in tensile tests, at temperatures below their glass transition temperature (Halary et al. 2011). Unmodified epoxy, on the other hand, exhibits yielding and plasticity under compression, even at low temperatures (Yamini and Young 1980; Cook et al. 1998). Strain rate, temperature, and hydrostatic pressure all play a role in the yielding phenomenon in epoxies. As the test strain rate rises or the temperature decreases, the yielding behavior of bisphenol A-based epoxy cured with amine hardener with different cross-link densities is seen to improve (Yamini and Young 1980).

Other researchers (Mayr et al. 1998; Behzadi and Jones 2005) confirmed the same pattern, confirming that the yielding behavior of unmodified epoxies is strain rate and temperature dependent. Several models are presented to illustrate how the yield behavior of epoxies is affected by pressure, temperature, and strain rate. These models were originally created to explain the yield behavior of thermoplastic polymers. These models can make excellent predictions up to the yield point, when applied to unmodified epoxies. This chapter only looks at one of these versions. As seen in Eq. 2, the modified von Mises criterion defines the pressure dependency of the yield activity of unmodified epoxies (Crist 1997; Ward 1971).

$$(\sigma_1 - \sigma_2)^2 + (\sigma_2 - \sigma_3)^2 + (\sigma_3 - \sigma_1)^2 = 6\left(\tau_y^0 + \mu p_{hs}\right)^2 \tag{2}$$

where σ_1, σ_2, and σ_3 are the principal stresses in the material, τ_y^0 is the shear stress in pure shear and under zero pressure, $p_{hs} = -\frac{(\sigma_1+\sigma_2+\sigma_3)}{3}$ is the hydrostatic pressure, and μ is the internal coefficient of friction. By allowing the shear stress, τ_y^0, to vary linearly with the fraction of the hydrostatic pressure, the standard von Mises yield criterion is updated.

Epoxies which are unmodified are usually vulnerable to brittle failure, where a tensile stress field dominates fracture and stress concentrations at defects (cracks)

become problematic. Epoxies are extremely brittle and only exhibit localized plastic deformation during fracture. Linear elastic fracture mechanics (LEFM) has been used to investigate their fracture behavior (Crist 1997). As a result, epoxies' resistance to fracture is typically expressed as a fracture energy or critical strain energy release rate, G_{Ic} (energy per unit area required to generate a new crack surface), or a critical stress intensity factor, K_{Ic} (in the presence of a natural crack, the value needed to cause catastrophic failure under simple uniaxial loading), in plane strain constrained conditions. Mostly, mode I (tensile mode) crack propagation is considered because it is theoretically more critical than the other crack propagation modes (mode II, in-plane shear, and mode III, out-of-plane shear) and provides the minimum value of fracture toughness, which is crucial in design considerations (see Fig. 11). At room temperature, the fracture energy (mode I) of unmodified epoxy systems is usually in the range of 90–2901 J/m^2 (Hull 1999).

Since the values of G_{Ic} are far higher than the energy measured theoretically for pure brittle fracture (Crist 1997), however, energy absorption processes such as plastic deformation must also occur during fracture. This hypothesis was confirmed by fractography observations of river line patterns caused by matrix fracturing that were spontaneously generated from the initial crack front (Hull 1999), as depicted in Fig. 12, to support this conclusion.

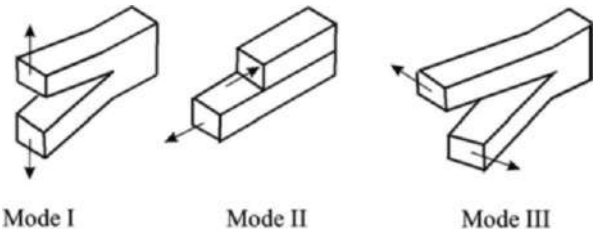

Fig. 11 Various cracking opening modes. Mode I (tensile), mode II (in-plane shear), and mode III (out-of-plane shear) (Bajpai 2018). (Reused with permission)

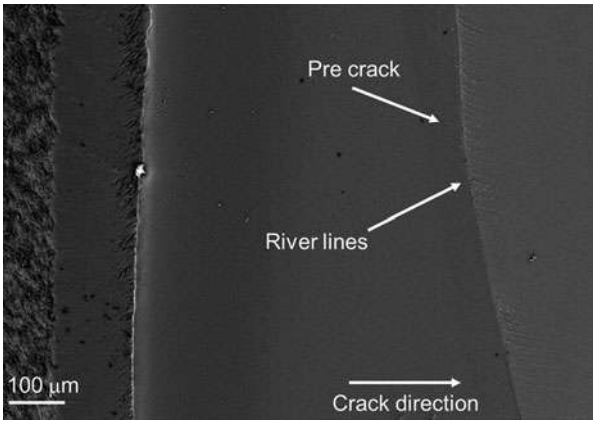

Fig. 12 River lines begin at the crack front of an unmodified amine-cured DGEBF epoxy in this SEM picture

In the fracturing of unmodified epoxies (also toughened epoxies), three major forms of crack propagation are observed, depending on the test temperature and test loading rate (Gannon 1986). Figure 13 depicts different types of crack propagation in epoxy systems. Since the yield stress governs the size of the plastic deformation zone and the crack tip blunting mechanism, the effect of strain rate and temperature on the fracture behavior of an unmodified epoxy is dependent on the yield stress' strain rate and temperature dependence (Pascault et al. 2002).

The radius of curvature of the blunting tip and the plastic deformation zone during crack propagation are inversely proportional to yield stress squared, according to Eq. 3. The fracture energy of unmodified epoxy (G_{Ic}) increases as the yield strength value decreases.

$$r_{pzu} = \left(\frac{1}{6\pi}\right)\left(\frac{1}{\sigma_{yt}}\right)^2 \frac{G_{Ic}E}{\left(1-\vartheta^2\right)} \tag{3}$$

Here, r_{pzu} is the plain strain plastic zone radius, σ_{yt} is the tensile true yield strength, υ is Poisson's ratio, and E is Young's modulus for an unmodified epoxy system. A

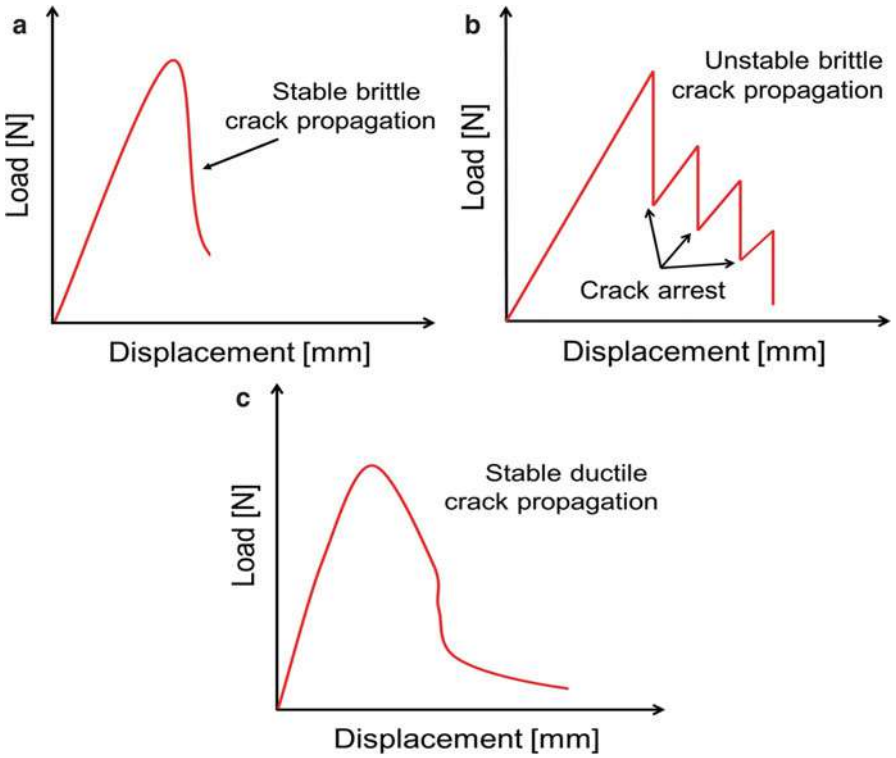

Fig. 13 Load displacement diagrams in compact tension specimens for different types of crack propagation in unmodified epoxy

drop in temperature leads to an increase in yield strength and facilitates a decrease in G_{Ic} for a constant strain rate. As a result, at low temperatures, stable brittle crack propagation occurs, while at higher temperatures, unstable brittle crack propagation occurs. Furthermore, at constant temperature, a lower strain rate reduces yield strength and raises G_{Ic}, resulting in stable brittle crack growth at faster strain rates but unstable semi-brittle crack growth at lower strain rates (Kinloch et al. 1983).

Synthetic Fibers

Reinforcing of epoxy resins is a common way of modifying the epoxies. The reinforcements improve both the thermal and mechanical properties. In epoxy composites, the most commonly used reinforcements in composite industries are synthetic/man-made fibers such as carbon, glass, and aramid. Table 1 provides a comparison of the properties of the common synthetic fibers for composite applications. The fibers are available in the form of continuous fibers, chopped fibers, rovings, woven textiles, and prepregs. These are further utilized to manufacture composite parts using various manufacturing techniques.

Historically, the growth and development of composite materials began in the 1940s (Cevahir 2017). This can further be classified into two major generations of development.

- First generation in the 1940s, which saw major developments in glass fiber-reinforced composites.
- Second generation in the 1960s, an era which saw the start of the development of high-performance composites. Carbon fibers were used for the first time as reinforcements in polymer composites for aircraft structures. In the 1980s–

Table 1 Comparison of the properties of the common synthetic fibers for composite applications (Cevahir 2017; Gao et al. 2004; Anandjiwala 2016; Sharma et al. 2014; Acatay 2017; Sathishkumar et al. 2014; Ertekin 2017; Chowdhury et al. 2020)

Fiber material	Elastic modulus (GPa)	Tensile strength (MPa)	Density (g/cc)	Potential application
Carbon (high modulus)	350–650	2500–4000	1.75	Spacecraft, high-end sporting goods, and industrial rollers
Carbon (high strength)	240	3500	1.95	Wingbox, pressure vessels, hydrogen storage tanks for fuel cell vehicles
E-glass	80–81	3100–3800	2.6	Aircraft radomes, antennae Wind turbine blades
S-glass	88–91	4380–4590	2.5	Military applications
Aramid	70–112	2900	1.44	Helicopter rotor blades, marine vessel hulls and sporting goods, armor applications

1990s, new markets emerged for composites, from sports to automobile industries (Erden and Ho 2017).

This chapter will discuss the characteristic properties of various synthetic fibers, including some recent developments in epoxy-synthetic fiber composites.

Carbon Fibers

Commercially available carbon fibers possess a carbon content of more than 92%. Carbon is manufactured via various precursor materials such as PAN, pitch, and rayon. The process of production of carbon fibers involves multi-stage heat treatment carried out under tension. The strength and stiffness of the carbon fiber depend on the final heat treatment cycle. High heat treatment (above 2000 °C) can produce high modulus-type fibers. This process is known as graphitization. An intermediate heat treatment (around and above 1500 °C) is generally associated with the high strength-type fibers. Low heat treatment (< 1000 °C) produces low modulus and low strength materials. Post-heat treatment, the fibers are sized with a thin polymeric coating applied in low concentration (0.3–1.5 wt.%). This promotes bonding with the matrix and reduces friction damage during fiber handling (Acatay 2017; Summerscales 2019; Davide and Wilhelm 2016). The modulus band in which the properties of carbon fibers fall is typically used to group them. High strength, intermediate modulus, high modulus, and ultra-high modulus are some of the terms used to describe these group. Most varieties have a filament diameter of 5–7 μm. Carbon fiber has the highest specific stiffness of any commercially available fiber and is extremely strong in tension and compression, and it is rust, creep, and fatigue resistant. Impact strength of carbon fibers, on the other hand, is lower than that of glass or aramid fibers, with HM and UHM fibers being especially brittle (Lavin and Hearle 2001).

The use of PAN-based carbon fibers in composites for military aircraft propelled the development of carbon fibers in the 1980s. Carbon fiber composites had a significant importance since they allowed for weight reduction as well as increased range, payload, and performance. Commercial aircraft adopted the technology in the 2000s and 2010s. Carbon fibers found their way into sporting goods, medical devices, industrial applications, and infrastructure because they enabled new levels of efficiency. PAN-based carbon fiber is divided into two categories: aerospace grade, which has stringent requirements for sensitive applications, and industrial grade, which is manufactured in larger tow sizes. Carbon fiber-reinforced plastics (CFRP) are widely used in applications with critical requirements of high strength, stiffness, low weight, and fatigue performance such as aeronautics, automotive, sport, wind turbine blade spars, compressed gas storage, and transport and recreation. The material maintains high modulus and strength, even at high temperatures. Additionally carbon fibers also have high thermal conductivity, electrical conductivity, and good chemical inertness, resistance to environmental degradation and corrosion, self-lubrication, and low linear coefficient of thermal expansion (Sharma et al. 2014; Chand 2000; Potter 2017).

Glass Fibers

Manufacturing of glass fiber started in 1893; however, it was during World War II that they were first used as reinforcements for structural parts of aircraft (Cevahir 2017; Sathishkumar et al. 2014). The constituents of glass fibers include various combinations of raw materials. Silica (55–74 wt %) is the principal ingredient. Other key components of glass fiber are alumina, boron oxide, calcium oxide, and alkali oxides, which determine the final properties of the fibers. Liquid glass is made by combining quarry materials at 1590 °C. Glass fiber filaments with diameters ranging from 5 to 25 μm are generated by passing liquid through micro-fine bushings and cooling them at the same time. To provide filament cohesion and protect the glass from abrasion, the filaments are drawn together into a strand or roving and coated with a sizing agent. Different types of glass may be made by altering the key ingredients. E-glass contains less alkali and is more durable than A-glass. The material has high tensile and compressive strength and stiffness, as well as good electrical properties and a low cost, but it has weak impact resistance. The cost of E-glass varies depending on the form. It costs about £1–2/kg. In polymer matrix composites, E-glass is the most common form of reinforcing fiber. Although glass fiber has lower stiffness compared to other synthetic fibers, its major advantage is in improved properties through reinforcement, at relatively lower cost. E-glass is the most widely used among various fibrous reinforcements, due to its low cost and low elastic modulus. Glass fiber-reinforced polymer composites are expected to grow at an annual 4% for another 5 years (Glass Fiber Reinforced). There are an increasing amount of interest and rise in demand for glass fiber forecast in marine and wind energy composites (Nash et al. 2019; Zangenberg et al. 2014). Two common glass fibers and their applications are described in Table 1. Sizing agents are applied to protect the glass fibers from breakage or disintegration during manufacturing, to improve fiber/matrix adhesion, and to inhibit static charge accumulation.

E-glass is available in the market in the form of rovings, yarns, and strand. A loosely connected bundle of untwisted filaments or strands is known as rovings. The diameter of each filament in a roving is the same, and it is normally between 14 and 24 μm. Rovings come in a variety of weights, with tex values ranging from 290 to 4700. Tex is a measure of linear density (grams per 1000 m of yarn). The resulting fiber bundle is known as a direct roving, where filaments are gathered immediately after the melting process. After the glass is made, several strands can be brought together separately to make what is known as an assembled roving (Jones and Hearle 2001).

Aramid Fibers

Aramid fibers are organic-based synthetic fibers formed from aromatic polyamide. The fibers are produced by dry-jet, wet spinning of a liquid crystal solution in sulfuric acid. The aramid fiber consists of a stiff aromatic ring, covalently bonded in the backbone chain through the para-linkage (1, 4 positions) in the fiber direction. The amide groups along the linear backbone chain interact with the adjacent chains

through extensive hydrogen bonding in the radial direction (Ertekin 2017; Andrews et al. 1997; Deng et al. 2010).

Aramid fibers have distinct properties that distinguish them from other fibers. Aramid fibers are easier to weave on fabric looms than relatively fragile fibers like glass, carbon, or ceramic. They also have a built-in tolerance to organic solvents, oils, lubricants, and flame exposure. Each type of aromatic polymer has distinct fiber properties, as a result of its fiber and intrinsic polymer structure. The mechanical properties of aramid fiber underpin its widespread industrial use in a variety of fields. It is thicker than steel wire and stiffer than glass, per unit of weight. The thermal stability is high, and both creep and the linear coefficient of thermal expansion are low. The latter properties, which are similar to those of inorganic fibers, are due to the extended chain morphology, high molar mass, and excellent orientation in a thermally stable, non-melting structure. Para-aramid fibers are useful because they combine superior properties with characteristics typically associated with organic fibers, such as low density, simple processability, and moderate fatigue and abrasion resistance. Aramid fibers are lightweight and possess high modulus, strength, toughness, chemical resistance, and thermal stability. They have poor transverse properties and compressive strength, however, resulting from weak hydrogen bonding (Andrews et al. 1997). The major disadvantages of aramid fibers are their tendency to absorb moisture and UV light, due to the aromatic nature of para-aramid (Ertekin 2017).

Dynamic mechanical properties of the aromatic polyamide fibers, as well as their viscoelastic behavior, which can be tailored through appropriate resin reinforcement, are ideal for use in impact-resistant systems for low or high velocities. Aramid polymers, especially meta-aramids, are well known for their high temperature tolerance and stability. This provided a powerful motivation to improve these materials for unique heat-resistant industrial applications. Specialized composites reinforced with aramid fibers have found widespread use in areas where their strength-to-weight and stiffness-to-weight ratios make them more appealing for use than traditional materials like aluminum and steel, especially in aerospace structural components. These components should not only withstand the full range of stresses and strains experienced during flight while remaining structurally sound, but they must also withstand a catastrophic impact. Carbon fibers are not ideal because, despite their stiffness and compressive strength, they are unyielding and prone to brittle fracture (Rebouillat and Hearle 2001).

End-use business segments, such as the substitution of asbestos with para-aramid pulps, have been rethought as a result of aramids. Other fields, such as transportation, will continue to change in response to the ever-increasing stringent requirements for energy efficiency. In this region, aramid plays a significant role. Clearly, aramids have greatly improved and adapted to modern technology, including transportation and delivery, recreational activities like sports, life support, health, and safety in general.

Other Synthetic Fibers

There are a number of other fibers that can be used in advanced composite structures, which are not very widely used, such as polyethylene, polyester, and boron.

The mechanical properties of ultra-high molecular weight polyethylene molecules in random orientation are very poor. The molecules become disentangled and aligned in the direction of the filament when dissolved and are drawn from solution through a filament by a method known as gel spinning. The filaments and resulting fibers have extremely high tensile strength due to the molecular alignment. These fibers have the highest specific strength of the fibers discussed here, due to their low specific gravity (c. 1.0). The fibers' tensile modulus and ultimate strength are marginally higher than E-glass and are lower than aramid or carbon, and the fiber produces a very low compressive strength when used in a composite laminate. Polyethylene fibers are seldom used in isolation for composite components due to these reasons, as well as the high cost and, more significantly, the complexity of making a strong fiber/matrix bond.

Polyester is a high-tenacity, low-density fiber with strong impact resistance with low stiffness values. Its lower stiffness values prevent it from being used in composite components, but it is useful in applications requiring low weight, high impact or abrasion resistance, and low cost. It's often used as a surfacing material because it's very smooth, light, and compatible with most resin forms.

To boost the overall properties of carbon or metal fibers, a coating of boron can be applied. Because of its very high price, this fiber is only used in high-temperature aerospace applications and advanced sporting equipment. A boron/carbon hybrid with carbon fibers intermixed among 80–100 μm boron fibers in an epoxy matrix will achieve properties that are superior to either fiber alone, with flexural strength and stiffness twice that of HS carbon and 1.4 times that of boron, and shear strength that is greater than either fiber (Hearle and Hearle 2001).

Processing of Epoxy Composites

Increased usage of epoxy composites is driven by the research and development of materials and manufacturing processes. Various manufacturing techniques have been developed in the past 50 years, ranging from labor-intensive to automated processes. In processing of epoxy composites, three critical stages can be identified.

- Preforming: The process of arranging fibers in one, two, or three dimensions, conforming to the approximate shape, contour, and thickness desired in the finished composite parts.
- Processing: In the processing stage, pressure and temperature are applied to infuse the resin (if necessary), cure the resin, and consolidate the final product.
- Post-manufacturing: Post-manufacturing involves finishing activities such as trimming, machining, and assembly of parts using mechanical or adhesive methods.

Some common processing of epoxy composites includes contact molding, resin transfer molding, filament winding, vacuum bagging/autoclave automated fiber/tape placement, etc. The fabrication techniques can be further classified into direct

processes where the fibers and resin are introduced at the time of molding (contact molding, resin transfer molding, filament winding, etc.) and indirect processes where a pre-impregnated fiber or fabric material is used (vacuum bagging, autoclave, compression molding).

Contact Molding

Contact molding, also known as hand layup/wet up, can use either a male or a female mold (Fig. 14). It is one of the simplest, oldest, and most globally used composite process. In this process, the resin is manually applied to the dry reinforcement, and compaction is carried out using a roller or vacuum to remove air pockets. A gel coat is used to give a good surface finish. The contact molding process enables manufacturing of large dimension structures; however, it is poor in terms of achieving low void content and high tolerances. Reliability is low, and the quality of the product depends upon the skill of the workforce. There can also be some health and safety issues with the handling of uncured epoxy resins, and volatile organic compounds (VOCs) can be released during layup. The process is flexible, however, and requires just a basic infrastructure to set up. It is very suitable for producing large-sized components in small numbers.

Vacuum Bagging/Autoclave

Vacuum bagging and autoclave processing are the most widely used closed-mold processes. In these processes, a pre-impregnated tape or fabric (prepreg) is used. The preformed prepregs are placed onto the tool surface, covered with release film, breather film, and a vacuum bagging film secured over the tacky tape (Fig. 15). The air is drawn out by creating a vacuum. Due to the action of atmospheric pressure, the part is compressed and consolidated. The tool can be placed in an oven or autoclave under positive pressure for curing. Epoxy/CF composites for aerospace applications are manufactured using this process.

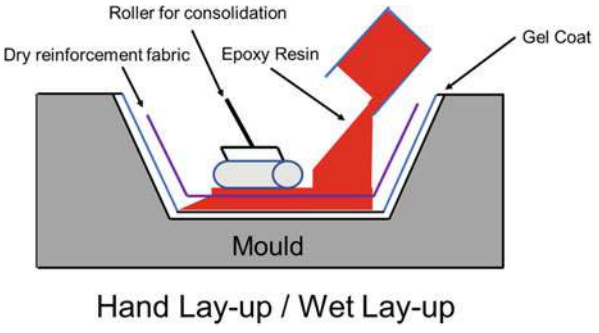

Fig. 14 Schematic of contact molding

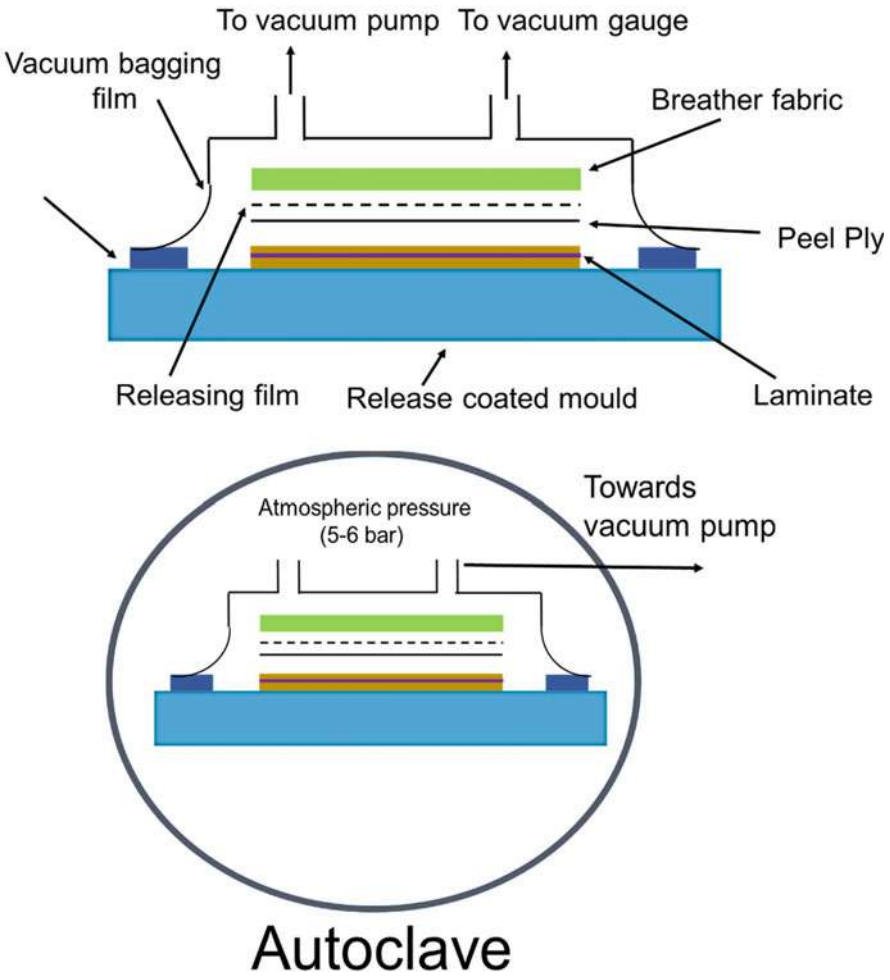

Fig. 15 Schematic of vacuum bagging and autoclave process

Resin Transfer Molding (RTM)

Potter suggests that the first patent of what is described as RTM appeared in the early and mid-1950s; however, it matured for general aerospace and automotive applications in the 1980s (Potter 1999). The major driver was automotive industries looking for high volume production and near net shape structural parts.

In this process, the fiber/fabric is draped onto the tool surface of the mold. In the case of complex geometries, various methods like the use of bindered tapes or stitching to prevent movement of the fibers are carried out. The mold is then closed, and the resin is injected under high pressure to enable complete wet out of the dry reinforcement (Fig. 16). The mold tool provides the required consolidation pressure. The process uses low viscosity resins, and care should be taken to control the resin

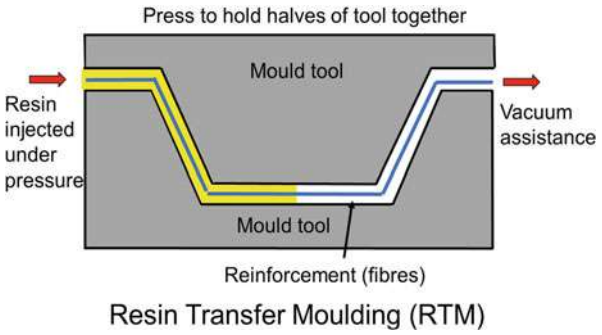

Fig. 16 Schematic of resin transfer molding

injection and flow to ensure complete wet out of reinforcement. Consolidation pressure can be varied to give the required fiber volume fraction (V_f). RTM can use a range of reinforcement systems ranging from UD-stitched cloths and woven fabrics to 3-D fabrics. RTM is used by various industries from aerospace, defense, automotive, marine, sport equipment, construction, etc.

Vacuum-Assisted Resin Transfer Molding (VaRTM)

RTM processes involve high cost for production of large structures, due to the tooling costs and presses involved. Hence, efforts toward the development of VaRTM were made, where one of the hard metal tools is replaced by a consumable vacuum bag. The process is operated at atmospheric pressure and temperature.

The three important stages of VaRTM process are molding, de-molding, and post-manufacturing like trimming of finished components. The molding process involves the following steps:

- Release agent is applied to the mold to ease the de-molding process.
- The dry preform is placed on the mold.
- Peel ply is laid on the fabric, to help de-mold the laminate. A distribution medium is also laid which acts as a flow medium in the process.
- A sealant tape is used on the entire boundary of the mold surface to achieve a good vacuum seal.
- The mold surface is covered by a vacuum bag to ensure an airtight setup. One end of the bag is connected to the vacuum pump, while the inlet is connected to the resin pot. A schematic of the process is shown in Fig. 17. The air is drawn out by the vacuum pump for consolidation. Vacuum integrity is checked.
- The resin and hardener are mixed prior to infusion process. The resin is drawn through the inlet valve. The resin then flows through the pore spaces in the dry reinforcement.
- After curing, the laminate is then de-molded.

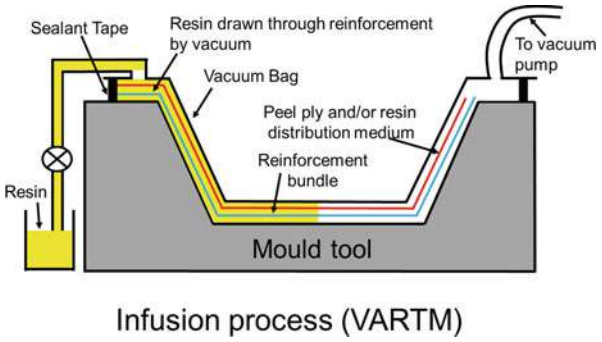

Fig. 17 Schematic of VaRTM infusion process

The major advantages of the VaRTM process are:

- Higher fiber volume fractions and higher productivity can be achieved compared to the hand layup process.
- Large structures can be manufactured at much lower costs compared to RTM.
- The VOCs and handling issues for health and safety reasons are much reduced.

Filament Winding

After World War II, filament winding was used to produce solid rocket motor case. In the early 1960s and 1970s, the technology was used to fabricate fiber-reinforced pipes, pressure vessels, and streetlight poles (Gardiner 2018). In recent years, due to interest in energy storage and hydrogen storage, new epoxy resin systems and manufacturing process are emerging to meet the requirements. The process is well suited for pressure vessels since they have defined stress directions, i.e., the hoop and longitudinal stresses.

In the filament winding process, the tows of the fibers are passed through the resin bath and wound over the revolving mandrel, keeping them in tension (Fig. 18). The fiber payout traverses longitudinally along the axis of the rotating mandrel. Also, a pre-impregnated tape can be used in filament winding. Maximum winding speeds of 1–2 m/s can be achieved, and a range of winding angles is possible in the case of a wet process. With a pre-impregnated tape, winding speeds of higher than 5 m/s can be achieved.

Manufacturing processes can have an impact on quality, properties, and production cost of the component. Potter (1996) has defined parameters on which an ideal process can be defined. This is based in terms of productivity, geometrical flexibility, material cost, property flexibility, finishing requirements, and reliability and quality of manufactured product. The selection criteria for a process, however, depend on the ideal requirements of the product.

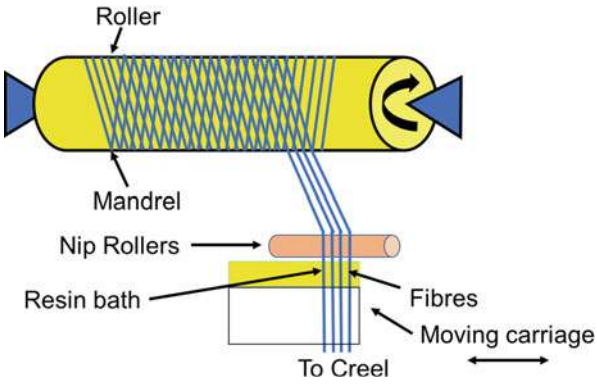

Fig. 18 Schematic of filament winding process

Material Properties of Epoxy Composites

Figure 19 shows a log-log Ashby plot of specific stiffness versus specific strength, mapping the areas of property space occupied by each material class. The charts help in the selection and design of hybrid materials and provide an estimated value of material properties. It is important to note that fiber-reinforced composites offer a high specific modulus and specific strength (i.e., properties divided by the material density).

Epoxy-based resins, due to their inherent properties such as high mechanical properties, good adhesion to various substrates, good processability, and excellent chemical and corrosion resistance, are widely adopted in the composite industry (Wong et al. 2010; Hodgkin et al. 1998). Use of unmodified epoxies, however, is limited in various applications due to their inherent fracture toughness limitations (Wong et al. 2010; Farooq et al. 2020). To prevent catastrophic material failure, designers typically have a maximum strain allowance of 0.4% in a dynamically loaded reinforced structure (Klingler et al. 2018). Several researchers have worked on improving the fracture toughness of fiber-reinforced epoxy composite by modifying the resin itself. The major approaches to toughening epoxy resins are:

(i) Use of a secondary polymeric phase (Kinloch et al. 2003; Klingler et al. 2018; Bajpai et al. 2018, 2020a; Wong et al. 2010, 2017; Di Pasquale et al. 1997; Daelemans et al. 2015)
(ii) Particulate toughening (Alam et al. 2019; Bajpai et al. 2016, 2020b; Bajpai and Wetzel 2019; Bajpai and Carlotti 2019; Chian et al. 2005)
(iii) Varying the cross-link density and molecular weight of epoxy (Mamalis et al. 2018, 2019; Maguire et al. 2019, 2020)
(iv) Incorporation of a flexible backbone in the epoxy chain

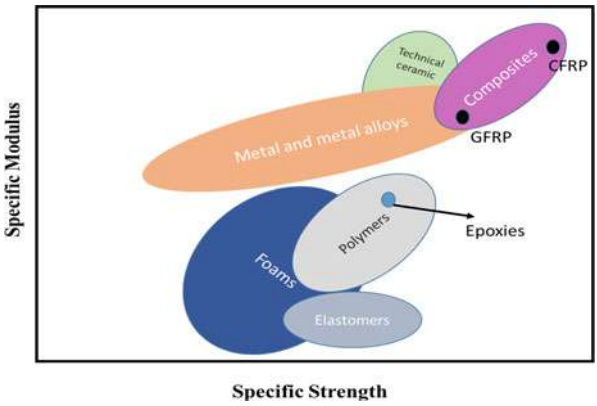

Fig. 19 Ashby plot of specific modulus versus specific strength for different materials

In the case of composites, however, the final properties of composites depend to a large extent on the interphase between the fiber and the matrix. The fracture behavior depends on properties of various phases; fiber content, orientation, and straightness; manufacturing techniques; void content; and durability aspects.

Kingler et al. (2018) carried out an extensive work on understanding the effect of different hybrid toughening agents on the morphology and fracture of epoxy-based carbon fiber-reinforced composites (CFRP). A core-shell rubber (CSR)-block copolymer (BCP) and hybrid CSR-BCP were used in the study. The effect of CSR-BCP on both bulk epoxy and epoxy-based carbon fiber-reinforced composite was investigated. The morphology evolution in the case of epoxy hybrid modified CFRP showed a strong influence of the carbon fiber. The BCP phase, which existed as a macro-phase separated structure, existed as a nanophase structure in CFRP. Figure 20 shows the interface of the fractured surface of CSR/BCP hybrid toughened epoxy-based CFRP laminates. Evenly dispersed cavities (80–100 nm) were observed in Region 1, and a finer morphology was observed in Region 2. The work suggested that by controlling the matrix morphology and the particle size to interparticle distance ratio, toughness-related properties could be controlled.

Ó Brádaigh et al. and group have pioneered the manufacturing of composites using powdered or solid epoxies. Powdered epoxies show a relatively low exothermic cure reaction (Maguire et al. 2019). The major advantage of powdered epoxy is that the degree of cure is low, even at temperatures above 100 °C, with cure normally only occurring above 150 °C. In addition, powdered epoxies are solid at room temperature and melt and flow at moderate temperatures, typically above 50 °C. The authors developed a cost-effective alternative to manufacturing out-of-autoclave components for marine and wind applications (Mamalis et al. 2018; Maguire et al. 2020; Robert et al. 2020).

A novel hand layup approach for powdered epoxies was the use of a fiber-tensioning apparatus to keep the carbon fibers under tension during the curing process. Figure 21a shows taped carbon fibers with deposited epoxy powder. The loading apparatus is shown in Fig. 21b, clamped at both ends and then tensioned to

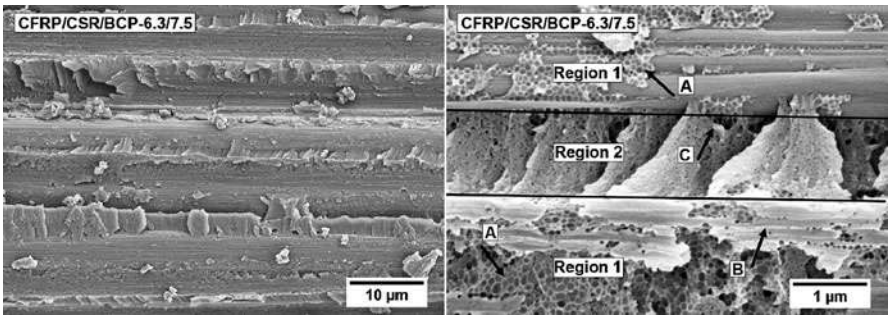

Fig. 20 Fracture surfaces of CSR/BCP hybrid toughened epoxy-based CFRP laminates (Klingler et al. 2018). (Reused with permission from Elsevier)

3000 N during processing. The manufactured CF composites are shown in Fig. 21c. The schematic of the layup with tension apparatus is shown in Fig. 21d (Mamalis et al. 2018, 2019; Maguire et al. 2020).

Effect of Sizing Agent and Manufacturing Technique

To achieve optimum performance from next-generation composites, the fiber and matrix must be effective. The sizing agents help in achieving an effective bond between the fiber and matrix. The amount and type of sizing agent influence the properties of the composites.

Mamalis et al. (Chian et al. 2005) studied the properties of carbon fiber powder epoxy composites manufactured using the technique described above with three different grades of sized carbon fibers: commercially available continuous tow carbon fibers T700S-24 K-50C (1% sizing agent), T700S-24 K-F0E (0.7% sizing agent), and T700S-24 K-60E (0.3% sizing agent) from TORAYCA® (Toray Industries, Inc.). Figure 22 shows the morphology of carbon fiber with different concentrations of sizing agent. The surface topology is distinct for these fibers with varying amounts of sizing agent. 50C shows bumps and higher roughness compared to F0E and 60E. With higher roughness in the case of 50C, it is expected to improve the mechanical interlocking.

The rule of mixtures can be utilized to determine the engineering physical properties of the composites. The theoretical Young's modulus, E_c, can be estimated using the well-established rule of mixtures as follows (Mamalis et al. 2018).

$$E_c = \kappa \eta_d \eta_I \eta_o V_f E_f + V_m E_m \tag{4}$$

where κ is the fiber area correction factor (set at unity for circular cross-section fibers), η_d is the fiber diameter distribution factor (set at unity for man-made fibers), η_I is the interface factor, and η_o is the fiber orientation distribution factor. Since the carbon fibers are unidirectionally oriented, η_o can be considered to have a value of unity. V_f is the fiber volume faction, V_m is the matrix volume fraction ($1 - V_f - V_V$),

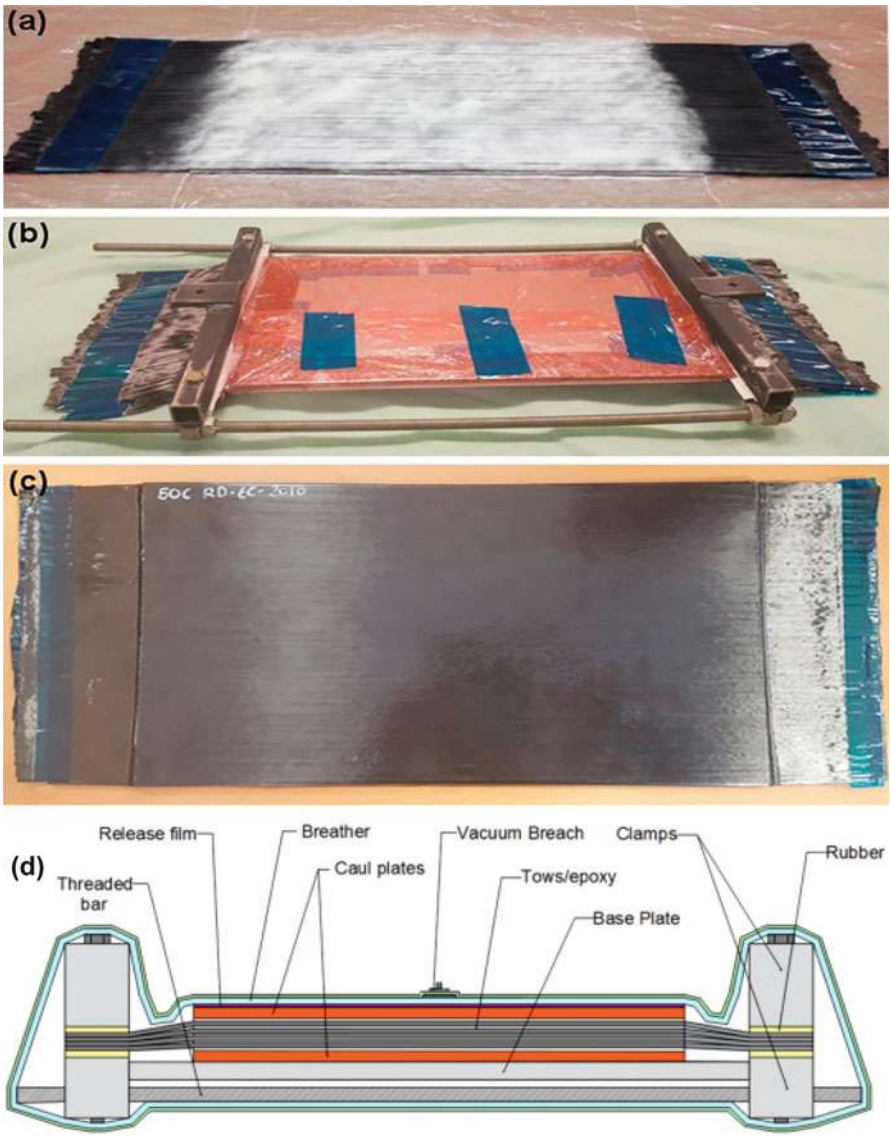

Fig. 21 Typical photographs of (**a**) no-tension carbon fiber (black) powder epoxy (white) layup, (**b**) apparatus for applying tension to the fibers during the processing cycle, (**c**) carbon fiber epoxy composite laminate produced. (**d**) Diagram of the tensioning apparatus used in the production of CFRP with improved fiber straightness (Mamalis et al. 2018, 2019). (Reused with permission from Elsevier)

V_V is the void volume fraction (which was reported to be less than 1% and hence neglected), E_f is Young's modulus of the fiber, and E_m is Young's modulus of the matrix, respectively.

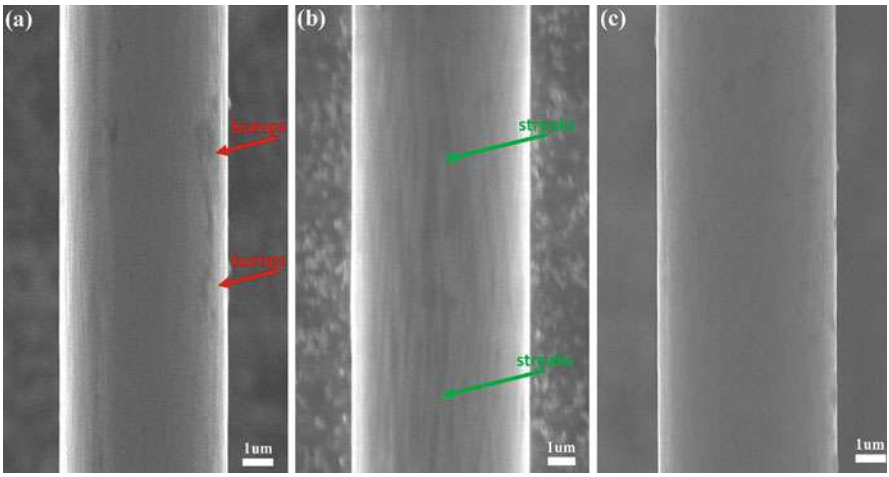

Fig. 22 SEM photographs of carbon fiber surfaces, (**a**) 50C, (**b**) F0E, and (**c**) 60E, with three separate sizing agent concentrations (and types): 1%, 0.7%, and 0.3%, respectively (Mamalis et al. 2018; Synergistic Toughening). (Reused with permission from Elsevier)

Table 2 Tensile properties and micromechanics predictions for CFRPs with different fiber sizings (Mamalis et al. 2018). (Reused with permission from Elsevier)

CFRP tensioned	Modulus (GPa)						η_I	Tensile strength (MPa) tested
	CF	V_f	Matrix	V_m	Theoretical	Tested		
50C	230	59.2	3	40.8	136.9	133.5	0.97	2600 ± 120
F0E	230	58.1	3	41.9	134.8	127.2	0.94	2310 ± 100
60E	230	58.0	3	42	134.6	121.3	0.90	2172 ± 105

Table 2 compares the theoretical and experimental E_c and calculated η_I. The interface factor was consistent with the amounts of the sizing agent on the fiber surface. The amount of sizing agent influences the properties of the composites. The tensile strength also followed similar trends. The experimental results show a higher degree of influence of sizing agent on the performance.

Effect of Tensioning during Manufacturing

Figure 23 shows the influence of fiber tension during the curing process. The no-tension 50C composites showed a drop in tensile strength of around 25% compared to their tensioned counterparts. F0E and 60E showed a drop of 8% and 7% compared to tensioned fibers. The modulus also showed similar trends, 14%, 7%, and 4% drop in modulus for 50C, F0E, and 60E compared to tensioned fibers.

The following conclusions were drawn from the studies.

- Tensioning during manufacturing and higher amounts of sizing agent improved the fiber straightness.

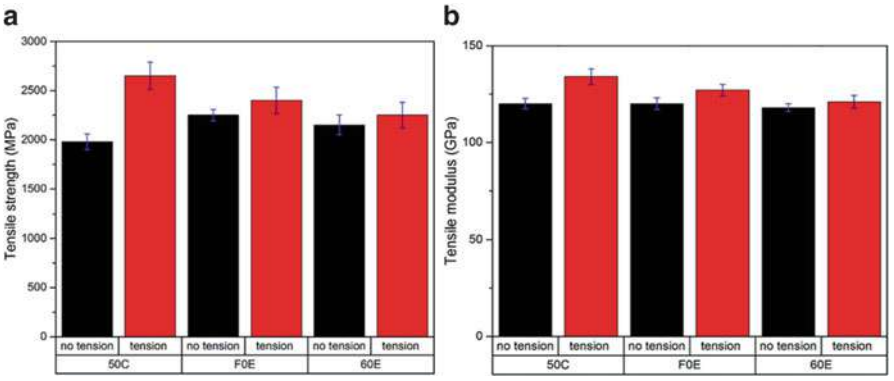

Fig. 23 Effect of tensioning during curing on tensile strength of composites (Mamalis et al. 2018). (Reused with permission from Elsevier)

- Properties of smaller amount of sizing agent were not affected by tensioning during curing.
- Fiber volume fraction was higher in the case of fiber with higher amount of sizing agent (50C).
- The tensile and longitudinal flexural properties were higher for 50C due to improved interfacial bonding.

Conclusion

Epoxies are an important class of resin system widely used in various composite industries. The demand for composites with requirements of high performance and fast production rates has led to research and development work on tailoring the properties of epoxy resins.

Novel epoxy powder manufacturing process is the latest development, which is emerging as an alternative, low-cost material with potential of automation and fast processing rates.

References

K. Acatay, *Carbon Fibers*, Elsevier Ltd, Fiber Technology for Fiber-Reinforced Composites, Woodhead Publishing, Duxford, United Kingdom (2017)

P. Alam, D. Mamalis, C. Robert, C. Floreani, C.M. Ó Brádaigh, The fatigue of carbon fibre reinforced plastics – A review. Compos. Part B Eng. **166**, 555–579 (2019)

M.C. Andrews, D. Lu, R.J. Young, Compressive properties of aramid fibres. Polymer (Guildf). **38**(10), 2379–2388 (1997)

A. Bajpai, Modification of epoxy systems for mechanical performance improvement. TU Kaiserslautern. pp. 10–12, 16–17, 20 (2018)

A. Bajpai, S. Carlotti, The effect of hybridized carbon nanotubes, silica nanoparticles, and core-shell rubber on tensile, fracture mechanics and electrical properties of epoxy nanocomposites. Nano **9**(7), 5 (2019)
A. Bajpai, B. Wetzel, Effect of different types of block copolymers on morphology, mechanical properties, and fracture mechanisms of bisphenol-F based epoxy system. J. Compos. Sci. **3**(3), 68 (2019)
A. Bajpai, A.K. Alapati, B. Wetzel, Toughening and mechanical properties of epoxy modified with block co-polymers and MWCNTs. Procedia Struct. Integr. **2**, 104–111 (2016)
A. Bajpai, A. Alapati, A. Klingler, B. Wetzel, Tensile properties, fracture mechanics properties and toughening mechanisms of epoxy systems modified with soft block copolymers, rigid TiO_2 nanoparticles and their hybrids. J. Compos. Sci. **2**(4), 72 (2018)
A. Bajpai, B. Wetzel, A. Klingler, K. Friedrich, Mechanical properties and fracture behavior of high-performance epoxy nanocomposites modified with block polymer and core–shell rubber particles. J. Appl. Polym. Sci. **137**(11) (2020a)
A. Bajpai, B. Wetzel, K. Friedrich, High strength epoxy system modified with soft block copolymer and stiff core-shell rubber nanoparticles: Morphology, mechanical properties, and fracture mechanisms. Express Polym Lett **14**(4), 384–399 (2020b)
S. Behzadi, F.R. Jones, Yielding behavior of model epoxy matrices for fiber reinforced composites: Effect of strain rate and temperature. J. Macromol. Sci. Part B **44**(6), 993–1005 (2005)
J.P. Bell, Mechanical properties of a glassy epoxide polymer: Effect of molecular weight between crosslinks. J. Appl. Polym. Sci. **14**(7), 1901–1906 (1970)
V. Bellenger, J. Verdu, E. Morel, Effect of structure on glass transition temperature of amine crosslinked epoxies. J. Polym. Sci. Part B Polym. Phys. **25**(6), 1219–1234 (1987)
V. Bellenger, W. Dhaoui, J. Verdu, J. Boye, C. Lacabanne, Internal antiplasticization in diglycidyl ether of bisphenol A diamino diphenyl methane non-stoichiometric epoxy networks. Polym. Eng. Sci. **30**(6), 321–325 (1990)
V.A. Bershtein, V.M. Yegorov, Y. A. Yemel'yanov, Relations between the main relaxation transitions in polymers and the length of segments and the character and degree of cooperation in molecular motion in the vicinity of Tg. Polym. Sci. U.S.S.R. **27**(11), 2757–2764 (1985)
J. Boye, J.J. Martinez, C. Lacabanne, Thermally stimulated creep spectroscopy for the study of DGEBA-DDM networks. J. Therm. Anal. **37**(8), 1775–1783 (1991)
A. Cevahir, *Glass fibers*, Elsevier Ltd., Fiber Technology for Fiber-Reinforced Composites, Woodhead Publishing, Duxford, United Kingdom (2017)
S. Chand, Carbon fibers for composites. J. Mater. Sci. **35**(6), 1303–1313 (2000)
W. Chian, C. Mallampalli, R.M. Winter, Nano-reinforcement of epoxy adhesives with POSS. NSTI-Nanotech **2**, 107–110 (2005)
I.R. Chowdhury, N.H. Nash, A. Portela, N.P. O'Dowd, A.J. Comer, Analysis of failure modes for a non-crimp basalt fiber reinforced epoxy composite under flexural and interlaminar shear loading. Compos. Struct. **245**, 112317 (2020)
W.D. Cook, A.E. Mayr, G.H. Edward, Yielding behaviour in model epoxy thermosets — II. Temperature dependence. Polymer (Guildf). **39**(16), 3725–3733 (1998)
B. Crist, Yield processes in glassy polymers, in *The Physics of Glassy Polymers*, ed. by R. N. Haward, R. J. Young, (Springer Netherlands, Dordrecht, 1997), pp. 155–212
L. Daelemans et al., Bisphenol A based polyester binder as an effective interlaminar toughener. Compos. Part B Eng. **80**, 145–153 (2015)
P. Davide, S. Wilhelm, Synthetic fibers for composite applications, in *Fibrous and Textile Materials for Composite Applications*, ed. by R. Sohel, P. Raul, (Springer), Singapore (2016)
L. Deng, R.J. Young, S. van der Zwaag, S. Picken, Characterization of the adhesion of single-walled carbon nanotubes in poly(p-phenylene terephthalamide) composite fibres. Polymer (Guildf). **51**(9), 2033–2039 (2010)
G. Di Pasquale, O. Motto, A. Rocca, J. T. Carter, P. T. McGrail, and D. Acierno, "New high-performance thermoplastic toughened epoxy thermosets," Polymer (Guildf)., 38, 17, pp. 4345–4348, Aug. 1997

S. Dixon, D. Jaques, S.B. Palmer, The development of shear and compression elastic moduli in curing epoxy adhesives measured using non-contact ultrasonic transducers. J. Phys. D. Appl. Phys. **36**(6), 753–759 (2003)
S. Erden, K. Ho, Fiber reinforced composites, in *Fiber Technology Fiber-Reinforced Composites*, (Woodhead Publishing, Cambridge, UK, 2017), pp. 51–79
M. Ertekin, Aramid fibers, in *Fiber Technology for Fiber-Reinforced Composites*, (2017), pp. 153–167. Woodhead Publication, Duxford, United Kingdom
U. Farooq, J. Teuwen, C. Dransfeld, Toughening of epoxy systems with interpenetrating polymer network (IPN): A review. Polymers (Basel). **12**(9), 8–21 (2020)
J.A. Gannon, History and development of epoxy resins, in *High Performance Polymers: Their Origin and Development*, (Springer Netherlands, Dordrecht, 1986), pp. 299–307
S.L. Gao, E. Mäder, S.F. Zhandarov, Carbon fibers and composites with epoxy resins: Topography, fractography and interphases. Carbon N. Y. **42**(3), 515–529 (2004)
G. Gardiner, Filament winding, reinvented, *Composites world*, pp. 24–27, 2018
J.K. Gillham, Formation and properties of thermosetting and high Tg polymeric materials. Polym. Eng. Sci. **26**(20), 1429–1433 (1986)
Glass Fiber Reinforced Polymer Market | 2020–2027 | Industry Report | Covid Insights. [Online]. Available: https://www.mordorintelligence.com/industry-reports/glass-fiber-reinforced-polymer-gfrp-market. Accessed: 04-Feb-2021
J.L. Halary, F. Laupretre, L. Monnerie, *Polymer Materials: Macroscopic Properties and Molecular Interpretations* (Wiley, Hoboken, 2011), p. 432
J.W.S. Hearle, Introduction, in *High-Performance Fibres*, ed. by J. W. S. Hearle, Elsevier, Woodhead Publishing Ltd, Cambridge, England (2001), pp. 1–22
J.H. Hodgkin, G.P. Simon, R.J. Varley, Thermoplastic toughening of epoxy resins: A critical review. Polym. Adv. Technol. **9**(1), 3–10 (1998)
D. Hull, *Fractography Observing, Measuring and Interpreting Fracture Surface Topography* (Cambridge University Press, Cambridge, 1999)
F.R. Jones, Glass fibres, in *High-Performance Fibres*, ed. by J. W. S. Hearle, Elsevier, Woodhead Publishing Ltd, Cambridge, England (2001), pp. 191–238
S.L. Kim, M.D. Skibo, J.A. Manson, R.W. Hertzberg, J. Janiszewski, Tensile, impact and fatigue behavior of an amine-cured epoxy resin. Polym. Eng. Sci. **18**(14), 1093–1100 (1978)
A.J. Kinloch, S.J. Shaw, D.A. Tod, D.L. Hunston, Deformation and fracture behaviour of a rubber-toughened epoxy: 1. Microstructure and fracture studies. Polymer (Guildf). **24**(10), 1341–1354 (1983)
A.J. Kinloch, J.H. Lee, A.C. Taylor, S. Sprenger, C. Eger, D. Egan, Toughening structural adhesives via nano- and micro-phase inclusions. J. Adhes. **79**(8–9), 867–873 (2003)
A. Klingler, A. Bajpai, B. Wetzel, The effect of block copolymer and core-shell rubber hybrid toughening on morphology and fracture of epoxy-based fibre reinforced composites. Eng. Fract. Mech. **203**, 81–101 (2018)
J. Lange, R. Ekelöf, G.A. George, Charge-recombination luminescence as a monitor of network formation during cure of epoxy resins. Polymer (Guildf). **40**(1), 149–155 (1999)
J.G. Lavin, Carbon fibres, in *High-Performance Fibres*, ed. by J. W. S. Hearle, Elsevier, Woodhead Publishing Ltd, Cambridge, England (2001), pp. 156–190
W.A. Lee, J.H. Sewell, Influence of cohesive forces on the glass transition temperatures of polymers. J. Appl. Polym. Sci. **12**(6), 1397–1409 (1968)
L.Z. Linganiso, R.D. Anandjiwala, *Fibre-Reinforced Laminates in Aerospace Engineering*, Elsevier Ltd, Advanced Composite Materials for Aerospace Engineering, Woodhead Publishing Duxford, United Kingdom (2016)
E.R. Mafi, M. Ebrahimi, M.R. Moghbeli, Effect of matrix crosslink density, varied by stoichiometry and resin molecular weight, on fracture behavior of epoxy resins. J. Polym. Eng. **29**(5), 293–308 (2009)

J.M. Maguire, P. Simacek, S.G. Advani, C.M. Ó Brádaigh, Novel epoxy powder for manufacturing thick-section composite parts under vacuum-bag-only conditions. Part I: Through-thickness process modelling. Compos. Part A Appl. Sci. Manuf. **136**, 105969 (2019) 2020
J.M. Maguire, K. Nayak, C.M. Ó Brádaigh, Novel epoxy powder for manufacturing thick-section composite parts under vacuum-bag-only conditions. Part II: Experimental validation and process investigations. Compos. Part A Appl. Sci. Manuf. **136**, 105970 (2020)
P.K. Mallick, *Fiber-Reinforced Composites*. CRC Press, Boca Raton, Florida, USA (2007)
D. Mamalis, T. Flanagan, C.M. Ó Brádaigh, Effect of fibre straightness and sizing in carbon fibre reinforced powder epoxy composites. Compos. Part A Appl. Sci. Manuf. **110**, 93–105 (2018)
D. Mamalis et al., Novel carbon-fibre powder-epoxy composites: Interface phenomena and interlaminar fracture behaviour. Compos. Part B Eng. **174**, 3 (2019)
A.E. Mayr, W.D. Cook, G.H. Edward, Yielding behaviour in model epoxy thermosets — I. Effect of strain rate and composition. Polymer (Guildf). **39**(16), 3719–3724 (1998)
S. Mostovoy, E.J. Ripling, Fracture toughness of an epoxy system. J. Appl. Polym. Sci. **10**(9), 1351–1371 (1966)
N.H. Nash, A. Portela, C.I. Bachour-Sirerol, I. Manolakis, A.J. Comer, Effect of environmental conditioning on the properties of thermosetting- and thermoplastic-matrix composite materials by resin infusion for marine applications. Compos. Part B Eng. **177**, 107271 (2019)
G.R. Palmese, R.L. McCullough, Effect of epoxy–amine stoichiometry on cured resin material properties. J. Appl. Polym. Sci. **46**(10), 1863–1873 (1992)
J. Pascault, R. J. J. Williams (eds.), *Epoxy Polymers*, Wiley, WILEY-VCH Verlag GmbH & Co. KGaA, Weinheim, Germany (2010)
J.-P. Pascault, H. Sautereau, J. Verdu, R.J.J. Williams, *Thermosetting Polymers*, CRC Press, Newyork, USA (2002)
E.M. Pearce, Principles of polymerization (third edition), by George Odian, Wiley-Interscience, New York, 1991, 768 pp. J. Polym. Sci. Part A Polym. Chem. **30**(7), 1508–1508 (1992)
E. Petrie, *Epoxy Adhesive Formulations*, 1st edn. (McGraw-Hill Professional, New York, 2005)
K. Potter, *Introduction to Composite Products: Design, Development and Manufacture* (Springer, Dodrecht, 1996)
K.D. Potter, Early history of the resin transfer moulding process for aerospace applications. Compos. Part A Appl. Sci. Manuf. **30**(5), 619–621 (1999)
K. Potter, 'But how can we make something Useful out of black string?' The development of carbon fibre composites manufacturing, in *The Structural Integrity of Carbon Fiber Composites*, ed. by P. W. Beaumont, C. Soutis, A. Hodzic, (2017), pp. 29–57. Springer International Publishing Switzerland 2017 Gewerbestrasse 11, 6330 Cham, Switzerland
S. Rebouillat, 2 – Aramids, in *High-Performance Fibres*, ed. by J. W. S. Hearle, (Woodhead Publishing, 2001), pp. 23–61
C. Robert, T. Pecur, J.M. Maguire, A.D. Lafferty, E.D. McCarthy, C.M. Ó Brádaigh, A novel powder-epoxy towpregging line for wind and tidal turbine blades. Compos. Part B Eng. **203**, 4 (2020)
T.P. Sathishkumar, S. Satheeshkumar, J. Naveen, Glass fiber-reinforced polymer composites – A review. J. Reinf. Plast. Compos. **33**(13), 1258–1275 (2014)
M. Sharma, S. Gao, E. Mäder, H. Sharma, L.Y. Wei, J. Bijwe, Carbon fiber surfaces and composite interphases. Compos. Sci. Technol. **102**, 35–50 (2014)
J. Summerscales, Materials selection for marine composites, in *Marine Composites*, Elsevier, Woodhead Publishing, Duxford, United Kingdom (2019), pp. 3–30
Synergistic Toughening of Epoxy Modified by Graphene and Block Copolymer Micelles. American Chemical Society ({ACS})
F.T. Wall, Principles of polymer chemistry. Paul J. Flory. Cornell Univ. Press, Ithaca, New York, 1953. Science (80-.). **119**(3095), 555–556 (1954)
I.M. Ward, Review: The yield behaviour of polymers. J. Mater. Sci. **6**(11), 1397–1417 (1971)
J.G. Williams, Fracture mechanics of polymers. Polym. Eng. Sci. **17**(3), 144–149 (1977)

G. Wisanrakkit, J.K. Gillham, The glass transition temperature (Tg) as an index of chemical conversion for a high-Tg amine/epoxy system: Chemical and diffusion-controlled reaction kinetics. J. Appl. Polym. Sci. **41**(1112), 2885–2929 (1990)

D.W.Y. Wong, L. Lin, P.T. McGrail, T. Peijs, P.J. Hogg, Improved fracture toughness of carbon fibre/epoxy composite laminates using dissolvable thermoplastic fibres. Compos. Part A Appl. Sci. Manuf. **41**(6), 759–767 (2010)

D.W.Y. Wong, H. Zhang, E. Bilotti, T. Peijs, Interlaminar toughening of woven fabric carbon/epoxy composite laminates using hybrid aramid/phenoxy interleaves. Compos. Part A Appl. Sci. Manuf. **101**, 151–159 (2017)

S. Yamini, R.J. Young, The mechanical properties of epoxy resins. J. Mater. Sci. **15**(7), 1823–1831 (1980)

A.F. Yee, J. Du, M. Thouless, Toughening of epoxies in polymer blends, in *Polymer Blends*, vol. 2, (Wiley, New York, 2000), pp. 225–267

J. Zangenberg, P. Brøndsted, M. Koefoed, Design of a fibrous composite preform for wind turbine rotor blades. Mater. Des. **56**, 635–641 (2014)

Chemical Modification and Fabrication of Epoxy/Synthetic Fiber Composites

2

N. H. Padmaraj

Contents

Abstract

Fiber-reinforced polymer composites with excellent chemical and mechanical properties were extensively used in aerospace, automotive, marine, civil, and sports applications. Mechanical and chemical durability of the polymer composites depended upon the interphase bonding between the fiber/matrix interphases. Surface modifications of synthetic fiber surface have profound importance as they improve wettability, adhesion, and surface roughness. This chapter provides an overview on surface treatments adopted for the synthetic fibers such as glass, carbon, and aramid. The common surface modification processes such as silane, plasma, acid treatments, and nanofiber coatings have been employed in the synthetic fiber industry. The surface treatments of the synthetic fibers increase the intensity of reactive sites in the matrix/fiber interphase and aid in improving the bonding between the matrix and the fibers.

Keywords

Surface treatment · Amine Group · Interphase · Covalent bond · Adhesion

N. H. Padmaraj (✉)
Department of Aeronautical and Automobile Engineering, Manipal Institute of Technology, Manipal Academy of Higher Education, Manipal, India
e-mail: Padmaraj.nh@manipl.edu

S. Mavinkere Rangappa et al. (eds.), *Handbook of Epoxy/Fiber Composites*,
https://doi.org/10.1007/978-981-19-3603-6_2

Introduction

The need for alternative materials has been increasing exponentially to meet the requirements of modern engineering applications. The researchers focused on developing new multifunctional materials by combining two different materials with excellent properties and finally developed multiphase composite materials. The properties of the newly developed composite materials have been optimized by combining two or more constituents together with the help of advanced material processing techniques. Fiber-reinforced polymers (FRPs) are one of the alternative materials developed by the researchers in the past decades by reinforcing fibrous materials with suitable matrix material (Gibson 1994; Mallick 2007). The FRPs have been widely used in various engineering applications as an alternative material for their low density, high fatigue resistance, low strength-to-weight ratio, high modulus, etc. These properties of the FRPs can be enhanced or customized by varying constituent material- or processing technique-related parameters (DiBenedetto 2001; Gore and Kandasubramanian 2018). The researchers focused on improving the properties by varying orientation of fibers, fiber/matrix volume fraction, hybridization of reinforcements, addition of fillers, surface modification of fibers, etc. Among these parameters, the surface modification of fibers is an important factor as it improves the wettability and the bonding of fiber/matrix interphase. The bonding of fiber/matrix interphase is the major deciding factor in the mechanical properties of the FRPs. The bonding between the fiber/matrix interphases depended on chemical composition, atomic arrangements of constituents, and surface morphology of the fibers. The surface modification of synthetic fibers removes the foreign particles from the surface, improves hydrophilic nature and hygrothermal stability, and reduces the residual stresses and improves the wettability and the properties of adhesion. Mechanical interlocking and chemical interactions generally explain the adhesion between the fiber/matrix interfaces. In the process of mechanical interlocking, the matrix material will penetrate the surface irregularities such as pores and holes of the reinforcement material. Synthetic fibers are considered a good example for the mechanical interlocking as they have a rough surface. The modification of these rough surfaces with chemical agents will enhance the adhesion between the fiber/matrix interfaces. In the chemical interaction, the van der Waals forces and the dipole interaction between the fiber/matrix interfaces are considered the major reasons for the adhesion (Garton and Daly 1985; Jang-Kyo Kim 1998).

Surface Treatments of Glass Fibers

Glass fiber-reinforced polymer composites have been extensively used in marine, automotive, aerospace, and wind energy industries. The glass fibers are considered very much compatible with the epoxy resin and are used as the most common matrix material. Chemical stability, better adhesion property, high glass transition temperature, and easy processing make the epoxy as an excellent choice in combination with the glass fibers (Sathishkumar et al. 2014; Padmaraj et al. 2019, 2021). Owing

to the advancement of technology and the need for the better adhesion between the glass/epoxy surfaces, the researchers focused on understanding the effect of silane coupling agent on the texture of the glass fiber surface. The effect of silane treatment on fiber/matrix interface is mainly explained by the theory of chemical interaction. The silane molecules available in the treated fiber surface act as a link between the epoxy and the glass fiber. The interaction of the silane group and the fiber formulates a new chemical bond and is known as siloxane bridge. The chemical structure of the multifunctional silane group is represented by $X_3Si–R$. The R represents the group, which can interact with the matrix, and the X represents the group, which reacts with the hydroxyl group of the glass fiber surface. The R group reacts with the functional group of the matrix such as methacrylate, amine, epoxy, etc. and forms a strong covalent bond with the matrix material. The formation of covalent bond between the fiber/matrix interfaces provides better adhesion and resistance to moisture intake and hygrothermal loading (Jang-Kyo Kim 1998).

The researchers attempted to understand the effect of the silane coupling agents on the mechanical properties of the glass/epoxy composites. Sever et al. (2008) treated E-glass fibers with 0.3% silane coupling agent for a duration of 1 h. The surface-modified E-glass fabrics were reinforced with the epoxy using the hand lay-up technique followed by compression molding.

The surface treatment of E-glass enhanced the flexural and the interlaminar shear strength (ILSS) of the composite structures. The flexural and the ILSS mainly depended upon the adhesion between the fiber and the matrix surface. The untreated fiber-reinforced specimens showed fiber pull out and smooth fiber surface in the failure region, whereas in the silane-treated fiber surfaces, a large amount of matrix material was adhered to the fiber surface and indicated the appropriate interlocking between the fiber/matrix surfaces as shown in Fig. 1.

Hydrolysis process can be used for the silane treatment of E-glass fibers. The silane solutions were prepared using ethanol (95%)-water (5%) and treated the fibers for 10 min. The treated fibers were dried at 110 ° C for 10 min to remove the moisture and create Si-O-Si structure. The treatment of fiber surface formed amine

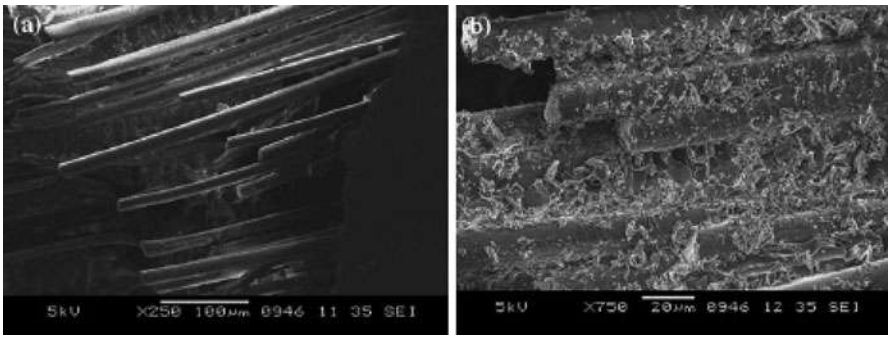

Fig. 1 Fiber/matrix interphase bonding: (**a**) untreated and (**b**) silane treated. (Reproduced with the permission of Springer Nature)

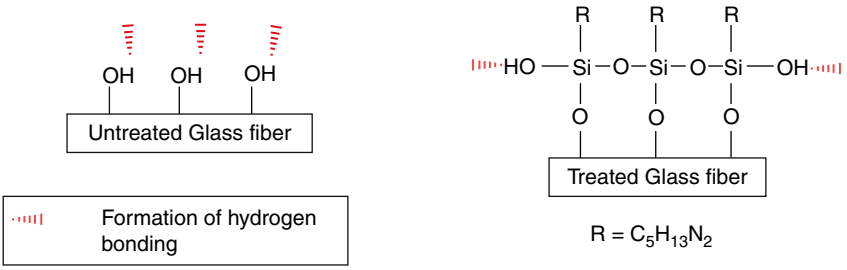

Fig. 2 Interaction of water molecules with the untreated and the treated glass fiber (Chen et al. 2021). (Reproduced with the permission of Elsevier)

functional group (NH_2) on the fiber surface and improved the matrix/fiber adhesion property. The treatment of the fiber with silane solution modified the fiber surface without altering the dimensions, whereas the surface treatment with the acid or base solutions reduced the fiber cross-sectional area due to leaching effect. The reaction site available in the treated fiber surface formed a covalent bond with the epoxide group and enhanced the ILSS as compared to the untreated epoxy/glass composites (Arun Prakash and Rajadurai 2017).

The resistance of moisture absorption of the glass/epoxy composites was improved by the silane treatment of the glass fibers. In the untreated fibers, a number of hydroxyl interaction groups were found to be higher as compared to the treated fibers. The R group of the silane coupling agent makes a strong covalent bond with the treated fibers as shown in Fig. 2. The strong interfacial bond between the epoxy and the silane group of the fiber surface prevents the penetration of water molecules into matrix/fiber interphase (Chen et al. 2021). The fiber treatment influenced the tensile failure pattern of the glass/epoxy composites. The untreated glass fiber-reinforced composites showed fiber pull out and very smooth fiber surfaces. However, the treatment of fibers brought about a rough failure surface due to the strong mechanical strain effect between the interfaces.

The studies conducted by Griswold et al. showed the variation in the thickness of fiber/matrix interphase with the absorption of percentage of coupling agent. The authors used γ-aminopropyl as the silane coupling agent and atomic force microscopy phase imaging (AFM-PI) for the measurement of interphase thickness. The fibers treated at 0.1% and 5% silane solution showed an interphase thickness of 110 ± 8.5 nm and 888 ± 30.3 nm, respectively. The presence of silane layer on the fiber surface reacted with the matrix material and played a vital role in the formation of strong interphase region (Griswold et al. 2005). The glass fibers treated with the amino silane and the epoxy silane coupling agent improved the tensile and the flexural loading conditions as compared to the untreated glass/epoxy composites. The amino silane groups on the fiber surface formed a strong covalent bond with the epoxy and improved the overall performance of the composite structure (Garg et al. 2016).

The bond between the coupling agent and the fiber surface can be monomeric, linear, or cross-linked. The formation of these bonds mainly depended upon the

chemical structure of the coupling agent. The linear and the cross-linked structures provide a better adhesion and improved the mechanical and the chemical characteristics for the composite structures (Iglesias et al. 2002). The silane treatment of glass fibers induced changes in the behavior of moisture absorption of the glass/epoxy composites. The fiber treatment reduced the amount of moisture uptake at equilibrium conditions. The high cross-linking density between the treated fiber and the matrix material led to low volume of free water molecules and improved the resistance to uptake moisture (Olmos and Lo 2006). The number of reaction sites on the fiber/matrix interphase region can be controlled by treating the fiber surface with the silane solution containing silane reactive and non-reactive group to the epoxy, and to enhance the fiber surface roughness, the silica nanoparticles can be added along with the silane coupling agent. The presence of chemical bonding agent and surface texturing particles improved the overall mechanical properties of the structures (Safi et al. 2018). Thus, the mechanical and the chemical stabilities of the glass/epoxy composites can be improved by modifying artificially the fiber/matrix interphase.

Surface Modifications of Carbon Fibers

Carbon fiber-reinforced composites have been extensively used in aerospace, automotive, and sports applications since the 1960s due to their excellent properties such as high specific strength, stiffness, high thermal stability, corrosion resistance, low weight to the structures, etc. The commercially available carbon fibers were manufactured by precursors such as polyacrylonitrile (PAN) and rayon (cellulose). The type of precursors and structure of graphite used for the production of the fiber influenced the chemical and the mechanical properties of the carbon fibers (P K Mallick 2007). The high bond strength of carbon atoms along with the fiber axis provides high modulus for the fiber. The weak van der Waals force between the neighboring layers leads to the low modulus of the fiber along the edge plane. This drawback of carbon layers provided the researchers a new area to explore, and it is possible to change the orientation of graphite crystals by modifying the carbon fiber surface with oxidative or non-oxidative agents. Plasma treatment is one of the methods of oxidative treatment and extensively used for improving the matrix/fiber interphase. Whiskerization and plasma deposition are the major types of non-oxidative treatments applied to carbon fibers to improve the adhesion with the matrix material (Sharma et al. 2014).

The plasma treatment chemically modifies the fiber surface by introducing excited groups such as hydroxyl, ether, and carbonyl on the surface. The addition of these groups to the fiber surface improves the strength of the fiber/matrix bonding by improving the wettability and the intermolecular bonding without altering the bulk properties. The plasma treatment of ex-PAN-based fibers showed a slight increment in the depth of striations as compared to the untreated fiber. The analysis of the Raman spectroscopy showed edge disorders on the treated fiber surface. The analysis of X-ray diffraction of the plasma-treated fibers showed that the treatment

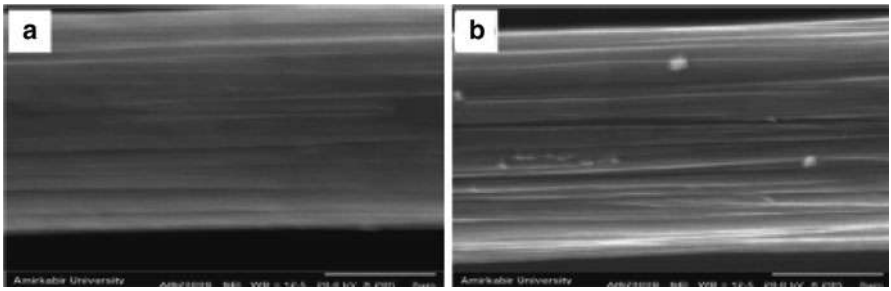

Fig. 3 Surface morphology of carbon fiber: (**a**) untreated and (**b**) plasma treated (Baghery Borooj et al. 2016a). (Reproduced with the permission of Elsevier)

affected only the external surface of the fiber (Montes-Morán and Young 2002). The plasma treatment introduces -OH and -C=O on the fiber surface and is responsible for providing excellent adhesion properties. The examination of surface morphology of the treated fiber showed deep grooves as compared to the untreated fibers, and the difference observed in the fiber surface is shown in Fig. 3. The change fiber texture improved the ILSS of the plasma-treated carbon/epoxy composites. The longer exposure of fiber to plasma source can partially destroy the fiber surface and may reduce the overall performance of the composite structures (Baghery Borooj et al. 2016a).

The treatment of low-pressure plasma of carbon fiber for a duration of 1 min improved the ILSS, whereas it reduced the ILSS when conducted for the durations of 3 and 5 min. As the duration of treatment increased, the concentration of the loose filaments increased and affected the overall strength. The shear strength also improved with the increase in the plasma power up to 125 W. The treatment etched the fiber surface and interlocked the fiber/matrix interphase better (Baghery Borooj et al. 2016b). The studies conducted by Li et al. showed that the plasma treatment can be used for improving the interlaminar fracture toughness of the carbon/epoxy composite structure containing multiwalled carbon nanotube (MWCNT) doped with conductive thermoplastic film (Li et al. 2018). The plasma treatment of carbon tape induced -OH and amide group on the fiber surface, and these groups improved the fracture toughness. The duration of the plasma treatment and the power plays a vital role in improving the ILSS and the flexural strength of carbon/epoxy laminates. The coating of fiber, the presence of polar site, and the removal of unwanted contaminations from the fiber surface improved the flexural and the ILSS (Dilsiz and Akovali 1995). The oxygen plasma treatment of carbon fiber surface improves the percentage of oxygen in the fiber. The treatment increases the density of carbonyl and the ester functional group in the fiber. The treatment also promotes the mechanical interlocking and wettability between the fiber/matrix surfaces due to the enhancement of surface roughness (Ma et al. 2010). Sai et al. investigated the combined effect of the plasma and the silane treatments on the interfacial performance of carbon/epoxy laminates. The combined treatment of the fiber improved the surface roughness and the interlocking of the fiber/matrix interphase. The ILSS of

the laminates increased with the duration of treatment process. The wear resistance of the carbon/epoxy can be improved by the plasma treatment of carbon fiber. Better adhesion between the fibers/matrices reduced the coefficient of friction and the mass loss from the carbon/epoxy surface (Shi et al. 2021).

The researchers developed silane and acid-based treatments for the carbon fibers to improve the property of adhesion of the matrix/fiber. The silane treatment of fibers formed a thin layer of siloxane oligomers. The hydroxyl groups of these layers improved the adhesion between fiber/matrix interfaces (Zheng et al. 2016). The treatment of carbon fibers with a strong acid medium introduces perforations on the fiber surface. However, in some cases, the strong acid medium may introduce pits and microcracks on the fiber strength and reduce the individual fiber strength. Nitric acid, sodium hydroxide, and maleic anhydride were commonly used to treat the carbon fibers (Wang et al. 2019).

Surface Modifications of Aramid Fibers

Due to the technological advancement in the defense technology, specifically in the ammunition and weapons, the researchers focused on developing protective anti-ballistic lightweight materials. The aramid fiber-reinforced polymers were used extensively in the defense applications due to enhanced impact resistance properties, high tenacity, high strength, and high modulus (Mallick 2007). The aramid fiber made up of polymer chain consists of aromatic rings. Each molecule of the polymer chain has a strong covalent bond and creates macromolecules. These macromolecules provide a high tensile modulus for the aramid fiber. The outer surface of the aramid fiber is chemically inert due to the absence of side groups and is enabled to make a strong bonding interphase with the surroundings. To enhance the bonding between the aramid fiber and the matrix material, different types of treatments modified the fiber surfaces. During the processing of aramid fibers, plasma treatments, acid treatments, and mechanical bonding, silane coupling agents are used extensively (Guo et al. 2009; Xu et al. 2017).

In the process of plasma treatment, the wetting of aramid fibers was enhanced by bombarding high energy plasma. The high energy plasma increases the intensity of the hydrogen bonds and the van der Waals attractive forces on the fiber surface. These bonds and forces were used to enhance the adhesion between the fiber and the matrix surface as shown in Fig. 4 (Palola et al. 2020).

In the acid treatments, the interaction between the fiber surface and the acidic medium introduces new reactive groups such as carboxylic or amine groups on the fiber surface. These groups create a strong adhesive bond between the fiber and the matrix surface as shown in Fig. 5. The major drawback of this treatment is the acidic nature of the treatment medium. The acid medium causes the degradation of the fiber surface and the core and will have negative impact on the impact resistance and the tensile properties of the structures.

In the mechanical bonding, the hierarchal structures created on the fiber surface by incorporating nanoscale particles, as shown in Fig. 6, improved the surface roughness. The incorporation of nanoscale particles into the fiber surface creates

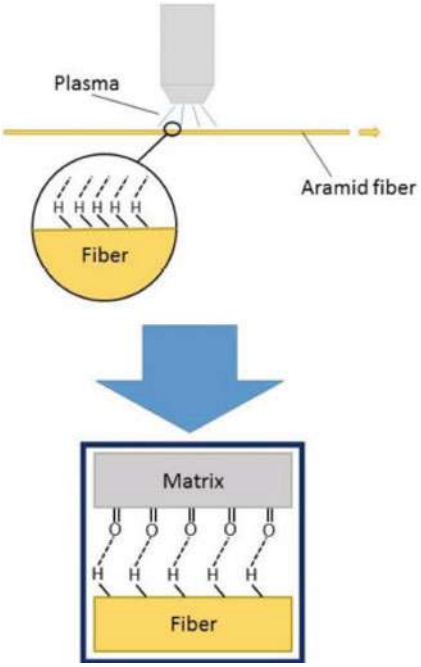

Fig. 4 Effect of plasma treatment and fiber/matrix bonding (Palola et al. 2020)

cavities and pultrusion and enhances the interlocking between the fiber/matrix interphases. The addition of nanoparticles helps in developing the structures of new multifunctional composite with properties such as electrical conductivity, self-healing, etc.

The silane surface treatment is mainly adopted to improve the adhesion between the aramid fiber and the matrix. The surface modification by the silane agent introduces new polar groups on the fiber surface, and these groups will react with the epoxy groups and partially improve the interlocking properties. The coupling agents used mainly for the aramid fibers are γ-(2,3-epoxypropoxy)propyltrimethoxysilane and γ-chloropropyltrimethoxysilane and γ-glycidyloxypropyltrimethoxysilane (Palola et al. 2020; Wang et al. 2016).

The treatment of aramid fiber with phosphoric acid solutions increased the presence of hydroxyl groups on the fiber surface. The high surface roughness increases the surface area and provides a good interlocking between the fiber and the matrix interphases. The significant increase of reaction group on the fiber surface increased the interfacial shear strength (IFSS) of the aramid/epoxy composites by 42% (Zhao 2013). The treatment of low-temperature plasma on the aramid fibers produced seashore kind of structures made up of convex and concave profiles on the fiber surfaces. This phenomenon is mainly attributed to the chemical etching of the fiber surface (Watanabe et al. 2000). The studies conducted by Sun et al. showed that the effect of the plasma treatment on the aramid fiber surface depended upon the

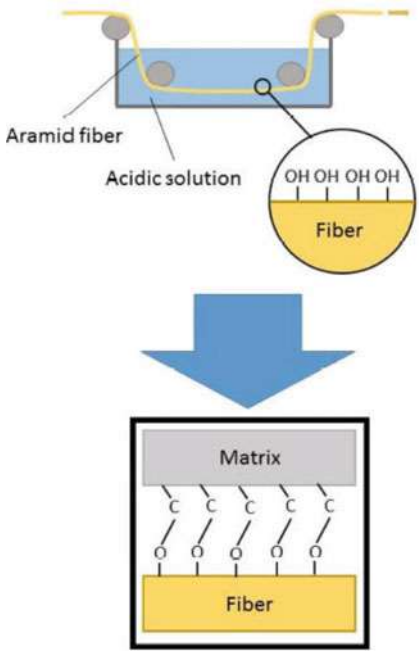

Fig. 5 Effect of acidic solution on aramid fiber/matrix interphase (Palola et al. 2020)

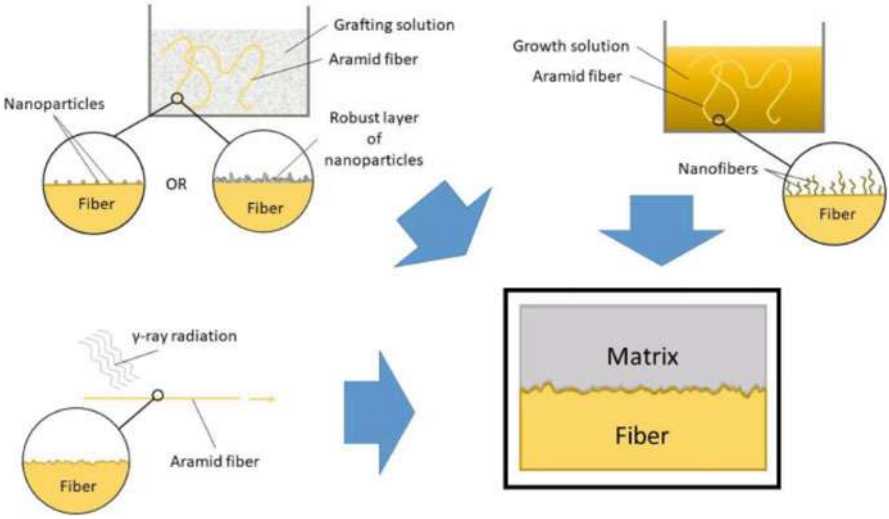

Fig. 6 Different techniques of mechanical bonding (Palola et al. 2020)

plasma power density, the treatment time, and the polymerization process (Sun et al. 2014). The introduction of polar groups into the aramid fiber surface during the plasma treatment reduced the water contact angle to 30° from 56°. The plasma

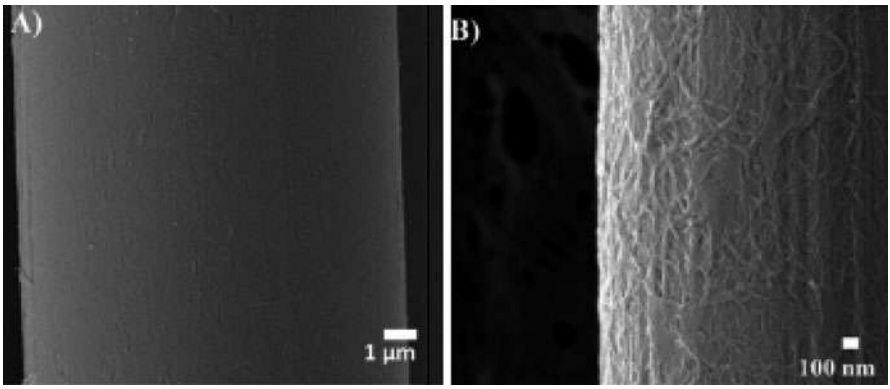

Fig. 7 A comparison of surface roughness of aramid fiber: (**a**) uncoated and (**b**) coated (Nasser et al. 2019). (Reproduced with the permission of Elsevier)

treatment also increased the concentration of both the oxygen and the nitrogen on the fiber surface (Ren et al. 2007). The improved adhesion between the aramid and the epoxy improved the IFSS by 75% over the untreated fibers.

The treatment of aramid with the epoxy chloropropane increased the interfacial bonding strength of the aramid/epoxy composites by 50%, and the presence of epoxy group and rough fiber surface improved the wettability of the fiber with the matrix (Tie-Min Liu and Yuan-Suo Zheng 2010). The coating of aramid nanofiber over the aramid fiber surface improved the adhesion properties. The coating of nanofiber covered the smooth surface of the aramid fibers (Fig. 7a) as shown in Fig. 7b. The nanofibers covered the fiber surface in the form of networks, and these morphological changes increase the surface roughness by 100%. This improved the interfacial properties between the fiber/matrix interphases. The coating of aramid fibers with the nanofibers improved the IFSS by 70.27% as compared to the uncoated fiber-reinforced specimens (Nasser et al. 2019).

Free radicals, reactive sites, or excited states on the fiber surface can be generated by performing ionizing radiation using γ-rays or X-rays. These intermediates form new bonds or hydrogen abstraction with the matrix material. The surface roughness of the aramid fiber depends on the absorption of radiation. As the energy levels or irradiation increase, the surface roughness also increases. The radiation process increased the number of polar groups and the wettability of the fiber surface. Hence, the IFSS of the aramid/epoxy composites increased by 45.17% at 400 kGy irradiation level (Xing et al. 2015).

Conclusion

The interfacial shear strength of the synthetic fiber-reinforced composites depends upon the interlocking mechanism between the fiber/matrix surfaces. To improve the adhesion properties, the physical and the chemical modifications of the fiber surface

are necessary. The treatments such as silane, plasma, and acid are used extensively in the synthetic fiber industry in improving the adhesion. These treatment processes increase the surface roughness. The introduction of new reactive sites and grafting nanofibers on the fiber surface are the major mechanisms used in improving the adhesion properties of the fiber/matrix. The tensile strength of fibers is a major concern during the process of treatment. In some treatments, the degradation of tensile properties was observed. This opens a new area to explore a variety of surface modification processes without compromising the strength of the synthetic fibers.

References

V.R. Arun Prakash, A. Rajadurai, Inter laminar shear strength behavior of acid, base and silane treated E-glass fibre epoxy resin composites on drilling process. Defence Technol. **13**(1), 40–46 (2017). https://doi.org/10.1016/j.dt.2016.11.004

M. Baghery Borooj, A. Mousavi Shoushtari, A. Haji, E. Nosratian Sabet, Optimization of plasma treatment variables for the improvement of carbon fibres/epoxy composite performance by response surface methodology. Compos. Sci. Technol. **128**, 215–221 (2016a). https://doi.org/10.1016/j.compscitech.2016.03.020

M. Baghery Borooj, A. Mousavi Shoushtari, E. Nosratian Sabet, A. Haji, Influence of oxygen plasma treatment parameters on the properties of carbon fiber. J. Adhes. Sci. Technol. **30**(21), 2372–2382 (2016b). https://doi.org/10.1080/01694243.2016.1182833

R.S. Chen, Y.H. Muhammad, S. Ahmad, Physical, mechanical and environmental stress cracking characteristics of epoxy/glass fiber composites: Effect of matrix/fiber modification and fiber loading. Polym. Test. **96**, 107088 (2021). https://doi.org/10.1016/j.polymertesting.2021.107088

A.T. DiBenedetto, Tailoring of interfaces in glass fiber reinforced polymer composites: A review. Mater. Sci. Eng. A **302**(1), 74–82 (2001). https://doi.org/10.1016/S0921-5093(00)01357-5

N. Dilsiz, G. Akovali, Effects of plasma surface modification on the mechanical properties of carbon fiber and carbon fiber/epoxy composite. Composite Interf. **3**(5–6), 344–369 (1995). https://doi.org/10.1163/156855496X00056

M. Garg, S. Sharma, R. Mehta, Processing of functionalized and pristine carbon nanotube epoxy composites with Silane-treated glass fiber. Mater. Manuf. Process. **31**(15), 2044–2056 (2016). https://doi.org/10.1080/10426914.2016.1176186

A. Garton, J.H. Daly, Characterization of the aramid: Epoxy and carbon: Epoxy interphases. Polym. Compos. **6**(4), 195–200 (1985). https://doi.org/10.1002/pc.750060403

R.F. Gibson, *Principles of Composite Material Mechanics* (MacGraw-Hill, Inc, 1994). https://doi.org/10.2214/ajr.159.6.1442392

P.M. Gore, B. Kandasubramanian, Functionalized aramid fibers and composites for protective applications: A review. Ind. Eng. Chem. Res. **57**(49), 16537–16563 (2018). https://doi.org/10.1021/acs.iecr.8b04903

C. Griswold, W.M. Cross, L. Kjerengtroen, J.J. Kellar, Interphase variation in silane-treated glass-fiber-reinforced epoxy composites. J. Adhes. Sci. Technol. **19**(3–5), 279–290 (2005). https://doi.org/10.1163/1568561054352649

F. Guo, Z.Z. Zhang, W.M. Liu, F.H. Su, H.J. Zhang, Effect of plasma treatment of Kevlar fabric on the tribological behavior of Kevlar fabric/phenolic composites. Tribol. Int. **42**(2), 243–249 (2009). https://doi.org/10.1016/j.triboint.2008.06.004

J.G. Iglesias, J. González-Benito, A.J. Aznar, J. Bravo, J. Baselga, Effect of glass fiber surface treatments on mechanical strength of epoxy based composite materials. J. Colloid Interface Sci. **250**(1), 251–260 (2002). https://doi.org/10.1006/jcis.2002.8332

Y.-W.M. Jang-Kyo Kim, *Engineered Interfaces in Fiber Reinforced Composites* (Elsevier Science Publishers B.V., 1998). https://doi.org/10.1016/b978-0-08-042695-2.x5000-3

W. Li, D. Xiang, L. Wang, E. Harkin-Jones, C. Zhao, B. Wang, Y. Li, Simultaneous enhancement of electrical conductivity and interlaminar fracture toughness of carbon fiber/epoxy composites using plasma-treated conductive thermoplastic film interleaves. RSC Adv. **8**(47), 26910–26921 (2018). https://doi.org/10.1039/c8ra05366a

T.-M. Liu, J.H. Yuan-Suo Zheng, Surface modification of aramid fibers with new chemical method for improving interfacial bonding strength with epoxy resin. J. Appl. Polym. Sci. **118**(5), 2541–2552 (2010). https://doi.org/10.1002/app.32478

K. Ma, P. Chen, B. Wang, X.X. Guiling Cui, A study of the effect of oxygen plasma treatment on the interfacial properties of carbon fiber/epoxy composites Keming. J. Appl. Polym. Sci. **116**(5), 2658–2667 (2010). https://doi.org/10.1002/app

P K Mallick. (2007). Fiber- Reinforced Composites Materials, Manufacturing and Design. CRC Press Taylor & Francis Group (Third). https://doi.org/10.1016/j.engfracmech.2008.09.002

M.A. Montes-Morán, R.J. Young, Raman spectroscopy study of HM carbon fibres: Effect of plasma treatment on the interfacial properties of single fibre/epoxy composites. Part I: Fibre characterisation. Carbon **40**(6), 845–855 (2002). https://doi.org/10.1016/S0008-6223(01)00212-3

J. Nasser, J. Lin, K. Steinke, H.A. Sodano, Enhanced interfacial strength of aramid fiber reinforced composites through adsorbed aramid nanofiber coatings. Compos. Sci. Technol. **174**(February), 125–133 (2019). https://doi.org/10.1016/j.compscitech.2019.02.025

D. Olmos, R. Lo, The nature of the glass fibre surface and its effect in the water absorption of glass fibre/epoxy composites. The use of fluorescence to obtain information at the interface. Compos. Sci. Technol. **66**, 2758–2768 (2006). https://doi.org/10.1016/j.compscitech.2006.03.004

N.H. Padmaraj, K.M. Vijaya, P. Dayananda, Experimental study on the tension-tension fatigue behaviour of glass/epoxy quasi-isotropic composites. J. King Saud Univ. Eng. Sci **xxxx**, 0–5 (2019). https://doi.org/10.1016/j.jksues.2019.04.007

N.H. Padmaraj, K.M. Vijaya, P. Dayananda, Experimental investigation on fatigue behaviour of glass/epoxy quasi-isotropic laminate composites under different ageing conditions. Int. J. Fatigue **143** (2021). https://doi.org/10.1016/j.ijfatigue.2020.105992

S. Palola, J. Vuorinen, J.W.M. Noordermeer, E. Sarlin, Development in additive methods in aramid fiber surface modification to increase fiber-matrix adhesion: A review. Coatings **10**(6) (2020). https://doi.org/10.3390/COATINGS10060556

Y. Ren, C. Wang, Y. Qiu, Influence of aramid fiber moisture regain during atmospheric plasma treatment on aging of treatment effects on surface wettability and bonding strength to epoxy. Appl. Surf. Sci. **253**(23), 9283–9289 (2007). https://doi.org/10.1016/j.apsusc.2007.05.054

S. Safi, A. Zadhoush, M. Ahmadi, S.P.R. Tehrani, Hybrid silane-treated glass fabric/epoxy composites: Tensile properties by micromechanical approach. Iranian Poly. J. (English Edition) **27**(1), 1–11 (2018). https://doi.org/10.1007/s13726-017-0578-1

T.P. Sathishkumar, S. Satheeshkumar, J. Naveen, Glass fiber-reinforced polymer composites – A review. J. Reinf. Plast. Compos. **33**(13), 1258–1275 (2014). https://doi.org/10.1177/0731684414530790

K. Sever, M. Sarikanat, Y. Seki, V. Cecen, I.H. Tavman, Effects of fiber surface treatments on mechanical properties of epoxy composites reinforced with glass fabric. J. Mater. Sci. **43**(13), 4666–4672 (2008). https://doi.org/10.1007/s10853-008-2679-x

M. Sharma, S. Gao, E. Mäder, H. Sharma, L.Y. Wei, J. Bijwe, Carbon fiber surfaces and composite interphases. Compos. Sci. Technol. **102**, 35–50 (2014). https://doi.org/10.1016/j.compscitech.2014.07.005

J. Shi, Y. Yamamoto, M. Mizuno, C. Zhu, Interfacial performance enhancement of carbon fiber/epoxy composites by a two-step surface treatment. J. Mech. Sci. Technol. **35**(1), 91–97 (2021). https://doi.org/10.1007/s12206-020-1208-y

Y. Sun, Q. Liang, H. Chi, Y. Zhang, Y. Shi, D. Fang, F. Li, The application of gas plasma technologies in surface modification of aramid fiber. Fibers Polym. **15**(1), 1–7 (2014). https://doi.org/10.1007/s12221-014-0001-x

L. Wang, Y. Shi, R. Sa, N. Ning, W. Wang, M. Tian, L. Zhang, Surface modification of aramid fibers by catechol/polyamine codeposition followed by silane grafting for enhanced interfacial

adhesion to rubber matrix. Ind. Eng. Chem. Res. **55**(49), 12547–12556 (2016). https://doi.org/10.1021/acs.iecr.6b03177

H. Wang, K. Jin, C. Wang, X. Guo, Z. Chen, J. Tao, Effect of fiber surface functionalization on shear behavior at carbon fiber/epoxy interface through molecular dynamics analysis. Compos. A: Appl. Sci. Manuf. **126**(August), 105611 (2019). https://doi.org/10.1016/j.compositesa.2019.105611

H. Watanabe, M. Furukawa, T. Takata, M. Yamamoto, Surface improvement of aramid fibers by physical treatments. Macromol. Symp. **159**(1), 131–141 (2000). https://doi.org/10.1002/1521-3900(200010)159:1%3C131::AID-MASY131%3E3.0.CO;2-J

L. Xing, L. Liu, Y. Huang, D. Jiang, B. Jiang, J. He, Enhanced interfacial properties of domestic aramid fiber-12 via high energy gamma ray irradiation. Compos. Part B **69**, 50–57 (2015). https://doi.org/10.1016/j.compositesb.2014.09.027

F. Xu, W. Fan, Y. Zhang, Y. Gao, Z. Jia, Y. Qiu, D. Hui, Modification of tensile, wear and interfacial properties of Kevlar fibers under cryogenic treatment. Compos. Part B **116**, 398–405 (2017). https://doi.org/10.1016/j.compositesb.2016.10.082

J. Zhao, Effect of surface treatment on the structure and properties of Para-aramid fibers by phosphoric acid. Fibers Polym. **14**(1), 59–64 (2013). https://doi.org/10.1007/s12221-013-0059-x

N. Zheng, J. He, D. Zhao, Y. Huang, J. Gao, Y.W. Mai, Improvement of atomic oxygen erosion resistance of carbon fiber and carbon fiber/epoxy composite interface with a silane coupling agent. Mater. Des. **109**, 171–178 (2016). https://doi.org/10.1016/j.matdes.2016.07.004

Electrical Properties of Synthetic Fiber/ Epoxy Composites

3

Priyanka Rani, Kalim Deshmukh, and M. Basheer Ahamed

Contents

Abstract

Polymer composites have gained tremendous attention due to their unique properties and potential application in various technological fields. These advanced materials obtained by the unification of two or more constituents and reinforced with various fillers especially in fiber forms produce a new kind of materials having diverse properties. Epoxy resins are insulating in nature, and their electrical properties can be influenced by incorporating various synthetic fibers. The combined properties of epoxy resins and synthetic fibers are advantageous for developing novel functional materials applicable in varied research fields.

P. Rani · M. Basheer Ahamed
Department of Physics, B. S. Abdur Rahman Crescent Institute of Science and Technology, Chennai, Tamil Nadu, India
e-mail: priyanka14035rani@gmail.com

K. Deshmukh (✉)
New Technologies – Research Center, University of West Bohemia, Plzeň, Czech Republic

S. Mavinkere Rangappa et al. (eds.), *Handbook of Epoxy/Fiber Composites*,
https://doi.org/10.1007/978-981-19-3603-6_5

Therefore, in this chapter, the electrical properties of synthetic fiber-based epoxy composites has been reviewed. The electrical properties including electrical conductivity, electrical resistivity, and dielectric strength are briefly discussed. The fiber interaction with epoxy chains and the motion of charge carriers affecting the electrical properties of composites are also discussed.

Keywords

Epoxy · Synthetic fibers · Polymer composites · Electrical properties · Conductivity

Introduction

In the past few decades, polymer composites have gained the attention of many researchers due to their interesting properties. The manufacturing industries are developing a variety of materials to accomplish improved properties such as strength, density, stiffness, durability, and lower cost with better sustainability. Polymer composites are emerging as excellent materials that possess great improvement in various properties. The development of polymer composites is increased due to their potential application (Deshmukh et al. 2020; Sankaran et al. 2018; Joseph et al. 2021). Polymer composites are advanced materials made by the unification of two or more constituents isolated by different interfaces. Here, the constituents have their unique and different physical/chemical properties, and in a unified form, they produce new kinds of materials having diverse properties in comparison to the specific constituents. Among the specified constituents, one is the polymeric matrix phase, whereas others are considered as reinforcing fillers which could be in nanoparticle or fiber form (Chand and Jain 2005; Mohanapriya et al. 2019; Haghgoo et al. 2019; Jawaid and Khalil 2011). The combined properties of various constituent materials give an advantage to develop novel functional materials applicable in different research fields. Generally, the matrix phase could be insulating or conductive polymers, and the most commonly used polymers are polyvinyl alcohol, polyester, polyvinylidene fluoride, polystyrene, epoxy, polypropylene, vinyl ester, phenolic, etc. (Deshmukh and Joshi 2015; Rani et al. 2020a, b; Jia et al. 2014; Akman et al. 2020; Nagaraj et al. 2020; Deshmukh et al. 2018). The incorporation of low content of nanosized fillers in the polymer matrix offers unique possibilities in achieving the desired physical and chemical properties.

In an insulating polymer matrix, the properties such as electrical, dielectric, or optical properties can be enhanced by the addition of conductive fillers which provides the significant formation of interconnected conductive networks within the polymer chains (Kumar et al. 2022; Thangamani et al. 2021a, b; Muzaffar et al. 2019). To improve the interfacial adhesion between the conductive filler phase and the polymer matrix is the main challenge in developing and designing the conductive polymer composites. Nanofillers acquiring large surface area, high aspect, and capability to form strong interfacial bonding with polymer matrix made researchers

to model and characterize polymer composites attaining improved properties such as high Young's modulus, corrosion resistance, hardness, high tensile strength, etc. (Remis et al. 2021; Ahmad et al. 2013). The improvement in the properties of polymer composites reliant on the compatibility, interfacial interactions, and polarity match between reinforced filler and polymer chain (Deshmukh and Pasha 2020). The various factors on which the distribution and dispersion of nanofiller depend are surface area, size, mixing time, dispersion techniques, and applied shear (Shen et al. 2020). These factors lead to the allocation of superior properties of nanofillers into the host polymer matrix. Moreover, the polymer composites formed through a variety of polymers and reinforced nanofillers or nanofibers provide excellent reinforcement effects which are quite useful for various applications such as electronic systems, solar cells, supercapacitors, memory devices, EMI shielding, drug delivery systems, sensors, etc. (Ibragimov et al. 2020; Nazir et al. 2016; Rani et al. 2020c; George and Ishida 2018; Muzaffar et al. 2020; Deeraj et al. 2020; Kshad et al. 2017; Sobolčiak et al. 2017).

The layered or sheet-like nanofillers are composed of two-dimensional layers in their crystal lattice with thickness around 1 nm, and their adjacent dimensions vary from 10 nm to 100 mm or larger. The layers stacked through van der Waals forces between the interlayers do not possess constant charge because of gaps between the layers. Generally, the higher aspect ratio of nanofillers is the main key factor to accomplish the improved properties (George and Ishida 2018). The most common layered silicates used in polymer composites are saponite, montmorillonite, hectorite, etc. (Ibragimov et al. 2020; Nazir et al. 2016; Rani et al. 2020c). The direct mixture of a polymer and layered nanofiller does not necessarily provide good results. There are different possibilities of occurring discrete phases which can cause poor physical interaction of nanofiller and polymer matrix leading to low physical or mechanical properties. However, the strong interactions of layered nanofillers and polymers due to a good level of dispersion will provide unique physical or mechanical properties (George and Ishida 2018).

Epoxy Resins

Among most of the commercially used polymers, epoxy is one of the exclusively used thermoset polymers. Epoxy with a wide range of properties gains special interest in the preparation of composites for the vast area of applications. The epoxy resins consist of a minimum of two epoxide groups (Gonon and Boudefel 2006). The structure of epoxy obtained after polymerization of monomer units consists of the cross-linked 3-D infusible network which resulted from the usage of curing agents. Cross-linking of monomers can be done by two methods, which are by coupling through intermediate having reactive tendency and through catalytic homopolymerization by directly coupling the resin molecules (Sasidharan and Anand 2020). Earlier epoxy resins were used as intermediates for surface coatings, and, it still remains a commercially major material for coating applications. The high adhesive strength makes these resins a potential material for protective coatings.

Epoxy owns unique properties including good heat resistance, high adhesive strength, toughness, high electrical resistance, high mechanical strength, etc. (Kausar 2019).

Composites based on epoxy have low cost and high specific strength which make them promising materials in load-bearing applications such as aerospace, construction, automotive, and marine industries (Rajak et al. 2019a). These reasons developed the greater need to explore the deformation performance of epoxy composites in wide-ranging loading conditions and are especially influenced by the added filler and the morphology of the epoxy matrix. Many investigations gave an insight for fiber-reinforced epoxy composites providing an extreme improvement in strength, stiffness, and easiness in complex molding (Megahed et al. 2019). The variation in processing conditions like the functionality of the hardener constituent or change in molecular weight can lead to an improvement in the properties of epoxy-based composites. Epoxy resins are developed as chemical intermediates to produce various products for technological applications (Mittal and Chaudhary 2018). Epoxy resins are significantly used in the synthesis of fiber-reinforced composites that offer a variety of applications especially in the aerospace or aircraft systems. The electrical, optical, and mechanical properties of epoxy-based composites are a great area of concern. However, these composites are still extensively investigated for numerous applications (Greiner et al. 2019; Li et al. 2018a).

Synthetic Fibers

Fibers introduced a new era in the field of research. The polymer composites reinforced with fibers bring quite interesting results in the electrical as well as mechanical properties. Various types of fibers are produced by polymerization of raw materials such as petroleum, petrochemicals, etc. into the linear chemical reacting with distinct chemicals. There are two kinds of fibers; natural fibers and synthetic fibers (Karikalan et al. 2017; Sanjay et al. 2016). The use of natural fibers is in concern with the environment as an embedded material for polymer composites. However, synthetic fibers are manmade and have a greater advantage in high mechanical strength, in stain resistance, and even in consumer-friendly functions. Almost in every field of fibers, synthetic fibers are preferred over other fibers. Natural fibers such as leaf, bast, fruit, and core fibers are explored due to their environment-friendly nature and degradability. Despite the non-degradability of synthetic fibers, they have gained more attention over a few decades. The synthetic fibers based on carbon, glass, Kevlar, and boron provide high stiffness and strength when being used as reinforcement material for the preparation of polymer composites (Ravichandran et al. 2020; Kasaragadda et al. 2020). Synthetic fibers are less expensive and readily available in the marketplace. The wide research on fiber-reinforced polymer composites suggested that the better adhesion of fibers is required to form an effective polymer composite with high durability. The composite properties are straightway influenced by the size, reinforcement, and chemical

constitution. However, these characteristics are prodigiously important for better adhesion between the reinforced fiber and the polymer matrix. The good adhesion makes the reinforced fiber exert its role effectively and consequently absorb the concentration in conjugation with the matrix. The reinforced materials can be either mineral fillers or fibers with ultra-high strength (Yu et al. 2018). When the fiber is used for reinforcement, then through the shear mechanism, the overall stress applied to the nanocomposite is transferred from the polymer matrix to the added fibers. Herein, the strong adhesion between the components of the nanocomposites is essential for the effective transfer of these stresses.

The production of commercial fibers is basically done via three different processes such as melt spinning, dry spinning, and wet spinning. In most cases, the mixing of polymer and fibers leads to some fractures in the polymer matrix, which are generally initiated due to the cracking of the fiber constituents reinforced in the matrix. The manner of initial fracture established will determine the nanocomposite toughness (Domun et al. 2015). In an isolated fiber, when a fracture arises along its length at any point, then to stabilize the fracture, the stresses in the vicinity of the crack carried by the fiber must be transferred to the respected matrix surroundings. If the fibers are able to withstand the stresses, then fracture can be controlled at that location, but the deformation remains continued at other locations. However, in some cases, this process needs to continue until the wide spreading of damage and the fractured fibers can no longer able to support the stress by the un-cracked matrix, and at this point, the ultimate fracture occurred in the composite (Breuer and Sundararaj 2004). However, to overcome this deformation, the fibers reinforced in the polymer matrix should include some properties such as high surface area, small diameter, and large length representing the geometric configuration, high volume, etc. Also, the increase in fiber concentration in the matrix interface will lead to an increase in the modulus of elasticity and high tensile strength (Rong et al. 2001). Synthetic fibers have good elasticity and can handle the heavy load without breaking. These fibers do not wrinkle or shrink, can retain good absorption capacity, and have good flexibility. The polymer composites embedded with synthetic fibers are widely accepted as aerospace components as well as in automotive industries (Zhang et al. 2020).

Classification of Synthetic Fibers

Carbon Fibers

The most abundant non-metallic element in the earth's crust is carbon. In various research applications, carbon is the most frequently used filler to form composites. Based on the necessity and variations, carbon or different derivatives of carbon can be significantly added to the matrix. Carbon derivatives such as carbon nanotubes, carbon-modified nanoparticles, activated carbon, carbon black, carbon fibers, etc. are required to enhance the properties of composite materials (Chuang et al. 2017). The development of carbon-based composite materials gain more attention due to the long-term stability, the cost evaluation, and the interaction mechanism between

the carbon-based filler and matrix. Among various carbon-based fillers, carbon fibers have numerous advantages together with low weight, high stiffness, high chemical resistance, low thermal expansion, high tensile strength, and high-temperature tolerance (Han et al. 2013). Carbon fibers as reinforcing fillers have remarkable usage particularly in a class of polymer composites. However, in the case of the non-polymer matrix, for example, in metals, the occurrence of corrosion has limited the success of metal-matrix composites. Carbon fibers are produced by bonding together the carbon atoms in crystals in a parallel alignment to the long axis to form a fiber. The crystal alignment gives a high strength-to-volume ratio to the formed fiber. A tow formed by bundling thousands of carbon fibers may be woven into fabric and can be utilized in textile industries (Forintos and Czigany 2019). Carbon fibers have quite high specific strength and are electrically conductive. Likewise, they are biologically inert and non-poisonous, with good tensile strength and a low coefficient of thermal expansion (Bhatt and Goe 2017). The numerous properties of carbon fiber have made them very popular in civil engineering, aerospace, motorsports, and the military. The carbon fibers are utilized as an electrode, an anti-static component, and a high-temperature gas filtrate (Bhatt and Goe 2017). Besides, several authors have demonstrated that the fire resistance properties of polymer composites can be substantially improved by molding carbon fibers into thin layers. Moreover, carbon fibers are also used in the production of electrically conductive concrete (Sassani et al. 2017).

Carbon fibers are ideal reinforcement for progressive nanocomposites. Besides the fabrication process, the most important aspects include the interfacial bonding strength to determine the properties of the nanocomposites. However, the surface of neat carbon fibers is quite smoother and inert, which sometimes results in a weak interfacial adhesion with the polymers (Islam et al. 2016). Thus, the surface modification of the fiber is required to increase the interface strength. Until now, carbon fibers are modified with several methods such as plasma treatment, acid oxidation treatment, polymer sizing, surface grafting, and so on. Tsotra et al. (Tsotra and Friedrich 2004) examined the effect of carbon fibers on the electrically conductive blends of polyaniline (PANI) and epoxy. Here, epoxy as a host polymer on blending with PANI leads to the enhancement in the electrical conductivity of the material with increasing content of PANI, whereas the mechanical properties were not much affected with the addition of PANI. Interestingly, on adding the carbon fiber in the polymer blend, an improvement in both the electrical and mechanical properties of the composite was reported. An obvious synergistic effect was observed between carbon fiber and PANI with respect to the electrical conductivity of the materials. The superior electrical conductivity values were the result of the fine conductive network of PANI which acts as a connector between the separated carbon fibers. Moreover, the existence of PANI was not affected by the reinforcing effect of carbon fibers (Tsotra and Friedrich 2004). In another study by Kupke et al. (2001), the electrical properties such as d.c. and a.c. measurements were investigated. This study reports the utilization of carbon fibers as sensors for d.c. measurements and functioning as electrical resistors. However, for a.c. measurements such as evaluation of capacitance and dissipation, the reinforced carbon fibers and their joining points

were functioning as resistors, whereas the gaps between the reinforced fibers were functioning as capacitors.

Basalt Fibers

Basalt is the most common rock present on the earth's surface which is rich in magnesium and iron. Basalt fibers are made through electrospinning (at ~1500 °C) of basalt rock, and this molten rock is further extruded to produce extremely fine continuous fibers of basalt. The composition of basalt fibers contains pyroxene, plagioclase, and olivine (Dhand et al. 2015). The structural properties of basalt fiber are similar to other fibers, i.e., carbon fiber or glass fiber, although the mechanical properties of basalt fibers are better than glass fiber and they are less expensive than carbon fiber. In the aerospace and automotive industries, basalt fibers are used as a fireproof textile. A wide range of products can be produced through composites reinforced with basalt fibers. These fibers contain interesting properties like higher oxidation resistance, higher shear strength, higher compression strength, and higher radiation resistance (Rill et al. 2010). Additionally, some interesting features of basalt fibers such as excellent shock resistance, good fatigue, high strength, corrosion resistance, and ease in processing and handling made them suitable for various applications. The formation of various fiber-reinforced composites is due to the compatibility of basalt fibers with many resins such as vinyl ester, phenolic, epoxy, unsaturated polyester, etc. Basalt fibers form various products like chopped strands, textile yarn, needled felts, and geogrids. One of the products made from basalt fiber is continuous basalt roving which is an inorganic fiber generally used as a protective material (Jamshaid and Mishra 2016). However, in the case of an explosive blast, it is used with ballistic materials as an explosive prevention function. It is utilized in the form of base material for the ceramic facing armoring system as it has no spalling or bounce. Various applications of basalt fiber include filament winding of various tanks or pipes, mesh fabrics, and repairing of infrastructure. Moreover, the chemical corrosion, super low temperature, and high-pressure properties of basalt fibers made them potential materials to be used as heat shields for tank gun turrets (Li et al. 2018b).

Basalt fiber-reinforced polymer composites are used as structural confinement and reinforcement material for the application in civil infrastructure. These materials display higher strength and modulus (approx. 20%), more chemical stability, and similar cost as compared to glass fiber and also efficiently work in a wide range of temperatures with much lesser cost than carbon fiber-reinforced polymer composites (Guo et al. 2013). Several studies have shown the creep behavior of basalt fiber-reinforced polymer composites. Banibayat (2011) investigated the creep properties of bars composed of basalt fiber and polymer. In this research, the alkaline corrosion was found to be influenced by high temperature. The measurements have shown the one-million-hour creep rupture stress level for the effective exposure and the converted time to be 11% and 15%, respectively. Meanwhile, there is no investigation on the creep behavior of bars under standard conditions so it was quite difficult to differentiate the rupture of basalt fiber-based polymer composites and whether it was induced by alkaline corrosion or the creep effect.

In another study, Wang et al. (2014) investigated the mechanical properties, namely, tensile strength and stress-strain behavior, of basalt fiber-reinforced polymer composites. They studied the relationship of strain and the sustained time which displayed various characteristics for various levels of applied stresses. However, the first stage of the rapid increase of strain was characterized under low stress and was triggered by the non-uniformity of basalt fibers in the polymer composites. However, high stress or stress redistribution results in continuous fracture among fibers analyzed under moderate and low levels of stress. Meanwhile, the second stage of long stable low rate has shown the increase of strain. In addition, the residual strength of composites reinforced with basalt fiber tendons after 1000 h of sustained load exhibiting a minor impact on the tensile strength of fibers with less scattering, reflects the creep degradation mechanism.

Glass Fibers

Among various non-crystalline amorphous solids, glass has widespread technological and practical applications. This material is often used for optical purposes, tableware, windowpanes, etc. Glass is manufactured by quenching or rapid cooling of the molten silica (quartz) and known as silicate glasses. Among the diverse variety of manufactured glasses, glass fiber is one of the widely used materials in the class of fibers. Glass fiber is comprised of several thin strands of silica which are extruded into fine fibers having small diameters. The mechanical properties of glass fibers are analogous to other fibers. Glass fibers are less rigid and cheaper as compared to carbon fiber. The composite materials reinforced with glass fibers are typically known as glass-reinforced plastics or fiberglass. These composites exhibited high strength and relatively lighter in weight (Ellyin and Maser 2004). This material was denser having no air or gas, which makes it a poor thermal insulator. Glass fibers are the most common reinforcement fiber compared to other fibers to synthesize polymer composites. These fibers are added to enhance tensile strength, impact resistance, flex modulus, dimensional stability, creep, and chemical resistance. Most often silanes are cast as sizing of glass fibers to expand the reinforcing effectiveness in various plastics. The glass fibers are available in a wide variety of shapes including staple fiber, roving, and chopped strands. Moreover, the continuous fibers are used for reinforcement in a variety of resins. The glass fibers exhibit a high strength-to-weight ratio but low elastic modulus which particularly reduces the elongation and increases the stiffness of the composite. Glass fibers have a large heat-absorbing capacity and quite high melting points nearly ranging from 1225 °C to 1360 °C. Meanwhile, glass fibers have a wide variety on the bases of different chemical compositions such as A-glass (alkali glass), C-glass being chemical resistant known as chemical glass, E-glass (electrical glass) a good electrical insulator, AE-glass (alkali-resistant glass), and S-glass (structural glass) which is known for its mechanical properties.

Glass fibers are employed for numerous applications including protection of docks from corrosion, food processing, power generation, chemical industry, automotive industry, and defense and aerospace industry (Sathishkumar et al. 2014). The glass fiber-reinforced polymer composites have excellent strength along the direction of fiberglass (Romanzini et al. 2013). However, the consistency of glass fiber with the

resin matrix is not strong enough, which makes them vulnerable to spall during a normal impact process. Few investigations have presented the mechanical behavior of glass fibers when reinforced in the polymer matrix. Yuan et al. (2007) have investigated the mechanical strength of glass fiber reinforced in the polyester resin and Ciba epoxy matrix. The mechanical studies conducted at 0–175 MPa resulted in low tensile stress which caused spallation within the specimens, and also it leads to the complete unloading of free surface particle velocity profiles up to no-spall levels. On increasing the impact stresses to 600 MPa, the tensile stresses were sufficiently high to cause in spall. When the impact stress was larger than 600 MPa, it results in substantially higher shock compression causing damage to the glass fiber-reinforced polymer composites, and no resistance to spall was registered (Yuan et al. 2007). Also, no pullback of free surface particle velocity profiles was reported. Generally, the performances of fiber-reinforced polymer composites are dependent and controlled by the corresponding properties of reinforced fiber and the matrix interface. Excellent interfacial adhesion is required to ensure the load transfer from the polymer matrix to the reinforced fiber. So, it is a prior requisite to understand the fundamental interfacial properties and the interfacial adhesion strength which can support in estimating the capabilities and the mechanical behavior of the composite materials. Numerous techniques have been developed to understand the interfacial adhesion of glass fiber-reinforced polymer composites (Yuan et al. 2007). Gu et al. (2000) reported that the vibration damping technique was more advantageous as it is non-destructive; besides, it is highly sensitive to analyze the interfacial region. An ordinary optical system was subsidized for the measurement of the damping factor of uniaxial glass fiber-induced polymer composites. The interfacial damping factors were correlated with the transverse tensile strength of the composites which provided an insight into glass fiber and matrix interface adhesion. The authors investigated four varied compositions of the prepared composites. For each composition, three types of surface treatments of glass fiber were carried out at varied volume fractions. The results showed that the damping contributed by the interface was inversely proportional to the transverse tensile strength of the composite.

Kevlar Fibers

Kevlar is an organic fiber having highly oriented and long molecular chains. Kevlar exhibits diverse chemical compositions and exclusive properties such as high modulus, high strength, thermal stability, and toughness that distinguish them from other fibers (Kabir and Ferdous 2012). Similar to silk, Kevlar chains tend to form planar sheets which are relatively rigid. The para-orientation of the benzene rings brings together the locking of chains through H-bonds forming a sheet consisting of very high tensile strength. The aromatic stacking interactions between the adjacent aromatic groups and the intermolecular hydrogen bonds provide greater strength to Kevlar fiber. However, in other synthetic fibers, the van der Waals interaction is less strong than the interaction found in Kevlar fibers. The relatively rigid molecules, forming planar sheet-like structure in Kevlar fibers, result in high mechanical strength and heat resistance. These features of Kevlar fiber are important for the formation of fiber-reinforced polymer composites. Kevlar fibers consist of various functionalities like lightweight, small diameter, flexibility, dielectric properties,

decomposes at ~450 °C, good mechanical strength, and chemical resistance (Oliwa 2020).

The fibers having significantly different properties than the polymer matrix are combined together with an obvious interface to acquire a novel material with superior properties. For structural applications, the fiber-reinforced polymer composites play a significant role because of the high stiffness and strength of fibers. Interdisciplinary research has been conducted on the diversified application of fiber-reinforced polymer composites. Among other synthetic fibers, Kevlar fiber known as the polyaramid fiber possesses exclusive properties (Chinnasamy et al. 2020). The chemical composition of Kevlar fiber is composed of nylon having extra benzene rings in the polymer chain which increases the stiffness of fiber. Kevlar fibers are utilized for widespread application in industries and innovative technologies such as helicopter blades, sporting goods, ballistic armor, etc. Kevlar fibers exhibit high tensile strength, high modulus, and significantly inferior fiber elongation. These fibers exhibit remarkable high-temperature properties when embedded with polymer materials. The development of polymer composites by reinforcing Kevlar fiber has gained the attention of many researchers. Bhaskar and Mohamed (2012) estimated the elastic properties of fiber-reinforced polymer composites by employing an analytical approach. The estimation was made separately to both fiber and the matrix interface due to the difference in the geometry of the finite element mesh regions. The parameters of fibers including type, orientation, geometry, volume fraction, and the degree of interfacial adhesion in the matrix affected the mechanical properties of the fiber-based polymer composites. The mechanical properties of the Kevlar fiber-reinforced polymer composites mainly depend on the extent of the interfacial adhesion of fibers in the polymer matrix. Kevlar fibers used in this study were highly crystalline in nature, and their surface was soother and inert which provides poor adhesion with the resin matrix. However, the adhesion between the fiber and matrix can be improved by surface modifications of Kevlar fibers. In a work done by Lin et al. (2000), the interaction of Kevlar fiber with bismaleimide (BMI) matrix was improved by chemically treating the fibers with chlorosulfonic acid. The thermal properties were also reported to be improved under a large processing temperature range lying between the initial polymerization temperature and the melting points, due to the decrease in the cross-link density of the cured resins without undergoing any significant reduction in the thermal resistance of the composite. The surface modifications with reactive functional groups were observed after the introduction of Kevlar fibers, which improved the interfacial shear strength and T-peel strength of the composite (Lin et al. 2000).

Methods of Synthesis of Epoxy/Synthetic Fiber Composites

There are various methods to prepare synthetic fiber-reinforced epoxy composites, and the most common methods are in situ polymerization, melt blending, and solution casting method. The in situ polymerization technique is a very effective method to uniformly disperse the nanofibers in the polymer matrix. In this method,

the monomers are mixed with nanofibers in a suitable solvent. Firstly, by adjusting the heat or temperature, polymerization is initiated by diffusing a suitable initiator. However, this method is most efficient in the case of thermally unstable or insoluble polymers for fusing it in solvents. This method is used for small to large scale, but during polymerization, the increase in viscosity limits its application. Moreover, the in situ polymerization method is not widespread for the synthesis of several materials due to lower elastomer viscosity. Also, it acquires low electrical conductivity because of the attachment of the polymer's macromolecular chain with the nanofibers causing the lack of interconnecting network formation.

The melt blending method is the most adaptable method explicitly for the preparation of fabric-reinforced polymer composites and has a greater advantage over the in situ polymerization technique. Generally, the polymer is melted at high temperature and then combined with the nanofiller or nanofiber by using an extruder in the molten polymer matrix. On the other hand, the dry mixture of the polymer and the intercalant filler is heated at high temperature in a mixer by applying shear. Typically, this method being eco-friendly and cost-effective is useful for industrial-based bulk production as it does not require a solvent for the intermixing of fabric into the polymer matrix. Injection molding and extrusion are some examples of this method. This method leads due to its toxic-free nature, whereas the poor dispersion of added filler in the polymer matrix especially at higher loadings limits its potential. Also, this method results in filler/fabric buckling due to stronger shear forces which cause low conductivity of formed composites.

The solution casting method is the most versatile and simplest method for the preparation of polymer composites. This method involves the dispersion of nanofibers and polymer in the same solvent. The dispersion obtained through this method is quite stable and uniform. The main factor on which the dispersion depends is the compatibility of nanofiber and the polymer with the same solvent. This method is very simple and most applicable due to ease in processing without requiring advanced equipments. Generally, the polymer is first dissolved in a suitable solvent, and subsequently, the desired amount of fillers/fibers is dispersed in the same solvent. Further, the homogenous solution is cast for the removal of the solvent. However, this method is not eco-friendly as it requires more amount of solvents and critical to remove the solvent by evaporation. This method is most convenient for small scale preparation of composites.

Electrical Properties of Epoxy/Synthetic Fiber Composites

Every material can conduct the electrical current. Several factors on which the electrical properties of composite depend are electrical resistivity, dielectric strength, electrical conductivity, and temperature coefficient of resistance. The non-destructive measurement of composites which defines the property to resist electric current flow through the composite is known as electrical resistivity of such composite. These values are measured in micro-ohm centimeter units. The electrical resistivity values depend on various factors including materials' cross-sectional area, length of

conductor, temperature, the thickness of composite, etc. (Ekhtiyari et al. 2020). It is also investigated to check the porosity level after doping a filler in the polymer matrix. However, this investigation is necessary but not sufficient. The electrical resistivity of materials can be given as;

$$\rho = R(A/L)$$

where R is the electrical resistance of the material, L length of the material, A cross-sectional area of the material, and ρ electrical resistivity of the material.

Another important measurement of composites is to calculate how strongly a material allows the flow of electric current through the composite. This parameter is known as the electrical conductivity of composites. It is the reciprocal of the electrical resistivity. In conductivity measurements, movement of electric charges which is defined as the ratio of current density to the electric field strength is identified throughout the composites.

Electrical conductivity is the reciprocal of the electrical resistivity given as:

$$\sigma = \frac{1}{\rho}$$

Here, electrical conductivity is related to resistivity as:

$$R = \frac{L}{\sigma A}$$

where R is the resistivity of the material, L length of the material, A cross-sectional area of the material, and σ electrical conductivity of the material.

For composites, various properties rely on the electrical conductivity values which provide information regarding inspecting the heat damage, purity level, and heat treatment of materials. Another main parameter is the dielectric strength which indicates the ability of the material to endure at high voltages without experiencing any electrical breakdown. The resistivity behavior of a material with temperature change is calculated by temperature coefficient values also called a temperature coefficient of resistance. Both resistivity and conductivity of composites depend on the temperature.

Electrical Properties of Carbon Fiber-Reinforced Epoxy Composites

The electrical properties of various epoxy/fiber composites are reported by many researchers. In research reported by Bekyarova et al. (2007), multiscale hybrid composites were fabricated via vacuum-assisted resin transfer molding. The multiwalled and single-walled nanotubes (MWCNTs and SWCNTs) were integrated into the carbon fiber bundles and reinforced in an epoxy resin matrix. The mechanical strength of NT-coated carbon fiber-based epoxy composites is higher (∼30%) than that of carbon fiber/epoxy composites. Similarly, the electrical conductivity for NT-coated carbon fiber-reinforced epoxy composites was also significantly improved. Figure 1

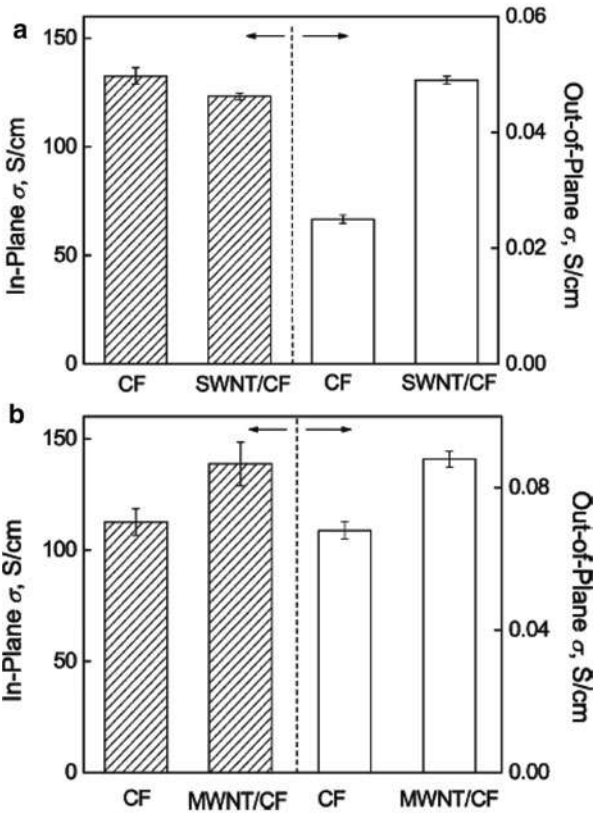

Fig. 1 The in-plane and out-of-plane electrical conductivity of carbon fiber (CF)/epoxy composites in comparison with the (**a**) single-walled nanotube (SWNT)- and (**b**) multiwalled nanotube (MWNT)-coated carbon fiber/epoxy composites. Reproduced with permission from Ref. (Bekyarova et al. 2007). Copyright 2007, American Chemical Society

represents the in-plane and out-of-plane electrical conductivity of NT-coated carbon fiber (CF)/epoxy composites (Bekyarova et al. 2007). The in-plane and out-of-plane electrical conductivity values of carbon fiber/epoxy composites were quite satisfactory. However, after coating with a small amount of NTs, carbon fiber/epoxy composites provide improved results for out-of-plane electrical conductivity, whereas the in-plane electrical conductivity remains unaffected. The difference was attributed to the thickness of the composites as originated due to the difference in the morphologies of NTs. The integration of NTs into carbon fiber bundles introduced a highly interconnected network and formed conducting paths throughout the carbon fiber/epoxy composites. Also, coating with a very small amount of NTs has significantly enhanced the electron transport channels causing improvement in the out-of-plane electrical conductivity of the composites.

In another study, Senis et al. (2019) reported the electrical conductivity for carbon fiber-reinforced epoxy composites. To reduce the heat damage of the composites along with enhanced electrical conductivity values, graphene oxide (GO) was introduced to a carbon fiber-reinforced epoxy composite system (Senis et al. 2019). The electrical

conductivity values were observed to be greater in the case of the longitudinal direction and lower in the case of transverse and through-thickness directions due to the fiber properties. Initially, the electrical conductivity in both transverse and through-thickness directions was assumed to be similar, but it is evident that the measured transverse conductivity values were about one order of magnitude greater than that of through-thickness conductivity. This was attributed to the formation of vacuum-infused and prepreg-based laminates, resin-rich interlaminar regions, and prepreg-based vacuum-infused laminates which leads to the substantial reduction in the through-thickness directional conductivity. However, on adding GO content in the carbon fiber-reinforced epoxy composite system, the through-thickness directional conductivity increased, and no effect was observed in transverse conductivity. The threefold increase was measured after reinforcing a very high concentration of GO in the epoxy. Moreover, the enhanced electric conductivity values were similar with or without GO for carbon fiber-reinforced epoxy system at low filler content (Senis et al. 2019).

In a study reported by Bhanuprakash et al. (2019), carbon fiber-reinforced epoxy hybrid composites coated with GO were fabricated through a simple electrophoretic deposition technique. Figure 2 illustrates the electrical conductivity of carbon fiber-reinforced epoxy hybrid composites measured for through-thickness and in-plane conductivity values (Bhanuprakash et al. 2019). The in-plane electrical conductivity values were observed to be significantly high as compared to through-thickness electrical conductivity values, resulting from the outspread of carbon fibers along the in-plane direction and the alternate layer arrangement of carbon fibers in the thickness direction. Generally, the epoxy resins are insulating in nature which reduces the electrical conductivity of the composite. In this study, carbon fiber-reinforced epoxy hybrid composites were later coated with GO to improve the electrical conductivity values of the composites. The in-plane conductivity for uncoated and coated composites was observed to be similar. However, the drastic improvement of almost 48% in through-thickness electrical conductivity values was observed after coating with GO. This enhancement was asserted to the restoration of graphite structure due to

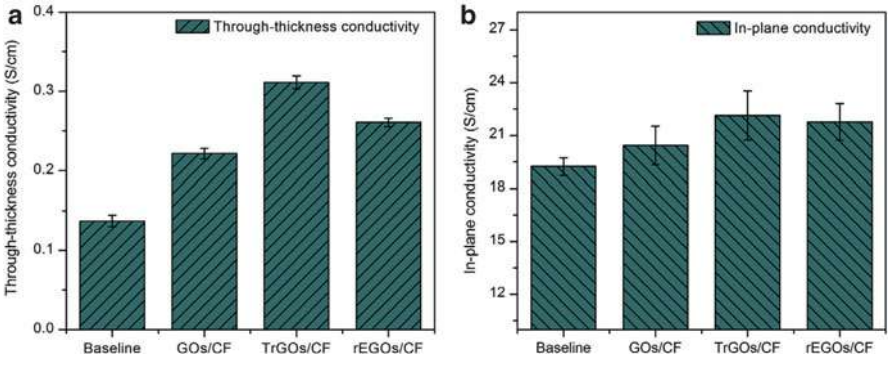

Fig. 2 Electrical conductivity values of composites for (**a**) through-thickness and (**b**) in-plane conductivity values. Reproduced with permission from Ref. (Bhanuprakash et al. 2019). Copyright 2019, Elsevier

reduction in filler size, chemical reduction, and thermal defunctionalization in the hybrid composite. The conductive graphene sheets within the epoxy matrix and the interaction of filler with carbon fibers contributed in enhancing the overall conductivity of the hybrid composite.

Electrical Properties of Basalt Fiber-Reinforced Epoxy Composites

In a report by Kim et al. (2019), the investigation on electrical properties of MWCNT-coated basalt fiber-reinforced epoxy composites obtained through cyclic dip-dry coating process and hand lay-up process was made. The electrical conductivity values of MWCNT-coated basalt fiber-reinforced epoxy composites were significantly increased from 3.25×10^{-9} S/cm to 1.44×10^{-1} S/cm as with the increment in the dip-dry coating cycle and represented in Fig. 3 (Kim et al. 2019). The main contribution to the improvement of electrical conductivity is the effective flow of electric charges along with the interconnected networks of basalt fibers coated with MWCNT in the epoxy composites (Kim et al. 2019). The electrical properties including the current-voltage (I-V) and power-voltage (P-V) characteristics of MWCNT-coated basalt fiber-reinforced epoxy composites are illustrated in Fig. 4 (Kim et al. 2019). In the I-V curves, no electric current over the applied voltages was observed for basalt fiber/epoxy composite demonstrating the insulating nature of composite. A significant increase in the slopes of the I-V curves and linear increase in electric current with applied voltage was reported after fabricating the MWCNT-coated basalt fibers with epoxy resins. This is attributed to the strongly interconnected network formation of MWCNT on the basalt fibers with higher dip-dry coating cycles. Similar results were reported for P-V curves experiencing the quadratically increased electric power with the applied voltage. Accordingly, the composites having high values of electrical conductivity exhibit outstanding electric heating performance characterizing the

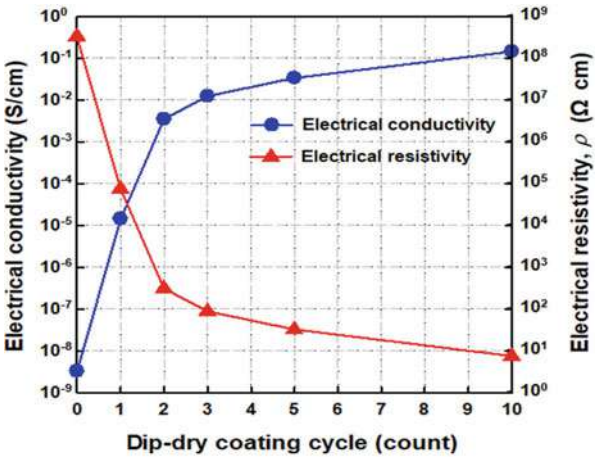

Fig. 3 Electrical conductivity and electrical resistivity of MWCNT-coated basalt fiber-reinforced epoxy composites with respect to dip-dry coating cycle. Reproduced with permission from Ref. (Kim et al. 2019). Copyright 2019, Elsevier

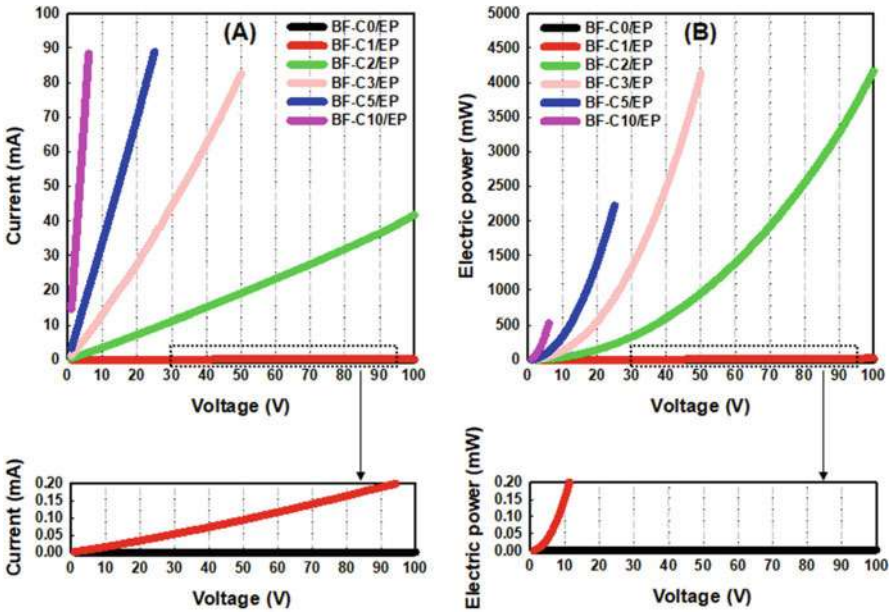

Fig. 4 The electrical properties including (**a**) current-voltage (I-V) and (**b**) electric power-voltage (P-V) curves of MWCNT-coated basalt fiber-reinforced epoxy composites. Reproduced with permission from Ref. (Kim et al. 2019). Copyright 2019, Elsevier

rapid temperature responsiveness to the applied voltage. Under the stepwise change in cyclic voltage, the operational stability and electric power efficiency were also reported to be high (Kim et al. 2019).

In another study, Wang et al. (2018) investigated the electrical resistivity and compared the results of carbon nanofiber (CNF) -reinforced epoxy composites with CNF-laminated basalt fiber-reinforced epoxy composites. The observed values of electrical resistivity decrease significantly with the increasing content of CNFs, and the resistivity values varied drastically after reaching the percolation threshold. The 3-D conductive network distribution was very poor for CNF/basalt fiber/epoxy composite than that of CNF/epoxy composite which is due to the insulating nature of basalt fibers. Additionally, the higher resistivity in CNF/basalt fiber/epoxy composites was observed as shown in Fig. 5 (Wang et al. 2018). The main reason is the incorporation of basalt fibers in CNF/epoxy composites which drastically increased the resistivity by restricting the conductive network formation. Thus, this increase in resistivity values leads to the lower electrical conductivity of composites.

Electrical Properties of Glass Fiber-Reinforced Epoxy Composites

One of the important parameters in investigating the electrical properties is measuring the dielectric strength of the composites. Panda et al. (2014) have reported an

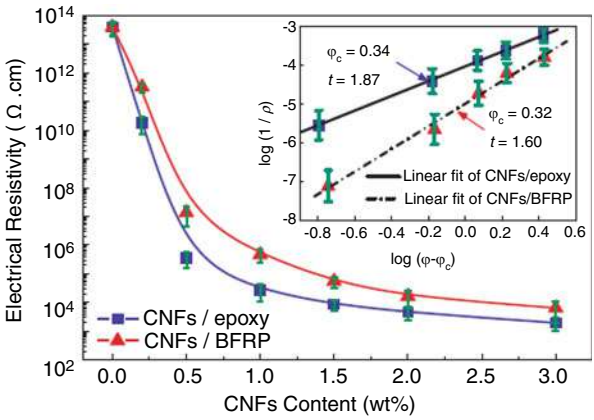

Fig. 5 Electrical resistivity of CNF/epoxy composites and CNF/basalt fiber-reinforced plastic laminates with respect to CNF content. Reproduced with permission from Ref. (Wang et al. 2018). Copyright 2018, Elsevier

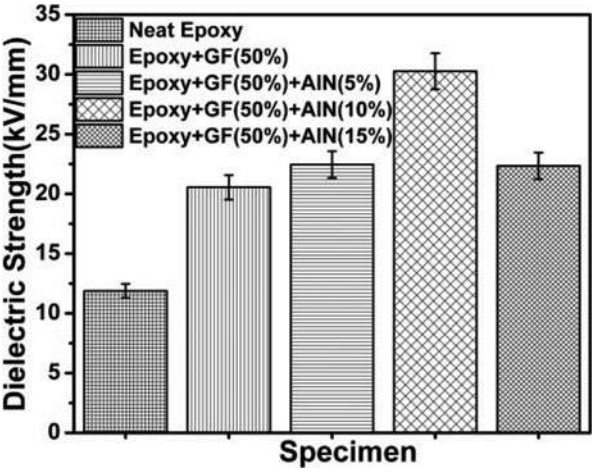

Fig. 6 Dielectric strength variation of epoxy reinforced with glass fiber and plasma-synthesized AlN powder at different wt%. Adapted from Ref. (Panda et al. 2014). Copyright 2013, Sage Publications

effort to understand the dielectric breakdown strength of glass fiber-reinforced epoxy composites and also incorporated various loading of aluminum nitride (AIN). The highest voltage at which the composite withstands before failing electrically is known as dielectric breakdown strength. Figure 6 represents the dielectric breakdown strength of epoxy composites with various contents of glass fiber and AIN loadings (Panda et al. 2014). According to this report, the breakdown strength increases significantly (~50%) after adding glass fiber in the neat epoxy matrix. However, with adding a low concentration of AIN, the breakdown strength remains almost the same. The similar values of dielectric strength after adding lower content of nanofiller in glass fiber-reinforced epoxy composites are due to the more interparticle distances and larger volume fraction of polymer layers allowing the

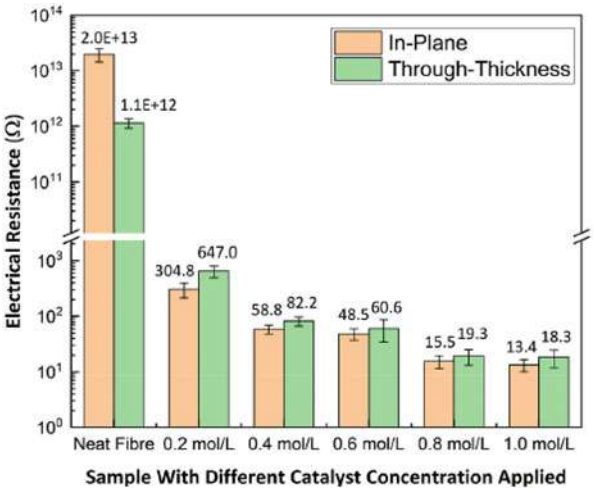

Fig. 7 Electrical resistivity of glass fiber-reinforced epoxy composite with or without CNT coating. Reproduced with permission from Ref. (Zhao et al. 2020). Copyright 2020, Elsevier

similar charge carrier transfer as that of breakdown strength in glass fiber/epoxy composites. Moreover, at a higher concentration of AIN, the breakdown strength was higher which was due to the high packing density and reduced accumulated charge. Thus, the dielectric breakdown strength was more with the addition of nanofiller in the glass fiber/epoxy composites.

In another research work, Zhao et al. (2020) prepared CNT-coated S-glass fiber/epoxy composites by flame synthesis method. The electrical resistance measured for both in-plane and through-thickness directions is represented in Fig. 7 (Zhao et al. 2020). The neat glass fiber laminates have an electrical resistivity value of about $\sim 2 \times 10^{13}$ Ω, and the values dropped significantly to 650 Ω with the coating of CNTs on glass fibers. In this regard, the electrical conductivity values which increase with the increase in the CNT loadings into the glass fiber/epoxy composites are illustrated in Fig. 8 (Zhao et al. 2020). The outstanding electrical conductivity of CNTs has enhanced the poor electrical properties of the glass fibers and epoxy by forming numerous conductive pathways and increasing the transfer of electrons between the coated CNT and the glass fiber layers. Also, the electrical resistance drops abruptly which also confirmed the formation of conductive pathways within the composite. Moreover, the thickness of composites also leads to an increase in conductive pathways and reduces the electrical conductivity of the composites.

Electrical Properties of Kevlar Fiber-Reinforced Epoxy Composites

Santhosh et al. (2018) have successfully prepared the hybrid epoxy composites reinforced with Kevlar/E-glass fiber laminates by vacuum-assisted resin transfer molding. The good flexural strength and high impact energy absorption were reported for the Kevlar/E-glass combination. The highest electrical conductivity

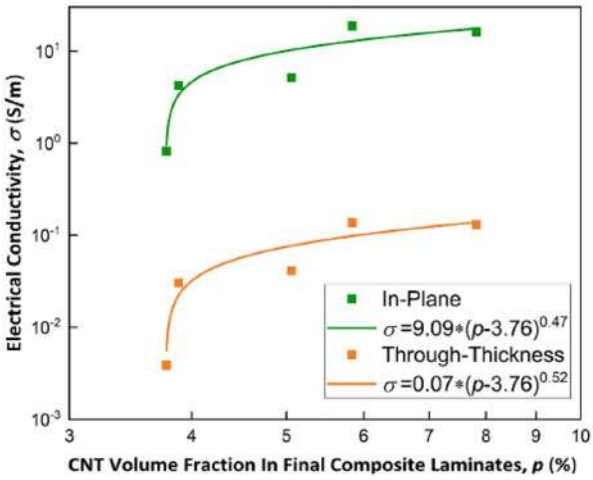

Fig. 8 Electrical conductivity of glass fiber-reinforced epoxy composite with or without CNT coating. Reproduced with permission from Ref. (Zhao et al. 2020). Copyright 2020, Elsevier

was observed for Kevlar/E-glass laminate samples. In this report, the Kevlar/E-glass laminate sample showed improved conductivity by 17% and lower resistivity values in comparison to other samples. This increase was attributed to the decrease in activation energy by incorporating Kevlar fibers in the composites (Santhosh et al. 2018). In another investigation, Anwar et al. (2017) have observed the variation of electrical conductivity over a range of γ-radiation doses. The measurements showed the decreasing behavior of electrical conductivity of about $2.7 \times 10^{-9}\ \Omega^{-1}\ m^{-1}$ for Kevlar fiber/epoxy composite samples with the increasing γ-dose (500 kGy) which are one-third values of the non-irradiated sample. This reduced conductivity was explained on the basis of chain scission causing the defect formation in the energy gap. These defects consequently created barriers and restricted the charge carrier's mobility, and hence due to the formation of voids, the conductivity reduces. Further on increasing in the gamma dose, branched-chain scissoring occurred and leads to increase in the free carrier mobility which increases the electrical conductivity at an irradiation dose of 750 kGy (Anwar et al. 2017).

In another study, Jackson et al. (2017) reported the dependence of electrical conductivity on frequency and temperature as shown in Figs. 9 and 10, respectively (Jackson et al. 2017). Kevlar fibers were incorporated into hybrid polymer composites by using the hand lay-up method. The variation of conductivity as a function of frequency (100 Hz–1 MHz) gives a clear insight that conductivity which is nearly constant at low frequency was frequency independent. As the frequency rises, a strong dispersion occurred in spectra due to the restricted motion of mobile ions and impurities. The anomalous behavior of conductivity was observed at high frequency (around 700 KHz) due to the increase in the collision between the charge carriers (Jackson et al. 2017). Furthermore, the authors studied the influence of temperature on Kevlar fiber-reinforced hybrid polymer composite and found that at low frequency, conductivity values remain almost constant and very small for all the temperatures.

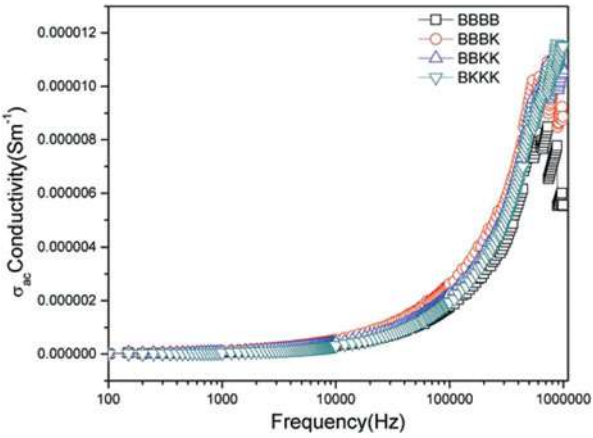

Fig. 9 Electrical conductivity as a function of frequency for Kevlar fiber-reinforced hybrid polymer composite. Adapted from Ref. (Jackson et al. 2017). Copyright 2017, Taylor & Francis

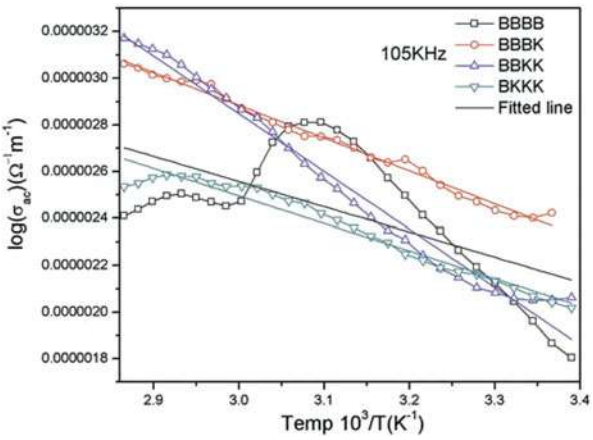

Fig. 10 Electrical conductivity as a function of temperature for Kevlar fiber-reinforced hybrid polymer composite. Adapted from Ref. (Jackson et al. 2017). Copyright 2017, Taylor & Francis

However, conductivity is significantly varied at a higher frequency with the temperature. This also indicates that low-frequency conductivity is independent of temperature (Jackson et al. 2017). Table 1 summarizes the electrical properties of different types of fiber-reinforced epoxy composites.

Epoxy/Metallic Fiber Conductive Composites

The fibers containing pure metals, alloys, metal salts, metal oxides, and metalloids are known as metal fibers or metallic fibers. They can be produced through different thermal and mechanical processes. Earlier gold and silver fibers were used in clothing and textile applications as yarns in fabric decoration. Lately, they were

Table 1 Literature survey of electrical conductivity studies of fiber-reinforced polymer composites

Synthetic fiber/ nanofiller	Matrix	Filler content	Electrical conductivity	Ref.
CF/SWNT	Epoxy	0.75/0.25 wt%	123 S/cm (in-plane) 0.05 S/cm (out-of-plane)	Bekyarova et al. (2007)
CF/MWNT	Epoxy	0.75/0.25 wt%	140 S/cm (in-plane) 0.089 S/cm (out-of-plane)	Bekyarova et al. (2007)
CF/GO	Epoxy	57/2.71 wt%	0.7 S/cm (in-plane)	Senis et al. (2019)
CF/rGO	Epoxy	–	0.3 S/cm (through-thickness) 22.3 S/cm (in-plane)	Senis et al. (2019)
MWCNT/basalt fiber	Epoxy	2.65/0.20 wt%	1.44×10^{-1} S/cm	Bhanuprakash et al. (2019)
CNT/glass fiber	Epoxy	2/20 wt%	9.09 (in-plane) 0.07 (through-thickness)	Zhao et al. (2020)
Glass fiber	Epoxy	–	$3.53 \times 10^{-9}\ \Omega^{-1}\ m^{-1}$	Anwar et al. (2017)
Kevlar fiber	Epoxy	–	$3.4 \times 10^{-9}\ \Omega^{-1}\ m^{-1}$	Anwar et al. (2017)
CF/rGO	Epoxy	10 + 80 wt%	1.12×10^{5} S/m	Alemour et al. (2019)
CNT/GNP/CF	Epoxy	50 vol %	5.26×10^{3} S/m	Li et al. (2018c)

CF carbon fiber, *SWNT* single-walled nanotube, *MWNT* multiwalled nanotube, *MWCNT* multi-walled carbon nanotube, *GO* graphene oxide, *rGO* reduced graphene oxide, *GNP* graphene nanoplatelets , *CNT* carbon nanotube

replaced by aluminum yarns, aluminized nylon yarns, and aluminized plastic yarns. Nowadays, the metal fiber industry has offered various fibers composed of nickel, copper, steel, aluminum, and titanium for various applications (Lukiyanchuk et al. 2018). The conductive textile industries manufactured electrically conductive fibers from conductive metals like stainless steel, ferrous alloys, aluminum, copper, nickel, etc. Metal fibers exist in the form of thin filaments with about 1 μm to 100 μm diameter range. They may also be shaved from foil, steel wool, or the bundles drawn from the wires of large diameter. Also, various forms of metal fibers include chopped fibers mostly employed in wet-laid operations and needle felt fibers used for the production of stiff rigid media or can be cast from the molten metal (Nturanabo et al. 2019). However, the highly conductive metallic fibers are quite expensive, heavy, and brittle in nature as compared to other textile fibers which make these fibers difficult to produce and be consumed for fabricating homogeneous blends. The fibers made from high-temperature-resistant alloys display high-temperature resistance which makes them a suitable material to be used as mats, filament yarns, woven and rovings. The processing of metallic fibers through the thermal process includes the direct extrusion from the melt via the melt spinning method. However, metal melt spinning is more challenging than melt spinning of glass or polymers, and this is due to the low melt viscosity of metals (about 100 times) than that of glass or

polymers (Wang et al. 2019). Therefore, there are greater chances for melt fractures to occur which can result in the formation of only droplets instead of fibers. However, metallic fibers can be produced by some methods including coagulation bath. Another way to produce melt-spun metallic fibers is by the usage of the melt extraction process. In this process, a water-cooled extraction roller was rotated in the melt batch, and this roller contains multiple blades of V-shaped edges which solidified the mass and pull out the short fibers. Also, the magnetic field prevents the waves which are occurring at the melt's surface (Gupta and Laubscher 2017). With this process, it is possible to process materials like tin and aluminum fibers which are quite difficult to process via other conventional methods because of their brittle nature.

Metallic fibers are widely used in composite materials as reinforced fibers to improve the breaking behavior and electrical conductivity. The other fibers like carbon or glass fiber are also used as reinforcement fibers but acquire very limited elongation possibilities and hence result in more brittle and explosive breaking behavior. Metal fibers are a good replacement for these fibers, and also these fibers absorb a considerable amount of energy before breaking. However, the processing is similar to other reinforcement fibers for fabricating the composite materials. Moreover, there is a great possibility to combine metallic fibers with the other synthetic fibers and that they can be transformed into a hybrid composite structure combining the benefits of all other fibers. The electrical resistance of metallic fibers is quite low in comparison to other fibers like carbon, glass, or natural fibers. However, these fibers are potential materials for applications which require electrical conductivity. Also, the excellent thermal resistance property helps the composite to withstand extreme temperatures. Metallic fibers exhibits various properties such as corrosion resistance, good mechanical properties, high failure strain, high porosity, shock resistance, ductility, sound insulation, and fire resistance (Rajak et al. 2019b).

The metallic fiber-reinforced polymer composites are a widely researched area. A lot of research work has been done to study the reinforcement effects and variation in different properties of polymer composites after the addition of metallic fibers in the polymer matrix. McBride et al. (2017) have investigated the mechanical and structural properties of the hybrid fiber composites composed of steel fiber and glass fibers embedded in the epoxy matrix. As other conventional fiber-reinforced polymer composites having high strength and stiffness provide low ductility and less ability to absorb energy before failure. To overcome this limitation, ductile steel fibers were combined with glass fiber-reinforced epoxy composites. The hysteresis behavior, stress-strain relationships, and insight into failure mechanisms were studied for non-hybrid and hybrid composites. By incorporating steel fibers into the glass/epoxy composites, a significant improvement was reported in the energy absorption and material recentering capabilities. The low concentration of steel fibers provided higher energy absorption to the composite. The tensile stress-strain relationships of composites showed that the introduction of steel in glass/epoxy composites helps to retain more strength even with a stress concentration present in the composite (McBride et al. 2017). Trzepiecinski et al. (2018) have synthesized the glass/epoxy composites embedded with aluminum fibers to investigate the

improvement in strength for adhesive applications. There are two types of fiber-metal laminates, among which one was composed of 3 M structural adhesive film AF 163-2 K being used as an intermediate layer between prepreg and adherend, while the other one was produced by coupling between the adherents using epoxy resin. The tensile/shear test and 90° peel test was used to measure the adhesion between the layers of fiber-metal laminate composite. The elasticity, fatigue life of the joint, and strength were increased with the addition of aluminum fibers. Additionally, peel strength was significantly increased by which the bonded laminates become very susceptible to normal stresses (Trzepiecinski et al. 2018). In another study by Guo et al. (2005), the tungsten fiber/epoxy matrix composite was fabricated, and interface debonding behavior was analyzed. The interface debonding was reported to be continuously growing, and debond length increased with the increment in the applied load. This was attributed to the interaction of the thermal residual stress and the stress induced by the applied load on the composite. However, there was no interface debonding crack propagation that was reported in the tungsten fiber/epoxy matrix composites. The thermal expansion coefficient of tungsten fiber was lesser than that of the epoxy matrix (Guo et al. 2005).

Epoxy/Polymer Fiber Conductive Composites

The recent development on fibers particularly the production and the intensive use of polymer fibers for various commercial and technological applications has gained the attention of many researchers. The formation of a fiber network can be obtained through natural as well as synthetic polymers. Natural polymers such as cellulose, collagen, and silk form network having attached cells and that can proliferate (Sofi et al. 2018), whereas synthetic polymers are widely used for the reinforcement to form composites and provide good mechanical support. Polymer fibers can be manufactured by three different approaches such as the melt spinning, electrospinning, and solution spinning. To fabricate thermoplastic polymer fibers, the melt spinning method is mainly used because of its simple processing. This method includes the solidification of polymer fibers by cooling and then their extrusion from the spinneret. However, among these different methods, electrospinning is considered to be the most preferred method to obtain a fibrous material especially for biomedical applications. The electrospun nanofibers offer biodegradability, good compatibility, and outstanding structural properties. The fabrication of polymer fibers via electrospinning involves the passing of a suitable polymer solution through a syringe with which a needle is attached to a metallic support role. In the electrospun mechanism, the high voltage is applied which stimulates the fiber formation in the collector. An electrical fill is generated that stimulates the production of fibers through the liquid drop formation known as the Taylor cone, by the injection of fluid. The collector rotates with an opposite electrical charge, and it attracts the final fiber produced which also forms a network at the end of the process (Beckers et al. 2015).

The polymer fiber composites are usually composed of nanofibers made of natural or synthetic polymers having a distinct dispersed phase and a polymer matrix. However, there are different reinforcements other than polymer fibers that are also used to fabricate the composites such as inorganic or metal nanoparticles, bioactive macromolecules, drug nanocarriers, or carbon nanostructures (Ravichandran et al. 2012). By the surface modification or phase blending of nanofibers, the fiber-reinforced polymer composites can be prepared. In medical applications, polymer fibers are a good option because of their unique properties and structure. The polymer fiber provides high toughness and stiffness. In the case of mechanical strength, they display advanced properties in tension and deprived properties in compression. The polymer fibers are ductile in nature, and there may be fractures that occurred by splitting into small fibrils. These fibers can be utilized for many applications which require relatively high temperatures and high specific strength and possess very low creep values. Moreover, different fiber-based composite materials can be designed by modifying the structural parameters or by changing the traditional electrospinning parameters (Guadagno et al. 2014). There are several reports on the analysis and investigation on improving the properties of the composite material by reinforcing polymer fibers. Dharmavarapu and Reddy (2020) investigated the effects of reinforcing a nanofiller in aramid fiber/epoxy composite. This work reported the importance of adding silane-modified nano-silica particles in the aramid fiber-reinforced epoxy resin hybrid composite to improve the mechanical properties of the composites (Dharmavarapu and Reddy 2020). The preparation includes the surface treatment of aramid fiber and nano-silica particles using 3-aminopropyltrimethoxysilane via acid hydrolysis process. The results show the improvement of tensile and flexural strength by adding the aramid fiber into nano-silica-toughened epoxy resin hybrid composite. The strength was increased about 102 MPa and 135 MPa of the hybrid composites. The results revealed that the limited penetration was observed for drop load impact penetration of the hybrid composite (Dharmavarapu and Reddy 2020). However, the hybrid composite containing 2 vol.% of nano-silica provided a very minor specific wear rate and low coefficient of friction. In addition, the study also shows that the introduction of aramid fiber and nano-silica particle offered good wear resistance, high modulus, stiffness, and fatigue life and it can be used as a potential material for applications such as wind turbine blades, automobile power transmission gears, farm-related machinery, and domestic equipment. Pan et al. (2014) have discussed the structural modifications and the tribological properties of epoxy/aramid fabric composite prepared through successive curing and a dip-coating method. The investigation on mechanical properties by introducing SBN in the epoxy/aramid fabric composite was reported concisely. The frictional and wear behaviors of composites were analyzed for the application in tribological fields. The study has shown that the improvement in the wear life of composites was found to be higher than that of the neat fibers, but the friction coefficient values were slightly decreasing. The morphological analysis predicted that the composite monocrystal occurred in the selected area, and it was due to the introduction of single-layer boron nitride at the worn surface. However, good compatibility of aramid fabric with epoxy leads to enhancement in the mechanical strength of the composite (Pan et al. 2014).

Conclusions

This chapter discusses the electrical properties of various synthetic fiber-reinforced epoxy composites. The influence of various electrical properties by reinforcing different synthetic fibers in the epoxy matrix with their performance is reviewed. The synthesis of epoxy hybrid composites by incorporating various nanofillers and synthetic fibers such as glass fiber, carbon fiber, Kevlar fiber, and basalt fiber is discussed. Different synthetic fibers reinforcement and distribution in an epoxy matrix made them a potential material for a wide range of engineering applications. These synthetic fiber/epoxy composites meet the universal demand of hybrid materials that gives potential results. The uniform distribution and interaction of fibers with the polymer matrix is a special feature to attain efficient electrical conductivity values. However, the electrical properties of fiber-reinforced epoxy composites can be improved by coating or incorporating various other nanofillers. Synthetic fiber-based composites have unique properties and provide a platform to develop hybrid composites that fulfill the greater material need for future technological applications.

References

J. Ahmad, K. Deshmukh, M. Habib, M.B. Hägg, Influence of TiO_2 nanoparticles on the chemical, mechanical and gas separation properties of polyvinyl alcohol-titanium dioxide PVA-TiO_2 nanocomposite membranes. Int. J. Polym. Anal. Charac. **18**, 287–296 (2013)

F. Akman, H. Ogul, M.R. Kaçal, H. Polat, K. Dilsiz, M.F. Turhan, Impact of lead (II) iodide on radiation shielding properties of polyester composites. Appl. Phys. A Mater. Sci. Process. **126**, 301 (2020)

B. Alemour, H.N. Lim, M.H. Yaacob, O. Badran, M.R. Hassan, Improving the electrical conductivity of carbon fiber reinforced epoxy composite using reduced graphene oxide. Mater. Res. Exp. **6**, 065607 (2019)

A. Anwar, D. Elfiky, A.M. Ramadan, G.M. Hassan, Effect of γ-irradiation on the optical and electrical properties of fiber reinforced composites. Radiat. Phys. Chem. **134**, 14–18 (2017)

P. Banibayat, Experimental investigation of the mechanical and creep rupture properties of basalt fiber reinforced polymer (BFRP) bars. Dissertation University of Akron (2011)

M. Beckers, T. Schlüter, T. Vad, T. Gries, C.A. Bunge, An overview on fabrication methods for polymer optical fibers. Polym. Int. **64**, 25–36 (2015)

E. Bekyarova, E.T. Thostenson, A. Yu, H. Kim, J. Gao, J. Tang, H.T. Hahn, T.W. Chou, M.E. Itkis, R.C. Haddon, Multiscale carbon nanotube−carbon fiber reinforcement for advanced epoxy composites. Langmuir **23**, 3970–3984 (2007)

L. Bhanuprakash, S. Parasuram, S. Varghese, Experimental investigation on graphene oxides coated carbon fibre/epoxy hybrid composites: Mechanical and electrical properties. Compos. Sci. Technol. **179**, 134–144 (2019)

P. Bhaskar, R.H. Mohamed, Analytical estimation of elastic properties of polypropylene fiber matrix composite by finite element analysis. Adv. Mater. Phys. Chem. **2**, 23–30 (2012)

P. Bhatt, A. Goe, Carbon fibres: Production, properties and potential use. Mater. Sci. Res. India **14**, 52–57 (2017)

O. Breuer, U. Sundararaj, Big returns from small fibers: A review of polymer/carbon nanotube composites. Polym. Compos. **25**, 630–645 (2004)

N. Chand, D. Jain, Effect of sisal fibre orientation on electrical properties of sisal fibre reinforced epoxy composites. Compos. Part A: Appl. Sci. Manuf. **36**, 594–602 (2005)

V. Chinnasamy, S.P. Subramani, S.K. Palaniappan, B. Mylsamy, K. Aruchamy, Characterization on thermal properties of glass fiber and Kevlar fiber with modified epoxy hybrid composites. J. Mater. Res. Technol. **9**, 3158–3167 (2020)
W. Chuang, J. Geng-sheng, L. Bing-liang, P. Lei, F. Ying, G. Ni, L. Ke-zhi, Dispersion of carbon fibers and conductivity of carbon fiber-reinforced cement-based composites. Ceram. Int. **43**, 15122–15132 (2017)
B.D. Deeraj, R. Harikrishnan, J.S. Jayan, A. Saritha, K. Joseph, Enhanced visco-elastic and rheological behavior of epoxy composites reinforced with polyimide nanofiber. Nano-Struct. Nano-Objects. **21**, 100421 (2020)
K. Deshmukh, G.M. Joshi, Embedded capacitor applications of graphene oxide reinforced poly (3, 4-ethylenedioxythiophene)-tetramethacrylate (PEDOT-TMA) composites. J. Mater. Sci. Mater. Electron. **26**, 5896–5909 (2015)
K. Deshmukh, S.K.K. Pasha, Room temperature ammonia sensing based on graphene oxide integrated flexible polyvinylidene fluoride/cerium oxide nanocomposite films. Polym. Plast. Technol. Eng. **59**, 1429–1446 (2020)
K. Deshmukh, S. Sankaran, M.B. Ahamed, S.K.K. Pasha, K.K. Sadasivuni, D. Ponnamma, M.A.A. AlMaadeed, Studies on the electrical properties of graphene oxide reinforced poly (4-styrenesulfonic acid) and polyvinyl alcohol blend composites. Int. J. Nanosci. **17**, 1760005–1760013 (2018)
K. Deshmukh, T. Kovářík, A. Muzaffar, M.B. Ahamed, S.K.K. Pasha, Mechanical analysis of polymers, in Polymer Science and Innovative Applications: Materials, Techniques, and Future Developments, ed. by M. A. A. AlMaadeed, D. Ponnamma, M. A. Carignano, (Radarweg 29, PO Box 211, 1000 AE Amsterdam, Netherlands, 2020), pp. 117–152
V. Dhand, G. Mittal, K.Y. Rhee, S.J. Park, D. Hui, A short review on basalt fiber reinforced polymer composites. Compos. Part B: Eng. **73**, 166–180 (2015)
P. Dharmavarapu, M.S. Reddy, Mechanical, low velocity impact, fatigue and tribology behaviour of Silane grafted aramid fibre and Nano-silica toughened epoxy composite. SILICON **30**, 1–10 (2020)
N. Domun, H. Hadavinia, T. Zhang, T. Sainsbury, G.H. Liaghat, S. Vahid, Improving the fracture toughness and the strength of epoxy using nanomaterials – A review of the current status. Nanoscale **7**, 10294–10329 (2015)
A. Ekhtiyari, M.M. Shokrieh, R. Alderliesten, Loading rate effects on mode-I delamination in glass/epoxy and glass/CNF/epoxy laminated composites. Eng. Fract. Mech. **228**, 106908 (2020)
F. Ellyin, R. Maser, Environmental effects on the mechanical properties of glass-fiber epoxy composite tubular specimens. Compos. Sci. Technol. **64**, 1863–1874 (2004)
N. Forintos, T. Czigany, Multifunctional application of carbon fiber reinforced polymer composites: Electrical properties of the reinforcing carbon fibers – A short review. Compos. Part B: Eng. **162**, 331–343 (2019)
J. George, H. Ishida, A review on the very high nanofiller-content nanocomposites: Their preparation methods and properties with high aspect ratio fillers. Prog. Polym. Sci. **86**, 1–39 (2018)
P. Gonon, A. Boudefel, Electrical properties of epoxy/silver nanocomposites. J. Appl. Phys. **99**, 024308 (2006)
L. Greiner, P. Kukla, S. Eibl, M. Döring, Phosphorus containing polyacrylamides as flame retardants for epoxy-based composites in aviation. Polymers **11**, 284 (2019)
W. Gu, H.F. Wu, S.L. Kampe, G.Q. Lu, Volume fraction effects on interfacial adhesion strength of glass-fiber-reinforced polymer composites. Mater. Sci. Eng.: A. **277**, 237–243 (2000)
L. Guadagno, M. Raimondo, V. Vittoria, L. Vertuccio, C. Naddeo, S. Russo, B. De Vivo, P. Lamberti, G. Spinelli, V. Tucci, Development of epoxy mixtures for application in aeronautics and aerospace. RSC Adv. **4**, 15474–15488 (2014)
S. Guo, K. Honda, Y. Kagawa, Interface debonding from bottom face and frictional transition during pushout testing of a tungsten fiber-epoxy matrix composite. Compos. Sci. Technol. **65**, 1808–1814 (2005)
H. Guo, Y. Zhan, Z. Chen, F. Meng, J. Wei, X. Liu, Decoration of basalt fibers with hybrid Fe_3O_4 microspheres and their microwave absorption application in bisphthalonitrile composites. J. Mater. Chem. A **1**, 2286–2296 (2013)

K. Gupta, R.F. Laubscher, Sustainable machining of titanium alloys: A critical review. Proc. Inst. Mech. Eng., Part B: J. Eng. Manuf. **231**, 2543–2560 (2017)

M. Haghgoo, R. Ansari, M.K. Hassanzadeh-Aghdam, M. Nankali, Analytical formulation for electrical conductivity and percolation threshold of epoxy multiscale nanocomposites reinforced with chopped carbon fibers and wavy carbon nanotubes considering tunneling resistivity. Compos. Part A: Appl. Sci. Manuf. **126**, 105616 (2019)

S.H. Han, H.J. Oh, H.C. Lee, S.S. Kim, The effect of post-processing of carbon fibers on the mechanical properties of epoxy-based composites. Compos. Part B: Eng. **45**, 172–177 (2013)

M.A. Ibragimov, N.N. Shishkina, E.G. Zinovjeva, Reinforcement of elastomers based on butadiene rubbers and their mixtures with layered silicates, in *Key Engineering Materials*, ed. by K. Svetlana, Z. Azamat, V. Amina, vol. 869, (2020), pp. 158–162

M.S. Islam, Y. Deng, L. Tong, S.N. Faisal, A.K. Roy, A.I. Minett, V.G. Gomes, Grafting carbon nanotubes directly onto carbon fibers for superior mechanical stability: Towards next generation aerospace composites and energy storage applications. Carbon **96**, 701–710 (2016)

S.T. Jackson, S. Samanta, H. Singh, Influence of kevlar hybridization on dielectric and conductivity of bamboo fiber reinforced epoxy composite. J. Nat. Fibers. **14**, 837–845 (2017)

H. Jamshaid, R. Mishra, A green material from rock: Basalt fiber – A review. J. Text. Inst. **107**, 923–937 (2016)

M.H. Jawaid, H.A. Khalil, Cellulosic/synthetic fibre reinforced polymer hybrid composites: A review. Carbohydr. Polym. **86**, 1–8 (2011)

J. Jia, X. Sun, X. Lin, X. Shen, Y.W. Mai, J.K. Kim, Exceptional electrical conductivity and fracture resistance of 3D interconnected graphene foam/epoxy composites. ACS Nano **8**, 5774–5783 (2014)

J. Joseph, K. Deshmukh, N.A. Nambiraj, S.K.K. Pasha, Electromagnetic shielding characteristics of $SrTiO_3$ nanoparticles induced polyvinylchloride and polyvinylidene fluoride blend nanocomposites. J. Inorg. Organomet. Polym. Mater. **31**, 3481–3495 (2021)

R.B. Kabir, N. Ferdous, Kevlar-the super tough fiber. Int. J. Text. Sci. **1**, 78–83 (2012)

L. Karikalan, M. Chandrasekran, S. Ramasubramanian, S. Baskar, Hybridization of composites using natural and synthetic fibers for automotive application. Int. J. Sci. Res. Sci. Technol. **7**, 916–920 (2017)

S. Kasaragadda, I.M. Alarifi, M. Rahimi-Gorji, R. Asmatulu, Investigating the effects of surface superhydrophobicity on moisture ingression of nanofiber-reinforced bio-composite structures. Microsyst. Technol. **26**, 447–459 (2020)

A. Kausar, Interpenetrating polymer network and nanocomposite IPN of polyurethane/epoxy: A review on fundamentals and advancements. Polym. Plast. Technol. Mater. **58**, 691–706 (2019)

M. Kim, T.W. Lee, S.M. Park, Y.G. Jeong, Structures, electrical and mechanical properties of epoxy composites reinforced with MWCNT-coated basalt fibers. Compos. Part A: Appl. Sci. Manuf. **123**, 123–131 (2019)

M.A. Kshad, C. D'Hondt, H.E. Naguib, Carbon nano fibers reinforced composites origami inspired mechanical metamaterials with passive and active properties. Smart Mater. Struct. **26**, 105039 (2017)

Y.R. Kumar, K. Deshmukh, M.M. Naseer Ali, G. Abhijay, W.A. Al-Onazi, A.M. Al-Mohamimeed, S.K.K. Pasha, Structure, morphology and modelling studies of polyvinyl alcohol nanocomposites reinforced with nickel oxide nanoparticles and graphene quantum dots. Environ. Res. **203**, 111842 (2022)

M. Kupke, K. Schulte, R. Schüler, Non-destructive testing of FRP by dc and ac electrical methods. Compos. Sci. Technol. **61**, 837–847 (2001)

G. Li, Y. He, P. Zhu, T. Zhao, R. Sun, D. Lu, C.P. Wong, Tailored surface chemistry of SiO_2 particles with improved rheological, thermal-mechanical and adhesive properties of epoxy based composites for underfill applications. Polymers **156**, 111–120 (2018a)

Z. Li, J. Ma, H. Ma, X. Xu, Properties and applications of basalt fiber and its composites, in *IOP Conference Series: Earth and Environmental Science*, vol. 186, (2018b), pp. 1755–1315

Y. Li, H. Zhang, Y. Liu, H. Wang, Z. Huang, T. Peijs, E. Bilotti, Synergistic effects of spray-coated hybrid carbon nanoparticles for enhanced electrical and thermal surface conductivity of CFRP laminates. Compos. Part A: Appl. Sci. Manuf. **105**, 9–18 (2018c)

T.K. Lin, S.J. Wu, J.G. Lai, S.S. Shyu, The effect of chemical treatment on reinforcement/matrix interaction in Kevlar-fiber/bismaleimide composites. Compos. Sci. Technol. **60**(9), 1873–1878 (2000)

I.V. Lukiyanchuk, V.S. Rudnev, M.M. Serov, B.L. Krit, G.D. Lukiyanchuk, P.M. Nedozorov, Effect of copper coating on fibers made of aluminum alloy, titanium, and FeCrAl alloy on surface morphology and activity in CO oxidation. Appl. Surf. Sci. **436**, 1–10 (2018)

A.K. McBride, S.L. Turek, A.E. Zaghi, K.A. Burke, Mechanical behavior of hybrid glass/steel fiber reinforced epoxy composites. Polymers **9**(4), 151 (2017)

M. Megahed, A. Fathy, D. Morsy, F. Shehata, Mechanical performance of glass/epoxy composites enhanced by micro-and nanosized aluminum particles. J. Ind. Text. **51**, 68–92 (2019)

M. Mittal, R. Chaudhary, Experimental investigation on the mechanical properties and water absorption behavior of randomly oriented short pineapple/coir fiber-reinforced hybrid epoxy composites. Mater. Res. Exp. **6**, 015313 (2018)

M.K. Mohanapriya, K. Deshmukh, K.K. Sadasivuni, G.J. Thangamani, K. Chidambaram, M.B. Ahamed, S.K.K. Pasha, Enhanced quality factor of polyvinyl formal (PVF) based nanocomposites filled with zinc oxide and carbon black nanoparticles for wireless sensing applications. Mater. Today: Proc. **9**, 199–216 (2019)

A. Muzaffar, M.B. Ahamed, K. Deshmukh, Hydrothermal synthesis of $ZnWO_4$-MnO_2 nanopowder doped with carbon black nanoparticles for high performance supercapacitor applications. J. Mater. Sci. Mater. Electron. **30**, 21250–21258 (2019)

A. Muzaffar, M.B. Ahamed, K. Deshmukh, S.K.K. Pasha, Dielectric properties and electromagnetic interference shielding studies of nickel oxide and tungsten oxide reinforced polyvinylchloride nanocomposites. Polym. Plast. Technol. Mater. **59**, 1667–1678 (2020)

N. Nagaraj, S. Balasubramaniam, V. Venkataraman, R. Manickam, R. Nagarajan, I.S. Oluwarotimi, Effect of cellulosic filler loading on mechanical and thermal properties of date palm seed/vinyl ester composites. Int. J. Biol. Macromol. **147**, 53–66 (2020)

M.S. Nazir, M.H. Kassim, L. Mohapatra, M.A. Gilani, M.R. Raza, K. Majeed, Characteristic properties of nanoclays and characterization of nanoparticulates and nanocomposites, in *Nanoclay Reinforced Polymer Composites: Nanocomposites and Bionanocomposites*, (Springer Publication, Singapore, 2016), pp. 35–55

F. Nturanabo, L. Masu, J.B. Kirabira, Novel applications of aluminium metal matrix composites, in *Aluminium Alloys and Composites*, ed. by K. O. Cooke, (IntechOpen, 2019). https://doi.org/10.5772/intechopen.86225

R. Oliwa, The mechanical properties of Kevlar fabric/epoxy composites containing aluminosilicates modified with quaternary ammonium and phosphonium salts. Materials **13**, 3726 (2020)

B. Pan, M. Xu, H. Wang, E. Ye, J. Liu, Y. Zhang, Tribological properties of epoxy/aramid fabric composites reinforced by boron nitride of single layer. Polym. Plast. Technol. Eng. **53**, 678–683 (2014)

P. Panda, G. Mishra, S. Mantry, S.K. Singh, S.P. Sinha, A study on mechanical, thermal, and electrical properties of glass fiber-reinforced epoxy hybrid composites filled with plasma-synthesized AlN. J. Compos. Mater. **48**, 3073–3082 (2014)

D.K. Rajak, D.D. Pagar, P.L. Menezes, E. Linul, Fiber-reinforced polymer composites: Manufacturing, properties, and applications. Polym. **11**, 1667 (2019a)

D.K. Rajak, D.D. Pagar, P.L. Menezes, E. Linul, Fiber-reinforced polymer composites: Manufacturing, properties, and applications. Polymers **11**(10), 1667 (2019b)

P. Rani, M.B. Ahamed, K. Deshmukh, Dielectric and electromagnetic interference shielding properties of zeolite 13X and carbon black nanoparticles based PVDF nanocomposites. J. Appl. Polym. Sci. **50107** (2020a)

P. Rani, M.B. Ahamed, K. Deshmukh, Electromagnetic interference shielding properties of graphene quantum-dots reinforced poly (vinyl alcohol)/polypyrrole blend nanocomposites. J. Appl. Polym. Sci. **137**, 49392 (2020b)

P. Rani, M.B. Ahamed, K. Deshmukh, Significantly enhanced electromagnetic interference shielding effectiveness of montmorillonite nanoclay and copper oxide nanoparticles-based polyvinylchloride nanocomposites. Polym. Test. **91**, 106744 (2020c)

R. Ravichandran, S. Sundarrajan, J.R. Venugopal, S. Mukherjee, S. Ramakrishna, Advances in polymeric systems for tissue engineering and biomedical applications. Macromol. Biosci. **12**, 286–311 (2012)

S. Ravichandran, E. Vengatesan, A. Ramakrishnan, Synthesis and dynamic mechanical analysis of fiber reinforced low-density polyethylene hybrid polymer composites. Mater. Today: Proc. **27**, 177–180 (2020)

T. Remis, P. Belsky, T. Kovarik, J. Kadlec, M.G. Azar, R. Medlin, V. Vavrunkova, K. Deshmukh, K.K. Sadasivuni, Study on structure, thermal behavior and viscoelastic properties of nano-diamond reinforced polyvinyl alcohol nanocomposites. Polymers **13**, 1426 (2021)

E. Rill, D.R. Lowry, W.M. Kriven, Properties of basalt fiber reinforced geopolymer composites, in *Ceramic engineering and science proceedings*, vol. 31, (2010), pp. 57–67

D. Romanzini, A. Lavoratti, H.L. Ornaghi Jr., S.C. Amico, A.J. Zattera, Influence of fiber content on the mechanical and dynamic mechanical properties of glass/ramie polymer composites. Mater. Des. **47**, 9–15 (2013)

M.Z. Rong, M.Q. Zhang, Y. Liu, G.C. Yang, H.M. Zeng, The effect of fiber treatment on the mechanical properties of unidirectional sisal-reinforced epoxy composites. Compos. Sci. Technol. **61**, 1437–1447 (2001)

M.R. Sanjay, G.R. Arpitha, L.L. Naik, K. Gopalakrishna, B. Yogesha, Applications of natural fibers and its composites: An overview. Nat. Res. **7**, 108–114 (2016)

S. Sankaran, K. Deshmukh, M.B. Ahamed, S.K.K. Pasha, K.K. Sadasivuni, D. Ponnamma, M.A. AlMaadeed, K. Chidambaram, Investigation on the electrical properties of lithium ion conducting polymer electrolyte films based on biodegradable polymer blends. Adv. Sci. Lett. **24**, 5496–5502 (2018)

M.S. Santhosh, R. Sasikumar, L. Natrayan, M.S. Kumar, V. Elango, M. Vanmathi, Investigation of mechanical and electrical properties of kevlar/E-glass and basalt/E-glass reinforced hybrid composites. Int. J. Mech. Product. Eng. Res. Dev. **8**, 591–598 (2018)

S. Sasidharan, A. Anand, Epoxy-based hybrid structural composites with nanofillers: A review. Ind. Eng. Chem. Res. **59**, 12617–12631 (2020)

A. Sassani, H. Ceylan, S. Kim, K. Gopalakrishnan, A. Arabzadeh, P.C. Taylor, Influence of mix design variables on engineering properties of carbon fiber-modified electrically conductive concrete. Constr. Build. Mater. **152**, 168–181 (2017)

T.P. Sathishkumar, S. Satheeshkumar, J. Naveen, Glass fiber-reinforced polymer composites – A review. J. Reinf. Plast. Compos. **33**, 1258–1275 (2014)

E.C. Senis, I.O. Golosnoy, J.M. Dulieu-Barton, O.T. Thomsen, Enhancement of the electrical and thermal properties of unidirectional carbon fibre/epoxy laminates through the addition of graphene oxide. J. Mater. Sci. **54**, 8955–8970 (2019)

X. Shen, Q. Zheng, J.K. Kim, Rational design of two-dimensional nanofillers for polymer nanocomposites toward multifunctional applications. Prog. Mater. Sci. **115**, 100708 (2020)

P. Sobolčiak, A. Ali, M.K. Hassan, M.I. Helal, A. Tanvir, A. Popelka, M.A. Al-Maadeed, I. Krupa, K.A. Mahmoud, 2D Ti_3C_2Tx (MXene)-reinforced polyvinyl alcohol (PVA) nanofibers with enhanced mechanical and electrical properties. PLoS One **12**, e0183705 (2017)

H.S. Sofi, R. Ashraf, M.A. Beigh, F.A. Sheikh, Scaffolds fabricated from natural polymers/composites by electrospinning for bone tissue regeneration, in *Cutting-Edge Enabling Technologies for Regenerative Medicine*, (2018), pp. 49–78

G.J. Thangamani, K. Deshmukh, T. Kovarik, N.A. Nambiraj, D. Ponnamma, K.K. Sadasivuni, H.P.S. Abdul Khalil, S.K.K. Pasha, Graphene oxide nanocomposites based room temperature gas sensors: A review. Chemosphere **280**, 130641 (2021a)

G.J. Thangamani, K. Deshmukh, N.A. Nambiraj, S.K.K. Pasha, Chemiresistive gas sensors based on vanadium pentoxide reinforced polyvinyl alcohol/polypyrrole blend nanocomposites for room temperature LPG sensing. Synth. Met. **273**, 116687 (2021b)

T. Trzepiecinski, A. Kubit, R. Kudelski, P. Kwolek, A. Obłój, Strength properties of aluminium/glass-fiber-reinforced laminate with additional epoxy adhesive film interlayer. Int. J. Adhes. Adhes. **85**, 29–36 (2018)

P. Tsotra, K. Friedrich, Short carbon fiber reinforced epoxy resin/polyaniline blends: Their electrical and mechanical properties. Compos. Sci. Technol. **64**, 2385–2391 (2004)
X. Wang, J. Shi, J. Liu, L. Yang, Z. Wu, Creep behavior of basalt fiber reinforced polymer tendons for prestressing application. Mater. Des. **59**, 558–564 (2014)
Y. Wang, Y. Wang, B. Wan, B. Han, G. Cai, R. Chang, Strain and damage self-sensing of basalt fiber reinforced polymer laminates fabricated with carbon nanofibers/epoxy composites under tension. Compos. Part A: Appl. Sci. Manuf. **113**, 40–52 (2018)
H. Wang, Y. Yao, Z. He, W. Rao, L. Hu, S. Chen, J. Lin, J. Gao, P. Zhang, X. Sun, X. Wang, A highly stretchable liquid metal polymer as reversible transitional insulator and conductor. Adv. Mater. **31**, 1901337 (2019)
K.Q. Yu, J.T. Yu, J.G. Dai, Z.D. Lu, S.P. Shah, Development of ultra-high performance engineered cementitious composites using polyethylene (PE) fibers. Constr. Build. Mater. **158**, 217–227 (2018)
F. Yuan, L. Tsai, V. Prakash, A.M. Rajendran, D.P. Dandekar, Spall strength of glass fiber reinforced polymer composites. Int. J. Solid Struct. **44**(24), 7731–7747 (2007)
R.H. Zhang, X.T. Shi, L. Tang, Z. Liu, J.L. Zhang, Y.Q. Guo, J.W. Gu, Thermally conductive and insulating epoxy composites by synchronously incorporating Si-sol functionalized glass fibers and boron nitride fillers. Chin. J. Polym. Sci. **38**, 730–739 (2020)
G. Zhao, H.Y. Liu, X. Du, H. Zhou, Z. Pan, Y.W. Mai, Y.Y. Jia, W. Yan, Flame synthesis of carbon nanotubes on glass fibre fabrics and their enhancement in electrical and thermal properties of glass fibre/epoxy composites. Compos. Part B: Eng. **198**, 108249 (2020)

Dynamic Fracture Toughness Prediction of Fiber/Epoxy Composites Using K-Nearest Neighbor (KNN) Method

4

Aanchna Sharma, Priyanka Madhushri, and Vinod Kushvaha

Contents

Abstract

Geometrical features like size and shape of the particles which are used to reinforce the composites affect the mechanical behavior of the resulting particulate polymer composites to a great extent. The aspect ratio of the reinforcing filler is of great importance specially when such composites are subjected to impact loading. Usually, an increase in the aspect ratio results in a significant increase in the energy-absorbing ability which ultimately improves the fracture toughness of the resulting composite. However, the experimental procedure followed for determining the fracture toughness of polymer composites reinforced with particles of varying aspect ratio is very complex and time-consuming. In this view, this chapter investigates the applicability of a machine learning algorithm known as K-nearest neighbor (KNN) for determining the dynamic fracture toughness of glass-filled polymer composites. The proposed methodology aims to predict the fracture toughness in terms of stress intensity factor with limited experimentation and maximum accuracy. The current framework of machine learning utilizes time, dynamic elastic modulus, aspect ratio,

A. Sharma · V. Kushvaha (✉)
Department of Civil Engineering, Indian Institute of Technology Jammu, Jammu, India
e-mail: 2018RCE0035@iitjammu.ac.in; vinod.kushvaha@iitjammu.ac.in

P. Madhushri
Stanley Black and Decker, Atlanta, GA, USA
e-mail: Priyanka.Madhushri@sbdinc.com

S. Mavinkere Rangappa et al. (eds.), *Handbook of Epoxy/Fiber Composites*,
https://doi.org/10.1007/978-981-19-3603-6_6

and volume fraction of the glass particles as the independent model parameters. The proposed KNN model predicts the fracture behavior of these composites with an accuracy of ~96%.

Keywords

K-nearest neighbor · Aspect ratio · Fracture toughness · Machine learning · Impact loading · Stress intensity factor

Introduction

Particulate polymer composites have been observed to undergo a very complex behavior when they are subjected to impact loading. The overall behavior of the resulting composite gets significantly affected by the characteristic properties of its constituent materials, especially the fillers (Hemath et al. 2020; Vinod et al. 2021). Inorganic particles like silica, mica, alumina, talc, etc., are a few examples of the commonly used fillers that are being utilized as reinforcements to epoxy matrix. These fillers play a major role in enhancing the stiffness and toughness of the epoxy matrix (Friedrich et al. 2005). A few parameters like size, shape, elastic modulus, and the amount of filler particles to be added in the polymer matrix considerably change the ultimate response of the polymer composites (Sharma and Kushvaha 2020). Microscaled and nanoscaled filler particles are known to have different impact on the overall behavior of the composite materials (Sharma et al. 2020a, b, c). The interphase developed between the matrix and the dispersed phase (reinforcement) accounts for the plastic yielding and failure mechanisms that take place after the composite has been subjected to external loads, and the development of the interfacial zone depends largely on the type of fillers used for the purpose of matrix reinforcement (Bharath et al. 2020). A research group (Zhang et al. 1993) reported the contribution of local plastic deformation in the interfacial region in increasing the fracture toughness of short carbon-reinforced polymer composite. The aspect ratio, volume fraction of fillers, interfacial properties. and the chemical composition of both the matrix and fillers decide the overall morphology of the polymer composites (G et al. 2021; Ramesh et al. 2021). Hence, the choice of filler particles has to be made very carefully keeping in mind the potential application of the final composite product (Sharma et al. 2021). Such polymer composites possess a very good combination of mechanical and acoustic properties along with being very light in weight. Unlike metals, polymer composites perform considerably well in the corrosive environments. Because of this reason, such composites are getting very popular in various industries like automotive, marine, and aerospace. For their application in these industries, studying the fracture toughness is imperative so as to get an idea of the material's resistance to crack growth.

A stress-based parameter, known as stress intensity factor (SIF) is used as the direct indicator of the material's fracture toughness (Kushvaha et al. 2019). In the literature, different experimental methods like digital image correlation, Moire

method, and coherent optical methods are reported to determine the stress intensity factor. A research group (McNeill et al. 1987) used the technique of digital image correlation to determine the stress intensity factor for different geometries of a plexiglass specimen. G. Pluvinage (Pluvinage 1998) analyzed the distribution of stress at the crack tip using the concept of stress intensity factor. He explained the initiation of fatigue and fracture based on the methodology of stress intensity factor considered at the notch in the brittle composite materials. Another research group (Park et al. 2000) found a linear relationship between the free surface energy and the critical stress intensity factor, and based on that, they demonstrated the effect of matrix-reinforcement interactions on the overall fracture toughness of the carbon fiber-reinforced polymer composite. A very important observation regarding the stress intensity factor was reported by Subramaniyan and Sun (Subramaniyan and Sun 2007). They considered three different types of crack (notch, blunt, and sharp) and calculated the stress intensity factor for all of the three cases. They concluded that the stress intensity factor could only be considered as a parameter if the concerned crack is sharp and the idea of the crack sharpness could be taken from the fractured morphology of the specimen. Digital image correlation (DIC) method was used to validate the stress intensity factor values obtained from finite element simulations for the determination of fracture toughness of single-edge notch bending specimens (Ayatollahi et al. 2019). Digital image correlation has been used successfully to analyze the linear and nonlinear fracture parameters and determine the fracture toughness of concrete (Golewski 2019). Three-dimensional digital image correlation was used to study the fracture behavior of a glass fiber-reinforced polymer composite in terms of strain and displacement fields (Mallon et al. 2014). Dynamic fracture (mode-1) was introduced by means of a shock tube apparatus. This study concluded that the stress intensity factor decreases as the angle of fiber reinforcement increases. Qian and his research group (Qian et al. 2021) used a microscale DIC technique to determine the crack tip opening displacement and hence to find out the fracture toughness of a polymer substrate. Thus, obtained stress intensity factors were then used to establish a failure criterion curve. This further helped them to calculate the adhesive strength of the polymer substrate reinforced with nanoparticles. Moire method is another technique used to determine the stress intensity factor. Moire interferometry has been used to study the residual stresses in graphite-reinforced epoxy composites (Shankar et al. 2004). This experimental technique of Moire interferometry has been used by many researchers to understand the mechanical behavior of different materials. It has been proven as a powerful technique for quantifying the residual stresses in different materials (Ifju and Han 2010).

The dependence of stress intensity factor and consequently the fracture toughness on the geometry and anisotropy of the reinforcement of composite material have been reported in the literature (Brinckmann et al. 2017). Stress intensity factor has been used successfully to determine the effect of varying aspect ratios of the surface cracks in the case of bending plates (Mahmoud and Hosseini 1986). To study the dynamic fracture toughness of these composite materials experimentally, a gas-gun setup is often used (Kushvaha and Tippur 2013, 2014), and this experimental methodology is very complex, expensive, and time-consuming. In addition to it,

the standardization of test methods for determining the dynamic fracture toughness is still at the developing stage (Prasad et al. 2011). This calls for an alternative technique which can reduce the need of such complex experiments and provide comparable results. There are various analytical and numerical techniques, which have been used in the past, to predict the material response under different types of loading conditions (Romanowicz 2012; Sun et al. 2013; Wani et al. 2021; Williams and Vaziri 2001). Approaches like boundary element methods and XFEM have also been used for predicting the damage caused because of the crack propagation in elastoplastic solids (Kumar et al. 2018). XFEM has been used to assess the structural integrity by considering the cracked composite specimens and different orientations of the fibers reinforced in them (Abdullah et al. 2019). It has also been used for predicting the damage initiation when the polymer prosthetics are subjected to fatigue (Wan et al. 2021). However, these techniques were found to be deficient considering the effect of anisotropy and heterogeneity of the resulting composite, and also, these methods are computationally very expensive (Hashin 1970, 1979). The nonconformity of the elements often results in erroneous predictions of fracture toughness (Citarella and Buchholz 2008; Radovitzky et al. 2011). Difficulty in convergence, more run-time, and the effect of the location of the crack tip in a considered element are the major limitations of the XFEM (Heidari-Rarani and Sayedain 2019).

However, using such computationally expensive approaches is not feasible (Xu et al. 1997). In the last two decades, a considerable development has been made in the field of artificial intelligence and machine learning, and this has attracted many material science researchers to utilize these techniques. Machine learning techniques are getting very popular among material scientists on the account of predicting the material response under different loading conditions considering the influence of different affecting parameters with utmost accuracy and much lesser computational time (Liu et al. 2015; Matos et al. 2019; Pathan et al. 2019; Garg et al. 2021; Sharma et al. 2021). In order to predict the compressive strength of glass fiber-reinforced polyester composites, artificial neural network, one of the commonly used machine learning algorithms, has been used (Seyhan et al. 2005). Glass fiber thickness and the quantity of binder were used as the input parameters, and a correlation between these two and the compressive strength of the resulting composite was developed using this machine learning algorithm. The same technique has been used to predict the conductivity of the carbon nanotube-reinforced polymer composites by making use of the limited data of the principal strains (Matos et al. 2019). The tensile strength of CNT-reinforced polymer composites has also been predicted successfully with the help of the Gaussian process (machine learning algorithm) by making use of the limited experimental data of mechanical properties of the matrix (polymer) and the weight fraction of the carbon nanotube added to reinforce the matrix (Le 2020). Machine learning has been professed as a very reliable tool for predicting the material behavior (Chen and Gu 2019; Kushvaha et al. 2020).

There are different algorithms of machine learning which can be utilized in material science, and K-nearest neighbor (KNN) is one of these. KNN is one of

the simplest algorithms under the head of supervised machine learning, in terms of its implementation (Wani et al. 2020). For different regression and classification problems, KNN is commonly used (Kumar 2015). This method is found to be the most suitable one when there is no prior information about the data distribution. KNN is considered as the most intuitive and simple nonprobabilistic classification machine learning algorithm that can be used in material science (Fukunaga and Hostetler 1973). The classification algorithm of K-nearest neighbor has been used efficaciously by many researchers in medicinal biochemistry (Chen et al. 2015; Chou 2017; Wang et al. 2020). Earlier, this algorithm has been used to predict the behavior of aluminum-based composites when subjected to uniaxial tensile forces (Thirumoorthy et al. 2019). Mechanical response of different types of composite materials has been successfully predicted by making use of K-nearest neighbor (Garg et al. 2020; Kessler and Rani 2007; Khan et al. 2019; Rahim et al. 2011; Wang et al. 2011). Thermal and mechanical behavior of latania reinforced polypropylene biocomposite has been successfully studied using K-nearest neighbor regressor (Daghigh 2020). The classification algorithm of K-nearest neighbor has also been utilized in quality assessment of carbon fiber-reinforced polymer composites (Koumoulos et al. 2020). It further helped in identifying the nano reinforcement (CNTs, nano fibers, graphene) present in the carbon-reinforced polymer composites by making use of the nano-indentation data.

In our previous study (Sharma et al. 2020a, b, c), an artificial neural network was used in order to predict the dynamic fracture toughness of particulate polymer composites in terms of stress intensity factor, and the results showed that it is a promising methodology for predicting the material response. In an attempt to inflate the possibility of applying machine learning in material science, this chapter explains the framework of KNN algorithm to predict the dynamic fracture toughness of glass-filled polymer composites considering the varying aspect ratios of the glass particles.

Testing Systems

The data used in this chapter was obtained from a gas-gun setup, the detailed description of which is reported elsewhere (Sharma et al. 2020a, b, c). The specimens, on which the dynamic fracture testing was performed, were made up of Bisphenol epoxy and glass particles. Glass particles of three different shapes (flakes, circular, and rods) were used to reinforce the epoxy matrix in a volume fraction of 0%, 5%, 10%, and 15%. Circular-, flake-, and rod-shaped fillers had an aspect ratio of 1, 6, and 80, respectively. A detailed discussion of the experimental procedure is reported in a previous study (Kushvaha 2016). The SIF histories were obtained within a time frame of -30 to 30 μs, out of which the time $t = 0$ indicated the time instance at which the crack originates. Since this chapter focuses on using the framework of KNN to predict the dynamic fracture toughness of glass-filled epoxy composites, time, dynamic elastic modulus, aspect ratio, and the volume fraction of the reinforcing particles have been used as the independent variables in the algorithm.

KNN Algorithm

Under the broad category of supervised machine learning, K-nearset neighbor (KNN) is one of the simplest algorithms to be used for predictive analysis. This algorithm does not assume anything about the new data; rather, it works on the principle of decision boundaries based on the K value (Patrick and Fischer 1970). K value refers to the number of the nearest neighbors, and the selection of which is entirely data dependent (Bezdek et al. 1986). This algorithm is advantageous in terms of providing fairly accurate results for linear and nonlinear problems (Kumar 2015). KNN algorithm is also famously known as instance-based learning. K-nearest neighbor is known to be one of the most simple and computationally inexpensive algorithms of machine learning when it comes to smaller datasets. This algorithm has the capability of providing fairly accurate output that is easy to interpret, in a comparatively lesser run-time (Wu et al. 2002). This machine learning algorithm aims to find out the class of a new dataset based on the number of the nearest neighbors (K) by making use of the idea that similar things lie in a close proximity (Silva 2009). The basic idea of this method is to assign uniform values of the weights to the query samples by considering the values of calculated distances (Ertuğrul and Tağluk 2017). In case of regression problems that means when continuous variables are given, each data point contributes unvaryingly in order to classify the query data points (García-Pedrajas et al. 2017). In such problems, the mean of the nearest neighbors is used to compute the labels assigned to the available query points (Biau et al. 2012; Song et al. 2017).

In this chapter, the KNN algorithm was implemented using MATLAB R2019b on the dataset explained in the previous section. The KNN architecture used here is shown in Fig. 1. Here, stress intensity factor is the variable that needs to be predicted corresponding to the four independent parameters (time, dynamic elastic modulus, aspect ratio, and the volume fraction). Based on the concept that similar data points lie in the same proximity, KNN makes use of a distance metric to calculate the distance between training and test datasets. Minkowski, Manhattan, Euclidean, Chebyshev, Cosine, Jaccard, and Hamming are the available metrics which can be used in KNN algorithm to calculate the distance between one data point and all the other data points (Chomboon et al. 2015). Depending on the data type in hand, a particular distance metric is selected. Owing to the wider acceptability and simplicity, this chapter utilizes the Euclidean distance metric. Then the calculated distances are sorted in ascending order, and based on the defined number of the nearest neighbors, the algorithm returns the values of the dependent variable.

Figure 2 is an illustration of how the algorithm works using the above architecture for the computation of SIF values. The model was trained using the dataset corresponding to the aspect ratio 1 and 80. The steps followed during the model training phase are shown in Fig. 2a. The available data corresponding to aspect ratio 1 and 80 was subdivided into training and cross-validation datasets. Training dataset is used to recognize the underlying patterns among the different variables, and the cross-validation dataset is used for tuning the model parameters along with

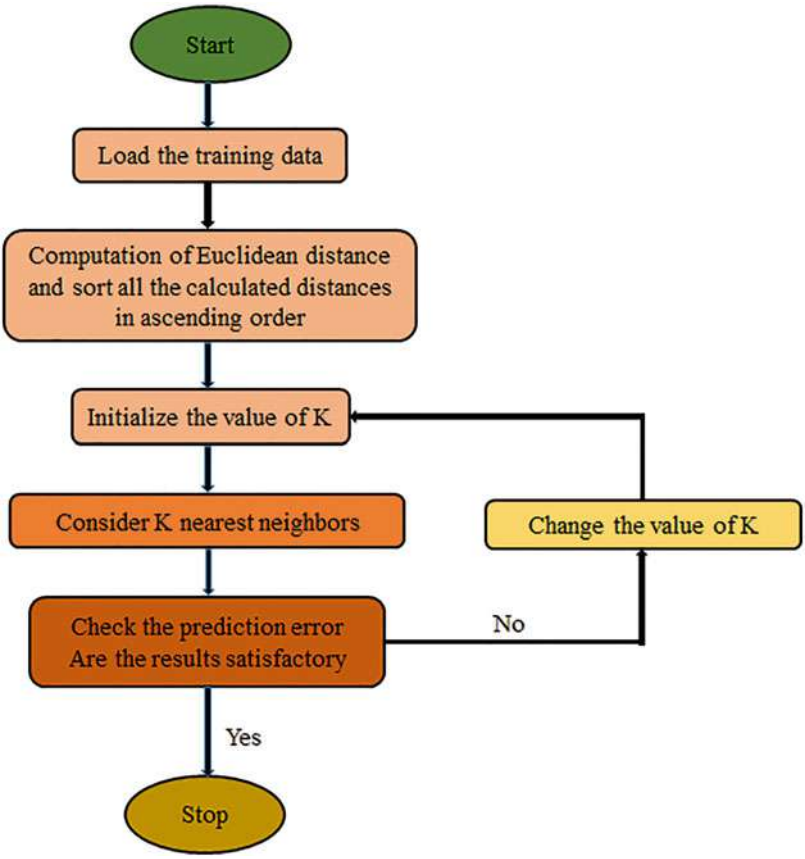

Fig. 1 Architecture of the used KNN algorithm

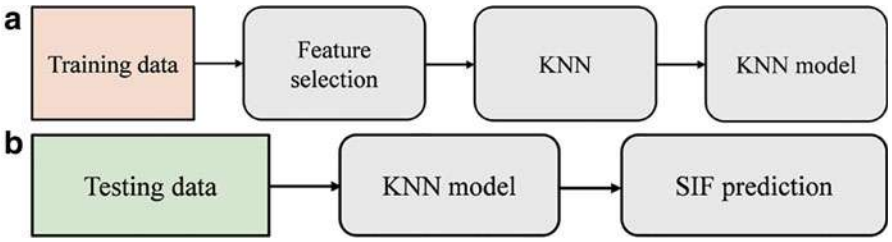

Fig. 2 Flowchart for predicting stress intensity factor

ensuring the learning ability of the model (Sharma et al. 2020a, b, c). In order to increase the generalization ability of the model and improve the predictions, feature selection is performed at the preliminary stage. In this step, redundant input parameters are dropped off, and only those parameters are selected, which

contribute most to the prediction of the dependent/target variable. For doing so, methods like filter, wrapper, embedded, and hybrid are available. In this chapter, the raw data corresponding to three different shapes of glass particles was available. To make sure that an appropriate and unbiased subset of data is selected for training purpose, random sampling in MATLAB was performed. Later, the dataset corresponding to aspect ratio 6 was used as testing data on which K-nearest neighbor regression was applied and the prediction for SIF values were made. Figure 2b shows the prediction flow of SIF values corresponding to different aspect ratios. This prediction was done corresponding to different values of K (nearest neighbors), and from this trial and error exercise, the value of K was brought down. The best value of K was then used for the SIF prediction of glass-filled epoxy composites corresponding to some random aspect ratios for which the experimental data was not available.

Summary

The entire available data was divided into training and testing datasets in the proportions of 70% and 30%, respectively. The accuracy of the trained KNN model was evaluated by means of the coefficient of determination (R^2) and the mean absolute percentage error. Figure 3 shows the goodness of fit between the predicted and the target values during the training phase.

Using the following equation, the mean absolute percentage error was calculated as 4.31%.

$$MAPE = \frac{100}{n} \sum_{i=1}^{n} \frac{|T_i - P_i|}{T_i} \tag{1}$$

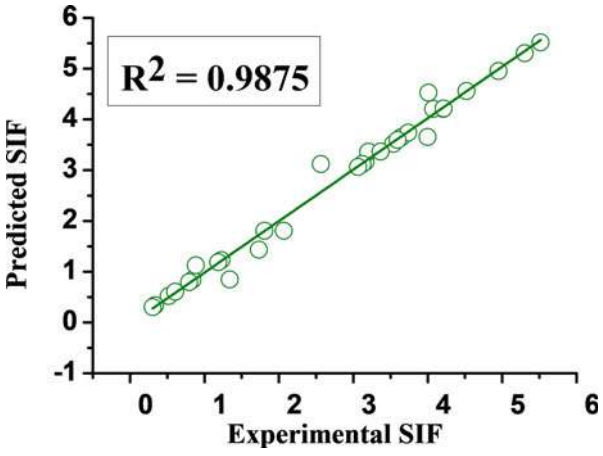

Fig. 3 Goodness of fit

where T_i = the, target value which was experimentally determined, P_i = the predicted value, and n = number of available data points. Predictions made for SIF using the proposed KNN model were quite close to the experimental SIF values, and the model was found to be ~96% accurate. The accuracy of the model largely depends on the value of number of the nearest neighbors (K) selected. Selecting the value of the nearest neighbors is the most crucial step of KNN implementation. If the value of the nearest neighbors is too small, then it will result in an algorithm extremely sensitive to the outliers, and a very large value might result in a very noisy and inaccurate model (Zhang et al. 2018). In this study, the number of the nearest neighbors was selected using a trial and error technique as shown in Fig. 4. Values of K = 1, 2, 3, 4, and 5 were tried, and the most appropriate K value was selected. Experimental and predicted values of the stress intensity factor corresponding to aspect ratio = 6 were compared based on a performance metric which is the mean absolute percentage error in this case. Table 1 summarizes the MAPE for different values of K, and the least error was found for K = 1. It was found that with the increasing value of K, predictions were

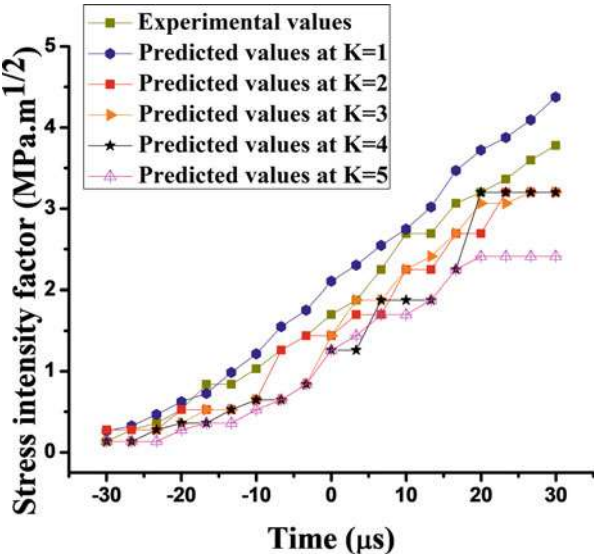

Fig. 4 Predictions for stress intensity factor at aspect ratio 6 using different values of the nearest neighbors

Table 1 Mean absolute percentage error (MAPE) for different values of K

K	MAPE (%)
1	4.31
2	12.59
3	16.19
4	22.32
5	31.11

diverging more from the target values, and this could be attributed to the fact that the data used in the study was less noisy (Beretta and Santaniello 2016). The type of dataset is the key factor for deciding the value of the nearest neighbors (Liu et al. 2019; Zhang et al. 2017). Therefore, for predicting the SIF value for some new unseen aspect ratio, K = 1 was used.

Considering the reported model accuracy of 96%, the same K-nearest neighbor framework was used to study the stress intensity factor history for new aspect ratio of 3.5 and 43. For these two aspect ratios, the experimental values of stress intensity factor were not available. But for comparison, SIF values were obtained corresponding to the following empirical relation (Kushvaha et al. 2014).

$$K_I = C_1 * \log(\mathrm{AR}) + C_2 \tag{2}$$

where K_I represents the crack initiation toughness, AR = aspect ratio, and C_1, C_2 are the constants having different values corresponding to different volume fraction.

Figures 5 and 6 show the closeness of predicted and empirically calculated stress intensity factor values. The coefficient of determination for aspect ratio 3.5 and 43 was found to be 0.9864 and 0.9873, respectively. In the following figures, time before zero second indicate the pre-crack initiation regime and at t = 0 s, the crack initiates and afterwards post crack-initiation regime is shown. It is evident from the graph that the stress intensity factor histories follow an increasing trend throughout the fracture event which ultimately results in improved fracture toughness of the resulting composite. Reinforcing the polymer matrix with fibers having higher aspect ratio results in increased energy dissipation by means of undergoing different failure mechanisms viz. matrix cracking, fiber pullout, fiber breakage, and fiber-matrix interphase separation (Greenhalgh 2009; Kushvaha and Sharma 2021).

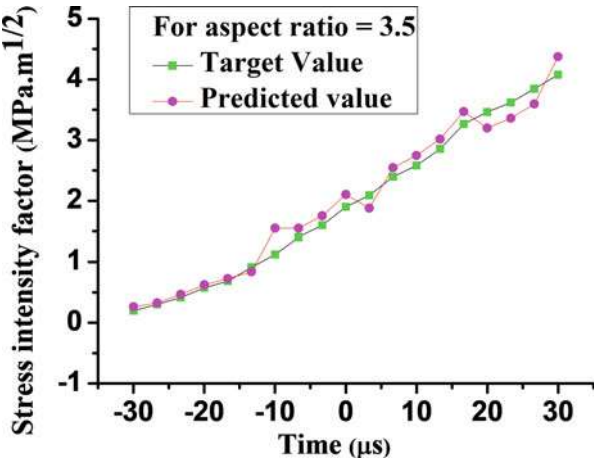

Fig. 5 Goodness of fit for SIF values corresponding to aspect ratio 3.5

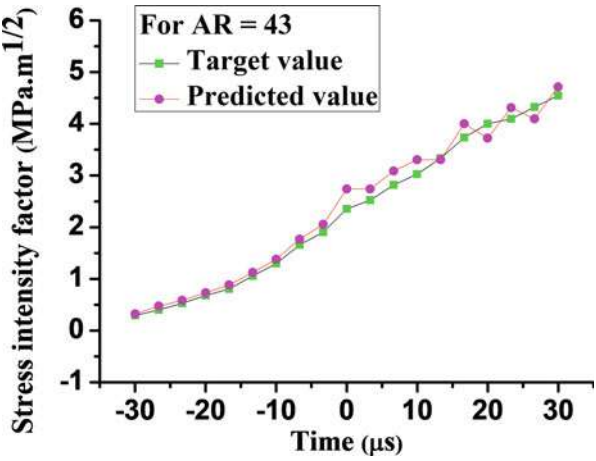

Fig. 6 Goodness of fit for SIF values corresponding to aspect ratio 43

Conclusion

The work presented in this chapter was an attempt to explore the feasibility of using machine learning algorithms in material science. The approach of KNN algorithm was found to be computationally inexpensive, and the key advantage was the accurate prediction of the material's behavior under dynamic loading. The optimized value of K was investigated by performing a sensitivity analysis, and for K = 1, the proposed model was found to be 96% accurate, which proves the efficacy of this model. This algorithm of KNN can be used successfully to predict the dynamic fracture toughness of glass-filled epoxy composites. Moreover, for predicting the wear and fatigue behavior of such composites, the same technique can be adopted.

References

N.A. Abdullah, M. Akbar, N. Wirawan, J.L. Curiel-Sosa, Structural integrity assessment on cracked composites interaction with aeroelastic constraint by means of XFEM. Compos. Struct. **229**, 111414 (2019). https://doi.org/10.1016/j.compstruct.2019.111414

M.R. Ayatollahi, B. Bahrami, A.M. Mirzaei, M. Yazid Yahya, Effects of support friction on mode I stress intensity factor and fracture toughness in SENB testing. Theor. Appl. Fract. Mech. **103**, 102288 (2019). https://doi.org/10.1016/j.tafmec.2019.102288

L. Beretta, A. Santaniello, Nearest neighbor imputation algorithms: A critical evaluation. BMC Med. Inform. Decis. Mak. **16**(3), 74 (2016). https://doi.org/10.1186/s12911-016-0318-z

J.C. Bezdek, S.K. Chuah, D. Leep, Generalized k-nearest neighbor rules. Fuzzy Sets Syst. **18**(3), 237–256 (1986). https://doi.org/10.1016/0165-0114(86)90004-7

K.N. Bharath, P. Madhushri, T.G.Y. Gowda, M.R. Sanjay, V. Kushvaha, S. Siengchin, Alkaline effect on characterization of discarded waste of Moringa oleifera fiber as a potential eco-friendly reinforcement for biocomposites. J. Polym. Environ. (2020). https://doi.org/10.1007/s10924-020-01818-4

G. Biau, L. Devroye, V. Dujmović, A. Krzyżak, An affine invariant k-nearest neighbor regression estimate. J. Multivar. Anal. **112**, 24–34 (2012). https://doi.org/10.1016/j.jmva.2012.05.020

S. Brinckmann, C. Kirchlechner, G. Dehm, Stress intensity factor dependence on anisotropy and geometry during micro-fracture experiments. Scr. Mater. **127**, 76–78 (2017). https://doi.org/10.1016/j.scriptamat.2016.08.027

C.-T. Chen, G.X. Gu, Machine learning for composite materials. MRS Commun. **9**(2), 556–566 (2019). https://doi.org/10.1557/mrc.2019.32

C.-H. Chen, W.-T. Huang, T.-H. Tan, C.-C. Chang, Y.-J. Chang, Using K-nearest neighbor classification to diagnose abnormal lung sounds. Sensors **15**(6), 13132–13158 (2015). https://doi.org/10.3390/s150613132

K. Chomboon, P. Chujai, P. Teerarassamee, K. Kerdprasop, N. Kerdprasop, An empirical study of distance metrics for k-nearest neighbor algorithm, in *International Conference on Industrial Application Engineering*, (2015)

K.-C. Chou, An unprecedented revolution in medicinal chemistry driven by the progress of biological science. Curr. Top. Med. Chem. **17**(21), 2337–2358 (2017). https://doi.org/10.2174/1568026617666170414145508

R. Citarella, F.-G. Buchholz, Comparison of crack growth simulation by DBEM and FEM for SEN-specimens undergoing torsion or bending loading. Eng. Fract. Mech. **75**(3), 489–509 (2008). https://doi.org/10.1016/j.engfracmech.2007.03.039

V. Daghigh, Mechanical and thermal behavior of multiscale bi-nano-composites using experiments and machine learning predictions (2020), https://ir.library.msstate.edu/handle/11668/16954

Ö.F. Ertuğrul, M.E. Tağluk, A novel version of k nearest neighbor: Dependent nearest neighbor. Appl. Soft Comput. **55**, 480–490 (2017). https://doi.org/10.1016/j.asoc.2017.02.020

K. Friedrich, Z. Zhang, A.K. Schlarb, Effects of various fillers on the sliding wear of polymer composites. Compos. Sci. Technol. **65**(15), 2329–2343 (2005). https://doi.org/10.1016/j.compscitech.2005.05.028

K. Fukunaga, L. Hostetler, Optimization of k nearest neighbor density estimates. IEEE Trans. Inf. Theory **19**(3), 320–326 (1973). https://doi.org/10.1109/TIT.1973.1055003

G, Y. G. T., A, V., P, M., Kushvaha, V., R, S. M., Siengchin, S, A new study on flax-basalt-carbon fiber reinforced epoxy/bioepoxy hybrid composites. Polym. Compos. **42**(4), 1891–1900 (2021). https://doi.org/10.1002/pc.25944

N. García-Pedrajas, J.A. Romero del Castillo, G. Cerruela-García, A proposal for local k values for k -nearest neighbor rule. IEEE Trans. Neural Netw. Learn. Syst. **28**(2), 470–475 (2017). https://doi.org/10.1109/TNNLS.2015.2506821

A. Garg, H. Huang, V. Kushvaha, P. Madhushri, V. Kamchoom, I. Wani, N. Koshy, H.-H. Zhu, Mechanism of biochar soil pore–gas–water interaction: Gas properties of biochar-amended sandy soil at different degrees of compaction using KNN modeling. Acta Geophys. **68**(1), 207–217 (2020). https://doi.org/10.1007/s11600-019-00387-y

A. Garg, I. Wani, H. Zhu, V. Kushvaha, Exploring efficiency of biochar in enhancing water retention in soils with varying grain size distributions using ANN technique. Acta Geotech. (2021).

G.L. Golewski, Measurement of fracture mechanics parameters of concrete containing fly ash thanks to use of Digital Image Correlation (DIC) method. Measurement **135**, 96–105 (2019). https://doi.org/10.1016/j.measurement.2018.11.032

E. Greenhalgh, *Failure Analysis and Fractography of Polymer Composites* (Elsevier, 2009)

Z. Hashin, Complex moduli of viscoelastic composites—II. Fiber reinforced materials. Int. J. Solids Struct. **6**(6), 797–807 (1970). https://doi.org/10.1016/0020-7683(70)90018-1

Z. Hashin, Analysis of properties of fiber composites with anisotropic constituents. J. Appl. Mech. **46**(3), 543–550 (1979). https://doi.org/10.1115/1.3424603

M. Heidari-Rarani, M. Sayedain, Finite element modeling strategies for 2D and 3D delamination propagation in composite DCB specimens using VCCT, CZM and XFEM approaches. Theor. Appl. Fract. Mech. **103**, 102246 (2019). https://doi.org/10.1016/j.tafmec.2019.102246

M. Hemath, S. Mavinkere Rangappa, V. Kushvaha, H.N. Dhakal, S. Siengchin, A comprehensive review on mechanical, electromagnetic radiation shielding, and thermal conductivity of fibers/inorganic fillers reinforced hybrid polymer composites. Polym. Compos. (2020). https://doi.org/10.1002/pc.25703

P.G. Ifju, B. Han, Recent applications of Moiré interferometry. Exp. Mech. **50**(8), 1129–1147 (2010). https://doi.org/10.1007/s11340-010-9404-9

S. Kessler, P. Rani, Pattern recognition for damage characterization in composite materials, in *48th AIAA/ASME/ASCE/AHS/ASC Structures, Structural Dynamics, and Materials Conference, Honolulu, Hawaii*, (2007, April 23). https://doi.org/10.2514/6.2007-2411

A. Khan, N. Kim, J.K. Shin, H.S. Kim, B.D. Youn, Damage assessment of smart composite structures via machine learning: A review. JMST Adv. **1**(1), 107–124 (2019). https://doi.org/10.1007/s42791-019-0012-2

E. Koumoulos, G. Konstantopoulos, C. Charitidis, Applying machine learning to nanoindentation data of (nano-) enhanced composites. Fibers **8**(1), 3 (2020). https://doi.org/10.3390/fib8010003

T. Kumar, Solution of linear and non linear regression problem by K nearest neighbour approach: By using three sigma rule. IEEE Int. Conf. Comput. Intell. Comm. Technol. **2015**, 197–201 (2015). https://doi.org/10.1109/CICT.2015.110

M. Kumar, I.V. Singh, B.K. Mishra, S. Ahmad, A.V. Rao, V. Kumar, Mixed mode crack growth in elasto-plastic-creeping solids using XFEM. Eng. Fract. Mech. **199**, 489–517 (2018). https://doi.org/10.1016/j.engfracmech.2018.05.014

V. Kushvaha, Synthesis, processing and dynamic fracture behavior of particulate epoxy composites with conventional and hierarchical micro-/nano-fillers (2016), https://etd.auburn.edu/handle/10415/5468

V. Kushvaha, A. Sharma, Dimensional analysis for predicting the fracture behavior of particulate polymer composite under the effect of impact loading, in *Fracture Failure Analysis of Fiber Reinforced Polymer Matrix Composites*, (Springer Singapore, 2021)

V. Kushvaha, H. Tippur, Effect of filler particle shape on dynamic fracture behavior of glass-filled epoxy, in *Dynamic Behavior of Materials*, ed. by V. Chalivendra, B. Song, D. Casem, vol. 1, (Springer, 2013), pp. 513–522. https://doi.org/10.1007/978-1-4614-4238-7_66

V. Kushvaha, H. Tippur, Effect of filler shape, volume fraction and loading rate on dynamic fracture behavior of glass-filled epoxy. Compos. Part B **64**, 126–137 (2014). https://doi.org/10.1016/j.compositesb.2014.04.016

V. Kushvaha, A. Branch, H. Tippur, Effect of loading rate on dynamic fracture behavior of glass and carbon fiber modified epoxy, in *Dynamic Behavior of Materials*, ed. by B. Song, D. Casem, J. Kimberley, vol. 1, (Springer International Publishing, 2014), pp. 169–176. https://doi.org/10.1007/978-3-319-00771-7_21

V. Kushvaha, S. Anandkumar, P. Madhushri, Dynamic fracture toughness index: A new integrated methodology for mode-I fracture behaviour of polymer composite under impact loading. Mater. Res. Exp. (2019). https://doi.org/10.1088/2053-1591/ab4e35

V. Kushvaha, S.A. Kumar, P. Madhushri, A. Sharma: Artificial neural network technique to predict dynamic fracture of particulate composite. J. Compos. Mater., 0021998320911418 (2020). https://doi.org/10.1177/0021998320911418

T.-T. Le, Prediction of tensile strength of polymer carbon nanotube composites using practical machine learning method. Sage **55**(6), 787–811 (2020). https://doi.org/10.1177/0021998320953540

R. Liu, A. Kumar, Z. Chen, A. Agrawal, V. Sundararaghavan, A. Choudhary, A predictive machine learning approach for microstructure optimization and materials design. Sci. Rep. **5**, 11551 (2015). https://doi.org/10.1038/srep11551

L. Liu, J. Su, X. Liu, R. Chen, K. Huang, R.H. Deng, X. Wang, Toward highly secure yet efficient KNN classification scheme on outsourced cloud data. IEEE Internet Things J. **6**(6), 9841–9852 (2019). https://doi.org/10.1109/JIOT.2019.2932444

M.A. Mahmoud, A. Hosseini, Assessment of stress intensity factor and aspect ratio variability of surface cracks in bending plates. Eng. Fract. Mech. **24**(2), 207–221 (1986). https://doi.org/10.1016/0013-7944(86)90052-4

S. Mallon, B. Koohbor, M.A. Sutton, Fracture behavior of prestressed composites subjected to shock loading: A DIC-based study. Exp. Mech. Int. J. **55**, 211–225 (2014). https://doi.org/10.1007/s11340-014-9936-5

M.A.S. Matos, S.T. Pinho, V.L. Tagarielli, Application of machine learning to predict the multiaxial strain-sensing response of CNT-polymer composites. Carbon **146**, 265–275 (2019). https://doi.org/10.1016/j.carbon.2019.02.001

S.R. McNeill, W.H. Peters, M.A. Sutton, Estimation of stress intensity factor by digital image correlation. Eng. Fract. Mech. **28**(1), 101–112 (1987). https://doi.org/10.1016/0013-7944(87)90124-X

S.-J. Park, M.-H. Kim, J.-R. Lee, S. Choi, Effect of fiber–polymer interactions on fracture toughness behavior of carbon fiber-reinforced epoxy matrix composites. J. Colloid Interface Sci. **228**(2), 287–291 (2000). https://doi.org/10.1006/jcis.2000.6953

M.V. Pathan, S.A. Ponnusami, J. Pathan, R. Pitisongsawat, B. Erice, N. Petrinic, V.L. Tagarielli, Predictions of the mechanical properties of unidirectional fibre composites by supervised machine learning. Sci. Rep. **9**(1), 1–10 (2019). https://doi.org/10.1038/s41598-019-50144-w

E. Patrick, F. Fischer, A generalized k-nearest neighbor rule. Inf. Control. **16**(2), 128–152 (1970). https://doi.org/10.1016/S0019-9958(70)90081-1

G. Pluvinage, Fatigue and fracture emanating from notch; the use of the notch stress intensity factor. Nucl. Eng. Des. **185**(2), 173–184 (1998). https://doi.org/10.1016/S0029-5493(98)00183-6

M.S.S. Prasad, C.S. Venkatesha, T. Jayaraju, Experimental methods of determining fracture toughness of fiber reinforced polymer composites under various loading conditions. J. Miner. Mater. Charact. Eng. **10**(13), 1263 (2011)

W. Qian, H. Zhang, J. Zhu, J. Li, J. Zhang, M. Zhang, Determination of fracture toughness of polymer coating using micro-scale digital image correlation technique. Polym. Test. **93**, 106896 (2021). https://doi.org/10.1016/j.polymertesting.2020.106896

R. Radovitzky, A. Seagraves, M. Tupek, L. Noels, A scalable 3D fracture and fragmentation algorithm based on a hybrid, discontinuous Galerkin, cohesive element method. Comput. Methods Appl. Mech. Eng. **200**(1–4), 326–344 (2011). https://doi.org/10.1016/j.cma.2010.08.014

I.M.A. Rahim, F. Mat, S. Yaacob, Comparison of classifying the material mechanical properties by using k-nearest neighbor and neural network backpropagation. Int. J. Res. Rev. Artif. Intell., 5 (2011)

M. Ramesh, L. Rajeshkumar, C. Deepa, M.T. Selvan, V. Kushvaha, M. Asrofi, Impact of silane treatment on characterization of ipomoea staphylina plant Fiber reinforced epoxy composites. J. Nat.Fibers **0**(0), 1–12 (2021). https://doi.org/10.1080/15440478.2021.1902896

M. Romanowicz, A numerical approach for predicting the failure locus of fiber reinforced composites under combined transverse compression and axial tension. Comput. Mater. Sci. **51**(1), 7–12 (2012). https://doi.org/10.1016/j.commatsci.2011.07.039

A.T. Seyhan, G. Tayfur, M. Karakurt, M. Tanoğlu, Artificial neural network (ANN) prediction of compressive strength of VARTM processed polymer composites. Comput. Mater. Sci. **34**(1), 99–105 (2005). https://doi.org/10.1016/j.commatsci.2004.11.001

K. Shankar, H. Xie, R. Wei, A. Asundi, C.G. Boay, A study on residual stresses in polymer composites using moiré interferometry. Adv. Compos. Mater. **13**(3–4), 237–253 (2004). https://doi.org/10.1163/1568551042580181

A. Sharma, V. Kushvaha, Predictive modelling of fracture behaviour in silica-filled polymer composite subjected to impact with varying loading rates using artificial neural network. Eng. Fract. Mech. **239**, 107328 (2020). https://doi.org/10.1016/j.engfracmech.2020.107328

A. Sharma, S. Anand Kumar, V. Kushvaha, Effect of aspect ratio on dynamic fracture toughness of particulate polymer composite using artificial neural network. Eng. Fract. Mech. **228**, 106907 (2020a). https://doi.org/10.1016/j.engfracmech.2020.106907

A. Sharma, V.C. Khan, G. Balaganesan, V. Kushvaha, Performance of nano-filler reinforced composite overwrap system to repair damaged pipelines subjected to quasi-static and impact loading. J. Fail. Anal. Prev. **20**(6), 2017–2028 (2020b). https://doi.org/10.1007/s11668-020-01013-6

A. Sharma, P. Madhushri, V. Kushvaha, A. Kumar, Prediction of the fracture toughness of silicafilled epoxy composites using k-nearest neighbor (KNN) method, in *2020 International Conference on Computational Performance Evaluation (ComPE)*, (2020c), pp. 194–198. https://doi.org/10.1109/ComPE49325.2020.9200093

A. Sharma, Y. Munde, V. Kushvaha, Representative volume element based micromechanical modelling of rod shaped glass filled epoxy composites. SN Appl. Sci. **3**(2), 232 (2021). https://doi.org/10.1007/s42452-021-04261-9

A. Sharma, T. Mukhopadhyay, M.R. Sanjay, S. Siengchin, V. Kushvaha, Advances in computational intelligence of polymer composite materials: Machine learning assisted modeling, analysis and design. Archives of Computational Methods in Engineering (2021).

D.F. Silva, Computacional (labic, L. D. I.), How k-nearest neighbor parameters affect its performance, in *Simposio Argentino de Inteligencia Artificial (ASAI 2009)*, (2009), pp. 95–106

Y. Song, J. Liang, J. Lu, X. Zhao, An efficient instance selection algorithm for k nearest neighbor regression. Neurocomputing **251**, 26–34 (2017). https://doi.org/10.1016/j.neucom.2017.04.018

A.K. Subramaniyan, C.T. Sun, Toughening polymeric composites using nanoclay: Crack tip scale effects on fracture toughness. Compos. A: Appl. Sci. Manuf. **38**(1), 34–43 (2007). https://doi.org/10.1016/j.compositesa.2006.01.021

Y. Sun, S.-L. Shen, X.-H. Xia, Z.-L. Xu, A numerical approach for predicting shakedown limit in ratcheting behavior of materials. Mater. Des. **47**, 106–114 (2013). https://doi.org/10.1016/j.matdes.2012.12.049

A. Thirumoorthy, T.V. Arjunan, K.L.S. Kumar, Experimental investigation on mechanical properties of reinforced Al6061 composites and its prediction using KNN-ALO algorithms. Int. J. Rapid Manuf. **8**(3), 161 (2019). https://doi.org/10.1504/IJRAPIDM.2019.100498

A. Vinod, T.G. Yashas Gowda, R. Vijay, M.R. Sanjay, M.K. Gupta, M. Jamil, V. Kushvaha, S. Siengchin, Novel Muntingia Calabura bark fiber reinforced green-epoxy composite: A sustainable and green material for cleaner production. J. Clean. Prod. **294**, 126337 (2021). https://doi.org/10.1016/j.jclepro.2021.126337

B. Wan, A. Entezari, Z. Zhang, T. Wilson, N. Yoda, K. Zheng, C. Wu, G. Sun, K. Sasaki, M. Swain, Q. Li, On fatigue failure prediction of prosthetic devices through XFEM analysis. Int. J. Fatigue **147**, 106160 (2021). https://doi.org/10.1016/j.ijfatigue.2021.106160

L.C. Wang, K.T. Tang, S.W. Chiu, S.R. Yang, C.T. Kuo, A bio-inspired two-layer multiple-walled carbon nanotube–polymer composite sensor array and a bio-inspired fast-adaptive readout circuit for a portable electronic nose. Biosens. Bioelectron. **26**(11), 4301–4307 (2011). https://doi.org/10.1016/j.bios.2011.04.015

C. Wang, Y. Long, W. Li, W. Dai, S. Xie, Y. Liu, Y. Zhang, M. Liu, Y. Tian, Q. Li, Y. Duan, Exploratory study on classification of lung cancer subtypes through a combined k-nearest neighbor classifier in breathomics. Sci. Rep. **10**(1), 5880 (2020). https://doi.org/10.1038/s41598-020-62803-4

I. Wani, A. Sharma, V. Kushvaha, P. Madhushri, L. Peng, Effect of pH, volatile content, and pyrolysis conditions on surface area and O/C and H/C ratios of biochar: Towards understanding performance of biochar using simplified approach. J. Hazard. Toxic Radioact. Waste **24**(4), 04020048 (2020). https://doi.org/10.1061/(ASCE)HZ.2153-5515.0000545

I. Wani, H. Kumar, S.M. Rangappa, L. Peng, S. Siengchin, V. Kushvaha, Multiple regression model for predicting cracks in soil amended with pig manure biochar and wood biochar. J. Hazard. Toxic Radioact. Waste **25**(1), 04020061 (2021). https://doi.org/10.1061/(ASCE)HZ.2153-5515.0000561

K.V. Williams, R. Vaziri, Application of a damage mechanics model for predicting the impact response of composite materials. Comput. Struct. **79**(10), 997–1011 (2001). https://doi.org/10.1016/S0045-7949(00)00200-5

Y. Wu, K. Ianakiev, V. Govindaraju, Improved k-nearest neighbor classification. Pattern Recogn. **35**(10), 2311–2318 (2002). https://doi.org/10.1016/S0031-3203(01)00132-7

X.-P. Xu, A. Needleman, F.F. Abraham, Effect of inhomogeneities on dynamic crack growth in an elastic solid. Model. Simul. Mater. Sci. Eng. **5**, 489–516 (1997). https://doi.org/10.1088/0965-0393/5/5/005

M. Zhang, H. Zeng, L. Zhang, G. Lin, R.K.Y. Li, Fracture characteristics of discontinuous carbon fibre-reinforced PPS and PES-C composites. Polym. Polym. Compos. **1**(5), 357–365 (1993)

S. Zhang, X. Li, M. Zong, X. Zhu, D. Cheng, Learning *k* for KNN classification. ACM Trans. Intell. Syst. Technol. **8**(3), 43:1–43:19 (2017). https://doi.org/10.1145/2990508

S. Zhang, X. Li, M. Zong, X. Zhu, R. Wang, Efficient KNN classification with different numbers of nearest neighbors. IEEE Trans. Neural Netw. Learn. Syst. **29**(5), 1774–1785 (2018). https://doi.org/10.1109/TNNLS.2017.2673241

Nondestructive Damage Detection of Epoxy/Synthetic Fiber Braided Composites

5

Xiaoyuan Pei, Wenjin Xing, Gang Ding, and Youhong Tang

Contents

Abstract

In engineering, nondestructive damage detection is a basic but very important technology, able to monitor the health state of composite structures in a noninvasive manner and guide the maintenance process for future service. This chapter introduces two nondestructive damage detection methods, established respectively on acoustic emission and vibration. Their basic principles of damage detection are described, as well as details of experimental testing, detection algorithms, and numerical analyses. The primary difference between two methods is that the acoustic emission-based method is a local detection

X. Pei
School of Textiles Science and Engineering, Tiangong University, Tianjin, China

Composites Research Institute, Tiangong University, Tianjin, China

W. Xing · Y. Tang (✉)
Institute for NanoScale Science and Technology, College of Science and Engineering, Flinders University, Adelaide, SA, Australia
e-mail: youhong.tang@flinders.edu.au

G. Ding
Department of Science and Technology, Tianjin Open University, Tianjin, China

S. Mavinkere Rangappa et al. (eds.), *Handbook of Epoxy/Fiber Composites*,
https://doi.org/10.1007/978-981-19-3603-6_7

method, while the other is a global method. However, both methods are demonstrated to be capable to detect and locate damage in epoxy resin/carbon fiber-braided composite structures, showing great promise in practical applications. The future development trend for nondestructive damage detection is discussed in the end.

Keywords

NDT · 3D braided composites · Damage and failure · Acoustic emission · Modal analysis · Signal processing

Introduction

Due to their appealing attributes including light weight, high strength, high modulus, and long lifespan, composite materials are commonly used in aerospace industry. While ensuring the sufficient load-bearing capability, the outstanding strength-to-weight ratio of composite materials helps largely reduce the weight of components and structures and consequently markedly improve the delivery efficiency of aircrafts (Huda and Edi 2013). In the early 1940s, the appearance of glass fiber-reinforced composites marked the beginning of modern composite industry. In the following decades, epoxy/carbon fiber composites gained increased interest in studies and applications, accompanying the continuing development of materials science and technology (Masuelli 2013). According to the different processing techniques of reinforcing fibers, basically epoxy resin/synthetic fiber composites can be categorized into braided, woven, knitted, and stitched composites (Ge et al. 2020; Yan et al. 2018; Pei et al. 2016b; Velmurugan and Solaimurugan 2007). Among them, engineers and researchers are highly concerned by the three-dimensional (3D) braided epoxy/carbon fiber composites. Since their reinforcing fibers form a three-dimensional layout in spatial multidirectional distribution, 3D braided epoxy/carbon fiber composites display much improved both strength and impact damage resistance in the thickness direction, compared to those of other composite classes (Gu et al. 2019).

In the processes of manufacturing, assembly, and service, the epoxy/synthetic fiber composites inevitably develop invisible internal defects or damage. When being very small, the defects typically do not greatly degenerate the mechanical performance of composite structures; however, they pose a potential threat to the structural integrity. If the defects were not detected early, the service life of composite structures would be limited by continuing damage progression up to the formation of an obvious crack. In the worst situations, sudden disasters occur without any indicating signs. Therefore, considering the safe operation of aircrafts, the effective detection and identification of defects or damage are essential for composites, especially those that function as main load-bearing structures.

Common Damage Forms in Epoxy/Synthetic Fiber Composites

The microstructure of composites is a complex multiphase system. Due to pervasive uncertainties and long-term use, the occurrence of defects is unavoidable during the manufacturing, assembly, and service stages of components (Mesogitis et al. 2014). A specific example is that significant randomness in the product quality can be attributed to imprecisely controlled human factors that bring about small defects during manufacturing and assembly. Conversely, in the cycles of service, the composite materials are affected in terms of developing defects by the surrounding environment. For example, rain and sand erosion and lightning may lead to irregular pits on the surface or internal damage. Additionally, severe damage occurs due to the impact on the surface from foreign objects with large kinetic energy, such as birds and runway stones. The generated defects and damage usually manifest as fiber fracture, matrix-fiber debonding, delamination, and other forms in the interior of the composite material. These distinct damage forms decrease the load-carrying capacity of the component and structure and are the major factors that are responsible for engineering accidents (Lemaitre 2012). According to the previous scientific research and engineering practice, the common damage forms in composite materials are pores, delamination, inclusions, fiber buckling, and uneven resin distribution (poor or rich). Other forms include cracks, poor interfaces between fibers and matrix, errors in fiber alignment, gaps and overlaps during layup, and so on. A few typical damage forms and their potential causes and effects are listed in Table 1.

Table 1 Different common damage forms in epoxy/synthetic fiber composites

Damage	Causes	Harmful consequences
Pores	The infiltration of resin and fiber is poor, and the air is difficult to squeeze out; during manufacturing, the solvent used for diluting the resin and the small molecules in the resin is volatilized	The bending, compression, fatigue, interlaminar shear, and fracture toughness properties are adversely influenced (Dong and Huo 2016)
Delamination	The thermal expansion coefficients of matrix, fiber, and mold are not matched; the interfacial bonding strength is very low; and the curing temperature of resin is limited	The delamination reduces the compressive strength and rigidity of the material and affects the integrity of the structure. Under mechanical or thermal load, the delamination in the structure may lead to the fracture (Zhang et al. 2018)
Fiber buckling	The coefficients of thermal expansion of fiber and matrix are inconsistent	Fiber buckling has a great influence on the tensile and compressive properties (Zhao et al. 2017)
Rich/poor resin	The resin content in the composite is higher or lower than the specified value	The mechanical properties in rich (poor) resin areas are reduced to a certain extent (Al-Shawk et al. 2018)

Recent Progress in NDT for Epoxy/Synthetic Fiber Composites

In most situations, it is essential to quantify the mechanical properties of composite materials. General static testing usually needs to in damage or even break tested components and structures to obtain desired measurements, seriously confining its application scope. To inspect defects or damage in composites, engineers are increasingly concerned by nondestructive testing (NDT) without any negative interference. As a safe and reliable noninvasive testing technology, NDT can locate defects and determine the characteristics of the defects such as size, shape, and orientation. NDT is surrounded by imaging technology, automation technology, and computer data processing and analysis and calls for material mechanics, fracture mechanics, and other disciplines, to make a comprehensive and accurate evaluation of the performance of the test pieces and products. The commonly adopted NDT techniques for composite materials consist of ray testing, ultrasonic testing, acoustic emission testing, etc. Critical comparisons among different NDT techniques can be found in comprehensive reviews (Gholizadeh 2016; Dwivedi et al. 2018).

One family of the primary NDT methods for composites is to detect damage at local regions of the structure. Examples include digital image correlation, acoustic emission, and ultrasonic testing (Caminero et al. 2013; Bashkov et al. 2017; Duan et al. 2019). Among them, acoustic emission provides real-time detection. It has been shown that this method is able to predict damage and fracture earlier than some other NDT methods such as ultrasonic testing (Zhang et al. 2020). Many functional acoustic emission signals are generated during the loading process of composites, owing to fiber fracture, fiber-matrix interfacial debonding, matrix cracking, and delamination. The extent and sequence of the different failure modes are necessary factors to evaluate the current health state and estimate the remaining service life for composite structures.

Another effective yet global NDT method is built upon vibration mode identification. The underlying principle for this global method is that some physical parameters (e.g., mass, stiffness, and damping) of the structure are sensitive to the accumulated internal damage, resulting in a varied dynamic response, in which the frequency response function and modal parameters differ from those in the initial and previous states of structures (Hammami et al. 2015; Katunin and Wronkowicz 2015). Damage location and severity in the degraded structure can be determined based on the changes in vibration features, thus informing the health state of the current structure. Compared with local NDT methods, this method can be used for the whole structure, attaining the overall health state, which brings about an expanded application scope, such as large and complex structures (Gibson 2000; Pei et al. 2016a).

Characteristics of 3D Braided Epoxy/Carbon Fiber Composites

Compared with laminated architectures, the reinforcement in 3D braided composites is characterized by a spatial network structure of multidirectional yarns with high

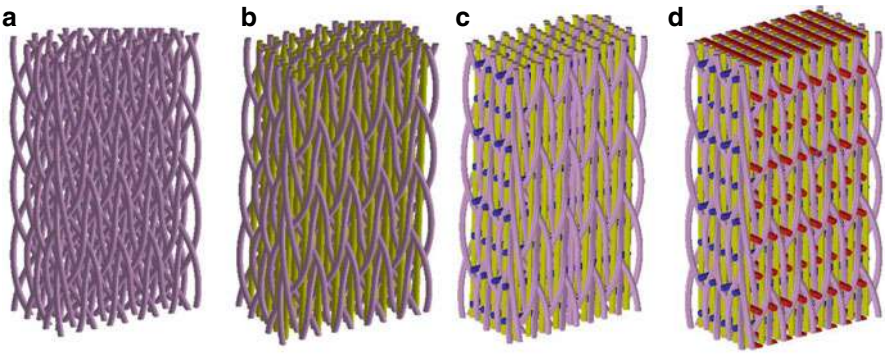

Fig. 1 3D braided composite reinforcements with different braided structures: (**a**) 3D four-direction, (**b**) 3D five-direction, (**c**) 3D six-direction, and (**d**) 3D seven-direction

integrity. The special yarn arrangement overcomes the disadvantage of poor interlaminar properties in laminated composites. 3D braided composites not only maintain the conventional advantages of light weight, high specific strength, and high specific modulus but also offer exceptional shear resistance and impact damage resistance. Moreover, 3D braiding technology supports preforms of complex shapes and different sizes, enabling the integrated design and manufacturing of composite components with net sizes. Since this type of reinforcement does not involve cutting and laminating, the damage to the fibers is minimized. The combination of 3D braided composites and resin transfer molding (RTM) technology simplifies the manufacturing of composite materials, thereby reducing potential environmental pollution and production cost (Laurenzi and Marchetti 2012).

The design space for 3D braided composite preforms is widely spanned (Fig. 1), making their composites ideal candidates as structural materials for high-performance main load-bearing members in aerospace. For example, 3D braided composites have been applied with great success in civil aircraft engines (El Mourid et al. 2015). Therefore, an in-depth understanding of the complicated damage modes and damage evolution process of 3D braided composites is fundamental to help develop reasonable strength and fracture criteria and to guide structural designs in aerospace industry. Moreover, this understanding can be enhanced by means of NDT technology.

Acoustic Emission and Vibration-Based NDT

In view of the anisotropic characteristics of 3D braided epoxy/synthetic fiber composites, two methods for detecting the damage of 3D braided composites will be described according to our previous work (Ding et al. 2019; Pei et al. 2016a). The first method (section "AE-Based Damage Detection") merges the acoustic emission (AE) technique and the improved Hilbert-Huang transform (HHT) analysis tool. The

HHT method is used to process the collected signals and help distinguish the damage modes as damage evolves. The damage sources in 3D braided composites are located by improving the four-point circular arc location method and the probabilistic neural network (PNN).

As a vibration-based technique, the second method (section "Vibration-Based Damage Detection") aims to study the effects of damage on the modal properties of 3D four-direction braided composite T-beams by means of experimental modal and finite element (FE) analyses. The experimental results show that the damage would affect the vibration mode of T-beam. The damage sensitivity of the mode shape curvatures of the T-beam provides an effective tool to identify and localize damage. The FE modeling of the damaged T-beam shows that the natural frequency of the damaged T-beam is more affected than the corresponding vibration mode when the damage exists. The results of experimental measurements and numerical analyses suggest that both AE and vibration-based techniques show considerable promise in detecting and characterizing damage in 3D braided composites in an effective and robust manner.

Materials and Structures

In both detection methods, carbon fiber braided composites are fabricated by a four-step 1 × 1 3D four-direction braiding process. The braided yarns of specimens are made of T700-12 k carbon fiber the density of carbon fiber is 1.76 g/cm^3. TDE86 epoxy resin is used to cure 3D braided preform by RTM process to prepare the composite. For the first detection, the technological parameters of the yarns are given as follows: the inner braiding angle is 32.1°, the fiber volume content is 45.0%, and the dimensions are 250 × 25 × 4 mm^3. Rectangular-shaped specimens are objects under detection. For the second detection, the braiding angle of the T-beam preforms is 30°, and the fiber volume fraction is 55%. The density of the T-beam is 1.58 g/cm^3. In Table 2, the properties of carbon fiber and epoxy resin matrix are listed. The geometry of the T-beam is displayed in Fig. 2.

AE-Based Damage Detection

After the propagation velocity of sound wave in solid medium is determined, traditional AE source location method is used to determine the location of AE source according to the arrival time interval of acoustic waves. However, the carbon fiber

Table 2 Properties of carbon fiber and epoxy of 3D braided composite T-beam

Material	E_{11}/GPa	E_{22}/GP)	G_{12}/GP)	G_{23}/GPa	μ_{12}
Carbon fiber T700	230.0	40.0	24.0	14.3	0.26
Epoxy	4.5	–	–	–	0.3

Reprinted with permission from (Pei et al. 2016a), © 2016, Elsevier

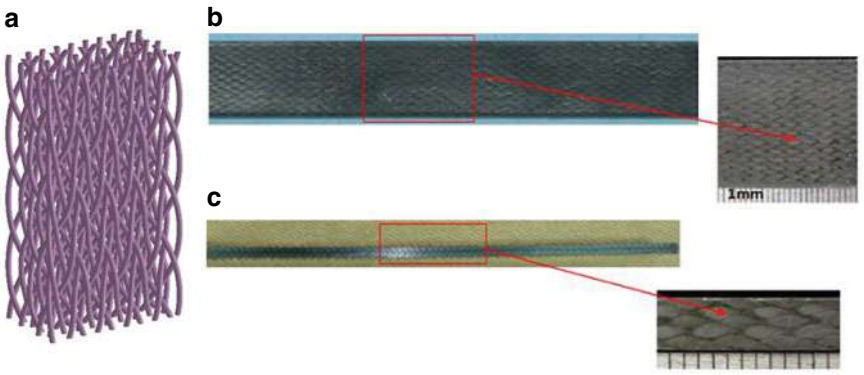

Fig. 2 Geometry of the T-beam: (**a**) Cross-section, (**b**) Isometric view. All dimensions are in mm. (Reprinted with permission from (Pei et al. 2016a), © 2016, Elsevier)

braided composites exhibit anisotropic properties since the reinforcing fibers constitute a spatial interweaving structure. The anisotropy complicates the identification process of the source location (Yamada et al. 2000; Ciampa and Meo 2010). Sound wave velocity may be affected by many factors, including material characteristics, specimen thickness, propagation angle, local damage, and environmental conditions. The results of the location of the source of damage will be disturbed by the change of acoustic velocity. To reduce the location error of the damage source, when the braided composites are tensile damaged, the time-frequency relationship of AE signal is compensated. At the first step, the damage in braided composites is identified in location. Next, the key parameters of PNN are optimized by chaos algorithm and fish swarm algorithm. The purpose is to improve the recognition accuracy of Drosophila algorithm, which can be applied to accurately locate the damage source of braided composites.

Testing System

A lead core with a diameter of 0.5 mm was used to simulate the AE source. The standard lead breaking test is used to determine the acoustic velocity. AE detection system (SAEU2S Acoustic Emission Signal Acquisition System) is used to obtain the information from the internal damage of braided composites during tensile testing. According to the requirements of the experimental device and conditions, the tensile test is carried out. Figure 3 shows the schematic illustration of the AE-based damage detection platform for the 3D braided composites.

AE Energy Evolution During Tension

The tensile load-AE energy-displacement curve of braided composite specimens during tensile testing is obtained. As an important acoustic signal, the evolution of AE energy during the specimen stretching is shown in Fig. 4, including the load-displacement curve.

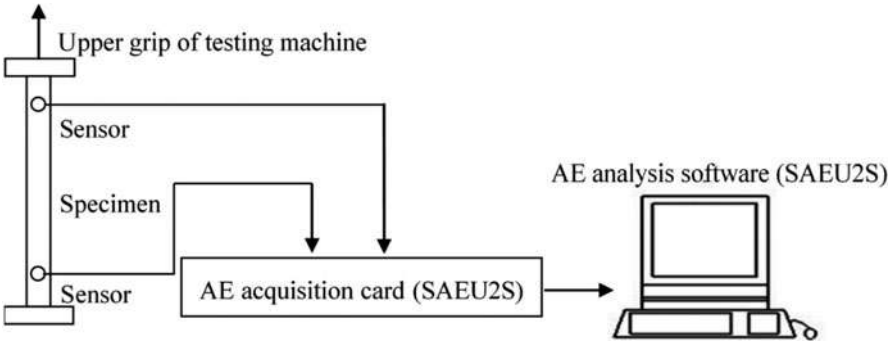

Fig. 3 The schematic illustration of the AE-based damage detection platform for the 3D braided composites (Ding et al. 2019)

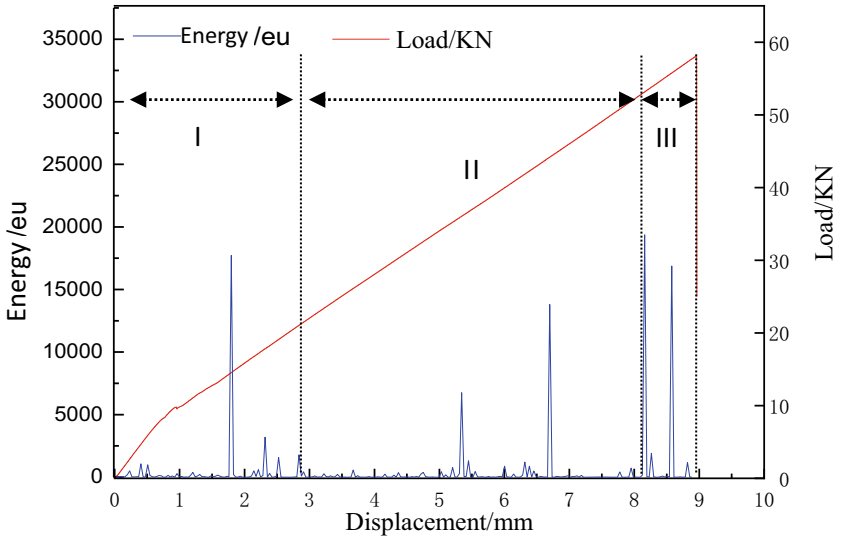

Fig. 4 AE energy and load as a function of displacement for a typical fiber braided composite structure under tension. (Reproduced with permission (Ding et al. 2019))

The red curve in Fig. 4 shows the relationship between the load and displacement during the tensile process of the composite. In the tensile process, the mechanical property curves of the specimens show good linear characteristics. With the increase of load, the damage and failure of braided composites are accumulated in the tensile process. The matrix cracks along the fiber direction are caused by impurities and holes in the specimens. With the tensile process going on, the influence of these internal micro defects on the specimen gradually decreases. The energy-displacement curve (blue) in Fig. 4 indicates that the damage extent of the specimen accumulates as the tensile load increases. The energy parameter variation can be clearly distinguished in the tensile process of the specimen. There are several

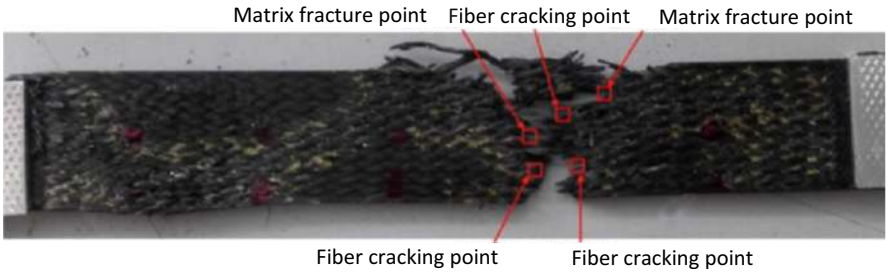

Fig. 5 Final fracture profile after tensile testing of a 3D braided composite specimen. The progressive failure process can be evaluated by using AE-based NDT. (Reproduced with permission (Ding et al. 2019))

abruptly varying points, indicating that energy is intensively released after a long period of accumulation. These intensive release moments correspond to the transition states of the specimen, experiencing significant changes.

In Fig. 4, according to the load and energy versus displacement curves, in the initial stage of tensile loading, the damage of braided composites is small, and the relative energy level is low. With the increase of load, the specimen appears to have a certain damage, and the relative energy increases gradually. As the load increases, the damage continues to accumulate. At about 8.2 mm, the relative energy increases sharply. At this time, the load is close to 52 kN, the damage propagation is intensified, and the specimen is about to fail. This indicates that a small amount of damage occurs in the initial stage of loading. Within this period, new micro defects start initiating at different spots, and initially present defects experience little progression. In the stage of microcrack propagation, the AE energy fluctuates only slightly. This indicates that the damage development in the specimen is progressive. The typical final fracture profile is displayed in Fig. 5. The obvious fiber fracture can be seen from Fig. 5. The reason may be that with the increase of load, the matrix cracks along the fiber direction, and the fiber pullout and fracture phenomenon will occur after the damage intensifies, which eventually leads to the fracture failure of the specimen.

HHT Analysis of AE Signal

At different damage stages, the specimens produce different AE signals. These AE signals are often superimposed together and present random and nonstationary distribution, which makes it difficult to identify AE signals (Aggelis et al. 2012). This brings difficulties to the recognition of AE signals. HHT is suitable for analyzing nonlinear and nonstationary AE signals (Hamdi et al. 2013). Herein, the adopted HHT consists of empirical mode decomposition (EMD) and Hilbert transform (Vazirizade et al. 2019). Herein, the adopted HHT consists of empirical mode decomposition (EMD) and Hilbert transform (Vazirizade et al. 2019). The EMD extracts individual signal modes of oscillation from a time series, presenting frequency-time distribution after preforming Hilbert transform. The HHT spectrum of the AE signal for the carbon fiber braided composite specimen under tension is shown in Fig. 6.

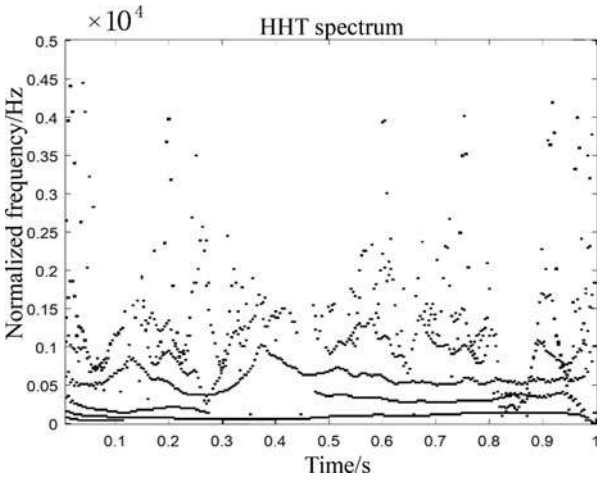

Fig. 6 HHT of the AE signal for the fiber braided composite specimen under tension. (Reproduced with permission (Ding et al. 2019))

In Fig. 6, the frequency of the AE signal mainly concentrates below 5 kHz. With time, the change in frequency shows oscillations. It can be seen from Fig. 6 that the energy spectrum of AE signal at the measuring point changes after the structure is damaged. In the tensile test of braided composites, the change of AE signal energy can be obtained by comparing the AE signal energy of the specimens, which can realize the preliminary judgment of different damage degrees of the specimens. In view of the noticeable variation in the AE signal, the progressive evolution of tensile failure can be identified.

Initial Locating by Four-Point Circular Arc Method

Four-point arc location method is a mature method in AE location technology, which is widely used in the research of structural damage location. The basic idea of this method is to determine the location of the damage by geometric method according to the different time of the sound wave arriving at each sensor. X, Y coordinates are used in the structure. Four piezoelectric elements are embedded in pairs of four points that are (x_1, y_1), (x_2, y_2), (x_3, y_3), (x_4, y_4), to form a rectangular plane detection area. It is assumed that the crack location is A (x, y), which is the acoustic emission source. The time for the sound wave to reach the piezoelectric element 1 is t_1, and the propagation time to piezoelectric elements 2, 3, and 4 is $(t_1 + \Delta t_2')$, $(t_1 + \Delta t_3')$, $(t_1 + \Delta t_4')$, respectively. For isotropic materials, the speed of sound propagation is equal. However, in the braided composites, the carbon fibers are distributed in a spatial network, and the sound velocity varies greatly in the structure. It is necessary to modify the acoustic velocity to reduce the damage location error caused by acoustic velocity difference (Mei et al. 2018). Taking the origin as the AE source, the time of sound wave arriving at a sensor is calculated by the lead breaking experiment.

According to the principle of sound wave propagation, the damage can be regarded as a secondary wave source in the process of signal propagation, which meets the requirements of damage location model in acoustic emission technology. The actual location of AE source is compared with the calculated location of four-point circular arc location. The results show that the four-point circular arc location method can be used to simply locate the damage location. However, because it cannot give the detailed characteristics of damage, such as size, damage degree, etc., it can only be used in the situation of low monitoring requirements. Moreover, the calculation error increases with the position close to the boundary of the specimen. The larger error may be due to the anisotropy of the spatial structure of carbon fiber braided composites or the attenuation of wave velocity. Therefore, it is necessary to improve the location accuracy of AE sources for carbon fiber braided composites by theoretical methods.

Accurate Location of Damage Sources

With the help of chaos search algorithm and crowding degree in fish swarm algorithm, the Drosophila algorithm can be optimized, which can not only determine the damage location of braided composites but also characterize the geometric characteristics and degree of damage to a certain extent. In the probabilistic neural network (PNN) calculation, the optimized Drosophila algorithm overcomes the shortcomings of the traditional Drosophila optimization algorithm in random search efficiency and poor convergence of the calculation results. It can effectively improve the global optimization performance of the algorithm to accurately locate the damage location.

Considering the characteristics of acoustic emission source, signal propagation path, environmental noise, measurement system, and other factors, the influence on the output waveform of braided composite AE signal is complex. Therefore, the improved Drosophila algorithm is used to optimize the PNN algorithm, and the coordinates calculated by the first four points arc positioning method are used as the initial positioning coordinates for damage detection and positioning, to improve the convergence speed and positioning accuracy of the algorithm.

The choice of smoothing coefficient directly affects the accuracy and convergence of the PNN. The selection of smoothing coefficient directly affects the accuracy and convergence of PNN, which determines the accuracy of prediction information. The improved Drosophila optimization algorithm has good global optimization performance. It can optimize the smoothing coefficient of PNN and improve the accuracy and convergence of probabilistic neural network (Ding et al. 2019). The procedure for accurate locating of damage sources based on the improved Drosophila optimization algorithm is outlined below, consisting of the following two major steps.

Construction of Optimal Function

As mentioned previously, selecting appropriate smoothing coefficients is important to enhance the PNN's capability to classify samples correctly. Therefore, the fitness function (optimization function) f_{fit} of PNN smoothing coefficient can be solved by optimization algorithm, which can be defined as:

$$f_{fit} = (\sigma_1, \sigma_2, \cdots, \sigma_s) = \frac{n_{coor}}{n_{not}} \tag{1}$$

where n_{coor} and n_{not} are correctly predicted sample and total sample numbers, respectively. Known samples are split into training and test sets. The training set is only used to construct the structure of PNN, not to optimize its smooth coefficients. The test set aims at optimization and evaluation for PNN.

Coefficient Optimization of PNN

The improved Drosophila optimization algorithm is used to optimize the PNN:

Step 1: Construct PNN according to the specific problem and number of known samples. If the number of modes is s, the parameters to be optimized for PNN are denoted as σ_1, σ_2, $\cdots$, σ_s. Smoothing coefficients (optimization parameters) are initialized in the definition domain.

Step 2: According to the complexity of PNN, in the process of optimization, chaos optimization parameters are introduced to update the position of Drosophila group and optimize the global search ability.

Step 3: Logistic map is chosen as the generation mechanism of chaotic sequence. The position of Drosophila population was updated and then iterated. The 2000 iterations were carried out to eliminate the effect of initial value selection on the optimization results.

Step 4: The distance between the Drosophila and the origin was estimated, and the taste concentration judgment value was calculated.

Step 5: The taste judgment value is substituted into the concentration judgment function.

Step 6: Drosophila individual concentration values are calculated: The concentration of Drosophila melanogaster is calculated by calculating the fitness function.

Step 7: In this Drosophila population, Drosophila individuals with the best taste concentration (fitness) were found.

Step 8: According to the best position of Drosophila, all Drosophila fly to the best position by using their vision.

Step 9: Conduct iterations until termination: Steps 4–8 are repeated until either the specified number of iterations or convergence is reached.

Through the location test of the damage source, the results show that the improved Drosophila algorithm based on chaos search algorithm and fish swarm algorithm has better optimization performance. Compared with the basic Drosophila algorithm, the positioning accuracy of the optimized algorithm has been greatly improved with an error of $\pm 1\%$. This comparison suggests that the two-step method has an important modification in locating accuracy by means of PNN and the modified Drosophila optimization algorithm, in contrast to the combination of PNN and the traditional Drosophila optimization algorithm.

Vibration-Based Damage Detection

T-beams are extensively used as structural elements in engineering structures. Compared to metal T-beams, composite T-beams are superior owing to their lower density, higher specific intensity, and higher modulus of the constituting material. Thereby, composite T-beams are often considered in aircraft, airfoil, and joints to achieve the conflicting goals of both the extensive weight saving and the satisfactory load-carrying capability. Furthermore, 3D braided composite T-beams have been widely recognized as ideal structural elements in the aerospace. However, the composite T-beam structure is prone to damage due to the external load, temperature and humidity, and other environmental factors, which leads to the reduction of the bearing capacity of the structure. Therefore, it is of great safety significance to identify the damage state of composite structures in time and effectively to prevent the occurrence of structural destructive damage accidents.

Investigation has been developed to forecast unknown damage using the vibration method. For example, Lou et al. (2014) researched the effects of local damage on the natural frequencies and the corresponding vibration modes of composite pyramidal truss core sandwich structures by means of vibration modal test. Their results indicate that the damage will reduce the stiffness of the composite material and affect the modal parameters of composite materials. To study the damage effect, the damage is simulated by the reserved hole in 3D braided composite T-beams. The modal parameters (namely, modal frequency, mode shape, and modal curvature) of 3D braided composite T-beam with and without holes are evaluated by experiment and numerical calculation.

Testing System

Experimental vibration modal analyses are conducted to implement nondestructive damage detection based on vibration. Along the length direction, the reinforcing and web of the composite are divided into ten equal parts. In the vibration modal experiment, the T-beam is given to the same boundary conditions as the cantilever beam. Under the boundary condition of cantilever beam, the right end of the T-beam is fixed, and the left end is free. Starting from the fixed end, the reinforcing plate of T-beam is divided into ten equal parts with a spacing of 30 mm, and the equal points are marked. Similarly, the web plate of T-beams is equally divided into ten parts with a spacing of 30 mm, and marks are made at the equidistant points. At the marked points, the T-beam is excited to vibrate freely. The acceleration sensor is fixed to the central axis of the reinforcing plate, which is located at a half distance from the fixed end. For each measurement, ten trials are repeated to obtain the average and standard deviation.

The modal parameters of T-beam are measured using the force hammer excitation method. The experimental setup and procedure are shown in Fig. 7. The piezoelectric acceleration sensor (LC0408T) is used in the experiment to receive the response. The acceleration sensor relates to ws-5921 network data collector through ws-2401

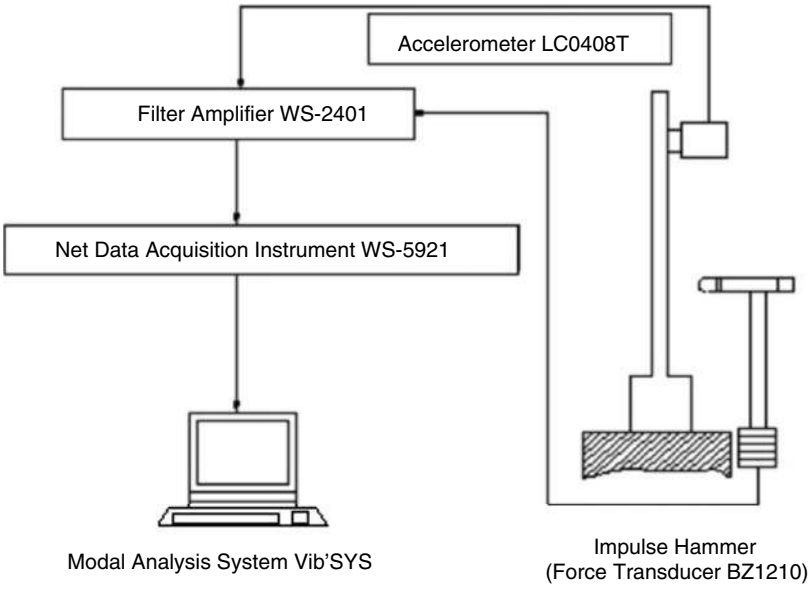

Fig. 7 Diagram of modal testing system for 3D braided composite T-beams. (Reprinted with permission from (Pei et al. 2016a), © 2016, Elsevier)

filter amplifier. The measuring points on the T-beam fixed at the right end are knocked one by one with a force hammer. The piezoelectric sensor (BZ1201) on the hammer collects the excitation signal as a function of time. Finally, the modal parameters (frequency response function, natural frequency, mode shape) of the system can be obtained by Fourier transform analysis of the attenuation time-domain response curves with modal analysis software (Vib'SYS modal analysis system). The damage location is mainly determined by consulting many statistical data about the damage location of 3D braided composite T-beam in practical application. Therefore, holes of different sizes are machined on the original beam. The holes, labeled as A, B, and C, are located on the reinforcing plate, whereas those holes, labeled as D, E, and F are located on the web plate. The depth of each hole is 4.5 mm.

Damage Influence on Braided Composite T-Beam

The frequency/response spectra are measured experimentally using the test setup. Along the length of the T-beam, the frequency response spectra of the original T-beam and the damaged T-beam at different locations and with different diameters are shown in Fig. 8.

As can be seen from Fig. 8, in the measurement frequency range of 0–2500 Hz. The frequency function curves of pristine T-beam and damaged T-beam will produce a resonance peak at a specific frequency. The change trend of the frequency function curve is consistent, and the position of the resonance peak is close. By comparing the frequency response curves of the T-beams at the same location, it is found that the

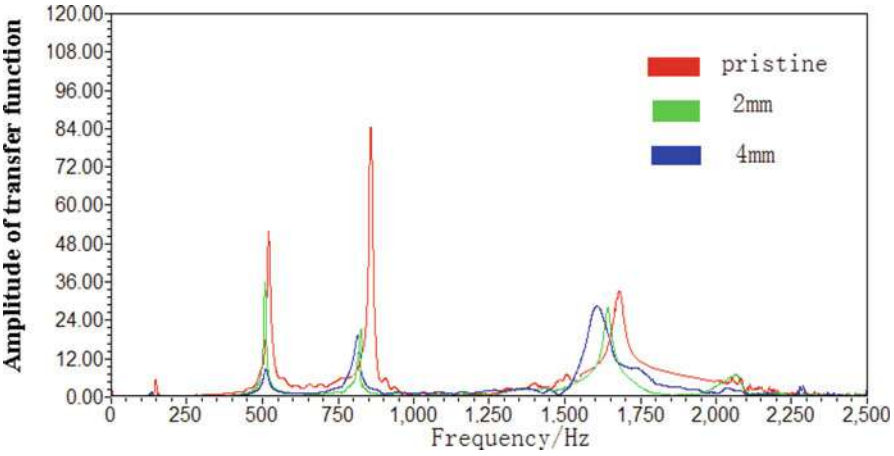

Fig. 8 Frequency response spectra of pristine and damaged T-beams. (Reprinted with permission from (Pei et al. 2016a), © 2016, Elsevier)

resonance frequency decreases as the damage area increases. Despite small differences in the frequency response spectra, these data do not appreciate the presence of holes in damaged T-beams statistically. According to the above analysis, it is not reliable to detect the damage of T-beam simply by changing the frequency response spectrum.

To further analyze the influence of damage on the time domain response curve of T-beam, the time domain response curves of undamaged and damaged T-beams are compared. When the hole diameters are 2 mm and 4 mm, there is no significant difference in the attenuation rate. So, it is not reliable to detect the damage of T-beam simply by changing the frequency response spectrum. The pristine and damaged T-beams all attenuate to zero at almost the same rate with increasing time. After expanding the hole diameter to 6 mm, the damaged T-beam seems to attenuate a little faster than the pristine T-beam. However, such an effect is insignificant to perceive easily. More importantly, the location and extent of damage cannot be exactly determined. According to the above analysis, it is not reliable to detect the damage of T-beam simply by changing the frequency response spectrum.

To identify the vibration mode of the structure through the experimental modal analysis, it is necessary to obtain the high-precision frequency response function first. On this basis, the frequency response function is further processed to identify the mode shapes of the structure. Based on the single-mode parameter identification method, the peak value of the resonance peak of the frequency response function is picked up, and then the displacement mode and curvature mode are further constructed.

Figure 9 showed the displacement mode shapes corresponding to the first four natural frequencies of the undamaged T-beam, corresponding to the natural frequencies of 171.55 Hz, 579.73 Hz, 955.92 Hz, and 1763.08 Hz, wherein the displacement modes corresponding to the first, second, and third natural frequencies are bending

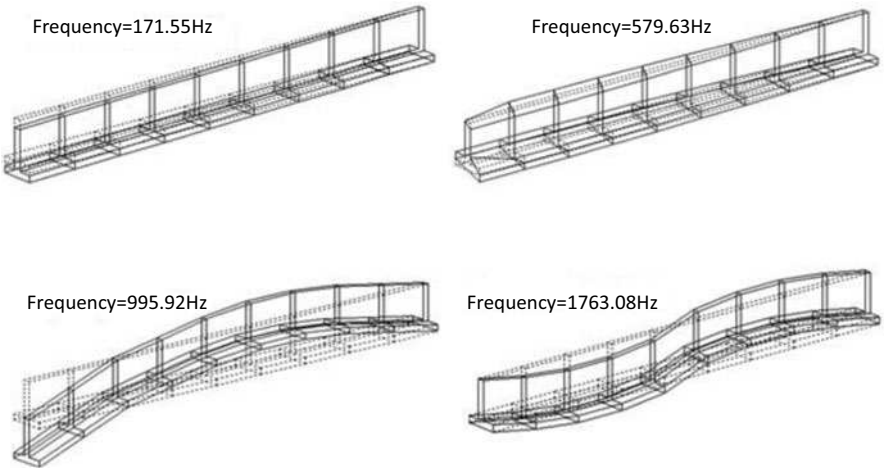

Fig. 9 The first four mode shapes of the pristine T-beam. (Reprinted with permission from (Pei et al. 2016a), © 2016, Elsevier)

modes. This showed that three of the first four mode shapes of the T-beam are bending dominant.

The vibration modes of the original T-beam and the damaged T-beam are compared. It is found that the size of the hole diameter and the location of damage have little influence on the first two mode shapes. Figure 10 compared and analyzed the third and fourth order displacement mode shapes of T-shaped beams with different damage degrees at points A and E. Comparing the third and fourth mode shapes of the pristine and the damaged T-beam, it is found that the damaged T-beam has obvious changes. At the damage location, the shape of the mode has continuous knuckle and displacement. When the hole diameter is relatively small, the displacement and knuckle are very small. However, as the hole diameter increases, the mode amplitude varies more significantly, and the knuckle becomes more acute at the damage location. It can be summarized that the change in local stiffness induced by damage only has a perceptible influence on the high-order mode shapes of the structure. However, the changes in mode shapes of the low-order frequencies of the damaged T-beam are negligible. Damage in the T-beam structure could not be determined using the mode shapes of the low-order frequencies, due to their poor sensitivity to existing damage.

As the displacement mode shape is not a very sensitive parameter to structural defects, to further understand the influence of subtle damage changes on its vibration characteristics, the mode curvature of T-beam has been studied. According to the mechanics of materials, the deformation formula of T-beam in bending is as follows:

$$\frac{1}{r} = \frac{M}{EI} \tag{2}$$

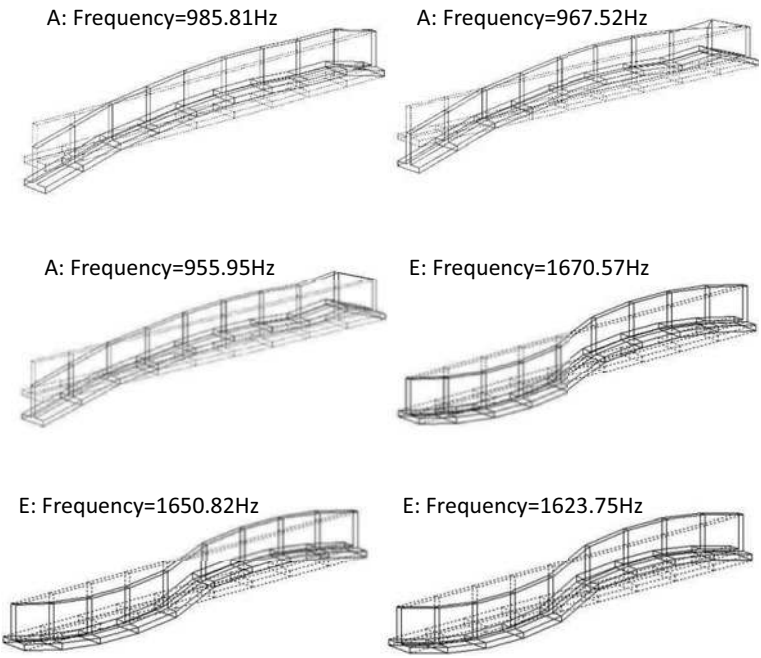

Fig. 10 The first four mode shapes of the pristine T-beam. (Reprinted with permission from (Pei et al. 2016a), © 2016, Elsevier)

In the formula, r is the curvature radius of the T-beam, the curvature is expressed by 1/r, the bending moment is expressed by M, and the flexural rigidity is expressed by EI. In the case of bending, the curvature of the T-beam is expressed as

$$\frac{1}{r} = \frac{u''}{\left(1 + u_y'\right)^{\frac{3}{2}}} \approx u_y'' \tag{3}$$

where u_y is the along the y-directional displacement of the T-beam bending deflection. If the structure is damaged, the local damage leads to a reduce in bending stiffness *EI*, and the curvature near the local damage region is then increased, as indicated by Eq. 2. Eq. 3 indicates that the mode shape curvature is the quadratic differential of the mode shape. Thus, the sensitivity to the change in displacements in the T-beam becomes amplified using the mode shape curvature. In this way, damage locations can be easily identified using the mode shape curvature rather than mode shapes. In practice, the mode shape curvature of a structure cannot be experimentally measured in a direct manner, but it can be calculated by means of numerical methods for differential equations. Applying the central difference approximation, the second-order derivative u_y'' can be approximated as

$$u_y'' \approx \frac{u_y^{n+1} - 2u_y^n + u_y^{n-1}}{l^2} \tag{4}$$

In Eq. 4, u_y^{n-1}, u_y^n, and u_y^{n+1} are the y-directional displacements of the mode amplitude at points n − 1, n, and n + 1; n means the experimental measurement point, and l is the distance between two adjacent measuring points. All displacement mode shapes are normalized to eliminate individual differences and facilitate the comparison of mode shape curvature of different samples. The modal curvature is the ratio of displacement modes between different nodes, so it is a dimensionless parameter.

It can be seen from the vibration mode shapes of T-beam that there is no significant difference among the other modes except the third and fourth modes. Therefore, it is difficult to find the location of the defect from the displacement mode shape curve. Therefore, according to the change of mode shape, only the curvature of the third and fourth modes are calculated, as shown in Fig. 11. In the damage location of T-beam, the peak appears on the mode curvature diagram, due to the decrease of local stiffness at the damaged position (Pandey et al. 1991; Ooijevaar et al. 2010). The 3D braided composite T-beams are overall structures. When the structures are damaged, fiber discontinuity may occur at the damage location, thus diminishing the constraints between the fibers. Reducing the restraint between fibers will affect the integrity of the structure. Since the mode shape curvature is very sensitive to such lessening

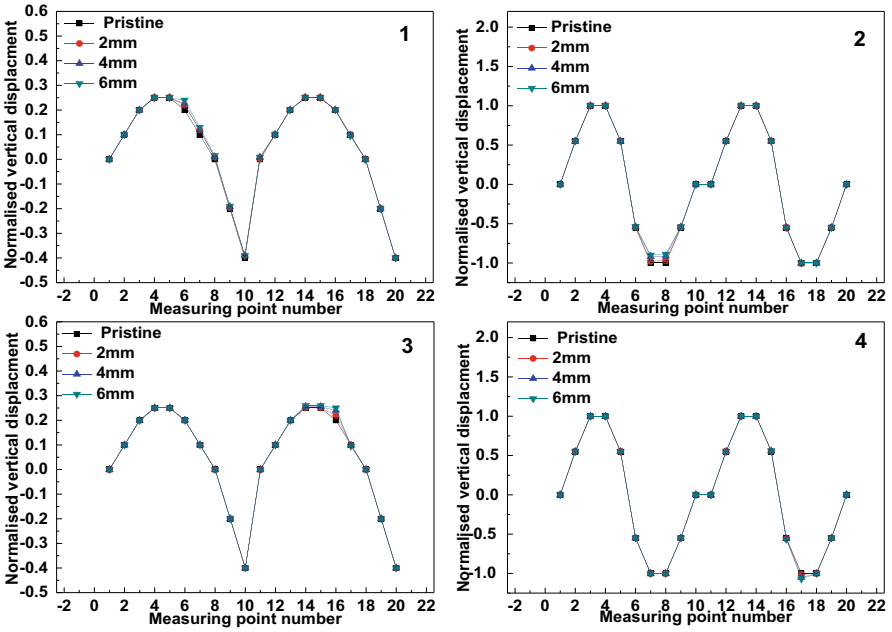

Fig. 11 The third- and fourth-order mode shape curvatures of pristine and damaged T-beams with different hole diameters: (1, 2) at point B; (3, 4) at point E. (Reprinted with permission from (Pei et al. 2016a), © 2016, Elsevier)

effects, the mode shape curvature is a powerful NDT parameter to analyze the influence of damage on structural vibration characteristics and locate the damage.

Finite Element Analysis

To verify the data of vibration test and study the influence of damage on the vibration characteristics of braided composite T-beam, the vibration characteristics of T-beam were simulated by finite element software. The simulation results are compared with the test results and verified with each other. The properties of the carbon fiber and epoxy in the FEM model are shown in Table 2. In ANSYS, PLAN42, and SOLID45 elements are used to calculate the elastic properties of T-beam by homogenization method. Using the free meshing scheme, the dynamic model of the whole system is established. SOLID187 elements discretize the 3D solid structure. According to the yarn orientation and damage characteristics in 3D braiding process, a local coordinate system is defined for each damage location. In the FEM modal analysis, the Maxwell's reciprocity theorem should be respected. Under this assumption, frequency response function (FRF) matrix, stiffness matrix, the mass matrix, and damping matrix of the structure become symmetric. It should be noted that the damping effect on the T-beam is not considered in the present simulation.

Under the boundary condition of cantilever beam, the finite element model of T-beam is analyzed by using the block Lanczos method, and the three-dimensional vibration mode diagram and natural frequency of the model can be obtained directly. The results show that the natural frequency of T-beam with damage is lower than that without damage. With the increase of damage degree, the decrease of natural frequency tends to increase. By comparison, it can be concluded that the natural frequencies obtained by the experiment and simulation match well within the maximum error of 4.5%, probably caused by no consideration of damping in the simulation. The four mode shapes of the pristine T-beam determined by the FEM are shown in Fig. 12. As shown in Fig. 12, The first and third displacement mode shapes are bending modes. The third and fourth displacement mode shapes are bending modes. However, the third mode shape calculated by the finite element method is different from the experimental data. The difference in the third mode shape can be explained as follows. For measuring the torsion mode, it requires that at least two sensors are simultaneously placed in the web plate and reinforcing plate in a symmetric manner in the experiment. In order to reduce the adverse effect of sensor-induced mass on the measurement of T-beam modal parameters, only one accelerometer is installed at the fifth excitation point. Thereby, only the bending mode can be captured in the experiment.

Conclusions

Two NDT methods, respectively, based on acoustic emission and vibration, have been described in this chapter. In the first NDT method, based on the basic idea and characteristics of HHT transform, the tensile damage experiment of carbon fiber braided composites is carried out, and the AE signal is extracted and processed by HHT transform. The relationship between the progressive failure process and the

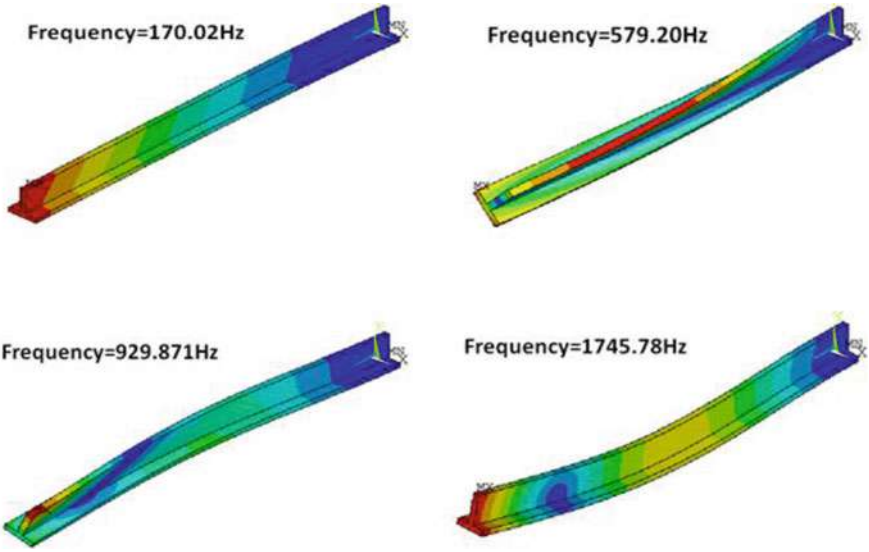

Fig. 12 Four mode shapes of pristine T-beam in FEM. (Reprinted with permission from (Pei et al. 2016a), © 2016, Elsevier)

evolution of AE signal is established. Afterward, a two-step method is presented to accurately locate damage. Aiming at the shortcomings of low precision and slow convergence speed of basic Drosophila optimization algorithm, a new Drosophila optimization algorithm based on chaos search algorithm and crowding degree of fish swarm algorithm is proposed. The locating error for the improved Drosophila optimization algorithm is about $\pm 1\%$, with much improvement in contrast with $\pm 5\%$ for the standard Drosophila optimization algorithm.

In the second NDT method, experiments and finite element simulation are used to analyze the vibration modal performance of pristine and damaged 3D braided composite T-beams. Taking natural frequency, displacement, and curvature mode shape as identification indexes, qualitative, positioning, and quantitative damage identification information was constructed. Moreover, the sensitivity of each index to damage was discussed. The results showed that the natural frequency and mode shape are two important vibration characteristic parameters of 3D braided composite T-beam. Compared with the intact condition, the natural frequencies of the damaged T-beam will be reduced. The mode shape is not very sensitive to small damage, while the mode shape curvature is a sensitive parameter to the location and size of structural damage.

Damage detection of composite components and structures in regular intervals is a necessary means to ensure their service safety. According to the testing conditions and specific purposes, it is significant to choose an appropriate detection method with high efficiency, accuracy, and robustness. NDT methods have different advantages and disadvantages. At present, the common NDT techniques for epoxy resin/synthetic fiber composites are likely under rapid development in the following directions.

Developing hybrid NDT techniques: These hybrid techniques integrate different NDT techniques and can exploit complementary advantages. The new techniques are anticipated to achieve quality evaluation, rapid detection, and reliable adaptability to extreme environmental conditions. This is a new trend of damage detection technology in the future. Establishing automatic high-speed detection system: Multichannel automatic scanning, real-time processing, automatic identification of defects and damage, phased array technology, automatic control systems, and robot technology are encouraged to apply to large-scale detection equipment, to reduce costs and, meanwhile, improve the efficiency of detection equipment. These technologies can not only improve the scanning speed but also greatly improve the automation level and effectively reduce the human error.

Integrating computer simulation and digital signal processing technology: Advanced numerical methods (such as finite difference, finite element, boundary element, and volume element) and signal processing methods (such as wavelet analysis, digital filtering, and power spectrum analysis) have become the necessary ingredients of non-contact NDT. With the comprehensive applications of digital imaging technology, the signal processing ability of composite damage detection equipment can be constantly improved, and the measurement accuracy can be steadily enhanced with the much-improved analyzing speed. Integration of miniature and portable testing equipment and devices: Electronic information technology and material synthesis and fabrication and sensor manufacturing have already entered a nearly mature state. Large-scale integration technology can help realize the rapid design and manufacture of electromagnetic transducer coils. The fabrication of small-array piezoelectric transducers and electromagnetic transducers should be promising candidates for embedding into large structures.

Development of online monitoring for structural health: Along with many emerging types of sensors, sensors that can be embedded in the structure will attract great attention. Soon, the structural health monitoring will develop in the direction of developing built-in networks of sensors. The current periodic inspection routines will be replaced by integral systems and platforms that are able to offer real-time health monitoring and immediate feedback. Composite structures will likely become intelligent structures with self-sensing and quick-responding capabilities.

In summary, we believe that the nondestructive damage detection for composite materials should evolve toward the objective of being faster in detection, more robust, more precise, more reliable, more convenient, but cheaper than the current detection methods. Our fearless outlook is inspired by rapid technological advancements. The damage detection technology for composite materials will continue to play a key role but in a more successful manner, in many sectors including aerospace, automotive industry, defense, civil infrastructure, and so on.

References

D. Aggelis, A. Mpalaskas, D. Ntalakas, T. Matikas, Effect of wave distortion on acoustic emission characterization of cementitious materials. Constr. Build. Mater. **35**, 183–190 (2012)

A. Al-Shawk, H. Tanabi, B. Sabuncuoglu, Investigation of stress distributions in the resin rich region and failure behavior in glass fiber composites with microvascular channels under tensile loading. Compos. Struct. **192**, 101–114 (2018)
O. Bashkov, A. Protsenko, A. Bryanskii, R. Romashko, Diagnostics of polymer composite materials and analysis of their production technology by using the method of acoustic emission. Mech. Compos. Mater. **53**(4), 533–540 (2017)
M.A. Caminero, M. Lopez-Pedrosa, C. Pinna, C. Soutis, Damage monitoring and analysis of composite laminates with an open hole and adhesively bonded repairs using digital image correlation. Compos. Part B **53**, 76–91 (2013)
F. Ciampa, M. Meo, A new algorithm for acoustic emission localization and exural group velocity determination in anisotropic structures. Compos. A: Appl. Sci. Manuf. **41**(12), 1777–1786 (2010)
G. Ding, C. Xiu, Z. Wan, J. Li, X. Pei, Z. Zheng, Location of tensile damage source of carbon fiber braided composites based on two-step method. Molecules **24**(19), 3524 (2019)
J. Dong, N. Huo, A two-scale method for predicting the mechanical properties of 3d braided composites with internal defects. Compos. Struct. **152**, 1–10 (2016)
Y. Duan, H. Zhang, X.P. Maldague, C. Ibarra-Castanedo, P. Servais, M. Genest, S. Sfarra, J. Meng, Reliability assessment of pulsed thermography and ultrasonic testing for impact damage of cfrp panels. NDT&E Int. **102**, 77–83 (2019)
S.K. Dwivedi, M. Vishwakarma, A. Soni, Advances and researches on nondestructive testing: A review. Mater. Today Proc. **5**(2), 3690–3698 (2018)
A. El Mourid, R. Ganesan, M. Brochu, T. Crochon, M. Levesque, Anisotropic oxidation due to aging in a triaxially braided composite and its influence on tensile failure. Compos. Part B **76**, 1–12 (2015)
L. Ge, H. Li, B. Liu, D. Fang, Multi-scale elastic property prediction of 3d five-directional braided composites considering pore defects. Compos. Struct. **244**, 112287 (2020)
S. Gholizadeh, A review of non-destructive testing methods of composite materials. Procedia Struct. Integr. **1**, 50–57 (2016)
R.F. Gibson, Modal vibration response measurements for characterization of composite materials and structures. Compos. Sci. Technol. **60**(15), 2769–2780 (2000)
Q. Gu, Z. Quan, J. Yu, J. Yan, B. Sun, G. Xu, Structural modeling and mechanical characterizing of three-dimensional four-step braided composites: A review. Compos. Struct. **207**, 119–128 (2019)
S.E. Hamdi, A. Le Duff, L. Simon, G. Plantier, A. Sourice, M. Feuilloy, Acoustic emission pattern recognition approach based on Hilbert-huang transform for structural health monitoring in polymer-composite materials. Appl. Acoust. **74**(5), 746–757 (2013)
M. Hammami, A. El Mahi, C. Karra, M. Haddar, Vibration behavior of composite material with two overlapping delaminations. Int. J. Appl. Mech. **7**(04), 1550054 (2015)
Z. Huda, P. Edi, Materials selection in design of structures and engines of supersonic aircrafts: A review. Mater. Des. **46**, 552–560 (2013)
A. Katunin, A. Wronkowicz, Inuence of parameters of modal analysis on vibration- based structural damage detectability. J. Vibroengineering **17**(8), 4153–4163 (2015)
S. Laurenzi, M. Marchetti, Advanced composite materials by resin transfer molding for aerospace applications, in *Composites and Their Properties*, ed. by N. Hu, (IntechOPen, UK, 2012)
J. Lemaitre, *A Course on Damage Mechanics* (Springer Science & Business Media, 2012)
J. Lou, L.Z. Wu, L. Ma, J. Xiong, B. Wang, Effects of local damage on vibration characteristics of composite pyramidal truss core sandwich structure. Compos. Part B **62**, 73–87 (2014)
M.A. Masuelli, Introduction of fibre-reinforced polymers-polymers and composites: Concepts, properties and processes, in *Fiber Reinforced Polymers-The Technology Applied for Concrete Repair*, (IntechOpen, UK, 2013)
Y. Mei, S. Fukai, D. Shaopeng, Acoustic emission source location for composite plate based on empirical wavelet transform. J. Beijing Univ. Aeronaut. Astronaut. **44**(7), 1395 (2018)

T. Mesogitis, A.A. Skordos, A. Long, Uncertainty in the manufacturing of fibrous thermosetting composites: A review. Compos. A: Appl. Sci. Manuf. **57**, 67–75 (2014)
T. Ooijevaar, R. Loendersloot, L. Warnet, A. de Boer, R. Akkerman, Vibration based structural health monitoring of a composite t-beam. Compos. Struct. **92**(9), 2007–2015 (2010)
A. Pandey, M. Biswas, M. Samman, Damage detection from changes in curvature mode shapes. J. Sound Vib. **145**(2), 321–332 (1991)
X. Pei, L. Chen, J. Li, Y. Tang, K. Chen, Effect of damage on the vibration modal of a novel three-dimensional and four-directional braided composite t-beam. Compos. Part B **86**, 108–119 (2016a)
X. Pei, B. Shang, L. Chen, J. Li, Y. Tang, Compression properties of multilayer- connected biaxial weft knitted carbon fiber fabric reinforced composites. Compos. Part B **91**, 296–305 (2016b)
S.M. Vazirizade, A. Bakhshi, O. Bahar, Online nonlinear structural damage detection using hilbert huang transform and artificial neural networks. Sci. Iran. Trans. A Civ. Eng. **26**(3), 1266–1279 (2019)
R. Velmurugan, S. Solaimurugan, Improvements in mode I interlaminar fracture toughness and in-plane mechanical properties of stitched glass/polyester composites. Compos. Sci. Technol. **67**(1), 61–69 (2007)
H. Yamada, Y. Mizutani, H. Nishino, M. Takemoto, K. Ono, Lamb wave source location of impact on anisotropic plates. J. Acoust. Emiss. **18**, 51 (2000)
S. Yan, X. Zeng, A. Long, Experimental assessment of the mechanical behavior of 3d woven composite t-joints. Compos. Part B **154**, 108–113 (2018)
C. Zhang, J. Zhao, T. Rabczuk, The interface strength and delamination of fiber-reinforced composites using a continuum modeling approach. Compos. Part B **137**, 225–234 (2018)
Y.-N. Zhang, W. Zhou, P.-F. Zhang, Quasi-static indentation damage and residual compressive failure analysis of carbon fiber composites using acoustic emission and micro- computed tomography. J. Compos. Mater. **54**(2), 229–242 (2020)
C. Zhao, B. Wang, J. Xiao, Macroscopic characterization of fiber micro-buckling and its influence on composites tensile performance. J. Reinf. Plast. Compos. **36**(3), 196–205 (2017)

Dynamic Mechanical Analysis of Epoxy/Synthetic Fiber Composites

6

Ibrahim M. Alarifi, Majid Khorami, Tarek M. A. A. EL-Bagory, and Ramazan Asmatulu

Contents

I. M. Alarifi
Department of Mechanical and Industrial Engineering, College of Engineering, Majmaah University, Al-Majmaah, Saudi Arabia

Engineering and Applied Science Research Center, Majmaah University, Al-Majmaah, Saudi Arabia
e-mail: i.alarifi@mu.edu.sa

M. Khorami
Facultad de Arquitectura y Urbanismo, Universidad UTE, Quito, Ecuador

T. M. A. A. EL-Bagory
Department of Mechanical Design, Faculty of Engineering Materia, Helwan University, Cairo, Egypt

R. Asmatulu (✉)
Department of Mechanical Engineering, Wichita State University, Wichita, KS, USA
e-mail: ramazan.asmatulu@wichita.edu

S. Mavinkere Rangappa et al. (eds.), *Handbook of Epoxy/Fiber Composites*,
https://doi.org/10.1007/978-981-19-3603-6_8

Abstract

This chapter presents the analysis of the dynamic mechanical properties of the epoxy/synthetic fiber-reinforced composites. It has highlighted the significant advantages of those composites, including low density, high mechanical and creep strengths, and different processing options for various sizes and complex shapes. These composites are extensively used in the automotive, aerospace, energy, and other production industries. The mechanical properties of single fiber-reinforced polymer composites can be enhanced through the carbonization process. The chapter also explains that the combination of high elongating fibers can enhance the epoxy/synthetic fiber composites' dynamic mechanical properties. On the other hand, the dynamic mechanical analysis (DMA) tests exhibit a shift in the synthetic carbon fibers composites' glass transition temperatures, which may be useful for these fiber-reinforced high-temperature applications of composites.

Keywords

Epoxy/synthetic fiber composites · Mechanical properties · DMA · Fiber-reinforced · Natural fiber-reinforced composites · Hybrid composites

Introduction

By nature, the composites are heterogeneous, with more than one solid phase close to each other on a microscopic scale. Figure 1 presents the typical classification of composite materials. Composite materials are made by reinforcing either synthetic or natural fibers within a polymer matrix. There are few benefits of natural fibers; therefore, synthetic fibers are replaced by natural fibers. These advantages included low density, environment friendly, increased flexibility, biodegradability, increased specific strength, low cost, abundant availability, nontoxicity, renewability, relative no abrasiveness, and easy processing (Thakur et al. 2014; Gupta and Srivastava 2016). Despite the great advantages of natural fibers, such as high moisture absorption properties and low impact strength, they have some limitations. However, the hybridization technique can be used to reduce these limitations.

The combination of supplementary fibers along with the single fiber in a polymer matrix makes up hybrid composites. The hybridization process shows a vital role in the increase of the composites' mechanical properties. Therefore, it is better to use two fibers with similar lengths and different diameters, as compared to using one fiber in a polymer matrix. It is recognized that the effective area for fiber-matrix adhesion increases in the presence of different fiber diameters because it allows the uniform transfer of stress (Gupta and Srivastava 2016; Boopalan et al. 2013). Moreover, hybridization is considered effective as the breaking of fiber with low elongation exerts load, with no matrix failure. This procedure effectively transmits stress to the matrix's fiber, further increasing the composites' mechanical properties (Sreekala et al. 2002).

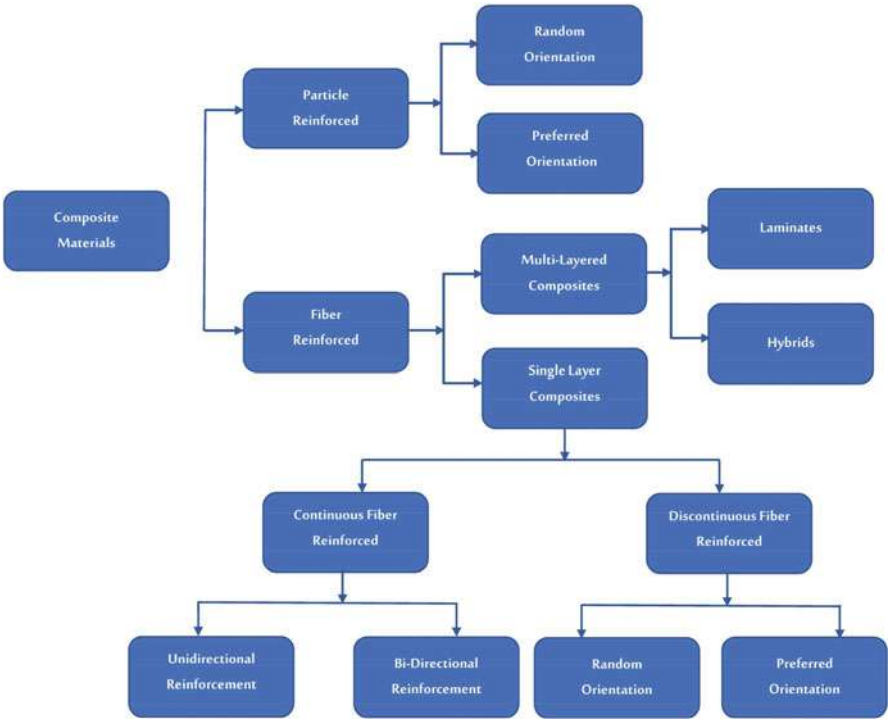

Fig. 1 Classification of the composite material

Therefore, the structure of the fiber is a pronounced effect on the mechanical properties of composite materials. The cellulose fibers are prepared from the helical wound cellulose microfibrils surrounded by an amorphous lignin matrix present in the natural plant fibers. The fiber's water is retained with lignin help, which protects against the biological attack and strengthens stems against wind and gravity forces. The hemicellulose acts as a compatibilizer between lignin and cellulose in the natural fibers. The cell wall's complex structure with multiple layers and a thin primary wall is shown in Fig. 2. This cell wall acts as the first deposited layer during the encircling of cell growth and the secondary wall formation. The secondary wall contains three layers, namely, S_1, S_2, and S_3, as shown in Fig. 2. The thickness of the middle layer mainly describes the mechanical properties of the fiber. The chains of helical curled cellular microfibrils are made with long-chain cellulose in the middle layer (Kabir et al. 2012). The angle between the microfibrils and the fiber axis is identified as the microfibril angle as shown in Fig. 2. This angle is altered according to the type of fibers.

At present, the natural fiber-reinforced polymer composites are used as construction materials and automotive parts and in electrical and mechanical industries (Huda et al. 2008). These composites materials are useful in the packaging industry because of their long durability and increased specific strength. It is known that the packaging industries use 42%, the building and construction industries use 20%, the automotive

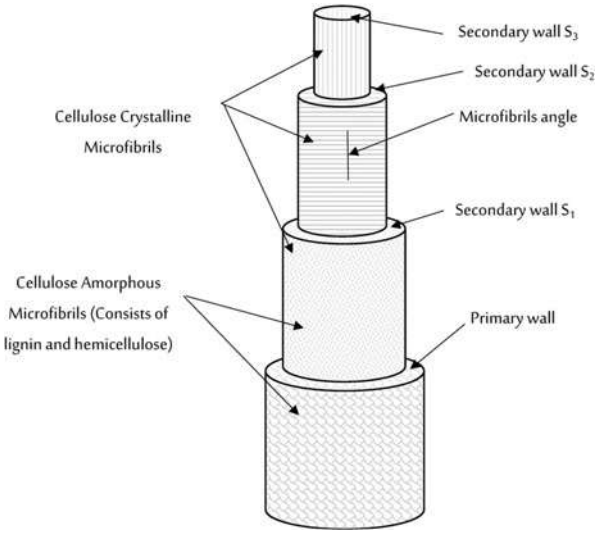

Fig. 2 Cell wall structure within a natural fiber

sector uses 8%, and other applications use 30% of the natural fibers (Majeed et al. 2013). Synthetic fiber-reinforced polymer (SRP) composites are used in altered parts of aerospace. The main features of SRP composites are very light; therefore, they are utilized in metal and ceramics composites in the automotive industries and aeronautical constructors. SRP composites can reduce weight by 10–50% and cost by 10–20% compared with metal composite materials (Gay 2014). Different parts of aircraft using SRP composites are listed below:

- Wing box, fuselage, and empennage box are used as primary structure components.
- Ailerons, high-lift device, a control component, and spoilers are used as control components.
- Fairings, landing gear trap doors, storage room doors, karmans, radomers, and front cauls are used as exterior components.
- Bulkheads, floors, doors, and partitions are used as an interior component.

The remaining part of this chapter presents the current examinations associated with the synthetic fiber composite mechanical properties. These properties included tensile modulus, flexural modulus, flexural strength, tensile strength, and hybrid composite impact.

Matrix Materials

The matrix in fiber-reinforced polymer composites is either thermoset or thermoplastic materials. The heating can soften, melt, and reshape the fiber's materials as many times

as desired, whereas thermoset materials lack this ability. The matrix's main significance is that it helps keep the fibers straight, and the entire load is transmitted to the fibers. Another feature of using the matrix in composite materials is that it protects, shapes, and makes the fiber rigid against corrosion and chemical effects. The thermoset polymers have several advantages to perform better, corresponding to their thermal stability, durability, mechanical properties, and chemical resistance (Yan et al. 2014). It is known that epoxy resin possesses high compressive and tensile strength properties; therefore, it is widely used in the polymer matrix (Eesaee and Shojaei 2014).

Similarly, the thermoplastic matrix materials wide usage corresponds to their design flexibility, easy fabrication, and low processing (Arthanarieswaran et al. 2014). The degradation of natural fibers is restricted within 230 °C in thermoplastic-based composites. However, it is possible to conduct the processing of thermoset-based composites at room temperature without fiber degradation. Furthermore, thermosets mechanical properties that further clarify that epoxy resin possesses better mechanical properties in evaluation to other composites.

Reinforcements

Reinforcements are responsible for the cumulative matrix mechanical properties. Different reinforcements in polymer matrix composites (PMCs) include:

- Synthetic fibers (glass, carbon, and Kevlar)
- Natural fibers (sisal, bamboo, jute, and banana)

Synthetic fibers have possessed high specific strength and low density; therefore, they are utilized in aerospace industries, unlike natural fibers. However, the synthetic fibers are replaced by natural fibers, considering that natural fibers are present in abundance and are made of renewable bio-based materials. The systematic classification of reinforcements in synthetic and natural fibers. The classification of fibers is divided into two groups from fibers, namely, natural and synthetic fibers. The natural fibers are classified into three types; animal, natural, and mineral fibers. On the other hand, synthetic fibers are divided into two types, namely, organic and inorganic fibers.

Fabrication Methods

The process of fabrication is conducted through different procedures based on the selected materials under various procedures. Polymer chemistry plays a significant role in determining the appropriate resin. The different fabrication methods to manufacture the composite materials are described as the following:

Human Layup

The layup method is the easiest way to handle thermoset-based synthetic fiber composites (Alarifi et al. 2016a, 2020). At the start of this fabrication process, the

liberating mediator is covered on the mold's surface to prevent the polymers from sticking to the surface. Later, thin plastic panes are used to cover the mold's top and bottom to give a perfect finished product. The top of the mold holds the fibers in the chopped or woven form as reinforcement. The surface of the mat that is already present on the mold is topped with a mixture of thermosetting resin along with a suitable hardener. The brush is used for the uniform spreading of the polymer. The polymer surface is then covered with the second layer of reinforcement, and the air and excess matrix present on the surface is removed using a cylindrical roller. This process is repetitive until the required thickness is attained for each layer of matrix and reinforcement. The relief agent is scattered on the internal surface of the topmost mold after placing the plastic sheet. It is then kept on the required thickness achieved with the application of pressure. The frame is opened after curing at 25 °C to take out the developed composite part for 60 minutes. The manufacture of hybrid composites through this procedure is done using polyester resin and epoxy resin.

Compression Molding

The closed molding process under high pressure is known as compression molding. This method uses two matched metal molds for fabricating the composite products. In the compression molder, the upper plate is movable, whereas the base plate is stationary. The metallic mold is placed with reinforcement and matrix, and these altogether are kept between the compression molder (Huda et al. 2006). The requirement of heat and pressure is contingent on the form and dimension of the composites. The pressure and heat application allow the flow of matrix and reinforcement present between the molder plates. After the composite material curing, the product is taken out from the mole to perform further processes at 25 °C temperature. This procedure is applicable in thermoplastic and thermoset-based fiber composites that may be natural or synthetic. The compression molding process is considered advantageous as it has a high fabrication speed and low fiber destruction (Huda et al. 2006). Therefore, this process is used in various parts of automobiles extensively.

Injection Molding

The injection molding is used for producing plastic parts with an excellent dimensional accuracy. This process is also used to produce products like packaging items, toys, housewares, furniture, medical disposal, syringes, appliances, and automobile parts. This process involves the formation of products under pressure by pushing melted plastic material into a frame. After the cooling process and solidifies, it is taken out by opening the mold (Huda et al. 2006).

Pultrusion

The pultrusion process is used to manufacture products with persistent cross sections like channels, golf club shafts, structural shapes, rod stock, beams, tubing, pipe, and fishing rods. This process involves continuous reinforcements using a resin bypassed via resin soak and lugged concluded steel die. The steel die strengthens the saturated reinforcement to control the ratio of fiber and resin that shapes the stock. The speedy cure of resin depends on the steel die (Huda et al. 2006). This process is widely used

to reinforce the thermoset polymer composites with either natural or synthetic fibers. Therefore, it is assumed that the pultrusion technique is useful in hybrid composite fabrication for different industries (Athijayamani et al. 2009).

Dynamic Mechanical Properties

A dynamic mechanical analysis tester was used to mechanically analyze the composite materials and determine the glass transition temperature (T_g). DMA is an extensively used method in composite characterization. In a typical DMA test, a sinusoidal mechanical excitation is applied for both force and elongation. On the other hand, the phase shift between elongation and force is determined as a temperature function. In this test, the model is supported at both ends, and sinusoidal stress is a function of the specimen mid-span. The model consists of two stationary clamps to support the specimen and one movable clamp to simulate the three-point bend test. The test specimen with dimensions of $5 \times 35 \times 3$ mm, as shown in Fig. 3, is prepared according to ASTM D7028-07 (2015).

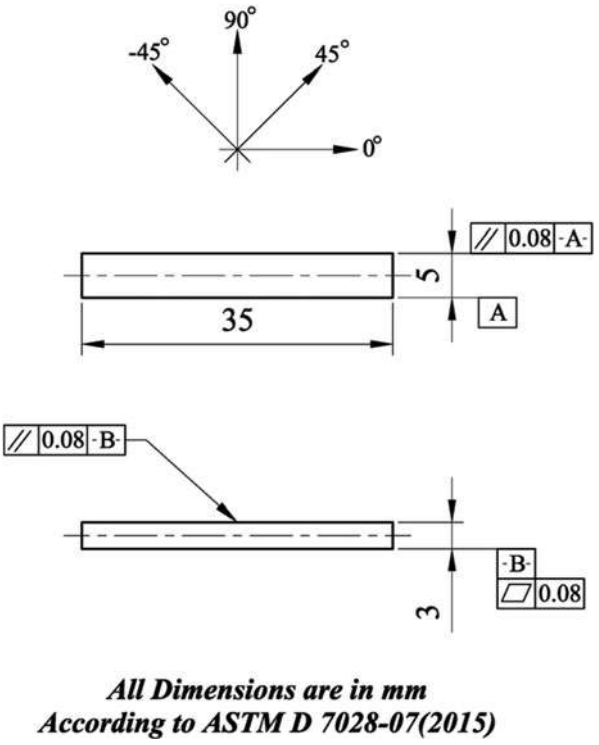

Fig. 3 Dimensions of DMA test specimen according to ASTM D7028-07 (2015)

Laminated Composites

The laminated composites are achieved by combining fibrous layers, each with different fiber orientations (Alarifi et al. 2015a, b, c; Saravanos and Pereira 1992). These layers are combined in a single component by keeping one layer over the other. Unlike the normal composites, these laminated composites tend to have directional strength and stability. Figure 4 represents the structure of a typical laminate composite that comprises of interlaminar damping layers. On the other hand, the fabrication process that involves laminated composites to be applied in engineering streams is presented in Fig. 5.

The capacity of prepared composites is identified through different tests, as these composites are widely used in many mechanical applications. The different structures, dynamic mechanical properties, and applications play a major role in most testing procedures. The damping layers are supported by modal damping's dynamic properties in laminated composite plates by utilizing discrete piece damping mechanics known as a semi-mathematical method (Saravanos and Pereira 1992).

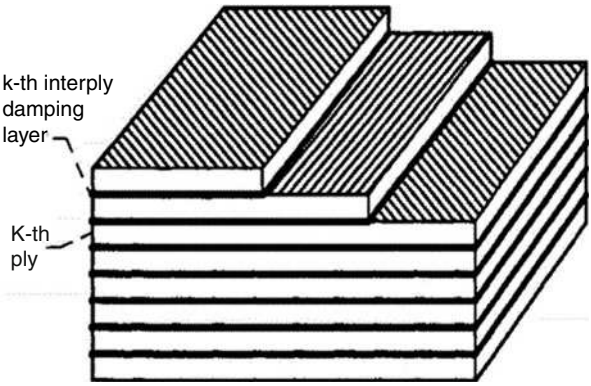

Fig. 4 The typical configuration of laminates composite with the damping layer (Saravanos and Pereira 1992). (Cite full required only)

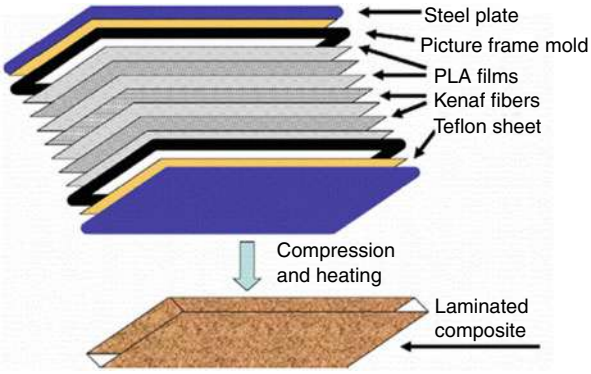

Fig. 5 Process of the laminated composite with heating and compression fabrication (Huda et al. 2008). (Copyright permission obtained)

The composite laminates dynamic mechanical characteristics which were made from jute fibers were studied at different temperatures. The nonwoven is treated chemically with cyano-ethyl. The cyanoethylation of the fibers in the prepared samples increased its storage modulus (E′). The surface-modified fibers are dignified as raw fiber-reinforced composites to increase stiffness and E′ in these composites. It is known that jute fiber (non-treated as well as chemically synthesized) and unsaturated resin show a remarkable decrease in the peak of damping factor (tan δ) (Saha et al. 1999). The layer sequencing and the fabrication architecture for dynamic analysis of reinforced polyester composites are studied with a special concentration of various fiber volume fractions. These reinforcements demonstrate useful consolidation to confer high strength to polyester. Increasing the number of layers helps to achieve the storage modulus (E′)' highest value, which is 3.5 GPa, and loss modulus (E″) with a value of 0.19 GPa. Moreover, the addition of maximum fabric layers increases the association between the fiber and the matrix (Pothan et al. 2005; Gupta and Bharti 2017). Figure 6 has provided a pictorial description of the complex modulus for the DMA test.

The dynamic mechanical characteristics of biocomposite laminates are analyzed as temperatures ranging between 20 °C and 100 °C. These laminates are made of kenaf and PLA fibers and testing using DM analyzer (TA 2980). This device is made with a dual-cantilever bending fixture that is heated continuously at 1 Hz frequency. This clearly shows that E′ rate is enhanced with higher flexural modulus in the fiber-reinforced composites that are chemically altered.

The fiber composites chemically treated with silane were observed to increase E′ rate, unlike other fiber composites. Moreover, E′ value of 8000 MPa was observed for composites with surface-modified fibers that is double compared to the observed values of the unsaturated fiber composites. This observation clarifies that there is a strong bond between the surface-modified kenaf fibers and the matrix. The improvement in thermal stability was observed through DMA results, which is achieved by adding silane-treated fibers in the composites (Huda et al. 2008). Wood composite fiber plays and PLA film-reinforced composites demonstrate approximately 64–66% of higher damping properties (Bogren et al. 2006).

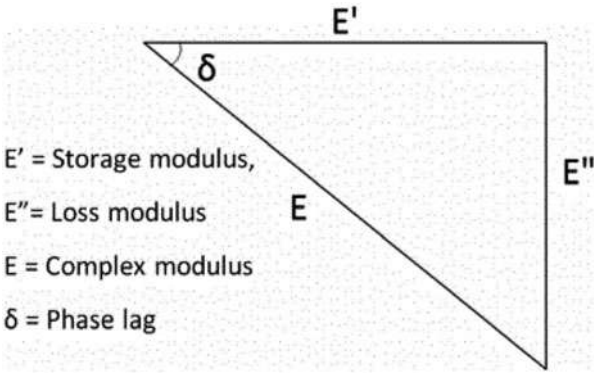

Fig. 6 Complex modulus of biocomposite laminates DMA (Gupta and Bharti 2017). (Cite full required only)

The new vibration-damping method was used to analyze thermoplastic composites based on natural and glass fiber composites to describe composite materials' nature at higher frequencies. Ashok et al. (2019) have shown that NFC's damping characteristics were greater than GFC at elevated compression range, with decreased trends at lower compaction. Therefore, GFCs are likely to be replaced with NFCs in most engineering applications, considering the dynamic mechanical characteristics (Di Landro and Lorenzi 2009). The flexibility of natural fiber composites made from Cordenka and flax epoxy is tested for high-performance structural applications. Laminated composites are made by soaking the commercially available reconstructed cellulose textiles and woven flax in resin. The specific energy absorption (SEA) procedure is used to analyze laminated composites' properties, and the diversity of SEA was shown between 21.2 and 34.3 kJ/kg (Okahisa et al. 2011). The testing of fiber loading in narrow film from DMA model Q800 showed increased storage and decreased moduli of kenaf fiber composites. These composite materials exhibit the increased value of E′, which is 16.15 MPa, and E″, which is 625 MPa. The value of the weight percentage of fiber is 17.5 in composites, unlike other composite combinations. However, 17.5% of intensified LPT decreased the value of E′ to 4.05 GPa and E″ to 152 GPa, in case of higher fiber loading (Salleh et al. 2014).

Dynamic mechanical properties like damping parameters are determined by testing the chemically treated and untreated coconut sheath incorporated within the epoxy composites. A higher value of E′ that is 3.3 GPa shows better intermolecular bonds of the hydroxyl group in treated coconut sheath epoxy composites. This also helped in achieving an increased amount of stiffness in the treated coconut sheath epoxy composites. There is an increase in the loss of factor among the untreated fiber composites (0.324) at 84.1 °C, unlike the treated fiber composites (0.269) at 82.4 °C. This happens because of an increase in E′ of fiber composites that are chemically treated, corresponding to polymeric molecular movements (Vickers 2017).

The sandwich fascia embraced with three thin layers of composites was studied using experimental and numerical analysis. It is probable to recognize the composites dynamic behavior as they contain recyclable pre-peg stable foam core and two face sheets made of glass-PP for flax-PE for panel A and panel B. The lower natural frequencies are determined based on the lower elastic moduli of flax-PE face sheets and glass-PP. A few basic modes' global dynamic performances are understandable through a statistical model with a congruent core (Vickers 2017).

Laminates are made using cotton waste and unsaturated polyester from the textile industries. The performance of glass and cotton fibers helps in determining the dynamic mechanical properties. At low temperatures, E′ of composite laminates increases with different stacking and glass fiber content. Laminates are prepared using the varying position of layers in jute and carbon fabric-reinforced laminate composites. These layers include two piles of carbon fabrics and two piles of jute fabric. The highest storage of 14 GPa and E″ of two GPa can be achieved for the composites with carbon fabric outer layer (Sezgin et al. 2016).

Hybrid Composites

There is a slight decrease in E′ value of jute fabrics as amine-cured epoxy resin and N-glass or E-glass sliced filament mats as hybrid laminates. These are arranged at 1 Hz a fixed frequency, unlike the glass-reinforced composites. It is known that the E′ values of glass-reinforced composites fall between 4–8 GPa, and 4–6 GPa for hybrid composites of glass and jute, respectively. The coupling type agent was similar to HC 5, and AR 504 is used to fabricate the composites and determine the composite properties such as E′ and stiffness (Wielage et al. 2003). Flax and temperature – fiber-reinforced polypropylenes helped in revealing these findings.

The glass hybrid/oil palm fiber-reinforced PF and palm fiber-reinforced phenol-formaldehyde composites demonstrated a fall in natural frequencies dynamic and modulus properties. There is a continuous enhancement in the E′, and tan δ values with fiber percentage as fibers are added. A reverse nature is demonstrated by E″ with improving the percentage of the fiber loading. Hybrid composites have possessed high mechanical dumping with reduced E′, unlike the hybridized oil palm fiber/PF composites (Wielage et al. 2003). Fabrication is done on the banana-glass woven fabric-reinforced polyester composites (Pothan et al. 2005). There is a significant impact of reinforcements that improve the rubbery plateau as the result of incorporating fabrics. The composites with four layers were found to have increased E′, that is, 3.5 GPa. However, three- and four-layered composites exhibited a slight difference in E″ in the gum, that is, the neat polyester.

Hybrid composites are studied for mechanical properties. They consist of an equal amount of wood flour (WF) and kenaf fibers (KF) as reinforcements in PP that result in PMCs formation. Hybrid WF composites exhibit great damping values at increased temperatures. KF composites exhibited impressive progress in the tan δ (0.08) value at 10 °C. On the other hand, an increase in temperature enhances the value of E′ (5.7 GPa) and E″ (0.28 GPa), unlike the WF and hybrid composites (Sen et al. 2004).

Moreover, enhancing the weight fraction of oil palm and sisal fibers present in natural rubber can improve E′ (755.5 MPa) and decrease tan δ (0.9). The increase in E′ value and decrease in tan δ correspond to expanded stiffness through increasing natural fiber content. The value of E″ was ranging between 2.5 and 3 MPa, and E′ equal to 3.5 MPa is likely to increase in the fibers imparted through a chemical treatment. There is a decrease in the damping characteristics for loading conditions; however, there was an increase in E″ in such conditions (Samal et al. 2009).

The dynamic mechanical characteristics of hybridized thermoplastic natural rubber with kenaf and carbon fibers were studied extensively. DMA revealed the real and TPNR-reinforced sliced kenaf definite performance and carbon fibers. Unlike the surface-modified composites, raw hybrid composites exhibit improved values for tan δ, E′, and E″ values. Irregular-oriented fibers and a decrease in the fiber aspect ratio characterize composites' low properties as recorded in DMA (Jacob et al. 2006).

Improvement in E′ (15 kPa) was recorded for the maleic anhydride-grafted polypropylene (MAPP) composites. These composites are reinforced with glass fiber and bamboo fiber. Improved E′ indicates improved stiffness of hybrid composites, unlike the raw fiber-reinforced composites. Tan δ spectra exhibit a coupling agent on α and polypropylene γ relaxation process and firm control of fiber contented (Samal et al. 2009). DMA helps in determining the measures of viscoelastic parameters. The results show an increase in the fiber contented by 15% and MAPP by 2% that further increased E′ (15 kPa) as the result of the hybridization of artificial fibers of glass (Nayak et al. 2009). The results also improve after treating fibers with MAPP, when polypropylene (PP) reinforced with short glass fiber and sisal hybrid composites are loaded with and without a coupling agent. Extension in measures of E′ (17.1 kPa) is exhibited by adding fibers and MAPP. This process is applied and shows effective results for glass hybridization, as well. Incorporating fibers and MAPP in the composites result in a decrease in the damping properties (Lehr et al. 2009).

The short jute fiber-reinforced polylactic acid composites and ramie exhibit the superior value of E′ for plain PLA composites. Increasing temperature to approximately 30 and 60 °C decreases E′ of the samples that range from 4000 to 1800 MPa, resulting from ramie/jute fibers in the PLA composites. Moreover, the maximum heat dissipation occurs at 30 °C and 60 °C due to an increase in E″ that ranges from 800 to 400 MPa. The transition temperature of fiber-reinforced composites increased in the presence of fiber. The transition temperature reduces PLA-based composites the damping properties, unlike the neat PLA (Nayak et al. 2009).

The results revealed that a considerable increase in the values of E′ and E″ is observed because of distinctive volume proportions between the glass, sisal, and other fiber loadings in glass/sisal hybrid composites. This growth corresponds to a shift toward higher comprehensive fiber volume and glass loadings – an increase in temperature results in diminished values of E′ and E″ (Ornaghi et al. 2010).

A decent dynamic modulus is exhibited by the fabrication of glass filaments (GF) and easily mixed hybrid composites with pineapple leaf filaments (PALF) in unsaturated polyester resin hybrid composites. The values of E′ and least dumping (0.1 at 95 °C) are likely to improve by the intimate mixing of hybrid composites with PALF/GF. The highest dumping behavior (0.15 at 150 °C) was exhibited by hybrid composites, unlike other composites (Devi et al. 2010). The glass hybrid composites show higher E's values (1E9.6 Pa). Adding a little amount of glass fiber enhances the loss of moduli and E′ (Ornaghi et al. 2011).

The DMA properties of oil palm empty fruit branches fiber-reinforced epoxy hybrid composites are examined according to tan δ, E′, and E″ values. The results revealed that the decrease in temperature decreases the value of E′. The peak height of tan δ was highest for the epoxy matrix and least for jute composites. The highest E′ value achieved for pure jute composites was 37.5 MPa, whereas the lowest E′ achieved for epoxy was 32.5 MPa. The addition of little amount of jute fibers to oil palm epoxy composites is likely to improve the hybrid composites' damping properties (Devi et al. 2010).

There is a significant impact of alkali, organoclay expansion, and silane treatment with coconut sheath surface on naturally available woven coconut as it strengthens

the hybrid polyester composites. It is shown that composites that are chemically treated with silane exhibit improved E′ (1.75E + 10 Pa) at room temperature, unlike the composites treated with alkali or untreated composites. The natural frequency and damping ratios are likely to increase by adding nanoclay to the least filler content in the composites that are either untreated, silane treated, or alkali treated. Rajini et al. (2013) have observed the surface preparation impact on E′ and E″ through DMA. Adding 2% of nanoclay to the composites improves the damping attributes as it enhances the matrix stiffness through the uniform distribution of clay. This mechanism was revealed that when naturally woven coconut sheath, nanoclay was synthesized in the form of hybrid composites using an unsaturated polyester matrix. The alkali fiber stacking sequences of coconut sheath composites are known to have improved the free vibration characteristics (Rajini et al. 2013). Enhanced bamboo weight fraction caused a decrease in value of E′, with almost diminished E″ value and rare establishment of damping for the glass and bamboo composites. The volume of fiber affects the bamboo and glass fiber-reinforced composites' DMA properties (Mandal and Alam 2012).

The hybridization impact of the glass fiber-reinforced composites was observed due to an increase in the fiber amount being reinforced in the composites in a decrease in E′ form. An increase in temperature for 75% glass and 25% ramie fiber composites showed a significant decrease in value of E″. Ramie and glass fibers showed diminished values for mechanical loss factor, unlike the neat resin composites (Romanzini et al. 2013).

Expanded estimation of E′ was also evaluated for jute fiber-reinforced epoxy hybrid of woven composites and oil palm empty fruit bunch (EFB) composites. Amendable deformations of filaments increase the epoxy matrix's ability to expand that further helps in the mechanical bounds. The stiffness and stress transfer of oil palm EFB and woven jute fiber composites increase after hybridization. Hybrid composites displayed the highest percentage of E″, unlike the pure jute fibers. This clearly explains the T_g critical role in the polymer matrix that is associated with fiber expansion at the reinforcing stage. Pure jute fibers are likely to have the highest E_{max} value (3.6 MPa), which is followed by pure EFB and woven jute fiber composites. It has been shown that tan δ increases in pure epoxy composites, while it decreases for pure jute fiber (Vickers 2017). The increase in fiber loading, along with the expansion of stress transfer, is likely to diminish the amount of E′ in jute and EFB hybrid composites. Expansion of jute fiber content demonstrates the expansion of E″ in the hybrid composites; however, there is a diminished marginal pattern of the rubbery area in the jute hybrid composites instance. The tan δ curves are brought down after evaluating T_g from E″. Hybrid composites contrasted with EFB composites and jute composites account for lower tan δ peak height that demonstrates improvement in fiber and matrix adhesion and reduced damping (Jawaid et al. 2013).

Almost all the fiber fractions with a different fiber content of ramie fibers and glass have demonstrated an enhancement in E′. There is an improvement in fiber content at the maximum value of E″ for pure resin overall among all glass-ramie proportions with complete temperature range and reduced damping characteristics (Romanzini et al. 2013).

At higher temperatures, decreased E′ is exhibited by the jute alkali-treated and fiber-reinforced hybrid composites palmyra palm leaf stalk fiber composites. However, E′ improves with increasing the content of jute fiber in hybrid composites. Moreover, E″ also increases with enhancement in the jute fiber content because it allows effective stress transfer (Vickers 2017). Ashok et al. (2019) have exhibited an increase in E′ value for jute composites and neat resin composites complemented with different compositions at low temperatures. The value of E′ for neat resin composites after adding jute fibers at 170 °C was calculated as 2150 kPa, which improved to 3390 kPa for jute and resin composite. However, the value of E′ diminishes with increasing temperature. E′s maximum value was exhibited by composites that are fabricated with jute fibers completely at reduced temperatures. At a low temperature that is 20 °C, the value of E″ was observed to be diminished for the hybrid composites; however, it is likely to expand at higher temperatures. The hybrid composites account for the highest value of E″ at 170 °C with 1880 kPa. The pure resin composites were observed to have a maximum tan δ (0.58), followed by 75% jute and 25% resin fiber composites.

The chemically modified jute and EFB fibers reduce their fibers hydrophilic properties, further increasing the wettability between the interface bonding of fiber and the matrix. This is likely to increase E′ and E″, which further increased the stiffness of hybrid composites. Poor results are presented in decreased E′ (below 3.6 MPa) for raw fiber composites. The molecular chain's portability is likely to be reduced at the interface in 2-HEA modified EFB and jute fibers due to solid collaboration between the matrix and fibers. This condition also exhibits diminished damping attributes for hybrid composites (Jawaid et al. 2013).

Their fundamental frequency of sisal and bagasse hybrid composites is increased by 1.15 times compared to the sisal composites. The difference in flexural stiffness of bagasse composites and sisal-bagasse composites results in a discrepancy in tan δ. In contrast, the difference in composites dynamic characteristics is yielded due to changes in the fiber angle. The greater value of tan δ is observed for sisal-bagasse fabric-reinforced epoxy hybrid composites, unlike the conventional composites (Sai et al. 2014).

Adding red mud helped establish the impact of various factors such as percentage weight and particle size in banana fiber-reinforced polyester composites with auxiliary reinforcing filler. The inherent modal characteristics and banana fiber-reinforced polyester composites show the highest damping properties by adding red mud as it comprises particles with a larger surface area. A decrease in natural frequency and tan δ is exhibited by silane-treated fibers that are added with red mud of particles with a size of 4 μm (Uthayakumar et al. 2014). Reduced biocomposite E′ is observed due to decreased stiffness of biocomposites, while an increase in fiber percentage corresponds to an increase in value to E′ (78 KPa). Observation through loss modulus revealed a shift of two T_g in composites. This behavior is due to including nanoclay that brings the fibers close to each other. This characteristic shows the similarity between nanoclay and biocomposites.

Moreover, the hybrid composites are characterized by less energy dispersion, as measured in the case of biocomposites. The bond between fiber and matrix enhances

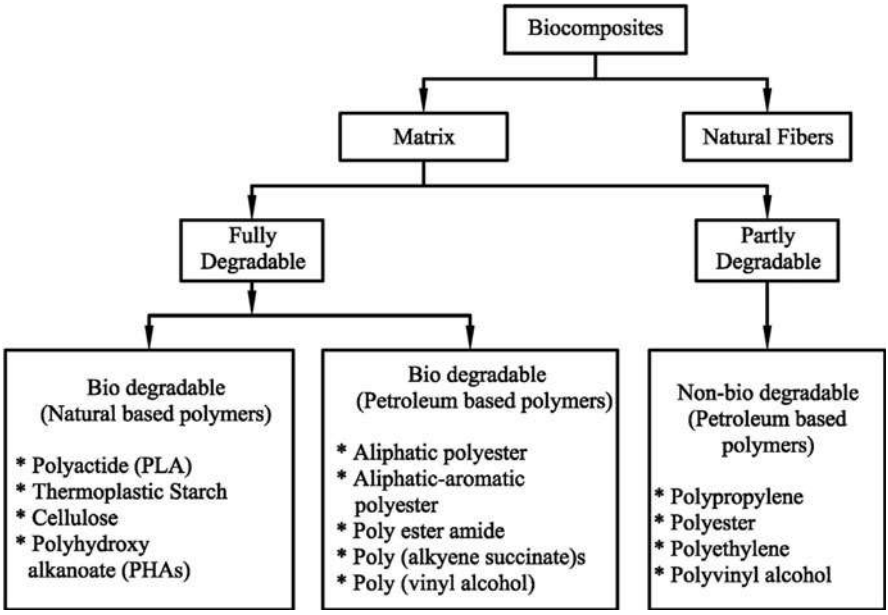

Fig. 7 Classifying biocomposite materials, considering the case of nanoclay (Ashok et al. 2019). (Copyright permission obtained)

after incorporating clay within biocomposites (Eng et al. 2014). Figure 7 provides the classification of biocomposites materials, considering the nanoclay case dispersed natural fiber hybrid interplay woven jute hybrid/banana polyester composites. The composite laminate, natural frequency improves till nano clay addition of 2 wt. %, whereas nanoclay content was higher than 2 wt.% would improve modular damping (Rajesh et al. 2016).

The fibers being treated with trichloro-vinyl silane and NaOH exhibit stress communication corresponding to tensile strength and impact strength within the hybrid and pure fibers (Fig. 7). Actual stacking can be achieved by splitting the coconut sheath layers in sisal for coconut sheath predominant hybrids and the sisal dominated hybrids. There is an increase in the natural frequency with independent hybrid fibers, sisal fiber composites, surface modified fibers, and coconut sheath for the pure and hybrid fibers. The order to enhance natural frequency for fiber composites is as follows: ST > CT > UT. The stiffness in the swan timber beans reinforced with glass fiber-reinforced polymers increases. They use the impressive reinforcements, providing a decrease in tan δ. Using glass-fiber-reinforced polymers offers favorable dynamic properties in reinforcements done by timber beams (Kumar et al. 2014; Bru et al. 2016).

Estimations were made for banana dynamic mechanical characteristics and jute woven polyester composites that hold fibers in a wavy pattern. The filaments are arranged like a wrap with weft angles in various compositions to study the impact of intra-ply hybridization. The jute and banana fibers hybridized with composites have shown enhancement in DMA properties with higher T_g values (Fig. 8). Moreover,

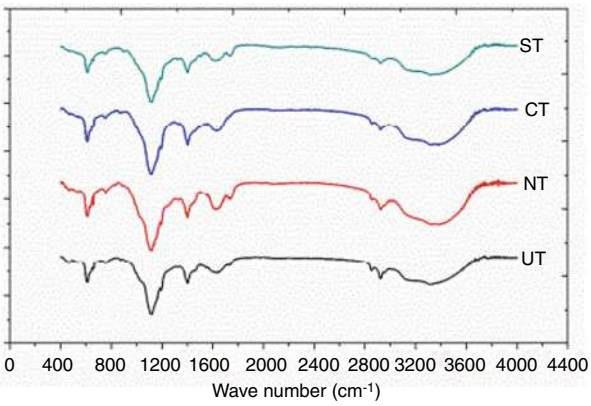

Fig. 8 The fibers treated with NaOH, $Ca(OH)_2$, and silane molecules (Kalusuraman et al. 2020). (Copyright permission obtained)

this favored higher dynamic mechanical properties, as associated with other combinations. Hybridization reinforcing natural fibers in a woven form increases the values of E′ and E″. The short and random fiber-oriented composites showed no change in their quantity of fiber loading.

Improving the sisal fibers weight fraction enhances E's value in the hybrid composite of jute and sisal fiber-reinforced epoxy resin. E′s value was observed to be equal to 2090 MPa for sisal fiber-reinforced epoxy composites and an equal 3500 MPa for jute fiber composites in the glassy region. The mobility within the matrix increases as there is an increase in the temperature; therefore, E″ in these composites increases in the initial phase, but later it decreases with increasing temperature. The decreased value of tan δ corresponds to the incorporation of an increased amount of sisal fibers. The hybrid composites were exhibited a good load-bearing capacity of the reinforced fibers (Huhtala et al. 2005). The higher value for E′ and E″ but a decrease in tan δ was detected in the vase of sisal and jute fiber reinforced with epoxy composites. The epoxy exhibits an increased value of tan δ that is 0.89, which favors better damping, unlike other composites (Gupta 2018).

The maximum natural frequency along different weight percentages was exhibited by sisal and banana fiber-reinforced polymer composites, which positively impacted material stiffness. The schematic presentation of different woven mats is shown in Figure 8 (Rajesh and Pitchaimani 2016). It is shown that the modulus of the material is expanded, and the composites' stiffness enhances as the result of surface modification (Rajesh et al. 2016). The DMA characteristics are studied for alkali-treated and alkali-untreated *Pennisetum purpureum* grass fiber and glass fiber-reinforced hybrid composites. It was displayed that the highest observation for E′ that is 4000 MPa, E″ that is 460 MPa, and tan δ 0.95 was recorded for alkali-treated *Pennisetum* glass-reinforced/purpureum composites, respectively. Moreover, compared to other combinations, the neat epoxy composites attained a high value of tan δ that is 0.88 (Dau et al. 2016).

In all the fiber composites, increasing temperature diminished nanofiller loading's impact on epoxy composites' E′ values. Including nanofiller in the epoxy composites

resulted in significant enhancement of E′, that is, 3700 MPa. Moreover, diminished E″ peak height was also observed for epoxy composites. An increase in internal fraction results in improved E″ height, which is evident through the epoxy hybrid nanocomposites' display. Among all the composite combinations, the epoxy composites showed an increased value of tan δ up to 0.44 (Saba et al. 2016).

The hybrid composites with equal proportions of sisal and jute fibers exhibited increased values for E′ and E″, along with a decrease in tan δ at a T_g of 80–100 °C and frequency of 1 Hz. This same pattern was followed for the frequency range of 5 and 10 Hz by jute and sisal fiber composites. The epoxy composites show the highest tan δ with no effect of change in temperature for different frequency ranges (1, 5, and 10 Hz) (Gupta 2017).

Analysis of intra-ply hybrid composites has also been done in which jute yarn and banana yarn are treated with potassium permanganate, saline, alkali, and benzoyl chloride. The treatment will include alkali, and benzoyl chloride has improved hybrid composites' DMA characteristics. The treating of the intra-ply fabric composites with benzoyl chloride significantly improved the natural frequency compared to other raw composites (Rajesh and Pitchaimani 2016).

Natural Fiber-Reinforced Composites

The DMA properties are evaluated to analyze composites with short sisal fibers and pure polystyrene. There is a decrease in E′ value with an escalation in segmental mobility as the temperature increases. The E′ value in these composites enhances by adding 10% of sisal fibers to the matrix and leveling off at peak loading. The natural fiber chemical adjustment enhances the adhesion between the matrix and the through benzoylation, which in turn shows a higher value of E, like the raw fiber composites. The activation energy for transition is expanded after matrix modification, with extreme transition observed for the benzoylated fabric composites. It is incorporating a higher percentage of fibers that results in diminished damping characteristics of the composites. As associated with the perfect PS matrix, the width of the damping peak of the composites was better, while the height of the damping peak for these composites was lower. It is shown that peaks are likely to fall, and the damping top width expands after fiber alterations (Nair et al. 2001). It is observed that 42 vol.% of fiber content in the jute fiber-reinforced epoxy composites shows the enhanced frequency and shear modulus, decreasing the log decrement. Similarly, an increase in jute fiber results' content enhances the growth of pure epoxy resin and jute composite materials (Bledzki and Zhang 2001).

Composite reinforcement with filaments increases E′ to 14.5 GPa and fiber loading by 35% to increase the interface's stress transfer. E's increased value corresponds to chemically modified fiber composites under standard temperature, as the temperature has a direct and significant impact on the concentrations within the composites. Surface treatment of natural fibers favors the bonding between the fiber and the resin (Ray et al. 2002).

The factors associated with the assessment of short sisal fiber-reinforced propylene composites' dynamic mechanical properties include fiber length, frequency, and impact of loading, temperature, and chemical modifications (Fig. 9). These composites are likely to exhibit increased values of E′ as the percentage of sisal fibers is increased. An increase in the fiber loading with a 2 mm fiber length higher dynamic modulus further increases the values of E′ and E″. Moreover, improved values of E′ and E″ have also been observed among the chemically modified sisal fiber composites. It is observed that these improved values create decent bonding between the fiber and matrix, unlike untreated ones (Joseph et al. 2003). The reinforcement volume fraction determines the value of the dynamic modulus of short banana fiber-reinforced polyester composites. This clarified the fact that the combination of fibers decreases the value of dynamic modulus. Improved properties selected as basic fiber loading were developed for 40% of the fiber loading that further expands the enhancement of attachment between the matrix and fiber. Supplementary peaks are perceived on tan δ curves because of the impact of interlaying (Fig. 10). The peak

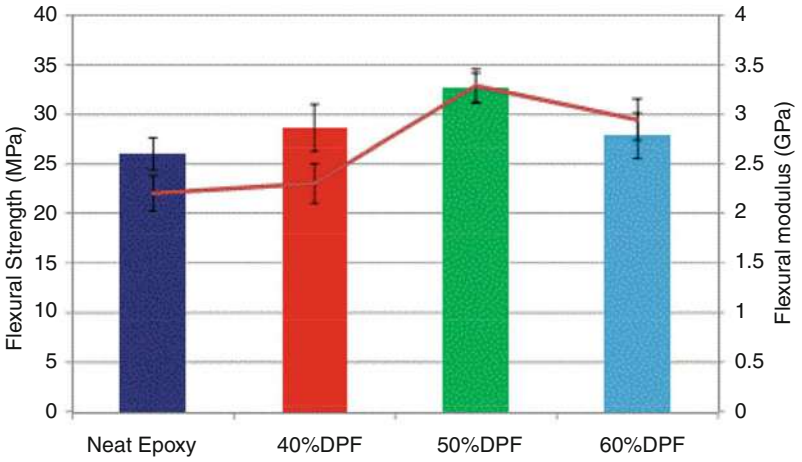

Fig. 9 Flexural strength loading impact and epoxy composites modulus (Gheith et al. 2019). (Copyright permission obtained)

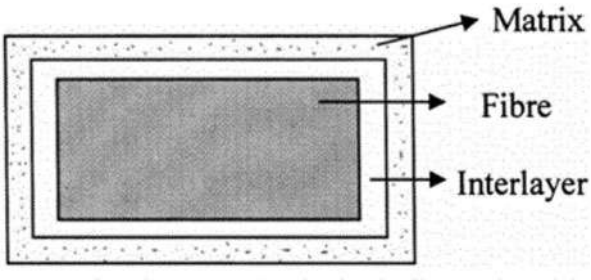

Fig. 10 Schematic presentation of interlaying (Devi et al. 2010). (Copyright permission obtained)

height of δ is further affected by adding more fibers as it further enhances the adhesion of matrix and fiber (Pothan et al. 2003).

Mechanical Properties of Synthetic Fiber Composites

The preparation of tensile test specimens for composite materials differs from that for ferrous, nonferrous, and polymeric materials. The standard tensile methods were recommended to use test specimen dimensions for composite materials according to fiber orientation. Figure 11 shows the tensile test specimen dimensions for composite materials according to ASTM D3039-17 based on type coupon with tabs. Specimens are cut from prepreg carbon fiber composites with a standard dimension of 250 × 25 × 3 mm; thickness, t = 3 mm; width, w = 25 mm; overall length, L_o = 250 mm; and gauge length, G = 138 mm. The rectangular cross-section tab area had the following dimensions: length = 56 mm, thickness = 1.5 mm, and bevel angle = 5°. The tab material is made from an aluminum plate with a tab thickness varying ±1%.

The mechanical properties Synthetic fiber composites mechanical properties along with thermal expansion coefficients of synthetic fibers observed in DMA analysis. The carbon nanotubes possess the lowest diameter, whereas the maximum diameter is observed in Kevlar fibers. Moreover, the SiC whiskers include the maximum value of tensile strength, unlike the carbon T 300 that includes the maximum tensile strength. SiC whiskers, unlike the high strength natural fiber nettle, are likely to exhibit about 300% of more tensile strength. For instance, the tensile strength possessed by SiC whiskers is much higher as compared to the tensile

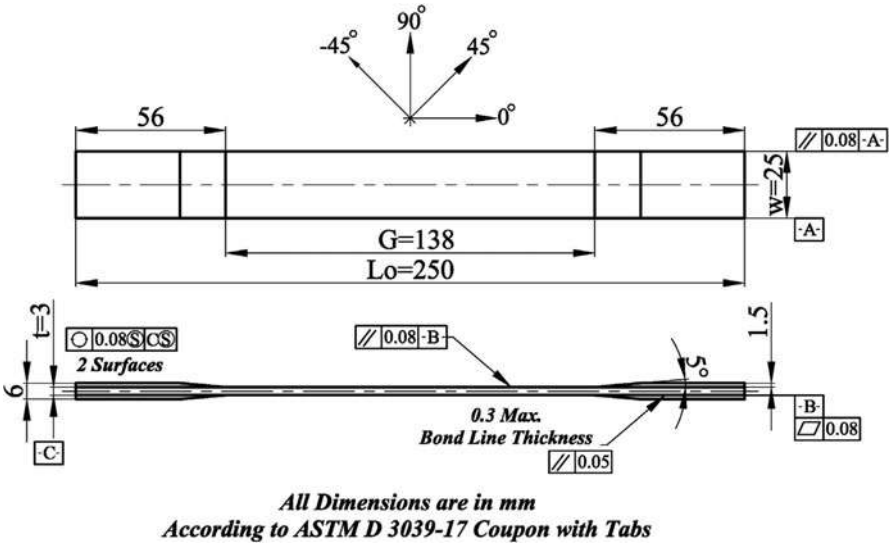

Fig. 11 Main dimensions of tensile test specimen used in composite materials, according to ASTM D3039-17

strengths of E-glass (50%), kevlar-49 (48%), carbon T-30 (47%), and S-glass (38%). E-glass and S-glass, respectively, show the maximum thermal expansion measure, the coefficient, and the percentage elongation. The synthetic fibers' mechanical properties are complementary compared to natural fibers and DMA experimental of synthetic carbon composite shown in Fig. 12.

The storage modulus has a typical glass transition curve, and the characteristic DMA curves are displayed loss modulus shown in Fig. 13. These elements were designed when each element chained atoms were the mechanical and laminate composites were tested and approved (Alarifi et al. 2016b, c). These elements are bonded together by a bond of synthetic carbon composite (Alarifi 2019).

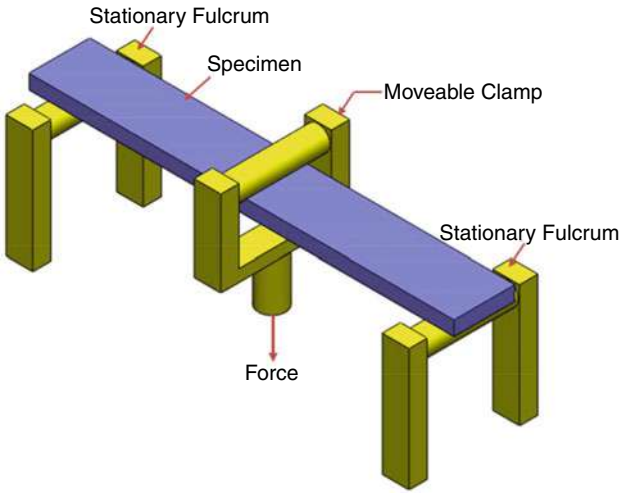

Fig. 12 Experimental setup specimen of solid carbon fiber composites mounted in a DMA three-point bending fixture (Alarifi 2020). (Copyright permission obtained)

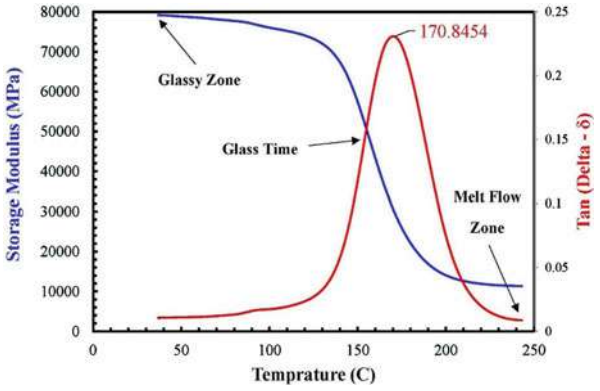

Fig. 13 Typical DMA curves of storage modulus and loss modulus of synthetic carbon fiber composites (Alarifi 2017). (From my Ph.D. dissertation)

Natural/Synthetic Fiber-Reinforced Thermosets Hybrid Composites

Recent investigations were performed to study the synthetic fiber effect on the natural fiber-reinforced mechanical properties with thermoset polymer composites. It is perceived that natural fibers' mechanical properties increase due to the incorporation of synthetic fiber in the natural fiber-reinforced thermoset composites. For instance, a combination of glass fibers in single natural fiber-reinforced thermoset composites increases their mechanical properties. AlMaadeed et al. (2012) have estimated tensile, chemical, and carbon/sisal fiber-reinforced polyester hybrid composites' flexural resistance properties. The outcomes depicted that hybrid composites incorporated with carbon fiber content result in increased tensile strength, tensile modulus, flexural strength, and flexural modulus. The glass fiber-reinforced composites' mechanical properties enhance through jute and sisal fiber (Pavithran et al. 1991). The maximum flexural load is exhibited by the glass, jute, and sisal composites. The maximum impact strength is exhibited by glass and sisal composites, while the maximum tensile strength is exhibited by glass and jute composites. Different types of composite materials are fabricated through the glass, jute, and abaca as reinforcement materials and epoxy matrix to increase flexural modulus, tensile modulus, and the composites reinforced with glass tensile strength, jute, and abaca, unlike the other composites (Ramnath et al. 2013). The maximum impact and flexural strength are also exhibited by the composites reinforced with glass, jute, and abaca.

Natural/Synthetic Fiber-Reinforced Thermoplastic Hybrid Composite

Nearby is a positive impact of hybridization on natural fibers' mechanical properties reinforced with thermoplastic polymer composites through synthetic fiber loading. Arthanarieswaran et al. (2014) have focused on the banana and glass fiber hybrid composites' mechanical properties with reinforced propylene. A hybrid composite is prepared through the molding process, in which different weight fraction fibers are injected. The test results showed that the combination of glass fibers within the propylene matric improved the prepared composites' mechanical properties. The tensile strength of composites is maximum for 7.5 wt.% of the fiber composites. Composites with 11wt.% of the fibers exhibit maximum flexural strength and impact strength. The maximum value of 24.59 MPa for tensile strength, 29.37 J/m for impact strength, and 227.81 MPa for flexural strength correspond to the values of 3%, 53%, and 19% for propylene matrix, respectively. The date palm glass fiber/wood flour hybrid composites reinforced with polypropylene are injected with date palm wood flour and E-glass fibers of various wt.%. There is an increase in pal polypropylene composites' tensile and modulus strength after reinforcement with glass fibers (Srinivasan et al. 2014).

Moreover, adding 5% of the glass fiber escalations the of the date palm propylene composites tensile strength by 18%. This presentation clearly shows that incorporating synthetic fibers increases the natural fiber-reinforced mechanical properties in thermoplastic composites.

Natural/Natural Fiber-Reinforced Mechanical Properties of Hybrid Composites

The natural fiber-reinforced synthetic fiber composites study obtained the mechanical properties composites mechanical properties escalation by incorporating natural fibers with comparable high elongation. The investigation of unidirectional stalk fiber/jute fiber-reinforced polyester matrix composites showed that their mechanical properties increase after adding jute fibers. Hybrid composites P50J50 exhibit increased flexural strength by 28% and the tensile strength by 11%, unlike the pal polyester composites (Fernandes et al. 2013). Similarly, the investigation of jute and banana fiber-reinforced epoxy hybrid composites revealed that their mechanical properties increase due to hybridization with jute fibers (Mishra et al. 2003). The human layup technique is used for preparing jute and banana fibers of different weight ratios, with constant wt. of the fiber at 30%. The highest measure of the mechanical properties is exhibited by a weight ratio of 50/50 of the composites. It is showed that the composite flexural strength J50B50 increased by 4.3%, tensile strength by 17%, and impact strength by 35.5%, unlike the jute epoxy composites. The sisal/banana reinforced epoxy composites mechanical properties are studied after the fabrication (da Silva et al. 2012). The maximum measure is flexural strength and tensile strength; the impact strength is exhibited by composite S50B50. As associated with the banana epoxy composites, the composite S50B50 shows improved flexural strength by 4%, tensile strength by 16%, and impact strength by 35%. The hand layup technique is used to prepare the woven jute and banana hybrid composites, whose flexural strength and tensile strength are better than those of an individual composite (Ahmed and Vijayarangan 2008; Zhang et al. 2013). As compared to other composites, the banana and jute hybrid composite's impact strength was found to be maximum. Moreover, better flexural and impact properties are exhibited by banana epoxy and flax hybrid composites arranged using the hand layup technique, unlike the glass-reinforced epoxy composites.

Natural/Natural Fiber-Reinforced Thermoplastic Hybrid Composites

The analysis of hybrid sisal/banana-reinforced polylactic acid composites showed that their mechanical properties increase due to incorporating banana fiber PLA composite to high strength sisal fibers (Khanam et al. 2010). However, this is not the case with banana-reinforced PLA and the neat PLA composite. The tensile modulus of hybrid sisal/banana composites improves by 40%, and tensile strength for hybrid sisal/banana composites improves by 21%. The study on agave fibers observed the reinforced high-density, and hybrid pine polyethylene composites presented that flexural strength, tensile strength, and pine high-density polyethylene composite impact strength increase agave fibers (Singh et al. 1995). Composites can also be prepared with 40 wt.% of fibers by the compression molding method. The natural fibers, including cotton, hemp, and kenaf, are used to analyze the PLA-based hybrid human-made fibers' mechanical properties, known as lyocell (Narendar et al. 2014).

Using hemp a mixture and lyocell increased the impact strength, elongation at break, and tensile strength, unlike the hemp-PLA composites. The injection molding method is used to study hybrid composites of synthetic cellulose and jute with polypropylene (Tzounis et al. 2014). It is shown that hybrid composites with 75 wt.% of Cordenka and 25 wt.% of jute exhibit better mechanical properties, unlike composites.

Synthetic/Synthetic Fiber-Reinforced Polymer Hybrid Composites

There is no substantial development in the reinforced polymer composites' mechanical properties after adding synthetic fiber (Alarifi et al. 2018). There is no improvement in the mechanical properties of carbon/glass-reinforced epoxy hybrid composites, unlike other composites' mechanical properties (Atiqah et al. 2014). The study about T77S carbon and E-glass fiber-reinforced epoxy composites showed that they are arranged through the hand layup method. Whereas, three-point bending test, according to ASTM D790-07, is used to study these composites the flexural properties (Naik et al. 2001).

It is shown that the hybridization process has no impact on improving the flexural strength; however, hybridization positively impacts the stimulation. It is also depicted that additional carbon nanotube reinforcement in the composites improves the flexural strength and the composites flexural modulus (Isa et al. 2013; Alarifi et al. 2015d, 2021).

Conclusions

The natural fibers and synthetic fiber are reinforced in the polymer matrix through various methods, such as bidirectional, unidirectional, and women mat form, or random orientation. Fibers of different weights and volume fractions are used for preparing composites through other manufacturing techniques. The most popular manufacturing techniques include human layup and compression molding techniques. Hybridization increases the single fiber-reinforced polymer composites' mechanical properties as it reduces its limitations. Moreover, the mechanical properties of natural fibers reinforced with polymer composites are increased through the combination of natural or synthetic fiber with comparable increased elongation properties. The main advantages of natural fibers are low density, recyclability, low cost, abundant availability, and eco-friendly nature. Moreover, synthetic fibers are replaced with natural fibers based on their distinct mechanical properties. The use of predictable materials is replaced with artistic materials because of issues in their density, chemical communications, availability, weight ratio, and use of matrix in the composites. It is shown that the majority of the natural fibers, such as sisal, pineapple leaf branches, jute, hemp, pine, and coconut sheath, are used as reinforcement materials. On the other hand, the natural fibers' main features are likely to build up a good association with the matrix. Hybridization plays an important role in

attaining new types of composite materials. Therefore, the performance of prepared composites boosts up by using natural and human-made fibers. The phase variations along with temperatures and variable frequency are measured through the technique known as DMA. It is shown that DMA test plays a significantly important role in searching for DMA properties, such as E′, damping, material behavior, and loss modulus. Some of the factors affecting the behavior for the dynamic mechanical properties of composite materials are the shape and size of the fibers, stacking sequences, fiber contented, and fibers' orientation. There is also a need to note the variation in natural frequencies and other dynamic mechanical properties of chemically treated composites. Therefore, it would not be wrong to conclude that DMA test plays a critical role in predicting the dynamic mechanical parameters. DMA is associated with fiber composites that ensure its design, safety, and replacements in various automobile parts and other structural parts. This chapter has clearly shown that natural fiber-reinforced composites' dynamic mechanical characteristics are far better than the human-made fiber composites. Therefore, it is stated that the use of normal or natural fiber composites is favored, rather than using human-made fibers in several industrial applications.

References

K.S. Ahmed, S. Vijayarangan, Tensile, flexural and interlaminar shear properties of woven jute and jute–glass fabric reinforced polyester composites. J. Mater. Process. Technol. **207**(1–3), 330–335 (2008)

I.M. Alarifi, Fabrication and characterization of electrospun polyacrylonitrile carbonized fibers as strain gauges in composites for structural health monitoring applications. Doctoral dissertation, Wichita State University (2017)

I.M. Alarifi, Investigation the conductivity of carbon fiber composites focusing on measurement techniques under dynamic and static loads. J. Mater. Res. Technol. **8**(5), 4863–4893 (2019)

I.M. Alarifi, Structural analysis of hexagonal and solid carbon fibers composite. Polym. Test. **84**, 106392 (2020)

I.M. Alarifi, Fabrication and characterization of Neem leaves waste material reinforced composites. Mater. Today: Proc. **47**(17), 5946–5954 (2021)

I.M. Alarifi, A. Alharbi, W.S. Khan, R. Asmatulu, Electrospun carbon nanofibers for improved electrical conductivity of fiber reinforced composites. In Electroactive polymer actuators and devices (EAPAD). International Society for Optics and Photonics, vol 9430, pp 943032 (2015a)

I.M. Alarifi, A. Alharbi, W.S. Khan, R. Asmatulu, Electrospun nanofibers for improved electrical conductivity of fiber reinforced composites. In SPIE smart structures/non-destructive evaluation conference, pp 8–12 (2015b)

I.M. Alarifi, A. Alharbi, W. Khan, R. Asmatulu, Structural health monitoring of composite aircraft. Adv. Mater. Sci. Res. **21**, 111–132 (2015c)

I.M. Alarifi, A. Alharbi, W.S. Khan, A. Swindle, R. Asmatulu, Thermal, electrical and surface hydrophobic properties of electrospun polyacrylonitrile nanofibers for structural health monitoring. Materials **8**(10), 7017–7031 (2015d)

I.M. Alarifi, A. Alharbi, W. Khan, R. Asmatulu, Carbonized electrospun polyacrylonitrile nanofibers as highly sensitive sensors in structural health monitoring of composite structures. J. Appl. Polym. Sci. **133**(13), 43235 (2016a)

I.M. Alarifi, W.S. Khan, A.S. Rahman, Y. Kostogorova-Beller, R. Asmatulu, Synthesis, analysis and simulation of carbonized electrospun nanofibers infused carbon prepreg composites for improved mechanical and thermal properties. Fibers Polym. **17**(9), 1449–1455 (2016b)

I.M. Alarifi, A. Alharbi, W.S. Khan, A.S. Rahman, R. Asmatulu, Mechanical and thermal properties of carbonized PAN nanofibers cohesively attached to surface of carbon fiber reinforced composites. Macromol. Symp. **365**(1), 140–150 (2016c)

I.M. Alarifi, W.S. Khan, R. Asmatulu, Synthesis of electrospun polyacrylonitrile-derived carbon fibers and comparison of properties with bulk form. PLoS One **13**(8), e0201345 (2018)

I. Alarifi, B. Prasad, M.K. Uddin, Conducting polymer membranes and their applications, in *Self-Standing Substrates*, (Springer, Cham, 2020), pp. 147–176

M.A. AlMaadeed, R. Kahraman, P.N. Khanam, N. Madi, Date palm wood flour/glass fiber reinforced hybrid composites of recycled polypropylene: mechanical and thermal properties. Mater. Des. **42**, 289–294 (2012)

V.P. Arthanarieswaran, A. Kumaravel, M. Kathirselvam, Evaluation of mechanical properties of banana and sisal fiber reinforced epoxy composites: influence of glass fiber hybridization. Mater. Des. **64**, 194–202 (2014)

R.B. Ashok, C.V. Srinivasa, B. Basavaraju, Dynamic mechanical properties of natural fiber composites – a review. Adv. Compos. Hybrid Mater. **2**, 1–22 (2019)

A. Athijayamani, M. Thiruchitrambalam, U. Natarajan, B. Pazhanivel, Effect of moisture absorption on the mechanical properties of randomly oriented natural fibers/polyester hybrid composite. Mater. Sci. Eng. A **517**(1–2), 344–353 (2009)

A. Atiqah, M.A. Maleque, M. Jawaid, M. Iqbal, Development of kenaf-glass reinforced unsaturated polyester hybrid composite for structural applications. Compos. Part B Eng. **56**, 68–73 (2014)

A.K. Bledzki, W. Zhang, Dynamic mechanical properties of natural fiber-reinforced epoxy foams. J. Reinf. Plast. Compos. **20**(14–15), 1263–1274 (2001)

K.M. Bogren, E.K. Gamstedt, R.C. Neagu, M. AÅkerholm, M. LindstroÖm, Dynamic–mechanical properties of wood–fiber reinforced polylactide: experimental characterization and micromechanical modeling. J. Thermoplast. Compos. Mater. **19**(6), 613–637 (2006)

M. Boopalan, M. Niranjanaa, M.J. Umapathy, Study on the mechanical properties and thermal properties of jute and banana fiber reinforced epoxy hybrid composites. Compos. Part B Eng. **51**, 54–57 (2013)

D. Bru, F.J. Baeza, F.B. Varona, J. Garcia-Barba, S. Ivorra, Static and dynamic properties of retrofitted timber beams using glass fiber reinforced polymers. Mater. Struct. **49**(1–2), 181–191 (2016)

L.J. da Silva, T.H. Panzera, V.R. Velloso, A.L. Christoforo, F. Scarpa, Hybrid polymeric composites reinforced with sisal fibers and silica microparticles. Compos. Part B Eng. **43**(8), 3436–3444 (2012)

F. Dau, M.L. Dano, Y. Duplessis-Kergomard, Experimental investigations and variability considerations on 3D interlock textile composites used in low velocity soft impact loading. Compos. Struct. **153**, 369–379 (2016)

L.U. Devi, S.S. Bhagawan, S. Thomas, Dynamic mechanical analysis of pineapple leaf/glass hybrid fiber reinforced polyester composites. Polym. Compos. **31**(6), 956–965 (2010)

L. Di Landro, W. Lorenzi, Mechanical properties and dynamic mechanical analysis of thermoplastic-natural fiber/glass reinforced composites. Macromol. Symp. **286**(1), 145–155 (2009)

M. Eesaee, A. Shojaei, Effect of nanoclays on the mechanical properties and durability of novolac phenolic resin/woven glass fiber composite at various chemical environments. Compos. A: Appl. Sci. Manuf. **63**, 149–158 (2014)

C.C. Eng, N.A. Ibrahim, N. Zainuddin, H. Ariffin, W.M. Yunus, Z. Wan, Y.Y. Then, Enhancement of mechanical and dynamic mechanical properties of hydrophilic nanoclay reinforced polylactic acid/polycaprolactone/oil palm mesocarp fiber hybrid composites. Int. J. Polym. Sci. **2014**, 715801 (2014)

E.M. Fernandes, J.F. Mano, R.L. Reis, Hybrid cork–polymer composites containing sisal fiber: morphology, effect of the fiber treatment on the mechanical properties and tensile failure prediction. Compos. Struct. **105**, 153–162 (2013)

D. Gay, *Composite Materials: Design and Applications* (CRC Press, Boca Raton, 2014)
M.H. Gheith, M.A. Aziz, W. Ghori, N. Saba, M. Asim, M. Jawaid, O.Y. Alothman, Flexural, thermal and dynamic mechanical properties of date palm fibers reinforced epoxy composites. J. Mater. Res. Technol. **8**(1), 853–860 (2019)
M.K. Gupta, Effect of frequencies on dynamic mechanical properties of hybrid jute/sisal fiber reinforced epoxy composite. Adv. Mater. Process. Technol. **3**(4), 651–664 (2017)
M.K. Gupta, Thermal and dynamic mechanical analysis of hybrid jute/sisal fiber reinforced epoxy composite. Proc. Inst. Mech. Eng. L J. Mater. Des. Appl. **232**(9), 743–748 (2018)
M.K. Gupta, A. Bharti, Natural fiber reinforced polymer composites: a review on dynamic mechanical properties. Curr Trends Fash. Technol. Text. Eng. **1**, 1–4 (2017)
M.K. Gupta, R.K. Srivastava, Mechanical properties of hybrid fibers-reinforced polymer composite: a review. Polym.-Plast. Technol. Eng. **55**(6), 626–642 (2016)
M.S. Huda, L.T. Drzal, A.K. Mohanty, M. Misra, Chopped glass and recycled newspaper as reinforcement fibers in injection molded poly (lactic acid) (PLA) composites: a comparative study. Compos. Sci. Technol. **66**(11–12), 1813–1824 (2006)
M.S. Huda, L.T. Drzal, A.K. Mohanty, M. Misra, Effect of fiber surface-treatments on the properties of laminated biocomposites from poly (lactic acid) (PLA) and kenaf fibers. Compos. Sci. Technol. **68**(2), 424–432 (2008)
M. Huhtala, J. Heino, D. Casciari, A. de Luise, M.S. Johnson, Integrin evolution: insights from ascidian and teleost fish genomes. Matrix Biol. **24**(2), 83–95 (2005)
M.T. Isa, A.S. Ahmed, B.O. Aderemi, R.M. Taib, I.A. Mohammed-Dabo, Effect of fiber type and combinations on the mechanical, physical and thermal stability properties of polyester hybrid composites. Compos. Part B Eng. **52**, 217–223 (2013)
M. Jacob, B. Francis, S. Thomas, K.T. Varughese, Dynamical mechanical analysis of sisal/oil palm hybrid fiber-reinforced natural rubber composites. Polym. Compos. **27**(6), 671–680 (2006)
M. Jawaid, H.A. Khalil, A. Hassan, R. Dungani, A. Hadiyane, Effect of jute fiber loading on tensile and dynamic mechanical properties of oil palm epoxy composites. Compos. Part B Eng. **45**(1), 619–624 (2013)
P.V. Joseph, G. Mathew, K. Joseph, G. Groeninckx, S. Thomas, Dynamic mechanical properties of short sisal fiber reinforced polypropylene composites. Compos. A: Appl. Sci. Manuf. **34**(3), 275–290 (2003)
M.M. Kabir, H. Wang, K.T. Lau, F. Cardona, Chemical treatments on plant-based natural fiber reinforced polymer composites: an overview. Compos. Part B Eng. **43**(7), 2883–2892 (2012)
G. Kalusuraman, I. Siva, Y. Munde, C.P. Selvan, S.A. Kumar, S.C. Amico, Dynamic-mechanical properties as a function of luffa fiber content and adhesion in a polyester composite. Polym. Test. **87**, 106538 (2020)
P.N. Khanam, H.A. Khalil, M. Jawaid, G.R. Reddy, C.S. Narayana, S.V. Naidu, Sisal/carbon fiber reinforced hybrid composites: tensile, flexural and chemical resistance properties. J. Polym. Environ. **18**(4), 727–733 (2010)
K.S. Kumar, I. Siva, N. Rajini, P. Jeyaraj, J.W. Jappes, Tensile, impact, and vibration properties of coconut sheath/sisal hybrid composites: effect of stacking sequence. J. Reinf. Plast. Compos. **33**(19), 1802–1812 (2014)
C.A. Lehr, C.S. Tan, J. Ysseldyke, Alternative schools: a synthesis of state-level policy and research. Remedial Spec. Educ. **30**(1), 19–32 (2009)
K. Majeed, M. Jawaid, A.A.B..A.A. Hassan, A.A. Bakar, H.A. Khalil, A.A. Salema, I. Inuwa, Potential materials for food packaging from nanoclay/natural fibers filled hybrid composites. Mater. Des. **46**, 391–410 (2013)
S. Mandal, S. Alam, Dynamic mechanical analysis and morphological studies of glass/bamboo fiber reinforced unsaturated polyester resin based hybrid composites. J. Appl. Polym. Sci. **125**(S1), E382–E387 (2012)
S. Mishra, A.K. Mohanty, L.T. Drzal, M. Misra, S. Parija, S.K. Nayak, S.S. Tripathy, Studies on mechanical performance of biofiber/glass reinforced polyester hybrid composites. Compos. Sci. Technol. **63**(10), 1377–1385 (2003)

N.K. Naik, R. Ramasimha, H.E.M.E.N.D.R.A. Arya, S.V. Prabhu, N. ShamaRao, Impact response and damage tolerance characteristics of glass–carbon/epoxy hybrid composite plates. Compos. Part B Eng. **32**(7), 565–574 (2001)

K.M. Nair, S. Thomas, G. Groeninckx, Thermal and dynamic mechanical analysis of polystyrene composites reinforced with short sisal fibers. Compos. Sci. Technol. **61**(16), 2519–2529 (2001)

R. Narendar, K.P. Dasan, M. Nair, Development of coir pith/nylon fabric/epoxy hybrid composites: mechanical and ageing studies. Mater. Des. **54**, 644–651 (2014)

S.K. Nayak, S. Mohanty, S.K. Samal, Influence of short bamboo/glass fiber on the thermal, dynamic mechanical and rheological properties of polypropylene hybrid composites. Mater. Sci. Eng. A **523**(1–2), 32–38 (2009)

Y. Okahisa, K. Abe, M. Nogi, A.N. Nakagaito, T. Nakatani, H. Yano, Effects of delignification in the production of plant-based cellulose nanofibers for optically transparent nanocomposites. Compos. Sci. Technol. **71**(10), 1342–1347 (2011)

H.L. Ornaghi Jr., A.S. Bolner, R. Fiorio, A.J. Zattera, S.C. Amico, Mechanical and dynamic mechanical analysis of hybrid composites molded by resin transfer molding. J. Appl. Polym. Sci. **118**(2), 887–896 (2010)

H.L. Ornaghi Jr., H.S.P. da Silva, A.J. Zattera, S.C. Amico, Hybridization effect on the mechanical and dynamic mechanical properties of curaua composites. Mater. Sci. Eng. A **528**(24), 7285–7289 (2011)

C. Pavithran, P.S. Mukherjee, M. Brahmakumar, A.D. Damodaran, Impact properties of sisal-glass hybrid laminates. J. Mater. Sci. **26**(2), 455–459 (1991)

L.A. Pothan, Z. Oommen, S. Thomas, Dynamic mechanical analysis of banana fiber reinforced polyester composites. Compos. Sci. Technol. **63**(2), 283–293 (2003)

L.A. Pothan, P. Potschke, R. Habler, S. Thomas, The static and dynamic mechanical properties of banana and glass fiber woven fabric-reinforced polyester composite. J. Compos. Mater. **39**(11), 1007–1025 (2005)

M. Rajesh, J. Pitchaimani, Dynamic mechanical analysis and free vibration behavior of intra-ply woven natural fiber hybrid polymer composite. J. Reinf. Plast. Compos. **35**(3), 228–242 (2016)

M. Rajesh, P. Jeyaraj, N. Rajini, Mechanical, dynamic mechanical and vibration behavior of nanoclay dispersed natural fiber hybrid intra-ply woven fabric composite, in *Nanoclay Reinforced Polymer Composites*, (Springer, Singapore, 2016), pp. 281–296

N. Rajini, J.W. Jappes, S. Rajakarunakaran, P. Jeyaraj, Dynamic mechanical analysis and free vibration behavior in chemical modifications of coconut sheath/nano-clay reinforced hybrid polyester composite. J. Compos. Mater. **47**(24), 3105–3121 (2013)

B.V. Ramnath, S.J. Kokan, R.N. Raja, R. Sathyanarayanan, C. Elanchezhian, A.R. Prasad, V.M. Manickavasagam, Evaluation of mechanical properties of abaca–jute–glass fiber reinforced epoxy composite. Mater. Des. **51**, 357–366 (2013)

D. Ray, B.K. Sarkar, S. Das, A.K. Rana, Dynamic mechanical and thermal analysis of vinylester-resin-matrix composites reinforced with untreated and alkali-treated jute fibers. Compos. Sci. Technol. **62**(7–8), 911–917 (2002)

D. Romanzini, A. Lavoratti, H.L. Ornaghi Jr., S.C. Amico, A.J. Zattera, Influence of fiber content on the mechanical and dynamic mechanical properties of glass/ramie polymer composites. Mater. Des. **47**, 9–15 (2013)

N. Saba, M.T. Paridah, K. Abdan, N.A. Ibrahim, Dynamic mechanical properties of oil palm nano filler/kenaf/epoxy hybrid nanocomposites. Constr. Build. Mater. **124**, 133–138 (2016)

A.K. Saha, S. Das, D. Bhatta, B.C. Mitra, Study of jute fiber reinforced polyester composites by dynamic mechanical analysis. J. Appl. Polym. Sci. **71**(9), 1505–1513 (1999)

N.V. Sai, P.N. Kishore, C.P. Kumar, Investigation on dynamic behaviour of hybrid sisal/bagasse fiber reinforced epoxy composites. Int. J. Innov. Res. Adv. Eng. **1**, 357–360 (2014)

F.M. Salleh, A. Hassan, R. Yahya, A.D. Azzahari, Effects of extrusion temperature on the rheological, dynamic mechanical and tensile properties of kenaf fiber/HDPE composites. Compos. Part B Eng. **58**, 259–266 (2014)

S.K. Samal, S. Mohanty, S.K. Nayak, Polypropylene – bamboo/glass fiber hybrid composites: fabrication and analysis of mechanical, morphological, thermal, and dynamic mechanical behavior. J. Reinf. Plast. Compos. **28**(22), 2729–2747 (2009)

D.A. Saravanos, J.M. Pereira, Effects of interply damping layers on the dynamic characteristics of composite plates. AIAA J. **30**(12), 2906–2913 (1992)

K. Sen, K. Babu, M., Studies on Indian silk. I. Macrocharacterization and analysis of amino acid composition. J. Appl. Polym. Sci. **92**(2), 1080–1097 (2004)

H. Sezgin, O.B. Berkalp, R. Mishra, J. Militky, Investigation of dynamic mechanical properties of jute/carbon reinforced composites. Composites **14**, 19 (2016)

B. Singh, M. Gupta, A. Verma, Mechanical behaviour of particulate hybrid composite laminates as potential building materials. Constr. Build. Mater. **9**(1), 39–44 (1995)

M.S. Sreekala, J. George, M.G. Kumaran, S. Thomas, The mechanical performance of hybrid phenol-formaldehyde-based composites reinforced with glass and oil palm fibers. Compos. Sci. Technol. **62**(3), 339–353 (2002)

V.S. Srinivasan, S.R. Boopathy, D. Sangeetha, B.V. Ramnath, Evaluation of mechanical and thermal properties of banana–flax based natural fiber composite. Mater. Des. **60**, 620–627 (2014)

V.K. Thakur, M.K. Thakur, R.K. Gupta, Raw natural fiber-based polymer composites. Int. J. Polym. Anal. Charact. **19**(3), 256–271 (2014)

L. Tzounis, S. Debnath, S. Rooj, D. Fischer, E. Mäder, A. Das, M. Stamm, G. Heinrich, High performance natural rubber composites with a hierarchical reinforcement structure of carbon nanotube modified natural fibers. Mater. Des. **58**, 1–11 (2014)

M. Uthayakumar, V. Manikandan, N. Rajini, P. Jeyaraj, Influence of red mud on the mechanical, damping and chemical resistance properties of banana/polyester hybrid composites. Mater. Des. **64**, 270–279 (2014)

N.J. Vickers, Animal communication: when I'm calling you, will you answer too? Curr. Biol. **27**(14), R713–R715 (2017)

B. Wielage, T. Lampke, H. Utschick, F. Soergel, Processing of natural-fiber reinforced polymers and the resulting dynamic–mechanical properties. J. Mater. Process. Technol. **139**(1–3), 140–146 (2003)

L. Yan, N. Chouw, K. Jayaraman, Flax fiber and its composites – a review. Compos. Part B Eng. **56**, 296–317 (2014)

Y. Zhang, Y. Li, H. Ma, T. Yu, Tensile and interfacial properties of unidirectional flax/glass fiber reinforced hybrid composites. Compos. Sci. Technol. **88**, 172–177 (2013)

Interface and Interphase in Carbon Nanotube-Based Polymer Composites

7

A Review

Harpreet S. Bedi and Prabhat K. Agnihotri

Contents

Abstract

The average mechanical properties of carbon fiber-reinforced polymer composites (CFRP) primarily depend on the properties of the constituents and the interaction between them. The strength of interaction is related to the extent of interface surrounding the fiber. Enhancing the interfacial area is one of the strategies to improve the interfacial strength and hence average mechanical properties of CFRP. To this end, a review is presented on the conventional and advanced approaches followed to improve the interfacial interaction. The advanced methods include the incorporation of nanofiller such as carbon nanotubes in the composite which act as secondary reinforcement in addition to the

H. S. Bedi (✉) · P. K. Agnihotri
Department of Mechanical Engineering, Indian Institute of Technology Ropar, Rupnagar, Punjab, India
e-mail: harpreet.bedi@iitrpr.ac.in; hsbedi88@gmail.com; prabhat@iitrpr.ac.in

S. Mavinkere Rangappa et al. (eds.), *Handbook of Epoxy/Fiber Composites*,
https://doi.org/10.1007/978-981-19-3603-6_9

primary fiber reinforcement. This is followed by a discussion on the importance of interphase region (a region having distinct properties from fiber and matrix) and the ways to process and characterize the same.

Keywords

Carbon fiber · Carbon nanotube · CFRP · Interface · Interphase · Multiscale and hybrid composite

Introduction

It is rightly quoted that technological and design developments are of no use without the availability of appropriate materials and "composite materials in this regard represent nothing but a giant step in the ever-constant endeavor of optimization in materials" (Chawla 2012). The term composite generally refers to materials that are processed with two or more components having significantly different physical and/or chemical properties. As per the context of this work, the emphasis is on polymer-based composites which consist of a polymer matrix reinforced with one or more different phases (in the form of fibers or micro- to nano-size particles) which are harder and stronger than the matrix. Both the matrix and filler have limited practical significance individually and hence are often combined together to make a composite in which the polymer matrix acts as a binder to hold the filler material together. Apart from this, the matrix transmits the applied load to the reinforcing filler which acts as the primary load carrying member in the composite. Therefore, the overall properties of a composite are a function of the properties of the constituents and the strength of their interaction. Consequently, the processed composite has characteristics not shown by any of the constituents in isolation. Because of their excellent specific properties, the reinforced polymer composites are finding increased use in the modern-day engineering. It is of no doubt that reinforced polymer composites hold the potential to fulfill the ever-widening scope of advanced applications. This can be achieved by choosing a right combination of the filler and matrix materials as per the requirements of an application.

At this point, it is extremely important to appreciate the inevitability of optimization in composite materials. This is because any deviation from the optimal performance would mean compensation in terms of either an increased weight or a reduced load carrying capacity of the composite. Of course, the choice of constituents (filler and matrix) available is the first thing to figure out the perfect match between the filler and matrix; the options available are still limited based on the demand, practicality, and ease of manufacturing. Although a lot of research is going on in the field of filler-reinforced polymer composites, one cannot ignore the existence of certain fixed classes such as glass fiber/polyester for furniture, electronics, boats, and automobile bumpers; carbon fiber/epoxy for aerospace and jet engines; and aramid fibers for ballistic protection armors, among others. The issue is, therefore, not just to find alternatives for the current set of composites (and their constituents) being used in

an industry; rather, the bigger challenge is to find ways to enhance the performance level of composites so as to fit them in a wider variety of applications.

Strength, stiffness, fracture toughness, and energy damping are the major requirements of structural load bearing components. Since the inherent properties of polymers are not up to the level of structural applications, the solution lies in reinforcing the polymer with some kind of filler material. Fiber-reinforced plastics (FRP) are the leading candidates that can offer high specific mechanical properties compared to their metal counterparts. Basically there are two broad categories of fibers to choose from: natural fibers (e.g., jute, hemp, wood, straw, rice husk, sisal, kenaf, and flax) and synthetic fibers (e.g., carbon, glass, aramid, boron, ceramic) (Chawla 2012). While the natural fiber composites are considered inappropriate for high stress conditions, the high-performance synthetic fibers are recommended for highly sophisticated areas like aircraft wings, helicopter rotor, wind turbine blades, etc. (Chawla 2012). Taking into account the functional requirements of such advanced applications, carbon fiber-reinforced polymer composites or carbon fiber-reinforced plastics (CFRP) are ahead of the other available options. This is due to the presence of strong carbon-carbon covalent bonds along the longitudinal direction of a carbon fiber and weak van der Waals forces between the graphite layers in the transverse direction of the fiber, making the fiber stiff and strong yet highly flexible (Soutis 2005). Due to their excellent structural properties such as high aspect ratio (length/diameter), high flexibility, lower imperfections owing to their small size, high resistance to corrosion, and fatigue failure (Chawla 2012), CFRP have not only served but have also assisted in the growth of a wide variety of industrial sectors like aeronautical and aerospace, automotive, high-speed trains, marine, military, sports, wind energy, civil infrastructure, pressure vessels, biomedical prosthetics, etc. (Kessler 2012). The tremendous potential held by FRP can be imagined from the fact that more than 50 wt% of modern aircrafts include composite materials in their fabrication (Kessler 2012). In all these real-world applications, CFRP are present in the form of laminated structural plates consisting of multiple layers (or laminas or plies) of fibers, with fibers in each lamina oriented in a particular direction (Fig. 1).

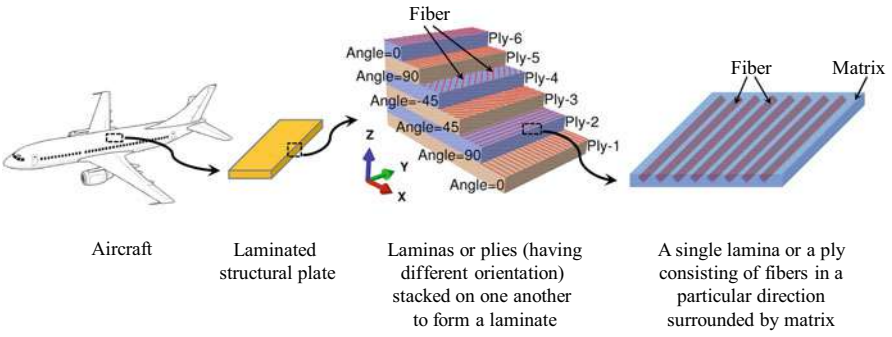

Fig. 1 Analysis of an aircraft structural member made of laminated composite. (Image source for aircraft: dumielauxepices.net)

Interface

In spite of their advantages and wide applicability, CFRP suffer from some limitations as well. Because of excellent properties in one direction and weak in other, there exists a high level of anisotropy in carbon fibers. This results in a mismatch of properties at the interface of individual fiber and matrix and also at the lamina/matrix interface. As a consequence of sudden change in properties, stress jumps are created at such interfaces leading to stress concentrations, thus limiting the load or stress to which the structural component may be subjected. Under the action of mixed and complex types of loading, structural composites may fail in many ways: fiber breakage, matrix cracking, fiber pull-out, fiber/matrix interface debonding, delamination, and diffused intralaminar (between the fibers in a lamina) and interlaminar (between alternating laminas) damage. Out of these, the delamination and interfacial failure are the two most critical failure modes that need urgent attention (Agarwal et al. 2006). If the induced stresses in a composite structure exceed the allowable limits, in-plane/intralaminar and/or out-of-plane/interlaminar failure may occur. So, the need is to develop a mechanism through which the adhesion between the fiber and matrix and the interaction between neighboring laminas can be enhanced.

As per the *rule of mixtures*, the strength and stiffness of a composite can be increased simply by increasing the fiber weight fraction. This, however, may prove counterproductive for fracture toughness, as strength and toughness are generally inversely related. Thus, augmenting the composite properties is not that straightforward as it appears. Fundamentally, the average properties of composites can be tailored at two scales of interest (Lubineau and Rahaman 2012): (1) tailorability at nano- to micro-scale (using nanofillers, fiber, and/or matrix treatment) and (2) tailorability at macro-scale (through lamina orientation, stacking sequence). Whatever the design route is followed, the level of adhesion at the fiber/matrix interface affects the average properties of the composite.

For manufacturing of composites, it is important to perform a detailed characterization of the interface so as to design the interface and hence the composite as per the needs of a specific application. This requires the knowledge of interface from three angles: mechanics, physics, and chemistry (Chen et al. 2018). The study of interfacial mechanics helps in building the constitutive relationships, understanding the unique interfacial microstructure, and prediction analysis and optimization of interface properties. The second angle, i.e., the interfacial physics, may help in better understanding the molecular forces operating at the nano- to micro-scale, the effect of surface forces, and the multi-phenomena occurring simultaneously at the nano-scale and micro-scale. Apart from the mechanics and physics, another interesting viewpoint of characterizing the interface is the interfacial chemistry where one can get important knowledge on the chemical bond formation at the interfacial region. Since the interfacial interactions influence the average properties of the composite, it is important to design the interface in order to get optimized outcomes.

Interface Designing: The Conventional Way

Nano- to Micro- scale Designing

The conventional ways to enhance the interfacial adhesion are oxidative and non-oxidative surface treatment of fiber (Tang and Kardos 1997). *Oxidative treatments* are intended to increase the interfacial area by texturing the fiber surface, by removing weak outer layers in fiber, and by the integration of some active groups to the fiber surface. This may be achieved by subjecting the fiber to electrochemical and chemical reactions; plasma oxidation; oxidation in air, oxygen, carbon dioxide, and ozone; and catalytic oxidation (Tang and Kardos 1997). However, such treatments are limited to low modulus fibers and require high temperatures that may compromise the in-plane properties of composites. The *non-oxidative treatments* involve depositing whiskers, polymer chains, or pyrolytic carbon on the surface of fiber, which reinforce the laminate in its thickness direction (Tang and Kardos 1997). However, such treatments affect the in-plane properties due to the need of excessively high temperatures of ~1800 °C, severely damaging the fiber. Further, the whiskerization method adds considerable weight to the composite, and the plasma-treated fibers are prone to surface deactivation of fibers.

Another way to tailor the interface is by coating a suitable thin polymer *sizing* on the fiber surface. This is almost always followed during fiber manufacturing so as to protect the fibers from environmental effects and for easier handling and retaining of fibers. Usually the composition of sizing is kept similar to that of matrix with which it is intended to be used. This allows cross-linking between the two polymer phases (sizing and bulk matrix), thereby modifying the interfacial properties. The objective behind all the abovementioned methods is to increase the surface roughness and surface reactivity of the fiber, thereby increasing the effectiveness of the interface.

Macro-scale Designing

The aforementioned techniques for nano- to micro-scale tailoring of composites make sense only if such improvements are reflected at the macro-level in a laminate. Fixing the fiber/matrix combination, the performance of a laminate is usually designed on the basis of the number, orientation, and stacking sequence of laminas. It is possible to reverse the nature of interlaminar normal stresses in the thickness direction from tensile to compressive by choosing a right stacking sequence (Jones 1999). This assists in seizing the laminas together as opposed to delamination. Furthermore, the stack geometry affects crack initiation as well as crack propagation (Soutis et al. 1993). It is true that a laminated construction allows us to design composites for specific applications; the same may lead to unexpected composite behaviors if the stacking sequence is not optimized (Pipes and Pagano 1994). The optimization of laminates has led to laminated composites having optimum in-plane properties, though the off-axis and out-of-plane laminate properties are compromised. This has resulted in laminates having lower in-plane shear strength compared to tensile and compressive strengths. While the off-axis angle $>15^\circ$ leads to in-plane shearing, a fiber orientation $>45^\circ$ leads to out-of-plane shearing.

The shear failure of off-axis laminates under axial loading indicates a failure mechanism dominated by the matrix (Tsai and Sun 2005). This is because of the possibility of matrix-rich regions, in between the fibers in a lamina and also between the alternating laminas, which act as weak links in laminated composites. The situation is further aggravated due to the weak transverse properties of carbon fibers compared to their longitudinal properties. Besides, the epoxy composites are brittle having poor damage tolerance even at low impact energies (5–10 J) which may delaminate the composite (Soutis 2005). This becomes even more crucial as the matrix provides lateral support to fibers against buckling and minimizes damage by deforming plastically. Consequently, the ability to bear shear and transverse loads, and hence the off-axis strength and interlaminar strength, of laminates is weak in comparison to the in-plane fiber-dominated properties.

Efforts have been made to improve the delamination strength by orienting the fibers in a lamina in the thickness direction, but the conventional techniques for manufacturing the fabric lack such capability. Other ways are to weave/stitch the fibers along thickness direction (Dransfield et al. 1998) or z-pinning to join laminas (Byrd and Birman 2006). However, such methods are exhaustive and require additional manufacturing processes and complex machinery and equipment that increase the cost of production. Besides, the research based on these fabric modification methods have produced contradicting results (Mouritz et al. 1997) possibly because of the involvement of a large number of parameters and the inherent shortcomings of these techniques such as fiber breaking or kinking, matrix cracking, resin-rich regions, etc.

Interface Designing: Using Carbon Nanotubes

In order to tackle the issues faced with conventional methods to design the interface, researchers have come up with the possibility of including secondary filler in FRP apart from the primary fibrous filler. For this purpose, several nano−/micro-size particles such as carbon nanotubes (CNT), carbon nanofibers, clay, graphene and graphene oxide, ZnO, TiO_2, nanorods, aluminum oxide, etc. have been tested (Lubineau and Rahaman 2012). The mechanical properties, especially the strength and modulus, of a solid material are basically a function of the nature of chemical bonds and the defects present in the solid. The presence of strong carbon-carbon covalent bonds in CNT, augmented with their defect-free 1D structure (owing to nanometer-length scales), makes them the primary choice of material scientists and engineers in a variety of applications. This along with the combination of high aspect ratio, low density, high thermal stability, and high thermal and electrical conductivity allows nanotubes to enhance the static mechanical, dynamic mechanical, and damping properties of polymer composites. CNT possess not only the mechanical properties but the capability to simultaneously improve the thermal and electrical properties of polymer composites as well.

As the interface between the filler and matrix is the most crucial thing that governs the filler/matrix adhesion, the sole purpose of adding nanotubes in FRP is

to enhance the fiber/matrix interfacial interaction (Coleman et al. 2004). Experimental and analytical studies are available investigating the effects of CNT addition on the mechanical properties of composites (Medina et al. 2015). In the recent past, CNT have been successfully incorporated for structural property enhancements in aircraft wings (Trimble 2011) and helicopter rotor blades (Army 2013). In their review article, Gohardani et al. (2014) have provided a list of research articles, projects, and patents actualized for implementing CNT in aerospace applications.

The straightforward approach to incorporate CNT in a composite is by dispersing the nanotubes in the matrix. Gojny et al. (2005a) have experimented by mixing different types of CNT in epoxy matrix, viz., single-walled, double-walled, and multiwalled nanotubes, and reported considerable improvements in the tensile strength, elastic modulus, and fracture toughness of epoxy. Further, it was shown that CNT concentrations as low as 0.05 wt% are sufficient to obtain significant modifications (Gojny et al. 2005a). Further, the nanoparticles in a composite deviate the micro-cracks and can augment the frictional component of adhesion, leading to an increased fracture toughness of the composite. Yokozeki et al. (2007) have shown an increase in the fracture toughness of CFRP, owing to the delayed crack initiation in the presence of CNT in epoxy matrix.

CNT addition also improves the interlaminar shear strength (ILSS) of laminated composites. When CNT-modified epoxy matrix is used to process glass fiber-reinforced laminates, the ILSS increased by 20% without influencing the in-plane modulus or strength of the FRP (Gojny et al. 2005a). Zhu et al. (2007) have achieved nearly 40% improvement in the ILSS by just coating 0.015 wt% of CNT on the middle two laminas of a glass fiber/vinyl ester composite. On the whole, the enhancements due to CNT addition are attributed to mechanisms such as matrix toughening, high strain to failure, fiber bridging, and reduced stress concentration by smearing the mismatch between neighboring plies and hence higher absorption of dissipation energy. All these phenomena are credited to a variety of possible fracture mechanisms of CNT such as nanotube debonding, CNT rupture, and telescopic fracture of multiwalled CNT (see Fig. 2), which allows the nanotubes to seize the cracks and prevent crack expansion and propagation (Gojny et al. 2005a).

Furthermore, the role played by interface between the nanofiller and the surrounding polymer matrix cannot be neglected. Wagner and Vaia (2004) have highlighted the importance of filler/matrix interface in CNT-based composites. CNT/polymer interface is known to possess shear strength of the order of 500 MPa and interfacial energy amounting to 300 J m^{-2} (Wagner et al. 1998). The molecular mechanics approach followed by Lordi and Yao (2000) attributes the strength of interface to the molecular-level entanglement between the nanotube and the surrounding polymer. Moreover, the nanoparticles in polymers hold the potential to enhance the nucleation of polymer crystals and increase the cross-linking density (Fiedler et al. 2006). Hence, the improvements due to CNT addition are a synergistic effect of reinforcing the polymer matrix with nanofillers having excellent mechanical properties and the ability of nanoparticles to augment the morphology of the matrix through physical interactions (Fiedler et al. 2006).

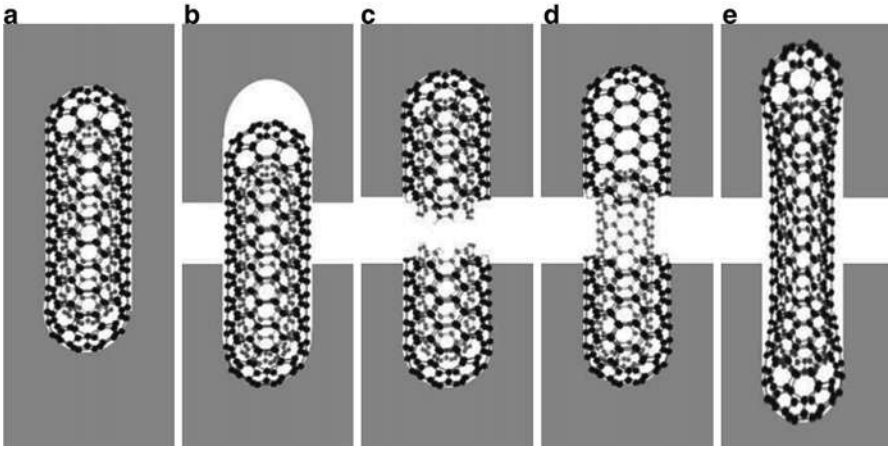

Fig. 2 Schematic description of possible fracture mechanisms of CNTs. (**a**) Original state of CNT; (**b**) weak interface leading to debonding of CNT from matrix; (**c**) strong interfacial adhesion leading to CNT rupture; (**d**) telescopic fracture of outer CNT layer due to strong interfacial bonding and pull-out of the inner tube; (**e**) local bonding to the matrix enabling crack bridging and partial interfacial failure in the non-bonded regions (Gojny et al. 2005). (©With permission of/courtesy of Elsevier)

Interfacial Interactions

It is clear, from the discussion in the previous section, that the usage of nanotubes in polymer composites is promising and can deliver excellent outcomes in terms of composite properties. All this is possible because of the different types of interactions playing at the interface of filler and the matrix. Interfacial interactions in FRP are one of the most important properties that need to be understood so as to predict and design the properties of composites. The different types of interactions that may occur at the filler/matrix interface are π-stacking, hydrogen bonding, weak van der Waals interactions, etc. However, the most general categorization of interfacial interactions can be in the form of either non-covalent or covalent interactions (Chen et al. 2018).

The *non-covalent technique* involves mechanical interactions between the filler and the matrix by introducing π-π stacking, CH-π stacking, and hydrogen bonding. This can be achieved by way of mechanisms such as polymer wrapping, bridging, encapsulation, and adsorption. On the other hand, *covalent interactions* happen due to the chemical bond formation between the filler and the matrix. In this technique, the sidewalls or open ends of the filler, such as nanotubes, are modified with chemical functional groups such as carboxylic acid group, hydroxide group, amine group, silane group, fluorination, etc. Because of the chemical bonding between the polymer chains and the filler material, the interfacial strength is high in covalent bonding, though this comes with the ill effects of adversely affecting the filler properties. The reader is suggested to refer to Rahmat and Hubert (2011) for more details on the covalent and non-covalent methods.

Interphase

The introduction of nanotubes in composites results in the formation of a third phase, known as interphase region. Interphase is defined as a region of finite thickness possessing properties different from that of the constituents of the composite. Interface can be considered as a line that separates the fiber from the matrix, whereas interphase is a solid region of finite thickness separating the fiber from the bulk matrix (Fig. 3). Because of its two-dimensional nature, the presence of interface leads to a jump in properties between the fiber and matrix. However, there is a gradual change in properties from fiber to matrix in the presence of an interphase region (Bedi et al. 2018a). The addition of nanotubes enhances the mechanical properties of the polymer matrix which has been attributed to an increase in the interphase region. Winey and Vaia (2007) predicted 63% increase in interphase volume fraction with the addition of only 1 vol% of nanoparticles in polymer. With increase in nanofiller fraction, interphase size increases gradually, and at a certain volume fraction, the whole matrix gets converted into interphase (Patel et al. 2008).

Interphase Processing Techniques

CNT Dispersion in Matrix

Although dispersing nanotubes in matrix is the simplest and direct way of preparing hybrid composites, it is not possible to keep on increasing the weight percent of CNT indefinitely in the matrix. There is always an upper limit on the amount of nanofiller that can be efficiently dispersed in the matrix so as to keep a check on the resin viscosity to allow it to flow within the fabric. Increase in CNT concentration beyond

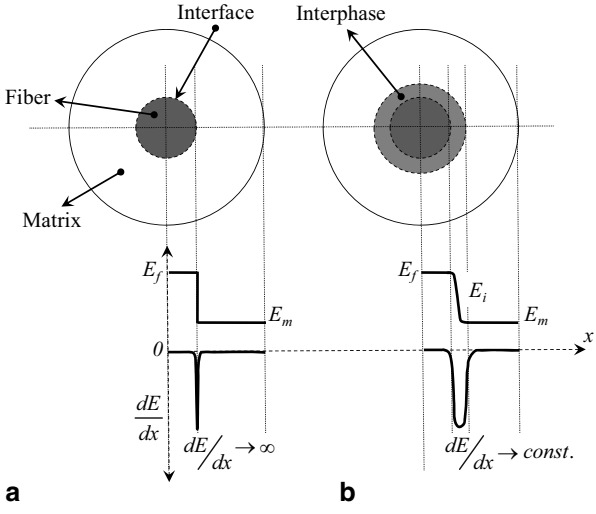

Fig. 3 Schematic of fiber-reinforced polymer matrix composite with (**a**) interface and (**b**) interphase having finite thickness. Subscripts *f*, *m*, and *i* refer to fiber, matrix, and interphase, respectively (Bedi et al. 2018). (©With permission of/courtesy of Elsevier)

a critical value may reduce the interparticle separation to such an extent that triggers the effects of van der Waals forces of attraction resulting in CNT agglomeration (Bakshi et al. 2010); see Fig. 4. In such a case, nanotubes lying inside of a CNT bunch are not bonded to matrix and can slip under the action of an applied loading, affecting the elastic properties of the composite. Moreover, the large aspect ratio offered by nanotubes is diminished once the aggregates are formed. Such CNT bundles in matrix then act as stress concentration sites and may result in premature failure of the composite (Zhou et al. 2008). The sole aim of adding CNT in matrix is to transfer the excellent mechanical, electrical, and thermal properties of CNT to the polymer. However, the non-reactive surface of nanotubes, their random distribution in matrix, and curled and entangled morphology are the issues that limit the extent of bonding between the nanotubes and the matrix (Ajayan et al. 2000).

CNT Purification and Functionalization

These issues along with the problem of agglomeration can be resolved if somehow the dispersion and bonding of nanotubes in matrix can be enhanced. A possible solution to tackle these two issues concurrently is to enhance the surface reactivity of nanotubes by way of purification and opening the CNT ends through oxidation (Xie et al. 2005); see Fig. 4. The surface reactivity of nanotubes can be further augmented by some chemical treatments known as functionalization. Functionalization (Fig. 4) involves the attachment of certain chemical groups at the surface defects and on the sidewalls and/or end caps of the nanotubes (Tasis et al. 2006). The level of chemical attack on nanotubes can further be raised by using, for example, the acid mixture H_2SO_4/HNO_3 which not only attacks the initial defect sites but also affects the integrated graphene structure of CNT by breaking the –C=C– bonds. This results in the generation of active –OH, –C–OH, and –C=O

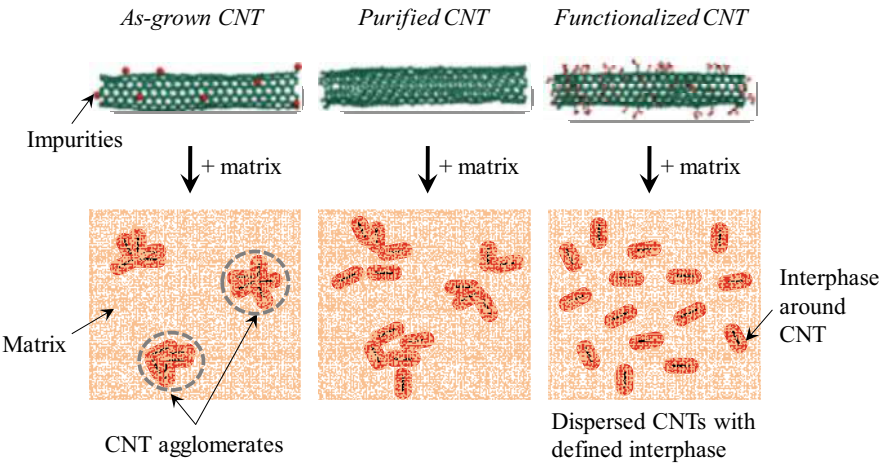

Fig. 4 Schematic showing the interphase processed by dispersing nanotubes in matrix

sites on the surface of nanotubes. These attached functional groups turn the hydrophobic nature of CNT to hydrophilic, which not only strengthens the chemical bonding with the matrix but also improves the dispersion of CNT in matrix owing to the electrostatic repulsions induced by functionalization (Mittal et al. 2015).

Therefore, in addition to the physical entanglement of CNT with matrix (as mentioned earlier), chemical attachments are introduced between the two. Yet, the harmful effects of chemical treatment on the structure and properties of nanotubes can never be ignored (Monthioux et al. 2001). It is, therefore, imperative to optimize not only the amount and dispersion level of nanotubes in matrix but also the dispersion process itself. All these complexities involved with the addition of nanotubes in matrix pose a challenge to fully harness the superior properties of CNT in improving the average properties of conventional composites.

CNT Suspension, Coating, and Sizing

To overcome the shortcomings faced during the mixing of nanotubes in matrix, alternate ways are developed to introduce CNT efficiently in composites. Some commonly followed approaches are to coat a CNT suspension on fiber (Sui et al. 2017) or by mixing nanotubes in the fiber sizing (Zhang et al. 2015) or by spray coating the CNT on the fabric (Li et al. 2016a). The reinforcing fibers used in FRP are usually coated with some polymer sizing during their manufacturing. This sizing layer promotes adhesion with the surrounding polymer matrix. However, in certain requirements, such as CNT grafting using chemical vapor deposition, the sizing can be easily removed either by chemical treatment with acetone or by oxidizing in air at elevated temperatures.

To further assist the fiber-matrix interaction, one simple processing technique can be followed, i.e., by coating the fiber with some suspension containing nanoparticles. The suspension media must have the characteristics of good dispersion ability and should be easy to evaporate upon drying. The removal of the suspension before preparing the composite is crucial so as not to deteriorate the overall composite properties. To this end, water (Xiao et al. 2018), ethanol (Yao et al. 2015), acetone (Awan et al. 2018), and ionic surfactants are the preferred choices. To facilitate the usage of nanoparticles on the fabric surface, spray coating comes out to be the simpler and effective technique. The nanofillers are first dispersed in some alcoholic medium such as ethyl alcohol (Rodríguez-González et al. 2017) or isopropyl alcohol (Yang et al. 2018) using the sonication procedure. The prepared nanofiller-based alcoholic solution is then sprayed uniformly on the fiber laminas using a spray gun. Electrospray deposition (Li et al. 2016a) is an advanced version of this process of spray coating in which the spray droplets disintegrate into further smaller droplets due to electrostatic repulsions. Usually, oxidation of the nanoparticle is done to achieve better dispersion in the sizing bath. This results in physical adsorption of the nanofillers in the interphase region through weak chemical interactions.

Electrostatic and Electrophoretic Deposition

Still, to get a uniform and homogeneous dispersion level through the abovementioned techniques of sizing, coating or spraying is a challenging task. To this end, researchers came out with the advanced methods of coating – electrostatic and electrophoretic deposition (Kamae and Drzal 2012). In these techniques, the nanofiller and the fiber are charged oppositely using electric potential, which helps the nanoparticles to travel toward and get physically adsorbed on the fiber/fabric. Pre-treatment of the fiber like thermal treatment (Wang et al. 2016) or electrochemical deposition of silver nanoparticles (Wang et al. 2017a) before carrying out the electrophoretic deposition process has resulted in composites with improved properties. However, before using these processes, it is important to remove the original sizing from the surface of the fiber; otherwise, the sizing layer can act as a hindrance. Although researchers have shown an improvement in the elastic modulus, strength, failure strain, and interlaminar shear strength, a number of parameters such as sonication frequency, applied voltage, inter-electrode distance, and bath acidity are required to be controlled and optimized. To assist on this, the functionalization of the reinforcing fiber and the nanofiller can always be followed to attain better dispersion and filler/matrix interaction.

CNT Grafting

A more advanced and versatile approach is to grow or graft CNT directly on the surface of fiber, as shown in Fig. 5, using *chemical vapor deposition (CVD)* technique (Agnihotri et al. 2011). The merit of using CVD is that it results in a strong grafting force (Wang et al. 2014) owing to the bridging function provided by the nanotubes between the fiber and matrix. Growing nanoparticles directly on fiber surface increases the fiber surface area that helps in capillary sorption of the matrix. The CNT-grafted fiber is then infiltrated with polymer matrix, resulting in a multiscale composite (Sharma et al. 2014). The grafting process further provides mechanical interlocking and local matrix stiffening, resulting in better stress transfer from the matrix to the fiber. Moreover, the radially grown nanotubes on the fiber surface provide transverse reinforcement, thereby improving the out-of-plane properties of the composite.

More often in today's scenario of multifunctional composites (Gibson 2010), the more significant task is not just limited to improving the properties but is to tailor the properties in an effective manner as per need. Such a requirement can be fulfilled by controlling the length (Li and Chou 2006), density (Agnihotri et al. 2011), type (Gojny et al. 2006), alignment (Wang et al. 2008), growth rate, and quantity of CNT, which is attainable through CVD. In catalytic CVD process, the fiber/fabric is first coated with a catalyst material (generally a transition metal like Co, Ni, and Fe) and then subjected to a combination of reactive gases such as hydrogen and acetylene. At suitable temperatures, the carbon from the precursor gas dissociates and diffuses into the catalyst particles deposited on the fiber. The gradual deposition of the carbon particles ultimately results in the growth of a nanotube on the fiber surface.

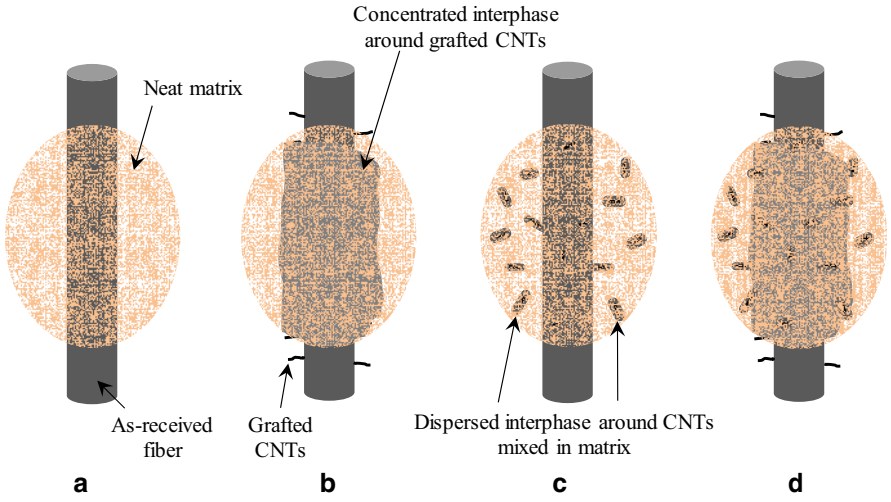

Fig. 5 Schematic representation of (**a**) distinct interface in a conventional CFRP, (**b**) concentrated interphase, (**c**) dispersed interphase, and (**d**) mixed interphase induced in CFRP using CNTs

Depending on the adhesion between the catalyst particle and the fiber, two growth phenomena can occur: *base growth* (catalyst particle remains on the fiber surface) or *tip growth* (catalyst particle moves with the nanoparticle) (Kotanjac et al. 2015). However, the coating of catalyst particles has been shown to erode the fiber and degrade the mechanical properties. Low-temperature CVD (De Greef et al. 2015), heat shielding zone (Lomov et al. 2011), and protective layering (Pozegic et al. 2016) are being explored as the possible solutions to the eroding action of the catalyst. Still, the overall effect of catalyst erosion on the bulk composite properties has been shown to be minimal (Bedi et al. 2018b). Furthermore, the issue of low yield of the CVD process has been tackled (Zheng et al. 2018) through non-covalent functionalization of the reinforcing fiber at low temperature.

In addition to the grafting of nanoparticles directly on the fiber surface, another approach could be to selectively place the nanofillers in between the reinforcing laminas. The concept of interleaving and buckypapers has shown simultaneous improvements in the mechanical, thermal, electrical, and electromagnetic properties (Xia et al. 2020). Such multiscale structures are efficient in stress transfer with increased resistance to crack initiation and crack propagation. The reader is further suggested to review the article by Thostenson et al. (2001) for details on the structure, processing, and characterization of nanotubes and by Kumar and Ando (2010) on the growth mechanism of CVD-grown CNT. It is, therefore, expected that the integration of nanotubes on fiber surface may help in overcoming the low interfacial shear strength and interlaminar shear strength in laminated composites, as the stresses at the nanotube/polymer interface can go as high as 500 MPa (Wagner et al. 1998).

Types of Interphase

Irrespective of the approach followed to incorporate nanotubes in the composite, the addition of nanotubes alters the microstructure at the filler/matrix interface and creates an interphase region having finite thickness (Bedi et al. 2018a). By mixing the nanotubes in matrix, a hybrid composite is obtained in which the interphase is dispersed throughout the matrix and is known as *dispersed interphase* (Fig. 5c). On the other hand, a *concentrated interphase* (Fig. 5b) and hence a multiscale composite are obtained by growing nanotubes directly on the fiber surface (Bedi et al. 2020). Wang et al. (2017b) processed a multiscale-hybrid composite by combining these two approaches. Such a composite has partly concentrated and partly dispersed interphase region and is termed as *mixed interphase* (Fig. 5d) that enhances the interlaminar shear strength (ILSS) of carbon fiber/epoxy composites. By varying the microstructure of interphase and incorporating different combinations of it in the composite, one can modify the interfacial chemistry, interfacial area, surface energy, etc. at the interfacial region. This offers a tool to design simultaneously the interfacial shear strength (IFSS) and interfacial fracture toughness (G_{ic}) as per the functional requirements of a particular application (Bedi et al. 2020). Enhancements in composite properties are attributed to improved bonding, better wetting, and higher glass transition temperature of CNT-modified CFRP.

Interface/Interphase Characterization

It is shown that interphase accounts for a significant volume fraction, so while predicting the composite properties, the contribution of interphase must be explicitly allowed in theoretical models. However, commonly used theoretical models, such as the *rule of mixtures*, do not include the effects of interphase on the overall composite properties. Even if the interphase is accounted for, one needs to know the volume fraction and modulus of the third phase, i.e., interphase, apart from that of fiber and matrix. Determining the volume fraction and modulus of fiber and matrix is straightforward; the same is not true in the case of interphase. Furthermore, very few studies have reported on the size and properties of interphase in composites. Surface energy of fiber, fiber texture, surface tension of matrix, wettability, method to introduce nanotubes in the composite, and the level of physical/chemical interaction between the filler and matrix are some of the parameters that influence the size, morphology, and properties of the interphase.

Experimental Techniques

Several experimental efforts have been made to engineer the interphase using CNT. Scanning electron microscopy (SEM), transmission electron microscopy (TEM), energy-dispersive X-ray microscopy (EDS), atomic force microscopy (AFM), and wettability are the primary techniques that are used to qualitatively characterize the

interface/interphase (Karger-Kocsis et al. 2020). These techniques can be used not only to establish the presence of an interphase region but to quantify the interphase size as well (Bedi et al. 2018a). VanLandingham et al. (1999) used AFM to study the interphase in carbon/epoxy and copper/epoxy composites. Using AFM, Mai et al. (1998) determined an interphase thickness of 1–3 μm in glass/polypropylene and carbon/epoxy composites. AFM further allows the measurement the adhesion level between the filler and the matrix (Moosburger-Will et al. 2017). X-ray photoelectron spectroscopy (XPS), Raman spectroscopy, and Fourier transform infrared (FTIR) spectroscopy are also used to perform the chemical analysis of the interface/interphase region (Moosburger-Will et al. 2017).

In order to quantify the mechanical properties of interface/interphase, especially the interfacial shear strength and interfacial fracture toughness, techniques such as fiber pull-out (Agnihotri et al. 2011), fiber fragmentation (Qian et al. 2010), fiber push-out (Battisti et al. 2014), microdebond (An et al. 2012), and nanoindentation (Gao et al. 2010) are widely used. All these tests are performed on a universal testing machine, and the output is in the form of load versus displacement curves from which the interfacial properties can be evaluated. A schematic of each of these tests is given in Fig. 6.

Pull-out Test

Single-fiber pull-out test is the most popular testing technique for interfacial characterization. A single filament of fiber is embedded in uncured matrix, the embedded length being sub-micron levels. Upon curing, the extended portion of the fiber is pulled out of the matrix, and a load versus displacement curve is generated as a result of overcoming the interfacial interactions. The peak force per unit embedded area gives the interfacial shear strength (IFSS). An added advantage of this test method is its ability to generate data on the frictional forces playing at the fiber/matrix interface post-interface debonding.

Fragmentation Test

Fiber fragmentation is another technique in which a single-fiber filament is fully embedded inside the matrix pool. The single-fiber composite is then carefully stretched until the fiber breaks into a number of smaller pieces. At some critical length, the fiber breaking seizes on further loading, and the test is stopped. The critical fiber length is then measured to evaluate the interfacial strength.

Nanoindentation and Push-Out Tests

Nanoindentation is widely used to get the stiffness, modulus, and hardness values in the interfacial region. In this testing method, a flat or pointed nanoindenter presses against the region of interest, often followed by a dwell period, and is then released. During the first phase, the load rises with respect to the indenter pressing against the specimen. Upon reaching the maximum value, the load curve becomes flat owing to the dwell period. The dwell period is introduced to account for the material recovery that may happen due to load release in case of soft materials such as polymers. During the last stage of load releasing, the slope of the load-displacement curve

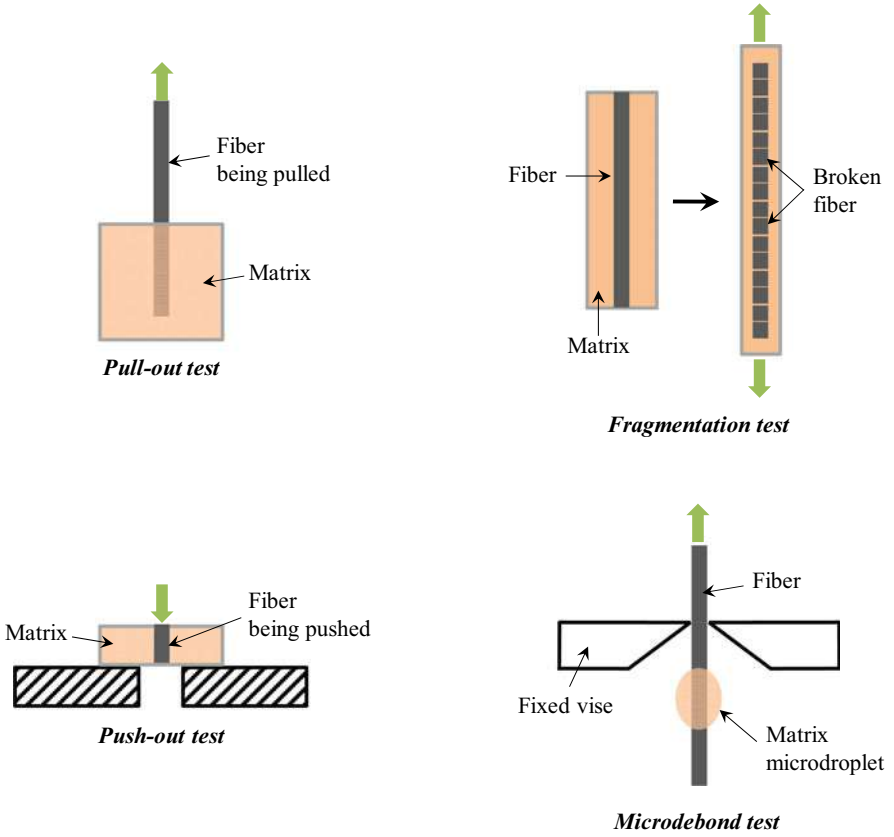

Fig. 6 Schematic showing different experimental techniques for characterizing the interface/interphase

becomes negative, and the load decreases with the movement of the indenter in the opposite direction. It is this negative slope of the curve which is used to evaluate the stiffness or modulus of the test specimen. Using nanoindentation technique on a single carbon fiber in epoxy matrix, the interphase size has been estimated to be less than 0.5 μm (Williams et al. 1990).

An extension of the nanoindentation method is the fiber push-out test where a single filament is pushed out of sub-micron matrix disc by the nanoindenter. The peak force per unit embedded area gives a measure of the IFSS of the composite.

Microdebond Test

Microdebond or microdroplet shear test is the direct testing method to evaluate the properties of FRP. In this method, a microdroplet of matrix adhering to the fiber surface is sheared off while making contact with a fixed jaw during the fiber longitudinal movement. The IFSS is obtained by dividing the force at which debonding of the microdroplet occurs with the surface area of contact of the droplet

with the fiber. Microdebond test method can be used to evaluate not only the IFSS but the interfacial fracture energy (G_{ic}) as well (Bedi et al. 2020). Because of the least amount of matrix used in the sample preparation, the microdebond test method becomes the only method that can be used to effectively to evaluate the properties of the interphase.

Numerical Techniques

Attempts have also been made to estimate the properties of interphase through numerical and modeling methods. Molecular dynamics, coarse grain simulations, and density functional theory are some of the modeling techniques used to measure the interfacial interactions in composites (Rahmat and Hubert 2011). Researchers have evaluated the effects of matrix cross-linking and curing conditions on the interfacial properties (Li et al. 2013). *Molecular dynamics* improved the understanding on the effect of grafted nanotubes on shear deformations in CFRP. The modulus and strength of the interphase are found to improve in the presence of grafted nanotubes (Yang et al. 2012). While the molecular dynamics approach evaluates the molecular interactions, the *coarse grain method* like Monte-Carlo simulations maps the atomistic picture. Density profile, radial distribution, viscosity, and glass transition temperature are the output parameters of *coarse grain techniques*. The electronic structure of the atomistic systems is examined by the density functional theory. The exact geometry of the stable state is evaluated by finding the energetically favorable states of molecular structures (Mylvaganam and Zhang 2004). This technique holds the potential to model the nanotube growth by simulating the interaction between the nanotube and the catalyst (Larsson et al. 2007). Further, the in situ polymerization inside the nanotubes can also be simulated by way of density functional theory (Kim et al. 2005).

Finite element analysis is another approach used to model interphase in a 3D environment. It has been shown that CNT influences stress distribution around the fiber in CFRP by reducing stress concentrations (Romanov et al. 2014). The combination of molecular dynamics and finite element or micromechanics approaches leads to the so-called *multiscale modeling* technique (Alian et al. 2015).

Conclusion

The structural composite panels are subjected to complex loading environment varying from quasi-static to dynamic loading. At one point, the functional requirement may demand high strength and stiffness; it may also be necessary for CFRP to provide high damping in some other situation. Since interfacial interactions depend on the extent of adhesion between the fiber and matrix, any way of modifying either fiber or matrix or both offers us a handle to design the composite. Such modifications usually involve playing with the interface/interphase region in composites, which can be done using carbon nanotubes. Incorporating CNT as a secondary filler to

reinforce FRP not only infuses the advantages of both the fillers (fiber and nanoparticle) in the resulting composite but also provides us with more choice to tailor the properties of the interphase either by dispersing nanotubes in matrix or by growing them on the surface of fiber. It, therefore, relies at the discretion of the design engineer to choose a desired type of strong or weak interphase depending on whether the intended application demands strength and stiffness or fracture resistance or both.

However, designing a composite with a certain level of strength and toughness and interfacial and interlaminar properties is a challenging task. The use of high-performance carbon fibers together with extremely versatile CNT appears promising, but before putting them into practice, one must fully understand the consequences that may happen at various scales in a composite. Hence, there is a need to characterize the size and properties of the interphase region, both qualitatively and quantitatively, and its effects on the performance of FRP in order to fully realize the potential of interphase in designing the composites. However, it should always be kept in mind that any type of modification carried out at micro- or even nano-scale may influence the average properties as well as the couplings in laminated composites. Even after so much progress, some aspects related to interphase are not clearly understood such as the size, structure, properties, and rate sensitivity of interphase. The need is not only to explore the effect of interphase on the interfacial, off-axis, and interlaminar properties of laminated composites but also to establish their inter-dependency to present a complete picture on how the interphase governs the micro-to-bulk phenomena in composites. In other words, the laminate couplings, the out-of-plane interlaminar properties, the in-plane interfacial properties, and the properties of the interphase are all interrelated and should be understood well in order to make a truly versatile composite for structural applications.

References

B.D. Agarwal, L.J. Broutman, K. Chandrashekhara, *Analysis and Performance of Fiber Composites* (Wiley, New Jersey, 2006)

P. Agnihotri, S. Basu, K. Kar, Effect of carbon nanotube length and density on the properties of carbon nanotube-coated carbon fiber/polyester composites. Carbon **49**(9), 3098–3106 (2011)

P.M. Ajayan, L.S. Schadler, C. Giannaris, A. Rubio, Single-walled carbon nanotube–polymer composites: Strength and weakness. Adv. Mater. **12**(10), 750–753 (2000)

A. Alian, S. Kundalwal, S. Meguid, Multiscale modeling of carbon nanotube epoxy composites. Polymer **70**, 149–160 (2015)

F. An, C. Lu, Y. Li, J. Guo, X. Lu, H. Lu, S. He, Y. Yang, Preparation and characterization of carbon nanotube-hybridized carbon fiber to reinforce epoxy composite. Mater. Des. **33**, 197–202 (2012)

U. Army Army researchers chase helicopter performance gains (2013)

F.S. Awan, M.A. Fakhar, L.A. Khan, U. Zaheer, A.F. Khan, T. Subhani, Interfacial mechanical properties of carbon nanotube-deposited carbon fiber epoxy matrix hierarchical composites. Compos. Interfaces **25**(8), 681–699 (2018)

S.R. Bakshi, D. Lahiri, A. Agarwal, Carbon nanotube reinforced metal matrix composites-a review. Int. Mater. Rev. **55**(1), 41–64 (2010)

A. Battisti, D. Esqué-de los Ojos, R. Ghisleni, A.J. Brunner, Single fiber push-out characterization of interfacial properties of hierarchical CNT-carbon fiber composites prepared by electrophoretic deposition. Compos. Sci. Technol. **95**, 121–127 (2014)

H.S. Bedi, M. Tiwari, P.K. Agnihotri, Quantitative determination of size and properties of interphase in carbon nanotube-based multiscale composites. Carbon **132**, 181–190 (2018a) https://doi.org/10.1016/j.carbon.2018.02.059

H.S. Bedi, S.S. Padhee, P.K. Agnihotri, Effect of carbon nanotube grafting on the wettability and average mechanical properties of carbon fiber/polymer multiscale composites. Polym. Compos. **39**(S2), E1184–E1195 (2018b)

H.S. Bedi, B.K. Billing, P.K. Agnihotri, Interphase engineering in carbon fiber/epoxy composites: Rate sensitivity of interfacial shear strength and interfacial fracture toughness. Polym. Compos (2020)

L.W. Byrd, V. Birman, Effectiveness of z-pins in preventing delamination of co-cured composite joints on the example of a double cantilever test. Compos. Part B **37**(4–5), 365–378 (2006)

K.K. Chawla, *Composite Materials: Science and Engineering* (Springer Science & Business Media, New York, 2012)

J. Chen, L. Yan, W. Song, D. Xu, Interfacial characteristics of carbon nanotube-polymer composites: A review. Compos. Part A **114**, 149–169 (2018)

J.N. Coleman, M. Cadek, R. Blake, V. Nicolosi, K.P. Ryan, C. Belton, A. Fonseca, J.B. Nagy, Y.K. Gun'ko, W.J. Blau, High performance nanotube-reinforced plastics: Understanding the mechanism of strength increase. Adv. Funct. Mater. **14**(8), 791–798 (2004)

N. De Greef, L. Zhang, A. Magrez, L. Forró, J.-P. Locquet, I. Verpoest, J.W. Seo, Direct growth of carbon nanotubes on carbon fibers: Effect of the CVD parameters on the degradation of mechanical properties of carbon fibers. Diam. Relat. Mater. **51**, 39–48 (2015)

K.A. Dransfield, L.K. Jain, Y.-W. Mai, On the effects of stitching in CFRPs – I. mode I delamination toughness. Compos. Sci. Technol. **58**(6), 815–827 (1998)

B. Fiedler, F.H. Gojny, M.H. Wichmann, M.C. Nolte, K. Schulte, Fundamental aspects of nano-reinforced composites. Compos. Sci. Technol. **66**(16), 3115–3125 (2006)

S. Gao, R.C. Zhuang, J. Zhang, J.W. Liu, E. Mäder, Glass fibers with carbon nanotube networks as multifunctional sensors. Adv. Funct. Mater. **20**(12), 1885–1893 (2010)

R.F. Gibson, A review of recent research on mechanics of multifunctional composite materials and structures. Compos. Struct. **92**(12), 2793–2810 (2010)

O. Gohardani, M.C. Elola, C. Elizetxea, Potential and prospective implementation of carbon nanotubes on next generation aircraft and space vehicles: A review of current and expected applications in aerospace sciences. Prog. Aerosp. Sci. **70**, 42–68 (2014)

F.H. Gojny, M.H.G. Wichmann, B. Fiedler, K. Schulte, Influence of different carbon nanotubes on the mechanical properties of epoxy matrix composites – A comparative study. Compos Sci Technol **65**(15–16), 2300–2313 (2005a) https://doi.org/10.1016/j.compscitech.2005.04.021

F.H. Gojny, M.H. Wichmann, B. Fiedler, W. Bauhofer, K. Schulte, Influence of nano-modification on the mechanical and electrical properties of conventional fibre-reinforced composites. Compos. Part A **36**(11), 1525–1535 (2005b)

F.H. Gojny, M.H. Wichmann, B. Fiedler, I.A. Kinloch, W. Bauhofer, A.H. Windle, K. Schulte, Evaluation and identification of electrical and thermal conduction mechanisms in carbon nanotube/epoxy composites. Polymer **47**(6), 2036–2045 (2006)

R.M. Jones, *Mechanics of Composite Materials* (Inc, 1999)

T. Kamae, L.T. Drzal, Carbon fiber/epoxy composite property enhancement through incorporation of carbon nanotubes at the fiber–matrix interphase–part I: The development of carbon nanotube coated carbon fibers and the evaluation of their adhesion. Compos. Part A **43**(9), 1569–1577 (2012)

J. Karger-Kocsis, H. Mahmood, A. Pegoretti, All-carbon multi-scale and hierarchical fibers and related structural composites: A review. Compos. Sci. Technol. **186**, 107932 (2020)

M.R. Kessler, Polymer matrix composites: A perspective for a special issue of polymer reviews. Polym. Rev. **52**(3), 229–233 (2012)

G. Kim, Y. Kim, J. Ihm, Encapsulation and polymerization of acetylene molecules inside a carbon nanotube. Chem. Phys. Lett. **415**(4–6), 279–282 (2005)
Ž. Kotanjac, L. Lefferts, V. Koissin, L. Warnet, R. Akkerman, Synthesis of carbon nanofibers on large woven cloth. C—J. Carbon Res. **1**(1), 2–15 (2015)
M. Kumar, Y. Ando, Chemical vapor deposition of carbon nanotubes: A review on growth mechanism and mass production. J. Nanosci. Nanotechnol. **10**(6), 3739–3758 (2010)
P. Larsson, J.A. Larsson, R. Ahuja, F. Ding, B.I. Yakobson, H. Duan, A. Rosén, K. Bolton, Calculating carbon nanotube–catalyst adhesion strengths. Phys. Rev. B **75**(11), 115419 (2007)
C. Li, T.-W. Chou, Multiscale modeling of compressive behavior of carbon nanotube/polymer composites. Compos. Sci. Technol. **66**(14), 2409–2414 (2006)
M. Li, Y.-Z. Gu, H. Liu, Y.-X. Li, S.-K. Wang, Q. Wu, Z.-G. Zhang, Investigation the interphase formation process of carbon fiber/epoxy composites using a multiscale simulation method. Compos. Sci. Technol. **86**, 117–121 (2013)
Q. Li, J.S. Church, M. Naebe, B.L. Fox, Interfacial characterization and reinforcing mechanism of novel carbon nanotube–carbon fibre hybrid composites. Carbon **109**, 74–86 (2016a)
Q. Li, J.S. Church, M. Naebe, B.L. Fox, A systematic investigation into a novel method for preparing carbon fibre–carbon nanotube hybrid structures. Compos. Part A **90**, 174–185 (2016b)
S.V. Lomov, L. Gorbatikh, Ž. Kotanjac, V. Koissin, M. Houlle, O. Rochez, M. Karahan, L. Mezzo, I. Verpoest, Compressibility of carbon woven fabrics with carbon nanotubes/nanofibres grown on the fibres. Compos. Sci. Technol. **71**(3), 315–325 (2011)
V. Lordi, N. Yao, Molecular mechanics of binding in carbon-nanotube–polymer composites. J. Mater. Res. **15**(12), 2770–2779 (2000)
G. Lubineau, A. Rahaman, A review of strategies for improving the degradation properties of laminated continuous-fiber/epoxy composites with carbon-based nanoreinforcements. Carbon **50**(7), 2377–2395 (2012)
K. Mai, E. Mäder, M. Mühle, Interphase characterization in composites with new non-destructive methods. Compos. Part A **29**(9), 1111–1119 (1998)
C. Medina, J.M. Molina-Aldareguía, C. González, M.F. Melendrez, P. Flores, J. LLorca Comparison of push-in and push-out tests for measuring interfacial shear strength in nano-reinforced composite materials. J. Compos. Mater.:0021998315595115 (2015)
G. Mittal, V. Dhand, K.Y. Rhee, S.-J. Park, W.R. Lee, A review on carbon nanotubes and graphene as fillers in reinforced polymer nanocomposites. J. Ind. Eng. Chem. **21**, 11–25 (2015)
M. Monthioux, B. Smith, B. Burteaux, A. Claye, J. Fischer, D. Luzzi, Sensitivity of single-wall carbon nanotubes to chemical processing: An electron microscopy investigation. Carbon **39**(8), 1251–1272 (2001)
J. Moosburger-Will, J. Jäger, J. Strauch, M. Bauer, S. Strobl, F.F. Linscheid, S. Horn, Interphase formation and fiber matrix adhesion in carbon fiber reinforced epoxy resin: Influence of carbon fiber surface chemistry. Compos. Interfaces **24**(7), 691–710 (2017)
A. Mouritz, K. Leong, I. Herszberg, A review of the effect of stitching on the in-plane mechanical properties of fibre-reinforced polymer composites. Compos. Part A **28**(12), 979–991 (1997)
K. Mylvaganam, L. Zhang, Nanotube functionalization and polymer grafting: An ab initio study. J. Phys. Chem. B **108**(39), 15009–15012 (2004)
R. Patel, B. Bhattacharya, S. Basu, Effect of interphase properties on the damping response of polymer nano-composites. Mech. Res. Commun. **35**(1), 115–125 (2008)
R.B. Pipes, N. Pagano, Interlaminar stresses in composite laminates under uniform axial extension, in *Mechanics of composite materials*, (Springer, 1994), pp. 234–245
T.R. Pozegic, K. Jayawardena, J.-S. Chen, J.V. Anguita, P. Ballocchi, V. Stolojan, S.R.P. Silva, I. Hamerton, Development of sizing-free multi-functional carbon fibre nanocomposites. Compos. Part A **90**, 306–319 (2016)
H. Qian, A. Bismarck, E.S. Greenhalgh, M.S. Shaffer, Carbon nanotube grafted carbon fibres: A study of wetting and fibre fragmentation. Compos. Part A **41**(9), 1107–1114 (2010)

M. Rahmat, P. Hubert, Carbon nanotube–polymer interactions in nanocomposites: A review. Compos. Sci. Technol. **72**(1), 72–84 (2011)
J. Rodríguez-González, C. Rubio-González, C. Meneses-Nochebuena, P. González-García, L. Licea-Jiménez, Enhanced interlaminar fracture toughness of unidirectional carbon fiber/epoxy composites modified with sprayed multi-walled carbon nanotubes. Compos. Interfaces **24**(9), 883–896 (2017)
V.S. Romanov, S.V. Lomov, I. Verpoest, L. Gorbatikh, Can carbon nanotubes grown on fibers fundamentally change stress distribution in a composite? Compos. Part A **63**, 32–34 (2014)
M. Sharma, S. Gao, E. Mäder, H. Sharma, L.Y. Wei, J. Bijwe, Carbon fiber surfaces and composite interphases. Compos. Sci. Technol. **102**, 35–50 (2014)
C. Soutis, Fibre reinforced composites in aircraft construction. Prog. Aerosp. Sci. **41**(2), 143–151 (2005)
C. Soutis, P. Curtis, N.A. Fleck, Compressive failure of notched carbon fibre composites. Proc. R. Soc. Lond. A Math. Phys. Sci. **440**(1909), 241–256 (1993)
X. Sui, J. Shi, H. Yao, Z. Xu, L. Chen, X. Li, M. Ma, L. Kuang, H. Fu, H. Deng, Interfacial and fatigue-resistant synergetic enhancement of carbon fiber/epoxy hierarchical composites via an electrophoresis deposited carbon nanotube-toughened transition layer. Compos. Part A **92**, 134–144 (2017)
L.G. Tang, J.L. Kardos, A review of methods for improving the interfacial adhesion between carbon fiber and polymer matrix. Polym. Compos. **18**(1), 100–113 (1997)
D. Tasis, N. Tagmatarchis, A. Bianco, M. Prato, Chemistry of carbon nanotubes. Chem. Rev. **106**(3), 1105–1136 (2006)
E.T. Thostenson, Z. Ren, T.-W. Chou, Advances in the science and technology of carbon nanotubes and their composites: A review. Compos. Sci. Technol. **61**(13), 1899–1912 (2001)
S. Trimble, *Lockheed Martin Reveals F-35 to Feature Nanocomposite Structures* (FliIn, 2011)
J.-L. Tsai, C. Sun, Strain rate effect on in-plane shear strength of unidirectional polymeric composites. Compos. Sci. Technol. **65**(13), 1941–1947 (2005)
M. VanLandingham, R. Dagastine, R. Eduljee, R. McCullough, J. Gillespie, Characterization of nanoscale property variations in polymer composite systems: 1. Experimental results. Compos. Part A **30**(1), 75–83 (1999)
H.D. Wagner, R.A. Vaia, Nanocomposites: Issues at the interface. Mater. Today **7**(11), 38–42 (2004)
H. Wagner, O. Lourie, Y. Feldman, R. Tenne, Stress-induced fragmentation of multiwall carbon nanotubes in a polymer matrix. Appl. Phys. Lett. **72**(2), 188–190 (1998)
Q. Wang, J. Dai, W. Li, Z. Wei, J. Jiang, The effects of CNT alignment on electrical conductivity and mechanical properties of SWNT/epoxy nanocomposites. Compos. Sci. Technol. **68**(7–8), 1644–1648 (2008)
C. Wang, Y. Li, L. Tong, Q. Song, K. Li, J. Li, Q. Peng, X. He, R. Wang, W. Jiao, S. Du, The role of grafting force and surface wettability in interfacial enhancement of carbon nanotube/carbon fiber hierarchical composites. Carbon **69**, 239–246 (2014)
C. Wang, J. Li, S. Sun, X. Li, F. Zhao, B. Jiang, Y. Huang, Electrophoretic deposition of graphene oxide on continuous carbon fibers for reinforcement of both tensile and interfacial strength. Compos. Sci. Technol. **135**, 46–53 (2016)
C. Wang, M. Zhao, J. Li, J. Yu, S. Sun, S. Ge, X. Guo, F. Xie, B. Jiang, E.K. Wujcik, Silver nanoparticles/graphene oxide decorated carbon fiber synergistic reinforcement in epoxy-based composites. Polymer **131**, 263–271 (2017a)
Y. Wang, S.K. Raman Pillai, J. Che, M.B. Chan-Park, High interlaminar shear strength enhancement of carbon fiber/epoxy composite through fiber-and matrix-anchored carbon nanotube networks. ACS Appl. Mater. Interfaces **9**(10), 8960–8966 (2017b)
J. Williams, M. Donnellan, M. James, W. Morris, Properties of the interphase in organic matrix composites. Mater. Sci. Eng. A **126**(1–2), 305–312 (1990)
K.I. Winey, R.A. Vaia, Polymer nanocomposites. MRS Bull. **32**(04), 314–322 (2007)

Q. Xia, Z. Zhang, Y. Liu, J. Leng Buckypaper and its composites for aeronautic applications. Compos. Part B Eng.:108231 (2020)
C. Xiao, Y. Tan, X. Wang, L. Gao, L. Wang, Z. Qi, Study on interfacial and mechanical improvement of carbon fiber/epoxy composites by depositing multi-walled carbon nanotubes on fibers. Chem. Phys. Lett. **703**, 8–16 (2018)
X.-L. Xie, Y.-W. Mai, X.-P. Zhou, Dispersion and alignment of carbon nanotubes in polymer matrix: A review. Mater. Sci. Eng. R: Rep. **49**(4), 89–112 (2005)
L. Yang, X. He, L. Mei, L. Tong, R. Wang, Y. Li, Interfacial shear behavior of 3D composites reinforced with CNT-grafted carbon fibers. Compos. Part A **43**(8), 1410–1418 (2012)
B. Yang, X. Tang, K. Yang, F.Z. Xuan, Y. Xiang, L. He, J. Sha, Temperature effect on graphene-filled interface between glass–carbon hybrid fibers and epoxy resin characterized by fiber-bundle pull-out test. J. Appl. Polym. Sci. **135**(19), 46263 (2018)
H. Yao, X. Sui, Z. Zhao, Z. Xu, L. Chen, H. Deng, Y. Liu, X. Qian, Optimization of interfacial microstructure and mechanical properties of carbon fiber/epoxy composites via carbon nanotube sizing. Appl. Surf. Sci. **347**, 583–590 (2015)
T. Yokozeki, Y. Iwahori, S. Ishiwata, Matrix cracking behaviors in carbon fiber/epoxy laminates filled with cup-stacked carbon nanotubes (CSCNTs). Compos. Part A **38**(3), 917–924 (2007)
S. Zhang, W. Liu, J. Wang, B. Li, L. Hao, R. Wang, Improvement of interfacial properties of carbon fiber-reinforced poly (phthalazinone ether ketone) composites by introducing carbon nanotube to the interphase. Polym. Compos. **36**(1), 26–33 (2015)
L. Zheng, Y. Wang, J. Qin, X. Wang, R. Lu, C. Qu, C. Wang, Scalable manufacturing of carbon nanotubes on continuous carbon fibers surface from chemical vapor deposition. Vacuum **152**, 84–90 (2018)
Y. Zhou, F. Pervin, L. Lewis, S. Jeelani, Fabrication and characterization of carbon/epoxy composites mixed with multi-walled carbon nanotubes. Mater. Sci. Eng. A **475**(1–2), 157–165 (2008)
J. Zhu, A. Imam, R. Crane, K. Lozano, V.N. Khabashesku, E.V. Barrera, Processing a glass fiber reinforced vinyl ester composite with nanotube enhancement of interlaminar shear strength. Compos. Sci. Technol. **67**(7–8), 1509–1517 (2007)

Rheology of Epoxy/Synthetic Fiber Composites

8

Mariacristina Gagliardi

Contents

Abstract

Rheology studies the deformation and the flow that materials show under the effect of external forces applied to bodies. So that, rheology can study a variety of materials, from elastic Hookean solids to viscous Newtonian liquids. Rheological analysis finds applications mainly in material development but also in several industrial aspects, such as their handling and storage.

Rheometry is the study of rheological properties. It comprises several ad hoc analyses able to identify the flow law and the mechanical constitutive models of

M. Gagliardi (✉)
NEST, Istituto Nanoscienze-CNR and Scuola Normale Superiore, Pisa, Italy
e-mail: mariacristina.gagliardi@nano.cnr.it

S. Mavinkere Rangappa et al. (eds.), *Handbook of Epoxy/Fiber Composites*,
https://doi.org/10.1007/978-981-19-3603-6_10

materials tested. Rheometry is also useful in those processes focused to the optimization of material properties, thanks to the possibility to predict the long-term behavior of tested materials in specific working conditions.

In synthetic fiber composites materials, rheological analysis can help to understand properties of raw materials and final products. In particular, rheology can give several information related to production processes, storage, ranges of optimal working conditions, and durability.

The first part of this chapter illustrates some basic aspects of rheology and the theory behind rheological tests. The fundamental terminology and the most common flow rules related to polymeric materials will be here explained. In the second part, the most important applications of rheology in fiber-reinforced epoxy composites will be illustrated to underline the importance of this science in the industrial world.

Keywords

Rheology · Rheometry · Viscosity · Flow curve · Chemorheology

Introduction

Rheology studies the flow of materials showing plastic flow rather than elastic deformation under the application of external forces. A very large number of materials can have plastic characteristics, thus rheological studies are related to liquid, soft, and solid matter materials.

Rheology investigates those properties deriving from the combination of non-linear viscous and plastic behaviors. So that, rheology aims at extend the domain of continuum mechanics (Fig. 1).

A complete rheological characterization provides a good prediction of the whole mechanical behavior of a system at the continuum-scale level.

On the basis of the microscale and the nanoscale material properties, results obtained from rheometry can be interpreted comprising also the effect of material structure, e.g., considering effects related to the molecular weight of polymers, the macromolecular architecture, size and geometry of fillers, and the energy balance at the filler/matrix interface.

In blends, rheology can give important information on the change of mechanical properties as a function of their components, their compatibility after mixing and the nonadditive laws.

In composite systems, rheological measurements are useful to understand the interactions between fillers and matrices, the effect of filler geometry (e.g., particles, fibers, . . .) and size (e.g., long or chopped fibers), and the arrangement of fillers in the matrix.

In general, rheological studies are well established in the following fields:

- Materials science, in particular for polymers, polymer melts, swellable polymer networks, gels and sol-gel systems, and colloids
- Food science and cosmetics, to study their stability with time, to develop suitable packaging and making them easy to use

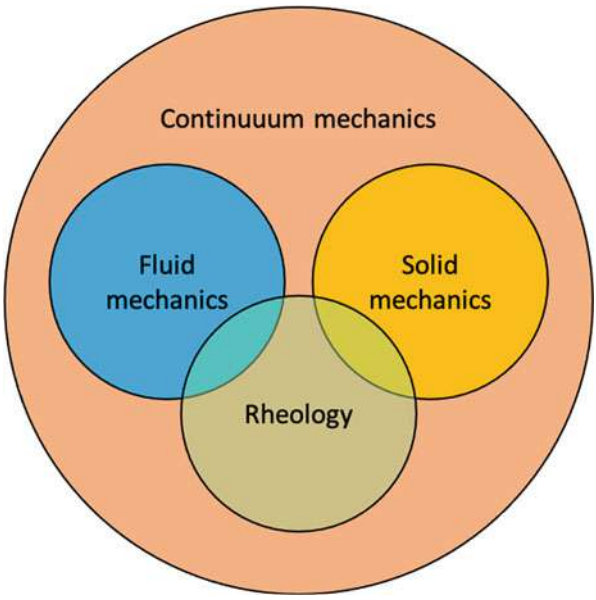

Fig. 1 The full domain of the continuum mechanics

- Geology, to understand and predict the flow of geological materials
- Physiology, for a better knowledge of body fluid motion, both in physiological and pathological conditions

Systems with "fluid" characteristics behave as a liquid, or flow under the effect of external loads. An external load generates a stress state in the fluid, defined as the applied force per area. Similarly to the solid mechanics approach, we can identify different stresses, such as torsional or shear, that can be applied to fluids. Thus, materials respond in different ways under the effect of different stresses.

Material response is strictly related to fundamental mechanical properties of the system, mainly depending on stress and strain tensors. It means that each stress type induces different deformations. The main aim of rheology is the identification of a relationship between external loads, internal stresses, and deformation.

In addition to the experimental rheometry, several studies can be completed with theoretical rheology principles. The theoretical rheology aims at mathematically explain the relationship between the external forces acting on the system and the generated internal stresses and strain gradients.

Basics of Rheology

Following there is a basic list of some key terms and concepts related to rheology.

Key Terms

We now list in this paragraph some introductory key terms. Their physical significance is following better clarified.

- The term rheology, the study of matter flow and deformation, derives from the Greek words "rheo" (to flow) and "logia" (the study of). This name fully circumscribes the domain of this science, focused on the flow rules of solid-like liquids and liquid-like solids.
- Rheological tests performed to identify the rheological law of a material are generally indicated as rheometry, comprising all experimental tests performed to discover the flow rule of a material.
- In the analysis of rheological systems, the most important material parameter to characterize is called viscosity. The viscosity, generally indicated with the symbol h, is the resistance of the material to flow, or the ratio between the shear stress and the shear rate (following defined).

Rheometry tests are designed to simulate both a standard analysis, for the calculation of key parameters, and the actual processing and working conditions that the system undergoes.

To cover all the aspects of how the system behaves under specific conditions, rheometric tests use several kinds of mechanical loadings. A deep knowledge of the stress states in the material is strictly important to maximize the knowledge of the system gained by rheological characterization.

The most important amounts that can be calculated in a rheometric test are:

- The shear stress, that is the force applied to a body in tangential direction
- The shear strain, or the deformation arising after the application of a shear stress
- The shear rate, or the rate of (temporal) change in strain

Results of rheometry tests are generally represented as plots of the measured physical quantity as a function of the applied external load. The most important plots obtained in rheometry are as follows:

- The flow curve, that is the plot of the shear stress versus the shear rate
- The viscosity curve, or the plot of the viscosity versus the shear rate

Rheological Models

Rheological models are mathematical laws that generally describe the rheological behavior of materials and systems.

Such mathematical laws were developed to simplify the interpretation of experimental data from rheometry tests but also to calculate, in most cases, the rheological parameters characteristic of the system.

Empirical and semiempirical models were developed, based on the coupling of elastic and viscous elements, to catch both material characteristics.

Before going in detail, it is fundamental to understand a basic classification in Newtonian and non-Newtonian fluids, widely used in rheology.

Newtonian Fluids (Viscous Liquids)

Isaac Newton formulated the first hypothesis on the resistance of a fluid to the motion promoted by its deformation (Philosophiæ Naturalis Principia Mathematica, 1686).

In his hypothesis, Newton stated that "the resistance which arises from the lack of slipperiness of the parts of the fluid, other things being equal, is proportional to the velocity with which the parts of the liquid are separated from one another." This hypothesized "lack of slipperiness" was attributed to an internal friction generated during the fluid motion. Newton was the first that named the internal friction as *viscous* friction.

About 150 years later, George Stokes perfected the Newton's theory. He studied the forces involved in a system composed of two sliding plates separated by a fluid thin layer. Stokes discovered that the force required to slide the plates over each other is linearly proportional to the differential plate velocity, and inversely proportional to the thickness of the fluid layer between them, the viscosity, and the overall surface of the plates involved in the contact with the fluid. Moreover, the stress profile across the thickness of fluid layer linearly changed, without any dependency on the spatial coordinate.

Those results indicated that the forces applied to the thin fluid layer were proportional to the rate of velocity change in the fluid across all the thickness. Fluids with this linear behavior are known as Newtonian fluids.

Generally speaking, a Newtonian fluid is a fluid characterized by a linear dependency of the shear rate upon the shear stress. The mathematical law used to describe the behavior of a Newtonian fluid contains a constant parameter, the so-called shear viscosity, that is used to relate shear stress and shear strain.

According to the given definition, in Newtonian fluids, all the applied forces are proportional to the rates of velocity vector in the fluid. Thus, viscous stress tensors and the strain rate are related each other by the constant viscosity tensor.

Let's we consider a single element of fluid surrounded by other equal elements of fluid. Our single element of fluid undergoes a stress state given by the forces exerted by the motion of surrounding elements. Such external forces are, mainly, viscous forces. So, our single element of fluid gets gradually deformed over time.

Forces acting on this single element can be mathematically approximated with a first-order law describing the viscous stress tensor $\boldsymbol{\tau}$ (note that the symbol is bold, this notation is conventionally used to indicate tensors).

At the same time, the deformation of the single element of fluid over time can be mathematically approximated with a first-order time-dependent strain tensor $\boldsymbol{\gamma}$.

The strain tensor has a first-order time derivative called strain rate tensor $\dot{\boldsymbol{\gamma}}$. The $\dot{\boldsymbol{\gamma}}$ tensor describes the change with time of the deformation in the fluid element.

Elements of the tensor $\dot{\boldsymbol{\gamma}}$ are also expressed as velocity gradient ∇v.

Elements composing cited tensors depend on the spatial coordinates. Thus, tensors are expressed by 3×3 matrices in the selected coordinate system.

In Newtonian fluids, the stress tensor and the velocity gradient tensor are related by Eq. 1:

$$\boldsymbol{\tau} = \mu(\nabla v) \tag{1}$$

$\boldsymbol{\mu}$ is a fourth-order tensor, and components are not affected by fluid velocity or its stress state.

A particular case of Newtonian fluids is represented by *isotropic* Newtonian fluids. "Isotropic" means that the physical properties of a material do not change when measured in different directions. In isotropic Newtonian fluids, the properties that do not vary are mechanical properties. Thus, the viscosity tensor is only composed by two real coefficients: the resistance to continuous shear deformation and the resistance to continuous expansion/compression.

On the other hand, also anisotropic Newtonian fluids can exist. "Anisotropic" means that physical properties of the material significantly change with the direction of measurements. In anisotropic Newtonian fluids, the tensor $\boldsymbol{\mu}$ relates the stress tensor with the deformation rate tensor. The last tensor contains the spatial derivatives of deformation rate as elements.

Non-Newtonian Fluids

Unlike Newtonian fluids, the rheological behavior of a non-Newtonian fluid is not described by the linear Newton's law of viscosity. Moreover, viscosity depends on stress or, most commonly, on shear rate or shear rate history.

In other terms, the relation between the shear stress and the shear rate in non-Newtonian materials is not linear and the value of the internal shear stress in the absence of applied shear rate could be nonzero.

Non-Newtonian fluids can also show a time-dependent viscosity, in some cases. For this reason, the viscosity is often not considered as a key parameter to adequately describe the behavior of these materials. To overcome this limitation, the behavior of such fluids is generally described by using the *apparent viscosity*.

Non-Newtonian fluids show a really complex behavior, characterized by several nonlinearities in the constitutive law. Thus, particular conditions are requested to perform a good rheological characterization of these materials. One widely used technique is the extensional rheometry, in which the applied external loads are purely extensional, with no shear loads. Another common technique is to perform the characterization in an oscillatory shear regime, in which the applied external loads follow a time-dependent law.

To recap, non-Newtonian fluids are classified as:

- Systems with a nonlinear viscosity
- Systems with a time-dependent viscosity

In the inventory of systems with a nonlinear viscosity, there are: viscoplastic (or Bingham) fluids, shear thinning (or pseudoplastic) fluids, shear thickening (or dilatant) fluids, and generalized non-Newtonian fluids.

- In viscoplastic fluids, the relationship between shear stress-shear rate is linear but the intercept of the curve, given by the value of the shear stress for a null shear rate, is not null. This characteristic indicates that a small but finite yield stress is required to activate the fluid flow.
- The main characteristic of shear thinning fluids is that the apparent viscosity decreases with an increased stress. This nonlinear behavior indicates that the more is the applied external force the simpler is the flow of the material.
- The opposite behavior of shear thinning is the shear thickening. In shear thickening fluids, we can find an increasing apparent viscosity with increased applied stress. In other words, shear thickening materials increase their resistance to flow under high stresses, assuming a solid-like behavior.
- In generalized Newtonian fluid, the viscosity is constant, the shear stress is a discrete or punctual function of the shear strain rate, and the internal stress state does not depend on the shear strain history.

Systems with a time-dependent viscosity are defined as: thixotropic fluids and rheopectic fluids.

- In thixotropic fluids, the viscosity decreases with the external load-application duration. It means that thixotropic materials have a tendency to become more fluids after a prolonged applied shear stress, or a prolonged shear strain.
- In rheopectic fluids, the apparent viscosity increases with the duration of the external load, thus they show a "more solid behavior," becoming less fluid, after prolonged applied loads.

The shear stress versus shear strain rate curves of Newtonians and non-Newtonian fluids with a nonlinear viscosity are illustrated in Fig. 2a, while the viscosity versus shear strain rate curves of non-Newtonian fluids with a time-dependent viscosity are reported in Fig. 2b.

Conditions Affecting the Rheological Properties of Materials

Rheological properties can be significantly affected by some specific conditions. In addition to the kind of external applied load and the loading frequency, the most relevant properties affecting rheology are:

- Temperature
- Structure of the system at the micro- or nanoscale

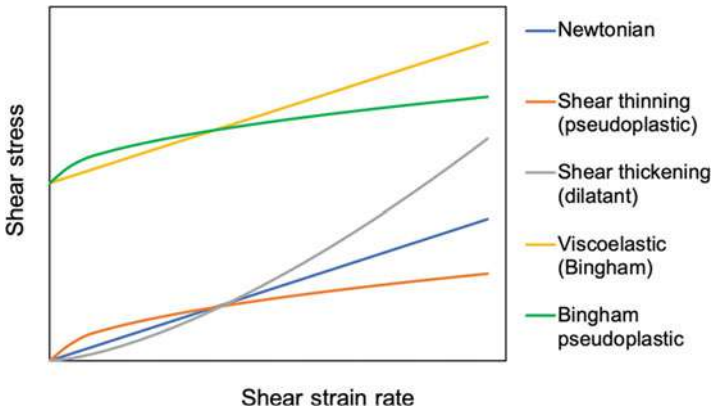

Fig. 2a Shear stress versus shear strain rate curves for different classes of rheological materials

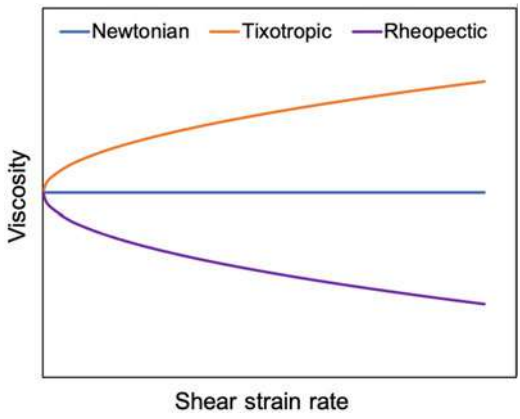

Fig. 2b Viscosity versus shear strain rate curves for different classes of time-dependent viscosity materials

Effect of Temperature

The temperature is one of the most important parameters affecting all materials properties, and strongly it affects rheological properties. The viscosity usually shows a very strong dependency on the temperature. This dependence is commonly treated as a separated function from the effect of all other parameters (e.g., the shear rate or the shear frequency). As a general rule, the viscosity depends on the temperature as:

$$\eta(\dot{\gamma}, T) = \eta(\dot{\gamma}) \cdot f(T) \tag{2}$$

and the function *f(T)* is defined for each material or system studied.

One of the simpler function form *f(T)* widely used is:

$$f(T) = exp\,(-\alpha \cdot \Delta T) \tag{3}$$

Here, the parameter a is called temperature sensitivity of the viscosity, while the temperature difference is calculated between the working temperature and the temperature at which viscosity is known.

In the case of composite rheology, an additional effect of the temperature during the curing should be considered. This aspect is deeply described in the second part of the chapter.

Structure of the System at the Micro- or Nanoscale

Rheological properties of a fiber composite material are affected by several aspects, mainly the properties of the matrix, the fiber aspect ratio, and the interface energy between matrix and fiber.

Concerning polymer matrices, rheological properties are mainly governed by the molecular architecture of the polymer. The molecular structure can strongly change by changing the physical status of the material, e.g., in polymer solutions or melts.

Basically, the mechanical properties of a polymer at the macromolecular scale are determined by the intramolecular and intermolecular interactions occurring between chain atoms and between chains.

Polymeric chains are a sequence of atoms covalently attached each other. Intramolecular forces acting in polymers are prevalently related to the C—C bond, while bonds between heteroatoms (e.g., C—N, C==N, C—O, C==O, C—S, and so on) are less frequent.

The energy of the C—C single bond is ~350 kJ/mol, and this value would lead to a theoretical material stiffness of 300–400 GPa. Anyway, polymers show in all cases a considerably lower stiffness in experimental tests than the theoretical value. The difference between theoretical and actual stiffness arises from the macromolecular misaligning. This observation leads to consider also the intermolecular interactions as important factor in polymer strength. Intermolecular interactions are mainly accounted to be Van Der Waals forces, and their entity is inversely proportional to the six-power of the distance between atoms. Thus, in the presence of solvents, plasticizers, or when heated, the distance between two macromolecules increases, the free volume increases, thus intermolecular interactions, and consequently stiffness, decrease.

The degree of polymerization, or the number of repeating units per macromolecule, is another factor affecting macromolecular interactions. Polymers with a low degree of polymerization are liquid or very soft at room temperature while, increasing the degree of polymerization, they gradually become stiffer at the same temperature and with the same additives.

However, while the stiffness rapidly tends to a plateau, the viscosity steadily increases with molecular weight, generally with a power law (Fig. 3).

In systems containing “soft” additives, such as macromolecular coils or clusters, soft particles or vesicles, rheological properties are also affected by deformation of these components.

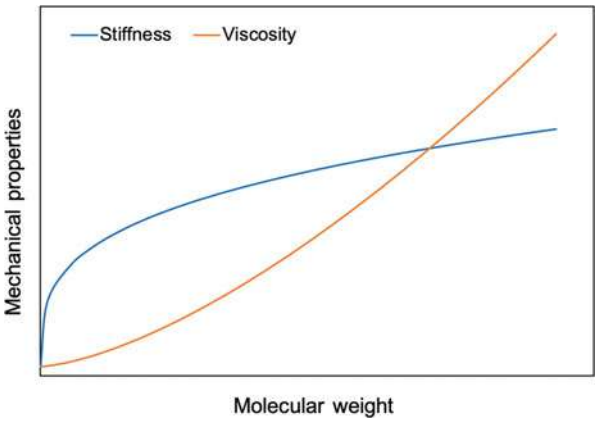

Fig. 3 Trends of mechanical properties (stiffness and viscosity) as a function of the polymer matrix molecular weight

As a general rule, deformable structures dispersed in a liquid phase tend to get deformed in the direction of load application, while non-deformable structures tend to get aligned in the load direction.

In the case of fiber composites, rheological properties are affected by the presence of fibers only if fibers are short and before curing. In this case, fibers dispersed in a liquid (pre-polymerized) matrix injected in a mold tend to align to the injection flow. In most cases, the general rule is that the uncured composite become shear thinning during load application, while thixotropy dominates when loading is stopped, and systems tend to return thicker with time.

Rheometry Measurements

The selection of the most useful experimental setup used to test rheological properties of materials depends on the macroscopic properties of the specimen.

As a general rule, the characterization of soft materials (e.g., gels and elastomers) is performed by the use of viscosimeters or rheometers rheometer, while in harder materials (e.g., metals, polymers, or highly viscous gels), the more appropriate characterization is obtained by dynamic mechanical analysis (DMA).

Viscometry

Rheological properties of epoxy materials can be assessed by means of several different tests. The selection of the proper characterization is given upon the sample properties and the information needed.

Rheological tests can be static, based on the application of a constant load, or dynamic, in which the applied load follows a cyclic function (e.g., sinusoidal).

In the case of static tests, a constant stress, or strain, is applied to study the creep of materials and to understand the effect of a static load for long-term applications.

In the same kind of static test, the load can be removed and the materials studied in order to evaluate the molecular relaxation.

Dynamic tests study the material response, in terms of stress or strain, under the effect of a cyclic load that can be applied as a steady shear or as an oscillatory regime. In addition to variable stresses or strain, also temperature and frequency can be cyclically varied. Steady shear loads are generally used to study the rheology of the epoxy matrix before curing. On the other hand, oscillatory tests are useful to understand the effects of curing kinetics. Dynamic tests are particularly interesting because they can give several information on viscoelastic properties of the matrix. The only restriction to the application of dynamic tests is the identification, prior to the characterization, of the linear viscoelastic range, in order to be sure that the molecular structure of the material does not change under the effect of the load and the material response does not depend on the magnitude of the load.

Rheometry

The instrumentation used to evaluate rheological parameters of soft materials are known as rheometers.

A rheometer applies several kinds of mechanical loads to trigger the flow and, at the same time, it registers the response of the material. Concerning applied loads, a rheometer that can control the applied shear stress or the applied shear strain (shear rheometer) or the extensional stress or extensional strain (extensional rheometers). The loading application is generally performed by applying constant or time-dependent shear rate functions.

Rheometry enables the calculation of all those functions and parameters, such as the apparent viscosity, the shear stress, the complex shear moduli, as a function of the shear rate, the time or the frequency of the entity of the applied load.

Dynamic Mechanical Analysis

The dynamic mechanical analysis (DMA) technique can be useful in the characterization of the viscoelastic behavior of a material. In this characterization, a cyclic stress is applied to the specimen while the deformation is calculated. The whole set of results allow calculating the complex elastic modulus of the material.

DMA is also coupled with frequency or temperature changes, in order to verify the effect of such parameters on the complex modulus.

Constitutive Rheological Laws

Experimental data gathered from rheometry are then used to identify an appropriate mathematical model for the studied material, or in other words the *constitutive law* of the system. The constitutive law correlates the shear stress and the shear strain, or the shear strain rate, each other.

Constitutive laws are mathematical equations that can analytically describe the material response, in terms of internal stress state, after the application of the external load. Thus, the main result of this calculation is the stress tensor.

The calculated stress tensor generally depends on the direction and orientation of the applied force in respect to the surface of application of the external load. To be defined, the velocity gradient needs that the direction along which the velocity varies is specified.

In steady shear flow analysis (Fig. 4a), the material lies between two flat plates. In this setup, one plate (generally, the top plate) can move and the other one (generally, the bottom plate) is fixed. The fluid is sheared by the motion of the moving plate in the direction of the motion.

If D_x is the displacement of the top plate in the x direction, and δ is the distance between the two plates, the shear strain in the xy plane, indicated by γ_{xy}, is given by:

$$\gamma_{xy} = \frac{D_x}{} \tag{4}$$

Indicating with u_x the velocity of the top plate in the x direction, the velocity gradient $\dot{\gamma}$, also called shear rate, is given by:

$$\dot{\gamma} = \frac{dv_x}{dy} = \frac{u_x}{\delta} \tag{5}$$

The velocity profile across the fluid layer thickness v_x arises from the stretching of the fluid given by the relative motion of plates. Considering a linear velocity profile (see Fig. 4a), the velocity profile function is $v_x = v_0$ at $x = 0$ at the interface with the resting plate, and $v_x = D_R \cdot v_0$ at $x = \delta$ at the interface with the moving plate, where D_R is the final displacement of the top plate.

In this test setup, the velocity profiles in directions y and z are zero.

The deformation between $x = 0$ and $x = \delta$ is indicated with γ_{xx} and it is calculated as:

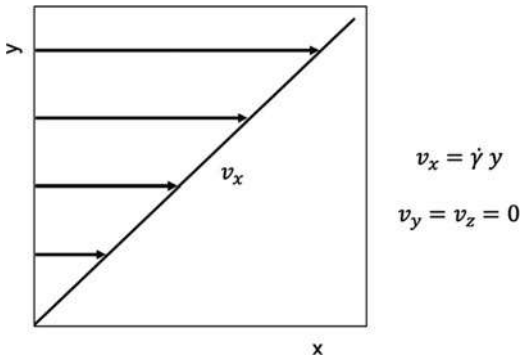

Fig. 4a Velocity profile across thickness in steady shear flow analysis

$$\gamma_{xx} = \frac{(D_R\ \nu_0)\ \Delta t}{\delta} \tag{6}$$

while the deformation in the y direction is given by $\gamma_{yy} = -\gamma_{xx}$.

The deformation γ is not a scalar. It is because this amount has multiple components in cartesian coordinates. Thus, it is described by the tensor $\boldsymbol{\gamma}$:

$$\boldsymbol{\gamma} = \gamma_{ij} = \begin{bmatrix} \gamma_{xx} & \gamma_{xy} & \gamma_{xz} \\ \gamma_{yx} & \gamma_{yy} & \gamma_{yz} \\ \gamma_{zx} & \gamma_{zy} & \gamma_{zz} \end{bmatrix} \tag{7}$$

The shear strain rate tensor $\dot{\boldsymbol{\gamma}}$ is the time derivative of $\boldsymbol{\gamma}$:

$$\dot{\boldsymbol{\gamma}} = \frac{\partial \gamma_{ij}}{\partial t} = \begin{bmatrix} \dot{\gamma}_{xx} & \dot{\gamma}_{xy} & \dot{\gamma}_{xz} \\ \dot{\gamma}_{yx} & \dot{\gamma}_{yy} & \dot{\gamma}_{yz} \\ \dot{\gamma}_{zx} & \dot{\gamma}_{zy} & \dot{\gamma}_{zz} \end{bmatrix} \tag{8}$$

Under the effect of the shear strain, a shear stress state with the same direction of the relative plate motion is generated within the material. Such shear stress state is another tensor, and its components are indicated with τ_{ij}. The shear stress state generated by the applied deformation is also called deviatoric stress. The calculation of components of the deviatoric stress tensor involves the viscosity function η. The mathematical equation used in this calculation is:

$$\tau_{ij} = -\eta \cdot \dot{\gamma}_{ij} \tag{9}$$

Also the overall stress state tensor comprises some additional components orthogonal to the surface over which the external load is applied. The normal components of the stress represent the hydrostatic pressure in the fluid. There are two normal components, generally indicated with N_1 and N_2, that are calculated as the difference between tangential stresses in different directions:

$$N_1 = \tau_{xx} - \tau_{yy} \tag{10}$$

$$N_2 = \tau_{yy} - \tau_{zz} \tag{11}$$

These components N_1 and N_2 are also called primary and secondary normal stress differences, respectively.

Normal components of the stress N_1 and N_2 are related to the shear strain rate by means of the following equations:

$$N_1 = -\psi_1 \cdot \dot{\gamma}^2 \tag{12}$$

$$N_2 = -\psi_2 \cdot \dot{\gamma}^2 \tag{13}$$

where ψ_1 and ψ_2 are the primary and the secondary normal stress coefficient, respectively.

Parameters η, ψ_1, and ψ_2 are function of the shear rate and are experimentally evaluated.

In Eqs. 12 and 13, normal stress components are proportional to the square of the shear strain rate in order to prevent changes in the shear direction, in the case of negative *y*, or by changing the shear direction through the test.

In dynamic rheological measures in oscillatory regime (Fig. 4b), the externally imposed shear varies with time, following a predefined cyclic law. The oscillatory regime is useful in the calculation of the phase angle between the imposed shear strain rate and the measured shear stress.

The linear viscoelastic region (LVR) shows a linear correlation between shear stress and shear strain. It involves that the stress response function perfectly fits the imposed shear strain function. Also in this test, velocity profiles in directions *y* and *z* are zero.

In dynamic tests, the oscillatory velocity field is given by:

$$v_x(t) = [\dot{\gamma}_{max} \cdot \cos(\omega t)] \cdot y \tag{14}$$

where $\dot{\gamma}_{max}$ is the maximum velocity gradient, and ω is the frequency of the cyclic applied shear strain.

The ratio between $\dot{\gamma}_{max}$ and ω is the maximum value of the shear strain γ_{max}. According to the previous definition of $v_x(t)$, the shear stress results:

$$\tau_{xy} = \tau_{max} \cdot \cos(\omega t - \varphi) \tag{15}$$

where τ_{max} is the maximum shear stress value registered in the test, and φ is the phase shift between the imposed strain and the measured stress.

The oscillatory stress measured in the test is a complex function in which one term is in-phase with the velocity and the other term is out-of-phase (orthogonal).

Now we define the complex viscosity η^* as follow:

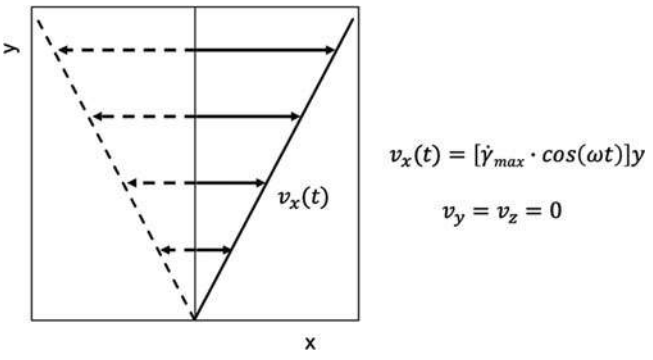

Fig. 4b Velocity profile across thickness in dynamic rheological measures in oscillatory regime

$$\eta^* = \eta' - i\eta'' \tag{16}$$

where η' and η'' are the two components used to define the complex viscosity. The complex viscosity is experimentally calculated as the ratio between values over time of the shear stress and the shear strain:

$$\eta^* = \frac{\tau_{xy}(t)}{\dot{\gamma}_{xy}(t)} \tag{17}$$

Combining Eqs. 9 and 15, the shear stress becomes:

$$\tau_{xy} = -\eta' \cdot \dot{\gamma}_{max} \cos(\omega t) - \eta'' \cdot \dot{\gamma}_{max} \sin(\omega t) \tag{18}$$

If the shear strain rate approaches zero and the applied shear frequency is significantly low, η' is approximatively the values of viscosity calculated in steady shear flow regime. This amount is generally indicated as dynamic viscosity.

Now we define the complex shear modulus G^* as:

$$G^* = G' - iG'' \tag{19}$$

Here, G' and G'' are, respectively, the storage and the loss modulus. Such two components are related to the dynamic viscosity coefficients through the frequency of the applied shear strain:

$$G' = \omega\, \eta' \tag{20}$$

$$G'' = \omega\, \eta'' \tag{21}$$

Reformulation Eq. 16 as a function of the complex shear modulus we obtain:

$$\tau_{xy} = -G' \cdot \gamma_{max} \cos(\omega t) - G'' \cdot \gamma_{max} \sin(\omega t) \tag{22}$$

We need to analyze the relationship between these physical amounts and the stress response upon the application of external loading to understand the importance such parameters.

G' linearly correlates with the component of the stress in-phase with the applied strain, and then it is strictly related to the recoverable elasticity of the material. On the contrary, G'' correlates to the orthogonal stress response to the applied strain, resulting in the dissipative energy losses in the material. Their ratio is called phase angle, and it is indicated with the symbol d. Accordingly, the G' function is pretty similar to the shear modulus calculated for an ideal rubbery material, in which the stress response is perfectly in phase with the applied shear strain. On the contrary, the G'' function has a physical meaning similar to that of the shear modulus in a purely viscous material, in which there is not elastic recovery and the energy resulting from applied external forces is fully dissipated by the viscous flow of molecules.

Components G' and G'' of the complex shear modulus generally depend on the frequency of the applied strain function, and this occurs more in macromolecular materials. Some materials tested under a frequency scan show a point called *cross-over*. At the crossover, G' and G'' have the same value. In materials crossover where the G'/G'' crossover occurs, one of two modules dominates the other at low frequencies and vice versa at high frequencies.

Constitutive Rheological Models

Each class of materials has its own constitutive rheological model.

The constitutive rheological law of Newtonian fluids has only one parameter, the viscosity. For this class of materials, the constitutive equation calculated by means of rheological tests is able to describe and predict the full flow behavior in every laminar flows. For Newtonian fluids, the constitutive law is:

$$\boldsymbol{\tau} = -\eta \cdot \dot{\boldsymbol{\gamma}} \tag{23}$$

Here $\boldsymbol{\tau}$ and $\dot{\boldsymbol{\gamma}}$ are both tensors.

As already reported in Eq. 9, the tensor $\boldsymbol{\tau}$, also called deviatoric stress tensor, is given by:

$$\boldsymbol{\tau} = \tau_{ij} = \begin{bmatrix} \tau_{xx} & \tau_{xy} & \tau_{xz} \\ \tau_{yx} & \tau_{yy} & \tau_{yz} \\ \tau_{zx} & \tau_{zy} & \tau_{zz} \end{bmatrix} \tag{24}$$

While, according to Eq. 1, we can define the strain rate tensor $\dot{\boldsymbol{\gamma}}$ as:

$$\dot{\boldsymbol{\gamma}} = \nabla \mathbf{v} + (\nabla \mathbf{v})^T \tag{25}$$

Here, ∇ is the gradient operator, $\nabla \mathbf{v}$ is the velocity gradient tensor, and the superscript T is the transpose operator. The velocity gradient is given by:

$$\nabla \mathbf{v} = \begin{bmatrix} \frac{\partial v_x}{\partial x} & \frac{\partial v_x}{\partial y} & \frac{\partial v_x}{\partial z} \\ \frac{\partial v_y}{\partial x} & \frac{\partial v_y}{\partial y} & \frac{\partial v_y}{\partial z} \\ \frac{\partial v_z}{\partial x} & \frac{\partial v_z}{\partial y} & \frac{\partial v_z}{\partial z} \end{bmatrix} \tag{26}$$

Components of the strain rate tensor (Eq. 25) are defined as:

$$\dot{\gamma}_{ij} = \frac{\partial v_i}{\partial x_j} + \frac{\partial v_j}{\partial x_i} \tag{27}$$

where v_i and v_j are the cartesian components of the velocity vector **v**, and x_i and x_j are the component of the position vector **x**. Combining Eqs. 27 and 9 for a steady shear flow, we obtain:

$$\tau_{xy} = -\eta\,\dot{\gamma}_{xy} = -\eta\,\frac{\partial v_x}{\partial y} \tag{28}$$

in which the component v_y is zero for this test (see the previous section).

Once calculated η, Eq. 28 can be applied to experimental data in the prediction of the Newtonian material behavior in each laminar flow.

The Newtonian constitutive rheological law can be generalized to be applied to non-Newtonian fluids. The generalization introduces a function of the shear rate as the viscosity parameter. This generalization needs to calculate the three invariants of the deformation rate tensor, and the second is the most important invariant. While the first invariant is empty for incompressible fluids, the second invariant of the deformation rate tensor contains both hydrostatic pressure and shear stresses. Finally, the third invariant is empty in shear-governed flows.

The second invariant of the shear rate tensor can be calculated as follows:

$$J_2 = \sum_i \sum_j \dot{\gamma}_{ij} \cdot \dot{\gamma}_{ji} \tag{29}$$

The viscosity is calculated as the square root of the halved second invariant, resulting:

$$\eta = \sqrt{\frac{1}{2}\,J_2} = \sqrt{\frac{1}{2}\sum_i \sum_j \dot{\gamma}_{ij} \cdot \dot{\gamma}_{ji}} \tag{30}$$

Combining Eqs. 28 and 30, we can calculate the constitutive equation in laminar flow for the majority of generalized Newton fluids.

There are some generalized Newton fluids for which the use of the proposed model is significantly hard to apply, mainly because of the difficult mathematical implementation. It is the case of transient flows or in fluids with not negligible normal stresses. To overcome this limitation, some semiempirical generalized flow laws, with a reduced number of parameters, were developed. Parameters of such semiempirical models are generally calculated by fitting experimental rheometric data.

One of the most used generalized flow models for the prediction of the viscosity is:

$$\eta = K\,\dot{\gamma}_{xy}^{(n-1)} \tag{31}$$

where K and n are fitting parameters, evaluated from experiments.

A simple two-parameters power law is easy to manage, and it is also reliable enough to be applied in the analysis of a large number of systems, in particular for polymer solutions.

However, this model fails for low flow rate regimes. In such cases, the power law model can be replaced by the Carreau model:

$$\frac{\eta - \eta_\infty}{\eta_0 - \eta_\infty} = \left[1 + \left(\lambda\, \dot{\gamma}_{xy}\right)^2\right]^{\frac{n-1}{2}} \tag{32}$$

In this equation, η_∞ and η_0 are viscosities at high and low shear rate, respectively, λ is a fitting parameter calculated at the shear rate of interest, and n is a fitting parameter of the overall set of data.

Rheology in Composites

Fiber-reinforced polymer composites are widely used for several applications, thanks to their versatile anisotropic mechanical properties and the processability by means of multiple technologies. However, production processes, like fiber/matrix mixing, injection molding or extrusion, need a deep knowledge of the rheological properties of the system to be processed.

The setup of a manufacturing process is often selected on the basis of the melt rheological properties, and final mechanical properties of the materials are mainly governed by production processed and thus by rheology.

To date, there are not specific standards or guidances for the rheological analysis of epoxies and their blends. The following standards are adapted to epoxy composites and blends:

- ISO 1133-1:2011: Plastics – Determination of the melt mass-flow rate (MFR) and melt volume-flow rate (MVR) of thermoplastics – Part 1: Standard method
- ISO 6721-10:2015: Plastics – Determination of dynamic mechanical properties – Part 10: Complex shear viscosity using a parallel-plate oscillatory rheometer
- ISO 11403-2: Plastics – Acquisition and presentation of comparable multipoint data – Part 2: Thermal and processing properties
- ISO 11443:2014: Plastics – Determination of the fluidity of plastics using capillary and slit-die rheometers
- ISO 20965:2021: Plastics – Determination of the transient extensional viscosity of polymer melts
- ISO 16790:2021: Plastics – Determination of drawing characteristics of thermoplastics in the molten state
- ISO 17744: 2004: Plastics – PVT determination of specific volume as a function of temperature and pressure (PVT diagram) – Piston apparatus method

Using Rheology to Monitor the Curing Process

In glassy amorphous materials, like epoxies are, rheology is important for the analysis of the pre-polymerized matrix before the curing process. At this stage, the

matrix is a viscous liquid to be spread and formed before polymerization and it could show, during this production process, large deformations and flow.

The analysis of large deformations in epoxy resins can be studied by means of chemorheology or microrheology. Both sciences belong to the analysis of fluid flow and are specifically developed for glassy matrices. Additionally, dynamic rheometric analysis can give important insights on the curing kinetics.

Chemorheology

The rheological analysis is a useful tool to evaluate the viscoelastic behavior of thermosets during the curing process. This part of rheology is commonly referred as *chemorheology*. More specifically, chemorheology is the study of the viscoelastic behavior of chemically reacting systems, which can be cured by heating or by applying a pressure, or both. This science regards the analysis of the changes in viscosity after a chemical reaction and/or some processing conditions, and the characterization of the molecular growth in infinite molecular networks and in the gelation process of a viscous liquid to a glassy state.

In a common curing process, viscosity is the most changing property. Chemorheology is able to gather information on viscosity changes occurring in the curing process. Viscosity changes mainly when the main transition states occur, identifying phenomena such as the gelling and the vitrification.

Viscosity of thermosetting resins is affected by several external parameters, like temperature, pressure, shear rate, time, but also by some chemical properties related to the resin blend, such as the chemical properties of the matrix, size, and dimension of fillers and the presence of compatibilization agents. In a common curing process, viscosity changes continuously, due to thermal effects of the process. Referring to Fig. 5, the viscosity initially decreases (from t_1 to t_2) due to the heating carried out on the mass to be polymerized. In this step, the decrease of viscosity due to the temperature increase is partially balanced by the increase of viscosity due to

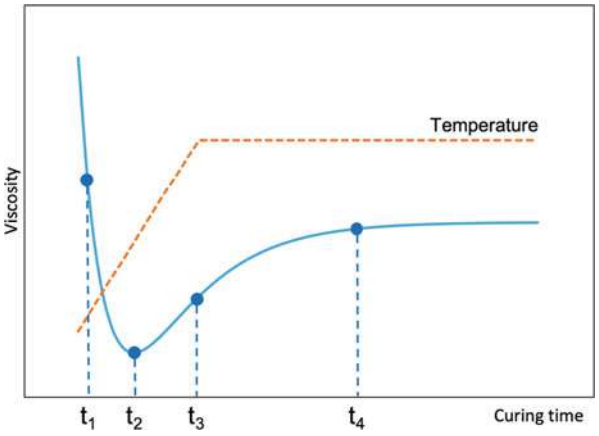

Fig. 5 Viscosity (—) and temperature (- - -) versus time in a typical curing process

the gelation process occurring in the mass from the starting fluidic state. At t_2, the temperature is still increasing while the viscosity function shows a minimum. At this stage, the pre-cured resin is applied to the mold. Between t_2 and t_3 the viscosity sharply increases, due to the formation of the crosslinked polymer network, and the material becomes an infusible solid. At t_3, the viscosity function shows an inflection point: before t_3, the slope of the function is maximum and the polymerization kinetics is the fastest achieved in the process; after t_3, the polymerization kinetics gradually slows down. After t_3, generally the temperature is kept constant until the complete curing of the resin (t_4).

From the knowledge of the viscosity function versus time in the non-isothermal curing process, important parameters like the activation energies of the processes can be calculated. On the other hand, if activation energies are known, the viscosity curve can be predicted.

Microrheology

Microrheology is an experimental technique used to determine the rheological properties of a medium by monitoring the path of a flow tracer in a microchannel. This measure related the microstructure of a polymer molecule with its flow properties, when molecules are solvated. Microparticles are generally used as flow tracer. The flow tracer is homogeneously dispersed in the sample before the measure. Common size of tracer particles is comprised between 0.3 μm and 2 μm. Particles can be added to the system or not, if the system to be analyzed already comprises particles that can be monitored.

The motion of the tracer is a visible indicator of the local rheological properties of the fluid. In fluid samples with a constant viscosity, particles are free to diffuse across the whole sample. In gelled or in partially cured samples, particle motion is hampered by the macromolecular structure and then they cannot freely diffuse.

Dynamic Rheometry

As previously reported, complex parameters like the complex modulus G* and the complex viscosity η* are evaluated by dynamic rheological measurements. This analysis is really useful to determine thermosetting resin transformations.

Epoxy resins commonly show an elastic shear modulus G' lower than the storage modulus G″ at an early stage of polymerization. It is because of the low monomer conversion at the beginning of the process. As the curing proceeds and the polymer chains grow, both moduli change, G′ raises until it reaches the same value of G″. This particular point is called *crossover* and it indicates the point at which a significant change of state, or the gelling, occurs.

The gelling of a resin can be also monitored by means of the phase angle, or the ratio between G′ and G″, that significantly changes during the process.

At the beginning of the curing, monomers are generally liquid or liquid-like and the phase angle is around 90°. At the end of the curing, the material is completely solid and the phase angle is close to 0°. In the middle of the process, the phase angle decreases from 90° to 0°, reaching the intermediate value of 45° at the gel point. This

trend is also clear in the viscosity function that steeply increases at the gelling, tending to an infinite value.

Thus, let's introduce the rheological definition of *gel point* as the time or the temperature at which the transition from a low molecular weight resin to a strongly crosslinked, fully connected, macromolecule occurs.

The selection of the best method to identify the gel point is given by some practical limitations, such as the available instrumentation and the formulation of the sample.

Another fundamental rheological transition occurring in epoxy curing is the vitrification. Vitrification is the point at which the material becomes a glassy material. The transition occurs when the curing temperature rises from the glass transition temperature to the cure temperature, which is an isothermal value. The estimation of the vitrification point can be done following several criteria, such as the arising of a time- or frequency-dependence of the G′ module, or the occurrence of a maximum in G″, or a maximum in the value of tan(δ).

Unlike gelling, vitrification is more difficult to evaluate due to limitations occurring in experimental measures (e.g., too high viscosity). Thus, additional techniques, such as spectroscopy to evaluate monomer conversion, or DMA analysis, are often needed at this stage.

The Rheology of Fiber/Melt Suspensions

Commonly, fibers act as a reinforcement for the matrix, and their presence strongly affects the behavior of the whole system, even when a Newtonian-like matrix is used. In the presence of a non-Newtonian-like matrix, the rheological behavior in the presence of fibers is even more complex to analyze.

The first study to predict the effect of a rigid filler on the viscosity of a matrix was given by Einstein for Newtonian fluids. The Einstein equation for the flow of a dilute suspension reads:

$$\eta = \eta_0(1 + k_E\phi) \tag{33}$$

where η and η_0 are the viscosities of the whole system and the disperse matrix, respectively, k_E is the Einstein coefficient, and ϕ is the volume fraction of the filler. The Einstein coefficient is strictly related to the shape of the filler, assuming lower values for spherical particles and higher values for elongated structures. In the case of uniaxially oriented fibers, oriented in the direction of the matrix flow, the Einstein coefficient is given by 2 L/D, where L is the length of the fiber, D its diameter, and L/D is called aspect ratio.

The Einstein equation is valid only for very diluted suspensions (<1% of filler) and thus not so much relevant in the field of fiber composites. It is mainly because the Einstein equation does not take into account any filler interaction, while in composites with high fractions of fillers, the increase of viscosity with the parameter ϕ is not linear.

Rheology of Cured Composites

The rheological behavior of cured epoxy resins filled with additional compounds is more complicated than that of neat epoxies. Complexities arise mainly from the structural transitions that are given by phase separations between matrix and fillers when heated. From this point of view, rheometry is a well-established technique to monitor phase separations, thanks to its capability to catch the viscoelastic changes of the analyzed materials.

The analysis of structural transitions in filled epoxy resins under curing started from early rheological studies based on the classical phase separation mechanism occurring in blends. According with this theory, the rheological analysis was devoted to the identification of all the structural changes related to separation mechanisms. This kind of changes are governed by the formulation properties and the processing parameters. The phase separation was generally identified by following the trends of the complex viscosity and the complex shear modulus. In the complex viscosity trace with temperature, the phase separation can be identified when a peak or a dip occurs.

More recently, this theory was significantly improved introducing the concept of the viscoelastic phase separation. Underlying this theory is the hypothesis that exists a correlation between changes in macromolecular arrangements, like gelation, vitrification, or phase separation, with the rheological model of the material, and thus with the related parameters. This goal is pretty difficult to be achieved due to the very wide variety of properties that epoxy resins-based composites can show, and for the large number of materials that can be used as fillers. However, some trends and characterization approaches can be generalized.

In addition to the conventional models used to describe the phase separation in solid or fluid materials, this novel approach takes into account the possibility that the final morphology of the composite is completely governed by the mechanical balance of thermodynamic and viscoelastic forces. A simple analysis of phase separation considers a binary phase in which the separation is assumed “symmetric” between the two components of the system. This property is called “dynamic symmetry.” The assumption of symmetry is valid in many systems, like an ideal mixture of liquid with similar dynamics. In the case of the viscoelastic phase separation, the theory is based on the hypothesis that a dynamic asymmetry between molecules occurs, and then the system components show marked differences in their dynamics, such as reactivity, melting, and so on. So that, the system is composed by “slow” and “fast” components interacting between them. Therefore, the equations describing a static system, like equations related to the evaluation of thermodynamic parameters or the time-independent constitutive laws, are coupled with the equations describing a dynamic system, like the equation of motion used in the calculation of transport coefficients or the relaxation properties.

It is noteworthy to underline that the morphology with two or more separated phases is crucial in filled composites because it is the main parameter affecting mechanical properties of the final manufact, causing the toughening of the composite. So that, phase separation can be considered the main desired property in

composite curing. This phenomenon is particularly marked in epoxy composited filled with thermoplastic additives.

After phase separation, the transition occurring in the material is very clear and results in a severe fluctuation of the complex viscosity. While the complex viscosity in the neat epoxy tends to constantly increase with time, due to the curing process, in composites the same parameter fluctuates when a phase change occurs. In formulations crosslinked with faster curing rates, phase separations occur earlier than in slow curing rates composites. It is related to the high temperatures applied to increase the curing rate, which lead to early phase separations.

Furthermore, the chemical composition of both matrix and fillers affects the phase separation. It is because the chemical composition dominates several parameters like viscosity, compatibility, solubility, interface energy, and so on.

Conclusions

Rheology, or flow science, can be successfully applied to the analysis of different classes of materials and also to fiber-reinforced epoxy composites. Due to their wide range of applications, it is necessary to calculate the rheological properties of epoxy composites in various industrial sectors, such as electronics, automotive, and aerospace. As previously stated, rheology includes a certain number of parameters useful in manufacturing, not only for the optimization of the production process but also for the maximization of the properties of the final products. Therefore, rheometry is considered a fundamental tool in the materials industry.

Different types of tests are developed ad hoc for tests on composites, with the aim of obtaining the desired characterization. Over the past 40 years, several efforts have been devoted to improving the understanding of epoxy composites and several specific characterizations have been developed for composite tests to obtain the calculation of the desired parameters. Furthermore, innovations in the design and construction of rheometers and viscometers have led to a "precision rheology" capable of analyzing and adapting conventional rheological analysis to very complex systems, such as composites. It is desirable that the evolution of rheology will continue in the future in order to gain even more knowledge of the rheology of epoxy composites.

Readings

P.J. Flory, *Principles of Polymer Chemistry* (Cornell University Press, Cornell, 1973)

J.W. Goodwin, R.W. Hughes, *Rheology for Chemists: An Introduction* (Royal Society of Chemistry, 2018)

B. Han, S. Sharma, T. Nguyen, L. Longbiao, K.S. Bhat, *Fiber-Reinforced Nanocomposites: Fundamentals and Applications* (Elsevier, 2020)

R.G. Larson, *The Structure and Rheology of Complex Fluids* (Oxford University Press, Oxford, 1998)

T.G. Mezger, *The Rheology Handbook* (Vincentz Network GmbH & C, 2014)

Newton I. Philosophiæ Naturalis Principia Mathematica, 1686
R. Pal, *Rheology of Particulate Dispersion and Composites* (CRC Press, 2006)
A.V. Shenoy, *Rheology of Filled Polymer Systems* (Springer, 1999)
Y.G. Yanovsky, *Polymer Rheology: Theory and Practice* (Springer Netherlands, 1993)
R. Zboncak, *Elastic Properties Prediction Models of Continuous Fibers Composites* (VÚTS, 2018)

Thermal Stability and Flame Retardancy of Epoxy/Synthetic Fiber Composites

9

Ruiqing Shen, Yufeng Quan, and Qingsheng Wang

Contents

Abstract

Epoxy is one of the most important and widely used thermosetting resins. Epoxy resins can further be reinforced with synthetic fibers to improve their performance from the aspects of stronger specific stiffness and strength, better fatigue endurance, and being more resistant to corrosion and chemicals. However, most neat epoxy-based thermosets are easily flammable. The presence of synthetic fiber reinforcements also affects the thermal decomposition process, pyrolysis kinetics,

R. Shen · Y. Quan · Q. Wang (✉)
Artie McFerrin Department of Chemical Engineering, Texas A&M University, College Station, TX, USA
e-mail: ruiqing@tamu.edu; yquan@tamu.edu; qwang@tamu.edu

S. Mavinkere Rangappa et al. (eds.), *Handbook of Epoxy/Fiber Composites*,
https://doi.org/10.1007/978-981-19-3603-6_11

and combustion behaviors of epoxy resins. Depending on epoxy monomers and curing agents, although most of the cured epoxy resins show flame retardancy to some extent, they are still not enough to pass a stringent industrial standard flammable test, so that their more extensive applications in engineering fields are still limited. Therefore, to reduce their inherent fire risk and widen their application range, different flame retardant strategies have been developed to enhance the thermal stability and reduce the flammability of epoxy-based materials, including phosphorus-based, silicon-based, nitrogen-based, nanomaterials-based, and metal-organic framework materials, etc. For these different systems, their specific flame retardant mechanisms are introduced in this chapter, and their advantages and shortcomings are also discussed.

Keywords

Flammability · Halogen-free · Flame retardant · Epoxy resin · Fiber-reinforced composite

Introduction

Epoxy Resins

Epoxy is one of the most important and popularly used thermosetting resins. Epoxy resins are characterized by many outstanding physical and chemical properties, for example, excellent dielectric properties, low shrinkage ratio, strong adhesion, good flexibility, and high chemical stability. Because of these properties, they have been widely used in various industrial applications as adhesives, coatings, and lamination materials. With the increasing demand from many industries, such as painting, coatings, wind energy, aerospace, construction, composites, and automotive, the global market for epoxy resins is still projected to grow constantly, and this trend will be kept to continue in the near future. Epoxy resins can further be reinforced with fibers, synthetic or natural, into the resin matrix to form composites, yielding fiber reinforced composites, for obtaining high specific stiffness and strength, good fatigue endurance, and excellent corrosion and chemical resistance. In the composite, the epoxy resin matrix is the binding material, which holds the fibers in place, transfers forces into and between the fibers, and is also responsible for improving the corrosion resistance, chemical resistance, fatigue endurance, and fire performance of the composite. The fibers are the reinforcement component, which provides strength and stiffness to the composite. In the aircraft industry, the primary use of epoxy is in the form of laminate. The epoxy laminate reinforced with carbon fiber can have very high strength-to-weight ratios in comparison to other traditional materials, such as steel and aluminum alloys (Xu et al. 2020). In the automotive industry, the primary use of epoxy is to be a structural glue and thus replaces traditional welding work. Additionally, it is also utilized to manufacture the press tools that are used for sheet metal during the production of new car models (Liu et al. 2018). However, when the

application temperature exceeds their glass transition temperature, for instance, when the aircraft structural parts are affected by the heat from running engines, the epoxy-based composites may reach the limit of their thermal properties, and it can result in thermal damage and mechanical performance degradation of those materials (Pecora et al. 2016). Moreover, in the majority, neat epoxy-based thermosets are highly flammable. Insufficient fire resistance is reported to be one of the most serious disadvantages of epoxy-based resins and their composites that has to be taken into consideration during applications (Xu et al. 2019). Depending on epoxy monomers and curing agents, although most of the cured epoxy resins have been found to have flame retardancy themselves, their performance is still not high enough to pass a stringent industrial standard flammable test, such as UL-94 V-0. Consequently, unless they are capable to pass the corresponding flammability tests, the epoxy-based materials are not allowed to be used in those field with demanding flame retardant requirements (interiors of public transport, etc.). Therefore, improving the thermal stability and reducing the flammability of epoxy resins are important and imperative to control the fire risk inherently associated with them.

Thermal Decomposition of Epoxy Resins

To understand the thermal decomposition and combustion of epoxy resins, it is fundamentally important to know the basic chemical structural elements of the cured epoxy network first. The final structure of the cured resin is determined by the type of epoxy monomer and curing agent used. The thermal properties of the cured resin will be directly affected by their chemical structure. Usually, the chemical linkages generated by reactions of glycidyl ethers are found to be less stable than other chemical linkages in the epoxy network (Levchik and Weil 2004). And nowadays, the most widely used epoxy monomers are the diglycidyl ether of bisphenol A (DGEBA) and its oligomers that are produced from the reaction of petroleum-based bisphenol A and epichlorohydrin, and they account for almost 90% of the world production of epoxy resins (Shibata and Ohkita 2017). Therefore, based on these facts, the structures formed by the glycidyl ethers and their thermal properties are to be mainly discussed in the following section. For these structures, the epoxy monomer component typically comprises the following epoxy or glycidyl group in Fig. 1.

The epoxy monomer is a low molecular weight oligomer containing one or more epoxy groups per molecule (more than one epoxy group per molecule is needed when crosslinking is required in the resultant material) (Azeez et al. 2013). Typically, the epoxy group will react with phenolic -OH groups and bisphenol-A-type resins to produce the following general structure as shown in Fig. 2.

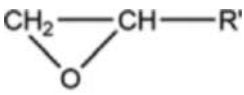

Fig. 1 Epoxy or glycidyl group (where R' is any aliphatic or aromatic residue)

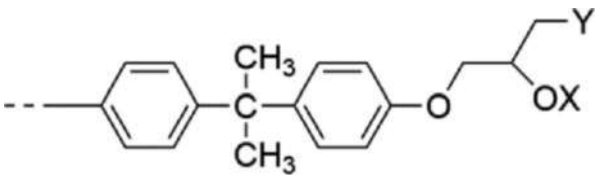

Fig. 2 General structure of a typical cured epoxy resin (where X can be H atom and the structure of Y depends on the curing agent)

In this relatively thermally stable structure, the ether linkages, -O-, are the weakest bonds. Aliphatic and aromatic diamines are two classes of curing agents that are the most widely used. With the proper catalyst, epoxy can be cured with aliphatic amines at room temperature, and aromatic amines and acid anhydrides are used for curing at a high temperature. There are also some specialized curing agents for epoxy, such as polyfunctional amines, polybasic carboxylic acids, mercaptans, and inorganic hardeners (Azeez et al. 2013).

Besides the monomer and curing agent structures, the thermal stability and flammability of epoxy resins will be also largely determined by the crosslink density in the resultant material. Typically, the higher the crosslink density, the better the thermal stability. However, it will also interact with the chemical structure of the epoxy resins. In general, even if the aliphatic networks may have higher crosslink densities, aromatic epoxy resins are found to have higher thermal stabilities than them. Usually, for any epoxy resin, the thermal decomposition reaction starts from the dehydration of the secondary alcohol, leading to the formation of vinylene ethers. The resulting allylic ether C-O bond is more vulnerable than the original C-O, and thus it is at the allylic position where the chain scission reaction mostly happens. Because the allylic amine C-N bond is less stable than the allylic ether C-O bond, commonly, the amine cured epoxy resins have lower stability than anhydride-cured epoxies (Levchik and Weil 2004).

During the early stages of thermal decomposition of epoxy resins, the reactions are mainly nonchain-scission type, whereas, as the reaction goes on, chain scissions occur at higher temperatures. For those nonchain-scission reactions, the most important ones are the competing dehydration and dehydrogenation reactions occurring in these resins, which are related to the secondary alcohol groups in the cured resin structures. From these reactions, methane, CO_2, formaldehyde, and hydrogen are basically the main products. Decomposition via random chain scission occurs over the temperature range of about 380–450 °C (Mouritz and Gibson 2007). During chain scission reactions, the aliphatic segments decompose to yield methane and ethylene (and possibly propylene), acetone, acetaldehyde, and methane (and probably CO and formaldehyde), all of which are flammable. From the decomposition of aromatic segments in the polymer, phenol is produced. For those resins cured by phthalic anhydride, phthalic anhydride is regenerated together with CO, CO_2, benzene, toluene, *o*- and *p*-cresols, and higher phenols. In addition to the main processes of chain scission mentioned earlier, there are also many secondary processes occurring during the whole thermal decomposition process. For example, cyclization occurs with aliphatic chain ends, rather than splitting off, which can

contribute to promoting the charring process and reducing the flammability. Overall, about 80–90% of the original epoxy resin weight is consumed by the scission reactions. In this process, different volatile compounds are produced, and the rest is converted into a highly porous char, which will start to oxidize above 550 °C in the air atmosphere (Mouritz and Gibson 2007). Compared with polyester resins, due to their crosslinking structure and char-forming behavior, the limiting oxygen index (LOI) values of epoxy resins are in the range of 22–23%, and thus they are less combustible.

The thermal decomposition processes are accelerated by the oxygen present in the air. In this case, the presence of an oxidant will lead to lower-onset thermal decomposition temperatures, and the detailed thermal decomposition process will become much more complicated by taking other factors into account, such as oxygen penetration depth below the surface of epoxy resins. Although the corresponding kinetic models have been proposed, the exact decomposition chemistry remains the subject of ongoing work (Celina et al. 2013). Basically, three mechanisms were proposed for the oxidation of epoxies: (1) oxygen attack on the methylene group, (2) oxidation of the tertiary carbons in the aliphatic portion of the chain, which is usually an ester-type crosslink in the resins cured with anhydride, and (3) oxygen attack on the nitrogen in the epoxies cured with amine. Any of these mechanisms results in the formation of carbonyl groups, which can further break down and result in chain splitting (Levchik and Weil 2004).

Fiber Categories

Fiber reinforcements in epoxy-based composites include both natural fiber and synthetic fibers. Natural fibers are those made from natural materials, such as plant fibers (bast, leaf, core fibers), animal-sourced fibers (silk, wool), and mineral-based fibers (asbestos, ceramic fibers). As a comparison, synthetic fibers are those made by humans through different chemical synthesis processes. These fibers are made from different raw materials based on chemicals or petrochemicals. These small molecular chemicals are polymerized into a long, linear chemical, and then they are used to produce various types of synthetic fibers with different chemical compounds. Some common examples of synthetic fibers made from polymers include nylon, polyesters, acrylics, polyurethanes, etc. Compared with natural fibers, synthetic fibers have a longer length and are more long lasting. Due to their high strength and stiffness, synthetic fibers are broadly used as aerospace components and in automotive industries. So far about half of all fiber usage is synthetic fibers (Asim et al. 2017). Currently, the three most common synthetic fibers used in composite industries are Kevlar (aramid), glass, and carbon fibers.

Kevlar Fiber

Kevlar fibers are made by reacting paraphenylene diamine with terephthaloyl chloride in an organic solvent to form polyparaphenylene terephthalamide (aramid) and then followed by extrusion, stretching, and drawing. In 1965, Stephanie Kwolek and

Herbert Blades, who are two scientists from DuPont, spun a fiber, called Kevlar, which has much higher performance than the nonaromatic polyamides from the aspects of strength and flexibility, such as nylon 6,6. From X-ray diffraction analyses, it was found that Kevlar fibers have a highly crystalline structure, and their long-molecular polymer chains are markedly oriented along the fiber axis. There is a very limited amount (a few percent) of unoriented crystalline components present, so the amorphous phase is nearly completely absent (Pegoretti and Traina 2018). The strong interchain bonding of the molecule contributes to the enhanced mechanical and thermal properties of Kevlar fibers. Typically, the mechanical properties of Kevlar fiber can be retained over a wide temperature range from very low temperatures up to 400 °C. The thermal shrinkage of this para-aramid fiber is very low. It is characterized to be self-extinguishing and has high flame retardancy. However, because of the costly manufacturing process and equipment, its price is high (Saba and Jawaid 2017).

Glass Fiber

Glass fibers are a very versatile class of materials. They are manufactured from melts, and their compositions are different by changing the ratio of raw materials like sand for silica, clay for alumina, calcite for calcium oxide, and colemanite for boron oxide (Seydibeyoglu et al. 2017). Depending on their composition, different types of glass fibers show different performances, for example, alkali resistance or high mechanical properties. Most glass fibers are based on silica (∼50–60% SiO_2), and they also contain a host of oxides of other metals, such as calcium, boron, sodium, aluminum, iron, etc. Glass fibers are lightweight, less brittle, extremely strong, and robust material, so they are extensively used as reinforcement of polymeric resins, such as epoxy resins, in various high-performance engineering fields. For these successful engineering applications, the high performance per cost ratio is one of the principal advantages of glass fiber reinforced polymeric composites. Glass fibers are also the most commonly used reinforcement in flame retardant polymer applications. Glass fibers are chemically inert in fire, and they can retain their chemical and physical stability even when they are exposed to an environment with high temperatures or high heat fluxes. For example, until being heated up to 830 °C and 1050 °C, E-glass and S-glass fiber will remain unaffected by the fire, respectively (Hicklin et al. 2008). However, glass fibers on the composite surface will cause the "candlewick effect," in which glass fibers can act to transfer and supply the fuel from the thermal decomposition of the polymer matrices to the flaming combustion zone by capillary action, accelerate the heat transfer back to polymers, and thus enhance the decompaction and burning of the polymers (Liu et al. 2011). Consequently, to achieve a UL-94 V-0 rating, more amount of flame retardants are needed for the glass fiber reinforced composites than the neat polymers to compensate for this effect. However, on the other hand, with a large amount of flame retardants being added to the polymer matrix, it will finally have side effects on other properties of polymers, especially the mechanical properties, which are deteriorating largely almost without expectation. Therefore, this "candlewick effect" makes it quite changeling to improve the flame retardancy of glass fiber reinforced composites while still maintaining their mechanical properties.

Carbon Fiber

Depending on the manufacturing methods, there are many different types of carbon fibers, and they have a wide range of strength and modulus values. About 90% of the carbon fibers are produced from polyacrylonitrile (PAN), and the rest is from rayon or petroleum pitch. Among these three, PAN precursors are the major precursors for the commercially large-scale production of carbon fibers, and 50% of total original fiber mass is produced from them (Saba and Jawaid 2017). As a class of reinforcements, carbon fibers are featured with strong stiffness and strength, but a low density. Furthermore, carbon fibers are highly resistant to creep, break stress, fatigue, and corrosive environments. The low coefficient of thermal expansion (CTE) is another important feature. In particular, carbon fibers have small, negative axial CTE when they are exposed to high temperature or high heat flux, so they can be used to produce carbon reinforced composites in aerospatial components, where the temperature of the part exposed to the sun is about 400–500 °C higher than that of the part in the shade (Tanzi et al. 2019). Carbon fibers also have some other advantages, such as high resistance to fatigue failure and strong thermal conductivity. However, it has to be admitted that carbon fibers also have some disadvantages. For example, the cost of carbon fibers is high, they have poor resistance to impact, and their failure strain is low. The onset thermal decomposition temperatures of PAN and pitch-based fibers are about 350 °C and 450 °C, respectively, so the surface of carbon fiber can be oxidized in the case of being exposed directly to a fire (Pereira and Martins 2014). In most types of fires, the degree of oxidation is found to be small and limited to the near-surface region only because the majority of carbon fibers are protected by char within the polymeric matrix.

Thermal Stability and Flame Retardancy of Epoxy Resins

Epoxy Resin Combustion Process

Being mainly composed of the elements of carbon and hydrogen, most epoxy resins are highly flammable. Being similar to the combustion process of other polymers, the flaming combustion of epoxy resins is comprised of multiple interacted steps involving both condensed phase and gaseous phase. A detailed schematic description of the self-sustaining polymer combustion process is shown in Fig. 3 (Wang et al. 2017). When the material is exposed to a high heat flux or temperature, thermoplastics tend to soften and flow, but thermosetting materials do not have a fluid state and they do not soften. Therefore, there are no physical transformations occurring in epoxy resins before decomposition. When the heat flux radiated from a fire is sufficiently large or the temperature is sufficiently high, various volatile gases, solid carbonaceous char, and airborne soot particulates (smoke) will be forced to yield from the intensive thermal decomposition of epoxy resins. Then these volatile components will mix with the surrounding air and create a combustible gaseous mixture. If the temperature is high enough to reach the auto-ignition temperature

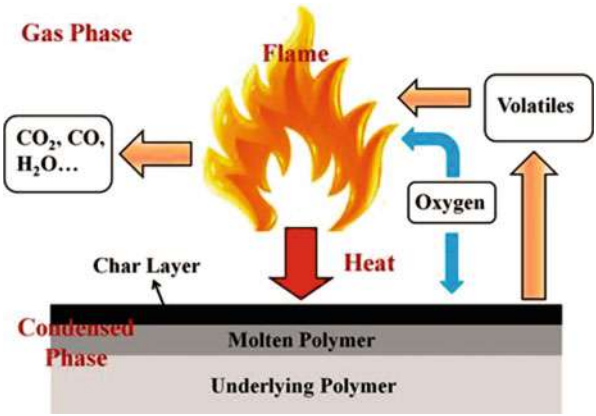

Fig. 3 Self-sustaining polymer combustion process. (Reprinted from Wang et al. 2017. With permission)

(defined as the temperature at which the activation energy of the combustion reaction is attained), this gaseous mixture can be ignited without any ignition source. Alternatively, with an external ignition source such as a spark or open flame, this gaseous mixture can also be ignited at a lower temperature when the temperature reaches the flashpoint of the fuel.

From the ignition, a large amount of heat is released from the combustion, a portion of which reradiates back into the unburned polymer in the condensed phase. This heat continues to drive the pyrolysis and the production of more flammable decomposition volatiles into the gaseous phase. The significant pyrolysis reactions of epoxy resins occur within a thin region in the interface between the flame and the solid epoxy resins. In this region, the temperature is maintained at or slightly above the onset thermal decomposition of epoxy resins for condensed phase decomposition reactions to occur. The oxygen diffuses in the flame zone from the air environment to support the flaming combustion. The combustion of more flammable volatiles will lead to the release of more heat. Subsequently, the flame becomes larger and larger until it is stable, and the combustion becomes a self-sustaining process when the heat released from the combustion reactions is sufficient to sustain the supply of flammable volatiles from the decomposition of the polymers to the flame. Finally, the flame will be extinguished due to the lack of oxygen, fuel, or heat. Obviously, this is a simplistic description of the complex combustion process, but it is basically true for almost all types of epoxy resins (Morgan and Gilman 2013).

Flame Retardant Mechanisms

Most polymers are vulnerable in a fire situation, including epoxy resins. The flammability of polymers is evaluated based on several processes and/or parameters under standard flammability tests, such as burning rates, spread rates (flame, pyrolysis, burn-out, smolder), ignition characteristics (delay time, ignition temperature,

critical heat flux for ignition), toxic species emissions, smoke production, etc. (Ahmed et al. 2018; Shen et al. 2017). The approach to rendering these polymers resistant to ignition or, if they are ignited, to burning less intensely to produce less smoke and toxic gases, is termed "flame retardance." If any step in the self-sustaining polymer combustion process can be chemically and/or physically prevented, minimized, or even stopped, the combustion reaction can be controlled, or even the flame can be extinguished. This principle is the basic theory behind the flame retardant mechanisms (Bar et al. 2015). Therefore, flame retardant systems are designed to inhibit or to stop one step or multiple steps in the polymer self-sustaining combustion as shown in Fig. 3. Depending on where they interfere with the combustion process, either the thermal decomposition of the polymer in the condensed phase or the combustion reactions in the gaseous phase, the specific flame retardant mechanisms are often classified as "condensed phase" or "gaseous phase" active (Levchik 2007; Mngomezulu et al. 2014). The "condensed phase" active flame retardant mechanisms include (Pereira and Martins 2014):

- Replacing part of combustible organic material with an inert filler to dilute the total amount of the combustibles
- Lowering the temperature of the composite by adding fillers having a high heat capacity to act as heat sinks
- Lowering the temperature of the composite through the endothermic decomposition of fillers
- Increasing the aromaticity of the polymer matrix to promote the formation of an insulating char layer as a barrier to slow down the heat transfer into the composite and reduce the release of flammable gas
- Forming a thermally stable ceramic surface layer composed mostly of nanoparticles that are combined with a relatively small amount of carbonaceous char

The "gaseous phase" active flame retardant mechanisms include:

- Releasing flame inhibition radicals, such as bromine, chlorine, or phosphorus-based radicals, to quench the exothermic combustion reactions by reacting with highly active H• and OH• radicals
- Releasing noncombustible vapors into the flame to dilute the concentrations of H• and OH• free radicals

Flame Retardant Strategies for Epoxy Resins

There are various methods to improve the thermal stability and flame retardancy of polymers, but generally, they all fall into three categories: (1) to use those polymers with inherent flame retardancy such as polyimide, poly (ether-ether ketone), and polyoxazoles; (2) to chemically modify the structure and property of existing polymers through copolymerization of other flame retardant monomers into the polymer chains; and (3) to embed flame retardant additives into the hosting polymer matrix to

form composites. For a given type of polymer, depending on its chemical structure, particular thermal decomposition chemistry, cost-performance ratio, and specific application requirements, different strategies can be adopted in practice. For epoxy resins, all these three methods have been used for enhancing their thermal stability and flame retardancy, and some products are commercially available now.

By developing epoxy resins with inherent flame retardancy, this method is designed to meet the special requirements of high-performance epoxy resins. As discussed earlier, both the epoxy components and curing agents, as well as the crosslinking density, strongly influence the flammability of a resin. Particularly, when very high contents of aromatic subunits are incorporated on epoxy materials, they can be intrinsically fire protected, and sometimes they even are rated as self-extinguishing. To name a few of them, naphthalene and biphenyl have been developed based on this strategy, and they are based on condensed aromatic hydrocarbons. Some of them have been commercially available for special high-performance applications. Moreover, there are also some curing agents that have been developed with rigid core structures. Highly aromatic diamines help to improve flame retardancy. Due to the high aromatic content, novolac-cured epoxies show the best intrinsic flame retardant performance. Dicyanamide and phenol novolacs are widely used to cure epoxy resins, especially for printed circuit boards. When both of these two components are combined in use, the cured epoxy materials are obtained with an extraordinarily high composition of aromatic moieties, such as glycidyl-functionalized novolac-based cured resins. For these materials, they show noticeably better performance from the aspect of the resistance to thermal decomposition and fire-related properties than those attained from conventional DGEBA or epoxy novolac resins (Ciesielski et al. 2017). For example, when naphthalene-based epoxy resins and special novolac curing agents (e.g., DIC Corporation, Japan; Huntsman, USA) are combined in use, they may show self-extinguishing behavior and may be classified as V-0 in UL-94 tests, so additional flame retardants are unnecessary. Some epoxy resins and curing agents with inherent flame retardancy are shown in Fig. 4 (Ciesielski et al. 2017). Because of the gradually growing awareness of sustainable development, environmental protection, and energy security, bio-based epoxy thermosets have also been developed with the intention to be used as renewable alternatives for petroleum-based counterparts over the past decades. However, similarly, most of these bio-based epoxy resins are also limited

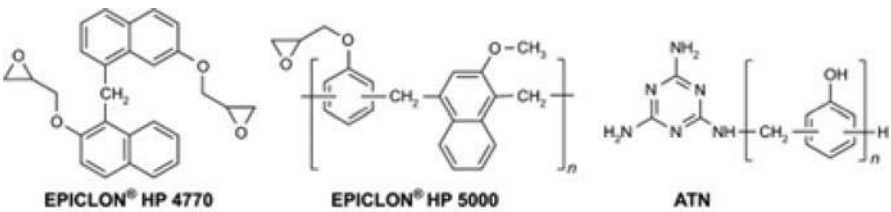

Fig. 4 Examples of epoxy resins and curing agent with inherent flame retardancy. (Reprinted from Ciesielski et al. 2017. With permission)

by their high flammability. Recently, some bio-based epoxy resins with inherent flame retardancy have been reported in the literature such as daidzein, furan, vanillin, etc. (Wang et al. 2019). Basically, they are designed by selecting those bio-based chemicals that are abundant in aromatic structures and have a strong capability to form char.

The second method is a structural modification strategy, which is to modify their final properties of epoxy resins by chemically incorporating the elements with flame retardant function into their molecular structures of epoxy components and/or curing agents. This method is also called reactive-type flame retardant. Typically, halogen, phosphorus, sulfur, nitrogen, or other suitable heteroatoms, or their flame retardant monomers, are introduced into the final chemical structures of epoxy resins by attaching a flame retarding unit either in the macromolecular backbone or as a pendant group through copolymerization. Because the flame retardant unit is incorporated in the epoxy resin matrix through strong covalent bonding, the leaching from the polymer during product processing or due to aging in use can be almost completely avoided. Moreover, these reactive-type flame retardants can be more effective to enhance the thermal stability and flame retardancy of composites at low concentrations without any loss of mechanical characteristics, i.e., <10 wt% of the resin mass (Biswas and Kandola 2011). Typically, this is also required by many high-performance applications. Thus, the main advantage of this type of flame retardant is to impart flame retardancy permanently while still maintaining the attractive physical properties of the original epoxy resins efficiently. For reactive-type flame retardants, the bromine-containing compound tetrabromobisphenol A (TBBPA) is a highly competent and cost-effective flame retardant for epoxy resins, and it still accounts for a big portion of the epoxy market by share (Pittinger and Pecquet 2018). In a fire, it will release volatile bromine radicals in the flame to scavenge hydrogen radicals there, form noncombustible hydrogen bromide gas subsequently, in turn diluting the concentration of the combustibles, and finally result in the interruption of the self-sustaining combustion cycle. However, in this process, toxic and corrosive gases are also released, which is the subject of health concerns. Mainly because of environmental concerns and end of life issues, the use of halogenated compounds has been limited or banned worldwide, and there is a growing interest in other non-halogenate-based techniques. Thus, the development of phosphorus-based reactive-type flame retardants has gained a considerable amount of attention to incorporate halogen-free alternatives into epoxy resins based on covalent bindings. To date, DOPO (9,10-dihydro-9-oxa-10-phosphaphenanthrene-10-oxide) and its derivatives have been regarded as an alternative promising solution as reported in many of the scientific studies (Ciesielski et al. 2017).

For the third method, it involves the physical blending of flame retardant additives to the polymer matrix of an epoxy resin to form composites. This method is also called additive-type flame retardant. This method exhibits numerous advantageous properties such as easy processing, low manufacturing cost, a broad variety of raw materials, and evident flame retardant performance. However, this method usually requires high loading of flame retardant additives to meet certain flame retardancy requirements. Because there is no chemical bonding between the flame retardant

additive and the polymer, unexpected migration and leaching of additives into the environment may occur during its service of life as time goes on. This could lead to the deterioration in mechanical strength and thermal stability. Moreover, it has a harmful effect due to human exposure in such an environment (Wang et al. 2019). Despite these shortcomings, this method is still considered the most economical and efficient strategy of promoting the flame retardancy of commercial polymers, and they take the biggest share in the market so far. Due to its diversity, a variety of additive-type flame retardants have been developed, and a lot of research has also been conducted in this field to overcome these drawbacks.

Flame Retardants for Epoxy Resins

There are abundant studies available in open literature both from academia and the industry to develop epoxy resins with higher thermal stability and flame retardancy. Among them, based on the flame retardant chemistry, common flame retardants can be categorized as halogen-based, phosphorus-based, nitrogen-based, silicon-containing compounds, nanocomposites, etc. Generally, halogenated flame retardants are based on the element of either chlorine or bromine, due to the fact that the bond between carbon and bromine/chlorine is relatively weak and thermally labile, so the chlorine or bromine radicals can be released into the gaseous phase at the decomposition temperatures of most polymers. These radicals are driven into the flame zone of the burning polymer where they interfere with the combustion process and inhibit key free radical reactions by removing or scavenging the high-energy H• and OH• radicals. This chemical interference with the radical chain mechanism can make flames burn unsteadily and even extinguish, and ultimately it has an overall effect of lowering heat release and reducing the burning intensity (Morgan 2019). Nevertheless, during this process, because of the incomplete combustion of carbon-containing species in the flame, more smoke will be released, and a large amount of corrosive gases (hydrogen halides) may also be produced, which will corrode metal components and cause damage to sensitive electronics. Moreover, due to the persistence, bioaccumulation, long-distance migration ability, and high biological toxicity of halogenated flame retardants as they continue to be found in the environment, they pose a serious threat to harm the environment and the health of the human being. Despite their high efficiency in improving flame retardancy, there has been a trend to move from traditional halogenated flame retardants toward non-halogenated alternatives. Recently, there is an increased interest in halogen-free environmentally friendly flame retardants from both academia and the industry, which will be reviewed briefly in the following sections. The advantages and shortcomings of different flame retardant systems are also discussed. For different flame retardant systems, the specific performance of some representatives is shown in Tables 1 (The flame retardancy performance of epoxy containing traditional flame retardants) and 2 (The flame retardancy performance of epoxy containing nanomaterial-based flame retardants) to give the readers some basic idea of this topic. A more thorough overview of recent advances in the flame retardant systems of epoxy resins has

Table 1 The flame retardancy performance of epoxy containing traditional flame retardants

EPs and Their Composites	wt%	LOI (%)	UL-94 Rating	Heat Flux (kW/m^2)	Peak-HRR (kW/m^2)	THR (MJ/m^2)	References
P-containing EPs	0 (P)	19	No rating	–	–	–	Hu et al. 2014
	0.5 (P)	24	V-2	–	–	–	
	1 (P)	26	V-1	–	–	–	
	1.5 (P)	32	V-0	–	–	–	
	2 (P)	34	V-0	–	–	–	
EP/DDS	0 (P)	22.5	No rating	50	1208	80.6	Huo et al. 2019
EP/DDS/DOPO	1.0 (P)	34.1	V-1	50	833	66.7	
EP/DDS/DIB-0.25	0.25 (P)	32.3	No rating	50	918	70.5	
EP/DDS/DIB-0.5	0.5 (P)	35.9	V-1	50	740	60.5	
EP/DDS/DIB-0.75	0.75 (P)	36.8	V-0	50	503	58.6	
EP/DDS/DIB-1.0	1.0 (P)	38.5	V-0	50	517	51.6	
EP	0 (P)	24.7	No rating	50	1420	143.6	Jin et al. 2019
2%ABD/EP	0.25 (P)	32.3	V-1				
3%ABD/EP	0.38 (P)	36.2	V-0	50	1043	101.5	
4%ABD/EP	0.51 (P)	39.1	V-0	50	933	94.3	
3%DOPO/EP	0.43 (P)	35.5	No rating	50	1182	91.9	
EP	0 (P)	25.3	No rating	–	–	–	Wang and Cai 2017
EP/DTA1	0.09 (P)	30.1	No rating	–	–	–	
EP/DTA2	0.17 (P)	32.4	V-1	–	–	–	
EP/DTA3	0.25 (P)	33.1	V-1	–	–	–	
EP/DTA4	0.34 (P)	34.8	V-0	–	–	–	
EP/DTA5	0.42 (P)	35.9	V-0	–	–	–	
EP/DTA6	0.51 (P)	36.5	V-0	–	–	–	
EP/ PEPATA	0	21.5	No rating	–	–	–	Wang et al. 2011
	5	26.0	No rating	–	–	–	
	10	28.5	V-1	–	–	–	
	15	31.0	V-1	–	–	–	
	20	33.0	V-0	–	–	–	
EP/ H-DPPA	0	24.1	No rating	35	862	175	Luo et al. 2016
	3.0	31.8	V-0	35	752	164	
EP/ HM-SiO_2	0	–	–	35	1377.7	86.6	Jiang et al. 2018
	0.5	–	–	35	1226.4	67.0	
	2	–	–	35	860.6	69.8	

(continued)

Table 1 (continued)

EPs and Their Composites	wt%	LOI (%)	UL-94 Rating	Heat Flux (kW/m^2)	Peak-HRR (kW/m^2)	THR (MJ/m^2)	References
EP	0	23.0	No rating	50	893	112	Qi et al. 2016
EP/DPP-POSS	5	33.2	V-0	50	489	94.1	
EP/DPOP-POSS	5	29.3	V-1	50	419	87.8	
EP/DOPO-POSS	5	30.0	V-1	50	433	91.1	
EP	0	23.0	No rating	50	1245	87.4	Qin et al. 2019
EP/DOPO + pristine CaMMT blend	8	33.0	V-1	50	874	74.9	
EP/DOPO-pristine CaMMT	8	34.1	V-1	50	712	65.6	
EP/DOPO-pristine CaMMT EtOH	8	33.2	V-1	50	774	70.5	
EP/OMMT-1.30P	8	29.4	No rating	50	973	90.0	
EP	0	21.5	No rating	35	1730.27	114.16	Tang et al. 2013
EP/APP	15	36	V-0	35	397.89	35.49	
EP/ MCAPP	15	38.5	V-0	35	283.09	44.00	

been conducted recently, in which the specific flame retardant performance of different systems has been summarized in tables, including their limiting oxygen index (LOI) values, UL-94 rating, heat release rate reduction under the cone calorimeter test, etc. (Liu et al. 2020).

Phosphorus-Based Flame Retardants for Epoxy Resins

Different kinds of additive and reactive approaches have been successfully developed to introduce phosphorous-based flame retardants into the structure of polymers to improve their flame retardancy, and so far, they are the most widely marked and available alternatives for halogenated flame retardants. Phosphorous-based flame retardants may act in the gaseous phase through a radical recombination mechanism to interfere with the combustion reactions and suppress the heat-releasing processes. It is reported that the PO-radical plays a major role (Schartel 2010) in such a process, and its efficiency in the gaseous phase was believed to be similar to or even higher than hydrogen halides like HBr, which are known to be highly efficient flame inhibitors (Babushok and Tsang 2000). Additionally, phosphorous-based flame retardants may also act in the condensed phase by promoting the formation of a char layer, which can act as a barrier to insulate the polymers underneath it from heat and air and also slow down the diffusion of volatile products into the flame. For different phosphorous-based flame retardants, their efficacy depends on the chemical structure of the polymer.

Table 2 The flame retardancy performance of epoxy containing nanomaterial-based flame retardants

EPs and Their Composites	wt%	LOI (%)	UL-94 Rating	Heat Flux (kW/m^2)	Peak-HRR (kW/m^2)	THR (MJ/m^2)	References
Carbon nanotubes epoxy composites	Neat	22	V-1	–	–	–	Kuan et al. 2010
	1 (CNT)	23	V-1	–	–	–	
	3 (CNT)	25	V-0	–	–	–	
	5 (CNT)	26	V-0	–	–	–	
	7 (CNT)	27	V-0	–	–	–	
	9 (CNT)	29	V-0	–	–	–	
EP	Neat	21.5	–	35	1730	113.1	Wang et al. 2014
EP/PPA	8	29.0	–	35	1124	61.3	
EP/PPA/g-GNS-2%	2	24.0	–	35	1154	63.4	
EP/PPA/g-GNS-4%	4	27.5	–	35	1120	60.6	
EP/PPA/g-GNS-8%	8	30.5	–	35	1016	56.9	
EP	Neat	25.0	No rating	35	1137.6	81.6	Feng et al. 2017
EP-RGO	1	24.3	No rating	35	972.5	79.8	
EP/FRGO	1	26.3	V-2	35	891.9	69.9	
EP-FRGO	3	28.2	V-1	35	753.2	70.3	
EP	Neat	21.8	No rating	–	–	–	Kaul et al. 2017
EP/MPP/LDH-1	15/1	23.8	V-1	–	–	–	
EP/MPP/LDH-5	15/5	24.4	V-1	–	–	–	
EP/MPP	15	23.4	V-1	–	–	–	
EP	Neat	22.4	No rating	50	1054	39.1	Xu et al. 2018
EP-SiO_2	2	26.0	No rating	50	727	34.4	
EP/ZIF-8	2	26.9	No rating	50	431	25.3	
EP/ZIF8@SiO_2	2	28.1	V-1	50	254	23.9	
EP	0	21.2	No rating	50	1146	56	Li et al. 2018
EP/ZIF-8@LDH	2	24.7	V-1	50	562	39	
EP/ZIF-67	2	23.6	No rating	50	817	42	
EP/ZIF-67@LDH	2	25.5	V-1	50	432	34	

Usually, they are found to be the most effective in oxygen-containing polymers such as epoxy resin. Furthermore, the specific flame retardant mechanism will also depend on the oxidization state of phosphorus. Generally, the main flame retardant mechanism of phosphine oxide is within the gaseous phase. However, when the oxidation state of phosphorous increases up to phosphate, the char-forming effect in the condensed phase becomes more and more predominant (Braun et al. 2006). The common examples of phosphorous-based flame retardants include red phosphorus, organophosphates, organophosphonates, polyphosphonates, and hybrid metal phosphonate salts.

As discussed earlier, in terms of high-performance epoxy resins, reactive-type flame retardants are a more desirable strategy because they have fewer negative effects on their physical properties, particularly the glass transition temperature and hydrolytic stability. The P-H bond has a high reactivity toward the epoxy group, and thus hydrogen phosphonates or phosphinates can be attached to an epoxy resin based on this reaction. Among various organophosphorus flame retardants, 9,10-dihydro-9-oxa-10-phosphaphenanthrene-10-oxide (DOPO) has attracted a lot of attention as a halogen-free flame retardant. It is a commercial product available on a large scale. Because of its high thermal stability, good oxidation resistance, and multiple structural diversifications by functionalization, it is widely used as a reactive-type flame retardant for epoxy resins (Salmeia and Gaan 2015). To meet the flame retardant requirements, the common practice is to pre-react DOPO with multifunctional novolac-type epoxy to achieve a high enough phosphorus content within the final product, about 3 wt% (Levchik 2014). The dominant flame retardant mechanism of DOPO is proposed to be related to the gaseous phase flame inhibition reactions, just as the halogenated flame retardants do. The flame retardant performance of DOPO-treated epoxy resins can be adjusted to meet a specific flame retardant requirement by independently modifying the amount of the epoxy component and/or curing reagent incorporated. For example, by having the phosphorus content in the cured matrix to be 3 wt%, a V-0 rating was obtained under the UL-94 test, and the LOI value was increased to 30% (Hu et al. 2014). Moreover, some examples of using DOPO as a part of the curing system have also been reported (Huo et al. 2019; Wang and Cai 2017). For example, using a 4 wt% DOPO-based triazole compound (DTA, P content: 8.9%) as a co-curing agent, the epoxy resins cured with diaminodiphenylmethane (DDM) achieved an LOI value of 34.8% and a V-0 rating in the UL-94 test (Wang and Cai 2017). The flame retardant effects were found both in the gaseous phase and condensed phase through releasing flame inhibition radicals and charring effect, respectively. However, for DOPO-modified epoxy resins, there are still several problems existing, such as the decreased glass transition temperature, high water absorptivity, and worse thermal stability, because the incorporation of the DOPO skeleton into the network structure of epoxy resin may affect its functionality and the property of cured epoxy resin will be affected finally. Since DOPO is reactive toward epoxide groups and only monofunctional, the network density will be decreased by the introduction of DOPO skeleton. To address these problems, a variety of DOPO derivatives combined with -OH, $-NH_2$, or -NH- active groups were developed to be used as multifunctional flame retardants as shown in Fig. 5. These novel DOPO derivatives are both a flame retardant agent and a curing agent and confer enhanced flame retardant property, higher glass transition temperatures, and better thermal stability on epoxy resins (Zhao et al. 2018).

Because they are thermally and hydrolytically stable, organophosphates or organophosphine oxides have been proposed to impart flame retardancy to epoxy resins by chemically pre-reacting. However, usually, the thermal stability and mechanical properties of epoxy resins will seriously deteriorate if the flame retardants containing P-O-C bond, such as phosphinates or phosphonates (e.g., triphenyl phosphate (TPP)), are incorporated into epoxy matrix (Liu et al. 2012). Cheng et al.

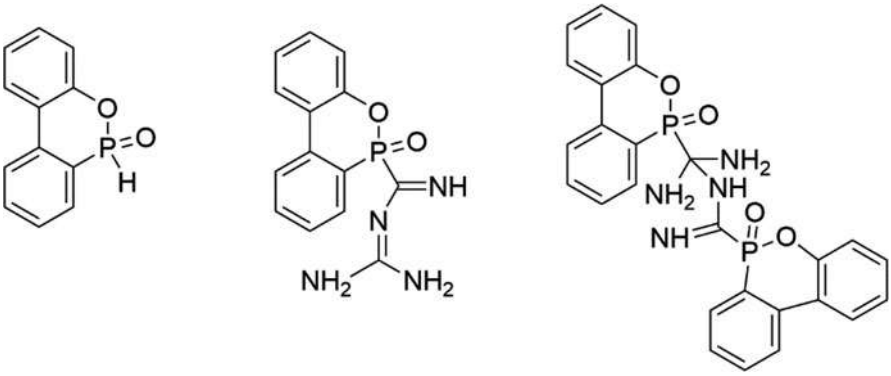

Fig. 5 Chemical structure of DOPO and some of its derivatives

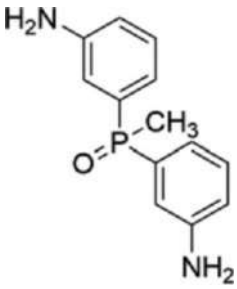

Fig. 6 Chemical structure of bis(aminophenyl) methylphosphine oxide

reported that di-epoxide containing phenyl phosphonate cured with diaminodiphenyl sulfone (DDS) had an LOI value of 29–31%. However, the thermal stability of the cured epoxy resin was lower, and better flame retardancy can be obtained with a higher % P content (Cheng et al. 2002). The thermal stability and flame retardancy of phosphine oxides are higher than those compounds containing P-O-C bond. Moreover, the thermal stability of epoxy resins will not be impacted by phosphine oxides too much. During burning, the radical scavengers, such as PO• radical, will be released from phosphine oxides, and they can react with H• or OH• free radicals to suppress the chain reactions in the gaseous phase. Meanwhile, in the condensed phase, they may provide acid sources to promote the dehydration of the polymer matrix and lead to the formation of a char barrier there. There are also many studies in the literature concerning curing epoxy resins with bis(aminophenyl)-methylphosphine oxide (shown in Fig. 6), and these cured epoxy resins are found to have improved flame retardant performance (Levchik 2014). Another study by Ren et al. showed that the phenyl phosphine oxide with bis-phenoxyl could help the epoxy resins cured with DDS to obtain an LOI value of 34% with a 7.8% P content and more char yield after the thermal decomposition tests at 800 °C in both air and nitrogen (Ren et al. 2007).

Metal salts of dialkyl phosphinates are known to be effective flame retardants, because they have a high efficiency of enhancing char formation. This behavior results from the reaction of phosphoric acids with decomposed polymers. Unlike other phosphorous-based flame retardants, metal phosphinates have some unique properties, such as high phosphorus content (~17%), good thermal stability (up to 320 °C), and lower affinity to moisture. Because the acidic degradation induced by the release of phosphoric acids is not acceptable during the processing and use, hydrolytic stability is an important property from this aspect (Rakotomalala et al. 2010). A wide variety of aluminum, calcium, and zinc salts of dialkyl phosphinates was investigated to be used as flame retardant agents, and among them, the aluminum salts of diethylphosphinic acid were commercialized under the trade name of Exolit OP 930 and Exolit OP 935, where with 10–30% content it is able to obtain the stringent flammability test, such as UL-94 V-0 (Pack 2015). Moreover, it has been reported that the effectiveness of metal phosphinates as flame retardant can be further enhanced in combination with a nitrogen-based synergist, such as melamine polyphosphate (MPP).

Silicon-Based Flame Retardants for Epoxy Resins

In response to the regulation pressure to develop non-halogenated flame retardants, another promising approach stemmed from the use of silicon-containing flame retardants. Silicon has different forms such as silicones, silica, organosilanes, silsesquioxanes, and silicates, as shown in Fig. 7. Almost all of them have been investigated as potential flame retardants to polymeric materials (Ciesielski et al. 2017). For silicon-containing compounds, they are very versatile in forms, and almost all of them are featured with high compatibility, low toxicity, and excellent thermal stability. Their dominant flame retardant mechanism is associated with the formation of a ceramic-like char layer upon decomposition. Meanwhile, with the component of silicone, the oxidation resistance and thermal stability of the carbon layer can also be improved. Not only the flame retardancy but also adding silicon-based flame retardants into the polymer improves its mechanical properties and heat resistance.

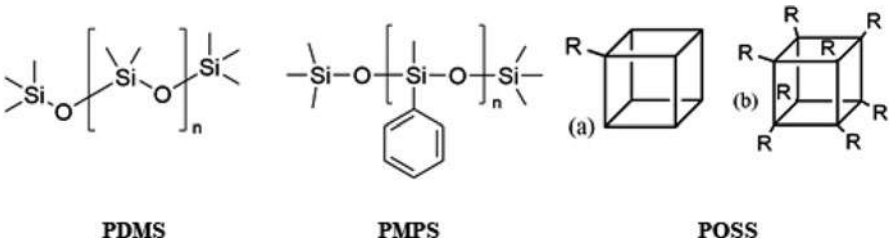

Fig. 7 Polydimethylsiloxane (PDMS), polymethylphenylsiloxane (PMPS), and the simplified chemical structure of cubic polyhedral oligomeric silsesquioxane (POSS) with eight (**a**) or one (**b**) functionality (R = hydrogen, alkyl, aryl, heteroatoms, etc.)

Silicon dioxide (or silica) has various types, such as amorphous, fused, fumed, crystalline, layered, and other forms. Silica is a commonly used filler to modify the properties of epoxy resins. Typically, the melting point of silica is very high (1600–1700 °C), but it can form a low melting siliceous barrier to act as a heat and mass transfer barrier during heating. This barrier delays the volatilization and diffusion of decomposition products, so the flammable volatiles available in the gaseous phase for burning are reduced and the burning intensity can be controlled. It was found that a thermal insulating layer on the resin surface can be formed by fumed silica and silica gel when they migrate there, whereas fused silica mostly remains in the resin core, and no such a thermal insulating layer can be formed. The simultaneous improvement on flammability and mechanical toughening of epoxy resin nanocomposite was achieved after the additions of nanosilica, and the improved ignition resistance is primarily due to a higher thermal diffusivity within the specimen, which can contribute to reducing the surface temperature and in turn slowing down the pyrolysis rate (Roenner et al. 2017). There are also some novel approaches to coat other flame retardant elements (chitosan (CS)/phosphorylated cellulose (PCL)) on the surface of silica to form multi-element silica derivative, based on the technology of layer-by-layer (LbL) assembly (Jiang et al. 2018). The results show that by adding only 2 wt% additive, a compact and dense char layer was formed to suppress the combustion and protect the epoxy resins.

Being a kind of important silicon-containing flame retardants, siloxanes have Si-O-Si bond as the main chain and alkyl, alkyl substituent, and phenyl as the side chain. They exhibit high flame retardant performance without generating toxic gases. Their glass transition temperature is low, but they have a high resistance to thermal oxidation. Their incorporation into the epoxy resins can increase the onset decomposition temperature and thus improves their thermal stability. Of polysiloxane polymers, the most important one is polydimethylsiloxane (PDMS). Typically, PDMS is synthesized via ring-opening polymerization of octamethyltetrasiloxane using diethyl ether as a solvent and sulfuric acid as a catalyst. One of the most characteristic and technologically important features of PDMS is its thermal properties. Due to the high flexibility of the Si-O bond, the irreversible decomposition of PDMS occurs at a temperature over 350 °C, so that it can retain its flexibility at relatively high temperatures (Kilinc 2014). During the combustion, the decomposition of PDMS segments results in the formation of stable silica structures and the subsequent migration of silica to the char surface, which forms a protective layer to prevents the char from further degrading at high temperatures.

Polyhedral oligomeric silsesquioxanes (POSS) are a kind of inorganic-organic hybrid nanomaterials, and they have a steady hexahedral cage composed of a silicon-oxygen framework, with a molecule size of 1–3 nm. Due to their better compatibility with a polymer matrix, environmental neutrality, strong heat resistance, and excellent thermal stability, POSS have attracted a lot of interest to be used as flame retardants (Zhang et al. 2017). The special structure also brings superior rigidity and stability for POSS. The general formula of POSS is $(RSiO_{1.5})_n$, where R may represent a hydrogen atom or an organic functional group. Based on their structure, these organic groups can be specially designed to be nonreactive or reactive, which

provides the opportunity for stem grafting and copolymerization of POSS to pristine polymer materials, such as epoxy resins. Generally, there are two ways that the terminal hydroxyl Si-OH groups (silanols) could react with epoxy resins to incorporate their network structure. The first one is to form a Si-O-C bond by reacting with mid-hydroxyl in the polymer chain. The second one is to form new hydroxyls first by reacting with the oxirane ring through a ring-opening reaction. Successively, these new hydroxyls can react with other terminal hydroxyl Si-OH groups (Zhang et al. 2017). Various functional POSS, such as glycidyloxypropyl-heptaphenyl POSS, glycidyloxypropyl-heptaisobutyl POSS, octaphenyl POSS, and octadiphenylsulfonyl POSS, were designed and applied as reactive-type flame retardants for epoxy resins. These reactive-type POSS can be incorporated into the epoxy network as either a junction point or a pendant group. The good dispersion of reactive POSS in epoxy resins is generally obtained. During the heating, a thermally stable ceramic-like layer can be formed from the decomposition of POSS, which interferes with the pyrolysis, ignition, combustion, or spread of flame. However, from the vast literature, almost no POSS can lead to the satisfactory improvement of epoxy resins in LOI or UL-94 tests so far, no matter whether they are reactive or inert, although it was observed that the peak heat release rate in cone calorimeter tests was reduced significantly. The phosphorous compounds are found to have a high-efficiency synergistic action with the silicon element, either being used as fire retardant together with POSS or as an atomic constituent in the POSS structure. This strategy is useful to further increase the flame retardant action of POSS in epoxy resins (Zhang et al. 2017). By combining octavinyl POSS with diphenylphosphine (DPP), diphenylphosphine oxide (DPOP), and DOPO, three different kinds of P-containing POSS were attained (Qi et al. 2016). By adding 5 wt% of DPP-POSS, DPOP-POSS, and DOPO-POSS, the flame retardancy of epoxy resins (EPs) can be remarkably improved. Under the LOI tests, their LOI value reached 33.2%, 29.3%, and 30.0%, respectively. EP/DPP-POSS passed the UL-94 V-0 test, and EP/DPOP-POSS and EP/DOPO-POSS passed the UL-94 V-1 test. Their peak heat release rate (PHRR) and total heat release (THR) were also significantly reduced under the cone calorimeter tests, and the amount of residues increased from 3.5% (neat EP) to 20.2% (EP/DPP-POSS), 17.9% (EP/DPOP-POSS), and 16.1% (EP/DOPO-POSS), respectively. These noticeable improvements are ascribed to the strong charring and intumescence effect in the condensed phase due to the synergistic effect between phosphorus and silicon in these three POSS. Thus, the P-containing POSS is a type of promising flame retardant, which is expected to be an interesting solution not only for epoxy resins but also for other polymers.

Silicate minerals are abundant on earth. Their common applications are in the form of additives to improve both mechanical properties and flame retardancy of epoxy resins. They have different compositions and structures, such as halloysite, kaolin, sepiolite, montmorillonite (MMT), etc. Generally, their morphology and crystal structure will largely determine if their efficiency as flame retardant fillers is high or not. For those lamellar silicates, they tend to generate an effective siliceous barrier, and for those needle-like silicates, they may contribute more to maintaining

the stability of the char (Kilinc 2014). Among them, owing to its natural abundance and high aspect ratio, MMT has drawn extensive attention and becomes the most promising candidate among layered silicates (Hu and Wang 2019). The thickness of a single MMT layer is around 1 nm, and the lateral dimensions can vary up to several microns. Because of this extraordinary high aspect ratio (>1000) in a delaminated structure, well-dispersed MMT fillers have a very extensive contact surface with the polymeric matrix, which helps to improve its thermal, physical, and mechanical properties even with a low loading. Generally, the fundamental flame retardant mechanism of MMT is based on the development of a multilayered carbonaceous-silicate structure on the surface of polymers from the collapse of their structure during burning (Kiliaris and Papaspyrides 2010). This layer can provide insulation to the underlying materials and slow the release of decomposition products into the flame. However, this effect mainly contributes to retarding flame spread in developing fires but is less efficient at the stage of ignition or in the case of fully developed fires. To improve their compatibility and dispersion within the polymer matrix, natural clays can be modified with organic cations (alkylammonium, alkyl phosphonium, and alkyl imidazol(idin)ium cations) to produce organomodified nanoclays. With the incorporation of 5 wt% bentonite modified with either ammonium or a phosphonium salt, impressive fire retardancy in terms of burning intensity reduction and slow fire growth rate was observed, especially when the external heat fluxes are high. However, the lower the external heat flux, the smaller the flame retardant effect, so the LOI values reveal a rather unnoticeable improvement from 18.3% to 19.6% (Hartwig et al. 2003). The flame retardant mechanism of tetraphenylphosphonium-modified layered silicate on epoxy resins was studied in detail, which shows that the heat insulation by the inorganic-carbonaceous residue on the surface is the main fire protection effect on epoxy resin, but its formation process is influenced by bubbling, migration, reorientation, agglomeration, ablation, and perhaps also delamination induced thermally by decomposition. Multiple, quite different mechanisms are relevant during this process, and the importance of each mechanism may be completely different depending on the specific type of nanocomposite system (Schartel et al. 2011). Currently, the more common approaches are reported to be by combing the use of organoclay with other conventional phosphorous flame retardants, such as DOPO, so that they can achieve a synergistic effect on the flame retardant performance (Qin et al. 2019).

Nitrogen-Based Flame Retardants for Epoxy Resins

Based on their mode of action, nitrogen-based flame retardants can be classified into two groups: gaseous phase and condensed phase active compounds. Ammonia, melamine, guanidine, urea, and their corresponding derivatives all belong to the first group. Their primary flame retardant effect is through the endothermic decomposition to release large amounts of nonflammable gases such as nitrogen and ammonia. For example, melamine is a thermally stable crystalline product with 67 wt% nitrogen in the molecule, and it is also featured with a high melting point

of about 345 °C. At about 350 °C, melamine undergoes the process of sublimation. During this process, it absorbs a significant amount of heat and thus decreases the temperature surrounding it. At high temperatures, ammonia will be yielded from the decomposition of melamine, which can dilute the concentrations of oxygen and combustible gases. Meanwhile, thermally stable condensates can be formed. The ammonia and melamine-based salts, such as ammonium polyphosphate (APP) and melamine polyphosphate (MPP), have high thermal stability and low volatility. They are the most widely used flame retardants in the nitrogen-based family by the mass so far (Ciesielski et al. 2017). However, due to their inorganic nature, their compatibility with the epoxy resin is very poor. Thus, in their composites, phase separation and/or bleeding out may occur during the application. Unfortunately, both of these two effects result in a lower flame retardancy. Thus, the surface modification treatment of these inorganic salts is required to improve the compatibility with polymers. One possible solution is to encapsulate APP and MPP with a polymeric shell to improve the compatibility with the epoxy resin. Furthermore, encapsulation enhances their water resistance. For example, APP was microencapsulated by glycidyl methacrylate (GMA). It was found that the unreacted epoxy group on the surface of the capsule not only enhanced the interface compatibility between the capsule and the epoxy matrix but also promoted the dispersion of microencapsulated APP. Under the reaction-to-fire test, an intumescent char layer was formed to protect the inner polymer matrix. Besides the significant reduction of burning intensity, excellent smoke suppression performance was also identified (Wang et al. 2015).

The second group of nitrogen-based flame retardants is characterized by a strong interaction with the polymer matrix where nitrogen exists in certain chemical structures, for example, in the backbone of epoxy resins or as a curing agent. In the condensed phase, their action of mode either leads to a change of decomposition pathway of the matrix polymer or results in intensive charring. However, the high performance of this mode of action relies on special interaction with the matrix polymer during decomposition. Consequently, in practice, the use of this type of nitrogen-based flame retardants is restricted to limited numbers of base polymers, such as phosphazenes in epoxy resins.

More commonly, due to their well-described synergistic effect, the flame retardant properties of the nitrogen-containing compounds show noticeable improvements when they are combined with other phosphorus-based flame retardant. This principle is widely applied in the intumescent system, which is a mix of different chemicals. In general, the ingredients of the intumescent system are composed of three components: a thermally activated acid source; a source rich in carbon to build the insulating foam; and some sort of foam "blowing agent" which is formed in situ at the right temperature and at the right time during thermal decomposition (Morgan 2019). Then after a series of reactions in sequence, they can form a thick but porous protective barrier through a combination of charring and foaming effect at the surface of the burning polymer. To enhance the fire safety of epoxy resins, nitrogen/phosphorus-based flame retardants, such as APP, MPP, and their derivatives, are important components of the intumescent system. As a single compound, they can act as both the blowing agent and the acid source after decomposition.

Nanomaterial-Based Flame Retardants for Epoxy Resins

Although phosphorus, silicon, and nitrogen-based flame retardants are efficient in flame retardancy with low toxicity, there remain some challenges to be resolved, such as the poor interfacial reaction with the organic polymers because of significant disparities in their polarities. Therefore, it is an important research area to develop and design some novel polymeric composites that have efficient flame retardancy as well as mechanical properties. In recent years, the development and advancement of nanomaterials provide an opportunity for flame retardants. In this part, some representative nanomaterials, including carbon-based nanomaterials and layered double hydroxides, are discussed.

Carbon Nanomaterials

Adding carbon nanomaterials into the epoxy resin as a polymeric composite is an effective way to improve their thermal stability and flame retardancy. In recent years, the progress of fullerene (C_{60}) polymeric composites has attracted interest because of the improvements in industrial production. Carbon nanotubes (CNTs) are competitive as additives in composites due to their low density, high aspect ratio, thermal stability, and extraordinary mechanical properties. Some 2D carbon nanosheets, such as graphene and its derivatives, are gradually commercially available in flame retardant fields considering their aspect ratio, thermal stability, and mechanical performance.

A series of benzalkoniumchloride-N-methyl pryrrolidine-fullerene (BEN-C_{60}-O) was designed and fabricated for the epoxy composites (Tsai et al. 2015). It was found that the LOI value increased from 22.5% in the neat epoxy to 30.0% in the Epoxy/CL88-C_{60}–O/BEN-3 wt%. With the incorporation of CL-88, it provides the silica layer and abundant C=C groups from C_{60}-O. During the combustion process, the pathway from the gaseous phase to the condensed phase is increased by the silica layers, and C=C groups work as a free radical trap. Moreover, the total heat release decreased from 92.0 MJ/m^2 to 86.5 MJ/m^2, and the peak heat release rate decreased from 599.03 MJ/m^2 to 567.77 MJ/m^2. The improved fire behaviors are ascribed to good dispersion of the fillers in the epoxy matrix and an increased char yield with the presence of C_{60}.

Carbon nanotubes, both multi-walled (MWCNTs) and single-walled (SWCNTs), are efficient flame retardants in epoxy composites. Their effectiveness on flame retardancy is highly related to their dispersion and concentrations in the polymeric matrix. The improved flame retardancy is related to the continuous char layers formed during the combustion, which is a good physical heat barrier to avoid heat transfer from the flame to the epoxy matrix. The -O-C_2H_5 group functionalized CNTs were added to the modified DGEBA epoxy resin (Kuan et al. 2010). The LOI value of the composite that contains 9 wt% CNTs is 29%, while the neat epoxy resin is only 22%. With 1 wt% CNTs, the UL-94 rating of the epoxy composite reaches a V-1 level, and with 3 wt%, the UL-94 rating reaches a V-0 level. These improvements are due to the structured network layer formed by CNT, which acts as heat and mass barriers and thus decreases the rate of polymer decomposition. In order to

enhance the dispersion efficiency, the CNTs can be modified via some hydrophobic functional groups. In this case, Im et al. developed montmorillonite (MMT) together with multi-walled carbon nanotube in epoxy resin. It was found that the MWCNT reduced the thermal degradation rate of the epoxy resin and increased the char yield, while the exfoliated MMT mainly acted as an energy storage medium to hinder thermal transfer within the epoxy resin. As a result, the LOI value increased from 21% to 31% in the presence of these additives. The activation energy E_a is used to describe the anti-oxidation behaviors and calculated by the equation below:

$$E_a = -\frac{R}{C}\left[\frac{\Delta \log \Phi}{\Delta(1/T_r)}\right]$$

where T_r is the rapid weight loss temperature, Φ is the heating rate (°C/min), C is a constant 0.4521, and R is the universal gas constant. When incorporating the additives into the epoxy composites, the calculated activation energy increased from 117 kJ/mol to 228 kJ/mol, indicating these additives make it harder to initiate the oxidization reactions of epoxy resin.

Graphene has attracted considerable interest from both academia and industry due to its high surface area, mechanical strength, abundance in nature, and low viscosity when compounded with polymers. The effect of graphene nanosheets (GNS) on thermal stability and flame retardancy of epoxy resins has also been investigated. Fewer gas products from the decomposition of epoxy resin, including epoxy group, aliphatic ether, and aromatic ring, were observed through TGA-FTIR within the temperature range of 400–430 °C. It can be proved that GNS changed the pathway of the epoxy resin decomposition, thus enhancing the thermal stability due to the incomplete decomposition compared with the neat epoxy resin. By adding 3 wt% GNS into the epoxy composite, the LOI value increased from 15.7% to 21.0%, while the total heat release reduced from 33.37 kJ/m^2 to 28.20 kJ/m^2 under the cone calorimeter test. It was also identified that if a small amount of GNS (less than 1 wt%) is added, few char residues and higher peak heat release are observed. This is because the thermal conductivity of GNS is much higher than the epoxy resin, which will accelerate the burning of epoxy resins. Instead, if the content of the GNS is higher than 1 wt%, the weight and compactness of the char residue improve significantly. In this case, the effect of the physical barrier from the contribution of GNS surpassed the effect of the thermal conductivity. The graphene can also be modified with some other kinds of traditional flame retardant, such as P-, N-, and Si-containing molecules, into polymer matrices via surface functionalization to obtain a synergistic effect. For example, a phosphorus-containing compound, polyphosphamide (PPA), was synthesized and covalently grafted onto the surface of GNS to obtain a novel flame retardant, PPA-g-GNS (Wang et al. 2014). The temperature of onset decomposition (the temperature corresponds to 5 wt% mass loss, $T_{5\%}$) under an air flow decreased when the filler was added into the epoxy resin, which is due to the decomposition of the phosphorus-containing components within the composites. Instead, when the decomposition temperature reached up to 700 °C, more char residue was left compared with the neat epoxy resin. The char residue can

work efficiently as a physical barrier to suppress the heat and mass transfer between the gaseous phase and the condensed phase. By adding 8 wt% fillers, the LOI value of the epoxy composites increased up to 30.5% as a comparison to only 21.5% for the neat epoxy. Under a cone calorimeter test, it was also observed that the peak heat release rate was reduced from 1730 kW/m^2 to 1016 kW/m^2, and the total heat release value was decreased from 113.1 MJ/m^2 to 56.9 MJ/m^2. It could be attributed to the barrier effect of the graphene to retard the permeation of the heat and mass transfer between the condensed phase and the flame. The catalytic effect of the filler for accelerating the carbonization process of the epoxy matrix contributes to the reduction of the total heat release rate. Another efficient graphene-based flame retardant was developed via adding phosphorus, nitrogen, and silica components onto the reduced graphene oxide (Feng et al. 2017). The wrapped flame retardant chains are responsible for improving the reduced graphene oxide (rGO) dispersion and compatibility efficiency within the epoxy matrix. In this study, total smoke production, total heat release, and the peak heat release rate were reduced by 30%, 14%, and 34%, respectively, compared to neat epoxy resin. From the char residue analysis, a stable char layer was obtained by adding the functional RGO. The silica-based group also enhanced the strength and oxidation resistance of the formed char layer.

Carbon nanomaterials can effectively inhibit the flammable drips, control the burning intensity, and reduce the total fire load available of epoxy composites through promoting epoxy matrices to form a compact, dense, and uniform protective char in the condensed phase, thus suppressing the combustible fragments diffusing into the flame region. However, it should be noticed that this char layer is not so effective as a heat barrier between the gaseous phase and condensed phase because of the high thermal conductivity of carbon nanomaterials. Another obstacle is the incompatibility of some pristine carbon-based filler with polymer matrix. In the future, some surface modification and hybrid functional materials may be a good strategy for enhancing the flame retardant performance of carbon-based nanomaterials.

Layered Double Hydroxides

Layered double hydroxides (LDHs) are a series of lamellar materials, and they are potentially efficient flame retardants due to their physical structures and chemical stability. Generally, they can be described by a formula $\left[M^{2+}_{1-x}M^{3+}_{x}(OH)_2\right](A^{n-})_{x/n}.mH_2O$, where M^{2+} is a divalent cation, M^{3+} is a trivalent cation, and A^{2+} is an inorganic or organic anion. LDHs can cool down the matrix via the endothermic decomposition, and the released water vapor can quench the flames and dilute flammable gases in the gaseous phase. The remained metal oxide residues in the condensed phase are an efficient physical barrier to suppress the heat and mass transfer between the polymeric matrix and the gaseous phase.

A modified Mg-Al-LDH was synthesized to improve the thermal properties and the flame retardant behaviors of epoxy resin. Mg-Al-LDH epoxy composite can reach an HB level under the UL-94 test. However, a relatively high loading of LDHs is often required to guarantee the final product to reach some fundamental flame retardancy requirements in the industry, such as UL-94 rating. Such high loading

levels sometimes are harmful to mechanical properties. Therefore, there are some emerging studies on combining LDHs with some other conventional flame retardants to improve their performance. Dodecyl sulfate (DDS) intercalated Mg-Al-LDHs and the melamine salt of pentaerythritol phosphate (MPP) were synthesized and used as additives for the preparation of epoxy nanocomposites (Kaul et al. 2017). The LOI value and UL-94 rating were improved to 24.4% and V-1 level, respectively. A dense and compact char residue was also observed after the combustion of the DDS-MPP-LDH-epoxy nanocomposite. MgAl-DDS is also a significant component for crosslinking MPP and epoxy resin by the dehydration of the hydroxyl groups. During the combustion, this crosslinking structure can prevent the phosphorus groups from diffusing into the gaseous phase, thus increasing the concentration of the phosphorus components available in the condensed phase to promote more carbonization formation.

In order to improve the dispersion efficiency of LDHs in the epoxy composites, the LDH was firstly modified by some bio-based components, phytic acid (Ph) and (hydroxypropyl) sulfobutyl-β-cyclodextrin sodium (CDBS), and subsequently Fe_3O_4 nanoparticles to obtain a Fe_3O_4 nanosphere@LDH (Kalali et al. 2016). With the assistant of the decorated Fe_3O_4 nanosphere (average size: 8 nm), the LDH-based flame retardant was well dispersed within the epoxy matrix. Compared with the neat epoxy resin, the peak heat release and total smoke production of the 8 wt% Fe_3O_4@Ph-CDBS-LDH epoxy composite were decreased by 55% and 34%, respectively. UL-94 rating also reached the V-0 level. A continual and compact char layer was formed after the combustion of the Fe_3O_4@Ph-CDBS-LDH epoxy composite.

The metal components in the LDHs framework are also important characters for designing novel flame retardants. A 3D NiCo-LDH@PZS hollow dodecahedral structure was designed and synthesized (Zhou et al. 2019). A reduction of 11.2% and 30.9% for total heat release rate and peak heat release rate was observed by adding 4 wt% NiCo-LDH@PZS into the epoxy matrix. The production of smoke and toxic gases during the combustion of polymers is the main concern for human safety and environmental protection. Surprisingly, with the addition of 4 wt% NiCo-LDH@PZS, it was found that the total amount of CO yield and smoke production was significantly suppressed compared with neat epoxy resin. However, through Fourier infrared gas analyzer, it was found that the production of these toxic gases was also reduced, due to the synergic assistance of the NiCo-LDH@PZS.

Metal-Organic Framework (MOF)-Based Flame Retardants for Epoxy Resins

Nowadays, metal-organic frameworks (MOFs) are a novel type of hybrid porous materials combining inorganic metal ions/clusters with organic ligands. Via varying the metal composition and organic linkers, the pore shape and size of the frameworks can be easily shaped and tuned. They are also found to be a new class of flame retardants for epoxy resins in recent years. Their excellent performance on flame

retardancy and smoke suppression is ascribed to their exceptional chemical compositions. During the thermal decomposition of the composite, metal oxides remain within the residue, which can work as a physical barrier to suppress the heat and mass transfer between the condensed phase and the gaseous phase. Similar to the effect of LDHs, the metal oxides can also efficiently catalyze the formation of the compact char layers. Some nonflammable gases, such as NH_3, can also be released to dilute the flammable gases in the flame.

For example, ZIF-8, a rhombic dodecahedral structure, is synthesized with zinc ions and 2-methylimidazole, which has a high surface area and thermal stability. The thermal decomposition process of ZIF-8 can be divided into three stages: (1) the evaporation of the absorbed small molecules within the pores, (2) carbonization of 2-methylimidazole, and (3) decomposition of the ZIF-8 nanocrystals and organic groups. The remained ZnO can efficiently catalyze the formation of the char residues, thus decreasing the oxygen supply to the condensed phase beneath the burning surfaces. By adding 2 wt% ZIF-8 into the epoxy matrix, the peak heat release rate was decreased from 1054 kW/m^2 to 431 kW/m^2, and total heat release was decreased from 39.1 MJ/m^2 to 25.3 MJ/m^2 (Xu et al. 2018). Compared with 67.8 m^2 from neat epoxy resin, the total smoke production was suppressed to 52.2 m^2, due to the high surface area structure and metal catalyst effects.

MOFs can also work efficiently with other flame retardants by only a small amount to impart the synergistic flame retardant effects to polymer composites. Due to the multiple active groups on the surface, it is easier for chemical surface modification to wrap the functional groups or compounds into the structure of MOFs. MgAl-layered double hydroxide (MgAl-LDH) was synthesized on the surface of ZIF-8 through electrostatic interactions (Li et al. 2018). It was found that 4.1 wt% of the total mass remained at 700 °C, while less than 0.1 wt% was left for neat epoxy resin. Due to the synergic effect between ZIF-8 and MgAl-LDH on the flame retardancy, a 50.9% and 30.4% reduction of peak heat release rate and total heat release were observed. Smoke production is another important factor to evaluate the flame retardant performance as it is the main factor for casualties during fire disasters. Compared with the neat epoxy resin, a 37.5% and 31.3% reduction of the smoke production rate and total smoke production were observed in ZIF-8@MgAl-LDH epoxy composites.

A Co-based MOF with P-containing groups was synthesized to investigate its influence on the flame retardancy of epoxy resin because of its good performance on char formation and smoke suppression (Hou et al. 2017). It was found that the char yield was as high as 36 wt% at 800 °C under N_2 conditions for the P-MOF epoxy composite. More importantly, the original shape of the P-MOF was still stable within the residue, but under an intumescent state. Therefore, the peak heat release rate and total heat release were decreased to 615 kW/m^2 (855 kW/m^2 for neat epoxy) and 70 MJ/m^2 (86 MJ/m^2 for neat epoxy) when filling 2 wt% of the P-MOF into the epoxy composite. In the presence of the P-MOF, a 15% reduction of the total smoke production was observed. Transition metal compounds can work efficiently on CO catalytic oxidation. Therefore, such a unique transition metal component is a potentially efficient catalyst for transforming CO to CO_2. A 52% reduction of CO release

and a 6.25% increase in CO_2 production directly confirm the excellent catalytic oxidation effect of P-MOF.

In summary, the general roles of MOFs and their composites are (1) producing metal oxides that can catalyze the formation of dense and compact char residues and (2) forming physical barriers to suppress the heat transfer and prevent the evaporation of flammable gases, thus delaying further combustion of flammable components within the matrix. Chemically functionalizing MOFs with some efficient phosphorus and/or nitrogen groups is a promising research area for developing efficient flame retardants.

Thermal Stability and Flame Retardants for Synthetic Fiber Reinforced Epoxy Resins

Only in a few research papers, the effect of fiber reinforcement on the thermal stability and flammability of epoxy composite was investigated. Carbon fiber and glass fiber are the two most popular synthetic fibers used in the industry. Herein, how these two kinds of fiber reinforcement affect the pyrolysis and combustion behaviors of epoxy composites is discussed. Moreover, how different flame retardants are developed and used for synthetic fiber reinforced epoxy resins are also reviewed. The specific improvements on the thermal stability and flame retardancy of the fiber reinforced epoxy composites are fully introduced, including weight loss during the decomposition, vertical burning (UL-94), LOI, heat release rate, etc.

Glass Fiber Reinforced Epoxy Composites

Glass fiber reinforced epoxy composites are widely used in different fields, such as aviation, marine, and chemical industry, due to their excellent mechanical properties and thermal insulation properties. Some equipment and fitting models are introduced to elucidate the effects of glass fiber on the thermal decomposition process and pyrolysis kinetics of epoxy composites.

Thermogravimetric analysis (TGA) with a pyrolizer was used to investigate the thermal decomposition process and evolved gas of the glass fiber reinforcement composites in a temperature range from 500 °C to 900 °C under different heating rates (Yun et al. 2014). The Friedman method can be simply described in the equation below to characterize different kinetic parameters, including activation energy (E), frequency factor (A), and conversion (X):

$$\ln\left(\frac{\mathrm{d}X}{\mathrm{d}t}\right) = \ln A + \mathrm{n}\ln(1-X) - \frac{E}{\mathrm{R}T}$$

where t is time, n is reaction order, and R is the universal gas constant. The kinetic parameters of glass fiber reinforced composites were derived from the Friedman method.

TGA-FTIR was used to obtain the thermogravimetric curves of the glass fiber reinforced epoxy composites and the infrared spectra of evolved gas during the pyrolysis process (Qiao et al. 2020). In addition to the Flynn-Wall-Ozawa method, a model fitting method Coat-Redfern equation is introduced as follows:

$$\ln\left(\frac{\mathrm{G}(\alpha)}{T^2}\right) = \ln\left(\frac{A\mathrm{R}}{\beta E_a}\left[1-\left(\frac{2\mathrm{R}T}{E_a}\right)\right]\right) - \frac{E_a}{\mathrm{R}T}$$

where G(α) is the integral form of the kinetic model, β is the heating rate, A is the pre-exponential factor, R is the universal gas constant, and E_a is the effective activation energy.

A linear positive correlation between the activation energy and the conversion rate was found during the thermal pyrolysis process of the glass fiber reinforced epoxy composites. Therefore, the reaction is controlled by one single reaction model from the overall degree of conversion. From the analysis of the FTIR data during the pyrolysis, the decomposition of glass fiber reinforced epoxy composites in the nitrogen atmosphere can be divided into two stages: (1) the main chain of the additives and epoxy resin matrix in the glass fiber reinforced epoxy composites are broken and decomposed into small molecules such as H_2O and CO_2 and a large amount of volatile macromolecular benzene with the temperature range from 290 °C to 460 °C, and (2) the volatile macromolecular benzene is further decomposed to generate a large amount of H_2O and CO_2 with the temperature range from 460 °C to 1000 °C (Qiao et al. 2020).

There are few studies focusing on using flame retardants to improve the fire resistance of the epoxy composite. Recently, a novel LDH/glass fiber epoxy composite was developed to improve its thermal and mechanical stability (Becker et al. 2012). It was found that the burning rate was decreased significantly by incorporating LDH together with the glass fiber. This improvement can be attributed to the accumulation of inorganic particles on the surface of the matrix. As a result, a carbonaceous coating can prevent heat and mass transfer from the condensed phase to the gaseous phase.

Carbon Fiber Reinforced Epoxy Composites

The effect of carbon fiber on the thermal decomposition of the epoxy composite can be fully investigated by pyrolysis analysis. Under a given heating rate, two obvious decomposition stages can be found in neat epoxy resin, while it shows three stages for carbon fiber reinforced epoxy resins. The first two stages have a similar decomposition temperature range, which means that the first two stages are for epoxy resin only and the third one is for carbon fiber. Furthermore, when increasing the heating rate, the starting and ending temperatures of different decomposition stages move toward a higher temperature range. The Kissinger model and Flynn-Wall-Ozawa model are two methods used to calculate the apparent activation energy and apparent pre-exponential factor for different polymer composites during the pyrolysis.

Kissinger Model

Combining the Arrhenius equation and the reaction rate equation, the general rate equation is obtained:

$$\frac{\mathrm{d}\alpha}{\mathrm{d}t} = \mathrm{k}(T) * \mathrm{f}(\alpha) = Z\,\mathrm{f}(\alpha)\exp\left[\frac{-E}{\mathrm{R}T}\right]$$

where α is the fraction of reactant remaining, t is time, f(α) is the "some-function-of α," E is the activation energy, Z is the Arrhenius pre-exponential factor, R is the universal gas constant (8.314 J/mol K), and T is the temperature (K).

If the general rate equation is differentiated by time (t), substituting T with exothermic peak temperature T_p, and assuming the decomposition reaction is first order, the following equation is derived:

$$\frac{\mathrm{E}\beta}{\mathrm{R}T_p^2} = Z\exp\left[\frac{-E}{\mathrm{R}T_p}\right]$$

By taking the logarithm on both sides of the equation, Kissinger equation is obtained:

$$\ln\left[\frac{\beta}{T_p^2}\right] = \ln\left[\frac{\mathrm{ZR}}{E}\right] - \frac{E}{\mathrm{R}T_p}$$

When combining the TGA data with the Kissinger model, it was found that for carbon fiber reinforced epoxy composites, the reaction rate of the first stage is faster than the other two stages. Comparing the carbon fiber reinforced epoxy composites with the neat epoxy resins, no obvious difference is identified for the first stage. However, higher activation energy is required for the carbon fiber reinforced epoxy composites within the second stage.

Flynn-Wall-Ozawa Method

Different from other kinetic models, the Flynn-Wall-Ozawa method is a model-free method and is not related to the Arrhenius-type temperature dependence. It measures the temperatures corresponding to fixed values of α from experiments at different heating rates, ln(α) is plotted against $1/T$, and the slopes of such plots give $-E_a$/R:

$$\log\beta = \log\left(\frac{AE_a}{\mathrm{RG}(\alpha)}\right) - 2.315 - 0.4567\frac{E_a}{\mathrm{R}T}$$

where G(α) is the integral form of kinetic model (i.e., G(α) = kt), β is the heating rate, A is the pre-exponential factor, R is the universal gas constant, and E_a is the effective activation energy.

It is found that the neat epoxy resin has a faster reaction rate in the beginning stage. Then, the reaction slows down gradually due to a higher energy barrier to break the bond, which is consistent with the activation energy results. In comparison,

carbon fiber reinforced epoxy composites are always under equilibrium in different reaction stages. Furthermore, no obvious activation energy changes indicate that the pyrolysis process is not under a big fluctuation.

In addition to the thermal stability, the effect of carbon fiber on the flammability of epoxy composite is also investigated. Specifically, the ignition time describes the time it takes for a specimen to ignite on the surface under a certain heat flux. The longer the ignition time, the better the ignition resistance. It was found that compared with the neat epoxy resin matrix, carbon fiber reinforced epoxy composite has a better ignition resistance. For instance, at a heat flux rate of 50 kW/m^2, the ignition time is prolonged from 15 s to 29 s when carbon fiber is reinforced into the epoxy resin (Wang and Zhang 2019). Under 50 kW/m^2, the neat epoxy resin only has 1% residue remained, while a carbon fiber/epoxy composite can have up to 63% residue remained. From the morphology analysis of different composites before and after combustion, a carbon layer can be found on the surface of the fiber reinforced epoxy composite's residue, which can efficiently inhibit the diffusion of the flammable gases toward the fire. As a result, both thermal stability and flammability are improved due to the developed physical barrier. No melting droplets or splashing phenomena were observed during the combustion experiments for the carbon fiber reinforced epoxy composites.

Carbon nanofiber has recently attracted more attention from researchers due to its good mechanical properties and renewability. Previous discussions on carbon-based nanomaterials demonstrate that it is a promising method to develop epoxy composites with conventional flame retardants and/or other nanomaterials.

Phosphorus-based materials are an efficient flame retardant system with low toxicity compared with other halogen-based commercial flame retardants. A facial layer-by-layer assembly method was developed for fabricating polyethyleneimine (PEI) and ammonium polyphosphate (APP) coating onto the surface of carbon fiber reinforced epoxy composites (Shi et al. 2018). By adding APP onto the surface of the composites, a decrease of the onset decomposition temperature was observed, which is due to the decomposition of the flame retardant instead of the epoxy matrix. These products during the decomposition can significantly influence the stability of the remaining epoxy matrix under higher temperatures. As a result, more residues were left compared with the neat carbon fiber reinforced epoxy composite. It gave LOI value rise to 39.0% $\pm$ 0.5% and passed the UL-94 V-0 test for both at 3.2 mm and 1.6 mm thickness. For neat carbon fiber reinforced epoxy composite, its LOI value was only about 31.0% $\pm$ 0.5%.

Silica-based flame retardants can improve the thermal stability of polymers by forming an accumulated SiO_2 protective layer on the surface of the polymer in the condensed phase. A novel carbon fiber reinforced epoxy/hybrid-silica composite was developed. To evaluate the thermal stability of this epoxy composite, the onset decomposition temperature increased a lot compared with the neat fiber reinforced composite. The self-extinguishing test shows that the UL-94 test can reach up to 20 s by introducing silica.

Similar to LDHs, boron-based flame retardants can also endothermically decompose into metal oxide and water, thus absorbing the heat from the epoxy resin matrix

in the condensed phase. Therefore, the boron carbide was used as an efficient additive for carbon fiber reinforced epoxy composite. The neat epoxy resin had a much smaller amount of residue compared with boron carbide/epoxy composite.

A new type of flame retardant by chemically grafting 9,10-dihydro-9-oxa-phosphaphenanthrene-10-oxide (DOPO) onto graphene was developed considering the good compatibility between nano-filler and polymer matrix (Sun et al. 2016). Chemically attaching the halogen-free functional groups onto the graphene can reduce the required amounts of additive fillers and have a competitive flame retardancy efficiency. By adding 3 wt% graphene-DOPO in the carbon fiber reinforced epoxy composite, the LOI value increased from 18.5% to 28.0%, and it was rated as a V-1 level under the UL-94 vertical flame test. Moreover, the total heat release was decreased from 16.1 kJ/g to 12.0 kJ/g.

Conclusions

In this chapter, the thermal decomposition and combustion behaviors of epoxy resins and their synthetic fiber reinforced composites are fully elucidated. For epoxy resins, their thermal stability and flammability are affected by their chemical structure, curing agent, and crosslink density. Three strategies can be implemented to further improve their thermal stability and flame retardancy: developing epoxy resins with inherent flame retardancy by introducing very high contents of aromatic subunits in their structures; chemically incorporating the elements with flame retardant function into the molecular structure of epoxy resins or their curing agents; and physically blending flame retardant additives into the matrix of an epoxy resin to form composites. Based on the basic principles of flame retardant mechanism in both the gaseous phase and condensed phase, different types of flame retardants are fully investigated to improve the thermal stability and fire resistance of the epoxy resins, including phosphorus-based, silicon-based, nitrogen-based, nanomaterials-based, and metal-organic framework materials. As a result, a variety of flame retardant epoxy composites has been successfully developed through individual components or combinations between different components to achieve a synergistic effect. Further, there has been some revolutionary progress in developing nanoscale-based flame retardants. Due to the improved dispersion within the organic matrix and the unique characteristics of nanomaterials, the flammability of the epoxy composites can be reduced significantly. The presence of synthetic fiber reinforcements also affects the thermal stability and flammability of epoxy resins, such as the thermal decomposition pathway, ignition mechanism, heat transfer within the epoxy matrix, etc. However, a very limited number of studies can be found in the open literature to improve the performance of synthetic fiber reinforced composites from the aspects of thermal stability and flame retardancy.

There are still some limitations on both traditional flame retardants and nanomaterials. Some high-aspect-ratio nanomaterials may aggregate during the preparation of the polymeric composites, thus deteriorating the flame retardant performance and mechanical properties as well. Most nanomaterial-based epoxy composites often

fail to obtain a V-0 rating under the UL-94 test or to obtain a higher LOI value. However, these two tests are important indicators in industries for evaluating the self-extinguishing behavior of a product. Moreover, typically, high loading of traditional additive-type flame retardants is required to meet certain flame retardancy requirements, which compromises the mechanical properties of the epoxy composites. Therefore, the combination of traditional flame retardants and nanomaterials is an innovative and promising strategy to develop advanced epoxy composites. Physical mixing is a simple and cost-effective method, but the aggregation of the nanomaterials is the main concern. Functionalization of nanomaterials with traditional flame retardants or corresponding groups is an alternative method. It can enhance the dispersion efficiency and achieve synergic effects between different flame retardants. However, this method currently is still limited on a lab scale.

References

L. Ahmed, B. Zhang, R. Shen, R.J. Agnew, H. Park, Z. Cheng, M.S. Mannan, Q. Wang, J. Therm. Anal. Calorim. **132**(3), 1853–1865 (2018)

M. Asim, M. Jawaid, N. Saba, M. Nasir, M.T.H. Sultan, in *Hybrid Polymer Composite Materials*, ed. by V. K. Thakur, M. K. Thakur, A. Pappu, (Elsevier, 2017), p. 1

A.A. Azeez, K.Y. Rhee, S.J. Park, D. Hui, Compos. Part B Eng. **45**(1), 308–320 (2013)

V. Babushok, W. Tsang, Combust. Flame **123**(4), 488–506 (2000)

M. Bar, R. Alagirusamy, A. Das, Fibers Polym. **16**(4), 705–717 (2015)

C.M. Becker, T.A. Dick, F. Wypych, H.S. Schrekker, S.C. Amico, Polym. Test. **31**(6), 741–747 (2012)

B. Biswas, B.K. Kandola, Polym. Adv. Technol. **22**(7), 1192–1204 (2011)

U. Braun, A.I. Balabanovich, B. Schartel, U. Knoll, J. Artner, M. Ciesielski, M. Döring, R. Perez, J.K. Sandler, V. Altstädt, Polymer **47**(26), 8495–8508 (2006)

M.C. Celina, A.R. Dayile, A. Quintana, Polymer **54**(13), 3290–3296 (2013)

K.C. Cheng, S.Y. Yu, W.Y. Chiu, J. Appl. Polym. Sci. **83**(13), 2733–2740 (2002)

M. Ciesielski, B. Burk, C. Heinzmann, M. Döring, in *Novel Fire Retardant Polymers and Composite Materials*, ed. by D.-Y. Wang, (Elsevier, Amsterdam, 2017), p. 3

Y. Feng, C. He, Y. Wen, Y. Ye, X. Zhou, X. Xie, Y.-W. Mai, Compos. Part A Appl. Sci. Manuf. **103**, 74–83 (2017)

A. Hartwig, D. Pütz, B. Schartel, M. Bartholmai, M. Wendschuh-Josties, Chem. Phys. **204**(18), 2247–2257 (2003)

R. Hicklin, R. Padda, G. Lenotte, in *Fire Retardancy of Polymers: New Strategies and Mechanisms*, ed. by T. R. Hull, B. K. Kandola, (Royal Society of Chemistry, Cambridge, 2008), p. 255

Y. Hou, W. Hu, Z. Gui, Y. Hu, Compos. Sci. Technol. **152**, 231–242 (2017)

Y. Hu, X. Wang (eds.), *Flame Retardant Polymeric Materials: A Handbook* (CRC Press, Boca Raton, 2019)

J. Hu, J. Shan, D. Wen, X. Liu, J. Zhao, Z. Tong, Polym. Degrad. Stab. **109**, 218–225 (2014)

S. Huo, J. Wang, S. Yang, C. Li, X. Wang, H. Cai, Polym. Degrad. Stab. **159**, 79–89 (2019)

S.-D. Jiang, G. Tang, J. Chen, Z.-Q. Huang, Y. Hu, J. Hazard. Mater. **342**, 689–697 (2018)

E.N. Kalali, X. Wang, D.-Y. Wang, Ind. Eng. Chem. Res. **55**(23), 6634–6642 (2016)

P.K. Kaul, A.J. Samson, G.T. Selvan, I. Enoch, P.M. Selvakumar, Appl. Clay Sci. **135**, 234–243 (2017)

P. Kiliaris, C.D. Papaspyrides, Prog. Polym. Sci. **35**(7), 902–958 (2010)

M. Kilinc, in *Non-Halogenated Flame Retardant Handbook*, ed. by A. B. Morgan, C. A. Wilkie, (Wiley, Hoboken, 2014), p. 169

C.-F. Kuan, W.-J. Chen, Y.-L. Li, C.-H. Chen, H.-C. Kuan, C.-L. Chiang, J. Phys. Chem. Solids **71**(4), 539–543 (2010)
S.V. Levchik, in *Flame Retardant Polymer Nanocomposites*, ed. by A. B. Morgan, C. A. Wilkie, (Wiley, Hoboken, 2007), p. 1
S.V. Levchik, in *Non-Halogenated Flame Retardant Handbook*, ed. by A. B. Morgan, C. A. Wilkie, (Wiley, Hoboken, 2014), p. 17
S.V. Levchik, E.D. Weil, Polym. Int. **53**(12), 1901–1929 (2004)
A. Li, W. Xu, R. Chen, Y. Liu, W. Li, Compos. Part A Appl. Sci. Manuf. **112**, 558–571 (2018)
Y. Liu, C.-L. Deng, J. Zhao, J.-S. Wang, L. Chen, Y.-Z. Wang, Polym. Degrad. Stab. **96**(3), 363–370 (2011)
H. Liu, K. Xu, H. Cai, J. Su, X. Liu, Z. Fu, M. Chen, Polym. Adv. Technol. **23**(1), 114–121 (2012)
S. Liu, V.S. Chevali, Z. Xu, D. Hui, H. Wang, Compos. Part B Eng. **136**, 197–214 (2018)
Q. Liu, D. Wang, Z. Li, Z. Li, X. Peng, C. Liu, Y. Zhang, P. Zheng, Materials **13**(9), 2145 (2020)
M.E. Mngomezulu, M.J. John, V. Jacobs, A.S. Luyt, Carbohydr. Polym. **111**, 149–182 (2014)
A.B.. Morgan, Polym. Rev. **59**(1), 25–54 (2019)
A.B.. Morgan, J.W. Gilman, Fire Mater. **37**(4), 259–279 (2013)
A.P. Mouritz, A.G. Gibson, *Fire Properties of Polymer Composite Materials* (Springer Science & Business Media, Dordrecht, 2007)
S. Pack, in *Flame Retardants: Polymer Blends, Composites and Nanocomposites*, ed. by P. M. Visakh, Y. Arao, (Springer International Publishing, Cham, 2015), p. 115
M. Pecora, Y. Pannier, M.-C. Lafarie-Frenot, M. Gigliotti, C. Guigon, Polym. Test. **52**, 209–217 (2016)
A. Pegoretti, M. Traina, in *Handbook of Properties of Textile and Technical Fibres*, ed. by A. R. Bunsell, (Elsevier, 2018), p. 621
C.M.C. Pereira, M.S.S. Martins, in *Polymer Green Flame Retardants*, ed. by C. D. Papaspyrides, P. Kiliaris, (Elsevier, Amsterdam, 2014), p. 551
C.A. Pittinger, A.M. Pecquet, Environ. Sci. Pollut. Res. **25**(15), 14361–14372 (2018)
Z. Qi, W. Zhang, X. He, R. Yang, Compos. Sci. Technol. **127**, 8–19 (2016)
Y. Qiao, O. Das, S.N. Zhao, T.S. Sun, Q. Xu, L. Jiang, Polymers **12**(11), 2739 (2020)
J. Qin, W. Zhang, R. Yang, Mater. Des. **178**, 107834 (2019)
M. Rakotomalala, S. Wagner, M. Döring, Materials **3**(8), 4300–4327 (2010)
H. Ren, J. Sun, B. Wu, Q. Zhou, Polym. Degrad. Stab. **92**(6), 956–961 (2007)
N. Roenner, K. Hutheesing, A. Fergusson, G. Rein, Fire Saf. J. **91**, 200–207 (2017)
N. Saba, M. Jawaid, in *Hybrid Polymer Composite Materials*, ed. by V. K. Thakur, M. K. Thakur, A. Pappu, (Elsevier, 2017), p. 57
K.A. Salmeia, S. Gaan, Polym. Degrad. Stab. **113**, 119–134 (2015)
B. Schartel, Materials **3**(10), 4710–4745 (2010)
B. Schartel, A. Weiß, H. Sturm, M. Kleemeier, A. Hartwig, C. Vogt, R. Fischer, Polym. Adv. Technol. **22**(12), 1581–1592 (2011)
M. O. Seydibeyoglu, A. K. Mohanty, M. Misra (eds.), *Fiber Technology for Fiber-Reinforced Composites* (Woodhead Publishing, 2017)
R. Shen, L.C. Hatanaka, L. Ahmed, R.J. Agnew, M.S. Mannan, Q. Wang, J. Therm. Anal. Calorim. **128**(3), 1443–1451 (2017)
X.-H. Shi, Y.-J. Xu, J.-W. Long, Q. Zhao, X.-M. Ding, L. Chen, Y.-Z. Wang, Chem. Eng. J. **353**, 550–558 (2018)
M. Shibata, T. Ohkita, Eur. Polym. J. **92**, 165–173 (2017)
F. Sun, T. Yu, C. Hu, Y. Li, Compos. Sci. Technol. **136**, 76–84 (2016)
M.C. Tanzi, S. Farè, G. Candiani, *Foundations of Biomaterials Engineering* (Academic, 2019)
T.-Y. Tsai, N. Bunekar, C.-C. Huang, Y.-S. Huang, L.-C. Chen, RSC Adv. **5**(116), 95649–95656 (2015)
P. Wang, Z. Cai, Polym. Degrad. Stab. **137**, 138–150 (2017)
H. Wang, L. Zhang, AIP Adv. **9**(12), 125110 (2019)
X. Wang, W. Xing, X. Feng, B. Yu, L. Song, Y. Hu, Polym. Chem. **5**(4), 1145–1154 (2014)

B. Wang, H. Sheng, Y. Shi, W. Hu, N. Hong, W. Zeng, H. Ge, X. Yu, L. Song, Y. Hu, Polym. Degrad. Stab. **113**, 96–109 (2015)
X. Wang, E.N. Kalali, J.-T. Wan, D.-Y. Wang, Prog. Polym. Sci. **69**, 22–46 (2017)
X. Wang, W. Guo, L. Song, Y. Hu, Compos. Part B Eng. **179**, 107487 (2019)
W. Xu, G. Wang, Y. Liu, R. Chen, W. Li, RSC Adv. **8**(5), 2575–2585 (2018)
Y. Xu, Y. Yang, R. Shen, T. Parker, Y. Zhang, Z. Wang, Q. Wang, Polym. Compos. **40**(12), 4530–4546 (2019)
Y. Xu, C. Lv, R. Shen, Z. Wang, Q. Wang, Polym. Compos. **41**(9), 3778–3786 (2020)
Y.M. Yun, M.W. Seo, G.H. Koo, H.W. Ra, S.J. Yoon, Y.K. Kim, J.G. Lee, J.H. Kim, Fuel **137**, 321–327 (2014)
W. Zhang, G. Camino, R. Yang, Prog. Polym. Sci. **67**, 77–125 (2017)
J. Zhao, X. Dong, S. Huang, X. Tian, L. Song, Q. Yu, Z. Wang, Polym. Degrad. Stab. **156**, 89–99 (2018)
X. Zhou, X. Mu, W. Cai, J. Wang, F. Chu, Z. Xu, L. Song, W. Xing, Y. Hu, A.C.S. Appl, Mater. Interfaces **11**(44), 41736–41749 (2019)

Morphology and Mechanical Properties of Epoxy/Synthetic Fiber Composites

10

Mattia Bartoli, Mauro Giorcelli, and Alberto Tagliaferro

Contents

Abstract

In this chapter, we provide an overview on the use of synthetic fibers for the production of performing epoxy composite materials. We choose to focus our effort on the description of works based on the utilization of carbon and glass fibers. Our decision is motivated by the diffusion of those fibers in plenty of key cutting edge applications and productions. Herein we report an introductive section where we describe the main features of carbon and glass fibers as well as those of epoxy.

M. Bartoli (✉)
Consorzio Interuniversitario Nazionale per la Scienza e Tecnologia dei Materiali (INSTM), Florence, Italy

Italian Institute of Technology, Torino, Italy
e-mail: mattia.bartoli@polito.it

M. Giorcelli · A. Tagliaferro
Department of Applied Science and Technology, Politecnico di Torino, Turin, Italy

Consorzio Interuniversitario Nazionale per la Scienza e Tecnologia dei Materiali (INSTM), Florence, Italy

S. Mavinkere Rangappa et al. (eds.), *Handbook of Epoxy/Fiber Composites*,
https://doi.org/10.1007/978-981-19-3603-6_12

Afterward, we discuss in detail the new discoveries in the field of synthetic fiber epoxy composites. Our aim is to guide the readers through the world of synthetic-based epoxy materials enlightening the main and most relevant issues.

Keywords

Carbon fibers · Glass fibers · Mechanical properties · Composites

Introduction

Synthetic fibers are one the most revolutionary materials of the twentieth century. Since their discovery, synthetic fibers have attracted a great scientific and commercial interest for their outstanding properties and consequent wide range of applications.

As years went by, a new class of fibers gained worldwide attention: high-performance fibers such as glass (GFs) and carbon (CFs) fibers. These materials have found their main application as reinforcement for the production of composites. Fiber-reinforced composites are a large family that regroups materials that can be divided into four classes based on the host matrix: (i) metal, (ii) ceramic, (iii) carbon/carbon, and (iv) polymer matrix.

Fibers containing polymer composites are the most widespread having a global marketplace of about 1 billion dollars.

Among the various polymeric matrices, epoxy resins are the most used thermoset polymeric host. Epoxy composites are one of the most extensively investigated fields of polymer and material science due to the large and common use of epoxy and epoxy-related materials in a wide range of real-world applications. The use of epoxy matrix combined with fibrous fillers is a very attractive route to produce high-performance composites materials.

GF- and CF-based epoxy materials are widely used by several strategic industries such as aeronautics and automotive.

Although the type of epoxy resin plays an unneglectable role, fibers are mainly accountable for all of the mechanical properties of the composites. However, the outstanding characteristics of the fibers can reinforce the whole composite only if a strong bonding between fibers and host material exist. Hence, the interaction between fibers and epoxy host is one of the key issues in the production of performing fiber-based composites.

In this chapter, we overview GF- and CF-filled epoxy materials through an updated review of recent literature providing as well a comprehensive introduction on the essential information about the properties of both fibers and epoxy host.

Synthetic Fiber Epoxy Composites: The Materials

Carbon Fibers

CFs are fibers with an average diameter ranging from 5 to 10 μm mainly composed by sp^2 carbon atoms as shown in Fig. 1.

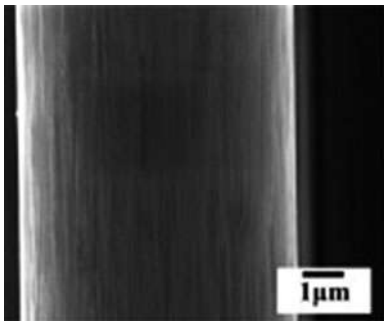

Fig. 1 Scanning electron microscope image of an uncoated CF. (Reprinted with permissions from Qin et al. (2015))

Nowadays, they are mainly produced by using a polymeric precursor. Poly (acrylonitrile) (PAN) fibers represent the common choice with only around 10 wt. % of CF produced by using alternative feedstock such as biomass.

CFs are industrially produced by treating the precursors at high temperature to convert it into a carbonaceous structure. The procedure is usually a three-stage process with a first step at around 300–350 °C, the second at around 1000–3000 °C and a final one for the surface oxidation. The first stage is called stabilization step, and it is necessary to provide a rearrangement of CF bonding pattern. Dunham and Edie (1992) identified three main reactions occurring in this step: dehydrogenation, oxidation, and cyclization. After the first step, a partially carbonized structure mainly made by a linear chain of pyridine moieties is formed accordingly with the original structure of PAN.

In the second stage, CF precursors are fully carbonized at temperatures ranging from 1000 °C up to 3000 °C in inert atmosphere under moderate pressure. In this stage, the heteroatoms such as nitrogen and oxygen are removed from the carbon skeleton that starts to rearrange itself in a graphitic like material. Several technologies have been used for this purpose ranging from tubular reactors to plasma processes.

Afterward, CFs undergo to the last step that is an oxidation process to improve their adhesion properties by tuning their interphase chemistry. Oxidation can be achieved by immersion using watery solution of oxidating agents such as sodium hypochlorite or nitric acid, by using plasma treatment or by exposing the fibers to oxidating gases (i.e., air, oxygen, carbon dioxide ozone) in appropriate conditions of temperature and pressure.

High-quality CFs produced by using PAN shows astonishing mechanical properties such as modulus of elasticity up to 531 GPa and a tensile strength up to 5600 MPa together with a high electrical and thermal conductivity.

The main drawback of CFs produced by using PAN is represented by their high cost, but it was estimated that the CF global market will reach up to 200 billion of dollar in 2022 due to the massive use in aerospace sector.

Several other CFs precursors have been investigated to simultaneously reduce the cost and the environmental impact. Recently, Mikkilä et al. (2020) reported a comprehensive study on the use of both cellulose and lignin to produce good-

quality carbon fibers. Authors used the fibrous structure of cellulose and the aromatic content of the lignin to simulate the PAN precursor with quite remarkable results. Kubo and Kadla (2005) blended lignin and polymers to improve the quality of the product but decrease the cost-price effectiveness of the use of natural feedstock. Kadla et al. (2002) used only kraft lignin for the production of CFs proving that also amorphous wasted biopolymers could lead to the formation of CFs.

Glass Fibers

GFs are a glass-derived compound formed though stranding of silica-based or other formulation extruded into many fibers with a very small average diameter as shown in Fig. 2.

There are two main types of GFs productive process: direct melt process and marble remelt process. Both of them are fed with solid form raw materials, silica, and other inorganic oxides. Feedstocks are mixed and melted together in a furnace at a temperature up to 1720 °C. Afterward for the marble process, the molten material is sheared and rolled into marbles and rapidly cooled. The blocks obtained could be easily remelted and extruded as fibers. On the contrary during the direct melt process, the molten feedstock in the furnace goes directly to the bushing for formation GFs. According to their compositions, GFs are classified as shown in Table 1.

GFs A are produced by using alkali-lime or soda lime glass and they are small-sized. They can be boron-doped, and the maximum content of alkaline oxides is 0.8 wt.%.

GFs C contain calcium borosilicate which increases structural equilibrium in both basic or acidic corrosive environments.

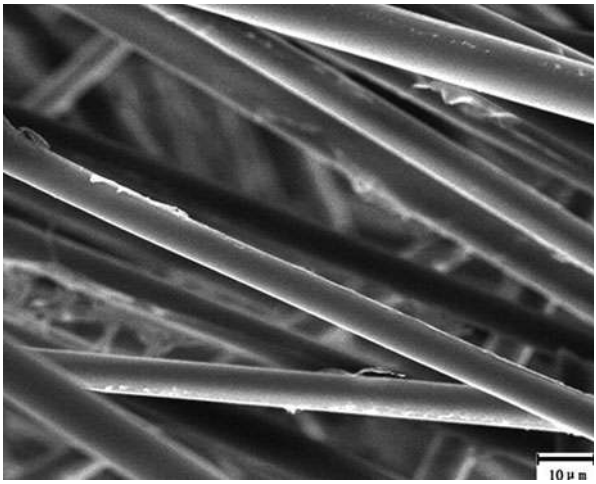

Fig. 2 Scanning electron microscope caption of an uncoated GF. (Reprinted with permissions from Di et al. (2013))

Table 1 Composition of main GFs types

	Composition [wt.%]									
	A	*C*	*D*	*E*	*Advantex*	*ECR*	*AR*	*R*	*S-2*	*Quartz*
SiO_2	63–72	64–68	72–75	52–56	59–62	54–62	55–75	56–60	64–66	>99.99
Al_2O_3	0–6	3–5	0–1	12–16	12–15	9–15	0–5	23–26	24–26	–
B_2O_3	0–6	4–6	21–24	5–10	<0.2	–	0–8	0–0.3	<0,05	–
CaO	6–10	11–15	0–1	16–25	20–24	17–25	1–10	8–15	0–0,2	–
MgO	0–4	2–4	–	0–5	1–4	0–4	–	4–7	0–4	–
ZnO	–	–	–	–	–	2–5	–	–	–	–
BaO	0–1	–	–	–	–	–	0–0.1	–	0–1	
Na_2O and K_2O	14–16	7–10	0–4	0–2	–	0–2	11–21	0–1	<0.3	–
TiO_2	0–0.6	–	–	0–0.8	–	0–4	0–12	0–0.3	–	–
Zr_2O_3	–	–		–	–	1–18	–	–	–	–
Li_2O	–	–	–	–	–	–	0–1.5	–	–	–
Fe_2O_3	0–0.5	0.8	0–0.3	0–0.4	–	0–0.8	0–5	0–0.5	0–0.1	–
F_2	0–0.4	–	–	0–1	–	–	–	0–0.1	–	–

GFs D contain a high percentage of boron, mainly as oxide, that leads to an enhancement of heat and thermal shock resistance. Furthermore, the presence of boron oxide decreases the dielectric constant making them suitable for the realization of optical cables.

GFs E are the most commonly used GFs and they are usually termed fiberglass. GFs E contain aluminum boron silicates and alkali oxide components such as aluminum oxide in concentration up to a maximum of 1 wt.%.

A GFs that were more recently made commercially available is the GFs Advantex produced since the early 1990s. Advantex are produced by using calcium aluminum silicates leading to a high content of calcium oxides. This induces a high corrosion resistance spreading GFs Advantex use in the oil and gas industry power plants, mining industry, and marine applications as well as in wastewater and sewage systems.

GFs ECR are also called electronic GFs due to their lower electrical leakage rate and high surface resistance. They show a good waterproofing, high mechanical strength, electrical acidic, and alkali corrosion resistance. They are boron oxide- and fluorine-free, so they are more environmentally friendly than GFs E.

GFs AR, alkali-resistant, were development targeting specifically concrete construction applications. GFs AR contain alkaline zirconium silicates, and they are able to effectively prevent concrete cracking by improving strength and flexibility of concrete. Due to their composition, they are very difficult to dissolve in any watery medium, and they are practically not affected by pH changes.

Other GFs reported in Table 1 are quite close to the composition of GFs E-type glass fibers, and they were developed for the aerospace and defense industries.

Table 2 Comparison between mechanical properties of GFs E and GFs S-2

	GFs E	GFs S-2
Ultimate tensile strength [MPa]	521	4890
Elongation at break [%]	4.8	5.7
Modulus of elasticity [GPa]	72.3	89.6
Poisson ratio	0.2	0.23
Shear modulus [GPa]	30	35

GFs S-2 are worth of a specific mention. They represent the top quality among GFs as they outperformed all the mechanical properties of GFs E as shown in Table 2. GFs S-2 are produced with a higher dense silica leading to the properties aforementioned.

Polymer-Based Fibers

CFs and GFs are the most used but not the only fibrous materials for the production of epoxy-based composites. Polymer-based fibers (PBFs) represent the other great family of fibers currently available for the production of composites with improved properties. The most used materials for the production of these compounds are polyamides, polyesters, polyaniline, and polysulfones; PBF classification is tricky, and properties dramatically change in each family with the change of molecular weight functionalization and preparation methodology. The great tunability and the facile production of PBFs counterbalance the inferior performances compared with CFs and GFs. Furthermore, they could be used for the production of self-standing materials.

Epoxy Resin

Epoxy resins are massively used for the production of reinforced plastics. Every year, worldwide market requires an increased amount of fibers containing composites for a lot of applications including automotive and aerospace industry. Among thermoset polymeric matrix, epoxy resins represent a special class due to their impressive mechanical properties. Epoxy is generally composed by a diglycidyl-ended prepolymer chain, an amine-based hardener and additives to improve workability. One of the most common epoxy resin formulations is based on diglycidyl bisphenol, a monomer that reacts with the hardener accordingly to the scheme of Fig. 3.

Epoxy resin polymerization is a two-step process. During the first step, low-molecular-weight chains having a poor reticulation are formed. This step is generally performed at room temperature. The second step is the most relevant and it is called curing step. During the curing the reticulation advances to completion and determines the final mechanical properties of the polymeric matrix. During the curing, the rheological properties of epoxy resin change accordingly to the increment in the reticulation degree. Epoxy matrix are generally resistant to corrosion, and they are stable in a wide temperature range.

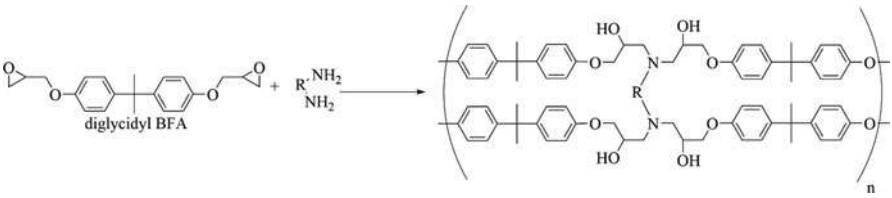

Fig. 3 Schematic pathway for the polymerization of diglycidyl BFA-based resin with amine curing agent

Synthetic Fiber Epoxy Composites

Fiber-reinforced epoxy composites have been used for decades for plenty of cutting edge applications where the mechanical properties of the filler paired to the stability of the epoxy matrix reached the optimum conditions for the application.

Several strategies have been applied to combine epoxy matrix with synthetic fibrous fillers ranging from longitudinal, woven mat, and chopped ones. All were aimed to enhance the mechanical and tribological properties of the composites.

The main drawbacks in the production of fiber-based epoxy composites are represented by brittleness and delamination. Synthetic fiber-based epoxy composite brittleness is related to their high elastic modulus and low maximum elongation of the fibrous filler compared to those of the epoxy matrix. So, when fibers reach their failing point, the polymer matrix is already beyond its limit. Accordingly, the composite undergoes a rapid crack propagation that can occur in three different modes. Mode I is due to stress orthogonal to the local plane of the crack surface, mode II is related to the stress parallel to the crack surface but orthogonal to the crack front, and mode III is due to the stress parallel to the crack surface and to the crack front. For CFs and GFs containing epoxy composites, the most relevant modes are I and II, due to the aforementioned mechanical properties. The delamination is the other key point that must be taken into account. It is due to the poor interphase bonding between the fibrous filler and the matrix. This creates local weaknesses in bonding between fibers and matrix that under solicitation and aging lead to debonding.

The interactions occurring on the interphase region could be summarized by two main mechanisms. The first is represented by mechanical coupling or interlocking on microscale of the fibrous filler and polymeric matrix. The second one is based on physical interactions though both weak forces and direct covalent bonding between the fibers and the resin and the matrix. Both mechanical and physical interactions generate a complex region close to the surface of the fibrous fillers.

In the following subsection, we present a comprehensive overview on the most remarkable results reached in the improvement of the properties of synthetic fibers containing epoxy composites taking into account the achievement and the remained unsolved issues.

Carbon Fiber Epoxy Composites

CF-based epoxy materials have undergone extensive studies during past years. Commonly, purchased CFs are covered by a thin layer of a polymeric coating known as prepreg (pre-impregnated carbon fiber) material that retains the main features of neat CFs together with an improved workability.

Newcomb (2019) studied the time-temperature transformation diagram of a commercially CF epoxy prepreg determining the gelation and vitrification behavior using small amplitude oscillatory shear and thermal analysis. Mphahlele et al. (2019) studied the curing process by using differential scanning calorimetry and investigated the rheology of the system showing that a slow curing process leads to the best epoxy properties. Wu et al. (2020a) reported a study on the interfacial improvement of CFs containing epoxy composites by tuning the content of curing agent during sizing process. Authors claimed to reach a maximum interfacial shear strength increment in the best conditions (15% stoichiometric curing agent in weight) of up to 30%. Based on the deep knowledge of CFs behavior, several authors improved their epoxy compositing by playing with many parameters.

Braided CFs improved significantly the toughness of epoxy composites. Tang et al. (2001) comprehensively described the fracturing behavior of braided CF epoxy composites aiming aerospace applications though explosive impact test. As clearly shown in Fig. 4b, CFs present in the surface ablation region were sheared off and pulled out. Furthermore, a damaged region was observed under the ablation layer (Fig. 4a). Fracture morphology observed in this region revealed that the epoxy matrix area between CFs showed crack growth traces similar to a "river pattern." This morphology was related to a brittle fracture, and the direction of the river pattern was toward the direction of crack spreading. The fracture process showed that damage formation occurred by CF shearing off and epoxy flaking off under the ablation region together with the propagation of a macro-crack path along the sheaf interface under the ablation region.

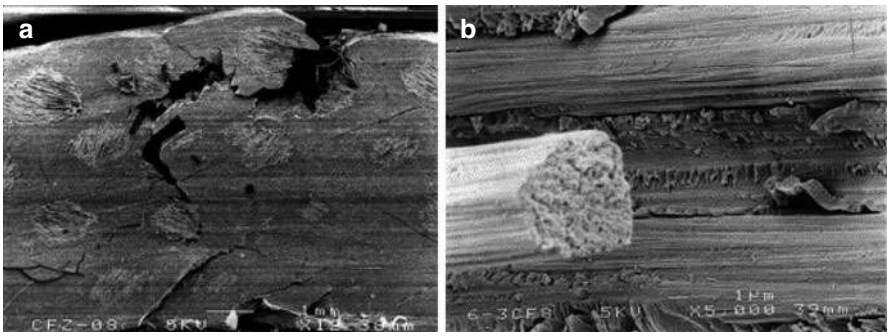

Fig. 4 Scanning electron microscopic captures of CFs composites after failing under static loading: (**a**) zigzag cracks in cross section of the specimens; (**b**) CF pullout from the epoxy matrix as reported by (Tang et al. 2001)

Khan et al. (2020) mixed CFs and GFs in different percentage enhancing the tensile strength up to ten times and the epoxy glass transition from 71 °C of up to 110 °C. Bisht et al. (2019) studied the role of 3D network of carbon nanofillers in improving the mechanical properties of CF epoxy-laminated composite. Authors tested graphene flakes, nanodiamond, and carbon nanotubes achieving an interlaminar and intralaminar mode I fracture toughness improvement of up to 260% and 5%, respectively, by using a with 1:1:2 ratio of carbonaceous fillers. Similarly, both tensile and interlaminar shear strength improved of up to 60% and 16%, respectively. This positive effect was induced by the high surface area of carbon fillers that induces an effective adhesion between matrix and CFs.

Hawal et al. (2020) proved synergetic effect of rubber on the tensile and flexural properties of graphene added CF-based epoxy composite. Authors produced CF epoxy composites containing from 0.1 wt.% to 0.3 wt.% of graphene and the same graphene-based composites with an addition of natural rubber of up to 30 wt.%. The addition of 10 wt.% of rubber improved the tensile and flexural strength of the hybrid composite of up to 20 wt.% compared with the others. Srivastava et al. (2019) coated CFs with graphene nanoplates and used them for the production of epoxy composites. Authors achieved a noticeable improvement of the flexural strength of the laminates due to the improvement of the interfacial properties of the CFs.

Sha et al. (2019) used a different approach based on the low-temperature plasma-assisted growth of vertical graphene plates on the CFs. Authors used a plasma-enhanced chemical vapor deposition operating at 400 °C. The presence of graphene nanoplates altered CF surface roughness, wettability, tensile strength, and interfacial shear strength between CFs and epoxy matrix improving the mechanical properties of CF-reinforced composites through the development of a multifunctional hierarchical structure.

Li et al. (2019) added reduced graphene oxide nanoplatelets (RGON) to CF epoxy composites for evaluating not only the mechanical properties but also the electromagnetic shielding ones. Authors used unidirectional CFs mixed with the nanofiller to produce epoxy laminate composites. The addition of reduced graphene oxide improved both the mechanical properties and electromagnetic shielding effectiveness of the composites. Although a worsening in the flexural strength occurs, the addition of reduced graphene nanoplates improves the mechanical property and EMI shielding effectiveness of the composites without sacrificing their thermal properties.

Kim et al. (2020) added graphene to highly loaded CF epoxy composites and investigated the interactions between the fillers and the matrix. They achieved a 250% improvement of the interlaminar shear strength and of 140% of the fracture toughness. This was due to the π-π interactions between graphene, CFs, and epoxy resin that induced a good filler dispersion and crack bridging.

The interaction between nanostructured carbon, CFs, and epoxy resin were deeply investigated by Wu et al. (2020b) by using polyether amine binder and graphene oxide. The first stage of the process involved the chemical bonding of amine binder on the CF surface. Afterward, polar residues of tailoring agent interact though hydrogen bonding and dipole interactions with graphene oxide. These interactions lead to an increment of interfacial shear strength by using covalent-

bonded CFs of up to 48%, while the ionic interacting ones showed a total improvement of 38%. The mixed interactions dramatically decreased the properties of the material due to an ineffective interfacial modification of CFs.

Wu et al. (2020c) added not only graphene oxide but also nanozirconia to CF-based epoxy composites. Authors achieved an improvement of interfacial shear strength up to 42% due to a more effective cracks deflection and energy dissipation due to an interfacial synergetic interactions of hydrogen bonding and π-π stacking.,

The simultaneous addition of nanosilica and the tailoring of epoxy matrix with silicon rubber were studied by Li and co-workers (2020). Authors claimed an increment in the tensile strength of epoxy composites by using a 5 wt. % of nanosilica of up to 49% and a tensile strength improvement of up to 17%. This was due to the combined ability of nanosilica and silicon rubber cooperating to transfer the stress from epoxy matrix to CFs.

Carbon nanotubes were also largely used for the CF epoxy resin improvement as reported for example by Park and Park (2020). Authors modified single-walled carbon nanotubes by oxidizing their surface using an ozone treatment on the surface properties. The surface-modified carbon nanotubes improved the interlaminar shear strength and fracture toughness up to 80% and 55%, respectively.

Yao et al. (2020) directly grow carbon nanotubes on CFs prior of the realization of composites by chemical vapor deposition technique. Authors improved interlaminar shear strength of up to 24% showing that the fracture surface morphology of the composites and the relative hardness modulus distribution at the interface was closely correlated with morphology of carbon nanotubes.

The carbon nanotube improvement was also investigated by simulation approach Reddy and Ramji (2020) using 3D finite element model achieving result in good agreement with experimental data.

The interfacial properties are a capital issue in CF epoxy-based materials, and plenty of materials have been used such as carboxymethyl cellulose, polymeric films, amphiphilic molecules, and hybrid formulations.

Modification of interfacial interaction between CFs and epoxy matrix drives the fracture process of CFs composites. As reported by Muralidhara et al. (2020), CF architecture marginally affected the mechanical properties of related epoxy composites. Substantial differences were not observed by using T700 or T800 CFs.

Cheng et al. (2020) produced uniformly aligned polyethersulfone CFs simultaneously improving mode I and mode II fracture toughness. Data reported showed that polyethersulfone filaments were not dissolvable at the temperature of the resin infusion process but only during the curing process. Authors achieved an enhancement of up to 120% and 69% on mode I and II fracture toughness, respectively. The fracture surface analysis enlightens that the interlaminar fracture toughness improvement was due to the interlaminar structures induced from the phase separation of polyethersulfone in epoxy resin. Additionally, authors observed an increment of the interlaminar shear strength and compression after impact of 18 and 43%, respectively, together with a limited enhancement of both tensile and flexural strength.

Wang et al. (2020) investigated the effect of nylon microparticles on mode I interlaminar fracture toughness of CF epoxy composites using both nylon 6 and 12. As clearly emerged from experimental data, the particle size is the driving force that regulates the toughness but only when the filler/epoxy matrix interfacial bonding is strong enough after the curing step. A good interfacial interaction allows the nylon particles to be plastically deformed while bridging the crack. Similarly, Quan et al. (2020) observed an analogue behavior studying mode II fractures in of aerospace-grade CFs containing epoxy using polyethylene terephthalate, polyphenylene sulfide, and polyamide-12.

The addition of polymeric additives could also improve the impact resistance as proved by using polyurethane and silane sized as additives. As proved by Salifu and co-workers (2020), CF-based epoxy resin could compete with aluminum 3105-H18 performances in high-velocity impact response.

Zhang et al. (2020) found a correlation between the CF plane orientation and the dynamic impact loading behavior of related composites, showing that failure mode is ductile-type one under higher strain rates. Marangonni et al. (2020) studied the fatigue behavior of woven CFs showing the huge influence on the damage mechanisms and the fatigue life of waviness. This morphological feature deeply affected tension/compression and compression/compression loadings and only in less appreciable way the stiffness loss.

Hendlmeier et al. (2019) studied the conductivity, current density, and sizings applied to CFs during manufacture and the related effect on the epoxy matrix adhesion. Authors explored the parameters for a large set of industrial CFs with an electrochemical oxidation treatment using ammonium hydrogen carbonate as electrolyte a conductivity value of the electrolytic medium varied between 8 and 24 μS/cm, while current density ranged between 0.5 and 1.5 A/m^2. Afterward, CFs were included into epoxy matrix, and interphase properties were evaluated showing that oxidation degree did affect appreciably the electrochemical parameters, but the typology of residual functionalities induced an enhancement of interfacial properties.

Hiremath et al. (2020) used low-cost textile-grade CFs for the production of effective epoxy composites for the automotive sector. Ming et al. (2020) developed a self-heating 3D-printed continuous CFs containing epoxy mesh for wind turbine deicing application. Authors achieved the conductivity of up to 131 S/cm at 25 °C that reached 148 S/cm at 200 °C. Additionally, mesh reinforcement reduced the deicing time by 85%.

CF-based epoxy composites undergo an aging process. Behera et al. (2020) evaluated the hygrothermal aging effect on both physical and mechanical properties of CF epoxy material at high temperature and humidity. Authors immersed the laminates into water at 70 °C for more than 6 months. Afterward, author observed that the moisture absorption follows a two-stage model where diffusion rate increased proportional to square root of immersion time followed by step of slowing down close to the saturation, a sluggish phase up to saturation. Aged materials mechanically failed due to the worsening of the bonding interaction between filler and matrix. A reduction of aging effect could be observed by adding an additive such graphene nanoplates or graphene aerogel as reported by Chiang et al. (2020).

The increment of CFs use together with their aging has promoted several approaches to recycled CF-based epoxy composites under the principles of the circular economy (Naqvi et al. 2018). Accordingly several studies tried to exploit the full potential of recycled CF epoxy materials as filler for construction building or after the degradation of polymer matrix as filler for the production of new composites.

Glass Fiber Epoxy Composites

GF epoxy-based composites are widely used in plenty of applications ranging from naval to aeronautic industries, insulation materials, and lightweight components production. Joshi et al. (2004) compared GFs with natural fibers production and applications showing that their log working life abundantly counterbalances the poor environmentally friendliness of their production.

The research work of Yang et al. (2000) enlighten some key issues in the failure process of GFs containing epoxy composites by using IITRI method (Bogetti et al. 1988). As shown in Fig. 5a, compressive loading resulted in the formation of a shear band during IITRI compression failure of the 0/90° non-crimp laminate. There was no relative displacement of the fibers across the failure and post-failure examination showed that the fracture band was oriented at 45° to the loading direction.

In Fig. 5b, IITRI compression failure in the plain weave fabric composite showed the appearance of interlaminar stresses due to local delamination together with a reduction of the local transverse support for the GFs and an overload in adjacent region of low waviness. In this case, a global microbuckling took place, and delamination and global buckling could be ascribed to a bending failure due to interlaminar stresses failing leading to relatively low compressive strength.

Dense stitching GFs showed a different failure mode as shown in Fig. 5c. A typical failure mechanism for the densely stitched biaxial woven composite was observed with localized failure in the form of a kink band close to the crack initiation.

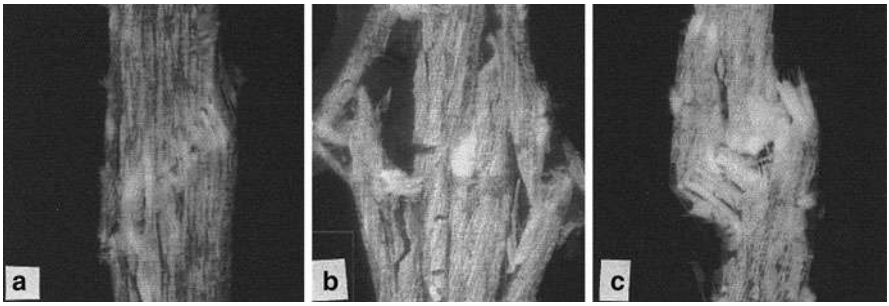

Fig. 5 Compressive failure in: (**a**) non-crimp laminate composite; (**b**) unstitched woven composite; and (**c**) biaxial stitched (stitching lines 5 mm apart) woven composite as reported by Yang et al. (2000)

Anjaneyulu et al. (2020) studied the mechanical behavior of GFs E epoxy composite laminates according to ASTM standards. Authors showed the linear relationship between the composites strength of composite and the GFs/matrix volume fractions. Furthermore, GF orientation dramatically contributes to the tensile strength of epoxy composite. A more exhaustive study on the relation between GF volume fraction and composite properties was reported by Swapnil et al. (2017). Authors investigated a GF volume fraction of 40 v/v%, 50 v/v%, and 60 v/v% in the total composition showing that the magnification of mechanical properties occurred for a volume fraction close to 50 v/v%. Minty et al. (2018) evaluated the relevance of the hardener/epoxy precursor ratio on the interfacial strength GF-based composites. The interfacial shear strength, glass transition temperature, storage modulus, and linear coefficient of thermal expansion were strongly related to the hardener/epoxy component ratio. Authors hypothesized that residual radial compressive interfacial stresses were influenced by the chemical bond network formed during the curing process. Similarly, Chakraverty et al. (2020) tested the thermomechanical response of GFs E epoxy composites after a plasma treatment of GFs. Authors reported an improvement of the interlaminar shear strength due to the improvement of curing process after the surface treatment. A different approach was for the first time described by Sangermano et al. (2018). Authors reported the UV-crosslinking of aGF-reinforced epoxy composites. Authors established a radical induced cationic frontal polymerization with a very fast kinetic that preserved the good thermomechanical properties. Another modification to the GF composites was reported by Sheinbaum et al. (2019) that used a brominated epoxy derivatives. The addition of brominated material to a non-brominated matrix induced an increment in glass transition temperature, toughness, strength, and elongation. Authors hypothesized an energy dissipating mechanism based on rough fracture surfaces, due to high interfacial bonding between the epoxy matrix and GFs.

GFs/epoxy composites interfacial properties can be easily tailored by adding an additive to the epoxy resin as in the case of CFs. One of the most used additive class is represented by graphene and related materials. Ojha et al. (2019) added graphene nanoplatelets to pultruded epoxy composites. Authors used unidirectional GFs pultruded by pulling the continuous GFs through the graphene containing epoxy resin. Authors observed an increment in ultimate tensile strength and the longitudinal modulus of up to 12% and 7%, respectively, by adding 0.1 wt.% graphene nanoplatelets. Prusty et al. (2017) extensively studied the effect of graphene oxide loafing on GF epoxy composites. Authors reported that the addition of graphene oxide up to 0.5 wt.% induced a flexural strength improvement of up to 21%. This was due to the interface interactions between graphene oxide/GFs/epoxy matrix that altered the viscoelastic properties of the composites and failure mechanisms. About failure mechanisms and creep propagation, Ghosh et al. (2018) published a very interesting computational study based on the use of time-temperature superposition principle to study the multilayered graphene GF epoxy composites. Flexural tests running in a temperature range from −196 °C up to 110 °C showed that the best flexural performances could be achieved by using 0.1 wt.% graphene oxide. The computational approach evaluated in billions of year the time required for the

naturally formation of cracks in the composites at 30 °C. Domun et al. (2019) proved that GF epoxy matrix mixed with graphene nanoplates could resist to ballistic impact in a more effective way than common GF epoxy composites dissipating up to 17% more energy.

Jena et al. (2020) added together multilayer graphene and nanosilica with a ratio close to 2 to GF epoxy composites inducing an enhancement in flexural strength. Hua et al. (2017) combined graphene oxide with carbon nanotubes increasing the transverse tensile strength of GF epoxy materials more than neat graphene oxide or carbon nanotubes addition. Anand et al. (2019) studied the effect of neat and oxidized carbon nanotubes on creep propagation of laminated GF epoxy materials in a temperature range from 50 °C to 110 °C. Authors clearly demonstrated the positive effect of surface-modified carbon nanotubes. Similarly, Gaurav and Singh (2018) improved interlaminar strength of up to 41% GF epoxy composites by adding carbon nanotubes modified by using arc discharged techniques.

The good dispersion of carbon nanotube is another key issue for the realization of improved GF epoxy materials. Ismail et al. (2020) evaluated this effect by using carbon nanotubes dispersed into watery media with different surfactants. Well-dispersed carbon nanotubes could be used to detect the defects inside the GF epoxy materials as demonstrated by the study of Slobodian et al. (2018). Authors use a carbon nanotubes buckypaper embedded in a polyurethane membrane to induce strain self-sensing property. This integrated sensor allowed a monitoring process due to the formation of micro-sized cracks pattern that altered its conductivity. The addition of carbon nanotubes to GF epoxy materials improved also the microwave shield effect.

Carbon nanotubes could be combined with inorganic fillers such as nanoclays as reported by Sen et al. (2020). Authors improved the flexural modulus of up to 12% by using a carbon nanotube/nanoclay ratio of 0.1 compared with GF composites containing only the same amount of carbon nanotubes. Bozkurt et al. (2019) used nanoclay up to 3 wt.% to improve GFs S epoxy composite buckling loads, both axial and lateral, achieving an improvement of up to 9%. The improvement of flexural properties could magnified by using nanoclay and nanosilica simultaneously with a ratio of 2 and a total loading of 3 wt.% as reported by Nayak et al. (2020). These materials showed a good improvement of flexural strength but a decrement of glass transition.

Kumar et al. (2020) combined GF epoxy materials with cellulose nanocrystals increasing the storage modulus of up to 56%, the flexural modulus of up to 50%, the flexural strength 55%, the tensile modulus of up to14%, and the tensile strength of up to 24%. These improvements were due to the strengthening of the interface interactions between GFs and epoxy matrix mediated by the presence of cellulose nanocrystals.

Plenty of nanofillers could be added to improve the interfacial interaction between epoxy resin and GFs such as fly ash, alumina, barium titanate nanoparticles, seashell maize, zinc oxide, carbon black, and polymers.

Other studies have proved that the addition to epoxy matrix of compounds such as 2-methylimidazole or encapsulated urea-formaldehyde formulation could lead to GF

epoxy composites with self-healing properties. Similar results could be achieved by treating the GF fibers using silane and silane derivatives.

Silane treatment could also be used to improve the interlaminar shear strength of GF composites as proved by Arun Prakash and Rajadurai (2017). Authors treated GFs E with a silane derivative, teh3-aminopropyletrimethoxysilane. Surface treatment induced interlaminar shear strength improvement of up to 155 MPa by using a 20 v/v% of GFs E.

The overall tuning of interfacial properties is aiming to improve the durability of the GF epoxy materials. Mohamed et al. (2019) evaluate the bending fatigue behavior of GF epoxy composites correlating the properties of GFs with the outcomes.

GF composite aging was studied under different conditions. Ahankari and Patil (2020) evaluate the accelerated aging effect of seawater on GF epoxy coating used to insulate steel pipes. Authors reported a reduction of 43% of strength and 15% modulus after 40 days of immersion at 80 °C in seawater proving that tough conditions could dramatically reduce the GF composite performances.

Similarly, Fitriah et al. (2017) studied the compressive behavior during hydrothermal aging of GF epoxy composite pipes from 60 °C to 80 °C for up to 1500 h. Results showed that the mechanical properties of the composites decreased with the increment of aging temperature.

As for CFs, GF epoxy composites could be recycled through thermochemical process. As reported by Hiremath et al. (2020), recovered CFs are not up to mark compared with neat GFs. Accordingly, the authors proposed the addition of carbon nanotubes to the matrix to improve the mechanical properties of related composites.

Polymer-Based Fiber Epoxy Composites

Polyamides are the most diffuse PBFs due to the facile production and good mechanical properties of commercial materials such as nylon-type ones. Polyamide-based epoxy composites have been deeply investigated for a wide range of application with a specific focus on compounds based on aromatic amines. In fact the ones containing aromatics amines are the most widespread due to high flame resistance and superior mechanical properties.

Aromatic poly(amide) fibers take the generic name of aramid. The most known aramids are Kevlar™, Nomex™, and Twaron™, and they are used for production of bullet shield textiles. Generally, aramid fibers are relatively light with a density close to 1.4 g/cm3, stiff with a Young's modulus up to 190 GPa, and strong with tensile strength reaching of up to 3.6 GPa. Additionally, aramid fibers showed good resistance to both impact and abrasion damage.

As for textiles, the main application of aramid containing epoxy composites is represented by the antiballistic use as reported by Braga et al. (2018). Authors tested an aramid-based epoxy multilayered armor by using high-energy bullet 7.62 mm. The shielding material was realized by using several layers of epoxy composites and ceramic and compared with neat ceramic and neat army grade aramid (Kevlar®).

Results clearly showed that epoxy composites met the requirements with comparable ballistic performance as the neat materials with a saving of up to 14% on the final cost-price. These good results were achieved by the unique stress absorption and subsequent deformation of the epoxy composite. As reported by Komai et al. (2002), this is a crucial point. Authors studied the stress waveform and water absorption on the tension-tension fatigue fracture behavior on ±45° angle-ply laminates of aramid fiber-based epoxy composite. Experiments run on dry samples showed a higher fatigue strength under negative pulse waveform than that under the positive pulse one. Fiber rotations on the longitudinal direction were evident by creep deformation caused by the cyclic loading superimposed on the maximum stress hold time inducing a decrement of the compliance and a simultaneous increment of the fatigue life under the negative pulse waveform. Authors observed a marked decrease of aramid/epoxy resin interfacial strength due to water impregnation that caused the swelling of the matrix with a decrement of the static tensile and fatigue strength. Moisture is not the only agent that could compromise the integrity of aramid-based epoxy composites. Xu et al. (2018) reported the damaging process of aramid composites by microwave irradiation. Authors used energy density ranging from 5.36 W/cm^2 to 16.09 W/cm^2 with exposure times from 2 min to 10 min studying several parameters such as equilibrium temperature, power thresholds, and damage morphologies of quasi-isotropic laminates and unidirectional composites. Results reported clearly proved that quasi-isotropic laminates displayed a greater shielding to microwaves compared to unidirectional composites with same thickness. Furthermore, the quasi-isotropic materials showed a fast temperature increment with circular damaged regions in the region of maximum microwaves irradiation.

Laminate aramid-based epoxy composites mechanical features could be improved by adding nanofillers into the epoxy matrix as mentioned above for both GFs and CFs. A more detailed study on aramid interaction with epoxy resin was reported by Qi et al. (2017). Authors evaluated the interaction between fibers and matrix by a model that took simultaneously into account the aramid skin and the core structure. Authors collected also an experimental set of data that showed the splitting of aramid fibers above the fracture surfaces. The fiber fracture was caused by tensile splitting, which was a typical fracture characteristic of the aramid fibers independently from the loading conditions. By combining the empirical data with the model, authors proved that the failure mechanism was due to an extensive interfacial failure coupled with some skin fibrils detached from the bulk aramid fiber.

Accordingly to the relevance of interfacial interaction with epoxy resin, aramid fibers were modified in order to appropriately tailor the fiber surface. Liu et al. (2008) modified aramid fibers by using ultrasonic treatment. Ultracavitation oxidized the aromatic moieties of aramid fibers promoting the creation of a solid network of hydrogen bonds in the composites. These additional interactions greatly improved the interlaminar resistance.

Similarly, Fan et al. (2018) functionalized the fibers surface by plasma treatment. The low-temperature plasma treatment on interfacial adhesion of aramid fiber type III-reinforced epoxy composites was studied and optimized through statistical analysis by using orthogonal experiments. After plasma treatment, authors observed

improved interfacial shear strength together with single-filament tensile stress decrement through single-fiber composite fragmentation tests. Authors reported that the observed behavior was mainly due to (i) rise in Van der Waals interactions due to increased surface area of post-treated fibers, (ii) mechanical interlocking of the rough fibers surface with the epoxy matrix, (iii) improved fibers surface wettability, and (iv) chemical bonding between oxygen-containing groups on the functionalized aramid and epoxy matrix.

Subsequently, the interfacial shear strength of aramid-based epoxy composites increased of up to 38.1% was compared with untreated based composite, reaching the value of 30.44 MPa together with a decrement of the tensile strength of up to 5.8%. These results were achieved by using a treatment power of 67.5 W for 11 min and a pressure of 2500 Pa.

The chemical modification of aramid was also performed through a multistep process as reported by Cheng et al. (2016). Firstly, a direct fluorination was used to generate aromatic C-F single bond on aromatic moieties by using fluorine at 100 °C. Afterward, a nucleophilic substitution reaction between the C-F and 3-aminopropyltriethoxysilane was induced to insert a silicon-based residue on the surface of aramid. Then, ethoxy residue were hydrolyzed directly on silicon producing a silicon-tailored aramid fibers used for the realization of epoxy composites. Through this procedure the interfacial wettability of resin to fiber was modified due to a surface energy increment of up to 25.01mN/m. This leads to an increment of interfacial shear strength up to 46.7%.

Xing et al. (2016) grafted aramid fibers in diethanolamine and epichlorohydrin promoting the formation of epoxy moieties directly bonded to aramid. Accordingly, authors observed that those sites acted as polymerization starter during epoxy resin curing. As a direct consequence of epoxylation, the resulting aramid-based epoxy composites showed an increase of both interlaminar shear strength and flexural strength of composites up to 511 MPa and 479 MPa, respectively.

Nonaromatic polyamine fibers were used by Meshram and co-workers (2018) to test the effect of combination between nylon 6,6 and epoxy resin. Authors prepared the nylon-based composites by using a simple hand layup technique that consists in the application of the epoxy resin on nylon fibers by using a handroller. The tensile test showed a remarkable effect of nylon fibers that induced an improvement of ultimate tensile strength from 266 N to 1311, of Young's modulus from 3 MPa to 763 MPa, and of yield stress from 4 MPa to 19 MPa. Simultaneously, authors observed a drastically decrement of maximum elongation from 1.2% to 0.5%.

Palazzetti et al. (2012) investigated the effect of electrospun nylon 6,6 fibers on mode I and the mode II fracture mechanics of modified epoxy laminates. Authors produced specimens composed of 20 plies of woven carbon fibers/epoxy resin prepregs and inserted nylon fiber mat in the midplane of beam-shaped specimens. Results clearly showed that nylon fibers (i) reduced maximum opening load that can be supported by stressed interface and (ii) increased the absorbable mechanical energy during the overall test. Nonetheless, the presence of nylon fibers did not affect the flexural modulus but enhanced the maximum value of the force that was required to initiate the longitudinal crack propagation. Furthermore, the presence of

nylon fibers induced a higher absorption of mechanical energy during interlaminar crack propagation. Considering the overall data set, authors concluded that the poly (amides) fibers enhanced composite delamination strength and damage tolerance due to a reduced damage progression sensitivity under mode I and mode II of fracture.

Moving on another class of polymers, polyesters were also considered as fibrous matrix for epoxy-based composites. Among them poly(ethylene terephthalate) is one of the most used due to the good mechanical and chemical properties. Teh et al. (2005) reported a very comprehensive study about the poly(ethylene terephthalate) fibers to toughen an intrinsically brittle epoxy resin with high glass transition temperature. Authors achieved a strong fiber/epoxy matrix adhesion by tailoring poly(ethylene terephthalate) fibers surface though a treatment with NaOH. Compared with neat epoxy resin, the fracture toughness of poly(ethylene terephthalate) fiber-based epoxy composites is almost doubled by using a fibers loading of only 1 wt.%. As shown in Fig. 6, the tailored poly(ethylene terephthalate) fibers presented a very high adhesion to the epoxy matrix without any appreciable debonding or delamination phenomena.

The last class of PBFs extensively used as fibrous component of epoxy composites is represented by polyolefin fibers.

Demir et al. (2014) produced a composite mixing epoxy resin with electrospinned poly(styrene) fibers. The quasi-static and high strain rate compression stress vs strain curves of poly(styrene) fiber-reinforced and neat epoxy resin showed the increment of both the elastic modulus and compression strength of the epoxy matrix after fiber addition. The increment of compressive strength of the poly(styrene) fiber-based epoxy composites at high strain rate was the main feature of the strain rate-sensitive compressive strength of the epoxy matrix. Conversely, the increment of strength at the quasi-static strain rate was mainly due to poly(styrene) fiber addition. The fracture surface of the specimens showed debonded fibers and a relatively flat fracture areas of the epoxy matrix with an evident strong interlocking on the

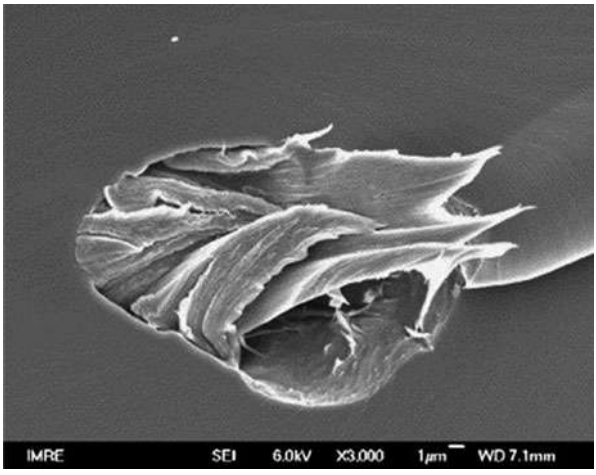

Fig. 6 Scanning electron microscopic capture of poly (ethylene terephthalate) embedded into a brittle epoxy matric as reported by Teh et al. (2005)

nanometer scale between the poly(styrene) fibers and the epoxy matrix. This was due to intrusions in the porosities on the fibers surface that led to an improvement of the load transfer from matrix to fibers.

Conclusions and Perspective on Carbon and Glass Fiber Epoxy Composites

In this chapter, we established some key point that can be used to better navigate the huge field of synthetic fibers composites reign:

(i) The interphase between CFs/GFs and epoxy matrix plays a crucial role in the production of tough long-life composites.
(ii) Addition of nanofiller reduces the intrinsic brittleness of fiber-based composites.
(iii) Surface tailoring of synthetic fibers promotes an improved interaction with the epoxy resin.

These points represent both the starting point and the final aim of the overall CF and GF research in the field of material sciences.

PBFs represent the other face of synthetic fiber-based composites. Even if PBF performances cannot reach CF- and GF-based materials properties, their affordability represents an unneglectable advance to spread their use in large markets around the world.

Furthermore, we believe that the future of the synthetic fibers will necessarily be encompassed in circular economy with an improved attention for the environmental impact of all production steps: from raw materials to productive plants and from ready to sell materials to end-of-life disposal.

References

S. Ahankari, A. Patil, Sea water effect on mechanical performance of steel pipes rehabilitated with glass fiber reinforced epoxy composites. Mater. Today: Proc. **22**, 2490–2498 (2020)

A. Anand, P. Banerjee, D. Sahoo, D.K. Rathore, R.K. Prusty, B.C. Ray, Effects of temperature and load on the creep performance of CNT reinforced laminated glass fiber/epoxy composites. Int. J. Mech. Sci. **150**, 539–547 (2019)

J. Anjaneyulu, M. Moizuddin, P. Chandra Kumar, Evaluation of mechanical behaviour of glass fibre-epoxy composite laminates. Mater. Today: Proc. **22**, 2899–2905 (2020)

V.R. Arun Prakash, A. Rajadurai, Inter laminar shear strength behavior of acid, base and silane treated E-glass fibre epoxy resin composites on drilling process. Defence Technol. **13**, 40–46 (2017)

A. Behera, M.M. Thawre, A. Ballal, Hygrothermal aging effect on physical and mechanical properties of carbon fiber/epoxy cross-ply composite laminate. Mater. Today: Proc. **28**, 940–943 (2020)

A. Bisht, K. Dasgupta, D. Lahiri, Investigating the role of 3D network of carbon nanofillers in improving the mechanical properties of carbon fiber epoxy laminated composite. Compos. A: Appl. Sci. Manuf. **126**, 105601 (2019)
T.A. Bogetti, J.W. Gillespie Jr., R.B. Pipes, Evaluation of the IITRI compression test method for stiffness and strength determination. Compos. Sci. Technol. **32**, 57–76 (1988)
Ö.Y. Bozkurt, M. Bulut, A. Erkliğ, W.A. Faydh, Axial and lateral buckling analysis of fiber reinforced S-glass/epoxy composites containing nano-clay particles. Compos. Part B **158**, 82–91 (2019)
A.P. Chakraverty, D. Parida, S. Dash, M. Parida, S. Beura, U.K. Mohanty, Thermo-mechanical response of post-plasma irradiated E-glass fibre/epoxy composite. Mater. Today: Proc. (2020)
Z. Cheng, B. Li, J. Huang, T. Chen, Y. Liu, X. Wang, X. Liu, Covalent modification of Aramid fibers' surface via direct fluorination to enhance composite interfacial properties. Mater. Des. **106**, 216–225 (2016)
C. Cheng, Z. Chen, Z. Huang, C. Zhang, R. Tusiime, J. Zhou, Z. Sun, Y. Liu, M. Yu, H. Zhang, Simultaneously improving mode I and mode II fracture toughness of the carbon fiber/epoxy composite laminates via interleaved with uniformly aligned PES fiber webs. Compos. A: Appl. Sci. Manuf. **129**, 105696 (2020)
C.-L. Chiang, H.-Y. Chou, M.-Y. Shen, Effect of environmental aging on mechanical properties of graphene nanoplatelet/nanocarbon aerogel hybrid-reinforced epoxy/carbon fiber composite laminates. Compos. A: Appl. Sci. Manuf. **130**, 105718 (2020)
M.M. Demir, N. Horzum, A. Taşdemirci, K. Turan, M. Güden, Mechanical interlocking between porous electrospun polystyrene fibers and an epoxy matrix. ACS Appl. Mater. Interfaces **6**, 21901–21905 (2014)
X. Di, Y. Gao, C. Bao, Y. Hu, Z.g. Xie, Optimization of glass fiber based core materials for vacuum insulation panels with laminated aluminum foils as envelopes. Vacuum **97**, 55–59 (2013)
N. Domun, C. Kaboglu, K.R. Paton, J.P. Dear, J. Liu, B.R.K. Blackman, G. Liaghat, H. Hadavinia, Ballistic impact behaviour of glass fibre reinforced polymer composite with 1D/2D nano-modified epoxy matrices. Compos. Part B **167**, 497–506 (2019)
M. Dunham, D. Edie, Model of stabilization for pan-based carbon fiber precursor bundles. Carbon **30**, 435–450 (1992)
F.d.O. Braga, T.L. Milanezi, S.N. Monteiro, L.H.L. Louro, A.V. Gomes, É.P. Lima, Ballistic comparison between epoxy-ramie and epoxy-aramid composites in multilayered armor systems. J. Mater. Res. Technol. **7**, 541–549 (2018)
W. Fan, H. Tian, H. Wang, T. Zhang, X. Yang, Y. Yu, X. Meng, X. Yu, L. Yuan, B. Xu, S. Wang, Enhanced interfacial adhesion of aramid fiber III reinforced epoxy composites via low temperature plasma treatment. Polym. Test. **72**, 147–156 (2018)
S.N. Fitriah, M.S. Abdul Majid, M.J.M. Ridzuan, R. Daud, A.G. Gibson, T.A. Assaleh, Influence of hydrothermal ageing on the compressive behaviour of glass fibre/epoxy composite pipes. Compos. Struct. **159**, 350–360 (2017)
A. Gaurav, K.K. Singh, Ilss improvement of quasi-isotropic glass fiber reinforced epoxy laminate enhanced with arc discharged multi-walled carbon nanotubes. Mater. Today: Proc. **5**, 8638–8644 (2018)
S.K. Ghosh, P. Rajesh, B. Srikavya, D.K. Rathore, R.K. Prusty, B.C. Ray, Creep behaviour prediction of multi-layer graphene embedded glass fiber/epoxy composites using time-temperature superposition principle. Compos. A: Appl. Sci. Manuf. **107**, 507–518 (2018)
T.T. Hawal, M.S. Patil, R.M. Kulkarni, S.N. Nandurkar, Synergetic effect of rubber on the tensile and flexural properties of graphene based epoxy-carbon fiber hybrid nanocomposite. Mater. Today: Proc. **27**, 515–518 (2020)
A. Hendlmeier, F. Stojcevski, R. Alexander, S. Gupta, L.C. Henderson, Examining conductivity, current density, and sizings applied to carbon fibers during manufacture and their effect on fiber-to-matrix adhesion in epoxy polymers. Compos. Part B **179**, 107494 (2019)
M.M. Hiremath, B.N.V.S. Ganesh Gupta K, R.K. Prusty, B.C. Ray, Mechanical and thermal performance of recycled glass fiber reinforced epoxy composites embedded with carbon nanotubes. Mater. Today: Proc. **33**, 5029–5034 (2020)

Y. Hua, F. Li, Y. Liu, G.-W. Huang, H.-M. Xiao, Y.-Q. Li, N. Hu, S.-Y. Fu, Positive synergistic effect of graphene oxide/carbon nanotube hybrid coating on glass fiber/epoxy interfacial normal bond strength. Compos. Sci. Technol. **149**, 294–304 (2017)

N.H. Ismail, J.O. Akindoyo, M. Mariatti, Solvent mediated dispersion of carbon nanotubes for glass fibre surface modification – Suspensions stability and its effects on mechanical, interlaminar and dynamic mechanical properties of modified glass fibre reinforced epoxy laminates. Compos. A: Appl. Sci. Manuf. **139**, 106091 (2020)

A. Jena, R.K. Shubham, B.C.R. Prusty, Mechanical and thermal behaviour of multi-layer graphene and nanosilica reinforced glass fiber/epoxy composites. Mater. Today: Proc. (2020)

S.V. Joshi, L.T. Drzal, A.K. Mohanty, S. Arora, Are natural fiber composites environmentally superior to glass fiber reinforced composites? Compos. A: Appl. Sci. Manuf. **35**, 371–376 (2004)

J. Kadla, S. Kubo, R. Venditti, R. Gilbert, A. Compere, W. Griffith, Lignin-based carbon fibers for composite fiber applications. Carbon **40**, 2913–2920 (2002)

Z.I. Khan, A. Arsad, Z. Mohamad, U. Habib, M.A.A. Zaini, Comparative study on the enhancement of thermo-mechanical properties of carbon fiber and glass fiber reinforced epoxy composites. Mater. Today: Proc. **39**, 956–958 (2020)

J. Kim, J. Cha, B. Chung, S. Ryu, S.H. Hong, Fabrication and mechanical properties of carbon fiber/epoxy nanocomposites containing high loadings of noncovalently functionalized graphene nanoplatelets. Compos. Sci. Technol. **192**, 108101 (2020)

K. Komai, K. Minoshima, K. Tanaka, T. Tokura, Effects of stress waveform and water absorption on the fatigue strength of angle-ply aramid fiber/epoxy composites. Int. J. Fatigue **24**, 339–348 (2002)

S. Kubo, J. Kadla, Lignin-based carbon fibers: Effect of synthetic polymer blending on fiber properties. J. Polym. Environ. **13**, 97–105 (2005)

S. Kumar, B.G. Falzon, J. Kun, E. Wilson, G. Graninger, S.C. Hawkins, High performance multiscale glass fibre epoxy composites integrated with cellulose nanocrystals for advanced structural applications. Compos. A: Appl. Sci. Manuf. **131**, 105801 (2020)

Y. Li, S.-t. Liu, J.-m. Sun, S. Li, J.-l. Chen, Y. Zhao, Effects of the oxygen content of reduced graphene oxide on the mechanical and electromagnetic interference shielding properties of carbon fiber/reduced graphene oxide-epoxy composites. New Carbon Mater. **34**, 489–498 (2019)

S. Li, D. Chen, C. Gao, Y. Yuan, H. Wang, X. Liu, B. Hu, J. Ma, M. Liu, Z. Wu, Epoxy-functionalized polysiloxane/Nano-SiO_2 synergistic reinforcement in cryogenic mechanical properties of epoxy and carbon fiber reinforced epoxy laminate. Compos. Sci. Technol. **198**, 108292 (2020)

L. Liu, Y.D. Huang, Z.Q. Zhang, Z.X. Jiang, L.N. Wu, Ultrasonic treatment of aramid fiber surface and its effect on the interface of aramid/epoxy composites. Appl. Surf. Sci. **254**, 2594–2599 (2008)

L. Maragoni, G. Modenato, N. De Rossi, L. Vescovi, M. Quaresimin, Effect of fibre waviness on the compressive fatigue behavior of woven carbon/epoxy laminates. Compos. Part B **199**, 108282 (2020)

P. Meshram, S. Sahu, M. Zahid Ansari, S. Mukherjee, Study on mechanical properties of epoxy and nylon/epoxy composite. Mater. Today: Proc. **5**, 5925–5932 (2018)

J. Mikkilä, M. Trogen, K.A. Koivu, J. Kontro, J. Kuuskeri, R. Maltari, Z. Dekere, M. Kemell, M.R. Mäkelä, P.A. Nousiainen, Fungal treatment modifies kraft lignin for lignin-and cellulose-based carbon fiber precursors. ACS Omega **5**, 6130–6140 (2020)

Y. Ming, Y. Duan, S. Zhang, Y. Zhu, B. Wang, Self-heating 3D printed continuous carbon fiber/epoxy mesh and its application in wind turbine deicing. Polym. Test. **82**, 106309 (2020)

R.F. Minty, L. Yang, J.L. Thomason, The influence of hardener-to-epoxy ratio on the interfacial strength in glass fibre reinforced epoxy composites. Compos. A: Appl. Sci. Manuf. **112**, 64–70 (2018)

Y.S. Mohamed, H.A. El-Gamal, M.N. Abouelwafa, W.A. Al-Tabey, Static and fatigue characterizations of fiber glass/epoxy tubes exposed to internal pressure and/or bending moment. Alex. Eng. J. **58**, 1247–1256 (2019)

K. Mphahlele, S.S. Ray, A. Kolesnikov, Cure kinetics, morphology development, and rheology of a high-performance carbon-fiber-reinforced epoxy composite. Compos. Part B **176**, 107300 (2019)
B. Muralidhara, S.P. Kumaresh Babu, B. Suresha, The effect of fiber architecture on the mechanical properties of carbon/epoxy composites. Mater. Today: Proc. **22**, 1755–1764 (2020)
S. Naqvi, H.M. Prabhakara, E. Bramer, W. Dierkes, R. Akkerman, G. Brem, A critical review on recycling of end-of-life carbon fibre/glass fibre reinforced composites waste using pyrolysis towards a circular economy. Resour. Conserv. Recycl. **136**, 118–129 (2018)
B.A. Nayak, R.K. Shubham, B.C.R. Prusty, Effect of nanosilica and nanoclay reinforcement on flexural and thermal properties of glass fiber/epoxy composites. Mater. Today: Proc. (2020)
B.A. Newcomb, Time-temperature-transformation (TTT) diagram of a carbon fiber epoxy prepreg. Polym. Test. **77**, 105859 (2019)
M. Ojha, P.K. Penumakala, G.V. Marrivada, P.K. Chaganti, A.K. Gupta, Processing of glass fiber pultruded composites using graphene nanoplatelets modified epoxy matrix. Mater. Today: Proc. **18**, 3298–3304 (2019)
R. Palazzetti, A. Zucchelli, C. Gualandi, M.L. Focarete, L. Donati, G. Minak, S. Ramakrishna, Influence of electrospun Nylon 6,6 nanofibrous mats on the interlaminar properties of Gr–epoxy composite laminates. Compos. Struct. **94**, 571–579 (2012)
S.-J. Park, S.-J. Park, Effect of ozone-treated single-walled carbon nanotubes on interfacial properties and fracture toughness of carbon fiber-reinforced epoxy composites. Compos. A: Appl. Sci. Manuf. **137**, 105937 (2020)
R.K. Prusty, S.K. Ghosh, D.K. Rathore, B.C. Ray, Reinforcement effect of graphene oxide in glass fibre/epoxy composites at in-situ elevated temperature environments: An emphasis on graphene oxide content. Compos. A: Appl. Sci. Manuf. **95**, 40–53 (2017)
G. Qi, B. Zhang, S. Du, Y. Yu, Estimation of aramid fiber/epoxy interfacial properties by fiber bundle tests and multiscale modeling considering the fiber skin/core structure. Compos. Struct. **167**, 1–10 (2017)
W. Qin, F. Vautard, L.T. Drzal, J. Yu, Mechanical and electrical properties of carbon fiber composites with incorporation of graphene nanoplatelets at the fiber–matrix interphase. Compos. Part B **69**, 335–341 (2015)
D. Quan, F. Bologna, G. Scarselli, A. Ivanković, N. Murphy, Mode-II fracture behaviour of aerospace-grade carbon fibre/epoxy composites interleaved with thermoplastic veils. Compos. Sci. Technol. **191**, 108065 (2020)
B.R. Reddy, K. Ramji, Modeling and evaluation of effective elastic properties of carbon nanotubes reinforced carbon fiber/epoxy multiscale composites. Mater. Today: Proc. **21**, 1099–1103 (2020)
S. Salifu, D. Desai, O. Ogunbiyi, R. Sadiku, O. Adesina, O. Adesina, Comparative study of high velocity impact response of aluminium 3105-H18 and carbon fibre-epoxy composite double hat bumper beams. Mater. Today: Proc. **38**, 712–716 (2020)
M. Sangermano, A. D'Anna, C. Marro, N. Klikovits, R. Liska, UV-activated frontal polymerization of glass fibre reinforced epoxy composites. Compos. Part B **143**, 168–171 (2018)
B. Sen, A.O. Fulmali, B.N.V.S.G. Gupta K, R.K. Prusty, B.C. Ray, A study of the effect of carbon nanotube/nanoclay binary nanoparticle reinforcement on glass fibre/epoxy composites. Mater. Today: Proc. **26**, 2026–2031 (2020)
Z. Sha, Z. Han, S. Wu, F. Zhang, M.S. Islam, S.A. Brown, C.-H. Wang, Low-temperature plasma assisted growth of vertical graphene for enhancing carbon fibre/epoxy interfacial strength. Compos. Sci. Technol. **184**, 107867 (2019)
M. Sheinbaum, L. Sheinbaum, O. Weizman, H. Dodiuk, S. Kenig, Toughening and enhancing mechanical and thermal properties of adhesives and glass-fiber reinforced epoxy composites by brominated epoxy. Compos. Part B **165**, 604–612 (2019)
P. Slobodian, S. Lloret Pertegás, P. Riha, J. Matyas, R. Olejnik, R. Schledjewski, M. Kovar, Glass fiber/epoxy composites with integrated layer of carbon nanotubes for deformation detection. Compos. Sci. Technol. **156**, 61–69 (2018)

A.K. Srivastava, V. Gupta, C.S. Yerramalli, A. Singh, Flexural strength enhancement in carbon-fiber epoxy composites through graphene nano-platelets coating on fibers. Compos. Part B **179**, 107539 (2019)

A.S. Swapnil, B. SatheSandip, P. ChaudhariBapu, S.J. Vishal, Experimental investigation of mechanical properties of glass fibre/epoxy composites with variable volume fraction. Mater. Today: Proc. **4**, 9487–9490 (2017)

G. Tang, Y. Yan, X. Chen, J. Zhang, B. Xu, Z. Feng, Dynamic damage and fracture mechanism of three-dimensional braided carbon fiber/epoxy resin composites. Mater. Des. **22**, 21–25 (2001)

S.F. Teh, T. Liu, L. Wang, C. He, Fracture behaviour of poly(ethylene terephthalate) fiber toughened epoxy composites. Compos. A: Appl. Sci. Manuf. **36**, 1167–1173 (2005)

W.-T. Wang, H. Yu, K. Potter, B.C. Kim, Effect of the characteristics of nylon microparticles on Mode-I interlaminar fracture toughness of carbon-fibre/epoxy composites. Compos. A: Appl. Sci. Manuf. **138**, 106073 (2020)

Q. Wu, R. Zhao, J. Zhu, F. Wang, Interfacial improvement of carbon fiber reinforced epoxy composites by tuning the content of curing agent in sizing agent. Appl. Surf. Sci. **504**, 144384 (2020a)

Q. Wu, J. He, F. Wang, X. Yang, J. Zhu, Comparative study on effects of covalent-covalent, covalent-ionic and ionic-ionic bonding of carbon fibers with polyether amine/GO on the interfacial adhesion of epoxy composites. Appl. Surf. Sci. **532**, 147359 (2020b)

Q. Wu, R. Zhao, T. Xi, X. Yang, J. Zhu, Comparative study on effects of epoxy sizing involving ZrO_2 and GO on interfacial shear strength of carbon fiber/epoxy composites through one and two steps dipping routes. Compos. A: Appl. Sci. Manuf. **134**, 105909 (2020c)

L. Xing, L. Liu, F. Xie, Y. Huang, Mutual irradiation grafting on indigenous aramid fiber-3 in diethanolamine and epichlorohydrin and its effect on interfacially reinforced epoxy composite. Appl. Surf. Sci. **375**, 65–73 (2016)

X. Xu, B. Zhang, L. Xing, K. Liu, M. Bai, D. Liu, Characterization and analysis of the thermal damages of aramid/epoxy composite laminates induced by the dielectric heating effect of microwaves. Compos. Struct. **200**, 371–379 (2018)

B. Yang, V. Kozey, S. Adanur, S. Kumar, Bending, compression, and shear behavior of woven glass fiber–epoxy composites. Compos. Part B **31**, 715–721 (2000)

Z. Yao, C. Wang, R. Lu, S. Su, J. Qin, Y. Wang, Z. Ma, H. Wei, Q. Wang, Fracture investigation of functionalized carbon nanotubes-grown carbon fiber fabrics/epoxy composites. Compos. Sci. Technol. **195**, 108161 (2020)

Z. Zhang, S. Hou, Y. Mao, L. He, X. Han, Rate-related study on the ply orientation of carbon fiber reinforced epoxy composite laminates. Int. J. Mech. Sci. **188**, 105968 (2020)

Miscellaneous Studies on Epoxy/Synthetic Fiber Composites

11

Sunan Tiptipakorn and Sarawut Rimdusit

Contents

S. Tiptipakorn
Department of Chemistry, Faculty of Liberal Arts and Science, Kasetsart University, Nakhon Pathom, Thailand
e-mail: faassntk@ku.ac.th

S. Rimdusit (✉)
Department of Chemical Engineering, Faculty of Engineering, Chulalongkorn University, Bangkok, Thailand
e-mail: sarawut.r@chula.ac.th

S. Mavinkere Rangappa et al. (eds.), *Handbook of Epoxy/Fiber Composites*,
https://doi.org/10.1007/978-981-19-3603-6_14

Abstract

In this chapter, epoxy resins (ERs) including its hardeners, benzoxazine resin (as curing agent), polybenzoxazine/epoxy alloy-based systems, and synthetic fibers were briefly overviewed. Besides the properties as discussed in the other chapters (electrical properties, dynamic mechanical properties, thermal stability, flame retardancy, morphology, and mechanical properties), the miscellaneous studies on the epoxy composites containing synthetic fibers (such as glass fibers, carbon fiber, and carbon nanotube) were discussed. The studies on shape memory behaviors, tribological properties (corrosion and friction coefficient), electromagnetic interference (EMI) shielding effectiveness, optically transparent properties, and environmental degradation have been reviewed. Moreover, it could be noted that the systems of epoxy incorporated with benzoxazine present the synergistic behaviors of glass transition temperature and exhibit favorable shape memory behaviors. Epoxy composites containing carbon fibers exhibit potential to be used for EMI shielding purposes.

Keywords

Epoxy resin · Synthetic fiber · Composites · Benzoxazine · Shape memory behaviors

Introduction

Epoxy resins (ER), or polyepoxides, are a class of greatly reactive low molecular weight pre-polymers or high molecular weight polymers containing epoxide functional groups including oxirane or glycidyl functional groups in their chemical structures. The crosslinked molecular compounds are rendered as products from catalytic polymerization with themselves or various types of hardeners or curatives, which are the chemicals in the family of polyfunctional amines and acid derivatives, i.e., amides, esters, acid chloride, anhydrides, and alcohols (Verma et al. 2020). In general, the cured ERs, as thermosetting polymers, possess many favorable properties (i.e., great mechanical properties, high thermal stability, and great chemical resistance); therefore, the applications are in the wide range such as great tension electrical insulators, electronic and electrical components, fiber-reinforced polymeric materials, and adhesives for many usage purposes (Wang et al. 2011).

Brief Overview of Epoxy Resins

Almost a century ago (ca. 1927), epoxy resins were first attempted to synthesize from epichlorohydrin in the United States. In 1936, Dr. Pierre Castan (of Switzerland) and Dr. S.O. Greenlee (of the United States) successfully developed diglycidyl ether of bisphenol A-based epoxy resins (DGEBA). The first epoxy patent was licensed by Ciba,

Table 1 Comparison on characteristics some widely used thermosets (Wang et al. 1999, 2011)

Thermoset	Characteristic				
	Approximated specific gravity	Tensile strength (MPa)	Tensile modulus (GPa)	Elongation at break (%)	Shrinkage rate (%)
Phenolic Paraformaldehyde	1.30	ca. 40–65	ca. 3	1.5–2.0	8–10
Polyester resin	1.10–1.50	ca. 40–70	ca. 2–4	5	4–6
Epoxy resin	1.10–1.20	ca. 85	ca. 3	5	1–2
Silicon resin	1.70–1.90	ca. 20–50	ca. 1	1	4–8

Ltd. (Switzerland). The company Ciba was one of the three resin manufacturers worldwide. After later several takeovers, in the late 1990s, the company Huntsman Advanced Materials from Basel (Switzerland) had run the business. Historically, Devoe & Raynolds was one of the manufacturers playing an important role in the epoxy resin industry of the United States. Later, the company was sold to Shell Chemicals, now a part of Hexion, Resolution Polymers. In the late period of the 1950s, epoxy resins were well known to be applied in the construction purposes. As previously mentioned, these resins have been well known as materials that possess many interesting properties. For instance, they could react with themselves or curing agent (hardener) to generate the network polymeric materials in forms of either liquid with various viscosities or solid. The resin could be produced from suitable curing agents in the wide range of curing temperatures from 0 °C to 180 °C. Table 1 presents the properties of epoxy resin in comparison with other thermosets (Wang et al. 1999, 2011).

Unlike other thermosetting resin, shrinkage rate of epoxy is generally lower than 2%. Due to great surface functionalities, e.g., ether groups (–O–) and hydroxy groups (–OH), the resin could strongly adhere to various surfaces of substrate (Verma et al. 2020). Moreover, the resins provide high mechanical properties and great insulative properties at various temperatures. The chemical stability and dimensional stability are also their favorable characteristics. The cured epoxy resins have superior corrosive resistance and ability to resist the microbial attack.

All mentioned properties could make them suitable as reagents for many productions. Nowadays, many companies from various countries have launched commercial epoxy, such as Gurit (Kassel) GmbH (Germany), M/S Vantico/Huntsman Corporation (Italy), Panjiva S&P Global (Brazil), Ciba Geigy India Ltd. (India), Nan Ya Plastics Corporation (Taiwan), Shankar Chemicals (India), M/S Covai Seenu & Company (Coimbatore, Tamil Nadu), Huntsman Corporation (Italy), Shell Chemicals/Hexion Inc. (Columbus, Ohio, USA), etc.

Types of Epoxy Resins

Typically, most of the epoxy monomers are synthesized from the reaction between epichlorohydrin and the compound with hydroxyl groups, which could be obtained

from dicarboxylic acids, aliphatic diols, polyols, or phenolic compounds. Another pathway to synthesize the resin is the reaction between either aliphatic or cycloaliphatic and peroxy acid. Some crucial types of the resins are presented as follows.

Bisphenol-Based Epoxy Resins

Bisphenol-based epoxy resins are synthesized from epichlorohydrin (ECH) and bisphenol resin. This resin type is most widely used and produced from bisphenol A and epichlorohydrin via two-stage chemical reaction, i.e., pre-polymerization between bisphenol A and ECH to produce bisphenol A diglycidyl ether (commonly designated as BADGE or DGEBA) and the condensation reaction between bisphenol A and BADGE with the by-product of sodium chloride and water as presented in Fig. 1. In the case of a few repeating unit, the epoxy product of viscous colorless liquid is obtained. For the repeating units in the range from ca. 3 to 30, the solid colorless resin is obtained. The variation of the ratio between bisphenol A and epichlorohydrin leads to the increase of the molecular weight of polyethers with the end of glycidyl groups, relating to properties of the products. When increasing the molecular weight of epoxy with decreasing the content of epoxide functional groups, the behaviors of the obtained resin product approach to thermoplastics. Another epoxy resin can be derived from the reactant of epichlorohydrin and bisphenol F or brominated bisphenols with the similar formation path as bisphenol A. The obtained products provide lower viscosity and higher epoxide groups with greater chemical resistance than that of bisphenol A.

Novolac-Based Epoxy Resins

Novolac resins are the polymers synthesized from formaldehyde (or methanal) and phenols (generally from a mixture of m- and p-cresols) with using carboxylic acids (such as oxalic acid) as catalysts. Moreover, hydrochloric acid, sulfuric acid, and toluene sulfonic acid could be used as catalyst as well. Typically, the reaction

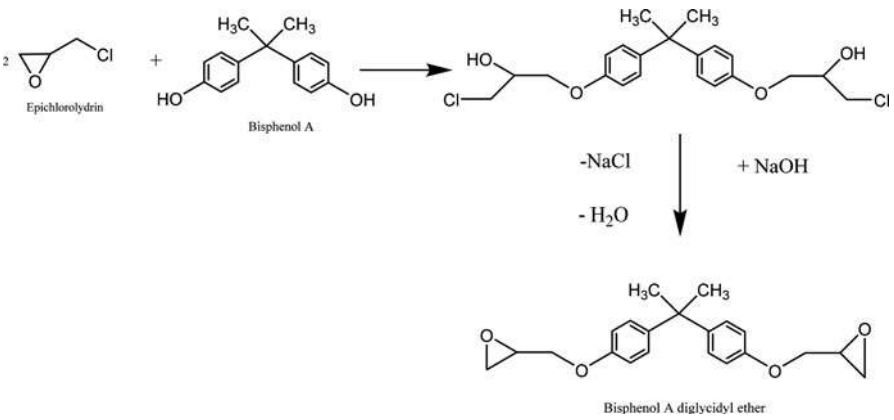

Fig. 1 Synthesis of bisphenol A-based epoxy resins (Wang et al. 1999; Dodiuk and Goodman 2013)

between novolac resin and epichlorohydrin generates epoxidized novolac with the repeating unit in the range from approximately 20 to 40 (Dodiuk and Goodman 2013). The properties of this epoxy resin type depend on the conditions of polymerization and the ratio of formaldehyde and cresols. The obtained resins are varied from greatly viscous liquid to solids. The cured products possess high chemical resistance with rather low flexibility. Generally, they could be used as photoresist materials for microelectronic devices (Dodiuk and Goodman 2013). The chemical structures of this epoxy resin type are presented in Fig. 2.

Aliphatic Epoxy Resins

Aliphatic epoxy resins (as presented in Fig. 3) could be classified into two categories as follows: (i) One is synthesized from epoxidation reaction of the alkene molecules and peroxy acid. The examples of this resin type are cycloaliphatic epoxides, which have at least one aliphatic ring and high oxirane content without chlorine in molecular structure. They possess low viscosity, high weather resistance, and high glass transition temperature. (ii) Another one is generated from the epichlorohydrin. The example of this type is aliphatic epoxy resin. Due to long curing time at room temperature, the proper accelerators and high temperature are required for polymerization of the resin.

Fig. 2 Novolac epoxy resin

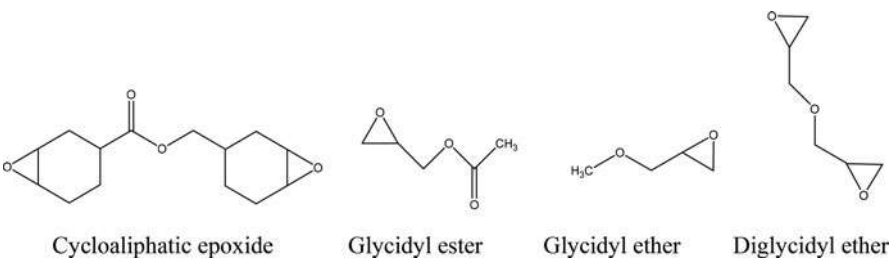

Fig. 3 Some examples of aliphatic epoxy resins

Halogenated Epoxy Resins

This epoxy resin type contains halogens, such as bromine or fluorine, in the chemical structure. The examples for this epoxy type are tetrabrominated bisphenol A and fluorinated epoxy resin. The applications of brominated epoxy resins are as reactive flame retardants and in electrical and electronics parts and equipment (Fig. 4).

Glycidyl Amine-Based Epoxy Resins

Glycidyl amine epoxy resins are a type of great functionality epoxies produced from the reaction between aromatic amines and epichlorohydrin. At room temperature, the viscosity of the obtained resin is varied from low to medium, which could be easy to handle. This kind of epoxy resin possessed high crosslink density, leading to great reactivity, high thermal and chemical resistance, good glass transition temperature, and high mechanical properties (Shang et al. 2015). The examples of this epoxy resins are 2,3,5-triglycidyl-4-aminophenol having three epoxide functionalities and 4,4′-methylenebis(*N*,*N*-diglycidylaniline) having four epoxide functionalities (as presented in Fig. 5). Because of their outstanding properties as mentioned above, the applications of the resin are for production of high-performance composites, coating, and adhesives in the aeronautical industries. Moreover, this type of resin could be used as diluents for highly viscous thermoplastics. However, the brittleness of the fully crosslinked glycidyl amine-based epoxy resin could limit their uses. In order to enhance the toughness, the resin could be blended with some thermoplastic (such as poly(ether ketone), polyether sulfone, and polyetherimides).

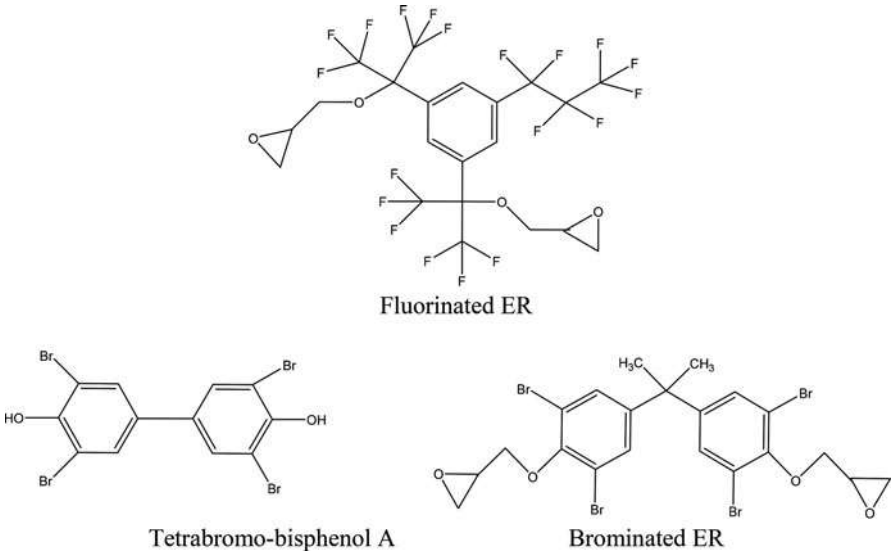

Fig. 4 Chemical structure of halogenated epoxy resins

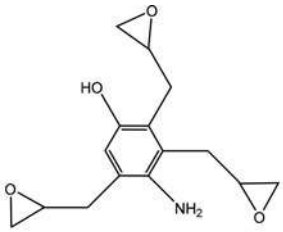

2,3,5-Triglycidyl-4-aminophenol

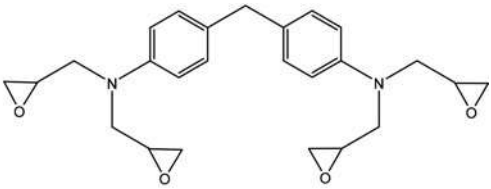

4,4′-Methylenebis(N,N-diglycidylaniline)

Fig. 5 Some examples of Glycidyl amine-based epoxy resins

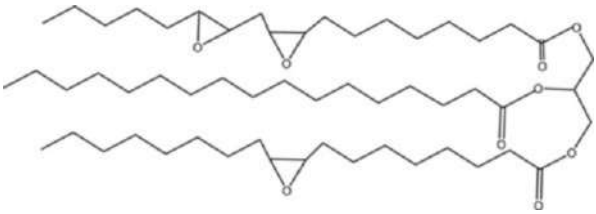

Fig. 6 Epoxided vegetable oil

Bio-Based Epoxy Resins

Nowadays, the raw materials, to produce various epoxy types in the industrial productions, are mainly derived from the petroleum sources. Approximately 90% of these resins are based on bisphenol A and epichlorohydrin (Ramon et al. 2018). These kinds of petroleum-based epoxy resins have been toxic, and their applications have been banned in many countries. Moreover, the awareness related to the reduction of fossil resources and emission of toxic gases have been increased. Due to environmental issues and to prevent global warming, at the present time, many bio-based epoxy resins have been produced. These resins have been derived from renewable resource, e.g., algae, wood dust, vegetable oils, rosin, lignin, furan, and itaconic acid. In the chemical structure of the bio-based epoxidized monomer, the epoxide groups accompanying the backbone chain could generate the three-dimensional epoxy network when curing with specific curing agents. That leads to the eco-friendly rigid products. The applications of the bio-based epoxy resin are varied, i.e., coating, paints, adhesive, and biomedicine. The examples of the bio-based epoxy are vanillin-diglycidyl ether (DGEVA, derived from lignin of wood flour), phloroglucinol (PHTE, derived from phloroglucinol from algae), and epoxidized vegetable oils as presented in Fig. 6.

Curing Agents for Epoxy Resins

As previously mentioned, three-dimensional networks of the resins take place from the reaction between their own molecules to generate homopolymer. As another path

to form the networks for copolymerization, the curing agents or hardeners have been applied. The hydrogen atoms of the curing agent can react with the epoxide functional group of the resin. In some cases, the reaction between the resin and the curing agent occurs at room temperature; many ones occur at high temperature from 150 °C to 200 °C. In the case of insufficient heat upon curing, incomplete curing leads to poor mechanical properties including low chemical and thermal resistance.

Many common types of used curing agents are introduced in order from the strongest reactivity to the weakest one as follows: thiol, amine, anhydride, and phenol. The thiol hardener, the most reactivity type, proceeds to the curing process at even room temperature. The reactivities of amine hardener are in the order as aliphatic amine (strongest reactivity), cycloaliphatic amine, and aromatic amine (weakest reactivity). The aromatic structures lead to the rigid structure than aliphatic one. As the most commercialized bio-based curing agents, phenalkamine hardener is obtained from the Mannich reaction of cardinol, formaldehyde, and some amine. Its chemical structure is presented in Fig. 7. The benefits of phenalkamine are short curing time with low curing temperature and high chemical and water resistance. Moreover, this kind of hardener is approved in contact with food or potable water.

Benzoxazine Resins as Hardener

Polybenzoxazines are a novel type of phenolic resins, being composed of nitrogen and oxygen in their heterocyclic macromolecules. The novel thermosets can be produced via ring-opening polymerization of benzoxazine resin. The thermosets are used as versatile materials having many outstanding properties, i.e., high flame retardance, great thermal properties, and good mechanical properties including great sound and noise absorbance. The polymerization of benzoxazine resin can be proceeded either with or without solvent. Upon thermal curing process, no need of curing agent or catalyst is required. During ring-opening polymerization of benzoxazine resin, there is great processability due to low viscosity and no generated by-products. The polymers have near-zero volumetric expansion or shrinkage. The thermosets render great char yield and low dielectric constant and high molecular design flexibility. Figures 8 and 9 present the synthesis path of BA-a monomer (common benzoxazine resin type) and thermal curing process of polybenzoxazine, respectively.

Polybenzoxazines possess favorable properties, i.e., these phenolic thermosets can be alloyed with other polymers such as polyurethane and epoxy. In addition, it has been reported that benzoxazine resin could play a role as hardener of epoxy (Rimdusit

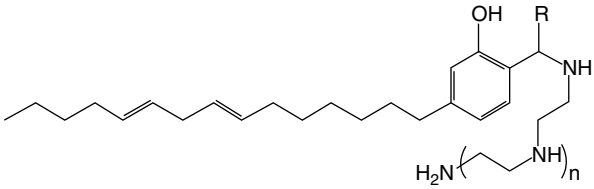

Fig. 7 Chemical structure of phenalkamine hardener

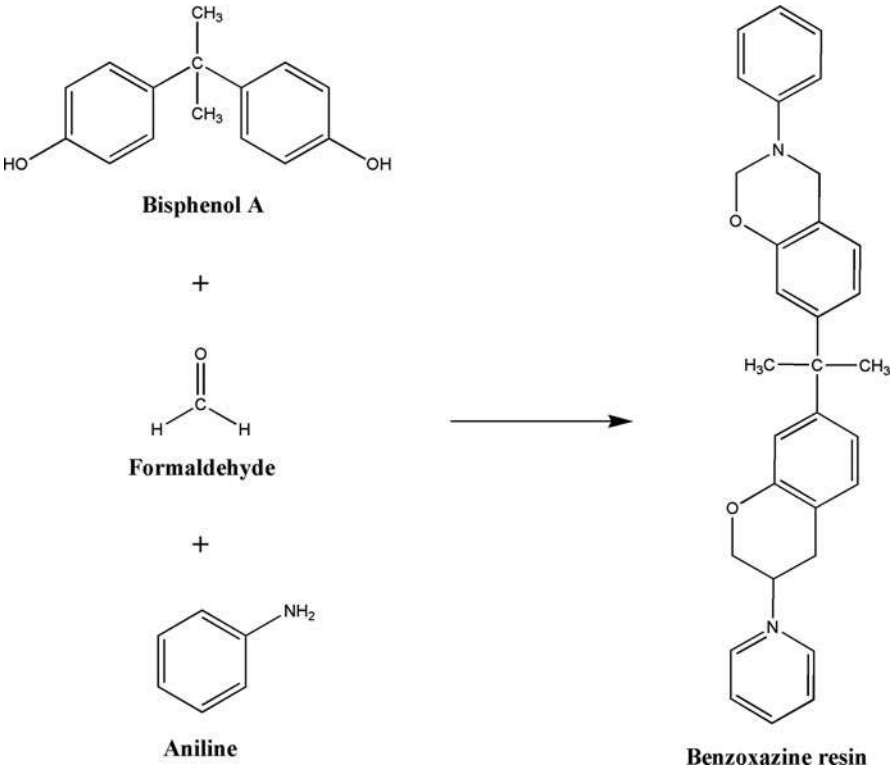

Fig. 8 Synthesis path of benzoxazine resins. (Reprinted with permission from Rimdusit et al. 2013a)

et al. 2013a). The chemical reaction between epoxy resin and benzoxazine resin is presented in Fig. 10. Interestingly, some properties of the copolymers between benzoxazine and epoxy copolymers represent synergism (Rimdusit et al. 2011, 2013b). In the ternary systems (derived from phenolic, epoxy, and benzoxazine resin), the synergistic behavior of glass transition temperature (T_g) was also observed. For the mass ratio of phenolic resin/epoxy/benzoxazine at 1/4/5, the highest value of T_g was reported at ca. 180 °C, which was higher than that of pure phenolic resin (approximately 170 °C), pure EPON825 epoxy resin (approximately 160–170 °C), and pure polybenzoxazine (approximately 170 °C) (Rimdusit et al. 2013a).

Synthetic Fiber for Epoxy Composites

Synthetic fibers are commonly derived from chemical or petrochemical substances. They have greater characteristic than natural fibers. For compositing, three kinds of synthetic fibers are generally applied in the industry, i.e., Kevlar fibers, carbon fibers, and glass fibers. Kevlar fibers are the aromatic polyamide synthesized from the

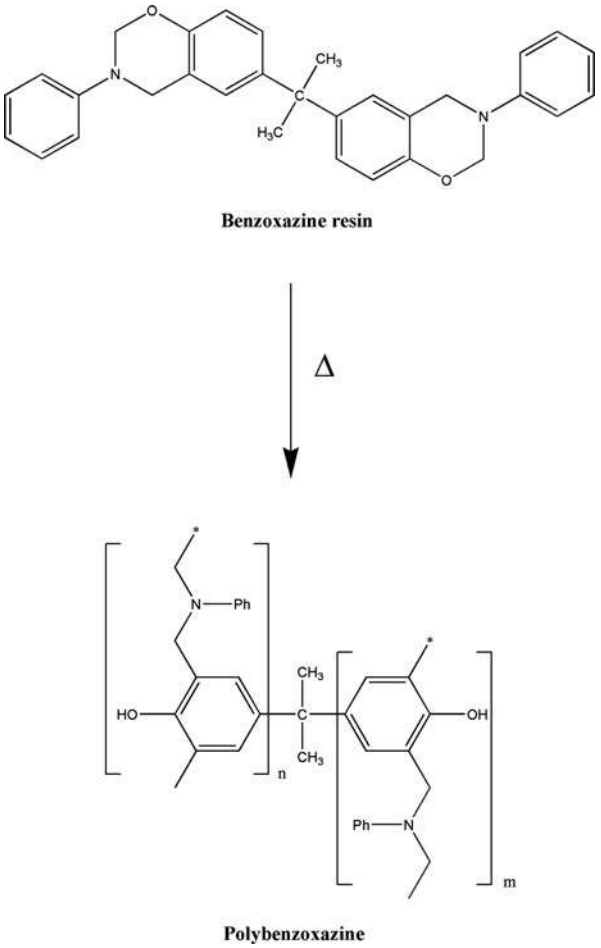

Fig. 9 Curing process of benzoxazine resins. (Reprinted with permission from Rimdusit et al. 2013b)

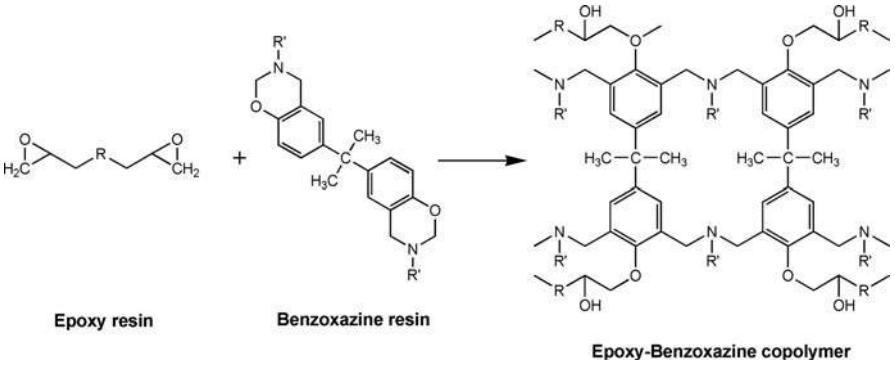

Fig. 10 Chemical reaction between epoxy resin and benzoxazine resin. (Reprinted with permission from Rimdusit et al. 2013b)

Table 2 Property comparison between glass fiber, carbon fiber, Kevlar, and epoxy (Shukla et al. 2015)

Property	E-glass fiber	Carbon fiber	Kevlar	Epoxy
Fiber strength (MPa)	ca. 3450	ca. 4130	ca. 2760	N/A
Strength by weight	ca. 560	ca. 1010	ca. 990	ca. 30
Young modulus (GPa)	ca. 30–40	ca. 130–180	ca. 70–110	3

condensation reaction between terephthaloyl chloride and 1,4-phenylenediamine. They are expensive because of high-priced production process and high-cost equipment. Carbon fibers are mostly derived from polyacrylonitrile (PAN). Some of the carbon fiber can be synthesized from rayon or petroleum pitch. The cost of carbon fiber is rather low. Due to the lowest cost, glass fibers are the most widely used in composite industries. The properties of three synthetic fibers are compared with epoxy and shown in Table 2.

Shape Memory Properties

Shape memory materials are smart substances which can recover their initial shape while using extrinsic triggers such as change of temperature, pH, etc. The properties of these materials can be tunable. The applications of shape memory materials are in many fields such as automobile actuators, smart medical devices, smart textiles, etc. Typically, common characteristics of shape memory materials can be represented, by the following terms such as shape fixity, recovery speed, recovery stress, recovery time, etc. (Rousseau 2008).

Shape Memory Epoxy-Based Materials

Shape memory epoxy-based materials have received attention from manufacturing and academic researchers. They possess more favorable characteristics than other shape memory materials in aspects of high mechanical and thermal properties with excellent processability. Shape memory epoxy polymers have been studied for many years ago. Bisphenol A diglycidyl ether (DGEBA)-based epoxy resins have been commonly applied for the production of shape memory epoxy composites. Wu et al. (2010) studied the effect of curing agent on the properties of shape memory materials. The study reported that the T_g value was increased with curing agent content. The derived shape memory polymers have high network structure resulting in great thermal stability. For several years ago, Parameswaranpillai et al. (2017) developed the shape memory polymer blends between DGEBA epoxy and poly (propylene glycol)-block poly(ethylene glycol)-block-poly(propylene glycol) (PPO-PEO-PPO) triblock copolymer. The obtained shape memory materials have great thermal stability and UV resistance. Wei et al. (2018) revealed that the shape memory rate of hydrogenated bisphenol A epoxy resin was higher than that of bisphenol A epoxy resin due to its chemical structure.

For polybenzoxazine/epoxy alloy-based shape memory polymer, the synergism of glass transition temperature was reported (Ishida and Allen 1996). Rimdusit et al. prepared shape memory of BA-a (benzoxazine resin), EPON 826 (aromatic epoxy), NGDE (aliphatic epoxy), and Jeffamine D230 (curing agent). They revealed that the recovery time of shape memory polymer alloys was decreased with the increase in epoxy contents. Also, the storage modulus and glass transition temperature were increased with increasing BA-a content. In the case of high temperature, the recovery force of the shape memory materials was increased because the chain mobility was promoted by heat (Rimdusit et al. 2013c). Typically, the shape memory epoxy polymers are consisted of aromatic epoxy; however, Tanpitaksit et al. (2015) synthesized the shape memory alloys from polybenzoxazine and NGDE aliphatic epoxy resin without using any hardener. Benzoxazine resin acted as hardener and a stable network portion. Furthermore, Rimdusit et al. (1994) reported that the reactions between benzoxazine resin and different epoxy resin types occurred without any curing agent. In addition, the alloying benzoxazine with epoxy at proper content could lead to a single broad switching transition region and the multiple shape memory behaviors. When increasing benzoxazine content, the shape recovery time tended to increase due to the molecular chain mobility impedance from the increase of crosslink density (Liu et al. 2010). Interestingly, Liu et al. (2010) reported that the recovery time of pure epoxy resin E-51 (WSR 618) hardened by aromatic amine was longer than that of aliphatic epoxy alloyed with benzoxazine resin. Moreover, the recovery time could be tunable by the content of benzoxazine resin to extend the usage range of shape memory alloys. The addition of benzoxazine to alloy with epoxy resin possesses many favorable properties, e.g., great shape fixity (closed to 100%) with short recovery time.

Because of environmental concern, bio-based benzoxazine resins based on furfurylamine, stearylamine, and eugenol have been synthesized by Thirukumaran et al. (2014). Recently, the shape memory materials derived from the blends of NGDE epoxy resin, furfurylamine-based benzoxazine, and eugenol-based benzoxazine resin (E-fa) were prepared. The results revealed that the increase of two bio-based benzoxazine content led to the increase of thermal stability and the shape fixity (up to approximately 99%). Recently, the shape memory polymers synthesized from copolymer of vanillin-based polybenzoxazine and castor oil-based epoxy were prepared without any curing agent by Rimdusit and Hombunma (2018). It was revealed that the shape recovery at T_g+20 °C was increased from 87% to 96% and the shape fixity at 25 °C was decreased from 93% to 86% when increasing castor oil-based epoxy.

Epoxy-Based Shape Memory Composites

In comparison with other shape memory polymers, shape memory epoxy resins have favorable characteristics such as great shape recovery ratios, high shape fixity, short recovery time, outstanding dimensional stability, and good processability (Liu et al. 2016). The properties of shape memory can be adjustable to meet the application

requirements. Compositing with fillers is one of the common methods to modify the characteristic of these smart materials. The synthetic fibers, commonly reinforced in shape memory epoxy resin, are glass fiber, carbon fiber, and aramid fiber. Moreover, the shape memory characteristics of shape memory epoxy filled with some fiber-shaped fillers, such as silicon carbide whisker (SiC_w) and carbon nanotube (CNT), are also reviewed in this section.

Zhu et al. prepared the shape memory epoxy composites filled with continuous glass fiber. In their study, common bisphenol A epoxy resins were hardened by anhydride to obtain high glass transition temperature (T_g). Glycidyl phenyl ether (PGE) was used as diluent to adjust the crosslink density, T_g value, and chain flexibility. The strain was enhanced when shape memory cycle was proceeded. The shape fixity was over 98%; the shape recovery ratio was closed to 100%. The T_g values were adjustable in the range of 80 °C to 140 °C (Zhu et al. 2018).

Recently, Liu et al. (2019) successfully synthesized shape memory epoxy composites reinforced with various short and continuous carbon fibers. In the curing process of epoxy resin E-51, methylhexahydrophthalic anhydride (MHHPA) and *N*, *N*-benzyldimethylamine (BDMA) were used as curing agent and accelerator, respectively. The obtained shape memory epoxy composites could provide high storage modulus at 37 GPa at room temperature with the highest recovery force (over 4.4 GPa) and favorable shape memory capacities. These properties were higher than those of other common shape memory polymers. The reason of such a high modulus could be attributed to the properties of carbon fibers and the ability to hinder crack growth in matrix. Also, Liu et al. fabricated the shape memory materials derived from DGEBA resin cured with MHHPA and reinforced with multiwalled carbon nanotube at 0.25 to 0.75wt%. The obtained composites rendered the wide range of T_g of ca. 65 to 140 °C (Liu et al. 2016). Zhang et al. prepared the shape memory composites of epoxy core layer and polycaprolactone shell layer (Zhang et al. 2015a). At testing temperature of 70 °C, a short recovery time was reported at approximately 6 s.

Abishera et al. studied the shape memory characteristics of the cold-programmed laminates of carbon fiber (CF)/multiwalled carbon nanotube (MWCNT)/epoxy mixture. Jeffamine 230 was used as curing agent. They reported that adding CF led to drastic changes in glass transition temperature and cold programmability of epoxy resin. The shape memory properties of the samples with different laminate configurations at various MWCNT contents were determined. The results revealed that the MWCNT at 1wt% lead to small change in T_g without any effect on cold programmability. The shape recovery of 100% was observed for all shape memory samples. Moreover, the configurations of laminate had great effect on the shape fixity. They investigated the effect of programming conditions such as strain rate, stress relaxation time, and strain level on the reversible plasticity shape memory characteristics of MWCNT-filled epoxy nanocomposites. The results exhibited that the excellent shape memory characteristics were observed under different programming conditions. Also, they reported that the addition of MWCNT could increase in reversible plasticity shape memory characteristics including shape fixity and recovery speed (Abishera et al. 2018).

Recently, shape memory epoxy resin composites reinforced with aramid fiber were prepared by Jing et al. (2020). Based on viscoelastic theory, the shape memory behaviors of the system in circular tube shape were analyzed by finite element model. The results from response tests of three reconfigurable structures (circular tube, curved tape, and flat tape) were compared. The results exhibited the strength failure upon the shape memory process. The study of viscoelastic parameters presented that the long-term modulus, in correspondence with the stationary phase, has an impact on the recovery process of the shape memory composites. The failure for the structure of curved tape and flat tape has more difficulty to detect than circular tube due to smaller local blending.

In recent years, the shape memory materials based on the ternary resin system of carboxyl-terminated butadiene acrylonitrile rubber (CTBN), JEF-2011 epoxy resin (ER), and bisphenol E type cyanate ester (CE) were prepared. The obtained shape memory polymers possessed great tensile and impact properties as well as outstanding shape memory characteristics. All tested samples exhibited shape recovery ratio in the range from 97% to 99% and shape fixity ranging from approximately 98% to 99%. This could be attributed to the reversible phase of CTBN and ER resin and the stationary phase of triazine rings in the structure. When the abovementioned ternary systems were also applied as prepreg for compositing with plain weave carbon fiber (CF), the mechanical properties of shape memory composites were significantly higher than those of neat shape memory polymers. When the mass ratio of CTBN/ER/CE was adjusted, the glass transition temperature was varied from approximately 180 to 120 °C. At the mass ratio of 3:3:10, the tensile strength and modulus values were reported at 570 MPa and ca. 37 GPa, respectively. The elongation at break of the shape memory composites was approximately 2% due to the properties of carbon fiber. The recovery time values of shape memory ternary resin and its shape memory composites filled with carbon fiber were reported at 64 and 35 s, respectively. The shape memory composites presented high shape fixity over 95% (after repeatedly conducting shape memory tests for 30 times) (Zhihua et al. 2019).

Benzoxazine/Epoxy Alloy-Based SMPCs

In the last few years, Plylaharn et al. (2018) successfully prepared shape memory composites derived from benzoxazine/epoxy alloy reinforced with woven carbon fibers. The almost 100% of shape recovery was presented. The recovery stress of the composites was improved from ca. 3 MPa (without filler) to ca. 29 MPa (at 47vol% of carbon fibers). The thermal stability determined from T_{d5} and char yield increased with the increase of carbon fiber. This was attributed to thermal properties of the filler. In recent years, Likitaporn et al. (2018) fabricated the shape memory composites synthesized from benzoxazine/epoxy alloys filled with silicon-carbide whisker (SiC_w). The T_g was reported to be increased with filler contents, i.e., 154 °C (without filler) to 170 °C (at 20wt%). Furthermore, the flexural strength and modulus of the composites at room temperature and T_g+20 °C were increased with increasing SiC_w. Enhancing thermal stability, the addition of filler could have barrier effect to prevent

heat transfer to matrix and hinder the decomposition process of polymer matrix. The char yield at 800 °C was increased with the increase of filler content, i.e., approximately 28 (without filler) to 43% (at 20 wt%). Moreover, the results from recovery test revealed that the addition of SiC_w provided the decrease in recovery time, i.e., ranging from ca. 3 to 5 min (for microwave induction) and from ca. 8 to 18 min (heating induction), respectively. In addition, the filler could significantly enhance the recovery stress from ca. 3 MPa (without filler) to ca. 11 MPa (at 20wt%) due to high modulus of the filler. The shape fixity of the composites was reported at approximately 99%.

Carbon nanotube is a fiber-shaped filler commonly added in shape memory materials. Recently, Prasomsin et al. successfully prepared bio-based benzoxazine resins derived from furfurylamine (fa), vanillin (V), and paraformaldehyde; the obtained V-fa benzoxazine resins were then reacted with epoxidized castor oil. Then, the copolymers were composited with multiwalled carbon nanotubes (MWCNT) (Prasomsin et al. 2019). The shape recovery and shape fixity tests were conducted as exhibited in Fig. 11. The addition of MWCNT could provide drastic enhancement in thermal, mechanical, and recovery properties of the shape memory composites. When the nanofiller contents varied from 0.1 to 0.3wt%, the shape fixity and shape recovery values were in the range from 92% to 93% and 96% to 98%,

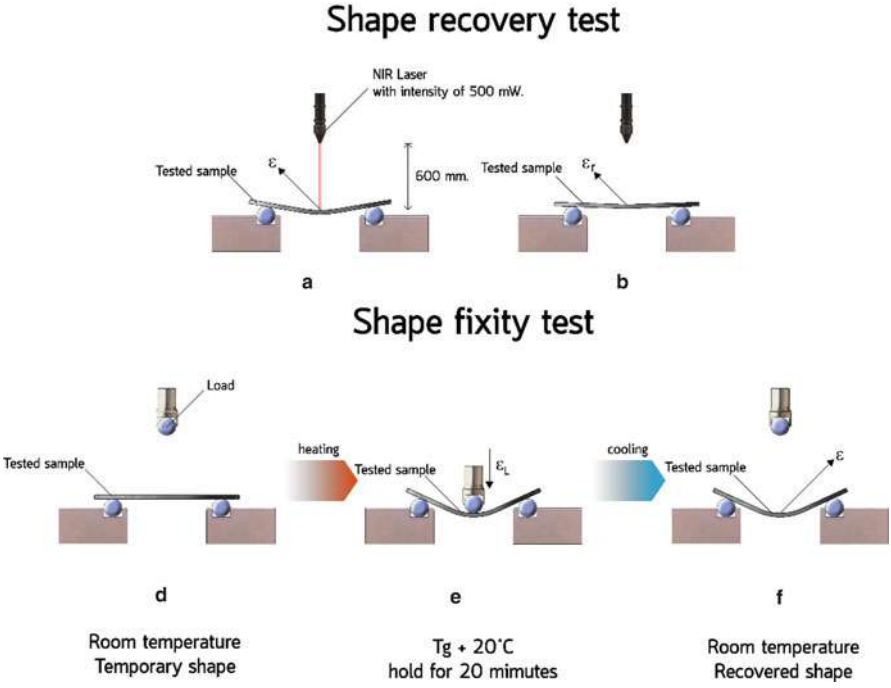

Fig. 11 Shape recovery and shape fixity test. (Reprinted with permission from Prasomsin et al. 2019)

respectively. The recovery time was decreased from 36 to 16 s. In comparison with different stimulation methods, the recovery time of the composites stimulated with near infrared was shorter than those stimulated with conventional heating.

Study on Tribological Properties

Epoxy resin is one of the frequently used polymers to composite with other reinforcing materials to develop anti-wear coating materials due to its outstanding erosive resistance, high processability, great flexibility, and inexpensiveness. In general, the tribological properties of the materials are related to the wear and friction characteristics. Many kinds of tribometers are used to determine these properties, i.e., an abrasive tribometer, a rolling sliding tribometer, and a pin- or ball-on disk tribometer. One of the most common analysis techniques is pin or ball-on disk test (Kalelia 2016) as presented in Fig. 12. In this technique, different moving modes of test can be conducted, e.g., unidirectional and complicated motion patterns. The tests can be carried out with the variation of load, sliding velocity, and abrasive surface. Typically, the determination of wear characteristics can be analyzed from the amount of removed substances after a wear test, which is related to the mass loss, volume loss, or dimensional change, that is dependent on the testing purpose, sample size, wear types, etc. A precision balance can be used for the direct measurement of weight loss of the sample, while a surface profilometer or a microscope can be applied to determine wear profile and dimensional data from wear track to calculate

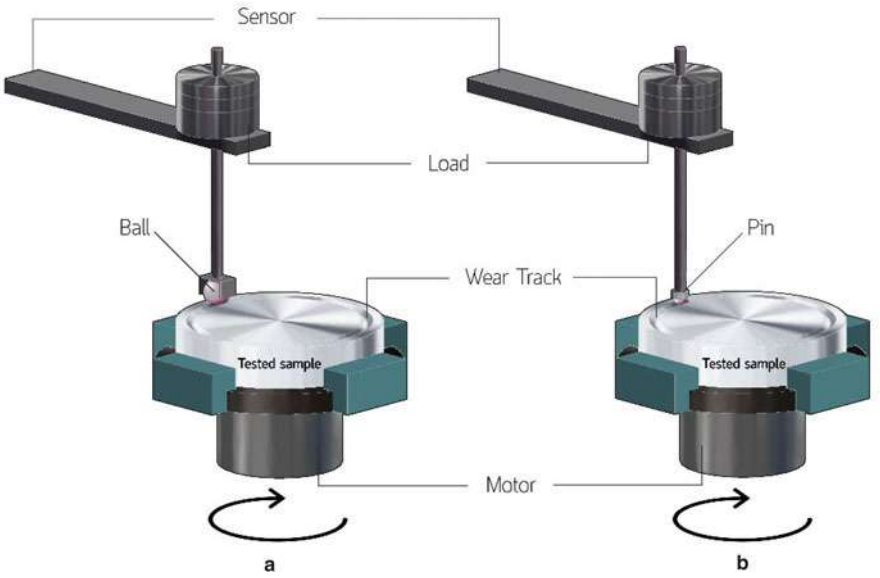

Fig. 12 Wear testing apparatus (**a**) ball-on-disk wear tester (**b**) pin-on-disk wear tester (Kalelia 2016)

volume loss, including dimensional change of the samples. From the calculation of the abovementioned parameters, the wear characteristics are commonly presented in terms of wear rate or specific wear rate. Wear rate of the tested materials is the parameter presenting the volume loss per unit of sliding distance, while the specific wear rate is the wear rate value per applied load that can be calculated according to Archard's equation, which is one of the most often used wear equations as follows (Horst et al. 2006).

$$k = \frac{V}{F \cdot d} \tag{1}$$

where k is the specific wear rate ($mm^3\ N^{-1}\ m^{-1}$), V is the loss volume of the material (mm^3), d is the sliding distance (m), and F is the applied load (N).

Erosion and Wear Resistance Properties of Epoxy-Based Fiber Composites

Erosion characteristic is a type of wear damage on the surface of materials. When solid or liquid particles impinge on the surface, the progressive loss of materials occurs. For polymeric composites, erosion properties relate to many factors that must be controlled during test, e.g., fiber orientation, fiber content, exposure time, impingement velocity, impingement angle, size of erodent, and standoff distance. In the present time, many studies relevant to erosion of epoxy-based composites filled with synthetic fibers (including glass fiber, carbon fiber, and aramid fibers) have been conducted (Vigneshwaran et al. 2017). In some studies, only one type of synthetic fiber was filled in the composites. For some studies, other types of either particulate shape filler or fiber shape filler can be incorporated with synthetic fiber. Barkoula and Kocsis (2002) prepared epoxy composites reinforced with unidirectional glass fiber (GF) and investigate the effect of fiber arrangement. Parallel and perpendicular directions of GF were arranged in the ER matrix. The erosion-resistant properties of the composites were exhibited at different impact angles. From their results, the impact angle of 90° provided the highest wear rate. The composites revealed brittle erosion characteristics with the highest weight loss at impingement angle of 90°. For the impingement angle of 30°, the higher erosion rate led to high roughness on the composites surface. Tewari et al. (2003) fabricated the ER composites reinforced with unidirectional glass and carbon fibers. The solid particle erosion characteristics were determined at various impact angle ranging from 15° to 90°. The fibers were arranged in three different orientations, i.e., 0°, 45°, and 90°. As particles for erosion evaluation, the steel ball with the diameter in the range of 300 to 500 microns and the impact velocity of 45 m/s were applied. At 60° impact angle, the highest erosion rate represented the semi-ductile erosion characteristics of the composites. They reported that the fiber orientation had significant effect on the erosion. Moreover, from the results of surface analysis of the tested composites, the delamination of fiber and matrix was observed. This poor bonding between matrix and fiber could lead to the

increase of erosion. They revealed that the highest erosion rate was observed as erodent particles passing parallel to the direction of fiber orientation. The fiber arrangement is a parameter having great effect on the erosion rate. Harsha and Jha (2008) prepared neat epoxy resin and the epoxy composites reinforced with different patterns, i.e., (i) unidirectional orientation of glass fiber, (ii) unidirectional arrangement of carbon fiber, and (iii) bidirectional direction of e-glass woven-reinforced epoxy composites. The effects of fiber arrangement and fiber types on the erosion resistance properties were determined. The fiber arrangement and fiber type have effects on the resistance properties of the composites. They reported that the erosion resistance of the composites reinforced with the bidirectional direction could possess the highest erosion characteristics.

Zhang et al. (2017) prepared the glass fiber-reinforced epoxy resin composites covered with surface protection layers of carbon nanosheets via the vacuum-assisted resin transfer molding process. The carbon sheets were composed of dense carbon nanofiber (CNF) network. The erosion resistance, electromagnetic interference shielding (EMI), and mechanical properties were determined. The thickness of composites was approximately 1.00 mm, while those of CNF nanosheet were 0.15 and 0.30 mm. The tests of sand erosion behaviors of the obtained composites were conducted. The results revealed that the sand erosion rates of neat glass fiber/epoxy composites and neat carbon fiber/epoxy composites were reported at 6.8 and 2.4 mg/s, respectively. That was attributed to intrinsic characteristics of each reinforcing fiber. The carbon fiber possesses higher tensile modulus and strength, leading to higher resistance to bombardment of sand particles. The erosion rate values for the composites coated with CNF nanosheet of 0.15 and 0.30 mm thickness were 1.2 and 0.9 mg/s, respectively. Moreover, the results revealed that the GF/epoxy composites coated with CNF nanosheet could attain EMI shielding effectiveness ranging from 33 to 40 dB at the frequencies in the range of 30 MHz to 1.5 GHz (Zhang et al. 2017). These results were corresponded to their previous work, which compared the surface erosion properties between the CF/ER composites with and without coating with carbon nanofiber (CNF) sheet (Zhang et al. 2013). The results exhibited that the CNF sheet coated on ER composites possessed higher erosion resistance than those without coating with CNF sheet. This could be due to great strength value of CNF sheet and its nano-sized structure.

Lv et al. (2018) studied the particle erosion resistance of glass fiber (GF)/epoxy resin (ER) composites added with thermoplastic polyurethane nonwoven textiles (TNT). The TNT was fabricated via melt-blown process, and the composites were prepared via vacuum-assisted resin transfer molding (VARTM) process. The erosion properties of TNT/GF/ER composites were compared with those of GF/ER composites. The results presented the enhancement of particle erosion resistance (i.e., varied from 99% to 493%) at various impingement angles (i.e., varied from 20° to 90°). In addition, the toughness of the composites was also improved with the incorporation of TNT component. The TNT/GF/ER composites that presented the values of the highest and lowest erosion rate were reported at 30° and 90°, respectively, while that of GF/ER composites was reported at 90°. In the research of Panda et al. (2014), the GF/ER composites filled with aluminum nitride (AlN) were

fabricated by hand lay-up process. The results from investigation of wear characteristics revealed that the addition of the AlN particle could improve the toughness and wear resistance of the composites. However, the tensile strength was decreased with increasing AIN.

In general, the impingement angles on the variation of erosion defect are important erosion properties on the properties of materials. In the case of ductile materials, the highest erosion generally takes place at small angle (not over 45°); for brittle materials, it takes place at 90°. This could be attributed that the three-dimensional network structures embedded into the composites could improve the energy absorption. In their study, the brittleness behaviors of GF/ER composites and the toughness behaviors of TNT/GF/ER composites could be observed and corresponded to the morphology analysis of eroded surface (Lv et al. 2018).

Zheng et al. (2016) prepared the carbon fiber (CF)/ER composites having resistance to atomic oxygen. This form of oxygen could lead to corrosion of spacecraft at low earth orbit altitude. In their study, a silane coupling agent was used on the surface of carbon fiber when fabricating the composites. The coupling agent was hydrolyzed and interacted with hydroxyl groups of carbonous filler. Then, uniform thin film layer of siloxane was finally formed and coated on the surface of carbon fiber. In their research, three kinds of silane coupling agent with various end-functional groups were treated with carbon fiber. For all types of used coupling agent, the atomic oxygen erosion resistance and shear strength of the obtained CF/ER composites were enhanced.

Zhang et al. (2007) determined the influence of carbon fiber length on the wear resistance properties of the epoxy composites reinforced with short carbon fiber. The composites filled with two different lengths of carbon fiber (90 and 400 microns) were compared. For either with or without the addition of graphite flakes and nano-TiO_2, the results revealed that the shorter fiber length could possess lower wear resistance than those of longer fiber length, which was attributed to the low bonding strength with epoxy matrix. These results were more obviously observed in the case of high contact pressures. In addition, the incorporation of graphite flakes and nano-TiO_2 could lead to drastically enhance the wear resistance of the composites. From the scanning electron microscope (SEM) images, the worn appearances of the composites with longer fiber were obviously smoother than those of the composites with shorter one. In their work, the smoother worn surface was corresponding to greater wear resistance. Furthermore, the shorter fiber could be more easily removed from the epoxy matrix.

Rao et al. (2015) studied erosion behaviors of carbon fiber (CF)-reinforced epoxy (ER) composites with and without graphite particulate by using sand particle as erodent at various impact angles. They studied the effect of impact angle and filler content on erosion rate of the CF/ER composites. The results revealed that both CF/ER composite unfilled and filled with graphite presented erosion behavior of semi-ductile materials as the highest wear rate at the impingement angle of 45°. The erosion resistance of graphite-filled composites was lower than that of unfilled ones. Moreover, the erosion weight loss was highest at graphite content of 4wt%. Papadopoulos et al. (2016) investigated the influence of carbon nanotube (CNT)

addition to the CF/ER composites. The synergistic behaviors of two inorganic fillers were observed, leading to the decrease of erosion rate for nearly 50%. The CF orientation in the composites had no significant effect on the erosion wear behaviors because of isotropy behaviors of the composites. According to the erosion characteristics, the ER systems presented as semi-brittle materials, while the composites exhibited as brittle ones.

In the recent year, Sharma and Kumar (2019) fabricated the epoxy composites reinforced with Kevlar fiber using VARTM technique. The slurry jet erosion test was used to determine erosive wear characterization. The fiber contents were different in the range from 52 to 58wt%. The Taguchi-based experiment design was applied to analyze the results. When the slurry concentration was 160 g/min, the lowest wear rate of the composites was observed at fiber content of 55wt%, impingement angle of 60°, and the impact velocity of 30 m/s.

The erosion behaviors between silicon carbide (SiC)-reinforced epoxy resin (ER) composites were investigated (Hooda et al. 2015). In comparison between pristine ER, the SiC-ER composites had lower amount of perviousness and greater micro-hardness. The dry sliding wear resistance properties were determined using the Taguchi design of experiment methods. The results exhibited that the sliding wear resistance of the ER was enhanced. The results presented that erosion resistance of the composite materials depended on many factors such as sliding velocity, applied load, and filler content. Moreover, the composites reinforced with SiC have great potential for various uses in environments, which are particularly vulnerable to wear, e.g., structural applications in desert or dusty environments. Recently, Antil et al. (2018) investigated the erosion behaviors of the epoxy composites reinforced with glass fiber (GF) and silicon carbide particles. The erosion behaviors of the composites were determined using different parameters, e.g., slurry pressure, standoff distance, and impingement angle. The results revealed that the addition of SiC could lead to enhancement of erosion resistance of the composites. The highest erosion rate with an impingement angle of 60° could exhibit semi-ductile properties. The increase of angle impingement could decrease the erosion rate. Moreover, it could be concluded that the types of erodent slurry drastically affected the erosion resistance of composite. In their research, the composites filled with 400 mesh size of SiC particles could have higher erosion resistance than those filled with 220 and 320 mesh size of SiC particles.

Carbon nanotube (CNT) is one of the fiber-shaped fillers commonly used as reinforcing elements in the composites. Chen et al. (2014) studied the influence of adding CNT with different alignments on the erosive wear resistance of epoxy-based composites. In their work, three patterns of CNT arrangement were prepared, i.e., (i) random dispersion, and (ii) vertical alignment of CNT array, and (iii) horizontal alignment of CNT array. They reported that the composite with CNT array in vertical alignment could provide greater erosive wear resistance than any other kinds of composites. The images from scanning electron microscope (SEM), which revealed the erosion wear mechanism of composites at different impact angles, presented that the erosion wear characteristics depended upon CNT alignment in ER matrix. The surface profilometer could exhibit the roughness of eroded surface, which related to the erosion rates.

Friction Coefficient of Epoxy-Based Fiber Composites

Attributed to their high specific characteristics, synthetic fiber-reinforced epoxy (ER) composites are widely applied in many advanced industries, which require durability and reliability (Kechaou et al. 2011). Friction coefficient is one of the tribological properties relevant to the industrial applications. Kechaou et al. (2008) investigated the friction behavior of epoxy-based industrial composite materials reinforced with glass fiber (GF). Their results revealed the enhancement of friction coefficient of the composites including great ability of electrical charge trapping at interface between fiber and matrix. They also studied on the effect of interfacial characteristics on the tribological and dielectric properties of three epoxy composites filled with glass fiber treated with different preparation methods, i.e., the GF treated with amino silane coupling agent (AC), polydimethylsiloxane (PDMS), and simple washing with ionized water (Kechaou et al. 2011). The tribological study revealed the nature of fiber/matrix interface affected the diffusion of electric charges, including the change of composite properties. For the GF treated with water, AC could generate new electric charge trapping areas, while that treated with PDMS could lead to electric charge spreading. To decrease the friction coefficient, the increase of electric charge trapping upon friction could lead to electrostatic cushion, resulting in the reduction of contact force.

The studies of friction coefficients of epoxy-based composites reinforced with carbon fiber (CF) have been conducted. Schön (2004a) determined the coefficient of friction (COF) of the ER composites in reciprocated sliding test of joint specimen. The wear mechanisms of the study were determined using scanning electron microscope (SEM). The values of initial COF and peak COF beyond wear were reported at 0.65 and 0.74, respectively. These high COF values exhibited a huge amount of load transferred by friction to a specimen at failure. Moreover, the slow wear of matrix and failure at the fiber/matrix interface were observed to be major wear mechanism. The researcher also conducted another study work of COF value for CF/ER composite in contact with aluminum (Schön 2004b). The results revealed that the initial COF value was increased with the increase of cycle number. Beyond the maximum COF value, gradual decrease of COF value was observed. In this case, the values of initial COF and peak COF beyond wear were reported at 0.23 and 0.68, respectively. The COF value did not have any relevance to normal load. Zhang et al. (2007) studied the effect of carbon fiber length on the COF value at different contact temperatures of the epoxy composites either with or without graphite flakes and nano-TiO_2. The test was conducted using a pin-on-disk wear tester. They exhibited that the average COF values was decreased with decreasing the average contact temperature. The length of carbon fiber added in the composites could have significant effects on COF values at steady period. The long carbon fiber led to the decrease of COF.

The friction and wear properties of epoxy composites reinforced with functionalized multiwalled carbon nanotubes (MWCNTs) were studied. The surfaces of MWCNTs were grafted with carbonyl and amino functional groups. Three types of MWCNTs were added into the resin, neat MWCNT, MWCNT with

carbonyl groups (a-MWCNT), and MWCNT with amino groups (b-MWCNT). The content of MWCNT was varied from 0 to 0.5wt%. The composites were tested with wear tester at various applied loads and sliding speeds. As seen in Table 3 and Fig. 13, the values of COF and wear rate were significantly increased with sliding speed. The enhancement of dispersibility of MWCNTs in the solvent was observed in a-MWCNT and b-MWCNT. The worn surfaces were observed via SEM. The results revealed that the composites reinforced with MWCNTs possessed less COF and wear rate values than pristine ER. Furthermore, when increasing the MWCNT content, the wear rate was decreased. The incorporation of MWCNTs in the composites could decrease the values of COF and enhance the wear resistance. In comparison with other composite types, the composites reinforced with 0.5wt% of b-MWCNTs rendered the highest wear resistance; the wear rate was lower by approximately 40% than pristine ER (Cui et al. 2013). Wang et al. (2013) studied the influence of adding carbon nanotube (CNT) on the friction and wear characteristics of epoxy (ER) composites reinforced with glass fiber (GF). The CNT surface treated with the acidic mixture of H_2SO_4 and HNO_3 could enhance the filler dispersion in the composites. As a result, the addition of CNTs with acid surface

Table 3 Approximated values of friction coefficient and wear rate of epoxy containing different types of MWCNTs (Cui et al. 2013)

	Friction coefficient		Wear rate ($\times 10^{-4}$ g/min)	
Type of filler	Low speed (r/min)	High speed (r/min)	Low speed (r/min)	High speed (r/min)
Pristine ER	0.61	0.70	2.3	25.5
Neat MWCNTs	0.58	0.68	2.3	25.0
a-MWCNTs	0.57	0.67	2.3	20.3
b-MWCNTs	0.58	0.65	2.2	20.0

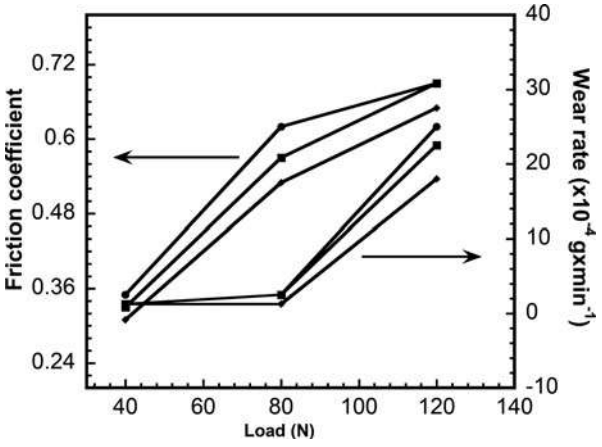

Fig. 13 Friction coefficient and wear rate of the epoxy composites at various loads (Cui et al. 2013)

Table 4 Approximated values of friction coefficient and wear rate of epoxy containing glass fiber and carbon nanotube at different sliding speeds (Wang et al. 2013)

	Friction coefficient		Wear rate ($\times 10^{-3}$ mm^3/Nm)	
Neat epoxy/composite	0.5 m/s	1.0 m/s	0.5 m/s	1.0 m/s
GF/ER	0.5	0.6	0.8	0.5
CNTs/GF/ER	0.4	0.5	0.4	0.3
a-CNTs/GF/ER	0.2	0.4	0.3	0.2

treatment could drastically decrease the COF values and enhance the wear resistance of the composites. In comparison with pure ER/GF composite at the sliding speed of 0.5 m/s, the COF values of the composites added with 0.5wt% of pure CNTs and treated CNTs were decreased for approximately 11% and 50%, respectively. As seen in Table 4, the specific wear rates of the composites added with 0.5wt% of pure CNTs and treated CNTs were decreased for approximately 58% and 67%, respectively (Wang et al. 2013). The tribological characteristics of epoxy composites reinforced with carbon nanotubes (CNTs) in forms of buckypaper were investigated by Han et al. (2015). In the study, the surface of CNTs was modified by ozone for enhancement of the interfacial adhesion. The results revealed that the COF value was decreased from ca. 0.7 (for pristine ER) to 0.3 (for ER composites with ozone-modified CNT buckypaper). Furthermore, ER/CNT composites consumed less time for COF values to become steady than pristine ER.

Study on Electromagnetic Interference (EMI) Shielding Effectiveness

EMI shielding properties have become interesting topics crucial for the protective applications of sensitive electronic devices and as the shelter for human being or environment. In general, the EMI shielding properties can be engendered by the reduction of signal moving throughout a system by certain ways such as wave absorption, backscattering of electromagnetic waves, multiple reflection, and decadence of the irradiation power in the materials (Munalli et al. 2019) as seen in Fig. 14. In general, many fillers to composite with polymeric materials are used, such as metals, intrinsically conductive polymers, carbon-based fillers, etc. Metallic components have great electrical conductivity; however, the corrosive sensitivity with great density and high difficulty of processing can restrict the applications of the filler.

As widely used for EMI shielding purposes, carbon fiber (CF) possesses many favorable properties such as outstanding electrical and mechanical properties with high corrosion resistance. However, the interfacial enhancement is needed due to poor compatibility to polymeric matrix (Wu et al. 2016). Munalli et al. (2019) developed the epoxy-based composites incorporated with continuous carbon fiber (CF). The results revealed the favorable EMI shielding effectiveness (SE) with the reflection mechanism. In the study, the related factors affecting the EMI-SE values

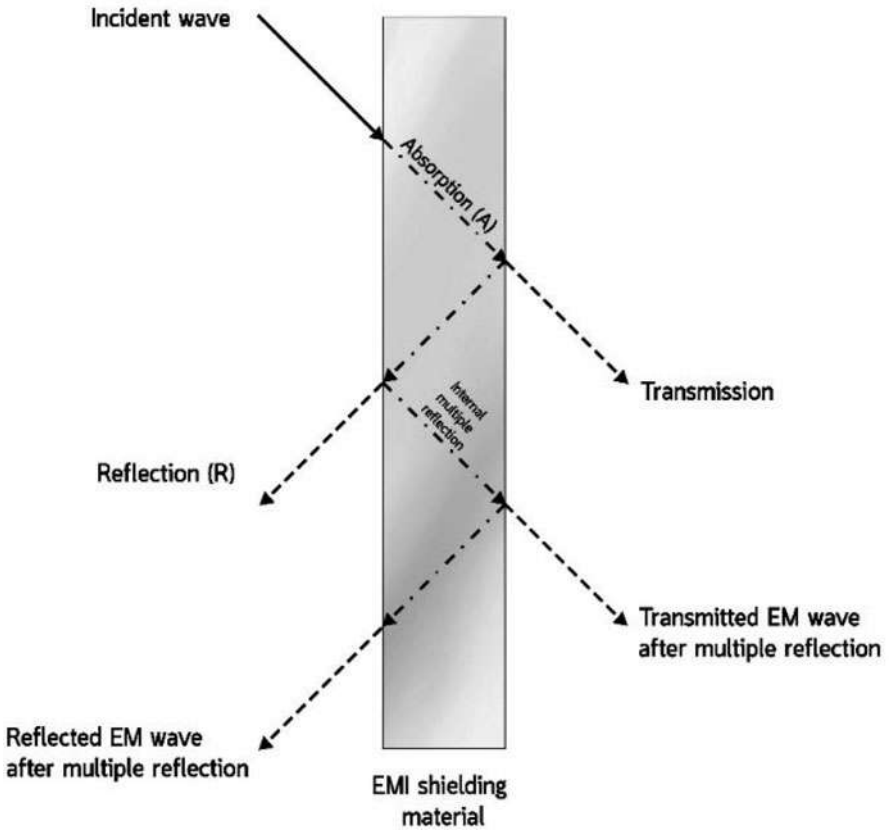

Fig. 14 Transmission and reflection of electromagnetic wave. (Reprinted with permission from Munalli et al. 2019)

were the volume ratio of fiber and number of layers. From the results, the epoxy resin reinforced with CF under the frequency in the range from 30 to 450 MHz provided the average EMI-SE values of approximately 73 and 82 dB for the composite samples reinforced with four and eight layers of CF fabric prepregs, respectively. Several years ago, in the work of Wu et al. (2016), carbon fiber modified with reduced graphene oxide (RGO) nanosheets was introduced in the epoxy resin. The reduction process was conducted using $NaBH_4$ solution. The composites were prepared via molding process. The electrophoretic condition on the shielding effectiveness (SE) was investigated. The Fourier transform infrared (FTIR) spectra exhibited that the RGO nanosheets were linked with surface of CF. The voltage and electrophoretic time had effects on shielding characteristics. The RGO/CF/ER composites have the highest value of EMI shielding effectiveness of approximately 38 dB at 21 Volts for 60 min, which was approximately 48% higher than CF/ER. At the same condition, the electrical conductivity was obtained at ca. 7 S/m. Moreover, the adjustment of electrophoretic conditions (i.e., RGO content, voltage, and time)

could lead to the high EMI shielding properties. The synergistic behaviors of EMI shielding effectiveness from the applications of both CF and RGO were observed. Li et al. (2015a) successfully incorporated graphene oxide (GO) into carbon fiber and epoxy composites by using wet process, leading to the improvement of interfacial characteristics between fiber and matrix. Furthermore, the EMI shielding properties were reported to be enhanced. The comparison between GO and RGO was conducted. The results exhibited that the dispersion quality of the fillers had an important effect on the properties of the composites. They also reported that the interfacial performance of CF/GO nanosheet/ER composites was improved by toughening effect. The addition of GO for 0.1 wt% could lead to 11% improvement of interlaminar shear strength. The enhancement for approximately 10 dB of EMI shielding effectiveness (SE) in the range of 5–20 GHz was observed; that was greatly a potential for industrial applications. The influence of oxygen content of RGO on the EMI shielding performance of CF/RGO/ER composites was investigated (Li et al. 2019). The composites were prepared by soaking the CFs in the acetone/epoxy solution consisting of RGO nanosheets. After that, the mixtures were heated for solvent evaporation and polymerization. The oxygen content of RGO could be tuned by reaction with hydrazine monohydrate and the adjustment of reaction temperature. The results presented that the incorporation of RGOs could increase the EMI shielding performance including its mechanical properties without the decrease of thermal properties. RGOs with higher oxygen content provided significantly higher EMI-SE value, while the ones with lower oxygen content possess greater mechanical properties. The developed high-performance composites showed potential to be used for advanced industrial sectors.

Li et al. (2015b) studied the EMI shielding performance of the composites derived from epoxy resin reinforced with low content of silver-plating carbon fiber (SPCF). On the CF surface, silver was coated with the thickness of 450 nm. At the SPCF content of 4.5wt%, the EMI-SE value at the X-band frequency ranging from 8.2 to 12.4 GHz was reported at 38–35 dB. The shielding mechanism was dominated by reflection.

Ucar et al. (2018) introduced continuous graphene oxide fiber (GOF), reduced graphene oxide fiber (RGOF), and multiwalled carbon nanotube (MWCNT) into the carbon fabric (CFA)/epoxy resin (ER) composites. They reported that the RGOF with two layers with the same orientation presented the increase of EMI-SE value, whereas the one with opposite orientation exhibited the decrease of EMI-SE value. The greatly rough surface of GOF and RGOF could lead to the lowering of EMI shielding performance because of the disruptive effect of multiple reflection from fiber roughness. Moreover, the MWCNT provides greater EMI shielding effectiveness than GOF and RGOF due to greater electrical conductivity without any disruptive reflection effect. The EMI shielding effectiveness of the composites filled with 15wt% MWCNT led to 32 dB of EMI-SE. However, the addition of either GOF or RGOF into the composites with 15wt% MWCNT led to the decrease of EMI-SE value due to disruptive effect of multiple reflection from rough fiber surface (Ucar et al. 2018). The EMI-SE values from this study are presented in Table 5.

Table 5 EMI-SE value of the tested composites (Li et al. 2015b)

Tested sample	EMI-SE value (dB)
ER + 2-ply CFA	12.3
ER + 2-ply CFA + 1.5wt% MWCNT	11.8
ER + 2-ply CFA + RGOF (2 layers/0°–0°) + 1.5wt% MWCNT	17.1
ER + 2-ply CFA + RGOF (2 layers/0°–90°) + 1.5wt% MWCNT	7.7
ER + 2-ply CFA + 15wt% MWCNT	32.0
ER + 2-ply CFA + GOF (2 layers/0°–90°) + 15wt% MWCNT	11.2
ER + 2-ply CFA + RGOF (2 layers/0°–90°) + 15wt% MWCNT	11.2

Zhang et al. (2015b) developed the epoxy composites reinforced with silicon carbide nanofibers of high aspect ratio (i.e., up to 300). The results revealed that at the frequency ranging from 26.5 to 40.0 GHz, the enhancement of EMI-SE values was observed to be greater than 10 dB at the content of 10wt%. The highest value was presented at 22.9 dB for 40 GHz. The incorporation of SiC could lead to the induction of effective conduction path and the increase of polarization of the composites. The mechanisms of shielding effects are mainly from absorption and minorly from reflection. The obtained high-performance composites had potentials for EMI shielding purposes.

Li et al. (2006) developed the epoxy composites reinforced with single-walled carbon nanotube (SWCNT). They reported the obtained composites could provide good EMI shielding performance with lightweight characteristics. The test frequency was conducted in the range from 10 MHz to 1.5 GHz. For the 15wt% of SWNT content, the maximum shielding effectiveness for 10 MHz was reported at ca. 49 dB, while that for the frequency range from 500 MHz to 1.5 GHz was reported in the range from 15 to 20 dB. The EMI shielding effectiveness was corresponding to the conductivity. Although carbon nanotube is one of the potential candidates to be composited with polymeric materials for EMI shielding applications, the low dispersibility should be considered.

Study on Optically Transparent Properties

The light transmission properties of composites have been a topic of interest for decades. Some transparent polymers, such as polymethyl methacrylate (PMMA) (Olson et al. 1992) and polycarbonate (PC) (Chrysostomou and Hashemi 1996), have been used as matrix. In general, the optical transparency of the fiber-filled composite systems depends on the fiber type and content. The fiber volume content should be low, and the difference of refractive index between matrix and fiber should be minimized. Glass fibers were commonly used due to its optical transparency in nature with preferable mechanical properties. Iba et al. (2002) fabricated epoxy composites reinforced with unidirectionally aligned continuous glass fiber. The diameter of the glass fiber in the system was varied, i.e., 18, 37, and 50 microns, with the volume fraction of the fiber in the range from 0.25 to 0.45. In the study, the

reflective index values of epoxy matrix and glass in bulk form were reported at 1.544 and 1.542, respectively. The transparent composites were successfully prepared. It was reported that for the wavelength in the range from 600 to 1100 nm, the light transmittance was ranging from 60 to 85%. Either the increase of fiber diameter or the decrease of fiber content could result in the increase of light transmittance. The tendency of light transparency was opposite to that of modulus and tensile strength.

Besides the effects of fiber content and reflective index, another factor related to the light transmission is fiber dispersion. Inam and Peijs (2006) prepared the epoxy composites reinforced with amino-modified multiwalled carbon nanotube composites (MWCNTs) via various dispersion methods, i.e., manual mixing, low power bath ultrasonication, high-power ultrasonic bath, tip ultrasonic process, twin screw mini-extrusion, high-speed mechanical mixing, and dual asymmetric centrifuging process. The amount of modified MWCNTs was as low as 0.05wt%. The light transmission of the composites was compared. The results revealed that the high-power ultrasonic bath provided the highest dispersion, while the low-power bath ultrasonication provided the lowest one. Transparent and flexible films derived from epoxy composites reinforced with MWCNTs with different aspect ratios were prepared by Saw et al. (2012). The results revealed that the composites filled with higher aspect ratio of MWCNTs (H-MWCNTs, with length of 5–15 microns and diameter of 10–20 nm) could provide lower electrical conductivity than those of composites with lower aspect ratio (L-MWCNTs, with length of 1–2 microns and diameter of 40–60 nm). This could be due to its better dispersion (i.e., lower agglomeration in nanoscale and uniform distribution of each nanofiller). Moreover, the high optical transparency in the range of 60–85% was observed at 550 nm. In general, the transparency of the composites depends on the properties of the filler including size, shape, and optical properties. When changing these filler properties, the reflection and light scattering related to transparency of the composites are changed. The results revealed that the light transparency of the composites containing H-MWCNTs was slightly higher than that of the composites containing L-MWCNTs. This could be attributed to the fact that L-MWCNT possess larger diameter, leading to higher reflection and light scattering.

Study on Environmental Degradation Behaviors

Degradation of Glass Fiber-Reinforced Epoxy Composites

Degradation characteristics are one of the crucial topics related to the durability of the materials in many fields (e.g., construction, automotive, and aerospace industries). The glass fiber and carbon fiber-reinforced composites are widely applied instead of steel and aluminum due to its favorable properties, such as high specific strength, corrosion resistance, good processability, and easiness to handing. The degradation behaviors after aging with different environments of the glass fiber-reinforced epoxy composites have been studied by Kajorncheappunngam et al. (2002). In the study, the commercial epoxy composites were immersed in four liquid

Table 6 Approximated weight percentage of main compositions for glass and basalt fiber

Type	SiO_2	Al_2O_3	Fe_xO_y	CaO	MgO	K_2O	TiO_2	Na_2O	B_2O_3
Glass fiber	53	14–15	0–1	19–20	4	0–1	0–1	–	8–9
Basalt fiber	48	15	15	8	5	2	4	3	–

Reprinted with permission from Wei et al. (2011)

medias (saturated salt, sodium hydroxide, distilled water, and hydrochloric acid) with the varied aging periods of 1, 3, and 5 months. The results revealed that the immersion of the composites in either hydrochloric acid at room temperature or the sodium hydroxide at 60 °C could lead to the decrease of the strength by not less than 70%, while the composites immersed in the saturated salt showed the least degradation effect on the mechanical properties. Wei et al. (2011) compared the degradation of the epoxy composites containing glass fiber and basalt fiber in seawater environment for various periods of treatment time. The approximated compositions of glass and basalt fibers are presented in Table 6. The mass gain ratio of the composites after treatment was obtained as presented in Eq. (2).

$$M = \frac{M_t - M_b}{M_b} \times 100\% \tag{2}$$

where M is the mass gain ratio and M_b and M_t are the mass before and after treatment, respectively. The change in mass gain could be attributed to two effects, i.e., water absorption and extraction of soluble materials. After immersion of the composite samples in seawater for 90 days, the color of seawater was turned from colorless to pale yellow. Many small channels were observed along the fiber direction. In addition, many cracks at the interface between the epoxy matrix and fibers were revealed. Although the main compositions of these two fibers are different, the corrosion behaviors of the composites containing glass and basalt fibers are small different. During immersion, the chloride ion and sodium ion including the molecules of water, oxygen, and carbon dioxide could penetrate the polymeric matrix as seen in Fig. 15. Some components (such as calcium and magnesium ions) could leak from the fibers. The degradation mechanism of the composites containing glass and basalt fibers is the reaction between ferrous ion (in the fiber) and chloride ion (in seawater) to form the rust at the interface which could absorb higher amount of water molecules.

Degradation of Carbon Fiber-Reinforced Epoxy Composites

Lv et al. (2006) studied the effect of environment on the degradation behaviors of the carbon fiber-reinforced epoxy composites. The unidirectional carbon fiber and weaved carbon fiber were incorporated in the composite systems. The tested samples were exposed to the irradiation from xenon lamp and ultraviolet light with varied humidity conditions and temperatures. The weight of two types of composites exhibited the similar trends, i.e., after 100-h exposure of ultraviolet, the weight values were drastically decreased. It could be due to the removal of material from

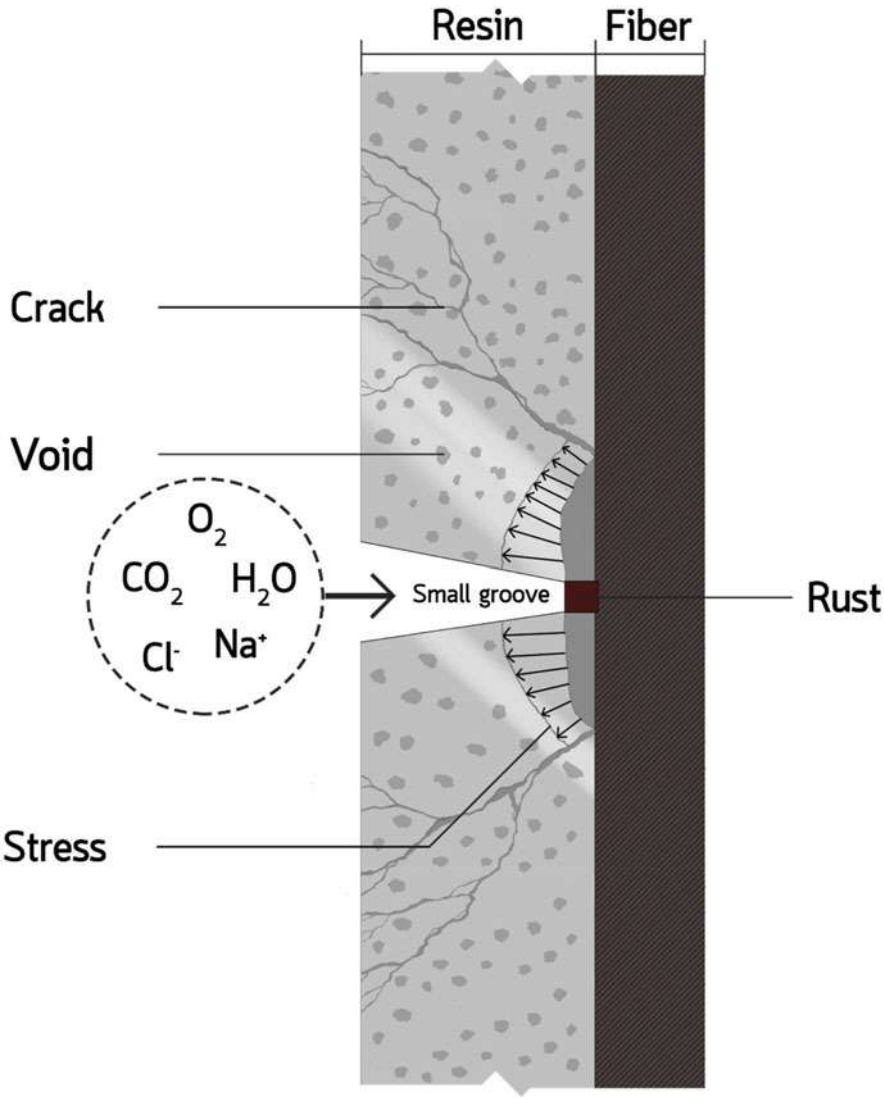

Fig. 15 Degradation of polymeric materials filled with basalt fiber in seawater. (Reprinted with permission from Wei et al. 2011)

the sample and the formation of some small cracks on the interface and the polymeric matrix. After 500-h exposure, the weight was significantly increased during humidity exposure attributed to the absorption of water. The change of weight loss was obviously observed in the case of the weaved fiber composites. These results corresponded to the work of Kumar et al. (2002) who reported that only the ultraviolet exposure for 500 h leads to ca. 0.3% decrease of weight, while only

the condensation exposure for 500 h results in ca. 0.9% increase of weight. The exposure of both ultraviolet and condensation could present the synergistic behaviors, engendering interfacial debonding and small cracks on matrix.

Conclusions

Epoxy resins (ERs) are the thermosets having been used for many decades. Many favorable properties of this polymer are high mechanical properties, great high thermal stability, and good chemical resistance. Many types of the thermoset are bisphenol-based epoxy resins, novolac-based epoxy resins, aliphatic epoxy resins, halogenated epoxy resins, glycidyl amine-based epoxy resins, and bio-based epoxy resins. Benzoxazine resins can be used as hardener of epoxy resins. The alloys of polybenzoxazine/epoxy resin were reported to possess synergistic behaviors of glass transition temperature (T_g). Moreover, the composites of ER alloyed with bio-based polybenzoxazine could provide favorable shape memory behaviors. It has been reported that the increase of curing agent could lead to the increase of T_g of the composites. The recovery time of pure epoxy resin hardened by aromatic amine was longer than that of the aliphatic epoxy alloyed with benzoxazine resin. The synthetic fibers, commonly reinforced in shape memory epoxy resin, are glass fiber, carbon fiber, and aramid fiber. In the study of tribological properties, epoxy composites containing synthetic fibers have been developed as anti-wear coating materials due to its outstanding erosive resistance. Many studies about EMI shielding materials derived from epoxy composites reinforced with carbon fibers have been conducted. In the study of optically transparent properties, many factors influence the transparency of the epoxy composites, i.e., fiber content, fiber type, reflective index, and fiber dispersion. For the study on the environmental degradation, many factors are relevant to the decomposition behaviors, such as fiber types, and environmental conditions. Moreover, the exposure of both ultraviolet and humidity could lead to synergy of composite decomposition.

References

R. Abishera, R. Velmuruga, K.V. Nagendra Gopal, Free, partial, and fully constrained recovery analysis of cold-programmed shape memory epoxy/carbon nanotube nanocomposites: Experiments and predictions. J. Intell. Mater. Syst. Struct. **29**(10), 2164–2176 (2018)

P. Antil, S. Singh, A. Manna, SiCp/glass fibers reinforced epoxy composites: Wear and erosion behavior. Indian J. Eng. Mater. Sci. **25**, 122–130 (2018)

N.M. Barkoula, J.K. Kocsis, Solid particle erosion on unidirectional GF reinforced EP composites with different fiber/matrix adhesion. J. Reinf. Plast. Compos. **21**, 1373–1388 (2002)

J. Chen, I.M. Hutchings, T. Deng, M.S.A. Bradley, K.K.K. Koziol, The effect of carbon nanotube orientation on erosive wear resistance of CNT-epoxy based composites. Carbon **73**, 421–431 (2014)

A. Chrysostomou, S. Hashemi, Influence of reprocessing on properties of short fibre-reinforced polycarbonate. J. Mater. Sci. **31**, 1183–1197 (1996)

L.J. Cui, H.Z. Geng, W.Y. Wang, L.T. Chen, J. Gao, Functionalization of multi-wall carbon nanotubes to reduce the coefficient of the friction and improve the wear resistance of multi-wall carbon nanotube/epoxy composites. Carbon **54**, 277–282 (2013)

H. Dodiuk, S.H. Goodman, *Handbook of Thermoset Plastics* (William Andrew, 2013), p. 800
J.H. Han, H. Zhang, P.F. Chu, A. Imani, Z. Zhang, Friction and wear of high electrical conductive carbon nanotube buckypaper/epoxy composites. Compos. Sci. Technol. **114**, 1–14 (2015)
A.P. Harsha, S.K. Jha, Erosive wear studies of epoxy-based composites at normal incidence. Wear **265**, 1129–1135 (2008)
R. Hooda, N. Kumar, Y. Sharma, Study and analysis on mechanical and wear behavior of SiC filled epoxy composite. Int. J. Recent Res. Civ. Mech. Eng. **2**, 241–252 (2015)
C. Horst, S. Tetsuya, S. Leslie, *Springer Handbook of Materials Measurement Methods* (Springer, 2006). https://doi.org/10.1007/978-3-540-30300-8
H. Iba, T. Chang, Y. Kagawa, Optically transparent continuous glass fibre-reinforced epoxy matrix composite: fabrication, optical and mechanical properties. Compos. Sci. Technol. **62**, 2043–2052 (2002)
F. Inam, T. Peijs, Transmission light microscopy of carbon nanotube-epoxy nanocomposites involving different dispersion methods. Adv. Compos. Lett. **15**(1), 7–12 (2006)
H. Ishida, D.J. Allen, Mechanical characterization of copolymers based on benzoxazine and epoxy. Polymer **37**, 4487–4495 (1996)
X. Jing, J. Wei, Y. Liu, B. Song, Y. Liu, Deployment analysis of aramid fiber reinforced shape memory epoxy resin composites. J. Eng. Sci. **11**, 44–53 (2020)
S. Kajorncheaqppunngam, R.K. Gupta, H.V.S. Gangarao, Effect of aging environment on degradation of glass-reinforced epoxy. J. Comps. Constr. **6**, 61–69 (2002)
H. Kalelia, New universal tribometer as pin or ball-on-disc and reciprocating pin-on-plate types. Tribol. Ind. **38**(2), 235–240 (2016)
B. Kechaou, C. Turki, M. Salvia, Z. Fakhfakh, D. Treheux, Dielectric and friction behavior of unidirectional glass fibre reinforced epoxy (GFRE). Wear **265**(5), 763–771 (2008)
B. Kechaou, M. Salvia, K. Benzarti, C. Turki, Z. Fakhfakh, D. Treheux, Role of fiber/matrix interphases on dielectric, friction, and mechanical properties of glass fiber-reinforced epoxy composites. J. Compos. Mater. **46**(2), 131–144 (2011)
B.G. Kumar, R.P. Singh, T. Nakamura, Degradation of carbon fiber-reinforced epoxy composites by ultraviolet radiation and condensation. J. Compos. Mater. **36**(24), 2713–2731 (2002)
N. Li, Y. Huang, F. Du, X. He, X. Lin, H. Gao, Y. Ma, F. Li, Y. Chen, P.C. Eklund, Electromagnetic interference (EMI) shielding of single-walled carbon nanotube epoxy composites. Nano Lett. **6**(6), 1441–1445 (2006)
Y. Li, Y. Zhao, J. Sun, Y. Hao, J. Zhang, X. Han, Mechanical and electromagnetic interference shielding properties of carbon/graphene nanosheets/epoxy composite. Polym. Compos. (2015a). https://doi.org/10.1002/pc.23436
J. Li, S. Qi, M. Zhang, Z. Wang, Thermal conductivity and electromagnetic shielding effectiveness of composites based on Ag-plating carbon fiber and epoxy. J. Appl. Polm. Sci. (2015b). https://doi.org/10.1002/APP42306
Y. Li, S.T. Liu, J.M. Sun, S. Li, J.L. Chen, Y. Zhao, Effects of the oxygen content of reduced graphene oxide on the mechanical and electromagnetic interference shielding properties of carbon fiber/reduced graphene oxide-epoxy composites. New Carbon Mater. **34**(5), 489–498 (2019)
C. Likitaporn, P. Mora, S. Tiptipakorn, S. Rimdusit, Recovery stress enhancement in shape memory composites from silicon carbide whisker-filled benzoxazine epoxy polymer alloy. J. Intell. Mater. Syst. Struct. **29**, 388–396 (2018)
Y. Liu, C. Han, H. Tan, X. Du, Thermal, mechanical and shape memory properties of shape memory epoxy resin. Mater. Sci. Eng. A **527**, 2510–2514 (2010)
Y. Liu, J. Zhao, L. Zhao, W. Li, H. Zhang, X. Yu, Z. Zhang, High performance shape memory epoxy/carbon nanotube nanocomposites. ACS Appl. Mater. Interfaces **8**, 311–320 (2016)
Y. Liu, Y. Guoa, J. Zhao, X. Chen, H. Zhang, G. Hud, X. Yue, Z. Zhang, Carbon fiber reinforced shape memory epoxy composites with superior mechanical performances. Compos. Sci. Technol. **177**, 49–56 (2019)
X. Lv, Q. Zhang, G. Xie, G. Liu, Degradation of carbon fiber/epoxy composites by Xe lamp and humidity. Int. J. Mod. Phys. B **20**, 3686–3691 (2006)
G. Lv, N. Zhanga, M. Huanga, C. Shena, J. Castroc, K. Tand, X. Liua, C. Liu, The remarkably enhanced erosion resistance and toughness properties of glass fiber/epoxy composites via

thermoplastic polyurethane nonwoven fabric. Polym. Test. (2018). https://doi.org/10.1016/j.polymertesting.2018.06.005
D. Munalli, G. Dimitrakis, D. Chronopoulos, S. Greedy, A. Long, Electromagnetic Shielding effectiveness of carbon fibre reinforced composites. Compos B Eng. **173**, 06906 (2019)
X. Ning, H. Ishida, Phenolic materials via ring-opening polymerization: Synthesis and characterization of bisphenol-A based benzoxazines and their polymers. J. Polym. Sci. Part A **32**, 1121–1129 (1994)
J.R. Olson, D.E. Day, J.O. Stoffer, Fabrication and mechanical properties of an optically transparent glass fiber/polymer matrix composite. J Comp Matter **26**, 1181–1192 (1992)
P. Panda, S. Manytry, S. Mohapatra, S.K. Singh, A. Satapathy, A study on erosive wear analysis of glass fiber–epoxy–AlN hybrid composites. J. Compos. Mater. **48**(1), 107–118 (2014)
A. Papadopoulos, G. Gkikas, A.S. Paipetic, N.M. Barkoula, Effect of CNT addition on the erosion wear response of epoxy resin and carbon fibre composites. Compos. Part A **84**, 299–307 (2016)
J. Parameswaranpillai, S.P. Ramanan, J. Seno, S. Siengchin, A. Magueresse, A. Janke, J. Pionteck, Shape memory properties of epoxy/PPO–PEO–PPO triblock copolymer blends with tunable thermal transitions and mechanical characteristics, industrial and engineering chemistry research. Am. Chem. Soc. **56**, 14069–14077 (2017)
J. Plylaharn, M. Okhawilai, S. Rimdusit, High recovery stress obtained in benzoxazine-epoxy shape memory polymers reinforced with carbon fiber, in *Proceeding in the 2018 Pure and Applied Chemistry International Conference (PACCON 2018)*, (Songklanakarin, Thailand, 2018)
W. Prasomsin, T. Parnklang, C. Sapcharoenkun, S. Tiptipakorn, S. Rimdusit, Multiwalled carbon nanotube reinforced bio-based benzoxazine/epoxy composites with NIR-laser stimulated shape memory effects. Nanomaterials **9**, 881 (2019). https://doi.org/10.3390/nano9060881
E. Ramon, C. Sguazzo, P.M.G.P. Moreira, A review of recent research on bio-based epoxy systems for engineering applications and potentialities in the aviation sector. Aerospace **5**, 110 (2018)
K.S. Rao, Y.S. Varadarajan, N. Rajendra, Erosive wear behavior of carbon fiber-reinforced epoxy composite. Mater Today Proc. **2**, 2975–2983 (2015)
S. Rimdusit, P. Hombunma, Shape memory polymer from Vanillin based Polybenzoxazine/castor oil-based epoxy copolymer, in *Proceeding in ICCE, July 15–21, 2018*, (France, 2018)
S. Rimdusit, P. Kunopast, I. Dueramae, Thermomechanical properties of arylamine-based benzoxazine resins alloyed with epoxy resin. Polym. Eng. Sci. **51**, 1797–1807 (2011)
S. Rimdusit, C. Jubsilp, S. Tiptipakorn, Alloys and composite of polybenzoxazines properties and application, in *Engineering Materials*, (Springer, 2013a). https://doi.org/10.1007/978-981-4451-76-5
S. Rimdusit, S. Tiptipakorn, C. Jubsilp, T. Takeichi, Polybenzoxazine alloys and blends: Some unique properties and application. React. Funct. Polym. **73**(2), 369–380 (2013b)
S. Rimdusit, M. Lohwerathama, K. Hemvichian, P. Kasemsiri, I. Dueramae, Shape memory polymers from benzoxazine-modified epoxy. Smart Mater. Struct. **22**, 075033 (2013c)
I.A. Rousseau, Challenges of shape memory polymers: A review of the progress toward overcoming SMP's limitations. Polym. Eng. Sci., 48090–49055 (2008)
L.N. Saw, M. Mariatti, A.R. Azura, A. Azizan, J.K. Kim, Transparent, electrically conductive, and flexible films made from multiwalled carbon nanotube/epoxy composites. Compos. Part B **43**, 2973–2979 (2012)
J. Schön, Coefficient of friction and wear of a carbon fiber epoxy matrix composite. Wear **257**, 395–407 (2004a)
J. Schön, Coefficient of friction for aluminum in contact with a carbon fiber epoxy composite. Tribol. Int. **37**, 395–404 (2004b)
C. Shang, X. Zhao, B. Sun, X. Yang, Y. Zhang, W. Huang, Synthesis and properties of novel trifunctional epoxy triglycidyl of 4-(4-aminophenoxy) phenol with high toughness. J. Appl. Polym. Sci. **132**, 41878 (2015)
C. Sharma, S.R. Kumar, *Erosion Analysis of Aramid Fiber-Epoxy Composite* (Springer, Singapore, 2019)
M.J. Shukla, D.S. Kumar, K.K. Mahato, D.K. Rathore, R.K. Prusty, C. RayB, A comparative study of the mechanical performance of Glass and Glass/Carbon hybrid polymer composites at different temperature environments. Mater. Sci. Eng. **75**, 012002 (2015)

T. Tanpitaksit, C. Jubsilp, S. Rimdusit, Effects of benzoxazine resin on property enhancement of shape memory epoxy: A dual function of benzoxazine resin as a curing agent and a stable network segment. Express Polym Lett **9**, 824–837 (2015)
U.S. Tewari, A.P. Harsha, A. Hager, Solid particle erosion of carbon fibre- and glass fibre-epoxy composites. Compos. Sci. Technol. **63**, 549–557 (2003)
P. Thirukumaran, A. Shakila Parveen, M. Sarojadevi, Synthesis and copolymerization of fully biobased benzoxazines from renewable resources. ACS Sustain. Chem. Eng. **2**, 2790–2801 (2014)
N. Ucar, B.K. Kayaoğlu, A. Bilge, G. Gurel, P. Sencandan, S. Paker, Electromagnetic shielding effectiveness of carbon fabric/epoxy composite with continuous graphene oxide fiber and multiwalled carbon nanotube. J. Compos. Mater. **52**, 3341–3350 (2018)
C. Verma, L.O. Olasunkanmi, E.D. Akpan, M.A. Quraishi, O. Dagdag, M.E.L. Gouri, E.L.M. Sherif, E.E. Ebenso, Epoxy resins as anticorrosive polymeric materials: A review. React. Funct. Polym. **156**, 104741 (2020)
S. Vigneshwaran, M. Uthayakumar, V. Arumugaprabu, A review on erosion studies of fiber-reinforced polymer composites. J. Reinf. Plast. Compos. **36**(14), 1019–1027 (2017)
T.S. Wang, J.K. Parng, M.D. Shau, The synthesis and properties of new epoxy resin containing phosphorus and nitrogen groups for flame retardancy. J. Appl. Polym. Sci. **74**, 413–421 (1999)
R.M. Wang, S.R. Zhang, Y.P. Zhang, *Polymer matrix composites and technology* (Elsevier, Cambridge, 2011)
Y. Wang, Z. Xu, L. Chen, Effect of carbon nanotubes on friction and wear properties of glass fiber/epoxy composites. Appl. Mech. Mater. **44–47**, 2181–2185 (2013)
B. Wei, H. Cao, S. Song, Degradation of basalt fiber and glass fiber/epoxy resin composites in seawater. Corros. Sci. **53**, 426–431 (2011)
J. Wei, S. Ma, H. Yue, S. Wang, J. Zhu, Comparison of hydrogenated bisphenol A and bisphenol A epoxies: curing behavior, thermal and mechanical properties, shape memory properties. Macromol. Res. **26**, 529–538 (2018)
X. Wu, H. Zheng, Y. Liu, Thermomechanical property of epoxy shape memory polymers. Int. J. Mod. Phys. B **24**, 2386–2391 (2010)
J. Wu, J. Chen, Y. Zhao, W. Liu, W. Zhang, Effect of electrophoretic condition on the electromagnetic interference shielding performance of reduced graphene oxide-carbon fiber/epoxy resin composites. Compos B Eng. **105**, 167–175 (2016)
H. Zhang, Z. Zhang, K. Friedrich, Effect of fiber length on the wear resistance of short carbon fiber reinforced epoxy composites. Compos. Sci. Technol. **67**(2), 222–230 (2007)
N. Zhang, F. Yang, C. Shen, J. Castro, J. Lee, Particle erosion on carbon nanofiber paper coated carbon fiber/epoxy composites. Compos B Eng. **54**, 209–214 (2013)
F. Zhang, Z. Zhang, Y. Liu, W. Cheng, Y. Huang, J. Leng, Thermosetting epoxy reinforced shape memory composites microfiber membranes: Fabrication, structure, and properties. Compos. Part A **76**, 54–61 (2015a)
Y. Zhang, Z. Wang, B. Zhang, G.L. Zhao, S.M. Guo, The electromagnetic interference shielding effectiveness of high aspect-ratio SiC nanofibers/epoxy composites. Spec. Publ. R. Soc. Chem. **5**, 93499–93506 (2015b)
D. Zhang, E. Cabrera, Y. Zhao, Z. Zhao, J.M. Castro, Improved sand erosion resistance and mechanical properties multifunctional carbon nanofiber nanopaper-enhanced fiber reinforced epoxy composites. Adv. Polym. Technol., 1–8 (2017)
N. Zheng, J. He, D. Zhao, Y. Huang, J. Gao, Y.W. Mai, Improvement of atomic oxygen erosion resistance of carbon fiber and carbon fiber/epoxy composite interface with a silane coupling agent. Mater. Des. **109** (2016). https://doi.org/10.1016/j.matdes.2016.07.004
L. Zhihua, H. Jiankang, M. Li, L. Hongxin, Shape memory CTBN/epoxy resin/cyanate ester ternary resin and their carbon fiber reinforced composites. J. Appl. Polym. Sci., 48756 (2019)
J. Zhu, G. Fang, Z. Cao, X. Meng, H. Ren, A Self-folding dynamic covalent shape memory epoxy and its continuous glass fiber composite. Ind. Eng. Chem. **57**(15), 5276–5281 (2018)

The Effect of Environmental Conditions on the Synthetic Fiber-Reinforced Epoxy Composites

12

Moslem Najafi, Reza Eslami-Farsani, Ali Saeedi, and Hossein Ebrahimnezhad-Khaljiri

Contents

Abstract

Fiber-reinforced epoxy (FRE) composites are increasingly utilized in a broad range of industrial applications where long-term reliable service in hostile environments is required. However, there are still unresolved questions regarding these materials' durability when exposed to different environmental conditions. The most important environmental factors contributing to degradation in

M. Najafi · R. Eslami-Farsani (✉) · H. Ebrahimnezhad-Khaljiri
Faculty of Materials Science and Engineering, K. N. Toosi University of Technology, Tehran, Iran
e-mail: moslem.najafi@kntu.ac.ir; eslami@kntu.ac.ir; ebrahimnezhad-k@email.kntu.ac.ir

A. Saeedi
Faculty of Mechanical Engineering, Iran University of Science and Technology, Tehran, Iran
e-mail: asaeedi@mail.iust.ac.ir

S. Mavinkere Rangappa et al. (eds.), *Handbook of Epoxy/Fiber Composites*,
https://doi.org/10.1007/978-981-19-3603-6_16

FRE composites include temperature variations, moisture, ozone, saltwater, ultraviolet radiation, corrosive solutions, elevated/cryogenic temperatures, etc. These factors can adversely affect the physical, chemical, and mechanical properties of FRE composites leading to various types of degradation mechanisms. Therefore, understanding the durability behavior of FRE composites is one of the major challenges facing these materials for wider use in more advanced applications. This chapter aims to cover a brief review of several aspects of environmental durability, with a large emphasis on common degradation mechanisms associated with FRE composites and their consequences on mechanical properties.

Keywords

Epoxy resins · Synthetic fiber-reinforced epoxy composites · Environmental conditions · Degradation mechanisms · Mechanical properties

Introduction

Over the past few decades, fiber-reinforced plastics (FRPs) have increasingly gained interest in many structural applications. The main reasons for this trend include their outstanding properties such as high specific stiffness and strength, ease of fabrication, excellent fatigue behavior, and corrosion resistance compared to traditional metal alloys such as steel (Ellyin and Maser 2004). Today, the various types of FRPs are used in the aerospace, marine, and automotive fields where high reliability must be maintained. On the other hand, aircraft, ships, and automobiles will experience contact with a wide range of cold, hot, dry, and humid environments during storage or operation. Regarding the long-term and frequent operation of these vehicles during their service life, it is necessary to preserve the original properties of their structural components as much as possible. Unfortunately, despite all the advantages of FRPs, most of them, especially those manufactured from traditional thermoset polymeric resins (e.g., epoxy, vinyl ester, and polyester), are highly sensitive to environmental conditions.

The structures and vehicles made from FRPs may experience a wide range of environmental conditions such as electromagnetic effects, fire, high and low temperatures, lightning and electric discharge, ozone, ultraviolet (UV) radiation, erosion by rain and sand, low-velocity impacts, moisture absorption, and contact with organic liquids (such as fuels, oils, acids, and alkalis) during their service life. However, moisture, high and low temperatures, and moisture/temperature fluctuations are often considered as major threats to composites structures in the long-term mode. Unlike industrial fluids (such as fuel and hydraulic oil), moisture is often present in the environment which can significantly affect both the physical and mechanical properties of all types of FRPs. The weight gain and degradation of mechanical properties are commonly considered as two undesirable consequences of the moisture absorption in FRP composite structures (Park et al. 2010). Since the

temperature can severely fluctuate due to solar radiation, the generation of internal stresses within the structure is an expected issue. In passenger aircraft, a significant number of deaths are related to fires. Unlike metallic materials, heat and fire can quickly reduce the strength and integrity of the FRPs and lead to catastrophic failure in structure, which is a critical issue in aerospace and marine structures (Liu et al. 2020).

In the case of thermoset plastics, it has been recognized that the cured epoxy resins have a densely cross-linked molecular structure. Therefore, they can exhibit better mechanical properties and higher resistance to environmental factors compared to other well-known thermoset plastics such as polyester or vinyl ester resins (Bai 2013). Thanks to their unique characteristics, nowadays, epoxy resins are extensively used in manufacturing applications such as coatings, adhesives, electronics, as well as automotive, marine, and aerospace structures. In advanced structural applications such as aviation and aerospace industries, where strength, stiffness, durability, and lightweight are strongly required, the fiber-reinforced epoxy (FRE) composites are typically considered as one of the best candidates (Bai 2013). Traditional synthetic fibers such as glass and aramid are mostly used for manufacturing the nonstructural FRE parts of some aircraft, whereas carbon and boron fiber-reinforced epoxy composites are specifically intended for more critical structural elements such as surfaces furniture and aircraft tail (Bai 2013). Due to the good chemical resistance of epoxy resins, they are also used to produce paints and protective coatings to protect metals against corrosion (Bai 2013). Several studies have shown that the FRE composites perform much better than polyester ones in aqueous environments due to their good chemical properties. Thus, besides the aerospace applications, they can be also of concern in the marine industry where seawater resistance is a crucial issue.

However, all the above discussed does not mean that FRE composites can fully retain their original properties in all environmental conditions. To ensure economical and safe operation during the entire lifetime, evaluating the environmental durability of such composites is critical. Therefore, this chapter's scope is to cover some aspects of degradation mechanisms and durability of epoxy-based composites reinforced by common synthetic fibers (e.g., glass, carbon, aramid, etc.) under exposure to different environmental factors, in particular moisture and temperature.

Effect of Moisture on the Synthetic Fiber-Reinforced Epoxy Composites

Synthetic fiber-reinforced epoxy composites are gaining widespread interest in recent years for use in aqueous and humid tropical environments, especially advanced marine applications including naval ships, patrol boats, manned or unmanned vehicles, submarines, propellers, and marine infrastructures. The emphasis on the use of epoxy resins in advanced marine structures is mainly because they do not emit volatile and dangerous products (e.g., styrene) during

the curing process, have a low shrinkage (only 3–4%), establish a high adhesion to several materials, and process higher resistance to water degradation than polyester ones (Bai 2013). Unlike the polyester and vinyl ester resins in which ester groups make them vulnerable to water degradation, the epoxy resins' molecular structure processes higher water-induced degradation resistance. However, exposure to harsh marine environments, including prolonged water immersion, hygrothermal influences, changing weather conditions, and salinity, remains as a crucial issue for each structural material considered for long-term application in marine conditions.

It is well-known that moisture ingress can induce physical and chemical changes in epoxy-based composites through two main processes. These mechanisms can reversibly alter the physical state and irreversibly change the chemical structure of the material. If water can penetrate the polymeric matrix, the interaction of the water polar molecules with the matrix polar groups may lead to plasticization as an outstanding physical phenomenon. Water molecules can push polymer chains apart and increase free volume (Kotsikos et al. 2007). This phenomenon is commonly accompanied by matrix softening, reduction in elastic modulus of the resin, as well as depressing its glass transition temperature (Tg) (Kotsikos et al. 2007). However, considering the plasticization is a physical mechanism, its resulting consequences are partially reversible upon drying, and the original properties may be recovered. The hydrolysis accompanied by the permanent change in T_g of polymer, especially in the unsaturated polyesters, is a typical chemical aging indication. The hydrolysis of ester groups can cut the network strands in polyesters, leading to generate organic molecules ultimately responsible for the osmotic cracking phenomenon (Davies and Rajapakse 2014). Chemical aging usually has more detrimental effects on the original properties of organic resins compared to physical ones.

The water absorption mechanisms in epoxy resins and their composites are mainly linked to the water molecules' diffusion within the micro gaps between epoxy chains and microcracks within the matrix. Water absorption is typically considered as a slow process that is mainly dependent on the diffusion coefficient of the material. Some high-performance epoxies with a relatively high hydrophilic nature can absorb water even up to 7 wt.% (Davies and Rajapakse 2014). The loss of mechanical properties in the amine cross-linked epoxy category is mainly due to water absorption and its swelling effect on the matrix. The absorbed water as a plasticizer can depress the T_g of the epoxy matrix, which ultimately reduces the mechanical properties of the FRE composite. On the other hand, the hydrolysis-induced failures can be greatly found in the anhydride cured epoxies category in which hydrophilicity is relatively low but having hydrolyzable groups (Davies and Rajapakse 2014).

It is well-known that the fiber-matrix interfaces contain several types of inherent defects related to the manufacturing process, e.g., curing-induced microcracks, micro-voids/air bubbles, and poor wetting of the fibers. These imperfections can act as a path for more water ingress during the hygrothermal aging process. As these imperfections grow, hygrothermal-induced mechanisms can dramatically influence the interfacial properties, involving significant decreases in mechanical properties of

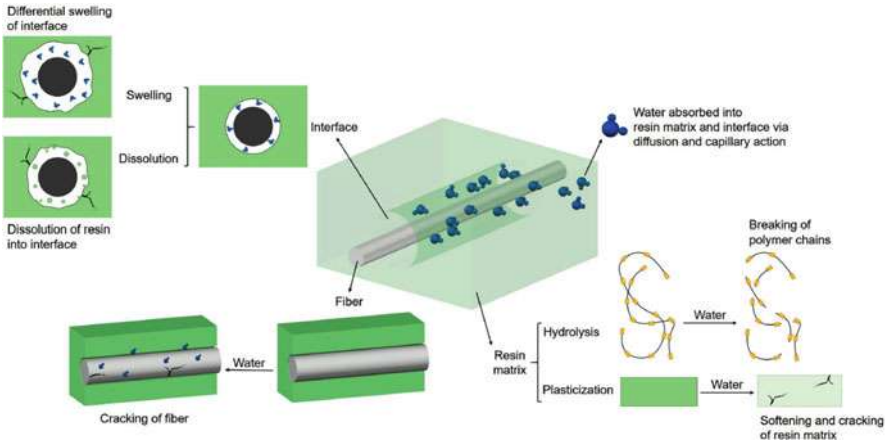

Fig. 1 Degradation mechanisms of FRPs exposed to hygrothermal conditions (Liu et al. 2020)

FRE composites. It was reported that fiber-matrix interfaces are very prone to hydrolysis and chemical attack. Additionally, water absorption can promote osmotic pressure within interfaces, contributing to the weakening of fiber-matrix interfacial bonding, and chemical decomposition of the synthetic fibers, particularly glass fibers (Weitsman 2012). Water absorption can also create microcracks on the surface of the fibers, which consequently leads to fiber rupture. While the moist environments have a negligible adverse effect on conventional synthetic fibers, especially carbon, the aramid fibers contain hydrophilic amide groups that are significantly susceptible to moisture-induced degradation. Figure 1 (Liu et al. 2020) schematically represents the various types of degradation mechanisms of FRPs under exposure to moist conditions.

Although FRE composites are mainly susceptible to moisture effects, however, this sensitivity is highly material-dependent. It means that the type and nature of fiber and epoxy resin, manufacturing method, curing process, imperfections, and quality of interfacial bonding between fibers and epoxy resin are determining factors in how the FRE composites respond to moist environments. Similarly, the water absorption behavior of FRE composites is controlled by three main factors of hydrophilic nature of resin and the fibers, fibers/resin interfacial bonding, and voids content in the composite.

Since hygrothermal aging, hygrothermal cycling, and saltwater are commonly considered as the main threatening environmental factors of FRE composites in moist environments, they are discussed separately below.

Hygrothermal Aging

Hygrothermal aging is a generic category of environmental conditioning in which the combination of moisture and temperature can degrade the material properties. During the hygrothermal aging process in polymeric resins, the amount and rate of

water absorbed as well as the structural response of resin profoundly depend on some characteristics of the resin such as its relaxation behavior in the presence of elevated temperature and moisture, void content, T_g, molecular structure, and morphology of the resin (Rull et al. 2015). It has been found that increasing the aging time and temperature has more detrimental effects on the original properties of the epoxy-based composite under exposure to hygrothermal aging. Elevated temperatures can significantly accelerate the saturation of the FRE composites due to increased diffusivity. The effect of moisture and temperature on the mechanical properties of glass/epoxy composites was investigated by Ellyin and Maser (Ellyin and Maser 2004). It was found that the moisture absorption rate of the composite specimens at high temperature (50 °C) is noticeably greater than those of room temperature (20 °C). The marginal reduction of stiffness and strength with the moisture absorption and increasing the temperature was also observed.

Typical mass change data for glass/epoxy (G-E), carbon/epoxy (C-E), and hybrid laminated bidirectional composites immersed in distilled water at 24, 70, and 90 °C is illustrated in Fig. 2. The results indicate that rising temperature could affect water molecules' activity, accelerating the water penetration and decreasing the necessary time to reach the plateau in hydrothermally aged epoxy-based composites. After the saturation level, at lower temperature, i.e., 24 °C, the water absorption tended to attain a plateau, in contrast, a reduction in the mass gain due to leaching of the epoxy matrix at higher temperatures was evident, as shown in Fig. 2b, c. It was found that the hydrophilic nature of glass fibers associated with its polarity led to the increase in both the diffusion coefficient and maximum moisture absorption of G-E composites compared to those contain carbon fibers (Guermazi et al. 2016).

Plots relating thermomechanical properties indicate the higher values of storage modulus for C-E composites compared to G-E ones, which can be attributed to the stiff character of carbon-reinforced epoxy composites, arresting the easy molecular chain movement when increasing the temperature. As shown in Fig. 3, plasticization and swelling caused by the hygrothermal aging process lowered the storage modulus of FRE composites and shifted T_g to lower values (Guermazi et al. 2016).

Several researchers made significant efforts to investigate the moisture absorption behavior and associated changes in mechanical properties of FRE composites under exposure to hygrothermal aging. Although the majority of these researches indicate the deterioration in original properties due to hygrothermal aging, the signs of enhancement are sometimes evident. It has also been reported that both the matrix and interface-dominated properties, such as the flexural and shear ones, are dramatically affected in this case. For example, Zhong et al. presented results from a study of the epoxy reinforced by unidirectional carbon fibers (C/Ep) composites aged in the water at 60 °C (Zhong and Joshi 2015a). The effect of hygrothermal aging at 80 °C for 54 days on Mode I fracture toughness of C/Ep composite through double cantilever beam (DCB) test was evaluated, as shown in Fig. 4. Accordingly, the hygrothermal aging could significantly increase the initiation energy release rate Mode I (G_{IC}) in the studied C/Ep composite. These observations were attributed to softness caused by moisture absorption which prevented the abrupt and rapid crack propagation in the aged specimens. On the other hand, it

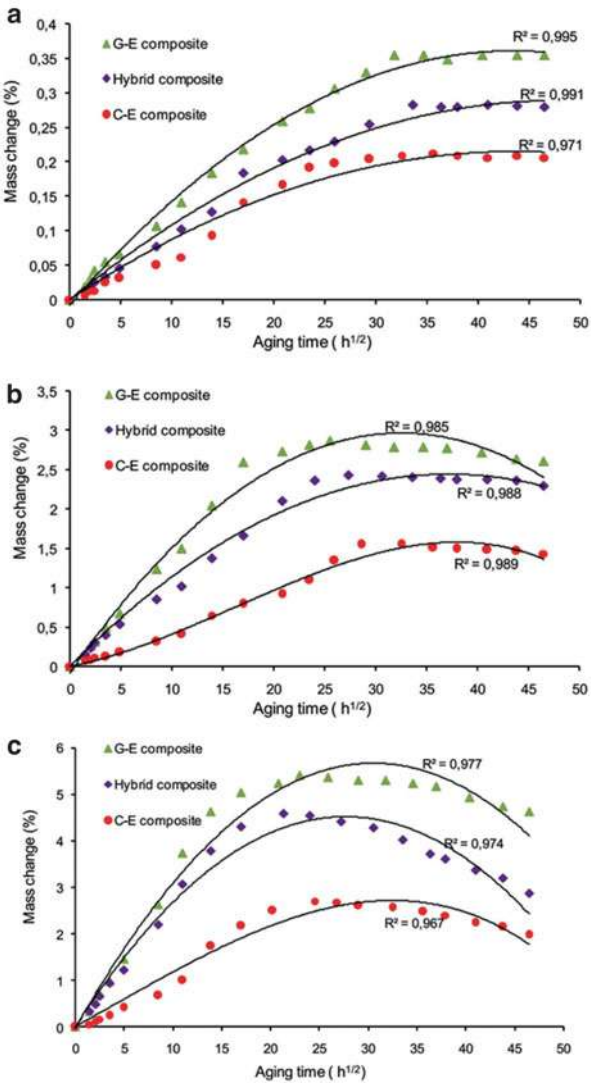

Fig. 2 Mass change as function of the square root of time ($h^{1/2}$) for the G-E (glass/epoxy), C-E (carbon/epoxy), and hybrid (glass/carbon/epoxy) composites under exposure to distilled water at, (**a**) 24 °C, (**b**) 70 °C, and (**c**) 90 °C (Guermazi et al. 2016)

is well-known that the Mode I fracture toughness of laminated composites is often considered as a matrix-dominated property, and both the strength and stiffness of the epoxy matrix can be adversely affected by the moisture uptake. Therefore, in hydrothermally aged specimens, the peeling resistance of the epoxy resin at the interlaminar region was likely to be decreased accompanied by a reduction in propagation G_{IC}.

The scanning electron microscopy (SEM) examination of surfaces of the mid-plane interface of DCB specimens demonstrates a large volume of the debonded

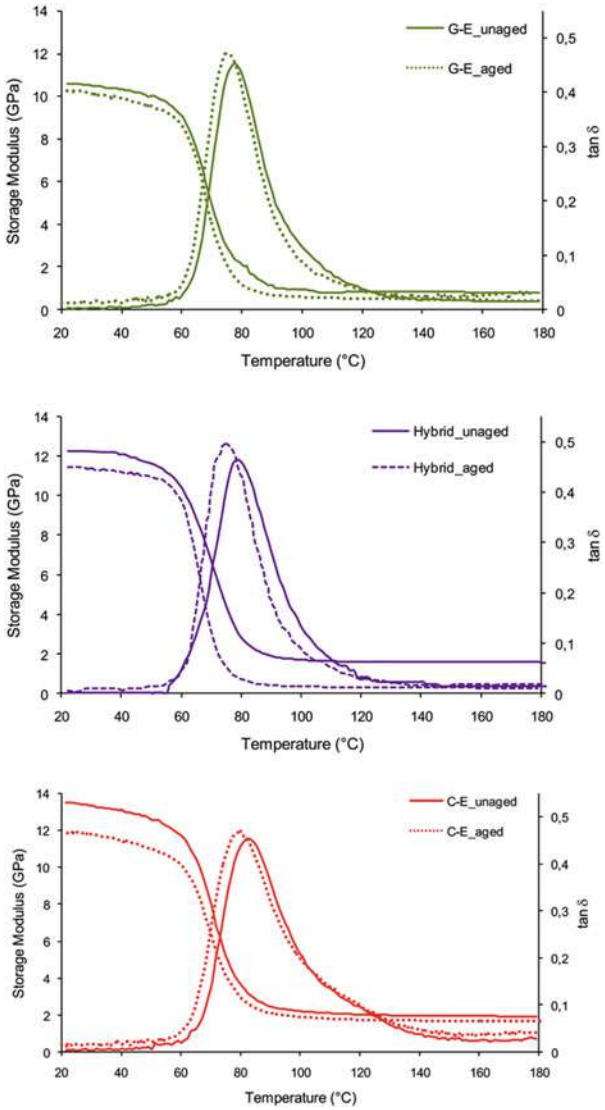

Fig. 3 Storage modulus and glass transition temperature for un-aged (dry) and aged (after 90 days of water immersion at 70 °C) for G-E (glass/epoxy), C-E (carbon/epoxy), and hybrid (glass/carbon/epoxy) composites (Guermazi et al. 2016)

fibers from the epoxy resin (Surface A) and a layer of pure matrix resin without any fibers at the inverse surface (Surface B) in aged CE specimens. This indicates the severe weakening of fiber/epoxy resin adhesion due to hygrothermal aging, as

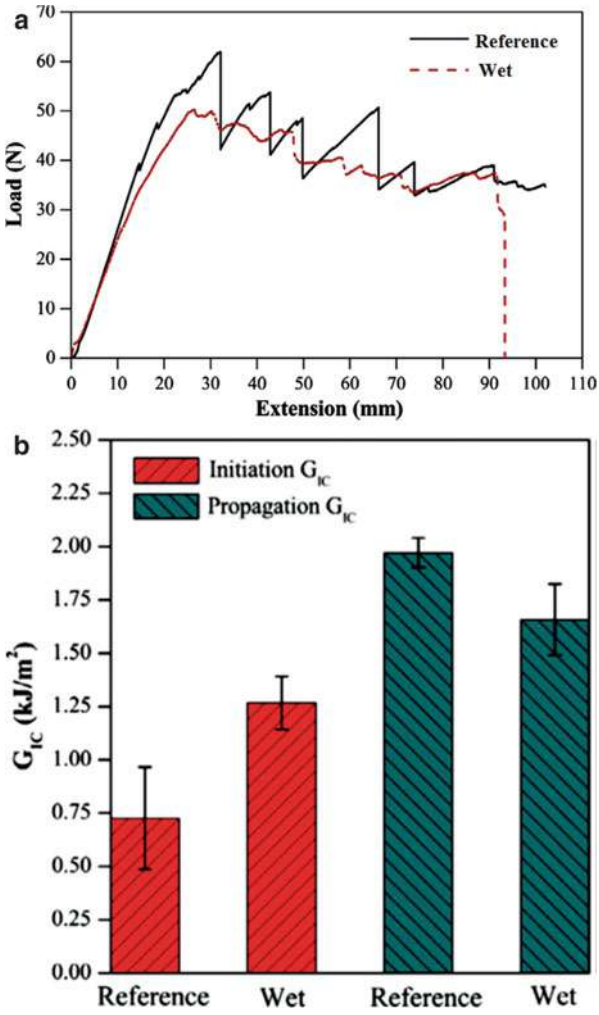

Fig. 4 Results of DCB tests, (**a**) typical load-extension curves, (**b**) comparison in G_{IC} values, for C/Ep composite before (reference) and after (wet) exposure to hygrothermal aging in distilled water at 80 °C for 54 days (Zhong and Joshi 2015a)

shown in Fig. 5a, b. In contrast, both surfaces of the reference specimen (Figs. 4d and 5c) after the DCB test are relatively impregnated by the epoxy resin, indicating good adhesion at the fiber-matrix interface (Zhong and Joshi 2015a).

Figure 6 depicts the measured mechanical properties of glass/epoxy (G/Ep) composite specimens before and after hygrothermal aging at 90 °C for 35 days. It can be observed that the water absorption had a negative effect on flexural properties. This can be attributed to the water diffusion into the whole structure of the epoxy resin as well as the subsequent plasticization in the polymeric part of the composite. It was also seen that the values of specific breaking energy of the aged specimen

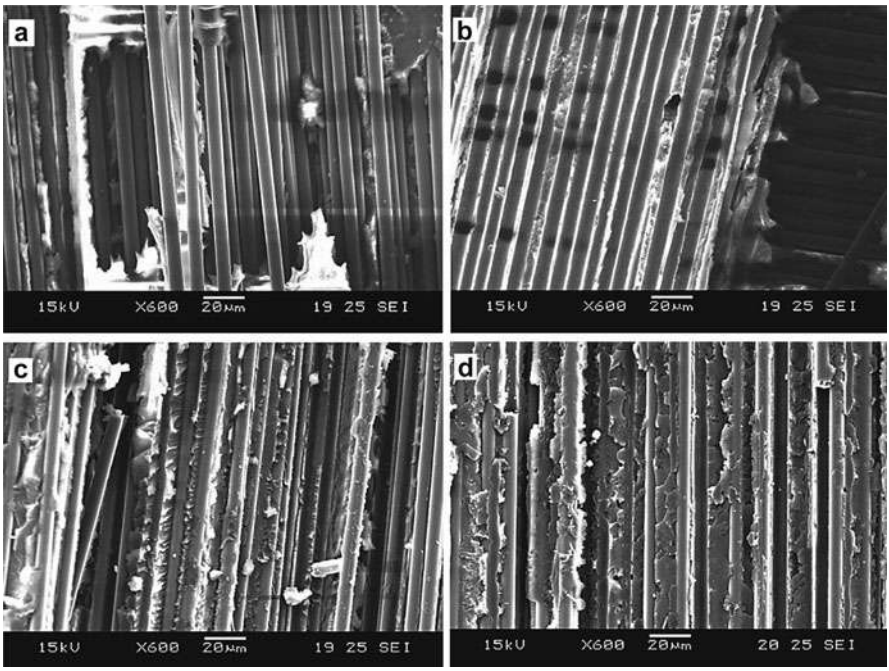

Fig. 5 Comparison between the surfaces A and B of the midplane interface of (**a**, **b**) wet, (**c**, **d**) Reference C/Ep composite specimens after Mode I fracture toughness testing (Zhong and Joshi 2015a)

decreased less than both the flexural stiffness and strength. Although the flexural stiffness and strength of aged specimens were reduced, however, increasing the ductility of material due to water absorption-induced plasticization caused less negative effects on specific breaking energy values (Najafi et al. 2017). In similar findings, Buehler and Seferis (Buehler and Seferis 2000) suggested the plasticization effect and increased fiber bridging as the possible reasons for the enhancement in fracture toughness of carbon fibers/epoxy composites after exposure to water conditioning for 1200 h.

It is noted that the impact properties of the G/Ep composite were not influenced by hygrothermal aging as much as the flexural ones (Najafi et al. 2017). Increasing the ductility of the epoxy matrix can be probably responsible for this less sensitivity of impact properties to hygrothermal conditioning. However, the confining factors, e.g., the stiffness and brittleness of fibers, can restrict the aging-induced ductility. The water may also weaken the interfacial bonding between the fibers and matrix and induce osmotic pressures. These events can amplify the activation of crack growth, and consequently decrease the toughness of FRPs (Weitsman 2012).

Typical flexural stress-strain curves for the dry and hydrothermally aged (80 °C for 10 weeks) of three epoxy-based composites, i.e., glass fibers/epoxy (G/Ep) composite

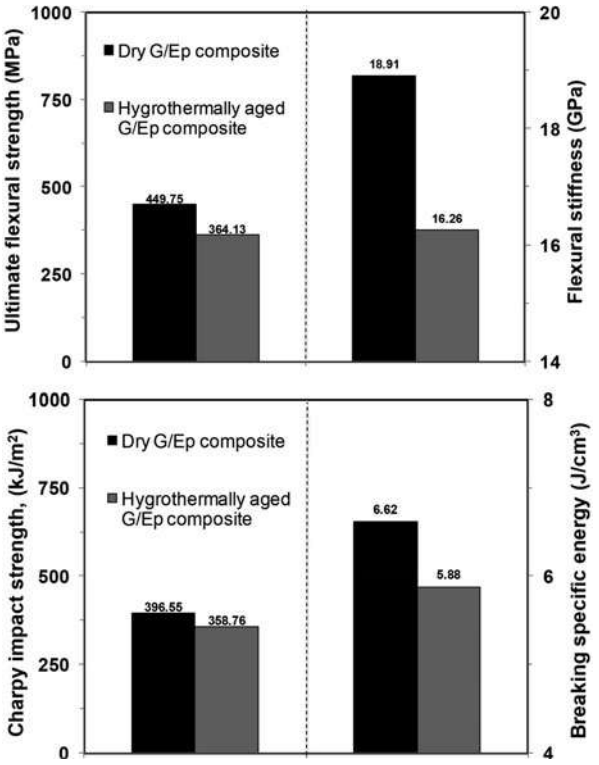

Fig. 6 Results of measured mechanical properties of G/Ep composite specimens before and after hygrothermal aging at 90 °C for 35 days (Najafi et al. 2017)

and glass/enriched epoxy with 3.0 wt.% (3 wt.% nano-G/Ep) and 5.0 wt.% nanoclay (5 wt.% nano-G/Ep) as well as the normalized degraded flexural properties relative to the reference properties are shown in Fig. 7. The strain at maximum strength was found to be increased in all types of hydrothermally aged specimens, suggesting the softening of these FRE composites. From Fig. 7b, it appears that after hygrothermal conditioning, the 3 wt.% nano-G/Ep specimens could remarkably preserve their flexural properties better than those of neat G/Ep and 5 wt.% nano-G/Ep ones (Najafi et al. 2018). Interestingly, Zainuddin et al. (2010) reported relatively similar findings. In their research, the catalytic effect of nanoclay was found to be the main reason for persevering the flexural properties of G/Ep composites hybridized with 1 and 2 wt.% nanoclay under hygrothermal aging. Nanoclay can postpone or subsidize the adverse effects of environmental conditions by accelerating the curing process and increasing the cross-linking between polymer chains (Zainuddin et al. 2010; Zhong and Joshi 2015b).

Figure 8 depicts the SEM micrographs from the morphology of fracture surfaces of flexural specimens. As shown in Fig. 8a, the fracture morphology of G/Ep composites indicates the brittle fracture characteristics which were characterized by the matrix cracking and extensive fiber breakage. From Fig. 8b, and in contrast to the dry specimens, a rougher fracture surface and more fiber pullout as the signs of

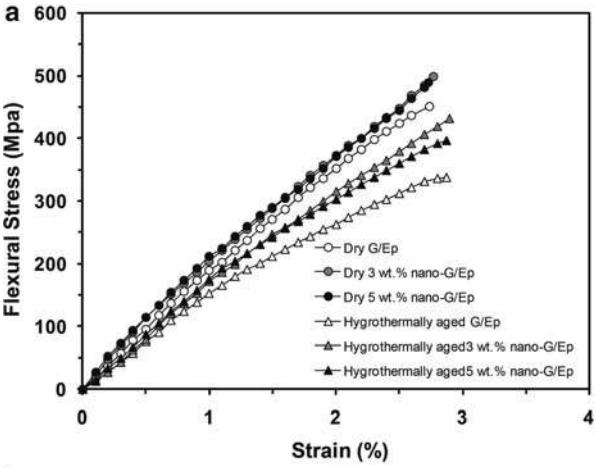

	Flexural Strength	Loss (%)	Flexural Stiffness	Loss (%)	Breaking Specific Eenergy	Loss (%)
G/Ep	0.75	24.76	0.81	18.98	0.91	9.35
3 wt.% nano-G/Ep	0.87	13.45	0.84	16.20	0.96	4.30
5 wt.% nano-G/Ep	0.82	18.45	0.82	17.62	0.88	11.99

Fig. 7 Results of flexural tests, (**a**) typical flexural stress-strain curves, (**b**) degradation of flexural properties, for G/Ep and its nanocomposites before and after exposure to hygrothermal aging in distilled water at 80 °C for 70 days (Najafi et al. 2018)

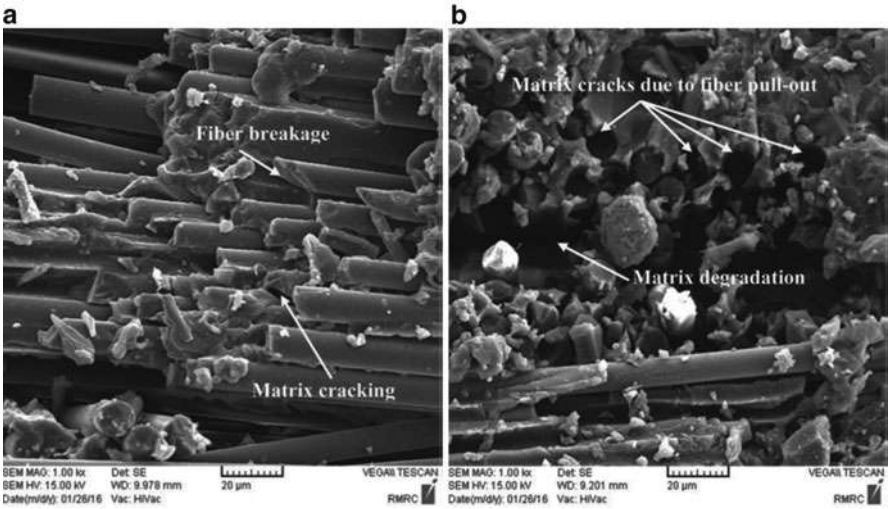

Fig. 8 Photographs of failure modes following flexural testing in the G/Ep composite specimens, (**a**) dry, (**b**) hydrothermally aged in distilled water at 80 °C for 70 days (Najafi et al. 2018)

ductility were observed in aged G/Ep composites, implying a more ductile behavior in aged G/Ep composites compared to those of dry (Najafi et al. 2018).

A wealth of data regarding the effect of hygrothermal aging on the different types of FRE composites are briefly listed in Table 1. Note for ease of use and better comparison, the values are given approximated and rounded to the closest.

Hygrothermal Cycling

FRE composites are frequently used in structural applications where they experience cyclic moisture and temperature. Repeated temperature/humidity changes are often known as hygrothermal cycling. In general, hygrothermal cycling can induce transverse matrix cracks initiating in surface plies of laminated composites and progress deeply with increasing the cycles (Martin 2008). These transverse matrix cracks often affect both the mechanical and thermal properties, which can reduce strength in matrix-dominated failure modes and contribute to higher moisture uptake in the laminate depth (Martin 2008). The micro-void generation, outer ply delamination, and surface blistering during rapid heating as other consequences of hygrothermal cycling may also occur even with no applied loads (Martin 2008). Therefore, hygrothermal cycles may impose some critical effects on the in-service structural durability of FRPs. Despite this, a review of the literature indicates a lack of published comprehensive researches regarding the effect of hygrothermal cycling on the mechanical properties of FRPs, especially FRE composites.

Several plots relating the effect of the number of hygrothermal cycles (eight cycles from 50 °C to 100 °C in distilled water) and conditioning temperatures on the mechanical properties of G/Ep composites are shown in Fig. 9. It was evident that both the impact load and the deflection at the maximum impact load for hydrothermally cycled unidirectional G/Ep specimens were adversely affected, indicating the softening and several damage initiations, which could reduce the stiffness of the specimens. The impact results also demonstrate that the cross-ply G/Ep specimens were less affected by hygrothermal cycling compared to those unidirectional. Additionally, it was found that the repeated hygrothermal cycles had a greater effect on the residual tensile strength after impact compared to low-velocity impact response. It was attributed to less sensitivity of impact test to the viscoelastic behavior and the hygrothermal cycling-induced damages (Li et al. 2000).

Figure 10 represents the flexural behavior of G/Ep specimens as well as normalized residual flexural and impact properties after enduring five hygrothermal cycles (from boiling saltwater to dry air at 50 °C) relative to the reference condition (Najafi et al. 2019a). As shown in Fig. 10a, in contrast to the dry specimens exhibiting a linear behavior before reaching peak load, the load-deflection curve for the hydrothermally cycled specimens showed a bilinear elastic response. Besides, both the stiffness and peak load in cycled specimens dramatically decreased. The reduction in flexural and impact properties of hydrothermally cycled specimens is more than 20% and 10%, respectively (Fig. 10b).

Table 1 Results of hygrothermal aging effects on different types of FRE composites

Material system	Environmental factor	Time (h)	T (°C)	Max. water uptake (%)	Change in original properties		References
					Property	(%)	
C/Ep	Water	1344	80	3.6	**Ultimate tensile strength** **Tensile modulus** **Ultimate tensile strain**	−16 −11 +1	Zhong and Joshi (2015b)
C/Ep	Distilled water	2160	24 70 90	@ 24 °C: 0.2 @ 70 °C: 1.6 @ 90 °C: 2.7	**T_g** (@ 70 °C) **Flexural strength** (@ 24 °C) **Flexural strength** (@ 70 °C) **Flexural strength** (@ 90 °C)	−3 −9 −14 −17	Guermazi et al. (2016)
G/Ep				@ 24 °C: 0.4 @ 70 °C: 2.9 @ 90 °C: 5.4	**T_g** (after aging at 70 °C) **Tensile modulus** (@ 24 °C) **Tensile modulus** (@ 70 °C) **Tensile modulus** (@ 90 °C)	−4 −18 −25 −28	
C/G/Ep (hybrid)				@ 24 °C: 0.3 @ 70 °C: 2.4 @ 90 °C: 4.6	**T_g** (after aging at 70 °C) **Tensile modulus** (@ 24 °C) **Tensile modulus** (@ 70 °C) **Tensile modulus** (@ 90 °C)	−5 −21 −27 −31	
G/Ep C/Ep	Water	1200	71	~4 ~5	**Mode I fracture toughness** (C/Ep) **Mode II fracture toughness** (C/Ep) **Flexural modulus** (G/Ep) **Flexural modulus** (C/Ep)	+14 −72 −32 −29	Buehler and Seferis (2000)
					Flexural strength (G/Ep) Flexural strength (C/Ep) **T_g** (G/Ep) **T_g** (C/Ep)	60 −54 −35 −36	

G/Ep	Distilled water	1000 3000	RT 65	RT @ 1000 h: 0.9 RT @ 3000 h: 1.7 65 °C @ 1000 h: 7.8	**Tensile strength** (RT @ 1000 h) **Tensile modulus** (RT @ 1000 h) **Strain failure** (RT @ 1000 h)	+1 −14 +18	Abdel-Magid et al. (2005)
					Tensile strength (RT @ 3000 h) **Tensile modulus** (RT @ 3000 h) **Strain failure** (RT @ 3000 h)	−35 −9 −32	
					Tensile strength (65 °C @ 1000 h) **Tensile modulus** (65 °C @ 1000 h) **Strain failure** (65 °C @ 1000 h)	−18 −29 +18	
A-G/Ep (hybrid) A/G/Ep (interlayer)	Distilled water	1344	70	A-G/Ep: 4.1 A/G/Ep: 4.4	**Compression strength** A-G/Ep A/G/Ep	 −28 −28	Imielinska and Guillaumat (2004)

C, carbon fiber; G, glass fiber; A, aramid fiber; Ep, epoxy resin

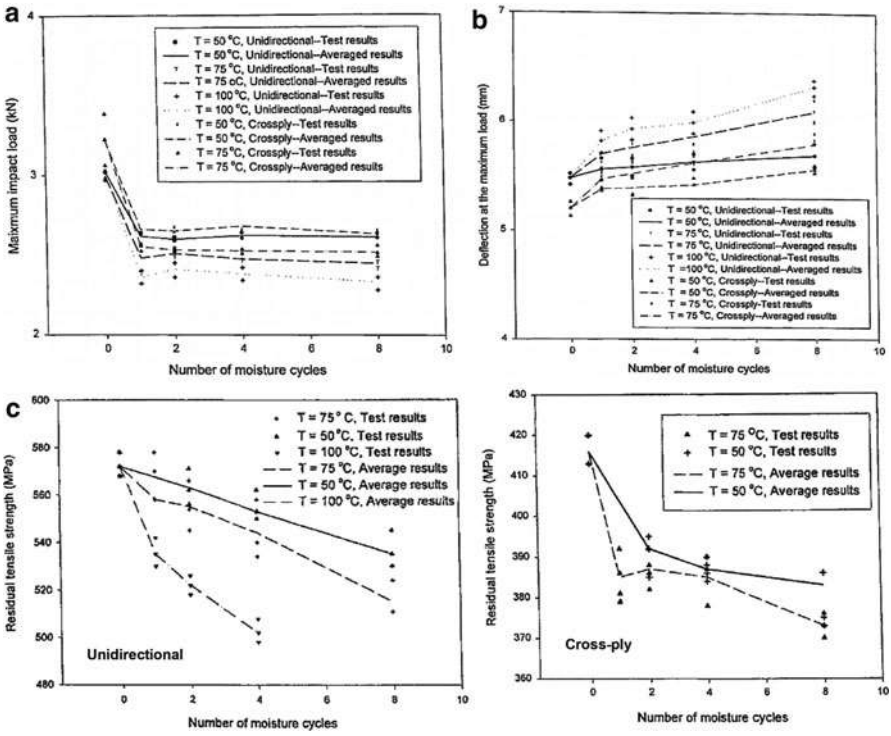

Fig. 9 Effect of hygrothermal cycling (8 cycles from 50 °C to 100 °C in distilled water) and conditioning temperatures on the, (**a**) maximum impact load, (**b**) deflection at the maximum impact load, (**c**) residual tensile strength after impact, for G/Ep composite specimens (Li et al. 2000)

Therefore, it was clearly found that the detrimental effects induced by hygrothermal cycling were more pronounced in flexural properties compared to impact ones. When an FRP is exposed to thermal cycling, the mismatch in coefficient of thermal expansion (CTE) between polymer matrix and fibers can promote high interfacial strains (Najafi et al. 2019a). If the thermal stresses associated with these strains exceed the tensile stress limit of the polymer matrix, the interfacial adhesion between fibers and matrix may be damaged, which can be accompanied by the reduction of flexural properties in FRP (Najafi et al. 2019a). Additionally, hygrothermal cycling in a moist environment can probably magnify the negative consequences of thermal cycling. When a laminated composite is exposed to moisture absorption conditions, the outer wet plies tend to swell, which is accompanied by the generation of compressive stresses. On the contrary, when desorption occurs, the outer plies experience tensile stresses due to restrictions created by wet swollen inner plies (Najafi et al. 2019a; Ray et al. 2007). Consequently, these stresses can initiate nonreversible failures such as matrix

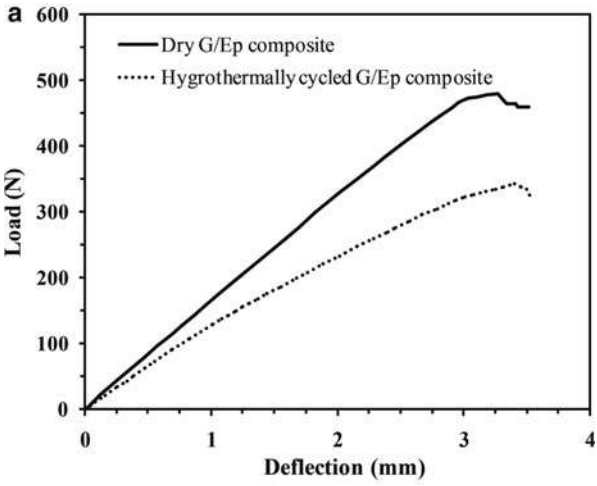

Fig. 10 Results of mechanical tests, (**a**) typical flexural load-deflection curves, (**b**) degradation of mechanical properties, for G/Ep composite after exposure to hygrothermal cycling from boiling saltwater to dry air at 50 °C (Najafi et al. 2019a)

cracking, fiber splitting, and delamination, which can adversely affect the durability of composite (Najafi et al. 2019a).

Figure 11a taken from a dry specimen exhibits most fibers are firmly fixed in the epoxy matrix and no significant microcrackin"g along the fiber surface is found. Limited evidence of fiber pullout can be considered as an indication of good adhesion between the epoxy matrix and fibers. In the case of hydrothermally cycled specimens (Fig. 11b), the fiber-matrix interfacial debonding is severe, and clean areas on the fiber surfaces suggested that fibers were totally separated from the epoxy matrix in a river mark form (Najafi et al. 2019a).

The effects of the hygrothermal cycling (from 50 to 100 °C in water) on the interlaminar shear behavior on epoxy reinforced by 55, 60, and 65% weight fraction of E-glass were studied by Ray (Ray et al. 2007). After nine cycles of moisture absorption, both the rate and maximum weight uptake of G/Ep

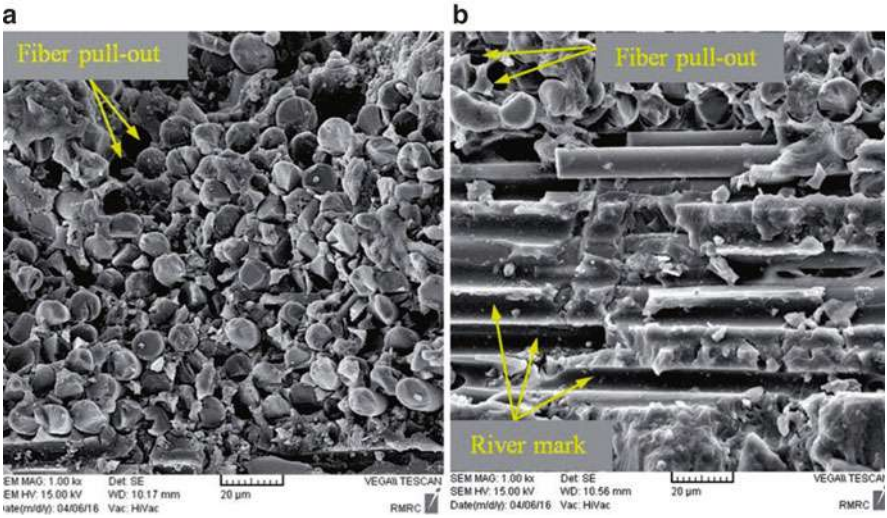

Fig. 11 SEM micrographs of failure modes following flexural testing in the G/Ep composite specimens, (**a**) dry, (**b**) hydrothermally cycled from boiling saltwater to dry air at 50 °C (Najafi et al. 2019a)

specimens containing 65 wt.% fibers were significantly higher than those of others. These results were attributed to the greater percentage of inter-facial area in 65 wt.% glass fiber-reinforced epoxy composites. Contrary to the moisture uptake results, the reduction in interlaminar shear strength value was interestingly higher in G/Ep composites with the lowest fiber weight fraction (i.e., 55%).

Tsotsis et al. (Tsotsis and Weitsman 1990) investigated the influence of hygrothermal cycling (five to six cycles from 40 °C at 100% relative humidity (RH) to 40 °C at 0% RH) on mechanical properties of G/Ep composites with differently oriented layups. Results showed a decrease of 34% and 11% in the tensile strength of hydrothermally cycled specimens with $[90°]_8$ and $[\pm 30°]_{2s}$ layup, respectively, while no statistically significant change was seen in the tensile modulus of both specimen types. It was also found that the moisture-induced cracks in unidirectional layup could propagate much more easily than that of angle-ply (here, i.e., $[\pm 30°]_{2s}$) layup.

Another study performed by Jana and Bhunia (Jana and Bhunia 2008) indicated that interlaminar shear strength for both the G/Ep and C/Ep composites gradually decreased with the number of hygrothermal cycles. Accordingly, the interlaminar shear strength of the G/Ep and C/Ep specimens was reduced by about 40% and 45% after 32 cycles of exposure. A reduction of about 39% and 34% in the value of delamination damage tolerance after 32 hygrothermal cycles was also found for the G/Ep and C/Ep specimens, respectively.

As highlighted by the abovementioned research works, the hygrothermal cycling in FRE composites generally involves some detrimental mechanisms leading to serious structural consequences, even at a relatively small number of cycles.

Seawater/Saltwater Exposure

As a major reliability concern, materials utilized in the construction of marine structures must be able to endure continuously in seawater and sultry environments (Najafi et al. 2019a). On the other hand, considering the ubiquitous use of E-glass-reinforced polyesters and vinyl esters composites in marine structures, only a few authors have directly instigated the influence of seawater/saltwater exposure on the epoxy-based composites. However, the growing demands for weight-lightening, increasing speed, and reducing fuel consumption in marine applications have recently led to great attention on FRE composites, especially those having carbon fibers.

It was reported that seawater exposure in FRE composites can change the thermophysical, chemical, and mechanical properties of the epoxy matrix via plasticization and hydrolysis (Mourad et al. 2010). On the other hand, determining the exact amount of seawater exposure-induced degradation in a real condition is an expensive and time-consuming process. Thus, accelerated aging in boiling seawater or artificial saltwater as an accepted procedure for reducing the time required to complete saturation of test specimens is frequently used. For example, the durability of G/Ep composites in a simulated marine environment was evaluated by accelerated aging in boiling saltwater (Najafi et al. 2019a). The normalized residual mechanical properties after 10 h aging in boiling saltwater are presented in Fig. 12. Considering that the G/Ep specimens used in this case study are exactly the same as those used in the section "Hygrothermal Cycling" (Najafi et al. 2019a), by comparing Figs. 10 and 12, it is well found that both types of conditioning in saltwater affect the mechanical properties of G/Ep specimens. However, this negative effect was much pronounced in hygrothermal cycling in comparison with the aging in saltwater. The penetration of saltwater into the different depths of structure and subsequent possible plasticization and/or hydrolysis of the polymer structure can be taken into account as the main reason for the structural deterioration of aged specimens (Najafi et al. 2019a).

Similar findings are reported by Stabik (Stabik 2005). The results showed that the short-term aging in boiling saltwater (only 87 h) could surprisingly reduce

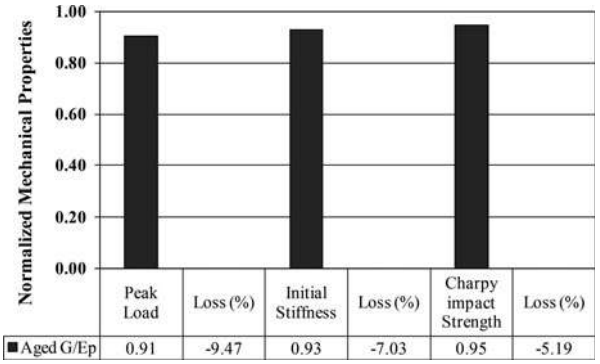

Fig. 12 Degradation of mechanical properties for G/Ep composite after exposure to boiling saltwater for a period of 10 h (Najafi et al. 2019a)

more than 20% of the flexural strength of the G/Ep composites. The swelling and weakening of the fiber-matrix interface during the boiling process were introduced as responsible for this noticeable reduction in flexural strength of G/Ep composites. Results also demonstrated that the flexural modulus did not change significantly with aging time.

Some authors have reported that exposure to hot seawater can change the failure mode of the G/Ep composite from the brittle matrix and ductile fiber to the ductile matrix and brittle fiber system (Mourad et al. 2010). For example, Fig. 13 illustrates several micrographs from the G/Ep composite specimens before and after exposure to 3 months and 1 year of immersion in seawater. Accordingly, the fractured surface in control (dry) specimens demonstrated a rough surface of broken fibers and epoxy matrix without any significant fiber pullout, indicating a good interfacial bonding at the fiber-matrix region, as shown in Fig. 13a. On the other hand, the microstructure of the G/Ep composite conditioned for 1 year at room temperature in Fig. 13b shows some fiber pullout and debonding, indicating the occurrence of deterioration at the fiber-matrix interfacial region. However, the rough surface of both the fibers and epoxy matrix implies a partially ductile failure and retention of interfacial strength. As shown in Fig. 13c, the smooth fiber surfaces, as well as a limited amount of fiber pullout, implies the indications of hydrolysis-induced deterioration at the fiber-matrix interface for G/Ep composite conditioned for 1 year at 65 °C. The effect of plasticization in terms of short fiber pullout and the stretched matrix can be observed in Fig.13c.

The surveyed researches about the effect of seawater/saltwater exposure on the different types of epoxy-based composites are summarized in Table 2.

Effect of Temperature on the Synthetic Fiber-Reinforced Epoxy Composites

FRE composites are being increasingly used in applications where they can be exposed to various thermal conditions such as elevated/low temperatures, thermal cycling, thermal shocks, fire, etc. The long-term durability of the composite structure facing with abovementioned factors is one of the difficult challenges for designers of composite structures. It is well-known that the epoxy resins can immediately soften and exhibit rubber-like behavior at elevated temperatures even slightly above T_g, leading to a considerable decrease in mechanical properties and structural integrity of the epoxy-based composite. The long-term exposure of polymeric composites to high temperatures is commonly referred to as thermal or thermo-oxidative aging. Although the epoxy matrix at sub-T_g preserves its glassy behavior, the chemical structure of the epoxy matrix may gradually change through mechanisms such as cross-linking or chain scission which is often not reversible. On the other hand, the long-term exposure to sub-T_g temperatures can only lead to the physical changes in the molecular structure of epoxy resins and their composite. At temperatures far beyond the T_g, most types of epoxy resins start to decompose. In these temperatures, synthetic fibers such as glass, aramid,

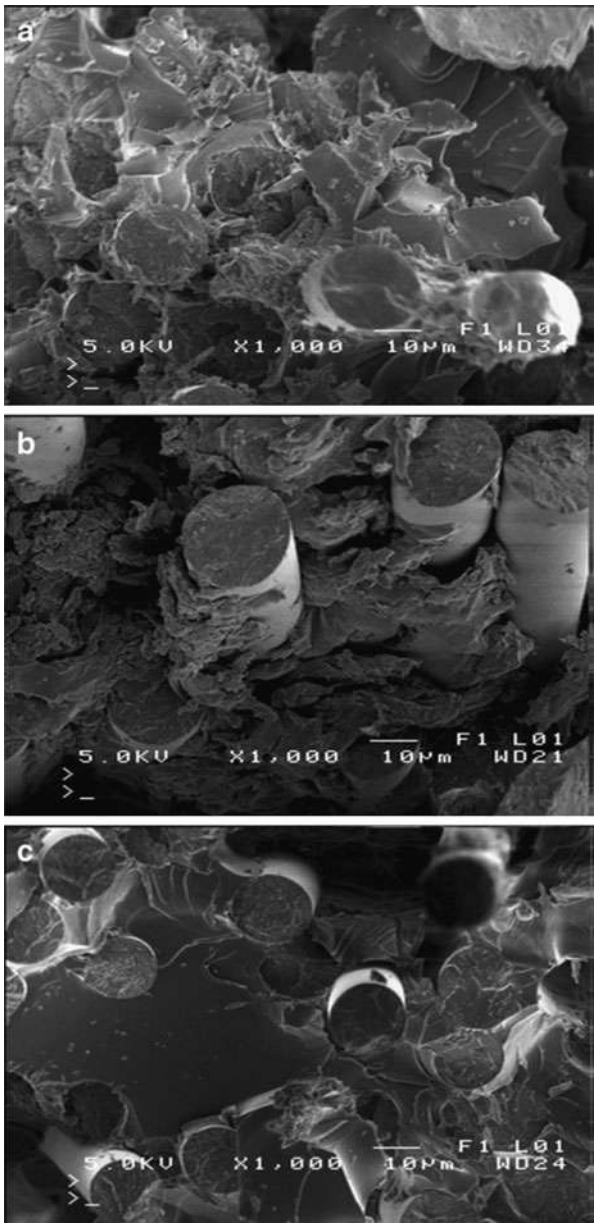

Fig. 13 SEM micrographs of fractured surfaces of G/Ep composite, (**a**) control specimen, (**b**) after exposure to saltwater at room temperature for 1 year, (**c**) after exposure to saltwater at 65 °C for 1 year (Mourad et al. 2010)

and carbon may even experience some degradation mechanisms, i.e., softening and oxidation. As the temperature varies, some original properties of both the polymeric resin and fiber-matrix interface can be adversely affected which is eventually accompanied by a drastic decrease in the mechanical properties of FRE

Table 2 Results of seawater/saltwater exposure effects on the FRE composites

Material system	Environmental factor	Time (h)	T (°C)	Max. water uptake (%)	Change in original properties		References
					Property	(%)	
G/Ep	Natural seawater	~2160 ~ 4320 ~8640	65	2160 h: 2.9 4320 h: 3.0 8640 h: 5.1	**Tensile strength** (@ 2160 h) (@4320 h) (@8640 h)	+1 −4 −6	Mourad et al. (2010)
					Tensile modulus (@ 2160 h) (@4320 h) (@8640 h)	−5 −9 −5	
					Strain to failure (@ 2160 h) (@4320 h) (@8640 h)	+20 +15 +10	
G/Ep	Natural seawater	~12,960	20 50	. . .	**Shear modulus** (20 °C) **Shear modulus** (50 °C) **Shear strength** (20 °C) **Shear strength** (50 °C)	−8 −18 −8 −22	Davies et al. (2001)

G/Ep	Saltwater	2160 3600	RT 60	...	**Tensile strength** (RT) (@ 2160 h) (@ 3600 h)	−2 +3	Kajorncheappunngam et al. (2002)
					Strain at failure (RT) (@ 2160 h) (@ 3600 h)	−3 0	
					Tensile strength (60 °C) (@ 2160 h) (@ 3600 h)	0 −19	
					Strain at failure (60 °C) (@ 2160 h) (@ 3600 h)	−1 −16	
G/Ep	Oxygenated seawater	300 1000 3000 10,000	RT	...	**Tensile strength** (@ 300 h) (@ 1000 h) (@ 3000 h) (@ 10,000 h)	−11 −8 −10 −13	Merah et al. (2010)
					Tensile modulus (@ 300 h) (@ 1000 h) (@ 3000 h) (@ 10,000 h)	16 −8 −16 −15	
					Fracture strain (@ 300 h) (@ 1000 h) (@ 3000 h) (@ 10,000 h)	7 −7 −3 −2	

(continued)

Table 2 (continued)

Material system	Environmental factor	Time (h)	T (°C)	Max. water uptake (%)	Change in original properties		References
					Property	(%)	
G/Ep (0°/90°) G/Ep (+45°/−45°) G/Ep (woven)	Artificial seawater	~2160	60	G/Ep (0°/90°):1.1 G/Ep (0°/45°):0.8 G/Ep (woven):0.7	**Energy required for incipient damage** G/Ep (0°/90°) G/Ep (+45°/−45°) G/Ep (woven)	 +20 +17 +3	Strait et al. (1992)
					Peak impact load G/Ep (0°/90°) G/Ep (+45°/−45°) G/Ep (woven)	 −13 −17 −17	
					Energy absorbed at peak load G/Ep (0°/90°) G/Ep (+45°/−45°) G/Ep (woven)	 −24 −27 −29	
					Energy required for penetration G/Ep (0°/90°) G/Ep (+45°/−45°) G/Ep (woven)	 −25 −18 −14	

C, carbon fiber; G, glass fiber; Ep, epoxy resin

composites. Another limitation with using FRE composites is related to the flammability of the epoxy resin. When an epoxy matrix is exposed to fire, it can ignite within a short time, which can catastrophically influence the integrity and load-carrying capacity of the structure. Microcracking as one of the major consequences of aging in low temperatures commonly occurs in FRE composites where thermal expansion mismatch between the fibers and the epoxy resin induces large residual stresses. To ensure a safe and durable design, different aspects of the structural performance of FRE composites when exposed to thermal conditions should be adequately evaluated.

Thermal/Thermo-Oxidative Aging

It has been well-established that long-term exposure to a relatively elevated temperature in the presence of oxidative environments has a detrimental effect on the mechanical performance of FRPs. Although fibers in the FRPs are generally intact, the matrix and the fiber-matrix interface can easily deteriorate at sufficiently elevated temperatures. In the first steps of thermo-oxidative aging, only the external surfaces of FRPs experience oxidation. This process then continues by gradually accelerating the oxygen diffusion rate and the oxidation reactions within the composite material. Subsequently, several failure mechanisms including deterioration at the fiber-matrix interfacial bonding, resin shrinkage, as well as the microcrack initiation and propagation caused by CTE mismatching between the matrix and fibers may probably happen during thermo-oxidative aging (Decelle et al. 2003). The mentioned microcracks not only can degrade the mechanical properties, particularly the failure properties of FRPs, but also facilitate new pathways for more oxygen and other corrosive materials to diffuse into the material. Some consequences of thermal aging including weight loss of polymeric matrix due to dehydration and evaporation of volatiles, material embrittlement, as well as chain scissions of the polymer can also affect the mechanical properties of FRPs (Fan et al. 2015).

The effect of thermal aging on the mechanical properties of epoxy-based composites has been the subject of numerous studies. For example, Birger et al. (Birger et al. 1989) evaluated the residual mechanical performance of graphite/epoxy composites after exposure to thermal aging at 170 °C temperature for 120, 240, and 626 h. While, no degradation in properties was detected at short durations, both the flexural and shear strength decreased at prolonged exposure time. The weakening of the fiber-matrix interface in terms of bare fibers as well as the transition of failure appearance from the ductile to brittle was also observed at the largest exposure time. Ozcelik et al. (Ozcelik et al. 2009) reported that thermo-oxidative aging significantly affects the weight loss and mechanical properties of graphite/epoxy composites. It was found that 5000 h of thermo-oxidative aging at 150, 175, and 200 °C could reduce weight by 0.81, 2.31, and 5.84%, respectively, which was also associated with 10.87, 33.07, and 49.86% reduction in short-beam strength, respectively. Moreover, after 5000 h of aging at 100 °C, the weight and strength of composites were almost unaffected. Lafarie-Frenot et al. (Lafarie-Frenot et al. 2006) investigated how the carbon/epoxy

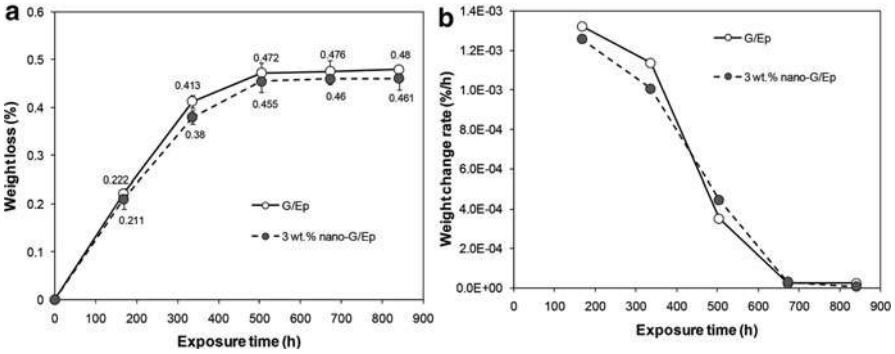

Fig. 14 Percentage of (**a**) weight loss and (**b**) weight change rate versus aging time, for G/Ep and 3 wt.% nano-G/Ep specimens thermally aged at 130 °C for 35 days (Najafi et al. 2019b)

composites were damaged under thermal aging. Microscopic observations indicated that the oxidation of the matrix on the surfaces directly subjected to thermal aging led to surface degradation in the form of matrix shrinkage and fiber-matrix debonding.

Figure 14a depicts the percentage of weight loss versus the time for two epoxy-based composites, i.e., glass/epoxy (G/Ep) composite and glass/enriched epoxy with 3 wt.% nanoclay (3 wt.% nano-G/Ep), during thermal aging at 130 °C for 5 weeks (Najafi et al. 2019b). It can be observed that both laminate types exhibit more weight loss as the time of thermal aging increases. The results also demonstrated that the incorporation of nanoclay had a moderate improvement in the thermal stability of the epoxy matrix (Najafi et al. 2019b). The positive effect of nanoclay on the reduction of weight loss was mainly attributed to the enhancement of fiber-matrix interfacial properties. Nanoclay also can successfully trap gaseous products in the matrix and prevent the diffusion of the high amount of oxygen into the composite as well as hinder the mobility of polymer chains during thermal aging (Najafi et al. 2019b). Since E-glass fibers are thermally stable at the abovementioned temperature (Zainuddin et al. 2010), the oxidation of fiber-matrix interfaces or thermo-oxidation of the matrix was responsible for the weight loss (Eslami-Farsani et al. 2013). Figure 14b demonstrates a high-rate weight loss up to 336 h of aging for both specimens which can be explained by degassing and/or desorption of moisture due to high-temperature conditioning (Ozcelik et al. 2009). After about 336 h of aging, the weight loss reduced with a lower rate and gradually tended to stability. Mechanical properties of both laminate types decreased after thermal aging which was mainly attributed to the embrittlement and degradation of the matrix through chain scission, matrix cracking in the external surface, weakening of fiber-matrix due to thermal stresses, and oxidation of matrix. The thermally aged nano-filled G/Ep specimens showed about 13, 13, and 11% reduction in flexural stiffness, maximum flexural load, and Charpy impact strength, respectively, while these values for thermally aged G/Ep specimens were approximately 20, 16, and 17%, respectively (Najafi et al. 2019b). It can be concluded that the addition of nanoclay into the epoxy matrix might lower the CTE of the matrix, followed by reducing the expansion of

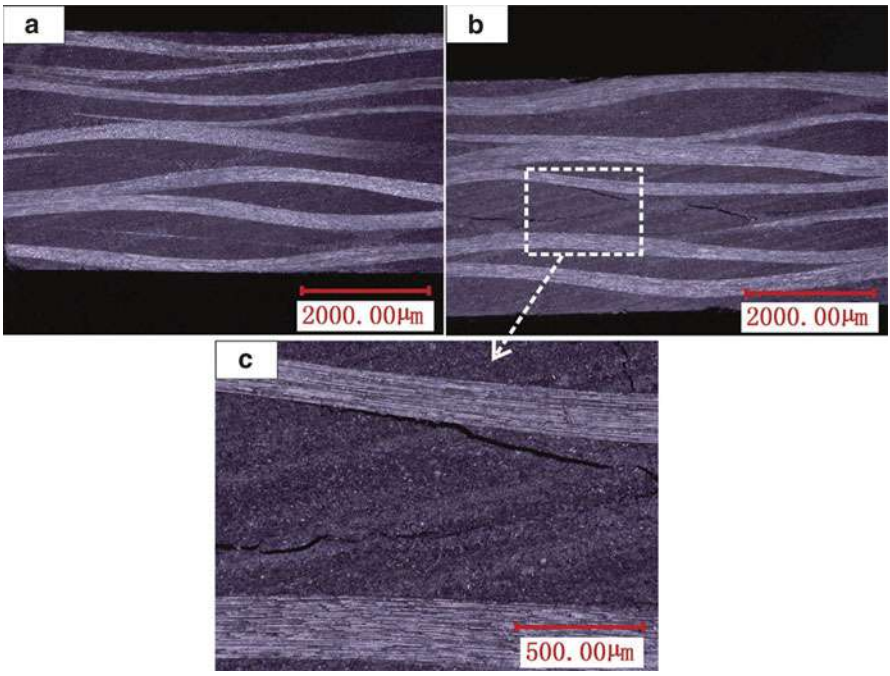

Fig. 15 The cross-sectional photomicrographs of the C/Ep specimen, (**a**) un-aged, and (**b**) thermally aged (140 °C for a period of 200 h), (**c**) zoom on thermo-oxidation-induced microcracks corresponding to (**b**) (Fan et al. 2016)

polymer chains during thermal aging. Finally, these modifications could probably decrease the thermal stress-induced microcracks formed due to prevented differential CTEs of the glass fibers and epoxy matrix (Najafi et al. 2019b).

Figure 15 illustrates the typical cross-section photomicrograph of the C/Ep composite laminate after aged at 140 °C for 1200 h compared to the un-aged ones (Fan et al. 2016). As shown in Fig. 15a, no visible damage can be seen on the un-aged specimen surfaces. In contrast, the appearance of thermally aged specimens exhibited severe microcracking (Fig. 15b, c).

In the case of thermo-oxidative aging on FRE composites, some useful results reported in the literature are listed in Table 3.

Elevated Temperatures and Fire

Unlike the majority of metallic materials, the mechanical properties of FRPs exposed to elevated temperatures can potentially be compromised. It is well-known that elevated temperatures, especially fire, can quickly undermine the structural integrity of the FRPs which can lead to the catastrophic failure of these materials. For an in-depth examination, it is necessary to consider some key factors involved in the

Table 3 Results of thermal/thermo-oxidative aging effects on the FRE composites

Material system	Environmental factor	Time (h)	T (°C)	Max. weight loss (%)	Change in original properties		References
					Property	(%)	
C/Ep	Thermo-oxidative aging	312	90 120 150 180	90 °C @ 312 h: 0.05 120 °C @ 312 h: 0.07 150 °C @ 312 h: 0.12 180 °C @ 312 h: 0.53	**Flexural strength** (@ 90 °C) (@ 120 °C) (@ 150 °C) (@ 180 °C)	−5 −8 −9 −9	Fan et al. (2015)
					Flexural modulus (@ 90 °C) (@ 120 °C) (@ 150 °C) (@ 180 °C)	2 −1 −3 −10	
G/Ep G/C/Ep	Thermo-oxidative aging	60	70 100	. . .	**Interlaminar shear strength** G/Ep @ 70 °C G/Ep @ 100 °C G/C/Ep @ 70 °C G/C/Ep @ 100 °C	−12 −22 0 −17	Shukla et al. (2014)
C/Ep (0°) C/Ep (90°) C/Ep (0°/90°)	Thermo-oxidative aging	336	200	. . .	**Impact strength** C/Ep (0°) C/Ep (90°) C/Ep (0°/90°)	−46 −80 −42	Chifu and Iroh (1996)
					Interlaminar shear strength C/Ep (0°) C/Ep (90°) C/Ep (0°/90°)	−13 0 −32	
					Flexural strength C/Ep (0°) C/Ep (90°) C/Ep (0°/90°)	+7 −55 +5	

C/Ep	Thermo-oxidative aging	2000	100 150 175 200	100 °C @ 2000 h: 0.2 150 °C @ 2000 h: 0.5 175 °C @ 2000 h: 1.3 200 °C @ 2000 h: 3.0	**Short-beam strength** (@ 100 °C) (@ 150 °C) (@ 175 °C) (@ 200 °C)	0 −10 −20 −35	Ozcelik et al. (2009)
C/Ep (0°) C/Ep (±45°)	Thermo-oxidative aging	1000 3000 5000 10,000	177	. . .	**Tensile modulus** C/Ep (0°) (@ 1000 °C) (@ 3000 °C) (@ 5000 °C) (@ 10,000 °C)	−3 −4 −5 −2	Tsotsis (1998)
					Tensile modulus C/Ep (±45°) (@ 1000 °C) (@ 3000 °C) (@ 5000 °C) (@ 10,000 °C)	+8 +3 −11 −22	
					Tensile strength C/ep (0°) (@ 1000 °C) (@ 3000 °C) (@ 5000 °C) (@ 10,000 °C)	+20 +15 +14 −49	
					Tensile strength C/Ep (±45°) (@ 1000 °C) (@ 3000 °C) (@ 5000 °C) (@ 10,000 °C)	−27 −30 −36 −69	

C, carbon fiber; G, glass fiber; Ep, epoxy resin

firing process of FRE composites, e.g., duration and intensity of heat flux, structural response of the composite constituents during the fire, thermal decomposition of the epoxy resin, residual properties of the composite after the fire, etc.

When the temperature increases close to the T_g, the FRE composites first exhibit reversible mechanical changes, such as viscous softening where the reduction of structural properties for the epoxy resin begins. It is known when the FRE composites are exposed to sufficiently high temperatures above the decomposition temperature of the resin, they experience a reaction releasing toxic and volatile gases, pyrolysis of the polymer matrix, and eventually the formation of the carbonaceous char. Another possible physical, chemical, and structural phenomenon during fire exposure includes the ignition of flammable reaction gas, an increase in internal pressure generated by the formation of volatile gas and evaporation of moisture, matrix cracking, interfacial debonding between resin and fiber, and delamination. Additionally, the oxidation and burning of fibers embedded in the polymeric matrix may occur at extreme temperatures (Burns et al. 2010). The durability and residual mechanical properties of FRE composites subject to fire or other elevated temperature sources have become an area of considerable interest for researchers. While some works have addressed the post-fire mechanical properties, others investigated the residual mechanical properties and the failure time of composite during the combined heating and loading process.

Figure 16 shows the typical stress-displacement relationship for a C/Ep composite under fire conditions and their corresponding failure modes (Wang et al. 2011). The results showed that the exposure to the elevated temperatures about 50, 100, 150, 200, 300, 400, 500, and 600 °C for 5 min could reduce the tensile strength of the C/Ep composite by about 10, 30, 40, 45, 45, 50, 55, and 80%, respectively. Surprisingly, the tensile strength of the specimens at the approximate peak temperature of 700 °C was found to be about only 7% of the value measured at room temperature (Fig. 16a). As shown in Fig. 16b, the brittle fiber rupture was observed within the range of 22–50 °C. The softening and gasification of the epoxy resin accompanied by partial loss of epoxy matrix followed by fiber rupture occurred between the temperature range 97–308 °C. From 395 to 625 °C, there was no epoxy left on the specimens since the epoxy had self-ignited at about 350 °C. Ultimately, complete burning of the epoxy matrix, as well as oxidation of about half of the carbon fibers, was seen for temperatures from 698 to 706 °C.

As another example, Burns et al. (Burns et al. 2010) investigated the compression failure of C/Ep composites when exposed to heat fluxes of 10, 25, and 50 kW/m^2. It was observed that the failure time decreased with increasing compression load or heat flux. The failure time for the case of 50 kW/m^2 was found to be only several hundred seconds, even when subjected to low levels of compression loads. As reported, while the specimens tested at 10 kW/m^2 experienced viscous softening (without decomposition), the heat flux of 25 kW/m^2 could heat the specimens above both the epoxy viscous softening temperature and the matrix decomposition temperature. The heat flux of 50 kW/m^2 was also enough to cause softening and decomposition of the epoxy matrix as well as the oxidation of the carbon fibers.

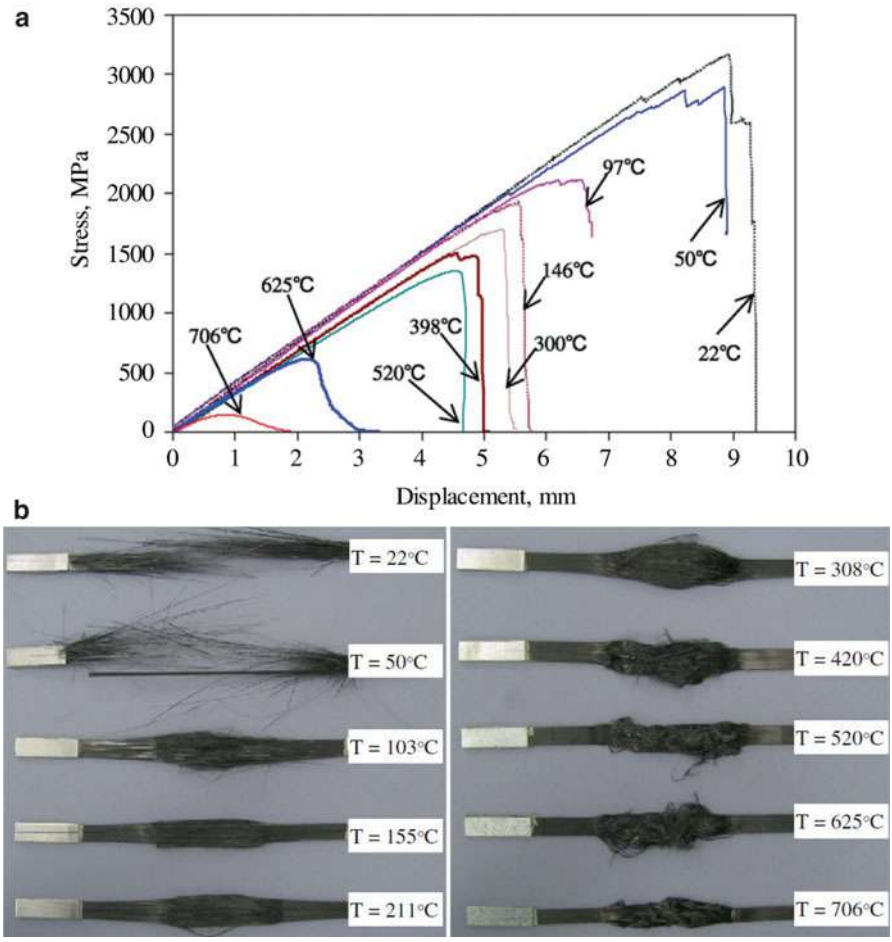

Fig. 16 Results of tensile test, (**a**) stress-displacement curves, (**b**) typical failure modes, for C/Ep composite specimens after exposure to elevated temperatures for 5 min (Wang et al. 2011)

Additionally, it was found that the failure times increase progressively with increasing the Tg for all levels of compression load.

It is known that the post-fire properties of FRE composites can quickly decrease with the increase of temperature or heating time of the fire source. Quach et al. (Quach et al. 2017) reported that short-term fire exposure dramatically affects the tensile properties of the carbon/epoxy composites with the stacking sequences of $\pm 45°$. After the fire exposure to a heat flux of 35 kW/m^2, at different durations of 130, 140, 150, 180, 200, and 220 s, the composite specimens exhibited a strength reduction of about 15, 18, 21, 40, 52, and 65%, respectively. Pering et al. (Pering et al. 1989) examined the residual tensile strength of the C/Ep composites following exposure to gas fires at the temperature range of 540–980 °C. The sudden and

great reduction of post-fire tensile strength, especially in the highest applied temperature was attributed to the rapid thermal decomposition of the epoxy matrix. According to the researches performed by Mouritz (Mouritz 2002), the rapid degradation of the epoxy matrix was suggested as the main responsible for dramatic reductions of the post-fire properties in carbon/epoxy, glass/epoxy, and aramid/epoxy composites.

Thermal Cycling

The cyclic temperature variation is considered as one of the critical service environments for FRPs usage (Eslami-Farsani et al. 2013). Traditional carbon fiber-reinforced epoxy composites still meet the basic design requisites for aircraft construction. However, these structures may encounter temperature excursions including ambient temperature fluctuations, exhaust gas, deicing, and engine operation during their service life (Eslami-Farsani et al. 2013). It is well-known that the C/Ep composites are very vulnerable to thermal cycling-induced microcracking (Eslami-Farsani et al. 2013). When carbon-reinforced polymers are exposed to temperature excursions, the large difference between the CTE of carbon fibers and polymer matrix can generate thermal stress in the composite. For example, when the temperature drops, the polymer matrix tends to contract more than the fibers. This can induce thermal stresses in the fiber and matrix, as well as fiber-matrix interfacial regions which may lead to thermal fatigue in the material (Eslami-Farsani et al. 2013). Because of the structural heterogeneity of composite materials, the thermal fatigue damage process is a rather complex phenomenon consisting of various failure modes such as matrix shrinkage, matrix cracking, fiber-matrix interfacial debonding, delamination between adjacent plies, and fiber fracture (Khalili et al. 2017; Papanicolaou et al. 2009). Timmerman et al. (Timmerman et al. 2002) reported that some fiber properties such as its modulus have a remarkable effect on the structural response of the C/Ep composites to thermal cycling. It was stated that the higher T_g of resin decreased the microcracking propensity of these epoxy-based composites. On the other hand, higher modulus and linear CTE of the carbon fibers compared to the epoxy matrix were suggested as responsible for increasing the microcrack density in the composite during the thermal cycling process. Paillous and Pailler (Paillous and Pailler 1994) studied the deterioration induced by a space environment exposure on graphite/epoxy composites. It was found that that thermal cycling could degrade the epoxy matrix via several mechanisms such as chain scission, cross-linking, and microcracking, leading to alter the mechanical properties of the composite.

Figure 17 illustrates an SEM micrograph of the free edge of the $[0_3/90_3]_S$ cross-ply C/EP laminate exposed to 100 thermal cycles in oxygen. Fiber-matrix interfacial debonding (Fig. 17a), matrix cracking (Fig. 17b), and permanent deformation of the matrix caused by shrinkage (Figs. 17a, c) as three different types of thermal cycling-induced damages was evident (Lafarie-Frenot and Rouquie 2004).

Another example of the abovementioned laminate that has sustained 500 thermal cycles, respectively, in nitrogen, in air, and oxygen, is shown in Fig. 18. The significant dark and deep hollows as a sign of matrix shrinkage only exist on the

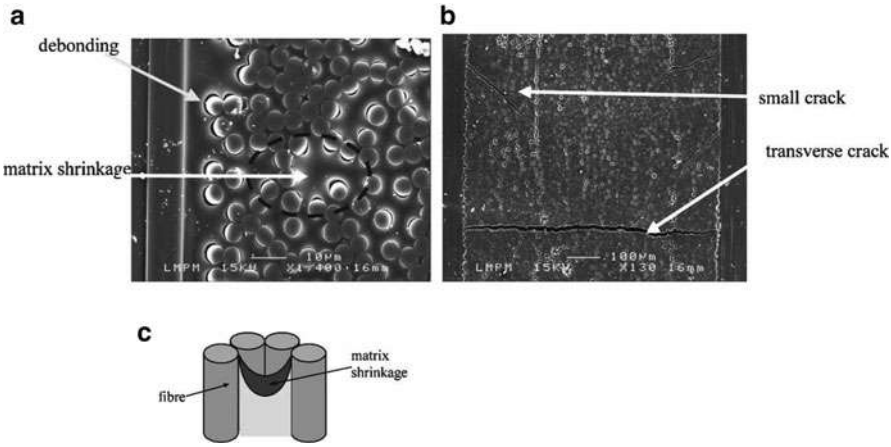

Fig. 17 Different types of damages in the $[0_3/90_3]_S$ cross-ply C/EP laminate subjected to 100 thermal cycles in oxygen (Lafarie-Frenot and Rouquie 2004)

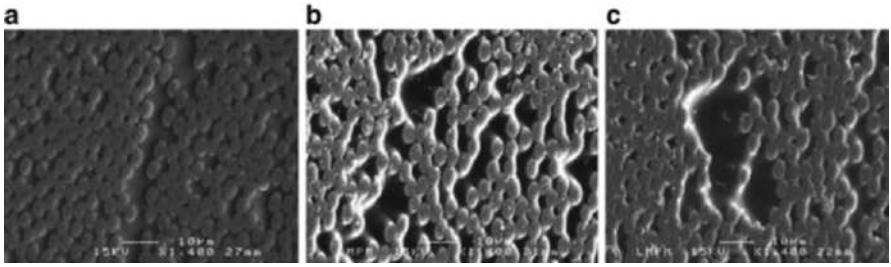

Fig. 18 SEM pictures of the polished edges of the $[0_3/90_3]_S$ cross-ply C/EP laminate subjected to 500 thermal cycles in, (**a**) nitrogen, (**b**) air, (**c**) oxygen (Lafarie-Frenot and Rouquie 2004)

specimens' edges cycled in oxidative environments (i.e., air and oxygen). In the case of thermal cycling in oxidative environments, a coupling between oxidation and cyclic thermomechanical stresses caused by the temperature variations can accelerate all the phases of the damage process (Lafarie-Frenot et al. 2006; Eslami-Farsani et al. 2013).

Thermal cycling can gradually reduce the stiffness and strength of the composite but has a more adverse effect on the matrix-dominated material properties (Eslami-Farsani et al. 2013). Shin and Kim (Shin et al. 2000) evaluated the residual properties of graphite/epoxy composite after exposure to simulated low earth orbit (LEO) environmental conditions, including UV radiation, high vacuum, and thermal cycles (80 cycles, +100 °C to −70 °C). As shown in Fig. 19, both the stiffness and strength of the graphite/epoxy composites after exposure to the abovementioned conditioning were found to be gradually decreased with increasing the thermal cycles. The severe drop in transverse flexural properties compared to other properties was attributed to the matrix loss at the composite surface.

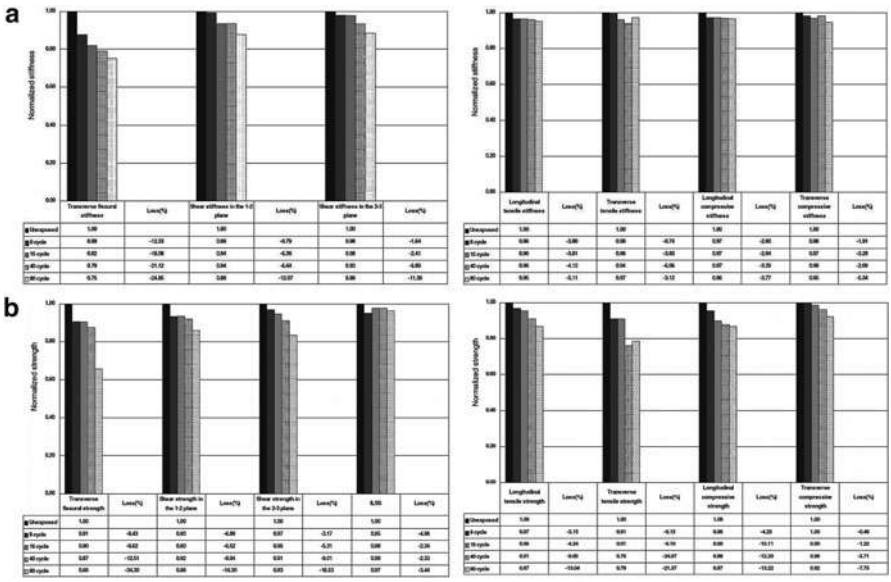

Fig. 19 Variations of, (**a**) stiffness, (**b**) strength, for the graphite/epoxy composite after exposure to the simulated LEO environmental conditions including high vacuum, UV radiation, and thermal cycles (80 cycles, +100 °C to −70 °C) (Shin et al. 2000)

Figure 20 shows the effect of thermal cycling (from +50 to −27 °C) on the creep behavior of G/Ep composites (Papanicolaou et al. 2009). One can see that strain response was reduced with increasing the number of thermal cycles (Fig. 20a). Surprisingly, the positive effect of thermal cycling on improving the mechanical properties of FRE composites has been reported in limited studies. For instance, the influence of thermal cycling (from +80 to −80 °C) on interfacial damage in the epoxy matrix reinforced with aramid fibers was examined by Ray (Ray 2003). He showed that the post-curing effects might lead to increase cross-linking density in the epoxy matrix and also improve fiber-matrix interfacial bonding. The thermal conditioning may alter the chemistry of the interface between the fiber and matrix via forming an interpenetrating network (Khalili et al. 2017) and also enhance the adhesion at the fiber-matrix interface by surface chemistry or mechanical interlocking mechanism (Khalili et al. 2017; Ray 2003). The cryogenic exposure at −80 °C for repeated times might generate different degrees of shrinkage compressive strength at the fiber-matrix interfacial region. This could probably strengthen the adhesion between the aramid fibers and epoxy matrix (Ray 2003).

Cryogenic Temperatures

Advanced FRPs, especially those of epoxy-based composites are considered as one of the possible materials for use in low-temperature applications such as aerospace

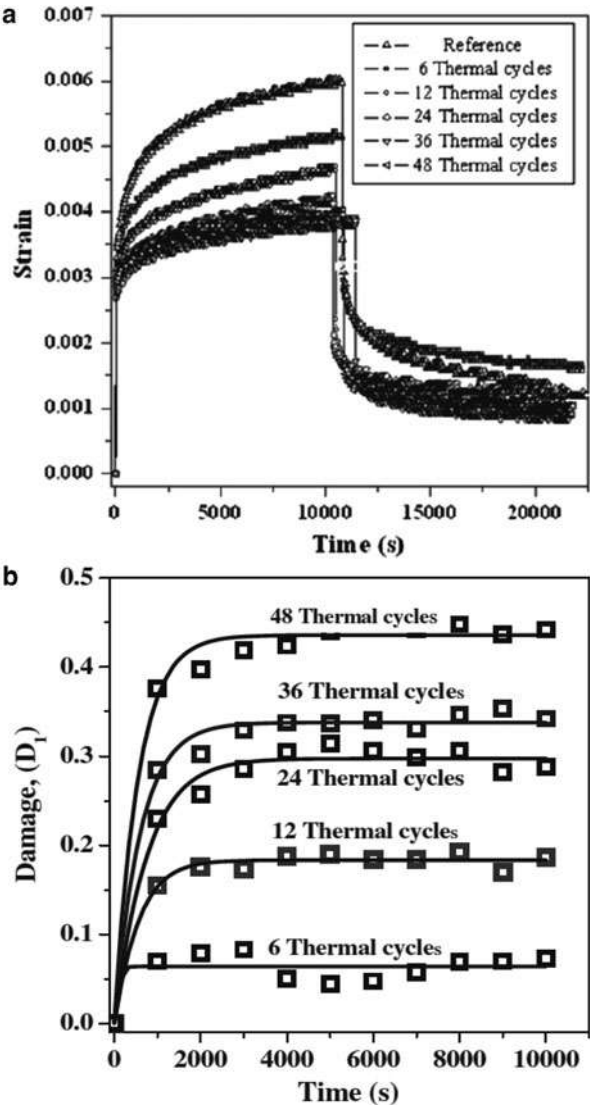

Fig. 20 The effect of thermal cycling on the creep behavior of G/Ep, (**a**) variation of strain with time, (**b**) variation of the degree of damage with time (Papanicolaou et al. 2009)

vehicles, superconductivity devices, and cryogenic liquids tanks (Cheng et al. 2019). On the other hand, in the case of long-term exposure to cryogenic conditions, the CTE mismatching between fibers and matrix can develop thermal stresses at their interfacial bonding as well as different plies of laminate. If the thermal stresses caused by cryogenic exposure can exceed the composite strength, the fiber-matrix interfacial debonding and, subsequently, matrix microcracking may happen. When these microcracks develop to a certain density and size, they coalesce to form macroscopic cracks as well as delamination damage, which can dramatically change

the mechanical strength. Additionally, the majority of epoxy resins exhibit more brittle behavior at low temperatures (Cheng et al. 2019) and, therefore, do not allow the relaxation of induced thermal stresses.

Although the majority of the previous researches have reported the negative effect of cryogenic conditioning on the mechanical properties of FRE composites, the significant indications of enhanced properties, especially in the case of mechanical testing under low-temperature condition were also observed. Kumar et al. (Kumar et al. 2009) examined the tensile and shear strength of the C/Ep composites after exposure to cryogenic aging. Results showed that the cryogenic aging for 1 h at −196 °C could enhance tensile strength but reduce the shear strength of composites. Besides, a large amount of matrix cracking and delamination cracks associated with the cryogenic-induced brittleness was observed. In another study conducted by the same previous authors, a clear sign of improvement in the interlaminar shear strength of G/Ep composites after cryogenic conditioning was detected. This improving effect was attributed to the thermal contraction of the epoxy matrix during cryogenic conditioning which could probably enhance the friction at the fiber-matrix interface (Kumar et al. 2008).

Typical flexural load-displacement curves of the unidirectional and orthogonal C/Ep composite specimens tested at 25, −15, and − 55 °C are displayed in Fig. 21. From 25 to −55 °C, enhancement in the flexural strengths and modulus is respectively evaluated as about 36% and 18% for the unidirectional and 45% and 16% for the orthogonal C/Ep composite specimens. It can also be observed that the peak loads for both laminate types increase with decreasing temperature but rapidly drop after the peak values with the decreased temperature (Cheng et al. 2019).

Putic et al. (Putic et al. 2007) conducted studies on the impact behavior of G/Ep composites at cryogenic temperatures and found the brittle failure with dramatically reduced impact strength. Ma et al. (Ma et al. 2016) reported that the size and depth of damaged areas, as well as absorbed energy for G/Ep composites, were considerably decreased when subjected to a low-velocity impact at low temperature (−196 °C) condition. The reduction in absorbed energy was attributed to the large extent of low temperature-induced contraction in epoxy which tightened the glass fibers, leading to an increase in resistance during fiber pullout. The increase in stiffness caused by the embrittlement of composite at cryogenic condition also resulted in decreased deflection in the impact test. Najafi et al. (Najafi et al. 2019c) studied the influence of cryogenic aging on the mechanical properties of G/Ep composites. It was found that the cryogenic aging in LN_2 at a temperature of −196 °C for 336 h could negatively affect the maximum flexural load, flexural stiffness, and impact strength of composites and decrease them by about 27, 5, and 14%, respectively. The accumulation of multiple microcracks generated from cryogenic aging was introduced as the main reason for the reduction in the matrix-dominant properties such as flexural properties.

The changes in the tensile, flexural, and shear properties of woven carbon/epoxy and woven Kevlar/epoxy laminates after exposure to short-term cryogenic aging were evaluated by Islam et al. (Islam et al. 2015). The principal finding was the deterioration of the fiber-matrix interface caused by cryogenic aging could noticeably affect the flexural properties compared with those of tensile properties. These observations were

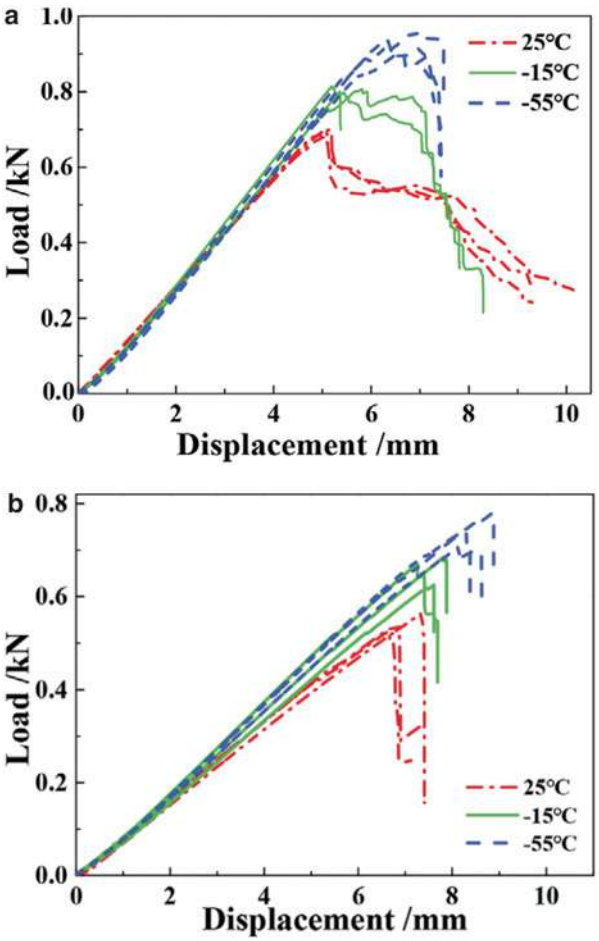

Fig. 21 Flexural load-displacement curves for, (**a**) unidirectional, (**b**) orthogonal, C/Ep composite specimens at 25, −15, and − 55 °C (Cheng et al. 2019)

attributed to the nature of flexural behaviors which are the matrix-dominated properties, and, therefore, the negative effects of cryogenic aging are more pronounced on the flexural properties. As shown in Fig. 22, after 6 h of exposure to LN_2 at a temperature of −196 °C, the flexural modulus and strength of carbon/epoxy composites decreased by about 3.7% and 3.5%, respectively. Also, the Kevlar/epoxy composites exhibited a remarkable reduction of 16.8% in shear strength.

Effect of Other Environmental Factors

Presently, FRE composites are widely used in outdoor applications where the material, in addition to the moisture and temperature fluctuations, is also exposed to corrosive factors and ultraviolet (UV) radiation. Several studies have shown that

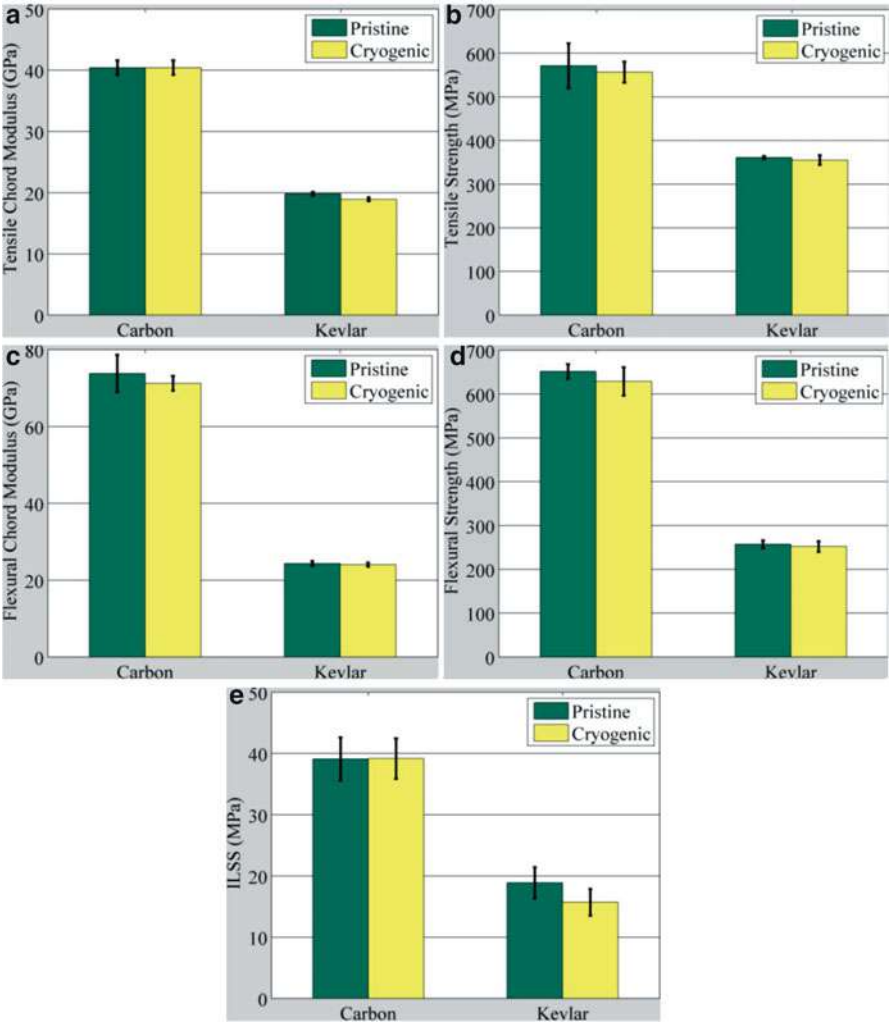

Fig. 22 Variations of, (**a**) tensile modulus, (**b**) tensile strength, (**c**) flexural modulus, (**d**) flexural strength, (**e**) interlaminar shear strength, for the carbon/epoxy and Kevlar/epoxy composites after exposure to 6 h cryogenic aging at −196 °C (Islam et al. 2015)

the durability of FRE composites can be seriously affected in these environments. The UV components of solar radiation incident on the earth's surface possess a wavelength between 290 and 400 nm. The energy associated with these wavelengths is comparable to the breakdown energies of covalent bonds which can lead to discolorations, chain scission-induced microscopic degradation, and reduction in mechanical properties of the polymer (Kumar et al. 2002). Since UV radiation on FRE composites is a surface process, it is mainly constrained to the degradation of

the epoxy properties and does not involve fiber degradation. Whereas the long-term exposure to UV radiation can dramatically decrease the matrix-dominated properties of FRE composites such as interlaminar shear strength as well as flexural stiffness and strength, fiber-dominated properties, e.g., tensile stiffness and strength, are generally not impressed remarkably (Shin et al. 2000; Kumar et al. 2002; Liau and Tseng 1998).

An experimental investigation (Kumar et al. 2002) on the effect of UV radiation on FRE composites showed that 500 h exposure to UV radiation decreased the weight of C/Ep composites by about 0.3%. This was attributed to the evaporation of volatiles and residual moisture from the FRE composites, similar to what happens in the case of thermo-oxidative aging. The FTIR analysis exhibited that UV radiation could probably increase the cross-link density of the epoxy followed by the excessive brittleness which resulted in microcracking. Additionally, the reductions of about 4% and 9%, respectively, in the transverse tensile modulus and strength were attributed to the effect of photo-oxidation on molecular chain scission of the epoxy matrix during the UV radiation exposure.

Liau and Tseng (Liau and Tseng 1998) examined the effects of UV radiation on the physical and mechanical properties of two types of epoxy-based composites reinforced by carbon and glass in the air and a near-vacuum system. It was found that the UV radiation-induced weight loss in specimens exposed to air was significantly higher than those of the near-vacuum system, especially for the G/Ep specimens. For both specimen types, the tensile strength decreased with increasing irradiation time. However, this reduction was not significant. The combined UV radiation and the elevated temperature had synergistic effects on the physical properties of the C/Ep composites, as demonstrated by Phelps and Long Jr. (Phelps and Long Jr 1980). Although short-term UV exposure could change the surface morphology of the C/Ep composites, no significant reduction in flexural properties of irradiated specimens was observed. Since the UV radiation on FRE composites is a surface mechanism, its dependence on the thickness of the exposed specimen is to be expected. Larsson (Larsson 1986) studied the effect of UV light exposure on the tensile properties of Kevlar/epoxy composite laminates with three thicknesses of 0.13, 0.25, and 0.50 mm. No degradation effect on the initial tensile elastic modulus was observed for three types of specimens. The strength reduction of a 0.13 mm laminate after 1000 h exposure was more than 40%, whereas no significant change was observed for both the 0.25 and 0.50 mm thick laminates.

It is well-known that corrosive fluids contain alkaline or acid seriously threaten metallic materials such as steel. Thus, in recent years there has been growing interest to introduce FRPs as an alternative to the traditional metals for applications in highly corrosive environments. For example, polyester and epoxy-based FRP pipes are commonly used in the chemical industry, building, and infrastructures (Amaro et al. 2013a). However, long-term exposure to these working environments can be harsh even for FRPs, resulting in the degradation of their original properties.

The effects of two different acid solutions, i.e., HCl and H_2SO_4, on the mechanical properties of G/Ep composite were studied by Amaro et al. (Amaro et al. 2013a). After 36 days of exposition, the reduction in flexural strength and modulus was

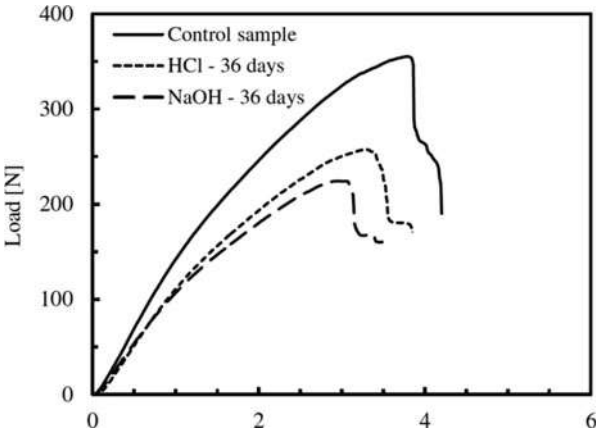

Fig. 23 Typical flexural load-displacement curves for G/Ep composites before (control specimen) and after exposure to HCl and NaOH for a period of 36 days (Amaro et al. 2013a)

about 16% and 22% for the specimens exposed to the HCl solution, respectively, while these values for the specimens immersed in H_2SO_4 solution were about 12% and 18%, respectively. In the case of impact properties, the composites immersed in HCl and H_2SO_4 solutions during 36 days exhibited an increase of the damaged areas about 21% and 19%, respectively, compared with those of un-aged specimens.

Figure 23 depicts the typical flexural load-displacement curves for G/Ep composite specimens before and after exposure to HCl and NaOH solutions that were reported in similar work, by the same authors. It can be observed that the aggressive effect of NaOH solution on flexural properties was more than the acid solution (i.e., HCl). The results showed the 36 days of immersion in NaOH solution led to the reduction of about 22% and 27%, respectively, in flexural strength and modulus of studied composites. Similarly, HCl solution could decrease flexural strength and modulus by around 16% and 22% for the same period of immersion. It was also found that, independently of the solution, the flexural properties decreased with the exposure time (Amaro et al. 2013b).

Figure 24 illustrates the evolution of the elastic energy (as the difference between the absorbed energy and the energy at peak load) with the impact number. It was found that the elastic energy decreased with increasing the number of impacts and exposure time. Similar to that for flexural properties, the elastic energy exhibited more reduction in alkaline solution compared to acidic one (Amaro et al. 2013b).

As shown in Fig. 25, the unexposed surface of specimens became gradually rougher accompanied by a noticeable increase of microcracks when the exposure time increased. Comparing Fig. 25d, g, it can be seen that the extent of damages that occurred for specimens exposed to NaOH was significantly higher than those exposed to HCl. The long cracks and the fiber exposition as a consequence of the matrix's dissolution are evident for specimens exposed to the NaOH solution (Fig. 25d). In contrast, for the specimens immersed in HCl, multiple cracks on the matrix occurred, but the bare fibers did not visible, as shown in Fig. 25g (Amaro et al. 2013b).

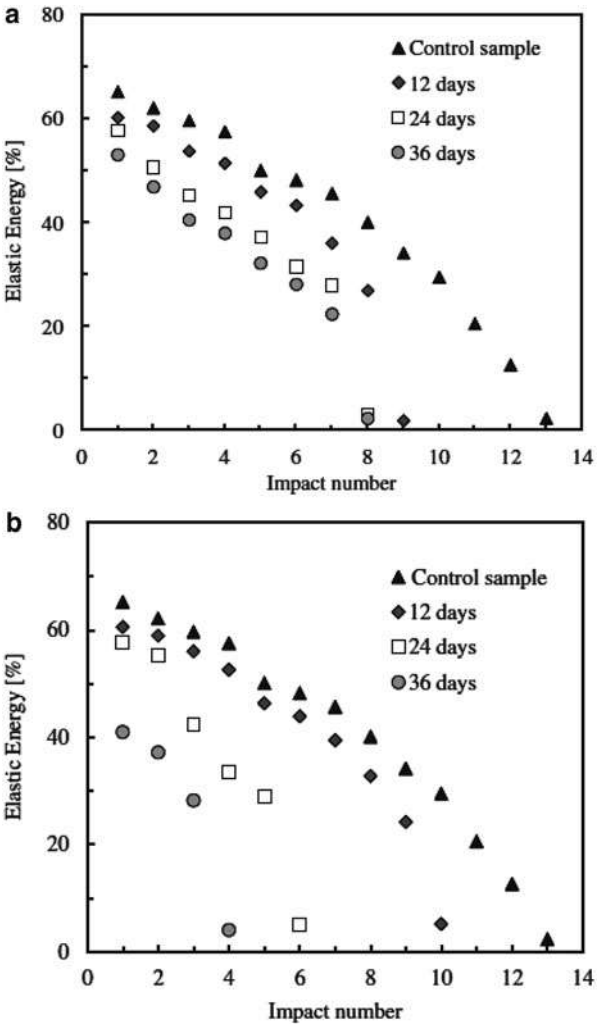

Fig. 24 Evolution of the elastic energy with the impact numbers for G/Ep composite specimens exposed to (**a**) HCl, (**b**) NaOH (Amaro et al. 2013a)

According to Kattaguri et al. (Kattaguri et al. 2019), the decrease observed in the flexural strength of G/Ep can be explained by the free electron of HNO_3 which might interfere with the hydrogen bonding between water molecules and hydrophilic groups within the epoxy matrix. In this way, HNO_3 can breakdown the polymer matrix and promote deterioration at the fiber-matrix interface. In comparison to acidic aging in HNO_3 solution, alkaline aging in KOH solution induced a greater extent of degradation in the flexural properties which is attributed to the combined action of water and KOH. KOH is known as a strong corrosive fluid and a highly nucleophilic anion which can attack the polar bonds of the polymer. When the FRE

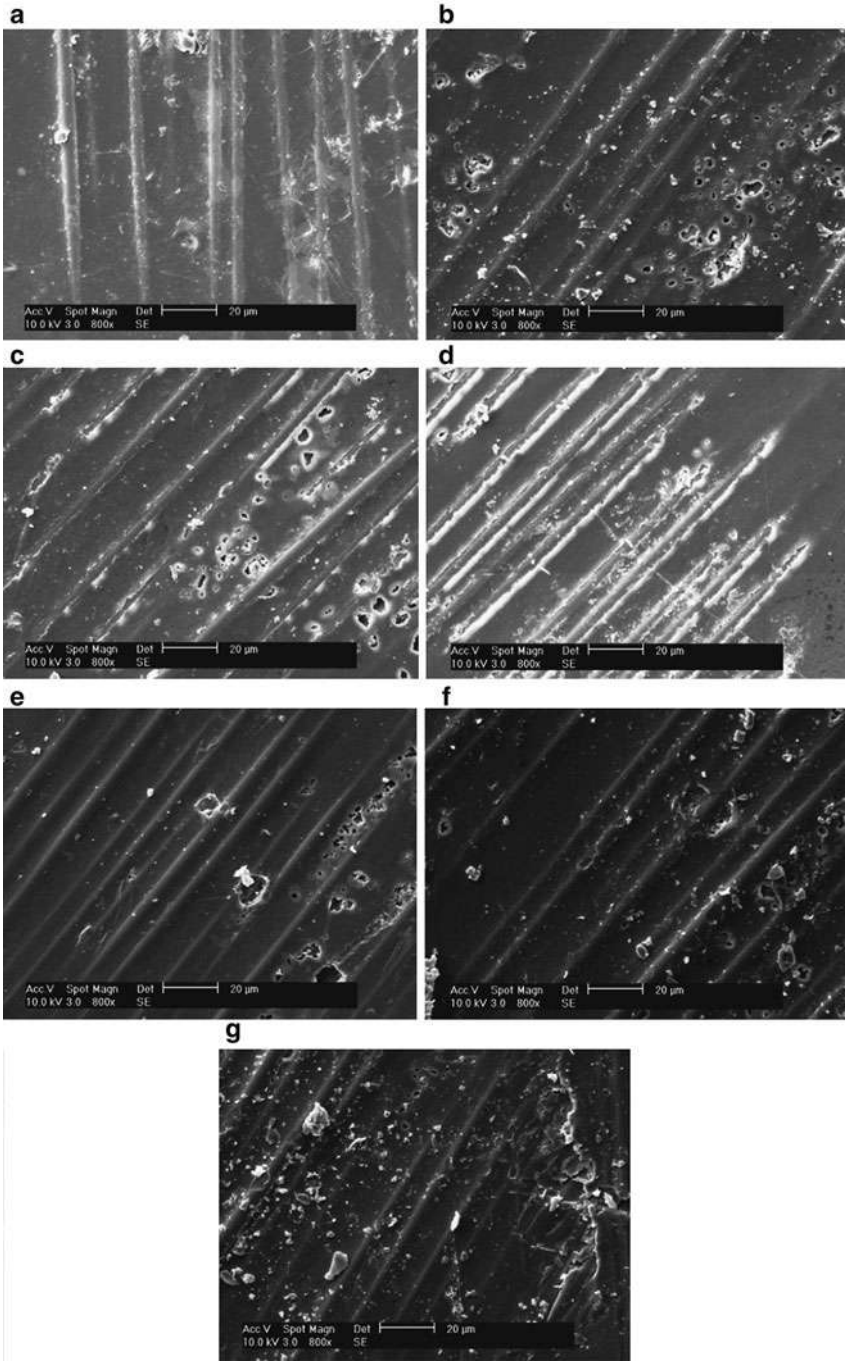

Fig. 25 (continued)

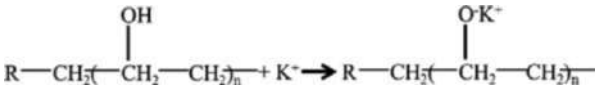

Fig. 26 Possible changes in polymer structure due to alkaline aging (Kattaguri et al. 2019)

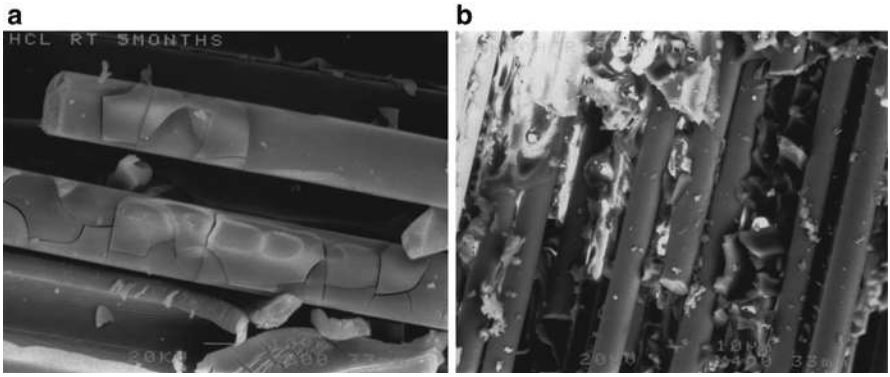

Fig. 27 SEM pictures for G/Ep composites aged in, (**a**) 1 molar HCl solution, (**b**) 5 molar NaOH solution, at room temperature for 5 months (Kajorncheappunngam et al. 2002)

composites are aged in the alkaline solution, hydrogen from the polymer chain can be replaced by potassium, as shown in Fig. 26 (Kattaguri et al. 2019). The significant reduction in the flexural strength of composites in alkaline aging could also be due to the direct chemical attack of KOH solution on the glass fibers, as reported by Bashir et al. (Bashir et al. 2018).

A review of similar researches in this context indicates that more sensitivity of FRE composites to alkaline solutions compared to acidic solutions is not a general rule. For example, it has been reported that the reduction in tensile strength of G/Ep composites in 1 molar HCl solution was significantly more than that in the alkaline medium (5 molar NaOH solution) at room temperature (Kajorncheappunngam et al. 2002). The dramatic reduction of 73% in ultimate tensile strength after 5 months of immersion in HCl solution was attributed to the degradation of glass fibers or the fiber-matrix interface, as shown in Fig. 27. Cracks visible on the fiber surface imply that the acid solution reached the glass fibers surface and attacked their integrity (Fig. 27a). In contrast, Fig. 27b demonstrates such cracks were not observed in fibers immersed in the alkaline solutions (Kajorncheappunngam et al. 2002).

A similar finding was reported on G/Ep composite pipes where the loss of flexural strength was about 36% in acidic solution (5% H_2SO_4), whereas it was around 18%

Fig. 25 SEM pictures for G/Ep composites, (**a**) control specimens, (**b**) specimens exposed to NaOH during 12 days, (**c**) specimens exposed to NaOH during 24 days, (**d**) specimens exposed to NaOH during 36 days, (**e**) specimens exposed to HCl during 12 days, (**f**) specimens exposed to HCl during 24 days, (**g**) specimens exposed to HCl during 36 days (Amaro et al. 2013a)

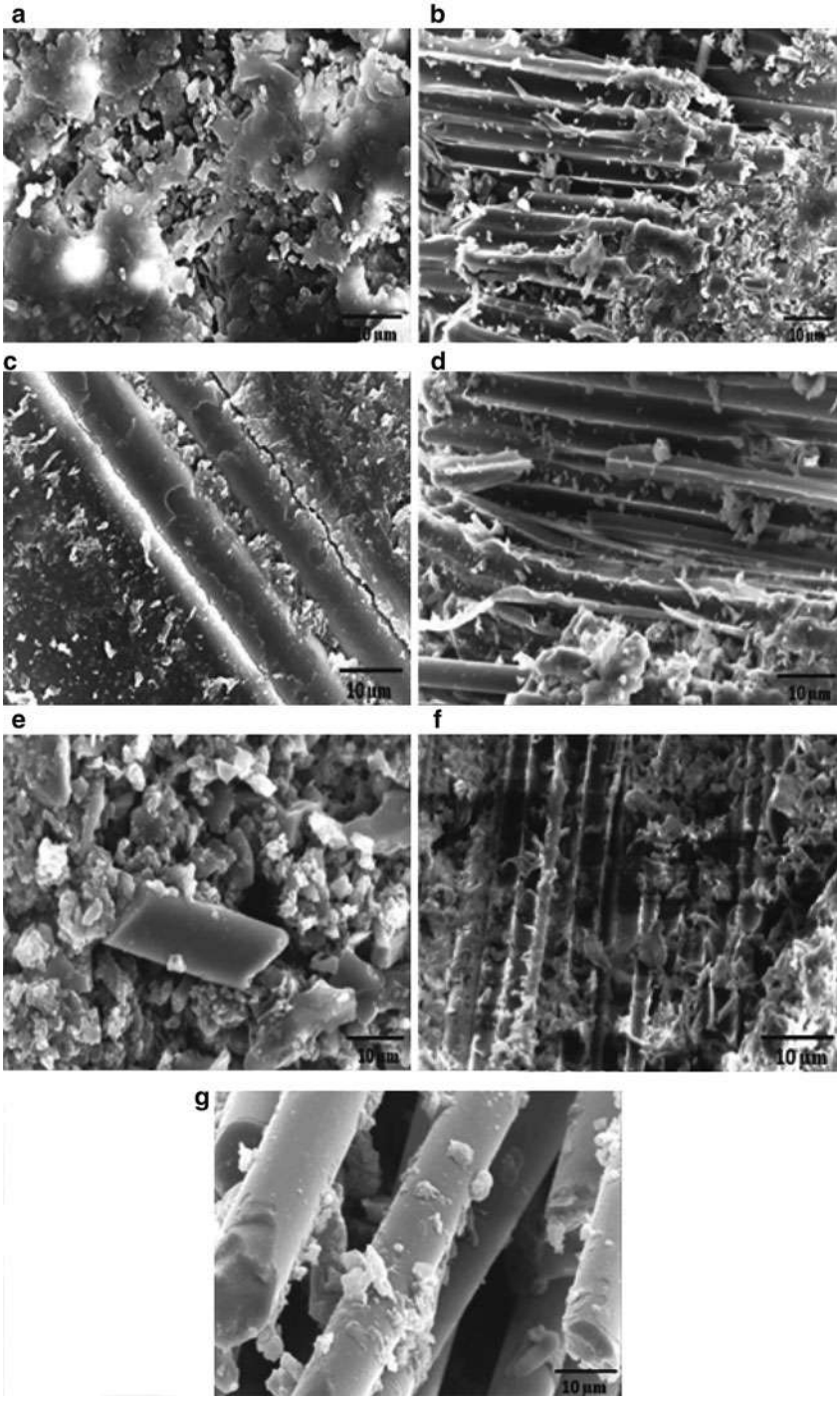

Fig. 28 (continued)

in alkaline solution (10% NaOH) at different aging schedules (Marru et al. 2014). As demonstrated in Figs. 28 and 29, the aging-induced degradations can be observed in the form of flake formation in the epoxy matrix and changes in glass fiber circularity. However, more damages to both the matrix and fiber were observed in the case of the acidic medium.

Even though aging at 55 °C after 5 months led to the breaking of the fibers into pieces, resin was completely dissipated in neither medium, as shown in Figs. 28e and 29e. According to Figs. 28g and 29g, the large void surrounding the glass fibers implies the extensive deterioration of the matrix in the case of aging at 65 °C after 5 months.

Long-Term Performance of the Synthetic Fiber-Reinforced Epoxy Composites at Outdoor Conditions

Although the environmental durability of the FRE composite has been frequently evaluated by several accelerated testing procedures, the higher degradation rates associated with these tests may alter the mechanisms differently from what actually occurs in realistic environments. Besides, the results of accelerated artificial methods are highly dependent on the test setup and are sometimes contradictory (Karbhari et al. 2003). To overcome uncertainties associated with such short-term methods, the most reliable method seems to be naturally exposing the material to long-term outdoor conditions. On the other hand, because the long-term outdoor exposure tests are generally time-consuming and expensive procedures, they are often utilized as the customized programs for the special organizations and industries consuming FRE composites. To the best of the authors' knowledge, there is currently limited comprehensive data available regarding the long-term durability of FRE composites.

Outdoor exposure tests are generally designed and conducted based on the geographical location where the material is intended to be served (such as natural weathering tests including a combination of UV exposure, high/low temperatures, ice, rain, etc.), or the ultimate application of the material (e.g., chemical durability tests on FRE composite transmission pipelines). Moreover, long-term outdoor conditioning can involve several environmental elements, i.e., mechanical stresses, contact with chemicals, moisture and temperature fluctuations, radiation, and biological attacks simultaneously (Martin 2008).

The outdoor weathering effects greatly depend on the climate divisions including tropical, dry, temperate, continental, and polar as well as the service media, e.g., space, aerial, marine, or general industrial. For example, the adverse effect of 1-year weathering in tropical monsoon climate such as Florida may be equivalent to 4–5 years in central Europe with humid continental climates (Martin 2008). It is

Fig. 28 SEM images of G/Ep composite specimens before and after aging in acidic medium, (**a**) un-aged, (**b**) 30 °C after 1 month, (**c**) 30 °C after 5 months, (**d**) 55 °C after 1 month, (**e**) 55 °C after 5 months, (**f**) 65 °C after 1 month, (**g**) 65 °C after 5 months (Marru et al. 2014)

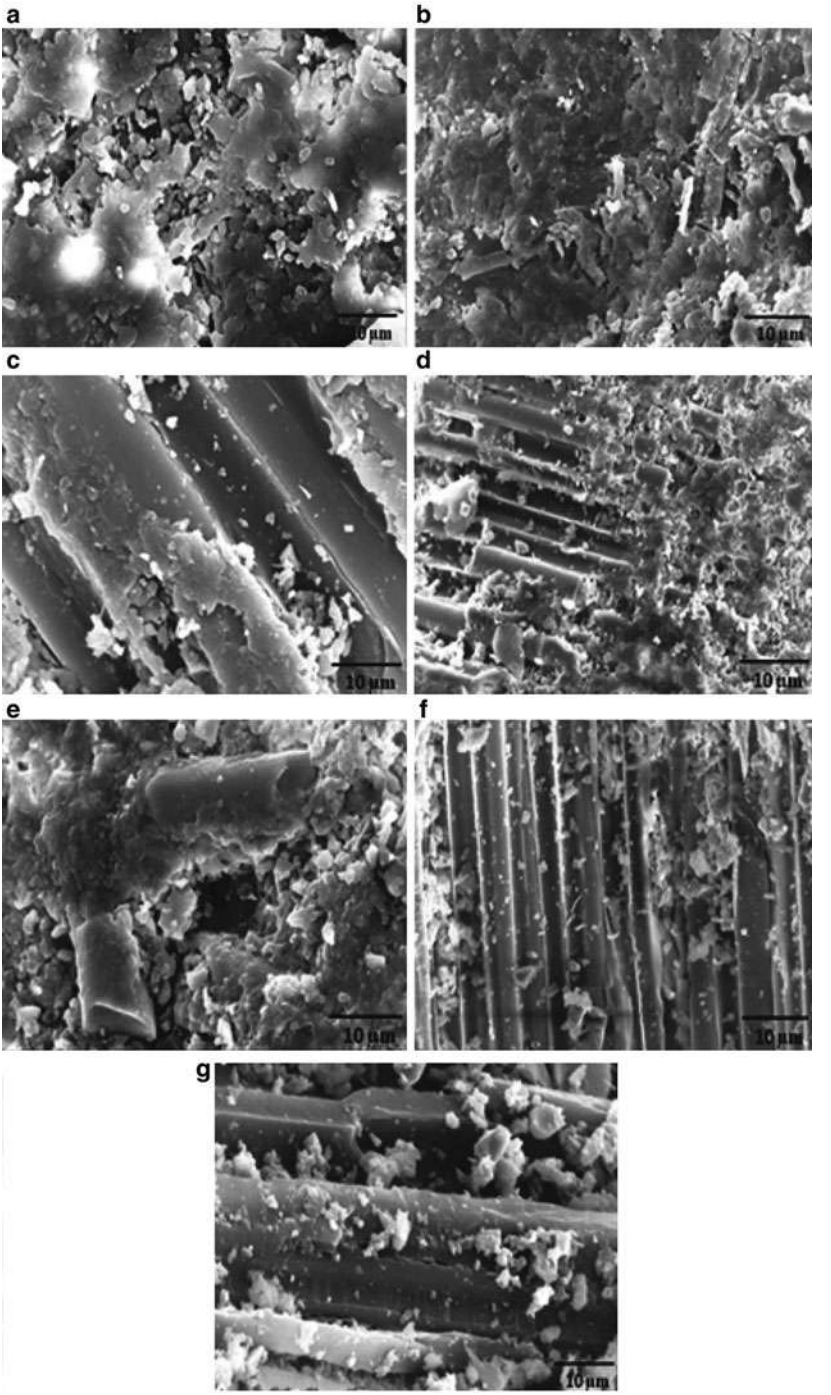

Fig. 29 (continued)

well-known that the effect of long-term outdoor exposure on FRE composites varies from merely cosmetic (i.e., color fading and darkening, loss of gloss and chalking, blooming, and yellowing) to serious structural integrity aspects (Martin 2008) depending on the material constituents and environmental factors.

The results obtained from research performed on T300/AD6005 graphite/epoxy composites exposed to 5-year natural weathering in Daejon, Korea (hot-summer humid continental climate) revealed that all the studied mechanical properties were dramatically reduced. It was found that the matrix-dominated properties (i.e., transverse ones) were affected the most, with the transverse flexural strength and stiffness decreasing by about 18% and 40%, respectively, while the loss of longitudinal flexural strength and stiffness was around 9% and 23%, respectively (Martin 2008). This vulnerability of matrix-dominated properties to natural weathering is generally attributed to the removal of the matrix due to thermal cracking caused by long-term exposure.

Dexter (Dexter 1987) conducted a worldwide outdoor exposure testing program in North America (Hampton, San Francisco, San Diego, Honolulu), Germany (Frankfurt), New Zealand (Wellington), and Brazil (Sao Paulo) on several advanced FRE composite laminates for 1, 3, 5, 7, and 10 years. In general, the 10-year outdoor exposure in various environments could deteriorate the studied mechanical properties of Kevlar/epoxy composites more than those of graphic/epoxy systems. The moisture absorption of Kevlar/epoxy systems was found to more than 2.2%, whereas this value for graphic/epoxy composites was in the range of about 0.6–1.2%. After 10 years of outdoor exposure in Hampton, the moisture absorption of 2.20% and 0.58% was recorded for the K-49/F-155 Kevlar/epoxy composite and T300/5209 graphic/epoxy system, respectively. These values were higher for specimens aged in New Zealand, i.e., 2.57% and 0.71% for K-49/F-155 Kevlar/epoxy and T300/5209 graphic/epoxy composites, respectively. The highest amount of moisture absorption in moist environments was reported for the FRE specimens aged in Brazil and New Zealand. For instance, the moisture absorption for the T300/5209 graphic/epoxy exposed to 10-year outdoor environments in Hampton, San Diego, Honolulu, Germany, New Zealand, and Brazil was found to be about 0.58%, 0.64%, 0.52%, 0.60%, 0.71%, and 0.71%, respectively. The most damages on both the epoxy resin and fibers occurred in Hawaii due to UV radiation, especially for the Kevlar-reinforced composites. The general strength drops for FRE composites were also in the order of 20–25%. It was found that the reduction in shear strength for Kevlar/epoxy systems was significantly more than those of graphic/epoxy composites. For example, the K-49/F-155 Kevlar/epoxy exhibited 12%, 22%, 25%, 17%, 25%, and 26% loss in shear strength after 10-year outdoor exposure in Hampton, San Diego, Honolulu, Germany, New Zealand, and Brazil, whereas these values were found to be less than 10% for T300/5209 graphic/epoxy composites. As a general rule, the

Fig. 29 SEM images of G/Ep composite specimens before and after aging in alkaline medium, (**a**) un-aged, (**b**) 30 °C after 1 month, (**c**) 30 °C after 5 months, (**d**) 55 °C after 1 month, (**e**) 55 °C after 5 months, (**f**) 65 °C after 1 month, (**g**) 65 °C after 5 months (Marru et al. 2014)

specimens exposed to Hampton and Germany environmental conditions suffered less shear strength reduction than others.

David and Margaret Roylance (Roylance and Roylance 1978) studied the effects of degradation induced by long-term weathering on a typical G/Ep composite. The composite specimens were exposed to natural outdoor environments for various times up to 2 years at the Panama Canal Zone (sunny, hot, and humid). The resin yellowing and deterioration were gradually more apparent with increasing the exposure time, especially in outer surfaces of specimens that were directly exposed to the sunlight. The results showed that after 2 years of outdoor exposure, the tensile strength decreased by less than 10%, while during the same period, loss of the flexural strength was more than 30%. These observations indicate that in this type of epoxy-based composites, the flexural properties may be more vulnerable to weathering-induced degradation compared to the tensile properties. The results also demonstrated that the Tg of composite specimens, especially at the outer surfaces, was seriously impressed by outdoor exposure. The reduction of Tg was strongly attributed to photolysis among the network of chemical bonds in the epoxy matrix.

The long-term environmental durability of FRE composite components used in some commercial aircrafts was evaluated by Pride (Pride 1987). Accordingly, six different FRE systems (i.e., T300–5209, T300–2544, AS-3501, and T300–5208 graphite/epoxy composites as well as K49-F155 and K49-F161 Kevlar/epoxy composites) were exposed to several ground-based outdoor environments (Seattle, San Francisco, San Diego, Honolulu, Frankfurt, Sao Paulo). For 3 years of outdoor ground-based worldwide exposures, there had been no significant indication of degradation in flexural, interlaminar shear, and compressive strength. It can be concluded that 3-year outdoor exposure was probably inadequate to seriously deteriorate the structural performance of the aforementioned high-quality FRE composites.

The effect of a warm humid climate (Batumi on the Black Sea coast) on the mechanical properties of different types of FRE systems for aviation application after a long-term real exposure was investigated by Startsev et al. (Startsev et al. 1999). Surprisingly, after 2 years of natural climatic exposure, the flexural strength of an aramid/epoxy system not only exhibited no loss, but also an indication of strength-increasing due to the post-curing of the epoxy matrix was evident. However, as time increased, the flexural strength was gradually impressed and after 6 years of aging reduced by about 18%. It was also found that the tensile fatigue strength had a higher sensitivity to the accumulation of weathering-induced surface damages compared with the tensile strength and flexural strength. After 2 years of climatic exposure, no adverse effect on the tensile strength and flexural strength of another type of aramid/epoxy composite was observed, while the tensile fatigue strength decreased by about 16% at the same exposure duration.

It is clear from both the abovementioned and other relevant investigations that evaluating the long-term performance of the FRE composites at outdoor conditions is a rather complex issue including numerous environmental- and material-dependent parameters. It means that the type and nature of synthetic fibers and

epoxy matrix, manufacturing method, fabrication quality, as well as climatic conditions, annual and seasonal changes, duration of exposure, etc. are determining factors affecting the long-term durability of FRE composites during their service life.

Conclusion and Future Trends

In this chapter, some aspects of environmental durability involving epoxy-based composites reinforced by synthetic fibers were discussed. It might provide some useful information concerning the fiber-reinforced epoxy (FRE) composites in different industrial sectors. Evaluating residual mechanical properties (i.e., tensile, flexural, shear, etc.) after exposure to the simulated real-service condition has been frequently employed as a convenient approach to predict the environmental durability of FRE composites. Besides, complementary scanning electron microscopy (SEM), dynamic mechanical analysis (DMA), differential scanning calorimetry (DSC), and thermomechanical analysis (TMA) may be performed to characterize the material degradation further. Although the degradation in FRE composites often occurs in a long-term mode, several accelerated testing protocols for reducing the time required for starting the deterioration have been scientifically accepted. A wide range of degradation agents was identified in this chapter, including hygrothermal/thermal aging, hygrothermal/thermal cycling, saltwater immersion, elevated temperatures and fire, cryogenic temperatures, UV radiation, and alkaline and acidic solution. Generally, most of the abovementioned environments have detrimental effects on the original properties of FRE composites. While some environmental conditions such as hygrothermal aging at medium temperatures may slowly degrade the properties of epoxy-based composites, other harsh conditions, e.g., fire, can quickly compromise their strength, leading to rapid catastrophic failure in the structure. The environmental degradation in the fiber-matrix interface has been also demonstrated that to be the most detrimental to the properties and performances of FRE composites. Although a good fundamental understanding of the mechanisms associated with environmental degradation processes in FRE composites has been currently established, in many cases this has not yet been formalized into the standardized testing methods. It is also strongly recommended that some unexpressed aspects associated with the environmental durability of FRE composites be addressed in future works, as follows:

1. Extend the study to other aggressive environments such as weathering (including rain, ozone, hailstone impact, and sand erosion), electrical stress (e.g., lightning stress and galvanic reactions), combined load (i.e., stress) and environmental exposures, microorganisms (e.g., fungi), etc.
2. Develop reliable nondestructive methods to characterize the environmental durability of FRE composites.
3. Understand the synergistic effect of different degradation mechanisms.
4. Develop testing standards to guide specific types of environmental conditions.

5. Increase the accuracy of comprehensive analytical models for simulation of degradation mechanisms in FRE composites.
6. Study the benefits promoted by the nanoparticles in this field.

References

B. Abdel-Magid, S. Ziaee, K. Gass, M. Schneider, Compos. Struct. **71**, 320–326 (2005)

A.M. Amaro, P.N.B. Reis, M.A. Neto, C. Louro, J. Reinf. Plast. Compos. **32**(14), 1018–1029 (2013a)

A.M. Amaro, P.N.B. Reis, M.A. Neto, C. Louro, Polym. Degrad. Stab. **98**, 853–862 (2013b)

J. Bai (ed.), *Advanced Fibre-Reinforced Polymer (FRP) Composites for Structural Applications* (Woodhead Publishing Limited, 2013)

S.T. Bashir, L. Yang, J.J. Liggat, J.L. Thomason, J. Mater. Sci. **53**, 1710–1722 (2018)

S. Birger, A. Moshonov, S. Kenig, Composites **20**(4), 341–348 (1989)

F.U. Buehler, J.C. Seferis, Compos. A **31**(7), 741–748 (2000)

L.A. Burns, S. Feih, A.P. Mouritz, J. Aircr. **47**(2), 529–533 (2010)

X. Cheng, L. Liu, X. Feng, L. Shen, Z. Wu, Low temperature-based flexural properties of carbon fiber/epoxy composite laminates incorporated with carbon nanotube sheets. Macromol. Mater. Eng. (2019). https://doi.org/10.1002/mame.201900247

A.F. Chifu, J.O. Iroh, Polym. Compos. **17**(3), 532–536 (1996)

P. Davies, Y.D.S. Rajapakse, *Durability of Composites in a Marine Environment* (Springer Netherlands, 2014)

P. Davies, F. Mazeas, P. Casari, J. Compos. Mater. **35**(15), 1343–1372 (2001)

J. Decelle, N. Huet, V. Bellenger, Polym. Degrad. Stab. **81**, 239–248 (2003)

H.B. Dexter, *Long-Term Environmental Effects and Flight Service Evaluation of Composite Materials*, NASA Technical Memorandum 89067 (January 1987)

F. Ellyin, R. Maser, Compos. Sci. Technol. **64**, 1863–1874 (2004)

R. Eslami-Farsani, S.M.R. Khalili, M. Najafi, J. Therm. Stress. **36**, 684–698 (2013)

W. Fan, J.L. Li, D. Guo, J. Compos. Mater. **49**, 3189–3202 (2015)

W. Fan, J. Li, Y. Zheng, T. Liu, X. Tian, R. Sun, Polym. Degrad. Stab. **123**, 162–169 (2016)

N. Guermazi, A. Ben Tarjem, I. Ksouri, H.F. Ayedi, Compos. B **85**, 294–304 (2016)

K. Imielinska, L. Guillaumat, Compos. Sci. Technol. **64**, 2271–2278 (2004)

M.D.S. Islam, E. Melendez-Soto, A.G. Castellanos, P. Prabhakar, Cryogenics **72**(1), 82–89 (2015)

R.N. Jana, H. Bhunia, Polym. Compos. **29**(6), 664–669 (2008)

S. Kajorncheappunngam, R.K. Gupta, H.V.S. GangaRao, J. Compos. Constr. **6**, 61–69 (2002)

V.M. Karbhari, J.W. Chin, D. Hunston, B. Benmokrane, T. Juska, R. Morgan, J.J. Lesko, U. Sorathia, D. Reynaud, J. Compos. Constr. **7**(3), 238–247 (2003)

R. Kattaguri, A.O. Fulmali, R.K. Prusty, B.C. Ray, Effects of acid, alkaline, and seawater aging on the mechanical and thermomechanical properties of glass fiber/epoxy composites filled with carbon nanofibers. J. Appl. Polym. (2019). https://doi.org/10.1002/app.48434

S.M.R. Khalili, M. Najafi, R. Eslami-Farsani, Mech. Compos. Mater. **52**, 807–816 (2017)

G. Kotsikos, A.G. Gibson, J. Mawella, Plast. Rubber Compos. **36**, 413–418 (2007)

B.G. Kumar, R.P. Singh, T. Nakamura, J. Compos. Mater. **36**(24), 2713–2721 (2002)

M.S. Kumar, N. Sharma, B.C. Ray, J. Reinf. Plast. Compos. **27**(9), 937–944 (2008)

M.S. Kumar, N. Sharma, B.C. Ray, J. Reinf. Plast. Compos. **28**(16), 2013–2023 (2009)

M.C. Lafarie-Frenot, S. Rouquie, Compos. Sci. Technol. **64**, 1725–1735 (2004)

M.C. Lafarie-Frenot, S. Rouquie, N.Q. Ho, V. Bellenger, Compos. A **37**, 662–671 (2006)

F. Larsson, J. Reinf. Plast. Comp. **5**, 19–22 (1986)

G. Li, S.S. Pang, J.E. Helms, Polym. Compos. **21**(5), 686–695 (2000)

W.B. Liau, F.P. Tseng, Polym. Compos. **19**, 440–445 (1998)

T.Q. Liu, X. Liu, P. Feng, A comprehensive review on mechanical properties of pultruded FRP composites subjected to long-term environmental effects. Compos. B (2020). https://doi.org/10.1016/j.compositesb.2020.107958
H. Ma, Z. Jia, K. Lau, J. Leng, D. Hui, Compos. B **92**, 210–217 (2016)
P. Marru, V. Latane, C. Puja, K. Vikas, P. Kumar, S. Neogi, Fibers Polym. **15**(9), 1935–1940 (2014)
R. Martin (ed.), *Ageing of Composites* (Woodhead Publishing, Cambridge, 2008)
N. Merah, S. Nizamuddin, Z. Khan, F. Al-Sulaiman, M. Mehdi, J. Reinf. Plast. Compos. **29**(20), 3104–3110 (2010)
A.H.I. Mourad, B.M. Abdel-Magid, T. El-Maaddawy, M.E. Grami, Appl. Compos. Mater. **17**, 557–573 (2010)
A.P. Mouritz, J. Mater. Sci. **37**, 1377–1386 (2002)
M. Najafi, R. Ansari, A. Darvizeh, Environmental effects on mechanical properties of glass/epoxy and fiber metal laminates, Part I: hygrothermal aging. Mech. Adv. Compos. Struct. **4**, 187–196 (2017). https://doi.org/10.22075/MACS.2016.507
M. Najafi, A. Darvizeh, R. Ansari, Fibers Polym. **19**(9), 1956–1969 (2018)
M. Najafi, A. Darvizeh, R. Ansari, Proc. Inst. Mech. Eng. L **233**(8), 1542–1554 (2019a)
M. Najafi, R. Ansari, A. Darvizeh, Proc. Inst. Mech. Eng. C J. Mech. Eng. Sci. **233**(19–20), 7003–7018 (2019b)
M. Najafi, R. Ansari, A. Darvizeh, Polym. Compos. **40**(6), 2523–2533 (2019c)
O. Ozcelik, L. Aktas, M.C. Altan, Exp. Polym. Lett. **3**, 797–803 (2009)
A. Paillous, C. Pailler, Composites **25**, 287–295 (1994)
G.C. Papanicolaou, A.G. Xepapadaki, G.D. Tagaris, Compos. Struct. **88**, 436–442 (2009)
S.Y. Park, W.J. Choi, H.S. Choi, Compos. Struct. **92**, 18–24 (2010)
G.A. Pering, P.V. Farrell, G.S. Springer, J. Compos. Mater. **14**, 54–66 (1989)
H.R. Phelps, E.R. Long Jr., J. Compos. Mater. **14**, 334–341 (1980)
R.A. Pride, *Environmental Effects on Composites for Aircraft*, NASA Technical Memorandum 78716 (May 1987)
S. Putic, M. Stamenovic, B. Bajceta, P. Stajcic, S. Bosnjak, J. Serb. Chem. Soc. **72**(7), 713–722 (2007)
T.H.Y. Quach, A. Benelfellah, B. Batiot, D. Halm, T. Rogaume, J. Luche, D. Bertheau, J. Compos. Mater. **51**(1), 17–29 (2017)
B.C. Ray, J. Mater. Sci. Lett. **22**, 201–202 (2003)
P.K. Ray, S. Mula, U.K. Mohanty, B. Ray, J. Reinf. Plast. Compos. **26**, 519–524 (2007)
D. Roylance, M. Roylance, Polym. Eng. Sci. **18**(4), 249–254 (1978)
N. Rull, R. Ollier, G. Francucci, E. Rodriguez, V. Alvarez, J. Compos. Mater. **49**(13), 1629–1637 (2015)
K.B. Shin, C.G. Kim, C.S. Hong, H.H. Lee, Compos. B **31**, 223–235 (2000)
M.J. Shukla, D.S. Kumar, K.K. Mahato, D.K. Rathore, R.K. Prusty, B.C. Ray, *A Comparative Study of the Mechanical Performance of Glass and Glass/Carbon Hybrid Polymer Composites at Different Temperature Environments*. Paper presented at 4th National Conference on Processing and Characterization of Materials, Rourkela (5–6 December 2014)
J. Stabik, Polym. Test. **24**, 101–103 (2005)
O.V. Startsev, A.S. Krotov, L.T. Startseva, Polym. Degrad. Stab. **63**, 183–186 (1999)
L.H. Strait, M.L. Karasek, M.F. Amateau, J. Compos. Mater. **26**(14), 2118–2133 (1992)
J.F. Timmerman, M.S. Tillman, B.S. Hayes, J.C. Seferis, Compos. A **33**, 323–329 (2002)
T.K. Tsotsis, J. Compos. Mater. **32**(11), 1115–1135 (1998)
T.K. Tsotsis, Y. Weitsman, J. Reinf. Plast. Compos. **9**(5), 420–445 (1990)
K. Wang, B. Young, S.T. Smith, Eng. Struct. **33**, 2154–2161 (2011)
Y.J. Weitsman, *Fluid Effects in Polymers and Polymeric Composites* (Springer US, 2012)
S. Zainuddin, M.V. Hosur, Y. Zhou, A. Kumar, S. Jeelani, Mater. Sci. Eng. A **527**(13–14), 3091–3099 (2010)
Y. Zhong, S.C. Joshi, Mater. Des. **65**, 254–264 (2015a)
Y. Zhong, S.C. Joshi, J. Compos. Mater. **49**(7), 829–841 (2015b)

Modeling and Simulation of Epoxy/Synthetic Fiber Composites

13

Mauricio Torres-Arellano and Saul Piedra

Contents

Abstract

Modeling and simulation of epoxy/synthetic fiber composites has gained a lot of attention in the last two decades, because of the numerous industries that employ such materials. In the last two decades, improvements of computational power have incremented the precision to simulate composite structures under multiple phenomena. Since the beginning of composite simulation, the transition from microscale to mesoscale and then to macroscale and vice versa has been one of the key issues to perform robust calculations and to obtain accurate results. In this chapter, we collect the improvements of modeling and simulation of epoxy/synthetic fiber composites by tackling two main topics for researchers: (1) interaction of resin fibers during manufacturing process and (2) mechanical

M. Torres-Arellano (✉) · S. Piedra
Center for Engineering and Industrial Development (CIDESI), National Council for Science and Technology of México (CONACYT), Santiago de Querétaro, Mexico
e-mail: mauricio.torres@cidesi.edu.mx; saul.piedra@cidesi.edu.mx

S. Mavinkere Rangappa et al. (eds.), *Handbook of Epoxy/Fiber Composites*,
https://doi.org/10.1007/978-981-19-3603-6_15

performance of consolidated composite. Both topics are addressed in the three scales, because material and structure, in the case of composites, are created at the same time. Fist part deals with the simulation of liquid composite manufacturing (LCM) by approaching the interaction of a liquid with transient viscosity (epoxy resin) and a porous media (synthetic fiber preform). Weaving, fiber waviness, closure factor, and type of fiber define the preform permeability, resulting in impregnation paths and finally defining the final physical properties of the composite. Also, resin manufacturing parameters, such as injection pressure, temperature, and inlet-outlet position, influence the resin flow path, and in consequence the surface quality, the appearance of inner flaws, and, finally, defining the performance of the consolidated material. The main goal of this type of numerical simulation is to improve the efficiency of the manufacturing process and to obtain a good-quality product. Second part deals with the simulation of mechanical performance of fiber composites, by approaching multi-scale models where the micromechanics, cohesive conditions between fibers and matrix, define the unit cell behavior (tows, weave, and resin), and then the macroscopic properties are calculated. Stratified theory and failure criteria coupled with damage mechanics at the mesoscale currently result in robust simulations where delamination and crack path can be identified. Moreover, cohesive zone models plus extended finite element method (XFEM) is currently used to compute crack propagation or even fatigue. This chapter wants to be a summary where the reader can find the current state-of-the-art and novel trends for modeling and simulating epoxy/synthetic fiber composites.

Keywords

Composites · Manufacturing · CFD · FEM · Multi-scale approach

LCM Process Modeling and Simulation

Introduction – Liquid Composite Moulding Process

Polymer composites are considered advanced materials made by combining a polymer with a technical textile (i.e., carbon or glass fibers). These composites have the advantage of being lightweight and corrosion-resistant and having a high mechanical performance, making them very versatile materials that are being adopted for a large number of applications ranging from aerospace, automotive, naval, and infrastructures (Carlone et al. 2018). However, manufacturing issues make difficult their introduction to some industrial applications, and the solutions with this kind of materials are still under developments. The most common and well-established manufacturing technique for high-performance structural applications is the autoclave curing. Nevertheless, autoclave curing requires high costs for installation, operation, and tooling. For this reason, the out-of-autoclave manufacturing techniques have gained many attention in order to reduce manufacturing costs especially for large and complex parts.

Many ways to combine a polymeric matrix with reinforcing fibers out of autoclave have been developed in the last decades (Mazumdar 2002). In particular, liquid

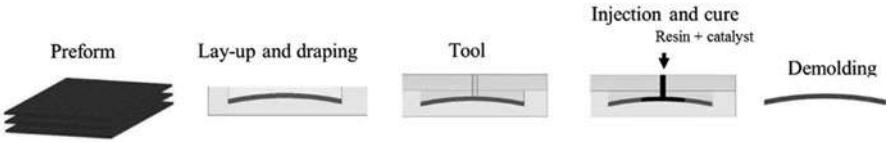

Fig. 1 Schematic steps of the LCM process. (Credits by the authors)

composite molding (LCM) processes are widely used to manufacture large and complex components in the automotive and aeronautic industry. The main stages of the LCM process are shown illustrated in Fig. 1 (Hoa 2009).

In the preforming stage, dry fibers are piled up in a preform with the geometry of the part to be fabricated. The dry fibers are usually random mats or woven fabrics. For complex parts adhesives are frequently utilized to hold the fibers on the preform. Once all the fibers layers are piled up in the preform, it is placed inside a mold that usually is conformed by two metallic parts or for specific processes (VARTM, SCRIMP) only one mold part is metallic, and the other is composed by a flexible membrane. The last save manufacturing costs especially for large and complex components. Additionally, if it is required, high pressure can be applied to the mold in order to enhance the quality of the final part (reduce void formation). In the next stage, resin is infused into the mold to impregnate the fibers and fill completely the preform. The resin infusion time depends on the size and complexity of the part and, also, on the curing kinetics of the polymer resin used. After the resin flows into the mold and filling the preform and for the case of polymer matrix composites, the solidification process is a cross-linking reaction called curing, which converts the polymeric resin in a hard, brittle solid (Pillai 2004). For this purpose, the resin is combined with catalysts before the infusion stage, and also heat sources can be used to accelerate the curing. Finally, after the curing process, the part is removed from the mold. LCM processes were developed in order to reduce the manufacturing cost for large and complex composite parts for which autoclave process becomes impractical. There exist many variants of the LCM that depends on the operating conditions of the process, the type of the mold used, the required fiber volume fraction, and the final application of the part. A description of the different LCM variants can be found in (Hoa 2009).

Flow Through Porous Media: Macroscopic Modeling for a LCM Process

The critical stage of the LCM processes is the resin infusion. During this stage, the resin flows through the preforms of fibers, and the porous must be fully filled by the resin in order to minimize defects in the final product. Also, the resin infusion must be performed at certain operating conditions in order to avoid changing the fibers orientations in the plies that conforms the preform.

The resin infusion depends on many factors: pressure, position of the inlet and outlet gates, fiber permeability and porosity, geometry of the preform, etc. Then, it is very difficult to design the mold and the process for a specific part only by designer

intuition or experience (Pillai et al. 1993). Additionally, trial-and-error methods to design and optimize composite manufacturing processes are time consuming and economically prohibitive (Tan and Pillai 2012).

In order to support and optimize the LCM design processes, computational simulations based on the mass, momentum, energy, and chemical reaction conservation equations are implemented. Several approximations have been proposed for the resin impregnation stage depending on the level of detail at which it is required to analyze the flow (Pillai 2004).

Usually, the resin flow through the preforms is treated as an incompressible flow in an anisotropic porous medium (Kang et al. 2000; Dusi et al. 1987; Hirt and Nichols 1981). In this situation, the resin flow can be analyzed by solving the so-called Darcy's law which relates the mean velocity flow through the porous medium with the pressure gradient:

$$\boldsymbol{v} = -\frac{\boldsymbol{K}}{\mu}\nabla P \tag{1}$$

where $\boldsymbol{v}$ is the volume average Darcy velocity, $\boldsymbol{K}$ is the permeability tensor of the porous medium, μ is the dynamic viscosity, and P is the averaged resin pressure. The Darcy's law is complemented by the mass conservation equation which for an incompressible flow is given by:

$$\nabla \cdot \boldsymbol{v} = 0 \tag{2}$$

The resin impregnation is a non-isothermal process since exothermic chemical reactions occurs while the polymer cures. Due to the high effect that the temperature has over the viscosity, the energy and a transport equation for the curing process must be also solved in order to have a good approximation of the process. The energy conservation equation for the resin fiber mixture in terms of temperature is (Kang et al. 2000):

$$\rho c \frac{\partial T}{\partial t} + \rho_r c_r \boldsymbol{v} \cdot \nabla T = k \nabla^2 T + \varphi \dot{G} \tag{3}$$

where T is the temperature, ρ, c, and k are the density, heat capacity, and thermal conductivity of the mixture, respectively, φ is the porosity, and $\dot{G}$ is the volumetric heat generation due to the chemical reaction of the curing process. In order to close the system and take into account the exothermic reaction and the resin kinetics, an equation for the degree of cure is integrated to the model:

$$\frac{\partial \alpha}{\partial t} + \frac{1}{\varphi} \boldsymbol{v} \cdot \nabla \alpha = \dot{m} \tag{4}$$

where α is the degree of cure and $\dot{m}$ is the generation of mass of cured resin that can be approximated by the following relation:

$$\dot{m} = (k_1 + k_2\alpha^m)(1-\alpha)^n \tag{5}$$

where constants k_1, k_2, m, and n can be determined by the methodology described in (Dusi et al. 1987), using experimental results from a differential scanning calorimeter (DSC). The heat generation $\dot{G}$can be calculated in terms of $\dot{m}$ as:

$$\dot{G} = \Delta H \dot{m} \tag{6}$$

where ΔH is the heat of the exothermic reaction. The set of partial differential equations is usually solved using a control volume finite element method (FEM-CV). Additionally, in order to track the resin interface, the volume of fluid (VOF) method is incorporated. Details of the VOF computational implementation can be found in (Hirt and Nichols 1981). For the purposes of the present work, only isothermal flows will be reviewed in the next sections.

Permeability: Theoretical and Measurement Methods

Permeability links the microstructure of the fiber reinforcement with the path for which the resin flows through it. Besides, this parameter depends on the resin properties and manufacturing process conditions. The determination of woven fibers permeability is one of the most important for predicting with a relative high precision the LCM processes. There exist different methodologies in order to compute the fibers reinforcement permeability, based on theoretical models (Gebart 1992; Yuan et al. 2019), experimental measurements (Naik et al. 2014), and numerical simulations (Fournier et al. 2005; Belov et al. 2004; Ngo and Tamma 2001).

In the simplest case, where the flow through fibers can be considered in a preferential direction, several models for computing the permeability have been developed; those models relate the volume fraction and tow geometry of the fibers with the permeability. The most known model is the Kozeny-Carman equation (Hoa 2009):

$$K = \frac{r^2}{4k_0}\frac{\left(1-V_f\right)^3}{{V_f}^2} \tag{7}$$

where K is the permeability in a preferential direction, r is the fiber radius, V_f is the volume fraction ($V_f = 1 - \varphi$), and k_0 is a constant that depends on the orientation of the fibers with respect to the flow direction (see Fig. 2).

For woven fibers, it is possible to estimate the permeability in plane directions *(x,y)* using the appropriate constants given in Table 1. The constants depend on the angle-ply laminate with respect to the flow direction.

As it was commented, several analytical and semi-analytical models have been developed to estimate the permeability in woven fabrics; a complete review of these

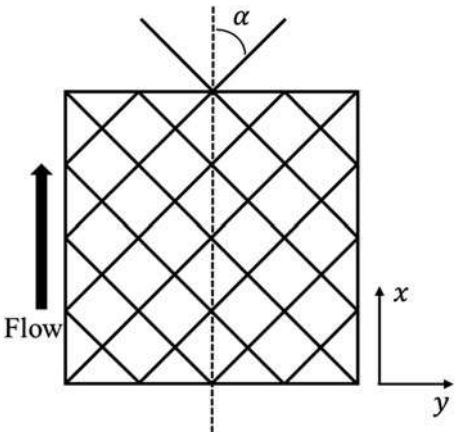

Fig. 2 Angle-ply laminate with respect to the flow direction. (Credits by the authors)

Table 1 In-plane Kozeny constants for a preform with α angle-ply laminate

α [°]	k_{0x}	k_{0y}
0	0.68	11
15	1.18	10.1
30	1.49	6.65
45	2.7	2.7

Courtesy of S.V. Hoa (2009)

models can be found in (Xiao 2012). A very useful analytical model is the proposed by Gebart (Gebart 1992) for predicting the permeability of fiber bundles for a flow perpendicular to and parallel with unidirectional filaments:

$$K^{\parallel} = \frac{8r^2}{53} \frac{\left(1 - V_f\right)^3}{{V_f}^2} \tag{8}$$

$$K^{\perp} = \frac{16}{9\pi\sqrt{6}} \left(\sqrt{\frac{V_{fmax}}{V_f} - 1} \right)^{2.5} r^2 \tag{9}$$

Equations 8 and 9 are widely used to compute the intra-tow permeability in the multi-scale modeling that will be discussed in the last section of this work.

When composite laminates are designed, different fiber orientations are considered depending on the required mechanical behavior. For these cases, analytical models must be used to calculate the individual permeability of each ply of the laminate, and an average can be used to calculate an effective laminate permeability and solve the porous media equations. However, an intrinsic error will be introduced since the interfacial effects between each composite ply are neglected.

Another way to compute the permeability is through experimental characterization. Several experimental methods have been developed to perform indirect measurements of the permeability. Very detailed studies about permeability characterization from

experimental results can be found in (Naik et al. 2014; Sharma and Siginer 2010; Karaki et al. 2019).

In general, the permeability measurements can be classified based on the saturation o unsaturation of the fiber preform as an initial condition for the experiment. Saturated permeability is quantified when the preform is wetted before the experiment. On the other hand, unsaturated permeability is measured, while the preform is filled by resin and is usually quantified by capturing the advance of the resin front in the dry preform (Sharma and Siginer 2010). Actually, this unsaturated permeability is the correct input parameter for macroscopic LCM process simulations. The permeability measurement methods can be also classified based on the flow configuration (one-direction or radial) and on the control operating conditions of the experiment (constant pressure or constant velocity injection). In the next subsections, two classic experimental methods for measuring the permeability are briefly described.

Radial Flow Experiments

In radial flow experiments, resin is injected through a central inlet port. The resin advances in the fibers forming an elliptical front (circular for quasi-isotropic materials). The main advantage of this experimental configuration is that the two in-plane permeability components can be computed. For orthotropic materials, the two components of the in-plane unsaturated permeability are calculated from the position of the resin front (x_f, y_f) at a specific time t and the coordinates of the inlet gate (x_0, y_0) (Weitzenbock et al. 1999):

$$K_{11}^{US} = \frac{\mu\varphi}{4t\Delta \mathrm{P}} \left\{ x_f^2 \left[2\, ln \left({}^{x_f}\!/_{x_0} \right) - 1 \right] + x_0^2 \right\} \tag{10}$$

$$K_{22}^{US} = \frac{\mu\varphi}{4t\Delta \mathrm{P}} \left\{ y_f^2 \left[2\, ln \left({}^{y_f}\!/_{y_0} \right) - 1 \right] + y_0^2 \right\} \tag{11}$$

Examples of measurements using the radial flow experiments can be found in (Alhussein et al. 2016), where the unsaturated permeability is estimated for three different 3D woven fabrics. In Fig. 3, the advance of the resin front for the three woven fabrics can be observed. The in-plane permeability components are oriented as the marked major and minor axes of the ellipse.

Channel Flow Experiments

The channel flow method is very similar to the Darcy's experiment (Brown 2001). This experimental method consists in use a rectangular mold where the resin is injected at constant velocity or pressure from one of the sides unidirectional to the opposite side (see Fig. 4). The other two sides are sealed tightly against the reinforcement so that the tow front becomes a straight line.

If the resin is injected to a constant pressure, the flow exhibits a linear pressure distribution between the injection gate and the resin front. Integrating the Darcy's law in terms of the resin front position, the permeability can be computed as:

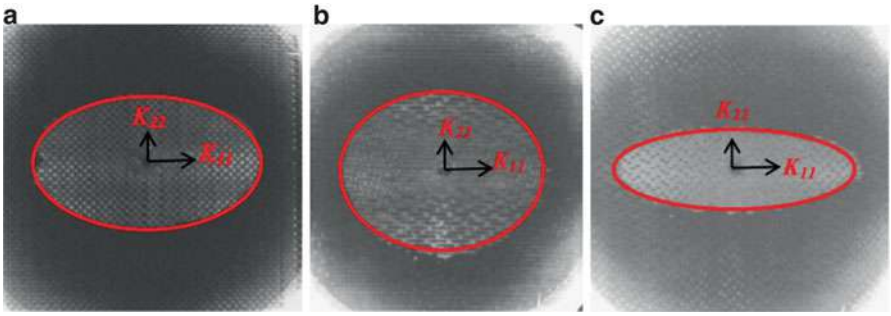

Fig. 3 Advance of the flow front during in-plane permeability tests for three different 3D woven fabrics architectures. (Courtesy of H. Alhussein, reproduced with thanks from Springer) (Alhussein et al. 2016)

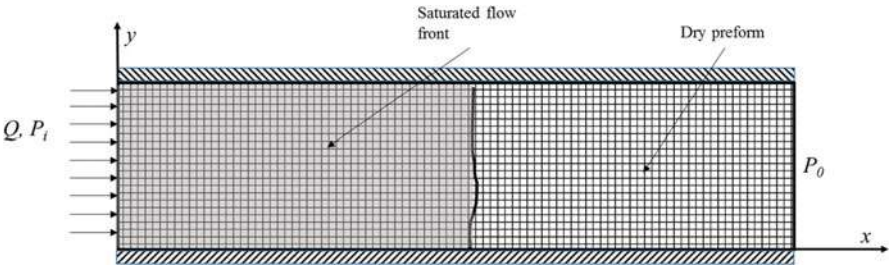

Fig. 4 Channel flow experiment arrangement. Boundary conditions are shown. (Credits by the authors)

$$K_x^{US} = \frac{x(t)^2 \mu \varphi}{2tP_i} \tag{12}$$

where x is the position of the resin front and P_i is the injection pressure. Alternatively, if the resin is injected to a constant flow rate, the flow front position increases linearly with time and the permeability is calculated by:

$$K_x^{US} = \frac{Q\mu L}{A\Delta P} \tag{13}$$

where A is the cross-sectional area of the composite, L is the length reached by the flow front, and Q is the flow rate.

As a practical example, the results reported by (Torres et al. 2019) are presented. The main goal of that work was to determine the mold filling time for a nonstructural component of a light sport aircraft using different inlet gate configurations. For this purpose, experimental characterization of the composite laminate was carried out using the channel flow method in order to compute the effective permeability and used as an input parameter for a CFD model. The model for resin flow through the cowling preform was based on the solution of the porous media equations in ANSYS

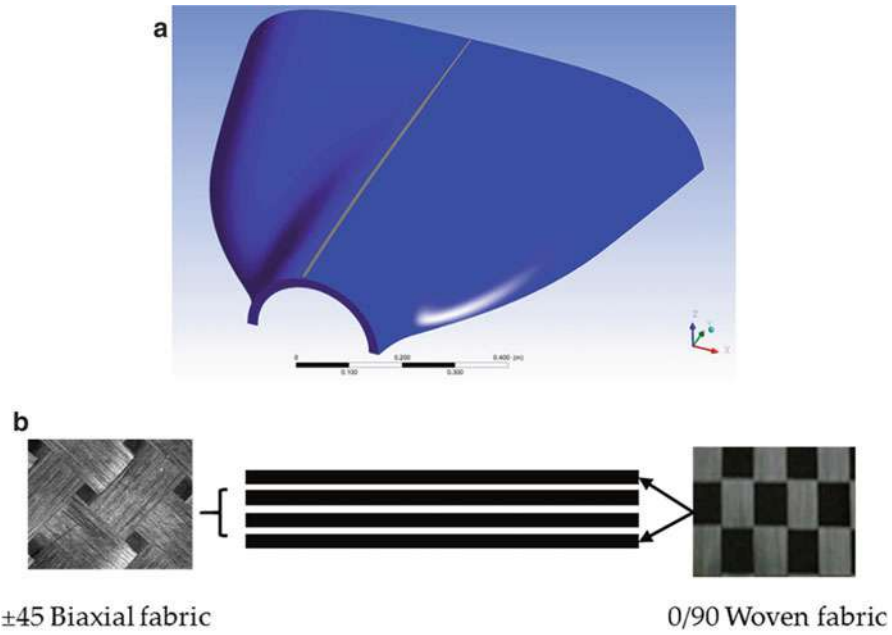

Fig. 5 (**a**) Geometry of the aircraft upper cowling; (**b**) laminate code. (Courtesy of the authors, reproduced with thanks from MDPI) (Torres et al. 2019)

Fluent. The boundary conditions implemented in the model and in the experimental characterization were based on the vacuum pressure that the aircraft manufacturer has been fixed for its VARI processes. The geometry of the aircraft upper cowling is shown in Fig. 5a. The laminate code for manufacturing the upper cowling is shown in Fig. 5b.

In Fig. 6, the filling process of the upper cowling is shown, through the contour map of the resin volume fraction for two different instants of time.

Permeability Estimation Using Numerical Simulations

In addition to analytical models and experimental measurements, several methods have been developed to predict the in-plane permeability tensor numerically. The main idea is to solve the flow at a mesoscale level defining a representative unit cell of the woven fabrics. Once the unit cell is chosen, the next step consists in characterize the geometrical properties of the woven fabrics and model the representative unit cell in a specialized software (i.e., WiseTex (Verpoest and Lomov 2005), TexGen (Lin et al. 2011)). This step is critical for the fidelity of the permeability calculations, since this parameter is highly affected by the geometry of the fabric, and then the most important features of the reinforcement must be taken into account when it is modeled, including yarn paths, cross sections of the yarns, inter-yarn porosity, and distribution of the fiber volume fraction in tows (Belov et al. 2004). Recently, in order to improve the fidelity of the geometrical model for the

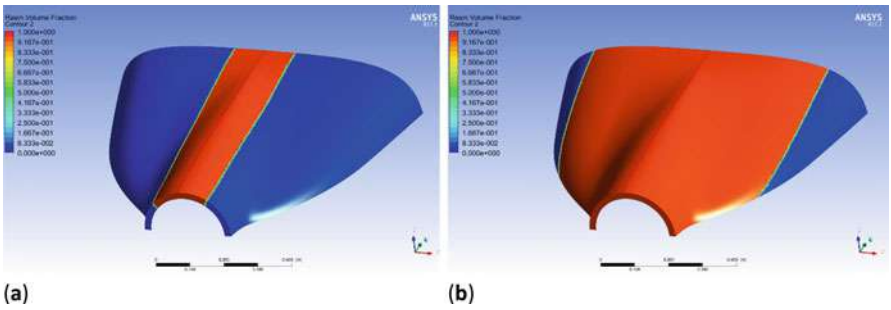

Fig. 6 Results from the computational simulation of the resin impregnation process for the upper cowling (**a**) t = 21 s, (**b**) t = 500 s. (Courtesy of the authors, reproduced with thanks from MDPI) (Torres et al. 2019)

woven fibers unit cells, sophisticated techniques as micro X-ray CT have been used to reconstruct high-fidelity representation of fibers arrangements (Soltani et al. 2017; Ali et al. 2019).

Once the unit cell is defined and constructed, computational fluid dynamics simulations are performed to calculate the pressure and velocity fields. Two different regions are identified in the unit cell with different microstructural levels. The first level consists of the intra-tow region where the fiber filaments are treated as arrays of impermeable cylinders and the second level that consists of the tows in a woven pattern and the fluid inter-tow region (Ngo and Tamma 2001) (see Fig. 7).

The two identified regions in the unit cell are modeled by two different sets of governing equations. On one hand, for modeling the inter-tow fluid region continuity and Stokes equations are utilized:

$$\nabla \cdot \boldsymbol{v} = 0 \tag{14}$$

$$\nabla P = \mu \nabla^2 \boldsymbol{v} \tag{15}$$

On the other hand, the intra-tow region is treated as a porous medium, and the flow is modeled by the continuity and Brinkman equations:

$$\nabla \cdot \langle \boldsymbol{v} \rangle = 0 \tag{16}$$

$$\nabla \langle P \rangle = \mu \nabla^2 \langle \boldsymbol{v} \rangle - \mu \widetilde{\boldsymbol{K}}_{tow}^{-1} \cdot \langle \boldsymbol{v} \rangle \tag{17}$$

The tow permeability $\widetilde{\boldsymbol{K}}_{tow}$ is estimated using empirical, analytical, or semi-analytical models. For instance, in (Belov et al. 2004), the authors assumed that the fiber consists of parallel filaments arranged in a periodic quadratic/hexagonal array; this allows to use the models presented by Gebart to compute the intra-tow permeability (Gebart 1992).

There exist several numerical techniques that can be used to solve the Stokes and Brinkman equations; particularly, three different strategies have been widely

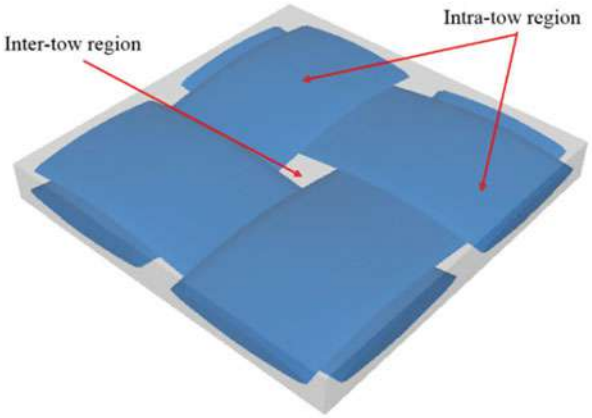

Fig. 7 Unit cell of reinforcement example. Inter-tow region corresponds to the gap between the fiber tows. (Credits by the authors)

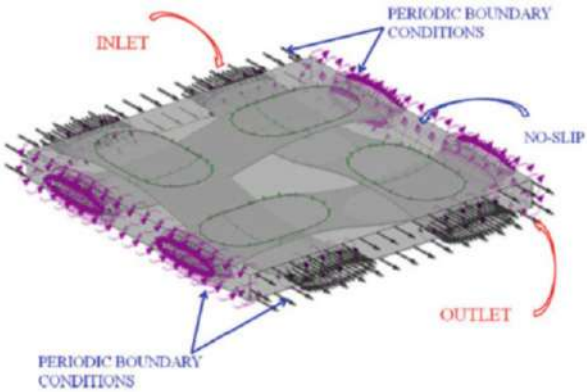

Fig. 8 Unit cell computational domain and boundary conditions that usually are used for computing the permeability. (Courtesy of Pierpaolo Carlone, reproduced with thanks from Springer) (Carlone et al. 2018)

reported in literature: finite element, finite difference, and Lattice-Boltzmann. A detailed description of numerical methods to estimate the permeability can be found in (Karaki et al. 2019). Typical boundary conditions used to solve Stokes and Brinkman equations are shown in Fig. 8. Once the Eqs. (14–17) are solved and the pressure gradient and velocity are computed, it is possible to substitute those values into the Darcy's law (Eq. 1) and calculate the effective permeability in the unit cell. This result can be used as input data for performing macroscopic simulations for large components manufacturing by an LCM process.

Multi-scale Modeling for LCM Processes

At this point, macroscopic models for predicting the resin impregnation stage of the LCM processes have been presented. Additionally, a mesoscopic formulation to

compute the permeability numerically was shown in the previous section. Although the macroscopic models using Darcy's law have been applied with satisfactorily results for large and complex components, several authors have reported important differences between the experimental results and computational simulations (Parnas and Phelan Jr. 1991). Tan and Pillai (Tan and Pillai 2012) explained carefully that the cause of the discrepancies is related to the difference of length scale of the flow in the intra-tow with respect to the inter-tow regions. In this case the woven fabrics behave as a dual porosity medium whose nature suggests the adoption of a multi-scale modeling methodology. The dual porosity medium representation is illustrated in Fig. 9. The resistance to the resin flow inside the fiber bundles (fiber tows in woven fabrics) are larger than outside exhibiting distinct impregnation rates. This produce a delay in the impregnation inside the bundles, and two different length scales must be taken into account for modeling the system.

In the multi-scale approach, the mass balance equation for macroscopic flow (Eq. 2) is modified by incorporation a negative sink term that accounts for the adsorption of resin from the inter-tow region into the tows promoted by their delayed impregnation (Carlone et al. 2018; Pillai and Advani 1998):

$$\nabla \cdot \boldsymbol{v_b} = -S \tag{18}$$

where subscript b refers to the bulk-based averaged quantity (inter-tow region). Analytical and semi-analytical expressions have been developed in literature in order to compute the sink term of Eq. (18) (Parnas and Phelan Jr. 1991; Zhou et al. 2006). However, numerical calculation of this sink term has been proposed turning the models into a multi-scale approach for a dual porosity medium. For instance, Tan and Pillai (2012) derived a well-established mathematical approach for mass and momentum balance for the resin flow through the dual porosity preform. For the interflow region, the flow is governed by the Darcy;s law only taken into account the permeability outside the tows:

$$\boldsymbol{v_b} = -\frac{\boldsymbol{K_b}}{\mu}\nabla P_b \tag{19}$$

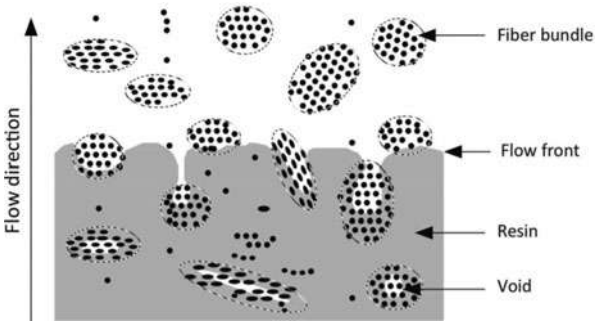

Fig. 9 Representation of the flow in a dual porosity medium. The delayed impregnation of the fiber bundles is shown by the formation of dry zones inside the tows. (Courtesy of Véronique Michaud, reproduced with thanks from Springer) (Michaud 2016)

For the intra-tow region, the flow inside the tows can be solved as a single-porosity medium without absorption by individual fibers. Then the governing equations for the intra-tow region stay as:

$$\nabla \cdot \boldsymbol{v}_t = 0 \tag{20}$$

$$\boldsymbol{v}_t = -\frac{\boldsymbol{K}_t}{\mu} \nabla P_t \tag{21}$$

where the subscript t means the tow-based averaging. The tow permeability can be find using the different strategies described in the previous sections; however, in order to have a quick solution, analytical models are preferred for compute this quantity. For instance, in references (Carlone et al. 2018; Tan and Pillai 2012), Gebart analytical model (Eqs. 8–9) is utilized for such purpose. In this multi-scale approach, the two-scale models are linked by the sink term; in (Tan and Pillai 2012) the authors utilized an integral expression for sink term applicable for any realistic dual-scale porous medium. The sink term is solved by integrating the velocities obtained from the unit cell model over the outer surface of tows inside unit cells. On the other hand, in (Carlone et al. 2018), an analytical formulation is proposed based on the results of numerical simulations of inter- and intra-tow flows at the mesoscale. This analytical expression relates the sink terms with the resin saturation inside the tows as can be observed in Fig. 10. The simulations are performed coupling the two sets of equations for inter and intra-tow regions.

Both approximations for the sink term have shown to improve the flow prediction compared with the single-porosity approximation. For instance, in Fig. 11, the monitoring for resin volume fraction as function of time is presented in three

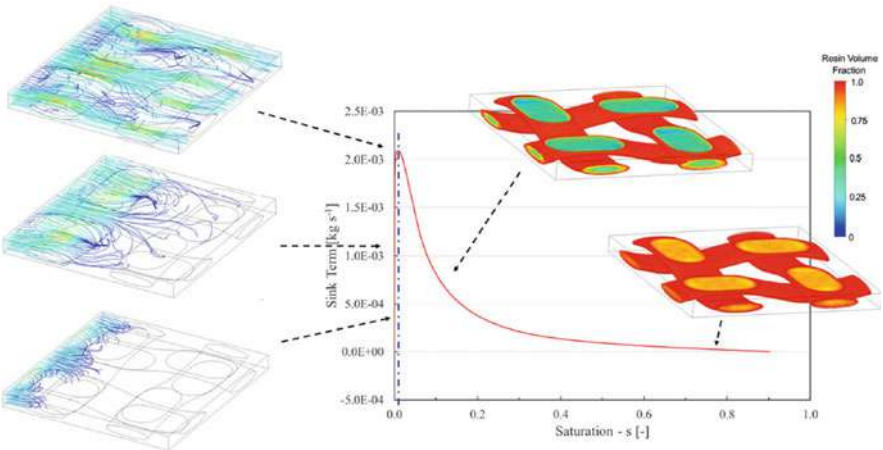

Fig. 10 Computing the sink term as a function of the saturation. (Courtesy of Pierpaolo Carlone, reproduced with thanks from Springer) (Carlone et al. 2018)

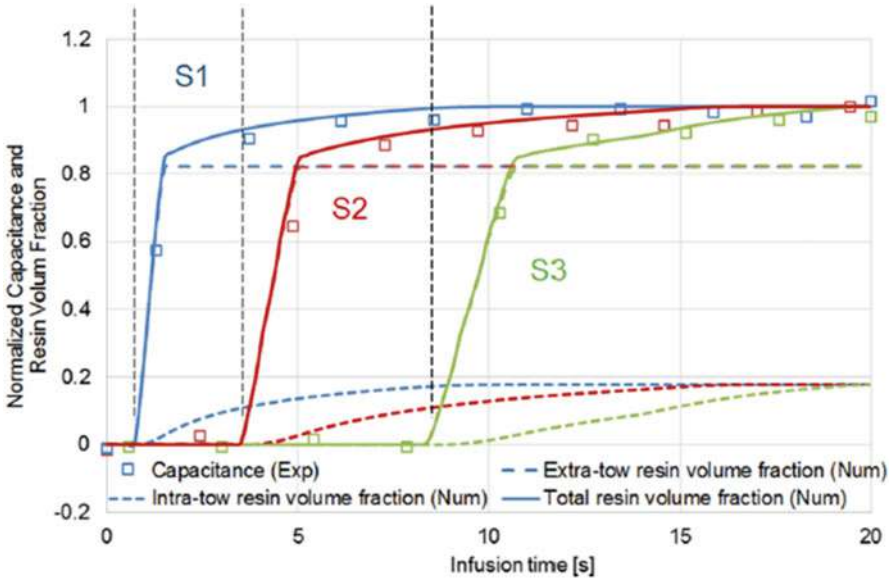

Fig. 11 Resin volume fraction as function of time for three monitoring points. (Courtesy of Pierpaolo Carlone, reproduced with thanks from Springer) (Carlone et al. 2018)

different points, and, as can be observed, the numerical results show a very good agreement with respect to experimental data collected by dielectric sensors.

To finalize this section, it is important to highlight multi-scale approach for flow during the resin infusion is one of the challenges in the LCM processes modeling, and then we hope that this issue continues its development and more research work be published during the next years.

Mechanical Modeling and Simulation of Epoxy/Synthetic Fiber Composites Introduction

Mechanical modeling and simulation of fiber-reinforced composites always have been treated at three scales: microscale, mesoscale, and macroscale (Beaumont 2020; Budarapu et al. 2019; Eshelby 1957). Each one of them deals with specific considerations to represent the physics involved with the interaction of non-continuous, heterogeneous, and anisotropic constituents (Fig. 12).

Microscale Mechanical Modeling and Simulation of Epoxy/Synthetic Fiber Composites

At the microscale, representative elementary volume (RVE) is modeled with a cylinder, representing the fiber reinforcement, surrounded by a prism, representing

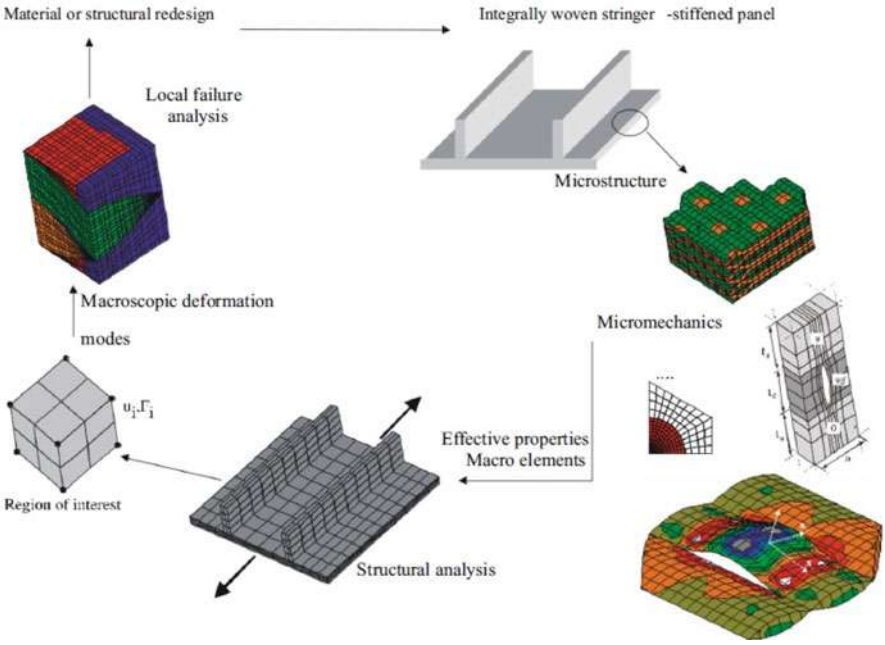

Fig. 12 A typical multi-scale challenge: a stringer-stiffened panel fabricated from a textile composite. (Courtesy of John Whitcomb, reproduced with thanks from Springer) (Beaumont 2020)

the continuous matrix. At this level, mechanical properties are based on micromechanics approach by the rule of mixtures, where the volume fractions define the behavior of the fiber composites. This approach is modeled by considering three aspects: (i) both constituents, separately, are continuous, homogeneous, and isotropic materials, (ii) there is a perfect interface between the contact areas of both constituents, and (iii) both work at the elastic regime (Beaumont 2020; Budarapu et al. 2019). To deal with modeling and simulation of the structural and nonstructural aspects of epoxy/synthetic fiber composites, several researchers have proposed mathematical models based on micromechanics to infer strength, stiffness, fracture toughness, thermal and electrical conductivities, and more recently self-damage detection, sensing capabilities, and electromagnetic shielding, when micro-fillers are added (Pal and Kumar 2016; Pan et al. 2016).

One key aspect, at microscale modeling, is the type of fiber composite to model, where two main kinds can be represented: (i) random short-fiber composites and (ii) angle-oriented long-fiber composites. In the first classification, modeling and simulation of epoxy/synthetic fiber composites are commonly estimated by the Mori-Tanaka approach (Eshelby 1957; Shabaze et al. 2019; Han et al. 2015). In the second classification, unit cell concept – cylindrical fibers embedded on epoxy prism – is the conceptualization of Eshelby model where one inclusion is embedded in a semi-infinite elastic, homogeneous, and isotropic medium (Eshelby 1957).

In the Mori-Tanaka model, the constitutive equations of a fiber-reinforced composite are expressed in terms of the average strain and stress by (Eq. 22):

$$\langle \sigma \rangle = C \langle \varepsilon \rangle \tag{22}$$

The effective average elastic moduli C is given by (Eq. 23):

$$\boldsymbol{C} = \left(V_m \boldsymbol{C}_m + V_f \boldsymbol{C}_f\right)\left(V_m \boldsymbol{I} + V_f \langle \boldsymbol{A} \rangle\right)^{-1} \tag{23}$$

where **I** is the fourth-order tensor identity tensor; $\mathbf{C}_\mathrm{f}$ and $\boldsymbol{C}_m$ are the fourth-order elasticity tensor of the fiber reinforcement and polymer matrix, respectively; and V_f and V_m are, as well, the volume fractions of the fiber reinforcement and the polymer matrix. **A** is the Eshelby strain concentration tensor which describes the relation between average strain ε_f and ε_m through (Eqs. 24 and 25):

$$\boldsymbol{\varepsilon}_f = \boldsymbol{A}\boldsymbol{\varepsilon}_m \tag{24}$$

$$\boldsymbol{A} = \left[\boldsymbol{I} + \boldsymbol{S}(\boldsymbol{C}_m)^{-1}\left(\boldsymbol{C}_f - \boldsymbol{C}_m\right)\right]^{-1} \tag{25}$$

where **S** is the Eshelby tensor. This approach is the most common used to predict the effective elastic moduli **C** of random straight fiber-polymer composites.

The orientation distribution of the reinforcement fibers could be written by a probability density function $p(\alpha, \beta)$, expressed by (Eq. 26):

$$\int_0^{2\pi}\int_0^{\pi/2} \boldsymbol{p}(\boldsymbol{\alpha},\boldsymbol{\beta}) \sin \boldsymbol{\alpha} d\boldsymbol{\alpha} d\boldsymbol{\beta} = 1 \tag{26}$$

with two Euler angles α and β as shown in Fig. 1. If the fibers are completely randomly oriented, it can be considered that $p(\alpha, \beta) = 1/2\pi$ (Fig. 13).

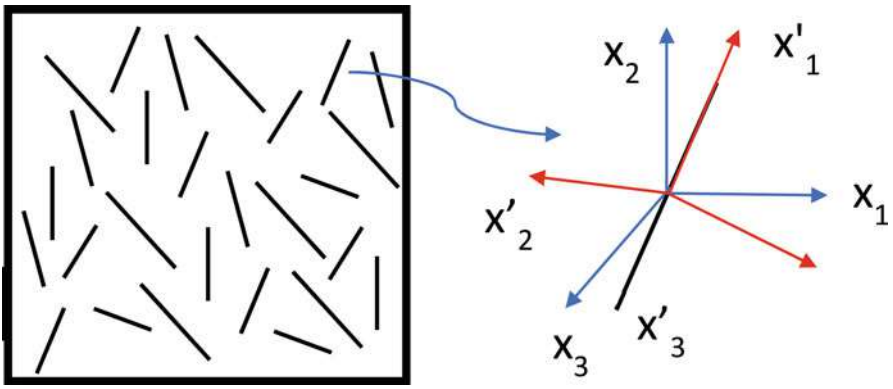

Fig. 13 Representative volume element (RVE) with randomly oriented short fibers (left) and a fiber with a global and local coordinate system (right). (Credits by the authors)

In the unit cell concept, Eshelby model is applied for cylindrical fibers embedded on epoxy prism. To calculate the effective elastic constants of unidirectional fiber-polymer composites, the rule of mixtures (ROM) is frequently applied (Eqs. 27–31) (Beaumont 2020; Shabaze et al. 2019). However, modeling and simulation of the two constituents at the microscale consider the RVEs were meshed using linear tetrahedron elements. This consideration is only valid if both constituents are considered as isotropic materials, which in the case of glass fibers and epoxy resins is true; however, due to the lamellar nature of the carbon fiber, it behaves more like an anisotropic material, but commonly it is treated as a transverse isotropic material.

A summary of the calculation of effective elastic constants is given below:

$$E_1 = E_m V_m + E_f V_f \tag{27}$$

$$E_2 = \left(V_m/E_m + V_f/E_f\right)^{-1} \tag{28}$$

$$\nu_{12} = \nu_m V_m + \nu_f V_f \tag{29}$$

$$\nu_{12}/E_1 = \nu_{23}/E_2 \tag{30}$$

$$G_{12} = \left(V_m/G_m + V_f/G_f\right)^{-1} \tag{31}$$

V_f and V_m are, as well, the volume fractions of the fiber reinforcement and the polymer matrix, assuming that $V_f + V_m = 1$ (Fig. 14).

From the equations of micromechanics, engineers can infer the following statements when dealing with modeling and simulation of epoxy-synthetic fiber composites: (a) the elastic properties of the fibers determine the properties of the composite in the fiber orientation and vice versa, ergo, the longitudinal elastic

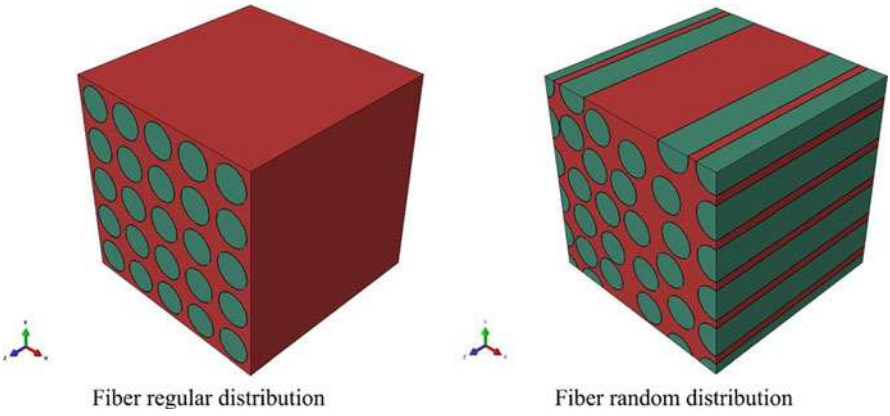

Fig. 14 Microscale RVE with regular distributed fibers (left) and random distributed fibers of synthetic fiber-epoxy composite. (Courtesy of Geng Han et al., reproduced with thanks from Springer) (Han et al. 2015)

modulus $E_1 = f(E_f)$; (b) the elastic modulus of the matrix and the fiber transverse elastic modulus have a significant effect on the composite transverse modulus $E_3 = f(E_f, E_m)$; (c) the in-plane shear modulus of the composite has a strong dependence on the fiber in-plane shear modulus and the matrix elastic modulus $G_{12} = f(G_{12f}, E_m)$; however, other effects (matrix Poisson's ratio, matrix shear modulus) cannot be ignored; and (d) the transverse shear modulus of the composite depends on the transverse shear modulus of the fiber, the in-plane shear modulus of the fiber, and the elastic modulus and Poisson's ratio of the matrix $G_{23} = f(G_{23f}, G_{12f}, E_m, \nu_m)$ (Huang and Ramakrishna 2002). Statements (a) and (b) serve to design composites in strength; statement (c) is important for out-of-plane loads; and statement (d) takes relevance when delamination failure needs to be avoided (Huang and Ramakrishna 2002; Catalanotti et al. 2017).

The intention of modeling and simulation of epoxy-synthetic fiber composites at the microscale is (1) to estimate the mechanical properties of the resulting composite (Han et al. 2015; Zhenchao et al. 2019; Desrumaux et al. 2000) and (2) to infer their specific damage initiation and failure propagation mechanism (Sharma et al. 2020). As epoxy-synthetic fiber composites are designed to undergo multiaxial loads during their service life, several failure models have been proposed, categorized in stress based (Sharma et al. 2020; Hashin 1980), strain based (Sun et al. 2004; Hart-Smith 1998; Puck and Schürmann 2004), and other phenomenology based (Totry et al. 2010). However, discrepancies have been encountered between the simulated and experimental failure envelopes. Those gaps are related to the genesis of the constituents and the idealization method used, which involves fiber, matrix, fiber distribution, orientation, and void content. Also, at the microscale, the nature of the fiber-matrix interfacial bonds (interface cohesion) and load transfer mechanics between epoxy and synthetic fibers play a huge role. Recent studies have proposed detailed computational micromechanical models to simulate UD and woven composites based on the following steps (Totry et al. 2010): (1) a RVE-generated random algorithms (random sequential adsorption (RSA) (Canal et al. 2012), nearest neighbor algorithm (NNA) (Naya et al. 2017)) to create a random fiber distribution; (2) to model interface damage with a bilinear traction separation law; and (3) to consider a matrix yield behavior (Mohr-Coulomb or Drucker-Prager plasticity model). One of the identified drawbacks, to correlate this micromechanics approach with the ply-level stress-strain behavior, is the lack of reliable fiber/epoxy interface data in the literature (Totry et al. 2010). Another important point is that epoxy matrix behaves differently at the microscale composite level compared with its bulk form. Generally, for the micromechanics calculations, the bulk epoxy properties are used (Shabaze et al. 2019; Totry et al. 2010). However, it has been proven that epoxy bulk mechanical properties are from 20% to 55% lower than the values obtained from nanoindentation and microscale test. This behavior is linked to the yield strength attributed to a scale phenomenon: the smaller the sample, the lower number of available weak bonds, and then the harder performance (Gregory and Spearing 2005; Wang et al. 2012) (Table 2).

Latest studies employ some variants of the three steps described above: (1) a RVE model from a microscopic image of the epoxy-fiber composite of interest, to capture

Table 2 Comparison between the bulk and the microscale properties of epoxy resins

	Bulk Kaddour and Hinton (2012)	In situ bulk Torres-Arellano et al. (2020)	Nanoindentation Naya et al. (2017)
Elastic modulus (GPa)	4	3.4	5.07
Poisson's ratio	0.38	0.36	0.35
Tensile strength (MPa)	99	66–68	121
Compression strength (MPa)	130	–	176
Flexural strength (MPa)	–	117	–

its inner nature, (2) a cohesive zone-friction damage-combined model, and (3) matrix yield behavior plus a non-dilatant flow rule (Sharma et al. 2020; Catalanotti et al. 2017). The accuracy of the calculation depends on the balance of two factors: (1) the placement of the fibers in the RVE should be representative of the fiber scattering from the composite ply of interest; and (2) the RVE must be large enough so, no matter its position or its size within the material, the average properties remain independent. In these terms, a non-periodical fiber distribution, normally around 50 fibers, is converted into a periodical one to represent a volume fraction like the macroscopic level and to capture the essential features of the microscopic composite structure (Fig. 15).

As the fiber-matrix interface is the Achilles tendon of the epoxy-synthetic fiber composites, its damage modeling has taken important relevance. Damage initiation is commonly modeled using maximum nominal stress or quadratic stress criteria; meanwhile, damage propagation is modeled employing mixed-mode criteria plus the Coulomb friction law (Sharma et al. 2020; Kaddour and Hinton 2012). The following expression resumes the behavior described above (Eq. 32):

$$\tau = (1-D)\begin{bmatrix} K_1 & 0 & 0 \\ 0 & K_2 & 0 \\ 0 & 0 & K_n \end{bmatrix}\begin{bmatrix} \delta_1 \\ \delta_2 \\ \delta_n \end{bmatrix} + D\begin{bmatrix} K_1 & 0 & 0 \\ 0 & K_2 & 0 \\ 0 & 0 & K_n \end{bmatrix}\begin{bmatrix} \delta_1 - \delta_1^{di} \\ \delta_2 - \delta_2^{di} \\ -\langle -\delta_n \rangle \end{bmatrix} \tag{32}$$

The first term defines the cohesive damage law, while the second term defines the frictional stress state on the damaged interface. In this expression, t_n, t_1, and t_2 are the normal, and the shear stresses at the epoxy-synthetic fiber (Modes I, II, and III) and δ_n, δ_1, and δ_2 are the corresponding displacements. K_n, K_1, and K_2 are the interface stiffness related to the Modes I, II and III, respectively (Catalanotti et al. 2017). The scalar D is the damage variable, which runs from "no damage," equal to zero, to "full damage," equal to one. Moreover, the terms $\delta^{di}{}_n$, $\delta^{di}{}_1$, and $\delta^{di}{}_2$ are the inelastic sliding due to friction, implying that compressive normal displacement does not affect the damage model. This approach seeks to couple numerical-experimental results, to predict biaxial failure envelopes as function of the microscale parameters. The damage microscopic profile obtained by finite element simulations, under transverse tensile load, shows

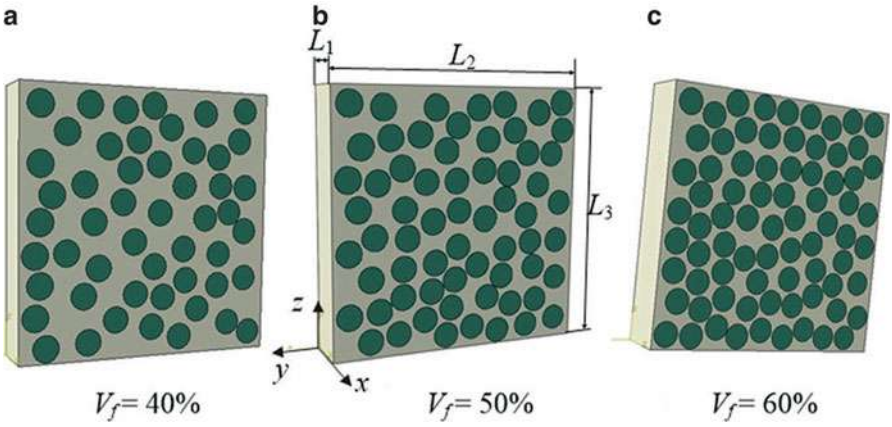

Fig. 15 RVE models generated to emulate synthetic fiber-epoxy composite microstructure. (Courtesy of Zhenyi Yuan et al., reproduced with thanks from Springer) (Yuan et al. 2019)

circumferential decohesion angles between 54° and 70°, which closely resemble to the experimental ones, between 64° and 70° (Sharma et al. 2020). Moreover, the behavior of the composite under transverse tension and compression is influenced by the curing residual stresses and fiber distribution (Han et al. 2015) (Fig. 16).

As depicted, microscale modeling and simulation of epoxy/synthetic fibers still get a lot of attention, focused recently in how to include the frictional sliding between fiber-epoxy interfaces. Most of numerical methodologies are validated for unidirectional composites (UD) and under uniaxial loading cases and now extrapolated for biaxial loading cases. The limitations of the microstructure are now extrapolated dominated region, an increment of the interface friction, and will have an impact in the biaxial strength. As epoxy-synthetic fiber composites need to be treated as a material and as a structure simultaneously, the next step is to account the geometry and configuration of both constituents at the mesoscale, where fiber waviness, fiber undulations, stacking sequence, interlaminar interface, and plies' bonding define also the mechanical behavior.

Mesoscale Mechanical Modeling and Simulation of Epoxy/Synthetic Fiber Composites

Modeling and simulation of epoxy/synthetic fiber composites at the mesoscale deal with two approaches, regarding the nature of the reinforcement. In the first case, fiber unidirectional plies (UD), at different orientations, are piled to form a laminate. To obtain the overall stiffness and strength, laminate theory is applied, by adding the orthotropic contribution of each ply (Beaumont 2020; Budarapu et al. 2019). In the second case, woven fabrics, with different waviness patterns and at different orientations, are stacked to create the laminate. The ply's stiffness and strength will depend on the diameter and width of yarns, weft/wrap cross section, the type of

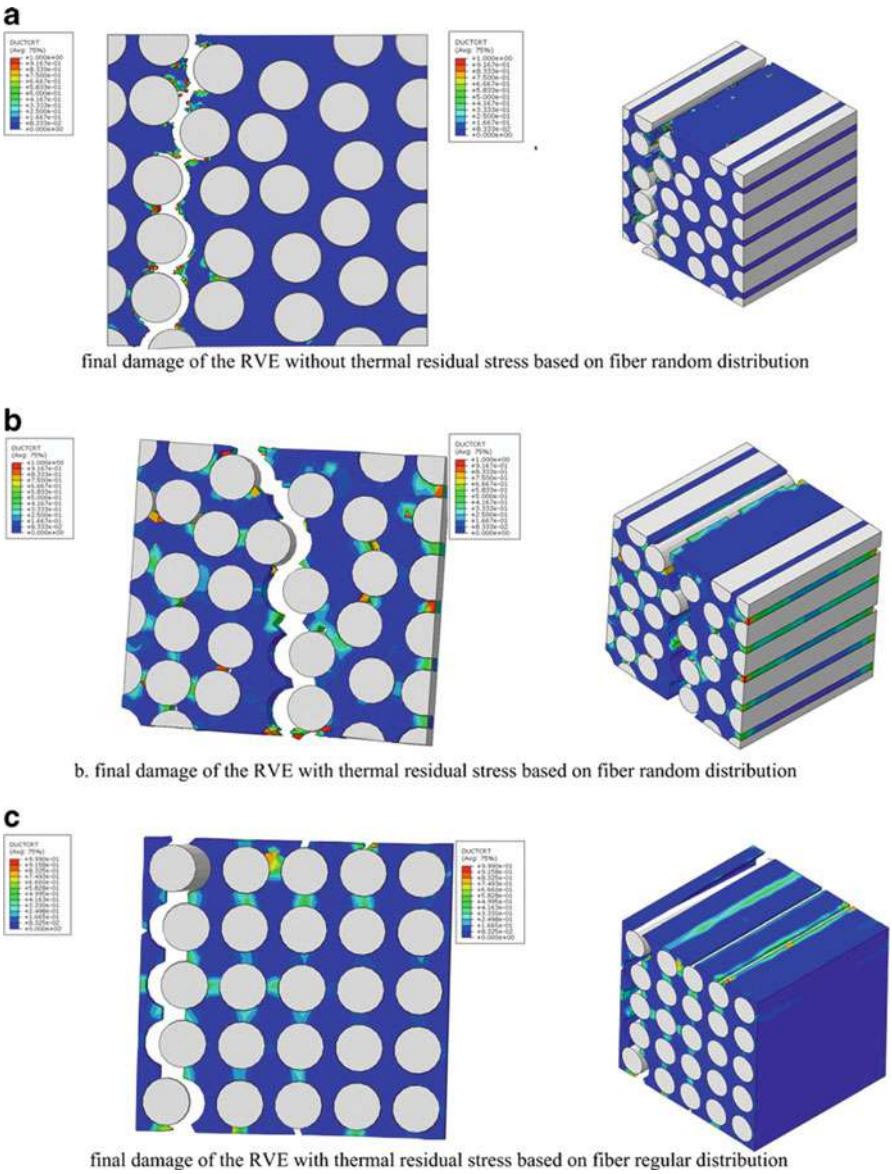

Fig. 16 Failure modes of the composites under transverse tension considering fiber distribution and curing residual stresses. (Courtesy of Geng Han et al., reproduced with thanks from Springer) (Han et al. 2015)

weave (2D, 2.5D, or 3D), and the fabric closure factor. All these parameters will define the microstructure of woven composites and, combined with the laminate theory, will define the overall stiffness and strength of a woven composite laminate (Zhang et al. 2017a; Guo et al. 2020).

The microstructure of woven composites must be captured following two conditions: first, it should be small enough, to be regarded as a point on the macroscale (RVE), and, second, it must be selected according to the periodicity of the material (repeating unit cell (RUC)). By combining both conditions, the smallest RUC turns to be the RVE, to create the unit cell model (UCM), which represents the composite at the mesoscale (Zhang et al. 2017b, 2018, 2019).

Textile composites, which are fabricated by weaving fibers and combining them with an epoxy matrix, have upraised with the advances in braiding and knitting technologies obtaining complex 2D, 2.5D, and 3D preforms. In the past decades, UCM were mainly employed to predict stiffness, strength, and even delamination, by using selective averaging method, orientation averaging method, or progressive damage method; however, these models do not consider the process factors influence such as binder yarns, weaving patters, and epoxy-synthetic fiber interface. More recently, the UCM have been improved by considering many factors such as variations in the weaving, surface extrusion, internal yarn extrusion, randomness, tow profiles, matrix wettability, compounding process, and void content. These considerations promote a higher-accuracy model, with the corresponding enhancement of the predicted results; nonetheless, the problematic to generate high-quality meshes for FEA remains a big drawback in practical applications (Guo et al. 2020; Zhang et al. 2017a, b, 2018, 2019). As an example, a statistical volume element (SVE) has been proposed by joining the characteristics of RVE and RUC. SVE assumes that the main weave geometric parameters: (i) warp cross section (WPCS) and (ii) weft cross section (WFCS) can be treated, respectively, as rectangular and elliptical random variables, which can be modeled from two sources, (a) actual woven micrographs (Zhang et al. 2017a, b) and (b) discrete random number generation (Guo et al. 2020).

In the case of woven composite materials whose weaving configuration only contains warp and weft yarns, the width and height of the WPCS (W_{1j}, W_{2j}) and the mayor and minor axes of the WFCS (W_{1w}, W_{2w}) work as geometric variables to set the regular periodic structure. The structure network is analyzed to include the horizontal and vertical distance as well as the rotation angle. Since most of the weaved fabrics are used to set the preform before liquid resin injection, yarns are squeezed, and, therefore, warp and weft yarns will offset, and they could modify their elliptical form, depending on their location, near the surface of the middle plane. Those experimental situations will lead to correct the warp-warp and warp-weft interferences by fitting spline curves in the model (Guo et al. 2020; Zhang et al. 2018). After generating the geometric model, by performing stretching and Boolean operations, it can be imported to a mesh generation software to create the corresponding finite element model, considering the common nodes between the different constituents. At this stage, we should note that periodic boundary conditions (PCB) are required when analyzing the mechanical properties of the SVE and they must be imposed on its surfaces, edges, and vertices (Guo et al. 2020) (Fig. 17).

At the mesoscale, due to the resolution of the constituents, researchers have found interest on develop progressive damage models as an effective way to analyze the

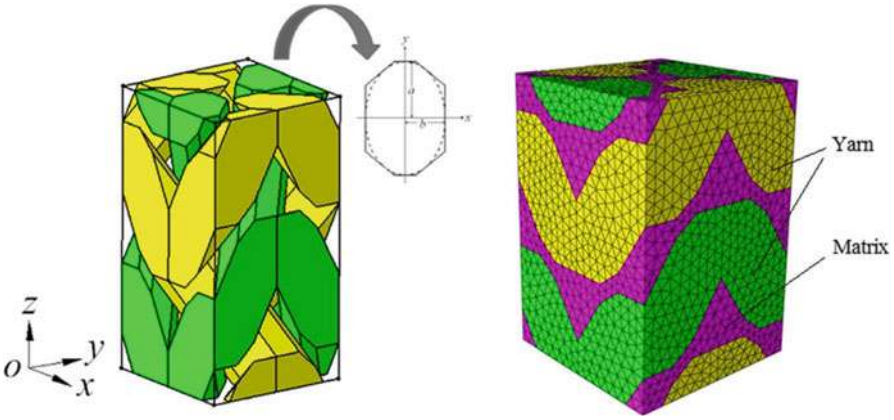

Fig. 17 Unit cell model (left) and its mesh (right) of a 3D braided composite at the mesoscale. (Courtesy of C. Zhang et al., reproduced with thanks from Springer) (Zhang et al. 2018)

damage propagation, which mainly involves three correlated parts: (i) stress analysis, (ii) damage onset criteria, and (iii) damage propagation law.

The stress analysis normally is performed based on (Eq. 33):

$$\int_{V_{n-1}} Q_{ijkl}^{n-1} \Delta\varepsilon_{kl} \delta(\Delta e_{ij}) dV + \int_{V_{n-1}} \sigma_{ij}^{n-1} \delta(\Delta\eta_{ij}) dV = \int_{S_\sigma} T_i^n \delta(\Delta u_i) dS - \int_{V_{n-1}} \sigma_{ij}^{n-1} \delta(\Delta e_{ij}) dV \tag{33}$$

where $\Delta\sigma_{ij}$, $\Delta\varepsilon_{ij}$, and Δu_i are the increment of stress, strain, and displacement from *n-1*th load step to *n*th load step, respectively; T_i^n is the surface force on the elements area by the boundary; ${\sigma_{ij}}^n$ is the stress inside the structure at the nth load step; Δe_{ij} and $\Delta\eta_{ij}$ are the linear and quadratic terms, respectively; and ${Q_{ijkl}}^{n-1}$ is the stiffness matrix at the *n-1*th load step.

In terms of damage onset criteria, some variants of the 3D Hashin failure criteria, for woven composites, have been developed with the aim to study both constituents inside the UCM: (i) the resin rich matrix and (ii) the yarns including weft-warp. The resin is considered as an isotropic material, meanwhile the yarns are assumed as transversely isotropic material, following the same microscale mechanics statements.

For the yarns, an improved 3D Hashin failure criterion is currently used (Eqs. 34 and 35) (Hashin 1980; Lu et al. 2013):

Longitudinal tensile damage of the yarn, for $\sigma_{11} \geq 0$:

$$\Phi_{1t} = \left(\frac{\sigma_{11}}{X_{11t}}\right)^2 + \left(\frac{\frac{\sigma_{12}^2}{2G_{12}} + \frac{3}{4}\alpha_s\sigma_{12}^4}{\frac{S_{12}^2}{2G_{12}} + \frac{3}{4}\alpha_s S_{12}^4}\right)^2 + \left(\frac{\frac{\sigma_{13}^2}{2G_{13}} + \frac{3}{4}\alpha_s\sigma_{13}^4}{\frac{S_{13}^2}{2G_{13}} + \frac{3}{4}\alpha_s S_{13}^4}\right)^2 \geq 1 \tag{34}$$

Transversal tensile damage of the yarn, for $\sigma_{22} > 0$:

$$\Phi_{2t} = \left(\frac{\sigma_{22}}{X_{22t}}\right)^2 + \left(\frac{\frac{\sigma_{12}^2}{2G_{12}} + \frac{3}{4}\alpha_s\sigma_{12}^4}{\frac{S_{12}^2}{2G_{12}} + \frac{3}{4}\alpha_s S_{12}^4}\right)^2 + \left(\frac{\sigma_{23}}{S_{23}}\right)^2 \geq 1 \tag{35}$$

For the pure matrix, Von Mises criterion is used. In the case of tensile damage of the resin matrix, for $\sigma_{11} + \sigma_{22} + \sigma_{33} \geq 0$ (Eq. 36):

$$\Phi_{mt} = \left(\frac{(\sigma_{11} - \sigma_{22})^2 + (\sigma_{22} - \sigma_{33})^2 + (\sigma_{11} - \sigma_{33})^2 + 6\left(\sigma_{12}^2 + \sigma_{13}^2 + \sigma_{23}^2\right)}{2X_{mt}^2}\right)^2 \geq 1 \tag{36}$$

where σ_{ij} ($i,j = 1, 2, 3$) are the stress components, X_{ik} ($i = 1, 2, 3$; $k =$ t, c) are the tensile or compressive strength of the yarns, S_{ik} ($i = 1, 2, 3$; $k =$ t, c) are the shear strength of the yarns, αs is the shear factor, and X_{mk} ($k =$ t, c) is the tensile or compressive strength of the resin matrix (If the reader wants to consult the expressions of all damage onset criteria, authors can refer him/her to (Guo et al. 2020)).

At the end, the damage propagation law must be proposed to denote that the element begins to damage when the stress state of the element reaches the cited criterion. Many researchers employ extended finite element method (XFEM), interface elements, cohesive zone models (CZM), or embedded discontinuities. Most of them are based on the conversion of elastic energy into fracture energy, as an example, the crack band theory proposes (Bažant and Oh 1983) (Eq. 37):

$$g_{ik} = \frac{G_{ik}}{l_{eq}} \ (\mathrm{i} = 1, 2, 3; \mathrm{k} = \mathrm{t}, \mathrm{c}) \tag{37}$$

where g_{ik} is the energy release density and G_{ik} is the breaking energy density and $l_{eq} = \sqrt[3]{V_{elem}}$ is the equivalent element length, which depends on the element volume. For woven composites, it is considered that if the material fails, the energy released by the element is equal to its elastic energy when undamaged (Eq. 38):

$$\frac{1}{2}\sigma_{eq}^{ik,f}\varepsilon_{eq}^{ik,f} = \frac{G_{ik}}{l_{eq}} \ (i = 1, 2, 3; k = \mathrm{t}, \mathrm{c}) \tag{38}$$

where $\sigma_{eq}^{ik,f}$ and $\varepsilon_{eq}^{ik,f}$ are the failed element equivalent stress and strain, respectively.

As baseline reference, we present the results obtained by Zhang et al. (Zhang et al. 2017a, 2018, 2019) where 3D braided composites were simulated based on meso-scale FEM models. In this research, solid tetrahedral elements are used to mesh the UCM. To predict the tensile properties of 3D woven composites in each direction, displacement loading mode is recommended (Zhang et al. 2018; Zhang et al. 2017c; Murakami 1988). As these types of composites are conceived to work at

multi-axis loading conditions, it is recommended to use force loading mode; thus the stress ratios can remain constant throughout the simulation process. A simulation of biaxial tension loading case is showed in Fig. 7. When stress ratio is equal (σx: σy = 1:1), the stress-strain curves are coincident, revealing that woven composite has the same properties in both directions, when stress ratio is different (σx: σz = 1: 4), stress-strain curves in x and z-axis have evident difference under biaxial tension loading.

One of the most powerful advantages of mesoscale modeling and simulation is the analyses of the damage evolution process and related failure mechanisms. The damage variables evolve from 0 to 1, describing the degradation of composite's stiffness until the failure is completed. This biaxial loading case shows that yarn T tensile and compressive shear failure, yarn Z tensile shear failure, and matrix cracking are the main failure modes. At the yarn/yarn contact zones, yarn T tensile shear failure propagates along the transverse direction of the braiding yarn. Matrix cracking appears after in the intersecting edges of the braiding yarns and matrix, resulting in many damaged elements (Fig. 18).

As described, mesoscale modeling and simulation of epoxy/synthetic fibers continuously get improvement, more recently in terms of including the three phases: braiding yarn, matrix, and interface. The most public interest is to simulate the damage evolution and predict the mechanical properties under quasi-static multiaxial loads. 3D Hashin criterion with gradual degradation scheme, such as Banzant and Oh crack band theory (Bažant and Oh 1983) or Murakami damage model (Zhang et al. 2017b; Murakami 1988), is applied to predict the damage evolution of yarns and matrix. More recently, a damage friction combination interface constitutive model is proposed to capture the interface debonding behavior, as is the case of the Camanho model (Catalanotti et al. 2017) and by using user-material subroutines where damage models of constituent are scripted. The next step is to agglomerate the concepts cited above and pull a modeling and simulation strategy for designing composite structures and products. The goal is to take engineering decisions based on optimized calculations to fabricate composites using novel process technique and estimate their performance under several loading scenarios.

Macroscale Mechanical Modeling and Simulation of Epoxy/Synthetic Fiber Composites

The principal objective of the macroscale modeling and simulation of composite materials is an attempt to ensure that a highly stressed component will function within its design lifetime. This goal only can be afforded by developing robust numerical models and by doing representative tests on instrumented composite structures (Torres et al. 2014, 2015).

The successful prediction of the mechanical behavior of an epoxy/synthetic fiber composite needs exhaustive characterization, first, in all scales and axis, and, second, in most of the possible loading cases across a wild spectrum of in-service conditions.

Nonetheless, the experimental campaign that will cover all possible and imaginable scenarios would be enormous and expensive. In this case, for the modeling and

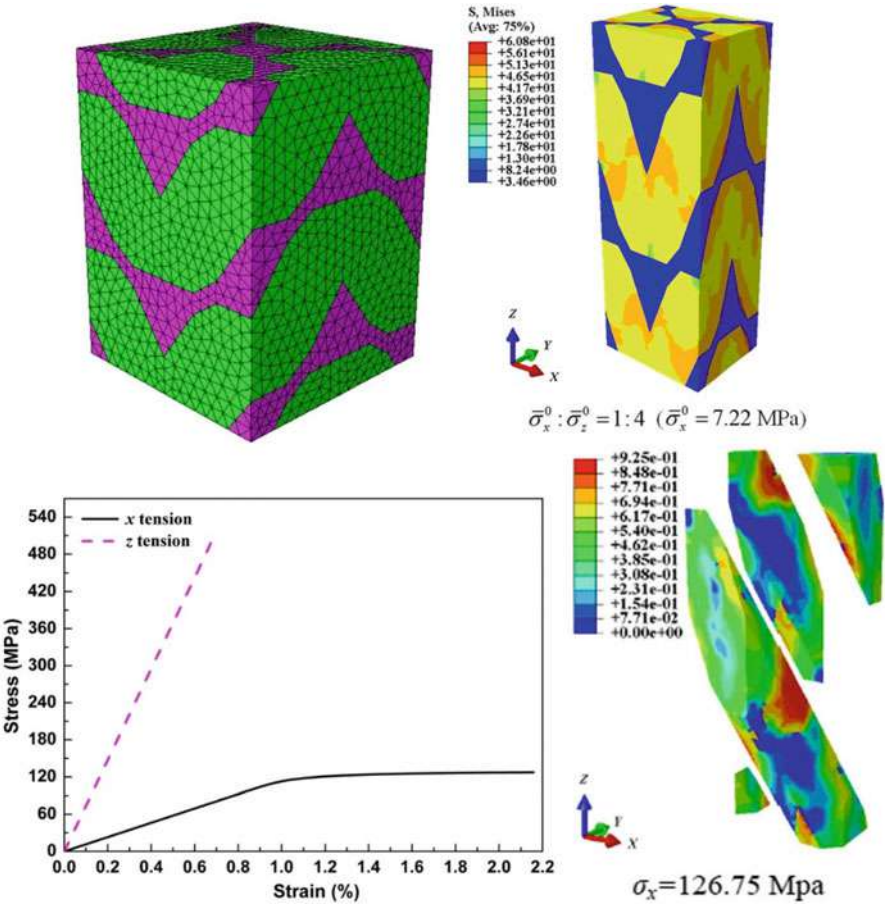

Fig. 18 Mesoscale modeling and simulation of a 3D braiding composites with optimal mesh (top-left), stress distributions of UCM (top-right), predicted stress-strain curve for σx: σz = 1:4 (bottom-left), and yarn Z tensile shear failure (bottom-right). (Courtesy of C. Zhang et al., reproduced with thanks from Springer) (Zhang et al. 2018, 2019; Lu et al. 2013)

design of a composite component, aeronautics and other industry sectors employ the "building block approach" also known as the "pyramid of tests" (Beaumont 2020; Torres et al. 2017).

In the first level, an extensive materials characterization needs to be performed for obtaining the elastic constants for the epoxy/synthetic fiber composite. Currently, the simplest modeling and simulation of composite standard coupons are carried out by using 2D linear multilayer shell elements and using in some cases, an offset-transfinite mesh to optimize the time cost (Torres et al. 2014, 2017). Depending on the loading case, boundary conditions are set. For tensile tests, the model is clamped at the bottom by means of the fixations along the X, Y, and Z axes, and rotation is

along the X axis. At the top, the fixations are set along the Y and Z axes, and rotation is along the Z axis. The machine displacement is imposed via the X direction.

Beyond that, 3D FEM models are used to represent the constitutive layup with better precision. The use of a 3D model lies on study the delamination and interlaminar fracture. Commonly, the ply-scale models are created with linear multilayer cubic elements. Each element through-the-thickness represents one epoxy-synthetic fiber ply. In some cases, inner flaws, such as resin pockets, are considered, and they can be modeled with tetrahedral isotropic elements (Fig. 19).

From second to fifth levels, numerical analysis is required for (i) exploring loading cases, (ii) defining manufacturing and assembly choices, and (iii) taking decisions on the configuration of each component, subassembly, and assembly to describe the baseline structural performance (Torres et al. 2015, 2017). This approach suggests working on modeling and simulation strategies that integrate the composite structure's reality and therefore its variability. These models should define pertinent target marks that regroup the physical behavior at the different scales of the composite structure. In the case of aeronautics, the failure probability of epoxy/synthetic fibers structural components is commonly fixed at 10–9 per flight hour. Therefore, numerical simulation for these components should be convenient to demonstrate that the accuracy and resolution of the predicted calculations present a similar failure probability (Torres et al. 2014, 2017).

An example of modeling and simulation at the macroscale of epoxy/synthetic fibers is the MITE toolbox (Multi-Instrumented Technological Evaluator) (Torres et al. 2015, 2017; Collombet et al. 2020). The MITE regroups four interactive aspects: (i) composite structure with singularity details, (ii) multiaxial modular testing machine, (iii) multi-scale numerical modeling, and (iv) multi-sensor instrumentation.

The first aspect, composite structure, can be adapted to analyze the current problematics found at it such as plies drop-offs, glued and/or fastened, or stiffener

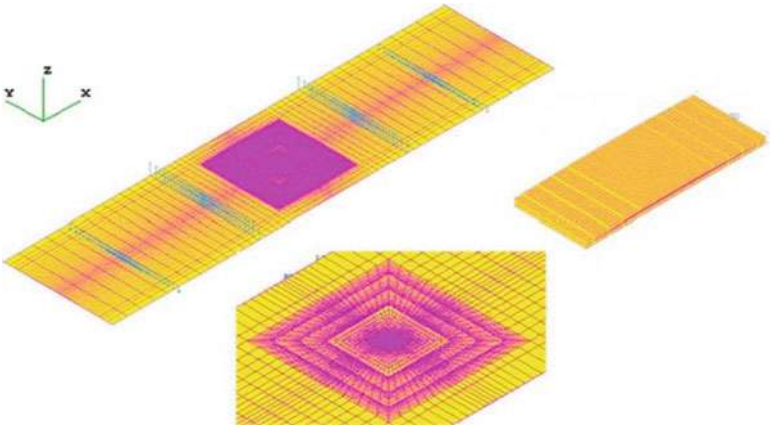

Fig. 19 FEM models developed for an instrumented composite: 2D model of the 4-point bending test (left), numerical zoom of the 2D model (middle) and 3D model of the instrumented zone (right). (Courtesy of Mauricio Torres et al., reproduced with thanks from Springer) (Torres et al. 2014)

plate assemblies. In the last decade, MITE composite structure has been tested in epoxy/synthetic fiber composite study cases (Torres et al. 2015, 2017). The second aspect, multiaxial modular testing machine, must be able to generate and to apply a group of mechanical, thermal, and/or electrical loads like those imposed on real composite structures.

The third aspect, dedicated to multi-scale numerical modeling, deals with 2D and 3D FEM models of the composite structure with the boundary conditions proposed on the multiaxial testing machine. The numerical modeling opens two lines of research. On the first one, fast and accurate results can be afforded by testing different layup configurations and numerous loading cases. These simulations, with 2D models, are carried out at the beginning of the analysis to identify possible failure scenarios and to obtain the fittest configuration. On the second one, 3D models are used, employing cohesive zone models, damage models, or even XFEM to get more judicious and specific results as delamination or buckling.

The fourth aspect, the multi-sensor instrumentation, takes advantage of the availability to place embedded sensors, such as fiber Bragg gratings (FBG), tunneling junction sensors (TJS), or piezoelectric elements (PZT), in the composite structure (Collombet et al. 2020).

The MITE toolbox looks to close the gap on the use of technologies well-known at laboratory scale but which are quite difficult to export to final industrial components. Also, it has the possibility to evaluate new materials, alternative design concepts, disruptive manufacturing concepts (automated fiber placement of additive manufacturing), or new sensor technologies.

As an example of the capabilities of the MITE toolbox for performing multi-scale analysis, a multi-axis modular testing machine with an epoxy-synthetic fiber composite plate with plies drop-offs was modeled by FEM (Fig. 20).

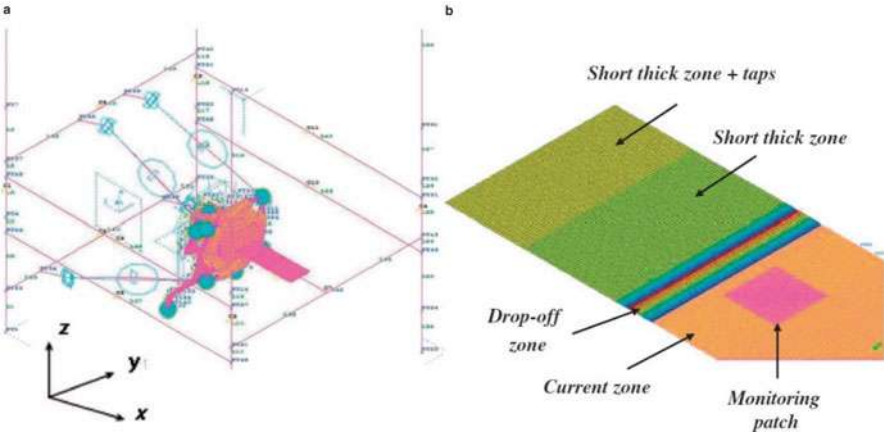

Fig. 20 Numerical FE models employed for an instrumented structure: (**a**) machine kinematics and (**b**) composite plate with an embedded monitoring patch. (Courtesy of Mauricio Torres, credits by the author) (Torres et al. 2017)

In (Torres et al. 2017) a 2D FE model is proposed Mindlin multilayer shell quadrangle elements. The size of the finest element is set to be same of the smallest sensor embedded, to have the stress and displacements at that scale. The instrumented zone, the monitoring patch, is modeled following the strategy of a transfinite mesh to optimize the plate's meshing and to reduce computational cost.

The goal of this work is to study the effects to apply two bending moments on a composite plate with plies drop-offs. This loading case is commonly seen in wing structures. The testing machine conceived is capable to generate a director torsion moment on the X axis and a bending moment on the Y axis, avoiding the buckling in the composite plate. When epoxy-synthetic fiber composite plates have thickness variations, the highest strains are concentrated near the drop-off zone. Stress field and Tsai-Hill criterion confirms stress intensification at the drop-off zone (Fig. 21).

This example shows, at macroscale, the possibility to optimize the FE models (2D and 3D) and to extend the explanations of the mechanical behavior of a composite plate. Then, the loss of stiffness as the delamination grows could be modeled, to improve the predicted strain field, by returning to the mesoscale modeling.

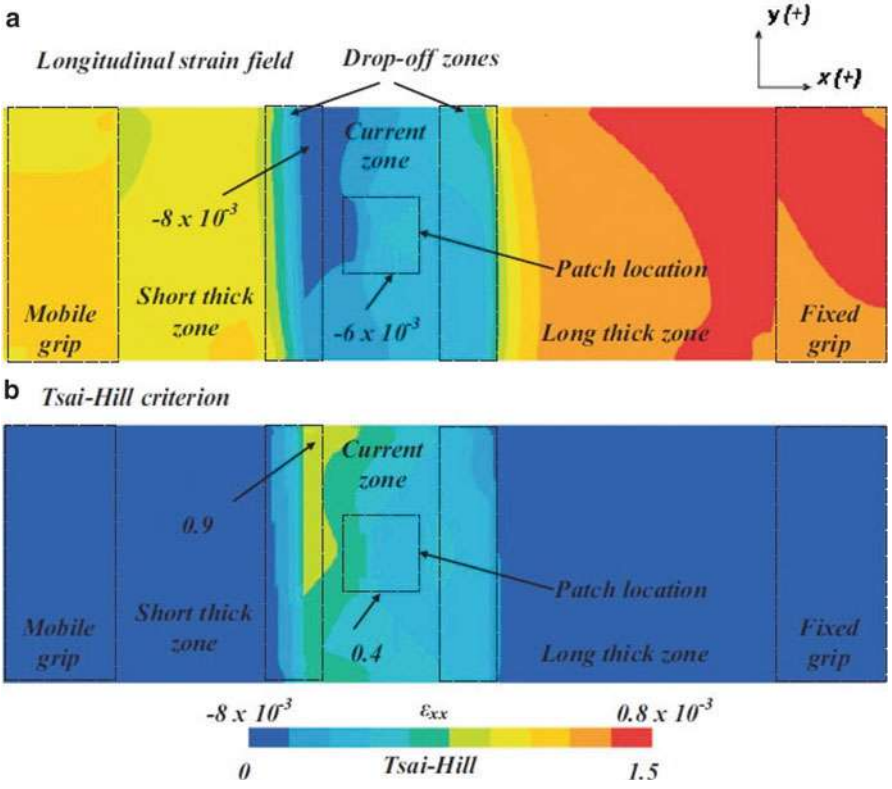

Fig. 21 Numerical results for torsion-bending test at the surface ply (0°) of the composite structure with a monitoring patch: (**a**) longitudinal strain field (σ_{xx}) and (**b**) Tsai-Hill criterion (time = 0.8/1). (Courtesy of Mauricio Torres, credits by the author) (Torres et al. 2017)

Conclusions

A major difficulty in modeling and simulation of epoxy-synthetic fiber composites is coupling the phenomena related to each scale and used to predict for one side, the resin flow during the LCM processes in order to improve the quality of the final part, and for the other side damage initiation, evolution, and safe in-service limits.

True challenges in modeling and simulation of epoxy-synthetic fiber composites are identified:

1. Formulate new multi-scale models that allows to solve the resin flow with strong coupled between the two-scale levels and be able to predict the inter and intra-tow void formation for large and complex components.
2. Formulate equations that combine continuum mechanics and discrete damage models in a single calculation. Currently, coupling finite element method by enriching the formulation (XFEM) or by adding other formulations (e.g., cohesive zone models) remains the current practice.

Some key aspects are still in development to be considered in modeling and simulation of epoxy-synthetic fiber composites:

- Delamination mechanism.
- Dissipation of energy.
- Surface treatment of fiber.
- Fatigue and crack propagation.
- Environmental effects (aging, moisture, thermal shock, lighting strike, fire resistance).

Acknowledgments Mauricio Torres-Arellano and Saul Piedra thank the opportunity to write and share our experience of 25 years combined in the field of modeling and numerical simulation of composite structures by CFD and FEM.

Some images show results from our latest projects, mainly funded by National Council for Science and Technology of Mexico (CONACYT) and Mexican Space Agency (AEM).

The authors also give appreciation to the Program "Cátedras CONACYT."

References

H. Alhussein, R. Umer, S. Rao, E. Swery, S. Bickerton, W.J. Cantwell, Characterization of 3D woven reinforcements for liquid composite molding processes. J. Mater. Sci. **51**, 3277–3288 (2016)

M.A. Ali, R. Umer, K.A. Khan, W.J. Cantwell, Application of X-ray computed tomography for the virtual permeability prediction of fiber reinforcements for liquid composite molding processes: A review. Compos. Sci. Technol. **184**, 107828 (2019)

Z.P. Bažant, B.H. Oh, Crack band theory for fracture of concrete. Mater. Constr. **16**, 155–177 (1983)

P.W.R. Beaumont, The structural integrity of composite materials and long-life implementation of composite structures. Appl. Compos. Mater. **27**, 449–478 (2020)

E.B. Belov, S.V. Lomova, I. Verpoesta, T. Petersb, D. Rooseb, R.S. Parnasc, K. Hoesd, H. Sold, Modelling of permeability of textile reinforcements: Lattice Boltzmann method. Compos. Sci. Technol. **64**, 1069–1080 (2004)

G.O. Brown, Henry Darcy and the making of a law. Water Resour. Res. **38**(7), 1106 (2001)

P.R. Budarapu, X. Zhuang, T. Rabczuk, S.P.A. Bordas, Multiscale modeling of material failure: Theory and computational methods. Adv. Appl. Mech. **52**, 1–103 (2019)

L.P. Canal, C. González, J. Segurado, J.L. Lorca, Intraply fracture of fiber-reinforced composites: Microscopic mechanisms and modeling. Compos. Sci. Technol. **72**, 1223–1232 (2012)

P. Carlone, F. Rubino, V. Paradiso, F. Tucci, Multi-scale modeling and online monitoring of resin flow through dual-scale textiles in liquid composite molding processes. Int. J. Adv. Manuf. Technol. **96**, 2215–2230 (2018)

G. Catalanotti, C. Furtado, T. Scalici, G. Pitarresi, F.P. van der Meer, P.P. Camanho, The effect of through-thickness compressive stress on mode II interlaminar fracture toughness. Compos. Struct. **182**, 153–163 (2017)

F. Collombet, M. Torres, B. Douchin, L. Crouzeix, Y.-H. Grunevald, J. Lubin, T. Camps, X. Jacob, G. Luyckx, K.-T. Wu, Multi-instrumentation monitoring for the curing process of a composite structure. Measurement **157**, 107635 (2020)

F. Desrumaux, F. Meraghni, M.L. Benzeggagh, Micromechanical modelling coupled to a reliability approach for damage evolution prediction in composite materials. Appl. Compos. Mater. **7**, 231–250 (2000)

M.R. Dusi, W.I. Lee, P.R. Ciriscioli, G.S. Springer, Cure kinetics and viscosity of fiberite 976 resin. J. Compos. Mater. **21**, 243–261 (1987)

J.D. Eshelby, The determination of the elastic field of an ellipsoidal inclusion, and related problems. Proc. R. Soc. London A Math. Phys. Eng. Sci. **241**, 376–439 (1957)

R. Fournier, T. Coupez, M. Vincent, Numerical determination of the permeability of fibre reinforcement for the RTM process. Revue Européenne des Éléments Finis **14**, 803–818 (2005)

B. Gebart, Permeability of unidirectional reinforcements for RTM. J. Compos. Mater. **26**, 1100–1133 (1992)

J.R. Gregory, S.M. Spearing, Nanoindentation of neat and in situ polymers in polymer-matrix composites. Compos. Sci. Technol. **65**, 595–607 (2005)

J. Guo, W. Wen, H. Zhang, H. Cui, J. Song, Representative cell modeling strategy of 2.5D woven composites considering the randomness of weft cross-section for mechanical properties prediction. Eng. Fract. Mech. **237**, 107255 (2020)

G. Han, Z. Guan, Z. Li, M. Zhang, T. Bian, S. Du, Multi-scale modeling and damage analysis of composite with thermal residual stress. Appl. Compos. Mater. **22**, 289–305 (2015)

L.J. Hart-Smith, Maximum-strain failure models for certain fibrous composite laminates. Compos. Sci. Technol. **58**, 1151–1178 (1998)

Z. Hashin, Failure criteria for unidirectional fiber composites. J. Appl. Mech. **47**, 329–334 (1980)

C.W. Hirt, B.D. Nichols, Volume of fluid (VOF) method for the dynamics of free boundaries. J. Comput. Phys. **39**(ll1), 201–225 (1981)

S.V. Hoa, *Principles of the Manufacturing of Composite Materials* (DEStech Publications, Inc, 2009)

Z.M. Huang, S. Ramakrishna, Towards automatic designing of 2D biaxial woven and braided fabric reinforced composites. J. Compos. Mater. **36**, 1541–1579 (2002)

A.S. Kaddour, M.J. Hinton, Input data for test cases used in benchmarking triaxial failure theories of composites. J. Compos. Mater. **46**, 2295–2312 (2012)

M.K. Kang, J.J. Jung, W. Lee, Analysis of resin transfer moulding process with controlled multiple gates resin injection. Compos. A. Appl. Sci. Manuf. **31**(5), 407–422 (2000)

M. Karaki, R. Younes, F. Trochu, P. Lafon, Progress in experimental and theoretical evaluation methods for textile permeability. J. Compos. Sci. **3**(73), 1–28 (2019)

H. Lin, L.P. Brown, A.C. Long, Modelling and simulating textile structures using TexGen. Adv. Mater. Res. **331**, 44–47 (2011)

Z. Lu, Y. Zhou, Z. Yang, Q. Liu, Multi-scale finite element analysis of 2.5D woven fabric composites under on-axis and off-axis tension. Comput. Mater. Sci. **79**, 485–494 (2013)

S. Mazumdar, *Composites Manufacturing: Materials, Product, and Process Engineering* (CRC Press, 2002)
V. Michaud, A review of non-saturated resin flow in liquid composite moulding processes. Transp. Porous Media **115**, 581–601 (2016)
S. Murakami, Mechanical modeling of material damage. ASME J. Appl. Mech. **55**, 280–286 (1988)
N. Naik, M. Sirisha, A. Inani, Permeability characterization of polymer matrix composites by RTM/VARTM. Prog. Aerosp. Sci. **65**, 22–40 (2014)
F. Naya, C. González, C.S. Lopes, S. Van der Veen, F. Pons, Computational micromechanics of the transverse and shear behavior of unidirectional fiber reinforced polymers including environmental effects. Compos. Part A Appl. Sci. Manuf. **92**, 146–157 (2017)
N.D. Ngo, K.K. Tamma, Microscale permeability predictions of porous fibrous media. Int. J. Heat Mass Transf. **44**(6), 3135–3145 (2001)
G. Pal, S. Kumar, Multiscale modeling of effective electrical conductivity of short carbon fiber-carbon nanotube-polymer matrix hybrid composites. Mater. Des. **89**, 129–136 (2016)
J. Pan, L. Bian, H. Zhao, Y. Zhao, A new micromechanics model and effective elastic modulus of nanotube reinforced composites. Comput. Mater. Sci. **113**, 21–26 (2016)
R.S. Parnas, F.R. Phelan Jr., Effect of heterogeneous porous media on mold filling in resin transfer molding. SAMPE Quart. **22**(2), 53–60 (1991)
K.M. Pillai, Modeling the unsaturated flow in liquid composite molding processes: A review and some thoughts. J. Compos. Mater. **38**(23), 2097–2118 (2004)
K.M. Pillai, S.G. Advani, A model for unsaturated flow in woven fiber preforms during mold filling in resin transfer molding. J. Compos. Mater. **32**(19), 1753–1783 (1998)
K.M. Pillai, T.L. Tuce, M.V. Bruschke, R.S. Parnas, S.G. Advani, Modeling the heterogeneities present in preforms during mold filling in RTM, in *Advanced Materials: Expanding the Horizons, 25, 25th International SAMPE Technical Conference*, (1993)
A. Puck, H. Schürmann, Failure analysis of FRP laminates by means of physically based phenomenological models. Fail. Crit. Fibre-Reinf.-Polym. Compos., 264–297 (2004)
M. Shabaze, P.K. Sahoo, V.L. Jagannatha Guptha, Multiscale material modelling and analysis of carbon fiber/MWCNT/epoxy composites to predict effective elastic constants. Mater. Today Proc. **19**, 521–527 (2019)
S. Sharma, D.A. Siginer, Permeability measurement methods in porous media of fiber reinforced composites. Appl. Mech. Rev. **63**, 020802 (2010)
A. Sharma, S. Daggumati, A. Gupta, W. Van Paepegem, On the prediction of the bi-axial failure envelope of a UD CFRP composite lamina using computational micromechanics: Effect of microscale parameters on macroscale stress–strain behavior. Compos. Struct. **251**, 112605 (2020)
P. Soltani, M. Zarrebini, R. Laghaei, A. Hassanpour, Prediction of permeability of realistic and virtual layered nonwovens using combined application of X-ray CT and computer simulation. Chem. Eng. Res. Des. **124**, 299–312 (2017)
C.T. Sun, J. Tao, A.S. Kaddour, The prediction of failure envelopes and stress/strain behavior of composite laminates: Comparison with experimental results. Fail. Crit. Fibre-Reinf.-Polym. Compos. **62**, 890–902 (2004)
H. Tan, K.M. Pillai, Multiscale modeling of unsaturated flow in dual-scale fiber preforms of liquid composite molding I: Isothermal flows. Compos. Part A Appl. Sci. Manuf. **43**, 1–13 (2012)
M. Torres, F. Collombet, B. Douchin, L. Crouzeix, Y.-H. Grunevald, Comparison between the classic sensor embedding method and the monitoring patch embedding method for composites instrumentation. Appl. Compos. Mater. **21**, 707–724 (2014)
M. Torres, L. Crouzeix, F. Collombet, B. Douchin, Y.H. Grunevald, Numerical and experimental value added of multi-instrumented technological evaluator for the analysis of thick monolithic composite structures with singularity details. Compos. Struct. **127**, 41–50 (2015)
M. Torres, F. Collombet, B. Douchin, L. Crouzeix, Y.-H. Grunevald, Assessments on the mechanical behaviour of a monolithic composite structure instrumented with a monitoring patch. J. Compos. Mater. **51**, 3597–3610 (2017)

M. Torres, S. Piedra, S. Ledesma, C.A. Escalante-Velázquez, G. Angelucci, Manufacturing process of high performance-low cost composite structures for light sport aircrafts. Aerospace **6**, 11–27 (2019)

M. Torres-Arellano, V. Renteria-Rodríguez, E. Franco-Urquiza, Mechanical properties of natural-fiber-reinforced biobased epoxy resins manufactured by resin infusion process. Polymers **12**, 2841–2285 (2020)

E. Totry, J.M. Molina-Aldareguía, C. González, J.L. Lorca, Effect of fiber, matrix and interface properties on the in-plane shear deformation of carbon-fiber reinforced composites. Compos. Sci. Technol. **70**, 970–980 (2010)

I. Verpoest, S.V. Lomov, Virtual textile composites software WiseTex: Integration with micro-mechanical, permeability and structural analysis. Compos. Sci. Technol. **65**, 2563–2574 (2005)

S. Wang, Y. Yang, L.M. Zhou, Y.W. Mai, Size effect in microcompression of epoxy micropillars. J. Mater. Sci. **47**, 6047–6055 (2012)

J.R. Weitzenbock, R.A. Shenoi, P.A. Wilson, Radial flow permeability measurement. Part A: Theory. Compos. A. Appl. Sci. Manuf. **30**, 781–796 (1999)

X. Xiao, *Modeling the Structure-Permeability Relationship for Woven Fabrics*. PhD thesis, Division of Materials, Mechanics & Structures Faculty of Engineering, The University of Nottingham (2012)

Z. Yuan, B. Zhang, G. Yang, Z. Yang, A. Tang, S. Li, Y. Li, P. Zhao, Y. Wang, Multi-scale modeling of curing residual stresses in composite with random fiber distribution into consideration. Appl. Compos. Mater. **26**, 983–999 (2019)

D. Zhang, L. Chen, Y. Sun, Y. Zhang, K. Qian, Multi-scale modeling of an integrated 3D braided composite with applications to helicopter arm. Appl. Compos. Mater. **24**, 1233–1250 (2017a)

C. Zhang, C. Mao, Y. Zhou, Meso-scale damage simulation of 3D braided composites under quasi-static axial tension. Appl. Compos. Mater. **24**, 1179–1199 (2017b)

D.T. Zhang, L. Chen, Y.J. Wang, Stress field distribution of warp-reinforced 2.5D woven composites using an idealized meso-scale voxel-based model. J. Mater. Sci. **52**, 6814–6836 (2017c)

C. Zhang, C. Mao, J.L. Curiel-Sosa, T.Q. Bui, Meso-scale finite element simulations of 3D braided textile composites: Effects of force loading modes. Appl. Compos. Mater. **25**, 823–841 (2018)

C. Zhang, J.L. Curiel-Sosa, T.Q. Bui, Meso-scale finite element analysis of mechanical behavior of 3D braided composites subjected to biaxial tension loadings. Appl. Compos. Mater. **26**, 139–157 (2019)

Q. Zhenchao, Z. Nanxi, L. Yong, C. Wenliang, Prediction of mechanical properties of carbon fiber based on cross-scale FEM and machine learning. Compos. Struct. **212**, 199–206 (2019)

F. Zhou, N. Kuentzer, P. Simacek, S.G. Advani, S. Walsh, Analytic characterization of the permeability of dual-scale fibrous porous media. Compos. Sci. Technol. **66**, 2795–2803 (2006)

Recycling Studies of Epoxy Fiber-Reinforced Composites

14

Young Nam Kim and Yong Chae Jung

Contents

Abstract

With the rapid urbanization of modern society, we live in a world in which we are surrounded by materials with various functions, especially composite materials. Although our lives have become very prosperous owing to this, on the flip side, we are also facing deep concerns about serious environmental pollution. To resolve this issue, numerous studies have focused on the development of material recycling technologies, and we are preparing for a healthy future with the development of new alternative materials. Within this context, this chapter reports present research on recycling studies focusing on fiber reinforcement composite materials.

Y. N. Kim
Institute of Advanced Composite Materials, Korea Institute of Science and Technology (KIST), Jeonbuk, Republic of Korea

Department of Chemical and Biomolecular Engineering, Yonsei University, Seoul, Republic of Korea
e-mail: tony0008@naver.com

Y. C. Jung (✉)
Institute of Advanced Composite Materials, Korea Institute of Science and Technology (KIST), Jeonbuk, Republic of Korea
e-mail: ycjung@kist.re.kr

S. Mavinkere Rangappa et al. (eds.), *Handbook of Epoxy/Fiber Composites*,
https://doi.org/10.1007/978-981-19-3603-6_46

Keywords

Recycle · Fiber-reinforced composites · Composite · Plastic

Introduction

The world is now simultaneously facing an "environmental" crisis evidenced by climate change and a "resource" crisis represented by high oil prices. The issue of climate change is significant as it not only causes meteorological disasters but also fundamentally disrupts the order of the ecosystem, which consequently threatens the survival of mankind. In addition, the economic development of developing countries and the continuous increase in the world's population are exacerbating the shortage of energy and resources, in turn accelerating price increases. However, several developed countries have already focused their national power into research on efficient and environment-friendly uses of resources, as "green industries" and "green technology" become more commonplace.

In recent years, there have been global movements toward regulating the fuel economy and carbon dioxide emission from vehicles in the automotive sector, as environmental issues gradually emerge. The average carbon dioxide emission from vehicles has been regulated to less than 120 g/km in the European Union (EU) since 2012, and the fuel economy has been regulated to 16.8 km/L or more in Japan since 2015 (Jacob 2011; Global CFRP 2016). In parallel, it has become essential to develop technology for reducing the weight of vehicles in order to increase the fuel efficiency and to reduce carbon dioxide emissions. Thus far, various car makers have set a goal to reduce vehicle weight by 30–40% by 2030 and are working on developing technology to achieve this goal (Jacob 2011; Global CFRP 2016). About 75% of the materials used in the body of general passenger cars are metallic materials such as steel, alloy steel, and aluminum. Accordingly, representative developments aim to reduce the weight of the transportation (car, plane, drone, etc.) body while maintaining the mechanical strength by gradually replacing the materials with carbon fiber-reinforced plastic (CFRP) (Ghobadi 2017; Rosato 2013). With the use of CFRP, it is possible to achieve a weight reduction of about 30% compared to using aluminum and a 50% weight reduction compared to using steel; thus, the fuel economy can be improved, and carbon dioxide emission can be reduced by greatly lightening the vehicle body.

Among the world's fiber-reinforced composite material markets, the carbon fiber (CF) market has continued to grow at ~20% annually, and the global market size is estimated to be about $ 46 billion with a usage of ~140,000 tons in 2020 (Global CFRP 2016). The CFRP market size is about ten times larger than that of the carbon fiber market, and the global market size of the former was about 180,000 tons and $ 38 billion in 2020 (Carbon fiber composites 2014). New applications of CFRP such as in medical devices, building materials, industrial cables, and electronic products, in addition to the main uses in automobiles and aircraft, are expected to grow rapidly.

With the increasing usage of carbon composite materials in recent years, the market demand for treatment of carbon composite wastes at their end of life is also gradually growing. The global demand for carbon composites is projected to reach approximately 245,000 tons in 2022 (The Global CFRP Market 2016), and the price of carbon composites is anticipated to reach $27,994/ton (Global Automotive Composites Market 2016). Therefore, the market for waste carbon composites is projected to reach approximately $690 million in 2022 if carbon composites are recycled at an estimated rate of 10%. The market for recycled carbon fiber is expected to be driven by the application of this material in various high-functional parts through functionalization and intermediate material manufacturing processes.

Currently, materials used in automobiles are subject to recycling regulations under the Registration, Evaluation, Authorization, and Restriction of Chemicals (REACH) stipulations for end-of-life vehicles in most countries. Under the EU's end-of-life vehicles (ELV) directive for 2015 and beyond, 85% of materials used in automobiles must be recycled, 10% of them can be incinerated, and only less than 5% of them can be landfilled (Commission Directive (EU) 2016/774 2016). However, depositing composite material waste in landfills has been completely banned in the EU, and thus various efforts are being made by the government, academia, and companies to recycle composite materials to respond to these regulations. For example, the EU's ELV has increased the material recycling rate from 80% in 2014 to 85% in 2015. In Germany, the reuse and recycling rate, including energy recovery has already been improved by more than 100% since 2010 (Commission Directive (EU) 2016/774 2016).

Despite its excellent mechanical properties and gradually increasing utility, CFRP is facing increasingly stringent demand for measures and methods of recycling carbon fibers (RCF) and carbon composites due to increased awareness of the global environment and the difficulty in waste treatment. To implement practical carbon composite material recycling techniques, it is important to develop technology that can reduce energy consumption by reducing the operating temperature and pressure while maintaining the physical properties of the recovered carbon fibers. However, because the currently available technology for recycling composite materials faces substantial difficulty due to the composition of the composite material, the cross-linking characteristics of the thermosetting resin, and the fusion with other materials, most of the waste is deposited in landfills at present.

In general, thermoplastic resins such as polyether ether ketone (PEEK) or thermosetting resins such as unsaturated polyester resin, phenolic resin, and epoxy resin are mainly used as the matrix for CFRP. Among them, epoxy resins are the most widely used due to their low viscosity, good compatibility with carbon fibers, and excellent heat resistance and mechanical properties. However, unlike thermoplastic resins that can be recycled by simply separating the matrix from the carbon fiber through drying processes, thermosetting resins suffer from the disadvantage that it is difficult to separate the matrix from the carbon fiber subsequent to curing. Therefore, CFRP using thermosetting resin is treated as industrial waste at its end of life, and mainly ends up in landfills. This treatment is problematic as carbon fibers are unrecyclable, landfill costs are enormous, and the material places a lot of burden on the global environment. In addition, the cost of producing new carbon fibers is twice as much as

Fig. 1 "The New Waste Framework Directive" published in 2008 by EU. (Source: Recyctec™) (Directive 2008/98/EC 2008)

that of producing aluminum and ten times as much as producing steel, and a lot of pollutants such as carbon dioxide are emitted during the production process.

Recently, due to these environmental and economic concerns, the importance of technology for recovering and recycling carbon fibers by decomposing the matrix from CFRP has grown. For example, the EU banned the reclamation of CFRP waste and stipulated that it should be recycled, which expands the scope of responsibility of waste producers in environmental pollution, as stated in "The New Waste Framework Directive" published in November 2008 (Fig. 1) (Directive 2008/98/EC 2008). Accordingly, when foreign companies enter the European market, it is necessary to secure recycling technology to cope with these regulations. However, unlike European and Japanese companies that currently possess over 95% of recycling technology, the level of recycling technology in other countries is estimated to be around 60%.

Therefore, it is necessary to secure recycling technology that creates new added value and to develop green technology that suppresses environmental pollution in the new carbon fiber-based material industry, which has rapidly emerged as a new material industry that will change the tides of the global economy. Representative examples are presented hereinafter in this report.

Methods of Recycling Fiber Composite Materials

At present, reducing the cost of part manufacturing by developing CF recycling technology and process reduction and minimizing waste disposal costs by producing parts using recycled materials have been realized in Germany, Japan, and the USA, but most of the related technologies remain in the early stage.

The BMW Automotive Group in Germany produces auto parts for its "i series" by simplification of the process using recycled CF wet compression molding. Further, joint research and development of CF recycling technology at the pilot-plant stage and commercialization of part processing technology are being conducted by Toho Tenax (Teijin Carbon), Mitsubishi Rayon, and Toray in Japan. Carbon Conversions in the USA is in the process of commercializing this technology by manufacturing cheaper wind turbine blades and reinforcing materials from CF scraps.

For the past 20 years, various recycling technologies, such as mechanical processes, pyrolysis, other thermal processes, and solvolysis, have been actively studied (Fig. 2).

Among the existing methods, pyrolysis is the only technique that has been successfully commercialized and is currently used by ELG Carbon Fiber Ltd. (ELGCF, UK). Adherent Technologies Inc. (ATI, USA) is recovering fiber reinforcement materials by chemically treating fiber-reinforced composite materials (ELG Carbon Fibre 2014). Additionally, Innoveox (France) is applying a technology that is based on supercritical hydrolysis (http://www.innoveox.com/; Morin et al. 2012). Supercritical fluids have continued to receive considerable attention as they afford control over various process conditions such as temperature, pressure, and volume, but the high equipment cost remains a major drawback.

Mechanical Recycling

In general, mechanical recycling is a commonly applied technique in which materials are initially crushed or shredded to form small pieces that are further grinded into finer particles (Molnar 1995; Steenkamer and Sullivan 1998; Palmer et al. 2009, 2010; Pickering 2006; Takahashi et al. 2007; Ogi et al. 2007). Recyclates, the sizes of which have been reduced by pulverization, comprise fine powders and resins with high resin content, and can be separated into coarse powders with relatively high fiber content through sieving. The mechanical grinding method has been mainly applied to glass fiber-reinforced composite materials (especially sheet molding

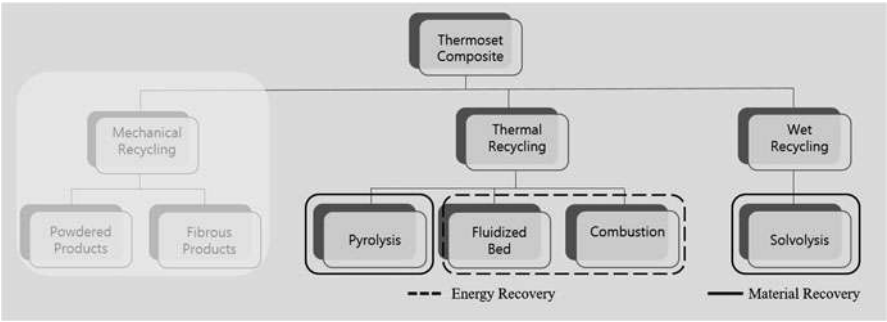

Fig. 2 Classification of recycling applications of carbon composite materials

compound (SMC) and bulk molding compound (BMC)), but applications to carbon fiber-reinforced thermoplastic composites (CFRC) have also been studied.

The mechanically recycled composite materials are typically used in new composite materials or in construction materials (artificial wood, asphalt, or mineral resources for cement). However, these materials are used as low-cost products, and thus mechanical recycling has been applied to improve their quality to maintain the quality of composite materials containing the recyclates. Schinner et al. studied CFRC using PEEK resin (Schinner et al. 1996). In that study, it was confirmed that the cutting mill can produce a more uniform fiber length distribution and longer fibers than the hammer mill, even though the cutting blade of the former becomes dull relatively faster. Injection molding with up to 50% of recycled material by weight was made possible by successfully mixing the pulverized material into unused virgin PEEK resin. Palmer et al. (2009) confirmed that the mixing time had an effect on the mechanical properties of the final materials by evaluating the effect of the mixing time when combining about 10% of the recycled fiber material recovered from SMC with dough molding compounds (DMC) as in the virgin fiber (Fig. 3) (Palmer et al. 2009). When the paste and the reusable materials were mixed for an extended period, the mechanical properties were further improved. These technologies have been employed to process glass fiber-reinforced composites (GFRC) by many companies such as Mixt Composites Recyclables (MCR), a subsidiary of Plastic Omnium in France and Filon Products Ltd. in the UK (Asmatulu et al. 2014; Yang et al. 2012).

Pyrolysis

Pyrolysis involves heat treatment in the presence of oxygen (Fig. 4) (Torres et al. 2000; Cunliffe and Williams 2003; Åkesson et al. 2012; Pakdel et al. 2020; Abdou et al. 2020; Dwivedi et al. 2020). Pyrolysis of organic molecules under an inert

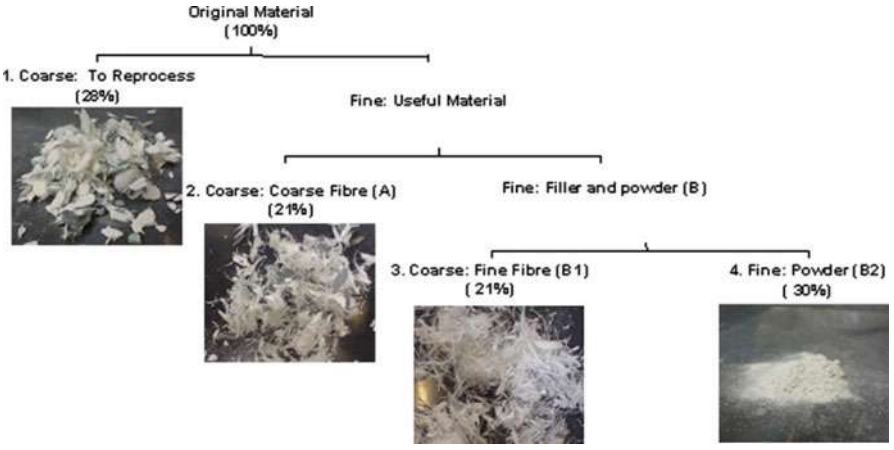

Fig. 3 Three stage air classification of the ground SMC recyclate (Palmer et al. 2009)

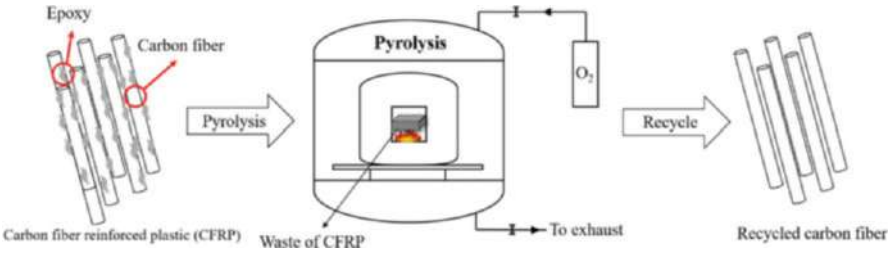

Fig. 4 Pyrolysis recycle process of fiber composite materials

atmosphere is one of the most widely used processes for CFRP recycling. CFRP is heated to 450–700 °C under oxygen-free conditions in the decomposition treatment vessel. During this process, the polymer resin is decomposed to low-weight molecules and evaporated. Subsequently, the carbonized fibers remain inactive and can be recovered at the end of the process.

As the composite materials decompose, they produce oil, gas, and solid products (fibers, fillers, and carbides). Therefore, the requirement for posttreatment to remove the carbides by burning off in a heating furnace at 450 °C is inconvenient because the recycled glass or carbon fiber is contaminated by these carbides.

In 2011, Pimenta and Pinho summarized the data from other research groups (Pimenta and Pinho 2011). Additional values were also found and are reported in Table 2. The results showed that the tensile strength can be reduced by 85%, but may not be affected by the treatment. Therefore, it can be confirmed that the process conditions have a strong impact on the physical properties of the fiber. In particular, it was found that the tensile strength of the fiber regenerated by heat treatment in the composite material was reduced to a lesser extent than that of the fibers without resin heat treated in air.

Epoxy resins are decomposed more easily under oxidative conditions than under inert conditions, and the resin residue can be completely decomposed at 500–600 °C (Meyer et al. 2009). It was reported that high-tenacity carbon fibers (HTA, Toho-Tenax co. Ltd) with a tensile strength of 95% or more can be recovered without surficial resin residue when treated under oxidative conditions subsequent to treatment at 550 °C for 2 h under nitrogen atmosphere (Meyer et al. 2009).

In 2009, Meyer et al. (2009) evaluated the thermal decomposition conditions for minimizing surface changes and deterioration of the physical properties of the recovered carbon fiber and found that thermal decomposition of the epoxy resin proceeds in the temperature range of 380–600 °C under nitrogen atmosphere, leaving about 19% waste, and the epoxy resin is completely decomposed at 310–580 °C under air atmosphere (Fig. 5). Because the mechanical strength of the recovered carbon fiber decreases when surface oxidation of the carbon fiber is initiated at ~600 °C under air atmosphere, a thermal decomposition method that can minimize deterioration of the fiber properties by heating the carbon fiber at 550 °C for 2 h under nitrogen atmosphere and cooling to 200 °C, followed by re-heating to 550 °C, was also reported.

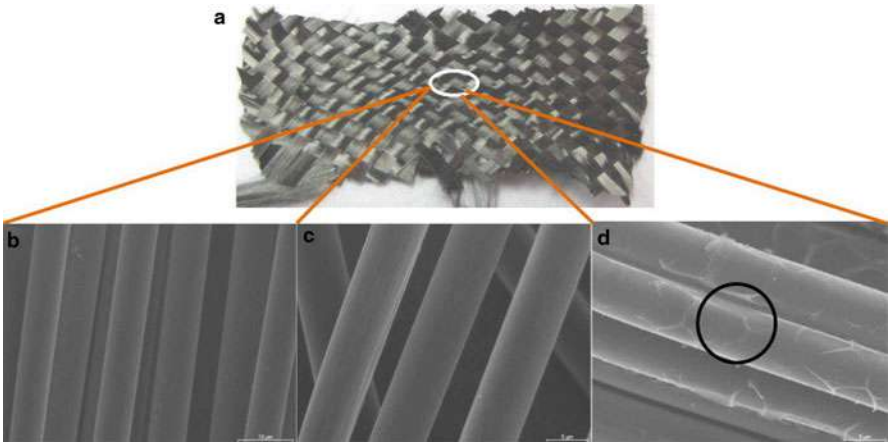

Fig. 5 (**a**) Carbon fibers recovered after thermolysis and gasification; (**b**) SEM images of carbon fibers recovered after thermolysis at 500 °C and gasification at 500 °C for 30 min; (**c**) after 60 min; and (**d**) after 180 min (López et al. 2013)

Moreover, Félix A. López reported the recovery of carbon fibers by the thermolysis and gasification of waste prepreg (López et al. 2013). The recovery of carbon fibers from aeronautical composite wastes was studied. At this time, it was confirmed that the types of gas and oil produced were different depending on the pyrolysis temperature. In addition, it was confirmed that the strength of the recycled carbon fiber varies depending on the treatment time (Fig. 5).

Solvolysis

Solvolysis is the technique in which a reaction medium (catalyst solution, benzyl alcohol, organic solvent, etc.,) at temperature below 350 °C is used to decompose the polymer resin in the composite material (Buggy et al. 1995; Onwudili et al. 2013; Yildirir et al. 2014). While polymerized resin, in general, decomposes into relatively large oligomers, the carbon fibers remain inert and can be collected at the end of the process (Fig. 6).

Thus far, many decomposition methods using various conditions and organic solvents have been attempted for recycling thermoplastics or thermoplastic polymers. Solvolysis has extensive potential owing to its broad operating parameters such as temperature, solvent, pressure, and catalyst and economic advantages due to its relatively low operating temperature compared to pyrolysis.

Chemical recycling of epoxy resins depolymerized by the soluble decomposition method is a remarkable research field in terms of recycling resins other than fibers. G. Tersac et al. (El Gersifi et al. 2006; Sánchez-Cadena et al. 2019; Vallee et al. 2004) reported on chemical recycling after decomposition of epoxy resins cured with bisphenol A diglycidyl ether (DGEBA). Epoxy resin was decomposed into

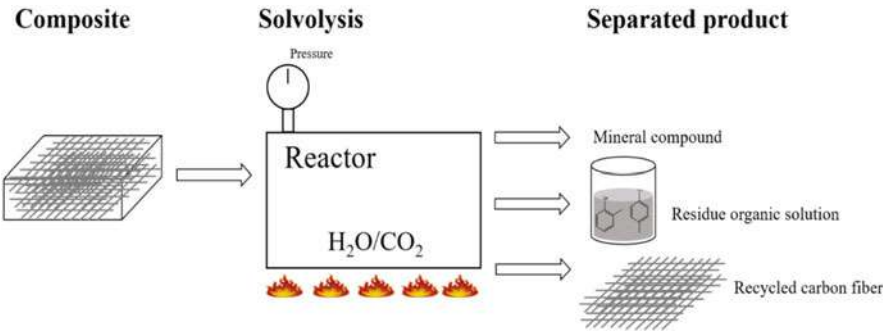

Fig. 6 Solvolysis recycle process of fiber composite materials

monomer units after depolymerization, and at this time, it was identified as esterdiols, tetraalcohols, and excess of glycol as process products. In addition, through NMR and Maldi-Tof analysis, it was confirmed that the reaction mechanism of the transesterification reaction and the existence of other side reactions of alcohol decomposition were observed as an effect on the characterization of depolymerization products. This report of research results suggests factors for higher recyclability of polymeric monomers and more stable depolymerization conditions after depolymerization using the solvent decomposition method (Fig. 7).

Supercritical Fluid

Since the 2000s, the supercritical fluid process has gained attention as the most environmental-friendly process (Taylor 1996; McHugh and Krukonis 2013; Perrut 2000). It has emerged as an underlying core technology for quality and efficiency improvement, environment-friendly processes, and energy-saving processes in various fields, such as polymer synthesis and processing, rapid expansion of supercritical solution (RESS), dyeing processes, extraction of organic matter, crystallization, absorption, drying, and cleaning.

In the recycling of composite materials using supercritical fluids, supercritical water (SCW, temperature >374 °C and pressure >221 bar) is the main solvent used for recycling CFRP to recover high-quality carbon fiber without concern for resin decomposition (Perrut 2000; Dauguet et al. 2015; Kim et al. 2019; Goto 2009; Li and Xu 2019). This is attributed to the superior quality and physical properties of carbon fibers recycled by SCW compared with those produced by other recycling methods. Supercritical fluids are also being researched and developed for recycling composite materials owing to their advantages such as high dissolving power, high mass and heat transfer, low viscosity, high diffusion coefficient, and high power for penetrating into micropores due to their low surface tension.

A supercritical fluid is defined as a substance at a temperature and pressure above its critical point, where the liquid phase and gas phase are indistinguishable from

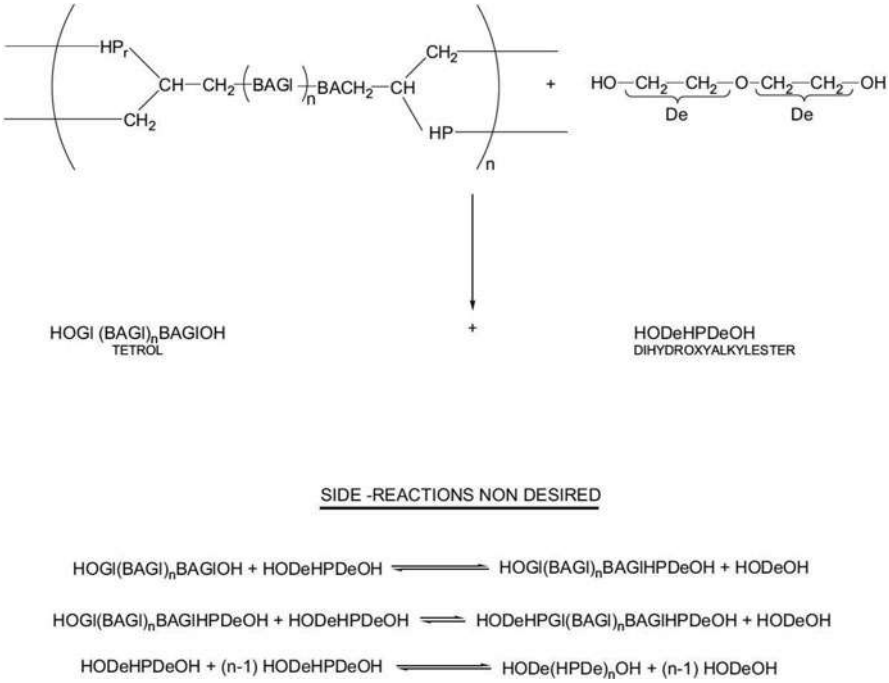

Fig. 7 Scheme of solvolysis reaction of a DGEBA/HP model network by DEG (El Gersifi et al. 2006)

each other, and functions as a highly active solvent as it is close to liquid in terms of viscosity and to gas in terms of the diffusion coefficient (Fig. 8).

A representative supercritical fluid is supercritical carbon dioxide ($Tc = 31$ °C, $Pc = 73$ atm), which has a critical point close to room temperature and is nontoxic, nonflammable, and very inexpensive; the use of carbon dioxide enables the development of eco-friendly and energy-saving processes. Carbon dioxide is a nonpolar substance and thus can be used as an alternative to nonpolar solvents such as *n*-hexane. Many studies have been conducted in the pharmaceutical, flavor, and food industries, in which active ingredients are extracted from natural products to take advantage of the lack of organic solvent residue afforded by this process. Recently, there have been many studies and commercialization of drug particle engineering, polymer synthesis, and polymer processing.

Due to its high polarity, water can dissolve inorganic salts such as NaCl, where the dielectric constant of water is temperature- and pressure-dependent (Shaw 1991). The dielectric constant of water at room temperature and atmospheric pressure is 78, which is very high compared to ~2–20 for other common polar organic solvents. When water reaches the supercritical state ($Tc = 374$ °C, $Pc = 218$ atm), with increasing temperature and pressure, the hydrogen bonds in water become weaker, and thus the dielectric constant decreases to ~2–30, which is similar to that of organic solvents such as *n*-hexane (dielectric constant: 1.8), acetone (dielectric

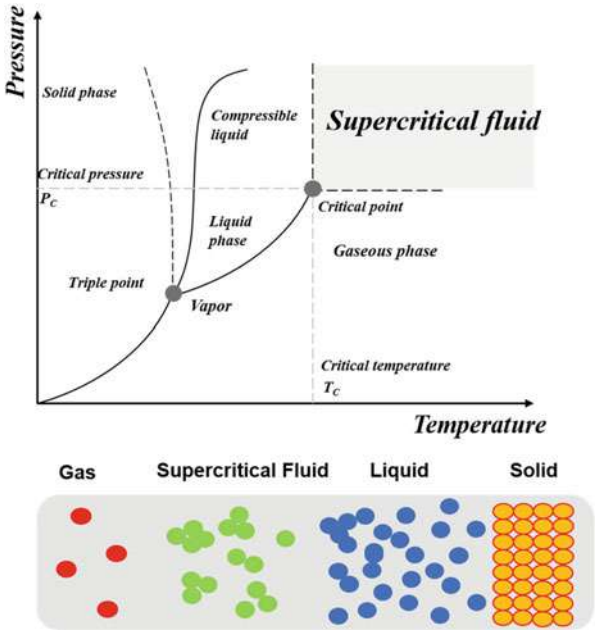

Fig. 8 Critical point of supercritical fluids

constant: 20.7), ethanol (dielectric constant: 24.5), and methanol (dielectric constant: 28). In other words, water can be changed from a polar solvent to a nonpolar solvent.

Supercritical water cannot dissolve inorganic salts such as NaCl as the bonding between molecules becomes weaker in the supercritical state but can be mixed with organic compounds such as benzene and dissolve gases such as oxygen and hydrogen completely. Therefore, supercritical water functions as an oxidizing agent or base catalyst by itself. Therefore, it is possible to produce fine particles or to control decomposition, synthesis, radical reactions, and ionic reactions of hardly decomposable substances.

Recycling Using Supercritical Organic Solvent

Supercritical water has attractive properties for the recovery of high-quality carbon fiber but requires special vessels that can withstand harsh hydrolysis conditions and high pressure. To alleviate the requirements, a study to develop alternative solvents that function under lower temperature and pressure conditions was reported using other supercritical fluids such as ethanol, methanol, *n*-propanol, and acetone, as well as water-containing additives or catalysts.

For example, supercritical alcohol or acetone requires a temperature similar to that of supercritical water from pure water to sufficiently remove resin from the carbon fibers, but the required pressure is much lower than that of supercritical water (comparing the same amounts of solvent, the required pressure of water is about 630 bar and that of 1-propanol is about 255 bar at 450 °C). The change in the decomposition conditions can lead to energy and cost savings for recycling processes.

In 2009, Goto and coworkers at Kumamoto University in Japan (Goto 2009) reported a synthesis/separation technique using supercritical or subcritical fluid for recycling FRP (insoluble PET/insoluble plastics) (Figs. 9 and 10).

Okajima and coworkers at Shizuoka University in Japan reported the development of a supercritical methanol-based technique for recycling CFRP (Figs. 11 and 12) (Okajima et al. 2014). In the study, thermosetting epoxy resins were decomposed by supercritical methanol and transformed into thermoplastic resins. The plain fabric sheet shape was maintained in the recovered carbon fiber, and the tensile strength was reduced by 9% compared to that of the pure carbon fibers. It was reported that the recovered carbon fibers could be used to make recycled CFRP, with strength similar to that of pure CFRP.

The recycling of CFRP containing amine-cured epoxy resin using either supercritical or subcritical fluids was also reported (Fig. 13) (Okajima et al. 2017). Either supercritical alcohol or ketone was used as a solvent for chemical recycling of the resin matrix of

Fig. 9 Recovered glass fiber (left) and carbon fiber (right) from treatment in BZA (Goto 2009)

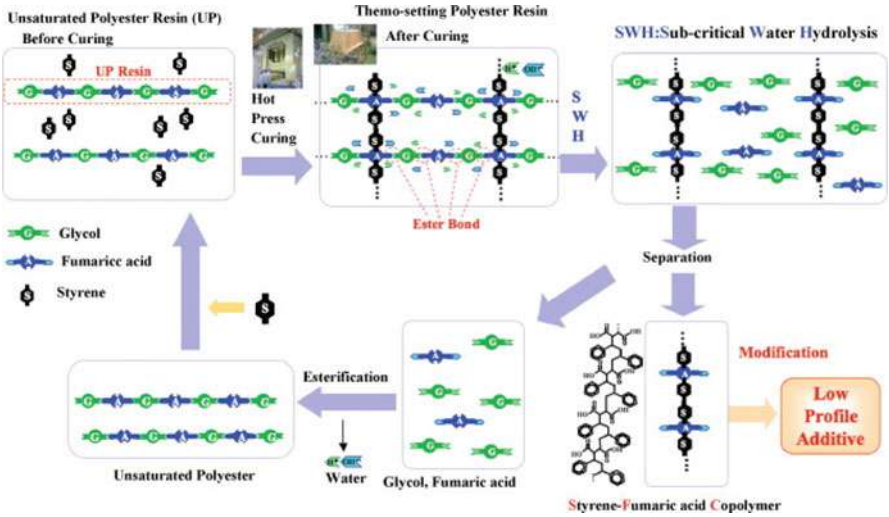

Fig. 10 A concept of FRP recycling developed at Matsushita Electric Works, Ltd. (Goto 2009)

Fig. 11 Appearance of recovered carbon fiber from CFRP at 270 °C, 8 MPa and 90 min: (**a**) CFRP before decomposition, (**b**) recovered carbon fiber after decomposition, and (**c**) SEM photo of recovered carbon fiber with 3000 magnification (Okajima et al. 2014)

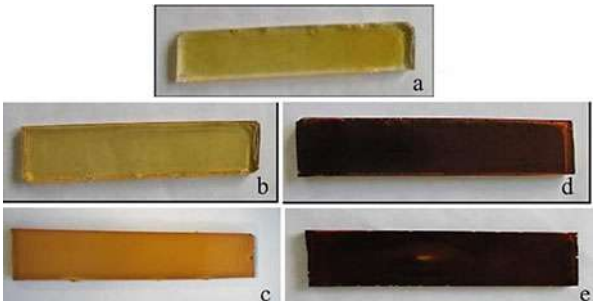

Fig. 12 Re-curing of recovered and virgin epoxy resins. Ratio of recovered resin: (**a**) 0%, (**b**) 25%, (**c**) 50%, (**d**) 75%, and (**e**) 100% (Okajima et al. 2014)

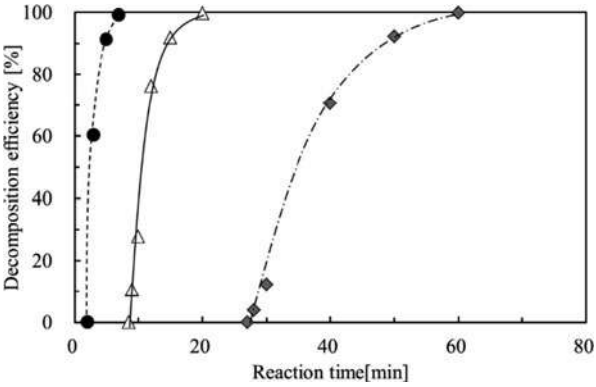

Fig. 13 Effects of reaction temperature and time on the decomposition of epoxy resin using supercritical acetone at a molar density of 3.64 mol/L. ◆,300 °C; △, 320 °C; ●, 350 °C (Okajima et al. 2017)

carbon fiber-reinforced plastic (CFRP) containing amine-cured epoxy resin. Supercritical fluids such as methanol, 1-propanol, 2-propanol, 1-butanol, 2-butanol, *tert*-butanol, acetone, and methyl ethyl ketone were used at 320 °C, and the reaction time ranged from 6 to 120 min, suggesting that the decomposition rate was solvent-dependent. Notably, supercritical acetone was the best solvent for rapidly decomposing the matrix resin.

Most recently, the recycling of fiber-reinforced composite materials using supercritical acetone was reported (Fig. 14) (Okajima and Sako 2019). By investigating the pressure-dependent decomposition of epoxy resin in CFRP with superheated and

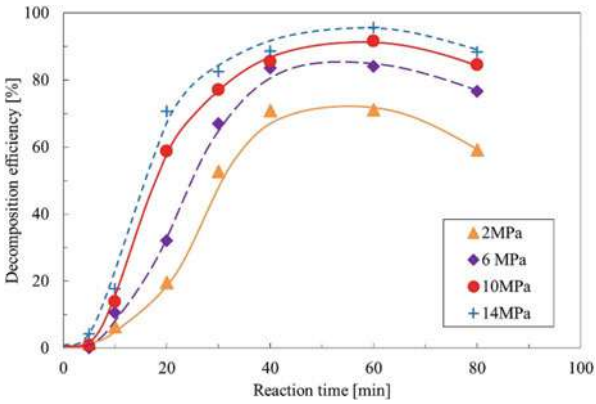

Fig. 14 Pressure dependence of decomposition efficiency of epoxy resin in CFRP using superheated and supercritical acetone at 350 °C (Okajima and Sako 2019)

supercritical acetone, it was found that the decomposition efficiency improved to 95.6% when the composite was treated at 350 °C and 14 MPa for 60 min as the reaction pressure and density of acetone increased. From the results, the rate of decomposition of the epoxy resin in CFRP using supercritical acetone was rationalized by the surface reaction and shrinking core model.

Haihong Huang's group reported the recycling and upcycling of CFRP based on a closed-loop recycling process using supercritical *n*-butanol (Liu et al. 2020). The decomposition of carbon fiber-reinforced epoxy resin composites was performed by controlling the ratio of the composite waste to *n*-butanol to achieve high recovery efficiency; the study provided insight into the changes in the properties and morphology of recycled carbon fibers (RCF). To evaluate the reusability of RCF in the remanufacturing process and the feasibility of the closed-loop recycling process for carbon fiber, the composite was remanufactured by mixing RCF with new epoxy resin and polypropylene, and the properties of the resultant composite were evaluated. Specifically, the effects on the physical properties of RCF during the regeneration process were attributed to degradation of the tensile properties and removal of the sizing agent, leading to changes in the interfacial bonding strength between RCF and the new resin, in turn affecting the performance of the recycled composite.

Recycling Using Supercritical Water

The effect of using supercritical water on the recycling of carbon fibers is excellent, but the high critical temperature and pressure required to reach supercritical conditions, as described earlier, can be considered a disadvantage. However, when only supercritical water is used, the composite material can be sufficiently recycled without commonly used oxidizing agents or catalysts, and thus this technique is considered very suitable for mitigating the environmental impact.

Table 1 presents a list indicating the types of solvents used, the use/nonuse of a catalyst, and the reuse technique applied to carbon fiber in the recycling process with various supercritical fluids. As seen in the table, high recyclability was mainly obtained with organic solvents or water containing a catalyst. However, Jung's

Table 1 Recycling rate according to supercritical water treatment conditions

Entry	Solvent	Catalyst	Decomposition rate (%)	Time (min)	Reuse (composite)	Ref
1	Water	KOH	99	180	–	(Liu et al. 2012)
2	Water	KOH	95	120	–	(Knight et al. 2012)
3	Acetic acid	$AlCl_3$	99	300	–	(Wang et al. 2015)
4	Ethanol	$ZnCl_2$	95	450	–	(Liu et al. 2017)
5	Acetone	Acid/ KOH	97	200	–	(Jiang et al. 2017)
6	Acetic acid	H_2O_2	98	300	–	(Das et al. 2018)
7	Water	–	99	120	O	(Kim et al. 2019, 2020)

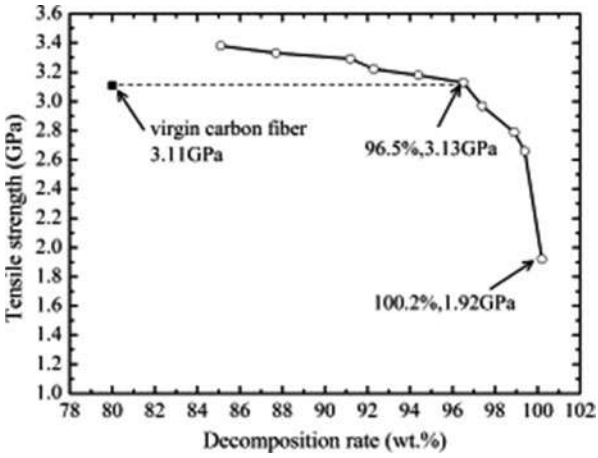

Fig. 15 The curve of tensile strength versus decomposition rate (Bai et al. 2010)

group reported a high recycling rate and technology for the reuse of recycled carbon fiber using supercritical water without a catalyst.

Zhi Wang's group reported the recycling of carbon fiber composites by adding oxygen to supercritical water (Fig. 15) (Bai et al. 2010). In other words, the recycling characteristics were improved by adding oxygen to the active supercritical water. The decomposition rate increased by up to 96% compared to that of the existing method, and very clean carbon fibers without any epoxy composite on the surface were acquired. Based on this result, it is thought that researchers are closer to an ideal recycling technology.

Generally, when CFRP is used in a supercritical fluid to obtain recycled carbon fiber, it is completely separated from the matrix and is obtained in a random form. Therefore, it is difficult to reuse the recycled carbon fiber to form a composite.

However, very recently Jung's group used CBT resin to easily shorten the RCFs and reapply the product as a conductive composite. In addition, we compared our recently published CFRP recycled paper and existing papers to emphasize that our system generated a conductive composite by using RCF, where the recycling system is environmentally friendly (Figs. 16 and 17) (Kim et al. 2019). Figure 16 shows the tensile test results to investigate the mechanical properties of the original CF and RCFs. The RCFs of tensile strength and modulus decreased about 18–36% compared to the original CFs, because of the decomposition epoxy resin and elimination of sizing agent on the surface of carbon fibers through SCF-W treatment (Das et al. 2018). Moreover, Jung's group reported recycled CFRP of bio-epoxy based as a polymeric matrix as shown in Fig. 18 (Kim et al. 2020). This

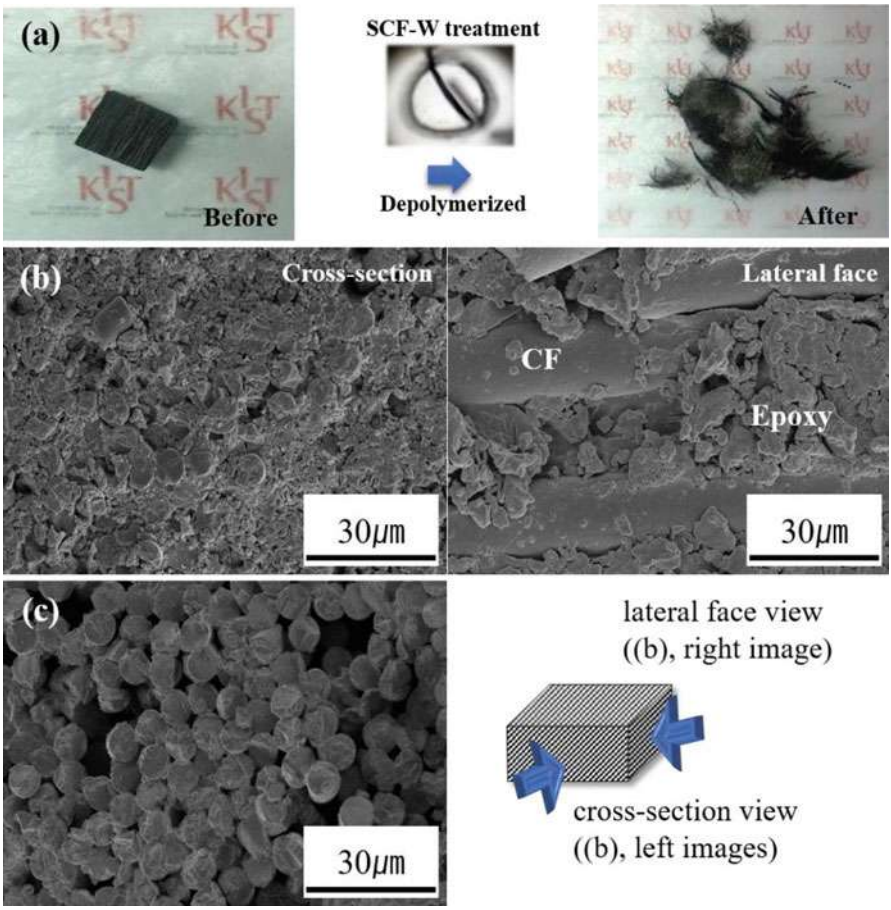

Fig. 16 (**a**) Photo images of untreated CFRP sample cubic (left) and RCFs (right); SEM photos (**b**) before SCF-W treatment (cross section and lateral face), and (**c**) after SCF-W treatment (Kim et al. 2019)

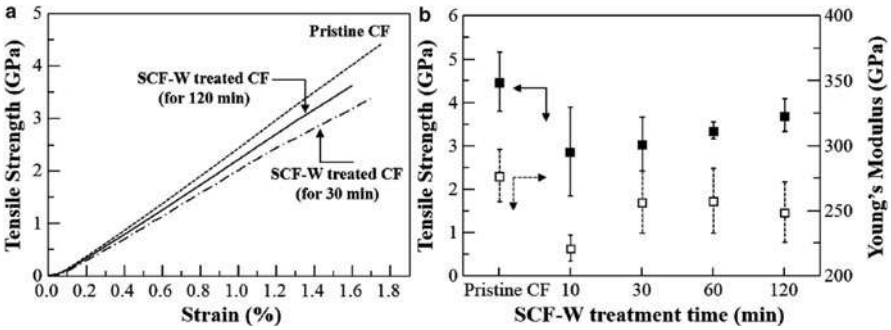

Fig. 17 Mechanical properties of single fiber of pristine CF and RCF at various supercritical fluid conditions: (**a**) strain-stress curves and (**b**) tensile strength and modulus specimens, respectively (Kim et al. 2019)

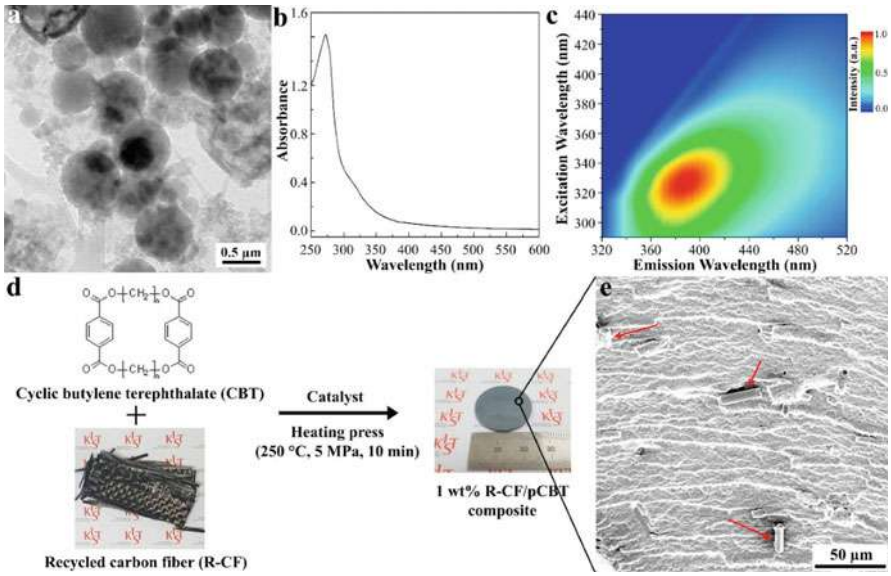

Fig. 18 (**a**–**c**) Characterization of degraded TA-based epoxy matrix obtained by treating scDW with T-CFRPs. Degraded materials were extracted from DW phase using ethyl acetate. (**a**) TEM image of degraded TA-based epoxy matrix. (**b**) UV spectroscopy and (**c**) 2D excitation-emission topographical map of the materials recovered by scDW treatment of T-CFRPs. (**d**) Scheme of fabrication of RCF/pCBT composite using heating press. (**e**) FE-SEM image of fractured surface of 1 wt% RCF/pCBT composite. Red-colored arrows indicate chopped CF fillers in composite (Kim et al. 2020)

research result for recyclable tannic acid-based CFRP. That sample can be treated with supercritical deionized water (scDW) with no additives, producing carbon spheres from the degradation of the epoxy matrix and clean CFs.

Conclusion

The world we are now living in is rapidly developing, and thus materials with various functions, especially composite materials, are being developed and used to meet the demands of modern life. Accordingly, while our lives have become very prosperous, on the flip side, we are deeply concerned about the serious pollution of the global environment. To overcome this, environmental regulations and eco-friendly recycling technology have been steadily developed over the last decade, and the development of new alternative materials is still a task that must be undertaken to achieve a healthy future. Within this context, research efforts in the development of eco-friendly materials and recycling technologies deserve strong recognition. This chapter described domestic and overseas markets and research trends for composite materials and the recent stages in the advancement of composite material recycling technologies. The summary is expected to contribute to better outcomes in the future based on the eco-friendly recycling technologies mentioned above.

Acknowledgments This work was supported by the KIST Institutional Program.

References

T. Abdou, A.B.. Junior, D.Espinosa, J. Tenório, Recycling of polymeric composites from industrial waste by pyrolysis: deep evaluation for carbon fibers reuse. Waste Manag. **120**, 1–9 (2020)

D. Åkesson, Z. Foltynowicz, J. Christeen, M. Skrifvars, Microwave pyrolysis as a method of recycling glass fibre from used blades of wind turbines. J. Reinf. Plast. Compos. **31**(17), 1136–1142 (2012)

E. Asmatulu, J. Twomey, M. Overcash, Recycling of fiber-reinforced composites and direct structural composite recycling concept. J. Compos. Mater. **48**(5), 593–608 (2014)

Y. Bai, Z. Wang, L. Feng, Chemical recycling of carbon fibers reinforced epoxy resin composites in oxygen in supercritical water. Mater. Des. **31**(2), 999–1002 (2010)

M. Buggy, L. Farragher, W. Madden, Recycling of composite materials. J. Mater. Process. Technol. **55**(3–4), 448–456 (1995)

Carbon fiber composites market update, the future of carbon fiber composites. Lux Research report, 2014

Commission Directive (EU) 2016/774 of 18 May 2016 amending Annex II to Directive 2000/53/EC of the European Parliament and of the Council on end-of-life vehicles (Text with EEA relevance)

A.M. Cunliffe, P.T. Williams, Characterisation of products from the recycling of glass fibre reinforced polyester waste by pyrolysis☆. Fuel **82**(18), 2223–2230 (2003)

M. Das, R. Chacko, S. Varughese, An efficient method of recycling of CFRP waste using peracetic acid. ACS Sustain. Chem. Eng. **6**(2), 1564–1571 (2018)

M. Dauguet, O. Mantaux, N. Perry, Y.F. Zhao, Recycling of CFRP for high value applications: effect of sizing removal and environmental analysis of the SuperCritical fluid solvolysis. Procedia CIRP **29**, 734–739 (2015)

Directive 2008/98/EC of the European Parliament and of the Council of 19 November 2008 on waste and repealing certain Directives (Text with EEA relevance) Special edition in Croatian: Chapter 15 Volume 034 P. 99 – 126

C. Dwivedi, S. Manjare, S.K. Rajan, Recycling of waste tire by pyrolysis to recover carbon black: alternative & environment-friendly reinforcing filler for natural rubber compounds. Compos. Part B Eng. **200**, 108346 (2020)
K. El Gersifi, G. Durand, G. Tersac, Solvolysis of bisphenol A diglycidyl ether/anhydride model networks. Polym. Degrad. Stab. **91**(4), 690–702 (2006)
ELG Carbon Fibre. http://www.elgcf.com/. Last accessed Jan 2014
A. Ghobadi, Common type of damages in composites and their inspections. World J. Mech. **7**(2), 24–33 (2017)
Global Automotive Composites Market, Forecast to 2021, Frost & Sullivan, 2016
Global CFRP Recycle Industry Report 2016, QYR Chemical & Material Research Center
M. Goto, Chemical recycling of plastics using sub-and supercritical fluids. J. Supercrit. Fluids **47**(3), 500–507 (2009)
http://www.innoveox.com/. Last accessed Jan 2014
A. Jacob, Composites can be recycled. ReinfPlast **55**(3), 45–46 (2011)
J. Jiang, G. Deng, X. Chen, X. Gao, Q. Guo, C. Xu, L. Zhou, On the successful chemical recycling of carbon fiber/epoxy resin composites under the mild condition. Compos. Sci. Technol. **151**, 243–251 (2017)
Y.N. Kim, Y.-O. Kim, S.Y. Kim, M. Park, B. Yang, J. Kim, Y.C. Jung, Application of supercritical water for green recycling of epoxy-based carbon fiber reinforced plastic. Compos. Sci. Technol. **173**, 66–72 (2019)
Y.-O. Kim, J. Cho, Y.N. Kim, K.W. Kim, B.W. Lee, J.W. Kim, M. Kim, Y.C. Jung, Recyclable, flame-retardant and smoke-suppressing tannic acid-based carbon-fiber-reinforced plastic. Compos. Part B Eng. **197**, 108173 (2020)
C.C. Knight, C. Zeng, C. Zhang, B. Wang, Recycling of woven carbon-fibre-reinforced polymer composites using supercritical water. Environ. Technol. **33**(6), 639–644 (2012)
K. Li, Z. Xu, A review of current progress of supercritical fluid technologies for e-waste treatment. J. Clean. Prod. **227**, 794–809 (2019)
Y. Liu, J. Liu, Z. Jiang, T. Tang, Chemical recycling of carbon fibre reinforced epoxy resin composites in subcritical water: synergistic effect of phenol and KOH on the decomposition efficiency. Polym. Degrad. Stab. **97**(3), 214–220 (2012)
T. Liu, M. Zhang, X. Guo, C. Liu, T. Liu, J. Xin, J. Zhang, Mild chemical recycling of aerospace fiber/epoxy composite wastes and utilization of the decomposed resin. Polym. Degrad. Stab. **139**, 20–27 (2017)
W. Liu, H. Huang, H. Cheng, Z. Liu, CFRP reclamation and remanufacturing based on a closed-loop recycling process for carbon fibers using supercritical N-butanol. Fiber Polym. **21**(3), 604–618 (2020)
F.A. López et al., Recovery of carbon fibres by the thermolysis and gasification of waste prepreg. J. Anal. Appl. Pyrolysis **104**, 675–683 (2013)
M. McHugh, V. Krukonis, *Supercritical Fluid Extraction: Principles and Practice* (Elsevier, 2013)
L.O. Meyer, K. Schulte, E. Grove-Nielsen, CFRP-recycling following a pyrolysis route: Process optimization and potentials. J. Compos. Mater. **43**(9), 1121–1132 (2009)
A. Molnar, Recycling advanced composites. Final report for the Clean Washington Center (CWC), December 1995
C. Morin, A. Loppinet-Serani, F. Cansell, C. Aymonier, Near-and supercritical solvolysis of carbon fibre reinforced polymers (CFRPs) for recycling carbon fibers as a valuable resource: state of the art. J. Supercrit. Fluids **66**, 232–240 (2012)
K. Ogi, T. Nishikawa, Y. Okano, I. Taketa, Mechanical properties of ABS resin reinforced with recycled CFRP. Adv. Compos. Mater. **16**(2), 181–194 (2007)
I. Okajima, T. Sako, Recycling fiber-reinforced plastic using supercritical acetone. Polym. Degrad. Stab. **163**, 1–6 (2019)
I. Okajima, M. Hiramatsu, Y. Shimamura, T. Awaya, T. Sako, Chemical recycling of carbon fiber reinforced plastic using supercritical methanol. J. Supercrit. Fluids **91**, 68–76 (2014)

I. Okajima, K. Watanabe, S. Haramiishi, M. Nakamura, Y. Shimamura, T. Sako, Recycling of carbon fiber reinforced plastic containing amine-cured epoxy resin using supercritical and subcritical fluids. J. Supercrit. Fluids **119**, 44–51 (2017)

J.A. Onwudili, E. Yildirir, P.T. Williams, Catalytic hydrothermal degradation of carbon reinforced plastic wastes for carbon fibre and chemical feedstock recovery. Waste Biomass Valorization **4**(1), 87–93 (2013)

E. Pakdel, S. Kashi, R. Varley, X. Wang, Recent progress in recycling carbon fibre reinforced composites and dry carbon fibre wastes. Resour. Conserv. Recycl. **166**, 105340 (2020)

J. Palmer, O.R. Ghita, L. Savage, K.E. Evans, Successful closed-loop recycling of thermoset composites. Compos. Part A Appl. Sci. Manuf. **40**(4), 490–498 (2009)

J. Palmer, L. Savage, O. Ghita, K. Evans, Sheet moulding compound (SMC) from carbon fibre recyclate. Compos. Part A Appl. Sci. Manuf. **41**(9), 1232–1237 (2010)

M. Perrut, Supercritical fluid applications: industrial developments and economic issues. Ind. Eng. Chem. Res. **39**(12), 4531–4535 (2000)

S.J. Pickering, Recycling technologies for thermoset composite materials – current status. Compos. Part A Appl. Sci. Manuf. **37**(8), 1206–1215 (2006)

S. Pimenta, S.T. Pinho, Recycling carbon fibre reinforced polymers for structural applications: Technology review and market outlook. Waste Manag. **31**(2), 378–392 (2011)

D. Rosato, *Designing with Plastics and Composites: A Handbook* (Springer Science & Business Media, 2013)

L.E. Sánchez-Cadena, G. Tersac, X. Coqueret, Z. Gamiño-Arroyo, Solvolysis of acrylate-urethane coatings cured by electron-beam and UV radiation. Prog. Org. Coat. **136**, 105268 (2019)

G. Schinner, J. Brandt, H. Richter, Recycling carbon-fiber-reinforced thermoplastic composites. J. Thermoplast. Compos. Mater. **9**(3), 239–245 (1996)

R.W. Shaw, Supercritical water a medium for chemistry. Chem. Eng. News **69**, 26–39 (1991)

D.A. Steenkamer, J.L. Sullivan, On the recyclability of a cyclic thermoplastic composite material. Compos. Part B Eng. **29**(6), 745–752 (1998)

J. Takahashi, N. Matsutsuka, T. Okazumi, K. Uzawa, I. Ohsawa, K. Yamaguchi, A. Kitano, *Mechanical Properties of Recycled CFRP by Injection Molding Method. ICCM-16* (Japan Society for Composite Materials, Kyoto, 2007)

L.T. Taylor, *Supercritical fluid extraction* (Wiley, New York, 1996)

The Global CFRP Market 2016, Experience Composites, 2016

A. Torres, I. De Marco, B. Caballero, M. Laresgoiti, J. Legarreta, M. Cabrero, A. Gonzalez, M. Chomon, K. Gondra, Recycling by pyrolysis of thermoset composites: characteristics of the liquid and gaseous fuels obtained. Fuel **79**(8), 897–902 (2000)

M. Vallee, G. Tersac, N. Destais-Orvoen, G. Durand, Chemical recycling of class A surface quality sheet-molding composites. Ind. Eng. Chem. Res. **43**(20), 6317–6324 (2004)

Y. Wang, X. Cui, H. Ge, Y. Yang, Y. Wang, C. Zhang, J. Li, T. Deng, Z. Qin, X. Hou, Chemical recycling of carbon fiber reinforced epoxy resin composites via selective cleavage of the carbon–nitrogen bond. ACS Sustain. Chem. Eng. **3**(12), 3332–3337 (2015)

Y. Yang, R. Boom, B. Irion, D.-J. van Heerden, P. Kuiper, H. de Wit, Recycling of composite materials. Chem. Eng. Process. Process Intensif. **51**, 53–68 (2012)

E. Yildirir, J.A. Onwudili, P.T. Williams, Recovery of carbon fibres and production of high quality fuel gas from the chemical recycling of carbon fibre reinforced plastic wastes. J. Supercrit. Fluids **92**, 107–114 (2014)

Electrospun Fiber-Reinforced Epoxy Composites

15

B. D. S. Deeraj, Jitha S. Jayan, Appukuttan Saritha, and Kuruvilla Joseph

Contents

Abstract

Electrospinning is a straightforward method to fabricate continuous nanofibers from polymer solutions. These fibers have unique characteristics like high aspect ratio, surface area, easy processability, and scaling-up ability that make these fibers attractive candidates as reinforcements. Fiber-reinforced composite is a class of composite systems with good mechanical and load-bearing abilities where carbon fibers, glass fibers, or Kevlar fibers are mainly used as reinforcements. Electrospun polymer fibers can be added to the polymer matrix to enhance the overall mechanical performance of polymer matrices. This chapter will bring together the details of preparation and characterization of electrospun fiber-reinforced polymer matrices, giving more importance to epoxy matrix. This chapter will also discuss the property enhancement of electrospun fiber-reinforced composites with respect to type, concentration, and variety of fibers. Further, a brief description of epoxy, electrospinning, and governing parameters is also provided.

B. D. S. Deeraj · K. Joseph (✉)
Department of Chemistry, Indian Institute of Space Science and Technology, Thiruvananthapuram, Kerala, India

J. S. Jayan · A. Saritha
Department of Chemistry, Amrita Vishwa Vidyapeetham, Amritapuri, Kerala, India

S. Mavinkere Rangappa et al. (eds.), *Handbook of Epoxy/Fiber Composites*,
https://doi.org/10.1007/978-981-19-3603-6_3

Keywords

Electrospinning · Epoxy · Reinforcements · Nanofibers · Fiber-reinforced composites

Introduction

Fiber-reinforced composites (FRCs) are currently the most versatile and popular class of engineered composite materials with attractive properties. These materials find potential applications in mechanical, civil, transport, military, aerospace, sports, and defense areas (Jiang et al. 2018; Puglia et al. 2005; Chand 2000; Brøndsted et al. 2005; Li et al. 2007; Al-Saleh and Sundararaj 2011). These fiber-reinforced polymer (FRP) materials mainly consist of a polymer matrix and reinforcing fibers. These fibers are embedded inside the polymer matrix, and the arrangement of these fibers and matrix can be controlled to tailor the composite properties to make it suitable for a particular application.

Mostly, polymer-based FRCs, are developed to obtain superior mechanical performance for structural applications (Zucchelli et al. 2011). These FRCs are generally used for structural, functional, electronic applications, and other functional fields. Fibers can be modified to impart better functional properties to the polymer matrix, such that thermal and mechanical properties, conductance, etc., can be tailored. Usually, conventional FRCs contain micrometer-range fibers as reinforcements (Deshpande et al. 2000; Summerscales et al. 2011; Correa et al. 1998; Lee 1992). For the preparation of advanced high-performing composites, the idea of incorporating nanofibers into polymer matrices is highly recommended. The use of nano-sized fibers instead of micro and hybrids of nano/microfibers provides a way to impart better mechanical properties (Zucchelli et al. 2011).

This chapter focuses on the use of nanofibers prepared from the electrospinning technique as reinforcement in the polymer matrix, mainly epoxy matrix. This chapter will give an idea about the methods of preparation of electrospun fiber epoxy composites, their properties, and their applications. In Figs. 1 and 2, the number of publications and classification of topics are presented, respectively.

Epoxy

Epoxy is one of the most used thermosetting polymers with a wide range of applications due to its properties (Konnola et al. 2019; Jayan et al. 2018). Its good mechanical and thermal properties make it an excellent choice for aerospace, defense, adhesive, and other advanced applications. These epoxy polymers have two or more oxirane rings in their structure. These are linear in nature and form a highly crosslinked structure when added with hardeners. The inherent brittleness of these epoxy composites after curing is a significant drawback, as this brittleness leads to poor fracture toughness. Adding secondary agents to epoxy is a common

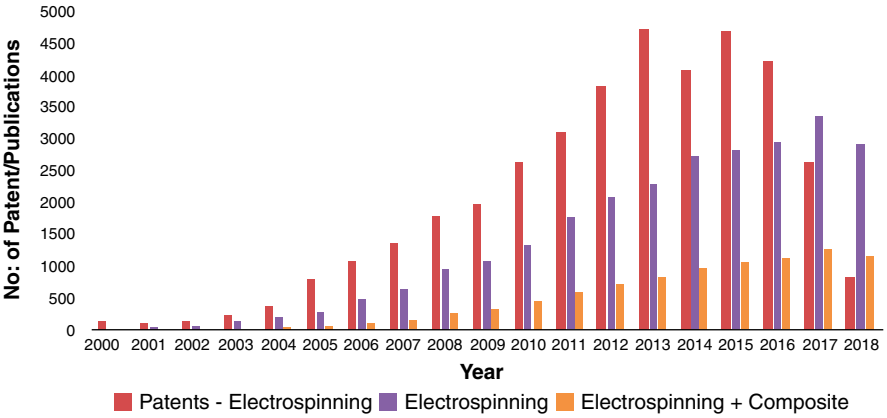

Fig. 1 No. of publications based on electrospinning-related topics (Vijay Kumar et al. 2019). (Reproduced with permission from Wiley)

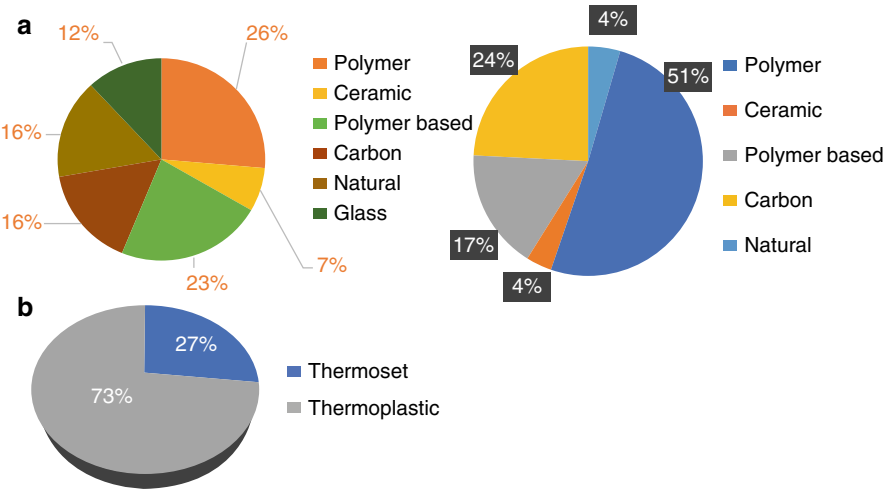

Fig. 2 Distribution of publications based on electrospinning-related topics. (**a**) Since 2018, (**b**) In 2018 (Vijay Kumar et al. 2019). (Reproduced with permission from Wiley)

approach to enhance its toughness. However, some tougheners are observed to reduce their mechanical performance. So, the challenge is to prepare toughened epoxy composites without compensating their mechanical performance. Many such studies are reported, and more work is being done in this area. Fillers like thermoplastics, particulate fillers, core-shell particles, block copolymers, etc., are being used to enhance the toughness of epoxy. However, the major disadvantage of few types of filler is the enhancement of toughness with the compensation of other properties like glass transition temperature and tensile strength. However, nanomaterials are considered a better choice for enhancing the toughness without altering

the other inherent properties. Researchers have successfully employed nanoparticles and nanoparticle-grafted polymer systems for effectively enhancing the overall properties of epoxy composites (Jayan et al. 2020a, b).

Konnola et al. (2019) prepared titanium oxide–based epoxy systems by using both titania nanoparticles and nanowires and compared the effect of shape on the performance of epoxy composites. They prepared titania nanowires from a simple hydrothermal process and prepared composites at 0.2 w% to 0.8 w% of epoxy. They found excellent toughening property at 0.6w% titania loading. They also found a maximum improvement of 26% in tensile strength, 16% in tensile modulus, and 136% in toughness. The dynamic mechanical storage modulus improved 11% at 30 °C, at 0.6% loading of titania. This work concludes that nanofillers can be excellent epoxy reinforcements at low loadings because of their high aspect ratio. In another work, nano titania–aggregated graphene oxide hybrids are prepared for toughening the epoxy (Jayan et al. 2020b). This hybrid material is observed to have a core-shell structure, titania forming the inner core and the graphene oxide the outer shell. This hybrid system is observed to improve the toughness by 200%. This work shows the significance of nanomaterial combinations as efficient reinforcements in epoxy. Jayan et al. (2020c) prepared graphene oxide–grafted polyethylene glycol (PEG) combinations to investigate their role in reinforcing epoxy composites. They observed an excellent improvement of 334% improvement in toughness at a low loading of 0.1w%. In other work, polyvinylpyrrolidone (PVP)-grafted graphene oxide is prepared from the "grafting from" technique to reinforce epoxy (Jayan et al. 2021). They observed an improvement of over 190% in fracture toughness. In Table 1, a few of the epoxy tougheners and percentage improvement are presented.

Microfibers are used as reinforcing agents in epoxy, but the incorporation of nanofibers offers better enhancement in toughness without the loss of tensile strength due to the high surface area. The preparation of fibers in the nano regime is considered a tedious process. Electrospinning is an effective method for the fabrication of nanofibers. This chapter focuses on various electrospun fibers used as toughening agents in epoxy matrix.

Electrospinning

Electrospinning is a versatile nanofabrication method to prepare polymeric fibers in the nanometric and micrometric scales (Zucchelli et al. 2011; Greiner and Wendorff 2007; Agarwal and Greiner 2011; Jian et al. 2018; Wu et al. 2013; Deeraj et al. 2019, 2020; Huang et al. 2003). These fibers are observed to have a high surface area and unique characteristics. Compared to other nanofabrication techniques, an easy scale-up facility and low cost make this technique more convenient for bulk sample preparation. These electrospun fibers can be prepared in different architectures by adjusting the setup and process parameters. This method gives an easy way to blend plastics, prepare nanocomposite fibers, carbon fibers, hollow fibers, and core-shell fibers with the desired property. Nanofibers find applications in a protective coating,

Table 1 List of epoxy tougheners and toughness improvement

S. no	Toughener	Toughness improvement (%)	Reference
1.	Alumina	100	McGrath et al. (2008)
2.	Carbon black	20	Kim and Park (2008)
3.	Nano-alumina	19	Ji et al. (2004)
4.	Epoxidized soybean oil (ESO) grafted with carboxyl-terminated poly(acrylonitrile-co-butadiene)	68	Bach et al. (2020)
5.	Amine-functionalized poly (styrene) microspheres	33	Chaudhary et al. (2015)
6.	9,10-Dihydro-9-oxa-10-phosphaphenanthrene-10-oxide (DOPO)-grafted epoxidized soybean oil	73	Vu and Bach (2020)
7.	Liquid carboxyl-terminated poly (butadiene-co-acrylonitrile) rubber	68	Chonkaew and Sombatsompop (2012)
8.	Epoxidized natural rubber	48	Chuayjuljit et al. (2006)
9.	Silane-coupling-agent-treated GNPs (KH-GNPs) and hydroxyl multi-walled carbon nanotubes	34	Yao et al. (2020)
10.	PES	60	Mimura et al. (2000)
11.	Graphene oxide and polyethylene glycol-b-polypropylene glycol-b-polyethylene glycol	400	Jayan et al. (2020a)
12.	HTPB	156	Thomas et al. (2008)
13.	Poly-(allyl amine)-grafted graphene oxide	87	Sahu and Raichur (2019)
14.	PSF	20	Huang et al. (1997)
15.	Polysiloxane	29	Ma et al. (2011)
16.	POSS-rubber core–shell nanoparticles	30	Thitsartarn et al. (2015)
17.	GO-g-CTBN	128	Konnola et al. (2015)
18.	Reactive hyper-branched polyurethane	128	Tang et al. (2014)
19.	Polysiloxane-based core-shell particles	109	Chen et al. (2013a)
20.	Poly (ether ether ketone)-grafted graphene oxide	31	Katti et al. (2017)
21.	PEP-PEO block copolymer	144	Liu et al. (2010)
22.	Core-shell rubber nanoparticles	125	Quan and Ivankovic (2015)

(continued)

Table 1 (continued)

S. no	Toughener	Toughness improvement (%)	Reference
23.	Silica	73	Blackman et al. (2007)
24.	Nanoclay	98	Wang et al. (2015)
25.	Aligned carbon nanotubes	51	Ma et al. (2015)
26.	Graphene	57	Chandrasekaran et al. (2014)
27.	Reduced graphene oxide/PCL-PPC-PCL	60	Liu et al. (2016)
28.	poly(ether sulfone)-grafted multi-walled carbon nanotube	125	Konnola et al. (2016)

energy storage and conversion, composite reinforcement, EMI shielding, biomedical fields, and so on (Huang et al. 2003; Li et al. 2002; Christopherson et al. 2009; Sun et al. 2007; Zeng et al. 2003; Shen et al. 2015; Xu et al. 2014a; Zhou et al. 2017; Reich et al. 2018; Xu et al. 2014b; Jose et al. 2009; Zeng et al. 2015; Im et al. 2008, 2011; Aussawasathien et al. 2005; Akangah et al. 2010; Bergshoef and Vancso 1999; Chen et al. 2016, 2018; Si et al. 2015; Wei et al. 2019; Inagaki et al. 2012).

Parameters that influence the electrospun fibers can be broadly grouped as solution parameters, controlled variables, and ambient parameters. Solution parameters include polymer concentration, polymer solution viscosity, surface tension, dielectric properties, and electrical conductivity. Controlled variables include flow rate employed, voltage, and distance between collector and needle tip. Ambient parameters like humidity and temperature are also observed to have an effect on the fibers. There are no universal electrospinning parameters as such suitable for all types of polymers. These parameters are to be altered based on the type of polymer (Jiang et al. 2018). The schematic representation of the electrospun technique is presented in Fig. 3. In Table 2, the influence of process parameters is shown.

Electrospun fibers are not limited to single-component polymers. It can also be made of polymer blends and polymers with additives (additives include metals, ceramics, carbons, bacteria and viruses, metal oxides, etc.) (Jiang et al. 2018). These fibers can be a single component, two component, and multi-component depending on the desired application. It is observed that two-component or multi-component electrospun fibers provide diverse compositions and functionalities (Jiang et al. 2018). When compared with bulk reinforcement, electrospun fibers have particular properties, which make them a promising candidate for reinforcing applications. These characteristics include a high aspect ratio, high axial molecular orientation, pore size, mechanical properties, and specific surface area. In Table 3, a list of few electrospun polymer fibers is presented. Electrospun polymers also offer better enhancement to the electrochemical properties of Li-ion batteries. Addition of fillers into the polymer matrix enhances the cycle life as well as rate of Li-ion batteries (Lan et al. 2021). Electrospun polymers are now considered as a candidate in biomedical application, due to the dissolution of water-soluble drugs from the electrospun polymers. Generally, combined use of electrospinning and e-jet printing process is

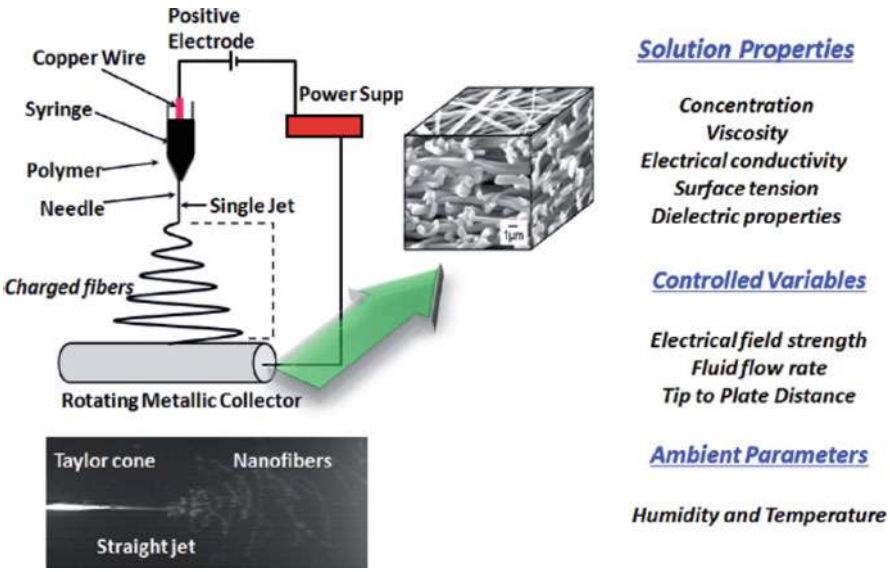

Fig. 3 Schematic representation of electrospinning setup and parameters (Gopiraman and Kim 2019). (Open access)

Table 2 Overview of the influence of parameters on electrospinning (Shirazi et al. 2020). (Open access)

Process parameter	Effect(s) on morphology	Highlights	Importance
Applied high voltage	Fiber diameter	Using high applied voltage can increase the fiber diameter.	***
		First, the solution jet carries more charges for fast elongation.	
		More jet can be ejected using high applied voltage	
Tip-to-collector distance	Bead formation	Longer tip-to-collector distance can increase the number of beads on the surface.	*
		Longer distance increases the jet elongation time.	
		It can form unstable nanofibers	
Needle gauge	Fiber diameter	Using needle with higher gauge (smaller inner diameter) can decrease the pore size.	***
		Smaller needle can also decrease the fiber diameter	
Dope injection rate	Fiber diameter and bead formation	Higher dope injection rate ejects more solution in a jet.	*
		So, it can increase the pore size.	
		It can also lead to bead formation due to electrospraying	

*less important
***more important

Table 3 List of electrospun fibers from different polymer sources

S. no	Polymer	Solvent	Reference
1.	Polyacrylonitrile (PAN)	DMF	Shakil et al. (2020)
2.	PA66	Formic acid	Ahmadloo et al. (2017)
3.	Cellulose acetate (CA)	Acetone/DMA	Liao et al. (2011)
4.	Lignin/PVA	Water	Lee et al. (2014)
5.	PLA	Chloroform	Sobczyk and Leluk (2018)
6.	PVA	Distilled water	Zhang et al. (2005)
7.	PVDF	*N*,*N*-Dimethylacetamide	Choi et al. (2004)
8.	PMMA	THF/DMF	Liu et al. (2009)
9.	SBS	Butyl acetate, LiBr, and crosslinker	van der Heijden et al. (2017)
10.	SIS	THF/DMF	Feng et al. (2009)
11.	Nylon 6	Formic acid	Ryu et al. (2003)
12.	PET	Trifluoroacetic acid	Ma et al. (2005)
13.	Polystyrene	THF/DMF	Lee et al. (2003)
14.	Polycarbonate	Chloroform, THF/DMF	Krishnappa et al. (2003)
15.	PVP	Ethanol	Zhou et al. (2009)

followed for the fabrication of electrospun hydrophilic polymer nanofibers for drug delivery applications (Bai et al. 2021). Electrospun nanofibrous polymers exhibit better ion-exchange properties over simple polymer membranes and hence are considered as promising candidates for fabrication of membranes for water purification application (Cseri et al. 2021). Mechanical as well as other significant properties of composites can be altered to a great extent by the addition of electrospun fibers. The coming section discusses about the reinforcing efficiency of electrospun nanofibers in polymer matrix (Uslu et al. 2021).

Electrospun Fibers as Reinforcements in Polymer Matrices

There are many examples available from literature for preparing electrospun fibers from polymer sources, but all of them cannot be used as reinforcements. Only a few polymers with electrospun fibers of good mechanical strength can be used as worthy reinforcements. A list of few electrospun fibers and their mechanical properties are presented in Fig. 4.

For developing polymer nanocomposites, weak polymer matrices are reinforced with advanced nanofillers to achieve resultant solid composites. Many types of nanofillers like carbon nanotubes, carbon fibers, nano inorganic materials, and nanoclay are used as reinforcements in polymer matrices. In addition, the use of electrospun fibers as potential reinforcements is an emerging and promising area of developing fiber-reinforced polymer composites. In Table 4, a list of polymer fibers and their matrices are presented.

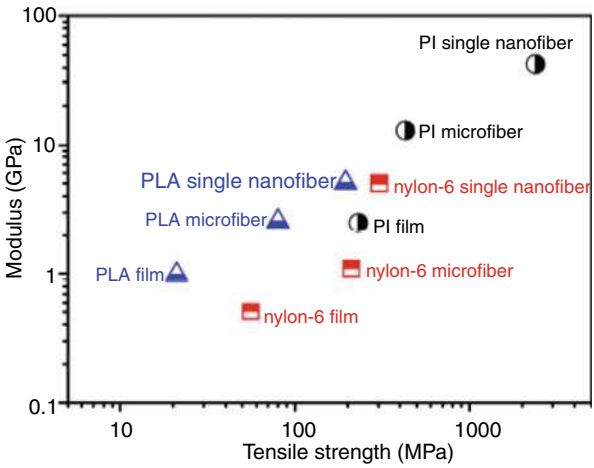

Fig. 4 Mechanical properties of electrospun single PLA, nylon-6, and polyimide (PI) nanofibers compared with other formations (Jiang et al. 2018). (Reproduced with permission from Royal society of chemistry)

Electrospinning of cellulose fibers was successfully done, and poly(butylene succinate) biocomposites were prepared (Han et al. 2008). They used *N*-methylmorpholine-*N*-oxide hydrate as a solvent for making cellulose fibers at 100 °C, and the average diameter of fibers is found to be 560 nm. The storage modulus of cellulose fiber-reinforced poly(butylene succinate) is 67% more than neat poly(butylene succinate) samples confirming the reinforcing ability of cellulose fibers. Electrospun graphene/PLA composite nanofibers with 1.3 wt.% graphene are employed as reinforcement in poly(butylene succinate) (PBS) matrix (Sisti et al. 2016). They found that the incorporation of 0.8 wt. % nanofibers increased the tensile strength and elongation at the break by 27% and 47%, respectively. These improvements were only 16% and 26%, respectively, for poly lactic acid (PLA) nanofiber-reinforced composites without graphene. Based on fracture surface observations, they discovered that these nanofiber mats made the cracks stop and deviate, contributing to the toughening effect. The reinforcing ability of electrospun polyhydroxybutyrate (PHB) nanofibers with two nano clays, that is, cationic Cloisite (CL) and anionic Perkalite (PK), was studied (Marega and Marigo 2015). It was found that PHB nanofibers with CL-reinforced PCL composites exhibited enhanced modulus and tensile strength than those of PHB nanofibers with PK-filled systems as well as those of the PCL matrix.

Graphene-loaded electrospun nylon 6 nanofibers (Gr/nylon-6)-reinforced polymethyl methacrylate (PMMA) nanocomposites were studied (Li et al. 2013). The nanofibrous mats were chopped and stacked layer by layer, followed by hot press molding to melt electrospun PMMA fibers and make nanocomposite films. The resulting Gr/nylon-6 nanofiber-reinforced nanocomposites displayed a noteworthy enhancement in overall mechanical properties at Gr loading of only 0.01 wt.%, that is, nearly 56%, 113%, and 250% improvement in tensile strength, Young's modulus, and fracture toughness, respectively, were achieved. Electrospun fibers are utilized as better reinforcing agent owing to its capability to fragment regular fibers after the

Table 4 List of electrospun fiber-reinforced polymer composites for different applications

S. no	Polymer fiber	Matrix	Reference
1.	Nylon-6	PMMA	Chen et al. (2009)
2.	PBI	SBR rubber	Js and Reneker (1999)
3.	Nylon-6	PVA	Stachewicz et al. (2012)
4.	Nylon-6	PANI	Romo-Uribe et al. (2009)
5.	Nylon-6	PCL	Neppalli et al. (2010)
6.	Cellulose	PVA	Tang and Liu (2008)
7.	Nylon-6	PLA	Neppalli et al. (2012)
8.	Cellulose	Protein	Chen and Liu (2008)
9.	Nylon-6	TPU	Jiang et al. (2012a)
10.	Nylon 6,6	Polyethylene	Neppalli et al. (2012)
11.	Polyimide	Polyimide	Jiang et al. (2013)
12.	Nylon 6	Melamine formaldehyde	Jiang et al. (2012b)
13.	Polybenzimidazole	Rubber	Js and Reneker (1999)
14.	Polyurethane	Silicon film	Tijing et al. (2013)
15.	Aligned PI	PI	Chen et al. (2011a)
16.	Cellulose	Cellulose diacetate	Chen et al. (2013b)
17.	PI	PA6	Chen et al. (2012)
18.	Poly (azo-naphthyl-imide)/carbon nanotube nanofiber	PI	Kausar (2016)
19.	PU	PU	Chang (2011)
20.	PMMA	PMMA	Matabola et al. (2011)
21.	PMMA	PCL	Lamastra et al. (2012)
22.	PAN-PMMA core shell	BIS-GMA/TEGDMA dental resin	Lin et al. (2008)
23.	Nylon 6/silicate crystals	BIS-GMA/TEGDMA dental resin	Tian et al. (2007)
24.	Nylon 6	BIS-GMA/TEGDMA dental resin	Fong (2004)
25.	PAN	PMMA	Wu et al. (2012)

(continued)

Table 4 (continued)

S. no	Polymer fiber	Matrix	Reference
26.	Cellulose	Soybean protein isolate	Chen and Liu (2008)
27.	PCL	Gelatin	Beachley and Wen (2009)
28.	PCL	PU	Guo et al. (2015)
29.	Nylon 6,6	HDPE	Lu et al. (2015)
30.	PS/TiO_2	Poly(butylene succinate-co-adipate)	Neppalli et al. (2014)
31.	Electrospun carbon nanofibers	PI	Xu et al. (2015)

application of stress. Hence, recently, PMMA fibers are utilized for the core-shell-structured polymer matrix. It was observed that stress and Young's modulus showed an improvement of about 260 and 630% respectively (Ura et al. 2021). It is also observed that electrospun polymer nanocomposites are capable of showing better photocatalytic efficiency and antifouling properties (Bode-Aluko et al. 2021). Complex, three-component core-sheath-structured electrospun monolithic composites were capable of showing combined properties of process-structure-performance relationship. Thus it is also possible to make multi-component-based nanofibers by electrospinning for advanced functional application (Chang et al. 2020).

Electrospun Fiber-Loaded Epoxy Composites

Epoxy is the mainly used thermosetting polymer for structural applications. Fiber-reinforced epoxy composites are advanced composite materials with excellent mechanical properties (Deeraj et al. 2019). The incorporation of electrospun fibers in epoxy composites is an exciting area of research as these fibers can be incorporated as chopped pieces or laminate mats or as interface mats. Thus it is possible to alter the properties. In Fig. 5, a schematic representation of the possible use of electrospun fibers as reinforcement is presented.

The initial work on the use of ultrafine nanofibers in the polymer matrix was carried out by Kim et al. in 1999 (Js and Reneker 1999). In that work, they employed electrospun nanofibers of Polybenzimidazole (PBI) in epoxy and SBR matrix. They found out that the non-woven fibers effectively reinforce the epoxy matrix. Furthermore, with the increase in fiber loading, Young's modulus, the fracture toughness, and the fracture energy of the resultant nanofiber-reinforced composites were observed to increase. The increase in toughness is due to the resistance offered by fibers to the crack front; as the fibers obstruct the crack propagation, the energy needed for crack propagation increases, thereby enhancing fracture toughness.

The performance of short polymethyl methacrylate (PMMA) nanofibers in the epoxy matrix is investigated by Al-Assafi and coworkers (Al-Assafi et al. 2016). In this work, PMMA nanofibers were (avg. dia.: 150–200 nm) chopped and mixed with

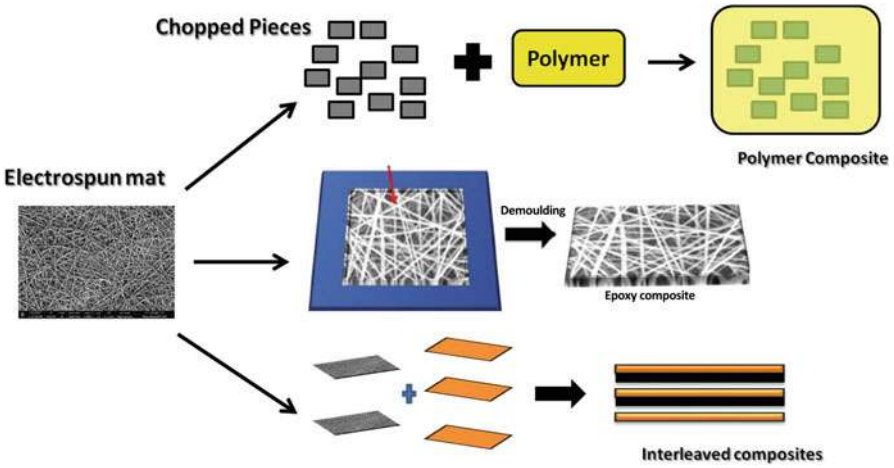

Fig. 5 Ways to prepare electrospun epoxy composites

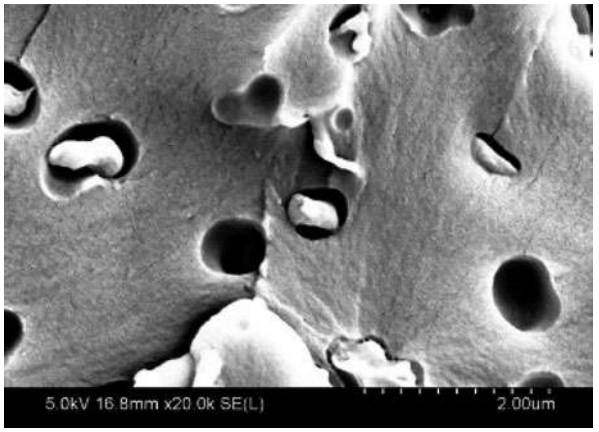

Fig. 6 SEM image of fractured samples at 5 w% loading (Al-Assafi et al. 2016)

bisphenol A-based epoxy resin and hardener. The cut size of the nanofiber mat is kept at 10 mm square pieces and loading percentage 0 to 5 w%. After curing, flexural and tensile testing was done to study the effect of fiber volume fraction on mechanical performance. They observed that there is no significant change in flexural properties, but the tensile strength of samples decreased with fiber loading. They concluded that no proper fiber/matrix adhesion and porosity as reasons for low mechanical properties. They also highlight that these results are not in synchronization with other results where nanofibers improved the mechanical properties. They indicated that detailed studies are needed to develop fiber coating to enhance the fiber/matrix adhesion. In Fig. 6, the scanning electron micrograph (SEM) image of the fractured surface is presented, where we can observe fiber pullout.

Our group investigated the reinforcing capability of chopped polyimide mats in the epoxy matrix (Deeraj et al. 2020). The schematic representation of composite preparation is presented in Fig. 7. Polyimide nanofibers were prepared from electrospinning and imidization of poly (amic acid) by optimizing all the spinning parameters. The transmission electron microscope (TEM) and atomic force microscope (AFM) images are presented in Fig. 8. By varying the fiber loading, the composites were prepared and characterized. The dynamic mechanical performance of PI/epoxy composites is found to be superior to neat epoxy composites, and the fracture toughness of composites displayed a noteworthy improvement of 20% at 1 w% PI loading. In addition, the thermal stability of PI-loaded epoxy is better than neat epoxy composites.

In another work, we have reinforced epoxy matrix with chopped poly (styrene-co-butadiene) copolymer (SBC) fibers and analyzed its mechanical performance (Deeraj et al. 2019). Electrospun fibers of SBC copolymer were successfully prepared by the electrospinning process. In that work, fibers are prepared at polymer concentration of 18 wt% at an electrical potential of 10 KV. These mats are chopped, and chopped fiber-incorporated epoxy composites were prepared by loading these manually cut mats at various weight ratios into the neat epoxy. The mechanical strength of the resultant samples obtained from universal testing machine (UTM) showed an enhanced tendency with an 18% increase at 2.5 wt % fiber loading. The

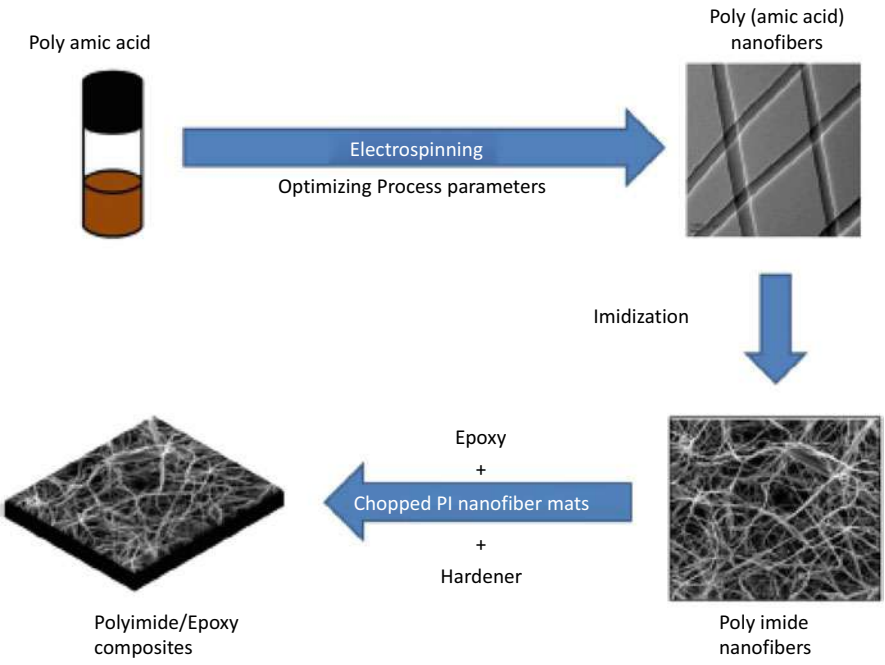

Fig. 7 Schematic representation of the preparation of polyimide/epoxy composites (Deeraj et al. 2020). (Reproduced with permission from Elsevier)

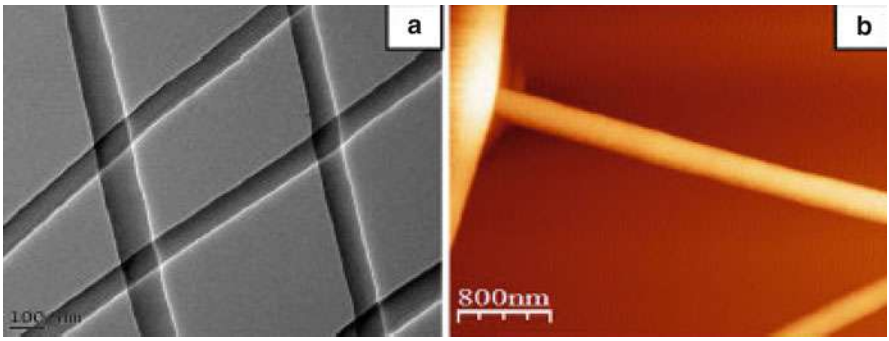

Fig. 8 (**a**) TEM and (**b**) AFM images of as spun fibers

toughness of the resultant samples was investigated, and a significant improvement of 104% at 2.5 wt % fiber loading was observed. The possible toughness-enhancing procedure was explained from the fractured morphology obtained using scanning electron micrographs as crack deviation, fiber pullout, and fiber breakage. The storage modulus of the electrospun SBC-reinforced epoxy samples revealed a significant enhancement than that of unloaded epoxy. The thermal stability of resultant epoxy samples was tested, and all the fiber-loaded samples are found to be thermally stable compared to neat epoxy.

The reinforcing capability of electrospun nylon yarns in epoxy is done by Ahmadloo and coworkers (Ahmadloo et al. 2017). They prepared PA66 fibers by dissolving the polymer in the formic acid solution for 5 h and subsequent electrospinning. To get the yarn morphology, they used an adversely charged setup. In Fig. 9, the SEM images of nanofiber yarns are presented at different magnifications. After getting the yarn fibers, they incorporated them in epoxy resin and hardener (ratio 100:30) and prepared epoxy composites. They prepared composites by varying the fiber percentage from 0 to 3 w% and tested the fracture properties. In the case of pure epoxy, a complete failure occurred, but in the case of yarn-loaded samples, plastic behavior is noticed because of fiber yarns. They observed that adding these nano yarns causes plastic work, which is absent in pure epoxy, and further, the plastic work increased with yarn loading (253% improvement from 0.5% to 3%).

The fracture toughness of these samples is tested and depicted in Fig. 10. From the graph, it is very clear that the toughness of these samples increased with an increase in the yarn content until 3w%. As the yarn percentage increases, the plastic deformations increase, so it displayed good toughness compared to neat epoxy. They stated that by increasing the nanofiber yarn loading in the epoxy, the elastic, plastic, and total works and the maximum load related to the initiation of crack propagation could be improved.

Investigations on the preparation of the cellulose nanofiber mat and its epoxy composites were done (Jahanbaani et al. 2016). In this work, a unique way of chemical treatments followed by electrospinning is employed to prepare cellulose

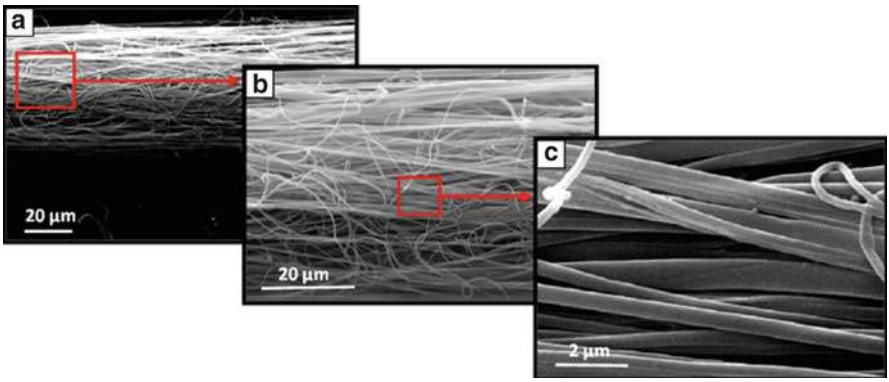

Fig. 9 SEM images of nanofiber yarns at a magnification of (**a**) 625X, (**b**) 1250X, and (**c**) 10000X (Ahmadloo et al. 2017). (Reproduced with permission from Elsevier)

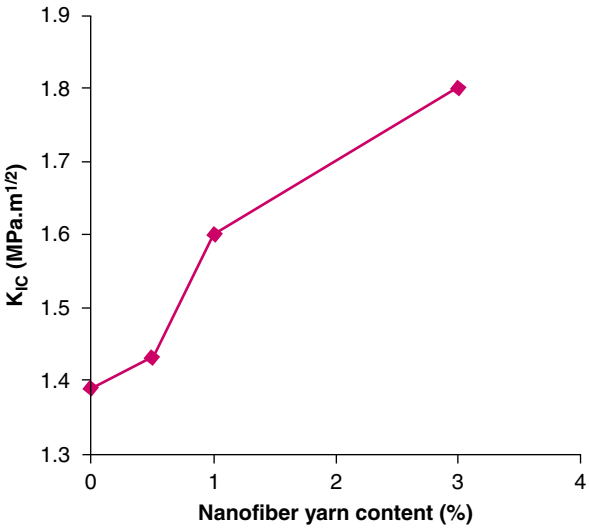

Fig. 10 Variation of fracture toughness with nanofiber yarn content (Ahmadloo et al. 2017). (Reproduced with permission from Elsevier)

from wheat straw. The chemical treatments include NaOH pretreatment, acid and alkali hydrolysis, and bleaching. After confirming the cellulose content by eliminating lignin and hemicelluloses, the electrospinning technique was followed to prepare cellulose nanofibers. By using different solvent systems, sodium hydroxide/urea/thiourea, pure trifluoroacetic acid (TFA), and TFA/methylene chloride, they prepared electrospun fibers. The earlier case failed to give fibers, while in the latter case cellulose fibers with a mean diameter of 120 nm are produced along with beads. So, 5 w% methylene chloride is added to the solution, and the conductivity increased and resulted in nanofiber production with a mean diameter of 150 nm. SEM image of prepared electrospun fibers is presented in Fig. 11.

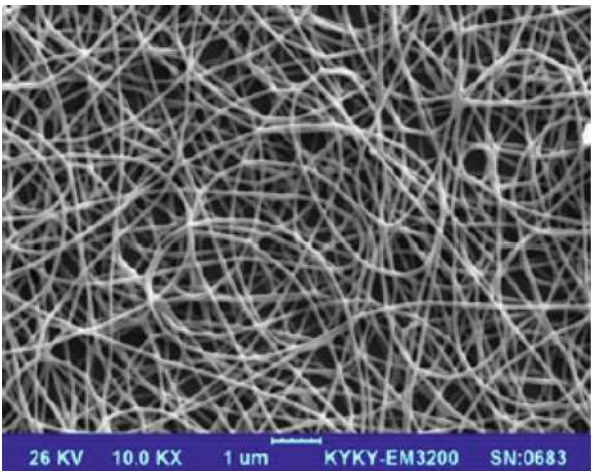

Fig. 11 SEM image of electrospun cellulose nanofibers in cellulose/TFA solution (7.5 wt.%) with 5 wt. % methylene chloride (Jahanbaani et al. 2016). (Reproduced with permission from Springer)

Table 5 The tensile strength, elongation, and modulus of samples(Jahanbaani et al. 2016)

	Tensile (MPa)		Elongation (%)		Modulus (MPa)	
	Average	Standard deviation	Average	Standard deviation	Average	Standard deviation
Epoxy resin	88.6	1.29	0.82	0.02	10,800.1	19.12
Microfiber-laminated composite	94.2	1.48	0.86	0.04	11,010.5	20.23
Nanofiber-laminated composite	117.3	2.90	0.96	0.01	12,537.6	23.87

Reproduced with permission from Springer

In the later stage, laminated composites were prepared by cellulose microfiber and electrospun nanofibers, using epoxy as the matrix polymer by hand lay-up technique. The mechanical characterization reveals that the ultimate tensile strength, modulus, elongation, and impact resistance of laminated composites are better than neat epoxy composites. In Table 5, the mechanical performance of these composites is presented. The SEM images of the fractured laminates reveal that the problem of epoxy brittleness can be handled by the nanofiber layer as there is good fiber/matrix interaction. Due to the high surface area, the electrospun nanofiber laminates are better than cellulose microfiber mat laminates. So, they concluded that electrospun cellulose nanofiber mats act as better reinforcing material than cellulose microfibers.

In another work, the mechanical interlocking between electrospun porous polystyrene fibers and an epoxy matrix was studied (Demir et al. 2014). They prepared electrospun fibers of polystyrene using THF as the solvent. These fibers are prepared at different weight fractions (10–30%), and the SEM images of those fibers are presented in Fig. 12a–c. These fibers are observed to be porous, and it is

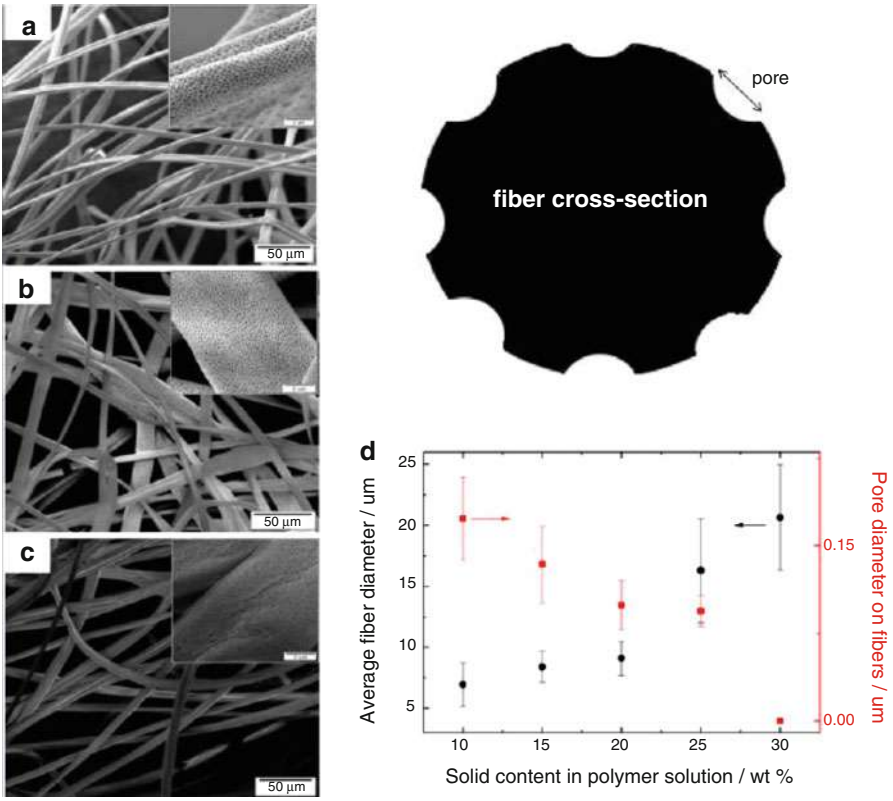

Fig. 12 SEM images of polystyrene fibers at different weight percentages (**a**) 0.10, (**b**) 0.15, (**c**) 0.20 (**d**) cartoon of c/s view of electrospun polystyrene fibers (**e**) Average fiber and pore diameter as a function of polymer concentration (Demir et al. 2014). (Reproduced with permission from American Chemical Society)

schematically presented in Fig. 12d. The average fiber diameter and pore size are shown in Fig. 12e. These fibers are used as reinforcement, and epoxy composites are prepared at a weight percentage of 0.2. These composites are compression tested at quasi-static and high strain rates, and it was observed that the compressive elastic modulus and strength of these composites are better than neat epoxy samples. SEM images of fractured surfaces of composites are presented in Fig. 13. From these microscopic studies, it is revealed that the surface pores contributed to enhancing interlocking and increased the deformation energy needed to deform the polystyrene-loaded epoxy composite.

In another report, the toughening effect of functionalized core-sheath PAN/SBS electrospun fibers was investigated (Guo et al. 2014). They prepared core-sheath co-axial fibers keeping PAN as the sheath material and SBS as the core material by co-axial electrospinning technique. These fibers after amination (by using diethylenetriamine) are employed to toughen epoxy composites. When compared

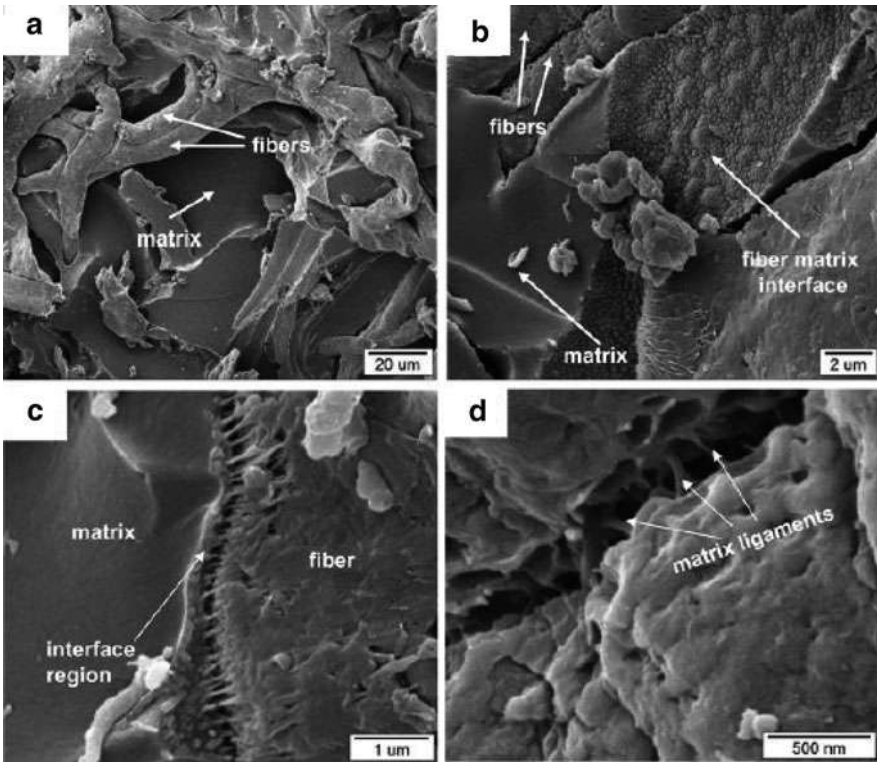

Fig. 13 SEM images of compression-tested PS fiber-reinforced epoxy showing (**a**) the fiber network on the fracture surface, (**b**) the ligaments of the fiber debonding, (**c**) the fiber-matrix interface, and (**d**) matrix ligaments at the fiber-matrix interface (Demir et al. 2014). (Reproduced with permission from American chemical Society)

to PAN-aminated fibers, SBS/PAN-aminated fibers are observed to act as more effective reinforcements. The Charpy impact energy of samples is observed to increase with electrospun fibers. The impact energy increased almost 150% when the core-sheath fibers are loaded at 4 w%. In Fig. 14, the impact energy values are presented, where we can clearly observe the improvement. The high impact resistance is because of the rubbery core of the fibers that have the ability to absorb and dissipate impact energy and the presence of bonding between the fibers and epoxy. The DMA results show that the storage modulus decreased, but the glass transition temperature of these fibers increased, indicating that heat resistance is not affected by these fibers.

Aziz and coworkers prepared epoxy composites using both electrospun carbon fibers and amine-functionalized electrospun carbon fibers (Aziz et al. 2021). For preparing carbon fibers, they used PAN polymer as the source and DMF as the solvent for making electrospun fibers. They prepared PAN solutions at 9 w% in DMF and prepared electrospun PAN fibers. These PAN fibers are stabilized at 250 °C and carbonized at 1100 °C in a nitrogen atmosphere to get carbon fibers.

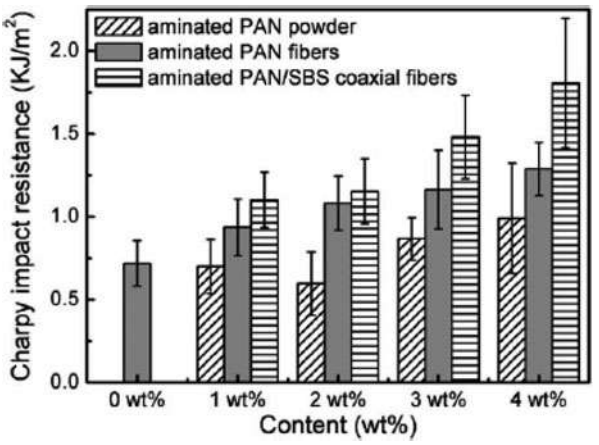

Fig. 14 Effect of aminated PAN/SBS fiber, aminated PAN fiber, and aminated PAN powder on the Charpy impact strength of epoxy resin (Guo et al. 2014). (Reproduced with permission from Wiley)

Further, these mats were acid oxidized with HNO_3 and amine functionalized. They used these amine-functionalized mats and prepared 0.5 to 10 w% epoxy composites; neat carbon fiber epoxy composites were also made for comparison. They investigated these composites for mechanical, thermal, and electrical properties. From dynamic mechanical studies, 82% improvement in storage modulus and 20% improvement in glass transition temperature were observed for 1 w% amine-functionalized samples. Furthermore, it was observed that the interaction between amine-functionalized carbon mats and epoxy provides better load transfer, enhanced tensile strength, and modulus. This chapter highlights that the electrospun carbon fibers are efficient reinforcements in epoxy composites for multi-functional applications.

Dzenis and Wen prepared PAN-based electrospun nanofibers and investigated its reinforcing potential in epoxy. They concluded that these carbon fibers have good potential to be employed as epoxy reinforcements (Dzenis and Wen 2001). In another work, a comparison of short electrospun nanofiber epoxy composites and electrospun nanofiber mat epoxy composites was made (Sancaktar and Aussawasathien 2009). They concluded that nanofiber mat-based composites are having better mechanical properties because of the homogeneity of the mats in the resin.

In another work, a composite nanofiber of MWCNTs/P(St-co-GMA) was employed to study its properties in epoxy matrix (Özden-Yenigün et al. 2012). In this work, they used MWCNTs as reinforcement in surface-functionalized P(St-co-GMA) nanofibers. The surface functionalization of these fibers with epoxy moieties helped in creating better interfacial adhesion with the epoxy matrix. Furthermore, they optimized the polymer concentration and MWCNT loading, and these composite fibers were used as reinforcement in the epoxy matrix. The mechanical performance revealed a noteworthy improvement of above 20% in flexural modulus. The increase is attributed to the dual effect of surface chemistry and inherent MWCNTs. The storage modulus of these reinforced materials is presented in Fig. 15. From Fig. 15a, we can observe that compared to neat epoxy, fiber-reinforced

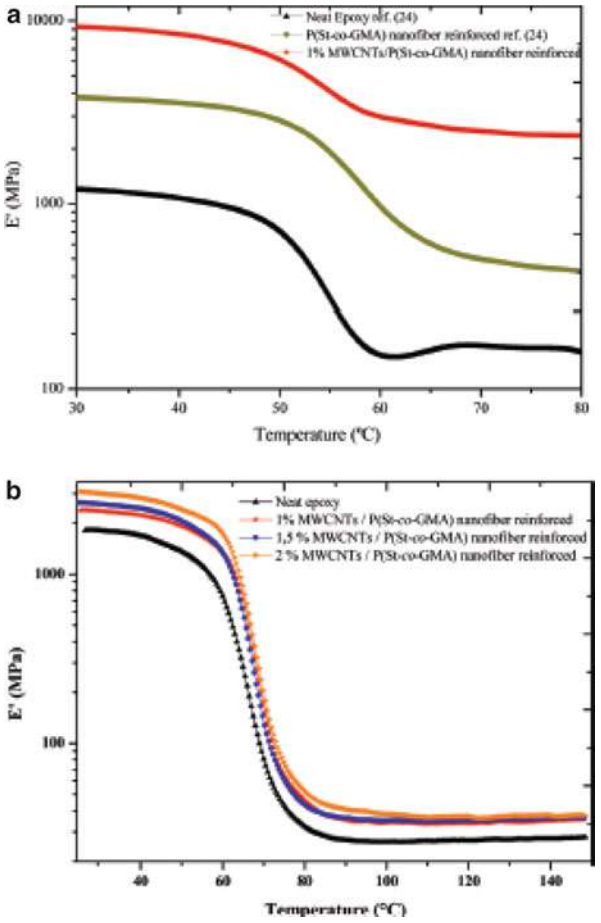

Fig. 15 (**a**) Storage modulus vs. temperature measurements on nanofiber-reinforced materials. (**b**) Storage modulus vs. temperature measurements on nanofiber-reinforced hybrid materials (Özden-Yenigün et al. 2012). (Reproduced with permission from American chemical Society)

samples are better, and from Fig. 15b, the variation of modulus with MWCNT loading can be observed. Thus, they concluded that they made a high-performance nanofiber/epoxy system by surface engineering and employing CNTs. In Table 6, a list of few electrospun fiber-reinforced epoxy composites is presented.

Fiber-reinforced composites are, to date, the best performing composite materials for structural applications because of their good stiffness and less weight. Thus, these composites are having many comparative advantages, but delamination is a significant disadvantage (Daelemans et al. 2020). Here, electrospun nanofibers can be employed as viable interlaminar toughening agents to resolve this problem. For this purpose, multi-scale analysis of the toughening mechanism by employing electrospun fibers was done by Daelemans and coworkers (2016). In this work, they have evaluated the performance at different levels, namely matrix level, interlaminar region level, and laminate level.

Table 6 List of electrospun fibers used to reinforce epoxy composites

S. no	Polymer fiber	Matrix	Reference
1.	PEO	Epoxy	Lee et al. (2004)
2.	PBI	Epoxy	Js and Reneker (1999)
3.	Nylon 4,6	Epoxy	Bergshoef and Vancso (1999)
4.	P(S-co-GMA)	Araldite epoxy	Ozden et al. (2010)
5.	Nylon 6,6	Epoxy	Borges et al. (2015)
6.	Nylon 4,6	Two-component phenolic epoxy	Bergshoef and Vancso (1999)
7.	Nylon 6,6	Gr-epoxy	Palazzetti et al. (2012)
8.	PC	Graphite/epoxy prepreg	Sihn et al. (2008)
9.	Nylon 6,6	Epoxy/carbon	Akangah et al. (2010)
10.	Nylon 6,6	Glass/epoxy	Saghafi et al. (2014)
11.	Nylon 6,6	Aramid/epoxy	Goodarz et al. (2017)
12.	PMMA	Epoxy	Iyengar et al. (2013)
13.	Nylon 6	Glass fiber/epoxy	De Schoenmaker et al. (2013)
14.	Nylon 6,6	Carbon/epoxy	Beckermann and Pickering (2015)
15.	PCL	Carbon epoxy	Zhang et al. (2012)
16.	PAPBI/CNT-PA	Epoxy	Kausar (2014)
17.	Electrospun carbon nanofibers	Epoxy	Chen et al. (2014)
18.	PAN	Carbon/epoxy laminate	Herwan et al. (2016)

They also conducted a multi-scale evaluation of toughening micromechanics by using PCL and PA6 nanofibers. The multi-scale approach is presented as a cartoon in Fig. 16. In Fig. 17, the mode I fracture toughness of PCL-loaded and PLA-loaded composites are presented. They observed that in level 1, the yielding of nanofibers and nanofiber bridging mechanism enhance the fracture toughness significantly. Thus, it is understood that the fracture toughness of the nano-toughened epoxy is determined by mechanical properties of nanofibers and their interaction with the matrix. In level 2, they observed the systemic analysis of the delamination path. It is shown that crossings in the interlaminar region are major contributors to enhancing interlaminar toughness. It is also seen that for the fully prepared interleaved composites, a fracture mechanism similar to level 2 is observed in level 3. The formation of interlaminar crossing hindered the delamination growth. In addition, the interlaminar crack through the nano-toughened interlayer contributes to toughening effect and locally increases the fracture toughness. Thus the multi-scale evaluation studies play a crucial role for both understanding the behavior of nanofiber-toughened composites and designing new damage-resistant materials.

In another work, styrene acrylonitrile (SAN) nanofibers were used for interfacial toughening of carbon/epoxy composites (Neisiany et al. 2018). First, by using the

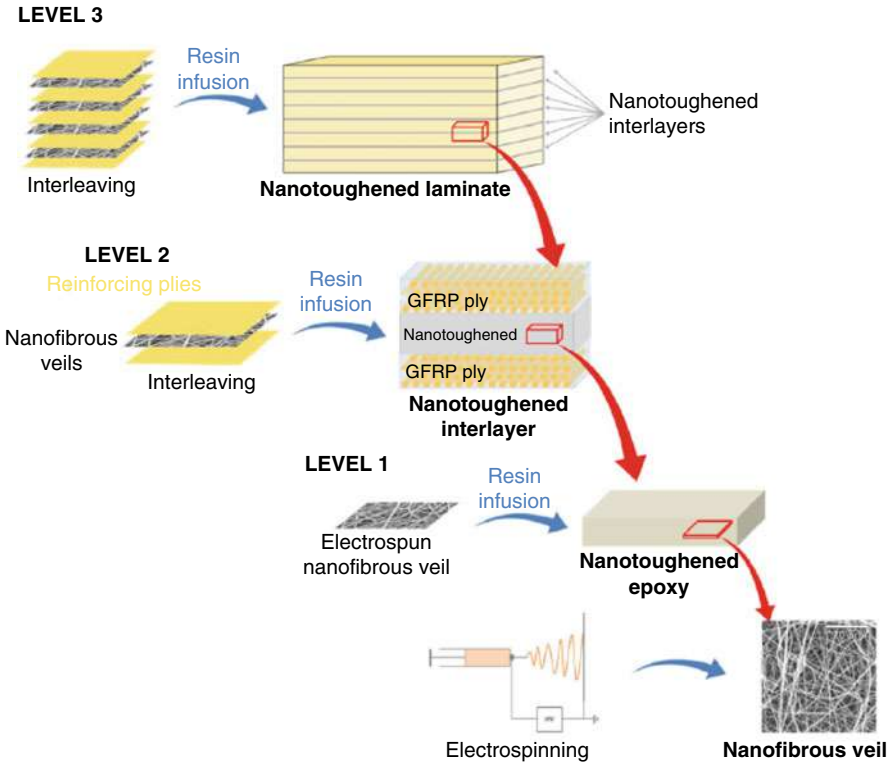

Fig. 16 Multi-scale approach to study the performance of electrospun nanofiber-interleaved composites (Daelemans et al. 2016). (Reproduced with permission from American chemical Society)

electrospinning technique, SAN nanofibers were deposited directly on the carbon fiber fabrics. Then, by employing vacuum assist resin transfer molding (VARTM), carbon/epoxy composites were prepared. The morphological investigation of prepared SAN electrospun fibers was bead free, smooth, and continuous, with mean diameters near 480 ± 102 nm. The resultant composite with SAN fibers displayed a 26% improvement in flexural strength, 27% gain in short beam shear strength, and 8% improvement in impact energy absorption. In addition, the SEM images of fractured composites confirm the positive effect of embedding fibers.

In another work, the effect of graphene-reinforced electrospun nano-interlayers on fiber-reinforced epoxy composites was studied (Goodarz et al. 2017). They prepared aramid/epoxy composites interleaved with electrospun graphene nanoplatelets/nylon 66 mats. They found that nanofibers with 1 w% GNPs have good mechanical properties. This increase is a combined effect of GNPs and the proper thickness of nanofibrous webs. They found that optimum thicknesses for pristine and reinforced interleaves are 35 and 17.5 μm, respectively. They concluded that composite nanofiber-interleaved FRPs are better performing materials than plain FRPs.

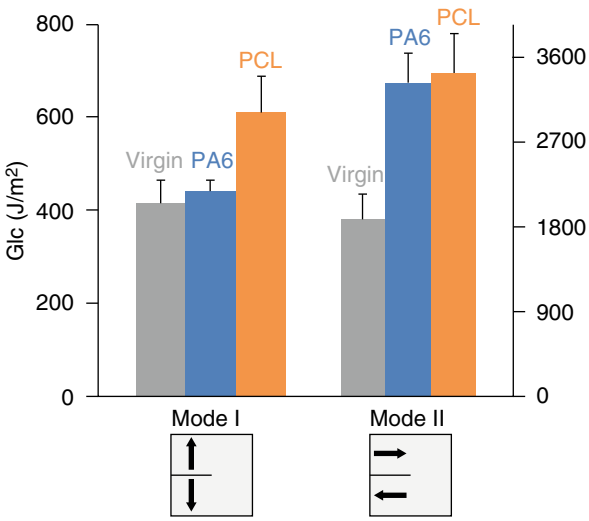

Fig. 17 Mode I interlaminar fracture toughness of interleaved composites (Daelemans et al. 2016). (Reproduced with permission from American chemical Society)

Some researchers have explored the use of electrospun carbon fibers as interlayers between carbon fabrics and developed multi-scale composites. In one such work, when these electrospun mats are used as intermediates, an improvement of 86% in interlaminar shear strength is observed (Chen et al. 2011b). In another work, electrospun carbon fibers are attached to the surface of conventional carbon fabrics, and composites were made (Chen et al. 2013c). Here an improvement in out-of-plane mechanical properties of electrospun carbon fiber surface-attached fabric composites is observed compared to traditional composites.

Conclusions and Future Outlook

Electrospinning is a versatile technique for the fabrication of nanofibers. It is possible to prepare nanofibers with different shapes, properties, and orientations by suitable electrospinning techniques. The incorporation of nanofibers in epoxy enhances the thermal, mechanical, and electrical properties of epoxy due to the enhanced aspect ratio, surface area, and better interlaminar interaction. By adjusting the alignment of nanofibers in the epoxy matrix, controlling the pore size, and incorporating functionalities, it is possible to alter the properties of epoxy to a great extent. The multi-component and core-shell nanofibers are effective over conventional nanofibers in enhancing the properties of epoxy due to the combined effect of the components present in it. Thus nanofibers are better choice for epoxy reinforcement. Nowadays, carbon nanofibers made by the carbonization of electrospun nanofibers are employed as effective reinforcement in epoxy. Thus by judicious selection of nanofiber, shape, orientation, and functionalities, one could make epoxy composites with desired properties and can be utilized for advanced applications.

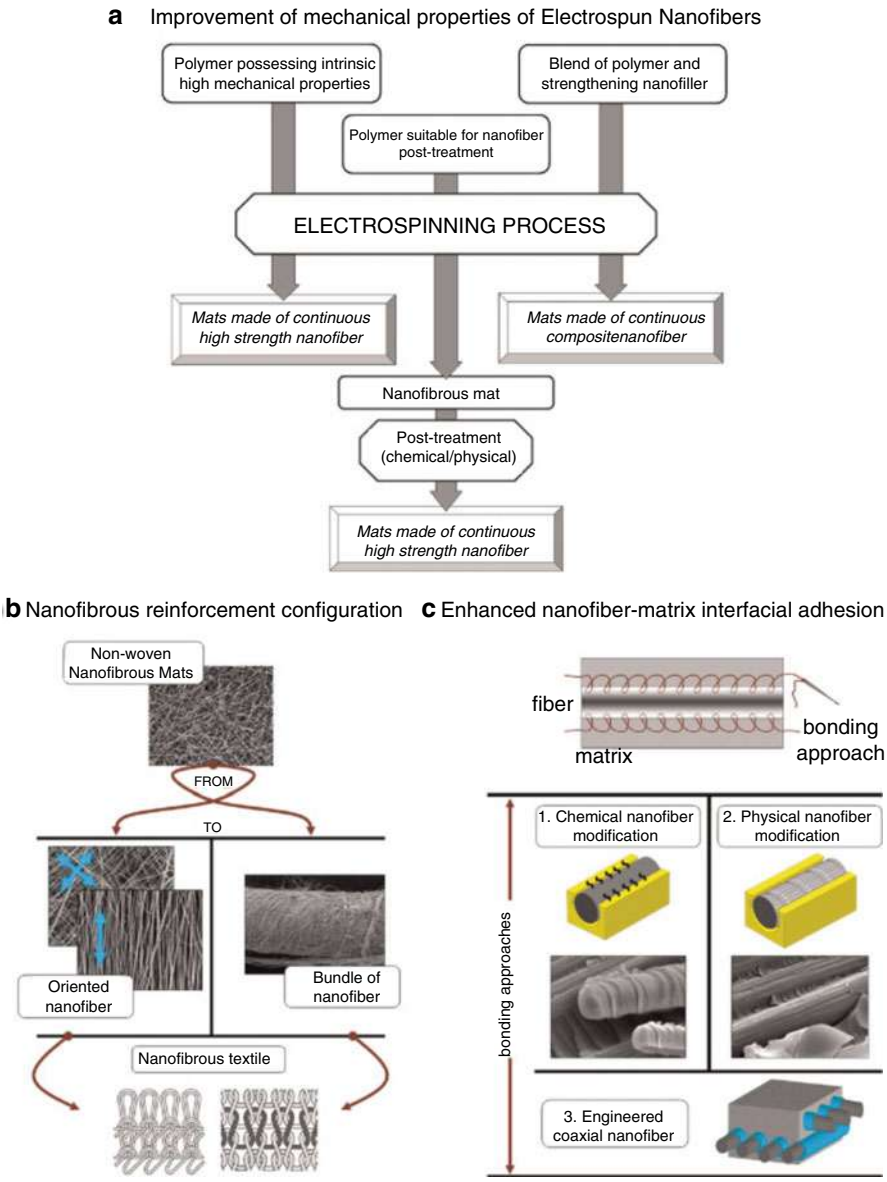

Fig. 18 Ways to improve the mechanical performance of electrospun fiber-reinforced composites (Zucchelli et al. 2011). (Reproduced with permission from Wiley)

Moreover, the orientation of nanofibers is more complicated, and a better method for controlling the alignment has to be developed so that properties of polymer composites can be controlled to a great extent. The development of biomass-derived nanofibers is in its infancy. The development of biomass-derived nano and carbon

fibers can be considered as an effective way in making environmental-friendly epoxy composites. Moreover, the biomass-derived fibers in bio-based epoxy composites can be considered as a step toward sustainable development. Currently, the development of epoxy vitrimers is gaining much research interest, and the incorporation of electrospun nanofibers in epoxy vitrimers could enhance the applications of self-healing epoxies. In Fig. 18, ways to improve the performance of electrospun polymer composites are presented. The ways include improving the properties of fibers themselves by modifying the orientation of fibers and nanofiber modifications to enhance fiber/matrix interface.

References

S. Agarwal, A. Greiner, Nanofibers by electrospinning. Polym. Adv. Technol. **3**(22), 293–294 (2011)

E. Ahmadloo, A. Gharehaghaji, M. Latifi, N. Mohammadi, H. Saghafi, How fracture toughness of epoxy-based nanocomposite is affected by PA66 electrospun nanofiber yarn. Eng. Fract. Mech. **182**, 62–73 (2017)

P. Akangah, S. Lingaiah, K. Shivakumar, Effect of Nylon-66 nano-fiber interleaving on impact damage resistance of epoxy/carbon fiber composite laminates. Compos. Struct. **92**(6), 1432–1439 (2010)

S. Al-Assafi, N. de Bruijn, A.M. Al-Jumaily, Processing and characterization of PMMA nanofiber reinforced epoxy composites. World J. Nano Sci. Eng. **6**(2), 58–63 (2016)

M.H. Al-Saleh, U. Sundararaj, Review of the mechanical properties of carbon nanofiber/polymer composites. Compos. A: Appl. Sci. Manuf. **42**(12), 2126–2142 (2011)

D. Aussawasathien, J.H. Dong, L. Dai, Electrospun polymer nanofiber sensors. Synth. Met. **154**(1), 37–40 (2005)

I. Aziz, H. Duran, M. Saleem, B. Yameen, S.N. Arshad, The role of interface on dynamic mechanical properties, dielectric performance, conductivity, and thermal stability of electrospun carbon nanofibers reinforced epoxy. Polym. Compos. (2021)

Q.-V. Bach, C.M. Vu, H.T. Vu, T. Hoang, T.V. Dieu, D.D. Nguyen, Epoxidized soybean oil grafted with CTBN as a novel toughener for improving the fracture toughness and mechanical properties of epoxy resin. Polym. J. **52**(3), 345–357 (2020)

Y. Bai, D. Wang, Z. Zhang, J. Pan, Z. Cui, D.-G. Yu, et al., Testing of fast dissolution of ibuprofen from its electrospun hydrophilic polymer nanocomposites. Polym. Test. **93**, 106872 (2021)

V. Beachley, X. Wen, Fabrication of nanofiber reinforced protein structures for tissue engineering. Mater. Sci. Eng. C **29**(8), 2448–2453 (2009)

G.W. Beckermann, K.L. Pickering, Mode I and Mode II interlaminar fracture toughness of composite laminates interleaved with electrospun nanofibre veils. Compos. A: Appl. Sci. Manuf. **72**, 11–21 (2015)

M.M. Bergshoef, G.J. Vancso, Transparent nanocomposites with ultrathin, electrospun nylon-4,6 fiber reinforcement. Adv. Mater. **11**(16), 1362–1365 (1999)

B. Blackman, A. Kinloch, J.S. Lee, A. Taylor, R. Agarwal, G. Schueneman, et al., The fracture and fatigue behaviour of nano-modified epoxy polymers. J. Mater. Sci. **42**(16), 7049–7051 (2007)

C.A. Bode-Aluko, O. Pereao, H.H. Kyaw, L. Al-Naamani, M.Z. Al-Abri, M.T.Z. Myint, et al., Photocatalytic and antifouling properties of electrospun TiO2 polyacrylonitrile composite nanofibers under visible light. Mater. Sci. Eng. B **264**, 114913 (2021)

A.L. Borges, E.A. Münchow, A.C. de Oliveira Souza, T. Yoshida, P.K. Vallittu, M.C. Bottino, Effect of random/aligned nylon-6/MWCNT fibers on dental resin composite reinforcement. J. Mech. Behav. Biomed. Mater. **48**, 134–144 (2015)

P. Brøndsted, H. Lilholt, A. Lystrup, Composite materials for wind power turbine blades. Annu. Rev. Mater. Res. **35**, 505–538 (2005)
S. Chand, Review carbon fibers for composites. J. Mater. Sci. **35**(6), 1303–1313 (2000)
S. Chandrasekaran, N. Sato, F. Tölle, R. Mülhaupt, B. Fiedler, K. Schulte, Fracture toughness and failure mechanism of graphene based epoxy composites. Compos. Sci. Technol. **97**, 90–99 (2014)
Z. J. Chang (ed.), *Development of a Polyurethane Nanocomposite Reinforced with Carbon Nanotube Composite Nanofibers. Materials Science Forum* (Trans Tech Publ, 2011)
S. Chang, M. Wang, F. Zhang, Y. Liu, X. Liu, D.-G. Yu, et al., Sheath-separate-core nanocomposites fabricated using a trifluid electrospinning. Mater. Des. **192**, 108782 (2020)
S. Chaudhary, P. Surekha, D. Kumar, C. Rajagopal, P. Roy, Amine-functionalized poly (styrene) microspheres as thermoplastic toughener for epoxy resin. Polym. Compos. **36**(1), 174–183 (2015)
G. Chen, H. Liu, Electrospun cellulose nanofiber reinforced soybean protein isolate composite film. J. Appl. Polym. Sci. **110**(2), 641–646 (2008)
L.S. Chen, Z.M. Huang, G.H. Dong, C.L. He, L. Liu, Y.Y. Hu, et al., Development of a transparent PMMA composite reinforced with nanofibers. Polym. Compos. **30**(3), 239–247 (2009)
D. Chen, R. Wang, W.W. Tjiu, T. Liu, High performance polyimide composite films prepared by homogeneity reinforcement of electrospun nanofibers. Compos. Sci. Technol. **71**(13), 1556–1562 (2011a)
Q. Chen, L. Zhang, A. Rahman, Z. Zhou, X.-F. Wu, H. Fong, Hybrid multi-scale epoxy composite made of conventional carbon fiber fabrics with interlaminar regions containing electrospun carbon nanofiber mats. Compos. A: Appl. Sci. Manuf. **42**(12), 2036–2042 (2011b)
Y. Chen, D. Han, W. Ouyang, S. Chen, H. Hou, Y. Zhao, et al., Fabrication and evaluation of polyamide 6 composites with electrospun polyimide nanofibers as skeletal framework. Compos. Part B **43**(5), 2382–2388 (2012)
J. Chen, A. Kinloch, S. Sprenger, A. Taylor, The mechanical properties and toughening mechanisms of an epoxy polymer modified with polysiloxane-based core-shell particles. Polymer **54**(16), 4276–4289 (2013a)
C. Chen, M. Cho, J.-D. Nam, Y. Lee, Cellulose diacetate reinforced with electrospun cellulose fiber: A new route to prepare an all cellulose-based composite. Compos. A: Appl. Sci. Manuf. **53**, 10–15 (2013b)
Q. Chen, Y. Zhao, Z. Zhou, A. Rahman, X.-F. Wu, W. Wu, et al., Fabrication and mechanical properties of hybrid multi-scale epoxy composites reinforced with conventional carbon fiber fabrics surface-attached with electrospun carbon nanofiber mats. Compos. Part B **44**(1), 1–7 (2013c)
Q. Chen, W. Wu, Y. Zhao, M. Xi, T. Xu, H. Fong, Nano-epoxy resins containing electrospun carbon nanofibers and the resulting hybrid multi-scale composites. Compos. Part B **58**, 43–53 (2014)
W. Chen, S. Chen, Y. Morsi, H. El-Hamshary, M. El-Newhy, C. Fan, et al., Superabsorbent 3D scaffold based on electrospun nanofibers for cartilage tissue engineering. ACS Appl. Mater. Interfaces **8**(37), 24415–24425 (2016)
C. Chen, Y. He, G. Xiao, Y. Wu, Z. He, F. Zhong, Zirconia doped in carbon fiber by electrospinning method and improve the mechanical properties and corrosion resistance of epoxy. Prog. Org. Coat. **125**, 420–431 (2018)
S.-S. Choi, Y.S. Lee, C.W. Joo, S.G. Lee, J.K. Park, K.-S. Han, Electrospun PVDF nanofiber web as polymer electrolyte or separator. Electrochim. Acta **50**(2-3), 339–343 (2004)
W. Chonkaew, N. Sombatsompop, Mechanical and tribological properties of epoxy modified by liquid carboxyl terminated poly (butadiene-co-acrylonitrile) rubber. J. Appl. Polym. Sci. **125**(1), 361–369 (2012)
G.T. Christopherson, H. Song, H.-Q. Mao, The influence of fiber diameter of electrospun substrates on neural stem cell differentiation and proliferation. Biomaterials **30**(4), 556–564 (2009)
S. Chuayjuljit, N. Soatthiyanon, P. Potiyaraj, Polymer blends of epoxy resin and epoxidized natural rubber. J. Appl. Polym. Sci. **102**(1), 452–459 (2006)

R. Correa, R. Nunes, W.F. Filho, Short fiber reinforced thermoplastic polyurethane elastomer composites. Polym. Compos. **19**(2), 152–155 (1998)
L. Cseri, F. Topuz, M.A. Abdulhamid, A. Alammar, P.M. Budd, G. Szekely, Electrospun adsorptive nanofibrous membranes from ion exchange polymers to snare textile dyes from wastewater. Adv. Mater. Technol. **2000955** (2021)
L. Daelemans, S. van der Heijden, I. De Baere, H. Rahier, W. Van Paepegem, K. De Clerck, Damage-resistant composites using electrospun nanofibers: A multiscale analysis of the toughening mechanisms. ACS Appl. Mater. Interfaces **8**(18), 11806–11818 (2016)
L. Daelemans, W. Van Paepegem, K. De Clerck, Effect of interleaved polymer nanofibers on the properties of glass and carbon fiber composites, in *Fiber-Reinforced Nanocomposites: Fundamentals and Applications*, (Elsevier, 2020), pp. 235–260
B. De Schoenmaker, S. Van der Heijden, I. De Baere, W. Van Paepegem, K. De Clerck, Effect of electrospun polyamide 6 nanofibres on the mechanical properties of a glass fibre/epoxy composite. Polym. Test. **32**(8), 1495–1501 (2013)
B. Deeraj, A. Saritha, K. Joseph, Electrospun styrene-butadiene copolymer fibers as potential reinforcement in epoxy composites: Modeling of rheological and visco elastic data. Compos. Part B **160**, 384–393 (2019)
B. Deeraj, R. Harikrishnan, J.S. Jayan, A. Saritha, K. Joseph, Enhanced visco-elastic and rheological behavior of epoxy composites reinforced with polyimide nanofiber. Nano-Struct. Nano-Objects **21**, 100421 (2020)
M.M. Demir, N. Horzum, A. Taşdemirci, K. Turan, M. Güden, Mechanical interlocking between porous electrospun polystyrene fibers and an epoxy matrix. ACS Appl. Mater. Interfaces **6**(24), 21901–21905 (2014)
A.P. Deshpande, M. Bhaskar Rao, R.C. Lakshmana, Extraction of bamboo fibers and their use as reinforcement in polymeric composites. J. Appl. Polym. Sci. **76**(1), 83–92 (2000)
Y. Dzenis, Y. Wen, Continuous carbon nanofibers for nanofiber composites. MRS Online Proc. Libr. **702**(1), 1–6 (2001)
S.Q. Feng, X.Y. Shen, Z.Y. Fu, Y.L. Ji, Studies on the electrospun submicron fibers of SIS and its mechanical properties. J. Appl. Polym. Sci. **114**(3), 1580–1586 (2009)
H. Fong, Electrospun nylon 6 nanofiber reinforced BIS-GMA/TEGDMA dental restorative composite resins. Polymer **45**(7), 2427–2432 (2004)
M. Goodarz, S. Bahrami, M. Sadighi, S. Saber-Samandari, The influence of graphene reinforced electrospun nano-interlayers on quasi-static indentation behavior of fiber-reinforced epoxy composites. Fibers Polym. **18**(2), 322–333 (2017)
M. Gopiraman, I.S. Kim, *Preparation, characterization, and applications of electrospun carbon nanofibers and its composites. Electrospinning and electrospraying-techniques and applications* (IntechOpen, 2019)
A. Greiner, J.H. Wendorff, Electrospinning: A fascinating method for the preparation of ultrathin fibers. Angew. Chem. Int. Ed. **46**(30), 5670–5703 (2007)
T. Guo, Z. Zhou, H. Guo, G. Xiao, X. Tang, M. Peng, Toughening of epoxy resin with functionalized core-sheath structured PAN/SBS electrospun fibers. J. Appl. Polym. Sci. **131**(23) (2014)
F. Guo, N. Wang, L. Wang, L. Hou, L. Ma, J. Liu, et al., An electrospun strong PCL/PU composite vascular graft with mechanical anisotropy and cyclic stability. J. Mater. Chem. A **3**(9), 4782–4787 (2015)
S.O. Han, W.K. Son, J.H. Youk, W.H. Park, Electrospinning of ultrafine cellulose fibers and fabrication of poly (butylene succinate) biocomposites reinforced by them. J. Appl. Polym. Sci. **107**(3), 1954–1959 (2008)
J. Herwan, E. Al-Bahkali, K.A. Khalil, M. Souli, Load bearing enhancement of pin joined composite laminates using electrospun polyacrylonitrile nanofiber mats. Arab. J. Chem. **9**(2), 262–268 (2016)
P. Huang, S. Zheng, J. Huang, Q. Guo, W. Zhu, Miscibility and mechanical properties of epoxy resin/polysulfone blends. Polymer **38**(22), 5565–5571 (1997)

Z.-M. Huang, Y.-Z. Zhang, M. Kotaki, S. Ramakrishna, A review on polymer nanofibers by electrospinning and their applications in nanocomposites. Compos. Sci. Technol. **63**(15), 2223–2253 (2003)

J.S. Im, S.-J. Park, T.J. Kim, Y.H. Kim, Y.-S. Lee, The study of controlling pore size on electrospun carbon nanofibers for hydrogen adsorption. J. Colloid Interface Sci. **318**(1), 42–49 (2008)

J.S. Im, J.G. Kim, T.-S. Bae, Y.-S. Lee, Effect of heat treatment on ZrO2-embedded electrospun carbon fibers used for efficient electromagnetic interference shielding. J. Phys. Chem. Solids **72**(10), 1175–1179 (2011)

M. Inagaki, Y. Yang, F. Kang, Carbon nanofibers prepared via electrospinning. Adv. Mater. **24**(19), 2547–2566 (2012)

P.K. Iyengar, K.A. Bhat, D. Sangeetha, T.V. Moorthy, Polymethyl methacrylate nanofiber-reinforced epoxy composite for shape-memory applications. High Perform. Polym. **25**(8), 1000–1006 (2013)

A.R. Jahanbaani, T. Behzad, S. Borhani, M.H.K. Darvanjooghi, Electrospinning of cellulose nanofibers mat for laminated epoxy composite production. Fibers Polym. **17**(9), 1438–1448 (2016)

J.S. Jayan, A. Saritha, K. Joseph, Innovative materials of this era for toughening the epoxy matrix: A review. Polym. Compos. **39**(S4), E1959–E1E86 (2018)

J.S. Jayan, A. Saritha, B. Deeraj, K. Joseph, Triblock copolymer grafted Graphene oxide as nanofiller for toughening of epoxy resin. Mater. Chem. Phys. **248**, 122930 (2020a)

J.S. Jayan, A. Saritha, B. Deeraj, K. Joseph, Synthesis of self-assembled and porous nano titania-graphene oxide hybrids for toughening the epoxy. Polym. Compos. **41**(10), 4093–4103 (2020b)

J.S. Jayan, A. Saritha, B.D.S. Deeraj, K. Joseph, Graphene oxide as a prospective graft in polyethylene glycol for enhancing the toughness of epoxy nanocomposites. Polym. Eng. Sci. **60**(4), 773–781 (2020c)

J.S. Jayan, K. Pal, A. Saritha, B. Deeraj, K. Joseph, Graphene oxide as multi-functional initiator and effective molecular reinforcement in PVP/epoxy composites. J. Mol. Struct. **1230**, 129873 (2021)

Q.L. Ji, M.Q. Zhang, M.Z. Rong, B. Wetzel, K. Friedrich, Tribological properties of surface modified nano-alumina/epoxy composites. J. Mater. Sci. **39**(21), 6487–6493 (2004)

S. Jian, J. Zhu, S. Jiang, S. Chen, H. Fang, Y. Song, et al., Nanofibers with diameter below one nanometer from electrospinning. RSC Adv. **8**(9), 4794–4802 (2018)

S. Jiang, G. Duan, H. Hou, A. Greiner, S. Agarwal, Novel layer-by-layer procedure for making nylon-6 nanofiber reinforced high strength, tough, and transparent thermoplastic polyurethane composites. ACS Appl. Mater. Interfaces **4**(8), 4366–4372 (2012a)

S. Jiang, H. Hou, A. Greiner, S. Agarwal, Tough and transparent nylon-6 electrospun nanofiber reinforced melamine–formaldehyde composites. ACS Appl. Mater. Interfaces **4**(5), 2597–2603 (2012b)

S. Jiang, G. Duan, J. Schöbel, S. Agarwal, A. Greiner, Short electrospun polymeric nanofibers reinforced polyimide nanocomposites. Compos. Sci. Technol. **88**, 57–61 (2013)

S. Jiang, Y. Chen, G. Duan, C. Mei, A. Greiner, S. Agarwal, Electrospun nanofiber reinforced composites: A review. Polym. Chem. **9**(20), 2685–2720 (2018)

R. Jose, V. Thavasi, S. Ramakrishna, Metal oxides for dye-sensitized solar cells. J. Am. Ceram. Soc. **92**(2), 289–301 (2009)

K. Js, D.H. Reneker, Mechanical properties of composites using ultrafine electrospun fibers. Polym. Compos. **20**(1), 124–131 (1999)

P. Katti, K. Kundan, S. Kumar, S. Bose, Improved mechanical properties through engineering the interface by poly (ether ether ketone) grafted graphene oxide in epoxy based nanocomposites. Polymer **122**, 184–193 (2017)

A. Kausar, Mechanical, thermal, and electrical properties of epoxy matrix composites reinforced with polyamide-grafted-MWCNT/poly (azo-pyridine-benzophenone-imide)/polyaniline nanofibers. Int. J. Polym. Mater. Polym. Biomater. **63**(16), 831–839 (2014)

A. Kausar, Synthesis and properties of polyimide nanocomposites self-reinforced with electrospun poly (azo-naphthyl-imide)/carbon nanotube nanofibers. J. Thermoplast. Compos. Mater. **29**(3), 312–326 (2016)
B.C. Kim, S.W. Park, Fracture toughness of the nano-particle reinforced epoxy composite. Compos. Struct. **86**(1–3), 69–77 (2008)
R. Konnola, J. Joji, J. Parameswaranpillai, K. Joseph, Structure and thermo-mechanical properties of CTBN-grafted-GO modified epoxy/DDS composites. RSC Adv. **5**(76), 61775–61786 (2015)
R. Konnola, C.R. Nair, K. Joseph, High strength toughened epoxy nanocomposite based on poly (ether sulfone)-grafted multi-walled carbon nanotube. Polym. Adv. Technol. **27**(1), 82–89 (2016)
R. Konnola, B. Deeraj, S. Sampath, A. Saritha, K. Joseph, Fabrication and characterization of toughened nanocomposites based on TiO2 nanowire-epoxy system. Polym. Compos. **40**(7), 2629–2638 (2019)
R. Krishnappa, K. Desai, C. Sung, Morphological study of electrospun polycarbonates as a function of the solvent and processing voltage. J. Mater. Sci. **38**(11), 2357–2365 (2003)
F. Lamastra, D. Puglia, M. Monti, A. Vella, L. Peponi, J. Kenny, et al., Poly (ε-caprolactone) reinforced with fibres of Poly (methyl methacrylate) loaded with multiwall carbon nanotubes or graphene nanoplatelets. Chem. Eng. J. **195**, 140–148 (2012)
F. Lan, H. Zhang, J. Fan, Q. Xu, H. Li, Y. Min, Electrospun polymer nanofibers with TiO2@ NiCo-LDH as efficient polysulfide barriers for wide-temperature-range Li–S batteries. ACS Appl. Mater. Interfaces **13**(2), 2734–2744 (2021)
S.M. Lee, *Handbook of Composite Reinforcements* (Wiley, 1992)
K. Lee, H. Kim, H. Bang, Y. Jung, S. Lee, The change of bead morphology formed on electrospun polystyrene fibers. Polymer **44**(14), 4029–4034 (2003)
J.-R. Lee, S.-J. Park, M.-K. Seo, J.-M. Park, Preparation and characterization of electrospun poly (ethylene oxide)(PEO) nanofibers-reinforced epoxy matrix composites. MRS Online Proce. Libr. Arch. **851** (2004)
E. Lee, Y. Song, S. Lee, Antimicrobial property and biodegradability of lignin nanofibers, Master's thesis, Yonsei University, Republic of Korea, 2014
W.J. Li, C.T. Laurencin, E.J. Caterson, R.S. Tuan, F.K. Ko, Electrospun nanofibrous structure: A novel scaffold for tissue engineering. J. Biomed. Mater. Res. **60**(4), 613–621 (2002)
X. Li, L.G. Tabil, S. Panigrahi, Chemical treatments of natural fiber for use in natural fiber-reinforced composites: A review. J. Polym. Environ. **15**(1), 25–33 (2007)
B. Li, H. Yuan, Y. Zhang, Transparent PMMA-based nanocomposite using electrospun graphene-incorporated PA-6 nanofibers as the reinforcement. Compos. Sci. Technol. **89**, 134–141 (2013)
H. Liao, Y. Wu, M. Wu, H. Liu, Effects of fiber surface chemistry and roughness on interfacial structures of electrospun fiber reinforced epoxy composite films. Polym. Compos. **32**(5), 837–845 (2011)
S. Lin, Q. Cai, J. Ji, G. Sui, Y. Yu, X. Yang, et al., Electrospun nanofiber reinforced and toughened composites through in situ nano-interface formation. Compos. Sci. Technol. **68**(15-16), 3322–3329 (2008)
Y. Liu, Y. Ji, K. Ghosh, R.A. Clark, L. Huang, M.H. Rafailovich, Effects of fiber orientation and diameter on the behavior of human dermal fibroblasts on electrospun PMMA scaffolds. J. Biomed. Mater. Res. A **90**(4), 1092–1106 (2009)
J. Liu, Z.J. Thompson, H.-J. Sue, F.S. Bates, M.A. Hillmyer, M. Dettloff, et al., Toughening of epoxies with block copolymer micelles of wormlike morphology. Macromolecules **43**(17), 7238–7243 (2010)
Y. Liu, S. Chen, S. Ye, J. Feng, A feasible route to balance the mechanical properties of epoxy thermosets by reinforcing a PCL-PPC-PCL toughened system with reduced graphene oxide. Compos. Sci. Technol. **125**, 108–113 (2016)
B. Lu, G. Zheng, K. Dai, C. Liu, J. Chen, C. Shen, Enhanced mechanical properties of polyethylene composites with low content of electrospun nylon-66 nanofibers. Mater. Lett. **140**, 131–134 (2015)

Z. Ma, M. Kotaki, T. Yong, W. He, S. Ramakrishna, Surface engineering of electrospun polyethylene terephthalate (PET) nanofibers towards development of a new material for blood vessel engineering. Biomaterials **26**(15), 2527–2536 (2005)

S. Ma, W. Liu, N. Gao, Z. Yan, Y. Zhao, Synthesis and properties of LED-packaging epoxy resin toughened by a novel polysiloxane from hydrolysis and condensation. Macromol. Res. **19**(9), 972–979 (2011)

C. Ma, H.-Y. Liu, X. Du, L. Mach, F. Xu, Y.-W. Mai, Fracture resistance, thermal and electrical properties of epoxy composites containing aligned carbon nanotubes by low magnetic field. Compos. Sci. Technol. **114**, 126–135 (2015)

C. Marega, A. Marigo, Effect of electrospun fibers of polyhydroxybutyrate filled with different organoclays on morphology, biodegradation, and thermal stability of poly (ε-caprolactone). J. Appl. Polym. Sci. **132**(31) (2015)

K. Matabola, A. De Vries, A. Luyt, R. Kumar, Studies on single polymer composites of poly (methyl methacrylate) reinforced with electrospun nanofibers with a focus on their dynamic mechanical properties, 2011

L.M. McGrath, R.S. Parnas, S.H. King, J.L. Schroeder, D.A. Fischer, J.L. Lenhart, Investigation of the thermal, mechanical, and fracture properties of alumina–epoxy composites. Polymer **49**(4), 999–1014 (2008)

K. Mimura, H. Ito, H. Fujioka, Improvement of thermal and mechanical properties by control of morphologies in PES-modified epoxy resins. Polymer **41**(12), 4451–4459 (2000)

R.E. Neisiany, S.N. Khorasani, J.K.Y. Lee, M. Naeimirad, S. Ramakrishna, Interfacial toughening of carbon/epoxy composite by incorporating styrene acrylonitrile nanofibers. Theor. Appl. Fract. Mech. **95**, 242–247 (2018)

R. Neppalli, C. Marega, A. Marigo, M.P. Bajgai, H.Y. Kim, V. Causin, Poly (ε-caprolactone) filled with electrospun nylon fibres: A model for a facile composite fabrication. Eur. Polym. J. **46**(5), 968–976 (2010)

R. Neppalli, C. Marega, A. Marigo, M.P. Bajgai, H.Y. Kim, S.S. Ray, et al., Electrospun nylon fibers for the improvement of mechanical properties and for the control of degradation behaviour of poly (lactide)-based composites, 2012

R. Neppalli, V. Causin, E.M. Benetti, S.S. Ray, A. Esposito, S. Wanjale, et al., Polystyrene/TiO2 composite electrospun fibers as fillers for poly (butylene succinate-co-adipate): Structure, morphology and properties. Eur. Polym. J. **50**, 78–86 (2014)

E. Ozden, Y.Z. Menceloglu, M. Papila, Engineering chemistry of electrospun nanofibers and interfaces in nanocomposites for superior mechanical properties. ACS Appl. Mater. Interfaces **2**(7), 1788–1793 (2010)

E. Özden-Yenigün, Y.Z. Menceloğlu, M. Papila, MWCNTs/P (St-co-GMA) composite nanofibers of engineered interface chemistry for epoxy matrix nanocomposites. ACS Appl. Mater. Interfaces **4**(2), 777–784 (2012)

R. Palazzetti, A. Zucchelli, C. Gualandi, M. Focarete, L. Donati, G. Minak, et al., Influence of electrospun Nylon 6, 6 nanofibrous mats on the interlaminar properties of Gr–epoxy composite laminates. Compos. Struct. **94**(2), 571–579 (2012)

D. Puglia, J. Biagiotti, J. Kenny, A review on natural fibre-based composites – Part II: Application of natural reinforcements in composite materials for automotive industry. J. Natl. Fibers. **1**(3), 23–65 (2005)

D. Quan, A. Ivankovic, Effect of core–shell rubber (CSR) nano-particles on mechanical properties and fracture toughness of an epoxy polymer. Polymer **66**, 16–28 (2015)

S. Reich, M. Burgard, M. Langner, S. Jiang, X. Wang, S. Agarwal, et al., Polymer nanofibre composite nonwovens with metal-like electrical conductivity. npj Flexible. Electronics **2**(1), 5 (2018)

A. Romo-Uribe, L. Arizmendi, M.A.E. Romero-Guzmán, S. Sepulveda-Guzmán, R. Cruz-Silva, Electrospun nylon nanofibers as effective reinforcement to polyaniline membranes. ACS Appl. Mater. Interfaces **1**(11), 2502–2508 (2009)

Y.J. Ryu, H.Y. Kim, K.H. Lee, H.C. Park, D.R. Lee, Transport properties of electrospun nylon 6 nonwoven mats. Eur. Polym. J. **39**(9), 1883–1889 (2003)
H. Saghafi, A. Zucchelli, R. Palazzetti, G. Minak, The effect of interleaved composite nanofibrous mats on delamination behavior of polymeric composite materials. Compos. Struct. **109**, 41–47 (2014)
M. Sahu, A.M. Raichur, Toughening of high performance tetrafunctional epoxy with poly (allyl amine) grafted graphene oxide. Compos. Part B **168**, 15–24 (2019)
E. Sancaktar, D. Aussawasathien, Nanocomposites of epoxy with electrospun carbon nanofibers: Mechanical behavior. J. Adhes. **85**(4-5), 160–179 (2009)
U.A. Shakil, S.B. Hassan, M.Y. Yahya, S. Nauman, Mechanical properties of electrospun nanofiber reinforced/interleaved epoxy matrix composites – A review. Polym. Compos. (2020)
Y. Shen, L. Chen, S. Jiang, Y. Ding, W. Xu, H. Hou, Electrospun nanofiber reinforced all-organic PVDF/PI tough composites and their dielectric permittivity. Mater. Lett. **160**, 515–517 (2015)
M.M.A. Shirazi, S. Bazgir, F. Meshkani, Electrospun nanofibrous membranes for water treatment. Adv. Membr. Technol. **57**(3), 467–504 (2020)
Y. Si, Q. Fu, X. Wang, J. Zhu, J. Yu, G. Sun, et al., Superelastic and superhydrophobic nanofiber-assembled cellular aerogels for effective separation of oil/water emulsions. ACS Nano **9**(4), 3791–3799 (2015)
S. Sihn, R.Y. Kim, W. Huh, K.-H. Lee, A.K. Roy, Improvement of damage resistance in laminated composites with electrospun nano-interlayers. Compos. Sci. Technol. **68**(3-4), 673–683 (2008)
L. Sisti, J. Belcari, L. Mazzocchetti, G. Totaro, M. Vannini, L. Giorgini, et al., Multicomponent reinforcing system for poly (butylene succinate): Composites containing poly (L-lactide) electrospun mats loaded with graphene. Polym. Test. **50**, 283–291 (2016)
K. Sobczyk, K. Leluk (eds.), *An Openwork Like Structures of Polylactide–Manufacturing and Properties. E3S Web of Conferences* (EDP Sciences, 2018)
U. Stachewicz, F. Modaresifar, R.J. Bailey, T. Peijs, A.H. Barber, Manufacture of void-free electrospun polymer nanofiber composites with optimized mechanical properties. ACS Appl. Mater. Interfaces **4**(5), 2577–2582 (2012)
J. Summerscales, W. Hall, A.S. Virk, A fibre diameter distribution factor (FDDF) for natural fibre composites. J. Mater. Sci. **46**(17), 5876–5880 (2011)
T. Sun, D. Norton, R.J. McKean, J.W. Haycock, A.J. Ryan, S. MacNeil, Development of a 3D cell culture system for investigating cell interactions with electrospun fibers. Biotechnol. Bioeng. **97**(5), 1318–1328 (2007)
C. Tang, H. Liu, Cellulose nanofiber reinforced poly (vinyl alcohol) composite film with high visible light transmittance. Compos. A: Appl. Sci. Manuf. **39**(10), 1638–1643 (2008)
B. Tang, X. Liu, X. Zhao, J. Zhang, Highly efficient in situ toughening of epoxy thermosets with reactive hyperbranched polyurethane. J. Appl. Polym. Sci. **131**(16) (2014)
W. Thitsartarn, X. Fan, Y. Sun, J.C.C. Yeo, D. Yuan, C. He, Simultaneous enhancement of strength and toughness of epoxy using POSS-Rubber core–shell nanoparticles. Compos. Sci. Technol. **118**, 63–71 (2015)
R. Thomas, D. Yumei, H. Yuelong, Y. Le, P. Moldenaers, Y. Weimin, et al., Miscibility, morphology, thermal, and mechanical properties of a DGEBA based epoxy resin toughened with a liquid rubber. Polymer **49**(1), 278–294 (2008)
M. Tian, Y. Gao, Y. Liu, Y. Liao, R. Xu, N.E. Hedin, et al., Bis-GMA/TEGDMA dental composites reinforced with electrospun nylon 6 nanocomposite nanofibers containing highly aligned fibrillar silicate single crystals. Polymer **48**(9), 2720–2728 (2007)
L.D. Tijing, C.-H. Park, S.-J. Kang, A. Amarjargal, T.-H. Kim, H.R. Pant, et al., Improved mechanical properties of solution-cast silicone film reinforced with electrospun polyurethane nanofiber containing carbon nanotubes. Appl. Surf. Sci. **264**, 453–458 (2013)
D.P. Ura, K. Berniak, U. Stachewicz, Critical length reinforcement in core-shell electrospun fibers using composite strategies. Compos. Sci. Technol. **108867** (2021)

E. Uslu, M. Gavgali, M.O. Erdal, Ş. Yazman, L. Gemi, Determination of mechanical properties of polymer matrix composites reinforced with electrospinning N66, PAN, PVA and PVC nanofibers: A comparative study. Mater. Today Commun. **26**, 101939 (2021)

S. van der Heijden, L. Daelemans, K. De Bruycker, R. Simal, I. De Baere, W. Van Paepegem, et al., Novel composite materials with tunable delamination resistance using functionalizable electrospun SBS fibers. Compos. Struct. **159**, 12–20 (2017)

V. Vijay Kumar, S. Ramakrishna, J.L. Kong Yoong, R. Esmaeely Neisiany, S. Surendran, G. Balaganesan, Electrospun nanofiber interleaving in fiber reinforced composites – Recent trends. Mater. Des. Process. Commun. **1**(1), e24 (2019)

C.M. Vu, Q.-V. Bach, Effects of DOPO-grafted epoxidized soybean oil on fracture toughness and flame retardant of epoxy resin/rice husk silica hybrid. Macromol. Res. **28**(9), 826–834 (2020)

M. Wang, X. Fan, W. Thitsartarn, C. He, Rheological and mechanical properties of epoxy/clay nanocomposites with enhanced tensile and fracture toughnesses. Polymer **58**, 43–52 (2015)

Y. Wei, Y. Shi, X. Zhang, Z. Jiang, Y. Zhang, L. Zhang, et al., Electrospinning of lightweight TiN fibers with superior microwave absorption. J. Mater. Sci. Mater. Electron., 1–9 (2019)

M. Wu, Y. Wu, Z. Liu, H. Liu, Optically transparent poly (methyl methacrylate) composite films reinforced with electrospun polyacrylonitrile nanofibers. J. Compos. Mater. **46**(21), 2731–2738 (2012)

J. Wu, N. Wang, Y. Zhao, L. Jiang, Electrospinning of multilevel structured functional micro-/nanofibers and their applications. J. Mater. Chem. A **1**(25), 7290–7305 (2013)

W. Xu, Y. Ding, S. Jiang, J. Zhu, W. Ye, Y. Shen, et al., Mechanical flexible PI/MWCNTs nanocomposites with high dielectric permittivity by electrospinning. Eur. Polym. J. **59**, 129–135 (2014a)

W. Xu, Y. Ding, S. Jiang, L. Chen, X. Liao, H. Hou, Polyimide/BaTiO3/MWCNTs three-phase nanocomposites fabricated by electrospinning with enhanced dielectric properties. Mater. Lett. **135**, 158–161 (2014b)

W. Xu, Y. Feng, Y. Ding, S. Jiang, H. Fang, H. Hou, Short electrospun carbon nanofiber reinforced polyimide composite with high dielectric permittivity. Mater. Lett. **161**, 431–434 (2015)

S.-S. Yao, C.-L. Ma, F.-L. Jin, S.-J. Park, Fracture toughness enhancement of epoxy resin reinforced with graphene nanoplatelets and carbon nanotubes. Korean J. Chem. Eng. **37**(11), 2075–2083 (2020)

J. Zeng, X. Xu, X. Chen, Q. Liang, X. Bian, L. Yang, et al., Biodegradable electrospun fibers for drug delivery. J. Control. Release **92**(3), 227–231 (2003)

Y. Zeng, X. Li, S. Jiang, S. He, H. Fang, H. Hou, Free-standing mesoporous electrospun carbon nanofiber webs without activation and their electrochemical performance. Mater. Lett. **161**, 587–590 (2015)

C. Zhang, X. Yuan, L. Wu, Y. Han, J. Sheng, Study on morphology of electrospun poly (vinyl alcohol) mats. Eur. Polym. J. **41**(3), 423–432 (2005)

J. Zhang, T. Yang, T. Lin, C.H. Wang, Phase morphology of nanofibre interlayers: Critical factor for toughening carbon/epoxy composites. Compos. Sci. Technol. **72**(2), 256–262 (2012)

J. Zhou, M. Zhou, Z. Chen, Z. Zhang, C. Chen, R. Li, et al., SiC nanotubes arrays fabricated by sputtering using electrospun PVP nanofiber as templates. Surf. Coat. Technol. **203**(20-21), 3219–3223 (2009)

S. Zhou, G. Zhou, S. Jiang, P. Fan, H. Hou, Flexible and refractory tantalum carbide-carbon electrospun nanofibers with high modulus and electric conductivity. Mater. Lett. **200**, 97–100 (2017)

A. Zucchelli, M.L. Focarete, C. Gualandi, S. Ramakrishna, Electrospun nanofibers for enhancing structural performance of composite materials. Polym. Adv. Technol. **22**(3), 339–349 (2011)

Microwave-Based Manufacturing of Epoxy/Fiber Composites

16

Rajeev Kumar, Manjeet Rani, and Sunny Zafar

Contents

R. Kumar · M. Rani · S. Zafar (✉)
Composite Design and Manufacturing Research Group, School of Engineering, Indian Institute of Technology Mandi, Mandi, Himachal Pradesh, India
e-mail: sunnyzafar@iitmandi.ac.in

S. Mavinkere Rangappa et al. (eds.), *Handbook of Epoxy/Fiber Composites*,
https://doi.org/10.1007/978-981-19-3603-6_54

Abstract

The development of fiber reinforced polymer composite (FRPC) has become essential owing to their exceptional mechanical, physical, and chemical properties. It includes high strength and stiffness to weight ratio, high corrosion resistance, better fatigue resistance against cyclic loading, remarkable corrosion resistance, and better dimensional stability in critical environment conditions. The demand of FRPCs has become essential in aerospace, marine, wind energy, and military sector. Several fabrication methods are available to fabricate FRPCs, such as resin transfer molding (RTM), high pressure-RTM (HP-RTM), compression molding, vacuum-assisted resin infusion microwave curing (VARIMC), and many more. For curing laminates conventional heating and microwave heating have been used. The factors degree of cure, interfacial adhesion of fiber and matrix, curing rate, and curing temperature are critical, and mechanical properties are influenced by these. The mechanical tests (tensile test, 3-point bending test, pull out test, fatigue test, etc.) were performed to determine various mechanical properties of FRPCs. The degree of cure was determined by DSC analysis. The SEM analysis was done for the fractured surface for the understanding of microstructure of FRPCs. The matrix cracking, fiber fracture, debonding between fiber and matrix or poor adhesion, and delamination of laminates were the leading causes of failure. The challenges and applications are also discussed.

Keywords

Fiber reinforced composites · Microwave curing · Thermal heating · Fabrication methods · Glass fiber · Carbon fiber · Kevlar fiber · Epoxy resin

Introduction

Fiber reinforced polymer composites (FRPCs) have the ability to provide customizable material properties and fabrication methods based on applications. The FRPCs have high mechanical performance, high resistance to critical environment, good structural stability and are lightweight and environmental- and economical-friendly structures (reduction in fuel cost and long service life). Composite is a multiphase material consisting of continuous phase as matrix and reinforcement phase as reinforcement material, i.e., glass fiber (GF), carbon fiber (CF), Kevlar fiber (KF), and many more. In composites, the fibers are typically used in the form of woven mats (unidirectional and bidirectional), continuous (long), short (chopped mats and particulates), and braids. Commonly used matrix materials are polyester, phenolic, and epoxy (Edwards 1998). Epoxy resins are used in critical structural applications. The

FRPC materials have shown magnificent and outstanding popularity because of their lightweight, good conductivity, high toughness, high specific strength, and stiffness compared to conventional metallic materials. Therefore, they become widely used materials in aircraft, aerospace, and wind and automotive industries. For the fabrication of microwave absorbing composites, epoxy resin is one of the most exclusively used polymers because of its resistance to corrosion, commercial availability, high fracture toughness, irreversible hardening, and ease of processing (Mondal 2016). With increasing commercial demand of the FRPCs, various fabrication and curing processes have been developed to improve the composites' mechanical properties, which are described in the subsequent section. With the development of fabrication and curing processes, various factors, i.e., quality, production cycle time, and overall production cost, have improved. The fabrication of fiber/epoxy-based composites depends on low content of voids and high glass transition temperature (T_g). The maximization of T_g should occur during the design of fabrication (curing) process. Autoclave processing for fabrication of composite is a well-known method. In this method, heat and pressure were applied simultaneously to cure the prepreg in autoclave chamber. Although fabricated composite parts have excellent mechanical and structural performance, they require long curing time due to low curing rate and incur high production costs. During prepreg curing with this process, first the air inside the autoclave chamber will heat up; after that composite part starts to heat up by convection (Kwak et al. 2015). In a recent development, high-pressure resin transfer molding (HP-RTM) has taken an initiative to reduce/compress the processing time. In this method, resin is injected at high pressure and temperature. The limitation of this process is that it has a high initial setup cost and energy cost also (Maenz et al. 2015). As reported in several studies, rapid curing (high curing rate) is an important parameter to increase energy efficiency, better process control, and production rate. However various attempts were carried out for replacement of conventional heating sources (induction, ultrasonic, and resistance) with different alternative ones (electron beam, ultraviolet radiation, infrared, and laser) (Endruweit et al. 2006; Abliz et al. 2013). However, fabricated composites were produced with some defects/degradation, which seems inevitable in critical applications. The reduction in ultimate tensile strength (>40%) was reported due to weak interfacial bonding. This reduction was attributed to less degree of cure and increased voids (the rapid curing rate due to change in ramp rate of temperature) using conventional heating source (Gupta and Ogale 2002). To improve mechanical properties of composites, void content should be minimized. The degree of cure is the fundamental measurement parameter by which cured and uncured epoxy-based composites could be identified. The degree of cure can be analyzed using differential scanning calorimetry (DSC). The presence of an exothermic peak is the indication of uncured condition (Chen et al. 1993; Mijović and Wijaya 1990).

In conventional heating or curing of FRPCs, CFs can influence thermal gradient across thickness of laminate, which results in improper curing of matrix material. This is owing to high thermal conductivity of CFs. To overcome these existing issues with conventional and other curing methods, there was a need of controllable accelerated curing of composites. Therefore, to reduce the energy cost, initial

setup cost, and high depth of penetration across thickness and production cycle time, the microwave curing process can become an optimal solution to existing problems. Microwave is well known or frequently presented for its volumetric heating/curing of FRPCs at the molecular level in a short span of time (Kwak et al. 2015; Mijović and Wijaya 1990). Microwave heating/curing mechanism involves conduction loss, dipolar loss, Eddy current loss, and hysteresis loss according to the type of materials (Mishra and Sharma 2016). Generally, epoxy (resin) used dipolar loss mechanism for heating or curing. Some other materials, i.e., water and ceramics, are heated through dipolar loss. These materials are subjected to an alternating electric field and applied field during microwave exposure to reorient dipoles in electric field direction. Dipoles try to resist their orientation due to presence of internal forces, i.e., inertial, elastic, frictional, and molecular interaction force. Therefore, dipoles start to vibrate and generated kinetic energy is converted into heat energy resulting in increase in temperature. Microwave curing/heating, owing to its characteristics, has the ability to heat the mold as well as composite material/parts in a short span of time and able to reduce the total production cost with saved energy consumption cost. The aforementioned advantages of microwave curing can be chosen as a replacement of the conventional curing for the same.

Microwave curing of epoxy resin has probable outcomes over thermal curing such as low energy consumption, moderate operating cost, less time for complete and uniform/consistent cure, enhanced mechanical/structural properties, and lower degradation (Chen et al. 1993). Similar outcomes have been observed in previous studies during the microwave curing of FRPC laminates (Hang et al. 2017; Kwak et al. 2015; Li et al. 2018; Rao et al. 2006; Zhou et al. 2016). The variation of microwave power and processing cycle time was studied to determine maximum flexural strength and modulus of glass fiber reinforced polymer composites (GFRPCs). The microwave power, i.e., 400 W, 600 W, and 800 W, were used with time range from 5 min to 20 min. At lower power, maximum cycle time was observed and vice versa. The maximum flexural strength was obtained with 800 W and 8 min (approximately). The maximum flexural strength was obtained with 600 W and 20 min cycle time (Boey and Lee 1991). In later 1990s studies, presence of voids was observed more in case of microwave cured composites than thermally cured ones. That was attributed to short curing time and lower pressure during cure process. However, increment in transverse tensile strength and modulus was reported based on experimental results. The transverse tensile strength depends on the interfacial strength of composite. Thus fast curing rate with low thermal gradient was the dominant factor for enhancing interfacial properties, not the short curing time (Bai and Djafari 1995). In another study, an attempt was made to reduce the defects (porosity) in carbon fiber reinforced polymer (CFRP) composite during the manufacturing process. The composite was fabricated using microwave curing (atmospheric pressure) and vacuum-assisted microwave curing (vacuum pressure) to observe the effect of vacuum on the properties of composite laminates. The microwave power 180 W and 360 W were used. The tensile strength was increased 1.16 (180 W) and 1.7 times (360 W) for vacuum-assisted microwave curing composites compared to without vacuum-assisted microwave cured composites.

For better strength, the reason was attributed to the uniform wetting of the fibers and proper adhesion boning between fiber and matrix material (Verma et al. 2020). The interfacial properties are essential to understand mechanical properties and failure mechanisms of composites. A similar study was carried out to investigate the influence of microwave and thermal curing on mechanical and interfacial properties of GFRPCs by Yue and Looi (1995). The pull-out test was conducted to find the interfacial properties. Comprehensive analysis of interfacial properties, i.e., interfacial shear bond strength, interfacial toughness, interfacial frictional shear stress, and coefficient of friction between fiber and matrix, was carried out from the experimental data (Yue and Looi 1995). Kumar et al. (2021) fabricated high-grade hybrid carbon fiber/glass fiber epoxy composites using vacuum-assisted resin infusion microwave curing (VARIMC) process. In traditional curing processes like autoclave, convective heat transfer mode heats the surface of composites, and further heat transfer to the core is due to conduction of heat. The multimode heating of composites results in nonuniform heating of composites and may result in lower mechanical properties, whereas microwaves directly couple with target materials and heat the composite more uniformly. Impact tests of the hybrid composites were conducted, and different modes of failures were analyzed, such as matrix cracking, delamination, and fiber cracking. The result showed the significant influence of the stacking sequence of laminates on its impact strength (Kumar et al. 2021).

Chen et al. compared the mechanical properties of the microwave and conventional cured samples made of epoxy/glass composites. The thickness of the glass fiber reinforced polymer (GFRP) laminates was kept 2 mm. Improved properties like higher T_g, flexural strength, tensile strength, and modulus were observed for microwave cured samples. Failure of thermally cured composite samples was correlated to the rupture of fibers and inferior adhesion between fiber and matrix material. Microwave cured samples failed with flat fracture surface attributed to better adhesion between fiber and matrix. This can be attributed to the improved interfacial bonding of the fiber and matrix (Chen et al. 2014). Mijović and Wijaya discussed the interaction between electromagnetic waves and composites. Authors provide information about the materials, microwave applicator, and modes of microwave energy (Mijović and Wijaya 1990). Claus et al. investigated the composites under penetrating impact loading. Composites were reinforced with structural fibers (carbon and glass) with different epoxy resin systems. Composites were fabricated with most popular composite fabricating technique (vacuum-assisted resin infusion) with thermal curing (Claus et al. 2020). Thostenson and Chou conducted experimental and simulation studies to investigate the processing time of conventional and microwave curing. Thick glass/epoxy laminates (about 24.5 mm) were fabricated with both heating processes. A drastic reduction was found during the microwave curing in both studies (Thostenson and Chou 2001). In another study, a combination of microwave and thermal curing was used to fabricate L-390 carbon fiber polymer-based composites. Optimum mechanical properties were obtained with respect to time and energy saving. As we know, sufficient time and energy (heat) is required to cure the polymers. In different studies, microwave curing showed the ability to cross-link the monomer network in less time

and energy to cure the composite with improved mechanical properties (Balzer and McNabb 2008).

Mgbemena et al. (2018) reviewed several studies or research papers related to accelerated curing of FRPCs using microwave heating or radiation. Although microwave curing has several advantages as reported in previous studies, i.e., volumetric heating, compressed processing time, and high energy efficiency (Abliz et al. 2013; Mijović and Wijaya 1990), it has several scientific challenges also that include presence of hotspots, uneven penetration depth of microwaves, shielding of fibers (CFs) to reduce sparking, and uneven curing. This study was focused to establish correlation between microwave frequency, depth of penetration, degree of cure, and dielectric properties of reinforced and matrix materials. The curing of epoxy matrix in composite plays a critical role in improvement of the structural and mechanical performance. The curing of epoxy depends on process parameters such as temperature, curing rate, and curing time. The curing variation leads to voids, poor adhesion, and interfacial properties between fiber and matrix material (Mgbemena et al. 2018). Xu et al. investigated compressive strength, molecular structure, degree of cure, and glass transition temperature (T_g) of microwave cured unidirectional CF/epoxy composites. A further comparison was made with thermally cured laminates. Laminates are stacked and fabricated using vacuum bagging method under one atmospheric pressure. For curing of vacuum bagged laminates, microwave heating was used. Microwave heating of laminates was carried out using multistep (2-step and 3-step) process to improve the compressive strength of laminates. Further, mechanical and physical properties of microwave and thermally cured samples were compared. Carbon fiber reinforced composites (CFRC) have lower compression load carrying capacity than tensile load. Therefore, in this study, much more attention was given to improve compressive strength of laminates by interfacial bonding between fiber and matrix. Results showed that increment in compressive strength of microwave cured laminates (2-step process) was about 1.22 times higher than thermally cured laminates. Significant reduction in processing cycle time (2/3 times) was also reported for the same (Xu et al. 2015). The GFRCs were fabricated with multistep microwave curing process. The mechanical properties were compared for microwave and thermally cured laminates. Single-step and multistep (2-step and 3-step) curing of laminates was performed using microwave at frequency of 2450 MHz, exposure time of 7.75 min, and microwave power of 800 W. The results showed better interfacial adhesion in multistep curing compared to single step. However, improvement in properties was observed in microwave cured laminates over thermal curing (Tanrattanakul and Jaroendee 2006). The (CFRPC) was fabricated using hand lay-up vacuum bagging method. Further, for curing, two methods, thermal and indirect microwave heating, were used. Indirect microwave heating was used to avoid arcing in CFs. Design of CF volume fraction was done based on dielectric constant (ε') and dielectric loss tangent ($\tan \delta$). The dielectric constant value was increased from 122.87 to 268.23 with volume fraction (V_f) 20% – 70% at constant frequency, i.e., 2.45 GHz. This showed that CF has ability to absorb microwave. The multidirectional CFRC laminate was fabricated with optimized V_f (50%). For the determination of the effectiveness of curing

process, mechanical properties of fabricated laminates were compared. The marginal improvement in compressive strength (4.8%) and interlaminar shear strength (ILSS ~7.2%) was observed in indirect microwave cured laminates (Li et al. 2018).

Park et al. (2019) investigated the mechanical properties (tensile strength, Young's modulus, flexural strength and modulus) of the microwave cured CF composites and further compared them with compression molding fabricated composites. In this study, microwave input power and curing/processing time effect were selected as the processing parameters. Mechanical testing (tensile and three-point flexural test) was conducted of the composites. At low microwave power (200 W) and 60 min processing time, inferior mechanical properties were observed compared to conventionally cured samples. This could be correlated to insufficient curing of matrix; therefore, weak adhesion was obtained between fiber mat and matrix. At higher microwave power (400 W and 700 W) with the same curing time, mechanical performance was enhanced. Comparable mechanical properties were obtained with microwave and conventionally cured samples with a significant reduction in curing time. The curing time was 60 min and 360 min of microwave and conventional cured samples, respectively. The void content and void ratio were decreased with increased power with constant time, as shown in Fig. 1. This study concludes that microwave curing can be considered an efficient alternative to conventional curing methods to reduce the composites' energy cost and overall fabrication cost (Park et al. 2019).

Kwak et al. proposed a method to predict maximum penetration depth in CFRPCs during microwave curing. The operating parameters and tool design (fixtures) can enhance fabricated composites' quality with repeatable consistency. In this study, polyacrylonitrile (PAN)-based unidirectional CF was selected as reinforcement material and epoxy as a matrix for fabrication of composite laminates. The thickness of the four-ply laminates was 2.4 mm. To avoid sparking, epoxy tape was used at the edges of the CFs during microwave exposure of stacked laminates. After stacking of laminates in vacuum bagging kit, thermal as well as microwave curing was carried out to compare the laminate properties. To control the microwave power level and

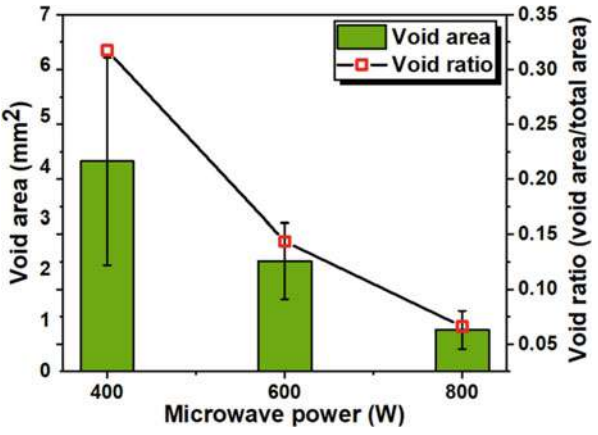

Fig. 1 The void area and void ratio variation with microwave power at constant processing time. (Data source: Park et al. 2019)

curing time, temperature measurement analysis was carried out using fiber-optic temperature probe. The depth of penetration was measured using a methodology, in which a thin-walled cylinder (made of high conductive material, i.e., aluminum) was filled with water. Further, exposure of microwave energy through perforated hole with constant microwave power of 1000 W and time of 10 min thermal gradient of water and laminate was measured using thermal imaging camera. To attain minimum change in temperature of water (<0.3 °C), various tests (with or without perforated hole) were conducted with variation of laminate thickness. Thus, reported method can be used to measure depth of penetration across the thickness for composite materials. The tensile, compression (ply lay-up: 0°/90°), in-shear plane (ply lay-up: ±45°), and indentation test were carried out for analysis of mechanical properties. The improvement in compressive strength, comparable ultimate tensile strength and small deviation in shear strength, and longitudinal and transverse elastic modulus of microwave cured samples were observed with reference to thermally cured samples (Kwak et al. 2015). In another study, Maenz et al. (2015) fabricated GFRCs using resin transfer molding (RTM) with the help of microwave and thermal heating. In this study, bidirectional roving mesh was used. Further comparison of mechanical properties was carried out based on heating method. Results showed similar mechanical properties. The improvement in heating time and production efficiency was found for microwave heating. The ash fragments of laminates after burning of samples in oven were used for porosity measurement. The average porosity was 1.1% ± 0.9% and 1.0% ± 1.2% for microwave cured and thermally cured, respectively (Maenz et al. 2015). To consider the advantage of cyclic heating and cooling with high rate in microwave curing, the CFRPCs were fabricated with 35.7% fiber volume fraction. Residual stresses in composite were measured with respect to change in stress level at fiber and matrix interface. This was attributed to difference in thermal expansion of the fiber and matrix. To reduce residual stresses, concept of alternate heating and cooling was proposed. The proposed method was based on heat transfer, curing kinetics, and residual stress formation (Li et al. 2017). The proposed method was similar to multistep curing method (Xu et al. 2015). In this study, effect of room temperature curing was compared with microwave and thermal curing of GFRCs. The custom-designed multimode microwave applicator with frequency of 2450 MHz and 1.2 kW was used (Rao et al. 2006). Some studies suggested that the interfacial adhesion of fiber and matrix could be improved by microwave heating. The chemical reaction and selective heating were identified and confirmed with the analysis of Fourier transform infrared spectroscopy (FTIR) for the same. The shear strength increased by 1.52 times and processing time decreased by 0.5 times positively with microwave heating than thermal (Zhou et al. 2016). The temperature measurement during the fabrication of composite is crucial. The temperature profile ensures the degree of cure of epoxy, which simultaneously affects mechanical properties of FRPCs. How the temperature profile can influence mechanical and structural performance was described in this study. The curing kinetics was similar in microwave and thermally cured. The results showed improvement in interlaminar shear strength (ILSS) and flexural but smaller decrease in tensile and compressive properties of microwave cured laminates. The SEM analysis of fractured surface

showed difference in matrix fiber interface of microwave and thermally cured samples. Although curing kinetics were the same, there was a significant difference in the heating/curing rate. This study concludes that the optimum heating rate may influence the mechanical performance of composite laminates (Hang et al. 2017). The short fibers were also in demand because of fabrication ease and being economically efficient. Sato and Hotta (2015) investigated the effect of microwave curing on composite. The short fibers were used to fabricate composite, and curing was done in three different ways, i.e., room temperature, thermal, and thermal with microwave curing. The random dispersion of short fibers was observed using SEM images. The fractured surfaces after flexural test were observed using SEM. In room temperature cured composite, fibers easily come out from epoxy matrix with clean and smooth surface. It indicated poor adhesion between fiber and epoxy. The presence of epoxy residue on fibers and attachment of fiber with epoxy matrix were observed in thermally cured and microwave cured laminates. It indicated better interfacial adhesion. The mechanical properties were well correlated with the SEM analysis (Sato and Hotta 2015). The summary of previous studies which were performed to investigate the mechanical and physical properties of the FRPCs has been presented in Table 1.

Improvement in interfacial properties of CF and matrix was done through surface treatment of CFs using microwave irradiation. The fiber/matrix interface adhesion is critical and can be improved with proper interaction between fiber and matrix and better fiber surface wettability with matrix. Presence of surface functional groups and active surface area are the dominating factors that improve the adhesion properties.

Fabrication of Thermoset Polymer Composites

Fiber reinforced polymer composites (FRPCs) are fabricated using different fibers as reinforcement and polymers as matrix materials. Fibers are available as short, continuous, woven (unidirectional, bidirectional), braided, etc. The selection depends upon application of the composite. The matrix material not only binds the fibers but also protects them from external atmosphere.

Matrix-Fiber Material

Matrix material is the component that holds the reinforcement (fibers) in the FRPCs. It is a homogeneous and monolithic material that surrounds the fibers. Various kinds of polymers available are used as matrix materials in FRPCs, depending upon applications. Broadly polymer matrix material is classified into two categories: thermoplastic and thermoset polymers. Thermoset polymer such as polytetrafluoroethylene (PTFE) and polyether ether ketone (PEEK) required heat to become moldable at glass transition temperature.

Table 1 Summary of FRPCs based on fabrication, curing method, and its properties

Fiber type	Volume fraction (V_f)	Fabrication method	Curing method	Properties	References
CF	57.56	Vacuum bagging	Microwave and thermal	Degree of cure, molecular structure, T_g and compressive strength	Xu et al. (2015)
CF	63	Vacuum bagging	Autoclave	Fatigue properties	Gamstedt and Talreja (1999)
GF and CF	–	Hand lay-up and vacuum bagging	Thermal	% elongation at break and tensile modulus	GuruRaja and HariRao (2013)
GF	55	Hand lay-up		UTS and stiffness, fatigue test	Ferdous et al. (2020)
GF	38.8	RTM	Microwave and thermal	Tensile strength, flexural strength and modulus, impact strength, degree of cure	Maenz et al. (2015)
CF	35.7	–	Cyclic microwave curing	Residual stress analysis	Li et al. (2017)
GF	62	Wet lay-up	Microwave, thermal, and room temperature	ILSS, T_g, and tensile strength	Rao et al. (2006)
CF	50	Hand lay-up with vacuum bagging	Indirect microwave and thermal curing	Degree of cure, compressive strength, and ILSS	Li et al. (2018)
GF	–	Vacuum bagging	Microwave and thermal	Flexural strength and modulus	Boey and Lee (1991)

On the other hand, thermoset polymers (resin) are initially viscous liquid at room temperature. The curing process in these materials starts either due to heating or through addition of curing agent, therefore causing well-defined irreversible network between its chemical components known as cross-linking. Thus cross-linking converts thermoset into a rigid and robust structure. Examples of thermoset polymers are epoxy, unsaturated polyesters, and phenolics.

Epoxy is one of the most commonly used matrix materials for the fabrication of the FRPCs. It has low viscosity and is capable of bearing high temperatures up to 200 °C. There are two basic categories of epoxy, glycidyl and non-glycidyl. Glycidyl comes under the category of glycidyl ether, glycidyl amine, and glycidyl ester. The non-glycidyl is either aliphatic or cycloaliphatic. The most common type of epoxy used commercially is a bisphenol, which comes under glycidyl ether. Bisphenol-A diglycidyl ether (DGEBA) is a type of epoxy resin with the lowest molecular weight.

Epoxy resin starts cross-linking when mixed with the cross-linker (hardener) such as amine-based, polyamide, aliphatic, and cycloaliphatic. The cross-linking also depends on the temperature and pressure conditions. An increase in temperature generally increases the curing rate of epoxy and hence results in high degree of cure.

The reinforcement used in the FRPCs is synthetic or natural fibers. These fibers generally provide strength and stiffness to the composite material. Fibers give the directional properties to the composite. If the composite is designed to bear only tensile load, then fibers can be placed only in one direction. Multidirectional fibers in the composite can result in isotropic properties. The ultimate properties of the composite depend not only on the properties of the fiber and matrix material but also on the interfacial bonding between them. Poor bonding can result in the delamination of the fibers. Woven fibers are generally made in the form of unidirectional and bidirectional mats. FRPCs with unidirectional laminate can have stacking sequences, which provide optimum strength and stiffness at low weight.

Most of the high-strength fibers are synthetic fibers. For example, carbon fiber has a very high strength value with significantly less weight; therefore, it is a prominent material to fabricate composite for aerospace, automobile, and sports industries. Aramid is another synthetic material used for making body armors due to its high impact energy-absorbing capacity. Natural fibers such as jute, coir, flex, etc., are used to fabricate composite for low load applications. But the cost and environmentally friendly nature of these fibers make them essential for the fabrication of FRPCs.

Effect of Stacking Sequence and its Orientation

The stacking sequencing of fiber mat is an important parameter to decide final properties of fabricated composites. There are different possible combinations of ply sequencing, such as unidirectional, cross-ply, sandwich-like, quasi-isotropic, etc. Fibers can be oriented in different directions during fabrication of the composites. Orientation decides the directional-specific properties of the composites. In the short fibers, it isn't straightforward to orient the fibers in a particular direction, resulting in more isotropic properties of the composites.

Fabrication Methods

There are various composite fabrication methods in the industries. The fabrication method depends on the material, design, and application of the composites. The properties of the FRPCs much depend upon the type of fibers (long, short, particulates) and their orientation in the matrix phase during the fabrication process. Proper fabrication methods play an essential role in the overall performance of the FRPCs.

Broadly fabrication methods are categorized for continuous fiber, and short fibers are shown in Fig. 2. For both types of fibers, mainly two types of fabrication methods are used: open mold fabrication and close mold fabrication. There are other special

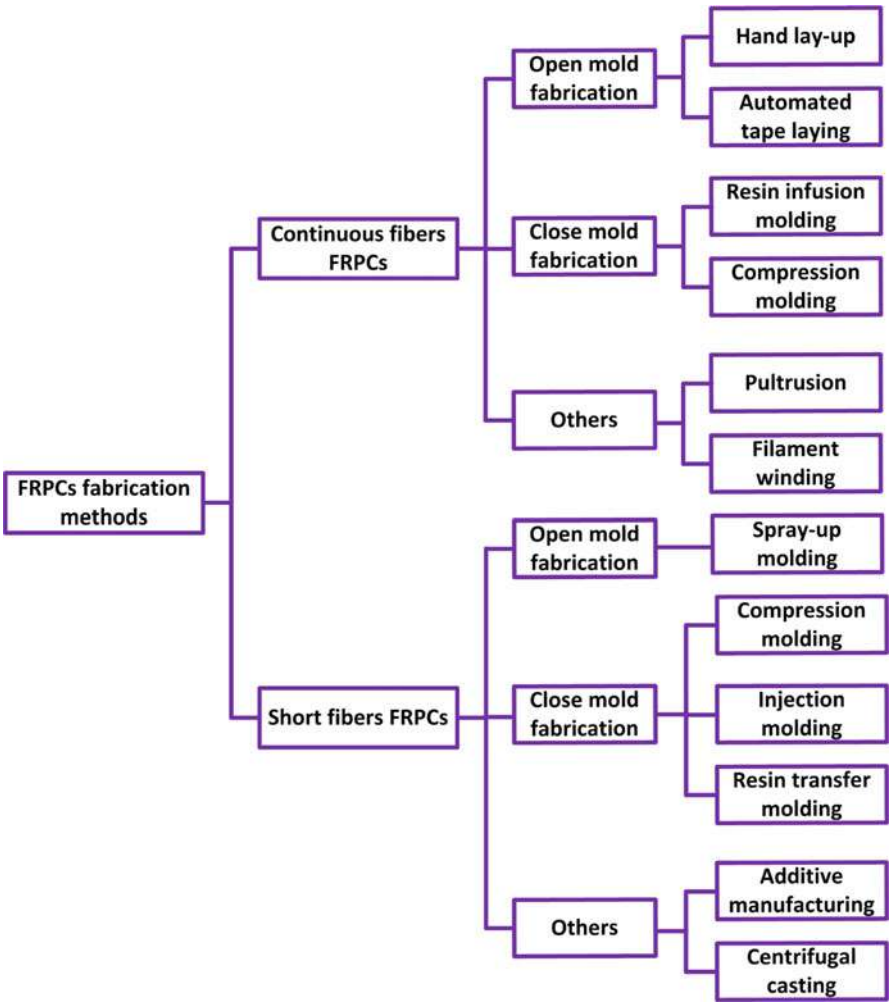

Fig. 2 Various fabrication methods used to fabricate FRPCs

types of fabrication methods used to fabricate FRPCs. The detailed fabrication methods are discussed below.

Open Mold Fabrication

Open mold is a low-cost fabrication method of FRPCs. This method includes hand lay-up, automated tape laying, and spray-up molding techniques. These methods are used to produce boats, truck cabs, fenders, tubs, showers, etc.

Hand Lay-Up Process

In the hand lay-up process, fiber mat is placed on the mold by hand, and a roller is used to spread the resin over the fiber mat as shown in Fig. 3. This is a manual

process for the fabrication of FRPCs. It is the least economical process and therefore used widely to fabricate composite materials with any reinforcing materials (long fibers, chopped fibers, and particulates). In this process, it is difficult to maintain the exact fiber to resin ratio.

Automated Tape Laying

This process comprises automatic laydown of tapes (fiber with resin) in mold with the help of rollers. This process can be used for fabrication of larger composites with higher speed and high accuracies. Stacking orientation can be changed automatically.

Spray-Up Molding

This method comprises a handgun, which sprays a mixture of resin and chopped fibers to the mold cavity until the desired thickness of the laminate is achieved. It is then cured at room temperature. A roller is also used to roll the fiber-resin mixture, to remove entrapped air from the composite. This method can be used for fabrication of large-sized composites. The properties of final composite depend upon the fiber orientations. The schematic of spray-up molding is shown in Fig. 4.

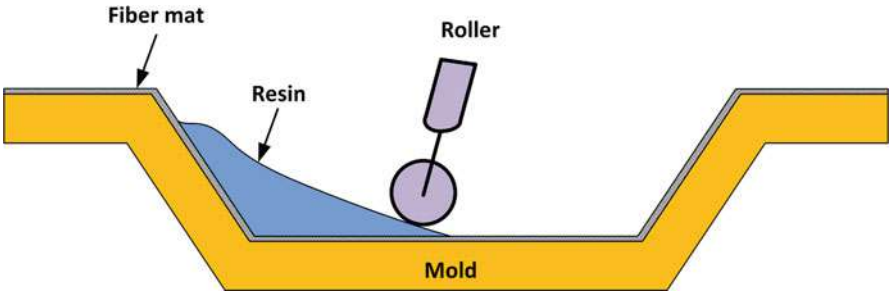

Fig. 3 Hand lay-up process for the fabrication of FRPCs

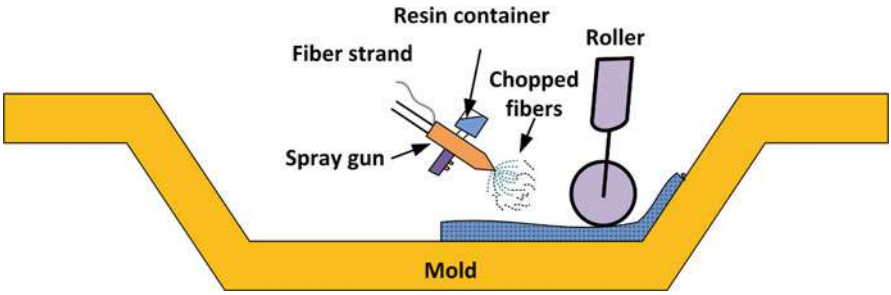

Fig. 4 Spray-up molding process for the fabrication of FRPCs

Close Mold Fabrication

In the close fabrication method, dry fibers are laid into the mold cavity, and resin can enter the mold using either pressure pump or vacuum pump. This method is known for its highly consistent fabrication process. A high production rate is ensured in this process due to reduced cycle time.

Resin Infusion Molding

The resin infusion process is also called a vacuum infusion process. In this process, dry fiber mat is first laid down in the mold cavity and vacuum is created in the cavity through vacuum pump. The resin is then sucked inside the fiber mat and is allowed to spread over it. It offers an optimized resin to fiber ratio due to constant vacuum pressure through vacuum hose pipe connected to vacuum pump as shown in Fig. 5.

Compression Molding

Compression molding is of two types: hot pressing and cold pressing. In hot pressing, mold charge is heated during pressing. Molding compounds and prepreg are generally hot pressed. Cold pressing results in curing of resin at room temperature. Parts made by hand lay-up process are generally cold pressed for better consolidation and better surface finish. This technique is used for both thermoset and thermoplastic polymer matrix composite materials. Mold consists of two parts, one cavity and a pressure plug, as shown in Fig. 6. Stacking of laminates is done inside the mold cavity and pressure is applied with the help of pressure plug. Adequate pressure ensures strong bonding between matrix and reinforcement. Hot compression reduces fabrication time of the composites and is generally used for the mass production of composites. The various advantages of this process are good reproducibility and dimensional accuracy. It has wide application in different industrial sectors, including the automobile industry.

Injection Molding

Injection molding is one of the most important techniques of manufacturing polymer composite parts. The schematic diagram (Fig. 7) shows that the pellets of polymer and fiber strands are mixed and fed to the hopper. A rotating screw advances the material through the barrel, where heaters are mounted to heat the material. After

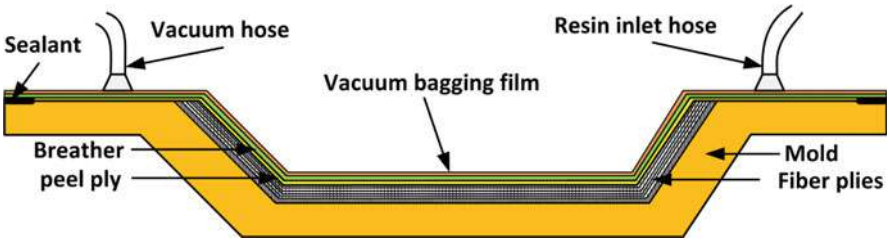

Fig. 5 Resin infusion process for the fabrication of FRPCs

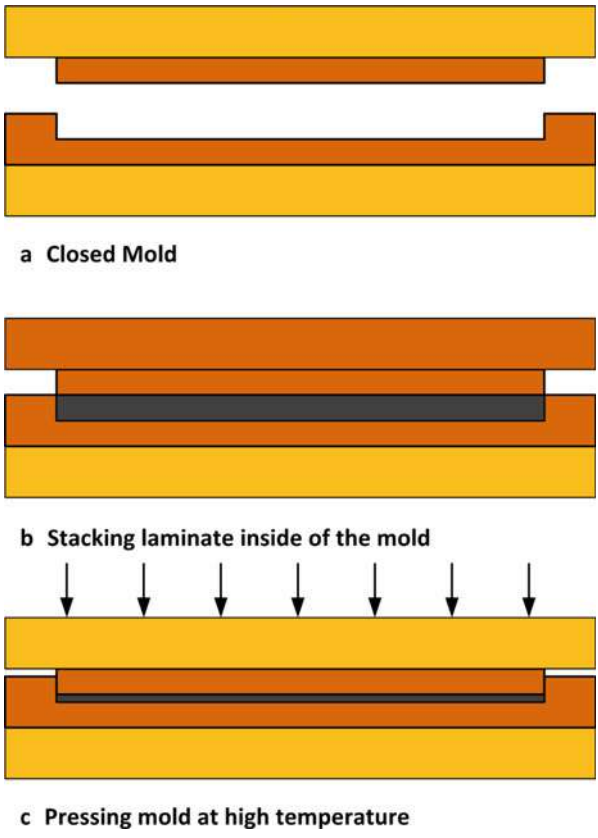

Fig. 6 Compression molding process for the fabrication of FRPCs

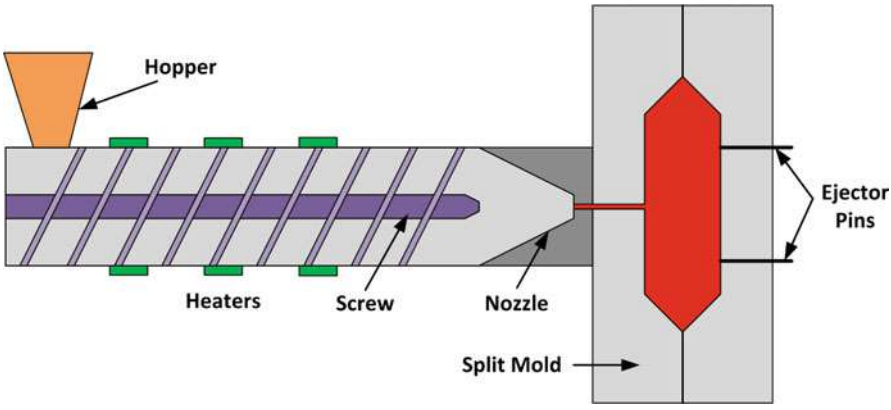

Fig. 7 Injection molding process for the fabrication of FRPCs

reaching the nozzle, material is pressurized to enter the mold cavity. Ejector pins are used to remove the composite after proper cooling. The parts produced by this method have exceptional physical and mechanical properties, but only short fiber composite can be fabricated using this method.

Other Fabrication Processes

Pultrusion

It is a continuous fabrication process of fiber reinforced composites. Uniform thickness is achieved in this process. This process is basically pulling the continuous fibers through polymer resin and curing at particular temperature. A very high-volume fraction can be achieved using this method, and this makes the process important for structural component manufacturing due to its high strength to weight ratio. Pultrusion is a widely used method to fabricate composites because of its low production cost and high production rate.

Filament Winding

Filament winding is similar to the pultrusion process. The only difference is that continuous fibers after impregnation are wound over the rotating mandrel. After adding sufficient layers of fibers on the mandrel, it is cured at a specific temperature. It can manufacture hollow and cylindrical components like storage tanks, pipes, pressure vessels, etc.

Additive Manufacturing

Additive manufacturing of FRPCs is known for its excellent capability to fabricate complex and customized parts. This method employs CAD files to fabricate layer-by-layer composites. High production rate can be achieved in this method.

Centrifugal Casting

In this process, chopped fiber is placed inside a rotating mold. Polymer resin is then added to it. The high rotational speed results in impregnation of the resin in the fibers. Due to centrifugal forces, void-free, high-strength FRPC can be fabricated using this technique.

Importance of Microwave in Fabrication

Heating accelerates the curing rate of polymer resin during fabrication of the composites. There is conventional method of heating the composite such as induction heating, coil heating, etc. These types of methods consume a lot of time and energy for the fabrication process. Microwave heating is an advantageous method that saves energy and a lot of time needed for fabrication process. Microwave is known for its selective, volumetric, and instantaneous heating. Due to selective heating of microwaves, it heats only the target material, resulting in comparatively less energy consumption. Microwave interacts with the material at molecular level

and results in volumetric heating. As heating with microwave is uniform, it greatly reduces the chances of burning the composites' surface. Also, microwave provides clean energy transfer, without producing harmful by-products. Therefore, using microwave instead of conventional heating methods results in more economical way of composite fabrication. The temperature during microwave fabrication can reach even more than 2000 °C.

In case of FRPCs, microwave curing results in strong resin-fiber bonding due to high degree of curing. The density of the composite also increases due to less void formation during fabrication processes. Uniform heating of composite results in less thermal stresses induced in the composites. Many researchers have found high mechanical properties (tensile, flexural, interlaminar shear stress, etc.) of composites fabricated using microwave energy compared to thermal curing techniques.

Microwave Heating and Curing Mechanism

Electric field present in the electromagnetic radiation in the microwave frequency is mainly responsible for generating heat in the FRPCs. There are two modes of microwave heating: dipolar rotation and ionic conduction. Ionic conduction is more dominant in the case of conducting metals such as aluminum, copper, etc. In case of the polymer, dipolar rotation is the main cause of heat generation under microwave exposure. The ability to absorb microwave energy by different fibers and polymer resin is dependent on their dielectric properties (dielectric constant and tangent loss). Figure 8 shows the microwave heating mechanism of carbon fiber reinforced polymer composites (CFRPCs), glass fiber reinforced polymer composites (GFRPCs), and aramid fiber reinforced polymer composites (AFRPCs). Carbon fiber is known for

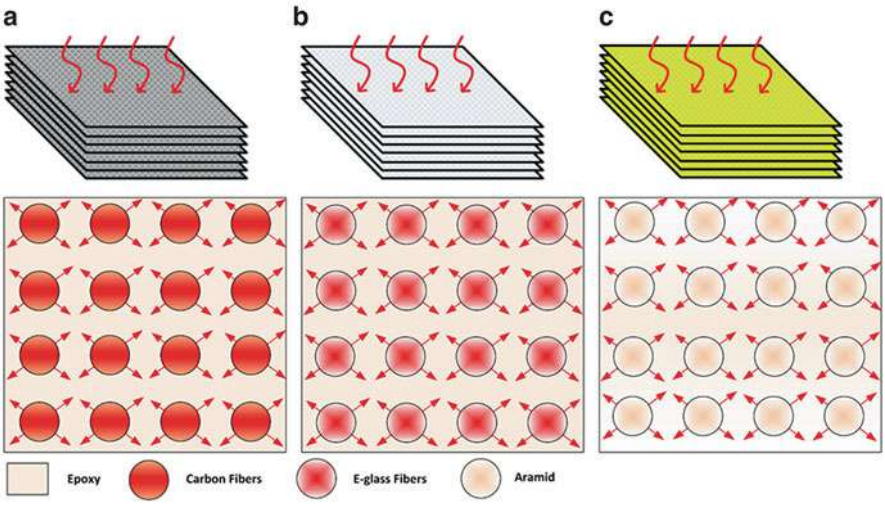

Fig. 8 Shows heating mechanism of (**a**) CFRPCs (**b**) GFRPCs (**c**) AFRPCs

Table 2 Dielectric properties of some fiber materials (Zoughi and Zonnefeld 1991)

Types of fibers	Dielectric constant	
	Horizontal polarization	Vertical polarization
Carbon fiber	29.4 ± 0.16	26.6 ± 0.2
Glass fiber	5.19 ± 0.6	17.8 ± 0.09
Kevlar	3.40 ± 0.05	4.63 ± 0.07

high microwave energy-absorbing capacity due to greater tangent loss values. During fabrication of the CFRPCs under microwave, heat is first generated in the carbon fiber and transferred to the nearby resin due to conduction. Thus, temperature near the fiber is more. In case of the GFRPCs, there is considerable difference in the dielectric properties of fiber and resin. Therefore, heating is more uniform. The aramid fiber in AFRPCs has low microwave absorbing capacity and resulted in more uniform temperature distribution along the composite. The values of dielectric constants for various fibers at 8 GHz frequency are shown in Table. 2.

Uniform heating of the composites generally results in better mechanical properties. This is because temperature gradient results in less cure of resin, more void generation, and induced stresses in the composite material. Different microwave power levels can be utilized to ensure more heating uniformity in the polymer composites.

In the case of matrix material such as epoxy and an amine, microwave exposure results in internal heat generation by the polar molecules. This heat accelerates the cross-linking reactions in the resin, and curing time is reduced.

As the microwave energy is absorbed by the composite material and dissipated as heat energy, the electric field energy is attenuated as it passes through the dielectric material. It is imperative in processing multi-ply (thick) composites. It is necessary to know how the electric field decreases as a function of distance from the surface into the sample. The penetration depth, defined as the distance from the surface where the power transmitted through the material has been reduced by a factor of 0.37 (1/e), is given by eq. 1:

$$d = \frac{C}{2\pi f \varepsilon_R' \tan \delta} \tag{1}$$

where C is the speed of light, f is frequency, ε_R' is relative dielectric constant of the material, and tan δ is loss factor of the material.

The typical value of the penetration depth for cured epoxy is around 30 cm.

Characterization Techniques of FRPCs

Tensile Test

Uniaxial tensile testing is performed to find out ultimate tensile strength, tensile modulus, percentage elongation at break, and reduction in the area of composite laminates. By these results, one can predict the behavior of material under different

loading conditions and for different applications also. The preparation of specimens was done according to ASTM standard 3039. The universal testing machine (UTM) was used for the testing. The machine's maximum load capacity was 100 kN with speed rate (crosshead) of 2 mm/min (GuruRaja and HariRao 2013; Maenz et al. 2015). While in another study, the tensile test was conducted according to ASTM D368 with crosshead speed of 5 mm/min. The gauge length of specimens was kept 50 mm (Tanrattanakul and Jaroendee 2006).

The tensile modulus (36.05 GPa) and elongation (1.33%) of the hybrid composite (GF/CF/matrix) were maximum for ply lay-up sequence of 0°/90° except other (±45° and 60°/30°) (GuruRaja and HariRao 2013). Maenz and coworkers performed tensile test of GFRCs. The reported tensile strength was 363 ± 34.4 MPa and 339 ± 42.7 MPa for microwave and thermally cured laminates (Maenz et al. 2015). The tensile strength of microwave cured GFRCs increased by 1.2 times compared to thermally cured (Rao et al. 2006). SEM analysis was done to observe porosities, delaminations, fiber misalignment, matrix cracking, fracture line formation, fiber pull-out, and fiber matrix interface (GuruRaja and HariRao 2013). In another study also, the tensile strength and tensile modulus were higher in microwave curing, while percentage of elongation decreased. The improvement in properties could be related to fiber matrix adhesion. At an optimum power level, the viscosity of epoxy was increased gradually. This increased wettability between fiber and matrix and thus helps to improve adhesion between fiber and matrix (Tanrattanakul and Jaroendee 2006).

Flexural Test of FRPCs and their Properties

A three-point bending test was performed to determine the flexural strength and flexural modulus of the FRPCs. The dimensions of the rectangle specimen were 120 mm long and 25 mm in width. The distance between supports and punch speed was 100 mm and 2 mm/min, respectively. The basic equations can be used to calculate flexural strength, flexural strength, and flexural modulus which were given elsewhere (Park et al. 2019). Boey and Lee (1991) conducted four-point bending test over three-point bending test. It is more precise and avoids direct intimation of loading fixtures on the failure-prone area. One more advantage was included that examines both tensile and compressive failure together. The test was conducted according to ASTM standard D-790-1. The distance between supports and thickness ratio was 32 (Boey and Lee 1991).

The composites' flexural properties in terms of flexural strength and modulus were 403 ± 46.5 MPa and 9.94 ± 0.86 GPa, respectively, for RTM-based microwave cured samples. Similar properties were also observed for thermally cured samples (Maenz et al. 2015). In another study, slightly lower flexural strength was reported for RTM-based thermally cured laminates with 50% volume fraction (Abraham et al. 1998). The flexural modulus was improved by 20% for microwave cured laminates. The decrease in flexural strength was reported due to insufficient wetting of fibers with epoxy. Further debonding of fiber and epoxy was propagated after matrix cracking (Boey and Lee 1991). In another study, inferior flexural strength and modulus were reported for microwave cured composites compared to autoclave cured. After analysis

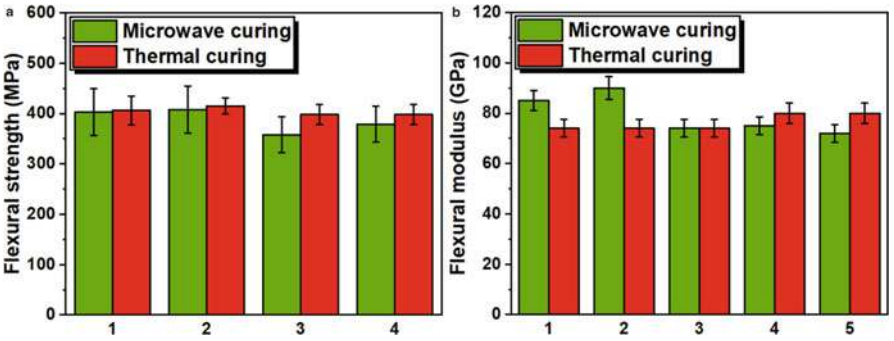

Fig. 9 Comparison of flexural strength and flexural modulus of microwave and thermally cured fiber reinforced epoxy composites. X-axis is representing reference. (Data source: Fig. 9 (**a**) 1 (Maenz et al. 2015), 2 (Abraham et al. 1998), 3, 4 (Nightingale and Day 2002). Figure 9 (**b**) 1, 2, 3 (Boey and Lee 1991); 4, 5 (Nightingale and Day 2002))

of previous studies, flexural strength and flexural modulus data of thermal and microwave cured composites are reported as shown in Fig. 9.

Impact Test of FRPCs and their Properties

Impact strength of the material is the measure of the resistance of material against suddenly applied force or load. The impact strength of composites can be measured by Izod and Charpy impact test. The impact behavior, energy absorption capability, and impact toughness of composite can be determined using an impact test. The impact test is categorized according to impact velocity as shown in Fig. 10.

For the Charpy impact test of GFRCs, DIN EN ISO 179-1 and ASTM D6110 standard are used. For the notched Izod impact test, ASTM D256 standard is used. The thickness of the specimen was 3.5 mm. The impact strength was reported to be 150 kJ/m^2 and 125 kJ/m^2 for microwave and thermally cured GFRCs (Tanrattanakul and Jaroendee 2006). In another study, impact strengths of 188.5 $\pm$ 21.8 kJ/m^2 and 190 $\pm$ 16.8 kJ/m^2 were reported for microwave and oven cured CFRPC laminates (Maenz et al. 2015). The comparison of impact strength is shown in Fig. 11.

Generally, fracture of fiber was observed with high impact energies, while matrix cracking and plies' delamination were observed with low impact energy. GFRPCs are less susceptible to impact loads compared to CFRPCs. CFRPCs are more brittle and tend to ease fracture, resulting in decreased stiffness and strength of composite laminates.

Interlaminar Shear Strength (ILSS)

To evaluate the interfacial properties of FRPCs, the ILSS was performed. In several components which are used in aerospace and marine industries, the ILSS is a critical

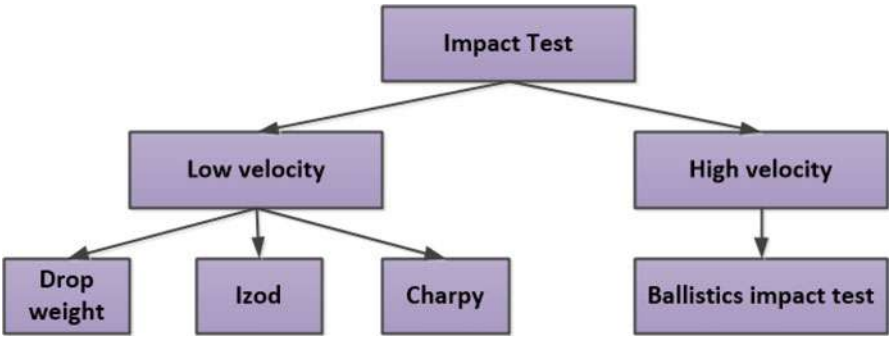

Fig. 10 Classification of impact test based on impact velocity

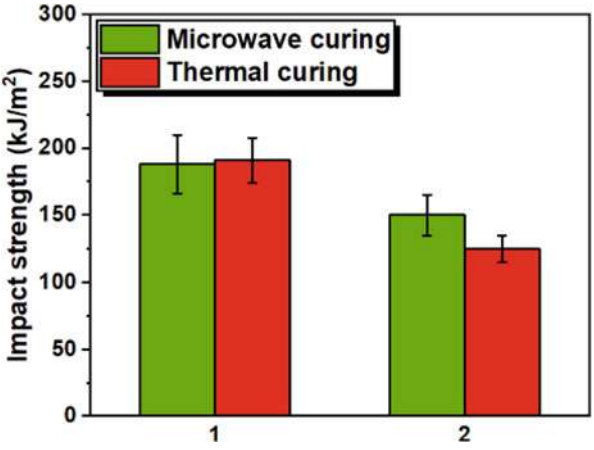

Fig. 11 Comparison of impact strength of microwave and thermally cured fiber reinforced epoxy composites. The X-axis is representing reference. Data source: 1 (Maenz et al. 2015), 2 (Tanrattanakul and Jaroendee 2006)

design criterion. The short beam shear method was used to determine the ILSS according to ASTM standard D 2344/D2344M. The equipment Instron Series IX Automated Material Tester software was used. The ILSS can be determined by using the formula which is given elsewhere (Rao et al. 2006). Many researchers have explored and proposed microwave curing as an effective process to improve the ILSS of FRCs. The improvement in ILSS of microwave cured laminates was 1.35 times of thermally cured laminates (Rao et al. 2006). Li et al. and coworkers (2018) used indirect microwave heating to fabricate CFRCs. The increment in ILSS was observed to be 7.2% against conventional thermal oven cured samples (Li et al. 2018). To validate the improvement in ILSS values, SEM analysis was carried out of fractured surfaces.

The evidence of epoxy residues on slight pull-out fibers indicated good adhesion of fiber and epoxy. Simultaneously, smooth fiber surface (no epoxy residues) indicated low adhesion properties and wettability. Further, some oxygen-containing functional groups could help to improve the surface energy of the fibers and the

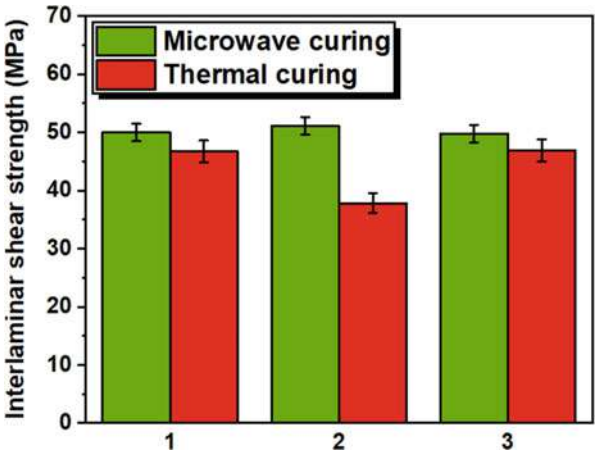

Fig. 12 Comparison of interlaminar shear strength of microwave and thermally cured fiber reinforced epoxy composites. X-axis is representing reference. Data source: 1 (Li et al. 2018), 2, 3 (Rao et al. 2006)

wettability behavior of fiber and epoxy. The comparison of ILSS has been summarized in Fig. 12. For microwave cured CFRP composites, the increment in ILSS was obtained. The enhancement in ILSS was correlated with change in viscosity during the initial stage of microwave curing. The low viscosity impregnated the fibers before curing and increased fiber to matrix bonding strength. Further, enhancement in ILSS was correlated with blunting of crack tip due to extended plastic deformation. The phenomena of plastic deformation can be observed through the presence of resin amount in between fibers. Using SEM microstructural analysis, amount of resin was higher for microwave cured composites compared to thermally cured composites. That also confirms better interfacial bonding between fibers and matrix for microwave cured composite laminates (Papargyris et al. 2008).

Fatigue Test of FRPCs

Most often, all engineering structures are subjected to cyclic loading conditions in their service life span. Fatigue is considered a continuous and progressive damage process of materials or structures. The initial level of fatigue is at microscale cracks, and with time, it converts or progresses to macroscale cracks. This happens due to micro-crack accumulations and further leads to complete failure of materials or components. The common factors that affect a material's fatigue properties are mechanical loading, thermal loading, and environmental conditions. The fracture mechanics of composites during fatigue loading are shown in Fig. 13. Composite system properties such as fiber/matrix material properties, volume fraction (V_f) of fiber, stacking sequence of fiber mats (Dong et al. 2016; Gamstedt and Talreja 1999), ply orientation, residual stresses, stress ratio, stress concentration, frequency, and manufacturing methods influence the performance of composites in a fatigue test.

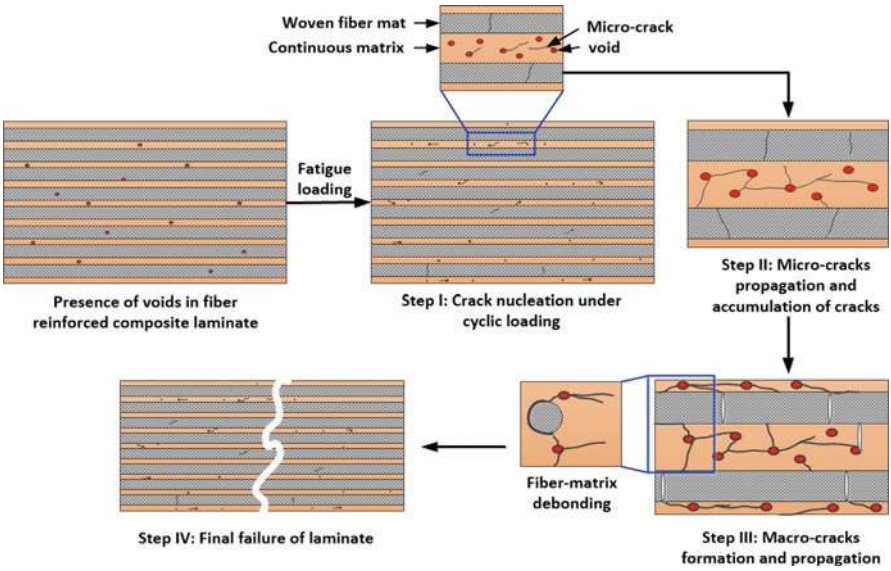

Fig. 13 Schematic diagram of possible composite failure mechanism under different loading conditions

For the fatigue test, the dimensions of the specimen were 127 mm × 12.7 mm × 0.5 mm (gauge length, width, and thickness) according to ASTM standard D3039. The fatigue test was performed on Instron 1272 tensile machine with the following parameters: stress ratio of 0.1, frequency of 10 Hz, and sinusoidal loading (Gamstedt and Talreja 1999). In another study, the effect of stress ratio, stress concentration, and frequency on GFRCs was investigated during the tension-tension fatigue test. Stress ratio and frequency were in the range of 0.25–0.80 and 2–8 Hz. The test was stopped either at the failure of specimens or the number of cycles (8×10^6). The specimens subjected to 1/4 times of UTS showed an infinite life cycle (Ferdous et al. 2020).

In uniaxial tension-tension fatigue loading, when the composite is subjected to the fiber direction, the failure of the composite depends on the stress ratio. In previous studies, the primary failure mechanisms (fiber cracking, matrix cracking, and fiber-matrix debonding) of composites are described in detail (Harris 2003; Talreja 1981). A possible mechanism of composite failure was shown in Fig. 13. A similar damage mechanism of chopped fiber mat/matrix composites was reported in another study (Owen and Howe 1972). Debonding in composites can be interpreted as a dark line between fiber and matric interface using SEM images. Fatigue properties of composite materials were successfully demonstrated by Talreja (1981) using fatigue-life diagram. A comprehensive analysis of several studies on multiaxial fatigue test of FRC laminates was reported by Quaresimin and coworkers (Quaresimin et al. 2010). Some important points like criteria to predict fatigue life, effect of design and fabrication parameters, evolution of damage, and understanding

of damage mechanics were discussed extensively. Initiation of micro-crack formation and propagation was observed after 3×10^6 and 8×10^6 cycles. Failure of laminates was random at any location. This was related to the inhomogeneity and anisotropic properties of laminates (Ferdous et al. 2020). Internal damage of FRCs can be due to matrix cracking, fiber cracking, debonding, and delamination. A similar theory was reported by others also (Harris 2003).

Damage Mechanism

Several damages and defects affecting FRCs can be categorized into manufacturing defects and in-service defects. Some defects are porosities, fiber misalignment, cracks in fiber and matrix, residual stresses due to large thermal gradient during fabrication, and formation of micro-cracks in fiber and matrix due to internal damage (De Luca and Caputo 2017). The failure mode analysis of FRPCs is an important phenomenon to get insight into causes of failure in FRPCs fabricated by different fabrication methods. There are four modes of failure reported in previous studies: (i) matrix cracking, (ii) fiber fracture, (iii) fiber/matrix debonding, and (iv) delamination (Quaresimin et al. 2010). Generally, there are two types of fracture, i.e., ductile and brittle fracture. High deformed surfaces and ribbons indicate ductile fracture, and a smooth matrix fracture surface indicates brittle fracture. Kwak et al. (2015) analyzed the fractured surface of microwave and oven cured composite and found that fiber disbanding and interfacial debonding were predominant in oven cured specimens. In microwave cured laminates, SEM images showed that almost all fibers were entirely covered with epoxy except a few. This was attributed to matrix and fiber failure for the same (Kwak et al. 2015). Some other studies also reported that the failure mode in microwave cured samples was a type of mix mode or multiphase failure (fiber and matrix failure).

Fourier Transform Infrared Spectroscopy (FTIR)

Fourier transform infrared spectroscopy (FTIR) is a vibrational spectroscopic technique, which may be used to study fiber reinforced composites for fiber identification, to detect organic matrix left, even after a very long time. FTIR is also found to be suitable in studying the effect of degradation on polymer composites at the molecular level. The cure characteristics of epoxy resin in fiber reinforced composites can be easily understood by using this technique. The resin curing characteristics under thermal heating and microwave heating are shown in Fig. 14 (Xu et al. 2016). Curve (a) shows the uncured peaks of epoxy ring at 908 cm^{-1}. The intensity of peak is found weak for both thermally cured and microwave cured composites. It suggests that epoxy group takes part in the curing reaction. Although both thermal and microwave curves have almost all the peaks at the same wavenumber, the peaks at 1365 cm^{-1} (bis-methyl symmetric deformation vibration of bisphenol-A) and 510–400 cm^{-1} (fingerprint region) are different. Also, a peak at 800–825 cm^{-1}

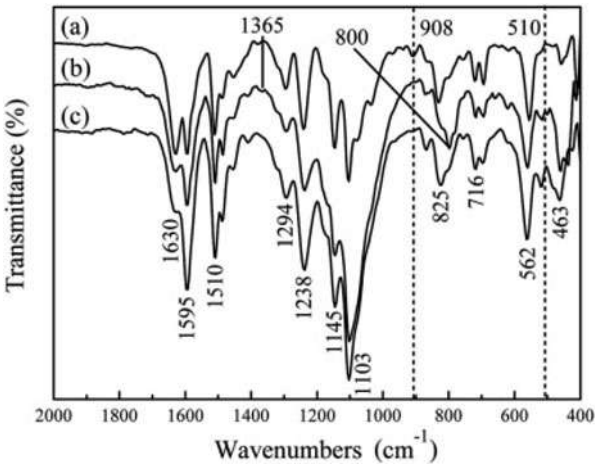

Fig. 14 FTIR spectra of (**a**) uncured, (**b**) thermally cured, and (**b**) microwave cured CFRPCs. (Reprinted with permission from (Xuehong Xu et al. 2016)©)

(benzene ring) has shown that microwave curing can change the methods of cross-linking and network structures in the fabricated composites. One other study was done to compare the FTIR results of microwave cured and thermally cured composites (Wu et al. 2017). The results reveal that more hydroxyl groups were present in thermally cured composites compared to the microwave cured composites. The hydroxyl group is responsible for forming hydrogen bonds due to the small size of oxygen and its high electronegativity. So, thermally cured composites result from more compaction and less small holes than microwave cured composites.

Differential Scanning Calorimetry (DSC)

Differential scanning calorimetry (DSC) monitors heat effects associated with phase transitions such as glass transition, melting, and crystallization. DSC is a thermal analysis technique in which heat flow into or out of the material is measured as a function temperature. DSC can be used for a wide range of materials, including composites, laminates, polymers, resins, adhesives, organic materials, chemicals, and biological samples. The properties of polymers such as glass transition temperature, specific heat capacity, cure process, and cross-linking degree linking in the resin and thermal stability can be evaluated using DSC. A small sample of 1 mg – 15 mg is placed inside a closed crucible in DSC study and placed inside a temperature-controlled DSC cell. Another empty crucible is used as a reference. The DSC run typically involves heating/cooling the sample at a controlled, steady state and examines the heat flow for characterizing the phase transition and cure reactions as a function of temperature. Other studies can involve multi-heating/cooling steps and isothermal mode. Figure 15a shows the DSC curves uncured carbon fiber laminates. The cross-linking of epoxy is an exothermic reaction, which means heat is evolved during curing process. The peak shows total heat

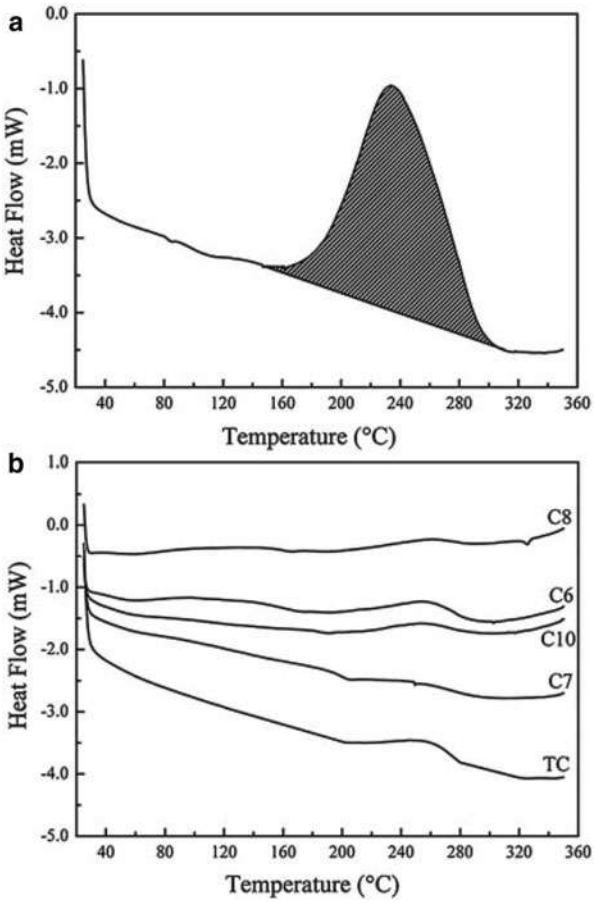

Fig. 15 DSC graphs of (**a**) uncured laminates (**b**) cured laminates. (Reprinted with permission from (Xuehong Xu et al. 2016)©)

evolved during the curing process and can be used as a reference to measure the degree of cure of the fabricated composites. Fig. 15b shows DSC curves for thermally cured (TC) and microwave cured specimens (C6, C7, C8, and C10) at different power conditions (Xu et al. 2016). The fully cured specimen will form no peaks in the curve, which means no further heat will be evolved. The small peaks in the curve indicate traces of uncured resin in the composites. It can be understood from the curve that microwave cured specimens have a low peak compared to the thermally cured composite. The exact value of the degree of cure can be calculated by using eq. 2:

$$\text{Degree of cure } (x) = \left(1 - \frac{\Delta H_x}{\Delta H_{\text{Ref.}}}\right) \times 100 \tag{2}$$

where ΔH_x is the residual exothermic enthalpy of the cured specimen in (J/g) and $\Delta H_{\text{Ref.}}$ is the total curing enthalpy of the raw laminates (J/g).

Another DSC study (Li et al. 2018) was done to compare the degree of cure of carbon fiber composites cured by microwave and thermal heating. The exothermic peaks observed in the DSC curve for both types of cured composites have almost same modes. Therefore, the author concluded that all the composites were found completely cured, and less impact was seen in the microwave and thermally curing composite methods. Another group of researchers (Rao et al. 2020) has analyzed and compared the effect of microwave power on the variation of the glass transition temperature of epoxy composites. At 915 MHz and 2450 MHz microwave frequencies, equivalent cure characteristics of composites were found compared to the thermally cured composites.

Thermogravimetric Analysis (TGA)

Thermogravimetric analysis (TGA) is a technique in which mass specimens in a specified atmosphere are observed against time and temperature. It measures mass change in a specimen and recognizes oxidation, evaporation, and decomposition by changing temperature. One of the critical applications of TGA for the characterization of fiber reinforced polymers is to determine fiber volume fraction in the composite. Maintaining proper fiber volume fraction is essential for the quality control of composites to ensure their accurate mechanical and physical properties. In a study (Moaseri et al. 2014), different functional groups attached to carbon fiber were exposed to the microwaves. TGA analysis was done, and the weight loss of sample was plotted against temperature. The degree of functionalization was calculated to know the functionalization yield. At higher microwave power, the functionalization degree is considerably improved. Another TGA study (Tanrattanakul and Jaroendee 2006) was carried out on glass fiber composites cured by multiple microwave power levels. The one type of microwave cured composite showed a two-step degradation process and started degraded at 200 °C. Another microwave cured composite followed one-step degradation and started degradation at around 240 °C. It has been concluded based on TGA results that higher thermal degradation was found in composites with higher cross-linking densities.

Nuclear Magnetic Resonance (NMR)

Nuclear magnetic resonance (NMR) is a helpful analytical technique to characterize organic and polymer-based composites. The application includes the molecular structure of the material, content, and purity of the material. The output of NMR depends upon the interaction of the nuclear magnetic moment and the magnetic field. The proton in the molecule behaves differently in a different chemical environment.

The application of NMR in epoxy composites includes the degree of cure, water absorption, environmental degradation, and aging. A solid-state NMR spectroscopy of microwave and thermally cured epoxy resin was done (Wallace et al. 2006). Powder of cured epoxy, both microwave and thermal, was taken and packed into 7 mm alumina and zirconia rotors. Cross-polarization/magic-magic angle spinning was used to get the spectra. The result showed that intense peaks for epoxy resin at 45 and 50 ppm arise from CH and CH_2 epoxide carbon, respectively. The residual epoxide peaks were found larger in microwave curing than thermal curing epoxy. It has been concluded that epoxy-amine reaction is more dominating under microwave exposure than thermal curing.

Ultraviolet-Visible (UV-Vis) Spectrophotometry

Ultraviolet-visible (UV-Vis) spectrophotometry is a method, which estimates light absorbance across ultraviolet and visible bands of the electromagnetic spectrum. Materials have the property of absorbing, reflecting, and transmitting light wave incidents on them. The absorbance of light in the UV-Vis range causes atomic excitation, which results in the transition of molecules from a low energy state to a high energy state. UV-Vis spectrophotometer measures the intensity of light transmitted through the material in a given range of wave lengths. Beer-Lambert law states that the amount of light absorbed is directly proportional to the concentration of the sample and the path length through which light travels through the material. A study has shown the UV-Vis absorption spectra of epoxy composites (Malekshahinezhad et al. 2020). A substantial absorption threshold for both neat epoxy and epoxy composites was found near the UV region. The resulting cross-linking in epoxy results in almost blocking of light through it.

Scanning Electron Microscopy (SEM)

The scanning electron microscope (SEM) generates various signals at the solid specimen surface by focusing on a high-energy electron beam. The interaction of the electron beam and surface of material reveals information about the material, including external morphology, chemical composition, and structure. The typical range of scanned areas for conventional SEM techniques lies from 1 cm to 5 μm. The magnification ranges from 20X to 30,000X with a spatial resolution of 50 to 100 nm. Figure 16a–d shows the SEM images of tensile and flexural fractured surfaces of carbon fiber composites cured by microwave techniques. Figure 10e, f are SEM images of tensile and flexural fractured specimens cured by autoclave (Li et al. 2017). The better adhesion of fiber and matrix material can be seen in the microwave cured specimens, ultimately resulting in better mechanical properties. SEM results also reveal fracture in the composites, such as fiber fracture, matrix cracks, and debonding.

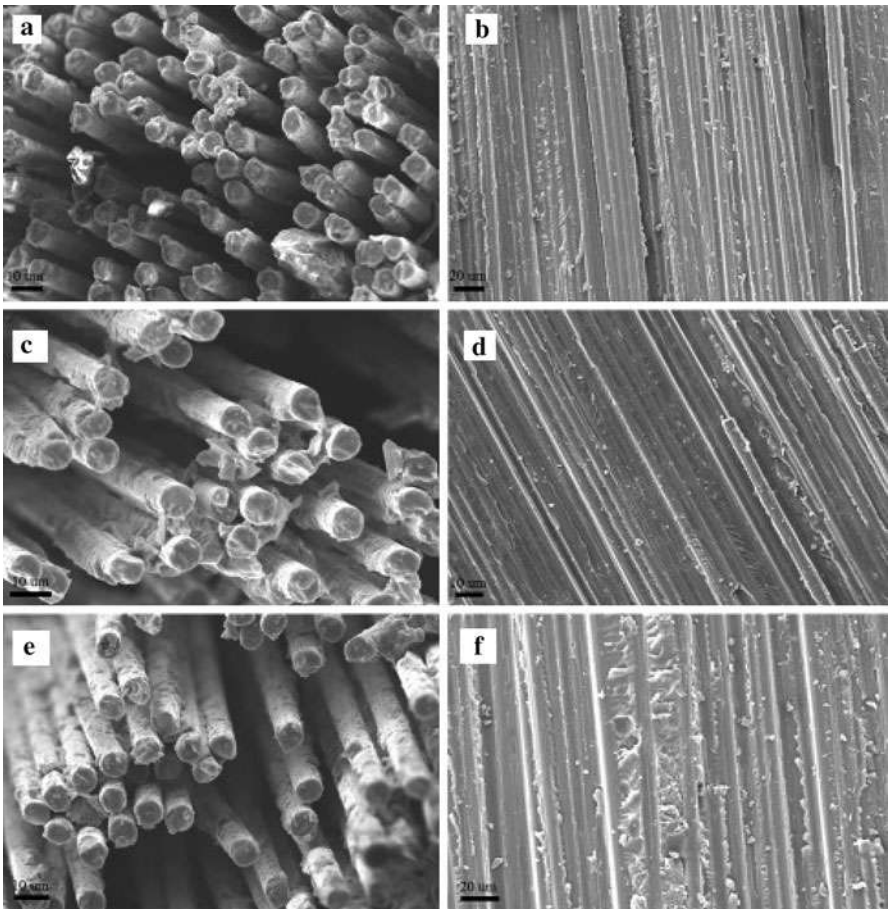

Fig. 16 SEM micrographs of samples cured by different processes showing the fracture surface after the tensile and three-point flexural test. (**a**) and (**b**) tensile and flexural test samples cured by new microwave process; (**c**) and (**d**) tensile and flexural test samples cured by current microwave process; (**e**) and (**f**) tensile and flexural test samples cured by autoclave. (Reprinted with permission from (Nanya Li et al. 2017)©)

Dynamic Mechanical Analysis (DMA)

Dynamic mechanical analysis (DMA) is a versatile and flexible analytical technique for determining dynamic characteristics of materials. It can measure the properties of a range of materials such as storage modulus (E′, G′), loss modulus (E″, G″), loss tangent (tanδ), glass transition temperature (T_g), etc. The dependency of these properties on temperature can also be analyzed using DMA. The dynamic oscillating is applied to a specimen, and the material's response to the cyclic force is analyzed. The curves plotted identify transition temperature based on noticeable changes in the

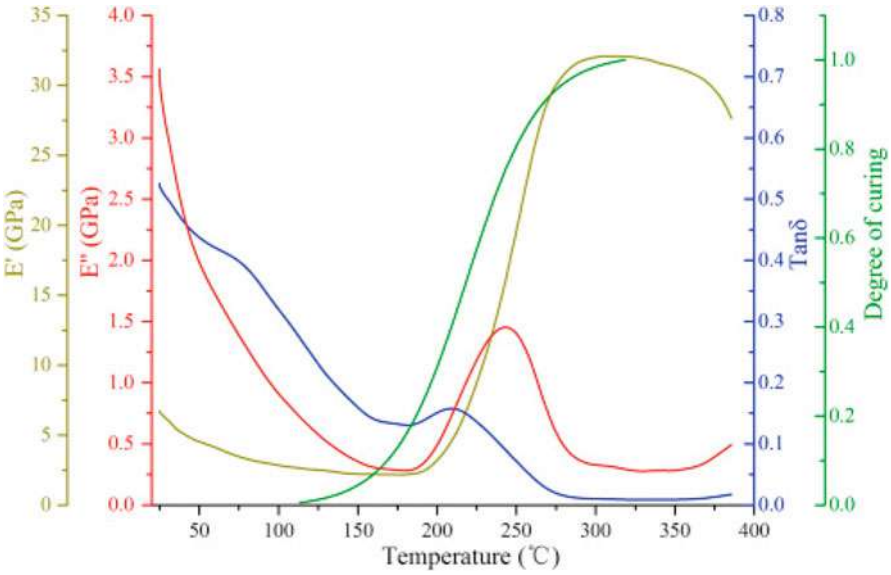

Fig. 17 Dynamic thermal mechanical analyzing results and degree of curing of composite sample. (Reprinted with permission from (Li et al. 2017)©)

curve. The DMA result of a CFRPC (Li et al. 2017) is shown in Fig. 17. The variation in the value of storage modulus (E′) ranges from 7 GPa to 30 GPa up to char temperature and reduced further. The viscoelastic material is given by loss modulus (E″). The value of E″ suddenly drops with an increase in temperature. A peak of storage modulus was found at the gelation point (240 °C).

The value of the degree of cure at this point was about 0.78. The value of loss tangent decreased first up to gelation point and decreased further after attaining a small peak. In another study, CFRP composites manufactured with RTM process are cured by microwave and thermal oven heating route. A difference in the cross-linking path of the molecular chain was observed with a change in shift of β-transition (solid state transition of cured polymer) peak in microwave cured composite (Papargyris et al. 2008). The viscoelastic behavior of the CFRP composite pipeline was evaluated to observe the heating rate and frequency on glass transition temperature. The measurement of material performance is evaluated using the activation energy concept. The composite material performance is important when environmental conditions are harsh, like variation in temperature, moisture, and chemicals. The composite materials are viscoelastic. Generally, the glass transition temperature plays a critical role to determine the application of composite material. The degradation rate of composite materials increased if the operating condition temperature of material is above T_g. Minor changes in T_g of FRPCs can be evaluated using DMA test (Goertzen and Kessler 2007).

Thermomechanical Analysis (TMA)

Thermomechanical analysis (TMA) is a technique in which deformation of the material is analyzed under non-oscillating force against time or temperature. Different types of stresses can be analyzed, such as compression, tension, flexural, and torsion. In this method, a sample is inserted into the furnace, which remains in contact with a probe. The probe is connected with the length detector and force generator. Also, a thermometer is placed near the specimen for accurately measuring its temperature. Change of temperature, thermal deformation, and softening of the specimen occur and are measured with the help of the probe movement. By applying force on the specimen from the force generator, there is a temperature change. This temperature is measured accurately with the help of the thermometer. TMA can also be used to find the glass transition temperature of epoxy composites. Zoughi and Zonnefeld (1991) have used TMA to compare the glass transition temperature of the DGEBA cured microwave and thermal heating. Microwave curing was done isothermally at three different temperatures. Thermal curing was done in a temperature adjustable thermal oven at three different temperatures. TMA thermographs were plotted for both microwave and thermally cured specimens. These graphs show well-defined transition at T_g. Microwave cured epoxy shows a significant increase at the 0.58 extent of cure.

X-Ray Diffraction Analysis (XRD)

X-ray diffraction is used to know the atomic and molecular structure of the material. It is a non-destructive technique that determines the crystallographic structure of the material. The working principle involves irradiation of material by X-rays and measuring the intensities of scattered X-rays and their scattering angles. The degree of dispersion of glass fibers in composites was determined. The peak was observed at Bragg's angle $2\Theta = 20.6^\circ$, representing the presence of crystalline silica in GFRP composites. No other peak was found, indicating the amorphous nature of the composite (Adekomaya et al. 2018).

Atomic Force Microscopy (AFM)

Atomic force microscopy (AFM) is a technique used to scan the surface of a material and has sub-nanometer-scale resolution. AFM is used to find the mechanical properties, electrical properties, and functional properties at non-scale. It is also famous for topography studies. The study of the surface of the material is done with the help of a micro-sized probe tip. The position of specimen material concerning the probe tip is measured to find its surface roughness. For measuring mechanical properties, a small amount of force is applied to the probe, and the tip of the probe penetrates the

material. By measuring this force, different mechanical properties can be calculated. AFM can be widely used for semiconductor science and technology, thin-film coatings, surface chemistry, tribology, polymer chemistry, energy storage materials, piezoelectric and ferroelectric materials, etc. AFM can also be used to characterize fiber reinforced composites. A recent technique (Zheng et al. 2018) to find adhesion force between fiber and epoxy is given in Fig. 18. The force of interaction between carbon fiber and epoxy is measured using a modified AFM probe tip with trimethoxysilane. The adhesion force was found around 17.9 nN, 22.5 nN, and 72.7 nN for three types of carbon fibers. The adhesion force between the sample surface and the probe tip is due to the material's surface properties in contact with the tip and interaction forces between tip and sample surface. The interaction forces include electrostatic force, van der Waals forces, etc. A more significant adhesion force is obtained between BAPPO-CF and epoxy functionalized tip by comparing all carbon fiber composites.

Challenges

There are two kinds of challenges associated with the microwave fabrication of FRPCs. One is associated with microwaves and the other is inherent with materials.

Challenges Associated with Microwave

The nonuniform composites' heating behavior of microwave results in thermal damage of its surface. Specific high microwave absorbing material such as carbon fiber causes problem of arcing during microwave exposure. This arcing results due to the accumulation of charge at the free surface of the composite. High arcing results in burning of the material and decreases its mechanical properties. Therefore, suitable arrangements like aluminum tape are required to seal the edges of fibers during microwave exposure. Microwave fabrication has the limitation related to the size of fabricated composite due to fixed size of microwave applicator and safety issues. There is a particular depth of composite material, up to which microwave can penetrate inside at specific frequency. If the composite's thickness is large, then microwave will not interact after certain depth, and result will be uncured resin in the composite. The microwave absorbing capacity of the material generally changes with change in temperature; therefore, real-time experimental material properties are challenging to obtain. The physical interpretation is very important to understand the effect of the electric field and magnetic field of microwave radiation on the composite materials. Modeling microwave behavior is also very difficult due to less experimental data available for validation of the results (Mishra and Sharma 2016). Also, the leakage of microwaves from microwave ovens is hazardous to human beings. So, all safety precautions must be followed before fabricating composite inside the microwave applicator.

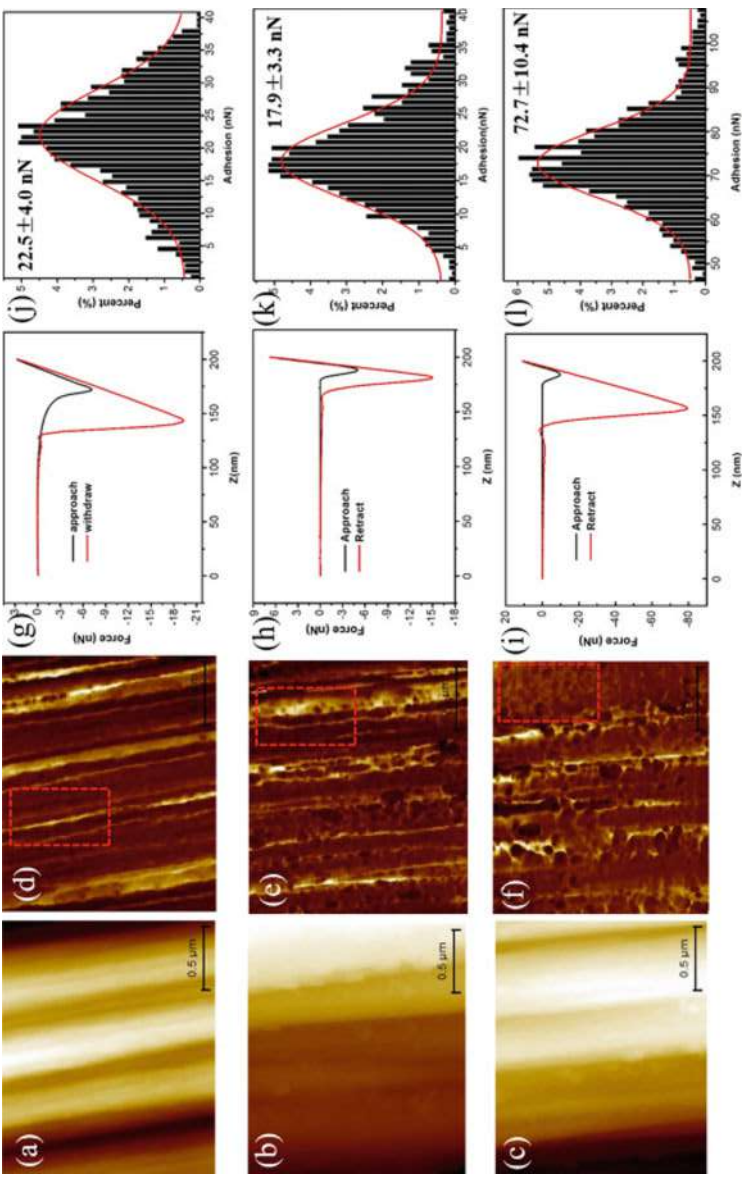

Fig. 18 Adhesion force measurement between the epoxy functionalized tip and CF samples. (**a**–**c**) AFM images of the as-received CF, de-sized CF, and BAPPO-CF used in adhesion force measurement, respectively. (**d**–**f**) The corresponding adhesion maps of **a**–**c**. (**g**–**i**) The representative force-displacement curves during the adhesion force measurement process. (**j**–**l**) Histograms of the measured adhesion forces between the epoxy functionalized tip and CFs. (Reprinted with permission from (Zheng et al. 2018)©)

Challenges Associated with the Composite Material

Homogeneous materials have uniform heating characteristics under microwave exposure. The heterogenous distribution of the fibers in the FRPCs results in anisotropic properties of the material. When these anisotropic materials are put under microwave exposure, nonuniform heating of the material takes place. The nonuniform heating results in formation of induced stresses in the composite material and ultimately reduces its mechanical properties (Mishra and Sharma 2016). Also, due to nonuniform heating, poor interfacial bonding occurs between the resin and fiber materials and lowers the properties of the composites. The other challenges are moisture content in polymer materials, difficulty maintaining the temperatures of different phases of the composites, and control on the curing rate of thermoplastic resin.

Applications

The development of materials with improved properties and performance has become essential to fulfill today's needs. Fiber epoxy composites may suit well in today's application frame as a structurally versatile material owing to their exceptional properties and performance in critical structural applications. The application of the FRPCs lies in various sectors, where the strength to weight ratio is an important design consideration. These composites are used in load-bearing applications such as aircraft, aerospace, marine, wind, automobile, and oil and gas industries.

Automotive Industry/Sector

FRPCs are nowadays used in manufacturing various automobile components, as shown in Fig. 19, because of their desirable properties such as high strength, wear resistance, and corrosion resistance. In automobile sectors, composites are gaining attention as a demanding/potential structural material because of savings of fuel due to lightweight components, excellent vibration and noise-dampening properties, ease of complex shapes like contours, low coefficient of friction, high wear resistance, and the aesthetic looks. In automobile sectors, several components were fabricated with FRPCs such as roof panels, fenders, hood, doors, trunk lid, decklid, and quarter panels due to flatness, smoothness, and high surface finish.

For the durability and corrosion resistance of automotive vehicles, especially in trucks, boats, and chemical-containing vehicles, the properties of GFRPCs have gained wide acceptance owing to their chemical and environmental stability. The surface degradation of FRPCs caused by chemical and environmental conditions does not affect mechanical properties. This holds good until the binding epoxy matrix has not degraded by these chemicals. The mechanical property degradation occurs on fracture of fibers.

Hybrid composites are also used over GFRPCs and CFRPCs in the automobile sector. Hybrid composites provide excellent impact resistance and fatigue resistance

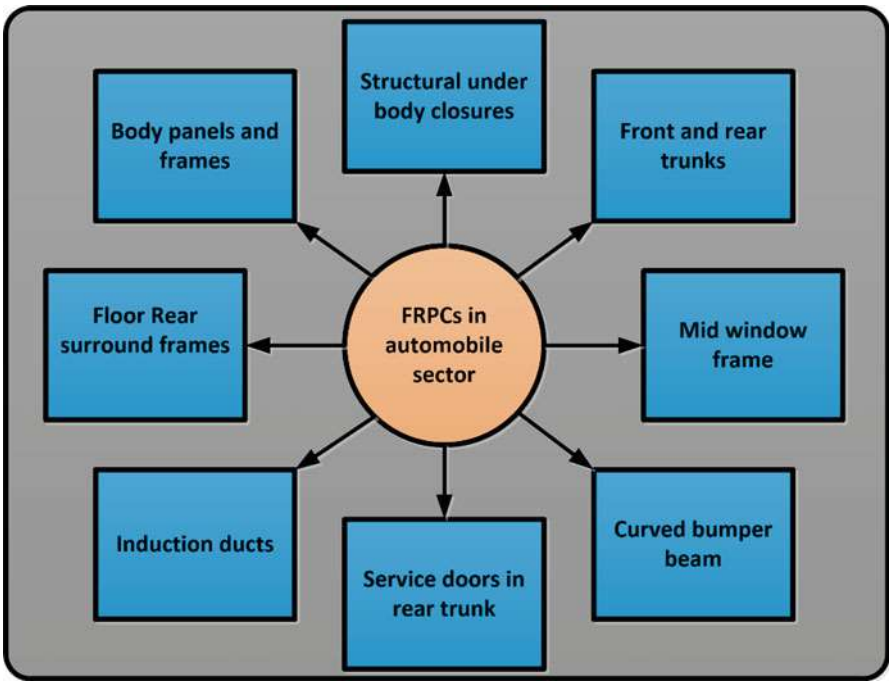

Fig. 19 The uses of FRPCs in several components of automobile

over individual fiber composites. It generally contributes to improving functional requirements by adding the synergistic effect of the mixture of two or more fibers in a single matrix. The use of hybrid composites in automobile components has increased rapidly. The components made of hybrid composites are piston, brake friction material, and anti-roll bar.

Aviation Sector

In aviation, the properties of the FRPCs, such as lightweight, high strength, high temperature resistance, and high wear resistance, make them a prominent material in the aerospace industry. Different parts of the aircraft fabricated using FRPCs are fuselage, wings, nose, doors, structural member struts, flaps, etc. The body parts of the rockets and missiles, pressure tanks, and fuel tanks are fabricated using FRPCs. Some parts such as frame, structural parts, and antenna are also fabricated using various FRPCs. Figure 20 shows the percentage use of the composite material in the aviation sector market up to the year 2022. Commercial aircraft will have the highest 199 M lb. market capacity, which is around 63% of the total market share by composites in the aviation sector. This shows the importance and need of lightweight composites in the future.

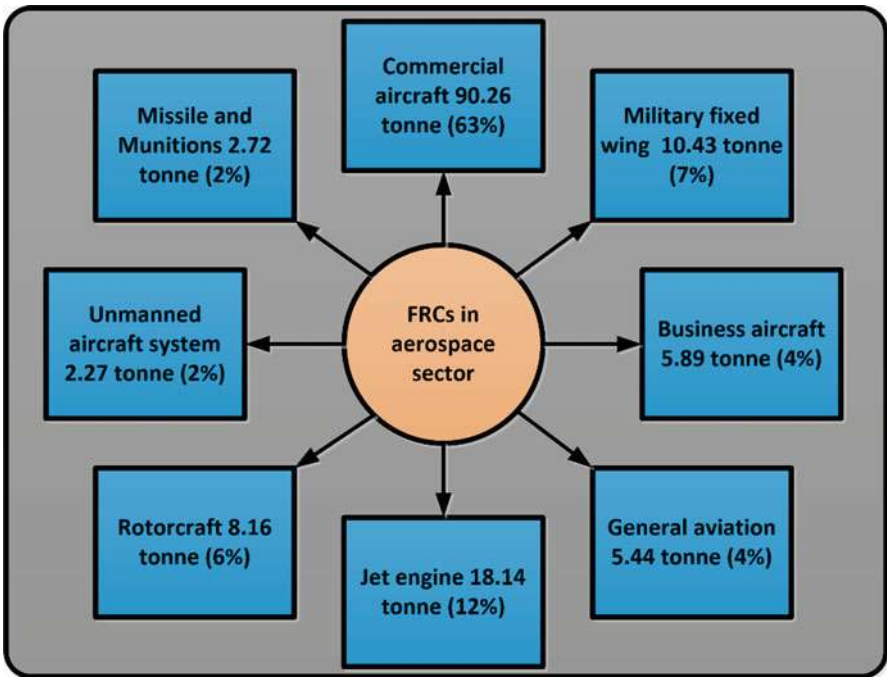

Fig. 20 Estimated market for aerospace composite structure up to year 2022. Data source: https://www.compositesworld.com/articles/the-outlook-for-thermoplastics-in-aerospacecomposites-2014-2023

Sports Sector

With the growth of economy, improvement in people's living standards has been observed. Now, people started to focus on the sports sector to improve and develop sports equipment. In most of the sports equipment (tennis racket, golf clubs, bikes, skis, etc.), human body movement is involved, so the requirement of lighter and stiffer equipment is generated. Generally, sports equipment was made of wood (natural composite), steel, and aluminum. Sports industries' interest has diverted to use composite materials due to their specific mechanical properties (high modulus and damping shock absorption), aesthetic appeal, and long service life.

Other Sectors

Other applications of FRPCs include energy sector, wind turbines, energy storage devices, pressure vessels, and oil and gas industries. FRPCs are also in increasing demand to manufacture domestic articles, e.g., furniture, ceiling material, rooftop, doors, and windows. Composites made of short fibers are extensively used as building construction material.

Conclusions

The microwave processing of the materials in the future appears very demanding for specialized applications, and probably it will have limited usefulness for producing heat in conventional processes. In domain of specialized applications, microwaves have distinct advantages as compared to conventional processing methods. Microwave processing applies to only certain types of materials, coupled with electromagnetic radiation and heat. The inadequate interaction among various researchers, engineers, and industrialists results in non-realization of the microwave processing's actual benefits. The basic type of microwave (generator, applicator, and power supply) is available commercially. However, customizing the equipment in terms of process design requires unique applicator design to accommodate process variations. It must be well recognized that material cannot be processed efficiently and uniformly if simply placed in a microwave oven without considering specific microwave/material interactions.

In the case of the FRPCs, microwave processing depends upon the constituents' individual properties (matrix and reinforcement). The significant difference in the ability to absorb microwave radiation may result in nonuniform heating of the composite. Therefore, the selection of fiber and matrix material is an important criterion to enhance the composite material's performance by microwave. Stacking sequence and fibers' orientation are the other important factors to decide the ultimate properties of the composites. Thermoset material such as epoxy has certain gelation point, where cross-linking of the polymer starts. Therefore, it is essential to keep it under microwave exposure until the desired temperature is reached. A high degree of cure results in better interfacial bonding with the fibers and decreases porosity. There are certain kinds of fiber, which have high microwave absorbing capacity. Under microwave exposure, these fibers interact more with the microwave and more heat is generated. Heat transfer to low temperature epoxy can result in temperature gradient, which ultimately affects the mechanical properties of the composite material. A proper combination of the fiber and matrix (having similar dielectric properties) may result in better properties of the composite materials.

Closed mold processes such as vacuum-assisted resin molding process and compression molding are known for their high precision and repeatability. However, the cost may be the other factor to decide the final method to fabricate the FRPCs. Although many researchers have shown the benefits of microwave-assisted composites, a lot of study and laboratory work is needed to shorten various challenges associated with FRPC fabrication.

Credit Authorship Contribution Statement **Rajeev Kumar:** Conceptualization, methodology, writing (original draft), data curation, and investigation. **Manjeet Rani:** Data curation, visualization, and investigation. **Sunny Zafar:** Funding acquisition, supervision, writing, review, and editing.

References

D. Abliz, Y. Duan, L. Steuernagel, L. Xie, D. Li, G. Ziegmann, Curing methods for advanced polymer composites – A review. Polym. Polym. Compos. **21**(6), 341–348 (2013). https://doi.org/10.1177/096739111302100602

D. Abraham, S. Matthews, R. McIlhagger, A comparison of physical properties of glass fibre epoxy composites produced by wet lay-up with autoclave consolidation and resin transfer moulding. Compos. A: Appl. Sci. Manuf. **29**(7), 795–801 (1998). https://doi.org/10.1016/S1359-835X(98)00055-4

O. Adekomaya, A.A. Adediran, K. Adama, Characterization and morphological properties of glass fiber reinforced epoxy composites fabricated under varying degrees of hand lay-up techniques. J. Appl. Sci. Environ. Manag. **22**(1), 110 (2018). https://doi.org/10.4314/jasem.v22i1.20

S.L. Bai, V. Djafari, Interfacial properties of microwave cured composites. Composites **26**(9), 645–651 (1995). https://doi.org/10.1016/0010-4361(95)98913-6

B.B. Balzer, J. McNabb, Significant effect of microwave curing on tensile strength of carbon fiber composites. J. Ind. Technol. **24**(3) (2008)

F.Y.C. Boey, T.H. Lee, Electromagnetic radiation curing of an epoxy/fibre glass reinforced composite. Int. J. Radiat. Appl. Instrum. Part **38**(4), 419–423 (1991). https://doi.org/10.1016/1359-0197(91)90118-L

M. Chen, E.J. Siochi, T.C. Ward, J.E. McGrath, Basic ideas of microwave processing of polymers. Polym. Eng. Sci. **33**(17), 1092–1109 (1993). https://doi.org/10.1002/pen.760331703

Y. Chen, Y. Li, Y. You, J. Xiao, Q. Song, Research on mechanical properties of epoxy/glass fiber composites cured by microwave radiation. J. Reinf. Plast. Compos. **33**(15), 1441–1451 (2014). https://doi.org/10.1177/0731684414524031

J. Claus, R.A.M. Santos, L. Gorbatikh, Y. Swolfs, Effect of matrix and fibre type on the impact resistance of woven composites. Compos. Part B **183**(December 2019), 107736 (2020). https://doi.org/10.1016/j.compositesb.2019.107736

A. De Luca, F. Caputo, A review on analytical failure criteria for composite materials. AIMS Mater. Sci. **4**(5), 1165–1185 (2017). https://doi.org/10.3934/matersci.2017.5.1165

H. Dong, Z. Li, J. Wang, B.L. Karihaloo, A new fatigue failure theory for multidirectional fiber-reinforced composite laminates with arbitrary stacking sequence. Int. J. Fatigue **87**, 294–300 (2016). https://doi.org/10.1016/j.ijfatigue.2016.02.012

K.L. Edwards, An overview of the technology of fibre-reinforced plastics for design purposes. Mater. Des. **19**(1–2), 1–10 (1998). https://doi.org/10.1016/s0261-3069(98)00007-7

A. Endruweit, M.S. Johnson, A.C. Long, Curing of composite components by ultraviolet radiation: A review. Polym. Compos. **27**(2), 119–128 (2006). https://doi.org/10.1002/pc.20166

W. Ferdous, A. Manalo, J. Peauril, C. Salih, K.R. Reddy, P. Yu, . . . T. Heyer, Testing and modelling the fatigue behaviour of GFRP composites – Effect of stress level, stress concentration and frequency. Eng. Sci. Technol. Int. J. **23**(5), 1223–1232. (2020). https://doi.org/10.1016/j.jestch.2020.01.001

E.K. Gamstedt, R. Talreja, Fatigue damage mechanisms in unidirectional carbon-fibre-reinforced plastics. J. Mater. Sci. **34**, 2535–2546 (1999)

W.K. Goertzen, M.R. Kessler, Dynamic mechanical analysis of carbon/epoxy composites for structural pipeline repair. Compos. Part B **38**(1), 1–9 (2007). https://doi.org/10.1016/j.compositesb.2006.06.002

A. Gupta, A.A. Ogale, Dual curing of carbon fiber reinforced photoresins for rapid prototyping. Polym. Compos. **23**(6), 1162–1170 (2002). https://doi.org/10.1002/pc.10509

M.N. GuruRaja, A.N. HariRao, Influence of angle ply orientation on tensile properties of carbon/glass hybrid composite. J. Miner. Mater. Charact. Eng. **01**(05), 231–235 (2013). https://doi.org/10.4236/jmmce.2013.15036

X. Hang, Y. Li, X. Hao, N. Li, Y. Wen, Effects of temperature profiles of microwave curing processes on mechanical properties of carbon fibre-reinforced composites. Proc. Inst. Mech. Eng. B J. Eng. Manuf. **231**(8), 1332–1340 (2017). https://doi.org/10.1177/0954405415596142

B. Harris, in *Ftigue in composites*, ed. by B. Harris, 1st edn., (Woodhead Publishing Limited, New York/Washington, DC, 2003)

R. Kumar, M. Rani, S. Zafar, Influence of stacking sequence on impact strength/hardness of CF/GF hybrid composites fabricated by VARIMC technique. Mater. Today Proc. **xxxx**, 1–5 (2021). https://doi.org/10.1016/j.matpr.2021.01.114

M. Kwak, P. Robinson, A. Bismarck, R. Wise, Microwave curing of carbon-epoxy composites: Penetration depth and material characterisation. Compos. A: Appl. Sci. Manuf. **75**, 18–27 (2015). https://doi.org/10.1016/j.compositesa.2015.04.007

N. Li, Y. Li, J. Jelonnek, G. Link, J. Gao, A new process control method for microwave curing of carbon fibre reinforced composites in aerospace applications. Compos. Part B **122**, 61–70 (2017). https://doi.org/10.1016/j.compositesb.2017.04.009

Y. Li, L. Cheng, J. Zhou, Curing multidirectional carbon fiber reinforced polymer composites with indirect microwave heating. Int. J. Adv. Manuf. Technol. **97**(1–4), 1137–1147 (2018). https://doi.org/10.1007/s00170-018-1974-1

S. Maenz, M. Mühlstädt, K.D. Jandt, J. Bossert, Mechanical properties of microwave cured glass fibre epoxy composites prepared by resin transfer moulding. J. Compos. Mater. **49**(23), 2839–2847 (2015). https://doi.org/10.1177/0021998314557295

K. Malekshahinezhad, A. Ahmadi-khaneghah, H. Behniafar, Amine-functionalized TiO2 nanoparticles covalently loaded into epoxy networks via thermal and microwave curing processes. Macromol. Res. **28**(6), 567–572 (2020). https://doi.org/10.1007/s13233-020-8067-3

C.O. Mgbemena, D. Li, M.F. Lin, P.D. Liddel, K.B. Katnam, V.T. Kumar, H.Y. Nezhad, Accelerated microwave curing of fibre-reinforced thermoset polymer composites for structural applications: A review of scientific challenges. Compos. A: Appl. Sci. Manuf. **115**, 88–103 (2018). https://doi.org/10.1016/j.compositesa.2018.09.012

J. Mijović, J. Wijaya, Review of cure of polymers and composites by microwave energy. Polym. Compos. **11**(3), 184–191 (1990). https://doi.org/10.1002/pc.750110307

R.R. Mishra, A.K. Sharma, Microwave-material interaction phenomena: Heating mechanisms, challenges and opportunities in material processing. Compos. A: Appl. Sci. Manuf. **81**, 78–97 (2016). https://doi.org/10.1016/j.compositesa.2015.10.035

E. Moaseri, M. Maghrebi, M. Baniadam, Improvements in mechanical properties of carbon fiber-reinforced epoxy composites: A microwave-assisted approach in functionalization of carbon fiber via diamines. Mater. Des. **55**, 644–652 (2014). https://doi.org/10.1016/j.matdes.2013.10.040

P. Mondal, *Improved Microwave Absorption of E-Glass- Epoxy Composites By Conducting Polymer Coated Carbon Nanotubes* (Indian Institute of Technology Hydrabad, India, 2016)

C. Nightingale, R.J. Day, Flexural and interlaminar shear strength properties of carbon fibre/epoxy composites cured thermally and with microwave radiation. Compos. A Appl. Sci. Manuf. **33**(7), 1021–1030 (2002). https://doi.org/10.1016/S1359-835X(02)00031-3

M.J. Owen, R.J. Howe, The accumulation of damage in a glass-reinforced plastic under tensile and fatigue loading. J. Phys. D. Appl. Phys. **5**(9), 1637–1649 (1972). https://doi.org/10.1088/0022-3727/5/9/319

D.A. Papargyris, R.J. Day, A. Nesbitt, D. Bakavos, Comparison of the mechanical and physical properties of a carbon fibre epoxy composite manufactured by resin transfer moulding using conventional and microwave heating. Compos. Sci. Technol. **68**(7–8), 1854–1861 (2008). https://doi.org/10.1016/j.compscitech.2008.01.010

E.T. Park, Y. Lee, J. Kim, B.S. Kang, W. Song, Experimental study on microwave-based curing process with thermal expansion pressure of PTFE for manufacturing carbon fiber/epoxy composites. Materials **12**(22) (2019). https://doi.org/10.3390/ma12223737

M. Quaresimin, L. Susmel, R. Talreja, Fatigue behaviour and life assessment of composite laminates under multiaxial loadings. Int. J. Fatigue **32**(1), 2–16 (2010). https://doi.org/10.1016/j.ijfatigue.2009.02.012

R.M.V.G.K. Rao, S. Rao, B.K. Sridhara, Studies on tensile and interlaminar shear strength properties of thermally cured and microwave cured glass-epoxy composites. J. Reinf. Plast. Compos. **25**(7), 783–795 (2006). https://doi.org/10.1177/0731684406063542

S. Rao, L. Vijapur, M.R. Prakash, Effect of incident microwave frequency on curing process of polymer matrix composites. J. Manuf. Process. **55**(September 2019), 198–207 (2020). https://doi.org/10.1016/j.jmapro.2020.04.003

K. Sato, Y. Hotta, Carbon fiber/epoxy composite materials cured thermally and with microwave irradiation. Compos. Interfaces **22**(1), 67–74 (2015). https://doi.org/10.1080/15685543.2015.988581

R. Talreja, Fatigue of composite materials: Damage mechanisms and fatigue-life diagrams. Proc. R. Soc. Lond. A Math. Phys. Sci. **378**(1775), 461–475 (1981). https://doi.org/10.1098/rspa.1981.0163

V. Tanrattanakul, D. Jaroendee, Comparison between microwave and thermal curing of glass fiber-epoxy composites: Effect of microwave-heating cycle on mechanical properties. J. Appl. Polym. Sci. **102**(2), 1059–1070 (2006). https://doi.org/10.1002/app.24245

E.T. Thostenson, T.W. Chou, Microwave and conventional curing of thick-section thermoset composite laminates: Experiment and simulation. Polym. Compos. **22**(2), 197–212 (2001). https://doi.org/10.1002/pc.10531

N. Verma, R. Kumar, S. Zafar, H. Pathak, Vacuum-assisted microwave curing of epoxy/carbon fiber composite: An attempt for defect reduction in processing. Manuf. Lett. **24**, 127–131 (2020). https://doi.org/10.1016/j.mfglet.2020.04.010

M. Wallace, D. Attwood, R.J. Day, F. Heatley, Investigation of the microwave curing of the PR500 epoxy resin system. J. Mater. Sci. **41**(18), 5862–5869 (2006). https://doi.org/10.1007/s10853-006-0321-3

X. Wu, Y. Li, N. Li, J. Zhou, X. Hao, Analysis of the effect and mechanism of microwave curing on the chemical shrinkage of epoxy resins. High Perform. Polym. **29**(10), 1165–1174 (2017). https://doi.org/10.1177/0954008316671794

X. Xu, X. Wang, Q. Cai, X. Wang, R. Wei, S. Du, Improvement of the compressive strength of carbon fiber/epoxy composites via microwave curing. J. Mater. Sci. Technol. (2015). https://doi.org/10.1016/j.jmst.2015.10.006

X. Xu, X. Wang, Q. Cai, X. Wang, R. Wei, S. Du, Improvement of the compressive strength of carbon fiber/epoxy composites via microwave curing. J. Mater. Sci. Technol. **32**(3), 226–232 (2016). https://doi.org/10.1016/j.jmst.2015.10.006

C.Y. Yue, H.C. Looi, Influence of thermal and microwave processing on the mechanical and interfacial properties of a glass/epoxy composite. Composites **26**(11), 767–773 (1995)

N. Zheng, J. He, J. Gao, Y. Huang, F. Besenbacher, M. Dong, Adhesion force measured by atomic force microscopy for direct carbon fiber-epoxy interfacial characterization. Mater. Des. **145**, 218–225 (2018). https://doi.org/10.1016/j.matdes.2018.02.060

J. Zhou, Y. Li, N. Li, X. Hao, C. Liu, Interfacial shear strength of microwave processed carbon fiber/epoxy composites characterized by an improved fiber-bundle pull-out test. Compos. Sci. Technol. **133**, 173–183 (2016). https://doi.org/10.1016/j.compscitech.2016.07.033

R. Zoughi, B. Zonnefeld, Permittivity characteristics of Kevlar, carbon composites, E-glass, and rubber (33% carbon) at X-band (8–12 GHZ). Rev. Prog. Quant. Nondestruct. Eval., 1431–1436 (1991). https://doi.org/10.1007/978-1-4615-3742-7_38

Impact Behaviors of Epoxy/Synthetic Fiber Composites

17

Manish Kumar Lila, Akarsh Verma, and Swapnil Sureshchandra Bhurat

Contents

Abstract

Synthetic fiber-reinforced epoxy composites have a broad spectrum in structural applications. The study of impact behavior of a structural element is a prime focus for any engineer or designer. The current chapter explain various impact testing methods, failure modes in impact testing, and factors affecting the impact strength of synthetic fiber-reinforced epoxy composites. Major testing methods used to analyze the impact behavior of composites are discussed in details along with

M. K. Lila
Department of Mechanical Engineering, Graphic Era Hill University, Dehradun, India

A. Verma (✉) · S. S. Bhurat
Department of Mechanical Engineering, University of Petroleum and Energy Studies, Dehradun, India

S. Mavinkere Rangappa et al. (eds.), *Handbook of Epoxy/Fiber Composites*,
https://doi.org/10.1007/978-981-19-3603-6_55

different failure modes. Energy transferred from matrix to reinforcing fibers and the fracture mechanism in different testing methods are also elaborated. The methods used to enhance the impact toughness of composites are also highlighted in different sections.

Keywords

Impact test · Composites · Epoxy resin · Synthetic fibers

Introduction

The applications of synthetic fiber-reinforced polymer matrix composites are increasing day by day in various engineering applications, such as automotive, aerospace, construction, etc., due to their exceptional mechanical properties, i.e., less moisture absorption, better thermal resistance, and chemical inactivity. These composites are usually lighter, stronger, and stiffer than unreinforced polymers and possess a competitive advantage of easy fabrication and mass production. The properties and forms of these composites can be customized to meet the specific needs of the desired application, and the properties are also a function of fabrication method and process parameters. Polymer matrix composites can be tailor-made according to the desired properties by varying the percent fraction of reinforcement (by weight or volume) and additives in the polymeric matrix. Parts are subject to various dynamic loads and stresses during their fabrication and use, highly depending on their working environment that may result in unanticipated damages. Epoxy resins possess superior chemical and physical properties and, therefore, are considered necessary for numerous engineering applications.

The most commonly used thermoset matrices in structural applications are epoxy and polyester (saturated/unsaturated) and have wide applications in the construction industry. Thermosets are brittle in nature, due to which the crack propagates instantaneously and results in poor impact strength of the materials. These brittle nature and poor impact properties have led the research fraternity to use synthetic fibers' thermoset matrices to enhance the impact properties for its use in structural applications. The impact strength of polymers is considerably altered, depending on the differences in monomeric units, prepolymers, or curing agents used (Miyamoto and Sugano 1974). Synthetic fiber-reinforced polymer (GFRP/CFRP) composites are considered as ductile one, proficient of captivating high projectile's kinetic energy, but have lesser ability with reference to deforming or fracturing due to impact by projectile (Naghizadeh et al. 2018). Impact test also exhibits the brittle or ductile nature of the composite materials at certain deformation speed.

In synthetic fiber-reinforced composites, the fibers impart strength as well as stiffness to the composite material and the matrix resin are responsible for transferring the load between the synthetic fibers. The matrix also shields the synthetic fiber reinforcement from any mechanical damage, environmental impact, etc. Fibers not only develop the toughness of the material but also restrict the crack propagation.

The presence of synthetic fibers highly influences the impact strength of most of the polymers due to their better mechanical properties as compared to the matrix.

Impact strength, also sometimes referred as impact toughness, is actually the maximum energy that can be absorbed by the material, when a sudden load is applied on it. In other words, it is a threshold of the force per unit of area before failure of the material. When the applied load, in terms of energy, surpasses the absorbing limit (impact toughness) of the material, it results in damage to the material in the form of fracture or tear. This damage can be seen in the form of localized damaged or complete disintegration, depending on the amount of energy of impact. Therefore, fibrous fillers are added to polymeric materials to increase the capability to absorb high energy and to avoid rupture. Fiber-reinforced composites exhibit elastic properties and distinctive fracture mechanism as the reinforcement imparts stiffness to the composite materials. The major drawback of synthetic fiber-reinforced composite materials, when compared to metals, is the vulnerability to damage caused by a foreign object impact; therefore, damage tolerance and damage resistance are the most vital features of synthetic fiber-reinforced composites. The global toughness of the developed composite is highly dependent on the fiber-matrix interfacial properties, geometry, construction, testing conditions, as well as nature of the components. Among these, the interfacial bonding is a function of the type of the epoxy resin, curing environment, functionalization of fiber, and the fabrication methods. Depending on the characteristics of constituents, the optimization and selection of reinforcing fiber and matrix, and arrangement and loading profile, the damage procedure can be deemed as an intricate amalgamation of energy absorption mechanisms, such as matrix cracking due to transverse fiber fracture, transverse shear, as well as delamination. Among these failure modes, delamination is quite unusual in composite structures and can greatly weaken the mechanical properties, which hampers the composite materials in replacing conventional materials. The other damages may also be unnoticeable on the surface of composite, but their presence also significantly decreases the overall properties of the developed composite and most commonly in-plane stiffness and strength (Hirai et al. 1998). The domain of impact testing is very intricate, due to a variety of tests available as well as the results, which may be entirely dissimilar from another test on the same composite. Different test comprises the use of different sample shapes, which subsequently tested under diverse types of stress as well as various criteria of impact. Difference may also come in the form of surface defects or the molecular orientation relative to the position of application of impact (Thomas 1973). Generally, impact test is an effective technique, used to evaluate the fracture resistance and fracture toughness under high-velocity impact conditions. Yet, the standard impact toughness tests provide only a limited data exhibiting influence of various parameters on material impact behavior. Only impact energy can be determined by a standard impact test to fracture the specimen, while the type of fracture is used to demonstrate the fraction of the ductile component or value of lateral expansion of the sample with fracture zone in overall fractured area. For a more precise analysis, the size of the data or information in the testing procedure can be further amplified by equipping modern systems for high-speed data registration, which further allows us to get a complete

figure of strain and fracture of test sample with a desired resolution. These advanced procedures and high-speed recording systems help in increasing the amount of data/information for conducted impact tests as well as assist in obtaining the additional opportunities for examination of courses of crack propagation and initiation. Nowadays, nuclear industries are employing subsized test specimens for the evaluation of level of metal degradation and exploring the possibilities to save the scarce metals as well as providing more data on process of testing (Kondryakov et al. 2019). The initiation and development of surface cracks during impact testing are incredibly significant in composite materials. In the same way, materials are expected to reveal mechanical behavior projected in design and retain the structural integrity under externally applied impact loads. Working life of composite materials depends on the chemical and mechanical effects, which may lead to notches or cracks on the surface of materials as even a small impact can exhibit a large effect due to the presence of notch of crack on the surface. The deterioration or the damage initiated in this manner led to a decrease in strength and rigidity of composite materials, and also the effect becomes more prominent under relatively higher loads. Sometimes, the crack formation and propagation can be seen also on the rear surface of the impacted object. Internal delamination between the layers of reinforcement and matrix is also exhibited after impact loading of composite specimens (Güneş and Şahin 2020).

Measurement of Impact Properties

The impact toughness of the material is established by measuring the energy absorbed during failure of material under impact loading. In all the tests, the energy is supplied by a striking hammer or impactor at a certain velocity. Based on the velocity of the striking hammer, the impact test can be listed as:

(a) High-velocity impact test.
(b) Low-velocity impact test.

When the velocity of striking hammer/impactor is in the range of 400–2000 m/s, the test is termed as high-velocity impact test (Hirai et al. 1998; Thomas 1973; Kondryakov et al. 2019; Güneş and Şahin 2020). Ballistic testing can be considered as a suitable example of high-velocity impact test. High-velocity impact test results in concentrated stress at a particular area and causes a localized damage. In low-velocity impact test, the energy is supplied by the mean of a swinging hammer or a dead weight. In low-velocity impact, the dynamic structural response of material is of much importance due to contact time between the impactor and the material. In case of high contact time, the complete structure is supposed to respond to the impact. While in high-velocity impact, this response is a function of the stress wave generation. The time of contact in high-velocity impact is comparatively very less; therefore, the material does not have time to respond to it, resulting in localized damage (Yadav and Srivastava 2015). Low-velocity impact on laminated composites can lead to different types of damages, which include fiber breakage, delamination,

matrix cracking, as well as fiber-matrix interfacial debonding, which are highly hazardous due to visual non-detection, and, subsequently, lead to a structural failure at lesser loads below the designed one.

Based on the type of impactor, low-velocity impact test can be further categorized as:

(a) Izod and Charpy impact test.
(b) Drop weight impact test.

The selection of test method depends on the composite material application, which will be explained in the upcoming section.

Charpy and Izod Impact Test

Measurement of the impact toughness in Izod and Charpy impact test is mainly done on impact testing apparatus based on swinging method, in which the amount of energy is transferred by the swinging weight on a pendulum, as shown in Fig. 1. The apparatus mainly consists of a sturdy base, a dial gauge, a pendulum with specific weight, and a specimen holder. The pendulum is attached to the pointer of a pre-calibrated energy gauge in the form of dial. While conducting the test, the pendulum arm is set at a spot, corresponding to a certain level of energy. The arm is subsequently released with the help of a lever, and its hammer end is allowed to

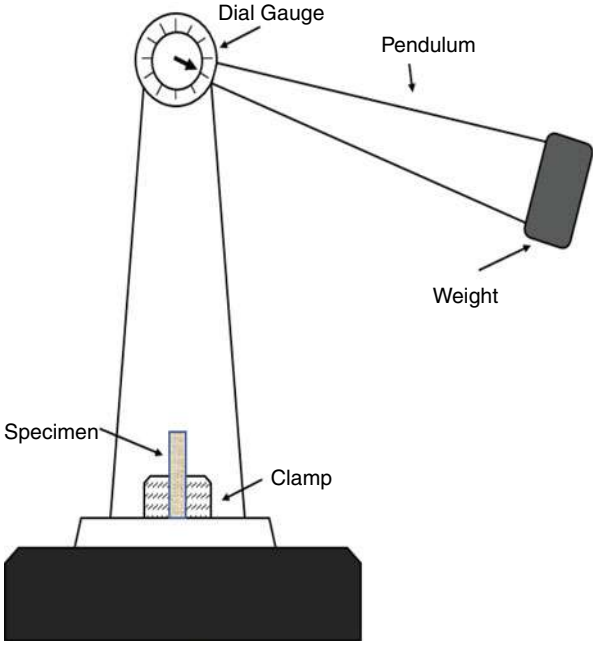

Fig. 1 Izod and Charpy impact testing apparatus

strike at the middle of the specimen place. The composite specimen impact strength is then determined by the amount of energy required to fracture or break the sample. Sometime, the friction losses are also considered and measured by swinging the pendulum arm freely, without placing the specimen and checking the readings. The energy absorbed in breaking the specimen is equal to the difference between the energy of the pendulum hammer at the instant of impact and the energy remaining in the pendulum hammer after breaking the sample (usually indicated by the pointer directly).

Based on the placement of the specimen, the impact test can be classified as:

(a) Izod impact test.
(b) Charpy impact test.

When the sample is kept as a vertical cantilever beam (one end is clamped while the other end is free), the test is known as the Izod impact test (refer to Fig. 2a). While in Charpy impact test, the specimen is placed horizontally as simply supported beam between two supports (refer to Fig. 2b).

The energy supplied to the composite specimen during the test is a function of the height attained by the impactor, prior to the impact and after the impact. The difference in the initial and final heights of the striking hammer is directly proportional to the amount of energy lost/absorbed for fracturing the sample.

The total energy of fracture is determined by

$$E_t = mg\left(h_i - h_f\right)$$

where E_t is the total energy resulted in the fracture, m is the mass of the hammer, g is the gravity (9.81 m/s^2), and h_i and h_f are the initial and final height of the hammer/

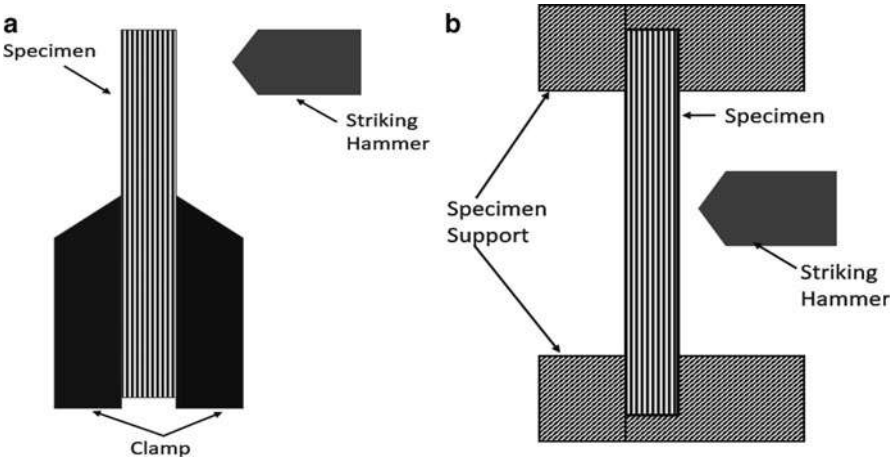

Fig. 2 (**a**) Izod impact test, (**b**) Charpy impact test

impactor, respectively. As it is mentioned earlier that the composite specimens can be unidirectional or multidirectional, therefore the impact energy depends also on the orientation of the composite specimens. Out of these two, the Charpy impact test provides a deep insight toward the localized damaged as well as the complete failure of the material; therefore, it is more preferred over the Izod impact test for the characterization of fiber-reinforced composites. In fiber-reinforced composites, the impact resistance is strongly affected by the direction and strain or ductility to the fracture of fibers. In the Izod test, when the impactor strike at the edge of the specimen, the impact load is distributed over the area between the striking point and the clamp, which further led to different modes of failure for similar composites and exhibiting different impact toughness for the same composite, while in the Charpy impact test, the load is imparted on the central point of the specimen, exhibiting similar type of fracture most of the time. When a predetermined mode of failure is studied, a notch is provided at the center of the specimen, which helps in concentrating the stress at a point and provides nearly the same results every time. The size and shape of the notch (V-notch or U-notch) depend on the standards used for testing. Generally, in fiber-reinforced composites, a V-notch is used having a depth of 2 mm and a 45° notch angle. The most common types of fractures are shown schematically in Fig. 3, in case of complete failure of the specimen.

Figure 3a exhibits the most common mode of failure, when the material in unreinforced or the fiber strength is comparatively lower in the case of reinforced composites. Fiber pullout is sometimes also visible due to poor interfacial adhesion between the fiber and matrix. Figure 3b exhibits a better interfacial bonding among the fiber and matrix, which results in uneven fractured surface attributed to delamination and debonding. The failure mode can be evaluated by fractography of the surface through a scanning electron microscopy (SEM). When the reinforcement is provided at a certain angle, the fracture (Fig. 3c) is visible, corresponding to the fiber orientation in unidirectional or bidirectional composite.

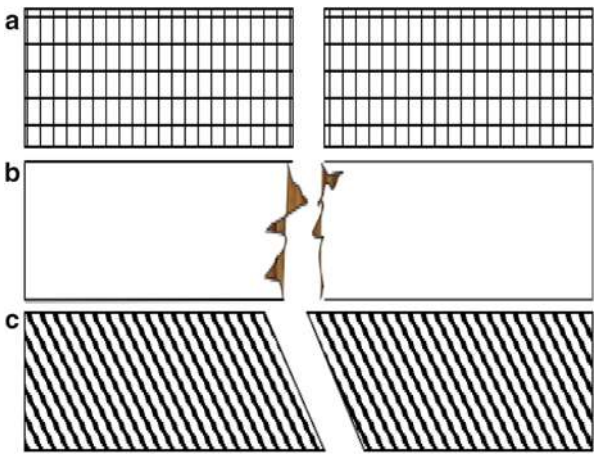

Fig. 3 Typical modes of fracture in the Charpy impact test specimens

The notch is provided on the test specimen to produce an increase in stress in a controlled and fixed manner. This also corresponds to a greater value of maximum tensile stress as well as a lower value of maximum shearing stress. This results in a reduction in the possibility of ductile failure, and that of a brittle fracture is greatly enhanced. In case of impact testing of polymeric material, this must be kept in mind that a strain is not only a function of time but also of stress. An increase in the rate of stress also results in an increase of the impact strength of composite sample. In practical conditions, a decrement can also be seen because of the dominant behavior of the notch that sometimes dictates that an increased rate of stress during an impact testing of composite may reduce the impact strength of the specimen.

Drop Weight Impact Test

The main drawback of Izod and Charpy impact test is that these tests provide the information only about the energy absorbed during the impact but not about the impact behavior. In recent time, the drop weight impact test method has become more prominent due to a wider range of testing parameters, and results are more readily investigated. Drop weight impact test is a low-velocity impact test, and the most common standard used for drop weight impact test is ASTM D-5628. A schematic of drop weight impact tester is shown in Fig. 4.

The drop weight impact tester consists of mainly three units:

1. Dynamic load cell (tup).
2. Data display system.
3. Signal conditioning unit.

In the drop weight impact testing, a specific metallic weight is kept at a predetermined height with the help of electromagnet. A tup, in the form of a hemispherical impactor, attached to the weight, is used to measure the overall strain during the impact. The specimen used in the testing is in the form of a rectangular or square plate in the form of composite laminate. Load cells (load measuring devices) are used either in the sample supporting platforms or in the tup to measure the impact. High-speed cameras are utilized to record the failure propagation and impact events. After adjusting the apparatus to its correct configuration, the weight is subsequently released and allowed to impact the plate, and the data is recorded with the help of data acquisition system. A curve is drawn between the load and time to analyze the impact behavior of the composite, the schematic of which is shown in Fig. 5.

When the impactor strikes the composite specimen, the load is initially transferred to the matrix and results in fracture in matrix and initializes the crack formation. Subsequently, the load is transferred by the matrix to the fibrous reinforcement. After attaining the allowable limit, the fiber tends to crack at the impact area and fiber fracture takes place. This limit is exhibiting the maximum load the composite can sustain and the corresponding energy is the impact toughness of the

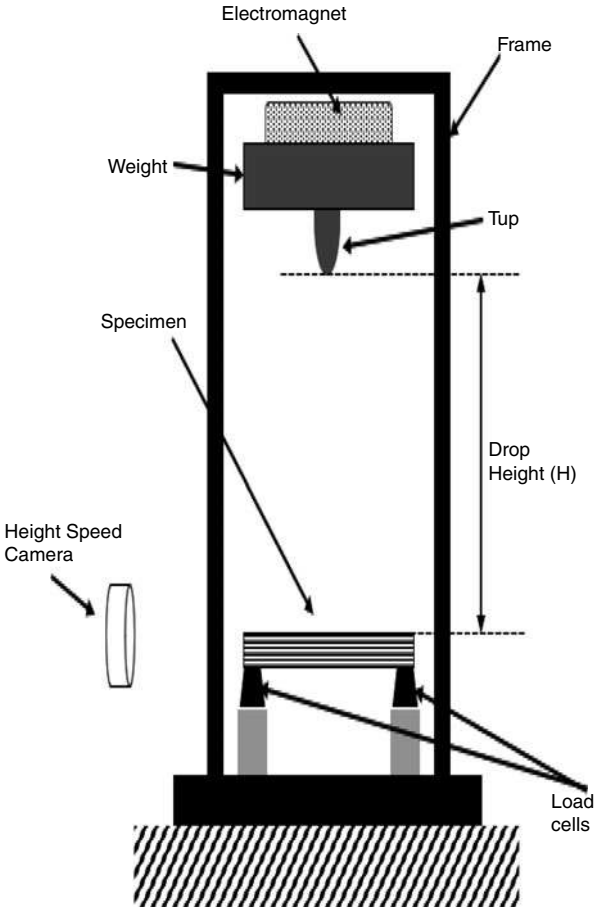

Fig. 4 Drop weight impact tester

composites. The load is further dispersed over the impact area and results in subsequent fracture in the matrix as well as fibers. Sometimes, a compression after impact (CAI) test is used in case of barely visible (or even non-visible) impact damage in the composite laminates.

High-Velocity Impact Test

As mentioned earlier, the impact resistant of composites is a function of various parameters, including materials of reinforcing fiber and matrix, architecture of fiber, layup sequencing, fabrication process, environmental conditions during fabrication and testing, geometry of specimen, specimen thickness, void percentage, fixtures and orientation, mass, type, orientation, and geometry of impact. The results are

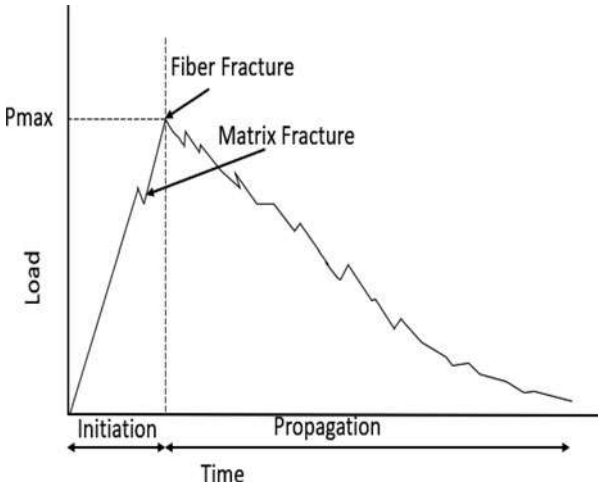

Fig. 5 Typical load-time curve for drop weight impact testing on composites

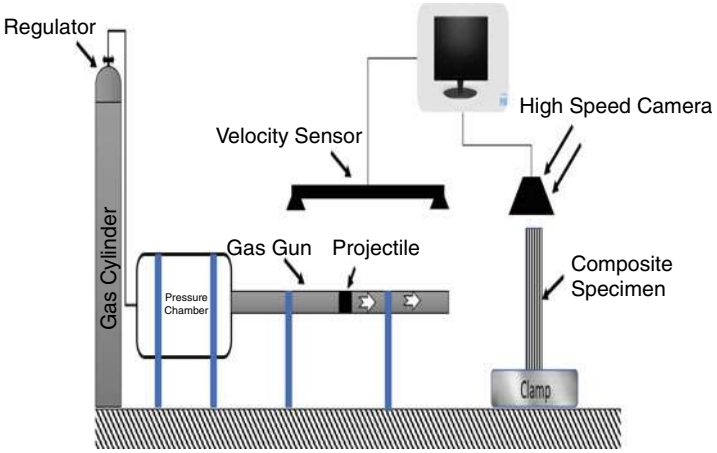

Fig. 6 Schematic of high-velocity impact testing apparatus

analyzed on the basis of the size and description of damage, impact velocity, and overall accuracy of the apparatus.

This type of impact is dominated by inertial forces, wave variation, and propagation in strength, stiffness, and fracture energy of the composite specimen due to a high strain rate. This test method is used for the testing of composite panels in which thickness dimension is small compared with the test panel length and width. High-velocity impact test is also employed to simulate the effect of the impact on the surface of aeroplane, space crafts, jet engine blades, etc. during operation. A schematic diagram of high-velocity impact testing apparatus is shown in Fig. 6.

Generally, a gas such as argon or nitrogen is fed to a pressure chamber located at one end of the gas gun. Gas is restrained by a plastic diaphragm or by some other means. When it attains a predetermined value based on experiment, this diaphragm is burst (by mechanical puncturing device or by electrical heating), which led to accelerating the projectile down gas gun to strike a component or sample supported vertically at the other end. These projectiles can be listed as hard, semihard, or soft, depending on the test as well as the specimen materials. Hard projectiles undergo negligible deformation during impact, semihard projectiles undergo some deformation, while soft projectiles experience considerable deformation. Velocity of the projectile is determined using velocity/acceleration sensor, prior to impact. Generally, these tests are not completely destructive in nature but commonly result in target perforation and/or large-scale damage on the composite specimen. High-speed cameras can also be utilized to study the instantaneous fracture behavior of the composite specimen. The obtained data can be analyzed using high end software.

Failure Modes in Composites

In low-velocity impact testing, the incident energy of projectile/striker is absorbed by the whole structure, while in high-velocity impacts, most of the energy is dissipated over a smaller zone near to the point of contact only. The dynamic response of the specimen in high-velocity impact is much localized, and geometrical effects are small. In drop weight impact testing, the contact time is higher and the target response is more noteworthy; therefore, geometrical effects are more vital. The damage made by low-energy impact is an intricate combination of delamination, transverse matrix cracking, fiber-matrix debonding, and fiber fracture (Sohn et al. 2000). In general, three major failure modes are visible in synthetic fiber-reinforced epoxy composites, namely, matrix cracking, fiber failure, and delamination. Energy captivated by a composite specimen over various fracture mechanisms is seen to be the distinctive characteristic between different composite systems.

Matrix cracking (the first type of failure) is caused by low-velocity impact test, which occurs in parallel to fiber mat, and caused due to a combination of tension, compression, or bending in the matrix layer. Matrix fracture happens in the form of various microcracks and can barely be seen with the naked eyes. This also resulted in a decrease in the interlaminar shear and compression strength on the fiber-resin interface.

Delamination is the most critical damage mechanism in composite laminates, which initiates after matrix cracking. When the threshold energy attains a certain value, the debonding between the matrix and fiber interface occurs and leads to the formation of different layers of fiber and matrix.

Fiber failure may occur in the form of fiber pullout and fiber fracture. Fiber failure depends on the mechanical properties of fibers and interface adhesion between the fiber and matrix. After the matrix cracking, the load/impact energy is transferred from the matrix to the adject layer of fibers, underneath. If the energy surpasses the interfacial bond strength, debonding occurs between the matrix and fiber up to a certain length and led to fiber pullout. Matrix cracking also lead to a reduction in the

cross-section area subjected to the impact loading, and in case of composites laminating with better interfacial bonding, the energy is concentrated over the area. When the energy surpasses the mechanical strength of the synthetic fibers, fiber fracture occurs.

A variety of failure modes may lead to perforation of the sample. Failure modes of the target will differ, depending on the projectile nose shape, impact velocity, target geometry, material's properties, relative mass of projectile and target, support conditions, etc. Most relevant failure modes in high-velocity impact testing are petaling and brittle fracture.

Factors Affecting Impact Behavior of Composites

In the previous section, we have seen that interfacial bonding highly affects the impact properties. Globally, the impact behavior of synthetic fiber-reinforced composites depends on many parameters, which directly or indirectly influence the interfacial bonding between the matrix and fiber.

Some of these are:

- Fundamental properties of the matrix.
- Fundamental properties of fibers.
- Fabrication process and parameters.
- Hybridization.
- Additives.
- Environment.

Fundamental Properties of Matrix

Polymer matrix is a key factor, which plays a major part in improving the toughness of composite through the energy dissipation mechanism. Epoxy is widely used as the matrix material in synthetic fiber-reinforced composites due to its better impact and mechanical properties. The main constituents are epoxy resin and hardener. When reinforced, the viscosity of the resin influences the interfacial adhesion, as the viscosity is low; the fluidity of resin is high, leading to better wetting of reinforcing fibers. However, low viscosity of resin led to high interfacial bonding but at the same time resulted in the compactness of the developed composite and led to a brittle fracture. When the interfacial adhesion level is high, the failure, due to impact, is brittle as relatively little energy is absorbed, while low levels adhesion led to multiple delamination among fiber and epoxy layers, instead of high energy absorption. This may result in catastrophic failure of composites. At intermediate levels of adhesion, progressive delamination occurs, which in turn produces high impact energy absorption, along with the viscosity of the resin, mixing of resin and hardener, temperature, etc., and also affects the intrinsic properties of the matrix. Neat epoxy and its composite are seemingly dissimilar when the crack propagates across them. These two materials exhibit similar characteristics in case of crack

initiation, but the fracture toughness in composites is comparatively higher (Al-Maharma and Sendur 2018). For better impact response of the composites, several studies for toughening of epoxy matrix by using additives are carried and reported, which are mention in the next sections. Some studies showing the effect of curing temperature on mechanical properties have also been reported by various researchers.

Fundamental Properties of Reinforcing Fibers

Intrinsic mechanical properties of reinforcing fibers also affect the impact response of the developed composites. The toughness and fracture properties of synthetic fiber-reinforced composites are largely affected by the type of synthetic fiber, fiber packing and weaving, etc. The tensile properties of different synthetic fibers are mentioned in Table 1.

Under the impact loading condition, fibers are subjected mainly to tensile load; therefore, the tensile strength of the synthetic fibers must be on the higher side. It can be seen that the tensile strength is highest for S-glass fiber. The Young's modulus and elongation properties may affect the nature of the fracture in the same type of resin as lower elongation may lead to a brittle fracture in the developed composites during impact test. Impact damage is generally not well thought-out to be a threat in aramid fiber-reinforced epoxy composites due to high elongation, capable of absorbing higher energy as compared to carbon and glass fiber.

Along with the fiber intrinsic properties, fiber length also plays a key role in defining the impact properties of composites. The fracture toughness is said to be directly proportional to the fiber length at equal fiber volume fraction in composites. For medium and high length of fibers (10–25 mm), the fracture toughness also improves at high fiber volume fractions.

Fabrication Process and Parameters

Hand layup is the most common fabrication method for synthetic fiber-based epoxy composites. This method is commercially feasible and consists of placing woven mat layers (plies) pre-impregnated with epoxy resin by hand composite laminate. Nowadays, vacuum-bagging or vacuum bag molding technique is being used to

Table 1 Typical tensile properties of synthetic fibers (Jawaid et al. 2017)

Fiber	Density (g/cc)	Young's modulus (GPa)	Tensile strength (MPa)	Elongation (%)
E-glass	2.5	70	2000–3500	2.5
S-glass	2.5	86	4500–4700	2.8
Aramid	1.4	63–67	3000–3200	3.3–3.7
Carbon	1.4	230–240	3500–4500	1.4–1.8

fabricate the composites, in which vacuum is used for compaction in sealed bags. The major difference in both the processes is of the compaction as in the vacuum bag molding; the epoxy resin is not only consolidated but also entrapped air in the resin mix which is also removed. In hand layup process, the entrapped air led to the creation of undesirable voids (air pockets) in the composite laminate that could affect the impact behavior of the composite. Therefore, applied pressure is a key parameter in defining the properties of developed composites. As curing takes place in the epoxy matrix, heat is generated due to the reaction between the resin and hardener. The thermal gradient is generated between the composite and ambience, resulting in thermal stresses and leading to inappropriate impact behavior of the composites.

Fiber fraction and orientation are the other parameters, which greatly influence all the mechanical properties of composites. Fracture toughness of epoxy composites increases with increased fiber fraction/loading, but at the same time, it can lead to fiber agglomeration. The agglomerated regions act as a stress concentrated zone and may result in reduced fracture toughness.

Orientation of reinforcing fibers also exhibits a great control on the impact toughness of developed composites. The capability of synthetic fibers to dissipate energy can be attributed to fiber orientation. The energy required for pulling out the fibers is comparatively higher, which are oblique relative to the direction of crack propagation compared to those with perpendicular fibers, and the contribution of transverse fibers to the impact toughness is lower than that of oblique fibers. Fracture toughness of the composite is much lower in case of fiber orientation parallel to the direction of crack propagation.

Hybridization

When more than one type of reinforcement is the same matrix or one type of reinforcement in a matrix mix, used to develop composites, it is termed as hybridization. Out of these two, the first one is used to fabricate hybrid composites, mainly due to incompatibility among different resins. The main purpose of hybridization is to achieve a synergistic result of the properties of constituents on the overall properties of composites. Hybridization results in an increase in energy absorption capacity as well as strain to failure of composite and further enhanced impact and toughness properties. A better impact toughness in hybrid composite can be attained by reinforcing long fibers in higher volume fraction than to short fibers. As mentioned earlier, agglomeration and void formation are considered as the key factor for improper fracture in case of long fibers; therefore, hybridization is performed with short fibers as higher strain localization is required to fracture the material. Therefore, a combination of short and long fibers increases the impact strength due to the combined effect.

Additives

The use of different additives and coupling agent has been reported widely in the last decade to improve the impact toughness of synthetic fiber-reinforced epoxy

composites. This also includes modification/toughening of epoxy resin by carboxyl-terminated butadiene acrylonitrile (CTBN), core shell rubber (CSR), silica nanoparticles, coating of synthetic fibers by ductile polymeric material, etc. (Naghizadeh et al. 2018; Deng et al. 2014; Park et al. 2015). In addition, the authors have a vast experience in the mechanical characterization of fiber-reinforced composites and other materials (Verma et al. 2016a, b; 2017, 2018a, b, c, d, e, 2019a, b, c, d, e, f, 2020a, b, c, d, e, f, g, h, 2021a, b; Verma and Parashar 2018a; Chaurasia et al. 2019; Jain et al. 2019; Verma and Singh 2016, 2019; Rastogi et al. 2020; Bharath et al. 2020; Singh et al. 2020; Verma and Parashar 2017, 2018b, c, 2020; Singla et al. 2018; Bharath et al. 2021; Marichelvam et al. 2021; Chaudhary et al. 2021a, b; Bisht et al. 2021).

Environment

Polymers will resist attack by most organic and inorganic reagents, except strong oxidizing acids (nitric acid, perchloric acid, chloric acid, chromic acid, etc.). Therefore, a reduction in impact strength can be observed, when these composites are immersed/placed in hydrochloric, nitric, and sulfuric acid environment. Strong alkali solutions as well as organic solvent also react with most of the polymers and exhibit a chemical reactions or dissolution with the polymer matrix in the composites. In GFRP composites, the polymeric matrix is being attacked and also results in crack generation due to stress concentration because of chemical reactions. The cracks generated in the composite material further allow the glass fibers to be subjected to chemical attack.

Conclusions

The present chapter exhibited the major research conducted in the domain of impact toughness of synthetic fiber-reinforced epoxy composites. Elaboration on high- and low-velocity impact test will help the readers to get a better insight about their application in different domains. The different failure modes exhibited in low-velocity impact test will help in understanding different failure modes in the composites.

Acknowledgments Monetary and academic support from the University of Petroleum and Energy Studies, Dehradun, India, is highly appreciable.

Conflicts of Interest "There are no conflicts of interest to declare by the authors."

References

A.Y. Al-Maharma, P. Sendur, Review of the main factors controlling the fracture toughness and impact strength properties of natural composites. Mater. Res. Exp. **6**(2), 022001 (2018). https://doi.org/10.1088/2053-1591/aaec28

K.N. Bharath, P. Madhu, T.G. Gowda, A. Verma, M.R. Sanjay, S. Siengchin, A novel approach for development of printed circuit board from biofiber based composites. Polym. Compos. **41**(11), 4550–4558 (2020)

K.N. Bharath, P. Madhu, T.Y. Gowda, A. Verma, M.R. Sanjay, S. Siengchin, Mechanical and chemical properties evaluation of sheep wool fiber–reinforced vinylester and polyester composites. Mater. Perform. Charact. **10**(1), 99–109 (2021)

N. Bisht, A. Verma, S. Chauhan, V.K. Singh, Effect of functionalized silicon carbide nano-particles as additive in cross-linked PVA based composites for vibration damping application. J. Vinyl Addit. Technol. **27**(4), 920–932 (2021)

A. Chaudhary, S. Sharma, A. Verma, Optimization of WEDM process parameters for machining of heat treated ASSAB'88 tool steel using response surface methodology (RSM). Mat. Today Proceed. (2021a)

A. Chaudhary, S. Sharma, A. Verma, WEDM machining of heat treated ASSAB'88 tool steel: A comprehensive experimental analysis. Mater. Today Proc. (2021b)

A. Chaurasia, A. Verma, A. Parashar, R.S. Mulik, Experimental and computational studies to analyze the effect of h-BN nanosheets on mechanical behavior of h-BN/polyethylene nanocomposites. J. Phys. Chem. C **123**(32), 20059–20070 (2019)

S.H. Deng, J.J. Zhao, Q.F. Lin, C.J. Fan, X.D. Zhou, Formation of interfacial network structure via photo-crosslinking in carbon fiber/epoxy composites. Express Polym Lett **8**(7), 505–516 (2014). https://doi.org/10.3144/expresspolymlett.2014.54

A. Güneş, Ö.S. Şahin, Investigation of the effect of surface crack on low-velocity impact response in hybrid laminated composite plates. J. Braz. Soc. Mech. Sci. Eng. **42**, 1–20 (2020). https://doi.org/10.1007/s40430-020-02422-2

Y. Hirai, H. Hamada, J.K. Kim, Impact response of woven glass-fabric composites – I: Effect of fibre surface treatment. Compos. Sci. Technol. **58**(1), 91–104 (1998)

N. Jain, A. Verma, V.K. Singh, Dynamic mechanical analysis and creep-recovery behaviour of polyvinyl alcohol based cross-linked biocomposite reinforced with basalt fiber. Mater. Res. Express **6**(10), 105373 (2019)

M. Jawaid, S.M. Sapuan, O.Y. Alotman, *Green Biocomposites Manufacturing and Properties* (2017), p. 409. https://doi.org/10.1007/978-3-319-46610-1

E. Kondryakov, O. Panasenko, A. Kravchyk, V. Kharchenko, Peculiarities of the crack initiation and propagation in different specimen types. Procedia Struct. Integr. **16**, 43–50 (2019). https://doi.org/10.1016/j.prostr.2019.07.020

M.K. Marichelvam, P. Manimaran, A. Verma, M.R. Sanjay, S. Siengchin, K. Kandakodeeswaran, M. Geetha, A novel palm sheath and sugarcane bagasse fiber based hybrid composites for automotive applications: An experimental approach. Polym. Compos. **42**(1), 512–521 (2021)

T. Miyamoto, T. Sugano, Impact strength of epoxy resin. Polym. J. **6**(5), 451–452 (1974)

Z. Naghizadeh, M. Faezipour, M.H. Pol, G.H. Liaghat, A. Abdolkhani, Improvement in impact resistance performance of glass/epoxy composite through carbon nanotubes and silica nanoparticles. Proc. Instit. Mech. Eng. L **232**(9), 785–799 (2018)

H. Park, H. Jung, J. Yu, M. Park, S.Y. Kim, Carbon fiber-reinforced plastics based on epoxy resin toughened with core shell rubber impact modifiers. E-Polymers **15**(6), 369–375 (2015). https://doi.org/10.1515/epoly-2015-0068

S. Rastogi, A. Verma, V.K. Singh, Experimental response of nonwoven waste cellulose fabric–reinforced epoxy composites for high toughness and coating applications. Mater. Perform. Charact. **9**(1), 151–172 (2020)

K. Singh, N. Jain, A. Verma, V.K. Singh, S. Chauhan, Functionalized graphite–reinforced cross-linked poly (vinyl alcohol) nanocomposites for vibration isolator application: Morphology, mechanical, and thermal assessment. Mater. Perform. Charact. **9**(1), 215–230 (2020)

V. Singla, A. Verma, A. Parashar, A molecular dynamics based study to estimate the point defects formation energies in graphene containing STW defects. Mater. Res. Express **6**(1), 015606 (2018)

M.S. Sohn, X.Z. Hu, J.K. Kim, L. Walker, Impact damage characterisation of carbon fibre/epoxy composites with multi-layer reinforcement. Compos. Part B **31**(8), 681–691 (2000). https://doi.org/10.1016/S1359-8368(00)00028-7

W.F. Thomas, Factors affecting the impact strength of glass-fibre-reinforced polyester composites. Composites **4**(3), 105–110 (1973). https://doi.org/10.1016/0010-4361(73)90583-1

A. Verma, A. Parashar, The effect of STW defects on the mechanical properties and fracture toughness of pristine and hydrogenated graphene. Phys. Chem. Chem. Phys. **19**(24), 16023–16037 (2017)

A. Verma, A. Parashar, Structural and chemical insights into thermal transport for strained functionalised graphene: A molecular dynamics study. Mater. Res. Express **5**(11), 115605 (2018a)

A. Verma, A. Parashar, Molecular dynamics based simulations to study the fracture strength of monolayer graphene oxide. Nanotechnology **29**(11), 115706 (2018b)

A. Verma, A. Parashar, Molecular dynamics based simulations to study failure morphology of hydroxyl and epoxide functionalised graphene. Comput. Mater. Sci. **143**, 15–26 (2018c)

A. Verma, A. Parashar, Characterization of 2D nanomaterials for energy storage, in *Recent Advances in Theoretical, Applied, Computational and Experimental Mechanics*, (Springer, Singapore, 2020), pp. 221–226

A. Verma, V.K. Singh, Experimental investigations on thermal properties of coconut shell particles in DAP solution for use in green composite applications. J. Mater. Sci. Eng. **5**(3), 1000242 (2016)

A. Verma, V.K. Singh, Mechanical, microstructural and thermal characterization of epoxy-based human hair–reinforced composites. J. Test. Eval. **47**(2), 1193–1215 (2019)

A. Verma, V.K. Singh, S.K. Verma, A. Sharma, Human hair: A biodegradable composite fiber–a review. Int J Waste Resour **6**(206), 2 (2016a)

A. Verma, V.K. Singh, M. Arif, Study of flame retardant and mechanical properties of coconut shell particles filled composite. Res. Rev. J. Mater. Sci. **4**(3), 1–5 (2016b)

A. Verma, A. Gaur, V.K. Singh, Mechanical properties and microstructure of starch and sisal fiber biocomposite modified with epoxy resin. Mater. Perform. Charact. **6**(1), 500–520 (2017)

A. Verma, A. Parashar, M. Packirisamy, Atomistic modeling of graphene/hexagonal boron nitride polymer nanocomposites: A review. Wiley Interdiscip. Rev. Comput. Mol. Sci. **8**(3), e1346 (2018a)

A. Verma, P. Negi, V.K. Singh, Physical and thermal characterization of chicken feather fiber and crumb rubber reformed epoxy resin hybrid composite. Adv. Civil Eng. Mater. **7**(1), 538–557 (2018b)

A. Verma, P. Negi, V.K. Singh, Experimental investigation of chicken feather fiber and crumb rubber reformed epoxy resin hybrid composite: Mechanical and microstructural characterization. J. Mech. Behav. Mater. **27**(3–4) (2018c)

A. Verma, K. Joshi, A. Gaur, V.K. Singh, Starch-jute fiber hybrid biocomposite modified with an epoxy resin coating: Fabrication and experimental characterization. J. Mech. Behav. Mater. **27**(5–6) (2018d)

A. Verma, A. Parashar, M. Packirisamy, Tailoring the failure morphology of 2D bicrystalline graphene oxide. J. Appl. Phys. **124**(1), 015102 (2018e)

A. Verma, P. Negi, V.K. Singh, Experimental analysis on carbon residuum transformed epoxy resin: Chicken feather fiber hybrid composite. Polym. Compos. **40**(7), 2690–2699 (2019a)

A. Verma, A. Parashar, M. Packirisamy, Effect of grain boundaries on the interfacial behaviour of graphene-polyethylene nanocomposite. Appl. Surf. Sci. **470**, 1085–1092 (2019b)

A. Verma, L. Budiyal, M.R. Sanjay, S. Siengchin, Processing and characterization analysis of pyrolyzed oil rubber (from waste tires)-epoxy polymer blend composite for lightweight structures and coatings applications. Polym. Eng. Sci. **59**(10), 2041–2051 (2019c)

A. Verma, R. Kumar, A. Parashar, Enhanced thermal transport across a bi-crystalline graphene–polymer interface: An atomistic approach. Phys. Chem. Chem. Phys. **21**(11), 6229–6237 (2019d)

A. Verma, C. Singh, V.K. Singh, N. Jain, Fabrication and characterization of chitosan-coated sisal fiber–Phytagel modified soy protein-based green composite. J. Compos. Mater. **53**(18), 2481–2504 (2019e)
A. Verma, A. Parashar, M. Packirisamy, Role of chemical Adatoms in fracture mechanics of graphene Nanolayer. Mater. Today Proceed. **11**, 920–924 (2019f)
A. Verma, K. Baurai, M.R. Sanjay, S. Siengchin, Mechanical, microstructural, and thermal characterization insights of pyrolyzed carbon black from waste tires reinforced epoxy nanocomposites for coating application. Polym. Compos. **41**(1), 338–349 (2020a)
A. Verma, A. Parashar, N. Jain, V.K. Singh, S.M. Rangappa, S. Siengchin, Surface modification techniques for the preparation of different novel biofibers for composites, in *Biofibers and Biopolymers for Biocomposites*, (Springer, Cham, 2020b), pp. 1–34
A. Verma, N. Jain, V.K. Avinash Parashar, S.M.R. Singh, S. Siengchin, Chapter 7: Design and modeling of lightweight polymer composite structures, in *Lightweight Polymer Composite Structures: Design and Manufacturing Techniques*, (Taylor & Francis Group (CRC Press), Boca Raton, 2020c), pp. 193–224
A. Verma, N. Jain, V.K. Avinash Parashar, S.M.R. Singh, S. Siengchin, Chapter 1: Lightweight graphene composite materials, in *Lightweight Polymer Composite Structures: Design and Manufacturing Techniques*, (Taylor & Francis Group (CRC Press), Boca Raton, 2020d), pp. 1–20
A. Verma, A. Parashar, S.K. Singh, N. Jain, M.R. Sanjay, S. Siengchin, Chapter 16: Modeling and simulation in polymer coatings, in *Polymer Coatings: Technologies and Applications*, (Taylor & Francis Group (CRC Press), Boca Raton, 2020e), pp. 309–324
A. Verma, N. Jain, S. Rastogi, V. Dogra, M.R. Sanjay, S. Siengchin, R. Mansour, Chapter 4: Mechanism, anti-corrosion protection and components of anti-corrosion polymer coatings, in *Polymer Coatings: Technologies and Applications*, (Taylor & Francis Group (CRC Press), Boca Raton, 2020f), pp. 53–66
A. Verma, N. Jain, S.M.R. Kalpana, S. Siengchin, M. Jawaid, Chapter 10: Natural fibers based bio-phenolic composites, in *Phenolic Polymers Based Composite Materials*, (Springer Nature, Singapore, 2020g), pp. 153–168
A. Verma, A. Parashar, N. Jain, V.K. Singh, S.M. Rangappa, S. Siengchin, Surface modification techniques for the preparation of different novel biofibers for composites, in *Biofibers and Biopolymers for Biocomposites*, (2020h), pp. 1–34
A. Verma, N. Jain, A. Parashar, A. Gaur, M.R. Sanjay, S. Siengchin, Lifecycle assessment of thermoplastic and thermosetting bamboo composites, in *Bamboo Fiber Composites*, (Springer, Singapore, 2021a), pp. 235–246
A. Verma, W. Zhang, A.C. van Duin, ReaxFF reactive molecular dynamics simulations to study the interfacial dynamics between defective h-BN nanosheet and water nanodroplets. Phys. Chem. Chem. Phys. **23**, 10822–10834 (2021b)
S. Yadav, V.K. Srivastava, Effect of thickness and crack length on the impact behaviour of particle loaded GFRP composite. Int. Res. J. Eng. Technol. **2**(02), 115 (2015)

Part II

Epoxy/Natural Fiber Composites

Introduction to Epoxy/Natural Fiber Composites

18

Hossein Ebrahimnezhad-Khaljiri, Reza Eslami-Farsani, Moslem Najafi, and Ali Saeedi

Contents

H. Ebrahimnezhad-Khaljiri · R. Eslami-Farsani (✉) · M. Najafi
Faculty of Materials Science and Engineering, K. N. Toosi University of Technology, Tehran, Iran
e-mail: ebrahimnezhad-k@email.kntu.ac.ir; eslami@kntu.ac.ir; moslem.najafi@kntu.ac.ir

A. Saeedi
Faculty of Mechanical Engineering, Iran University of Science and Technology, Tehran, Iran
e-mail: asaeedi@mail.iust.ac.ir

S. Mavinkere Rangappa et al. (eds.), *Handbook of Epoxy/Fiber Composites*,
https://doi.org/10.1007/978-981-19-3603-6_19

Abstract

Although, the epoxy composites reinforced with the synthetic fibers like carbon, glass, and Kevlar fibers had the incredible progress in the last decades, the environmental issues are one of the most important challenges about them. Therefore, replacing the natural fibers with the synthetic fibers in many aspects of engineering is one of the simplest ways for these issues. The natural fibers can be categorized according to their natural sources. Although, these fibers can be extracted from mineral, animal, and plant sources, the natural plant fibers and in some cases animal natural fibers have capability to be used as reinforcement or filler into the epoxy resins. The natural plant fibers can be extracted from the seed, bast, leaf, straw, grass, and fruit. Having the various plant sources has caused that these natural plant fibers have different features, which proper them in many applications. In this chapter, the feature of each plant fiber sources as reinforcement into the epoxy resin, the new ideas and applications of plant fibers/epoxy composites, and capability of these composites were introduced. Also, the animal fibers/epoxy composites were investigated in the separate section.

Keywords

Epoxy composites · Natural fibers · Eco-friendly composites · Bio-composites · Plant fibers

Introduction

Although, the concrete and metal materials are used in the various industries such as building, aerospace, marine, etc., replacing them with the advanced composite materials especially the composites reinforced with glass, carbon, and Kevlar fibers has extremely grown in the last decade. So, it can be expected that the polymeric matrix composites reinforced with fibers will be remarkably used, in the near future, due to having advantages like high strength, low weight, corrosion resistance, and low maintenance cost. The researches show that one of the most commonly used polymeric materials as matrix in the composite structures is the epoxy resins and their families. This is due to the mechanical and physiochemical properties of epoxy resin, as compared with the other resins. Despite of mentioned advantages about the polymeric composites, these materials have environmental issues, which are one of the most important challenges about them. Therefore, studying on the green structures in many aspects of engineering has caused to replace some of them with the eco-friendly composite structures. Hence, to reduce the environmental issues, the engineers and researchers have focused to fabricate the environment-friendly

composites with a biodegradability and recyclability features (Ebrahimnezhad-Khaljiri and Eslami-Farsani 2017).

One of the proper ways for responding to environmental issues is to replace the natural fibers with the synthetic fibers (like glass, carbon, and Kevlar fibers) into the composite structures. The natural fibers, in the simplest definition, are the fibers that not to be synthetic or man-made. In the viewpoint of some researchers, according to the production resources, the natural fibers can be classified into plant and animal natural fibers major groups. But, some other researchers believe that the fibers with mineral resources such as asbestos and brucite can be introduced as third major groups of natural fibers. The recent reviews depict that the new introduced fibers like modal, lyocell, and viscose are defined as natural/man-made fibers (Azwa et al. 2013).

Figure 1 illustrates the schematic representation of synthetic/natural fiber classifications. Based on this figure, it can be seen that the plant natural fibers have more variety, as compared with the animal or mineral natural fibers. Based on the investigations of Sanjay et al. (2019), reported as review papers, the plant natural fibers can be categorized as primary and secondary subject to their application. The primary plants like jute, hemp, etc. are cultivated because of their fibers, while, banana, pineapple, etc., as secondary plants, are grown due to their fruits, and their fibers are byproduct of them.

Like other materials, the natural fibers have their special features, which influence on their applications. Sanjay et al. (2019) collected these features, reported as review papers, in which the outcomes of those were listed in Table 1. Based on these data, these researchers mentioned the capability of natural fibers for using in the various applications, which have been listed in Table 2. Based on Table 2, it can be seen that the natural fibers can be good candidates for using instead of glass, carbon, or Kevlar fibers as synthetic reinforcements into the composite structures. In order to have deeper and more comprehensive viewpoint, it is require that the features of these fibers into the composite structures as reinforcement be investigated. Pickering et al. (2016) collected these features, which have been reported in Table 3.

The variety of plant natural fibers, which can be used as reinforcement into the epoxy resins, has been illustrated in Fig. 1. In general, based on the production resources, these fibers can be classified into the six different groups, which are bast, leaf, seed, straw, grass, and fruit fibers. The high variety of plant natural fibers has caused these fibers be of proper choices for using instead of synthetic fiber in the composite structures for various applications. The properties of natural fibers have depended to their structures. Therefore, a brief study on these structures is so necessary. The structure of these fibers has been illustrated in Fig. 2. These fibers have complex layered structures, which consist of a primary cell wall and three secondary cell walls. Among primary walls, three second cell walls have important role on the mechanical properties of plant natural fibers. The main structure of each cell wall is the cellulose/lignin-hemicellulose composite. Also, other components of these cell walls are a minor amount of pectin, oil, and waxes. The cellulose acts as reinforcement in the lignin/hemicellulose matrix. The percentage of cellulose into the plant natural fibers has an important role on the mechanical properties of them, while the percentage of hemicellulose influences on the thermal and biological

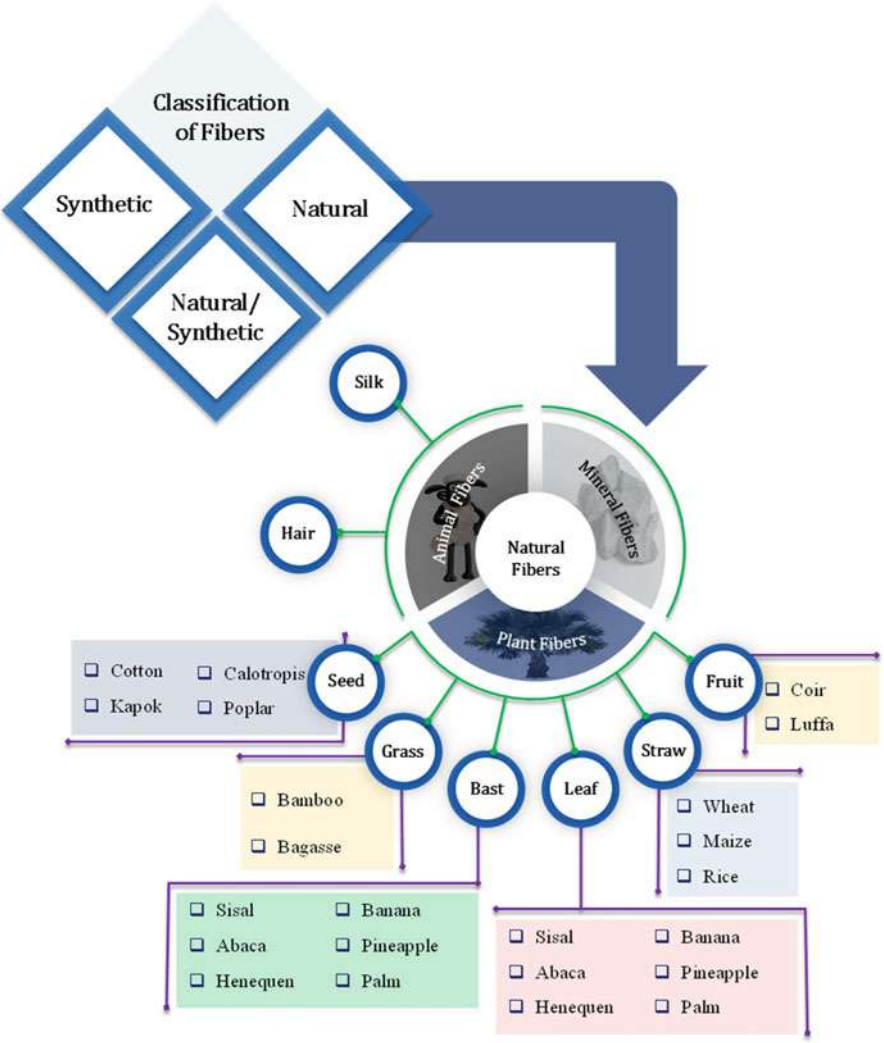

Fig. 1 The classification of fibers

degradation properties of those (Azwa et al. 2013). Therefore, the comprehensive cognition about the structure of plant natural fibers is so necessary, so, based on this cognition, the selection of fibers for desired application can be easier.

Given up the researches, the epoxy/natural fibers composites can be studied in the seven separate parts. The first to sixth sections can be epoxy-based composites, which were reinforced by seed, bast, leaf, straw, grass, and fruit-based fibers, respectively. By reviewing in the various literatures, it can be seen that many of researchers extracted the cellulose as nanomaterials from plant natural fibers by different chemical methods. The nano-cellulose can be added as reinforcement in the different matrices especially

Table 1 The features of natural fibers

Advantages	Disadvantages
Lower specific weight and higher specific strength than glass	Lower strength, especially impact strength
Renewable resources	Variable quality
Low production cost	Moisture absorption
Friendly fabrication process	Restricted maximum processing temperature
High electrical resistant	Lower durability
Good insulation for thermal and acoustic application	Poor fire resistant
Biodegradability	Weak bonding with the polymeric materials
Good thermal and acoustic insulating	Price fluctuation due to agricultural politics

Adapted from Sanjay et al. (2019) with the permission of Elsevier

Table 2 The potential applications of natural fibers

Industry	Application
Aerospace	Tails, wings, propellers, helicopter fan blades
Automotive	Door frames, door shutters, window frame, mirror casing
Marine	Boat hulls, fishing rods
Building and construction	Roofing sheets, bricks, furniture panels, storage tanks, pipelines
Sports and leisure goods	Ice skating boards, bicycle frames, baseball bats, tennis racket, fork, helmet, postboxes
Electronics	Laptop and mobile cases, chip boards, projector, and voltage stabilizer cover
Others	Pipes carrying coal dust, construction of weapons, textiles, industrial fans, paper, and packaging

Adapted from Sanjay et al. (2019) with the permission of Elsevier

Table 3 Advantages and disadvantages of natural plan fibers composites

Advantages	Disadvantages
Low density and high specific strength and stiffness	Lower durability than for synthetic fiber composites but can be improved considerably with treatment
Fibers are a renewable resource, for which production requires little energy and involves CO_2 absorption, while returning oxygen to the environment	High moisture absorption, which results in swelling
Fibers can be produced at lower cost than synthetic fiber	Lower strength, in particular impact strength compared to synthetic fiber composites
Low hazard manufacturing processes	Greater variability of properties
Low emission of toxic fumes when subjected to heat	Lower processing temperatures limiting matrix

Adapted from Pickering et al. (2016) as open access source of Elsevier

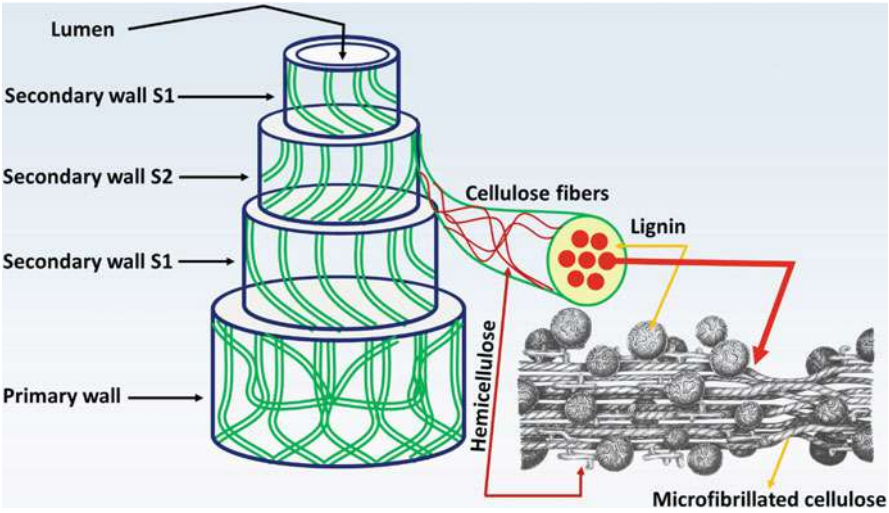

Fig. 2 The structure of natural fiber. (Adapted from Azwa et al. (2013) with the permission of Elsevier and Stokke et al. (2014) with the permission of John Wiley and Sons)

epoxy-based materials. Therefore, some admirable research works were collected and reviewed into the six introduced sections. It should be noted that the research about the animal-based natural fibers is too limited. So, it can be said that only the silk fibers can be used as filler or reinforcement into the epoxy resins. In the seventh section, the animal-based natural fibers/epoxy composites are investigated.

The Seed-Based Natural Fibers/Epoxy Composites

Cotton Fiber-Reinforced Epoxy Resin

One of the seed-based fibers for using into epoxy matrix is the cotton fibers. These fibers can be used in the different forms into the epoxy composites. Based on the researches, it can be found that the many researchers worked on the using the waste cotton fibers into the epoxy matrix. As we know, China is one of the biggest producers and consumers of cotton fibers, so, in the year of 2017, the cotton has been harvested about 5486 thousand tons into this country. The developed extraction methods of cotton with the high production efficiency make it good choice for using as reinforcement into the epoxy composites. Based on the reported researches, over the period of 2011 to 2015, about 140 million tons of the waste textiles have been produced in China. These waste cotton fibers have special properties like low density and high specific strength (Shao et al. 2020). Also, these fibers can be degraded and recycled. So, they can be good candidates for using into epoxy matrix as reinforcement. For example, Shao et al. (2020) fabricated the cotton fibers/epoxy composite. The fabrication process of this composite has been illustrated in Fig. 3. They reported that the cotton fibers had the positive role on the tensile strength, tensile

modulus, flexural, and impact strength. Also, the cotton fibers changed the fracture behavior of the epoxy matrix, so, the epoxy composite had the tougher fracture surface, in comparison with the neat epoxy.

Although, the cotton fibers can be used into the epoxy matrix, they have a weak interface with the epoxy matrix, because of their hydrophilic nature. Therefore, during the fabrication of epoxy composite with the cotton fibers, the fibers should be surface modified. One of the interesting research works about this modification is the work of Wang et al. (2016). The aim of these researches was to fabricate the cotton-epoxy composites as super-hydrophobic coating for protecting the aluminum sheets under the harsh working conditions. Confirming the fabrication of this coating was done by FTIR and water contact angle methods, which can be seen in Fig. 4.

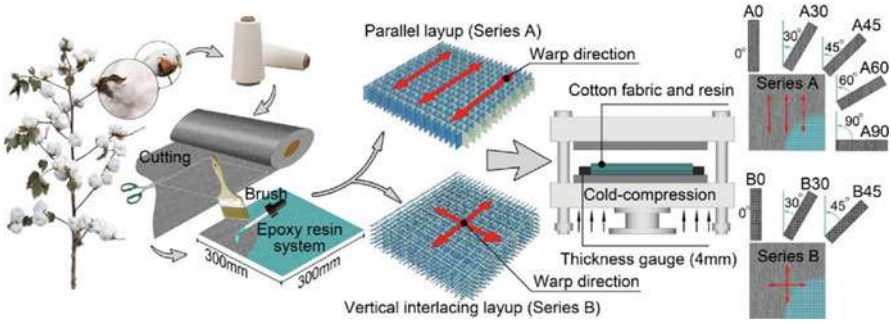

Fig. 3 The Schematic illustration of the fabrication of cotton fabric reinforced epoxy laminates. (Reprinted from Shao et al. (2020) with the permission of John Wiley and Sons)

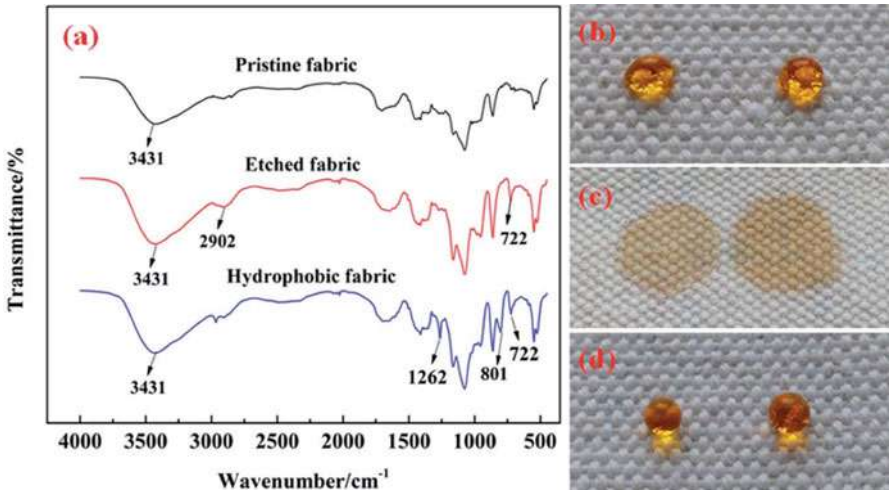

Fig. 4 The cotton-epoxy composites as super-hydrophobic coating for protecting the aluminum sheets, (**a**) confirming that by FTIR method, (**b**) pristine cotton, (**c**) etched cotton fibers, (**d**) etched super-hydrophobic fabrics. (Reprinted from Wang et al. (2016) with the permission of Royal Society of Chemistry)

Extracting the cellulose fibers from the cotton fibers and using them into the epoxy matrix is an interesting subject about the cotton ingredients into the epoxy composites. In the study of Tang and Weder (2010), they extracted the cellulose whiskers or nanofibers from cotton by solvent exchanging and lyophilization processing methods. Then, they fabricated the cotton cellulose whiskers/epoxy nanocomposites, which can be seen in Fig. 5.

One of the novel ideas for using the ingredients of cotton into the epoxy matrix was introduced by Ramprasad et al. (2018). These researches used the cotton dust waste as reinforcement into the epoxy matrix. They mentioned that the cotton dust is one of the industrial wastes, which are formed during the weaving the cotton fibers in the textile mills. These dust wastes have similar properties to the cotton fibers. In practical, these researches found the new application for using the waste fibers, which can be used instead of synthetic fibers into the epoxy matrix in the conventional applications. Although, many researches focused on using the cotton fibers into the epoxy matrix for fabricating the eco-friendly structures, adding these fibers into the bio-based epoxy resins is the new approach for substituting the eco-friendly structures instead of conventional composite structures.

Kapok Fiber-Reinforced Epoxy Resin

The second seed-based natural fibers/epoxy composites belonged to the kapok (*Ceiba pentandra*) fibers, which extracted from kapok trees. Based on the researches, the kapok trees are one of the Bombacaceae families and grow in Asia, Africa, and South America. Kapok fibers have been composed of two major layers, which have different cellulose microfibrillar orientations. In the outer layer, the microfibrillar is oriented transversely to the fiber axis, whereas, in the inner layer,

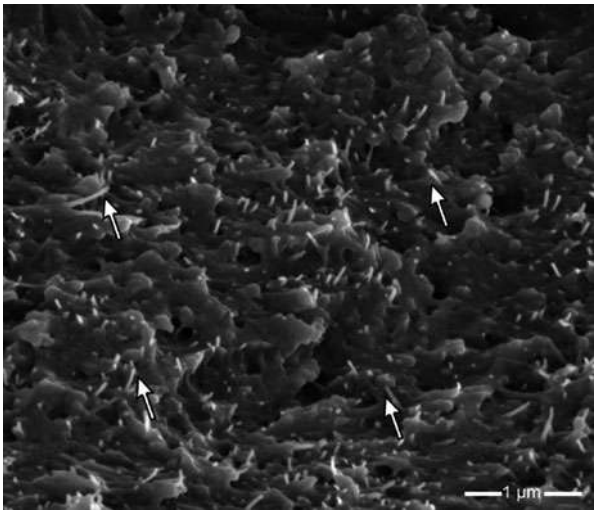

Fig. 5 The SEM image from the fractured surfaces of cellulose whisker/epoxy nanocomposite. (Adapted from Tang and Weder (2010) with the permission of American Chemical Society)

they oriented nearly parallel to that axis. The kapok fibers are eight times lighter than cotton fibers (Nilsson and Björdal 2008). This feature can be due to the hollow structure of that. Based on the researches, it can be estimated that the kapok fibers have near the 80% hollowness in their structures. Because of these hollow structures, the kapok fibers can be used as reinforcement into the composites, which have been designed for special applications like sound and energy absorbers. Although, this feature limits their usages, by blending them with the cotton fibers, they can be used in the various composites. The research about the kapok fibers into the epoxy matrix is too limited. The only noteworthy research about adding them into the epoxy was done by Wu et al. (2018) in order to investigate flame retardancy of epoxy composites. This research group capsulated the triphenyl phosphate as flame retarding agent into the hollow kapok fibers and then dispersed them into the epoxy resin. The obtained results showed that the mechanical properties were stable and not the noteworthy variations but the thermal behavior of that improved.

Calotropis Fiber-Reinforced Epoxy Resin

The third route of seed fibers for using as reinforcement into the epoxy matrix is *Calotropis*. In this plant, in addition to the extraction of fibers from seeds, the stem can also be used as a source of natural fiber. The reported researches about this plant showed that the two famous species of *Calotropis* can be used as an additive in the epoxy matrix, which are *Calotropis gigantea* and *Calotropis procera*. The extracted fibers from the seed of *Calotropis* have hollow structures like kapok fibers, but the stem fibers of that have bundles structures (seen Fig. 6) (Gao et al. 2020; Ramasamy et al. 2018). In comparison with the cotton fibers, the stem fibers of *Calotropis* have higher density and tensile and abrasive strengths, so, they can be used into the composites with the higher mechanical properties. In addition to the stated applications, the seed of *Calotropis* can be a proper source for extracting the nano-cellulose

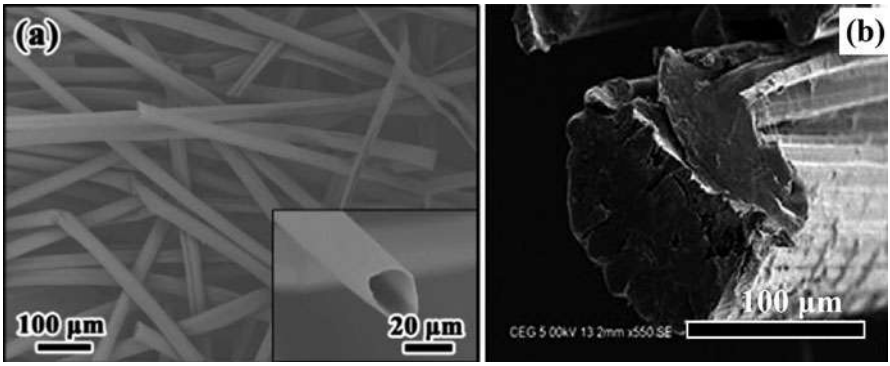

Fig. 6 The SEM image from, (**a**) the seed of *Calotropis*. (Adapted from Gao et al. (2020) with the permission of Elsevier, (**b**) the stem of *Calotropis*. Adapted from Ramasamy et al. (2018) with the permission of Taylor & Francis)

fibers to use as reinforcement into the epoxy resins. Also, the extracted powders from the stem of *Calotropis* can be added as second reinforcing agent into the epoxy resins (Gao et al. 2020).

Poplar Fiber-Reinforced Epoxy Resin

The fourth seed-based fibers for using into polymeric composites are poplar fibers. Poplar catkin fibers are cotton-like substance that surrounds the seed on the branches of poplar tree (seen Fig. 7) (Zhang et al. 2018), although these fibers cannot directly be used into the epoxy resins for improving the mechanical performances. However, they can be used for fabricating the hollow carbon fibers, due to having a tubular structure. Also, they can be used as reinforcement into the epoxy resin for sound absorber applications. They can be good choice for extracting the cellulose nanofibers for using into epoxy-based composites. Based on Fig. 7d, it can be said that these fibers can be used as healing agent containers into the vascular based smart epoxy composites.

The Bast-Based Natural Fibers/Epoxy Composites

Flax Fiber-Reinforced Epoxy Resin

As previously mentioned, one of the extraction sources of plant fibers is their bast. Among the various natural fibers, the flax known as *Linum usitatissimum* is extensively used into the composite materials. The reported results showed that the flax fibers have the best mechanical performance as compared with other natural fibers. The density of flax is about 1.45 g/cm^3, and, also, the stiffness of that has been reported approximately 70 GPa, which is even higher than the stiffness of glass fibers (George et al. 1999). Therefore, it can be a good candidate for using instead of glass fibers. Hence, many efforts have been done to use the flax fibers into the epoxy matrix by different research groups. The flax fibers are extracted from plant by retting method. The technical fibers with the dimension of 30–90 cm occur in bundles within pericycle. Each stem has approximately 15 bundles, each containing about 12 to 40 elementary fibers (seen Fig. 8) (Jia and Fiedler 2020). The length of each elementary fiber is about 30 to 90 mm. The presence of hydrogen group in the flax fibers improves the adhesion of them with the epoxy resins. It should be noted that the seed of this plant has linseed, which is used for producing the linseed oil. This oil has capability to be used as precursor for fabricating the bio-based epoxy resins (George et al. 1999). In the light of the above, it can be said that by harvesting the flax plant, the bio-fibers and bio-epoxy resins can be produced, which can be used to fabricate the eco-friendly composites.

Moudood et al. (2019) fabricated the flax/epoxy composites and exposed them on the different environmental conditions to investigate the effect of those on the mechanical properties of composites. These conditions were water immersion,

Fig. 7 The Photos from, (**a**) the poplar tree, (**b** and **c**) poplar catkin fibers, (**e** and **f**) SEM image of poplar fibers. (Reprinted from Zhang et al. (2018) as open access source of Springer Nature)

water humid environment, and freeze-thaw conditions. They reported that the mechanical properties were clearly reduced by water aging, which were about 9, 57, 64, and 70% for tensile strength, elastic modulus, flexural strength, and modulus, respectively. The mentioned mechanisms for these reductions were damaging the epoxy matrix by hydrolysis and plasticization via water molecules. They also concluded that the warm humid environments and freezing-thawing cycles had a slightly effect on the mechanical properties of these composites.

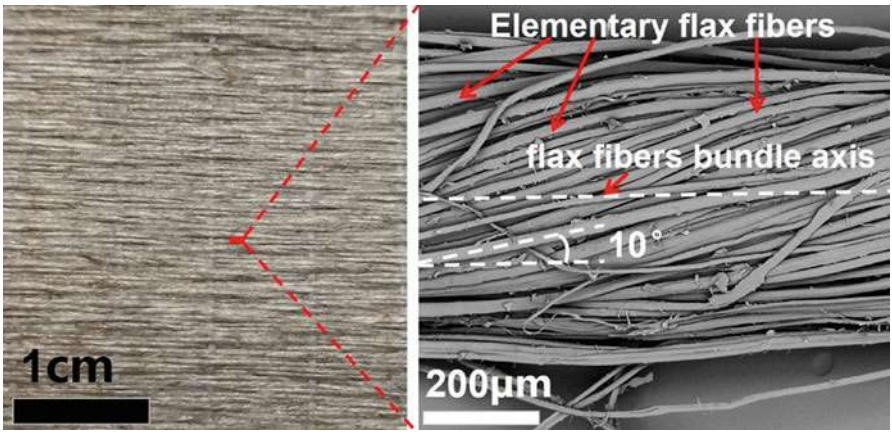

Fig. 8 The UD flax fibers fabric (left) and a SEM picture of an as received flax fiber bundle (right). (Reprinted from Jia and Fiedler (2020) with the permission of Elsevier)

Berges et al. (2016) surveyed the effect of moisture conditions on the static-cyclic and dynamic behavior of flax/epoxy composites. The obtained results showed that the diffusion of water molecules improved the tensile and fatigue behavior of these composites. They mentioned that the water sorption activated the hardening mechanisms of flax fibers into the epoxy matrix. These hardening mechanisms are the cellulose microfibrils reorientations and stress-induced crystallization of amorphous cellulose in the fiber wall.

Scida et al. (2013) discussed about the water absorption on the mechanical properties of flax/epoxy composites. They mentioned that waters acted as a plasticizer. It means that the water increased the microfibrils movements, which caused to reduce the mechanical properties. In the light of the above, it can be said that the two special features of flax fibers are plasticizer and recrystallization of the microfibrils, which the competition between them into the epoxy matrix has the important role on the mechanical behaviors of flax/epoxy composites under the different mechanical loadings.

Having these features has caused the flax fibers to be a good choice for using in the fatigue applications, which has attracted the attentions of many researchers. For example, Asgarinia et al. (2015) surveyed the tension-tension fatigue behavior of flax fibers/epoxy composites. They found that the reorientation of misaligned fibers in the viscoelastic matrix under the tension was the reason of stiffening effect of these composites, which improved the fatigue behavior of that. In another work, Liang et al. (2014) investigated the fatigue behavior of this composite with the different configurations of flax fibers. The characterized phenomena from fatigue tests showed that annealing of the epoxy matrix and reorienting the flax fibers' microfibrils reduced the effect of damage mechanisms.

Due to environmental issues, many researchers have tried to fabricate the complete bio-based composite structures with the acceptable mechanical properties for

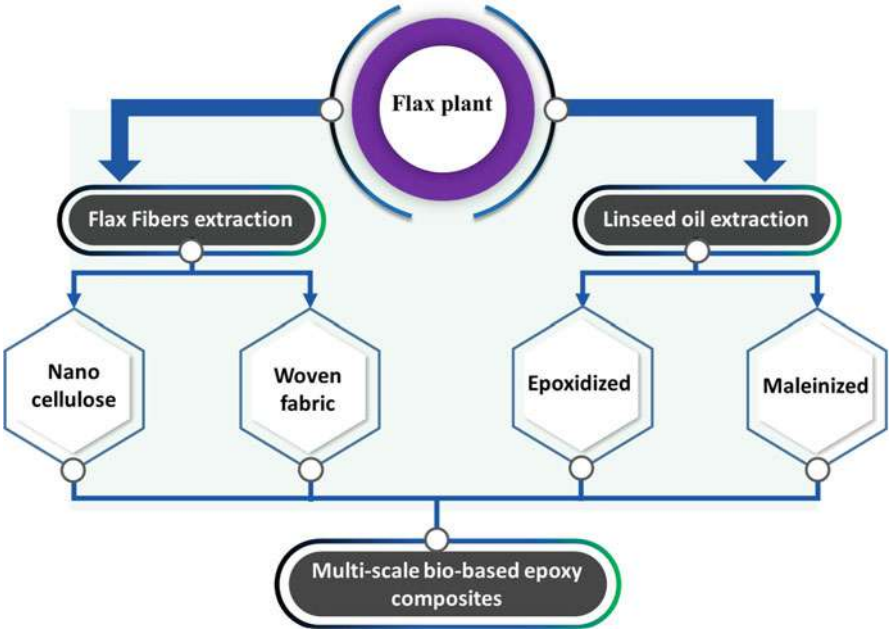

Fig. 9 The schematic flowchart of fabrication process of bio-based multi-scale composite structures

substituting those with the conventional epoxy composites, which reinforced with the high-performance fibers such as glass, carbon, Kevlar, or ultrahigh-molecular-weight polyethylene fibers (Ebrahimnezhad-Khaljiri et al. 2020a; Bigdilou et al. 2020). One of the best candidates for reaching this goal is the flax plant. Figure 9 illustrates the schematic flowchart of fabrication process of bio-based multi-scale composite structures. The extracted linseed oil from the seed of flax plant can be epoxidized and maleinized for producing the bio-epoxy and bio-hardener. Also, the extracted flax fibers can be used for fabricating the woven fabrics or synthesizing the nano-cellulose fibers, which both of them can be used as reinforcement. By using these bio-epoxy and bio-hardener and flax fabrics, Fombuena et al. (2019) fabricated the bio-composite structure, which had the approximately 78% bio-based content.

Hemp Fiber-Reinforced Epoxy Resin

Among the various kinds of natural fibers, the hemp (*Cannabis sativa*) as bast fibers is one of the most attractive fibers, due to having the special features. Fast-growing, capability to grow around the world, low cost, high specific strength, increasing the stiffness and strain of composites, and having high cellulose content are the features of hemp fibers. As we know, the cellulose has crystal structure. So, by increasing the content of that into the hemp fibers, it can be said that the hemp fibers have

noteworthy mechanical properties, which can be comparable with the glass and Kevlar fibers (Thygesen et al. 2007). Based on the researches, the cellulose in the hemp fibers consists of β-1,4-linked glucan chains and is organized into the microfibrils interlocked by xyloglucan, which can increase the mechanical properties of that (Liu et al. 2016). The common producing method of hemp fibers is the defibration by water retting method, which the hemp stem is placed under water and then the microorganisms attack to the hemp stem. After this production process, the cellulose content and stiffness of hemp fibers can be about 74% and 88 GPa, respectively (Thygesen et al. 2007).

Due to these features, the researchers have done many efforts to fabricate the hemp fibers/epoxy composites via various methods like the resin transfer molding and resin powder molding methods. Boccarusso et al. (2018) developed the new continuous process for fabricating the hemp/bio-epoxy grid structures. Their production process had five steps, which were impregnation, resin absorption, resin content reduction, cutting, and polymerization. In the impregnation step, the hemp fibers were pulled and impregnated to the resin bath. Then, the impregnated hemp fibers were squeezed via two rolls. In the following, for reducing the excess resin, the hemp fibers passed under the air jet system. In the following, the hemp fibers/epoxy was cut by scissors. In the final step, the hemp/epoxy layers were stacked into the mold. After reaching to required numbers of these layers for fabricating the part, the mold was closed under the controlled temperature and pressure to polymerize the epoxy resin. In the other study, Xu et al. (2018) added the self-exothermic curing agent to the epoxy resin for fabricating the hemp fibers/epoxy composites in the room temperature with the proper thermal and mechanical properties. In practical, these researchers by blending the acrylic acid with the 4,4′-diaminodiphenylmethane increased the curing rate of epoxy in the ambient temperature. The obtained results showed that this composite had the proper mechanical and thermal properties. In the light of the above, it can be mentioned that many efforts have been done to fabricate the hemp/epoxy composites. Therefore, it can be expected that these composites can be used instead of conventional composites.

Jute Fiber-Reinforced Epoxy Resin

Jute is the common name of extracted fibers from the *Corchorus* plants. The dark and white jute fibers extracted from the bast layers of *Corchorus olitorius* and *Corchorus capsularis*, respectively. It has the polar groups in the chemical structure. Therefore, the bundles of jute fibers have features like hydrophilicity, biodegradability, and moderate mechanical properties. But, these bundles have some drawbacks like coarseness, low extensibility, ready susceptibility to microbial attack, having shrinkage after the washing, and poor abrasion resistance. However, the jute fibers are recognized as low-cost and eco-friendly fibers. The production and research trends of jute fibers/epoxy composites during the last few years show that they have been used instead of synthetic fibers/epoxy composites as secondary or tertiary structural composites (Masoodi and Pillai 2012). Although, the jute fibers/epoxy composites

have moderate mechanical properties, as compared with the synthetic fibers/epoxy composites, many researches have been done to improve the mechanical properties of those by surface modifying of jute fibers, adding nanoparticles, and hybridizing with the other fibers (Ebrahimnezhad-khaljiri et al. 2020b). Because of having moderate mechanical properties, the jute fibers/epoxy composite can be a good choice for comparing that with the mechanical properties of various natural or synthetic fibers/epoxy composites, which have been reviewed in the following.

The comparison study between jute fibers/epoxy and hemp fibers/epoxy composites was done by Santulli and Caruso (2009). The content of reinforcement into the epoxy matrix in this work was about 45 vol.%. The obtained results showed that the elastic and flexural modulus of plain weave jute fibers/epoxy composite was about 4.8 and 2.8 GPa, respectively, whereas, both of those properties in the hemp fibers/epoxy composite were reported about 5.5 and 4.2 GPa, respectively. The outcome of this research showed that the hemp fibers had the better mechanical performance, as compared with the jute fibers.

In the study of Boopalan et al. (2013), the mechanical and thermal properties of epoxy composites reinforced by jute and banana fibers were compared. The reported results showed that the banana/epoxy composite had the higher tensile strength, elastic modulus, flexural strength and modulus, and impact strength than the jute/epoxy composite. Also, the heat deflection of banana/epoxy composite was higher approximately 20% than that of jute/epoxy composite. Also, the absorbed water by jute fibers was lower than the banana fibers into the epoxy composites. The efficiency comparison between flax and jute fibers into the epoxy as polymeric matrix was studied by Fiore and Calabrese (2019). These researchers included the unmodified and modified jute and flax fibers into the epoxy composites for comparing the mechanical and thermomechanical performance of those. It should be noted that the surface modification in this work was done by sodium bicarbonate. Based on the reported results between untreated jute and flax fibers, the jute fibers had the higher mechanical and thermomechanical properties. But by using the surface modification process, the performance of flax fibers into the epoxy matrix was incredibly improved, so, the highest reported mechanical properties belonged to the treated flax fibers/epoxy composite. The effect of this treatment on improving the adhesion in flax fibers and reducing that in the jute fibers were the reasons of this behavior.

The study on the mechanical properties of kenaf fibers/epoxy and jute fibers/epoxy composites was done by Sanjay and Yogesha (2018). The tensile and flexural results indicated that the jute fibers/epoxy composite had the lower mechanical properties, as compared with the kenaf fibers/epoxy composite. The higher void content in the jute fibers/epoxy composite can be the reason for having the lower mechanical properties. Comparison between the jute and bamboo fibers into the epoxy matrix was investigated by Daniel et al. (2019). In this work, the bamboo/epoxy composite had the higher tensile strength, as compared with the epoxy composite containing the jute fibers. But, the impact strength of jute/epoxy composite was twice that of bamboo/epoxy composite. The flexural strength of these composites had the similar trend like tensile strength. By substituting the bamboo

fibers with the jute fibers into the epoxy matrix, the compressive strength was increased more than five times. The improper adhesion between jute and epoxy and higher void content in this composite were the reasons of this weak performance in the compression loadings.

Kenaf Fiber-Reinforced Epoxy Resin

The other plant source for extracting the natural bast fibers is the *Hibiscus cannabinus* L. with the trade name of kenaf fibers. The kenaf plant can be grown in 4 or 5 months after sowing the seeds and is able to reach the height of more than 3 m with the diameter of 3 to 5 cm. Also, this plant is compatible with the various weather conditions (Sanjay and Yogesha 2016). For this reason, it is one of the abundant, renewable, and biodegradable lignocellulose sources for using into epoxy matrices. These fibers with the density of 1.3 g/cm^3 can be one of the lightest fibers, which proper them for using as reinforcement into the epoxy resins instead of synthetic fibers like carbon or glass fibers in the secondary or tertiary applications. Also, the kenaf fibers can be hybridized with the synthetic fibers for reducing the weight and production costs of composite structures. For this reason, many efforts have been done to develop the kenaf fibers/epoxy composites. The research areas about these composites are very wide. Therefore, these areas can be categorized in the three major groups.

Some research groups have been focused on the improving the properties, optimizing the performances, and characterizing the features of kenaf fibers/epoxy composites. Kumar et al. (2017) distributed the kenaf fibers with the various length of 5 to 50 mm and different weight fractions of 25 to 40 wt.% to enhance the dynamic mechanical properties of kenaf fibers/epoxy composites. Investigating the thermal performance of kenaf fibers/epoxy composites was done by Azwa and Yousif (2013) through exposing these composites to high temperatures. The reported results showed that adding the kenaf fibers into the epoxy resin slightly improved the thermal stability of that. Also, the alkalization surface treatment reduced this improving trend. Up to 150 °C, increasing the exposure time caused the higher weight loss of this composite. But at the higher temperatures, the effect of that on the weight reduction had the lower influences. By using the SEM method, they found that the fiber/matrix debonding was the reason of mechanical degradations. Finding the optimum volume fraction, customizing the stacking sequence, and selecting the proper pattern of kenaf fibers by experimental and analytical methods are the examples of efforts of various research groups, which have been done to improve the performance of kenaf fibers/epoxy composites.

The second research field about the kenaf fibers/epoxy composites can be surface modification of kenaf fibers and fabricating process of their epoxy-based composites. The effect of alkaline treatment on the mechanical properties of these composites can be one of them. The third category about applied research works on the kenaf fibers/epoxy composites can be hybridization of kenaf fibers with the other fibers or with the nanoparticles. Hybridizing the kenaf fibers with the glass fibers or aramid

fibers is one of the interesting subjects, which was studied by various research groups. Given up the researches, it can be said that the kenaf fibers have proper capability to hybrid with the other natural fibers like jute and bamboo fibers, because of having the low density and proper specific strength (Sanjay and Yogesha 2016).

The Leaf-Based Natural Fibers/Epoxy Composites

Sisal Fiber-Reinforced Epoxy Resin

The third generation of natural plant fibers/epoxy composites is the leaf-based plant fibers. One of the proper choices of leaf-based fibers for using as reinforcement into the epoxy matrix is the sisal fibers. The sisal leaves have three types of fibers, which can be seen in Fig. 10. Based on the researches, the name of these fibers are mechanical, ribbon, and xylem. The sisal fibers are recognized as hard fibers, which extracted from the leaves of *Agave sisalana* plant. Yearly, about 4.5 million tons of sisal fibers are fabricated in the world. These fibers are grown in the tropical regions like Africa, the West Indies, and Far East. The sisal plants have 200–250 leaves, and each leaf contains 1000–1200 fiber bundles. The cellulose content of sisal fiber is about 78 wt.%. Also, the length and diameter of that are about 1–1.5 m and 100–300 μm, respectively (Li and Shen 2015).

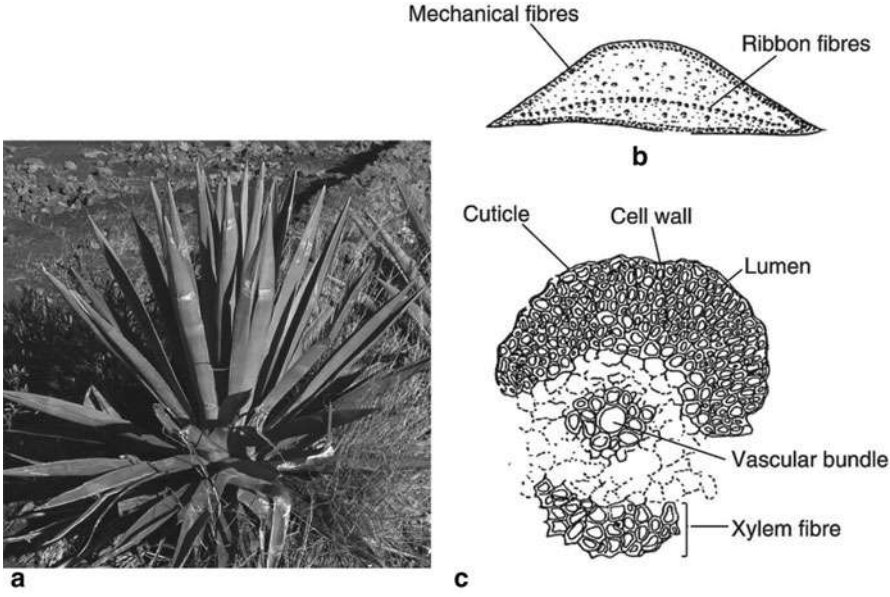

Fig. 10 The sisal, (**a**) the photograph of a sisal plant, (**b**) a sketch of the cross section of sisal leaf, (**c**) cross section of a ribbon-fiber bundle. (Reprinted from Li and Shen (2015) with the permission of Elsevier)

Like other natural fibers, the sisal fibers have OH (hydroxyl group) on their structures. So, they have low wettability with the epoxy resins, so, the surface modifications of those are so necessary. Therefore, many researchers focused to modify the surface of these fibers for using into epoxy matrix. Using the sodium hydroxide solution was one of the modification methods, which was recognized as alkaline surface modification. The other studied method was grafting the silane agent. The interesting modification was done by sodium bicarbonate, which was introduced as eco-friendly modification by Fiore et al. (2016).

Given up the applied researches, it seems that some researchers studied on the wear application of sisal fibers/epoxy composites. The influence of sisal fiber orientation and adding the short sisal fibers into the epoxy matrix for using on the wear conditions are the examples of these researches. The sisal fibers/epoxy composites have proper potential for using in the electrical applications. Using these composites as insulator was done by Shalwan et al. (2017). Also, modifying the sisal fibers for characterizing the electrical properties of those composites like dielectric constant, dielectric dissipation factor, and AC conductivity into the epoxy matrix was done by various research groups.

Abaca Fiber-Reinforced Epoxy Resin

The second leaf-based fiber, which can be used as reinforcement into the epoxy matrix, is the abaca fibers. The botanical name of these fibers is *Musa textilis*, which is a kind of banana grown extensively in the Philippines. Also, another name of these fibers is Manila hemp. These fibers are extremely harvested in the Philippines, and researches showed that this country can produce about 50,000 tons abaca fibers every year. Abaca fibers have interesting properties. The great mechanical strength, specific flexural strength near the glass fibers, resistance to the salt water, resistance to rotting, sustainability, and length about 3m are the features of these fibers. For this reason, the Mercedes Benz used the abaca composite parts. Also, using the abaca composites instead of glass fibers composites can save the energy about 60% in the automobiles (Punyamurthy et al. 2014).

Abaca fibers have vascular structures. Therefore, these fibers can only use as secondary or tertiary applications of composites. But, these structures can proper these fibers for using in the impact or thermal conductivity applications. Anisotropic thermal conductivity of abaca fibers, the physicochemical structures of abaca fibers on the thermal conductivity, and the effect of chemical treatment of abaca fibers on the thermal conductivity are the investigated researches about the thermal conductivity of these fibers into the epoxy matrix (Liu et al. 2012). It is worth noting that having the vascular structure reduces the density of these fibers, as compared with the other natural fibers. So, these fibers can be used into the epoxy composites as second or third reinforcement for reducing the weight of composite parts. In other words, the abaca fibers can be used in form of hybrid fibers into the epoxy resins. The hybridization of these fibers with the jute, flax, and glass fibers into the epoxy matrix has been investigated by various research groups.

Banana Fiber-Reinforced Epoxy Resin

Out of all natural fibers, the banana fibers are one of the emerging natural plant fibers for using into polymeric matrices especially epoxy resins, due to their proper specific strength and rotting resistance. The banana fibers have high cellulose content, which is about 60–65%. Also, these fibers have low microfibrillar angle (11°). The banana fibers are the waste product of banana cultivations. Hence, without any additional cost, these fibers can be one of the fiber sources for using as the reinforcement into the epoxy resins. The banana fibers can be comparable with the glass fibers. Also, the density of these fibers is lower than that of glass fibers. The main drawbacks of these fibers are high moisture absorption, low thermal stability, and weak bonding with the polymeric matrices (Gunge et al. 2019). Having the low density and noteworthy specific strength caused to use the banana fibers in form of hybrid fibers into the epoxy composite structures. Hybridizing the banana fibers with the synthetic fibers like carbon and glass fibers and most of the natural plant fibers such as sisal, hemp, flax, kenaf, and coir have been investigated by different research groups.

Henequen Fiber-Reinforced Epoxy Resin

The henequen fibers with the botanical name of *Agave fourcroydes* are another leaf-based natural plant fibers, which are similar to sisal fibers. These fibers grow in the Yucatan, Mexico, and obtain from 60 to 120 cm long leaves of agave plants. These cellulose-based fibers have a large number of hollow-type cells in each fiber. In other words, the structure of these fibers is tubular. Therefore, they are proper for using energy absorption applications and thermal and acoustic insulations (Cho et al. 2007). Having this structure was the main reason of rare research for using into polymeric composites especially epoxy resins, as compared with other natural plant fibers. In addition to the mentioned applications, these fibers can be used as container into the smart composite structures like the self-healing vascular system (Mohammadi et al. 2020) and producing the hollow carbon fibers for using into epoxy matrices. Also, these fibers have high cellulose content, which is about 77 w. %. So, it can be used for extraction of the cellulose nanofibers and as reinforcement or compatible agent into the other natural fibers/epoxy composites.

Pineapple Fiber-Reinforced Epoxy Resin

The fifth plant source for extracting the leaf fibers is the pineapple with the botanical name of *Ananas comosus* (Jain et al. 2019). The leaf fibers of pineapple are one of the waste materials in the agriculture sectors (Asim et al. 2015). These leaf fibers have the highest cellulose content as compared with other natural sources, which is more than 80% (Jain et al. 2019). Therefore, it can be mentioned that these fibers have superior mechanical strength and they can be good choice for using into polymeric materials like epoxy resins. In practical, the density of these fibers is about 1.5 g/cm^3 which is

more than other famous natural fibers like kenaf fibers. Also, the weak adhesion between these fibers and epoxy matrix is the major problem of those for using into epoxy composites. These drawbacks have caused that the researches about the pineapple/epoxy composites be limited. So, before the year of 2015, the noteworthy study about these composites had not been done, which the reported by Asim et al. (2015) in their review literature about the pineapple composites.

Palm Fiber-Reinforced Epoxy Resin

One of the wide leaf sources for extracting the natural fibers for using into epoxy matrix is the palm plant. Given up the applied investigations, it can be said that at least ten different types of palm fibers have been used as reinforcement into the epoxy resins, which can be seen in Fig. 11. Based on this figure, it can be seen that the cellulose content of each palm source is different. As previously mentioned, the cellulose has crystal structures into the natural fibers, and increasing the weight percentage of that enhances the mechanical properties of the natural fibers/epoxy composites. So, having various cellulose content creates the different behaviors into the epoxy matrices. Most of the applied researches by different scientific groups in the world have been done on the oil, date, and sugar palm fibers/epoxy composites. Investigating the effect of other palm fibers on the properties of epoxy resins and their composites has been rarely done by researchers.

The oil palm with the botanical name of *Elaeis guineensis* Jacq is the highest-yielding edible oil crop in the world. It is harvested in the 42 countries in the region of West Africa, Latin America, and Southeast Asia. The oil palm can be extracted

Fig. 11 The different palm plant fibers, the cellulose, hemicellulose, and lignin contents

from trunk, frond, and fruit mesocarp and empty fruit bunch (EFB) (Shinoj et al. 2011). Among them, the EFB has potential for using into epoxy resins which has hollow structure. EFB can be used in form of nano-filler or second reinforcement for improving the properties of other natural fibers into the epoxy resins. Using these fibers in form of mat fibers for enhancing the mechanical performances of jute and kenaf fibers has been done by various research groups (Hanan et al. 2020).

The second famous palm fibers source is the date palm fibers. The botanical name of date palm fibers is *Phoenix dactylifera*. This plant is one of the oldest plants, which are cultivated by human. The natural fibers in this plant can be extracted from leaf stalk, fruit bunch stalk, leaf sheath, and tree trunk. Also, the seed of that can be used as nano-filler into the epoxy resins for fabricating the epoxy based bio-composites. The extracted fibers from fruit bunch stalk with the 44 wt.% cellulose have the highest cellulose in its structure, as compared with other extracted fibers. Therefore, it can be expected that the fruit bunch stalk fibers had the most influence on the improvement of mechanical properties of epoxy resins. Comparing the various palm fibers into the epoxy resins was investigated by Alshammari et al. (2019). The obtained results showed that the best performance in the mechanical properties was achieved by adding fruit bunch stalk fibers/epoxy composite, whereas, the best performance in the resistance to the water absorption belonged to the epoxy resin with the leaf stalk in the various immersion times.

The third palm plant, which can be developed for using in the epoxy resins, is sugar palm with the botanical name of *Arenga pinnata*. This candidate grows in the tropical countries such as Indonesia, Malaysia, and the Philippines (Bachtiar et al. 2009). Up to now, the usage of sugar palm fibers has progressed as another natural fibers in the engineering applications. So, the obtained results show that they have proper potential for composite applications. As per the applied researches, most of the scientific groups have focused on the surface modification of these fibers for using into epoxy matrices. So, it can be said that the researches about the sugar palm fibers/epoxy composites are still located in the initial levels and can be predicted that these composites have progressive trend for using instead of conventional composites. Also, these fibers have proper cellulose content, which proper them for extracting the cellulose nanofibers and using them into epoxy composites (Ilyas et al. 2018).

As previously mentioned, there are some other palm plants, which the limited researches have been done about them and their composites. Some of these admirable researches are introduced in the following. Oladele et al. (2020) added the modified palm kernel shell and particulate cassava peel as biodegradable agro-waste into the epoxy matrix. Ganesh et al. (2020) characterized the effect of stacking sequence of areca sheath palm leaf on the mechanical and water absorption of epoxy composites. The obtained results showed that the cellulose content of these fibers was about 57.3%, which is recognized as one of the high cellulose content of palm fibers. It seems that these fibers can be good candidate for using into epoxy resins.

Peach palm tree is another source for extracting the cellulose-based fibers. Cordeiro et al. (2017) investigated the properties of peach palm/epoxy composites. Given up this research work, it can be said that to create the proper situation for using these composites into the various applications, more investigations should be done.

Like peach palm fibers, piassava, *Mauritiella armata*, toddy, and Palmyra fibers need more studying to use them into the epoxy resins. Among these fibers, the Palmyra fibers with the cellulose content of 58.58 wt.% have the highest cellulose content. Therefore, by modifying the surface of them, improving the adhesion between these fibers and epoxy resins, adding cellulose nanofibers, and including the nanoparticles, the Palmyra/epoxy composite can be one of the proper choices for using in the different applications in the near future.

The Straw-, Stalk-, and Husk-Based Natural Fibers/Epoxy Composites

Wheat-, Maize-, and Rice-Reinforced Epoxy Resin

The next plant natural fibers with the proper capability for using as reinforcement into the epoxy resins are the straw-, husk-, or stalk-based fibers. Based on reviewed researches, the most applicable sources for these groups of natural fibers are wheat, maize, and rice plants. It seems that these sources have lower capability to be used as reinforcement into the epoxy composites, as compared with the other plant fiber sources, because the extracted fibers from these natural sources can be in form of chopped or mat fibers. So, their performance in the epoxy resins is limited. In other words, most of the times, they are used as a filler into the epoxy resins. However, some of those have interesting features, which are reviewed in the following.

As previously mentioned, one of the straw fiber sources is the wheat plant. The worst drawback of these fibers is incompatibility between them and polymeric materials like epoxy resins. Having hydroxyl (OH) and carboxylic acid (COOH) groups in their structures is the reason of this incompatibility. Also, the existing microvoids and insufficiently wet regions reduce the load transferring, which limits their usage. Many efforts have been done to modify these fibers. The admirable of those is using the plasma treatment, which was done by Huner et al. (2018). It seems that wheat is one of the important sources for extracting the cellulose nanofibers.

Maize fiber is another straw-based fiber. It can be used as short fibers into the epoxy resin. Based on the reported researches, it seems that these fibers have proper thermal stability. The admirable work about maize stalk into the epoxy resins was done by Agunsoye et al. (2020). These researchers extracted the nanoparticles from maize stalk and then added them into the epoxy resin. As compared with the wheat and maize plant, it seems that the rice plant is more applicable for using into epoxy composites. The husk, ash, and straw of that can be used as reinforcement into the epoxy resins. Given up the researches, it can be said that the most of the researches about the rice husk is the extracting the nanosilica from that and using into epoxy resins. Comparing the effect of silica fume (synthetic silica) and rice husk silica (bio-based silica) on the performance of epoxy composites was done by Garcia-Mejia et al. (2020). Although, the composites containing the synthetic silica had the higher mechanical properties, this superiority was not noteworthy. So, the bio-based silica can be used instead of synthetic silica in the epoxy composites. One of the

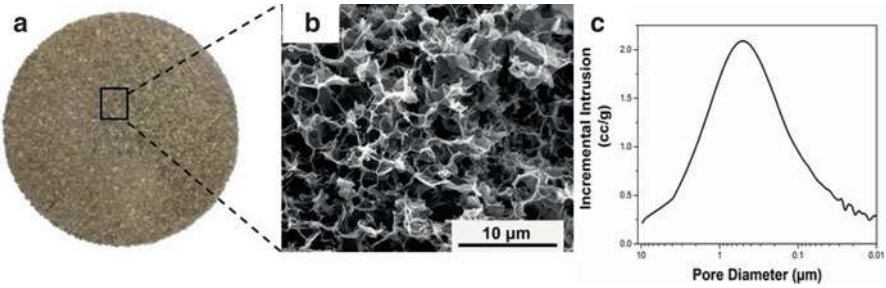

Fig. 12 The lignocellulosic foam, (**a**) digital image, (**b**) SEM image, (**c**) pore size range of that. (Reprinted from Zaman et al. (2020) with the permission of Elsevier)

creative ideas for using these straw fibers is fabricating the lignocellulose foam from those, which was done by Zaman et al. (2020). These researchers firstly fabricated the lignocellulose foam from rice straw and then produced the foam/epoxy composite structure. The features of this bio-foam can be seen in Fig. 12.

The Cane-, Grass-, and Reed-Based Natural Fibers/Epoxy Composites

Bamboo Fiber-Reinforced Epoxy Resin

The other plant sources for extracting the fibers and using into polymeric materials as reinforcement is the cane-, grass-, or reed-based plants. Among the various types of these plants, only bamboo and bagasse had the progressive trend for using into epoxy resins. Nowadays, bamboo is one of the most favorable fibers sources, due to its the low density and high mechanical properties. In other words, the bamboo fibers have high specific stiffness and strength (Osorio et al. 2011). China as the biggest producer of bamboo plant has around 67,000 hectares of bamboo forest. Utilization of this natural source was still rarely low, so, only about 40% of that is used. The extraction methods of bamboo fibers are retting, stem explosion, alkali treatment, degumming, etc. (Lu et al. 2013). Bamboo fibers have hollow structure. So, adding these fibers into the epoxy matrices reduces the density of composites. In other words, the composites containing the bamboo fibers have proper specific mechanical properties (Osorio et al. 2011). The erosion and wear properties of bamboo fibers/epoxy composites were compared with the glass fibers/epoxy composites by Biswas and Satapathy (2010). The comparative study showed that although the bamboo-based composites exhibited relatively inferior mechanical properties, their erosion wear performance was better than glass based composites.

Given up researches, the bamboo fibers can be used into the epoxy matrix in form of mat fabrics, bidirectional roving, plain woven, and micro-/nanofibrils. Therefore, it can be said that these fibers have proper capability to be used into the structural applications, even if they have lower mechanical properties, as compared with the advanced fibers like glass fibers. With this point, many efforts have been done to

improve the mechanical properties of bamboo/epoxy composites. Applying the various surface modifications on the bamboo fibers and adding the different nanoparticles into the epoxy resins are the conventional methods for improving these composites (Lu et al. 2013). The creative idea, which can be used for other hollow natural fibers as reinforcement into the epoxy resins, was done by Kalali et al. (2019). Actually, these researchers filled the hollow structures of bamboo fibers with the infiltration method. Firstly, these researchers soaked the bamboo fibers into the water solution containing 2.5 mol/L sodium hydroxide and 0.4 mol/L sodium sulfite for delignification of bamboo fibers. As previously mentioned, the lignification process removes the hydrophilic structures of natural fibers, so, the adhesion between those and epoxy resins improves. In the following, they put these fibers into a container and by using the vacuum method under the pressure of 200 Pa infiltrated the mixture of epoxy resin and hardener into the hollow structure of bamboo fibers.

Bagasse Fiber-Reinforced Epoxy Resin

The second candidate as cane source fibers for using into epoxy resins is the bagasse fiber. In practical, the bagasse fibers are the major waste of sugarcane industry. Some part of those can be used as fuel in the industries. Sugarcane waste has caused that the bagasse fibers be in form of short fibers. So, these fibers can be directly added to the epoxy resins or used in form of mat fabrics (James et al. 2020). The cellulose content of these fibers is about 52.42%, which proper them for using as a source for extracting the cellulose nanofibers and using them into the epoxy resins. As previously mentioned these fibers are used as fuel into the various industries. After the burning, the remaining ash from these fibers can be used as filler for improving the mechanical or thermal properties of epoxy composites.

The Fruit-Based Natural Fibers/Epoxy Composites

Coir- and Luffa-Reinforced Epoxy Resin

The last group of natural plant fibers/epoxy composites is composites containing the fruit-based fibers. The extracted fibers from coconut (coir fibers) and luffa can be used into the epoxy-based composites. As compared with other natural fibers, the fruit-based fibers had the lower development for using into epoxy composites. The coir fibers as fruit-based fibers are the waste of natural resources and can cause environmental pollution. Therefore, many efforts have been done to use them in the new applications. These fibers have the highest lignin as compared with the other natural fibers. Also, thermal conductivity of fabricated composites from those fibers is lower than that of other natural fibers (Das and Biswas 2016). These fibers have hollow structures, which proper them for using in the epoxy composites for energy absorption applications or wear conditions. For examples, Rashid et al. (2011) hybridized the coir and Kevlar fibers into the epoxy resin for investigating the flexural and impact properties of these composites.

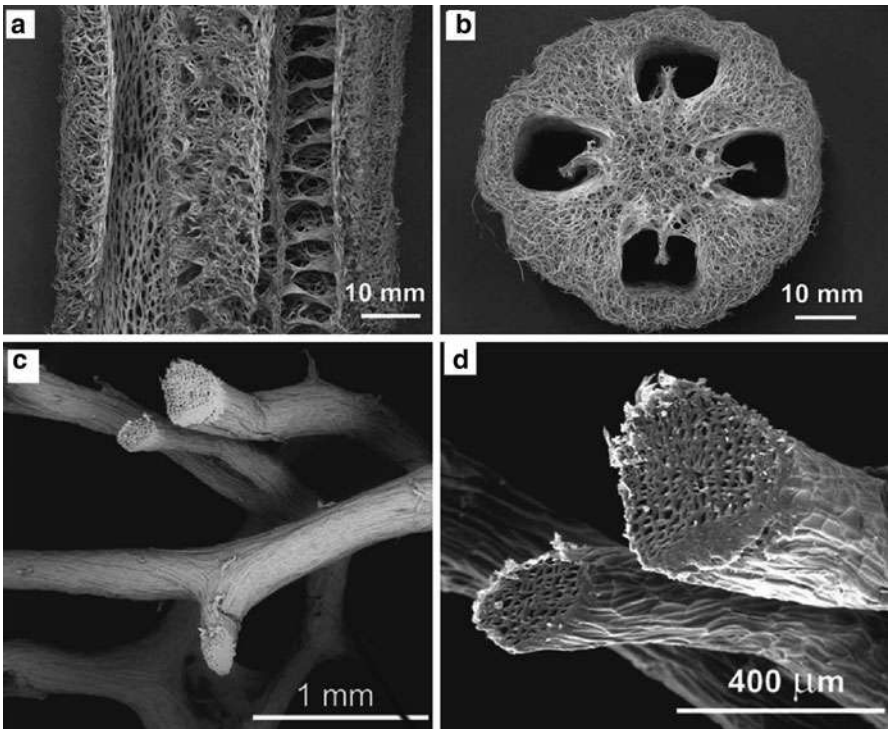

Fig. 13 The luffa sponge, (**a**) luffa gourd vertical cross section, (**b**) top view, (**c** and **d**) SEM micrographs of the luffa sponge struts. (Adapted from Zampieri et al. (2006) with the permission of Elsevier)

The luffa sponge (aegyptica or cylindrica), is locally known as vegetable sponge (seen Fig. 13). Luffa is cultivated in the tropical countries of Asia and Africa and some subtropical areas. Luffa sponge has special features like environment-friendly, non-toxicity, biomass degradation, and physical or chemical stability (Zampieri et al. 2006). Using that into the epoxy composites is too limited. It can be said the epoxy-based composites of this natural fibers source can be used in the conventional structures like door or window panel, partition board, and false ceiling. Also, the luffa sponge can be used as a foam part of epoxy-based sandwich panels in the engineering applications.

The Animal-Based Natural Fibers/Epoxy Composites

Silk Fiber-Reinforced Epoxy Resin

Another natural source for using as reinforcement or filler into the epoxy resins is the animal natural fibers. Given up the researches, it can be said that only silk fibers can be used into epoxy resins. As we know, the low production cost and high availability

are the features of these fibers. To understand how the performance of silk fibers into the epoxy resins, Shah et al. (2014) compared the epoxy composites containing the silk fibers, flax fibers as natural plant fibers, and glass fibers as synthetic fibers. The obtained results showed that the nonwoven silk/epoxy composite had lower tensile strength as compared with the composites containing the flax and glass fibers. Based on this work, it can be said that although the specific mechanical properties of silk/epoxy composite is proper, the mechanical strength of that is so weak, as compared with the other composites. Therefore, it can be mentioned that this composite has proper capability for using in the lightweight composite structures like sandwich composite panels. For example, Wen et al. (2020) fabricated the silk/epoxy pyramidal structures for using as core into the sandwich panels. Other admirable research work was done by Ude et al. (2013). These researchers used the silk fibers/epoxy composite as face sheet into the sandwich panels to investigate the impact resistance of that under the low velocity impact loadings.

Conclusion

Many efforts by different scientists have been done in the last decade for using the natural fibers/epoxy composites instead of the conventional polymeric composites, due to the environmental issues, recyclability of those, and reduction of production costs. The proper natural fibers as reinforcement into the epoxy resins can be extracted from plants and in some cases animal sources. Some of the plant fibers like jute and hemp directly are harvested because of their fibers, whereas the other plant fibers such as banana and pineapple are the byproduct of plants. The high variety of natural plant fibers causes that the natural plant fibers/epoxy composites be proper for various applications. For this reason, having the deep and comprehensive viewpoint about the features of these composites is so necessary. Recognizing the plant sources of natural fibers, identifying the structures of these fibers, modifying the surface of these fibers, knowing the fabrication process of natural fibers/epoxy composites, and selecting these composites for proper application are the subjects, which have been investigated in the past years by various research groups in the world.

Future Trend

Up to now, the natural fibers/epoxy composites have remarkably grown in the last decade. The natural fibers can be used in form of woven fabrics, chopped fibers, hybridized fibers, and cellulose nanofibers as well as in form of filler into the epoxy resins. The new hopeful researches indicate that some of these fibers like hemp, jute, and flax fibers have proper capability for using instead of glass fibers. To achieve this goal, the new modifications like adding the cellulose nanofibers for improving the adhesion between epoxy resins and these fibers will be continued by researchers. Some of these fibers like kapok, poplar, henequen, and bamboo have hollow structures. Therefore, they can be used as containers for producing the smart

epoxy composites. Also, they can be used as precursor for fabricating the hollow carbon fibers and using them into the epoxy resins. Other unconventional plant fibers like wheat, maize, and rice can be used as cellulose sources. Fabricating the nano-cellulose mat fabric and using them into the epoxy resins is one of the subjects, which will progress in the near future. Some admirable research works show that the natural fibers/epoxy composites with the lower mechanical properties and density can be used as complicated structures like pyramidal composites into the sandwich panels.

References

H. Ebrahimnezhad-Khaljiri, R. Eslami-Farsani, Thermal and mechanical properties of hybrid carbon/oxidized polyacrylonitrile fibers-epoxy composites. Polym. Compos. **38**, 1412 (2017)

Z.N. Azwa, B.F. Yousif, A.C. Manalo, W. Karunasena, A review on the degradability of polymeric composites based on natural fibres. Mater. Des. **47**, 424 (2013)

M.R. Sanjay, S. Siengchin, J. Parameswaranpillai, M. Jawaid, C.I. Pruncu, A. Khan, A comprehensive review of techniques for natural fibers as reinforcement in composites: preparation, processing and characterization. Carbohydr. Polym. **207**, 108 (2019)

K.L. Pickering, M.G.A. Efendy, T.M. Le, A review of recent developments in natural fibre composites and their mechanical performance. Compos. Part A Appl. Sci. Manuf. **83**, 98 (2016)

D.D. Stokke, Q. Wu, G. Han, *Introduction to Wood and Natural Fiber Composites* (Wiley, 2014)

B. Shao, Y. Fang, B. Chen, J. Shen, S. Xu, R. Ou, Q. Wang, Statistical distribution of mechanical properties and energy absorption of laminated cotton fabric reinforced epoxy composites. Polym. Compos. **41**, 2829 (2020)

H. Wang, R. Wang, R. Tao, Y. Zhu, C. Lv, Y. Zhu, Fabrication of superhydrophobic fiber fabric/epoxy composites coating on aluminum substrate with long-lived wear resistance. RSC Adv. **6**, 95556 (2016)

L. Tang, C. Weder, Cellulose whisker/epoxy resin nanocomposites. ACS Appl. Mater. Interfaces **2**, 1073 (2010)

S. Ramprasad, M.V. Ramana, M.M. Hussain, Development and comparison of cotton dust waste – Jute and cotton dust waste – Glass fiber reinforced epoxy based hybrid composites. Indian J. Eng. Mater. Sci. **25**, 465 (2018)

T. Nilsson, C. Björdal, The use of Kapok fibres for enrichment cultures of lignocellulose-degrading bacteria. Int. Biodeterior. Biodegrad. **61**, 11 (2008)

H. Wu, S. Araby, J. Xu, H.C. Kuan, C.H. Wang, A. Mouritz, Y. Zhuge, R.J.-T. Lin, T. Zong, J. Ma, Filling natural microtubules with triphenyl phosphate for flame-retarding polymer composites. Compos. Part A Appl. Sci. Manuf. **115**, 247 (2018)

A. Gao, H. Chen, J. Tang, K. Xie, A. Hou, Efficient extraction of cellulose nanocrystals from waste Calotropis gigantea fiber by SO42-/TiO2 nano-solid superacid catalyst combined with ball milling exfoliation. Ind. Crop. Prod. **152**, 112524 (2020)

R. Ramasamy, K. Obi Reddy, A. Varada Rajulu, Extraction and characterization of Calotropis gigantea bast fibers as novel reinforcement for composites materials. J. Nat. Fibers **15**, 527 (2018)

X. Zhang, Z. Li, Y. Yu, H. Wang, Characterizations of poplar catkin fibers and their potential for enzymatic hydrolysis. J. Wood Sci. **64**, 458 (2018)

J. George, J. Ivens, I. Verpoest, Mechanical properties of flax fibre reinforced epoxy composites. Die Angewandte Makromolekulare Chemie **272**, 41 (1999)

Y. Jia, B. Fiedler, Tensile creep behaviour of unidirectional flax fibre reinforced bio-based epoxy composites. Compos. Commun. **18**, 5 (2020)

A. Moudood, A. Rahman, H.M. Khanlou, W. Hall, A. Öchsner, G. Francucci, Environmental effects on the durability and the mechanical performance of flax fiber/bio-epoxy composites. Compos. Part B Eng. **171**, 284 (2019)
M. Berges, R. Léger, V. Placet, V. Person, S. Corn, X. Gabrion, J. Rousseau, E. Ramasso, P. Ienny, S. Fontaine, Influence of moisture uptake on the static, cyclic and dynamic behaviour of unidirectional flax fibre-reinforced epoxy laminates. Compos. Part A Appl. Sci. Manuf. **88**, 165 (2016)
D. Scida, M. Assarar, C. Poilâne, R. Ayad, Influence of hygrothermal ageing on the damage mechanisms of flax-fibre reinforced epoxy composite. Compos. Part B Eng. **48**, 51 (2013)
S. Asgarinia, C. Viriyasuthee, S. Phillips, M. Dubé, J. Baets, A. Van Vuure, I. Verpoest, L. Lessard, Tension-tension fatigue behaviour of woven flax/epoxy composites. J. Reinf. Plast. Compos. **34**, 857 (2015)
S. Liang, P.B. Gning, L. Guillaumat, Properties evolution of flax/epoxy composites under fatigue loading. Int. J. Fatigue **63**, 36 (2014)
H. Ebrahimnezhad-Khaljiri, R. Eslami-Farsani, E. Akbarzadeh, Effect of interlayer hybridization of carbon, Kevlar, and glass fibers with oxidized polyacrylonitrile fibers on the mechanical behaviors of hybrid composites. Proc. Inst. Mech. Eng. Part C J. Mech. Eng. Sci. **234**, 1823 (2020a)
M.B. Bigdilou, R. Eslami-Farsani, H. Ebrahimnezhad-Khaljiri, M.A. Mohammadi, Experimental assessment of adding carbon nanotubes on the impact properties of Kevlar-ultrahigh molecular weight polyethylene fibers hybrid composites. J. Ind. Text. (2020). https://doi.org/10.1177/1528083720921483
V. Fombuena, R. Petrucci, F. Dominici, A. Jordá-Vilaplana, N. Montanes, L. Torre, Maleinized linseed oil as epoxy resin hardener for composites with high bio content obtained from linen byproducts. Polymers (Basel) **11**, 301 (2019)
A. Thygesen, A.B.. Thomsen, G. Daniel, H. Lilholt, Comparison of composites made from fungal defibrated hemp with composites of traditional hemp yarn. Ind. Crop. Prod. **25**, 147 (2007)
M. Liu, A.S. Meyer, D. Fernando, D.A.S. Silva, G. Daniel, A. Thygesen, Effect of pectin and hemicellulose removal from hemp fibres on the mechanical properties of unidirectional hemp/epoxy composites. Compos. Part A Appl. Sci. Manuf. **90**, 724 (2016)
L. Boccarusso, M. Durante, A. Langella, Lightweight hemp/bio-epoxy grid structure manufactured by a new continuous process. Compos. Part B Eng. **146**, 165 (2018)
Y. le Xu, A.Q. Dayo, J. Wang, A.R. Wang, D. Lv, A. Zegaoui, M. Derradji, W.B. Liu, Mechanical and thermal properties of a room temperature curing epoxy resin and related hemp fibers reinforced composites using a novel in-situ generated curing agent. Mater. Chem. Phys. **203**, 293 (2018)
R. Masoodi, K.M. Pillai, A study on moisture absorption and swelling in bio-based jute-epoxy composites. J. Reinf. Plast. Compos. **31**, 285 (2012)
H. Ebrahimnezhad-khaljiri, R. Eslami-farsani, S. Talebi, Investigating the high velocity impact behavior of the laminated composites of aluminum/jute fibers- epoxy containing nanoclay particles. Fibers Polym. **21**, 2607 (2020b)
C. Santulli, A.P. Caruso, A comparative study on falling weight impact properties of jute/epoxy and hemp/epoxy laminates. Malay. Polym. J. **4**, 19 (2009)
M. Boopalan, M. Niranjanaa, M.J. Umapathy, Study on the mechanical properties and thermal properties of jute and banana fiber reinforced epoxy hybrid composites. Compos. Part B Eng. **51**, 54 (2013)
V. Fiore, L. Calabrese, Materials effect of stacking sequence and sodium bicarbonate treatment on quasi-static and dynamic mechanical properties of flax/jute epoxy-based composites. Materials (Basel). **12**, 1363 (2019)
M.R. Sanjay, B. Yogesha, Studies on hybridization effect of jute/kenaf/e-glass woven fabric epoxy composites for potential applications: Effect of laminate stacking sequences. J. Ind. Text. **47**, 1830 (2018)

D. Jafrey Daniel, G. Sai Krishnan, P. Velmurugan, Investigation on the characteristics of bamboo/jute reinforced hybrid epoxy polymer composites. Mater. Res. Express **6**, 105346 (2019)
M.R. Sanjay, B. Yogesha, Study on water absorption behaviour of jute and kenaf fabric reinforced epoxy composites: Hybridization effect of e-glass fabric. Int. J. Compos. Mater. **6**, 55 (2016)
R. Kumar, Enhanced dynamic mechanical properties of kenaf epoxy composites. Adv. Mater. Process. **2**, 749 (2017)
Z.N. Azwa, B.F. Yousif, Characteristics of kenaf fibre/epoxy composites subjected to thermal degradation. Polym. Degrad. Stab. **98**, 2752 (2013)
Y. Li, Y.O. Shen, The use of sisal and henequen fibres as reinforcements in composites, in *Biofiber Reinforcements in Composite Materials*, ed. by O. Faruk, M. Sain, (Woodhead Publishing, 2015)
V. Fiore, T. Scalici, F. Nicoletti, G. Vitale, M. Prestipino, A. Valenza, A new eco-friendly chemical treatment of natural fibres: Effect of sodium bicarbonate on properties of sisal fibre and its epoxy composites. Compos. Part B Eng. **85**, 150 (2016)
A. Shalwan, M. Alajmi, A. Alajmi, Insulation characteristics of sisal fibre/epoxy composites. Int. J. Polym. Sci. **2017**, 7312609 (2017)
R. Punyamurthy, D. Sampathkumar, B. Bennehalli, R. Patel, S.C. Venkateshappa, Abaca fiber reinforced epoxy composites: Evaluation of impact strength. Int. J. Sci. Basic Appl. Res. **4531**, 305 (2014)
K. Liu, H. Takagi, R. Osugi, Z. Yang, Effect of physicochemical structure of natural fiber on transverse thermal conductivity of unidirectional abaca/bamboo fiber composites. Compos. Part A Appl. Sci. Manuf. **43**, 1234 (2012)
A. Gunge, P.G. Koppad, M. Nagamadhu, S.B. Kivade, K.V.S. Murthy, Study on mechanical properties of alkali treated plain woven banana fabric reinforced biodegradable composites. Compos. Commun. **13**, 47 (2019)
D. Cho, H.S. Lee, S.O. Han, L.T. Drzal, Effects of e-beam treatment on the interfacial and mechanical properties of henequen/polypropylene composites. Adv. Compos. Mater. Off. J. Japan Soc. Compos. Mater. **16**, 315 (2007)
M.A. Mohammadi, R. Eslami-Farsani, H. Ebrahimnezhad-Khaljiri, Experimental investigation of the healing properties of the microvascular channels-based self-healing glass fibers/epoxy composites containing the three-part healant. Polym. Test. **91**, 106862 (2020)
J. Jain, S. Jain, S. Sinha, Characterization and thermal kinetic analysis of pineapple leaf fibers and their reinforcement in epoxy. J. Elastomers Plast. **51**, 224 (2019)
M. Asim, K. Abdan, M. Jawaid, M. Nasir, Z. Dashtizadeh, M.R. Ishak, M.E. Hoque, Y. Deng, A review on pineapple leaves fibre and its composites. Int. J. Polym. Sci. **2015**, 950567 (2015)
S. Shinoj, R. Visvanathan, S. Panigrahi, M. Kochubabu, Oil palm fiber (OPF) and its composites: A review. Ind. Crop. Prod. **33**, 7 (2011)
F. Hanan, M. Jawaid, P. Md Tahir, Mechanical performance of oil palm/kenaf fiber-reinforced epoxy-based bilayer hybrid composites. J. Nat. Fibers **17**, 155 (2020)
B.A. Alshammari, N. Saba, M.D. Alotaibi, M.F. Alotibi, M. Jawaid, O.Y. Alothman, Evaluation of mechanical, physical, and morphological properties of epoxy composites reinforced with different date palm fillers. Materials (Basel). **12**, 2145 (2019)
D. Bachtiar, S.M. Sapuan, M.M. Hamdan, The influence of alkaline surface fibre treatment on the impact properties of sugar palm fibre-reinforced epoxy composites. Polym.-Plast. Technol. Eng. **48**, 379 (2009)
R.A. Ilyas, S.M. Sapuan, M.R. Ishak, Isolation and characterization of nanocrystalline cellulose from sugar palm fibres (Arenga pinnata). Carbohydr. Polym. **181**, 1038 (2018)
I.O. Oladele, I.O. Ibrahim, A.A. Adediran, A.D. Akinwekomi, Y.V. Adetula, T.M.A. Olayanju, Modified palm kernel shell fiber/particulate cassava peel hybrid reinforced epoxy composites. Results Mater. **5**, 100053 (2020)
S. Ganesh, Y. Gunda, S.R.J. Mohan, V. Raghunathan, J.D.J. Dhilip, Influence of stacking sequence on the mechanical and water absorption characteristics of Areca sheath-palm leaf sheath fibers

reinforced epoxy composites. J. Nat. Fibers (2020). https://doi.org/10.1080/15440478.2020.1787921
E.P. Cordeiro, V.J.R.R. Pita, B.G. Soares, Epoxy–fiber of peach palm trees composites: The effect of composition and fiber modification on mechanical and dynamic mechanical properties. J. Polym. Environ. **25**, 913 (2017)
U. Huner, H.A. Gulec, I. Damar Huner, Atmospheric pressure plasma jet treatment of wheat straw for improved compatibility in epoxy composites. J. Appl. Polym. Sci. **135**, 1 (2018)
J.O. Agunsoye, A.A. Bamigbaiye, S.A. Bello, S.B. Hassan, Mechanical properties of maize stalk nano-particle reinforced epoxy composites. Arab. J. Sci. Eng. **45**, 5087 (2020)
G. Garcia-Mejia, G. Saavedra-Intriago, A. Rigail-Cedeño, A. Rivas-Ferrín, C.V. Tapia-Bastidas, Effect of silica fume and rice husk silica in bio-epoxy composites. Mater. Today Proc. (2020). https://doi.org/10.1016/j.matpr.2020.06.498
A. Zaman, F. Huang, M. Jiang, W. Wei, N. Kadhim, Z. Zhou, Fabrication of enhanced epoxy composite by embedded hierarchical porous lignocellulosic foam. Renew. Energy **150**, 1066 (2020)
L. Osorio, E. Trujillo, A.W. Van Vuure, I. Verpoest, Morphological aspects and mechanical properties of single bamboo fibers and flexural characterization of bamboo/epoxy composites. J. Reinf. Plast. Compos. **30**, 396 (2011)
T. Lu, M. Jiang, Z. Jiang, D. Hui, Z. Wang, Z. Zhou, Effect of surface modification of bamboo cellulose fibers on mechanical properties of cellulose/epoxy composites. Compos. Part B Eng. **51**, 28 (2013)
S. Biswas, A. Satapathy, A comparative study on erosion characteristics of red mud filled bamboo-epoxy and glass-epoxy composites. Mater. Des. **31**, 1752 (2010)
E.N. Kalali, Y. Hu, X. Wang, L. Song, W. Xing, Highly-aligned cellulose fibers reinforced epoxy composites derived from bulk natural bamboo. Ind. Crop. Prod. **129**, 434 (2019)
J.D. James, S. Manoharan, G. Saikrishnan, S. Arjun, Influence of bagasse/sisal fibre stacking sequence on the mechanical characteristics of hybrid-epoxy composites. J. Nat. Fibers **17**, 1497 (2020)
G. Das, S. Biswas, Physical, mechanical and water absorption behaviour of coir fiber reinforced epoxy composites filled with Al_2O_3 particulates. IOP Conf. Ser. Mater. Sci. Eng. **115** (2016)
A.H.A. Rashid, R. Ahmad, M. Jaafar, M.N. Roslan, S. Ariffin, Mechanical properties evaluation of woven coir and Kevlar reinforced epoxy composites. Adv. Mater. Res. **277**, 36 (2011)
A. Zampieri, G.T.P. Mabande, T. Selvam, W. Schwieger, A. Rudolph, R. Hermann, H. Sieber, P. Greil, Biotemplating of Luffa cylindrica sponges to self-supporting hierarchical zeolite macrostructures for bio-inspired structured catalytic reactors. Mater. Sci. Eng. C **26**, 130 (2006)
D.U. Shah, D. Porter, F. Vollrath, Can silk become an effective reinforcing fibre? A property comparison with flax and glass reinforced composites. Compos. Sci. Technol. **101**, 173 (2014)
J. Wen, Y. Zeng, C. Wu, J. Guan, H. Guo, Silk lattice structures from unidirectional silk fiber–reinforced composites for breaking energy absorption. Adv. Eng. Mater. **22**, 1900921 (2020)
A.U. Ude, A.K. Ariffin, C.H. Azhari, An experimental investigation on the response of woven natural silk fiber/epoxy sandwich composite panels under low velocity impact. Fibers Polym. **14**, 127 (2013)

Chemical Modification and Fabrication of Epoxy/Natural Fiber Composites

19

Shakuntala Ojha, Vasavi Boggarapu, Rakesh Kanakam, Gujjala Raghavendra, and P. Subash Chandra Bose

Contents

Abstract

The present chapter review the recent literature on natural fiber epoxy composites with regard to chemical modifications. The major drawback with natural fibers is their incongruity with the hydrophobic matrices such as epoxy. As a result, the interfacial bonding between the fiber and the matrix is not proper to attain sufficient strength. To overcome this problem, chemical treatment of fibers is

S. Ojha
Department of Mechanical Engineering, Kakatiya Institute of Technology and Science, Warangal, Telangana, India

V. Boggarapu · R. Kanakam · G. Raghavendra (✉) · P. S. C. Bose
Department of Mechanical Engineering, National Institute of Technology, Warangal, India
e-mail: raghavendra.gujjala@nitw.ac.in; subhash@nitw.ac.in

S. Mavinkere Rangappa et al. (eds.), *Handbook of Epoxy/Fiber Composites*,
https://doi.org/10.1007/978-981-19-3603-6_20

accomplished to make it least hydrophilic in nature. The latest trends in the fabrication and characterization of chemically treated natural fiber epoxy composites are discussed. Alongside, the mechanisms of different chemical modification methods have also been explained. The enhanced mechanical and tribological properties of composites were also reviewed.

Keywords

Polymer Composites · Epoxy · Chemical Modification · Natural Fibre · Mechanical and Tribological Properties

Introduction

Nowadays, the synthetic fibers such as glass, carbon, etc. were replaced with the natural fibers owing to their low cost, light weight, and environmental traits. In the past centuries, natural fibers like jute, flax, hemp, and sisal were widely used in the preparation of clothes, baskets, and ropes. With the progression in material science, these fibers were now utilized in polymer composites to prepare the industrial components. The selection of fiber depends upon the required properties of composites such as mechanical or tribological (Mochane et al. 2019; Boggarapu et al. 2020). In view of environmental regulations, sustainability, economic awareness, and ecological conditions, there has been significant demand for natural fiber-reinforced composites (NFRCs). These fibers impart high characteristics such as stiffness, elastic modulus, flexibility, and impact resistance compared to conventional materials. Moreover, NFRCs are low in cost and less dense and have least vibrational damping. NFRCs are abundantly available in nature and have no health hazards and least resistance toward abrasion. Presently, few of the aerospace and automotive components made of aluminum and steel were replaced with NFRCs (Zampaloni et al. 2007). It was predicted that substitution of metallic components with natural fiber and plastics shows a decrement of 15% in total weight of automotive (Mohanty et al. 2002). Compared to synthetic fibers, the natural fibers retain lower density which makes the composite lighter than conventional composite materials. The production of natural fibers requires less than 60% of energy when compared to synthetic fibers (Brosius 2006). Natural fibers are categorized into six distinct groups as portrayed in Fig. 1.

Depending on the type of fiber, the chemical composition is being varied. In general, any fiber comprises of cellulose, hemicellulose, lignin, and pectin. Each element contributes a distinct property to the fiber. Lignin divulges the thermal stability, but it is accountable for ultraviolet degradation. The hemicellulose element is responsible for moisture absorption, thermal degradation, and biodegradation owing to its minimal resistance. The content of these elements alters for various natural fibers. Commonly, fibers have 60–80% of cellulose, 5–20% of lignin, and 20% of moisture content (Saheb and Jog 1999). Among the different thermoset matrices, epoxy is widely used in polymer matrix composites due to its superior

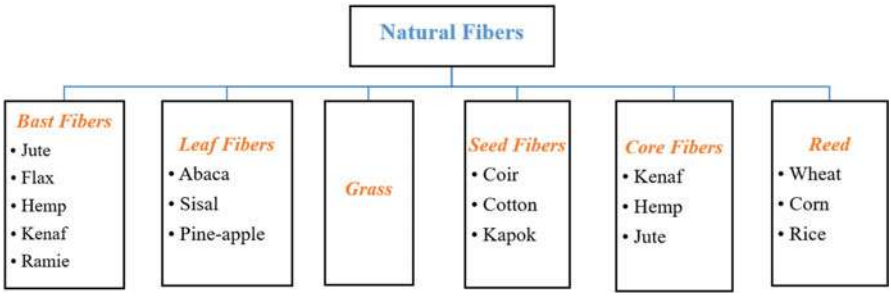

Fig. 1 Classification of natural fibers

thermo-mechanical and tribological properties. The strengthening of epoxy resin is acquired with the incorporation of reinforcement such as fibers (synthetic and natural) and filler particles. The drawbacks with natural fiber as reinforcement in polymer matrix are high moisture absorption and poor matrix-reinforcement compatibility. As a result, the strength of the composite decreases which leads to premature failure under hard working conditions. Therefore, surface chemical modification of natural fibers is crucial to enhance the matrix and fiber bonding. This chapter discourses the different chemical treatments and their mechanisms used for natural fibers. Alongside, the fabrication and characterization of epoxy composites added with chemically treated natural fibers were also discussed.

Chemical Modification Techniques on Natural Fibers

In this section, some of the chemical modification methods and their mechanisms that are adopted for natural fibers are discussed below.

Alkali Treatment

This treatment increases the content of amorphous cellulose than crystalline cellulose. From the network structure, removal of hydrogen bonding takes place. Eq. 1 represents the occurrence of reaction due to alkali treatment.

$$\text{Natural Fiber} - \text{OH} + \text{NaOH} \rightarrow \text{Fiber} - \text{O}^{-}\text{Na}^{+} + \text{H}_2\text{O} \quad (1)$$

Due to alkali effect, the cellulose fiber experiences swelling due to which its crystalline structure gets relaxed. In nature, the cellulose exhibits monoclinic crystalline structure which is then transformed into a polymorphous structure with thermal or chemical treatments. The concentration of commonly used alkali such as KOH, LiOH, and NaOH effects the swelling of lattice transformation in the cellulose. The studies depicted that the diameter of Na + ion is favorable to enlarge the pores and it gets penetrated into the lattice plane. Moreover, the higher swelling is shown in NaOH

chemical treatment. As a result, the sodium cellulose lattice is formed which showed a greater distance between cellulose molecules which are then filled with H_2O molecules. The OH groups in cellulose are transformed into ONa groups which increases the size of molecules. With the successive rinsing in water, sodium ions are removed which imparts a new crystalline structure to the cellulose that is thermodynamically much stable. Compared to other alkali, NaOH transforms the cellulose structure completely. Alkali treatment effects the cellulose and non-cellulose components such as lignin, hemicellulose, and pectin. The alkali treated jute fiber polymer composites have shown improved flexural strength (Sinha and Rout 2009). The rise in soaking time during NaOH treatment of kenaf fibers causes the damage which effects the characteristics of composites. Similarly, the concentration of alkali solution has a substantial effect on the strength of composites. The fibers treated with 5% of NaOH solution exhibit greater tensile strength than 10% concentration (Mohd Yuhazri et al. 2011). The possible reason may be the delignification of natural fiber at higher alkali concentration, which lowers the fiber resistance toward damage. The considerable decrease in the strength of composites is noticed beyond the optimal NaOH concentration. In contrast, the study stated by Edeerozey et al. (2007) concluded the 6% concentration of NaOH is optimal to attain better mechanical strength. Substantial amount of alkali concentration induces good interfacial bonding between the fiber and matrix which yields in the improvement of mechanical properties. The NaOH is employed to break the hydrogen bonding present in the fiber's cellulose structure and increase its surface roughness. Moreover, alkali treatment removes wax, fatty acids, oils, and lignin from the cell wall of fibers. It also de-polymerizes the cellulose network which enhances the properties. The confirmation tests were performed through SEM (scanning electron microscopy), chemical analysis, and DMA (dynamic mechanical analysis). Along with mechanical properties, the natural fibers were enriched with dielectric strength with the alkali treatment as reported by Venkatesha Prasanna et al. (2020). On the contrary, Srinivasa and Bharath (2011) used KOH solution of 10% concentration to treat the areca fibers. The fibers were added to epoxy matrix to prepare the composites. The hardness and impact strength of alkali treated fiber-reinforced composites were shown higher than the untreated fibers. Additionally, authors have inferred the influence of curing time on the mechanical performance of epoxy composites. The combined alkali and silane treatments were carried out on *Borassus* fibers by Obi Reddy et al. (2015). When compared to alkali treatment alone, the epoxy composites with combined treated *Borassus* fiber have exhibited greater tensile strength. Besides, the chemical resistance of fibers was enhanced as a result of combined treatments. A similar treatment on roselle fibers was reported by Nadlene et al. (2018). An improvement in chemical and thermal properties was noticed with the combined alkali and silane treatments. Additionally, the moisture absorption capability of treated fiber is less compared to untreated fibers. A study on alkali treated alfa fibers at different concentrations was stated by the researchers Mansour Rokbi et al. (2011). Flexural strength of composites increases with an increase in NaOH concentration of 10%, beyond which a decrement in trend is observed due to delignification. The optimal alkali concentration of 7% is preferred in the treatment of alfa fibers to attain better mechanical properties (Benyahia et al. 2014).

Silane Treatment

The chemicals have hydrophilic compounds of various groups related to silicon wherein the two ends react with the matrix and hydrophilic fiber, respectively. The intake of silane depends on factors such as temperature, hydrolysis time, pH, and silane organo-functionality nature. Hydroxyl groups are capable of bonding with the alkoxy-silanes. Besides, silanols are able to transform poly-siloxane structures when reacted with hydroxyl groups present in the natural fibers. Silanes will undergo the sequence of stages, namely, hydrolysis, condensation, and bond formation. Silanes experience condensation on the surface layer of cellulose fiber, and amino silane molecules get interacted with the OH groups in the cellulose through basic Bronsted amino groups. The work cited by Franco et al. (1997; Herrera-Franco and Aguilar-Vega 1997) reported on the effect of different silane coupling agents on the performance of polymer composites reinforced with henequen fiber. The results obtained from FTIR and X-ray spectroscopy indicated the temperature greater than 708 °C is suitable for the reaction between silanes and cellulose. The silane treatment reaction is shown in Eq. 2.

$$CH_2CHSi(OH)_3 + \text{Fiber} - OH \rightarrow CH_2CHSi(OH)_2O - \text{Fiber} + H_2O \quad (2)$$

Abdelmouleh et al. (2007) investigated the performance of cellulose fibers when treated with different silane coupling agents. Fibers treated with methacryloxypropyltrimethoxy and mercaptopropyltrimethoxy have shown superior mechanical properties compared to hexadecyltrimethoxy-silanes. It can be concluded from their studies that the silane agent has a noticeable effect on the performance of polymer composites. Asim et al. (2016) studied the influence of combined alkali and silane treatments on kenaf and pineapple leaf fibers. These treatments promote the amputation of impurities from the surface of fibers. The silane-treated fibers have displayed high interfacial strength than alkali and combined treated fibers. Similar results were exhibited by sisal fiber-reinforced epoxy composites as reported by Bisanda and Ansell (1991). Sabarinathan et al. (2020) presented the characterization of silane-treated palm tree fibers. The vinyl-triethoxy silane at various concentrations is utilized as a coupling agent in the process. FTIR analysis shows that cellulose content in the fibers is not affected by silane treatment. The strength of composites increases with the concentration of coupling agent up to 5%. Further increase in concentration makes the fiber brittle which leads to reduction of mechanical performance. Vijay et al. (2020) experimented on silane-treated *Leucas aspera* fiber-reinforced epoxy composites. The silane treatment has removed excess amount of lignin, hemicellulose, and wax which improved the bonding characteristics among the fiber and matrix. Such composites have displayed better tensile strength combined with thermal stability. Liu et al. (2019) studied the influence of silane treatment on the strength of corn stalk fiber-reinforced polymer composites. Silane-treated corn fibers have shown high crystallinity index and size as illustrated from XRD studies. The 5% silane-concentrated composites revealed greater tensile strength than the untreated ones.

Acetylation Treatment

It is an attractive methodology for the surface treatment of natural fiber to make it much hydrophobic in nature. The chemical reaction reduces the swelling of wood when immersed in water and is extended to lignocellulose materials. The principle of this methodology is that whenever the hydroxyl (OH) groups of fiber get reacted with the acetyl (CH_3CO) groups that yield the hydrophobic nature to the surface of the fiber, the OH groups get reacted with the minor elements of the fiber such as lignin, hemicellulose, and amorphous cellulose. The natural fiber consists of crystalline regions which are strongly packed by hydroxyl groups with interchain bonding. As a result, the fibers turn inaccessible toward chemical reagents. The process of acetylation is represented in Eq. 3.

$$\begin{aligned} \text{Natural Fiber} - \text{OH} \quad &+ \text{CH}_3\text{CO} - \text{O} - \text{OC} - \text{CH}_3 \xrightarrow[Conc.\ \ H2SO4]{CH3COOH} \\ \text{Natural Fiber} - \text{O} - \text{CO} - \text{CH}_3 \quad &+ \text{CH}_3\text{COOH} \end{aligned} \tag{3}$$

Acetylation also reduces the moisture absorption capability of natural fibers. As reported by Bledzki et al. (Bledzki and Gassan 1999), the acetylation-treated jute fibers have shown 50% reduction in moisture absorption. Similarly, pine fibers exhibited 65% moisture reduction due to chemical treatment (Zafeiropoulos et al. 2002). The interfacial bonding is improved in flax fiber polymer composites with acetylation. The acetylated wood fibers have shown 30% improvement in strength when immersed in water (Joffre et al. 2017). A study reported by Amaury et al. (Lepetit et al. 2017) observed a least enhancement in mechanical strength of cellulose fibers when treated with acetic anhydride. Yet, there is a great reduction in moisture absorption capability of composites. Similar results were also exhibited by kenaf fibers with acetylation treatment. The 6% concentration of acetylation treatment removed the swelling effect on palm fibers which are then utilized as reinforcement in polymer resin. Such composites can be employed for door panels and automobile interiors (Chung et al. 2018). Acetylation of pineapple fibers and coffee husk improved the rheological properties of polymer composites (Bellili et al. 2020; Okpanachi et al. 2020). Abdul Khalil et al. (2000) studied the mechanical characteristics of natural fibers like jute, coir, flax, and palm which are chemically treated with acetic anhydride under non-catalyzed environment. The fibers having high lignin content were more prone toward acetylation.

Benzoylation Treatment

The conversion of benzoyl chloride and organic synthesis results in benzoylation, which is used for the treatment of natural fibers. This treatment decreases the moisture absorption capability and improves the interaction between the fiber and matrix. The chemical process of benzoylation is represented in Eqs. 3 and 4. As reported by Joseph et al. (2000), the sisal fibers were chemically treated with 10% of sodium hydroxide (NaOH) and benzoyl chloride (C_6H_5COCl) solutions for 15 min,

respectively. The OH groups present in lignin and cellulose were stimulated with the alkaline treatment. After the process, fibers were rinsed in ethanol to escape benzoyl chloride followed by drying.

$$\text{Fiber} - \text{OH} + \text{NaOH} \rightarrow \text{Fiber} - \text{ONa} + \text{H}_2\text{O} \tag{4}$$

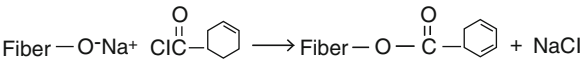

(5)

Zheng et al. (2007) employed benzoic acid in treating the bagasse fibers. These fibers were added to the polymer matrix to evaluate their strength. It was noticed that the mechanical strength of chemically modified fibers was 35% more than the untreated fibers which indicates good adhesion. The researchers Wang et al. (2004) performed the various chemical modifications such as alkali, peroxide, and benzoylation on flax fiber. The fibers were added to polymer resin to investigate the mechanical as well as physical properties of fabricated composite samples. A new type of fiber named Isora was explored by Mathew et al. (2007). This fiber resembles like a jute fiber in appearance but possesses more strength and durability. These fibers were chemically treated with alkali, toluene diisocyanate, and silane coupling agents to enhance their mechanical properties. Isora fibers have great potential as a reinforcement in polymer composites. The authors have observed high tensile strength with alkali treatment compared with other methods. Lopattananon et al. (2006) examined the chemically treated pineapple leaf fibers in the natural rubber. Fibers were subjected to alkali and benzoylation at various concentrations. It was inferred from their studies that 5% of NaOH and 1% of benzoyl peroxide provide 28% and 57% more strength when compared with untreated fiber composite samples, respectively. In the peroxide treatment, firstly fibers were immersed in acetone after pre-treatment with alkali. As the decomposition of peroxide occurs at elevated temperature, the resultant NFRCs can withstand high tensile stress to strain levels. Up to optimal peroxide concentration, the increase in tensile strength is being noticed. Besides, this treatment provides the decrement in hydrophilicity of fibers that contribute to enhanced performance (Rashdi et al. 2010; Laranjeira et al. 2006).

Fabrication Methods for NFRC

Fabrication of epoxy/fiber composites is very simple compared to other composite fabrications. Preforms are prepared from fibers earlier and then reinforced with matrix materials by using different types of fabrication techniques. The fiber preforms may be knitting, braiding, weaving, and stitching of long sheets are short mats. The basic classification of molding is open-type and closed-type molding.

Open Molding

In case of open molding techniques the entire process is carried out in the open atmosphere.

Hand Layup Process

The most widely and commonly used fabrication in open mold composites is the hand layup as shown in Fig. 2. It is an easy method even non-skilled person can also perform it. At first, a gel coat is added to the open mold, and then fibers are put by hand on the mold. Then the resin is applied on fibers (reinforcements) by using a brush. For better interaction between layers, pressure is applied by using the roller. Only one surface is smooth in this process. Higher cycle times are not possible in hand layup. Sivasaravanan et al. (2019) used hand layup technique to fabricate natural fibers along with GFRP and CFRP.

Spray-Up Process

The spray-up process is also an open mold process almost similar to the hand layup process, wherein a handgun is used, which sprays chopped fibers and resin onto a mold. A roller is also used to fuse these fibers into the matrix material simultaneously. The chopped fibers provide excellent conformability and quite faster than the hand layup process. Fig. 3 illustrates the fabrication procedure. This process is ideal for lower volumes, and also automation is possible. Mohd HanafeeZi et al. (Zin et al. 2019) had used the spray-up method for the fabrication of pineapple leaf fiber-reinforced hybrid composites.

Filament Winding Process

The filament winding method is specifically used for typically circular, hollow, oval-sectioned parts, such as pipes and tanks. This is also an open-type molding process as shown in Fig. 4. Operation is also very simple compared to others. Continuous strands of fibers are fed through the resin bath onto the rotating mandrel in a predetermined direction. The orientation gives a higher strength-to-weight ratio. Supian et al. worked on hybrid composites according to the winding orientation effect. Till the required thickness, the fibers are fed and then cured for a predetermined time. Depending on the requirement, collapsible mandrels are also used. Filament winding is completely automated which is controlled by a computer that results in higher precision. High volume is also possible with this process.

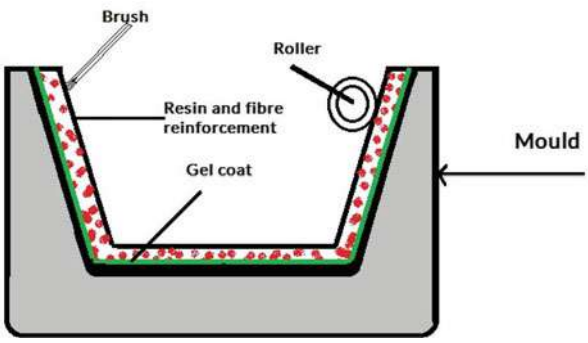

Fig. 2 Schematic diagram of the hand layup process

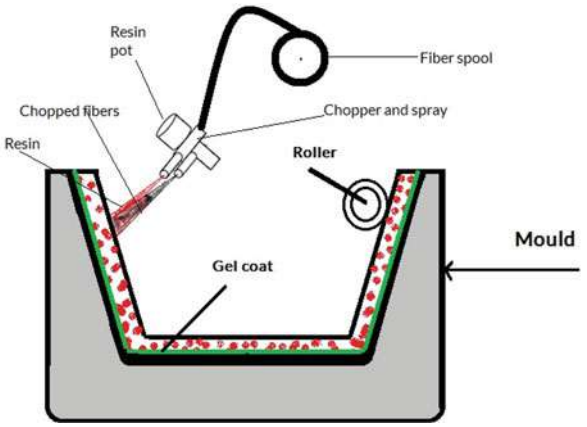

Fig. 3 Schematic diagram of the spray-up process

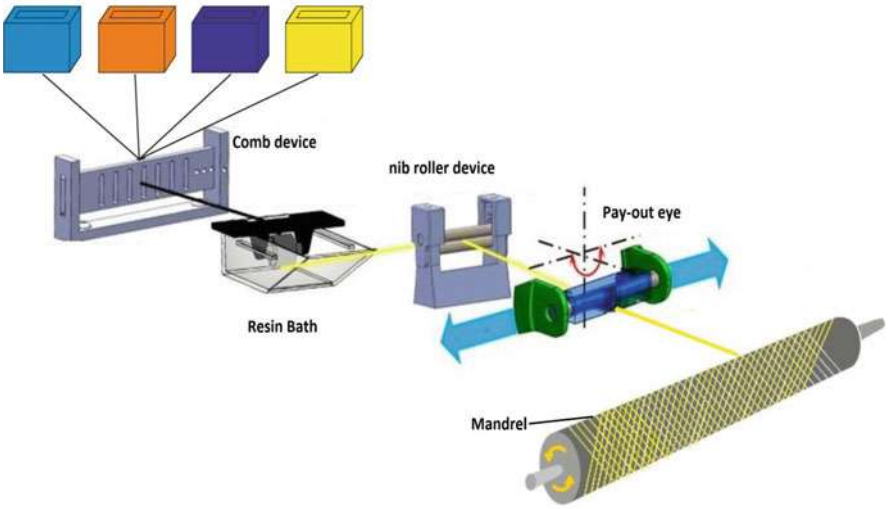

Fig. 4 Schematic diagram of the filament winding process

Closed Molding

In case of closed molding techniques, the entire process is carried out in a closed environment.

Vacuum Bag Molding

The vacuum bag molding is also one kind of closed mold process as displayed in Fig. 5. Firstly, laminates are made by hand layup and then placed in the wet mold; in this process, flexible films made by polyethylene, polyvinyl alcohol, or nylon are used on the top layers for the easy removal of resin and breathing. The wet layer of

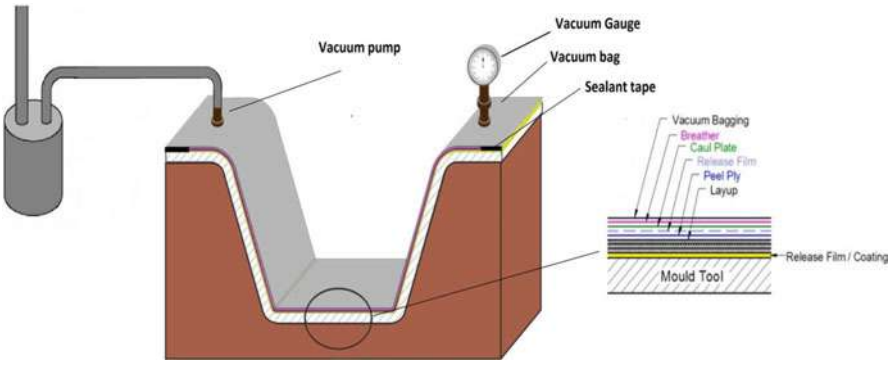

Fig. 5 Schematic diagram of the vacuum bag molding process

resin is applied on the mold, and then laminates are placed according to the requirement. Then the complete mold is sealed with vacuum packing. Now by using the vacuum pump, entrapped air is drawn out. Vacuum pump creates the maximum pressure on the mold so that all laminates and resin bond firmly. And also, excess resin will also be collected which can be used further. In some of the advanced uses, the entire setup is also placed in the autoclaves, in which both external pressure and heat are applied along with atmospheric pressure. Higher percentage of fiber reinforcement is achieved in vacuum bagging. According to Jauhar Fajrin (2016), natural fiber (sisal fiber) composites fabricated by vacuum bagging have shown better mechanical properties. For better curing of laminates, they must be cured in autoclave that yields a good strength to the composites.

Resin Transfer Molding (RTM)

The resin transfer molding technique is a closed-type mid-volume molding process as illustrated in Fig. 6. This is well known as liquid molding process. In this process, preforms of reinforcements (fibers) are placed on the bottom part of the mold. Then the mold is closed and entire set-up is preheated. If required, gel coating is applied on the mold before placing the fibers. Then resin is injected onto the preforms with the help of injectors with external pressure. Depending upon the requirement, temperature is maintained. Most of the times, RTM is used for the tooling. Complex shapes can be made in RTM. Surface is also an added advantage of the process. And also, wastage of resin is reduced in RTM. Rouison et al. (2004) investigated the fabrication of hemp/kenaf fiber-unsaturated polyester composites using the resin transfer molding (RTM) process, and this process has shown better mechanical properties depending on the curing time.

Vacuum Infusion Process

The vacuum infusion process is one of the closed mold processes in which vacuum pressure drives the resin into the laminate mold as shown in Fig. 7. Initially, the mold is gel coated if required, and dry laminates are placed on the mold, and in between,

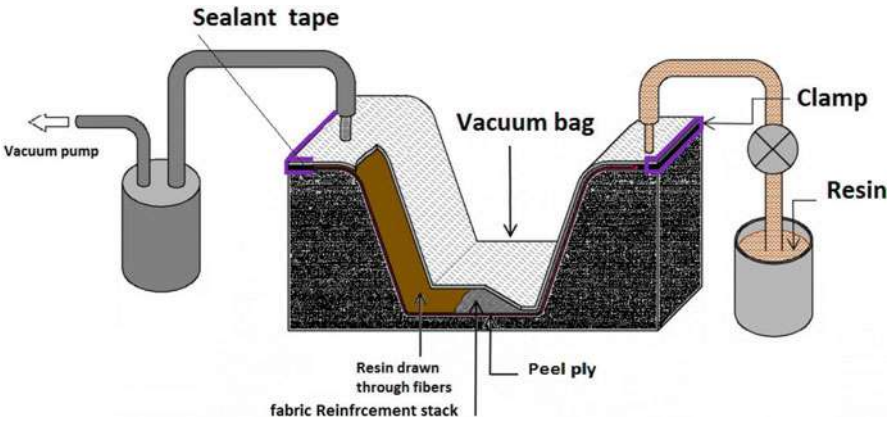

Fig. 6 Schematic diagram of resin transfer molding

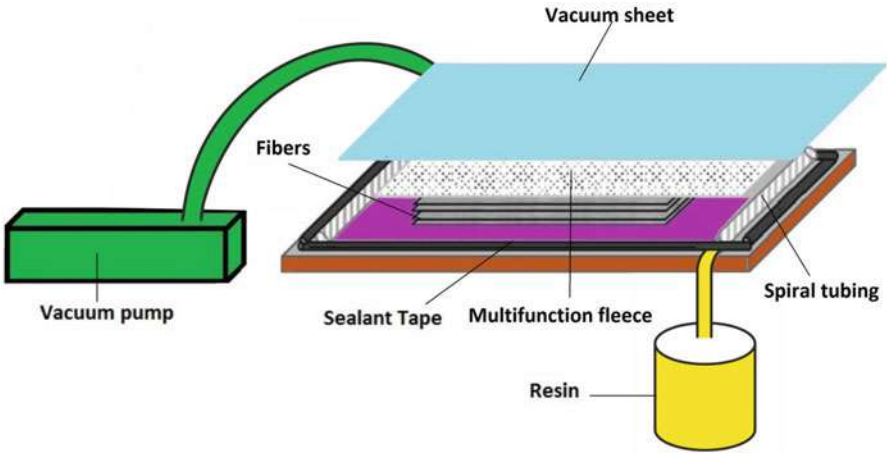

Fig. 7 Schematic diagram of the vacuum infusion process

perforated sheets are provided. Then the mold is sealed with the vacuum bagging or upper mold, vacuum is applied onto the laminates. The excess air is removed from the gap when the required resin-to-glass ratio is achieved. Then resin is applied onto the laminates which absorbers the required resin and excess is removed. Because of perforation sheets or tubes, less wastage of resin is achieved. Basically, low viscosity resins are preferred for infusion which allows easy permeation of reinforcement. This process is preferred for the very large structures and low volume molding processes. Mark C Symington et al. (2008) have used vacuum infusion process for the fabrication of abaca, flax, kenaf, sisal, and hemp fiber-reinforced composites which have shown better properties. Reusable silicone molds have shown less wastage of operating cost.

Pultrusion Process

The pultrusion process is a highly automated and continuous process as portrayed in Fig. 8. This process is mostly used for constant cross-sectional profiles like beams, rod stocks, fishing rods, and structural shapes in mass volume. The process is also very simple in nature; the reinforcing fibers are pulled through the resin bath and preheated dies by powerful traction mechanism. Dies are preheated in such a way that resins are cured instantly. Depending upon the materials used, die materials are selected. Most probably, thermosetting resins are used, and different strands of fibers are used. Very high strengths are achieved in this process, and complex shapes are fabricated using the pultrusion method. In some of the recent advancements, injected dies are used instead of external resin bath. Martin et al. (Martin 2013) stated that urethane resin offers the highest loading of glass compared to polyester and vinyl ester and therefore has flexural composite properties which approach aluminum properties. The work on pultruded kenaf composites went from characterization to product development (Fairuz et al. 2015).

Compression Molding

Compression molding is one of the closed molding process which is shown in Fig. 9. It is a high-pressure, high-volume process that is used for complex shape products. Hydraulic press is used in which the two molds are mounted on it. The preform and resins are placed on preheated lower mold and closed with upper mold by applying the pressure on it. Depending upon the materials, resins, and desired properties, the cure time is maintained approximately at 400 °C. The thickness of the product is also a factor for curing time. After curing, the finished product is removed from the molds. Most of the complex shapes are molded in this process. Surface finish of the products obtained is good. This entire process completes in maximum of 5 min. Faster cycles are achieved in compression molding. Aji et al. (2009) investigated that this process reduces the changes in the physical properties and also can help to retain the isotropic properties of the composites. The compression process produces high-impact strength composites. Davoodi et al. (2010) examined the tensile properties of kenaf fiber reinforced with different types of polymer composites known as

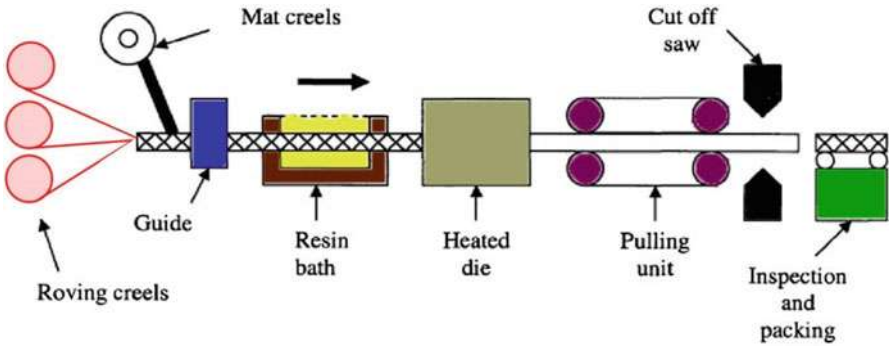

Fig. 8 Schematic diagram of the pultrusion process

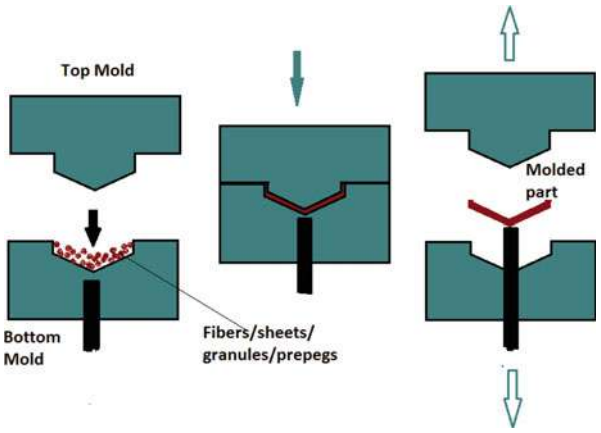

Fig. 9 Schematic diagram of compression molding

polypropylene (thermoplastic) and epoxy (thermoset). Liu et al. (2007) observed compression-molded biocomposites that show a high-impact strength compared to injection molding composites.

Reinforced Reaction Injection Molding (RRIM)

This process is also a closed molding process which has a higher production rate, low mold clamping pressure and low wastage, and very fast cycle times. It can be automated according to the requirement. RRIM is different to the reaction molding process. Figure 10 shows the illustration of the process. The reinforcements and resins are mixed in the mixing chamber outside the mold and injected into the chamber under high pressure. Metering is accomplished by high-pressure pumps and injection cylinders. Even though high pressure is applied, the mixer has low viscosity. Even we can use milled fibers or flakes to the resin before mixing in the chamber. Polymerization takes rapidly without the aid of heat treatment. RRIM has many advantages compared to other polymer fabrication processes. It has reduced thermal expansion, polymerization shrinkage, and low scrap rate. Most of the times, RRIM need special reinforcements and resins like epoxies, polyurethane, nylons, and polyesters. Most of the applications of RRIM are automobile industry.

Centrifugal Molding

Centrifugal molding is also one of the closed molding processes. The manufacturing process of this molding is very simple. Figure 11 shows the illustration of the process. Both the resin and the reinforcements are sprayed inside of the rotating mold. Because of centrifugal force, materials hold to it till cured. Curing time is dependent on the type of composites needed. Outer surface of the laminate has good surface finish, and for the inner surface of the laminate, additional neat coat or pure resin is to be added. Large-sized composite cylindrical pipes or tanks are manufactured by centrifugal molding/casting. Jamian S. et al. (2006) found that the hardness value of the specimen increases with the increment of fiber content.

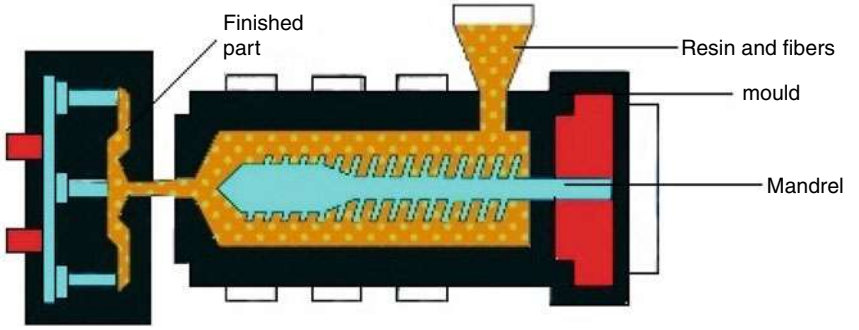

Fig. 10 Schematic diagram of RRIM

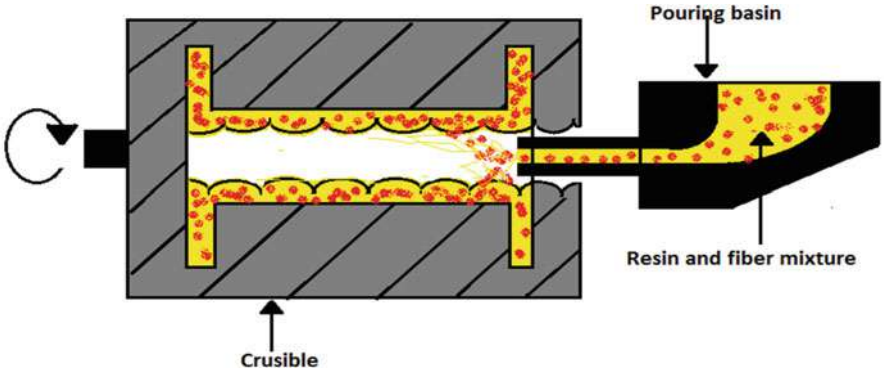

Fig. 11 Schematic diagram of centrifugal molding

Furthermore, from the inside to outside of the specimen, the porosity increases. Overall, the addition of fiber would give the mechanical properties of the polymer composites a strong impression. In addition, the mold's rotational speed influences FGNF/epoxy mechanical properties.

Mechanical Characterization of Chemically Treated NFRC

The following experiments were performed to study the mechanical properties and behavior of the NFRCs.

Tensile Testing

A material's tensile strength is the highest stress that can exist at point of instability. The normal tensile test specimen is the long piece as per the ASTM standards. The uniaxial stress of both ends of the specimen will be applied during the examination.

Example dimensions are $150 \times 10 \times 5$ mm^3. Typical points of concern for testing materials include the "ultimate tensile strength" (UTS) or peak stresses and the "offset yield strength" (OYS), which is an area that approaches the initiation of permanent deformation and the rupture point (R). The tensile test is conducted on the universal test machine (UTM) as seen in Fig. 12. Irawan et al. (2011) have fabricated ramie epoxy composites which have obtained higher tensile strengths of 90 MPa. George et al. (George and Verpoest 1999) have fabricated flax-reinforced epoxy composites and compared them with the banana fiber-reinforced epoxy composites. Tensile strength of banana fiber composites was 59 Mpa. While flax fiber composites showed 59.85 Mpa which is greater as compared to previous. Chittaranjan et al. (Deo and Acharya 2010) have observed the least value of tensile strength of 19.08 MPa for lantana added epoxy composites. It was noticed that bast and leaf fiber-reinforced composites exhibited better values of tensile strength as compared to other fiber-reinforced epoxy composites due to the enrichment of cellulose content and strong interface bonding between the natural fiber and matrix. Raghavendra et al. (2012) observed the optimal results on the tensile strength of banana fiber-incorporated epoxy composites at a fiber length of 4 mm. (Coura et al. 2020) studied the results of papaya composites and observed a specific tensile strength and specific tensile modulus of 22% and 47% less when compared to flax fiber-reinforced composites. It is evident that the layers of papaya bast fiber are favorable for polymer-added composites. Sisal/epoxy-based composites have the maximum tensile strength of 80.45 MPa. Sisal epoxy based composites have shown maximum tensile strength

Fig. 12 Universal testing machine

of 80.45 Mpa which was 16.88% greater as compared to banana fiber composite materials. The flexural stress behavior mainly depends on shear force, and this shear force is influenced by the layering patterns of fibers. The probability of delamination is increased as the layers increase in composites (Siva et al. 2020). The results reported that the five-layered ramie composites have shown enhanced mechanical properties (σ_{UTS} = 54.88 MPa) than the five-layered SPF-based composites as well as SPF-ramie-based hybrid composites. It is also noticed that the RSRSR-alternated stacking-sequenced composites gave a superior strength (12.47% more) than the SRSRS-sequenced composites (Siregar et al. 2020). Chaudhary et al. (Siva et al. 2020) stated a similar conclusion that incorporation of natural fibers in the epoxy matrix enhances the tensile strength of the composite produced by interfacial adhesion of the matrix with different natural fiber mats to a different extent. The experimental data shows that the tensile strength of sisal-epoxy composite is 24.5 MPa higher in average than the banana/epoxy as well as 32.28% higher than the sisal-banana-sisal composites. The tensile result has demonstrated excellent adhesion of the sisal-epoxy- as well as banana-epoxy-based composites to the epoxy matrix, which incidentally provides strong interfacial bonding of composite fibers and matrix (Mohammed et al. 2015).

Flexural Test

Flexural strength is also known as the transverse rupture strength or modulus of rupture. It is defined as the ability of a material to withstand the load deformation. The "short beam shear" (SBS) tests on the composite samples are performed to find the importance of "interlaminar shear strength" (ILSS). The dimension of the specimen is $20 \times 150 \times 5$ mm^3. The loading of desired forms (6×6inch) with a length of at least three times the depth is measured. The 3-point bend test promotes interlaminar shear failure and is tested on UTM as per ASTM standard. Venkateshappa et al. (2012) have observed least flexural strength in areca-incorporated epoxy composites, and Irawan et al. (2011) observed higher value of flexural strength in ramie-epoxy composites. Coura et al. (2020) studied that the specific flexural strength of papaya-based composites is 47% less and the specific flexural modulus is 30% less compared to flax fiber-based composites. This comparison shows that fiber layers of papaya bast have a promising strengthening in polymer composites.

Impact Test

The Charpy impact assessment represents a standardized high-strain test that calculates how much energy a material absorbs when a fracture occurs and tests the durability of a specific material. This energy absorption examination is a test of the durability of the objective material. It is widely used in the industry as planning and management for straightforward and the results are easy to obtain. Verma et al.

(2012) have studied and identified that flax fiber-added epoxy composites reported better value of impact strength behavior, whereas coir fiber-added epoxy composites have shown lower value of impact strength. Egala et al. (Egala and Setti 2018) showed a 5.8 times improvement in impact strength for the epoxy/castor oil plant cortex fiber composite compared to neat epoxy system. Gairola et al. (2020) found that impact energy at 10 wt. % as well as 20 wt. % of fiber loading was noticed as 1.6 J and 1.9 J, respectively. Impact energy rises from 30% to 40% with the increasing percentage of banana fiber. Siva et al. (2020) investigated sisal-epoxy composites that have shown a superior impact strength of 1.76 J, which is 10% more than banana-epoxy composites and 2.92% higher than sisal-banana-sisal composites. Highly dependent on the existence of adequate interface regions and good homogeneous filler distribution within the matrix results in greater impact force of sisal/epoxy composite. This helps to significantly avoid breakage and increases the efficiency of stress distributors between the fiber and matrix.

Izod Impact Test

Izod impact tests the energy needed to break a specimen by hitting a pendulum on a certain size bar as represented in Fig. 13. Izod refers generally to a notched effect of the specimen. Unknown specimens are however examined in certain circumstances. Researchers have also described the intensity of impact as the propensity of polymer-based composites to sustain high-energy impacts without rupture or fracture. The reports also show that the material properties are dependent on the individual fiber properties for hybridization and interlaminar as well as interfacial adhesion between the fibers and matrix in fiber-incorporated composites as well as hybrid composites

Fig. 13 Impact test apparatus

(Saba et al. 2016). Sarikaya et al. (2019) have studied palm fiber-reinforced epoxy composite which has shown best impact result of 0.130 J absorption energy. Eucalyptus fiber-reinforced epoxy-based composite absorbed significantly less impact energy of 0.124 J. Birch fiber-incorporated epoxy composite has the impact energy of 0.105 J. For eucalyptus-reinforced composites, the higher tensile strength and bending stress of 45.25 MPa and 79.92 MPa were noticed. Palm fiber-incorporated composite had the superior impact energy of 130 J.

Tribological Characterization of Chemically Treated NFRC

The authors have been inspired by tribology as the basic elements for the selection of materials in manufacturing and strict environmental regulations. The present study therefore focuses on the tribological behavior of natural fiber-incorporated composites. The study has been classified on the type of natural fibers and work on epoxy-based composites explored by different researchers. Nirmal et al. (2012) studied the adhesive wear performance of bamboo fiber-reinforced epoxy composites at different fiber orientations. Testing was conducted on the pin-on-disc tribological testing machine as represented in Fig. 14. Constant load of 30 N, 1–4 km of sliding distances, and sliding velocity of 1.7–3.96 m/s were used for testing. In comparison with the parallel oriented (PO) and randomly oriented (RO) (MBBFRE), it was identified that the antiparallel orientation (APO) gave the best result. Based on the study, 60% specific wear rate is achieved at 2.22 m/sec compared to neat epoxy under APO orientation. Boopath et al. (Paul et al. 2020) have studied the tribology of the *Borassus* fruit fiber-added epoxy composites. They analyzed the performance of fiber length on wear and friction. They have tested under the dry sliding conditions, considering different parameters like load, sliding velocities under constant time. They have achieved optimum wear rate and friction for 5 mm fiber length compared

Fig. 14 Pin-on-disc wear test

to neat epoxy. Tribological behaviors of flax-reinforced epoxy-based composites under the contact of dry sliding conditions were investigated by Choudhary et al. (2019). The bi-directionally mate fiber has been reinforced. Parameters taken into consideration for the study are sliding speed, load, and sliding distance. In comparison with the neat epoxy composites, specific wear rate of 31.34% was achieved at optimum conditions of sliding speed of 1 m/sec and a load applied at below 10 N.

Sabeel et al. (Ahmed et al. 2012) studied the tribological behavior of jute-added epoxy composites filled with additional ceramic fillers. Experimentation was tested on pin-on-disc method. In this study, the major parameter is weight fraction of the fillers in addition to applied load, sliding speed, and sliding distance. The studies stated that the use of ceramic fillers for jute-epoxy composites significantly improves wear resistance. SEM images also showed that there was a higher wear for SiC composites. In addition to that, higher friction performances resulted in a lower wear loss of 15 wt.% of filler material of Al_2O_3-based composite. Nasir et al. (Talib et al. 2017) have studied the wear behavior of gunny (jute fibers)-reinforced epoxy composites. Tribological studies have been performed using the pin-on-disc (POD) apparatus. Loads applied varied between 5 N and 35 N; slides varied between 1.12 and 22.56 m/s. The results were compared to the enhanced epoxy-based composites of honeycomb. Authors found that, as compared to reinforced honeycomb composites, the wear efficiency of the gunny composites increased by 76.7%. Yousif et al. (Yousif and Chin 2012) have examined the adhesive wear behavior of kenaf fiber-reinforced epoxy composites under wet sliding contact conditions. Authors have treated kenaf fibers with 6% NaOH solution. The experimentation technique used was block on disc (BOD). The authors found that specific wear rate was sensitive to changes in the applied loads as well as sliding distances. Results have also shown that composites can withstand higher application loads in wet contact conditions and also orientation has influenced the wear behavior. An enhancement of 46% was noticed in wear for a normal orientation (N-O) composite. Chin et al. (Chin and Yousif 2009) have also studied adhesive wear and frictional behavior of kenaf-reinforced epoxy-based composites. BOD experimental setup was used in this study. Parameters taken into consideration for the study are applied load, sliding distance, and speed. Wear and friction of the composites were improved by kenaf reinforcements. For kenaf-epoxy composites with normal orientation, wear performance was increased by 85% compared to neat epoxy. Kumar et al. (Kumar and Anand 2018) studied the tribology of Indian ramie-epoxy composites. Test was examined on POD apparatus under the dry load conditions. The input parameters considered for the analysis are applied load, sliding speed, as well as sliding distance. Different weight fractions of ramie fiber such as 10, 20, 30 and 40% were prepared. The friction coefficient for composites produced is improved with fiber loading according to the author. Ashok Kumar et al. (2010) have studied the frictional behavior of sisal-glass-epoxy composites for treated as well as untreated sisal fibers. Testing was conducted on POD apparatus under dry load conditions. The researchers found that composite materials with treated sisal fibers (5% NaOH) had higher frictional characteristics compared to composites with untreated sisal fibers.

Composites with fiber lengths of 2 cm, both treated and untreated composites, showed the lowest friction coefficient.

Conclusions

The chemically treated natural fibers enhance the interfacial bonding between hydrophilic fiber and hydrophobic matrix. Formation of covalent bonds promotes the fiber-matrix adhesion, subsequently improving the strength of epoxy composites. It is evident from the literature that alkali treatment is an efficient and extensively used chemical modification for natural fibers. The other chemical modification is silane treatment which uses the coupling agents in the reaction. Yet, the coupling is viable at extreme temperature environment and existence of moisture. The further research must be focused toward the extraction of coupling agents from natural resources. Further research is necessary in the development of new techniques for chemical modification and to extract fiber-matrix interfacial reactions.

References

M. Abdelmouleh, S. Boufi, M.N. Belgacem, A. Dufresne, Short natural-fibre reinforced polyethylene and natural rubber composites: Effect of silane coupling agents and fibres loading. Compos. Sci. Technol. **67**(7–8), 1627–1639 (2007)

K.S. Ahmed, S.S. Khalid, V. Mallinatha, S.A. Kumar, Dry sliding wear behavior of SiC/Al_2O_3 filled jute/epoxy composites. Mater. Des. (1980–2015) (36), 306–315 (2012)

I.S. Aji, S.M. Sapuan, E.S. Zainudin, K. Abdan, Kenaf fibres as reinforcement for polymeric composites: A review. Int. J. Mech. Mater. Eng. **4**(3), 239–248 (2009)

M. Ashok Kumar, G. Ramachandra Reddy, Y. Siva Bharathi, S. Venkata Naidu, V. Naga Prasad Naidu, Frictional coefficient, hardness, impact strength, and chemical resistance of reinforced sisal-glass fiber epoxy hybrid composites. J. Compos. Mater. **44**(26), 3195–3202 (2010)

M. Asim, M. Jawaid, K. Abdan, M.R. Ishak, Effect of alkali and silane treatments on mechanical and fibre-matrix bond strength of kenaf and pineapple leaf fibres. J. Bionic Eng. **13**(3), 426–435 (2016)

N. Bellili, H. Djidjelli, A. Boukerrou, B. Dairi, R. Bendib, Effect of acetylation on composite materials based on polypropylene/coffee husk waste. Comp.: Mech. Comput. Appl.: Int. J. **11**(4), 309–322 (2020)

A. Benyahia, A. Merrouche, Z.E.A. Rahmouni, M. Rokbi, W. Serge, Z. Kouadri, Study of the alkali treatment effect on the mechanical behavior of the composite unsaturated polyester-Alfa fibers. Mech. Industry **15**(1), 69–73 (2014)

E.T.N. Bisanda, M.P. Ansell, The effect of silane treatment on the mechanical and physical properties of sisal-epoxy composites. Compos. Sci. Technol. **41**(2), 165–178 (1991)

A.K. Bledzki, J. Gassan, Progress in Polym. Science **24**, 221 (1999)

V. Boggarapu, R. Gujjala, S. Ojha, A critical review on erosion wear characteristics of polymer matrix composites. Mater. Res. Express **7**(2), 022002 (2020)

D. Brosius, Natural fiber composites slowly take root. Comp. Technol. **12**(1), 32–37 (2006)

V. Chaudhary, K. Ram, F. Ahmad, Reprocessing and disposal mechanisms for fiber reinforced polymer composites, in *Reinforced Polymer Composites: Processing, Characterization and Post Life Cycle Assessment*, (2019)

C.W. Chin, B.F. Yousif, Potential of kenaf fibres as reinforcement for tribological applications. Wear **267**(9–10), 1550–1557 (2009)

T.J. Chung, J.W. Park, H.J. Lee, H.J. Kwon, H.J. Kim, Y.K. Lee, T.Y. Tze, W., The improvement of mechanical properties, thermal stability, and water absorption resistance of an eco-friendly PLA/kenaf biocomposite using acetylation. Appl. Sci. **8**(3), 376 (2018)

G.L.C. Coura, R.T.S. Freire, J.C. dos Santos, L.Á. de Oliveira, F. Scarpa, T.H. Panzera, Tensile and flexural properties of epoxy laminates with natural papaya bast fibre cellular layers. Comp. Part C: Open Access **2**, 100017 (2020)

M.M. Davoodi, S.M. Sapuan, D. Ahmad, A. Ali, A. Khalina, M. Jonoobi, Mechanical properties of hybrid kenaf/glass reinforced epoxy composite for passenger car bumper beam. Mater. Des. **31**(10), 4927–4932 (2010)

C. Deo, S.K. Acharya, Effect of moisture absorption on mechanical properties of chopped natural fiber reinforced epoxy composite. J. Reinf. Plast. Compos. **29**(16), 2513–2521 (2010)

A.M. Edeerozey, H.M. Akil, A.B. Azhar, M.Z. Ariffin, Chemical modification of kenaf fibers. Mater. Lett. **61**(10), 2023–2025 (2007)

R. Egala, S.G. Setti, Impact characterization of epoxy LY556/ricinus communis L plant natural fiber composite materials. Mater. Today: Proc. **5**(13), 26799–26803 (2018)

A.M. Fairuz, S.M. Sapuan, E.S. Zainudin, C.N.A. Jaafar, Pultrusion process of natural fibre-reinforced polymer composites, in *Manufacturing of Natural Fibre Reinforced Polymer Composites*, (Springer, Cham, 2015), pp. 217–231

J. Fajrin, Mechanical properties of natural fiber composite made of Indonesian grown sisal. INFO-TEKNIK **17**(1), 69–84 (2016)

S.P. Gairola, Y.K. Tyagi, B. Gangil, A. Sharma, Fabrication and mechanical property evaluation of non-woven banana fibre epoxy-based polymer composite. Mater. Today: Proc, **44**, 3990–3996 (2020)

J. George, J.I.I. Verpoest, Mechanical properties of flax fibre reinforced epoxy composites. Die AngewandteMakromolekulareChemie **272**(1), 41–45 (1999)

P.J. Herrera-Franco, M.D.J. Aguilar-Vega, Effect of fiber treatment on the mechanical properties of LDPE-henequen cellulosic fiber composites. J. Appl. Polym. Sci. **65**(1), 197–207 (1997)

P. Herrera-Franco, A. Valadez-Gonzalez, M. Cervantes-Uc, Development and characterization of a HDPE-sand-natural fiber composite. Compos. Part B **28**(3), 331–343 (1997)

A.P. Irawan, T.P. Soemardi, K. Widjajalaksmi, A.H. Reksoprodjo, Tensile and Flexural Strength of Ramie Fiber Reinforced Epoxy Composites for Socket Prosthesis Application. Int J Mech Mater Eng, **6**(1), 46–50 (2011)

S. Jamian, S.N. Ayob, M.R.Z. Abidin, N.H.M. Nor, Fabrication of Functionally Graded Natural Fibre/Epoxy Cylinder Using Centrifugal Casting Method (2006)

T. Joffre, K. Segerholm, C. Persson, S.L. Bardage, C.L.L. Hendriks, P. Isaksson, Characterization of interfacial stress transfer ability in acetylation-treated wood fibre composites using X-ray microtomography. Ind. Crop. Prod. **95**, 43–49 (2017)

K. Joseph, L.H.C. Mattoso, R.D. Toledo, S. Thomas, B.J. Carvalho, L. Pothen, S. Kala, Natural fiber reinforced thermoplastic composites. Nat. Polymer Agro Fiber Based Comp., **4**, 159–200 (2000)

H.A. Khalil, H.D. Rozman, M.N. Ahmad, H. Ismail, Acetylated plant-fiber-reinforced polyester composites: A study of mechanical, hygrothermal, and aging characteristics. Polym.-Plast. Technol. Eng. **39**(4), 757–781 (2000)

R. Kumar, A. Anand, Dry sliding friction and wear behavior of ramie fiber reinforced epoxy composites. Mater. Res. Express **6**(1), 015309 (2018)

E. Laranjeira, L.H. De Carvalho, De L. Silva, S.M, J.R.M. d'Almeida, Influence of fiber orientation on the mechanical properties of polyester/jute composites. J. Reinf. Plast. Compos. **25**(12), 1269–1278 (2006)

A. Lepetit, R. Drolet, B. Tolnai, R. Zerrouki, D. Montplaisir, Effect of acetylation on the properties of microfibrillated cellulose-LDPE composites. J. Appl. Polym. Sci. **134**(32), 44933 (2017)

W. Liu, L.T. Drzal, A.K. Mohanty, M. Misra, Influence of processing methods and fiber length on physical properties of kenaf fiber reinforced soy based biocomposites. Compos. Part B **38**(3), 352–359 (2007)

Y. Liu, X. Lv, J. Bao, J. Xie, X. Tang, J. Che, Y. Ma, J. Tong, Characterization of silane treated and untreated natural cellulosic fibre from corn stalk waste as potential reinforcement in polymer composites. Carbohydr. Polym. **218**, 179–187 (2019)

N. Lopattananon, K. Panawarangkul, K. Sahakaro, B. Ellis, Performance of pineapple leaf fiber–natural rubber composites: The effect of fiber surface treatments. J. Appl. Polym. Sci. **102**(2), 1974–1984 (2006)

P. Martin, Polyurethane pultrusion resin. ReinfPlast **57**, 13 (2013)

L. Mathew, K.U. Joseph, R. Joseph, Isora fibre: Morphology, chemical composition, surface modification, physical, mechanical and thermal properties – A potential natural reinforcement. J. Natl. Fibers **3**(4), 13–27 (2007)

M.J. Mochane, T.C. Mokhena, T.H. Mokhothu, A. Mtibe, E.R. Sadiku, S.S. Ray, I.D. Ibrahim, O.O. Daramola, Recent progress on natural fiber hybrid composites for advanced applications: a review. Express Polym Lett **13**, 159–198 (2019)

L. Mohammed, M.N. Ansari, G. Pua, M. Jawaid, M.S. Islam, A review on natural fiber reinforced polymer composite and its applications. Int. J. Polymer Sci. 1–5 (2015)

A.K. Mohanty, L.T. Drzal, M. Misra, Novel hybrid coupling agent as an adhesion promoter in natural fiber reinforced powder polypropylene composites. J. Mater. Sci. Lett. **21**(23), 1885–1888 (2002)

Y. Mohd Yuhazri, P.T. Phongsakorn, H. Sihombing, A.R. Jeefferie, P. Perumal, A.M. Kamarul, K. Rassiah, Mechanical properties of kenaf/polyester composites. Int. J. Eng. Technol, **11**(1), 106–110 (2011)

R. Nadlene, S.M. Sapuan, M. Jawaid, M.R. Ishak, L. Yusriah, The effects of chemical treatment on the structural and thermal, physical, and mechanical and morphological properties of roselle fiber-reinforced vinyl ester composites. Polym. Compos. **39**(1), 274–287 (2018)

U. Nirmal, J. Hashim, K.O. Low, Adhesive wear and frictional performance of bamboo fibres reinforced epoxy composite. Tribol. Int. **47**, 122–133 (2012)

C.B. Okpanachi, E.B. Agbaji, S.A. Yaro, Effect of acetylation on the mechanical and water absorption properties of pineapple peel reinforced polypropylene composites. FUDMA Rec. Chem. Sci **1**(3), 28–35 (2020)

R. Paul, K. Gouda, S. Bhowmik, Effect of different constraint on tribological behaviour of natural fibre/filler reinforced polymeric composites: A review. SILICON. **13**, 1–23 (2020)

G.V. Prasanna, T. Jayadeep, N. Poornabhodha, Chemical treatment, influence of fiber content, and optimization of hybrid natural fiber-reinforced composites, in *Advances in Materials and Manufacturing Engineering*, (Springer, Singapore, 2020), pp. 325–335

S. Raghavendra, P. Balachandrashetty, P.G. Mukunda, K.G. Sathyanarayana, The effect of fiber length on tensile properties of epoxy resin composite reinforced by the fibers of Banana. Int. J. Eng. Res. Technol. **1**(6), 2278–0181 (2012)

A.A.A. Rashdi, S.M. Sapuan, M.M.H.M. Ahmad, A.J.I.J. Khalina, Combined effects of water absorption due to water immersion, soil buried and natural weather on mechanical properties of Kenaf fibre unsaturated polyester composites (KFUPC). Int. J. Mech. Mater. Eng. **5**(1), 11–17 (2010)

K.O. Reddy, C.U. Maheswari, K.R. Reddy, M. Shukla, E. Muzenda, A.V. Rajulu, Effect of chemical treatment and fiber loading on mechanical properties of borassus (toddy palm) fiber/epoxy composites. Int. J. Polym. Anal. Charact. **20**(7), 612–626 (2015)

M. Rokbi, H. Osmani, A. Imad, N. Benseddiq, Effect of chemical treatment on flexure properties of natural fiber-reinforced polyester composite. Proc. Eng. **10**, 2092–2097 (2011)

D. Rouison, M. Sain, M. Couturier, Resin transfer molding of natural fiber reinforced composites: Cure simulation. Compos. Sci. Technol. **64**(5), 629–644 (2004)

N. Saba, M.T. Paridah, K. Abdan, N.A. Ibrahim, Effect of oil palm nano filler on mechanical and morphological properties of kenaf reinforced epoxy composites. Constr. Build. Mater. **123**, 15–26 (2016)

P. Sabarinathan, K. Rajkumar, V.E. Annamalai, K. Vishal, Characterization on chemical and mechanical properties of silane treated fish tail palm fibres. Int. J. Biol. Macromol. **163**, 2457–2464 (2020)
D.N. Saheb, J.P. Jog, Natural fiber polymer composites: a review. Adv. Polym. Technol. **18**(4), 351–363 (1999)
E. Sarikaya, H. Çallioğlu, H. Demirel, Production of epoxy composites reinforced by different natural fibers and their mechanical properties. Compos. Part B **167**, 461–466 (2019)
E. Sinha, S.K. Rout, Influence of fibre-surface treatment on structural, thermal and mechanical properties of jute fibre and its composite. Bull. Mater. Sci. **32**(1), 65 (2009)
J.P. Siregar, M. Zalinawati, T. Cionita, M.R.M. Rejab, I. Mawarnie, J. Jaafar, M.H.M. Hamdan, Mechanical properties of hybrid sugar palm/ramie fibre reinforced epoxy composites. Mater. Today: Proc. **44**, 3692–3696 (2020)
R. Siva, B. Kesavaram, J.J. Martin, G. Mathiselvan, K.B. Navas, M. Sangeetha, Mechanical behavior of sisal and banana fiber reinforced hybrid epoxy composites. Mater. Today: Proc. (2020)
S. Sivasaravanan, V.B. Raja, K.A. Babu, B.C. Mouli, Mechanical characterization of GFRP/CFRP/natural fiber laminated in epoxy resin composite. Mater. Today: Proc. **16**, 934–938 (2019)
C.V. Srinivasa, K.N. Bharath, Impact and hardness properties of areca fiber-epoxy reinforced composites. J. Mater Environ. Sci. **2**(4), 351 (2011)
A.B.M. Supian, S.M. Sapuan, M.Y.M. Zuhri, E.S. Zainudin, H.H. Ya, H.N. Hisham, Effect of winding orientation on energy absorption and failure modes of filament wound kenaf/glass fibre reinforced epoxy hybrid composite tubes under intermediate-velocity impact (IVI) load. J. Mater. Res. Technol. **10**, 1–14 (2021)
M.C. Symington, O.S. David-West, W.M. Banks, R.A. Pethrick, Vacuum infusion of natural fibre composites for structural applications, in *13th European Conference on Composite Materials (EECM 13)*, Wiley VCH, Germany (2008)
N. Talib, R.M. Nasir, E.A. Rahim, Tribological behaviour of modified jatropha oil by mixing hexagonal boron nitride nanoparticles as a bio-based lubricant for machining processes. J. Clean. Prod. **147**, 360–378 (2017)
S.C. Venkateshappa, S.Y. Jayadevappa, P.K.W. Puttiah, Mechanical behavior of areca fiber reinforced epoxy composites. Adv. Polym. Technol. **31**(4), 319–330 (2012)
D. Verma, P.C. Gope, M.K. Maheshwari, R.K. Sharma, Bagasse fiber composites–A review. J. Mater. Environ. Sci **3**(6), 1079–1092 (2012)
R. Vijay, S. Manoharan, S. Arjun, A. Vinod, D.L. Singaravelu, Characterization of silane-treated and untreated natural fibers from stem of leucas aspera. J. Natl. Fibers **18**, 1–17 (2020)
B. Wang, S. Panigrahi, L. Tabil, W. Crerar, Effects of chemical treatments on mechanical and physical properties of flax fiber-reinforced rotationally molded composites, in *2004 ASAE Annual Meeting*, (American Society of Agricultural and Biological Engineers, 2004), Michigan p. 1
B.F. Yousif, C.W. Chin, Epoxy composite based on kenaf fibers for tribological applications under wet contact conditions. Surf. Rev. Lett. **19**(05), 1250050 (2012)
N.E. Zafeiropoulos, C.A. Baillie, J.M. Hodgkinson, Engineering and characterisation of the interface in flax fibre/polypropylene composite materials. Part II. The effect of surface treatments on the interface. Compos. A: Appl. Sci. Manuf. **33**(9), 1185–1190 (2002)
M. Zampaloni, F. Pourboghrat, S.A. Yankovich, B.N. Rodgers, J. Moore, L.T. Drzal, A.K. Mohanty, M. Misra, Kenaf natural fiber reinforced polypropylene composites: a discussion on manufacturing problems and solutions. Compos. A: Appl. Sci. Manuf. **38**(6), 1569–1580 (2007)
Y.T. Zheng, D.R. Cao, D.S. Wang, J.J. Chen, Study on the interface modification of bagasse fibre and the mechanical properties of its composite with PVC. Compos. A: Appl. Sci. Manuf. **38**(1), 20–25 (2007)
M.H. Zin, K. Abdan, N. Mazlan, E.S. Zainudin, K.E. Liew, M.N. Norizan, Automated spray up process for pineapple leaf fibre hybrid biocomposites. Compos. Part B **177**, 107306 (2019)

Spectroscopic Analysis of Natural Fiber/Epoxy Composites

20

Manoj Panchal, Gujjala Raghavendra, Bhargav, Md. Alamgir, Shakuntala Ojha, V. Suresh Babu, and B. Satish Ben

Contents

M. Panchal · M. Alamgir
Department of Mechanical Engineering, RGM College of Engineering and Technology, Nandyal, Andhra Pradesh, India

G. Raghavendra (✉)
Department of Mechanical Engineering, National Institute of Technology, Warangal, India
e-mail: raghavendra.gujjala@nitw.ac.in

Bhargav · V. S. Babu · B. S. Ben
Department of Mechanical Engineering, NIT Warangal, Warangal, Telangana, India

S. Ojha
Department of Mechanical Engineering, Kakatiya Institute of Technology and Science, Warangal, Telangana, India

S. Mavinkere Rangappa et al. (eds.), *Handbook of Epoxy/Fiber Composites,*
https://doi.org/10.1007/978-981-19-3603-6_21

Abstract

The critical climate change and pollution have led scientists to research natural material. In the field of composites, natural fibers have started to replace synthetic fibers owing to their biodegradability, easy availability, good specific properties, etc. All research related to materials requires their characterization, whether it is the characterization of physical, chemical, or mechanical properties, spectroscopic techniques are of tremendous use, especially in natural composites where the natural fibers itself are made of complex carbohydrates, characterization of their properties is of utmost importance. The manufacturing of composite leads to many significant changes in their morphology, physical bonding, chemical bonding, etc., which is why it is important to observe these changes, which will directly affect the chemical, mechanical, and thermal properties. These changes can be easily identified with spectroscopic techniques. Moreover, the check for certain properties such as mechanical properties and tribological properties involves damage or breaking of material. By investigating the fracture, one can identify the fracture or wear phenomenon. For the study of all aforementioned phenomena, spectroscopy comes in very handy. This chapter deals with the study of epoxy/natural fiber composites using various phenomena like bonding, fracture, wear, etc. with the help of spectroscopic techniques.

Keywords

Natural fiber · Epoxy · XRD · SEM · FTIR · NMR · Raman Spectroscopy

Introduction

For the past few decades, polymers and polymeric materials have found their way into engineering applications and have become an important class of engineering material. For decades, polymers have been tremendously used in everyday life due to their applicability in routine work. The inception of the polymers can be traced back to the early nineteenth century. The term "polymer" was first introduced by J. J. Berzelius (Feldman 2008). The common chemical property which distinguishes polymers from another kind of materials is a high molecular weight, due to repeating units of covalent bonds. Some very important physical characteristics which are influenced by high molecular weight are high viscosity, a wide range of elasticity, good strength, etc. One of the first polymers was synthesized in the nineteenth century, by adding camphor to nitrocellulose, thus forming a polymer called celluloid (Feldman 2008). The rapid growth of polymers began in the early twentieth century with the introduction of Bakelite, polyester, and PVC and later polyethylene, epoxies, PEEK, etc.

The industrial production of polymers began during World War II, with the production of PVC for insulation (Feldman 2008). Polymers have a wide range of usage ranging from household appliances to space applications. Some applications of polymers are consumable goods, food and packaging, medical applications (capsules and tablets), insulators, pipe and pipe fittings, constructions (doors, windows, ceilings), automobile body parts, coatings, sealings, etc. Polymers lack certain properties such as strength, hardness, and wear resistance and they have low thermal resistance. They provide good compatibility with other materials when used in combination.

With the advent of composites, polymers have been widely used for the manufacture of polymer matrix composites. A composite is called a polymer composite when the polymer is matrix material while the reinforcement is fibers or particulates. The objective of polymer composites is to exploit the superior properties of both matrix and reinforcement and form new tailor-made properties.

Owing to the availability of a wide variety of matrix and reinforcements, polymer composites provide much more options in terms of design parameters compared to the metal matrix and ceramic matrix composites. The reinforcement can be fiber or particulate. Furthermore, the fiber can be natural or man-made fibers. Some examples of man-made fibers are carbon fiber, glass fiber, aramid fiber, boron fiber, etc. While natural fibers are acquired from agricultural resources such as bamboo fiber, jute fiber, hemp fiber, and coir fiber. Besides, fiber particulates are also used for enhancement of certain properties such as wear resistance, thermal stability, and hardness. Sometimes these filler materials are used in combination fibers to make hybrid composites. Polymer composites have an extensive array of engineering applications due to special characteristics of polymers such as lightweight, corrosion resistance, and self-lubrication and some of the applications are gears, bushes, cams, etc.

In polymer composites, epoxy composites are the most widely used composites owing to low cost, decent mechanical properties, high-specific properties, good adhesiveness with fibers, good thermal resistance (Abdellaoui et al. 2019), etc. Glass fiber (Fu et al. 2000; Safi et al. 2016; Jefferson et al. 2019; Hwang 2011) and carbon fiber (Elleithy 2000; Liu et al. 2014) are extensively used as reinforcement materials with epoxy composites. However, as we jumped in the field of plastics, a major concern is the environment, so the natural biodegradable materials have become a major point of attraction. In the field of composite where the carbon and glass fibers are dominating, the natural fibers have started to replace them for certain applications. Natural fiber composites are very much an area of research now. Natural fibers are made of complex carbohydrates and their function group, composition, etc. have to be analyzed. Natural fiber is made up of lignin, cellulose, hemicellulose, pectin, etc. As we talk about the research and development, analysis, application, and significance of natural fiber/epoxy composite in today's world, One of the most significant aspects of the analysis is concerned with the spectroscopic analysis of prepared material. A spectroscopy technique is based on the principle of interaction of light with material, that is, refraction, reflection, or absorption. This phenomenon reveals entire chemistry of material, and the material interaction of light shows some astonishing behavior. The behavior of material depends on the kind of spectrum it exposed to. The importance of the spectroscopic techniques was well defined by Robert B. Leighton, Professor of

Physics at the California Institute of Technology: "Of all the techniques that have been used to the study of the detailed structure of matter, it can be said that spectroscopy has been used in more ways to more problems, and has produced more fundamental information, than any other" (Hellman 1968).

Based on the spectrum of electromagnetic radiation the spectroscopic techniques are divided into different spectroscopy techniques, namely, Infrared Spectroscopy, Electron Microscopy, X-ray diffraction, Raman Spectroscopy, NMR Spectroscopy, UV Spectroscopy, etc., which are some of the most widely used techniques for characterization of natural fiber composites. The basic idea is the same for all spectroscopic techniques. In this chapter, we are going to explore research work that has been carried out with the aid of some of the most widely used spectroscopic techniques for characterization of natural fiber/epoxy, and we will discuss the results of previous research and their significance and future directions.

We will begin the discussion with the introduction of epoxy and natural fiber and then jump into natural fiber epoxy composites.

Epoxy

Epoxy is extensively used in the composite industry owing to its good mechanical, thermal, and electrical properties. Also, its ability to cure at room temperature and low shrinkage during curing are added advantages over other polymers. The term "epoxy resin" encompasses both pre-polymer and cured resin. Epoxy resins are designated by 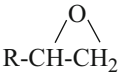 epoxy group. An epoxy resin is generally developed by the reaction of bisphenol-A with epichlorohydrin. Epoxy resin is also known by the name Diglycidyl-Ether of Bisphenol-A (DGEBA). DGEBA is extensively used in industries owing to its low viscosity, easy processability, and good mechanical properties. The XRD analysis of epoxy exhibits two amorphous peaks at 2θ value of 20.50 and 22.50 (Ismael Abdullah and Ansari 2015). Table 1 shows mid region infrared spectroscopy of epoxy at different frequency.

Natural Fibers

Broadly speaking, plants are made up of three parts, namely, roots, leaves, and stem, and each of these has specific functions. Their reproduction results in growth of nutrition-rich flowers or fruits or both. Each of these is made of several plant tissues, which in turn are made up of plant cells. The plants cells consist of different organelles which are same as human organelles. However, plants do have some features that humans don't. Those are cell wall, cell membrane, central vacuole, and plastids. The function of cell wall is to provide structural support and protection, and it acts as a transferring media that allows transfer of fluids such as water and gases such as CO_2 and O_2 (Cosgrove 2005). The cell wall is a composite structure

Table 1 Characteristic bands of DGEBA in the mid-IR (González et al. 2012)

Band (cm^{-1})	Assignment
3500	O–H stretching
3057	C–H stretching the oxirane ring
2965–2873	C–H stretching of CH_2 and CH aromatic and aliphatic rings
1608	Stretching C=C of aromatic rings
1509	C–C stretching of aromatic rings
1036	C–O–C stretching of ethers
915	C–O stretching of oxirane group
831	C–O–C stretching of oxirane group
772	CH_2 bending

containing hemicellulose, cellulose, lignin, and pectin, which comes under the category of lignocellulosic material (Siró and Plackett 2010; Chen and Chen 2014). Some intracellular substances come under category of lignocellulosic material. These intracellular substances are called extractives. Each of these chemical compounds has variable concentrations of carbon. The cell wall is the natural fiber. Natural fibers are composites of cellulose fiber embedded in lignin and hemicellulose matrix (Siró and Plackett 2010; Chen and Chen 2014). These fibers are made up of microfibrils throughout the length of the fiber. The hydrogen bonding and functional groups are responsible for strength and stiffness of fibers. The characteristics of each properties of each ingredient are accountable for imparting the properties to the fiber. The biodegradation, thermal degradation, and moisture absorption of the fiber material is due to the presence of hemicellulose. The presence of lignin provides the thermal stability; however, lignin degrades when exposed to ultraviolet radiation. The fraction of individual constituents differs for a variety of fibers. Usually, the variation is 60–80% cellulose, 5–20% lignin, and up to 20% moisture. Cellulose is one of the most abundant biopolymers existing on our planet (Siró and Plackett 2010). It serves as the reinforcing phase in plant structures as mentioned above. The reinforcement is (cellulose) an orderly arrangement of microfibrils of cellulose, which are coated with a layer of matrix polysaccharide. Matrix materials are in the form of complex polysaccharides, that is, lignin and hemicellulose. The strength of a natural fiber reinforced composite depends on amount cellulose content, morphology of fiber surface, diameter of fiber, cross section of fiber, etc.

Electron Microscopy for Morphology Analysis of Natural Fiber/Epoxy Composite

Working Principle of Electron Microscopy

In electron microscopy (EM) a beam of electron is used as source for generating images. Most widely used and most common type of electron microscope is scanning electron microscope. A scanning electron microscope (SEM) creates the image

of a sample by scanning with the concentrated electron beam. The electrons come in contact with atoms in the sample, which results in emission of secondary electron from the atom or back scattering of electron or transmission of electron (Gauglitz and Vo-Dinh 2003). The secondary electron contains information about the surface morphology and configuration of the sample.

For powdered sample very small quantity of sample was taken and attached to carbon tape. For nonconducting sample, a coating of conductive materials is required, gold being a very common material for coating purpose. Other electron microscopes are Field Emission Scanning Electron Microscope (FE-SEM) and Transmission Electron Microscope (TEM); these microscopes provide very high quality of image unlike conventional scanning electron microscope. A FE-SEM is used to picture very small topographical details on the surface or entire or divided objects. FE-SEM can be utilized to observe topographical details as small as 1 nm (Raghavendra et al. 2015). The difference between a SEM and FE-SEM lies in electron generation, in SEM (or TEM) electrons are generated by heating the filament, while in FE-SEM tungsten filament is cooled down to generate the electron source. A transmission electron microscope uses transmitted electron unlike scanning electron microscope which uses secondary electron or backscattered electron. The sample is a very thin film through which an electron beam is transmitted. TEM provides details about crystal structure, grain structure, and grain boundaries. High resolution can also be utilized to examine the quality, shape, size of nano wires, quantum dots, nanoparticles, etc. Among all the electron microscopy technique, SEM is most widely used technique due available and cost criterion.

Nowadays, a scanning electron microscope comes with EDX (energy-dispersive X-ray spectroscopy). EDAX (energy-dispersive X-ray spectroscopy) is a technique for identification of elements present in the sample.

Electron Microscopy Analysis of Natural Fiber/Epoxy Composites

An EM analysis is most important characterization technique along with X-ray diffraction and almost every material characterization research includes EM, whether it is surface morphology of prepared composite or whether it is fractured surface analysis or a wear analysis. Imaging is very important part of characterization of material surface. In area of composite, it is used at various stages of characterization beginning with inspection of morphology of fiber and then the morphology of prepared composite to see the bonding and interfacial adhesion. Imaging can be of tremendous use to assess the mechanism of physical phenomenon the material went through during the concerned testing of sample i.e., for mechanical testing whether it is a brittle or ductile failure, and path of crack propagation, for tribological analysis, kind of wear mechanism it follows. Likewise, there are innumerable examples, where EM is a primary method for investigation of surface morphology. Sometimes the EM and SEM are used interchangeably because of the popularity of SEM analysis.

Fractography Analysis

Fractography analysis involves analysis of fracture surface and investigation of failure mechanism. Scanning electron microscopy analysis is a precise tool to do it. Almost all research that involves failure analysis uses SEM as a primary tool for investigation. In the present segment, we will review the failure mechanism of different natural fiber reinforced epoxy composites.

Harish et al. (2009) prepared coconut coir/epoxy composite and performed the mechanical characterization for evaluation of tensile strength, flexural strength, and toughness. The fractography analysis was performed with SEM to see the failure mechanism. Fractography of tensile and flexural tested sample reveals the appearance of river patterns with voids and a fiber pull-out. SEM image of impact tested sample showed fiber cracking which indicates that there was energy absorbed during testing. It was concluded that failure is due to the fiber pull-out in case of tensile loading and flexural loading condition. Furthermore, the SEM fractography also reveals the poor interfacial bonding at the interface leading to failure. Similar research was performed elsewhere and it was observed that failure is due to fiber pull-out owing to poor interfacial bonding (Das and Biswas 2016). In yet another research a thorough comparison of PALF (pineapple leaf fiber) and coir fiber epoxy composite was made (Da et al. 2018). It was concluded through the SEM analysis of fiber surface and fractography analysis of composites that the PALF provides better adhesion compared to coir fiber, and it was observed that coir fiber had lower cross-section area and a smoother surface compared to PALF which may be the reason behind poor bonding between coir and epoxy. It can be concluded from the fractography analysis of previous research that surface of fiber plays a significant role for enhancement of strength, and it was observed through fractography analysis that the epoxy and coir fiber showed poor wettability and consequently poor interfacial bonding (Da et al. 2018). The solution to this problem could be solved by enhancing the interfacial adhesion either by surface treatment and/or adding another fiber in conjunction with coir fiber. In this direction, Yan et al. (2016) contrasted the SEM fractography of treated and untreated coir fiber reinforced epoxy composite. It was uncovered that the alkali treatment makes the surface rough, which in turn helps with the adhesion. Owing to the better adhesion, the fiber pull-out is less in untreated coir fiber epoxy composite. In yet another research it was concluded that the treated coir fiber in addition to carbon fiber reinforcement greatly influences the interfacial bonding (Singh et al. 2020). It was observed in SEM fractography that there is proper distribution of coir fiber in the matrix. It can surely be concluded here that coir fibers are not much efficient for reinforcement with epoxy resin, and does not provide good adhesion with epoxy due to the smoothness of fiber surface; however, surface treatment does improve adhesion and subsequently the strength.

We further explore the surface adhesion phenomenon along with the morphology of fractured surface to see the failure mechanism with help of microscopy analysis.

Biswas et al. (2015) compared unidirectional bamboo and jute epoxy composite. A good interface quality between the fiber surface and matrix was detected. The

SEM micrographs revealed that for bamboo fiber composite the failure is due to fiber pull-out rather than braking while the fiber braking is a cause of failure for jute fiber. This establishes the fact that there might be mechanical bonding or chemical bonding at the interface.

Khan et al. (2017) performed the fracture analysis of bamboo fiber reinforced epoxy composite. To check the fracture toughness a crack was introduced in the test sample, and then the tensile test was conducted. Fractography examination using SEM revealed that fiber breaking, matrix cracking, debonding, and fiber pull-out were the main phenomena involving failure of composite.

Osorio et al. (2011) examined the morphology of fractured surfaces of bamboo epoxy composite surface. It was observed that bamboo fibers provide good adhesion with epoxy. The fracture phenomenon involves fiber pull-out. However, fiber defibrillation and fiber delamination were also observed in some cases. These are the typical failure modes for natural fibers.

Rahul Kumar et al. (2019) analyzed the fractured surface of bamboo filled epoxy-based composite samples after the fracture test. The SEM images represent the debonding and void creation due to drawing out of bamboo fibers. A clear separation of fibers and matrix was observed owing to pull out. However, the interfacial bonding was good between fiber and matrix. The macropores were also visible at the site of the fracture surface. It was postulated that these pores (or voids) are possibly the source for crack initiation and propagation.

Zhang et al. (2018) checked the morphology of NaOH-treated bamboo fiber epoxy composites. It was established through the outcomes of experimental analysis that the composite fracture toughness and flexural modulus enhanced with fiber span and percentage. The fracture surfaces observed by SEM revealed the following major failure mechanism: fiber breakage, matrix cracking, and debonding due to fiber drawing out.

Here a concluding remark about bamboo fiber reinforced composite can be made, that is, they provide good adhesion and consequently better strength. The failure mechanism involves fiber pull-out besides fiber breakage and debonding.

Raghavendra et al. (2015) performed a morphology analysis tensile test and flexural test of jute fiber reinforced composites. Through the SEM image shown in Fig. 1 for the tensile tested sample, it can be noticed that the failure is due to fiber breakage and pull-out. In the SEM image shown in Fig. 2 for the flexural tested sample, it is pretty clear that breakage is due to the fiber breakage, and additionally, there is no proper bonding between fiber and matrix. They have also noted that there is very little stretching of fiber owing to the brittle nature of fiber.

Jabbar et al. (2017) characterized the fractured surface of jute fiber-green epoxy composites prepared with variable percentage of nanocellulose coating, viz., CF0 (uncoated), CF3 (3 wt.%), CF5 (5 wt.%), and CF10 (10 wt.%). Figure 3a–d shows fractography images for various percentage nanocellulose coated jute fiber reinforced epoxy composites. From Fig. 3, fiber breaking, fiber being drawn out, and some voids can be observed for all composites. However, fiber pull-out is a little more pronounced phenomenon for nanocellulose coated composites as can be appreciated from the figures.

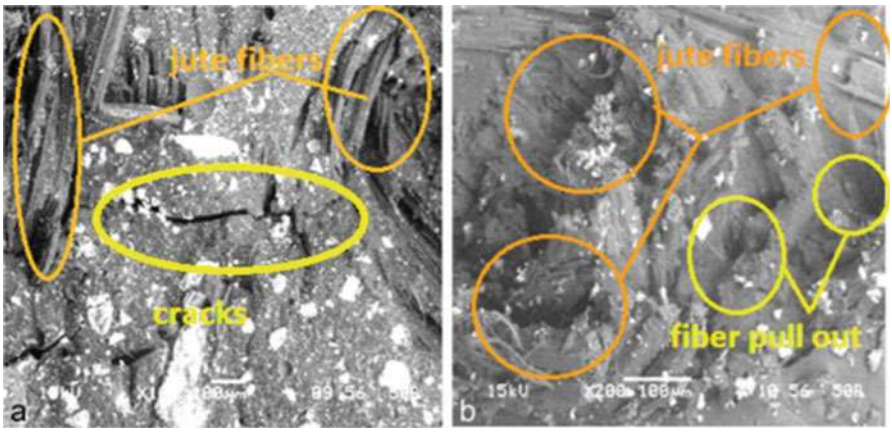

Fig. 1 (**a**, **b**) SEM micrograph of tensile tested jute fiber epoxy composite. (Reprinted with permission from Raghavendra et al. 2015)

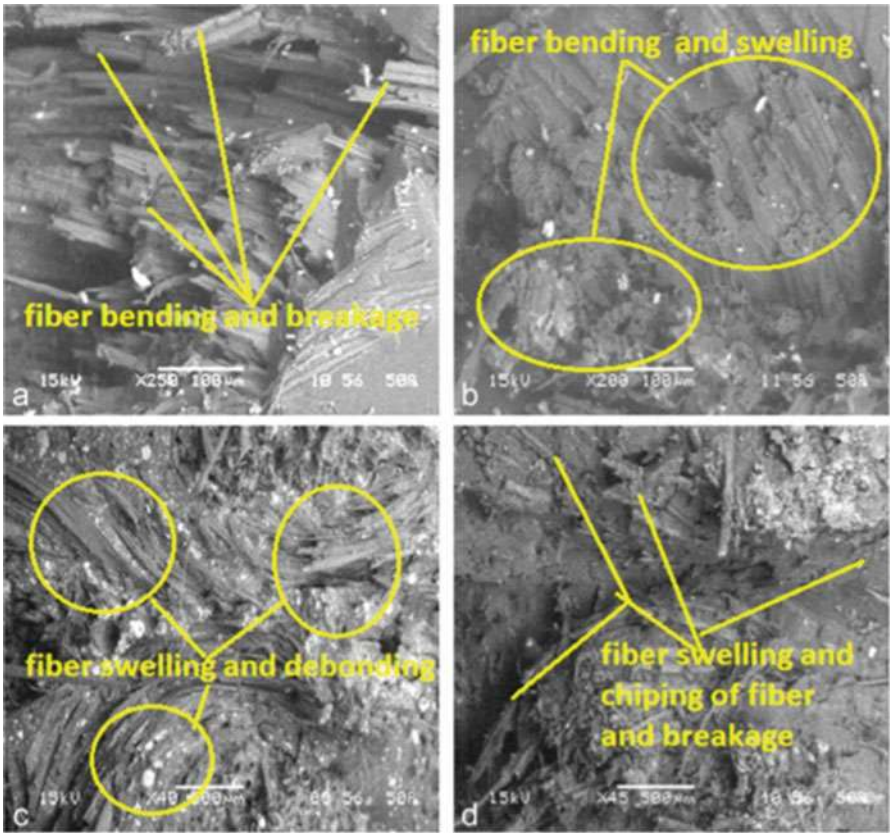

Fig. 2 (**a**–**d**). SEM micrograph of flexural-tested jute fiber composites. (Reprinted with permission from Raghavendra et al. 2015)

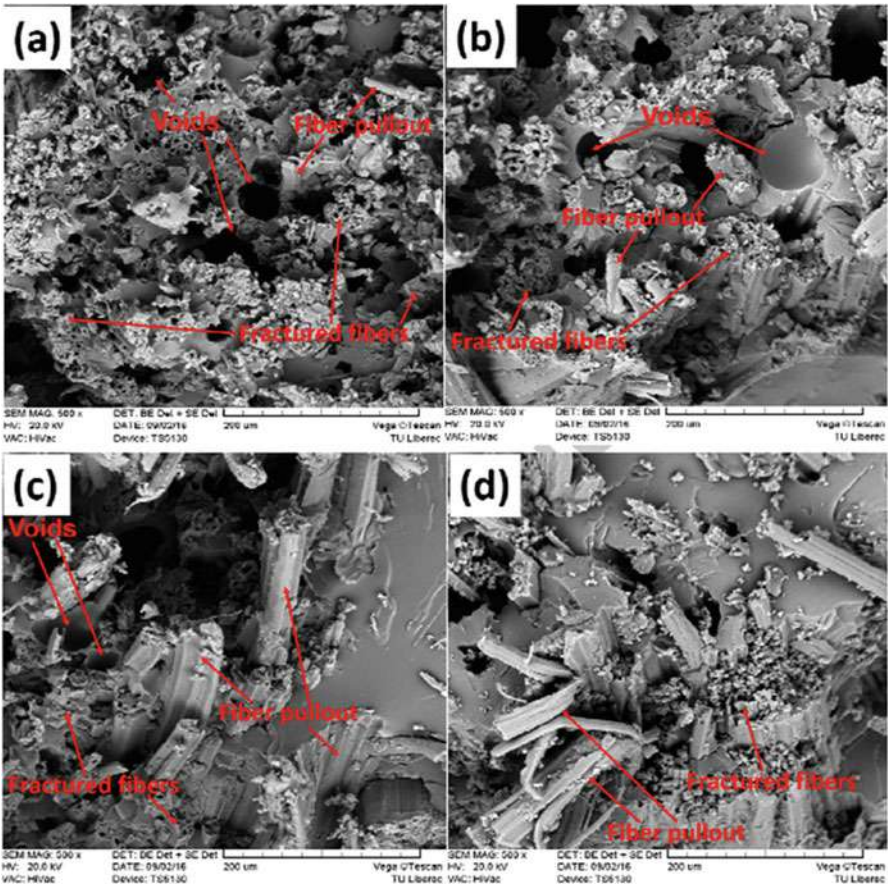

Fig. 3 Fracture surface morphology of jute/green epoxy composites: (**a**) CF0, (**b**) CF3, (**c**) CF5, and (**d**) CF10. (Reprinted with permission from Jabbar et al. 2017)

Dinesh et al. (2020) performed mechanical characterization of jute fiber/epoxy composites filled with Rosewood and Padauk wood dust and compared with neat jute fiber reinforced epoxy composites. In the fractography analysis of fractured surfaces of both the composites, the Padauk filled jute-epoxy composite showed very good interfacial interaction, and also there was negligible pull-out in case of Padauk dust filled jute fiber epoxy composite in contrast to Rosewood dust jute fiber epoxy composite. In the case unfilled jute fiber composite, many fracture phenomena, that is, fiber tear, fiber pull-out, resin cracking, fiber bending, and cracks, were observed owing to poor adhesion.

Another similar work with jute fiber was performed by R Vijay et al. (2020); they added *Azadirachta indica* seed powder and *Camellia sinensis* powder, and the amalgamation in jute fabrics/epoxy composites was compared with neat jute/epoxy composite. SEM studies of fractured surface revealed fiber cracking, tearing, crack

bridging, pull-out, and debonding in neat jute composite (JC-1). While for the spent *Camellia sinensis*-filled composites (JC-2) SEM images revealed that the voids were partially filled. Moreover, the various failure mechanisms like fiber tear, voids, pinning, crazing, filler debonding, and improper wetting of fiber were also observed in SEM. In case of *Azadirachta indica* seed powder filled Jute Composite (JC-3) voids were significantly covered. Moreover, good interfacial was visualized in SEM. In case of composite (JC-4) filled with both kinds of the filler materials fiber pull-out was observed. It was concluded that *Azadirachta indica* seed powder provided good additive when used in combination with jute in epoxy resin.

Yadav and Gupta (2019) performed chemical treatment with different chemicals such as alkali, benzoyl, and sodium bicarbonate along with PLA coating of jute fiber to enhance the adhesion of jute fiber with epoxy, which consequently enhanced the performance of composite. It was observed through morphology analysis of fractured surface that the coating along with chemical treatment greatly improved the adhesive bonding, and the benzoyl was the best chemical treatment among others. Good interfacial adhesion and proper distribution of fibers was detected after benzoylation.

Anand et al. (2018) investigated the mechanical characteristics of hybrid natural Jute/Kenaf fiber composite. It was observed through morphology analysis that natural fiber lacks the wettability with resin. It was also observed that hybrid composite provided good adhesion, although there are a few defects such as voids due to air entrapment. An intra-fiber delamination was observed in SEM.

Concluding remarks about jute fiber composite can be made from spectroscopic analysis that jute fiber does not provide good adhesion with epoxy; however, hybridization and surface treatment are one way to go.

Petrucci et al. (2013) have prepared flex and hemp fiber/epoxy composite, and their hybrid composites with basalt fiber and glass fiber, and the morphology analysis of flex fiber and hemp fiber laminates and hybrid composite was performed. The fractography analysis of the tensile tested sample of flex fiber and hemp fiber laminates is shown in Figs. 4 and 5, respectively. It can be observed from Fig. 4 that flax reinforced laminates show brittle failure owing to fiber pull-out and wear interfacial adhesion. In the case of hemp fiber reinforced it was fibrillation that causes failure as observed in Fig. 5. However, the hybridization with basalt fiber as core significantly improved tensile strength.

Sometimes hybridization provide the better interfacial bonding as stated before in that direction,

Arun Prakash and Viswanthan (2019) have used scanning electron microscopy to analyze fractured surfaces of raw and treated sea-urchin spike filler and kenaf fiber mat-reinforced neem oil blended epoxy composite. The fractography of neem-epoxy matrix reveals the homogeneous ridges on the surface of the fractured specimen which indicates the proper mixing of neem oil with epoxy. Fractography of pure kenaf fiber in epoxy-neem biocomposite reveals the fiber pull-out. But the case of treated kenaf fiber reinforced neem oil epoxy composite shows better bonding between kenaf fiber and matrix.

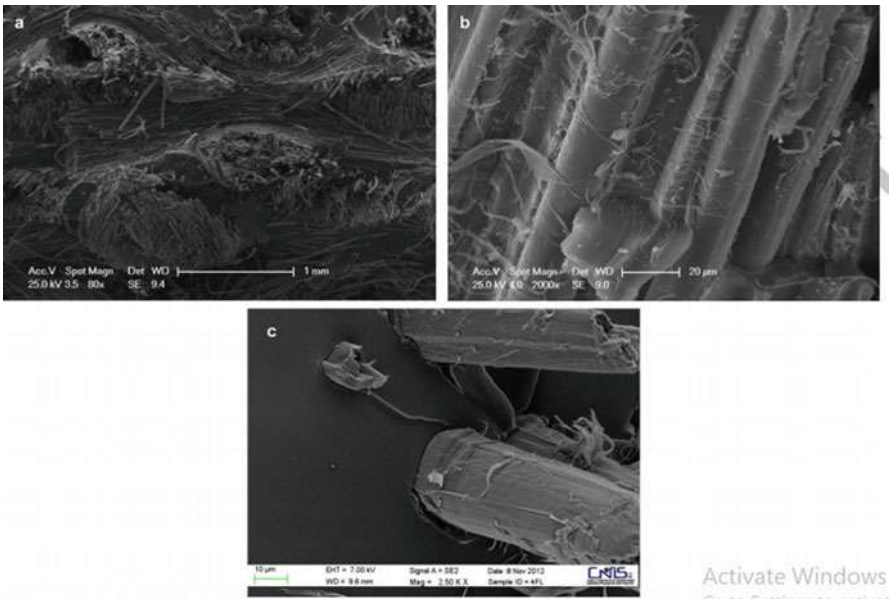

Fig. 4 SEM images of the fracture surface of flax fiber reinforced laminates. (Reprinted with permission from Petrucci et al. 2013)

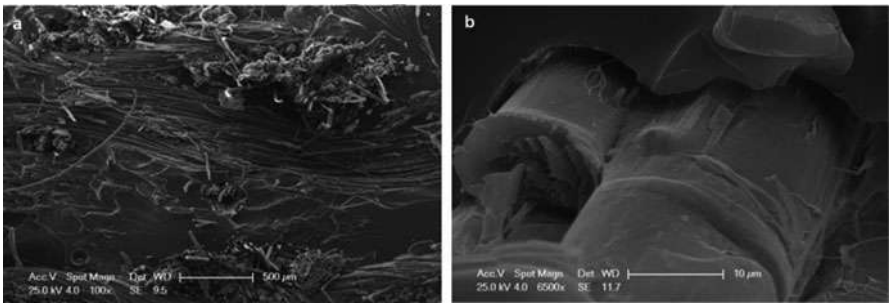

Fig. 5 SEM images of the fracture surface of hemp fiber reinforced laminates. (Reprinted with permission from Petrucci et al. 2013)

Saba et al. (2019) have developed magnesium hydroxide (MH) filler/kenaf fiber epoxy hybrid composite. It was concluded through morphology analysis that MH addition makes the surface rougher which in turn enhances the adhesion between fiber and resin. The same phenomenon was observed for all mechanical test, that is, tensile, flexural, and impact.

Vivek and Kanthavel (2019) developed hybrid biocomposite using a different combination of natural fiber such as banana/flax (HBF), banana/kenaf (HBK), sisal/kenaf (HSK), and sisal/flax (HSF) with Bagasse Ash (BGA). Morphological analysis was performed to study the fractured surface after the flexural test of the specimen

using a SEM. SEM images of fractured surfaces are shown in Fig. 6. In Figure 6a, d HBK and HSF filled with BGA indicates better compatibility between fiber and polymer matrix with few voids. While SEM images shown in Fig. 6b, c for HBF and HSK composite suggest poor interfacial adhesion owing to fiber accumulation and damage during fiber pull-out. It can be concluded here that the combinations of banana and flax and sisal and flax are a good for use with while the other two combinations, that is, banana/kenaf and sisal/kenaf, are not so good. Moreover, all the natural fibers were alkali treated before fabrication, which enhances the adhesion.

Suresh Kumar et al. (2014) fabricated and analyzed untreated and treated coconut sheath fiber reinforced epoxy (TCSE) composite for mechanical properties. The SEM images of untreated (raw) and treated coconut sheath fiber surfaces were observed. There was a cloud pattern observed on raw coconut sheath fiber surface owing to agglomeration of impurities while a clear surface was observed for treated coconut sheath fiber. The SEM image of tensile fractured surfaces of untreated composite and treated revealed that the fractured surface of untreated fiber epoxy composite had some cavities and debonding of fiber. The fractured surface of TCSE composite revealed that there were no voids and showed better adhesion bonding fiber and resin. For flexural and impact tested fractured surfaces the same was observed in the case of treated fiber epoxy composite, that is, broken fiber with no voids.

Raghu and Goud (2020) analyzed the fractured surface morphology of the *Calotropis procera*/glass fiber reinforced epoxy hybrid composites by using a

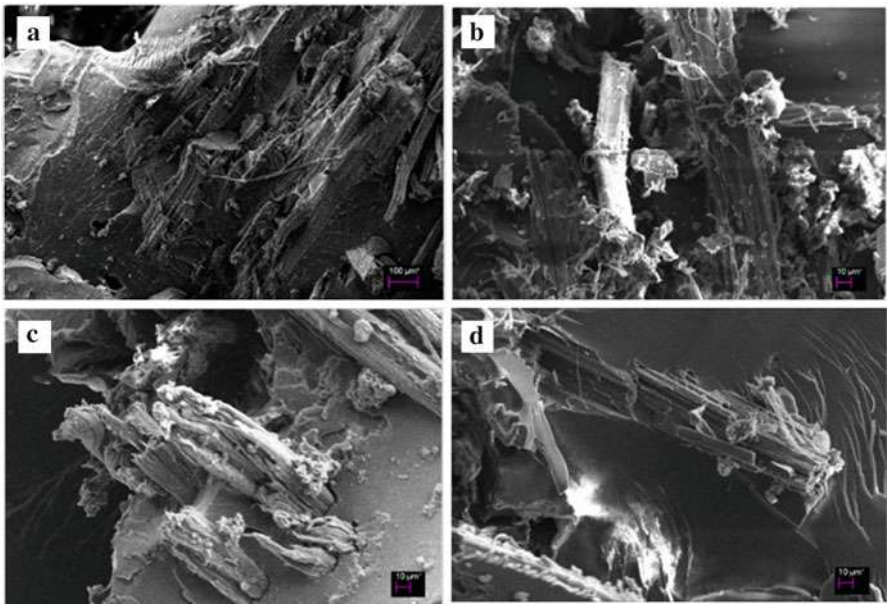

Fig. 6 SEM images of fractured specimens of a flexural test of (**a**) HBK, (**b**) HBF, (**c**) HSK, and (**d**) HSF. (Reprinted with permission from Vivek and Kanthavel 2019)

scanning electron microscope (SEM). They observed that the low fiber content, that is, 5 wt.%, of *Calotropis procera* and high fiber content of glass fiber provide better adhesion and consequently better stress transfer.

We have seen fractography analyses of various natural fiber epoxy composites, it was found out that for all the natural fiber epoxy composite the failure is either due to the fiber breakage or fiber pull out. It can be concluded from the observation that if adhesion is good, the failure is due to fiber breakage, and if adhesion is poor, the fiber pull-out causes the failure. The majority of natural fiber does not provide very good adhesion with resin; however, alkali treatment was found to be one way to enhance adhesion, and the secondary option could be hybridization.

Wear Mechanism Analysis

Wear is simply the removal of material through the interaction of external body by either direct contact or indirect contact (corrosion). There are plenty of examples such as outer body parts of automobile, high-speed aircraft body parts, piston and cylinder, lathe tool, drilling machine tools and body parts, milling machine, and abrasive machines where a part has to survive wear in one way or another. It can be rightly said that wherever there is an interaction between two bodies there will be wear. Finding wear properties of any material is of extreme importance; however, without finding the wear mechanism the wear analysis is not complete. For the establishment of wear phenomenon involved, in particular wear analysis, morphology analysis plays a huge role.

Erosion Wear Behavior

Erosion wear is the damage of the material due to the impact of hard particles. The erosion wear analysis is important where the part is moving with velocity and hit by sand particles/hard particles; such kinds of application are found especially in the field of automobile. Nowadays many automobile exterior parts are made of natural fiber composites, and it has become vital to study the erosion wear behavior of natural fiber composite. The morphology analysis comes in handy in identification of erosion wear mechanism.

Gupta et al. (2011) analyzed the effect of various parameters on erosion wear behavior of bidirectional roving bamboo fiber reinforced epoxy composites. They performed morphology analysis of worn-out surface after dry sand erosion test, observed through SEM analysis that at different sand impingement angle the erosion wear varies, and also observed the size of the crater and small cracks varies with wear angle. The maximum crater size and wear debris found at 60° of sand impingement angle as shown in Fig. 7e, f. In the SEM image shown in Fig. 7 a, b, wear debris can be seen; however, as impingement angle increases the wear debris and crater size increase, which can be observed in Fig. 7b, c and e, f. The lowest crater size was found at 90° of impingement angle as shown in Fig. 7g, h. It was concluded that the separation and braking of fiber was characterized as a wear mechanism.

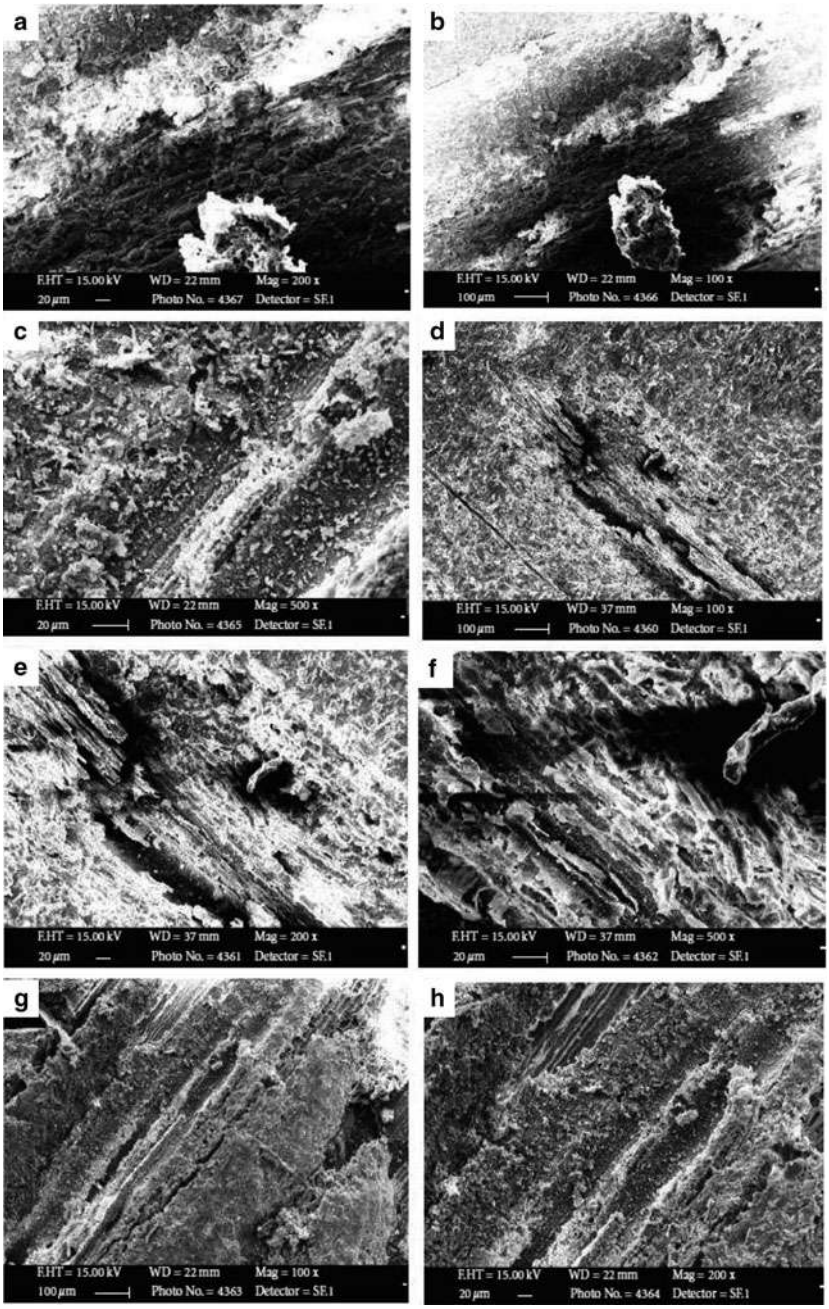

Fig. 7 SEM observations of eroded samples with the impingement angle (**a**–**b**) 30°, (**c**–**d**) 45°, (**e**–**f**) 60°, and (**g**–**h**) 90°. (Reprinted with permission from Gupta et al. 2011)

Furthermore, Biswas and Satapathy (2010) performed comparative wear analysis of red mud filled bamboo fiber reinforced epoxy composite and bamboo fiber epoxy composite. They concluded from SEM micrograph that the wear phenomenon is mixed, that is, it is neither ductile nor brittle, and that at lower velocity, the erosion of surface is due to braking of hard brittle debris of epoxy. However, as velocity increases, the fiber separation and braking starts. The micro-cracking, micro-cutting, and pulverization of matrix and fibers are the primary geographies in the micrograph.

Latha et al. (2016) investigated the erosion wear mechanism of near bamboo fiber and bamboo/glass fiber hybrid composite. It was clearly identified that the bamboo fibers are easily debonded due to the weak interfacial adhesion.

Raghavendra et al. (2014) performed morphology analysis of glass fiber composite and jute fiber composites. Figure 8a shows morphology analysis of glass fiber epoxy composite. In Fig. 8a, the formation of large voids due to erosion of material can easily be seen. From SEM of jute fiber epoxy composite, as shown in Fig. 8b, it is found that there are no cracks, and also good mechanical bonding with the epoxy was observed. In Fig. 8c, it can be noticed that fly ash filler erosion is less.

Dry Sliding Wear Analysis

This type of wear is generally referred to as adhesion wear, and the failure is due to adhesion of parts. However, in case of natural fiber composites its failure mechanism depends on fiber orientation unlike metals. The analysis of wear mechanisms for natural fiber polymer composites is an area of intense research (Menezes et al. 2012) due to the wide variety of applications of natural fiber composite. Fiber orientation is a critical phenomenon that needs to be understood to recognize the failure mechanism of natural fiber polymer composite. There are mainly three types fiber orientations relative to the sliding counterpart: parallel, anti-parallel, and normal (Stachowiak and Batchelor 2013).

The wear phenomenon of various mechanisms can be understood from Fig. 9. For normal orientation of fibers relative to sliding counterpart fibers, fibers are subjected to continuous bending which leads to debonding of fibers from the matrix. For parallel orientation of fiber the failure may be due fiber breaking and debonding of fiber. Of all the orientation the parallel orientation is preferred followed by the anti-parallel types. With normal orientation, there is a risk of sudden seizure owing to gouging of fiber into the counter face (Stachowiak and Batchelor 2013).

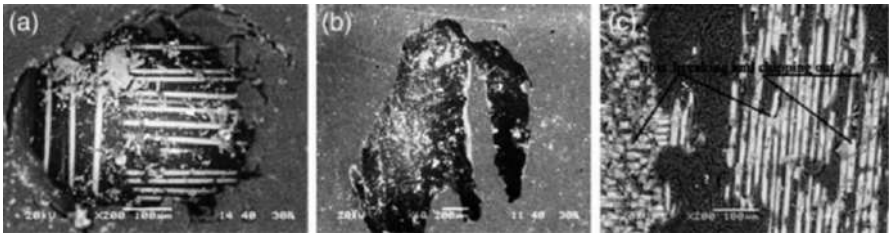

Fig. 8 Eroded surface of (**a**) glass fiber-composites, (**b**) jute fiber composites, and (**c**) Glass-fly ash and epoxy. (Reprinted with permission from Raghavendra et al. 2014)

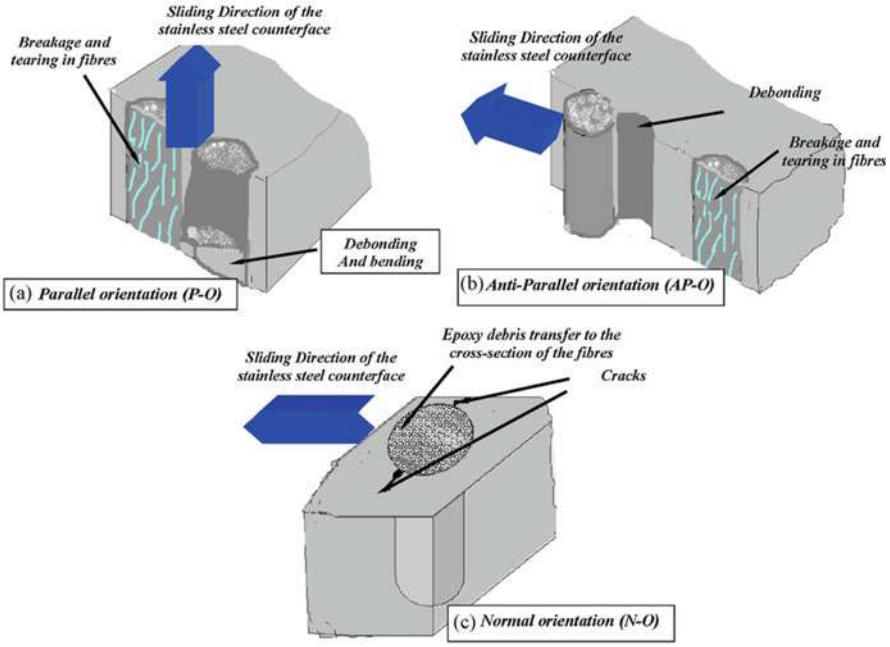

Fig. 9 Different orientations of fiber and their wear mechanism: (**a**) parallel orientation (P-O); (**b**) anti-parallel orientation (AP-O); and (**c**) normal orientation (N-O). (Adapted from Chin et al. reprinted with permission from Chin and Yousif 2009)

Kumar et al. (2020) used SEM for examination of dry sliding wear mechanism of Himalayan bast fibers (Nettle fiber (NF)/*Bauhinia vahlii* fiber (BF) and their hybrid composite. It was revealed in surface morphology of worn-out surface that with addition of fiber content the fiber breakage decreases, for 6 wt.% fiber loading the fiber breakage was virtually zero. From the SEM images of the worn surface, it was inferred that fatigue abrasion might be the dominant wear mechanism for 2 wt.% NFC, BFC, and NBFC; however, it transforms into adhesive abrasion for 6 wt.% fibers loading.

Zaer-Miri and Khosravi (2019) investigated the effects of variable percentages (0.5, 1, 3, and 5 wt.%) of surface-treated nano-TiO_2 on the dry-sliding wear properties of jute fiber/epoxy composite. The worn surfaces of the specimens were examined by SEM. It was concluded through SEM pictograph of the worn surface composites that compared to the neat jute fiber/epoxy composite, 3 wt.% TiO_2-loaded sample showed significantly less worn out. For the worn surface of the 3 wt.% TiO_2-filled sample fiber pulling out and fiber breakage were not visualized and the surface was found to be very smooth, which led to its improved wear properties.

Chin and Yousif (2009) studied the sliding wear properties of kenaf fibers epoxy for bearing applications. The dry sliding wear test was conducted for a range of applied loads, sliding distances, and sliding velocities, and the effect of the fiber orientations with respect to the sliding direction was evaluated. The morphology of

the worn exterior of the composite was examined using SEM as shown in Figs. 10 and 11. It was found through morphology analysis of worn surface, as shown in Fig. 10, that the wear mechanisms of the composite were dominated by microcracks in normal orientation, and while debonding it was dominant in parallel orientation as observed in Fig. 11.

Chaudhary et al. (2018) examined the dry sliding wear behavior mechanism of three natural fiber (jute, hemp, and flax) and their hybrid (jute/hemp/epoxy, hemp/flax/epoxy, and jute/hemp/flax/epoxy) composite. Fiber drawing out and fiber breaking, and microcracking were evident in the SEM micrograph of jute/epoxy composite and hemp/epoxy. For flax/epoxy composite, SEM images displayed very less matrix cracking, debonding, fiber fracture, and pull-out which led to the lowest specific wear rate among all the composites prepared. SEM analysis also revealed that, even at elevated, load fiber detachment and fiber pull-out were barely visualized in flax/epoxy composite. SEM micrograph of jute/hemp/epoxy composite clearly showed fiber pull-out, matrix breakage, and debris formation. These failures were less in jute/hemp/flax/epoxy composite as appreciated from SEM analysis, and moreover, the fibers were still in good condition.

Reddy et al. (2020a) evaluated the dry sliding wear mechanism of natural fibers like *Prosopis juliflora* (PJ), *Abuliton indicum* (AI), and Tapsi (T) fibers in the form of straws. All composite samples contain microcracks and grooves which are due to the

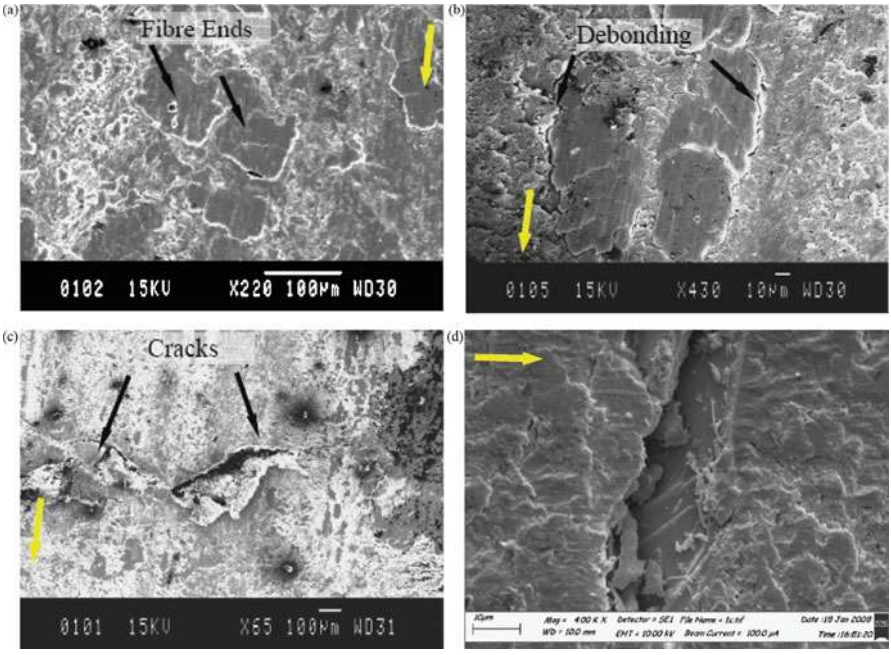

Fig. 10 Worn surface of the KFRE composite tested in N-O. (Reprinted with permission from Chin and Yousif 2009)

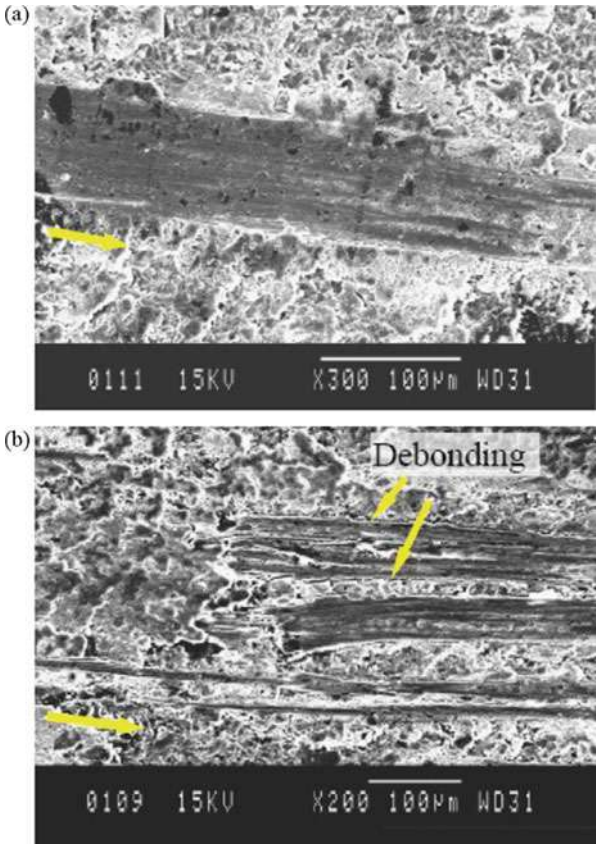

Fig. 11 Worn surface of the KFRE composite tested in P-O. (Reprinted with permission from Chin and Yousif 2009)

abrasive action between the composite samples and the disc. Morphology analysis reveals ploughing action was responsible for the removal of grooves at higher rate, which controls the subtraction of material from composite specimen. From SEM analysis it was clearly understood that load is transmitted to the fibers because of the good linkage between matrix and reinforcement.

Rajeshkumar (2020) performed morphology analysis of the worn-out surface of the dry sliding wear tested specimen of *Phoenix* sp. fiber-reinforced epoxy composites. It was inferred from morphology analysis that the fiber pull-out, debonding, and fiber cracking were major failure mechanisms in fiber-reinforced composites. It is concluded that the failure is due to poor bonding at fiber and matrix interface.

Abrasive Wear Mechanism

Abrasive wear as the name indicates is the removal of material by rubbing action of hard materials against soft materials. The failure mechanism involves removing material through asperity contact. There are plenty of examples where the abrasive wear analysis, plays a significant role in selection of material. The most common

example is the brake pad, where the wear has to minimal with high friction is required. Generally, asbestos material is used in brake pad, brake linings, brake couplings, etc., as reinforcement while the polymeric material is used as a binder along with friction modifiers and fillers (Menezes et al. 2012). However, due to the environmental hazardous nature, asbestos has been banned for use. Several other material like antimony trisulfides, copper, lead, tin, potassium titanate, silicon carbide, etc., which have been widely used in the past, are now being replaced by natural materials due to the environmental concerns. Numerous researches have been performed in recent years to replace man-made fibers with natural fiber composites (Menezes et al. 2012; Kukutschová et al. 2009; Roubicek et al. 2008; Bledzki and Gassan 1999). A few of recent research have been discussed here.

Swain and Biswas (2017) evaluated the abrasive wear behavior of jute fiber/epoxy composites with various weight fractions of fiber loading, and variable chemical treatments (alkaline and benzoyl chloride treatment) have been applied to jute. A scanning electron microscope (SEM) analysis revealed that the failure mechanism involves micro-ploughing, debris removal, microcracking, and debonding. For chemically treated sample, it was inferred from SEM analysis that fiber cracking and ploughing were minimized as compared to the untreated sample. This might be due to the better adhesion between treated fiber and matrix.

Mishra and Acharya (2011) studied the abrasive wear behavior of bagasse fiber/epoxy composite in various orientation, viz. parallel orientation (PO), antiparallel orientation (APO), and normal orientation (NO). It was inferred from worn surfaces analyzed using SEM that, in parallel orientation, micro-ploughing was the dominant wear phenomenon, while in antiparallel and normal orientation it was due to micro-cutting.

X-Ray Diffraction Analysis

Working Principle of X-Ray Diffraction (XRD) Analysis

An X-ray diffraction procedure is extensively used for the study of crystal structure and the structure of a material. XRD is a nondestructive procedure for identifying concentrations of distinct phases present in a given sample. It may be used for the estimation of d spacing for the crystal structure of the material. A clear perception of the composition of the material is obtained by XRD analysis. Bragg's Law is the main principle for XRD analysis. If d is the lattice spacing between two atomic planes of a crystal and x-rays with wavelength λ impinges on the crystal at an angle θ, then according to Bragg's Law the path difference between two beams may be given by Eq. 1 (Vereda 2016).

$$2dsin\theta = n\lambda \tag{1}$$

where n is the integral multiple of wavelength λ. In XRD, the X-ray impinges at a distinct angle θ on the sample and hence the intensities of the reflected light are

recorded, respectively. The diffractogram obtained in XRD gives a peak for constructive interference. The position of peaks represents the constituents present in the material, the distance between peaks identifies the crystal spacing, and the area under peak represents the concentration of the different constituents present. The crystallite size may be computed using the Scherrer equation 2 (Zsigmondy and Scherrer 1912). The degree of crystallinity or percentage crystallinity may be calculated using Eq. 3.

$$d = \frac{K\lambda}{\beta Cos\theta} \tag{2}$$

$$\%\text{Crystallinity} = \frac{\text{Area of crystalline peaks}}{\text{Total area of all the peaks}} \tag{3}$$

X-Ray Diffraction Analysis of Natural Fiber/Epoxy Composites

XRD analysis was mainly performed for hybrid composite to see the phase change due to filler composite. XRD analysis of a few natural fiber epoxy composite is discussed below.

Arun Prakash and Viswanthan (2019) studied the XRD schemes before and after calcinated sea urchin specimens. An intense peak was observed at $2\theta = 29°$ which approves the presence of $CaCO_3$ phase state untreated sea urchin particles. Other small peaks were recognized at $2\theta = 36°$,40°, 44°, 48°, 58°, and 61°. Peak at $2\theta = 31°$ designates the occurrence of $MgCO_3$ in untreated sea urchin specimen. The calcinated particles display $Ca(OH)_2$, $Mg(OH)_2$, CaO, and MgO phases. The appearance of hydroxide is owed to an uncertain phase of CaO and MgO in the environment, which then react with moisture and formulate $Ca(OH)_2$ and $Mg(OH)_2$ instantly.

Vivek and Kanthavel (2019) investigated Bagasse ash (BGA) filled biocomposite reinforced with sisal, flax, banana, and kenaf fiber. Phases present in BGA samples were identified using X-ray diffraction. The XRD examination of BGA specimens showed the existence of silica as the main component. The associated high peaks of silica in the bagasse ash occur due to the collapse of sugarcane from the soil during accumulation. The concerned BGA has large strength metal oxide which controls novel characteristics, viz. high thermal stability, solid lubricants, and chemical inertness. Hence recognition of BGA as filler material will develop the mechanical and thermal characteristics of epoxy.

Jain and Gupta (2018) studied the influence of sal woodland flour hybridization on the mechanical, thermal, and water penetration characteristics of teak woodland composite. This experiment was to determine the crystallinity of woodland composites of XRD models of the hybrid woodland composites, viz. T0S100, T25S75, T50S50, T75S25, and T100S0. It was be recognized from the diffractograms that the crystalline peaks of different samples have different crystallinity. The highest peak was produced by hybrid woodland composite T50S50.

Kumar et al. (2019) have characterized the bamboo epoxy composite. Crystallinity evaluation of alkali-treated and raw bamboo filler was accomplished through

the XRD investigation. The diffractogram of primary and alkali-treated bamboo filler uncovers that NaOH treatment resulted in a significant increment in crystallinity of treated filler comparative with the raw bamboo. The crystallinity index of treated and raw filler is discovered to be 0.83 and 0.46. It was elucidated that as a result of alkali treatment the crystallinity was enhanced.

Movva and Kommineni (2019) focused on the development of gram husk cellulose-based hybrid nanocomposites. The crystallinity contents of nanocellulose were determined by using the XRD procedure. XRD patterns at distinct planes of chemical treatment represent the main peak at $2\theta = 22^\circ$ and a peak in section 14–17° designate the appearance of cellulose I. When compared to alkali-treated and bleached samples, the acid hydrolyzed samples exhibited an enlarged crystallinity index. It was postulated that the rise in crystallinity index owed to the removal of non-cellulosic ingredients and amorphous sections of cellulose. The crystallinity index of untreated, alkali-treated, bleached, and acid hydrolyzed cellulose was found to be 59, 64, 67, and 73%, respectively.

Infrared Spectroscopy

Working Principle of FTIR Spectroscopy

Fourier-Transform Infrared Spectroscopy, abbreviated as FTIR, is an optical spectroscopic technique that uses infrared transmission to probe the working group present in any chemical compound. Infrared spectroscopy is one of the most frequently used spectroscopic methods in the characterization of materials. Ease of handling and easy sample preparation along with rapid results and sensitiveness to the different chemical compounds can be attributed to its great success and widespread use. Moreover, FTIR presents an easy way for the evaluation of qualitative and quantitative results. It works on the principle that different functional groups have different molecular "fingerprints" and based on transmitted spectra the functional group can be identified. On the frequency of infrared radiation, the particles absorb certain emissions and transmit others. The characterization of the sample functional group is based on the principle that a wavelength of absorption bands, the intensity of absorbed spectra, and the shape of spectra have a direct relation with the molecular structure of a compound. Different particles have several significant vibrations of an atom it is bound to. The incidence of IR radiation causes fundamental vibrations of bound atoms. Absorption of infrared strength results in vibration of these atom results, that is, they exhibit IR absorption bands. For data analysis, a curve is plotted between transmittance [%T] versus wavenumber [cm^{-1}], As per IUPAC recommendation the wavenumber reduction is plotted along the positive X-axis and the transmittance along the Y-axis (Gauglitz and Vo-Dinh 2003). FTIR analysis is very much used for the characterization of natural fiber/epoxy composites, as the natural fibers are made up of complex carbohydrates. Analysis of bonding among the different functional groups is important as FTIR analysis represents a big role.

FTIR of Natural Fiber/Epoxy Composites

As explained above FTIR analysis does the identification of functional. For natural fiber composite it is usually used as a tool to identify the functional group in natural fiber before and after the surface treatment. Generally, an FTIR is used along with SEM to verify the bonding phenomenon between fiber and resin. In this direction, some of the work can be found below.

Reddy et al. (2020b) investigated the effect of alkali treatment on the performance of *Setaria italic* fiber using FTIR. The results of FTIR findings are given in Table 2. It was found that the alkali treatment reduces the lignin and hemicellulose content, thereby enhancing the adhesion with resin.

Similar research was performed by Sumesh and Kanthavel (2020) who utilized the Fourier transform infrared (FTIR) spectroscopy to observe to change in functional group of treated and untreated coir and banana fibers. The cellulose content in banana and coir fiber was significantly improved by alkali treatment of fiber. Different peaks in FTIR spectra showed improvement in cellulose content in treated fibers based on the CH_2 symmetric bending and C-H symmetric deformation. Ionization of the –OH groups was observed in 5% NaOH treated fiber due to removal of –OH group. The design for the peak at a particular wavelength represents the presence of the hemicellulose. The NaOH treatment diminishes the hemicellulose and lignin content in the natural fibers. The peaks at distinct wavelengths with NaOH (5%) in coir fibers are expected to show the same effect in the case of working groups as banana fiber due to alkali treatment. The high appearance of cellulose also shows an effect on the crystalline properties of natural fibers.

Sumesh et al. (2020) analyzed the effect of cellulose micro filler (CMF) incorporation, which was extracted from peanut oil cake fiber (POCF) on mechanical and thermal properties of pineapple/flex hybrid composite. They performed FTIR analysis to show how the conversion of POCF to CMF leads to a reduction in lignin and hemicellulose. In their findings of FTIR analysis of NaOH treated POCF and untreated it was found that the existence of groups with acetyl and uronic ester have the presence of lignin and hemicellulose. While in FTIR analysis of CMF the lignin and hemicellulose content was found to be very less (Table 3).

It was observed through literature findings that FTIR spectroscopy was used along with another spectroscopy technique such as XRD and SEM. The FTIR

Table 2 FTIR findings of *Setaria italic* fiber (Foxtail millet)

Wavelength (cm^{-1})	Untreated *Setaria italic* fiber	Treated *Setaria italic* fiber
3200–3500	-OH group	-OH group
2921		-OH group (cellulose presence)
1610	C=O (carboxyl and acetyl for hemicellulose)	
1498	C-H (methyl for lignin)	
558	Si-O	

Table 3 FTIR findings of various natural fiber epoxy composites

Authors	Fiber/Filler	FTIR Findings	References
Movva et al.	Green gram husk cellulose and banana fiber	FTIR findings of raw, alkali treated, bleached and acid hydrolyzed matter. This treatment leads to removal of lignin (disappearance peak at 1179 cm^{-1}) and hemicellulose (disappearance of peak 1768 cm^{-1}).	Movva and Kommineni (2019)
Kumar et al.	Bamboo	Alkali treatment leads to removal of hemicellulose (appearance weaker spectra at peak 2899–2912 cm^{-1}), pectin, and lignin (disappearance of peak at 1721 cm^{-1}).	Kumar et al. (2019)
Suresh Kumar et al.	Coconut sheath fiber	The untreated coconut sheath fiber composite showed intense peak at 1738 cm^{-1} which reveals the presence of C=O stretching owing to the presence of hemicelluloses (Yan et al. 2016). However, alkali treated composite does not show such peaks.	Suresh Kumar et al. (2014)
Sepe et al.	Hemp fiber	Untreated hemp fibers showed cellulose, hemicellulose, and lignin. After alkali treatments a gradual decrease of peak at 1734 cm^{-1} is visualized due to decrease in concentration of hemicellulose.	Sepe et al. (2018)

spectroscopy was mainly used to distinguish chemical modification that happened in fibers after chemical treatment. Most literature reports FTIR analysis of treated and untreated fiber, and the main finding in all of the research is that the chemical treatment leads to a decrease in concentration of hemicellulose, lignin, and pectin content.

Raman Spectroscopy

Raman spectroscopy uses a monochromatic laser beam, and the incident of light causes a scattering effect. The incident of photons transfers energy to the sample, and the scattered light has positive or negative energy than the incident beams. The Raman spectra show a variation of intensity of scattered light with frequency. Raman and FTIR spectroscopy differ in some key fundamental ways. In Raman spectroscopy relative frequencies of scattering are measured while FTIR calculates the absolute frequencies as the sample absorbs the incident radiation (Gauglitz and Vo-Dinh 2003). One another major distinction between Raman and FTIR is that FTIR is OH group sensitive, while Raman is not, and therefore Raman can be used for an aqueous solution. The Raman spectroscopy also can distinguish between C-C, C=C, and C≡C bonds. In FTIR the dipole moment is changed upon the incident of IR radiation, while in Raman spectroscopy polarizability of a molecule is changed.

Raman Spectroscopy of Natural Fiber/Epoxy Composites

Raman spectroscopy was used to detect the change in the chemistry of fiber upon chemical treatment, and also there have been examples where the shift in Raman spectra was used to map the micromechanical deformation in natural fiber composites. Some of the examples are provided below.

Qin et al. (2008) examined the Raman spectra of ramie fiber and unmercerized and mercerized composites. It was observed in Raman spectra that there is a difference in intensity of unmercerized and mercerized composites. The difference was attributed to mercerization of ramie which causes the transformation of cellulose I into cellulose II.

Eichhorn and Young (2004) analyzed the micro deformation of hemp fiber and epoxy resin droplet. It was observed that a peak at 1095 cm^{-1} l shifts linearly with stress and strain. This peak corresponds to the stretching of cellulose to a lower wavenumber which is due to molecular deformation. It was concluded that this peak shift could be a gauge to measure the strength of the composite.

Mottershead and Eichhorn (2007) studied the deformation phenomenon involved in cellulose fiber epoxy composite with aid of Raman spectroscopy. Initially, the single fiber was deformed and Raman spectra was recorded at specific strain increment. Furthermore, the composite samples with resin droplets were examined throughout their length. The peak shift at a frequency of 1095 cm^{-1} was observed for a single fiber. The Raman shift data obtained for single fiber deformation were calibrated to obtain the deformation of composites. It was observed that there was a sudden drop of stress at the edges of droplets and symmetrically increased and decreased through the center.

Bulota et al. (2021) investigated the deformation characteristics at the fiber-matrix interface of Ion cell cellulose fiber epoxy composite with help of Raman spectroscopy. As it was already discussed the peak at 1095 cm^{-1} shifts with a strain rate of single fiber under tensile loading. It was confirmed that the Raman spectra provide the direct measurement of deformation at the matrix fiber interface. It was observed through Raman spectra analysis that shift rate of 1095 cm^{-1} with strain and stress was decreased by around 40% as compared to the neat fiber which corresponds to theoretical Young's modulus values.

UV-Vis Spectroscopy

UV-visible spectroscopy measures concentration based on the absorbance of ultraviolet or visible light by a sample. UV-visible spectroscopy covers a spectral range from 200 to 800 nm. UV-visible spectroscopy was used for both qualitative and quantitative evaluations of samples. The absorption of the visible spectrum of light results in a change of colour of certain chemicals, which then help in the identification of the chemical compound. The absorbance of visible or ultraviolet light is based on Beer Lambert law which provides details of the concentration of a particular chemical compound (Gauglitz and Vo-Dinh 2003; Förster 2004).

UV-Vis Spectroscopy of Natural Fiber Epoxy Composite

Peng et al.(2018) investigated the adsorption capacity of graphene oxide-cotton fiber epoxy composite for purification of polyphenols. The adsorption capacity was found to be 51 mg/g and polyphenol recovery was estimated to be 73%.

NMR Spectroscopy

Nuclear magnetic resonance spectroscopy, most commonly known as NMR spectroscopy, is a spectroscopic technique to identify organic compounds, proteins, and other complex molecules. There are two most common kinds of NMR: H-NMR (proton-NMR) and C-NMR (carbon-13 NMR) spectroscopy. The sample to be tested is placed in a constant magnetic field and nuclei are excited by radio waves, which results in magnetic resonance of nuclei. Magnetic resonance signals are detected with radio receivers, which provides details about the electronic structure of the molecule and its functional group (Gauglitz and Vo-Dinh 2003).

NMR Spectroscopy of Natural Fiber/Epoxy Composite

In an investigation the effect of silane-treated sea-urchin spike filler and kenaf fibre mat-reinforced neem oil blended epoxy resin composite has been studied. In this study, an epoxy-neem matrix was produced. The epoxy was mixed with neem oil and heated at 80 °C and cooled down. The chemical composition of the epoxy neem matrix was analyzed through nuclear magnetic resonance (NMR) spectroscopy. The NMR shows the presence of acetic acid in the epoxy neem matrix. The blend was further heated to 120 °C to eliminate the acetic acid from the epoxy-neem matrix. 1H and 13C NMR spectroscopy was conducted before and after heating the blend at 120 °C. The peak between 2.1 and 2.4 ppm was observed in the matrix, which confirms the presence CH_3CO from acetic acid. The presence of the ketone group, which confirms the bonding of neem and epoxy, was confirmed through 13C NMR spectroscopy. The NMR spectra of the blend after heating at 120 °C does not show any peak between 2.0 and 2.7 ppm, which indicates the elimination of acetic acid; however, it does show the ketone group at 192 ppm (Arun Prakash and Viswanthan 2019).

Branda et al. (2016) investigated the effect of silica coating on fire-retardant properties of hemp fiber/epoxy composites. The hemp fibres were coated with silica through waterglass treatment of hemp fibers. The bonding of silica and hemp fiber was investigated through 13C NMR spectroscopy. The 29Si spectra of both the sample waterglass and untreated samples were superimposed to the change in intensity of spectra. It was confirmed through 13C NMR solid-state analysis that there was a presence of strong –C–O–Si– bond between the coated hemp fiber and untreated hemp fiber. It was concluded that the coating was significantly effective for fire resistance.

Shih (2007) prepared the bamboo husk fiber/epoxy composites and investigated their mechanical and thermal properties. The bamboo husk was treated with silane coupling agent, and the NMR spectroscopy was used to inspect the change in the chemical structure of bamboo husk fiber before and after the treatment with a silane coupling agent. It was found through 13C NMR spectroscopy that the cellulose fiber in bamboo husk fiber changes from type I cellulose to type II cellulose. Furthermore, the crystallinity of fiber is low.

Paluvai et al. (2017) used unsaturated polyester for toughening of epoxy and investigated its effect of sisal fiber reinforcement on thermal and mechanical properties. The effect of unsaturated polyester toughening was analyzed through 1H-NMR spectroscopy. The presence various functional groups in epoxy, unsaturated polyester and epoxy/unsaturated polyester were analyzed and compared. It was concluded through the analysis that the reaction between epoxy and unsaturated polyester was positive, and polyester could be employed for toughening of epoxy.

An investigation was conducted by Newman et al. (2007) on deacetylated phormium tenax leaf fibres/Epoxy composites. The fibres were deacetylated and the degree of deacetylation was determined by NMR spectroscopy. It was observed through NMR spectroscopy that spectra of acetyl group are invisible in NaOH treated fiber, and the xylan and glucose content was also found to decrease.

Dielectric Spectroscopy

Dielectric spectroscopy provides the analytical measure of the dielectric characteristics of the medium with respect to frequency. When the external field is applied the dipole moment of sample changes and the change in dipole moment is presented in terms of permittivity.

Dielectric Spectroscopy of Natural Fiber/Epoxy Composite

Arous et al. (2007) conducted dielectric relaxation spectroscopy of Alfa fiber/epoxy composite to identify the dielectric properties. There were four relaxations processes recognized for composite. They were orientation, polarization, mode relaxation, a process associated with conductivity which results from the diffusion of charge carrier observed at high temperature and low frequency, and Maxwell Wagner-Sillars relaxation associated with charge accumulation at fiber-matrix interface.

Omri et al. (2019) examined the dielectric properties of E-glass fabrics, jute fabrics, and kenaf fabrics epoxy composite by using dielectric relaxation spectroscopy. The bare epoxy showed four relaxation processes, while the glass fiber epoxy composite showed one other relaxation process identified as Maxwell–Wagner–Sillar polarization. The composite with jute and kenaf reinforcement two additional processes were recognized, one attributed to water dipole polarization and the other to the interfacial polarization effect.

X-Ray Photoelectric Spectroscopy

X-ray photoelectric spectroscopy (XPS) is used to detect the elements present on the surface of the material, and it can also identify their chemical state and electronic state unlike the X-ray diffraction technique; XPS is a surface analysis technique (Polini and Yang 2017). It provides the quantitative and qualitative details of surface particles. Its working principle is based on photoelectric effect, and when the sample is irradiated with X-rays, it releases the electrons. Based on the kinetic energy of released electron and the number of electrons escaped from the surface, the surface characteristics of the specimen are quantified (Benelmekki and Erbe 2019).

X-Ray Photoelectron Spectroscopy of Natural Fiber/Epoxy Composite

Le Duigou et al. (2014) prepared flax fiber epoxy composites and studied the surface chemistry at fiber-matrix interface. The XPS analysis was performed to evaluate the surface properties of flax fiber. The C1s peak and O/C ratio was measured. The calcium content is linked with the presence of pectin. The O/C ratio of the lignin and wax value is approximately 0.35, and for the pectin, hemicellulose, and cellulose it is about 0.83 which matches with the existed data in the literature. Therefore, it was concluded that the fiber surface was covered with lignin or wax-like constituents. Due to the presence of the organic binding the O/C ratio of the Electra was higher than Hermes. The C1 peak for both Hermes and Electra is observed to be almost same. The C1s ratios revealed that the C1 carbon type is main constituent of fiber surface while small amount of C2, C3 and C4 also observed. C1 carbon type describes C-C and C-H bonds while C2, C3 and C4 represents the C-O-C, C-OH, C=O, O-C-O and O-C=O respectively. The surface of the Hermes fiber is covered by polysaccharide with C-C bond which is difficult for the primary cell wall. It was observed to be difficult to differentiate between the Hermes and Electra fibres in the analysis of the superficial surface.

Prasad et al. (2021) studied the mechanical properties of TiO_2 nanocoated flax fibres/epoxy composites. The surface chemistry analysis of the raw and TiO_2 nanocoated flax fibers was performed with XPS. The surface analysis was performed by varying the weight percentage of the TiO_2 nanoparticles to the spectrum of the raw and 0.6 wt.% TiO_2 coated fiber surface C1 aliphatic carbon at particular binding energy (eV) which was considered as the main peak as a result of carbon-carbon (C–C) bond observed in the case of cellulose fiber. The C-O-C bonds represented by a particular peak reveal the functional group in the silane coupling agent. The C-OH group of the fiber represented by the peak. The O1 peaks represent the O=O bond. The reduction in the intensity of the OH peak was observed in the case of coated fiber when compared to untreated fiber. An improvement was observed in the case of Si-O-Si bond peaks in TiO_2 coated surface, and this peak corresponds to the formation within the SCA groups during the siloxane formation.

Kılınç et al. (2018) investigated the surface chemistry of cellulose fiber extracted from *Conium maculatum* for potential use in polymer composites. The surface chemistry of the newly extracted unvalued *Conium maculatum* plant fiber was analyzed by XPS. The fiber surface is observed to be hydrophobic in nature which is indicated by of O/C ratio of the *Conium* fiber, which is lower than hemp, henequen, kenaf, and jute. As the O/C content decreases the fiber becomes more hydrophobic in nature. The oxygen and carbon content are more compared to silicon, calcium, nitrogen, and chlorine in the case of *Conium maculatum* fibers. The spectrum analysis of the fiber surface reveals the formation of C-C/C-H (highest percentage) groups and O=C groups. The carbonyl group is present in the form of lignin and hemicellulose in the fiber. The hemicellulose content is more due to the high concentration of carbonyl group at the surface of the fiber.

Lu et al. (2008) examined the surface properties of modified micro-fibrillated cellulose for potential use in epoxy composites. An X-ray photoelectron spectroscopy (XPS) spectrum was used to study the surface of treated and untreated micro-fibrillated cellulose (MFC). As the silane is bonded with the MFC the removal of the silane was performed with Soxhlet extracted with acetone. The O/C ratio and atomic concentration of untreated and ASP treated MFC were measured by XPS spectra. Due to the presence of the adventitious carbon on the surface of the MFC the O/C ratio is observed to be slightly changed than the formulated value. Better bonding between silane and MFC was observed after treating the MFC with silane due to the presence of nitrogen and silicon. Various types of carbon bonding like C-C(C1), C-O (C2), and O-C-O(C3) were observed. APS treatment leads to drastic decrease of C1 peak in addition to the decrease in C2 and C3 peaks. The slight increase and slight decrease of C1, C2, and C3 was observed in case of GPS treatment. When compared to GPS the APS treatment shows good adsorption behavior with respect to MFC substrate due to the presence of NH_2 group in APS (Safi et al. 2016).

Reale Batista and Drzal (2018) studied the surface chemistry of carbon fiber/epoxy matrix composite modified with cellulose nanocrystals. The surface modifications of the carbon fiber epoxy composites filled with cellulose nanocrystals (CNCs) were analyzed by XPS. The CNC composite was functionalized with 3 aminopropyltriethoxysilane (APTES-CNC). The treated CNC spectrum reveals the peak of silicon and nitrogen which are the characteristics of APTES. After treatment the silicon and nitrogen content on the surface of the cellulose increases even after extraction process was completed, which may be due to the reaction of APTES and CNCs. The C1, C2, and C3 peaks represent the C-C, C-O, and O-C-O bonds, respectively. Intense C1 peak was observed after treatment which represents the propyl groups on APTES. The intensity of C2 peak decreased and C3 slightly increased (Jefferson et al. 2019).

Shen et al. (2014) studied the effect of carbon nanotube addition on mechanical properties of natural fiber composites. The surface of the ramie fiber epoxy composite incorporated with carbon nanotubes (CNT) was analyzed by using an X-ray photoelectron spectroscopy. The spectra of the surface obtained before and after adding of CNT in epoxy was observed. Different peaks represent the functional groups like C–C, –C–OH, –C=O, and –COO in the spectra. The functional groups

with oxygen content were much influenced by the addition of CNT. The increased C/O ratio was found in case of CNT filled composite while oxygenated group was found in the absence of CNT. The C-C bond also increased due to the incorporation of CNT with accompanying decrease in C–O and C=O/epoxide functional groups.

Wang et al. (2020) evaluated the bending properties of sandwich structures with wood facing and jute fabrics/epoxy composites cores. The changes of surface chemistry of treated and untreated jute fiber reinforced epoxy laminated composite were examined. In case of untreated jute fiber composite O1 and C1 are the main constituents and rest are nitrogen and sodium at a particular binding energy. The KH-560 modified fiber composite revealed that the peak of Si2p and Si2s is higher than untreated, and moreover the Si-O-Si content increases, which may be due to the reaction between silanol group of the fiber and the Si-OH of KH-560. It was observed that the treatment showed slight increase in O/C ratio. The total carbon content and C-C and O-C-O carbon decreased but the C-O carbon content increased, which is due to reaction of KH-560 with the hydroxyl groups of jute fiber, and forms the C-O-Si bands. The treatment influences the compatibility between fiber and matrix which leads to increase in mechanical properties.

Shih (2007) evaluated the effect of bamboo husk fiber reinforcement on mechanical and thermal properties of epoxy composite. The waste water bamboo husk fibers were treated with silane before fabrication of composite and the effect of silane treatment was examined by XPS. It was found in XPS analysis that dominant peaks are C1 and O1. In addition to these peaks two silicon peaks were found in silane treated sample, viz. the Si2s and Si2p. It was concluded that the there was a sol–gel reaction between the coupling agents and the fibers.

Conclusion

We have seen that there is a huge application of spectroscopy technique for characterization of natural fiber composites. We have seen the application of spectroscopy for fractography analysis, wear mechanism analysis, functional group analysis, and phase identification.

From the present study the following conclusion can be drawn:

- It was observed from fractography analysis using scanning electron microscopy that natural fibers do not provide the best adhesion with epoxy.
- The fractography analysis of different fibers reveals that major phenomena involved in fracture are fiber breaking, pull-out, and matrix cracking. It was also observed that whenever there is good bonding fiber and matrix fiber, breaking is the dominant fracture phenomenon, while for poor fiber, pull-out is the dominant phenomenon.
- The wear mechanism analysis through SEM suggests that for erosion wear after initial removal of material, the fiber breaking is the dominant phenomenon, and abrasion and adhesion wear also follow the similar trend.

- The FTIR spectroscopy was majorly performed whenever there was a treatment of fiber in the composite. It was observed in FTIR analysis that the fiber treatment results in the removal of the hemicellulose and lignin.
- XRD analysis was performed to see phases present in the filler used in natural fiber reinforced epoxy hybrid composite.
- The XRD and FTIR were used in conjunction with SEM analysis for overall characterization of composite, and FTIR and XRD alone do not provide the sufficient information; however, scanning electron microscopy can be used for various analyses.
- The Raman spectroscopy was used for the micromechanical analysis of natural fiber composites.
- The NMR spectroscopy and XPS were used to analyze the change in the surface chemistry due to fiber or matrix modification.
- Dielectric spectroscopy was usually used to examine the dielectric properties of composites.

References

H. Abdellaoui, M. Raji, R. Bouhfid, A. el kacem Qaiss, Investigation of the deformation behavior of epoxy-based composite materials, in *Failure Analysis in Biocomposites, Fibre-Reinforced Composites and Hybrid Composites*, (Elsevier, 2019), pp. 29–49

P. Anand, D. Rajesh, M. Senthil Kumar, I. Saran Raj, Investigations on the performances of treated jute/Kenaf hybrid natural fiber reinforced epoxy composite. J. Polym. Res. **25**, 1–9 (2018). https://doi.org/10.1007/s10965-018-1494-6

M. Arous, I. Ben Amor, S. Boufi, A. Kallel, Experimental study on dielectric relaxation in alfa fiber reinforced epoxy composites. J. Appl. Polym. Sci. **106**, 3631–3640 (2007). https://doi.org/10.1002/app.26885

V.R. Arun Prakash, R. Viswanthan, Fabrication and characterization of echinoidea spike particles and kenaf natural fibre-reinforced Azadirachta-Indica blended epoxy multi-hybrid bio composite. Compos. A: Appl. Sci. Manuf. **118**, 317–326 (2019). https://doi.org/10.1016/j.compositesa.2019.01.008

M. Benelmekki, A. Erbe, Nanostructured thin films–background, preparation and relation to the technological revolution of the 21st century, in *Frontiers of Nanoscience*, (Elsevier Ltd, 2019), pp. 1–34

S. Biswas, A. Satapathy, A comparative study on erosion characteristics of red mud filled bamboo–epoxy and glass–epoxy composites. Mater. Des. Reigate **31**, 1752–1767 (2010) Elsevier

S. Biswas, S. Shahinur, M. Hasan, Q. Ahsan, Physical, mechanical and thermal properties of jute and bamboo fiber reinforced unidirectional epoxy composites. Proc. Eng. **105**. Elsevier Ltd, 933–939 (2015)

A.K. Bledzki, J. Gassan, Composites reinforced with cellulose based fibres. Prog. Polym. Sci. (Oxford) **24**, 221–274 (1999)

F. Branda, G. Malucelli, M. Durante, et al., Silica treatments: A fire retardant strategy for hemp fabric/epoxy composites. Polymers **8**, 313 (2016). https://doi.org/10.3390/polym8080313

M. Bulota, S. Sriubaite, A. Michud, et al., The fiber-matrix interface in Ioncell cellulose fiber composites and its implications for the mechanical performance. J. Appl. Polym. Sci. **138**, 50306 (2021). https://doi.org/10.1002/app.50306

V. Chaudhary, P.K. Bajpai, S. Maheshwari, An investigation on wear and dynamic mechanical behavior of jute/hemp/flax reinforced composites and its hybrids for tribological applications. Fibers Polym. **19**, 403–415 (2018). https://doi.org/10.1007/s12221-018-7759-6

H. Chen, H. Chen, Chemical composition and structure of natural lignocellulose, in *Biotechnology of Lignocellulose*, (Springer Netherlands, Dordrecht, 2014), pp. 25–71

C.W. Chin, B.F. Yousif, Potential of kenaf fibres as reinforcement for tribological applications. Wear **267**, 1550–1557 (2009). https://doi.org/10.1016/j.wear.2009.06.002

D.J. Cosgrove, Growth of the plant cell wall. Nat. Rev. Mol. Cell Biol. **6**, 850–861 (2005)

L.F.S. Da, F.J.H.T.V. Ramos, L.F.C. Nascimento, et al., Critical length and interfacial strength of PALF and coir fiber incorporated in epoxy resin matrix. J. Mater. Res. Technol. **7**, 528–534 (2018). https://doi.org/10.1016/j.jmrt.2018.04.025

G. Das, S. Biswas, Effect of fiber parameters on physical, mechanical and water absorption behaviour of coir fiber–epoxy composites. J. Reinf. Plast. Compos. **35**, 644–653 (2016). https://doi.org/10.1177/0731684415626594

S. Dinesh, P. Kumaran, S. Mohanamurugan, et al., Influence of wood dust fillers on the mechanical, thermal, water absorption and biodegradation characteristics of jute fiber epoxy composites. J. Polym. Res. **27**, 1–13 (2020). https://doi.org/10.1007/s10965-019-1975-2

S.J. Eichhorn, R.J. Young, Composite micromechanics of hemp fibres and epoxy resin micro-droplets. Compos. Sci. Technol. **64**, 767–772 (2004). https://doi.org/10.1016/j.compscitech.2003.08.002

R.H. Elleithy, Hierarchical structure and flexure behavior of woven carbon fiber epoxy composite. Polym. Compos. **21**, 716–723 (2000). https://doi.org/10.1002/pc.10225

D. Feldman, Polymer history. Des. Monomers Polym. **11**, 1–15 (2008). https://doi.org/10.1163/156855508X292383

H. Förster, UV/VIS Spectroscopy, in *Molecular Sieves – Science and Technology*, ed. by H. G. W. J. Karge, (Springer, Berlin, Heidelberg, 2004), pp. 337–426

S.Y. Fu, B. Lauke, E. Mäder, et al., Tensile properties of short-glass-fiber- and short-carbon-fiber-reinforced polypropylene composites. Compos. A: Appl. Sci. Manuf. **31**, 1117–1125 (2000). https://doi.org/10.1016/S1359-835X(00)00068-3

G. Gauglitz, T. Vo-Dinh, *Handbook of Spectroscopy* (Wiley, Weinheim, 2003)

M.G. González, J.C. Cabanelas, J. Baselga, Applications of FTIR on epoxy resins–identification, monitoring the curing process, phase separation and water uptake, in *Infrared Spectroscopy-Materials Science, Engineering and Technology*, ed. by T. Theophile, (IntechOpen, Rijeka, 2012), pp. 262–284

A. Gupta, A. Kumar, A. Patnaik, S. Biswas, Effect of different parameters on mechanical and erosion wear behavior of bamboo fiber reinforced epoxy composites. Int. J. Polym. Sci. **2011** (2011). https://doi.org/10.1155/2011/592906

S. Harish, D.P. Michael, A. Bensely, et al., Mechanical property evaluation of natural fiber coir composite. Mater. Charact. **60**, 44–49 (2009). https://doi.org/10.1016/j.matchar.2008.07.001

H. Hellman, *Spectroscopy* (US Atomic Energy Commission, Division of Technical Information, 1968)

H.Y. Hwang, Electromechanical characteristics of unidirectional glass fiber epoxy composites. Polym. Compos. **32**, 558–564 (2011). https://doi.org/10.1002/pc.21076

S. Ismael Abdullah, M. Ansari, Mechanical properties of graphene oxide (GO)/epoxy composites. HBRC J. **11**, 151–156 (2015). https://doi.org/10.1016/j.hbrcj.2014.06.001

A. Jabbar, J. Militký, J. Wiener, et al., Nanocellulose coated woven jute/green epoxy composites: Characterization of mechanical and dynamic mechanical behavior. Compos. Struct. **161**, 340–349 (2017). https://doi.org/10.1016/j.compstruct.2016.11.062

N. Jain, M.K. Gupta, Hybrid teak/sal wood flour reinforced composites: mechanical, thermal and water absorption properties. Mater. Res. Express **5**, 125306 (2018). iopscience.iop.org

A.J. Jefferson, S.M. Srinivasan, A. Arockiarajan, Effect of multiphase fiber system and stacking sequence on low-velocity impact and residual tensile behavior of glass/epoxy composite laminates. Polym. Compos. **40**, 1450–1462 (2019). https://doi.org/10.1002/pc.24884

Z. Khan, B. Yousif, M. Islam, Fracture behaviour of bamboo fiber reinforced epoxy composites. Compos. Part B **116**, 186–199 (2017) Elsevier

A.Ç. Kılınç, S. Köktaş, Y. Seki, et al., Extraction and investigation of lightweight and porous natural fiber from Conium maculatum as a potential reinforcement for composite materials in transportation. Compos. Part B **140**, 1–8 (2018). https://doi.org/10.1016/j.compositesb.2017.11.059

J. Kukutschová, V. Roubíček, K. Malachová, et al., Wear mechanism in automotive brake materials, wear debris and its potential environmental impact. Wear **267**, 807–817 (2009). https://doi.org/10.1016/j.wear.2009.01.034

R. Kumar, K. Kumar, S. Bhowmik, et al., Tailoring the performance of bamboo filler reinforced epoxy composite: insights into fracture properties and fracture mechanism. J. Polym. Res. **26**, 54 (2019) Springer

S. Kumar, K.K.S. Mer, B. Gangil, V.K. Patel, Synergistic effect of hybrid Himalayan Nettle/Bauhinia-vahlii fibers on physico-mechanical and sliding wear properties of epoxy composites. Def. Technol. **16**, 762–776 (2020). https://doi.org/10.1016/j.dt.2019.08.006

P.S. Latha, M.V. Rao, V.K. Kumar, et al., Evaluation of mechanical and tribological properties of bamboo–glass hybrid fiber reinforced polymer composite. J. Ind. Text. **46**, 3–18 (2016). https://doi.org/10.1177/1528083715569376

A. Le Duigou, A. Kervoelen, A. Le Grand, et al., Interfacial properties of flax fibre-epoxy resin systems: Existence of a complex interphase. Compos. Sci. Technol. **100**, 152–157 (2014). https://doi.org/10.1016/j.compscitech.2014.06.009

W. Liu, S. Zhang, B. Li, et al., Improvement in interfacial shear strength and fracture toughness for carbon fiber reinforced epoxy composite by fiber sizing. Polym. Compos. **35**, 482–488 (2014). https://doi.org/10.1002/pc.22685

J. Lu, P. Askeland, L.T. Drzal, Surface modification of microfibrillated cellulose for epoxy composite applications. Polymer **49**, 1285–1296 (2008). https://doi.org/10.1016/j.polymer.2008.01.028

P.L. Menezes, P.K. Rohatgi, M.R. Lovell, Studies on the tribological behavior of natural fiber reinforced polymer composite. Green Energy Technol. **49**, 329–345 (2012)

P. Mishra, S. Acharya, Anisotropy abrasive wear behavior of bagasse fiber reinforced polymer composite. Int. J. Eng. Sci. Technol. **2**, 104–112 (2011). https://doi.org/10.4314/ijest.v2i11.64558

B. Mottershead, S.J. Eichhorn, Deformation micromechanics of model regenerated cellulose fibre-epoxy/polyester composites. Compos. Sci. Technol. **67**, 2150–2159 (2007). https://doi.org/10.1016/j.compscitech.2006.11.003

M. Movva, R. Kommineni, Effect of green gram husk nanocellulose on banana fiber composite. J. Nat. Fibers **16**, 287–299 (2019). https://doi.org/10.1080/15440478.2017.1414658

R.H. Newman, E.C. Clauss, J.E.P. Carpenter, A. Thumm, Epoxy composites reinforced with deacetylated Phormium tenax leaf fibres. Compos. A: Appl. Sci. Manuf. **38**, 2164–2170 (2007). https://doi.org/10.1016/j.compositesa.2007.06.007

M.A. Omri, M.R. Sanjay, A. Triki, et al., Dielectric properties and interfacial adhesion of jute, kenaf and E-glass fabrics reinforcing epoxy composites. Polym. Compos. **40**, 2142–2153 (2019). https://doi.org/10.1002/pc.25001

L. Osorio, E. Trujillo, A.W. Van Vuure, I. Verpoest, Morphological aspects and mechanical properties of single bamboo fibers and flexural characterization of bamboo/epoxy composites. J. Reinf. Plast. Compos.Journal of Reinforced Plastics and Composites **30**, 396–408 (2011). https://doi.org/10.1177/0731684410397683

N.R. Paluvai, S. Mohanty, S.K. Nayak, Unsaturated polyester-toughened epoxy composites: Effect of sisal fiber on thermal and dynamic mechanical properties. J. Vinyl Addit. Technol. **23**, 188–199 (2017). https://doi.org/10.1002/vnl.21491

R. Peng, Q. Wu, J. Chen, et al., Isolation of ellagic acid from pomegranate peel extract by hydrophobic interaction chromatography using graphene oxide grafted cotton fiber adsorbent. J. Sep. Sci. **41**, 747–755 (2018). https://doi.org/10.1002/jssc.201700896

R. Petrucci, C. Santulli, D. Puglia, et al., Mechanical characterisation of hybrid composite laminates based on basalt fibres in combination with flax, hemp and glass fibres manufactured by vacuum infusion. Mater. Des. **49**, 728–735 (2013). https://doi.org/10.1016/j.matdes.2013.02.014

A. Polini, F. Yang, Physicochemical characterization of nanofiber composites, in *Nanofiber Composites for Biomedical Applications*, (Elsevier Inc., Duxford, 2017), pp. 97–115

V. Prasad, K. Sekar, M.A. Joseph, Mechanical and water absorption properties of nano TiO2 coated flax fibre epoxy composites. Constr. Build. Mater. **284**, 122803 (2021). https://doi.org/10.1016/j.conbuildmat.2021.122803

C. Qin, N. Soykeabkaew, N. Xiuyuan, T. Peijs, The effect of fibre volume fraction and mercerization on the properties of all-cellulose composites. Carbohydr. Polym. **71**, 458–467 (2008). https://doi.org/10.1016/j.carbpol.2007.06.019

G. Raghavendra, S. Ojha, S. Acharya, S. Pal, Jute fiber reinforced epoxy composites and comparison with the glass and neat epoxy composites. J. Compos. Mater. **48**, 2537–2547 (2014). https://doi.org/10.1177/0021998313499955

G. Raghavendra, S. Ojha, S.K. Acharya, S.K. Pal, Influence of micro/nanofiller alumina on the mechanical behavior of novel hybrid epoxy nanocomposites. High Perform. Polym. **27**, 342–351 (2015). https://doi.org/10.1177/0954008314550889

M.J. Raghu, G. Goud, Development of *Calotropis procera* -glass fibers reinforced epoxy hybrid composites: dynamic mechanical properties. J. Nat. Fibers, 1–8 (2020). https://doi.org/10.1080/15440478.2020.1745119

G. Rajeshkumar, A new study on tribological performance of *Phoenix Sp*. fiber-reinforced epoxy composites. J. Nat. Fibers, 1–12 (2020). https://doi.org/10.1080/15440478.2020.1724235

M.D. Reale Batista, L.T. Drzal, Carbon fiber/epoxy matrix composite interphases modified with cellulose nanocrystals. Compos. Sci. Technol. **164**, 274–281 (2018). https://doi.org/10.1016/j.compscitech.2018.05.010

P.V. Reddy, R.V.S. Reddy, P. Rajendra Prasad, et al., Evaluation of mechanical and wear performances of natural fiber reinforced epoxy composites. J. Nat. Fibers **1–14** (2020a). https://doi.org/10.1080/15440478.2020.1807441

R.V.S. Reddy, D. Mohana Krishnudu, P. Rajendra Prasad, P.V. Reddy, Alkali treatment influence on characterization of Setaria italic (Foxtail millet) fiber reinforced polymer composites using vacuum bagging. J. Nat. Fibers, 1–13 (2020b). https://doi.org/10.1080/15440478.2020.1788494

V. Roubicek, H. Raclavska, D. Juchelkova, P. Filip, Wear and environmental aspects of composite materials for automotive braking industry. Wear **265**, 167–175 (2008). https://doi.org/10.1016/j.wear.2007.09.006

N. Saba, O.Y. Alothman, Z. Almutairi, M. Jawaid, Magnesium hydroxide reinforced kenaf fibers/epoxy hybrid composites: Mechanical and thermomechanical properties. Constr. Build. Mater. **201**, 138–148 (2019). https://doi.org/10.1016/j.conbuildmat.2018.12.182

S. Safi, A. Zadhoush, M. Masoomi, Effects of chemical surface pretreatment on tensile properties of a single glass fiber and the glass fiber reinforced epoxy composite. Polym. Compos. **37**, 91–100 (2016). https://doi.org/10.1002/pc.23158

R. Sepe, F. Bollino, L. Boccarusso, F. Caputo, Influence of chemical treatments on mechanical properties of hemp fiber reinforced composites. Compos. Part B **133**, 210–217 (2018). https://doi.org/10.1016/j.compositesb.2017.09.030

X. Shen, J. Jia, C. Chen, et al., Enhancement of mechanical properties of natural fiber composites via carbon nanotube addition. J. Mater. Sci. **49**, 3225–3233 (2014). https://doi.org/10.1007/s10853-014-8027-4

Y.F. Shih, Mechanical and thermal properties of waste water bamboo husk fiber reinforced epoxy composites. Mater. Sci. Eng. A **445–446**, 289–295 (2007). https://doi.org/10.1016/j.msea.2006.09.032

Y. Singh, J. Singh, S. Sharma, et al., Fabrication and characterization of coir/carbon-fiber reinforced epoxy based hybrid composite for helmet shells and sports-good applications: influence of fiber surface modifications on the mechanical, thermal and morphological properties. J. Mater. Res. Technol. **9**, 15593–15603 (2020). https://doi.org/10.1016/j.jmrt.2020.11.023

I. Siró, D. Plackett, Microfibrillated cellulose and new nanocomposite materials: A review. Cellulose **17**, 459–494 (2010)

G. Stachowiak, A. Batchelor, *Engineering Tribology* (Elsevier Science B.V, 2013)
K. Sumesh, K. Kanthavel, Optimizing various parameters influencing mechanical properties of banana/coir natural fiber composites using grey relational analysis and artificial neural network models. J. Ind. Text., 152808372093030 (2020). https://doi.org/10.1177/1528083720930304
K.R. Sumesh, K. Kanthavel, V. Kavimani, Peanut oil cake-derived cellulose fiber: Extraction, application of mechanical and thermal properties in pineapple/flax natural fiber composites. Int. J. Biol. Macromol. **150**, 775–785 (2020). https://doi.org/10.1016/j.ijbiomac.2020.02.118
S.M. Suresh Kumar, D. Duraibabu, K. Subramanian, Studies on mechanical, thermal and dynamic mechanical properties of untreated (raw) and treated coconut sheath fiber reinforced epoxy composites. Mater. Des. **59**, 63–69 (2014). https://doi.org/10.1016/j.matdes.2014.02.013
P.T.R. Swain, S. Biswas, Abrasive wear behaviour of surface modified jute fiber reinforced epoxy composites. Mater. Res. **20**, 661–671 (2017). https://doi.org/10.1590/1980-5373-MR-2016-0541
F. Vereda, Introduction to standard spectroscopic methods: XRD, IR/Raman, and Mössbauer, in *Iron Oxides*, ed. by D. Faivre, (Wiley, 2016), pp. 293–324
R. Vijay, A. Vinod, R. Kathiravan, et al., Evaluation of *Azadirachta indica* seed/spent *Camellia sinensis* bio-filler based jute fabrics–epoxy composites: Experimental and numerical studies. J. Ind. Text. **49**, 1252–1277 (2020). https://doi.org/10.1177/1528083718811086
S. Vivek, K. Kanthavel, Effect of bagasse ash filled epoxy composites reinforced with hybrid plant fibres for mechanical and thermal properties. Compos. Part B **160**, 170–176 (2019). https://doi.org/10.1016/j.compositesb.2018.10.038
X. Wang, X.-l. Shi, Q.-k. Meng, et al., Bending behaviors of three grid sandwich structures with wood facing and jute fabrics/epoxy composites cores. Compos. Struct. **252**, 112666 (2020). https://doi.org/10.1016/j.compstruct.2020.112666
A. Yadav, M.K. Gupta, Development and characterization of jute composites for sustainable product: Effect of chemical treatments and polymer coating. Mater. Res. Express **7**, 15306 (2019). https://doi.org/10.1088/2053-1591/ab5bd9
L. Yan, N. Chouw, L. Huang, B. Kasal, Effect of alkali treatment on microstructure and mechanical properties of coir fibres, coir fibre reinforced-polymer composites and reinforced-cementitious composites. Constr. Build. Mater. **112**, 168–182 (2016). https://doi.org/10.1016/j.conbuildmat.2016.02.182
S. Zaer-Miri, H. Khosravi, Assessment of the wear behavior and interlaminar shear properties of modified nano-TiO_2/jute fiber/epoxy multiscale composites. J. Ind. Text., 152808371989371 (2019). https://doi.org/10.1177/1528083719893718
K. Zhang, F. Wang, W. Liang, et al., Thermal and mechanical properties of bamboo fiber reinforced epoxy composites. Polymers **10**, 608 (2018). https://doi.org/10.3390/polym10060608
R. Zsigmondy, P. Scherrer, Bestimmung der inneren Struktur und der Größe von Kolloidteilchen mittels Röntgenstrahlen, in *Kolloidchemie Ein Lehrbuch*, (Springer, Berlin/Heidelberg, 1912), pp. 387–409

Dielectric Properties of Epoxy/Natural Fiber Composites

21

P. Lokanatha Reddy, Kalim Deshmukh, and S. K. Khadheer Pasha

Contents

Abstract

Natural fiber-based polymer composites have been widely explored as a promising substitute for conventional synthetic composites owing to their ease of preparation, non-toxicity, desirable mechanical properties, biodegradability, and eco-friendliness. Epoxy resins have been widely used for several industrial applications such as adhesives, coatings, microelectronic components, laminated circuit boards and fiber-reinforced composites owing to their high tensile strength and stiffness and favorable electrical, thermal, and chemical properties. However, epoxy resin exhibits a few limitations which restrict their state-of-the-art applications. Therefore, epoxy resins have been often reinforced with natural and synthetic fibers or blending of both to achieve desired properties and to widen their applications in aerospace, automobile, electrical, and electronic industries.

P. L. Reddy
Department of Physics, School of Advanced Sciences, VIT University, Vellore, Tamil Nadu, India

K. Deshmukh (✉)
New Technologies – Research Center, University of West Bohemia, Plzeň, Czech Republic

S. K. K. Pasha
Department of Physics, VIT-AP University, Guntur, Andhra Pradesh, India

S. Mavinkere Rangappa et al. (eds.), *Handbook of Epoxy/Fiber Composites*,
https://doi.org/10.1007/978-981-19-3603-6_23

Over conventional composite materials, the epoxy/fiber composites possess several advantages such as high mechanical strength, good thermal stability, higher specific strength, recyclability, easily availability, and environmentally friendliness. This chapter reviews the new developments in the dielectric properties of natural fiber-reinforced epoxy composites. Several examples of epoxy/natural fiber composites are shown regarding their possible use as a dielectric material, and the related mechanisms have been discussed.

Keywords

Natural fibers · Epoxy · Epoxy/fiber composites · Dielectric properties

Introduction

Recently, a lot of attention has been paid to natural fibers as they exhibit extraordinary properties as compared with synthetic materials (Faruk et al. 2012; Kumar and Hiremath 2020). Natural fibers are generally cheaper, renewable, sustainable, lightweight, biodegradable, nonabrasive and possess low density, flexibility, compatibility, stiffness, impact resistance, and high specific properties (Reddy et al. 2019a). Natural fiber mainly depends on the nature of the plant, locality, age, procedure of extraction, and processing techniques. Most of the natural fibers are obtained from animal, mineral, and plant fibers. The animal fibers comprise proteins (e.g., feather, human hair, silk, wool etc.). Examples of mineral fibers are asbestos which are classified as chrysotile asbestos, anthophyllite asbestos, actinolite asbestos, tremolite asbestos, crocidolite asbestos, and amosite asbestos. Besides, there are different kinds of plant extracted natural fibers available which are classified as reed fibers (rice, corn, and wheat), core fibers (jute, hemp, and kenaf), seed fibers (kapok, cotton, and coir), leaf fibers (pineapple, sisal, and abaca), bast fibers (kenaf, ramie, hemp, flax, and jute), and other types of fibers (roots and wood) (Nassar et al. 2017). The natural fibers have potential applications in several fields such as automotive, aerospace, electronics, and marine industry. However, natural fibers have possessed some drawbacks such as low -dimensional stability and high biodegradability when exposed to the environment, low thermal stability, low processing temperature, limited compatibility with several thermoplastic matrices, swelling, and high moisture absorption (Pujari et al. 2017).

In recent decades, polymers are considered the most interesting materials because they can be used as substitute for other materials such as ceramics, wood, and metals. The polymers are generally reinforced with several fillers or blended with other polymers in order to enhance or modify their properties (Deshmukh and Pasha 2020). Today polymer composites have become one of the major aspects in the field of science and technology due to the combination of intrinsic properties of constituents involved and also due to their potential applications in various fields (Rackesh et al. 2018; Pickering et al. 2016; Deshmukh et al. 2019; Sankaran et al. 2019). Natural fiber-reinforced composites have emerged as the most promising

materials because of their outstanding structural, optical, mechanical, thermal, and electrical properties. Also, there is an increased necessity of natural fiber-based composites in the social, economic, and ecological awareness, sustainability concepts, and environmental regulation aspects due to their several advantages (Pujari et al. 2017). These composite materials mainly depend on porosity, composite manufacturing process, fiber orientation, fiber dispersion, interfacial strength, and selection of the matrix (Pickering et al. 2016; Deshmukh et al. 2019; Sankaran et al. 2019; Deshmukh et al. 2018). The polymer composites reinforced with natural fibers exhibit enhanced mechanical, electrical, and thermal properties. Also, these composite materials are used as printed circuit boards, switches, industrial and household plugs, terminals, and connectors in the electrical and electronic industry (Pathania and Singh 2009). Moreover, the natural fiber-reinforced composites have several applications in various fields such as in packaging, decoration, construction, disposable accessories, and the automotive industry (Reddy et al. 2019a). Thus, natural fiber-reinforced composites are becoming very popular in the field of polymer science and technology especially in the category of sustainable and renewable materials (Väisänen et al. 2017).

Epoxy resin has been considered as one of the most promising thermosetting polymer materials because of its versatile characteristic and diversity than other synthetic polymers. Epoxy resin exhibits several intriguing properties, namely, high electrical resistance, good heat resistance, high adhesion strength, and high thermal stability (He et al. 2001a). Moreover, epoxy resins also possess excellent corrosion resistance, impact resistance, perfect damage tolerances, long shelf life, nonmagnetic properties, outstanding chemical and moisture resistance, good mechanical and fatigue strength, and minimum shrinkage during curing (Saba et al. 2016). Due to their intriguing properties, the epoxy resins are used for various applications such as fiber reinforcement materials, adhesives, potting, surface coatings, castings, electronic component encapsulations, and laminated circuit boards (Jin et al. 2015). However, there are certain limitations in the applications of epoxy resins in the high-performance fields due to their poor fracture toughness, inherent brittleness, low impact resistance, etc. (Unnikrishnan and Thachil 2006). This can be surmounted by incorporating the fillers into the epoxy resin matrix thereby improving or modifying their physiochemical properties. For the past few years, epoxy resins have been reinforced with natural fibers to prepare epoxy/natural fiber composites for various potential applications (Saba et al. 2016). Several research groups reported the preparation, properties, and various applications of epoxy/natural fiber composites which showed better properties when compared with the synthetic polymer composites (Parbin et al. 2019; Mittal et al. 2016; Sadasivuni et al. 2018; Khadija et al. 2019). Moreover, the epoxy/natural fiber composites can be utilized as dielectric materials in several applications such as circuit boards, switches, connectors, terminals, parts of transformers, and microchips (Jayamani et al. 2014). Hence, there is a need to evaluate the effect of natural fibers on the dielectric behavior of the epoxy resins to fulfill the requirements of scientific and technological applications. Therefore, in this chapter, a detailed review of the dielectric properties of various natural fiber-reinforced epoxy composites is presented, and the related mechanisms are discussed.

Dielectric Mechanisms

Dielectric spectroscopy is one of the famous techniques which give information about the interaction between the constituent materials over other analytical techniques (Pandey et al. 2014; Reddy et al. 2019b). This technique can be employed to investigate the sample response subject to the external electric field as a function of fixed or variable frequency (Reddy et al. 2019b; Muzaffar et al. 2020). The dielectric spectroscopy also deals with the dipoles having reorientation mobility in materials with applied alternating electric fields (Kumar et al. 2021). Some important material properties such as energy density (U), breakdown strength (E_{BD}), dielectric constant (ε) and dielectric loss (tan δ), DC electrical conductivity (σ), and molecular dynamics can be evaluated using the dielectric spectroscopy (Reddy et al. 2020; Bouaamlat et al. 2020; Khutia et al. 2015). It also provides information about the current and voltage (AC system with phase and amplitude) parameters of the given sample. Depending upon the requirement, the dielectric spectroscopy can be operated from lower-frequency (μHz) range to higher-frequency range (THz) (Schönhals and Kremer 2003; Charkhesht et al. 2018).

The dielectric constant (ε) in terms of the polarizability of dielectrics can be given as

$$\varepsilon = \varepsilon' - j\varepsilon'' \tag{1}$$

where ε' is the real part or dielectric constant and ε'' is the imaginary part or dielectric loss or loss factor (Psarras 2018). For addressing the substantial independence from the electric field, the relative dielectric constant is given as

$$\varepsilon_r = \frac{\varepsilon}{\varepsilon_0} = \varepsilon_r' - j\varepsilon_r'' \tag{2}$$

Here ε_0 is called the permittivity of free space (8.854×10^{-12} F/m).

Generally, the energy stored in the material is represented with ε_r' which can be represented in terms of dielectric constant (Yang et al. 2019). In the field of microelectronics, if the relative dielectric constant (ε_r) of the dielectric materials is greater than the conventional SiO_2 ($\varepsilon_r = 3.9$), then such materials are called high dielectric constant (*high-k*) materials (Nketia-Yawson and Noh 2018; Dang et al. 2012). If the frequency of the applied electric field and relaxation time are similar, then the dissipation phenomenon will occur in the dielectric material (Li et al. 2018). Generally, the loss tangent can be used to determine the dissipative behavior of the dielectric material (Dang et al. 2012). The expression for the dielectric loss factor is given as

$$\tan\ \delta = \frac{\varepsilon''}{\varepsilon'} \tag{3}$$

From the above expression, it is clear that the dissipation factor or loss factor is the ratio of the dissipation of electrical power of dielectric material to the total power

which circulates in the circuit. It measures the loss of electric energy in the form of heat, which may accelerate deterioration; raising the temperature causes failure in the material (Haseena et al. 2007).

Breakdown strength in the dielectric studies is also considered an important parameter for the dielectrics. Conductive properties may be shown by the dielectric materials if they are kept under the strong applied electric field. In general, without conduction in the dielectric material, the maximum electric field which can be applied is called breakdown strength (E_{BD}). The major causes for the occurrence of the breakdown in the dielectric materials are the heterogeneous distribution of electric field and their electrical contrast (conductivity and dielectric constant) between the matrix and the fillers in the materials and states of the fillers (agglomeration, distribution, shape and size) (Huang et al. 2019). Besides, the breakdown strength is affected by the humidity, temperature, experimental condition, electrode contact and geometry, applied frequency, voltage, and thickness of the sample (Thakur and Gupta 2016).

The energy density (U) is also considered as one of the significant parameters in the dielectrics. The energy density of any dielectric material subject to an electric field (E) is given as

$$U = \int EdD \tag{4}$$

where "D" is electric displacement and it can be represented by the expression

$$D = \varepsilon_0 E + P \tag{5}$$

where P is polarization induced in the material (Psarras 2018). When the electric field is applied, the electric displacement and polarization changes linearly for the material with nonpermanent dipoles as in the case of linear dielectrics (Deshmukh et al. 2017). This phenomenon can be expressed as

$$D = \varepsilon_r \varepsilon_0 E \tag{6}$$

$$U = \frac{1}{2} \varepsilon_r \varepsilon_0 E^2 \tag{7}$$

Dielectric Polarizations

Polarization in the dielectric material is defined as the reorganization of charges in a regular manner in the presence of an external electric field. Normally, polarization occurs via stretching or rotation. In the generation of polarization, various mechanisms are involved, and the majority of the molecules display polarization subject to a strong external electric field. There are four types of polarization mechanisms that occur in the dielectrics which are commonly classified as ionic, orientation, atomic, and electronic polarization (Psarras 2018; Deshmukh et al. 2017).

Ionic Polarization

Ionic polarization which is also termed displacement polarization generally occurs in ionic solids. This polarization may happen due to displacement of anions and cations in the opposite direction which gives net dipole moment subject to an applied external electric field thereby sharing of electrons asymmetrically in different atoms involving molecules of the material. This leads to the shifting of the electron cloud towards the strong-binding atoms exhibiting opposite charge polarity (Deshmukh et al. 2017). The dielectric constant of the material generally enhances due to the shifting of ionic species which takes place due to the application of an electric field (Deshmukh et al. 2017). The ionic polarization is independent of thermal energy, and it is generally observed in ceramics, glasses, and inorganic crystals (Deshmukh et al. 2017).

Orientation or Dipolar Polarization

Dipolar dielectric materials having permanent dipoles generally exhibit orientation polarization (Noguchi et al. 2012). A permanent dipole moment takes place within the material caused by the ionic bonds created due to the transfer of a few valance electrons between two molecules. In the dipolar materials, all the dipoles move casually without any external electric field, and after applying the electric field, they have the tendency to align themselves in the direction of an electric field. Furthermore, the rate of dipolar orientation depends mainly on inter- and intramolecular interactions in the material. Therefore, the orientation of dipoles of the molecules takes place in the various frequency regions, and it depends on how easy the dipoles rotate (Ruan et al. 2002). At higher frequencies (microwave region), with the rapidly changing electric fields, the dipoles orient themselves easily toward the applied electric field resulting in the orientation polarization (Khaled et al. 2016).

Electronic or Atomic Polarization

Electronic polarization generally happens in neutral atoms at higher frequencies in which the movement of electrons takes place corresponding to the nucleus having a positive charge when the electric field is applied. Conversely, the atomic polarization occurs at lower frequencies because of the deformation of alignment of the nuclei of an atom in a molecule (Deshmukh et al. 2017). Normally, in the absence of an electric field, the electrons symmetrically rotate around the nucleus. The asymmetric shape and a temporary dipole moment occur in all the atoms of the material when the dielectric material is located in the external electric field. The atomic polarization is closely related to electronic polarization, and it is also termed vibrational polarization (Psarras 2018; Deshmukh et al. 2017). The atomic polarization generally appears in the infrared region, whereas the electronic polarization appears in the

optical band. Moreover, the electronic polarization primarily occurs in all the dielectric materials, and it is independent of temperature (Deshmukh et al. 2017).

Interfacial or Space-Charge Polarization

The interfacial or space-charge polarization usually occurs in dielectric materials exhibiting charge carriers which are able to migrate to a certain distance through the bulk material and consequently cause a macroscopic field distortion. This migration may occur through hopping, fast ionic conduction, or diffusion process. The distortion in the macroscopic field leads to an increased capacitance value, and it is generally identical to the rise in the dielectric permittivity. The macroscopic charge transfers can be observed in such type of polarization only. Generally, space-charge polarization is categorized into hopping and polarization and interfacial polarization (Jammula et al. 2015). The hopping of the electrons and holes or ions and vacancies (commonly known as localized charges in dielectrics) from one place to another in a dielectric material can cause the hopping polarization. However, the separation of positive and negative mobile charges with the application of an electric field is called as interfacial polarization. This polarization is also called Maxwell–Wagner–Sillars polarization (MWS) polarization (Prodromakis and Papavassiliou 2009).

Dielectric Properties of Epoxy/Natural Fiber Composites

The dielectric composites have become one of the most popular materials; therefore, it is necessary to study the dielectric properties of the natural fiber-based polymer composites. Several studies have demonstrated the dielectric behavior of natural fiber-filled epoxy composites for varied applications. Arous et al. (2007) fabricated cellulose fiber-reinforced epoxy composites reinforced with 40 vol% cellulosic fiber and performed the dielectric relaxation measurements of lignocellulosic alfa fiber-reinforced epoxy composites as a function of temperature ranging from room temperature to 200 °C and frequency ranging from 0.1 Hz to 100 kHz. These results indicate that relaxation was analogous with the MWS interfacial polarization. The MWS polarization occurs due to the electric charge between the interfaces of the epoxy resin and the alfa fibers. Goud and Rao (2012) prepared the *Roystonea regia*/epoxy composites using a hand layup process by reinforcing alkali-treated *Roystonea regia* fiber into the epoxy matrix and investigated their dielectric behavior at various frequencies loaded with *Roystonea regia*/glass fiber at 20% of total fiber content. From the results, it can be seen that the alkali-treated fiber composites showed a dielectric constant and loss tangent with lower values, whereas the untreated fiber composites exhibit higher values. However, an increase in frequency can cause an increase in both dielectric constant and dielectric loss values. In addition, the higher loss factor values exhibit MWS relaxation. Three relaxations were noticed as (i) the α relaxation which corresponds to the glass transition of the host polymer, (ii) water dipoles polarization, and (iii) MWS interfacial polarization.

Zhan et al. (2011) prepared the epoxy/chicken feather fiber (CFF) composites with various loadings of CFF. The dielectric experiments of these composites were performed with respect to CFF fiber loading and frequency. The dielectric constant values of the epoxy/CFF fiber composites are decreased with an increase in the CFF fiber content and the frequency, while the dielectric constant values are somewhat higher in the neat epoxy matrix which could be suitable for applications in printed circuit boards (PCBs).

Kumar et al. (2011) synthesized the bamboo fiber and nanoclay-reinforced epoxy (BFRE) composites and studied their dielectric properties at various frequencies with respect to various time periods of silane, and alkali-treated BFRE composites. It has been observed that the orientation, ionic, and interfacial polarization strongly contributed to the dielectric properties of NFRP composites at various frequencies and temperatures (Rana and Singha 2015; Zhang et al. 2020). The 0° and 90° oriented BFRE composites dielectric constant plots are shown in Figs. 1a, c, and 2a (Kumar et al. 2011). Also, the dielectric dissipation factors of 0° and 90° oriented BFRE composites are depicted in Figs. 1b, d, and 2b (Kumar et al. 2011).

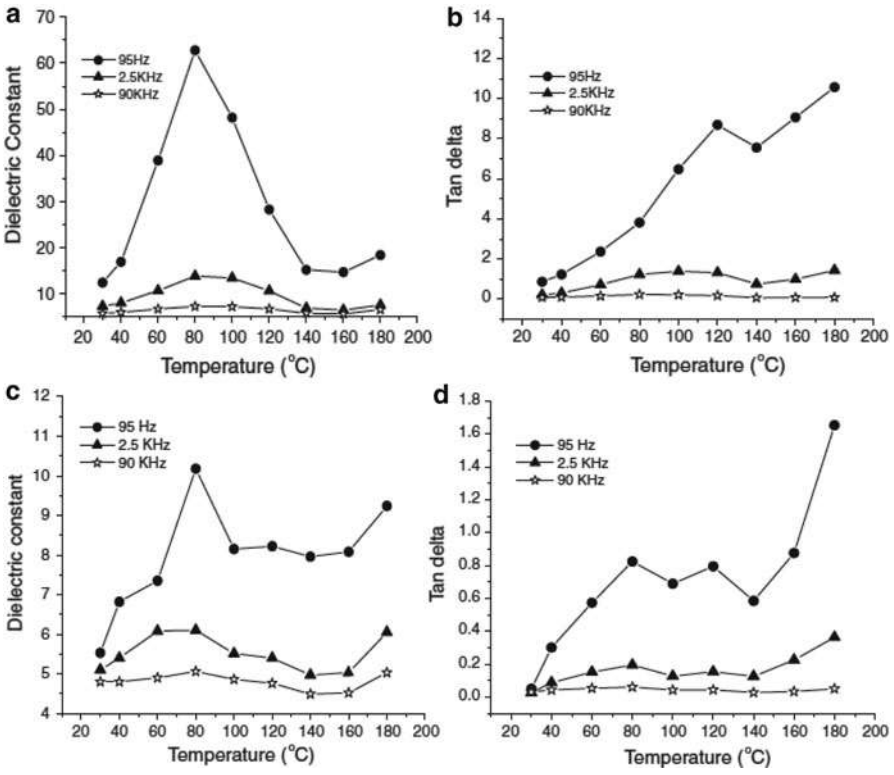

Fig. 1 (**a** and **b**) Real part of ε' and tan δ at different frequencies and temperatures (**c** and **d**) bamboo/epoxy composites oriented with 0°and 90°. (Adapted from Kumar et al. 2011. Copyright 2011, Springer Nature)

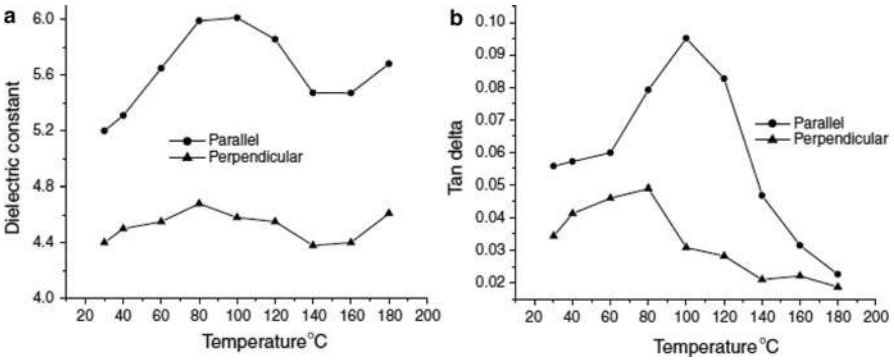

Fig. 2 Orientation dependence of (**a**) ε' and (**b**) tan δ at 2 MHz frequency. (Adapted from Kumar et al. 2011. Copyright 2011, Springer Nature)

For intermediate and lower frequencies, the dielectric constant and dielectric dissipation factor can occur because of strong interfacial, space-charge, and orientation polarization in the BFRE composites. At higher frequencies, the orientation polarization of the composites decreases since the molecules do not have enough time to align in the same orientation, and as a result, the dielectric constant and dielectric loss values of the BFRE composites decrease with an increase in frequency. At 80 °C and 95 Hz, the dielectric constant of 90° oriented BFRE composites was observed as 10.18, while at room temperature, it is in the range 5.53 to 4.4 in the frequency range 95 Hz–2 MHz. The values of ε' and tan δ increase as the temperature rises to ~80 °C for both 0° and 90° oriented BFRE composites. From Fig. 1a, c, the ε' value decreases in the temperature range 80–140 °C, and in between 140 °C and 160 °C, it is almost constant in the composites. The fiber molecular degradation was started beyond this temperature. During the decomposition stage, the samples might have undergone interfacial polarization, and hence the ε' values have decreased when the frequency was increased. Thus, it was concluded that the 0° oriented BFRE composites exhibit a better dielectric constant over 90° oriented BFRE composites since the parallel combination of dielectric constant is higher than the series combination (Ramajo et al. 2008). Besides, the alkali-treated bamboo fiber mattings were incorporated in epoxy resin to enhance the dielectric behavior of the BFRE composites. The dielectric constant of 90° oriented alkali-treated BFRE composite at 1 MHz was found to be 3.12 as depicted in Fig. 3.

Chand and Jain (2005) prepared the epoxy composites by reinforcing with sisal fiber using the compression molding technique and investigated the dielectric constant and dissipation factor of the prepared samples. The experiment was conducted under varying frequencies from 1–20 kHz and temperature from 24 to 180 °C. It has been concluded that with the temperature rise, the dielectric constant and loss factor values are increased. Furthermore, ε and tan δ values decrease with an increase in frequency. Jayamani et al. (2015) fabricated luffa/epoxy composites loaded with different contents (wt.%) of alkali-treated luffa fiber and untreated composites and studied their dielectric properties. The dielectric constant of

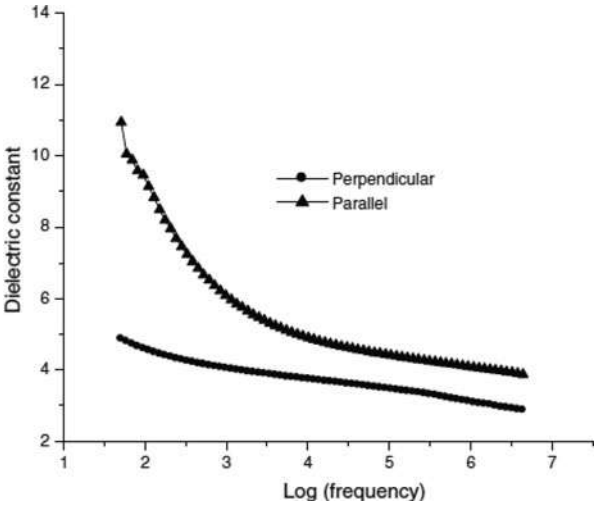

Fig. 3 Real part of dielectric constant plots having orientation dependence of alkali-treated bamboo-epoxy composites. (Adapted from Kumar et al. 2011. Copyright 2011, Springer Nature)

untreated fiber-reinforced composites was found to be greater than alkali-treated fiber composites. This is because of the hydrophilic nature of cellulose fibers which can increase the conductivity of composites. Further, the effect of loading of fibers on the dielectric constant of luffa fiber/epoxy composites was evaluated. It was noted that over the entire frequency range, the dielectric constants of luffa/epoxy composites are increased with increasing lignocellulose fiber content. These dielectric constant values are lower at high frequencies and higher at lower and medium frequencies. Generally, the increase in the orientation polarization leads to the enhancement in the dielectric constant with the increase in natural fibers loading in the host matrix. Besides, the dissipation factors of luffa/epoxy composites for different fiber loadings were studied. It was noted that the dissipation factor of the composites decreased with increasing frequency. With an increase in the contents of the fibers in the epoxy matrix, the dissipation factor exhibits a significant variation in the low-frequency region. The dissipation factor values were least for neat epoxy matrix, and it was maximum for 35 wt.% luffa fiber-reinforced epoxy composites. The authors investigated the loss factor of various compositions of fiber-reinforced epoxy composites as a function of frequency and observed that with an increase in frequency, there was a decrease in the loss factor of the composites. Generally, the dissipation factor increases in the composites due to orientation polarization. The loss factor was the highest for the 35 wt.% fiber content in the composites. Thus, the increase in polarization of the composite is due to the enhancement in the heterogeneity with the increase of fiber content (Sreekumar et al. 2012).

Dhal and Mishra (2013) prepared brown grass flower broom-reinforced epoxy LY 556 (bisphenol A diglycidyl ether) composites with different contents of filler and examined the dielectric properties of with respect to frequency. Figure 4 depicts the variation of the dielectric constant of the composites. The increase in the volume fraction of the filler in the composites led to the improvement in the dielectric

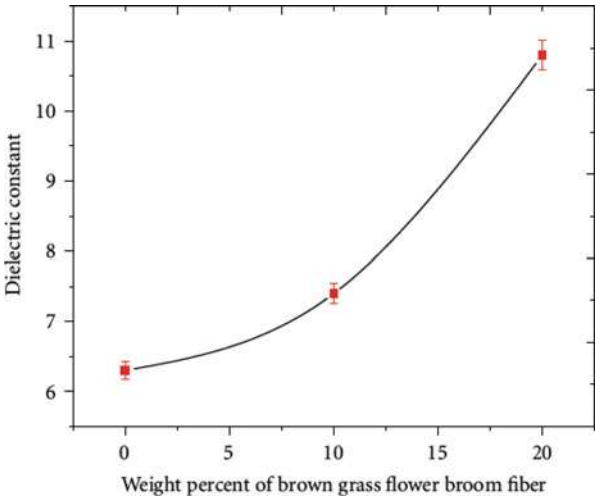

Fig. 4 Variation of dielectric constant with amount of fiber reinforcement. (Adapted from Dhal and Mishra 2013. Copyright 2013, Hindawi Publications)

constant values at 100 Hz. Figures 5 and 6 demonstrate the plots of dielectric constant and dielectric loss, respectively. It was observed that with an increase in frequency, both the values of dielectric constant and loss were initially lower and then reached a steady state. These results generally occur because of the dependence of dielectric behavior on the properties such as porosity and interface bonding of composites. Further, it was meant that due to dielectric relaxation in the materials, the dielectric constant decreases with an increase in frequency. Normally, with the application of an electric field, there is no rapid motion in the polar molecular rotational motion for the attainment of equilibrium, and it may decrease the dielectric constant of the composite material. So, with the increase in the content of the filler in the epoxy matrix, the dielectric constant increases. However, with an increase in frequencies, the stabilizing trend has been noticed in the dielectric loss values which may be useful for a suitable application.

Dash and Bisoyi (2020) synthesized the raw sunn hemp-reinforced epoxy composites (RSHC) with different loadings (5, 10, 15, 20, and 25 vol.%) using the hand layout technique. The prepared composites were labeled as RSHC5, RSHC10, RSHC15, RSHC20, and RSHC25, respectively. The dielectric properties of these prepared samples were studied at varying frequencies (100 Hz–100 kHz) and at ambient temperature. Figure 7 exhibits the dielectric constant and dielectric loss plots of the prepared samples having various contents of sunn hemp fiber. It can be seen that both the values of ε' and tan δ are increased with an increase in the content of filler. Generally, it may happen because of MWS interfacial polarization. This indicates that as the fiber content in the composite increases, the polar groups in it increases and enhances its amorphous phase which causes the enhancement in both the values of ε' and tan δ. Also, it has been studied that there is very low variation in both ε' and tan δ values in the samples RSHC5, RSHC10, and RSHC15 and is because of very low contents of fiber loadings in the composites which leave the

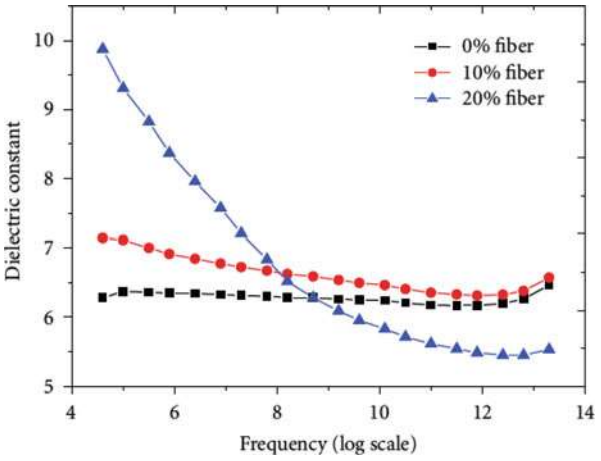

Fig. 5 Dielectric constant plots with frequency. (Adapted from Dhal and Mishra 2013. Copyright 2013, Hindawi Publications)

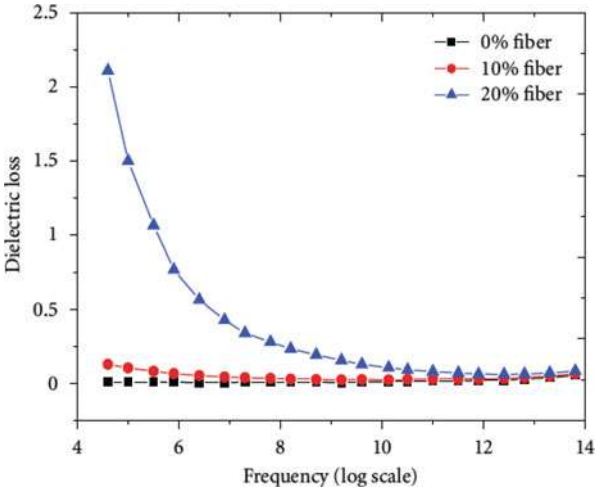

Fig. 6 Dielectric loss plots with frequency. (Adapted from Dhal and Mishra 2013. Copyright 2013, Hindawi Publications)

voids at the interface between natural fiber and the matrix. Cured epoxy resin (CER) shows very low values of dielectric constant and dielectric loss which are very near to RSHC5, RSHC10, and RSHC15, and this may be assigned to the hydrophobic and nonpolarity characteristics of the polymer chain which reins the instantaneous electronic and atomic polarization. The significant and sudden catastrophic increase in the values of ε' and tan δ from RSHC15 to RSHC20 and RSHC25 might point out the presence of polar groups (-OH) which are submerged in the reinforced fibers. The gaps in the resin flow region can be overcome with the incorporation of higher volume fraction of filler in the matrix which may cause a higher degree of dipolar and interfacial polarizability at lower frequencies as compared with higher

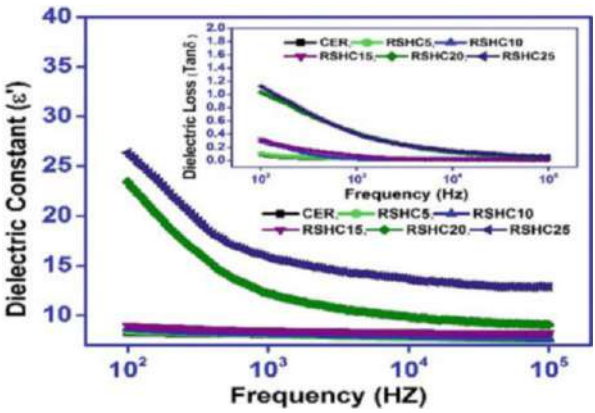

Fig. 7 (**a**) Dielectric constant and loss factor (inset) of RSHC with frequency under various fiber loadings. (Reproduced with permission from Dash and Bisoyi 2020. Copyright 2020, AIP Publishing. https://s100.copyright.com/CustomerAdmin/PLF.jsp?ref=36265e30-4232-4805-9cf7-ec8c0c73f650)

frequencies. This may be attributed to the conformational motion and partial rotation of dipoles in the polymer amorphous chains. The gradual enhancement of dielectric loss values of the composites with the increment of the fiber content may cause the consumption and accumulation of charges in semicrystalline fiber (amorphous phase) that leads to dissipation of heat energy in the sample.

Nimanpure et al. (2018) employed compression molding technique to prepare untreated and sodium hydroxide (NaOH)-treated sisal fibril based epoxy composites (termed as USFRE and TSFRE, respectively) with various compositions (10, 20, 30, and 35 wt.%). The incorporation of various contents of untreated sisal fibril-reinforced epoxy composites was designated as USFR10E, USFR20E, USFR30E, and USFR35E. Similarly, NaOH-treated composites were named USFR10E, USFR20E, USFR30E, and USFR35E, respectively. The authors investigated the dielectric properties of the prepared composites at varied frequencies and temperatures. The dielectric constant (ε') plots of both USFRE and TSFRE composites with different filler loadings (wt.%) in the temperature range 30–150 °C and in the frequency range 1 Hz–10 kHz are depicted in Figs. 8 and 9. It has been noted that with the increase in the filler loading, for both the TSFRE and USFRE composites, the ε' value increases. Also, with the increase in frequency, the ε' value decreases in the composites. At 1 kHz, 30 °C, the reported ε' values of TSFR10E and USFR10E composites are found to be 5.21 and 5.65, respectively. The reported ε' values of USFR10E, TSFR10E, USFR35E, and TSFR35E are 10.11, 9.71, 12.95, and 11.29, respectively, for the same frequencies, and with increased temperature. The reported ε' values of USFR10E and TSFR10E composites are 4.96 and 3.59, respectively, with increased frequency from 1 to 10 kHz at 30 °C. For USFR10E, TSFR10E, USFR35E, and TSFR35E, the dielectric constant values are found to be 9.49, 8.99, 10.52, and 9.78 for the increase in temperature (30–150 °C). For a change in frequency, and at various temperatures, the sisal fibril/epoxy composites exhibit higher sensitivity. This is because of the interfacial and orientation polarizations that occur with the increase in filler loadings. Also, the TSFRE and USFRE

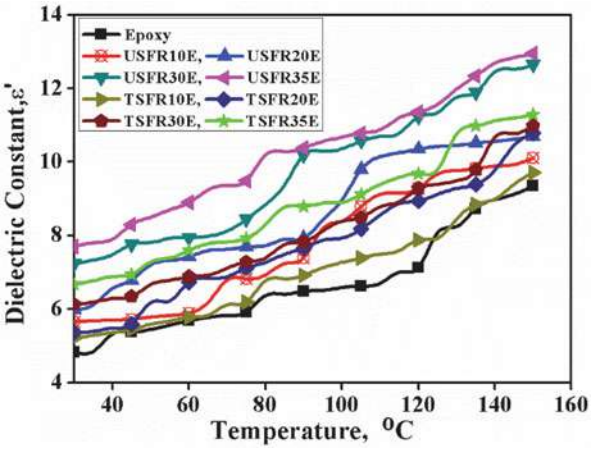

Fig. 8 Variation in the dielectric constant plots of USFRE and TSFRE composites at 1 kHz. (Adapted from Nimanpure et al. 2018. Copyright 2018, IEEE Publication)

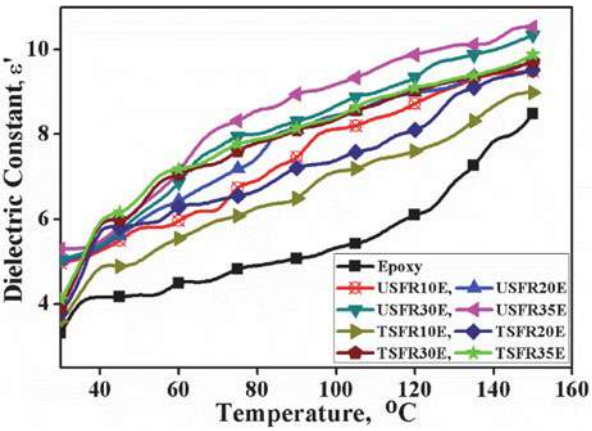

Fig. 9 Variation in the dielectric constant plots of USFRE and TSFRE composites at 10 kHz. (Adapted from Nimanpure et al. 2018. Copyright 2018, IEEE Publication)

composites exhibit better dielectric constants at a lower-frequency (1 kHz) and higher-frequency regions (10 kHz).

Figures 10 and 11 display the tan δ of different filler contents (wt.%) of USFRE and TSFRE composites at frequencies 1 and 10 kHz within the temperature range 30–150 °C. The dissipation factor increased with an increase in the filler loadings, whereas it decreased with increased frequency for both the USFRE and TSFRE composites owing to the interfacial polarization mechanism which is a function of frequency (Chen et al. 2017). Because of the alkali treatment of sisal fibril in the TSFRE composites, it exhibits a better dissipation factor than USFRE composites. At 1 kHz and 30 °C, the reported tan δ values of TSFR10E and USFR10E composites were 0.0049 and 0.0055, respectively (Fig. 10). However, at the same frequency, the reported values of tan δ for TSFR10E and USFR10E composites are

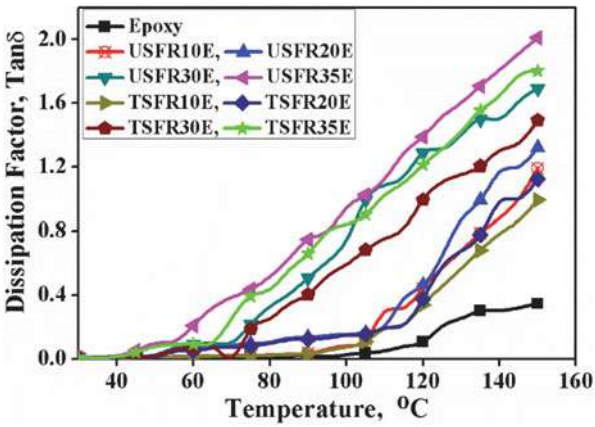

Fig. 10 Dissipation factor plots of USFRE and TSFRE composites at 1 kHz. (Adapted from Nimanpure et al. 2018. Copyright 2018, IEEE Publication)

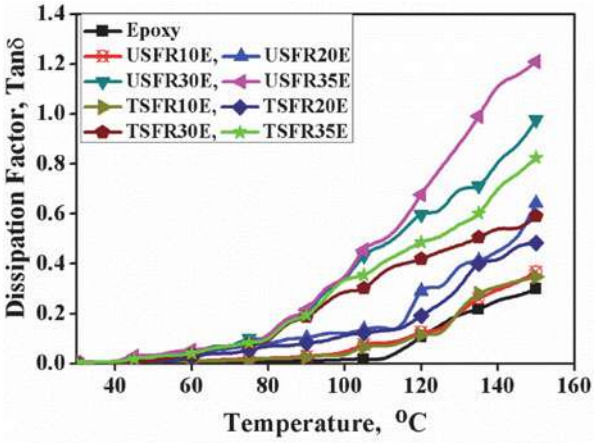

Fig. 11 Dissipation factor plots of USFRE and TSFRE composites at 10 kHz. (Adapted from Nimanpure et al. 2018. Copyright 2018, IEEE Publication)

0.9931 and 1.1908, respectively, with the rise in temperature from 30 to 150 °C. Moreover, the reported tan δ values of TSFR10E and USFR10E are 0.0011 and 0.0021, respectively, at 30 °C and for an increase in frequency (1–10 kHz) (Fig. 11). Further, TSFR10E and USFR10E composites show the tan δ values as 0.3478 and 0.3678, respectively, for the rise in temperature (30–150 °C). At 30 °C, the obtained tan δ values of TSFR35E and USFR35E composites are 0.0076 and 0.0082, whereas, at 150 °C, these values are changed to 1.8024 and 2.0098, respectively, for the same frequency (1 kHz). At 10 kHz frequency, the obtained tan δ values of TSFR35E and USFR35E composites are 0.0038 and 0.0056 at 30 °C, whereas these values were changed to 0.8244 and 1.2096, respectively, at 150 °C.

Figures 12 and 13 display the dielectric loss factor (ε'') of USFRE and TSFRE composites for 1 and 10 kHz frequency at various filler loadings and temperatures. It was revealed that the ε'' value was improved with the temperature rise and decreases

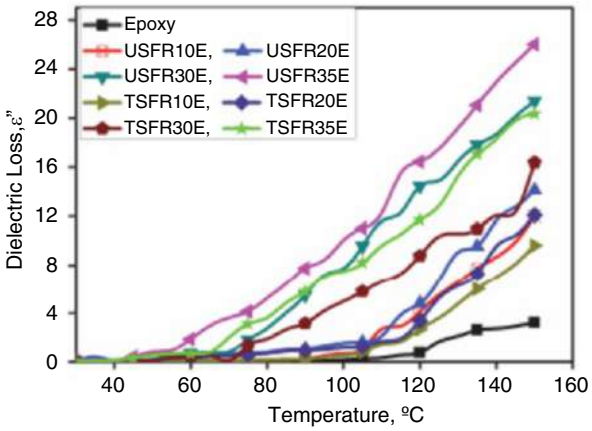

Fig. 12 Dielectric loss plots of USFRE and TSFRE composites at 1 kHz. (Adapted from Nimanpure et al. 2018. Copyright 2018, IEEE Publication)

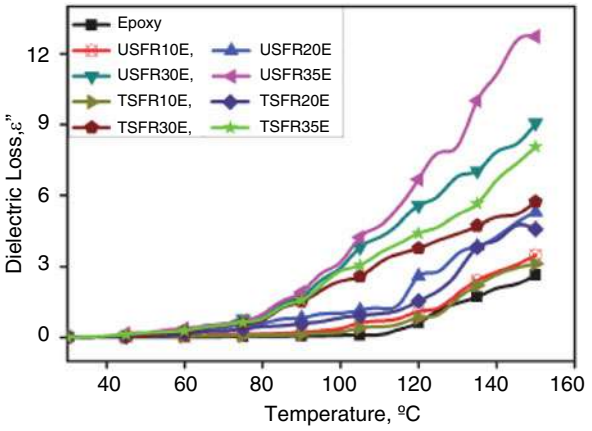

Fig. 13 Dielectric loss plots of USFRE and TSFRE composites at 10 kHz. (Adapted from Nimanpure et al. 2018. Copyright 2018, IEEE Publication)

with an increase in frequency. Also for both USFRE and TSFRE composites, the dielectric loss values increased with an increase in filler content. It has been observed that USFR35E and USFR10E exhibit the dielectric loss values as 0.0631 and 0.0310, respectively, at 1 kHz and 30 °C. On the other hand, for the USFR35E and USFR10E composites, the dielectric loss values are found to be 26.02 and 12.03, respectively, at 150 °C and 1 kHz. For the same filler loading, the TSFRE composites show a better dielectric loss factor than USFRE composites. The presence of hydrophilicity of the lignocellulosic sisal fibril fiber has led to increased dielectric loss factors in the epoxy composites with an increase in the temperature. Thus, it is studied that the alkali-treated sisal fibril-reinforced composites exhibit better dielectric properties.

Santhiarsa et al. (2014) fabricated palm sugar fiber reinforced epoxy composites using the molding injection method and studied the influence of alkali treatment and

weight fraction on the dielectric properties of composites. The authors concluded that the dielectric constant decreases because of the polarization effects after the treatment of different base strengths of alkaline solutions. Also, it was revealed that the dielectric constant of composites increases with the increase in weight fractions of various fillers in the epoxy composites. Mani et al. (2012) synthesized raw kapok fiber-reinforced epoxy composites and reported the room temperature dielectric properties in the frequency range of 100 Hz–1 MHz. The authors concluded that both dielectric constant and dielectric loss are decreased with increased frequency. Ridzuan et al. (2020) fabricated epoxy composites reinforced with natural fibers, namely, jute, kenaf, and napier fibers and studied their dielectric behavior at wet and dry conditions. Figure 14a–c shows the influence of natural fiber incorporation on the dielectric properties of epoxy composites at different wet and dry conditions.

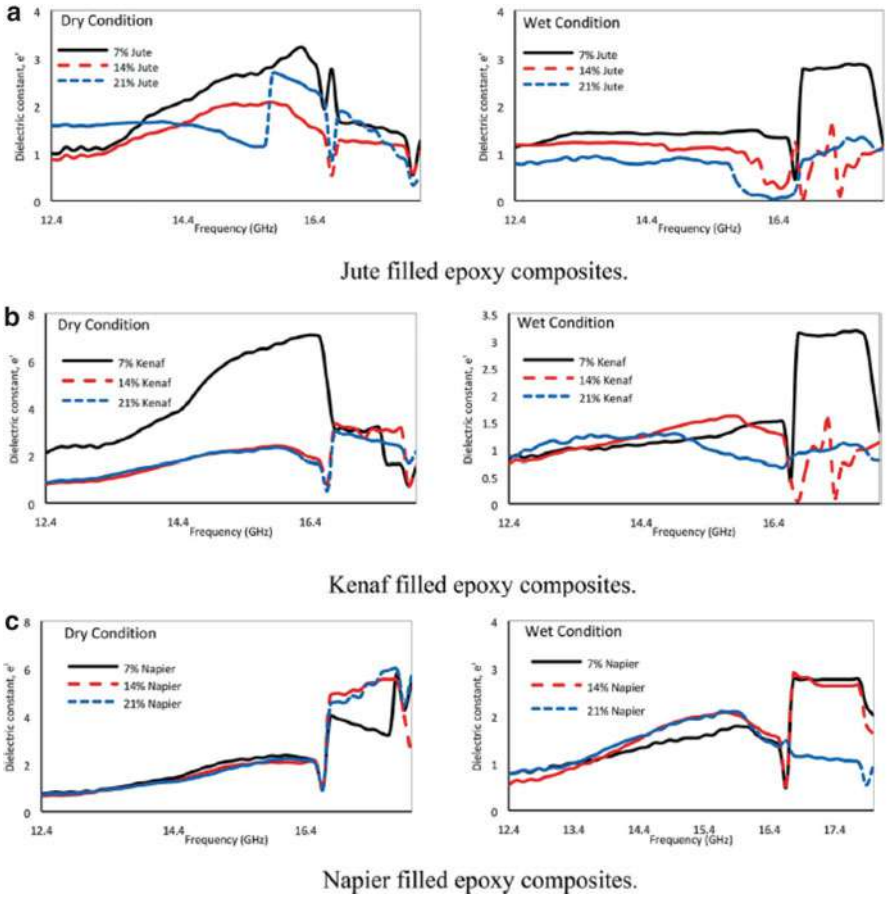

Fig. 14 Dielectric constant plots of natural fiber/epoxy composites. (Reproduced with permission from Ridzuan et al. 2020. Copyright 2020, Elsevier. https://s100.copyright.com/CustomerAdmin/PLF.jsp?ref=cc3bd47a-bb2e-4524-8069-25049fc36a3f)

From Fig. 14a, it can be observed that for jute/epoxy composites, the dielectric constant values were in the range between 0.33 and 3.23 for the dry conditions in the entire frequency range. Further, under wet conditions, the dielectric constant of the jute-reinforced epoxy composites are increased with a decrease in filler loadings in the frequency range 12.4 GHz–16.65 GHz. This may be due to the dependence of the dielectric constant on the water molecules which act as a plasticizer for cellulose (Ivanovska et al. 2019). The molecular vibrations are high in the frequency range 16.7 GHz–18 GHz, and, consequently, the complete orientation did not occur in the jute/epoxy composites, and hence, under wet conditions, the dielectric constant fluctuated. Figure 14b depicts the dielectric constant plot of kenaf-filled epoxy composites. It was noted that under dry conditions, the dielectric constant of 7 vol % filler-reinforced composites show higher values in the 12.4 GHz–16.2 GHz frequency range than the 14 and 21 vol% of kenaf/epoxy composites. However, under wet conditions, a minor difference in the dielectric constant was noted for the same filler loading which may be due to the increased porosity of epoxy materials with filler loading thereby reducing the number of molecules and hence decrease in the dielectric constant (Ridzuan et al. 2017). There is slight variation in the dielectric constant for the kenaf/epoxy composites reinforced with 7, 14, and 21 vol% filler content in the frequency range 16.2 GHz–18 GHz. Under wet conditions, for different filler loadings, the fluctuations are observed in the dielectric constant in the kenaf/epoxy composites. Moreover, the kenaf/epoxy composites reinforced with 7 vol% filler loading show a better dielectric constant over the 14 and 21 vol% in the frequency range 16.66 GHz–18 GHz. The epoxy composites reinforced with different contents (vol%) of napier filler is displayed in Fig. 14c. Under both dry and wet conditions, there was no considerable variation in the dielectric constant across the frequencies. The 7 and 14 vol% napier-reinforced epoxy composites show better dielectric constants compared with the 21 vol% napier-reinforced epoxy composites in the frequency range 16.66 GHz–18 GHz. Under dry conditions, when compared with the other natural fiber-based epoxy composites, the napier/epoxy composites show the lowest dielectric constant.

Zhang et al. (2018) employed the hot-pressing method to prepare flax fiber-reinforced epoxy composites with different filler contents (30, 45, and 60 vol%) and investigated the dielectric behavior in the frequency range 0.1–10 MHz at room temperature. Figure 15a, b depicts the dielectric constant and dielectric loss plots of epoxy/flax fiber composites reinforced with various filler loadings (Zhang et al. 2018). The synchronous augmentations in the dielectric properties are observed in the plots with an increase in the fiber loading in the epoxy matrix. The decrease in both the values of ε and tan δ was noticed with an increase in the frequency, and after that relatively stable values were obtained, while typical apolar behavior independent of frequency was observed in the neat epoxy matrix (Triki et al. 2015). An additional contribution to the charge carrier quantity was occurred due to higher loadings of fibers which multiply the interfacial polarization of introduced interfaces and hence enhancement in the dielectric constant (Triki et al. 2015). The higher degree of ultimate polarization takes place due to the engagement of more polar groups (–OH) in the material. For the composite system containing the augmented

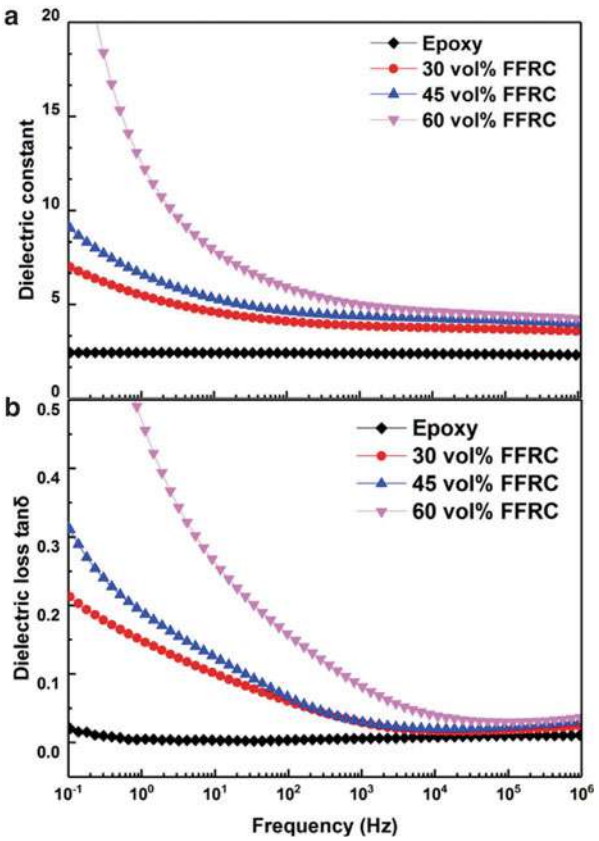

Fig. 15 Dielectric properties of FFRCs (**a**) dielectric constant and (**b**) dielectric loss. (Reproduced with permission from Zhang et al. 2018. Copyright 2018, Elsevier. https://s100.copyright.com/CustomerAdmin/PLF.jsp?ref=263dc365-744f-42fc-92e5-48bd5c96a6b3)

crystal region, the same trend was observed for the tan δ values. Further, the disturbance occurring in the orientation of dipoles at higher frequencies exhibits weak orientation polarization which causes frequency dependency of both ε and tan δ in the samples (Patra and Bisoyi 2011). Also, lower values of tan δ less relaxation have been observed with the change of frequency which may be due to the randomly arranged dipoles. The authors also compared the dielectric constant and dielectric loss of plant fiber-reinforced composites (PFRCs), man-made glass, and carbon fiber-reinforced composites (GFRCs and CFRCs) measured at 9.375 GHz with 60 vol% of fillers (Fig. 16). It can be noted that the ε values were almost the same for both GFRCs and PFRCs, whereas the values were slightly higher for CFRCs. Moreover, less energy dissipation has occurred in the PFRCs when compared to the GFRCs. Since the carbon fibers possess an excellent conductivity, the CFRCs exhibit distinguished values of ε and tan δ (Zhang et al. 2018). Also, it was noted that the ramie fiber-reinforced composite exhibits the least value of ε and the highest value of tan δ among three types of plant fibers because ramie possesses the highest crystallinity.

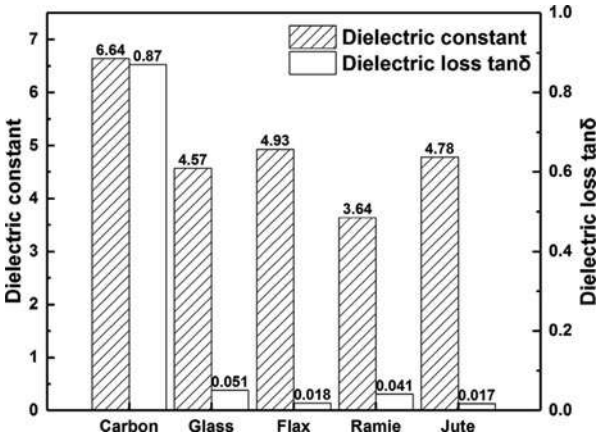

Fig. 16 Dielectric properties of epoxy/fiber composites. (Reproduced with permission from Zhang et al. 2018. Copyright 2018, Elsevier. https://s100.copyright.com/CustomerAdmin/PLF.jsp?ref=263dc365-744f-42fc-92e5-48bd5c96a6b3)

Singh et al. (2017) fabricated the bamboo fiber-reinforced epoxy composites using the hand layup method and investigated the effect of Kevlar hybridization on dielectric properties of the composites as a function of frequency in the range 1 kHz–1 MHz and temperature range 22–120 °C. Various compositions (wt.%) of bamboo and Kevlar fibers are added to the epoxy matrix to prepare these composites. The dielectric constant and tangent loss plots with respect to frequency for all the composites at room temperature are depicted in Fig. 17a, b. It was noted that the values of dielectric constant and dielectric loss were decreased as frequency increases. In general, at different frequencies and temperatures, the variation in the dielectric properties of the various natural fiber-based polymer composites arises due to the contribution of orientation, ionic, and interfacial polarization (Pothan et al. 2007). The main reason for the decrement in the values of both ϵ and tan δ is that the molecules do not have sufficient time for orientation at higher frequencies. Since Kevlar fiber exhibits a lower value of ε, its effect was felt on the composites and hence decreases their dielectric constant. Also, an increment in the Kevlar content in the host matrix increases the tan δ value of the composites. Further, it was observed that the composite consisting of one Kevlar and three bamboo laminas (termed as BBBK in Fig. 17a, b) showed the highest value of tan δ. Further, the investigation on dielectric properties of the composites was carried out as a function of temperature. It was noted that both the values of ε and tan δ increased with an increase in the temperature and it becomes the maximum up to critical temperature (T_c). When the temperature crosses the T_c, then there was a decrease in both the values of ε and tan δ. This may happen because of the scattering of charge carriers (thermally activated) and mobility enhancement in the water dipoles of the bamboo fibers (Navin et al. 2006).

Amor et al. (2010) reported the fabrication of palm tree fiber-reinforced epoxy composites using the classic contact method and examined their dielectric properties in the frequency range from 1 to 100 kHz and in the temperature range from 40 to 200 °C. Figure 18a, b shows the isothermal runs of the real part of permittivity (ε'),

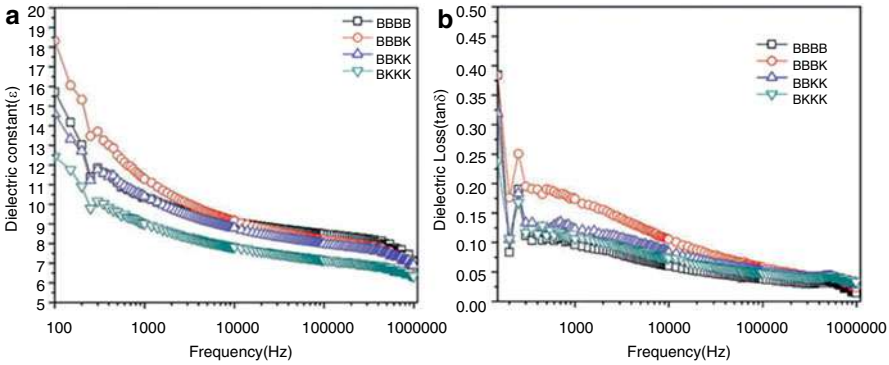

Fig. 17 Frequency dependence of (**a**) ε and (**b**) tan δ of composite samples. (Adapted from Singh et al. 2017. Copyright 2017, Taylor & Francis)

the loss factor (ε''), and tan δ. With the increase in the temperature, the permittivity of the composites reached the maximum values at lower frequencies. Generally, the presence of impurities in the palm fiber can increase the ε' value of composites. Also, improved conductivity in the composites at higher temperatures can cause an increase in the ε' value. The amplification in the loss effect takes place in the incorporation of filler in the host matrix when compared with the unfilled matrix which is directly related to the interface of palm fiber/epoxy resin or only the filler (Hammami et al. 2006). During the manufacturing process of the composites, the existence of free or immobilized charges in heterogeneous media which was arising from the polymeric phase induced the MWS relaxation. These ions may travel through the interface of the composites due to the variation in the permittivity, and conductivity thereby producing an interfacial polarization. At lower frequencies, the dielectric loss factor reaches maximum values, and with an increase in the frequency, the values will retain the normal values which indicate the presence of the dielectric relaxation.

Triki et al. (2015) synthesized epoxy composites reinforced with alkali-treated woven flax fibers. The authors named the untreated, leached, bleached, and mercerized woven flax fiber-filled epoxy composites as UWFFRE, LWFFRE, BWFFRE, and MWFFRE. Further, they examined the dielectric behavior of these samples in the temperature range 40–170 °C and the frequency range 0.1 Hz–1 MHz. It was observed that for all the composites, the dielectric permittivity (ε') increases with a decrease in frequency and vice versa. Due to the dipole polarization in the samples, the value of ε' was enhanced in all composites at the lower frequencies and at the lower temperatures. After mercerization and leaching treatments, the ε' value decreases, while it was increased after bleaching treatment in the composites. With increased temperature, the conductivity of the composites increases, and hence the dielectric permittivity increases. For the UWFFRE composite, at low temperatures and low frequencies, the ε'' value exhibits a decreasing trend with an increase in frequency. The low-frequency dispersion was found to be a dominating characteristic of the composite systems which can be explained according to the cluster model

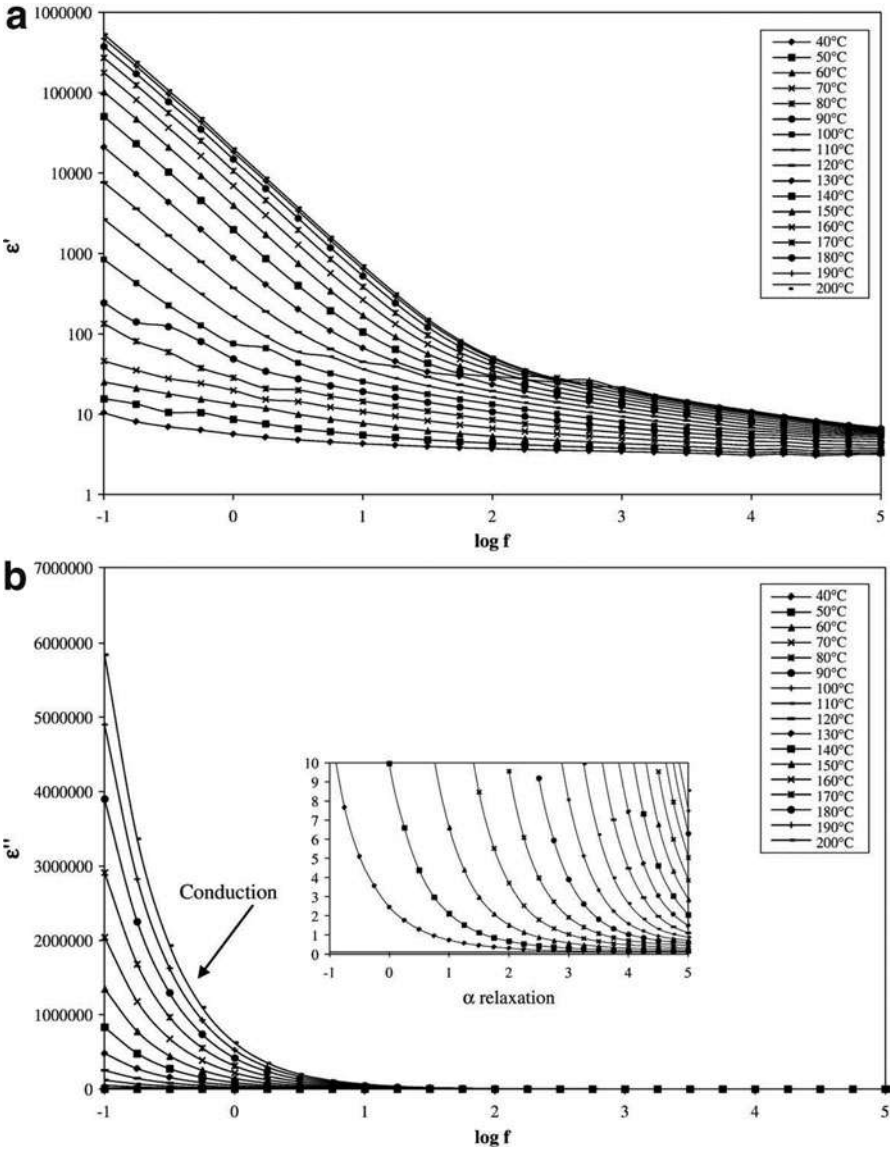

Fig. 18 Isothermal runs of (**a**) ε' and (**b**) ε'' versus frequency for the composites. (Reproduced with permission from Amor et al. 2010. Copyright 2010, Elsevier. https://s100.copyright.com/CustomerAdmin/PLF.jsp?ref=ed08a37a-9cfb-44b3-b51f-63e18c8c6fe7)

(Tuncer et al. 2002). The dispersion mechanism was decreased by leaching and mercerization and increased by the bleaching treatment in the composites.

Omri et al. (2019) prepared three laminated epoxy composites filled with five woven layers of E-glass, jute, and kenaf fabrics using the hand layup technique. The

dielectric properties of the prepared composites were studied in the frequency range of 0.1 Hz–1 MHz and the temperature range of 20–180 °C. The isothermal runs of the dielectric real permittivity (ε') and imaginary permittivity (ε'') of the epoxy matrix are depicted in Fig. 19a, b which showed four relaxation processes. The secondary β relaxation process was observed at the high frequency and low temperature in the first relaxation process (Hassan et al. 2016). The second relaxation process was noticed at low temperatures and low frequencies below the glass to rubber transition temperature (T_g). With the increase in frequency, the decreasing tendency of both the part of the permittivity and the loss factor was observed for the isothermal curves. This situation can be represented with the characteristic of the systems dominated by the carriers at low-frequency dispersion (Omri et al. 2019). The sites containing charge carriers in the dielectric materials are the existing

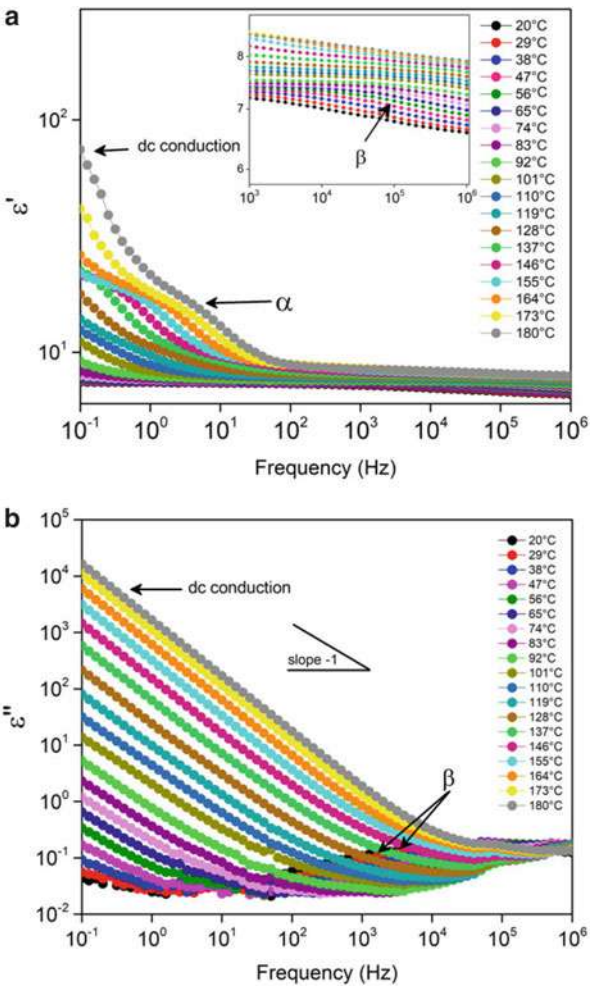

Fig. 19 (**a**) Real and (**b**) Imaginary parts of permittivity of epoxy. (Adapted from Omri et al. 2019. Copyright 2018, John Wiley & Sons)

clusters. With the application of an alternating voltage, the charges may move outside (inter-cluster movement) or inside (intra-cluster motion) the clusters. However, the inter-cluster motion takes place if the size of the cluster is lower than the displacement of the charges. At high temperatures and low frequencies, continuous conduction will occur for the mobile charges which can be affected by the inter-cluster motion.

To examine the adhesion of reinforced fillers, namely, E-glass, jute, and kenaf weaved fibers in the epoxy matrix (sample codes L1, L2, and L3, respectively), the authors performed the dielectric measurements. Figures 20a–c and 21a–c display the real and imaginary part (ε' and ε'') of permittivity plots of the composites L1–L3 as a function of frequency and the temperature. It was noted that for the composites L2 and L3, the values of ε' are increased at lower frequencies and decreased at higher frequencies. But, the permittivity was higher for the composites when compared with the neat epoxy matrix in the temperature range 70–100 °C. This enhancement in the permittivity was because of water dipoles polarization in the jute and kenaf fabric (Jayamani et al. 2014). The hydrogen bonding in the cellulose and lignin which hold the water molecules can cause the polarity in the fillers. For all composites, above the 100 °C, two types of dielectric relaxations are noticed at the intermediate frequency range. The first process is associated with glass rubbery transition and is known as the α relaxation process, and the second process is regarded as MWS effect or interfacial polarization (Omri et al. 2019).

Kumar and Kumar (2012) studied the dielectric behavior of silane- and alkali-treated bamboo fibers and nanoclay-reinforced epoxy resin composites in the frequency range from 95 Hz to 1 MHz at room temperature. The dielectric constant of bamboo fiber-reinforced epoxy composite (BFRE) at various periods of alkali treatments is depicted in Fig. 22. It can be seen that bamboo fiber with 0.5 h NaOH treatment enhances the dielectric constant of BFRE composites due to unfinished wetting of fiber (Kushwaha and Kumar 2009). The crystal structure of natural fiber can be damaged due to the prolonged alkali treatment which influences the water resistance of natural fiber composites. This damaging effect overshadowed the effect of eliminating artificial impurities, hemicelluloses, lignin, cuticle, and pectic substances (Kushwaha and Kumar 2010). Due to these factors, 5 h NaOH-treated bamboo-epoxy composites exhibit a high dielectric constant.

The dielectric constant plot of silane and alkali-treated BFRE composites is displayed in Fig. 23. It was noted that, with the increment in the frequency, the dielectric constant decreased in the composites. Because of low water resistance, the greater value of a dielectric constant can be achieved in the untreated BFRE composites. For untreated, silane and alkali-treated BFRE composites, the dielectric constant values decrease with the increase in frequency. Thus it can be said that the dielectric constant increases at lower frequencies and decreases at higher frequencies. In general, the dielectric properties of natural fiber-filled plastic composites strongly depend on the orientation, ionic, and interfacial polarization (Pothan et al. 2007). The decrease in the dielectric constant with an increase in frequency was due

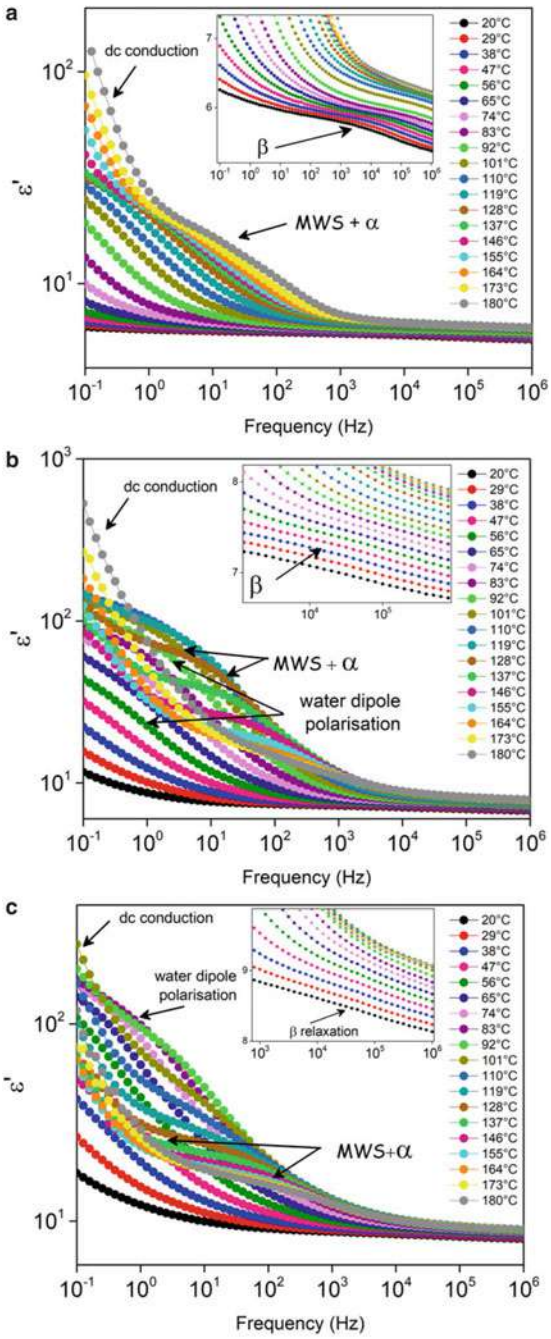

Fig. 20 Isothermal runs of ε' of (**a**) L1, (**b**), L2 and (**c**) L3. (Adapted from Omri et al. 2019. Copyright 2018, John Wiley & Sons)

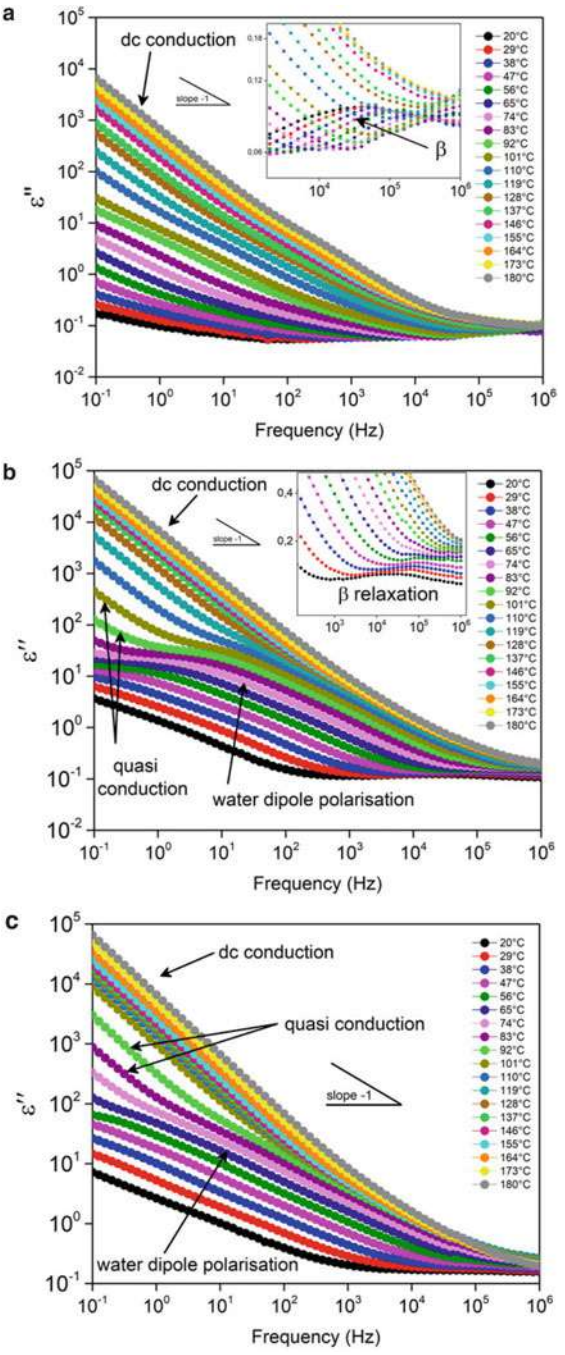

Fig. 21 Isothermal runs of ε'' of (**a**) L1, (**b**), L2 and (**c**) L3. (Adapted from Omri et al. 2019. Copyright 2018, John Wiley & Sons)

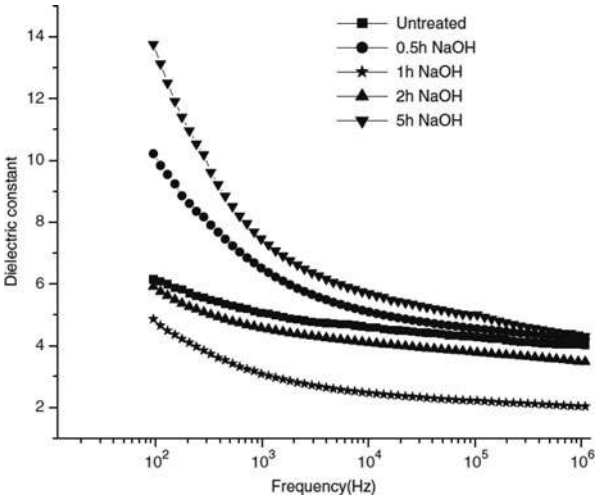

Fig. 22 Dielectric constant of BFRE composites with respect to various periods of alkali treatments. (Adapted from Kumar and Kumar 2012. Copyright 2012, Sage Publishing)

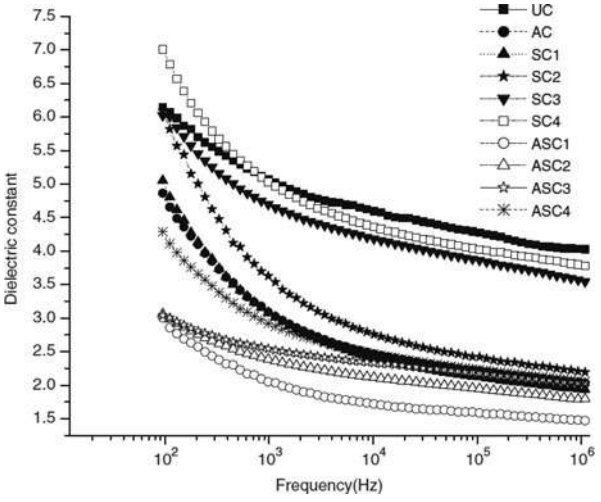

Fig. 23 Dielectric constant of silane and alkali-treated BFRE composites with frequency. (Adapted from Kumar and Kumar 2012. Copyright 2012, Sage Publishing)

to the decreased contribution of orientation polarization. Also, it was observed that, for all the frequencies, untreated composites exhibit higher dielectric constants than the alkali-treated BFRE composites.

The dielectric constant plot of nanoclay-filled bamboo-epoxy nanocomposites is shown in Fig. 24. It was observed that nanoclay (3 wt.%)-filled composites exhibit a lower dielectric constant than that of other filler loadings at all the frequencies. This may be due to the immobility of epoxy chains by nanoparticles of the

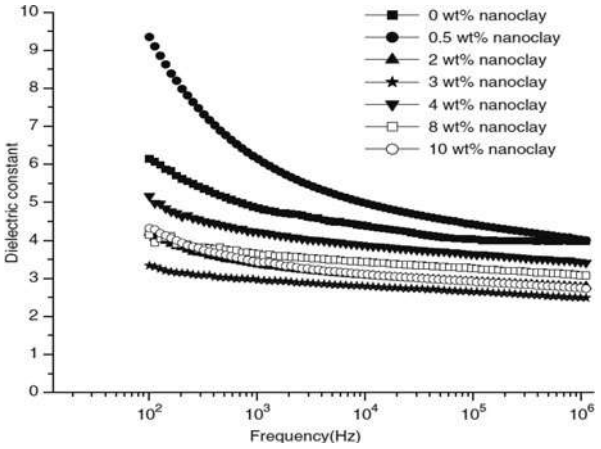

Fig. 24 Dielectric constant plots of bamboo/epoxy nanocomposites at various nanoclay content. (Adapted from Kumar and Kumar 2012. Copyright 2012, Sage Publishing)

nanocomposites. The predominance of intercalated clay can increase the dielectric constant, whereas it may be decreased due to exfoliated nanoclay in the nanocomposites (Pluta et al. 2007). Further, it was noted that the dielectric constant of 3 wt.% nanoclay-filled nanocomposites showed reduced intercalated structures and increased exfoliated structures. The authors further investigated the effect of the combination of silane treatment and nanoclay reinforcement on the dielectric behavior of the BFRE composites. The dielectric constant plots of bamboo-epoxy nanocomposites treated with mercerized silane and alkali materials are shown in Fig. 25. It was noted that in the frequency range 2.4 to 1.77 (95 Hz–1 MHz), mercerized aminopropyl triethoxysilane-treated bamboo/epoxy nanocomposites exhibit low dielectric constant. These properties of BFRE composites make them an important dielectric material for the applications in PCBs (Ehrler 2002).

Figure 26a, b displays dielectric dissipation factor plots of silane and alkali-treated and nanoclay (0 and 3 wt.%)-reinforced bamboo fiber epoxy resin composites as a function of frequency, respectively. These plots clearly show that for all composites, there is a decrease in the dissipation factor that takes place with an increase in the frequencies. In general, due to the contribution of interfacial, space-charge and orientation polarization in the BFRE composites can cause the dissipation factor at an intermediate and lower frequency. Further, at high frequency, the decrease in the dissipation factor of BFRE composites can occur since the molecules do not have enough time to acquire their direction and hence the contribution of orientation polarization. It has been observed that the silane treatment and nanofiller concentration strongly affects the dissipation factor of the composites. It can be seen that the nanoclay filler and the chemical treatment can decrease the dissipation factor of bamboo/epoxy composites. Moreover, the lowest dissipation factor values were noted for mercerized 3-trimethoxysilyl propyl methacrylate-treated BFRE nanocomposites. Thus, these results evidenced that these nanocomposite materials are promising for various dielectric applications (Kumar and Kumar 2012).

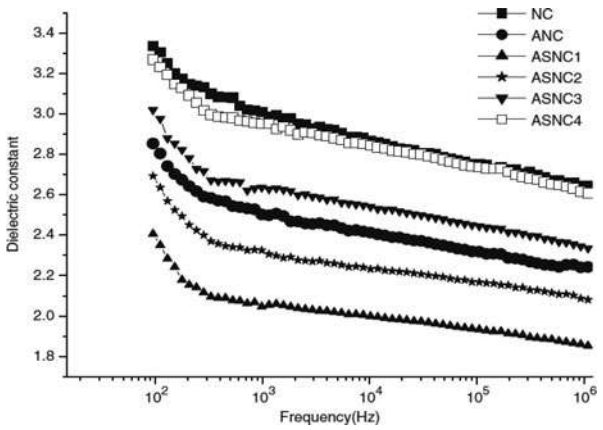

Fig. 25 Dielectric constant plots with frequency for silane and alkali-treated BFRE nanocomposites. (Adapted from Kumar and Kumar 2012. Copyright 2012, Sage Publishing)

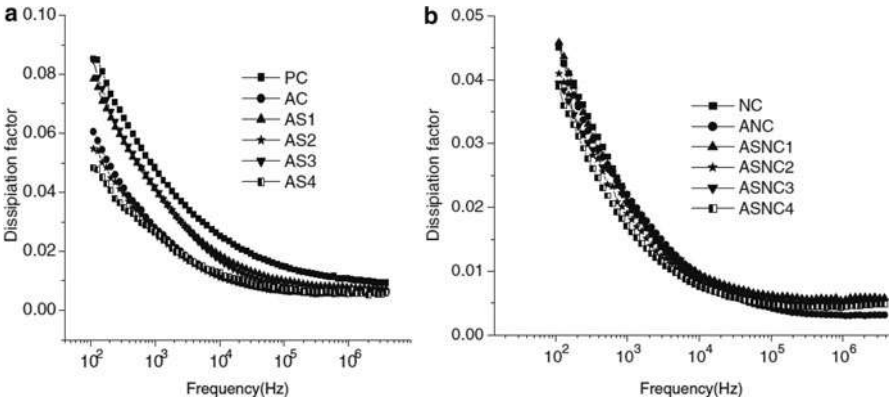

Fig. 26 Dissipation factor plots with frequency for silane- and alkali-treated bamboo fiber (**a**) without nanoclay, (**b**) with 3 wt.% nanoclay-reinforced epoxy composites. (Adapted from Kumar and Kumar 2012. Copyright 2012, Sage Publishing)

Table 1 summarizes the dielectric properties of epoxy composites reinforced with natural fibers as a function of frequency and temperature.

Conclusions and Future Perspectives

In the last decades, epoxy/natural fiber composites are developed for various dielectric applications. In this chapter, an overview of dielectric mechanisms such as dielectric constant, dielectric loss, breakdown strength, and energy density have been explored. Further, the basics of various dielectric polarization in dielectrics are discussed. Finally, the dielectric properties such as dielectric constant, dielectric loss, and dissipation factor of epoxy composites reinforced with different loadings of

Table 1 Dielectric properties of epoxy/natural fiber composites as a function of frequency and temperature

Natural fiber as a filler	Natural fiber loading (wt.%)	Dielectric constant range	Dielectric loss range	Frequency range (Hz)	Temperature range (°C)	Reference
Chicken feather fiber	26.49–66.92 (vol%)	~3.7–5.4	0.06–0.13	10 kHz–5 MHz	Room temperature	Zhan et al. (2011)
Bamboo fiber	–	4.4–10.18	0.01–6	95 Hz–2 MHz	30–180	Kumar et al. (2011)
Sisal fiber	–	2–30	0–1.3	1–20 kHz	24–180	Chand and Jain (2005)
Luffa fiber	10–35 (wt.%)	~1–7	0–4	1 kHz–1 MHz	70	Jayamani et al. (2015)
Brown grass flower broom fiber	10 and 20%	~5–11	~0–2.25	100 Hz–1 MHz	–	Dhal and Mishra (2013)
Raw sunn hemp fiber	5–25 vol%	~0–30	~0–1.2	100 Hz–100 kHz	Ambient temperature	Dash and Bisoyi (2020)
Sisal fibril fiber	10–35 (wt.%)	~3–14	~0–28	1–10 kHz	30–150	Nimanpure et al. (2018)
Kapok fiber	–	~0–350	~0–1.4	100–1 MHz	Ambient temperature	Mani et al. (2012)
Flax fiber	–	$\sim 10^2$–10^6	$\sim 10^2$–10^6	0.1 Hz–1 MHz	40–170	Triki et al. (2015)
Sisal fiber	–	~5–70	~0–2.5	180 Hz–1 MHz	~27–200	Patra and Bisoyi (2011)
Bamboo fiber	45.48–100 (wt.%)	5–19	0–0.4	1 KHz–1 MHz	22–120	Singh et al. (2017)
Palm tree fiber	–	~10–700,000	~0–140	0.1 Hz–100 kHz	40–200	Amor et al. (2010)
Jute and kenaf fiber	–	~ 0.1–10^3	0.01–10^5	0.1 Hz–1 MHz	20–180	Omri et al. (2019)

natural fiber are discussed. From these studies, it has been concluded that the epoxy/natural fiber composites have been considered as one of the best dielectric materials over synthetic fiber-reinforced polymer composites for various applications in the future. The most popular natural fibers obtained from the plants for the preparation of polymer composites are bamboo, sisal, kenaf, coconut, abaca, hemp, and jute. In particular, epoxy/natural fiber composites have become one of the most extensively

studied materials because of their economic viability, technical feasibility, and environmental suitability. Moreover, various treatments (ultrasonic, silane, alkaline, etc.) and coupling agents (cloisite, tourmaline, nanoclays, alumina, and zinc oxide) were employed to improve interfacial adhesion and the compatibility between the matrix and the filler and to enhance the performance of the epoxy/natural fiber composites. However, theoretical modeling for the prediction of dielectric constant and dielectric loss values of various natural fiber-based epoxy composites is not fully explored yet. Therefore, more work should be carried out on the theoretical investigations of dielectric properties of epoxy/natural fiber composites given their future applications.

References

I.B. Amor, Z. Ghallabi, H. Kaddami, M. Raihane, M. Arous, A. Kallel, Experimental study of relaxation process in unidirectional (epoxy/palm tree fiber) composite. J. Mol. Liq. **154**, 61–68 (2010)

M. Arous, I.B. Amor, S. Boufi, A. Kallel, Experimental study on dielectric relaxation in alfa fiber reinforced epoxy composites. J. Appl. Polym. Sci. **106**, 3631–3640 (2007)

H. Bouaamlat, N. Hadi, N. Belghiti, H. Sadki, M.N. Bennani, F. Abdi, T. Lamcharfi, M. Bouachrine, M. Abarkan, Dielectric properties, AC conductivity, and electric modulus analysis of bulk ethylcarbazole-terphenyl. Adv. Mater. Sci. Eng. **2020**, 8689150 (2020)

N. Chand, D. Jain, Effect of sisal fibre orientation on electrical properties of sisal fibre reinforced epoxy composites. Comp. Part A Appl. Sci. Manuf. **36**, 594–602 (2005)

A. Charkhesht, C.K. Regmi, K.R. Mitchell-Koch, S. Cheng, N.Q. Vinh, High-precision megahertz-to-terahertz dielectric spectroscopy of protein collective motions and hydration dynamics. J. Phys. Chem. B **122**, 6341–6350 (2018)

X. Chen, J. Tseng, I. Treufeld, M. Mackey, D.E. Schuele, R. Li, M. Fukuto, E. Baer, L. Zhu, Enhanced dielectric properties due to space charge-induced interfacial polarization in multilayer polymer films. J. Mater. Chem. C **5**, 10417–10426 (2017)

Z. Dang, J. Yuan, J. Zha, T. Zhou, S. Li, G. Hu, Fundamentals, processes and applications of high-permittivity polymer–matrix composites. Prog. Mater. Sci. **57**, 660–723 (2012)

C. Dash, D.K. Bisoyi, Significance of dielectric and mechanical properties on fiber loading of sunn hemp reinforced epoxy composite. AIP Conf. Proceed **2220**, 080027 (2020)

K. Deshmukh, S.K.K. Pasha, Room temperature ammonia sensing based on graphene oxide integrated flexible polyvinylidene fluoride/cerium oxide nanocomposite films. Polym.-Plast. Technol. Eng. **59**, 1429–1446 (2020)

K. Deshmukh, S. Sankaran, M.B. Ahamed, K.K. Sadasivuni, S.K.K. Pasha, D. Ponnamma, P.S.R. Sreekanth, K. Chidambaram, Dielectric spectroscopy, in *Spectroscopic Methods for Nanomaterials Characterization*, ed. by S. Thomas, R. Thomas, A. K. Zachariah, R. K. Mishra, vol. 2, (Elsevier, Amsterdam, 2017), pp. 237–299

K. Deshmukh, S. Sankaran, M.B. Ahamed, S.K.K. Pasha, K.K. Sadasivuni, D. Ponnamma, M.A.A. Al-Maadeed, Studies on the electrical properties of graphene oxide reinforced poly (4-styrenesulfonic acid) and polyvinyl alcohol blend composites. Int. J. Nanosci. **17**, 1760005–1760013 (2018)

K. Deshmukh, S. Sankaran, M.B. Ahamed, S.K.K. Pasha, Biomedical applications of polymer composite nanofibers, in *Polymer Nanocomposites in Biomedical Engineering Applications*, ed. by K. K. Sadasivuni, D. Ponnamma, R. Mariappan, M. B. Ahamed, J. J. Cabibihan, (Springer, Cham, 2019), pp. 111–165

J.P. Dhal, S.C. Mishra, Processing and properties of natural fiber-reinforced polymer composite. J. Mater. **2013**, 1–6 (2013)

S. Ehrler, Properties of new printed circuit board base materials. Circ. World **28**, 38–45 (2002)
O. Faruk, A.K. Bledzki, H. Fink, M. Sain, Biocomposites reinforced with natural fibers: 2000–2010. Prog. Polym. Sci. **37**, 1552–1596 (2012)
G. Goud, R.N. Rao, Mechanical and electrical performance of roystonea regia/glass fibre reinforced epoxy hybrid composites. Bull. Mater. Sci. **35**, 595–599 (2012)
H. Hammami, M. Arous, M. Lagache, A. Kallel, Experimental study of relaxations in unidirectional piezoelectric composites. Comp. Part A Appl. Sci. Manuf. **37**, 1–8 (2006)
A. Haseena, G. Unnikrishnan, G. Kalaprasad, Dielectric properties of short sisal/coir hybrid fibre reinforced natural rubber composites. Compos. Interface **14**, 763–786 (2007)
M.K. Hassan, S.J. Tucker, A. Abukmail, J.S. Wiggins, K.A. Mauritz, Polymer chain dynamics in epoxy based composites as investigated by broadband dielectric spectroscopy. Arab. J. Chem. **9**, 305–315 (2016)
S. He, K. Shi, J. Bai, Z. Zhang, L. Li, Z. Du, B. Zhang, Studies on the properties of epoxy resins modified with chain-extended ureas. Polymer **42**, 9641–9647 (2001a)
S. He, K. Shi, J. Bai, Z. Zhang, L. Li, Z. Du, B. Zhang, Studies on the properties of epoxy resins modified with chain-extended ureas. Polymer **42**, 9641–9647 (2001b)
X. Huang, B. Sun, Y. Zhu, S. Li, P. Jiang, High-*k* polymer nanocomposites with 1D filler for dielectric and energy storage applications. Prog. Mater. Sci. **100**, 187–225 (2019)
A. Ivanovska, D. Cerovic, N. Tadic, I.J. Castvan, K. Asanovic, M. Kostic, Sorption and dielectric properties of jute woven fabrics: Effect of chemical composition. Ind. Crop. Prod. **140**, 111632 (2019)
R.K. Jammula, S. Pittala, S. Srinath, V.V.S.S. Srikanth, Strong interfacial polarization in ZnO decorated reduced-graphene oxide synthesized by molecular level mixing. Phys. Chem. Chem. Phys. **17**, 17237–17245 (2015)
E. Jayamani, S. Hamdan, M.R. Rahman, M. Khusairy, B. Bakri, Comparative study of dielectric properties of hybrid natural fiber composites. Procedia Eng. **97**, 536–544 (2014)
E. Jayamani, S. Hamdan, M.R. Rahman, M.K.B. Bakri, Dielectric properties of lignocellulosic fibers reinforced polymer composites: Effect of fiber loading and alkaline treatment. Mater. Today Proceed **2**, 2757–2766 (2015)
F. Jin, X. Li, S. Park, Synthesis and application of epoxy resins: A review. J. Ind. Eng. Chem. **29**, 1–11 (2015)
Z. Khadija, S. Waseem, K.K. Sadasivuni, K. Deshmukh, A. Muzaffar, M.B. Ahamed, M.A.A. AlMaadeed, Processing and industrial applications of sustainable nanocomposites containing nanofillers, in *Sustainable Polymer Composites and Nanocomposites*, ed. by Inamuddin, S. Thomas, R. Mishra, A. M. Asiri, (Springer, Cham, 2019), pp. 451–478
D.E. Khaled, N.N. Castellano, J.A. Gazquez, A.J. Perea-Morena, F. Manzano-Agugliaro, Dielectric spectroscopy in biomaterials: Agrophysics. Materials **9**, 310–336 (2016)
M. Khutia, G.M. Joshi, K. Deshmukh, M. Pandey, Optimization of dielectric constant of polycarbonate/polystyrene modified blend by ceramic metal oxide. Polym.-Plast. Technol. Eng. **54**, 383–389 (2015)
S.S. Kumar, S.S. Hiremath, Natural fiber reinforced composites in the context of biodegradability: A review, in *Encyclopedia of Renewable and Sustainable Materials Reference Module in Materials Science and Materials Engineering*, ed. by S. Hashmi, I. A. Choudhury, vol. 5, (Elsevier, 2020), pp. 160–178
V. Kumar, R. Kumar, Dielectric and mechanical properties of alkali- and silane-treated bamboo-epoxy nanocomposites. J. Compos. Mater. **46**, 3089–3101 (2012)
V. Kumar, P.K. Kushwaha, R. Kumar, Impedance-spectroscopy analysis of oriented and mercerized bamboo fiber-reinforced epoxy composite. J. Mater. Sci. **46**, 3445–3451 (2011)
A.H. Kumar, M.B. Ahamed, K. Deshmukh, M.S. Sirajuddeen, Morphology, dielectric and EMI shielding characteristics of graphene nanoplatelets, montmorillonite nanoclay and titanium dioxide nanoparticles reinforced polyvinyledenefluoride nanocomposites. J. Inorg. Organomet. Polym. Mater. **31**, 2003–2016 (2021)

P.K. Kushwaha, R. Kumar, Enhanced mechanical strength of BFRP composite using modified bamboos. J. Reinf. Plast. Compos. **28**, 2851–2859 (2009)
P.K. Kushwaha, R. Kumar, Studies on water absorption of bamboo-epoxy composites: Effect of silane treatment of mercerized bamboo. J. Appl. Polym. Sci. **115**, 1846–1852 (2010)
Q. Li, F. Yao, Y. Liu, G. Zhang, H. Wang, Q. Wang, High-temperature dielectric materials for electrical energy storage. Annu. Rev. Mater. Res. **48**, 219–243 (2018)
G.K. Mani, J.B.B. Rayappan, D.K. Bisoyi, Synthesis and characterization of kapok fibers and its composites. J. Appl. Sci. **12**, 1661–1665 (2012)
V. Mittal, R. Saini, S. Sinha, Natural fiber-mediated epoxy composites – A review. Compos. B Eng. **99**, 425–435 (2016)
A. Muzaffar, M.B. Ahamed, K. Deshmukh, S.K.K. Pasha, Dielectric properties and electromagnetic interference shielding studies of nickel oxide and tungsten oxide reinforced polyvinylchloride nanocomposites. Polym.-Plast. Technol. Eng. **59**, 1667–1678 (2020)
M.M.A. Nassar, R. Arunachalam, K.I. Alzebdeh, Machinability of natural fiber reinforced composites a review. Int. J. Adv. Manuf. Technol. **88**, 2985–3004 (2017)
C. Navin, J. Deepak, N. Archana, Investigation on gradient dielectric characteristics of bamboo (Dendrocalamus strictus). J. Appl. Polym. Sci. **102**, 3489–3494 (2006)
S. Nimanpure, S.A.R. Hashmi, R. Kumar, A. Nigrawal, A. Naik, Electrical and dynamic mechanical analysis of sisal fibril reinforced epoxy composite. In IEEE Trans. Dielect. Electr. Insulat. **25**, 2020–2028 (2018)
B. Nketia-Yawson, Y.Y. Noh, Recent progress on high-capacitance polymer gate dielectrics for flexible low-voltage transistors. Adv. Funct. Mater. **28**, 1802201 (2018)
Y. Noguchi, Y. Miyazaki, Y. Tanaka, N. Sato, Y. Nakayama, T.D. Schmidt, W. Brütting, H. Ishii, Charge accumulation at organic semiconductor interfaces due to a permanent dipole moment and its orientational order in bilayer devices. J. Appl. Phys. **111**, 114508 (2012)
M.A. Omri, M.R. Sanjay, A. Triki, B. Yogesha, A. Kallel, Dielectric properties and interfacial adhesion of jute, kenaf and E-glass fabrics reinforcing epoxy composites. Polym. Compos. **40**, 2142–2153 (2019)
M. Pandey, G.M. Joshi, K. Deshmukh, M. Khutia, N.N. Ghosh, Optimized AC conductivity correlated to structure, morphology and thermal properties of PVDF/PVA/Nafion composites. Ionics **20**, 1427–1433 (2014)
S. Parbin, N.K. Waghmare, S.K. Singh, S. Khan, Mechanical properties of natural fiber reinforced epoxy composites: A review. Procedia Comput. Sci. **52**, 375–379 (2019)
D. Pathania, D. Singh, A review on electrical properties of fiber reinforced polymer composites. Int. J. Theo Appl. Sci. **1**, 34–37 (2009)
A. Patra, D.K. Bisoyi, Investigation of the electrical and mechanical properties of short sisal fiber-reinforced epoxy composite in correlation with structural parameters of the reinforced fiber. J. Mater. Sci. **46**, 7206–7213 (2011)
K.L. Pickering, M.G.A. Efendy, T.M. Le, A review of recent developments in natural fibre composites and their mechanical performance. Comp. Part A: Appl. Sci. Manuf. **83**, 98–112 (2016)
M. Pluta, J.K. Jeszka, G. Boiteux, Polylactide/montmorillonite nanocomposites, structure, dielectric, viscoelastic and thermal properties. Eur. Polym. J. **43**, 2819–2835 (2007)
L.A. Pothan, C.N. George, M. Jacob, S. Thomas, Effect of chemical modification on the mechanical and electrical properties of banana fiber polyester composites. J. Compos. Mater. **41**, 2371–2386 (2007)
T. Prodromakis, C. Papavassiliou, Engineering the Maxwell–Wagner polarization effect. Appl. Surf. Sci. **255**, 6989–6994 (2009)
G.C. Psarras, Fundamentals of dielectric theories, in *Dielectric Polymer Materials for High-Density Energy Storage*, ed. by Z. Dang, (Plastics Design Library, 2018), pp. 11–57
S. Pujari, A. Ramakrishna, K.T.B. Padal, Comparison of ANN and regression analysis for predicting the water absorption behaviour of jute and banana fiber reinforced epoxy composites. Mater. Today Proceed **4**, 1626–1633 (2017)

J.K. Rackesh, R. Indirajith, S. Krishnan, R. Robert, S.K.K. Pasha, K. Deshmukh, D. Sastikumar, S.J. Das, A high sensitivity isopropanol sensor based on Cr_2O_3-SnO_2 heterojunction nanocomposites via chemical precipitation route. J. Nano Sci. Nano Tech. **18**, 5454–5460 (2018)

L. Ramajo, M. Reboredo, D. Santiago, M. Castro, D. Ramajo, Computational approach of dielectric permitivities in $BaTiO_3$-epoxy composites. J. Compos. Mater. **42**, 2027–2037 (2008)

A.K. Rana, A.S. Singha, Dielectric, flammability and physico-chemical properties of surface functionalized Cannabis indica fibers reinforced composite materials. Polym. Sci. Ser. A **57**, 221–232 (2015)

P.L. Reddy, K. Deshmukh, K. Chidambaram, M.B. Ahamed, K.K. Sadasivuni, D. Ponnamma, R. Laxmipathy, D. Dayananda, S.K.K. Pasha, Effect of polyethyleneglycol (PEG) on structural, thermal and photoluminescence properties of CdO nanoparticles for optoelectronic applications. Mater. Today Proceed **9**, 175–183 (2019a)

P.L. Reddy, K. Deshmukh, K. Chidambaram, M.M.N. Ali, K.K. Sadasivuni, Y.R. Kumar, R. Lakshmipathy, S.K.K. Pasha, Dielectric properties of polyvinyl alcohol (PVA) nanocomposites filled with green synthesized zinc sulphide (ZnS) nanoparticles. J. Mater. Sci. Mater. Electron. **30**, 4676–4687 (2019b)

P.L. Reddy, K. Deshmukh, T. Kovářík, D. Reiger, N.A. Nambiraj, S.K.K. Pasha, Enhanced dielectric properties of green synthesized nickel sulphide (NiS) nanoparticles integrated polyvinylalcohol nanocomposites. Mater. Res. Exp. **7**, 064007 (2020)

M.J.M. Ridzuan, M.S.A. Majid, S.M. Hafis, K. Azduwin, The effects of alkali treatment on the mechanical and morphological properties of pennisetum purpureum/glass-reinforced epoxy hybrid composites. Plast Rubb. Comp. **46**, 421–430 (2017)

M.J.M. Ridzuan, M.S.A. Majid, A. Khasri, E.M. Cheng, Z.M. Razlan, Effect of natural filler loading, multi-walled carbon nanotubes (MWCNTs), and moisture absorption on the dielectric constant of natural filled epoxy composites. Mater. Sci. Eng. B **262**, 114744 (2020)

C. Ruan, L. Yang, Y. Li, Immuno biosensor chips for detection of escherichia coli O157:H7 using electrochemical impedance spectroscopy. Anal. Chem. **74**, 4814–4820 (2002)

N. Saba, M. Jawaid, O.Y. Alothman, M.T. Paridah, A. Hassan, Recent advances in epoxy resin, natural fiber-reinforced epoxy composites and their applications. J. Reinf. Plast. Compos. **35**, 447–470 (2016)

Sadasivuni KK, Rattan S, Deshmukh K, Muzaffar A, Ahamed MB, Pasha SKK, Mazumdar P, Waseem S, Grohens Y, Kumar B (2018) Hybrid nanofiller for value added rubber compounds for recycling. In: Kim JK, Thomas S, Saha P, Haponiuk J (eds) Rubber Recycling: Challenges and Developments, RSC Publications, 310-329.

Sankaran S, Deshmukh K, Ahamed MB, Pasha SKK (2019) Electrospun polymeric nanofibers: Fundamental aspects of electrospinning processes, optimization of electrospinning parameters, properties and applications. In: Sadasivuni KK, Ponnamma D, Mariappan R, Ahamed MB, Cabibihan JJ (eds) Polymer Nanocomposites in Biomedical Engineering Applications, Springer, 375–409.

N. Santhiarsa, S.A.A. Pratikto, E. Marsyahyo, Effects of alkali treatment and weight fraction on electrical properties of palm sugar fibre-epoxy composite. Contemp. Eng. Sci. **7**, 907–914 (2014)

A. Schönhals, F. Kremer, Broadband dielectric measurement techniques (10^{-6} Hz to 10^{12} Hz), in *Broadband Dielectric Spectroscopy*, ed. by F. Kremer, A. Schönhals, (Springer, Berlin/Heidelberg, 2003)

T.J. Singh, S. Samanta, H. Singh, Influence of Kevlar hybridization on dielectric and conductivity of bamboo fiber reinforced epoxy composite. J. Nat. Fibers **14**, 837–845 (2017)

P. Sreekumar, J.M. Saiter, K. Joseph, G. Unnikrishnan, S. Thomas, Electrical properties of short sisal fiber reinforced polyester composites fabricated by resin transfer molding. Comp. Part A Appl. Sci. Manuf. **43**, 507–511 (2012)

V.K. Thakur, R.K. Gupta, Recent progress on ferroelectric polymer-based nanocomposites for high energy density capacitors: Synthesis, dielectric properties, and future aspects. Chem. Rev. **116**, 4260–4317 (2016)

A. Triki, M. Karray, C. Poilâne, P. Picart, M. Gargouri, Dielectric analysis of the interfacial polarization of alkali treated woven flax fibers reinforced epoxy composites. J. Electrost. **76**, 67–72 (2015)
E. Tuncer, Y.V. Serdyuk, S.M. Gubanski, Dielectric mixtures: electrical properties and modelling. IEEE Trans. Dielectr. Electr. Insul. **9**, 809–828 (2002)
K.P. Unnikrishnan, E.T. Thachil, Toughening of epoxy resins, designed monomers and polymers. **9**, 129–152 (2006)
T. Väisänen, O. Das, L. Tomppo, A review on new bio-based constituents for natural fiber-polymer composites. J. Clean. Prod. **149**, 582–596 (2017)
W. Yang, L. Jiao, W. Liu, H. Dai, Manufacture of highly transparent and hazy cellulose nanofibril films via coating Tempo-Oxidized wood fibers. Nanomaterials (Basel) **9**, 107 (2019)
M. Zhan, R.P. Wool, J.Q. Xiao, Electrical properties of chicken feather fiber reinforced epoxy composites. Comp. Part A Appl. Sci. Manuf. **42**, 229–233 (2011)
S. Zhang, Y. Li, Z. Zheng, Effect of physiochemical structure on energy absorption properties of plant fibers reinforced composites: Dielectric, thermal insulation, and sound absorption properties. Compos. Commun. **10**, 163–167 (2018)
Y. Zhang, Z. Yang, T. Pan, H. Gao, H. Guan, J. Xu, Z. Zhang, Construction of natural fiber/polyaniline core-shell heterostructures with tunable and excellent electromagnetic shielding capability via a facile secondary doping strategy. Comp. Part A Appl. Sci. Manuf. **137**, 105994 (2020)

Dynamic Mechanical Analysis of Epoxy/Natural Fiber Composites

22

Ali Saeedi, Reza Eslami-Farsani, Hossein Ebrahimnezhad-Khaljiri, and Moslem Najafi

Contents

Abstract

Due to their environmentally friendly properties and proper mechanical behavior, natural fiber composites have attracted huge attentions during the recent years, and employing them for a wide range of industrial applications is on the rise. Considering the excellent mechanical properties of the epoxy resin as the host polymer, our focus in this chapter is on the natural fiber-reinforced epoxy resin composites. For employing the natural fiber composite products for different applications, a full characterization of their mechanical properties is required. Regarding the various loading and environmental conditions that may be applied on the composites, time and temperature-dependent behavior of such composite structures should be clearly determined. Among various experimental, numerical,

A. Saeedi
Faculty of Mechanical Engineering, Iran University of Science and Technology, Tehran, Iran
e-mail: asaeedi@mail.iust.ac.ir

R. Eslami-Farsani (✉) · H. Ebrahimnezhad-Khaljiri · M. Najafi
Faculty of Materials Science and Engineering, K. N. Toosi University of Technology, Tehran, Iran
e-mail: eslami@kntu.ac.ir; ebrahimnezhad-k@email.kntu.ac.ir; moslem.najafi@kntu.ac.ir

S. Mavinkere Rangappa et al. (eds.), *Handbook of Epoxy/Fiber Composites*,
https://doi.org/10.1007/978-981-19-3603-6_24

and analytical methods for investigating the mechanical properties of the composites as a function of time and temperature, dynamic mechanical analysis (DMA) method has been extensively used by the researchers. According to the literature, for the epoxy-based natural fiber composites, in addition to the fiber type, volume fraction, and geometrical shape, the bonding properties between the reinforcing fibers and the surrounding epoxy polymer significantly affect the DMA parameters for the resulting natural composites. Therefore, extensive attempts have been done in order to modify the interfacial properties in the natural fiber composites. In the following chapter, the effective parameters on the DMA properties of the natural fiber composites are investigated by reviewing some previously published results on the subject.

Keywords

Dynamic mechanical analysis · Natural fibers · Storage modulus · Loss modulus · Loss factor · Viscoelastic properties

Introduction

Recently, due to environmental issues and increasing price of petroleum products, natural fiber composites have attracted tremendous attentions in composite industries. Employing natural fibers for the design and fabrication of fiber-reinforced polymer composites (FRPs) delivers significant benefits that lead to the enhancement of physical and mechanical properties of the resulting composites (Mohammed et al. 2015; Gholampour and Ozbakkaloglu 2020). Such green reinforcement materials are renewable, recyclable, and environmentally friendly. Moreover, natural fiber composites generally are economically efficient and present lower energy consumption. However, the durability of the presented structures in their working life and their poor fire resistance and high moisture absorption are considered as the major limitations for using natural fiber composites.

Natural fibers can be sourced from animals or plants. Bamboo (Okubo et al. 2004; Thwe and Liao 2003), sugarcane bagasse (Cerqueira et al. 2011), jute (Thwe and Liao 2003; Corrales et al. 2007), kenaf (Ochi 2008; Huda et al. 2008), flax (Wang et al. 2007; Ibrahim et al. 2014), and grass (Sathishkumar et al. 2012; Rao et al. 2007) are the most common natural fibers that are recently employed in the industries. Geometrical and chemical properties of the natural fibers significantly affect the mechanical behavior of the fibers and their composites (Thwe and Liao 2003; Corrales et al. 2007). The time and temperature-dependent properties of natural fiber composites significantly affect the mechanical behavior of the products within their service life (Thomason and Yang 2011; Torres and Cubillas 2005; Demir et al. 2017; Eslami-Farsani 2015; Fathi et al. 2019). In other words, time and temperature-dependent behavior of the natural fiber composites can be considered as the most critical aspects of their performance for different applications.

Viscoelastic properties of polymers and polymer composites are generally investigated to ensure the proper performance of the products in long-term applications (Chen and Bogue 1972; Fetters et al. 1994). In fact, viscoelastic property of the composites can be considered as a tool that relates the macroscopic mechanical behaviors of the composites to the interactions between the components, such as interfacial shear strength between the reinforcing fibers and the polymeric matrix (Thomason and Yang 2011; Torres and Cubillas 2005; Demir et al. 2017; Eslami-Farsani 2015; Fathi et al. 2019). The effects of time, temperature, and loading rate (strain) on the short- and long-term behavior of composite structures can be obtained by using the viscoelastic analysis of the materials and structures. There are several experimental methods for the characterization of the viscoelastic properties of the composite structures, including creep tests (Luo et al. 2012), vibration tests (Butaud et al. 2014), mechanical indentations (VanLandingham et al. 2005), dynamic mechanical analysis (DMA) (Menard and Menard 2006; Costa et al. 2016; Jones 1999), etc. In the experimental methods, an action is applied to the structure (generally force), and the response of the specimen (generally displacement or strain) is recorded.

As an effective tool for characterizing the mechanical behavior of composite structures, DMA can be employed to examine the functionality of the composites at various ranges of the applied temperatures. In a DMA instrument, a cyclic load (tensile or flexural) with a specific frequency is applied to the specimen, and the displacement is measured using a linear variable differential transformer (LVDT) sensor. A wide range of loading frequencies and temperatures can be investigated on the mechanical behavior of composites using the DMA instrument.

Employing the natural fiber composites in various industrial applications needs a comprehensive property characterization of the natural composite products. Among the important mechanical properties of such structures, time and temperature-dependent behavior are of high importance for both short-term and long-term performance and serviceability. In the present chapter, the focus is on the DMA method for characterizing the mechanical properties of natural fiber composites. Employing the DMA method, structural parameters including the storage and loss moduli, the loss factor, and the glass transition temperature can be investigated on the polymer composites and specially natural fiber composites. The role of the composite components (fiber geometry and structure, the type of the matrix, and the interfacial behavior between the fibers and the matrix) is presented in the following sections.

Natural Fiber Composites and Their Viscoelastic Properties

Considering the proper mechanical properties and environmental aspects together introduces the natural fiber composites as the ideal candidates for a wide range of applications (Holbery and Houston 2006; Ticoalu et al. 2010). In the present chapter, the main focus is on the natural fiber-reinforced epoxy resin composites. In such composite structures, the animal- or plant-sourced fibers are being employed to

fabricate natural fiber epoxy-based composite structures. The physical and mechanical properties of the natural fibers are difficult to be modified, and they generally have complex physical and geometrical structures. However, there are some treatments that can be used to modify the surface properties of the natural fibers (Thomason and Yang 2011; Torres and Cubillas 2005; Demir et al. 2017; Eslami-Farsani 2015; Fathi et al. 2019). Therefore, a comprehensive characterization of the mechanical properties of different types of the natural fibers is required for the design and analysis of natural fiber composite structures.

The viscoelastic properties of the composites depend strongly on the interfacial properties between the host matrix and the reinforcement. In natural fiber composites, the geometrical shape and surface roughness of the fibers play a major role in defining the interfacial properties and consequently viscoelastic properties of the resulting composites. The structures of natural fibers are usually complicated and are consist of several layers (AL-Oqla et al. 2014). Generally, natural fibers are made of hollow cellulose fibrils held together by the lignin. The structure of the natural fibers should be properly characterized prior to employing them for a specific application. The fiber structure varies for different types of the plant- or animal-sourced natural fibers.

A list of the commercially available natural fibers and their chemical compositions is presented in Table 1. The chemical composition of the fibers is an effective parameter on the bonding properties between the fibers and the host matrix and should be considered in the design and analysis of natural fiber composites. The mechanical properties of some frequently used natural fibers are summarized in Table 2.

Table 1 The chemical composition of the mostly used natural fibers with the weight ratios of the cellulose, hemicellulose, lignin, and wax

Fiber	Cellulose (wt.%)	Hemicellulose (wt.%)	Lignin (wt.%)	Wax (wt.%)
Bagasse	55.2	16.8	25.3	–
Bamboo	26–43	30	21–31	–
Flax	71	18.6–20.6	2.2	1.5
Kenaf	72	20.3	9	–
Jute	61–71	14–20	12–13	0.5
Hemp	68	15	10	0.8
Ramie	68.6–78.2	13–16	0.6–0.7	0.3
Abaca	56–63	20–25	7–9	3
Sisal	65	12	9.9	2
Coir	32–43	0.15–0.25	40–45	–
Oil palm	65	–	29	–
Pineapple	81	–	12.7	–
Curaua	73.6	9.9	7.5	–
Wheat straw	38–45	15–31	12–20	
Rice husk	35–45	19–25	20	–
Rice straw	41–57	33	8–19	8–38

Reprinted with permission from AL-Oqla et al. (2014)

Table 2 Mechanical properties of some natural fibers

Fiber	Density (kg/m^3)	Tensile strength (MPa)	Elongation at (%)	Young's modulus (GPa)
Flax	1380	343–1035	1.2–3	27.6
Jute	1230	187–773	1.5–3.1	13–26.5
Hemp	1350	580–1110	1.6–4.5	70
Kenaf	1200	295–930	2.7–6.9	53
Ramie	1440	400–938	2–4	61.4–128
Sisal	1200	507–885	1.9–3	9.4–22
Pineapple	1500	170–1627	1–3	34.5–82.5
Banana	1350	529–914	3–10	8–32
Cotton	1500	287–587	7–8	5–13

Reprinted with permission from Fan and Fu (2016)

Employing the natural fibers for the fabrication of natural fiber composites has several advantages in comparison with the synthetic fiber composites. The renewability and biodegradability of the natural fibers are the main benefits that have attracted the tremendous attentions in the field of natural composites. Besides the abovementioned properties, natural composites also exhibit other advantages. For example, they can consume the greenhouse gases, and they don't produce extra greenhouse gasses after their lifetime (in comparison with burning synthetic fiber composites). Moreover, the natural fiber composites are more recyclable than the commercial composites, due to their natural structures (Bledzki and Gassan 1999).

As was previously mentioned in this chapter, employing the natural fibers in the natural composites needs a holistic characterization of the physical and mechanical properties of the fibers itself and the interfacial properties between the fibers and the surrounding matrix. Complex structure of the natural fibers makes the theoretical approach difficult to reach the exact characterization of such composites. Therefore, experimental and semi-empirical approaches can help to obtain the required mechanical properties of the natural fiber composites and make the analytical and numerical approaches more beneficial for a holistic characterization of the natural composites.

Dynamic Mechanical Analysis

Regarding the complex structure and the various ranges of applications for the natural fiber composites, it is necessary to implement an efficient analysis method for predicting the mechanical behavior of the natural fiber composites. Static and dynamic behaviors of the natural composites can be characterized by using experimental methods. Tensile, flexural, compressive, and shear tests are the most common experiments on the natural composites in static loading (Asadzadeh et al. 2012; Khalili et al. 2019). For dynamic characterization, low-velocity impact (drop-weight test), high-velocity impact, and low- and high-cycle fatigue experiments are the most frequent experimental tests (Khalili et al. 2011; Zareei et al. 2019). Moreover, some

experiments can be performed on the natural composites in order to examine the interfacial properties between the matrix and reinforcing natural fibers, including the fiber pull-out tests (Khalili and Saeedi 2017). The DMA experiment as will be described in the next session is a powerful tool for characterizing a wide range of the mechanical properties of the composite materials and structures.

The Advantages of Dynamic Mechanical Analysis

Among the various analysis techniques for evaluation of the mechanical properties of the natural fiber composites, DMA is of high interest (Menard and Menard 2006). By employing DMA method, the mechanical properties of the natural fiber composites can be determined as a function of the loading cycles (frequency) and the temperature. Therefore, the DMA method can be considered as a useful tool for characterization of both static and dynamic mechanical properties of the natural fiber composites.

Dynamic mechanical analysis can also be considered as an efficient tool for determining the viscoelastic properties of the polymers and the polymer-based composites (Menard and Menard 2006). Using the DMA experimental method, the stiffness and damping properties of the specimens can be obtained as a function of the temperature and the frequency. Moreover, the glass transition temperature of the polymers (T_g) can be accurately determined using DMA experiments.

Dynamic mechanical analysis experiment is performed by applying a sinusoidal force on the specimen. The applied force can be either axial or flexural, depending on the desired type of the test. The DMA experiments can be performed on the polymers and the polymer composites using the DMA testing machine. A sample of the DMA testing machine and its axial and torsional loading functions are presented in Fig. 1 (Menard and Menard 2006).

The DMA method is the most useful tool for characterizing the viscoelastic properties of the composites. The longtime behavior of the natural fiber composites

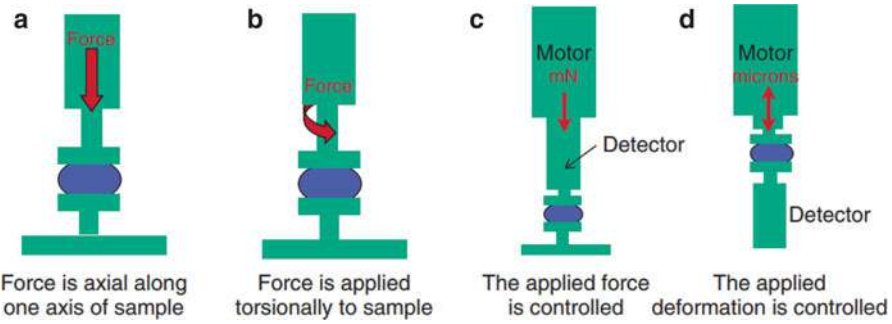

Fig. 1 A schematic of the various loading functions of the DMA testing machine: (**a**) axial loading, (**b**) torsional loading, (**c**) load control condition, and (**d**) displacement control conditions. (Reprinted with permission from Menard and Menard 2006)

can also be determined using the DMA method. In this regard, by obtaining the time-temperature shift factor for the composites, the working life of the structure under environmental and mechanical conditions can be predicted. The shift factor can be calculated by evaluating the effect of physical aging on the DMA parameters of the composites. Such an influence is achievable by accelerated tests on the composite specimens (Hafiz 2020). This test method is applicable on various types of natural fiber composites including thermoset-, thermoplastic-, and elastomer-based composites (Menard and Menard 2006).

Dynamic mechanical analysis can be performed for axial, torsional, and flexural loadings on the specimen. By employing the DMA method, the intended stiffness of the material can be obtained as a function of time (frequency) and temperature. An important advantage of the DMA method is that wide ranges of temperatures and frequencies can be applied to the test specimen. Therefore, the effect of each parameter or a combination of the parameters can be studied on the composites. It is noteworthy to mention that the DMA method can also be employed for the accelerated aging experiments to predict the expected working life of the composite structures. In this regard, the effects of the mechanical and the environmental parameters, such as loadings, working temperature, and humidity, on the viscoelastic properties of the composites are studied to predict the durability of the composite structures subjected to the abovementioned conditions (Fukushima et al. 2009). Such characterizations are critical for the designing the natural fiber composites for long-term service lives. In the following section, the most important parameters for the DMA method are presented, and afterward, the results of the DMA experiments on the various types of the natural fiber composites are reviewed.

Theoretical Aspects of the Dynamic Mechanical Analysis

A proper characterization of the mechanical properties of the natural fiber composites using the DMA method requires a good knowledge of the theoretical aspects of the DMA method. Because of this, a short review on the related parameters and definitions is presented in this section. In the following sections, the introduced parameters are used to describe the mechanical properties of the natural fiber composites.

There are several mechanical parameters that can be studied using the DMA method. The storage modulus ($\boldsymbol{E'}$) indicates the stiffness of the material. This parameter presents the tendency of the materials for storing the applied energy (Jawaid et al. 2013). The loss modulus ($\boldsymbol{E''}$) indicates the tendency of the material to dissipate the applied energy. It usually depends on the microstructural behavior of the material such as molecular motions that produce internal friction within the material. The ratio between the loss and the storage moduli is indicated by $\boldsymbol{\tan\delta}$ which is presented in Eq. 1 (Lakes and Lakes 2009):

$$\tan\delta = \frac{\boldsymbol{E''}}{\boldsymbol{E'}} \tag{1}$$

The parameter **tanδ** is expressed as the mechanical damping factor. T_g is another important parameter that can be obtained by using the DMA method. The T_g of the specimen can be defined as the temperature in which the maximum loss factor occurs.

The DMA experiments are performed by applying a cyclic stress (load) to the specimen and recording the response of the specimen to the applied actuation. The variation of the stress and the strain of the specimen with time is shown in Fig. 2. As can be seen in Fig. 2, by applying a sinusoidal force, there is a shift in the strain response of the specimen due to the viscoelastic properties of the material.

Considering the applied cyclic stress as a sinusoidal function of time, as Eq. 2:

$$\sigma(t) = \sigma_0 \sin(2\pi\upsilon t) \tag{2}$$

The strain response in the specimen (with a phase shift due to viscoelastic response) can be described by using Eq. 3 (Lakes and Lakes 2009):

$$\varepsilon(t) = \varepsilon_0 \sin(2\pi\upsilon t - \delta) \tag{3}$$

where $\boldsymbol{\sigma_0}$ and $\boldsymbol{\varepsilon_0}$ are the constant stress and strain components, respectively, t indicates the time, $\boldsymbol{\nu}$ is the frequency, and $\boldsymbol{\delta}$ is the lagging phase angle according to Fig. 3.

The phase lag between the stress and the strain response in viscoelastic materials leads to the generation of the complex stiffness ($\boldsymbol{E}^*$) for the structure. The real and imaginary parts of the complex stiffness are presented by Eq. 4.

$$\boldsymbol{E}^* = \boldsymbol{E}' + \boldsymbol{i}\boldsymbol{E}'' \tag{4}$$

where $\boldsymbol{E}'$ and $\boldsymbol{E}''$ are the frequency-dependent components of the complex modulus and are defined as the storage and loss moduli, respectively. The indicator i represents the imaginary unit. For a polymer, the variation of the storage and loss

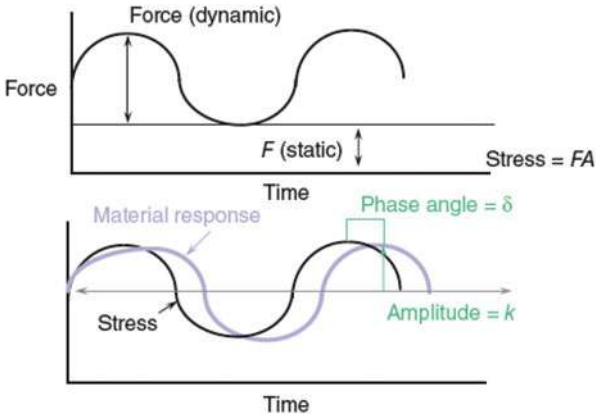

Fig. 2 The relation between the applied stress and obtained strain in the viscoelastic material which presents a phase shift between the applied force and displacement response. (Reprinted with permission from Menard and Menard 2006)

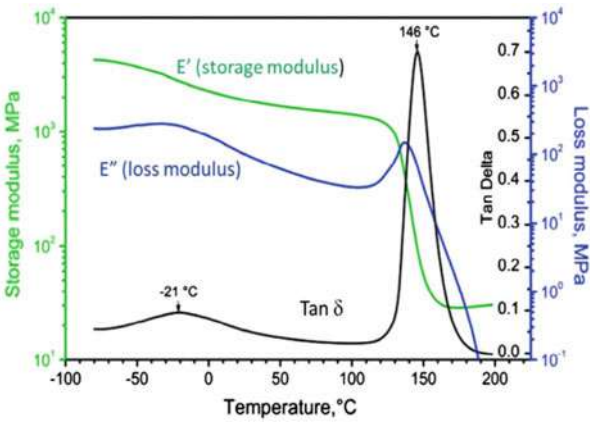

Fig. 3 The relation between the viscoelastic parameters (storage modulus, loss modulus, and loss factor) for a viscoelastic polymer. (Reprinted with permission from Saba et al. 2016)

moduli and the damping ratio (the loss factor) with temperature are illustrated in Fig. 3 (Saba et al. 2016).

The crosslinking density of polymers can also be calculated using DMA test method. For the partially crosslinked polymers, the plateau after T_g in the modulus vs temperature diagram will extend until complete failure of the polymer, while for the completely crosslinked polymers, a rise in the diagram after T_g will exist. It is noteworthy to mention that the storage modulus in the plateau region of the diagram is related to the number of crosslinks. Equation 5 can be employed for calculation of the molecular weight (M_c) between the crosslinks as follows (Barszczewska-Rybarek et al. 2017):

$$M_c = \frac{3RTd}{\boldsymbol{E}'} \tag{5}$$

where R, T, and d are the gas constants, temperature, and density of the polymer, respectively. The crosslink density (q) can now be obtained by employing Eq. 6.

$$q = \frac{M_W}{M_c} \tag{6}$$

M_W represents the molecular weight of the monomer. The degree of crystallinity is another parameter that can be obtained using DMA analysis and is reported in some research studies (Khanna 1989). The calculation of degree of crystallinity can be performed by comparing $\boldsymbol{E}'$ below and above of T_g for two types of crystalline and amorph polymer. Similar method can also be employed for the determination of the degree of crosslinking (DX) as presented in Eq. 7 (Khanna 1989).

$$DX = 1 - \frac{\Delta \log \boldsymbol{E}'}{3.22} \tag{7}$$

Along with the crosslinking density, the interfacial properties between the fibers and surrounding polymers can also be determined by using the storage modulus of the polymer and reinforcing fibers. As a well-known method for calculation of the interfacial shear stress between the fibers and the matrix, pull-out tests can be performed on the cylindrical specimens containing one fiber surrounded by the polymer. For the pull-out experiments, the interfacial shear strength is obtained from Eq. 8 (Khalili and Saeedi 2017).

$$\tau_{\max} = \left(\frac{\gamma}{2}\right)[M \ \sin h(2\gamma s) + N \ \cos h(2\gamma s)]\sigma \tag{8}$$

where

$$\gamma = \sqrt{\frac{1}{Q(1+\upsilon)}\left(\frac{S_f}{S_m} + \frac{E_m}{E_f}\right)}$$

$$Q = -0.25 + b^2\frac{2b^2 \ln\left({}^{b}\!/_{a}\right) - b^2 + a^2}{2\left(b^2 - a^2\right)}$$

$$M = -\frac{S_f E_f}{S_f E_f + S_m E_m}$$

$$N = \operatorname{csch}(\gamma s) - M \ \tan h(\gamma s) \tag{9}$$

In Eq. 9, a and b are the radii of the fiber and surrounding matrix, respectively. The cross-sectional area and storage modulus are presented by S and E. The subscripts m and f are representing matrix and fiber properties, respectively. Using Eq. 8, the effect of moduli of the matrix and fiber on the interfacial shear strength in the composites can be calculated. The presented formulation can also be employed for characterizing the interfacial properties in the natural fiber-reinforced composites.

Dynamic Mechanical Analysis of Epoxy/Natural Fiber Composites

After reviewing the important parameters related to the DMA method of the polymers and the composites, in this section, the main focus is on the DMA method for the characterization of epoxy polymer and epoxy-reinforced natural fiber composites. At first, we will have a look at the DMA characterization of the epoxy resin itself and will study the effective parameters on the mechanical behavior of the matrix phase. Afterward, the composites consisting of epoxy resin and natural fibers will be considered. In the composite specimens, as has already presented, besides the mechanical properties of the matrix and the reinforcing fibers, the interfacial behavior (interfacial shear strength) plays an important role on the overall mechanical properties of the resulting composites. Therefore, for characterizing the DMA properties of the natural fiber-reinforced epoxy resin, the most attention should be on the fiber/matrix interaction.

Dynamic Mechanical Analysis of Epoxy Resin

Epoxy resins are extensively employed in composite industries for the fabrication of high-performance composite structures. Excellent mechanical properties of the epoxy polymers as well as their temperature and corrosion resistance make the epoxy resin as the first choice for most of the composite applications. Epoxy resins have been also extensively used as the matrix for natural fiber composite structures. In general, polymer-based composite structures exhibit very high damping capacity, in comparison to traditional materials such as metals. Such vibrational properties make composite structures ideal candidates for employing in vibrational absorbers to significantly modify the natural frequencies and mode shapes of the base structures. The damping properties of the polymer-based composites can be tuned by proper selection of the effective parameters including resin and fiber material properties, reinforcement volume fraction, stacking sequence of the laminates, etc. A review on the damping properties of the polymer-based composites was presented by Treviso et al. (2015) in which the theoretical models for damping properties of composites are summarized. The mechanical properties of the epoxy resins depend on the curing process of the polymer (i.e., time and temperature of curing). The T_g for the polymers can be studied to determine their proper working temperature. By employing the DMA method, the T_g of the polymers can be obtained by a high level of accuracy. Therefore, besides evaluation of the storage and the loss moduli for the polymers or polymeric composites, determination of T_g is also of high importance for the mechanical characterization of the specimen. As was previously mentioned, the T_g of the specimen can be indicated as the temperature of maximum loss factor. The T_g can also be defined as a temperature in which a sudden drop in the storage modulus of the specimen occurs (McAninch et al. 2015; Deng et al. 2007).

For the epoxy resins, just like other thermoset polymers, the T_g depends on the curing time and curing temperature. The higher curing temperatures lead to higher T_g of the epoxy. Room temperature curing of the epoxy results in the lowest possible T_g of all for that resin. It is noteworthy to mention that T_g of the epoxy resin also strongly depends on some material parameters such as the structural features of the resin and hardener and also the resin-to-hardener ratio. Moreover, for most of aliphatic hardeners, complete curing occurs at room temperature. However, for a resin and hardener system, if the curing is not completed at the room temperature, then a higher T_g will be achieved for curing at an elevated temperature. A sample of experimental DMA results for epoxy resin is demonstrated in Fig. 4 (Sperandio et al. 2010).

Dynamic Mechanical Analysis of Natural Fiber/Epoxy Composites

In this section, the dynamic mechanical properties of the natural fiber-reinforced epoxy resin are considered, and some investigations on the DMA parameters of the abovementioned composites are reviewed. Regarding the complicated structure and surface roughness of the natural fibers, the interfacial properties should be thoroughly studied using experimental, theoretical, or numerical methods.

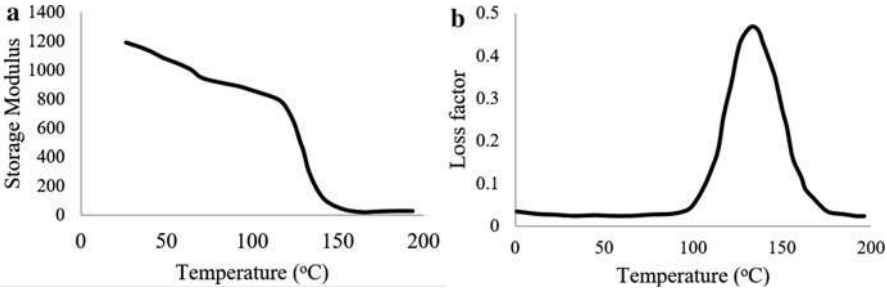

Fig. 4 (**a**) Storage modulus and (**b**) loss factor of epoxy resin obtained by DMA experiments. (Extracted from Sperandio et al. (2010)

A general review on the DMA properties of the natural fiber-reinforced polymer composites has been presented by Saba et al. (2016). They have studied the recent experimental works on the natural composites with various host polymers including thermosets, thermoplastics, and hybrid polymers.

There are several geometrical, physical, and mechanical properties that affect the DMA properties of the natural fiber composites. Some of the most effective parameters are as follows:

- The type of the polymer matrix and reinforcing fibers
- The geometrical shape of the reinforcements (fibers, particles, plates)
- The length or aspect ratio of the reinforcing fibers (long fibers, short fibers)
- The surface roughness of the reinforcements
- The volume fraction of the reinforcements within the composites
- The curing procedure (time and temperature) for the composites
- The modifications of bonding behavior between the fibers and the host matrix

One or more effective parameters were considered in each published investigation on the DMA properties of the polymer-based composites and especially natural fiber-reinforced epoxy composites.

In this section, we concentrate on the DMA properties of the natural fiber-reinforced epoxy composites. In Table 2, some previously published experimental studies on the natural fiber-reinforced epoxy composites are presented. Various types of the reinforcing natural fibers have been investigated in the previous works, as are presented in Table 3. In some of the investigations, a combination of the reinforcing fibers has been employed that resulted in hybrid natural fiber composites. Moreover, in some of the experiments, different geometrical arrangements of a specific type of natural fibers are investigated. As an example, in an experimental study, De Rosa et al. (2010) investigated the DMA properties of the *Phormium tenax* leaf fiber-reinforced epoxy resin composites. They fabricated two types of the natural fiber composites arranged as either short fibers or quasi-unidirectional ones and compared their mechanical properties.

Table 3 A list of the previously published investigations on the DMA properties of the natural fiber-reinforced epoxy polymer composites

Reference	Reinforcement type	Resin type	Laminate type	Treatment	Test method
Towo and Ansell (2008)	Sisal fiber	Epoxy Ly5052	Short-fiber composites	NAOH treatment	Single cantilever mode
De Rosa et al. (2010)	*Phormium tenax* leaf fiber	Epoxy Ampreg 26	Random fiber molding	–	Tensile, 3-point bending
Margem et al. (2010)	Ramie fiber	Epoxy DGBA	Short-fiber composites	–	3-point bending DMA
Mylsamy and Rajendran (2011)	Treated and untreated agave continuous fiber	Epoxy 3554A	Short-fiber composites	Alkali treatment	3-point bending
Jawaid et al. (2013)	Oil palm empty fruit bunch fiber	Epoxy A331	Bi-layer composites	–	3-point bending DMA
Suresh Kumar et al. (2014)	Untreated and treated coconut sheath fiber	Epoxy Ly556	Five-layered composite	Sodium hydroxide and acetic acid	3-point bending DMA
Duc et al. (2014)	UD and twill 2/2 flax fiber	Epoxy L235	UD, Twill, [0/90]	–	Single cantilever mode
Ram et al. (2018)	Palmyra sprout fiber	Epoxy	Random fiber hand lay-up	–	3-point bending
Prasob and Sasikumar (2019)	Jute fibers	Epoxy LY556	Random fiber hand lay-up	–	3-point bending
	Flax woven	Epoxy VBR8912	Four-layered composites	Alkali and silane treatment	3-point bending
Gargol et al. (2021)	Waste hemp fibers	Epoxy Epidian 5	Short-fiber composites	–	3-point bending

In the following sections, we will have a closer look with more details on the obtained results for the DMA properties of the natural fiber-reinforced composites with various reinforcement fibers and various types of the epoxy resins.

Sisal Fiber-Reinforced Epoxy Resin

Tensile, fatigue, and DMA properties of the sisal fiber-reinforced epoxy resins were studied experimentally by Towo and Ansell (2008). The fabricated specimens were first subjected to fatigue loading at the loading levels of 75, 60, 50, and 35% of the static tensile strength. The failed specimens after fatigue tests were subjected to the dynamic mechanical thermal experiments to study the effect of loading on the

glass transition temperature of the composites. Their experiments were performed at a frequency of 1 Hz and the temperature rate of 2 °C/min. The temperature range was selected to be between a minimum temperature of −50 °C and a maximum temperature of 180 °C. The minimum temperature was chosen to be well below the T_g of the resin matrix, while the maximum temperature was selected due to the deterioration of sisal fibers at higher temperatures.

The storage modulus diagram for the specimens subjected to different levels of fatigue loading is presented in Fig. 5. The variations of the storage modulus for the specimens subjected to fatigue tests show a shift to the left of the un-fatigued specimen for the untreated sisal fiber epoxy matrix composites. This shift indicates the reduction in the glass transition temperature of the untreated fiber composites subjected to fatigue tests. In order to improve the interfacial properties between the sisal fibers and the epoxy resin, a modification method was considered. In this regard, the sisal fibers were treated by NaOH solution for the surface modifications. The effect of the treating process on the storage modulus of the fatigued specimens is shown in Fig. 6. According to their obtained results, the glass transition temperature for the fatigued untreated composite specimens ranges from 75 to 82.5 °C, while that for the fatigued treated specimens ranges from 106.25 to 115 °C. From the obtained results, the authors concluded that T_g for fatigued treated specimens shows a smaller shift in comparison with fatigued untreated specimens. Therefore, it is obvious that the treatment has modified the resin to fiber bundle interface (Towo and Ansell 2008).

Ramie Fiber-Reinforced Epoxy Resin

Ramie fibers that are categorized as a plant-sourced natural fiber exhibit excellent mechanical properties for being used in the polymer-based composites. This type of fiber is extracted from the stem of the ramie plant. Figure 7 shows the ramie-extracted ramie fibers for composite fabrications (Giridharan 2019). In recent years, some experimental investigation has been done on employing ramie fibers

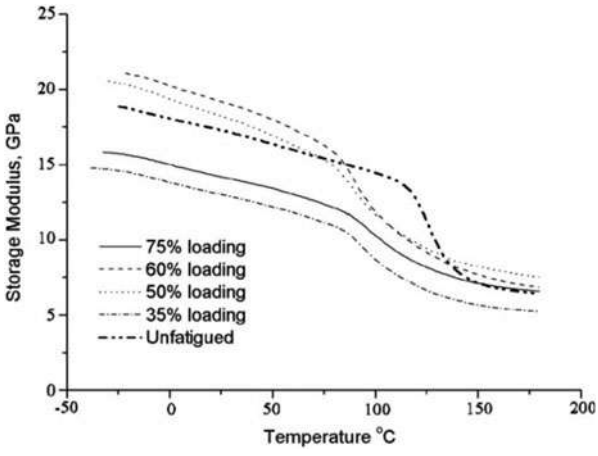

Fig. 5 The variations of the storage modulus of the fatigued and un-fatigued specimens with temperature for the untreated sisal fiber-reinforced epoxy natural composites. (Reprinted with permission from Towo and Ansell (2008))

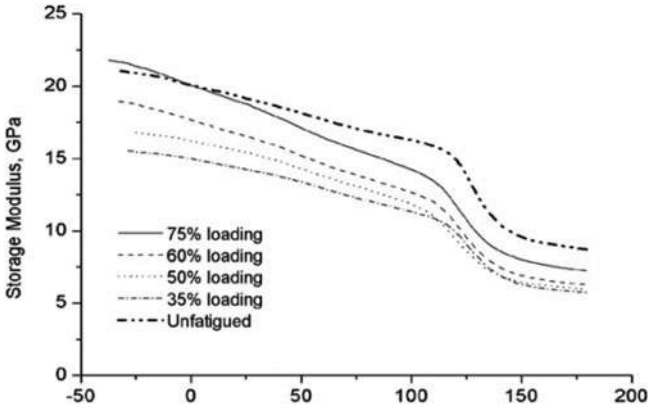

Fig. 6 The variations of the storage modulus of the fatigued and un-fatigued specimens with temperature for the treated sisal fiber-reinforced epoxy natural composites. (Reprinted with permission from Towo and Ansell (2008)

Fig. 7 The long ramie fibers for reinforcing composites. (Reprinted with permission from Giridharan 2019)

as the reinforcements in composites (Park et al. 2006; Nam and Netravali 2006a; Nam and Netravali 2006b). Margem et al. (2010) performed an experimental study to investigate the dynamic mechanical parameters of ramie fiber-reinforced epoxy matrix composites. They fabricated the DMA test specimens containing 0 to 30 wt.% of the ramie fibers and investigated DMA parameters.

The variation of the storage modulus with the ramie fiber content was reported as a function of temperature as shown in Fig. 8. Their obtained results showed that the storage modulus increased by increasing the fiber content at all temperatures. For example, at 25 °C, an enhancement of 113% was observed for the storage modulus of 30% ramie fiber-reinforced epoxy composites, in comparison with the neat epoxy resin. They also studied the variations of the loss modulus and **tanδ** with the temperature. According to the reported results, the loss modulus curves showed broad peaks with distinct amplitude and temperature positions, as compared to the neat epoxy peak. These can be related to the α peak and suggest a more complex structural relaxation behavior by the composites. According to Mohanty et al.

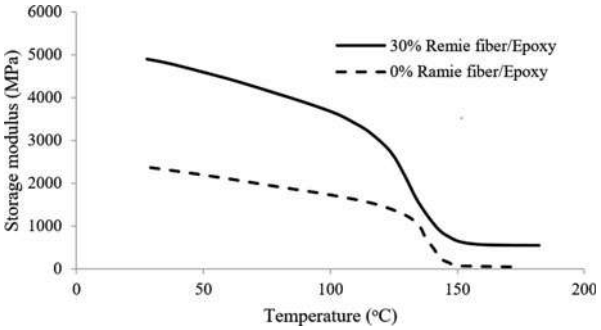

Fig. 8 The variation of storage modulus for ramie fiber-reinforced epoxy. (Extracted from Margem et al. (2010)

(2006), such relaxation can be related to the chain mobility of the polymeric matrix. In addition, the movement of the peaks to the lower temperatures occurs due to increase in flexibility of the polymer chains.

Treated and Untreated Agave Continuous Fiber

Agave fibers are one of the mostly used types of the natural fibers in the textile industry. Agaves are succulent plants of a large botanical genus of the same name, belonging to the family Agavaceae (Mylsamy and Rajendran 2011). In recent years, utilizing the agave fiber in polymer composites for the fabrication of the natural fiber agave/polymer composites has been considered. An experimental example is the study performed by Mylsamy and Rajendran (2011) on the mechanical properties of agave fiber-reinforced epoxy composites. In their study, the effect of fiber geometry (long or short fibers) and fiber treatment (for improvement in the bonding behavior between the fibers and the matrix) was considered.

Mylsamy and Rajendran (2011) conducted an experimental study on the mechanical properties of alkali treated continuous agave fiber-reinforced epoxy composite (TCEC) and untreated continuous agave fiber-reinforced epoxy composite (UTCEC). The preparation of the natural fibers is as follows: After harvesting the agave leaves, they were dried naturally to remove excess moisture. Retting of the leaves was performed by immersing them in water. Afterward, the leaves were manually beaten to remove the flesh. Moreover, for modifying the fiber surfaces for an enhanced debonding with the surrounding polymers, the fibers were treated chemically. In this regard, the raw agave fiber was washed and then was immersed in 5% sodium hydroxide solution and after 30 min washed with very dilute hydrochloric acid (HCl) to remove the excess alkali. The resulting treated agave fibers were prepared for being employed in the fabrication of the agave/epoxy natural composites.

The DMA parameters for the two types of the abovementioned composites (TCEC and UTCEC) are shown in Fig. 9. Their obtained results revealed that the movement of polymer chains is highly influenced by the presence of fibers, which in turn influenced the elastic characteristics of the epoxy (Mylsamy and Rajendran 2011).

The amount of E'' of TCEC increases by 10%, due to alkali treatment of fiber, compared to those UTCEC specimens.

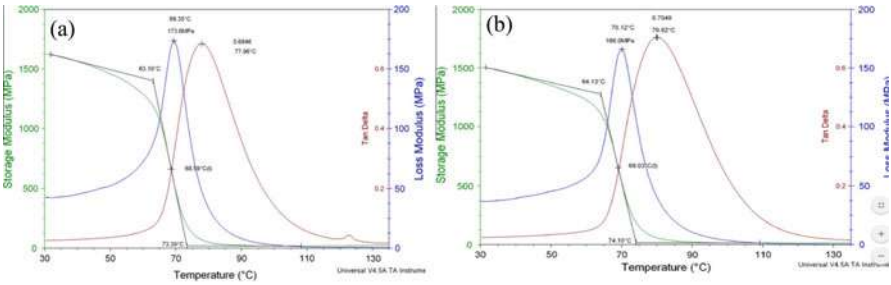

Fig. 9 Dynamic mechanical analysis (DMA) parameters for (**a**) alkali treated continuous agave fiber-reinforced epoxy composite (TCEC) and (**b**) untreated continuous agave fiber-reinforced epoxy composite (UTCEC). (Reprinted with permission from Mylsamy and Rajendran 2011)

Oil Palm Empty Fruit Bunch Fiber-Reinforced Epoxy

Of the other most usable natural fibers for reinforcing composites, oil palm fibers and jute have been utilized in recent years for reinforcing different types of polymers. An investigation on the abovementioned fibers with the epoxy for examining the mechanical properties of the resulting composites, especially the DMA parameters, is described as follows:

Jawaid et al. (2013) conducted an experimental study on the DMA properties of epoxy-based hybrid composites reinforced with jute and oil palm fibers. They employed 3-point bending mode of the DMA test with the frequency of 1 Hz and the temperature range between -150 and 150 °C. The variations of the storage modulus, loss modulus, and loss factor, with the jute weight fraction, are illustrated in Figs. 10, 11, and 12, respectively. The effects of the different ratios between the oil palm empty fruit bunch (EFB) and jute fibers are considered on the results at the frequency of 1 Hz.

The reported results revealed that by increasing jute fiber content in the hybrid composites, the interfacial properties between the fibers and the matrix are improved, due to more efficient stress transfer within the composites. Moreover, by increasing the jute fiber volume fraction in the specimens, the loss modulus increased, and a reduction in the rubbery stage was observed. The lower $\tan\delta$ in the hybrid composites shows lower damping and enhanced interfacial properties in the composites.

Coconut Sheath Fiber-Reinforced Epoxy Resin

The coconut sheath fibers can be considered as huge waste plant-based material. Finding a proper way for utilizing this type of the fibers for the industrial applications is of high interest. Employing the coconut sheath fibers for reinforcing the polymers and the polymer composites (for hybrid composites) can be considered as a proper solution. Regarding the main focus of the current chapter which is on the epoxy-based composites, an experimental study on the coconut sheath fiber-reinforced epoxy resin is explained. Just like other types of the natural fibers, the bonding properties between the coconut sheath fibers and epoxy resin are a major issue.

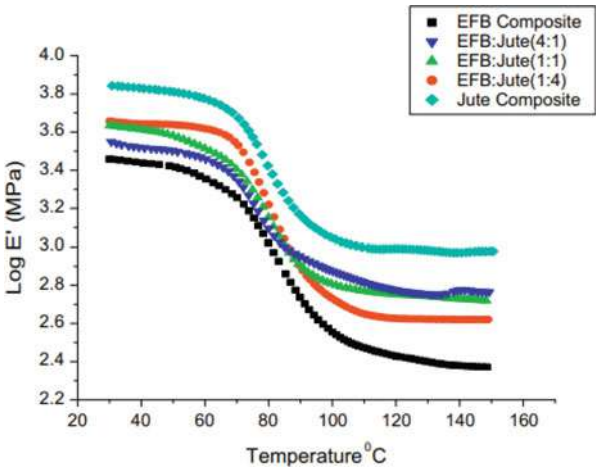

Fig. 10 The variations of storage modulus with the temperature for different relative weight fractions between the oil palm empty fruit bunch (EFB) and the jute fibers at the frequency of 1 Hz. (Reprinted with permission from Jawaid et al. 2013)

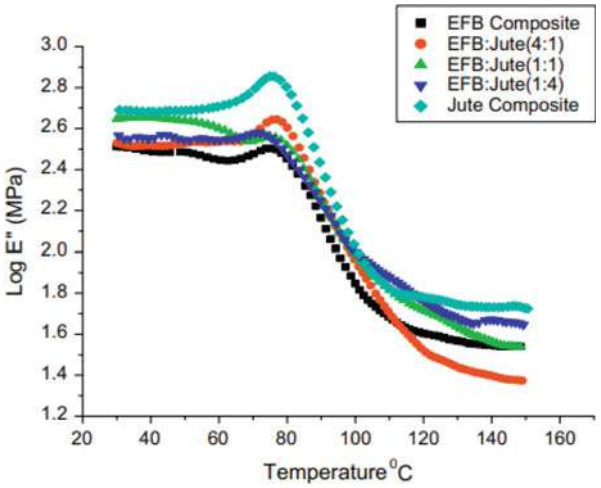

Fig. 11 The variations of loss modulus with the temperature for different relative weight fractions between the oil palm empty fruit bunch (EFB) and the jute fibers at the frequency of 1 Hz. (Reprinted with permission from Jawaid et al. 2013)

An experimental study on the DMA parameters of the coconut sheath fiber-reinforced epoxy resin was conducted by Suresh Kumar et al. (2014). They investigated the effect of two reinforcing types of untreated coconut sheath-reinforced epoxy (UTCSE) and treated coconut sheath-reinforced epoxy (TCSE) on the mechanical properties of the composites. Figure 13 shows the geometrical configuration for the DMA experiments.

Figure 14 demonstrates the changes in the storage modulus with temperature for different types of the specimens (UTCSE and TCSE). According to the reported results, TCSE specimens exhibit higher storage modulus in comparison

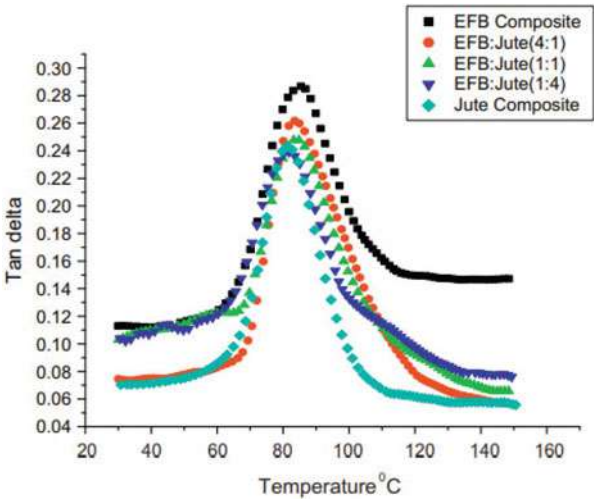

Fig. 12 The variations of the loss factor with the temperature for different relative weight fractions between the oil palm empty fruit bunch (EFB) and the jute fibers at the frequency of 1 Hz. (Reprinted with permission from Jawaid et al. 2013)

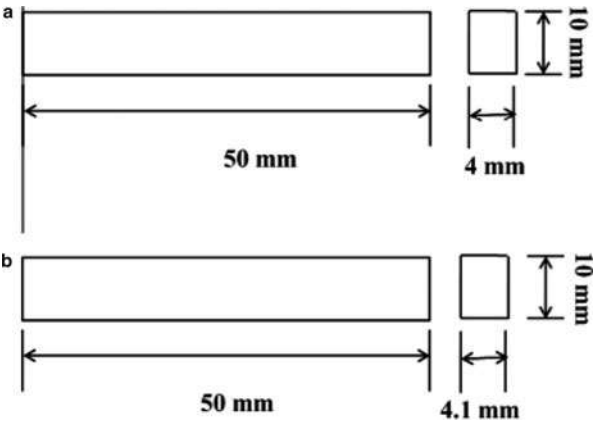

Fig. 13 The DMA test specimen geometry for (**a**) untreated coconut sheath-reinforced epoxy (UTCSE) and (**b**) treated coconut sheath-reinforced epoxy (TCSE). (Reprinted with permission from Kumar et al. 2014)

to UTCSE specimens. Such an improvement occurs because of the creation of hydrogen bonding and packing of the cellulose chain in TCSE composites (Kumar et al. 2014).

Figure 15 illustrates the variation of tanδ with temperature for UTCSE composite and TCSE composites. The frequency of the experiment is 1 Hz. According to the results, the treated fibers showed reduced tanδ in comparison with untreated fibers. The main reason for this phenomenon is the restricted movement of polymeric molecules in TSCE specimens. The reduction in tanδ for TSCE composites shows higher interfacial properties compared to UTSCE specimens (Kumar et al. 2014).

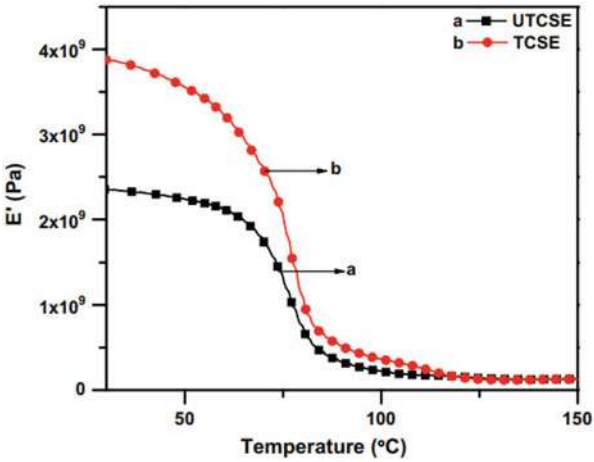

Fig. 14 The variations of the storage modulus with the temperature for the untreated coconut sheath-reinforced epoxy (UTCSE) and treated coconut sheath-reinforced epoxy (TCSE) composite specimens at the frequency of 1 Hz. (Reprinted with permission from Kumar et al. 2014)

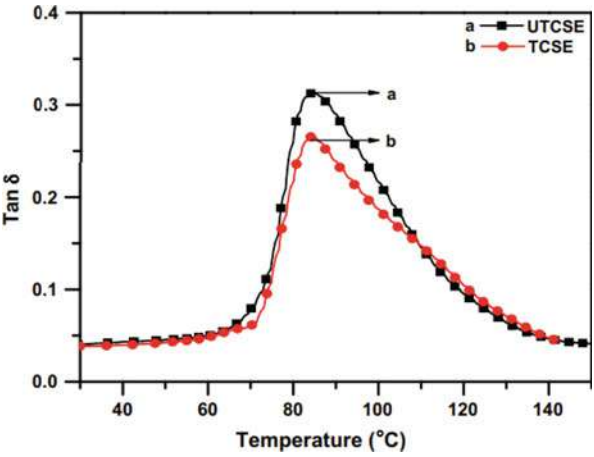

Fig. 15 The variations of the loss factor with the temperature for the untreated coconut sheath-reinforced epoxy (UTCSE) and treated coconut sheath-reinforced epoxy (TCSE) composite specimens at the frequency of 1 Hz. (Reprinted with permission from Kumar et al. 2014)

Flax Fiber-Reinforced Epoxy Resin

For the most of natural fibers, it is required to use spinning methods to fabricate the strong yarns for the reinforcement applications. The spinning parameters such as twisting can be significantly effective on the obtained results from the resulting composites. In this regard, Duc et al. (2014) employed the DMA method to evaluate the temperature-dependent mechanical properties of flax fiber-reinforced epoxy composites. They prepared six types of the textile fabrics for their specimens, as illustrated in Fig. 16, and their configurations are presented in Table 4. Different types of the fabrics with the specified spinning and sizing parameters are named FP, FD, FT, P, B, and H. UD and TW are representatives for unidirectional and twill fabrics.

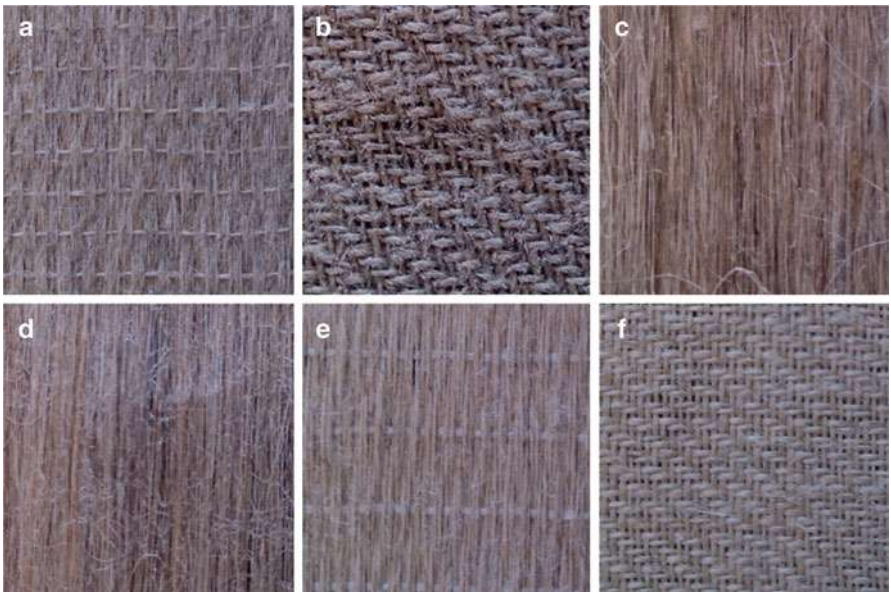

Fig. 16 The various textile fabrics types: (**a**) FP_UD, (**b**) FP_TW, (**c**) FT_UD, (**d**) P_UD, (**e**) B_UD, and (**f**) H_TW. (Reprinted with permission from Duc et al. 2014)

Table 4 The properties of the fabricated textile fabrics and their spinning parameters

Fabrics	Architecture	Twist angle (°)	Epoxy sized fabrics	FAW (g/m^2)
FP	Quasi-UD	13	Yes	180
FP	TW	13	Yes	300
FD	Quasi-UD	13	No	180
FT	UD	0	No	200
P	UD	0	Yes	122
B	Quasi-UD	13	No	300
H	TW	16	No	200

Reprinted with permission from Duc et al. (2014)

The storage modulus and the loss factor for the previously introduced specimens are presented in Fig. 17. According to the results, employing TW fabrics leads to the reduction of the storage modulus of the composites due to the crimp effect. In TW specimens, less sliding behavior between the fiber and matrix caused that for the temperatures above T_g, the storage modulus of TW composites was higher than that of the 0/90 composites. Figure 18 demonstrates the loss factor of different specimens at the frequency of 1 Hz. According to the results, there is no significant variation in the peak value between UD and 0/90 composites. The lower loss factor of the TW composites is due to material stiffening related to the limited sliding behavior as was previously introduced (Duc et al. 2014).

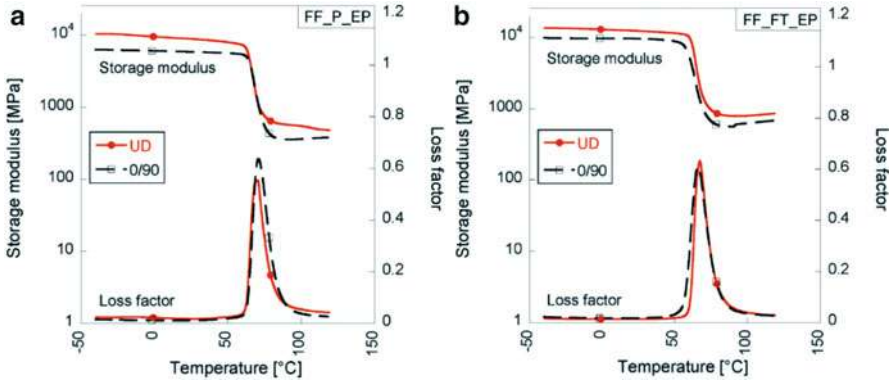

Fig. 17 The variation of the storage modulus and loss factor with the time for (**a**) FF_P_EP_UD and FF_P_EP_0/90 and (**b**) FF_FT_EP_UD and FF_FT_0/90 at the frequency of 1 Hz. (Reprinted with permission from Duc et al. 2014)

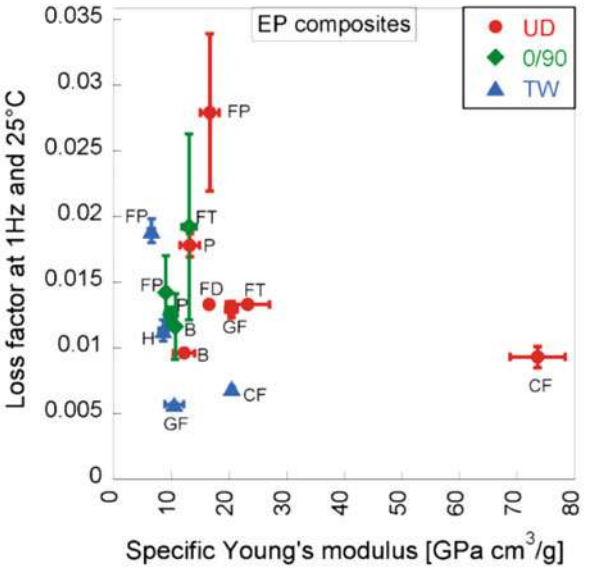

Fig. 18 The variations of loss factor with the specific Young's modulus for the different types of the flax fiber-reinforced epoxy composites. (Reprinted with permission from Duc et al. 2014)

Future Works

By studying the available investigations on the DMA parameter of the natural fiber composites, it is revealed that so far, valuable research studies on the effective parameters which can significantly improve the mechanical properties of the natural fiber composite structures have been conducted. However, there is still a long way

toward obtaining the optimum mechanical properties along with the high economic efficiency. The possible modifications that can be considered for the future improvements can be categorized as follows:

– Improvement in the mechanical properties of the natural fibers

The tensile mechanical properties of the fibers can be enhanced during the fabrication process of the fibers. By modifying the twisting parameters of the fiber clusters in the spinning process, the optimum mechanical properties of the yarns can be expected. Moreover, the woven fabrics which are produced by the natural fibers can be subjected to optimization process for obtaining the best performance. Numerical methods, especially finite element method (FEM), are the proper tools for performing such optimization and enhancing the overall mechanical properties of the natural fibers.

– Enhancement of the bonding properties between the natural fibers and the host polymer

As was previously mentioned within the present chapter, the interfacial properties are the best candidate for being improved in order to obtain the enhanced mechanical properties of the natural fiber-reinforced epoxy polymer composites. Several physical and mechanical techniques can be utilized for improving the bonding properties between the fibers and the matrix. Among them, the chemical treatment method has been extensively used in the previously published investigations. However, other effective methods can be examined. Modifying the coating type of the fibers in the manufacturing process can be considered as a solution. Another modification method could be mechanical modifications of the fibers by means of indentation. As another effective modification method, addition of the nanoparticles to the interface or to the host polymers by the well-known dispersion methods may lead to significant enhancements in the bonding properties and consequently on the overall mechanical properties of the resulting natural composite structure.

– Fabrication of the hybrid composites with multi-functional behavior

In order to achieve the modified mechanical properties from the natural fibers, hybridization techniques can be considered. In this regard, different types of the natural fibers can be hybridized in the fiber fabrication process or later in the composite manufacturing step. Moreover, a combination of the natural fibers and the common synthetic fibers can be considered for obtaining the enhanced mechanical properties of the natural composites. In addition, as was mentioned earlier in this section, nanoscale materials can be utilized in the natural fiber composites to improve the load transfer and consequently macroscopic mechanical properties of the multi-scale natural composites. It is noteworthy to mention that along with the mechanical properties of the structure, other limitations of the natural composites can be treated using the micro- and nano-sized reinforcements (Shokrieh et al. 2014).

Enhancements in the fire resistance of the natural composites and their corrosion resistance, electrical performance, aging parameters, etc. are the examples of nano- or microhybridization.

Conclusion

The natural composites generally consist of one or more types of the natural fibers and a synthetic polymer as the host matrix. So far, various animal- and plant-sourced fibers with different physical and mechanical properties have been used as the reinforcements in natural composites. The DMA test apparatuses are able to apply axial, torsional, and flexural cyclic loads on the test specimens and record the structural response of the composites to the applied loads. By employing the DMA method for characterizing the natural composites, the storage modulus, the loss modulus, and the loss factor for the composites can be obtained over a wide range of the temperatures and frequencies. The dynamic mechanical analysis parameters for the natural fiber-reinforced epoxy composites have been studied in the present chapter. Coconut sheath, jute, kenaf, flax, grass, and bamboo are of the most common natural fiber sources for the reinforcing purposes. The storage modulus, the loss modulus, the loss factor, and the glass transition temperature of the natural composites as the functions of time and temperature are presented for different types of natural fiber-reinforced epoxy polymers. By reviewing the previously published results on the DMA parameters of the natural fiber-reinforced epoxy resin, the most effective parameters were the geometrical shape of the reinforcing fibers (long or short fibers) and the interfacial properties between the reinforcing natural fibers and the surrounding epoxy resin. According to the available research results on the DMA parameters of the natural fiber-reinforced epoxy composites, some conclusions can be extracted. In the following, the main results of the experimental studies are summarized:

- The glass transition temperature of the natural composites that indicates the bonding properties of the fiber-matrix interface can be significantly affected by the applied loading conditions. In this regard, the results revealed that fatigue loading has modified the resin to fiber bundle interface to such an extent that the apparent glass transition temperature is shifted downward.
- For the natural fiber composites, like other types of the polymer-based composite structures, increasing the volume fraction of the reinforcing fibers leads to the improvement in the storage modulus of the resulting composite structure. The reported experimental results on the DMA properties of the natural fiber-reinforced composites revealed that the movement of polymer chains in the matrix phase is highly influenced by the presence of fibers, which in turn influenced the elastic characteristics of the epoxy.
- Utilizing natural fibers for reinforcing epoxy resin leads to a complex structural relaxation behavior in the composites. Such relaxation can be attributed to the chain mobility of the polymeric matrix. In addition, the translation of the peaks of

the loss factor diagram to lower temperatures occurs due to increase in flexibility of the polymer chains.

– The experimental results revealed that in the natural fiber composites, the interfacial properties between the fibers and the matrix can be improved, by hybridizing the reinforcements and employing the second type of reinforcing fibers for more efficient stress transfer within the composites. By using such hybridization method, the loss modulus increased, and a reduction in the rubbery stage was observed.
– The bonding properties between the natural fibers and epoxy polymer and consequently the DMA parameters are influenced by the spinning method. The spinning process which is performed on the fiber clusters to produce the yarns can be effective on the sliding behavior between the reinforcing fibers and matrix. By modifying the twisting parameters for the fibers and by utilizing fiber treatments as the secondary modification process, the sliding behavior can be limited, and therefore, the DMA parameters of the resulting natural fiber composites (especially the loss factor and glass transition temperature) can be improved.

References

F.M. AL-Oqla, O.Y. Alothman, M. Jawaid, S. Sapuan, M. Es-Saheb, Processing and properties of date palm fibers and its composites, in *Biomass and Bioenergy*, (Springer, 2014), pp. 1–25

M. Asadzadeh, S. Khalili, R. Eslami Farsani, S. Rafizadeh, Bending properties of date palm fiber and jute fiber reinforced polymeric composite. ADMT J. **5**(4) (2012)

I.M. Barszczewska-Rybarek, A. Korytkowska-Wałach, M. Kurcok, G. Chladek, J. Kasperski, DMA analysis of the structure of crosslinked poly (methyl methacrylate) s. Acta Bioeng. Biomech. **19**(1) (2017)

A.K. Bledzki, J. Gassan, Composites reinforced with cellulose based fibres. Prog. Polym. Sci. **24** (1999)

P. Butaud, M. Ouisse, V. Placet, E. Foltête, Experimental investigations on viscoelastic properties of a shape memory polymer, in *Smart Materials, Adaptive Structures and Intelligent Systems*, (American Society of Mechanical Engineers, 2014), p. V001T001A029

E. Cerqueira, C. Baptista, D. Mulinari, Mechanical behaviour of polypropylene reinforced sugarcane bagasse fibers composites. Proc. Eng. **10**, 2046–2051 (2011)

I.J. Chen, D. Bogue, Time-dependent stress in polymer melts and review of viscoelastic theory. Trans. Soc. Rheol. **16**(1), 59–78 (1972)

F. Corrales, F. Vilaseca, M. Llop, J. Girones, J.A. Mendez, P. Mutje, Chemical modification of jute fibers for the production of green-composites. J. Hazard. Mater. **144** (2007)

C. Costa, A.C. Fonseca, A.C. Serra, J.F.J. Coelho, Dynamic mechanical thermal analysis of polymer composites reinforced with natural fibers. Polym. Rev. **56** (2016)

I.M. De Rosa, C. Santulli, F. Sarasini, Mechanical and thermal characterization of epoxy composites reinforced with random and quasi-unidirectional untreated Phormium tenax leaf fibers. Mater. Des. **31**(5), 2397–2405 (2010)

B. Demir, L.C. Henderson, T.R. Walsh, Design rules for enhanced interfacial shear response in functionalized carbon fiber epoxy composites. ACS Appl. Mater. Interfaces **9**(13), 11846–11857 (2017)

S. Deng, M. Hou, L. Ye, Temperature-dependent elastic moduli of epoxies measured by DMA and their correlations to mechanical testing data. Polym. Test. **26**(6), 803–813 (2007)

F. Duc, P.-E. Bourban, J.-A.E. Månson, Dynamic mechanical properties of epoxy/flax fibre composites. J. Reinf. Plast. Compos. **33**(17), 1625–1633 (2014)

R. Eslami-Farsani, Effect of fiber treatment on the mechanical properties of date palm fiber reinforced PP/EPDM composites. Adv. Compos. Mater. **24**(1), 27–40 (2015)
M. Fan, F. Fu, *Advanced High Strength Natural Fibre Composites in Construction* (Woodhead Publishing, 2016)
H. Fathi, M. Shokrieh, A. Saeedi, A theoretical and experimental investigation on the stress distribution in the interface of pre-strained SMA wire/polymer composites. Compos. Part B **175**, 107100 (2019)
L. Fetters, D. Lohse, D. Richter, T. Witten, A. Zirkel, Connection between polymer molecular weight, density, chain dimensions, and melt viscoelastic properties. Macromolecules **27**(17), 4639–4647 (1994)
K. Fukushima, H. Cai, M. Nakada, Y. Miyano, Determination of time-temperature shift factor for long-term life prediction of polymer composites, in *Proceedings of ICCM*, (2009)
M. Gargol, T. Klepka, Ł. Klapiszewski, B. Podkościelna, Synthesis and thermo-mechanical study of epoxy resin-based composites with waste fibers of hemp as an eco-friendly filler. Polymers **13**(4), 503 (2021)
A. Gholampour, T. Ozbakkaloglu, A review of natural fiber composites: Properties, modification and processing techniques, characterization, applications. J. Mater. Sci., 1–64 (2020)
R. Giridharan, Preparation and property evaluation of Glass/Ramie fibers reinforced epoxy hybrid composites. Compos. Part B **167**, 342–345 (2019)
T. Hafiz, Life prediction of carbon fiber reinforced polymers using time temperature shift factor. Int. J. Eng. **33**(7), 1340–1346 (2020)
J. Holbery, D. Houston, Natural-fiber-reinforced polymer composites in automotive applications. JOM **58**(11), 80–86 (2006)
M.S. Huda, L.T. Drzal, A.K. Mohanty, M. Misra, Effect of fiber surface-treatments on the properties of laminated biocomposites from poly (lactic acid)(PLA) and kenaf fibers. Compos. Sci. Technol. **68**(2), 424–432 (2008)
H. Ibrahim, M. Farag, H. Megahed, S. Mehanny, Characteristics of starch-based biodegradable composites reinforced with date palm and flax fibers. Carbohydr. Polym. **101**, 11–19 (2014)
M. Jawaid, H.A. Khalil, A. Hassan, R. Dungani, A. Hadiyane, Effect of jute fibre loading on tensile and dynamic mechanical properties of oil palm epoxy composites. Compos. Part B **45**(1), 619–624 (2013)
D.S. Jones, Dynamic mechanical analysis of polymeric systems of pharmaceutical and biomedical significance. Int. J. Pharm. **179**(2), 167–178 (1999)
S. Khalili, A. Saeedi, Experimental investigation on the debonding strength in shape memory alloy wire reinforced polymers. Mech. Adv. Mater. Struct. **24**(6), 490–495 (2017)
S. Khalili, R.E. Farsani, S. Rafiezadeh, An experimental study on the behavior of PP/EPDM/JUTE composites in impact, tensile and bending loadings. J. Reinf. Plast. Compos. **30**(16), 1341–1347 (2011)
S. Khalili, R. Eslami-Farsani, A.A. Jaferzadeh Khoramabadian, S. Hayati, Investigation of tensile characteristics of an epoxy matrix composite with uni-directional and hybrid tissue natural hemp fibers. Mech. Adv. Compos. Struct. **6**(2), 181–190 (2019)
Y. Khanna, Estimation of polymer crystallinity by dynamic mechanical techniques. J. Appl. Polym. Sci. **37**(9), 2719–2726 (1989)
S.S. Kumar, D.A. Duraibabu, K. Subramanian, Studies on mechanical, thermal and dynamic mechanical properties of untreated (raw) and treated coconut sheath fiber reinforced epoxy composites. Mater. Des. **59**, 63–69 (2014)
S.V. Kumar, K.S. Kumar, H.S. Jailani, G. Rajamurugan, Mechanical, DMA and sound acoustic behaviour of flax woven fabric reinforced epoxy composites. Mater. Res. Exp. **7**(8), 085302 (2020)
R. Lakes, R.S. Lakes, *Viscoelastic Materials* (Cambridge University Press, 2009)
W. Luo, C. Wang, X. Hu, T. Yang, Long-term creep assessment of viscoelastic polymer by time-temperature-stress superposition. Acta Mechanica Solida Sinica **25**(6), 571–578 (2012)

F.M. Margem, S.N. Monteiro, J.B. Neto, R.J.S. Rodriguez, B.G. Soares, The dynamic-mechanical behavior of epoxy matrix composites reinforced with ramie fibers. Revista Materia **15**(2), 167–175 (2010). https://doi.org/10.1590/s1517-70762010000200012

I.M. McAninch, G.R. Palmese, J.L. Lenhart, J.J. La Scala, DMA testing of epoxy resins: The importance of dimensions. Polym. Eng. Sci. **55**(12), 2761–2774 (2015)

K.P. Menard, N. Menard, Dynamic mechanical analysis, in *Encyclopedia of Analytical Chemistry: Applications, Theory and Instrumentation*, (2006), pp. 1–25

L. Mohammed, M.N. Ansari, G. Pua, M. Jawaid, M.S. Islam, A review on natural fiber reinforced polymer composite and its applications. Int. J. Polym. Sci. **2015** (2015)

S. Mohanty, S.K. Verma, S.K. Nayak, Dynamic mechanical and thermal properties of MAPE treated jute/HDPE composites. Compos. Sci. Technol. **66**(3-4), 538–547 (2006)

K. Mylsamy, I. Rajendran, The mechanical properties, deformation and thermomechanical properties of alkali treated and untreated Agave continuous fibre reinforced epoxy composites. Mater. Des. **32** (2011)

S. Nam, A.N. Netravali, Green composites. I. Physical properties of ramie fibers for environment-friendly green composites. Fibers Polym. **7**(4), 372–379 (2006a)

S. Nam, A.N. Netravali, Green composites. II. Environment-friendly, biodegradable composites using ramie fibers and soy protein concentrate (SPC) resin. Fibers Polym. **7**(4), 380–388 (2006b)

S. Ochi, Mechanical properties of kenaf fibers and kenaf/PLA composites. Mech. Mater. **40**(4–5), 446–452 (2008)

K. Okubo, T. Fujii, Y. Yamamoto, Development of bamboo-based polymer composites and their mechanical properties. Compos. Part A **35**(3), 377–383 (2004)

J.-M. Park, T.Q. Son, J.-G. Jung, B.-S. Hwang, Interfacial evaluation of single Ramie and Kenaf fiber/epoxy resin composites using micromechanical test and nondestructive acoustic emission. Compos. Interfaces **13**(2-3), 105–129 (2006)

P. Prasob, M. Sasikumar, Viscoelastic and mechanical behaviour of reduced graphene oxide and zirconium dioxide filled jute/epoxy composites at different temperature conditions. Mater. Today Commun. **19**, 252–261 (2019)

A.J.K.S. Ram, M.A. Kumar, M.I. Reddy, Dynamic mechanical analysis of Asian palmyra sprouts fiber reinforced epoxy composites. (2018)

K.M.M. Rao, A.R. Prasad, M.R. Babu, K.M. Rao, A. Gupta, Tensile properties of elephant grass fiber reinforced polyester composites. J. Mater. Sci. **42**(9), 3266–3272 (2007)

N. Saba, M. Jawaid, O.Y. Alothman, M. Paridah, A review on dynamic mechanical properties of natural fibre reinforced polymer composites. Constr. Build. Mater. **106**, 149–159 (2016)

T. Sathishkumar, P. Navaneethakrishnan, S. Shankar, Tensile and flexural properties of snake grass natural fiber reinforced isophthallic polyester composites. Compos. Sci. Technol. **72**(10), 1183–1190 (2012)

M. Shokrieh, A. Saeedi, M. Chitsazzadeh, Evaluating the effects of multi-walled carbon nanotubes on the mechanical properties of chopped strand mat/polyester composites. Mater. Des. (56), 274–279 (2014)

C. Sperandio, A. Laachachi, D. Ruch, C. Poilâne, P. Bourson, J.-P. Salvestrini, S. Ahzi, Use of functionalized nanosilica to improve thermo-mechanical properties of epoxy adhesive joint bonding aluminium substrates. J. Nanosci. Nanotechnol. **10**(4), 2844–2849 (2010)

J. Thomason, L. Yang, Temperature dependence of the interfacial shear strength in glass–fibre polypropylene composites. Compos. Sci. Technol. **71**(13), 1600–1605 (2011)

M.M. Thwe, K. Liao, Durability of bamboo-glass fiber reinforced polymer matrix hybrid composites. Compos. Sci. Technol. **63**(3-4), 375–387 (2003)

A. Ticoalu, T. Aravinthan, F. Cardona, A review of current development in natural fiber composites for structural and infrastructure applications, in *Proceedings of the Southern Region Engineering Conference (SREC 2010)*, (Engineers Australia, 2010), pp. 113–117

F.G. Torres, M.L. Cubillas, Study of the interfacial properties of natural fibre reinforced polyethylene. Polym. Test. **24** (2005)

A.N. Towo, M.P. Ansell, Fatigue evaluation and dynamic mechanical thermal analysis of sisal fibre–thermosetting resin composites. Compos. Sci. Technol. **68**(3-4), 925–932 (2008)

A. Treviso, B. Van Genechten, D. Mundo, M. Tournour, Damping in composite materials: Properties and models. Compos. Part B **78**, 144–152 (2015)

M.R. VanLandingham, N.K. Chang, P. Drzal, C.C. White, S.H. Chang, Viscoelastic characterization of polymers using instrumented indentation. I. Quasi-static testing. J. Polym. Sci. B Polym. Phys. **43**(14), 1794–1811 (2005)

B. Wang, S. Panigrahi, L. Tabil, W. Crerar, Pre-treatment of flax fibers for use in rotationally molded biocomposites. J. Reinf. Plast. Compos. **26** (2007)

N. Zareei, A. Geranmayeh, R. Eslami-Farsani, The effect of different configurations on the bending and impact properties of the laminated composites of aluminum-hybrid basalt and jute fibers-epoxy. Fibers Polym. **20**(5), 1054–1060 (2019)

Study of Interface Properties of Epoxy Filled Nanocellulose of Natural Fiber-Based Composites

23

T. P. Mohan, Oluwatoyin Joseph Gbadeyan, and K. Kanny

Contents

T. P. Mohan (✉) · O. J. Gbadeyan · K. Kanny
Composite Research Group, Department of Mechanical Engineering, Durban University of Technology, Durban, South Africa
e-mail: MohanP@dut.ac.za; kannyk@dut.ac.za

S. Mavinkere Rangappa et al. (eds.), *Handbook of Epoxy/Fiber Composites*,
https://doi.org/10.1007/978-981-19-3603-6_22

Abstract

This chapter reviews recent progress on the development and application of cellulose of different types. Several cellulose sources such as plant, lignocellulosic materials, bacterial, and green growth cellulose were discussed. Standard techniques used for extracting cellulose and their characterization were also evaluated. The utilization of cellulose arranged in different sorts, including but not limited to cellulose microcrystalline (MCC), cellulose nanocrystal (CNC), cellulose nanofibers (CNF), and all forms of nano-cellulosic structures such as fibers, whiskers, and miniaturized scale fibrillated cellulose (MFC) were examined. The polymer's development and characterization, such as epoxy reinforced with the cellulose of different sizes extracted from various sources, were evaluated. The mechanical, thermal, and physical properties of cellulose reinforced composite were examined, and matrix-filler interface characteristics were highlighted. These properties were evaluated based on cellulose percentage loading, and composite properties with cellulose extracted from different sources were also compared. The present application of cellulose reinforced biocomposite with their future scope of this material was also considered.

Keywords

Biocomposite · Cellulose microcrystalline (MCC) · Cellulose nanocrystal (CNC) · Cellulose nanofibers (CNF)

Introduction

The pronunciation of nanocellulose depicts the cellulose fibril or crystallite comprising a nanoscale range of particles, which could be synthesized from or mechanical treatment is given to wood mash or vegetable cellulose (Mishra et al. 2018; Nissilä et al. 2019). Nevertheless, the utilization of nanocellulose depends on the supplementary such as properties relationship. Given this, they are generally arranged in different categories. These categories include but are not limited to nano-fibrillated cellulose (NFC), fibrillated cellulose (MFC), cellulose microcrystalline (MCC), miniaturized scale, nano-fibrillated cellulose (NFC), nanorods, or cellulose stubbles (Lu et al. 2019;

Alavi 2019; Trache et al. 2016; Yadav et al. 2020; Li et al. 2021; Siró and Plackett 2010). This nanocellulose is sourced from natural resources, including plant, bacterial cellulose, lignocellulosic materials, tunic cellulose, and green growth cellulose (Frone et al. 2011; Ramamoorthy et al. 2015; Ciolacu et al. 2010; Kalia et al. 2011; de Oliveira et al. 2017). This naturally sourced material is incorporated into polymeric material such as epoxy to produce nanocomposite for different applications. Epoxy is a thermosetting polymer manufactured from two fundamentally complicated substances, known as gum and hardener (Gbadeyan et al. 2020a). The fundamental motivation behind epoxy is to be utilized as a glue because of its high solidness. Epoxy gum glue frames a magnificent holding operator. The pitch holding can be created to yield a few specific items, each with its one-of-a-kind applications. Epoxies are typically used to manufacture composites with better mechanical properties and obstruction than destructive fluids and situations (Nehra and Chauhan 2021). Furthermore, it is used to accomplish great electrical properties, excellent execution at high temperatures, a great attachment to the substrate (Alamri and Low 2012; Hadjadj et al. 2016; Jonoobi et al. 2014a).

History of Epoxy and Nanocellulose

The world's principal cellulose innovative organization has established a nanocellulose division (Mohan and Kanny 2021). Along these lines, what precisely is nanocellulose, how is it created, what decisively would it be able to achieve, and is there any explanation showing that it wasn't used previously? have been continually asked until the Chinese figured out how the paper could be produced in 150 B.C. More answers were provided to the above-stated question when cellulose specialists saw that cellulose in plants, just as in harvests, comprises millimeter-sized strands that contain logically more minimal microfibers (Siró and Plackett 2010; Nakagaito and Yano 2005). These microfibers further contain microfibrils of nanometer estimates and build up the crucial structure squares of cellulose from practically all sources (Chun et al. 2020). The first business opportunities for epoxy tars were acknowledged in Switzerland by Pierre Castan of De Three pointer Freres and in the Joins States by Woody Greenlee of DeVoe and Raynolds. In 1936, Castan delivered a bisphenol A-based epoxy tar utilizing response with epichlorohydrin and, in this way, arranged a thermoset synthesis after the response of the pitch with phthalic anhydride. The utilization of the solidified sap was predicted in dental items; however, initial efforts to advertise the tar was ineffective. The licenses were authorized to CIBA AG of Basel, Switzerland (presently CIBA-GEIGY), and primary epoxy cement appeared at the Swiss Ventures Reasonable in 1946 (Jonoobi et al. 2014a; Chun et al. 2020).

In 1939, Woody Greenlee delivered a high atomic weight pitch from bisphenol A and epichlorohydrin, which was esterified with unsaturated fats to give an air-drying covering. This discovery led to the first patent, submitted in 1948. Aerospace was the primary business field where epoxies could explore in the mid-1950s. It took over two decades for epoxies to get its presentation (Henriksson et al. 2011). Epoxies have advanced toward private applications, and as a ground surface choice for

parking garages inside the 1970s as a deck, the replacement has demonstrated a drawn-out life span, simplicity of clean, and scratch verification properties (Gehri 2010). Epoxy is currently a worldwide compound with 12 achievements throughout the century and has now gotten the world's ideal and most utilized mixes. Today epoxy glues are sold in nearby home improvement shops, typically utilized as fasteners under ledges or floor coatings (Heckmann et al. 2019).

Types of Nanocellulose

Cellulose Nanocrystals

The word "cellulose nanocrystal" depicts a pole similar to the nanocrystal arrangement. Corrosive hydrolysis strategy is utilized to kill the formless locales present in local cellulose, and the strikingly translucent area in local cellulose is typically intact by caustic treatment technique delivering a bar-like structure as cellulose nanocrystal (CNC) is accomplished at last introduced with nanocrystalline cellulose or cellulose hairs (Iwamoto et al. 2011; Håkansson et al. 2014), as Fig. 1 shows. Cellulose nanocrystal tolerates an extensive scope of properties, counting immense superficial zone, exceptional dependability, excellent mechanical properties with distinctive visual characteristics, and chemical structure, as shown in Fig. 2 (Kalia et al. 2011; Henriksson et al. 2011). Cellulose nanocrystal shows a nearly elevated level of approximately 54–88% crystallinity. The cellulose nanocrystal components are demanding based on how to source the material and regularly involves running a mill measurement of 3–30 nm in breadth just as 100 nm to 1–2 lm long (Ramesh et al. 2019). The size range revealed that all nanocrystalline cellulose elements are really in the nano-size range. Furthermore, this material is often utilized in mechanical fortifying specialists, medication conveyance vehicles, and blends in nanocomposite material just as protein immobilization substrate (Henriksson et al. 2011).

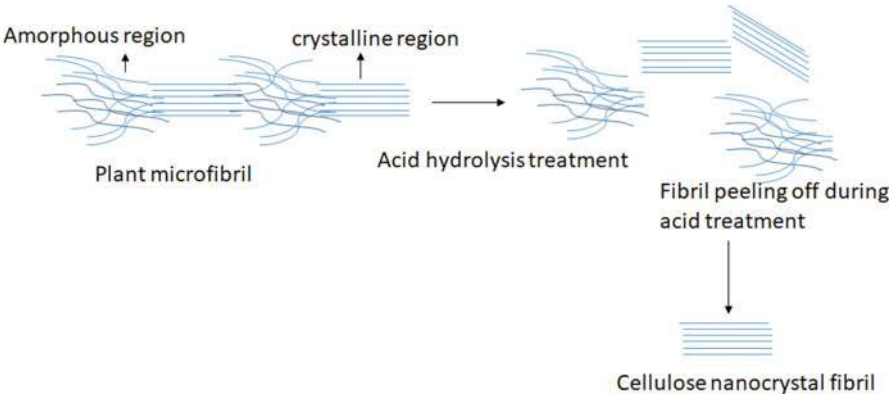

Fig. 1 Extraction of cellulose nanocrystal (CNC) fibrils using acid treatment from plant fiber

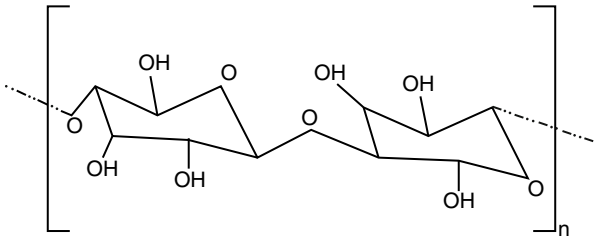

Fig. 2 Chemical structure of cellulose molecule

Cellulose Microcrystalline (MCC)

Microcrystalline cellulose is distinguished as a glasslike assembly of cellulose-containing totals of unequivocally hydrogen-fortified packs, which are multi-sized cellulose microfibrils (Alavi 2019; Trache et al. 2016). When thinking about small-scale cellulose highlights, the fine powder has molecule sizes ranging from 10 to 50 mm in width. The essential wellspring of cellulose microcrystalline is to make wood filaments, and it is acquired from these sources using dying procedures, which often results in sulfuric corrosive treatment strategy. The extraction procedure and relationship between different types of cellulose structures is shown in Fig. 3.

Bacterial Nanocellulose

Figure 4 shows different categories of cellulosic structure. The word "Nanocellulose" depicts managing nanostructured cellulose, which could be cellulose nanofibers (CNF) known as nanocrystalline cellulose (NCC or CNC) (Fig. 4a), micro fibrillated cellulose (MFC) (Fig. 4b), or bacterial nanocellulose as monocrystalline cellulose (Fig. 4c) (Siró and Plackett 2010; Sharma and Bhardwaj 2019; Akhlaghi et al. 2020). Microscopic organisms, tunicate, and wood are primary sources of cellulose nanofibers and nanocrystalline cellulose extracted by employing normal hydrolysis circumstances (corrosive, enzymatic, Beat interceded oxidation, and mechanical) (Håkansson et al. 2014; de Mendonça Neuba et al. 2020), CNCs, distinguished as rod-like, having a more prominent translucent part in correlation with CNFs that are fibrillar. CNCs sizes and perspective proportions assessments depend on a wellspring of the cellulose. The more drawn-out filaments were also thicker in bacterial sulfate, keeping up their perspective proportion low (Håkansson et al. 2014).

The Challenges of Nanocellulose Fibers and Matrix Interface

Nanofiber's utilization becomes conceivable due to their reinforcing capacity alongside filler ability in the polymeric material framework (Siró and Plackett 2010; Lu et al. 2014). The lacking scattering restricts its support capacity in the matrix grid. One other issue commonly watched is that the filler's agglomeration, especially at

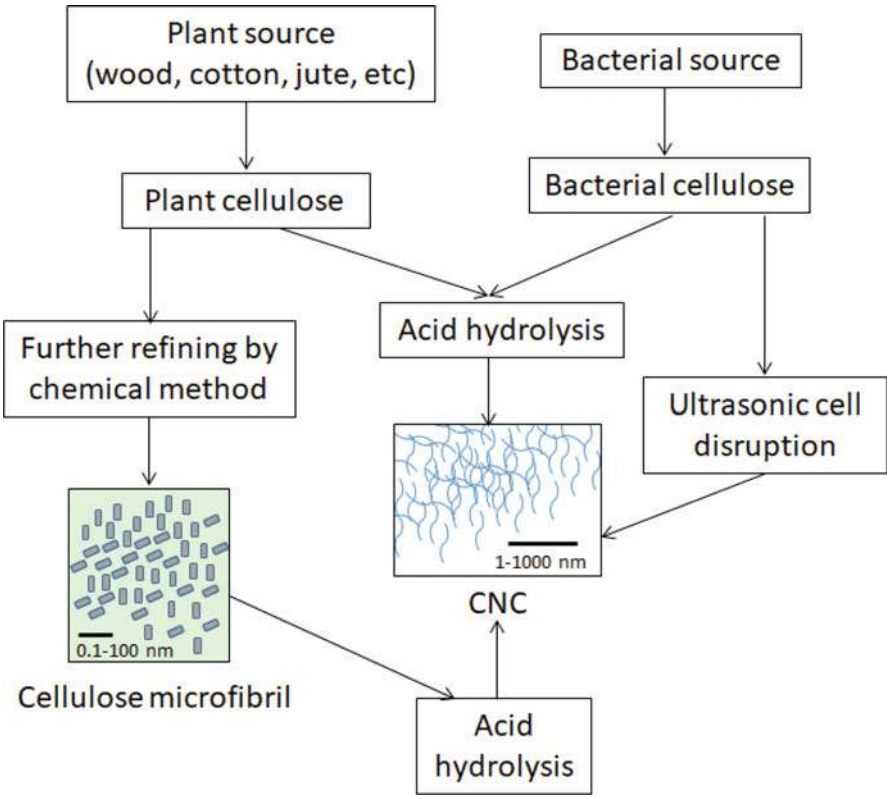

Fig. 3 Extraction and relationship between different types of cellulose structures

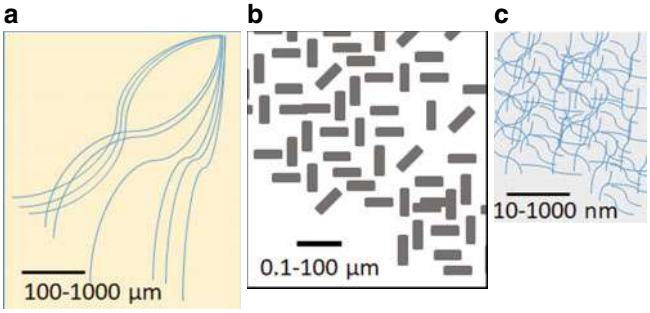

Fig. 4 Diagram showing different categories of nanocellulose, (**a**) cellulose fiber, (**b**) micro fibrillated cellulose, and (**c**) monocrystalline cellulose fiber

whatever point, is utilized to reinforce polymeric materials (Håkansson et al. 2014; Gbadeyan et al. 2020b). The nanomaterials with the colossal explicit surface region's more and huge estimation of thermodynamic budding (G) of the nanomaterials result in the absence of nanomaterial soundness (Puglia et al. 2017). As indicated by thermodynamics, DG = r DS (where r represents explicit surface vitality), it is all

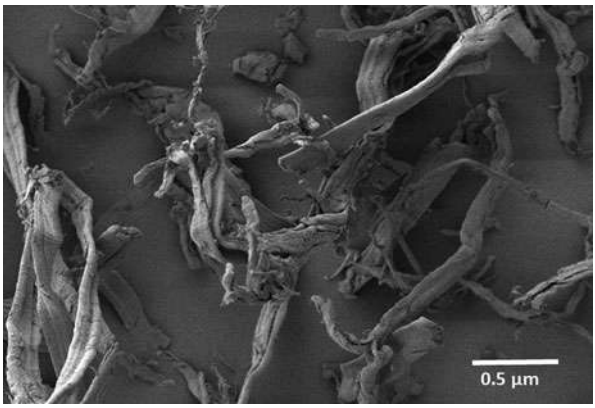

Fig. 5 Cellulosic nanofibers extracted from banana fiber

around perceived that the framework's solidness represents by presenting its particular surface territory (Mishra et al. 2018).

Subsequently, the Nano-sized materials' extremely explicit zone considers the advancement of more excellent structures by methods for conglomeration, just like nanomaterials' agglomeration. Subsequently, the composites' mechanical highlights are contrarily impacted by the deficient scattering just as conveyance (accumulation) of the filler in the polymeric grids. The dynamic gatherings(− Goodness) display on the outside of cellulosic nanofibers, such as cellulose nanofiber extracted from banana fiber shown in Fig. 5, potentially made the bonds with neighboring – bunch through feeble hydrogen holding. This procedure is identified with the agglomeration or trap of the nanofibers. Consequently, it is proposed to keep up the nanofibers in the type of water suspension (polar suspension) at whatever point obtained after chemical and mechanical treatment. Cellulose nanofibers (CNF) have a strong tendency to create hydrogen bonds with nearby fibrillation, which might increase insufficient scattering in nonpolar solvents. An additional significant issue identified with nanofibers is the worry of redispersion of nanofibers after drying. This worry might stretch out to an irrevocable accumulation of the fibrils identified with the occasion alluded as "horrification" and material presentations ivory-like qualities, which are not exhorted to utilize in rheological purposes or composite applications. The central system to forestall horrification is the consideration of a steric hindrance or electrostatic gatherings.

Type of Epoxy

Bisphenol F Epoxy

In this type of resin, viscosity is low and mean epoxy content per gram is higher than bisphenol A, and chemical resistance increases once cured. Bisphenol F with chemical structure in Fig. 6 undergoes epoxy resin formation similar to bisphenol (Mohan and Kanny 2021; Gbadeyan 2017).

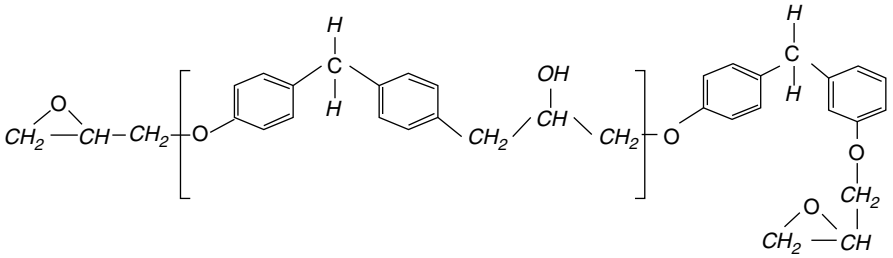

Fig. 6 Chemical Structure of bisphenol F epoxy

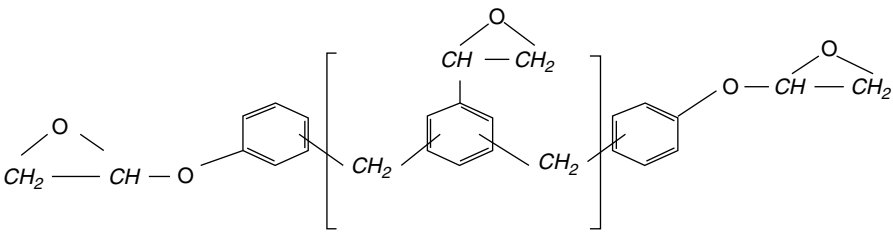

Fig. 7 Chemical structure of Phenol Novolac Epoxy

Phenol Novolac Epoxy Resin

Yielding epoxidized novellas is accomplished by phenolic response among ensuing glycosylation and formaldehyde, alongside epichlorohydrin, similar to epoxy cresol novellas (ECN) and epoxy phenol novellas (EPN) (Puglia et al. 2017). The accompanying gums contrasted with strong saps are extraordinarily gooey and typically include epoxide usefulness. High epoxide usefulness creates an especially cross-connected polymer, prompting substance opposition and high temperature with low flexibility. Figure 7 shows the substance structure during phenols' reaction among ensuing glycosylation and formaldehyde, alongside epichlorohydrin, to deliver Phenol Novolac epoxy tar.

Manufacturing Process of Epoxy Filled with Nanocellulose Composite

Cellulose Nanofiber (CNF) Using Aerogels

The cellulose nanofiber was synthesized using mechanical fibrillation techniques by bleaching softwood pulp with 10% spruce and 90% pine and milled to achieve fine particle sizes. A Super Masscolloider with ultrafine grinder was used to achieve milling pulp suspension. Before pouring, the gap between the Super Masscolloider grinding stone was adjusted to −90 μm relative to the initial contact point. A 2 wt%

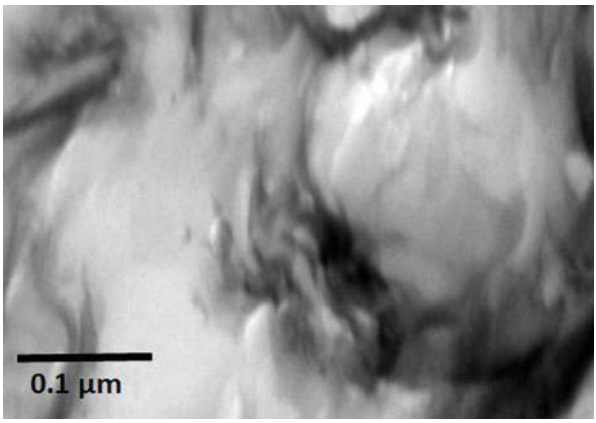

Fig. 8 TEM image of CNF surface morphology extracted from banana fiber showing fiber length in the nanometer range

suspension of 7.5 kg pulp was poured into the Super Masscolloider in two batches and processed for approximately 210 mins for each batch. The result in Fig. 8 shows a CNF suspension mostly of nanofibers obtained after milling was 1.88 wt% concentration (Nissilä et al. 2019).

FESEM investigation was conducted on the fibers carefully gathered from a dilute suspension on a polycarbonate membrane and prepared for FESEM imaging by freezing in liquid nitrogen; after that, freeze-dried. Platinum was used to sputter-coat the samples prepared for FESEM imaging. For TEM investigation, a dilute suspension drop on a carbon-coated grid was applied on fiber samples; the fibers were dry and later stained with uranyl acetate.

Sample Preparation

Figure 9 shows the two main methods of CNC-based nanocomposite preparation. Ice- templating techniques were used to fabricate 1.0 and 1.5 wt% CNF water suspensions to produce CNF aerogels (Nissilä et al. 2019). CNF water suspensions were stirred with the aid of a magnetic stirrer for 30 min to enhance the nanofiber dispersion. After that, this mixture was degassed using the planetary mixer to eliminate air bubbles in the mixture before casting. As shown in Fig. 9a, the suspension was decanted into a polytetrafluoroethylene mold with a copper bottom plate, and its temperature is controlled by a PID-controlled heating component attached to the rod. The mold was later placed on a copper rod in nitrogen solution, which gradually froze the suspension from 0 °C and was later reduced to 40 °C/h until the suspension was solidified. The solidified suspension was placed in a freeze-dryer for 5 days to obtain a dry and porous CNF.

A vacuum infusion procedure was used to fabricate aerogels infused bio-epoxy resin nanocomposites shown in Fig. 9b. The image represents the infusion techniques conducted. CNF aerogel was positioned on a flat metal surface with a plastic

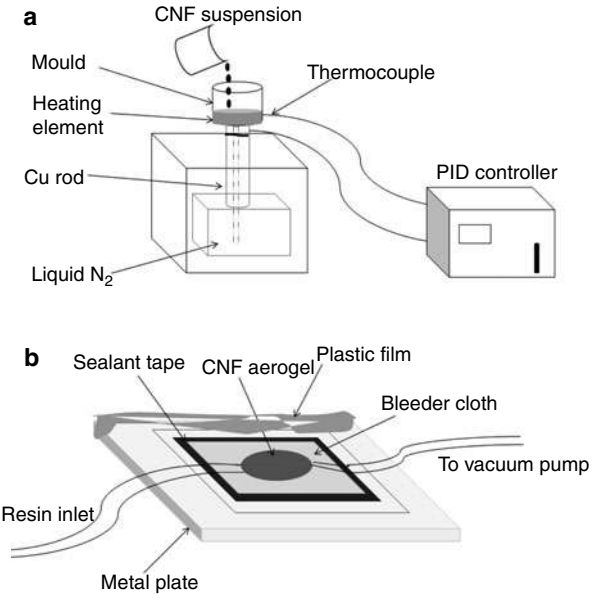

Fig. 9 A schematic diagram showing process adopted for CNC-based nanocomposite fabrication, (**a**) ice-templating, and (**b**) vacuum infusion methods

film glue on it with sealant tape. The set consists of two lines: the resin inlet, which directs the resin flow, and the outlet pipe connected to the vacuum pump. After vacuuming the air available around CNF aerogel, the resin inlet was opened to allow the resin's flow into the cold pathway using a vacuum pump. Before opening the inlet, epoxy and catalyst were premixed in a beaker and degassed for 5 mins to remove unwanted bubbles in the solution. The metal plate was then placed on a hot plate heated up to 60 °C to enhance uniform dispersion by decreasing the resin's viscosity. After the resin has covered the CNF aerogel, the outlet and the inlet were fastened for 60 mins. Equal pressure under the same ambient temperature was ensured across the infusion system. The metallic mold's temperature was increased to 80 °C and allowed to cure for another 60 mins, and the mold was taken off the hot plate (Nissilä et al. 2019). The mold was allowed to cool down to room temperature, and the nanocomposite was demolded. The control sample (epoxy and catalyst) was prepared by pouring epoxy and catalyst solution into a petri dish and subjected under the same temperature used for developing the nanocomposite.

Characterization

CNF suspensions and the bio-epoxy resin viscosity were determined on a rheometer (HR-1, TA USA). The viscosity investigation of the suspension was conducted at 25 °C, and the shear rate ramp was from 0.1 to 1000 1/s using a cone-plate with 40 mm diameter, at 1.999° angle, and 52 μm truncation. Resin viscosity was determined at 20 °C to 120 °C temperature sweep, with the other four isothermal

cure tests (at 20, 40, 60, and 80 °C). This investigation was conducted on a cone-plate with the same diameter and angle used to determine the suspension's viscosity. The plate-plate geometries 25 mm diameter, 500 or 1000 μm gap, torques (10 and 50), and frequencies (1 and 10 rad/s) used are conditional to the sample; the shear rate of 100 1/s was adopted as a substitution to oscillation for the isothermal cure investigated at 80 °C, and proper torque comeback was achieved.

Furthermore, a thin cross-sectional according to the freezing pathway of aerogel was cut and characterized under an optical microscope. This investigation was done to study aerogel structural formation. Similarly, the structure of cellulose nanocomposite samples was investigated using a scanning electron microscope ZEISS ULTRA FE-SEM. The sample was cut and prepared by putting the sample in liquid nitrogen and was allowed to be frozen. A pair of pliers was then used to collect the fracture surfaces and stick them on a holder with a carbon tape aid, later sputter-coated using a thin platinum layer.

The porosity of aerogel is the apparent density of the aerogel, and CNFs density was presumed to be 1.5 g/cm^3. Therefore, aerogel weight was obtained after freeze-drying, then apparent density was determined using Eq. 1.

$$\frac{\text{Weight}}{\text{Volume}} \tag{1}$$

The volume of the samples was determined by measuring five different points with the aid of a digital caliper, and the arithmetic means were determined. Fiber and matrix weight fraction was determined with respect to aerogel's weight before and after infusion processes, and densities were calculated based on the weights and dimensions obtained and were also used to calculate nanocomposite porosity using Eq. 2.

$$\phi = (1 - \rho m/\rho t) \times 100 \tag{2}$$

where

ρ_m = composite material density
ρ_t = theoretical density (calculated using volume fractions and densities of the fiber and epoxy phases)

A video recorder with image analyzer software was used to record the Vacuum infusion experiment processes. The recorded video was used to calculate the in-plane permeability of the aerogels with unsaturated one-dimensional. The permeability K was calculated according to Darcy's law shown in Eqs. 3 and 4

$$q = -\frac{K}{\mu}\nabla \mathrm{p} \tag{3}$$

$$L^2/t \tag{4}$$

N.B: $\mathrm{q} = L^2/t$, and it was obtained from the linear regression line slope calculated for the initial 10 min of the experimental filling distance/time curve

where

q = instantaneous flow rate
L = filling distance
μ = resin's viscosity
t = filling period
ΔP = pressure difference across the vacuum infusion system

Viscosity average value obtained at the first 10 mins of the curing process showed that the resin viscosity rose from 57 to 91 mPas. This viscosity change equation was used to validate the output, which was later compared with the polynomial curve. The polynomial curve proved that the obtained output correctly fit the available bio-epoxy viscosity data obtained in the first 100 mins and integrated with Darcy's law findings (Henriksson et al. 2011). The mechanical properties such as flexural and tensile of epoxy (control) and nanocomposite samples were investigated on the universal testing machine (Zwick/Roell Z2.5, Germany) furnished with a 1 kN load cell.

According to ISO 527 and ISO 790 standards, the investigation was conducted to determine the sample's tensile and flexural properties. A rectangular composite sample (50 × 4–5 × 1 mm^3) was cut into transverse and longitudinal specimens along the freezing pathway during the ice-templating process and set aside at 23 °C and 50% relative humidity for 8 h. They were later investigated for tensile and flexural properties at a 5 mm/min testing speed. However, the testing speed was reduced to 1%/min speed for determining modulus between the strains of 0.05 and 0.25%. A pre-set gauge length of 20 mm and 30 mm was used for tensile and flexural properties test, respectively. At least five specimens were investigated for each material, and the average value of five samples was reported.

The effect of aerogel loading in the suspension on the ice-templating process is as shown in Fig. 10. Figure 10a shows the macroscopic image of CNF based aerogel material. It was observed that the result revealed self-standing and foam-like material. Moreover, samples with suspension with 1.0 wt% of aerogel in Fig. 10c, referred to as 1.0 wt% aerogels, show a lax and smooth surface with an interlocking structure that elastically yielded minor compression stress. The suspension with 1.5 wt% aerogels (henceforth referred to as 1.5 wt% aerogels) revealed a stiffer and irregular surface formed by tiny air pockets trapped into the material when manually filling the suspension into the mold cavity before the freezing of the suspension. Air pockets formation increases with suspension's thickness were observed. This output can be directly attributed to increasing the viscosity and gel-like nature of the 1.5 wt% suspensions shown in Fig. 10b.

A shrink in transverse cross-sectional size of CNF suspension after vacuum infusion frozen processes was observed. Significantly, the transverse cross-section sizes of aerogels (102 × 58 × 18 mm^3) difference from the initial size of unfrozen CNF suspension in the mold cavity. This output depicts that transverse cross-sectional become smaller during the curing and drying process. However, the sample size increases along the longitudinal direction, and this enlargement was attributed to

the water expansion and freezing forced that occurred when opening the mold. The porosity of 99.2 and 98.9% obtained for 1.0 and 1.5 wt% aerogels corresponds to 11.6 and 16.4 kg/m^3 of densities obtained and is directly related to water and CNFs freezing suspension. It is well known that the higher the quantity of water in the suspension, the higher space inside the material after freeze-drying, as far as there are no noteworthy variances in the degree of shrinkage.

Besides, aerogel possesses an inner structure made up of open polygon pores, which could be filled with polymeric material molecules, as shown in Fig. 10c, d. These holes having diverse diameters from 10 to 100 micrometers were formed by transferred ice, and pore walls having CNFs were formed when pushed between mounting ice crystals during ice templating. The water crystals provided different shapes in the pores; most of the pore's cross-section revealed a stray from the idealized and expected shapes, while some show hexagonal shapes. Consequently, this uniform shape may influence the fiber-fiber interface bonding and CNFs moisture absorption rate when exposed to atmospheric conditions as the pore structure determines the properties of CNF-based aerogels. Furthermore, pores' shapes solely depend on two factors: fiber loading and the freezing rate. Pores with bigger diameters are often achieved when slower freezing is employed, which offered a larger space to be occupied by polymer and perhaps fillers.

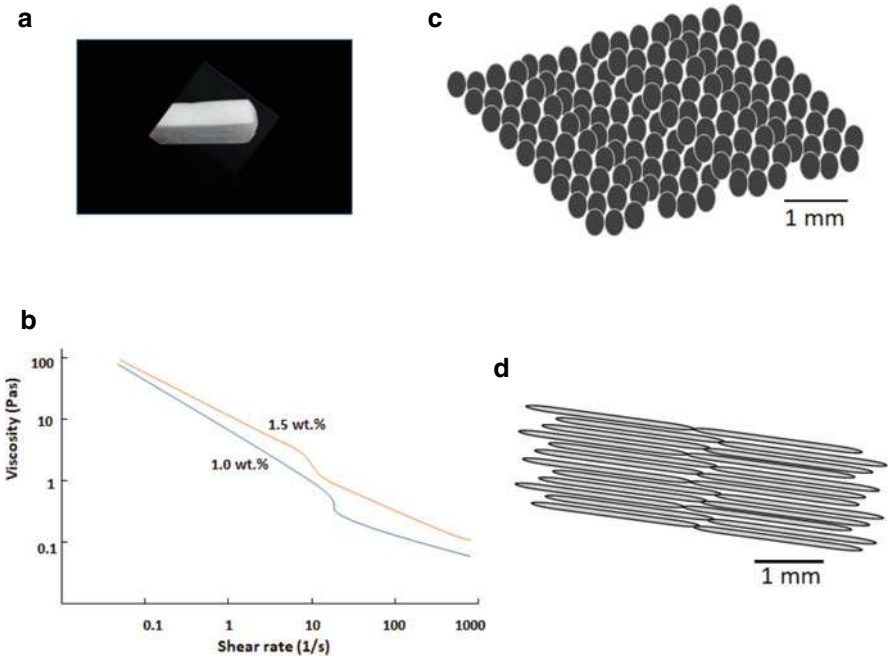

Fig. 10 Representation of (**a**) micrograph of an aerogel produced from suspension with 1.0 wt% CNF using ice-templating, (**b**) shear viscosities of the 1.0 and 1.5 wt% suspensions used as raw material, and optical microscope images of (**c**) transverse and (**d**) longitudinal cross-sections

As shown in Fig. 10, 1.0 wt% aerogels structure looked more consistent with better orientation as almost all the pores aligned vertically. However, some of these pores appeared aligned in a dendritic manner instead of strictly vertical and did not look well-formed. However, more uniform compares with 1.5 wt% aerogels that offered a more random structure. This structural formation may be attributed to more gel-like nature and sophisticated initial suspension viscosity. In this kind of structure, the increasing ice crystals' solidified forward-facing often contends with the fiber interface. However, the contention can be prevented by forming a vertical pore structure through the high loading of fiber content.

It is well-known that information about the orientation of fiber structure at a single nanofiber is most of the time not provided at a microscopic level. Therefore, the fiber strand may or may not be aligned along the freezing direction, irrespective of whether the pore structures are unidirectionally oriented. However, more effective approaches such as wide-angle X-ray scattering could obtain fiber orientation, but a scanning electron microscope is used for this study.

Vacuum Infusion

Figure 11 presented the viscosity measured before the vacuum infusion experiments. It was observed that the bio-epoxy resin viscosity decreases with a corresponding increase in temperature up to 80 °C; a significant acceleration in curing rate was observed afterward, resulting in a speedy rise in viscosity. It is noteworthy that the initial suspension viscosity can be reduced by more than 20-fold by increasing temperature from 20 °C to 80 °C, as confirmed by the four isothermal curing test results reported. In this regard, 60 °C was chosen for measuring viscosity and the trial vacuum infusion experiment for fabricating cellulose nanocomposite samples. Temperature 60 °C was used after discovering that the curing may happen before impregnation since either the curing rate or viscosity is too high when using different temperatures within the range mentioned above. The 1.0 wt%. aerogel was produced before and after the vacuum pressure is applied. The aerogel preforms positioned on a mold experiencing compaction, and the resin was infused along the freezing direction of the compressed structure, which is the pore route. These pores function as conduits that allow a speedy flow of resin. In this case, the more opened these pores are during the filling process, the final material's compaction is produced.

Figure 11a, b shows in-plane permeabilities along pore direction for 1.0 and 1.5 wt% aerogels calculated from the infusion direction against the flow duration using Eq. 3. It was observed that 1.0 wt% aerogels exhibited 1.78×10^{-12} ($\pm 0.43 \times 10^{-12}$) and 1.5 wt% aerogels have 4.15×10^{-12} ($\pm 0.23 \times 10^{-12}$) m^2 in-plane permeabilities. These results were corresponding with results 1.77×10^{-12} ($\pm 0.40 \times 10^{-12}$) and 3.93×10^{-12} ($\pm 0.19 \times 10^{-12}$) m^2 obtained using Eq. 4. This output showed that 1.5 wt% aerogels have an in-plane permeabilities value higher compared with those gained from recycled paper (3.60×10^{-13}) (Ray and Iroegbu 2021) and a bit comparable with that of wood fiber mats (Chu et al. 2020) This output significantly depicts that the aerogels possess the possibility to be exploited as

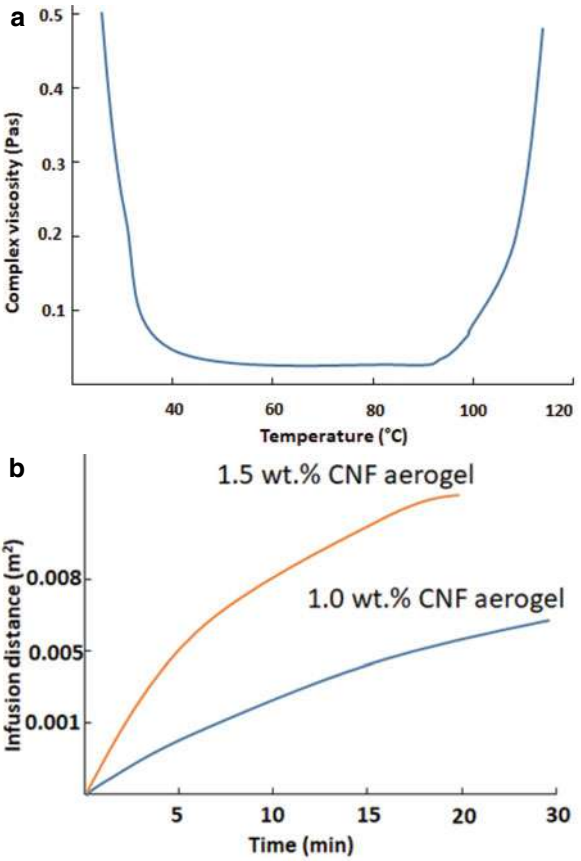

Fig. 11 Graph showing (**a**) a temperature ramp curing for the bio-epoxy resin and (**b**) Infusion distance/time curves on the effect of different wt% of CNF aerogel

a preform material. This higher in-plane permeability of 1.5 wt% aerogels may be attributed to easier impregnating due to lower compaction degree under vacuum compression, which kept pores wall structure more open in these samples. This opened structure allowed the resin to flow effortlessly through the sample and plug into the pore walls' spaces.

The infusion distance presented in Fig. 11b shows the variance among the two preforms types. Practically, the 10 cm long 1.5 wt% aerogels take about 900 s to fill; however, 1.0 wt% aerogels take a longer time and are very tough to impregnate entirely before the resin's viscosity increases seriously. Furthermore, another thing that affects is the degree of compaction. If compaction degree varies, it affects the composites with *higher* density aerogels that have a *lower* fiber content than those with lower density aerogels. Although samples with less fiber loading curbed inside a smaller volume often exhibit lower density, which reduces permeability, resulting in thinner and fiber-rich final composite sheets. This relationship is comparable to what is experienced among the fiber volume fraction and permeability, usual in

liquefied composite molding procedures (Ray and Iroegbu 2021; Chu et al. 2020; Thomas et al. 2020; Xu et al. 2020). However, the porosity and infusibility of aerogels presented in this study are critically affected by the vacuum conditions due to material compressibility. This compressible nature of the materials increases the possibility of controlling the permeability and fiber concentration, resulting in composite, making the aerogels a multipurpose and fascinating preform material.

Composite Morphology

A thin translucent shell cellulose nanocomposite shown in Fig. 12 was fabricated using a vacuum infusion process. It was observed that the typical length and width of the developed nanocomposite are similar to that of aerogel preforms. However, compression pressure during the vacuum process led to the fabrication of nanocomposite with significantly smaller thickness. The 1.0 aerogels-based composite thickness was 1.18 mm, and 1.5 wt% aerogels have 2.36 mm thickness.

The micrograph of composite fracture surfaces shown in Fig. 12c, d revealed aerogel pores attributed to the collapsed structures aerogel-filled polymer nanocomposite. Furthermore, hexagonal and later polygonal pores were observed on the sample's horizontal cross-section. This structure may be attributed to the sample's flattened due to compression pressure during the infusion process. SEM image of Fig. 12 also revealed that polymer reinforced pores produced a unidirectional edifice along the freezing direction. A discontinuous CNFs sheet with epoxy layers possibly formed an instinctively strong composite structure comparable to composites deliberated on available pieces of literature study (Nissilä et al. 2019).

Mechanical Properties of the Composites

Figure 13 and Table 1 present cellulose nanocomposites elastic moduli results investigated in longitudinal and transverse directions. Noteworthily, cellulose-filled nanocomposite exhibited higher elastic moduli than neat epoxy in both testing directions. The addition of 13 vol% CNFs enhances tensile and flexural moduli of neat epoxy by 30% and 74%. These improvements may be attributed to aerogel forming a synergistic network matrix, functioning as a reinforcement phase inside the matrix, which resulted in material stiffness. Meanwhile, testing direction influences moduli results as different moduli values were obtained for longitudinal and transverse directions, particularly flexural test results revealed an anisotropic network structure (Nissilä et al. 2019).

The effect of orientation was found to be noticeable in 1.0 wt% aerogels reinforced with 13 vol% composites. This orientation effect may be due to the improved configuration of the pores in the 1.0 wt% aerogels. It could be seen in Fig. 13 that 1.0 wt% aerogels exhibited homogeneous structure, which eventually enhances the properties of composite with higher fiber loading, making longitudinal exhibited flexural modulus of about 25% more outstanding compared to transverse.

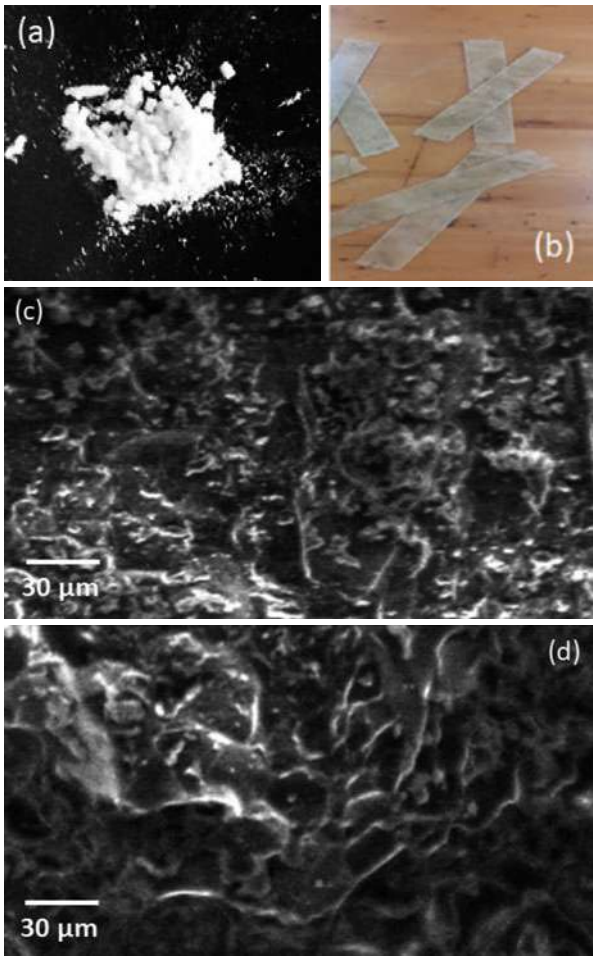

Fig. 12 CNF reinforced epoxy composites, (**a**) photograph of CNF particles, (**b**) epoxy filled CNF composite, (**c**) SEM fracture surfaces along the transverse direction (10 vol.% CNF), and (**d**) SEM fracture surface along the longitudinal direction (10 vol.% CNF)

The improvement in elastic modulus of the composite is moderately comparable with other reported studies. A study on epoxy-filled CNF composite via loading paper nanocellulose into the epoxy polymer was studied (Kumar et al. 2020). The study claimed to have increased the modulus from 2.1 to 5.9 GPa by incorporating 15 vol% of fiber. The notable variance in the result obtained for these studies can be attributed to the different nanofiller used (Kumar et al. 2020).

Furthermore, it was observed from these studies that paper nanoparticles could produce more robust networking in the matrix than aerogels. The current study suggested other techniques, such as solvent exchanger for better separation and dispersion of CNFs in the polymeric matrix. This technique may provide a better CFN network in the matrix with a higher specific surface area and lesser fiber agglomeration, enhancing mechanical properties. This suggested technique's

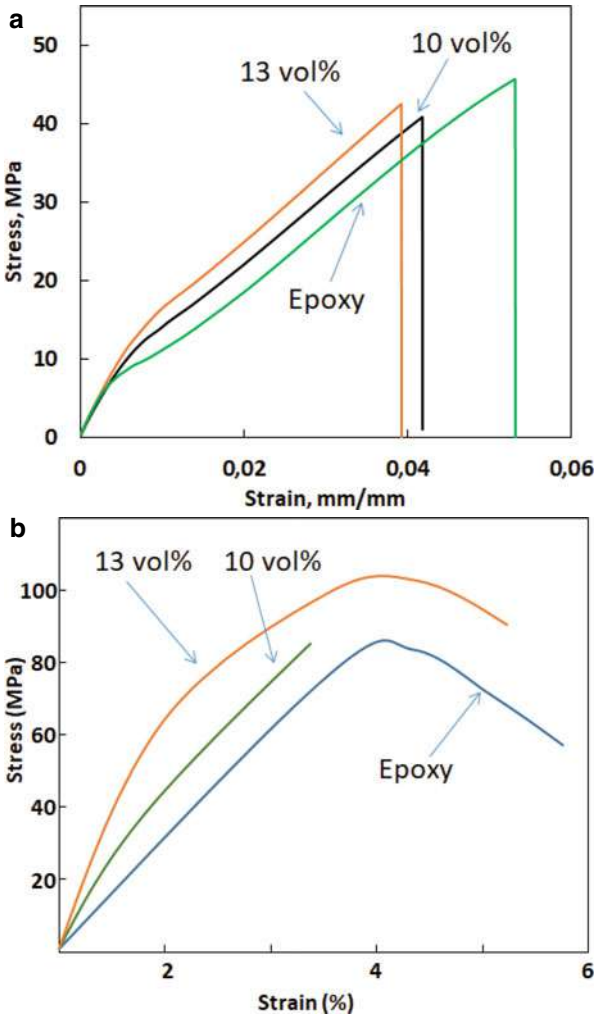

Fig. 13 Representative (**a**) tensile and (**b**) flexural stress-strain curves for the neat epoxy and the CNF reinforced epoxy composite investigated in the longitudinal direction

restriction includes time-consuming, use of a solvent is not required, and compliance issues that harmfully affect the composite's properties as extensometer were not used to determine the composite's strain shown in Table 1 (Nissilä et al. 2019; Puglia et al. 2017).

Besides, composite with 13 vol% fiber concentration offered higher longitudinal strength than neat epoxy. This composite series exhibited higher tensile and flexural strength of about 20–30% improvement over neat epoxy. However, the longitudinal strength of 10 vol% composites was practically unaffected as samples break prematurely under testing compared to the composite with higher fiber loading. This performance can be ascribed to the void content in the composite, taking with

Table 1 E-modulus (E), ultimate strength (σ), and strain at break (ε) of the epoxy/CNF composites measured in the longitudinal (∥) and the transverse (⊥) directions

	Fiber concentration in vol%	E (GPa)	σ (MPa)	ε (%)
Tensile	0	1.1 ± 0.1	52 ± 3	8 ± 1.0
	10 ⊥	1.3 ± 0.1	26 ± 2	2 ± 0.3
	10 ∥	1.2 ± 0.1	49 ± 3	4 ± 0.4
	13 ⊥	1.4 ± 0.1	30 ± 2	2 ± 0.2
	13 ∥	1.5 ± 0.1	66 ± 3	6 ± 1
Flexural	0	2.5 ± 0.1	88 ± 3	10–13
	10 ⊥	3.1 ± 0.1	37 ± 2	1 ± 0.1
	10 ∥	3.4 ± 0.1	87 ± 4	3 ± 0.4
	13 ⊥	3.5 ± 0.1	44 ± 2	1 ± 0.1
	13 ∥	4.4 ± 0.1	107 ± 3	5 ± 0.3

caution. Composite with higher fiber loading of 13 vol% offered 2% void content, and 10 vol% composites exhibited 4 vol% of void content (Nissilä et al. 2019).

A significantly lower strength value (Kumar et al. 2020) was also observed in this study. This less mechanical strength of epoxy/CNFs composite was due to the impregnation process used. Figure 13 shows that single impregnation did not appear to have happened at the single-fiber level, which eventually affected the fiber-matrix structural network (aerogel as a whole), resulting in poor mechanical properties. The study conducted by Lee et al. (2014) confirmed the structure observed for most resin-impregnated CNF networks. Furthermore, a notable difference in the mechanical properties of composite was investigated in the two testing directions. These results can be attributed to aerogels' anisotropic properties, consistent with a substantial variance in strength at longitudinal and transverse directions seen in an earlier research report. It is well known that if fiber functions as a whole network, anisotropy in the aerogels structure, not fiber orientation, determine the variance in composite longitudinal and transverse properties, and this is the reason for the difference in mechanical stiffness and strength observed for epoxy/CNFs tested at a different direction. Fiber and matrix poor interfacial bonding could be another reason for non-ideal properties observed.

Furthermore, an unexpected lesser strength was observed at the transverse direction of the samples. This decrease in strength may be attributed to weaker interfacial bonds and the irregular structure of epoxy/CNF structure, resulting in a brittle structure along the transverse direction. Agglomerated CNFs of sheet-like pore walls may have initiated the crack, which happens when impregnation does not occur at the single fiber level. This output required increasing the two components' compatibility and minimalizing the fiber agglomeration, increasing strength and stiffness. This study suggested that this kind of technique for nanocomposites where CNFs reinforcement potential is fully utilized. The mechanical properties of composite and nanocomposite may be enhanced by increasing the fiber concentration, reducing aerogels' fiber content, and making the material softer and more compressible, leading to the production of a final material with improved strength and stiffness. Lowering the concentration of aerogel fiber reduces pore walls and becomes thinner with the lesser fiber agglomerated (Nissilä et al. 2019).

Viscoelastic Properties of the Composites

DMA investigation was conducted to validate the mechanical properties observed in Table 1. The DMA results shown in Fig. 14 are similar tensile and flexural strength and stiffness presented in Table 1. In Fig. 14, an increase in storage modulus from 2.8 GPa to 4.2 GPa was observed. This enhancement corresponds with the results reported in previous studies. An improvement in storage modulus with a corresponding increase in fiber concentration was observed. A storage modulus value obtained for longitudinal direction was higher than the value obtained in the transverse direction, which can be directly attributed to the significance of anisotropy of fiber due to the vertical growth of ice crystals observed during aerogel development.

Furthermore, the storage modulus observed for the composite was more significant compared to what polymeric material was shown at temperatures directly above the *Tg* temperature. This performance may be ascribed to a constant fiber linkage, providing structural reliability even when the polymeric material is in a rubbery state. This finding corresponds with what is reported elsewhere for CNF filled epoxy composites (Jonoobi et al. 2014b) and other polymers.

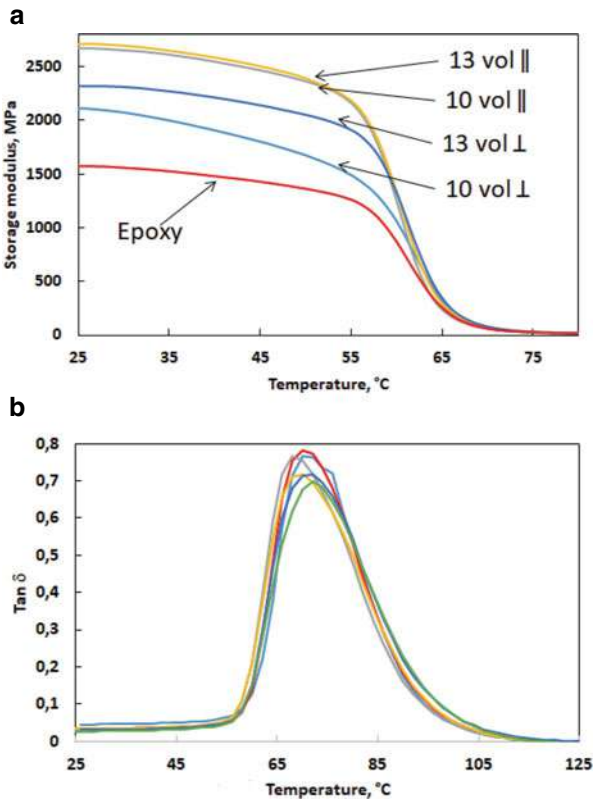

Fig. 14 The epoxy/CNF composites viscoelastic properties, temperature-dependent (**a**) storage modulus, and (**b**) tan delta conducted at the longitudinal (‖) and the transverse (⊥) directions

Despite the enhancement in storage modulus observed, the tan delta temperature peak lifted towards lower values, which depicts an insufficient interaction between fibers and matrix interface. This structure often indicates that the applying stress is not shared or transferred from the matrix to CNFs structure, which influences tensile and flexural results reported earlier. Improving mechanical properties required enhancement of compatibility between these two components (matrix and fiber) for aerogel to offer full reinforcing potential. The optimistic shift in tan delta temperature peak can be ascribed to good interfacial adhesion, and this output is similar to what was reported in a study for composites produced using a similar method at a lower temperature. This result shows that a variation in the processing temperature, the ambient temperature increased to 60 °C, harmfully affects the fiber-matrix interface interaction and structure. Also, alterations in the cured epoxy resin's contraction probably contributed to the differences in results observed. The challenges such as shrinkage and poor interfacial interaction suggest seeking another technique for manufacturing bio-based filled composite with improved compatibility of the component such as CNF and matrix, which improves the strength and stiffness of composite material. This search leads to the discovery of an LCM process, which is discussed in the next section.

Manufacturing of CNF Composites Using an Improvised Liquid Composite Molding (LCM) Process

An improvised Liquid Composite Molding process is a viable technique for developing CNF filled bio-based epoxy composite, where CNF aerogels serve as a preform and bio-based polymer function as a matrix. The technique uses a vacuum-assisted resin transfer molding (VARTM) procedure, and a vacuum pressure up to 100 kPa is employed to draw resin into the preform inside a mold. Apparatus such as a vacuum pump, a resin strap, and a "micro" LCM mold are needed to set up this process. An aluminum sealed at the top of the cap by a polycarbonate produces the micro LCM mold used for preparing specimens using this procedure. This experimental setup has two portable aluminum inserts placed inside the slab's base to form tensile and flexural specimens. The mold was air sealed, and the movement of the resin into the mold was tracked using a transparent Lexan® cap.

Furthermore, Super-Sap Entropy synthesized from industrial waste, such as wood pulps with bio-content of about 50%, was used as the bio-based resin. The bio-based resin is conditioned to cure under ambient temperature, and resin processability could be enhanced during the VARTM procedure. The fabrication method involves the positioning of CNF preform inside the mold and fastened Lexan® cap on the top to facilitate resin flow through the preform. An outlet opening was then linked to a container with curing resin and connected to the resin trap. The linking of curing resin beaker and resin connected carefully avoids resin leakage into the vacuum pump. The resin was then allowed to flow through the porous preform along the mold cavity; after this, the resin was allowed to exit from the outlet vent to the resin trap. The resin was left for 24 h to cure, and later the specimen was demolded. Well-cured specimens post-cure inside the oven at 130 °C for 20 min.

It is well known that aerogel has a meager sold-phase volume fraction. Due to this, the aerogel CNF composite was manufactured at very low fiber volume fractions (FVF) loading. The fiber volume fractions used for this study ranged from 0.9% to 1.4%. A cylindrical sample with hemispherical-shaped tips machined was used for tribological studies.

Manufacturing Process

Cellulose Nanofiber Preforms

A Kraft pulp (Aracruz Cellulose) was used to prepare the TEMPO-oxidized cellulose nanofibrils used as a raw material in this study. According to Saito et al. (Xu et al. 2020), research procedure (Xu et al. 2020), these nanofibrils were synthesized by the Kraft pulp received in dry form using a commercially supplied bleached eucalyptus. Chemical treatment was given to the pulp in phases. Pulping of fiber was conducted by washing it in acid solution, then soaked at 2% solids, pH 2, and 2 wt% $NaClO_2$ solution for 24 h, and later washed and fitted to remove chemical residues. The pre-treated pulp was carboxylated utilizing 2, 2, 6, 6-tetramethylpiperidine-1-oxyl (TEMPO), sodium chlorite, and sodium hypochlorite as the reactants at 60 °C for 72 h. Then carboxylation was performed by following Saito et al. research procedure (Xu et al. 2020).

Afterward, TEMPO-oxidized pulp fibers were thoroughly washed using reverse osmosis-purified (RO) water, making fibers uniform in a disk refiner, resulting in the separation of fibril bundles. Centrifugation techniques were used to dilute fiber slurry to enable separation of coarse and fine fractions, which also rejected the coarse fraction. A solid concentration of about 0.6% nanofiber suspension was later collected using ultrafiltration. The collected nanofiber suspension was allowed to pass through a Micro fluidizer (M-110EH-30) with 200- and 87-μm chambers in a series for final clarification. Similarly, reacted pulp fibers' carboxylate content was determined to be 0.65 mmol Coonan per gram of pulp using titration according to TAPPI Test Method T237 cm-98. Then CNF preforms with 18 cm thickness were fabricated by pouring the nanofiber suspension into a tray and frozen. Dog-bone shaped tensile samples investigated on the Universal Testing Machine shown in Fig. 15 were cut using Universal Laser Systems® (PLS6.75) 40 W laser cutter with a nitrogen purge to reduce burning samples. Following lyophilization, the laser-cut samples were positioned in a glass vacuum desiccator above 1 mL of trimethoxyoctadecyl silane per 5 tensile bars and placed in a vacuum oven at 1 in of Hg and 120 °C for 18 h. Some samples were cut without lyophilization to examine the effect of the treatment.

Production of Cellulose Nanocomposites Using an Improvised LCM Process

CNF filled nanocomposite was fabricated using an improvised LCM process, a hybrid of the Resin Transfer Molding (RTM) and Vacuum-Assisted Resin Transfer Molding (VARTM) procedures. CNF was used as the filler, and epoxy was

Fig. 15 CNF performs samples for tensile testing

permeated as the polymeric material. A negative (vacuum) pressure (VARTM) was used to substitute positive pressure commonly used for resin injection used in RTM to draw the resin into and over the CNF preform. Nevertheless, polycarbonate and aluminum made mold was inflexible, as in RTM, so that CNF preform can be prevented from progressive compression pressure experienced during the infusion process. Besides, a vacuum was used inside the mold to prevent air trapping, causing bubbles and dry sport, resulting in porosity or void in the final material. The whole injection set of the RTM mold, vacuum pump, and resin trap is as shown in Fig. 16. A resin trap serves to avert resin from getting sucked into the pump, and the installed pressure gauge was used to measure prompt pressure during experimentations.

An LCM mold created from aluminum and polycarbonate commonly used for RTM was employed in this study. This mold has an aluminum base block and a removable two-piece spacer-plate insert, having dog-bone-shaped patterns for producing tensile test samples. The mold also has a polycarbonate top-plate, used as an air seal, also acted as a window to sense resin flowing into the CNF preform. It is designed solely to produce dog-bone tensile samples by allowing the resin to pass through the inlet to the CNF preform compressed into the dog-bone pattern at the center of the mold and outlet trap out excess resin. However, inadequate resin infusion into CNF preform was experienced in this setup because of tracking race factors. In this setup, CNF skin prevents resin penetration as the resin has a habit of passing through the edges forming dry spots (void) in the specimen center (Ramnath et al. 2014; Arthanarieswaran et al. 2014). In this study, the dry spot formation was removed by redesigning the LCM mold. The mold was designed so that resin was permitted to flow in from one side, covered parallel along the CNF preform, and afterward trapped at the other side. This arrangement allows the resin to penetrate

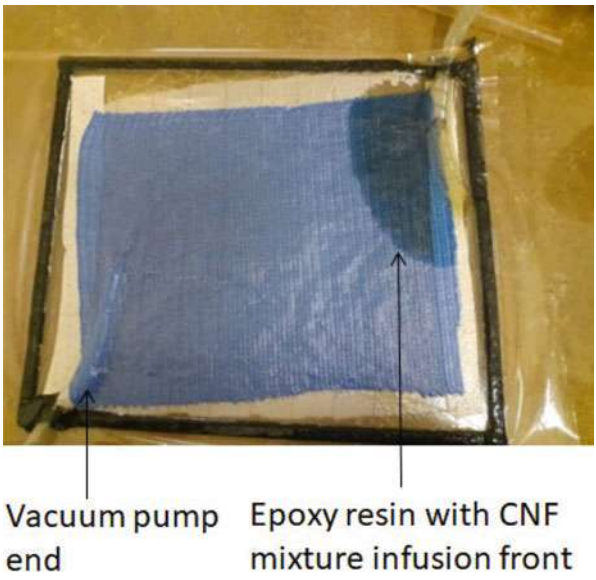

Fig. 16 LCM setup used for producing epoxy-CNF composite

and soak the more permeable inner core of CNF, enhancing the soaking of the preform with resin, leading to producing a final composite with improved properties.

Development of Epoxy Filled with Nanocellulose Using Okra Plant

Material Background

Abelmoschus Esculentus with chemical structure shown in Fig. 17, placed with the Malvaceae family known as okra plants, originated from Egypt. This plant also grows in the timberland close to Nekonda of the Warangal area in Telangana, India. It has strands of 2.4 m lengthy and utilized instead of jute, commonly used to produce rope, paper, and other materials. Additionally, a fiber extracted from a banana stem, as shown in Fig. 18, is often used to produce rope and other material produced using Jute fiber. Okra filaments are the superlative strands that are extracted from the branches of this vegetable.

Extraction and Purification of Nanocellulose from Okra Fibers and Nanocellulose Layer

Extraction Procedure

A corrosive hydrolysis procedure was used to extract cellulose from the okra plant. The filaments within 1–1.5 m long are chopped and reduced to 5–10 mm (Fortunati

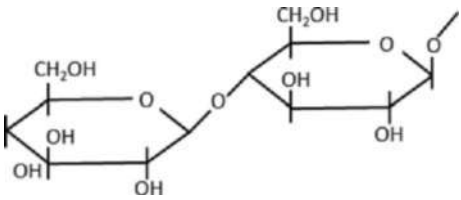

Fig. 17 Chemical Structure of *Abelmoschus esculentus* Plant

Fig. 18 Raw fiber stripes from the banana plant

et al. 2013). The chopped strands were put into measuring utensil and decontaminated by washing for 20–30 min using water, and stove dried at 80 °C for 24 h. Then the dried fiber strands were de-waxed in Toluene/ethanol (2:1 vol/vol) solution purged in the cup; then the filaments were placed in a piece of fabric and situated in the Soxhlet extractor and bubbled at 70 °C for 360 mins.

NaOH Treatment

Alkaline treatment was given to fibers strands for de-waxing (Cai et al. 2016; Sinha et al. 2017). This process was conducted in stages, as shown in Figs. 19 and 20. The strands were washed in ethanol for 30 min and later dehydrated for 4 h. Afterward, 0.1 M NaOH having 56% volume of ethanol was measured in a beaker containing the de-waxed fiber and constantly stirred at 47 °C for 3 h using a magnetic stirrer (Gbadeyan et al. 2020b).

Bleaching

The fibers were bleached with H_20_2 at pH = 10.5 (buffer solution) performed at 45 °C in a solution with different concentrations, viz., (I) 0.50% H_20_2, (II) 1.0% H_20_2, (III) 2.0% H_20_2 and (IV) 3.0% H_20_2 for 3 h each under constant agitation (Rayung et al. 2014).

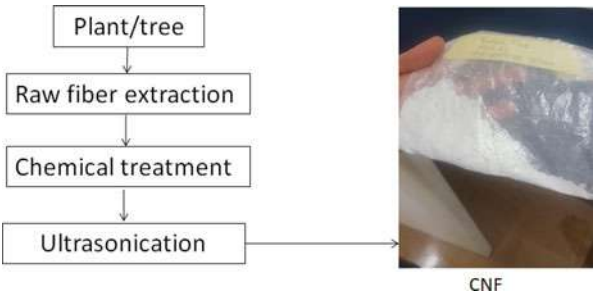

Fig. 19 Extraction procedures of cellulose nanofibrils

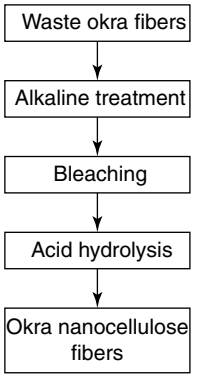

Fig. 20 Procedure used for extracting and purifying cellulose nanofibrils obtained from okra plant fibers

Chemical Treatment

At that point, every strand has been treated using 11.2% w/v NaOH + 1.1% w/v Na2B4O710 H_20 O solution at 32 °C and stirred consistently for 900 mins. The strands are presently treated with the above blend in a container put on a stirrer plate and warmed at 32–40 °C for 15 h under the consistent unsettling influence. Subsequently, the blend was safeguarded with HNO3, 70%, HAC, 80% mixed using volume ratio 1:10 at 100 °C for 1200 s. In concluding this procedure, cellulose remnants were washed away in a 95% ethanol solution, washed in water, and dried out in a broiler at 60 °C until the weight stays consistent. The cellulose acquired was washed using the hydrolysis process. The suspension cooled, the fibrils were removed and washed a while to arrive at the lack of bias. The clean fibrils are separated from this point forward, and the acquired CNFs are suspended in ethanol and sonicated for 10 min in the ice shower. The sonicated fibrils are stove dry at 60 °C for achieving a dry individual normal CNF.

Composite Processing

Okra nanocellulose composite was developed with changing weight rate (1–6 wt%) covered in epoxy gum using a pressure embellishment with VARTM procedure. The polymer was strengthened by adding various weight rates of (0,1,2,4,5 and 6) okra

nanocellulose fibril blended with an attractive stirrer at 850 rpm for 45 min at ordinary room temperature (Fortunati et al. 2013). Eventually, the jacket okra textures were dried at 80 °C for 3 h and later put in 95% ethanol solution for 20–30 min, afterward washed in water and dry in a broiler at 60 °C until the weight arrived nonstop worth. At that point, the filaments are ground to acquire as a powder.

Okra nano fibrillated the pressure shaping technique readied cellulose of composite cover with okra cellulose for creating a unique nanofibril. A metal with $180 \times 70 \times 3$ mm^3 dimensions was for composite, which is the most straightforward strategy for creating nano-fibrillated cellulose fortified composites. Nano fibrillated cellulose composites pay extraordinary solidarity to-weight proportions (Bhatnagar and Sain 2005). Creating pale weight parts is censorious to businesses determined as allocation, store, and aviation for various explanations. Nano fibrillated cellulose fortified composites with the okra cellulose nanofibrils expansion likewise remained finished in the comparative way (0, 1, 2, 4 and 6 wt%) is utilized as a filler considerable what's more, blended into the epoxy sap in advance the nano fibrillated cellulose is fortified in the grid. The shape discharge wax was applied to the metal form divider's internal surface to smooth the nanocellulose composite sample's light partition. A gauge amount of LY 556 epoxy pitch, HY951 hardener (proportion of 10:1 by weight Rate), was blended using stirrer at 800 rpm for 35 min at room temperature. At that point, the example is post relieved at room temperature for another day.

Characterization and Properties

Water Absorption

Samples shown in Figs. 21, 22, and 23 were cut intermittently from developed composite and were used for this investigation. Each sample's initial weight was measured before being soaked in water for 720–4320 mins, later they were wiped with a napkin to remove water on the sample's surface, and the final weight was taken using a digital to determine the water uptake of the samples. The impact of dampness ingestion on arranged composites was determined as per ASTM D 570 standard. Water Retention test shelters the assurance of the family member's

Fig. 21 Samples before for absorption properties

Fig. 22 Composite samples after testing

Fig. 23 Image of composite samples before water immersion test

pace of water assimilation by fiber when drenched. The dampness substance is related to properties, including dielectric misfortunes, electrical protection opposition, mechanical quality, presence, and dimensions.

The dimensional stability of okra nano fibrillated cellulose composites was controlled by conducting a water retention test. The heaviness of composites was estimated employing ASTM (Chun et al. 2020) by computerized offset with three critical numbers. Five tests of every crossbreed were drenched and afterward estimated; the average worth was recorded. Samples loads and thickness were estimated and afterward inundated again in a jar of purified water at 27 °C. Samples were removed from the purified water, and all wet surface was cleaned with an unblemished dry wipe and weighed to the closest 0.001 mg until soaked. The sample weight increase at a given inundation time was recorded at standard time t frames. From that point, the water retention rates (weight gain) were resolved to utilize the accompanying condition:

$$\text{Water absorption}\% = \frac{W2 - W1}{W1} \times 100$$

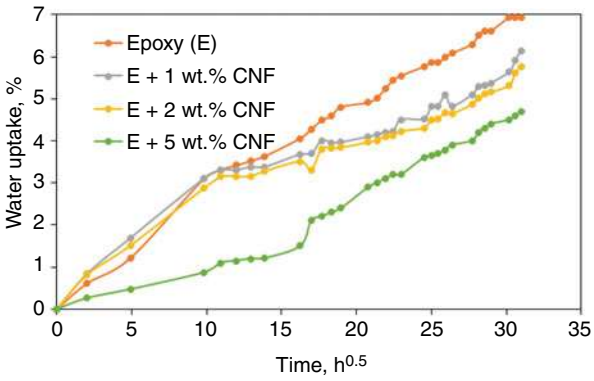

Fig. 24 Water absorption curve of CNC filled composite series

where W1 = initial weight of nano fibrillated cellulose composites before the test and W2 = weight of okra nano fibrillated cellulose composites soaked in water

The fibrillating of composite 2 wt% of okra nano cellulose showed the most noteworthy as illustrated in Fig. 24 – dampness assimilation level of 2.08%. The 1%, 4%, and 6% composite has retained marginally less water ingested contrasted with 2% composites. The gum showed the most reduced % of Water retention (0.71%). The 2% Okra nano fibrillated cellulose composite showed the most elevated dampness retention rate of 1.663%. The 5% and 10% cellulose Nano fibril composite has ingested somewhat less water retained contrasted with 15% cellulose composites. The pitch displayed the most reduced level of Water retention (0.185%) (Serroukh et al. 2018).

This fiber is inclined to water ingestion, causing insecurity in the properties of the composites. It is demonstrated in the writing that water assimilation and thickness expanding of okra fibrillated and other cellulose nanofibrils' fuse improves strengthened composites. When the water assimilation conduct of characteristic fiber composites is explored, and small-scale splits of the okra cellulose nanofibrils lessen the interfacial bond of fibril with the framework, bringing about the water atoms infiltrated prompts thickness expanding happened.

Compression Property

For the most part, the pressure investigation was carried out on round and hollow poles composite samples. Pressure testing of the epoxy tar and hardener as framework material is led to an idea of value control. The compressive investigation was completed on the composite samples to decide the pressure quality using a general testing machine and gauge the samples' pressure properties. The standard test strategy according to ASTM standard D695, the samples were cut in the tube-shaped pole form with the extent of (165 × 12.7 × 3) mm and figure barrel-shaped bar tallness 25.4 mm with a width of 12.7 mm represented in Fig. 25.

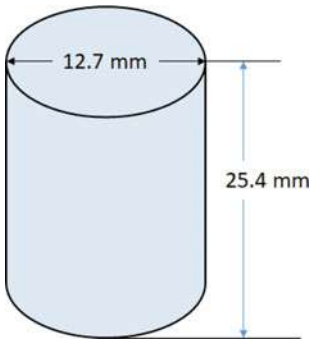

Fig. 25 Dimension of the sample used for compression test

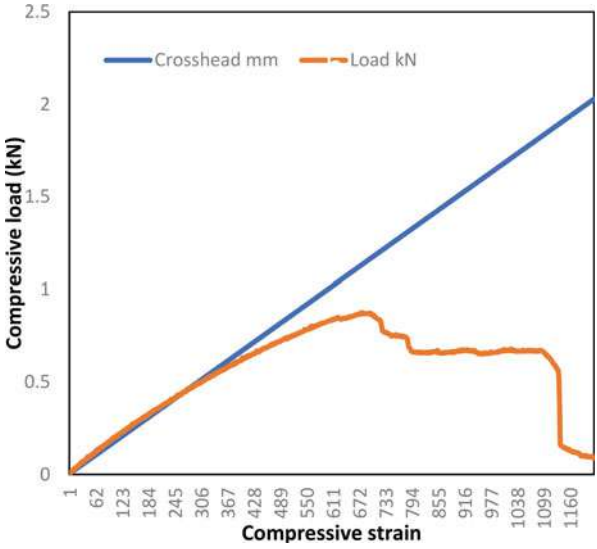

Fig. 26 Typical compressive load-elongation curve of 5% CNF filled epoxy composite

A typical load-extension curve of 5 wt% CNF filled epoxy composite is shown in Fig. 26. The 2 wt% of CNF filled epoxy composite showed the most extraordinary level of pressure quality of 68.6 MPa, as shown below. The CNF (1 wt%, 2 wt%, and 5 wt%) of composite has ingested the marginally less pressure quality contrasted with 4 wt% CNF filled fibrillated cellulose composites. The pitch showed a minor level of pressure test (Ramnath et al. 2013). The 4 wt% CNF filled epoxy composite showed the most noteworthy % of pressure quality of 68.6 MPa, as illustrated in Fig. 26.

Impact Property

It is well known that impact test is generally affected by sample level directions. In the standard test technique, as indicated by ASTM D 256. A rectangular sample

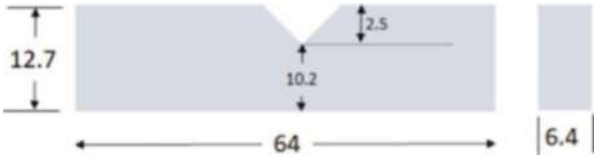

Fig. 27 Typical dimension of the notched impact test sample

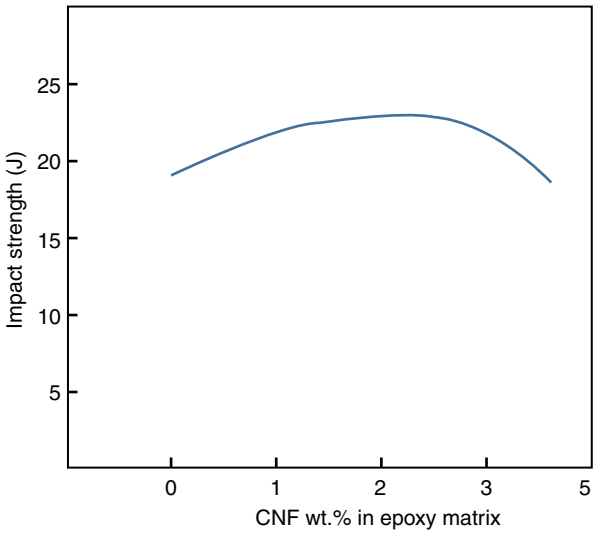

Fig. 28 Impact strength of okra nano fibrillated cellulose composites

having a 63.5 × 12.7 × 3 mm dimension with a 'V' indent of 2.5 mm at the center of the sample focal points was investigated. The test was conducted at an effective speed of 4 m/s and an episode vitality of 5.4 J using an Izod sway analyzer. The representation of the sample size of the test is shown in Fig. 27. This test directs the reason for the protection from breaking by flexural stun. At least five samples were examined, and the normal of five estimations of effect quality is estimated. A typical impact testing dimension is shown in Fig. 27. Figure 28 shows the impact result of CNF filled in epoxy composite series. The addition of CNF has a positive effect on impact property improvement.

Interfacial Property

The pressure, water retention investigation, and epoxy nanocomposites properties improve with a corresponding increase in nanocellulose constituent up to 4% due to increment in inclusive adhesion between fiber-matrix interface. Also, the framework and the rest of the rates of CNF cover are diminished. The flexural quality, flexural modulus, elasticity, and tractable stiffness of epoxy sap composites were recuperated to change with the brought-up drenching of nanocellulose spread with fibril composite.

An increase in mechanical properties was observed for 3–4 wt% of CNF epoxy composite. It is reliable that this work provides effective methodology towards improving the properties, taking the shape of cutting-edge composite materials significantly with new nanofillers as a potential research area to explore.

Significantly, composite with 3 wt% CNF epoxy composite showed higher impact resistance than other composites. Based on the impact strength result shown in Fig. 28, composite with 3–4 wt% of CNF shows superior properties to other samples, which may be due to voids formation in those samples.

Kenaf Fibre Reinforced Composites

Kenaf fiber is extracted from the *Kenaf plant*, known as Hibiscus cannabis. It comprises 56–64% of cellulose, 21–35% of hemicellulose, 8–14% of lignin (Khan et al. 2020), and trivial amounts of ash. Samples of unidirectional kenaf fiber-filled epoxy composites were tested. Increased tensile strength and stiffness were observed with corresponding fiber loading increases shown in Figs. 29 and 30.

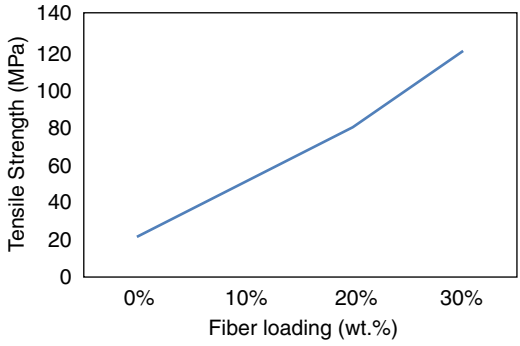

Fig. 29 Tensile strength (MPa) per volume content of kenaf fiber reinforced epoxy composite

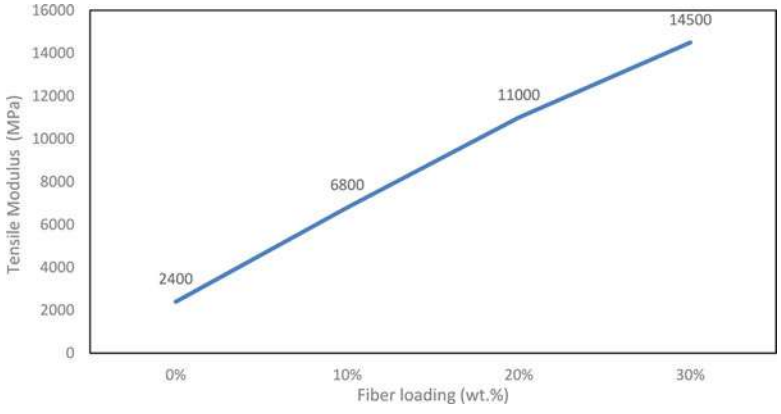

Fig. 30 Tensile modulus (MPa) per volume content of kenaf fiber-filled epoxy composite

Mechanical and Thermal Properties of Nanocellulose

Thermal Properties

The warm debasement of lignocellulosic materials begins with an underlying disintegration of hemicelluloses, the underlying period of pyrolysis of lignin, depolymerization, and ends with powerful blazing burning, just as scorch oxidation. Furthermore, cellulose nanofibrils comprise a high corruption temperature beginning (350 °C) and a much better warm execution contrasted with hemicellulose, gelatine, and lignin. Then again, the beginning of the warm corruption of nanocrystals, as a rule, happens at 200–300 °C. Cellulose nanocrystals with lesser sulphate sum have more helpful warm soundness than banana cellulose.

Mechanical Properties

Incorporating nanomaterials in fillers in composite materials improved inflexibility, solidness, versatility, hindrance highlights, and fire retardancy by being cultivated in examining the 100% unadulterated polymer material (Lee et al. 2014). The presentation of the constrained extent of nanomaterial is adequate for these upgrades because of the immense surface zone of the nanoparticles. In contrast with carbon nanotubes, cellulose nanofibers from wood have just a quarter of the quality; in any case, the valuing concerning cellulose nanofibers are less expensive than the costs for carbon nanotubes (Gbadeyan et al. 2017).

Permeation Properties of Nanocellulose

Fume hindrances confine the amount of water fume passing all through the structure because of unmistakable fume pressures. A fume obstruction is utilized to restrict the dissemination of water fume all through a material. As a fume obstruction, they are ready to manage the dampness stream's pace where present. Permeance is determined in perms. One perm is characterized as one drop of water fume passing through one square foot of a layer every hour, encouraged using a fume pressure distinction of one inch of mercury over the two surfaces. Porousness is typical for a material. Permeance is dependent on the thickness of the material, and it could be an abilities evaluation and not an attribute of a material (Mishra et al. 2018).

Epoxy Filled with Nanocellulose Reinforced by Graphene Oxide

Epoxy nanocomposite reinforced with graphene oxide-nanocellulose offer structure plays a significant role in engineering applications because of little moisture absorption and high-temperature performance (Mohan and Kanny 2021). Epoxy exhibits undesirable properties' brittle with small fracture resistance due to its structure.

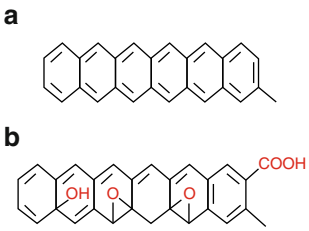

Fig. 31 Chemical structure of (**a**) graphene and (**b**) graphene oxide

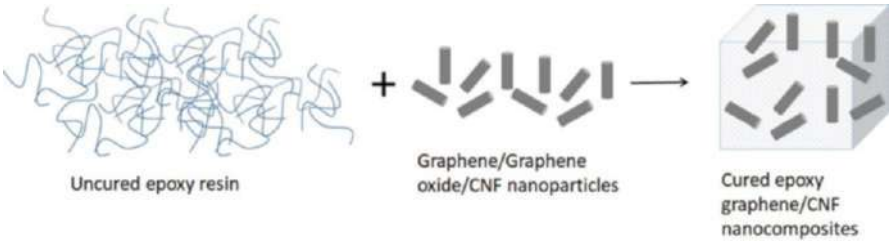

Fig. 32 Schematic illustration of the process for preparing the epoxy graphene (graphene oxide)

The interfacial area strongly influences these polymers in Fig. 31 its shows the graphene oxide structure.

The graphene oxide is added to advance the epoxy composite's mechanical properties, including robustness and strength. It also enhances the composite's brittle fracture toughness.

This added graphene oxide to the composite has been scientifically proven that it improved the strength by 42% and toughness by 58% at lesser filler loading of 0.2w %, resulting in better interfacial connections between graphene oxide and Epoxy. Furthermore, composite fracture toughness was higher than the most reported and tensile strength.

Processing of the GO-NCC/EP Nanocomposite

The preparation procedure of graphene oxide nanocellulose crystals (GO-NCC) based nanocomposites is shown in Fig. 32. These nanocomposites are manufactured by dispersed nanofillers in acetone using an ultrasonic cleaner. Subsequently, TED-85 was incorporated into the GO-NCC/acetone solution and stirred for 12 h using a mechanical stirrer. TED-85/ GO-NCC/acetone was later heated to 60 °C for 5 h to evaporate the solvent and further heated to 70 °C for 12 h under vacuum to eliminate acetone wholly. TDE-85 and the curing agent (mDP) were mixed using a 100:18 mixing ratio, then allowed to cure at 80 °C for 2 h and 120 for 4 h. However, 0.1, 0.3, and 0.5 wt % GO/EP were also prepared differently under similar conditions (Yan et al. 2019).

Mechanical Properties of GO-NCC/EP Nanocomposite

- The working temperature of the EP is much less compared to its glass transition temperature (Tg = 150–160) °C.
- The pristine EP naturally shows brittle fracture when subjected to tensile stress.
- Nanocomposite with 0.3 wt% GO-NCC/EP offered improved tensile strength and elongation at a break of 90.33% and 101.36%, respectively (Yan et al. 2019).

Strengthening Mechanisms of GO-NCC/EP Nanocomposite

The trademark fragility with a lesser crack sturdiness of the unblemished EP results from its high cross-connecting thickness, which brings about helpless ingestion of vitality during the crack. These variables habitually lead to reflect like break surfaces. Evidence of the hardening brought about by GO or GO-NCC pull-out, burst, and break spanning is frequently noticeable on the cracked GO or GO-NCC-strengthened EP composite surfaces. Considering the examples, GONCC/EP's cracked surface was harsher, and rugged multiplanar designs showed up additional, so more vitality was required. When a break experiences a nanofiller, it is restrained, and its spread was privately interrupted. To continue, the broken front curves itself, expanding the vitality essential for spread. If the break interfaces with GO or GO-NCC, the break must tilt or bend at more prominent points to pass the nano-fillers. The split-tip opening uprooting (CTOD) will be a lot bigger than that of the flawless EP (Yan et al. 2019).

Conclusions

This chapter provides information on several research studies on cellulose sources, extraction processes. The extraction and incorporation processes of cellulose and nanofiber of different categories extracted from different sources such as softwood, coir fiber, aerogels, and okra were deliberated extensively. The chapter touches on how epoxy was invented, where it was invented, and by whom. The role of reinforcements such as cellulose plays in improving the properties of polymeric material was also discussed. It also highlighted the uses and synthesizing processes of the cellulose-based composite.

Furthermore, the challenges of incorporating micro or nanocellulose into polymeric material to fabricate either bio-based composite or nanocomposite were studied. Different methods for determining the thermal and mechanical properties of the cellulose-based composite were reported. It was discovered that cellulose loading increases polymeric material properties; however, improvement in properties was influenced by fiber extraction, and treatment methods as interfacial bonding of components were challenging. Several techniques used to combat these challenges, such as alkaline chemical treatment and different composite fabrication

techniques, were provided in the chapter. It was observed that the techniques used for fiber extraction determine fiber/matrix interfacial interaction.

Furthermore, it was deduced that the techniques used for cellulose-based composite or nanocomposite have advantages over one another. It is still at the trial-and-error stages, which give room for further studies. Comparing cellulose-based composite properties with synthetic nanofiber reinforced composite may be another area of research to explore.

References

M.A. Akhlaghi, R. Bagherpour, H. Kalhori, Application of bacterial nanocellulose fibers as reinforcement in cement composites. Constr. Build. Mater. **241**, 118061 (2020)

H. Alamri, I.M. Low, Characterization of epoxy hybrid composites filled with cellulose fibers and nano-SiC. J. Appl. Polym. Sci. **126**(S1), E222–E232 (2012)

M. Alavi, Modifications of microcrystalline cellulose (MCC), nanofibrillated cellulose (NFC), and nanocrystalline cellulose (NCC) for antimicrobial and wound healing applications. E-Polymers **19**(1), 103–119 (2019)

V. Arthanarieswaran, A. Kumaravel, M. Kathirselvam, Evaluation of mechanical properties of banana and sisal fiber reinforced epoxy composites: Influence of glass fiber hybridization. Mater. Des. **64**, 194–202 (2014)

A. Bhatnagar, M. Sain, Processing of cellulose nanofiber-reinforced composites. J. Reinf. Plast. Compos. **24**(12), 1259–1268 (2005)

M. Cai, H. Takagi, A.N. Nakagaito, Y. Li, G.I. Waterhouse, Effect of alkali treatment on interfacial bonding in abaca fiber-reinforced composites. Compos. A: Appl. Sci. Manuf. **90**, 589–597 (2016)

Y. Chu, Y. Sun, W. Wu, H. Xiao, Dispersion properties of nanocellulose: a review. Carbohydr. Polym. **250**, 116892 (2020)

H. Chun, S.-Y. Park, S.-J. Park, Y.-J. Kim, Preparation of low-CTE composite using new alkoxysilyl-functionalized bisphenol A novolac epoxy and its CTE enhancement mechanism. Polymer **207**, 122916 (2020)

D. Ciolacu, J. Kovac, V. Kokol, The effect of the cellulose-binding domain from Clostridium cellulovorans on the supramolecular structure of cellulose fibers. Carbohydr. Res. **345**(5), 621–630 (2010)

L. de Mendonça Neuba et al., Promising mechanical, thermal, and ballistic properties of novel epoxy composites reinforced with cyperus malaccensis sedge fiber. Polymers **12**(8), 1776 (2020)

J.P. de Oliveira et al., Cellulose fibers extracted from rice and oat husks and their application in hydrogel. Food Chem. **221**, 153–160 (2017)

E. Fortunati, D. Puglia, M. Monti, C. Santulli, M. Maniruzzaman, J.M. Kenny, Cellulose nanocrystals extracted from okra fibers in PVA nanocomposites. J. Appl. Polym. Sci. **128**(5), 3220–3230 (2013)

A.N. Frone, D.M. Panaitescu, D. Donescu, Some aspects concerning the isolation of cellulose micro-and nano-fibers. UPB Bull. Stiintific Ser. B Chem. Mater. Sci. **73**(2), 133–152 (2011)

O.J. Gbadeyan, Low friction hybrid nanocomposite material for brake pad application (2017)

O.J. Gbadeyan, K. Kanny, T.P. Mohan, Influence of the multi-walled carbon nanotube and short carbon fibre composition on tribological properties of epoxy composites. Tribol. – Mater. Surf. Interfaces **11**(2), 59–65 (2017). https://doi.org/10.1080/17515831.2017.1293763

O.J. Gbadeyan, S. Adali, G. Bright, B. Sithole, A. Omojoola, Studies on the mechanical and absorption properties of achatina fulica snail and eggshells reinforced composite materials. Compos. Struct. **239**, 112043 (2020a). https://doi.org/10.1016/j.compstruct.2020.112043

O.J. Gbadeyan, S. Adali, G. Bright, B. Sithole, S. Onwubu, Optimization of milling procedures for synthesizing nano-CaCO3 from achatina fulica shell through mechanochemical techniques. J. Nanomater. **2020**, 4370172 (2020b). https://doi.org/10.1155/2020/4370172
E. Gehri, High performing jointing technique using glued-in rods, in *11th World Conference on Timber Engineering 2010*, vol. 2010, (WCTE, 2010)
A. Hadjadj et al., Effects of cellulose fiber content on physical properties of polyurethane based composites. Compos. Struct. **135**, 217–223 (2016)
K.M. Håkansson et al., Hydrodynamic alignment and assembly of nanofibrils resulting in strong cellulose filaments. Nat. Commun. **5**(1), 1–10 (2014)
T. Heckmann, J.P. McEvoy, K. Markantonakis, R.N. Akram, D. Naccache, Removing epoxy underfill between neighbouring components using acid for component chip-off. Digit. Investig. **29**, 198–209 (2019)
M. Henriksson, L. Fogelström, L.A. Berglund, M. Johansson, A. Hult, Novel nanocomposite concept based on cross-linking of hyperbranched polymers in reactive cellulose nanopaper templates. Compos. Sci. Technol. **71**(1), 13–17 (2011)
S. Iwamoto, A. Isogai, T. Iwata, Structure and mechanical properties of wet-spun fibers made from natural cellulose nanofibers. Biomacromolecules **12**(3), 831–836 (2011)
M. Jonoobi, Y. Aitomäki, A.P. Mathew, K. Oksman, Thermoplastic polymer impregnation of cellulose nanofibre networks: morphology, mechanical and optical properties. Compos. A: Appl. Sci. Manuf. **58**, 30–35 (2014a)
M. Jonoobi, Y. Aitomäki, A.P. Mathew, K. Oksman, Thermoplastic polymer impregnation of cellulose nanofibre networks: morphology, mechanical and optical properties. Compos. Part A Appl. Sci. Manufac. **58**, 30 (2014b)
S. Kalia, B. Kaith, I. Kaur, *Cellulose Fibers: Bio-and Nano-Polymer Composites: Green Chemistry and Technology* (Springer Science & Business Media, 2011)
A. Khan, A.M. Asiri, M. Jawaid, N. Saba, Effect of cellulose nano fibers and nano clays on the mechanical, morphological, thermal and dynamic mechanical performance of kenaf/epoxy composites. Carbohydr. Polym. **239**, 116248 (2020)
V. Kumar, P. Pathak, N.K. Bhardwaj, Waste paper: an underutilized but promising source for nanocellulose mining. Waste Manag. **102**, 281–303 (2020)
K.-Y. Lee, Y. Aitomäki, L.A. Berglund, K. Oksman, A. Bismarck, On the use of nanocellulose as reinforcement in polymer matrix composites. Compos. Sci. Technol. **105**, 15–27 (2014)
T. Li et al., Developing fibrillated cellulose as a sustainable technological material. Nature **590**(7844), 47–56 (2021)
Y. Lu, H.L. Tekinalp, C.C. Eberle, W. Peter, A.K. Naskar, S. Ozcan, Nanocellulose in polymer composites and biomedical applications. TAPPI J. **13**(6), 47–54 (2014)
Z. Lu et al., Study on the wet-web strength and pressability of paper sheet during the press process with the addition of nano-fibrillated cellulose (NFC). Carbohydr. Polym. **210**, 332–338 (2019)
R.K. Mishra, A. Sabu, S.K. Tiwari, Materials chemistry and the futurist eco-friendly applications of nanocellulose: status and prospect. J. Saudi Chem. Soc. **22**(8), 949–978 (2018)
T.P. Mohan, K. Kanny, Synthesis and manufacturing of epoxy composites, in *Epoxy Composites*, (Wiley-VCH, 2021), pp. 23–59
A.N. Nakagaito, H. Yano, Novel high-strength biocomposites based on microfibrillated cellulose having nano-order-unit web-like network structure. Appl. Phys. A **80**(1), 155–159 (2005)
P. Nehra, R. Chauhan, Eco-friendly nanocellulose and its biomedical applications: current status and future prospect. J. Biomater. Sci. Polym. Ed. **32**(1), 112–149 (2021)
T. Nissilä, M. Hietala, K. Oksman, A method for preparing epoxy-cellulose nanofiber composites with an oriented structure. Compos. A: Appl. Sci. Manuf. **125**, 105515 (2019)
D. Puglia, M.A.S. Al-Maadeed, J.M. Kenny, S. Thomas, Elastomer/thermoplastic modified epoxy nanocomposites: the hybrid effect of 'micro' and 'nano' scale. Mater. Sci. Eng. R. Rep. **116**, 1–29 (2017)
S.K. Ramamoorthy, M. Skrifvars, A. Persson, A review of natural fibers used in biocomposites: plant, animal and regenerated cellulose fibers. Polym. Rev. **55**(1), 107–162 (2015)

A. Ramesh, N.V. Srinivasulu, M. I. Rani, Development and evaluation of water absorption, compression and impact properties of okra nanocellulose fibers reinforced epoxy composites. Materials Today: Proceedings, **19**, 748–754 (2019)

B.V. Ramnath et al., Evaluation of mechanical properties of abaca–jute–glass fibre reinforced epoxy composite. Mater. Des. **51**, 357–366 (2013)

B.V. Ramnath, V. Manickavasagam, C. Elanchezhian, C.V. Krishna, S. Karthik, K. Saravanan, Determination of mechanical properties of intra-layer abaca–jute–glass fiber reinforced composite. Mater. Des. **60**, 643–652 (2014)

S.S. Ray, A.O.C. Iroegbu, Nanocellulosics: benign, sustainable, and ubiquitous biomaterials for water remediation. ACS Omega **6**(7), 4511–4526 (2021)

M. Rayung, N.A. Ibrahim, N. Zainuddin, W.Z. Saad, N.I.A. Razak, B.W. Chieng, The effect of fiber bleaching treatment on the properties of poly(lactic acid)/oil palm empty fruit bunch fiber composites. Int. J. Mol. Sci. **15**(8), 14728–14742 (2014). [Online]. Available: https://www.mdpi.com/1422-0067/15/8/14728

S. Serroukh, P. Huber, A. Lallam, Adsorption behavior of optical brightening agent on microfibrillated cellulose studied through inverse liquid chromatography: the need to correct for axial dispersion effect. J. Chromatogr. A **1533**, 17–29 (2018)

C. Sharma, N.K. Bhardwaj, Bacterial nanocellulose: present status, biomedical applications and future perspectives. Mater. Sci. Eng. C **104**, 109963 (2019)

A.K. Sinha, H. Narang, S. Bhattacharya, Effect of alkali treatment on surface morphology of abaca fibre. Mater. Today Proc **4**(8), 8993–8996 (2017)

I. Siró, D. Plackett, Microfibrillated cellulose and new nanocomposite materials: a review. Cellulose **17**(3), 459–494 (2010)

P. Thomas et al., Comprehensive review on nanocellulose: recent developments, challenges and future prospects. J. Mech. Behav. Biomed. Mater. **110**, 103884 (2020)

D. Trache et al., Microcrystalline cellulose: isolation, characterization and bio-composites application – a review. Int. J. Biol. Macromol. **93**, 789–804 (2016)

J. Xu et al., High-strength, transparent and superhydrophobic nanocellulose/nanochitin membranes fabricated via crosslinking of nanofibers and coating F-SiO2 suspensions. Carbohydr. Polym. **247**, 116694 (2020)

M. Yadav, K. Paritosh, V. Vivekanand, Lignocellulose to bio-hydrogen: an overview on recent developments. Int. J. Hydrog. Energy **45**(36), 18195–18210 (2020)

M. Yan, W. Jiao, G. Ding, Z. Chu, Y. Huang, R. Wang, High strength and toughness epoxy nanocomposites reinforced with graphene oxide-nanocellulose micro/nanoscale structures. Appl. Surf. Sci. **497**, 143802 (2019)

Rheology of Epoxy/Natural Fiber Composites

24

Dheeraj kumar Gara, Gujjala Raghavendra, Shakuntala Ojha, M. Om Prakash, and P. Syam Prasad

Contents

D. k. Gara
Department of Mechanical Engineering, NIT Warangal, Warangal, Telangana, India
e-mail: dk720045@student.nitw.ac.in

G. Raghavendra (✉)
Department of Mechanical Engineering, National Institute of Technology, Warangal, India
e-mail: raghavendra.gujjala@nitw.ac.in

S. Ojha · M. O. Prakash
Department of Mechanical Engineering, Kakatiya Institute of Technology and Science, Warangal, Telangana, India

P. S. Prasad
Department of Physics, NIT Warangal, Warangal, Telangana, India
e-mail: syamprasad@nitw.ac.in

S. Mavinkere Rangappa et al. (eds.), *Handbook of Epoxy/Fiber Composites*,
https://doi.org/10.1007/978-981-19-3603-6_25

Abstract

The need for high strength to weight ratio, high wear resistance, and high thermal resistance have challenged the materials to have multifaceted properties in a single sheet in the form of composite. Recent advances in the materials such as natural polymer composites received an ample attention in the scientific community and found their applications toward aerospace, automotive, and biomedical industries. As not much commercial aspect has received in the industry due to their complexities involved in processing the raw material to a finished product, most of the work is still constrained to laboratory. Alongside an assignment of rheological behavior has very limited research in literature which actually is more crucial in dictating the desired composite property. In lieu of this, the current paper discourses the types of natural fibers and their processing routes followed by rheological studies which allows the understanding of basic characteristic of processing of natural fiber composites.

Keywords

Natural Polymer Composites · Rheology · Glass transition · Cure kinetics · Shear and extension viscosity

Introduction

Natural polymer composites are generally a blend of natural reinforcements with polymer resin. The gap between demand and supply of conventional materials is widening day by day due to rapid industrialization across the world. In order to compensate the gaps, researchers started using renewable resources. One such invention was natural polymer composite material in which the naturally available materials are blended with some polymer resins to attain the desired structural properties for appropriate applications. Many researchers have explored the application of various natural materials such as filler content in composite fabrication. As these materials are abundantly available in nature, fabrication of natural composites will be cost-effective. Some of the areas where natural fibers surpass synthetic reinforcements are in low density, have low cost, and are recyclable and biodegradable (Saheb and Jog 1999). Previous studies show that natural fiber composites possess good mechanical strength, stiffness, and damping properties, low energy consumption, high tilling levels, and good carbon dioxide sequestration. Some of the natural reinforcements used in the past were kenaf, sisal, coir, jute, bamboo, wood

flour, coconut shell powder, etc. Summerscales et al. (2010) reviewed the bast fiber composite materials and concluded that jute, kenaf, hemp, and flax fiber composites have better properties.

Unlike the conventional reinforcements, the natural reinforcements are not uniform; the properties of natural reinforcement composite materials depend on the type of reinforcements. Ku et al. (Vlaev et al. 2009) surveyed tensile strength of various natural composites and showed that strengths are affected by the interfacial bonding of matrix and fiber. Relevant work has shown that fiber content influences the mechanical properties of final composite product. It was then concluded that by varying the fiber fraction, it was possible to enhance the properties of fiber composites. Natural fiber composites' application in found in automotive industry, and there are also reports that they are capable of replacing the synthetic fiber composites. Pandey et al. (2015) emphasized various properties of natural fiber composites; from the study it was reported that with the proper modification of resin or natural fiber, bio-composite materials can be suitably designed for a wide range of applications, e.g., aerospace and electronics like biosensors.

Apart from natural fibers, natural materials in particulate forms are also widely used as reinforcements in polymer composite. Researchers found rice husk flour as a reinforcement in polymer composite and investigated mechanical properties. From the experimental study, it was reported that increment of filler loading results in poor tensile properties. They attributed the decrease in strength to poor interfacial bonding between hydrophilic reinforcement and hydrophobic resin. Lai et al. (2003) experimented on improving mechanical properties of wood flour polyethylene composites by maleate polyolefin compatibilizers. From their study, it was evident that the inclusion of liner low- and high-density polyethylene improved the tensile and impact strength properties.

It is also equally important to emphasize on the basics of rheology and intuition in understanding the rheological characteristics with respect to composite materials. From the scientific investigations, we realize that dynamic mechanical analysis (DMA) plays a crucial role in attainment of desired mechanical and thermophysical parameters. The curing behavior can be evaluated using DMA which can detect the transition and is found to be better a method than differential scanning calorimetry (DSC) and dynamic thermal analysis (DTA). This method is widely accepted due to its operating principle that predicts the glass transition temperature for the polymers with phase change behavior during curing process. Interestingly the mechanical properties that can be derived from the DMA characterization are elastic modulus G′ (referred to as storage modulus hereafter), viscous modulus G″ (referred to as loss modulus hereafter), and damping coefficient *tan Δ* as function of temperature and strain. Analytically rheological properties such as storage, loss modulus, and damping are evaluated from DMA procedure as follows:

1. Stress and strain at any given point at any given time can be given in terms of phase component (in and out) as

$$\sigma(t) = \sigma_0 \sin(\omega t + \delta)$$

$$\varepsilon(t) = \varepsilon_0 \sin(\omega t)$$

2. The in-phase component of the stress is referred to as storage modulus, and the out-phase is referred to as loss modulus and inferred as

$$G' = (\sigma_0 \cos\delta)/\varepsilon_0$$

$$G'' = (\sigma_0 \cos\delta)/\varepsilon_0$$

3. Finally, the phase component will be the ratio of loss modulus to storage modulus and is referred to as damping and given as

$$\text{Tan}\,\delta = \frac{G''}{G'}$$

where E' is obtained through tension and E'' through compression test. It is now important to realize how to identify the glass transition temperature (T_g) from dynamic mechanical thermal analysis (DMTA) which actually consists of storage and loss modulus followed by damping of the material. For an instance, plot in the figure below replicates how modulus and damping of a polymer look like. From the figure below, T_g is evaluated from maximum deviation observed in the E' or E''. In most of the scientific literature, it can be inferred that G' and G'' coincide, and hence it is observed to be glass transition, i.e., transition to rubber state and hence sometimes referred to as rubber transition temperature.

Few works pertaining to the rheological behavior of the various epoxy/natural fiber composites and their parameters such as G', G'', and *Tan* δ will be discussed in brief. In this context, Pallikari-Viras et al. (1996) investigated thermal analysis of poly-methyl methacrylate impregnated porous gel silica glasses, and it was observed that there were three exothermic peaks which we get directly without the calculation of storage and loss modulus which are about 120 °C, 160 °C, and 200 °C. An interesting work from (Martínez-Hernández et al. 2007) on dynamic mechanical thermal analysis keratin biofibers extracted from chicken feathers interestingly found that storage modulus enhanced 1% and 2% wt of keratin fibers and also identified that at higher temperatures the polymer reinforcement provided higher stability. Intuitively from generosity of *Tan* δ, peaks indicate the strong interfaces, and this is observed in the work. This can be justified by optical image spectroscopy.

As discussed earlier, in mechanical perspective, DMTA gives an emphasis on measurement of glass transition from the behavior of the storage and loss modulus followed by the damping. Meeting this standard procedure, an imperative work from (Pereira and Oliveira 2000) measures the T_g by DMTA. G' and G'' followed by *Tan* δ has shown excellent configuration allowing to measure T_g at the interface. From few of the discussed works above, mostly it is observed that there are more than one exothermic peak, because of the very little loss of water, whereas in most cases, because of the moisture content, there is an observed increase in G' due to hardening.

But one must realize the fact that it involves lot of complexities due to influence of various parameters on the determination of T_g such as experimental setup, test

apparatus, processing conditions, and fiber reorientation, to name a few. The lags that measuring system impacts on the evaluation of $T_g$include heating rate and system, testing and starting temperature, testing mode, and clamping system. Alongside the same lieu, the specimen properties are geometry, types of fibers and fillers, heat capacity, orientation of fibers, moisture, curing, aging, thermal conductivity, and post-curing.

Over time, it is reviewed thoroughly that these parameters influence the final thermal and physical properties of the composite, and this is a requisite to meet the required applications/industries. These tests have been configured to give other important physiological properties which are amenable to biomedical applications such as creep, stress relaxation, quasi-static mechanical behavior, hydrogel swellings, and identification of softening transitions. Applications in context to the polymers will be emphasized in the next section followed by various aspects of the DMTA that will be emphasized in detail.

It is important that the processing of composites involves aqueous solution (resin) and solid which interface each other forming a solid network of composite. This is followed by a heat treatment process and would definitely involve change of phase and viscosity. Hence, it is important to study the viscosity under varying temperatures and change in viscosity on the event of stress or when the resin is subjected to strain and to evaluate stress. Measuring the rheological behavior, i.e., viscosity, stress strain, and temperature, is one of the crucial calibrations which enables us to identify and control the processing parameters. Similar to dynamic mechanical thermal analysis, the results will be plotted for storage and loss modulus against the typical shear oscillatory stress. The control parameters include shear stress, frequency, time, and temperature, whereas output data will be G', G'', and $Tan\ \delta$ and viscosity (μ) (transient analysis). These rheological measurements predict the type of the material behavior such as elastic, viscous, plastic etc.

Rheological experiments are basically performed in two cases, large and small deformation. Small deformation is performed to study the microstructure of the material, whereas large deformations are for the Hookean materials. Hookean materials exhibit elastic behavior under rheological environment, and Newtonian fluids exhibit viscoelastic behavior. Alongside, interestingly rheometers can also perform transient and dynamic experiments. The linear elastic behavior of the specimen whether Newtonian and non-Newtonian fluids is an area of interest and is referred to as linear viscoelastic region (LVR).

A work in this context can be extracted from (Wu et al. 2008) which measured the linear viscoelastic behavior of the multiwalled carbon nanotubes (MWCNTs)/polypropylene composites. They have evaluated the nanocrystalline and nucleation effect by the inclusion of the weight percent of nano-MWCNTs. Another work provided a brief insight on the evaluation of viscoelastic properties of the wood plastic composites (WPCs). The measurements include various flow curves such as shear stress vs shear strain, wall shear stress as a function of average velocity, viscosity against shear rate, and shift factors against fiber composition. However, there are more works on various composites to study their rheological properties which will be

discussed in the characterization section. The section also emphasizes on the types of rheometers, and lacunae in calibration techniques will be discussed in detail.

Applications

To reduce the dependency on the conventional metal materials and to increase the utilization of renewable resources, researchers applied natural fiber polymer composites in various industries. The addition of natural fiber/filler into a polymer matrix gives composite material significant mechanical properties. As the natural fibers are light weight and are biodegradable, natural fiber polymer composites found to be promising in many applications such as automobile industry and aerospace industry.

Automobile industry is one of the rapid-growing sectors in the world. Any automobile is assembled with different parts, and these parts were made up with various engineering materials mainly nonrenewable, costly, and high-density metals. Utilization of high-density metals adds weight to the vehicle and increases fuel consumption which is undesirable. In order to reduce the economy and ecological effects, many researchers have embraced utilization of natural fiber epoxy composites in the automobile industry to cut down the weight and reduce the overall cost. As natural fibers are abundantly available in nature, the replacement of conventional materials with natural fiber epoxy composites is found to be economical and environmentally friendly. Low density of natural fibers when reinforced into epoxy matrix yields light weight and high specific strength natural fiber epoxy composites. The application of natural fiber epoxy composites to automobile body parts will reduce overall weight of the automobile, thereby increasing fuel efficiency and reducing braking power. Light weight also assists in enhancing accelerating power and engine performance. Since the early period of the twentieth century, extensive research has been carried out by many automotive industries and research laboratories to employ natural fiber epoxy composites in automobiles. Most of the automotive industries started exploring the utilization of natural epoxy composites for different automobile parts in the early 1990s.

In the year 1996, leading automobile company Mercedes Benz successfully applied jute fiber epoxy composite for door panels in its E class vehicles. Benz also achieved pronounced vehicle performance with flax fiber epoxy composites as interior panels. Niranjan et al. (2013) studied mechanical properties of abaca fiber epoxy composites and concluded that abaca natural fiber epoxy composites can be extensively used for automobile applications. In an overview of application of natural fiber polymer composites in automotive industry, authors discussed potential of different natural fiber epoxy composite materials for different parts of automobile. Prasad et al. (2019) experimented fabrication of mudguard of a two-wheeler using natural fiber epoxy composites.

In view of reducing the cost and weight of vehicle, authors attempted developing mudguard using ramie, sisal, and pineapple filler epoxy composites. Composites were fabricated by stacking ramie, sisal, and pineapple fiber layer by layer with different sequential order. From results of mechanical tests, authors claimed that

pineapple-sisal-ramie fiber composite has high tensile strength of 24.43 MPa with compression load of 0.32 KN and impact load of 6 J. Davoodi et al. (2010) worked on the hybridization of kenaf fiber with glass fiber for fabrication of kenaf/glass fiber epoxy polymer for car bumper beam application. In their research authors tested the hybrid kenaf/glass fiber epoxy polymer bumper beam for mechanical properties, and results were compared with typical glass mat thermoplastic bumper beam. From the experimental results, it was observed that mechanical properties like Young's modulus, flexural strength, and tensile strength of kenaf hybridized glass epoxy composites were similar to the typical bumper beam.

Rwawiire et al. (2015) studied strength of bark cloth/epoxy composites to apply natural composites in car dashboard or interior panels. Authors noticed that bark fiber/epoxy composites have Young's modulus of 4 GPa and 33 MPa tensile strength. It was concluded that bark fiber/epoxy composites were suitable for the development of interior panels of automotive applications. Ramasubbu et al and his coworkers fabricated (Ramasubbu and Madasamy 2020) fabricated car bumper using sisal/kenaf fiber hybrid epoxy composites. Natural epoxy composite car bumper was developed by reinforcing 30% natural fibers (21% sisal and 9% kenaf) and 70% polymer by simple hand lay-up technique. Authors concluded that lightweight natural fiber hybrid composite is suitable for car bumper applications. Guduru et al. (2019) also worked on hybrid natural fiber epoxy composites for automobile hood application. In their study authors developed sisal-kenaf fiber hybrid epoxy composites by using vacuum-assisted resin transfer molding method. The researchers also explored the hybridization of conventional synthetic fiber epoxy composites with some of the natural fibers for automobile applications. Murugu Nachippan et al. (2020) worked on glass/hemp fiber hybrid epoxy composites, and from the results of mechanical tests, authors concluded that fabricated hybrid composite is best suited for automobile application where low tensile strength and high impact strength are desirable. Kenaf- aramid hybrid composites were fabricated with different fiber orientations and studied for mechanical behavior for spall-liner automotive application by Yahya et al. (2015).

Polymer composite materials were also extensively tested for aerospace application because of their light weight and high specific strength. In early period before polymer composite materials were commercialized, metals were used in the fabrication of aircraft. Still today aluminum is the dominant metal used in the fabrication of aircraft due to its excellent mechanical properties. To reduce the weight of the aircraft, aluminum was replaced with conventional synthetic fiber polymer composites. Though the synthetic polymer composites proved to be promising alternatives for metals in aircraft development, due to their high cost and non-renewability, researchers started working on replacing synthetic polymer composites with natural fiber epoxy composites. Natural fiber epoxy composites were experimented for the development of interior parts of the aircraft cabin. They presented detailed review about the utilization of bast fiber polymer composites for aircraft components. Authors claimed that bast fiber green epoxy composites have enough potential to be applied for developing interior structures of an aircraft. Boeing research department carried research work on flax epoxy composites for aircraft interior

applications. It was found that natural epoxy composites were 35% lighter when compared to carbon epoxy composites for similar application.

Apart from their excellent mechanical properties, natural epoxy composites also possess significant tribological properties such as high wear resistance, low material loss, and high coefficient of friction. In general, thermoset epoxy material is a brittle material; however many researchers found that with the inclusion of natural fibers/fillers into epoxy, the brittle behavior was changed. There was extensive research done on fiber reinforced polymer composites to improve wear resistance and reduce friction coefficient. From the past research works, it was noticed that addition of natural reinforcements in epoxy polymer enhanced the wear properties of composite materials.

High flexural strength and better resistance against impact loading natural epoxy composites were exploited for defense applications. Multilayer ballistic armor system is one of the significant defense applications where most researchers experimented to use natural/epoxy composites. Multilayer ballistic armor is a personal protective system which is in general made up of ceramic, synthetic fiber composites and ductile materials. Researchers experimented with different natural fiber epoxy composites to replace synthetic fiber composites to reduce cost and weight. Marsyahyo et al. (2009) worked on ramie fiber epoxy composites for bulletproof application. Authors fabricated ramie epoxy composites by using simple hand lay-up technique and subjected to ballistic test. It was observed that ramie fiber epoxy composite panels are lighter in weight compared to conventional bulletproof panels. From experimental bulletproof testing results, authors noticed that ramie fiber epoxy composites could able to withstand up to impact level II with minor fractures.

Nascimento et al. (2017a) experimented use of malva fiber epoxy composite for ballistic applications. Authors conducted ballistic experiments on malva fiber epoxy composites and compared results with aramid fiber composites. From the observations of experimental results, it was concluded that malva fiber epoxy composites are suitable for personal protection bulletproof application against 9 mm caliber ammunition. David et al. (2017) investigated the ballistic performance of basalt epoxy composites for different fiber orientations. Authors worked on the estimation of number of layers required for protection against threat level II NIJ standard 0101.04. It was concluded that 38 and 39 layers of basalt fiber composite are best suited for military application. Monteiro et al. (2015) carried out experimental studies on curaua fiber reinforced epoxy to replace the Kevlar fiber composites for military applications. From results of ballistic test, authors noticed that depth of indentation on natural fiber epoxy composites is relatively less when compared with armor having aramid fiber. It was concluded that curaua fiber/epoxy composite are best possible replacements for aramid synthetic fiber in ballistic armor.

Rohen et al. (2015) investigated the ballistic performance of sisal fiber epoxy composites. Authors noticed that 30% sisal fiber epoxy composite when utilized in multilayered ballistic armor in place of conventional materials were 20% more efficient than aramid armor. Da Luz et al. (2017) worked on coir fiber epoxy composite for ballistic armor application. From the study authors claimed the coir/

epoxy composites to have better ballistic characteristics compared to synthetic Kevlar fiber. Da Cruz et al. (2015) investigated potential of bamboo epoxy composites for ballistic armor application. Nascimento et al. (2017b) explored the possible utilization of jute fiber epoxy composites in ballistic armor application. Recent studies experimented utilization of piassava fiber/epoxy composite in ballistic armor and studied ballistic behavior against high-energy ammunition.

Processing Methods

In general, polymer composites are fabricated by using different techniques. Selection of fabrication techniques will be mainly based on type of filler/fiber, percentage of reinforcement, and area of application. There are many fabrication techniques in use for developing polymer composites; some of them are resin transfer molding, injection molding, simple hand lay-up technique, pultrusion, compression molding, filament winding, vacuum bagging, extrusion, etc. Because of distinct characteristic properties, low thermal degradation, and geometrical cross sections of natural filler, researchers hardly used these fabricating techniques in developing natural filler polymer composites.

Hand Lay-Up Technique

Hand lay-up technique is the most flexible and often used for fabrication of natural fiber epoxy composites. It is an open mold fabrication method as shown in Fig. 1 (Deo and Acharya 2010), where reinforcement (particulates or fibers) and epoxy blends are poured into mold and held for curing. If the reinforcement is in fiber form, the fiber laminates are placed in desired orientations onto the resin-coated mold, and layers of laminates are place one over the other by spraying or brushing the epoxy resin polymer at each intermediate layer which acts as adhesive material. It can also be used for making complex shapes. Fabrication of composites by reinforcing

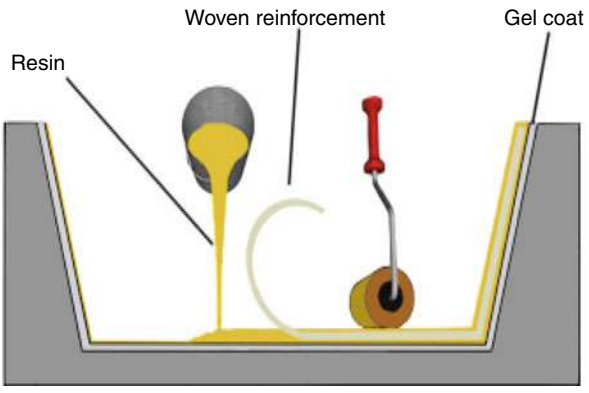

Fig. 1 Hand lay-up process. (Reused with permission from (Deo and Acharya 2010))

chopped natural fibers into epoxy polymer reported that composites prepared exhibited good mechanical properties. Ojha et al. (2014) successfully developed jute/Kenaf hybrid natural fiber composites using hand lay-up technique. Shotton-Gale et al. (2010) developed wood apple and coconut shell particulate epoxy composites and carried comparative study of mechanical properties of both the composite materials. From the past research, it is evident that hand lay-up technique can be employed for all types of natural reinforcements (i.e., particulate, short fiber, and long fiber).

Filament Winding

Filament winding is also an open mold fabrication method mainly employed for fabricating composites with fiber reinforcements. In filament winding, fibers are winded over a mandrel which as mold as shown in Fig. 2 (Shrigandhi and Kothavale 2021). This method is generally adopted for fabricating composites with cylindrical and rotational symmetric geometry products. Dai et al. (Dai and Fan 2014) experimented fabricating flax and viscose fiber epoxy composites. The authors concluded that low viscous epoxy resin could yield composites with better mechanical properties.

Resin Transfer Molding (RTM)

Resin transfer molding is usually a closed mold fabrication method. In this method, liquid resin is transferred into the mold in which reinforcement is present. The transfer of epoxy resin is carried by injection tool. The resin transfer velocity within the mold and between the reinforcements may result in micro-void defects. To reduce and eliminate the void formation and homogeneity, this method is carried out with a vacuum assistance. Understanding the rheology of the resin is significant before performing the resin transfer molding method (Park and Seo 2011) as shown in Fig. 3.

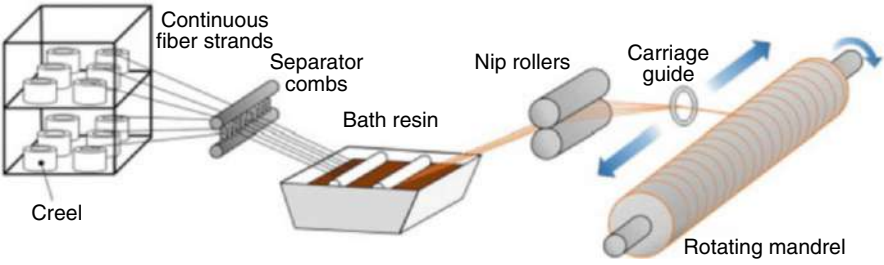

Fig. 2 Filament winding. (Reused with permission from (Shrigandhi and Kothavale 2021))

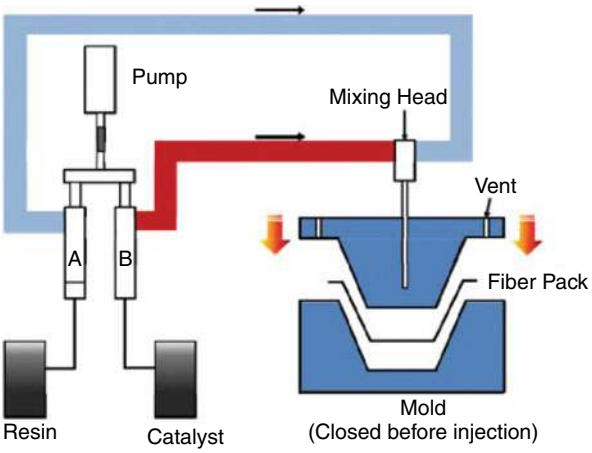

Fig. 3 Resin transfer molding. (Reused with permission from (Park and Seo 2011))

In resin transfer molding, liquid resin has to reach all the fiber laminates of proper adhesion and interfacial bonding. Epoxy resin is generally cured with a catalyst (hardener), so during flow of resin into the mold, chemical reaction takes place for curing. There are applications where the requirement of fiber loading will be large; in such cases there will high resistance to resin flow which may lead to curing of resin at intermediate flow paths. Hence it is important to have knowledge of viscosity of epoxy resin and chemical reactions involved during curing for obtaining the high-performance epoxy composites using RTM method. RTM method proved to be a cost-effective fabrication method for obtaining natural fiber epoxy composites. Bell et al. (Bell 1969) developed different natural fiber epoxy composite materials by reinforcing different natural fibers using resin transfer fabrication method. From the investigation of mechanical properties of composites, the authors concluded that resin transfer molding is a promising technique for fabricating natural fiber polymer composites.

Characterization Techniques (Rheometry)

It is intuitive to realize the mechanical properties of the composite materials, and hence a realization in this aspect can be cited in the literature through characterization techniques. The initial works cited in the literature revealed that orientation and flow fibers in the matrix play a crucial role in achieving the desired properties. As a result, there is development of rheometers that are capable to control the flow behavior in material processing. This enables the process to be carried out in three stages as compacting pellets, alignment of fibers, and unfilled polymer processing. This process achieved a proper flow orientation of short fiber composites. With this little understanding of how complex it is for a thermoset resin to cure properly to achieve desired properties, an intuition to this complexity was investigated; the

chemo-rheological transition during cure under the differential scanning calorimeter (DSC) and thermomechanical analysis (TMA) were reported. Acknowledgment for highlighting the challenges involved with cure kinetics derives the motivation for the current discussion and is outlined as follows:

1. Exothermic reactions due to thermal activation of polymers
2. Raise in glass transition temperature
3. Increase in length of viscoelastic-elastic temperature range
4. Appearance of equilibrium elastic response over glass transition temperature
5. Loss of continuity due to cavitation and void formation

Alongside the following characterization, experimental setups are used to determine the physical parameters during cure which include spectroscopic methods such as magnetic resonance spectroscopy (MRS), Fourier transform infrared (FTIR), mid-infrared (MIR), and near-infrared (NIR) and remote spectroscopy.

Exothermic Reaction Studies

It is imperative to discuss from the literature that exothermic reactions play an important role in studying the dynamic behavior of the curing process. In a specific way, we call them as peak exothermic reactions which trigger the heating rate during curing process. The study of these exothermic peaks gives an accurate measurement of activation energy for any kind of reactions. As a result, to study these exothermic peaks, we used differential scanning calorimetry (DSC) characterization technique, and the analysis referred to the calibrations is termed as thermogravimetric (TG) curves. For an instance, consider Fig. 4 that shows a TG curve for acetylated jute fibers with a peak 370.8 °C.

The above figure is DSC thermogram for an untreated jute fiber. With this simple understanding, we shall now discuss the cure kinetics of various epoxy/natural fibers

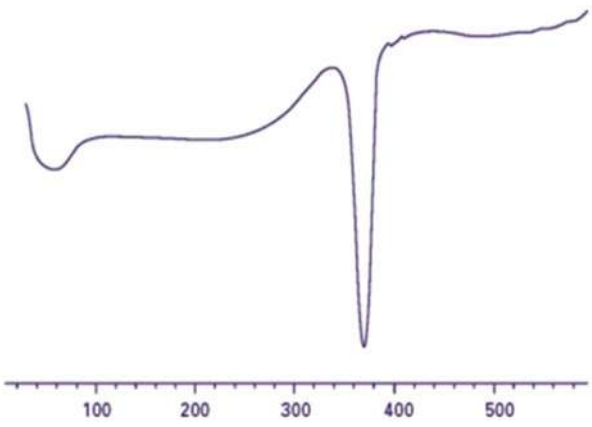

Fig. 4 DSC curve for an untreated jute fiber

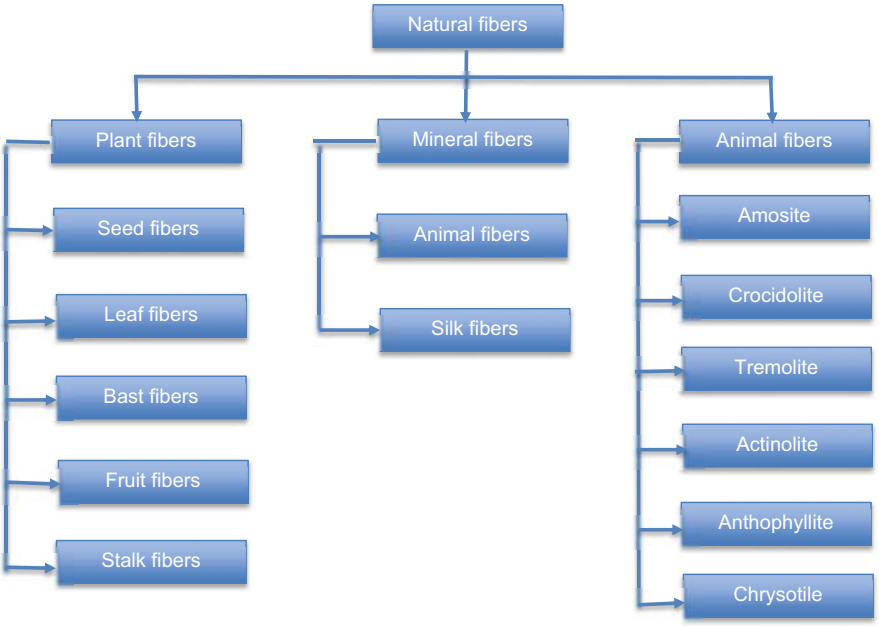

Fig. 5 Classifications of natural fibers

from the scientific literature and from author's perspective that will enable the readers to realize the need for monitoring the cure kinetics that affects the mechanical properties. From the scientific literature, many researchers have done ample contributions to the global community in the development of natural fiber-based composites. From many review works, the natural fibers are classified as shown in Fig. 5.

We shall now briefly discuss on various epoxy-based natural fibers, where an ample amount of research has progressed in the global community. In this context, a work from Mittal et al. (Mittal and Chaudhary 2018) has investigated the curing process for a jute fiber-based composite and suggested an optimization of parameters that are possible for controlling cure kinetics. The authors emphasized on the effect of temperature, fiber twist, and content of the fiber volume on the curing process. The studies suggest that the higher the curing temperature, the faster the curing reaction and residual strains. Actually these residual strains incline toward a stability when the curing reaction is about to complete. Fiber twist and their arrangement have a similar trend just like the effect of temperature, i.e., the greater the fiber twist and the tighter the fiber arrangement result in poor thermal conductivity and cause a lag in the curing process. However, this difference in thermal coefficient doesn't have significant effect in the residual strain, whereas when the fiber content is increased, there is a decline in residual strain and peak exotherm can be earliest.

An interesting discussion was made regarding the thermal decomposition for a coir fiber shows three steps of loss of mass. The maximum rate of thermal

degradation from the DSC curve exotherm peaks reflects to higher restrictions of debonding of molecular chains with the increase in the coir fiber content but revealing lower thermal stability; this occurs because of the presence of more crystalline cellulose in fiber. From DMTA, increase in the coir fiber content enhances the storage modulus which results in constrain of molecular mobility which slackens the stress relaxation process. Alongside, a work on leaf fibers also received significant attention, and in this context, a work from Asim et al. (2018) investigated the effect of pineapple leaf fiber (PALF) loading on thermal and mechanical properties extensively. The incorporation of PALF into phenolic matrix reduced the thermal stability which is evidential from the TGA curves; the weight loss after adding PALF increased the range of temperature, because of the thermal decomposition of hemicellulose and lignin of cellulose natural fibers. Whereas when PALF is added to alkali and silane enhanced the thermal stability of the fibers, this is because of thermal de-polymerization of hemicellulose. DTMA analysis has revealed that increase in the PALF fiber in the matrix enhanced the storage modulus up to 50 wt % but upon the increase, the stiffness reduces. This occurs due to the agglomerates present within composites, which enables uneven dispersion of fibers reducing the stiffness.

More scientific insights are available in the literature due to the ample amount of scientific interest received in the global community. Study of various plant fibers has contributed to development of new class of composite materials; in lieu of this, a work from (Muralidhar 2013) explored the dynamical and thermal characteristics of flax fibers, and interesting insights were provided. It was observed that thermal stability of matrix declined with increase in flax volume fraction under two-step degradations. The first step of thermal degradation corresponds to glycoside linkages, whereas in the second step, thermal degradation of lignin takes place. The glycoside linkages are attributed to lower thermal degradation because of the hydrophilic nature of flax fiber. It is evidential from the work that there is a significant shift in the glass transition temperature though flax fibers exhibit low thermal stability, but the fibers exhibited enhancement in the stiffness at the same time; there is no significant decline in the stiffness during the glass transition, but typically there is decrease in stiffness upon increasing in the temperature further. A typical material behavior however is expected but found to be amenable to applications to retain stiffness during glass transition temperature. Improving the thermal stability has received a specific interest by researchers in global community; as result, *Moringa oleifera* fruit fibers have been thoroughly investigated in (Nayak and Khuntia 2019) and found that thermal stability of the composite has improved. In most cases, the problem with the natural composites is its difficulty in retaining the stiffness and storage modulus of the composite without compromising the thermal stability. Increment in temperature after glass transition will decrease the modulus due to softening of matrix at high temperature which refers to not as much of observation in composite.

The abovementioned literature works are relevant to plant fibers; however there are substantial works available in the context of mineral and animal fibers, which will be concisely discussed. An excellent work from (Ivanič et al. 2020) had studied

the thermal and physical properties of mineral wool made from basalt glass fibers, and the following observations were discussed. The interesting facet in characteristic of this mineral wool has a first step thermal degradation as evaporation of the absorbed moisture content which is completely different from the discussed plant fibers earlier. In the similar stretch, few have investigated the thermal properties of dragline silk retrieved from the spider *Nephila clavipes*, and the following observations were made.

It was found that these fibers exhibited exceptional characteristics and mechanical properties with good thermal stability. A two-step transition takes place indicting the localized transition in the amorphous domain and the later polymer chain movement associated with the partial melt. It is also observed that further heating attributed to increase in stiffness; this may be due to the loss of moisture and improved crystallinity.

Similar works on various silks include *Antheraea yamamai* silk, *Bombyx mori* silk, etc., to name a few. However, a thorough examination of the silk fibers indicates that they have less fiber strength but intuitively good creep resistance presumably due to evaporation of moisture and their enhancement in crystallinity during heating. Nowadays, hybrid composites that use various series of natural fibers with distinct properties are integrated together to achieve multidirectional properties within a single composite material. Hence in the current context, we shall see few works that pertain to the curing kinetic behavior in terms of thermal degradation and stability which are shown in Table 1 from the literature.

Raise in Glass Transition Temperature

From Table 1, it is clear that glass transition temperature (T_g) for natural fiber epoxy resin-based composites has close analogy of range of T_g. We shall now discuss

Table 1 Glass transition temperatures of various fibers

S. no.	Type of the fiber	Type of resin	Glass transition temperature	Citation
1	Jute	Epoxy	56.7 °C	(Jabbar et al. 2016)
2	Kenaf	Epoxy	87.0 °C	(Fiore et al. 2015)
3	Banana	Epoxy	90 °C	(Venkateshwaran et al. 2013)
4	Empty fruit bunches	Epoxy	85.37 °C	(Jawaid and Khalil 2011)
5	Bamboo husk fiber	Epoxy	75 °C	(Shih 2007)
6	Hemp	Epoxy	65 °C	(Di Landro and Janszen 2014)
7	CFRP	Epoxy	130 °C	(Gabr et al. 2010)
8	Hybrid pineapple leaf fiber	Epoxy	65 °C	(Doddi et al. 2020)
9	Silk	Epoxy	79.5 °C	(Hamidi et al. 2018)
10	Caranan fiber	Epoxy	64 °C	(Souza et al. 2020)

further what happens with the increase in T_g and which material characteristic supports this enhancement. Understanding T_g is so important that it defines the thermal stability of the desired composite, in a classical way temperature at which polymers undergo the transition from glassy to rubbery state. Increase in the T_g of natural fiber/epoxy composites enhances the range of T_g due to stages of thermal degradation and weight loss. This indicates that the first stage of thermal gradation in most of the natural fiber-based composites exhibits slight weight loss due to absorbed moisture evaporation from the composites. Natural fibers exhibit shifts in T_g due to improper adhesion of fibers to epoxy and composition of epoxy and natural fibers.

From the definition of T_g, apart from low temperature weight loss due to absorbed moisture, with a decent temperature of 250–300 °C for rice hulls and wood flour composites, the decomposition takes place in three stages: the low temperature stage where thermal degradation of lignocellulose components takes place, the second stage with decomposition of cellulose, and finally the third stage wood flour exhibiting combustion where it is nonexistent in the case of rice hulls. An excellent insight on the effect of thermal degradation of natural fibers was well emphasized in various works, where degradation occurs in two stages: say, low temperature degradation of cellulose and high temperature degradation of lignin. Cellulose, which is generally hydrophilic in nature, readily absorbs moisture resulting in poor processability.

Increase in Length of Viscoelastic-Elastic Temperature Range

Viscoelastic-elastic temperature range is least studied in the literature because of the complexity of realizing the behavior of the sample during curing process; most of the literature often refers close to glass transition temperature. But it is very important as the viscoelastic characterization with temperature has significant effect on storage modulus. Storage modulus is an important viscoelastic parameter that determines the elastic response of a viscoelastic material during mechanical loading. When the same viscoelastic material is subjected to elevated temperatures, there is a degradation of mechanical property due to energy dissipation in the form of heat, and this is referred to as viscous modulus. By the above statements, it is clear that there is complexity involved in determining the viscoelastic nature of the material during the curing; hence theoretic formulations have received significant attention in the scientific community.

The only method to measure dissipation is through vibro-acoustic response of a system, and this is measured as input frequency to measured response from which energy dissipation is measured in terms of damping. It was found from the classical Arrhenius model which relates frequency and glass transition temperature via an activation energy. One more method to estimate the viscoelastic response uses master curves to identify the shift in temperature and frequency scanning accordingly.

Appearance of Equilibrium Elastic Response over Glass Transition Temperature

It is highly intricate to realize the mechanical behavior of the composite at glass transition temperature during curing process; however a new methodology was adopted to realize this behavior with fully liquid phase rather than solid phase. An elastic wave-based model is proposed to study the problems of glass transition in the literature. An important observation accounts to large-scale rearrangement of atoms after glass transition temperature, which is referred to as local relaxation event (LRE). The problem with the LRE is that they last for a Debye vibration period of 0.1 ps, which is a very short time scale, a very short range elastic medium. This appearance of equilibrium elastic response for a short period of time over a glass transition temperature is observed in recent literatures in the scientific community. The magnitude of transition is generally measured from the amount of change of C_p.

An interesting work which established a relation between gelation and crossover dynamic $G^{'}$ and loss storage moduli $G^{''}$ has been cited in (Sgriccia and Hawley 2007); however it lacked mathematical framework, but interesting conceptual insights were discoursed. But the existence of an underlying thermodynamic phase transition has still been a subject of debate. This mechanism was visually examined in the first-order melting transition similar to a melting of crystal. The authors also recommended that first-order glass transition is interpreted as less long-range elasticity of fluid to a solid of quasistatic microscopic shear modulus which is one of the crucial understanding of first-order glass transition. In analogy to this, a work from (Koushyar et al. 2012) studied the equilibrium elastic response which exists for a short time suggesting that equilibrium modulus increases vividly with T_g conversion during early stages of reaction, i.e., first-order glass transition.

The master curve in Fig. 6 provides the evidence of this observation; the shifting has produced master curves indicating all stages of glass transition where the absence of the peak plateau implicates the presence of equilibrium modulus and its unambiguous behavior in the early reaction. It shows how important a master curve is which actually predicts how fast the material behavior as fully glass-like manner and time required for the substantial relaxation to occur.

Loss of Continuity Due to Cavitation and Void Formation

A work from (Campbell et al. 1995) has investigated the interlaminar shear strength (ILSS) of carbon reinforced epoxy composites declined exponentially with increase in void content. Another work conferred that there is a decline in mechanical properties such as tensile strength and flexural strength and flexural modulus with increase in void content. Few works from the literature have traced that voids are primarily formed because of mechanical air entrapment in laminate during hand lay-up process, moisture absorbed during material storing, moisture dissolved in resin, and volatiles exposed out of chemical reactions. After which following the

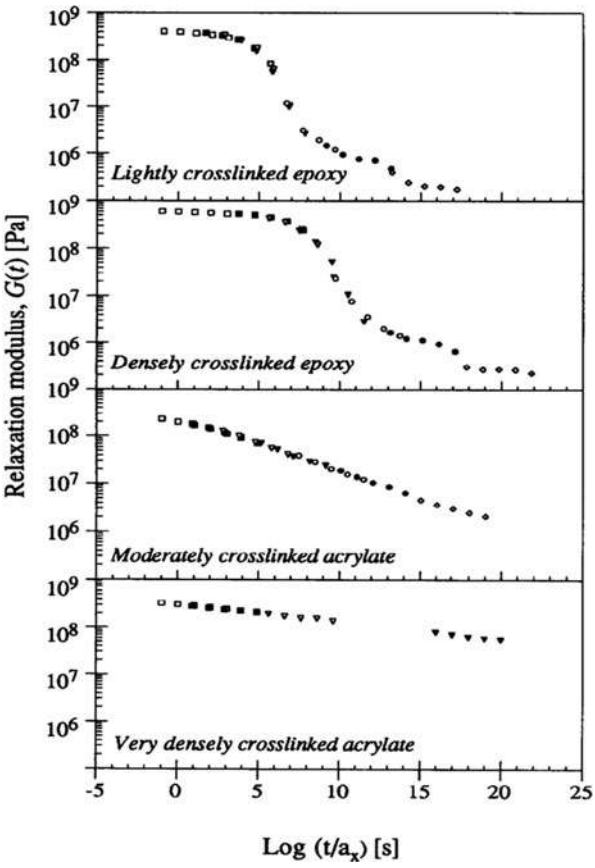

Fig. 6 Master curves to trace equilibrium modulus. (Reused with permission from (Koushyar et al. 2012))

curing process will enable to increase the growth of voids during the increment in the temperature, thus declining the mechanical properties. In context of natural fibers, most of the natural fibers exhibit hydrophilic property and when they are combined with hydrophobic epoxy resin induces voids at the interface between fibers and resin due to poor impregnation (Mosavian et al. 2018).

The ultrasonic C-scan image in Fig. 7 emphasizes voids on the laminate which is implicative that the red color represents the healthy material and yellow color represents the voids on the laminate. The respective optical microscopy image shown in Fig. 8 is absolute replication of the above ultrasonic C-scan. It appeared to be very clear that voids are appearing not only between the interfaces of fiber and matrix but also between the yarns.

It is also observed that as the curing pressure is increased, the air bubbles trapped inside the voids can be squeezed out. However as the curing pressure is further increased, it may cause voids within the yarns. Recent works in the scientific community received significant attention in studying the voids deteriorating the resin flow during curing.

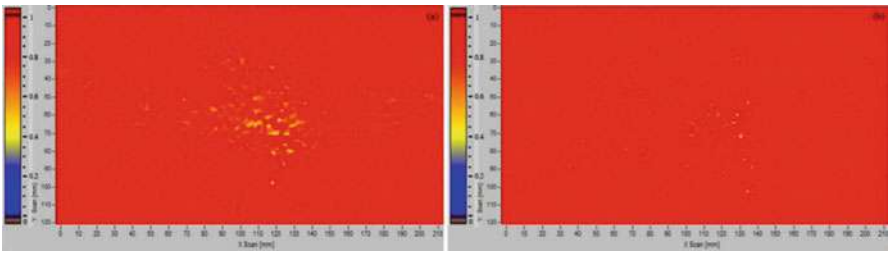

Fig. 7 Ultrasonic C-scan showing voids. (Reused with permission from (Mosavian et al. 2018))

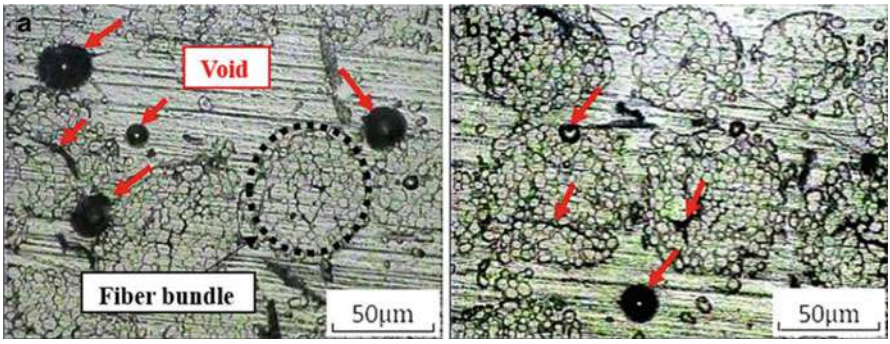

Fig. 8 Optical microscopy indicating voids on surface and fibers. (Reused with permission from (Mosavian et al. 2018))

Dynamic Mechanical Thermal Analysis

DMTA involves the thermal transition in the polymers that describes the free volume changes and relaxation times. The free volume can be monitored based on the change in the stiffness and the release of the heat associated with the latent heat. As regards moving from lower temperatures to the higher temperatures, the first variations in the system would be solid-state transitions. As the material starts heating during the early stages, there is bond bending, and stretching can result in side chain movements; this phenomenon is referred to as γ-transitions. As the chains can displace freely upon further increase in the temperature, the material starts to develop some toughness which is referred to as β-transitions. These β-transitions for most of the researchers in the scientific community have a disambiguation of toughness alone, but for a multicomponent system, the blend would undergo displacements, i.e., the secondary component, and even this is also inferred to as glass transition temperature T_g.

The next phase in the chain displacements is the interesting actual T_g where amorphous regions will start to melt and further heating would reflect crystalline or semi-crystalline with noticeable slippage of the crystallites past each other. However,

these slippage phenomena are not universally accepted as only few literatures on the very limited polymers are available and hence didn't receive scientific attention. Finally melting phase (T_m) is achieved and material starts to flow.

Without any disambiguation, the glass transition parameters influence the final mechanical properties of the system. But interestingly, the sub- T_g during curing plays an important role, and this cannot be pursued from DSC alone, and hence DMA is suggested. Few works pertaining to DMA in light of rheology will be emphasized in the current section.

A work from (Jacob et al. 2006) investigated the dynamic properties of sisal and oil palm fibers reinforced natural rubber composites which were estimated as a function of temperature. It was observed that the $G'$was found to increase due to the stiffness imparted by the fibers, while damping is found to decrease. However for the chemically modified fibers, there is a substantial increment in the G' and G''. This is in contrast to the earlier discussion on phases of curing, the mobility of the chains is in frozen state, and the addition of fibers increases the stress transfer at the interface, thus resulting in enhanced storage modulus; alongside, the loss modulus has shown slight broadening in the curve intimating energy absorption due to addition of fibers. As regards damping as one of the important aspects as discussed, increasing damping is implicative to increase in mobility.

Another excellent work on one of the most naturally existing polymers, chitosan, and its blend with polyvinyl alcohol (PVAL) and hydroxypropylcellulose (HPC) has been investigated for its DMA characteristics. Chitosan being hydrophilic in nature, upon increasing the temperature, the mobility in chains is attributed to the dissociations of hydrogen bonds. It is also evident from the literature that T_g of PVAL gets strongly influenced with the water content and hence with the addition of PVAL increased the T_g for about 10–70 °C. Relevant to similar context, by adding the silica nanoparticles to the chitosan at various compositions, a featured work to enhance the thermal stability was investigated in (Al-Sagheer and Muslim 2010). The results patterned with the increase in silica content from 0% to 30% reduced the damping while increasing storage modulus as discussed earlier. The mobility of chains while increasing in temperature has reduced their rate due to the good thermophysical properties that silica poses, and hence damping reduced drastically.

It is always intuitive to learn how influence of an element in various systems or a system with various elements plays a crucial role to realize the characteristic of the element and the system that allows us to monitor and alter the parameters. In lieu to the above works, we have considered influence of various elements such as PVAL and silica on chitosan and realized how chitosan behaves with various fillers. But now, we emphasize on how silica alters the behavior of a poly-methyl methacrylate (PMM). In this context, a work from (Etienne et al. 2007) investigated the DMA characteristics where authors observed that incorporation of silica into PMMA nanocomposites enhanced the $G'$by 65% at 30 °C. This is because of the proper interactions between the silica nanoparticles and polymers and better dispersion of nanoparticles into PMMA.

In a similar context, a work investigates DMA nature of polyether ether ketone (PEEK) with dispersed zirconia nanoparticles for a wt % up to 3%. With agreement

to the general scientific behavior, the work also revealed the similar behavior of enhancement of thermal stability and G' which is due to uniform dispersion of nanoparticles in the PEEK composites and proper interaction of zirconia nanoparticles in PEEK matrix. It was observed that mechanical properties such as tensile and flexural strength have been consistently increased with the increase in the wt% of zirconia nanoparticles in the PEEK matrix. Without a significant change in the T_g, there is considerable enhancement of the G' and damping characteristics.

Recently wood polymer composites (WPCs) received significant attention in the scientific community due to their wide availability and inherent excellent dynamical properties; a work in this pretext is reported in (Mishra et al. 2012), where authors have selected few species of tropical wood available in the demography and converted to WPC by treating with sodium meta-periodate. This is then followed by further chemical treatment wherein the WPCs are referred to as post-treated WPCs (PTWPC). The dynamical analysis concluded that G' and $Tan\delta$ depend on the type of wood species, whereas the $T_g$was found to be much lower for WPC and PTWPC when compared to raw wood. From the notch of the literature, it is conclusive that natural fibers decrease the damping of the composites.

Due to the advent of technologies, the move toward sustainable development goals led a motive toward renewable energy system. In this context, most of the scientific community has rigorously worked on converting industrial and agriculture waste as a source for renewable energy reserve.

In this context, a work from (Barczewski et al. 2019) have investigated the mechanical and thermal properties of various agricultural wastes as filler materials in epoxy-based composites. The agricultural wastes such as sunflower husk, hazelnut shell, and walnut shell were used in their investigation; however physio-mechanical properties have not been evaluated for the raw system but were added as a filler particle in the epoxy. The DMA characteristic has shown that improved stiffness and hardness, i.e., G' and thermal stability, are reported while decreasing the damping of the composite as accepted from the literature and previous discussions. But mechanical properties such as tensile and flexural strength were declined upon adding the fillers to the epoxy. A detailed investigation on the mechanism involved for the degrading of mechanical properties can be reviewed thoroughly from (Barczewski et al. 2019). A more advanced polymers processed through VARTM say, ELO, cured with various hardness such as (NMA, MTHPA) and various other catalysts are well cited in the literature. As regards DMA characteristics for G' and G'' for NMA-cured formulation at 120 °C, here an important abstract in terms of identifying the degree of material infusion, it was found that either viscosity curve or gel time couldn't capture degree of material infusion.

Linear Viscoelastic Measurements (Rheometers)

As discussed earlier, rheometers are the first of its kind used to measure the nature of the materials that exhibit inelastic, elastic, or combination of both. This kind of sophisticated behaviors is generally possessed by biomaterials in physiological

conditions, but sooner other industries such as aerospace and automotive industries received significant attention. This sudden focus toward rheometry is due to the materials that were in line with these industries such as composite materials. Almost all the composite materials due to their inherent nature which involves the aqueous solution with dispersed materials as reinforcement upon heat treatment finally ends in solid composite. Firstly, we shall discuss on the type of commercially available shear rheometers such as linear shear, pipe or capillary, dynamic shear, rotational cylinder, cone, and plate. Alongside, the types of extensional rheometers such as acoustic, falling plate, and capillary/contraction flow and dynamic shear rheometers. A typical fat characteristic can be perceived in Fig. 9 which disseminates loss and storage modulus and damping against shear oscillatory stress using a controlled stress rheometer as shown in Fig. 10 (Fernanda 2018).

A work from (Banerjee et al. 2021) investigated melt rheological measurements of PP/MWCNT composites in nitrogen environment using strain-controlled rheometer for a linear viscoelastic region. It was observed that as the concentration of MWCNT particle increases, the behavior changes from Newtonian to non-Newtonian at low frequency. It is inclusive from the same article that for higher concentrations at higher frequencies, property of shear thinning takes place. This behavior of shear thinning is applicable for bio-composites whose viscosity must be altered upon application of load. However, paper didn't highlight shear thinning application, but from the current author's area of research, this property has an interesting significance in the drug delivery medication. The effect of this shear thinning is because of the rheological percolation, i.e., "network-like" structures, viz., "polymer/polymer," "polymer/MWCNT," and MWCNT/MWCNT networks. When G' is plotted against G'', if we were to draw the curves, the curves above the diagonal of the axis represent elastic behavior and below the axis are referred to as viscous behavior.

In a similar context, a stress-controlled rheometric analysis to evaluate the gelation process of composite alginate/casein emulsion gels is studied; with the addition of alginate, the gelation time of emulsion gels was found to be reduced. This is because of the aggregation of caseins which is also the result of enhancing the repulsion between caseins and alginates. Behl et al. (2021) have investigated dynamic oscillatory shear strain behavior of FRC with micro-sized fibers and found that as the concentration of

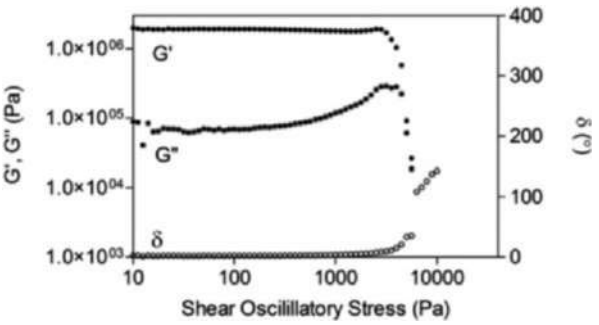

Fig. 9 Characteristics of fat under rheological study. (Reused with permission from (Fernanda 2018))

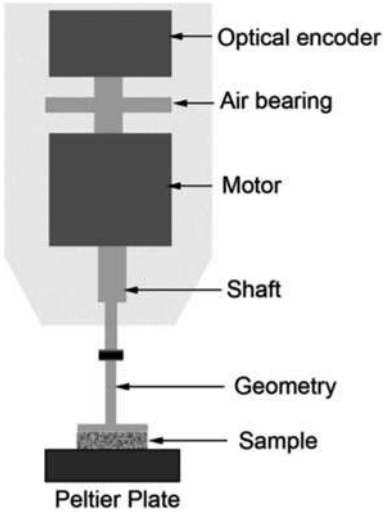

Fig. 10 Schemata of stress-controlled rheometer. (Reused with permission from (Banerjee et al. 2021))

microfibers increased, there is a deviation from ideal condition from flowable composites. The weight composition and ratio of the constituents influence the rheological characteristics of the composites which in fact can be observed from the above literature works also. An interesting understanding which most of the researchers should be sensitive to is identifying a yield point. This is the point where material initiates irreversible elastic behavior (starts to flow) which ultimately dominates the reversible elastic behavior. This attributes to no shearing and further reflects the decrement in storage and loss modulus before the plateau in the calibration.

Apart from evaluating the mechanical properties of the composites, rheometers are also used to study the network formations and microstructural changes in the composites. In this context, researchers have evaluated the dynamic frequency measurements of the PUC/OMTT nanocomposites for different loading of OMTT. To realize the impact of the addition of the nano-clay dispersion in the composite, a low frequency test is carried out for various compositions, and it is found that with the addition of nano-clay, there is a substantial increment in the G' and G''. This increase is attributed to the better particle-particle interface and bonding between filler and polymer. Recently lignin received significant attention by the material scientists to see the amenability for the use of lignin as a reinforcement in the composite due to their excellent mechanical characteristics. But a preliminary work to understand the rheological behavior of the lignin has been reported in (Yuan et al. 2021). The morphology of lignin-containing cellulose fibers exhibited poor gel behavior and low viscosity as lignin can easily disrupt the fibrous network. It was suggestive that a proper choosing of lignin content plays a vital role to tailor the desired rheological properties.

On a concluding remark, it would be important that the rheological characteristics of the composite materials depend on the type of the nanoparticles, reinforcements, and the

processing parameters. An intense care must be taken to evaluate the characteristics from the post-calibration. G' and G'' as a function of frequency, time, and temperature will give the gel characteristics, and G' and G'' against ω gives the morphology of the network chain in the composite material. Hence these analyses when corroborated with scanning electron microscopy (SEM) give the surface morphology which is equally important to see how G' and G'' influence the phase nature of the composite.

Cure Kinetic Models

Development of various classes of materials exhibits intriguing and complicated behavior which is difficult to realize from experiments or needs a sophisticated experimental technique to predict. As a result, just like constitutive models for classical metals, it has been important equally to have kinetic models that define the constitutive behavior of the composite materials during curing. As curing process is very instinctive, parameters in the curing process decide the mechanical properties of the final composite material. The following few methods have been developed by the researchers and are widely used in the scientific community:

1. Dynamic kinetic analysis (DKA)
2. Isothermal kinetic analysis (IKA)
3. Flynn-Wall-Ozawa method (FWOM)
4. Kamal model
5. Kissinger model

Dynamic Kinetic Analysis

Model is based on the proportionality between the reaction rate of chemical changes involving solids and the surface areas of an initial solid and solid product (Montserrat and Málek 1993). The rate equation is given as

$$\frac{d\alpha}{dt} = k\alpha^{\frac{2}{3}}(1-\alpha)^{2/3}$$

where α is fraction reacted at time t and k is rate constant. The calibrated kinetic parameters give a provision to construct time-temperature-transformation (TTT) diagram which indicates behavior of epoxy during isothermal curing. The TTT diagram also implicates restricted mobility where the vitrification occurs.

Isothermal Kinetic Analysis

The rate constants were determined and used in the model to predict the progress of the cure reaction at different temperatures. Agreement with experimental reaction rate data is within $\pm 5\%$, The rate equation in this case is given as

$$\frac{d\alpha}{dt} = k_1 C(1-\alpha)(\beta-\alpha) + k_2\alpha(1-\alpha)(\beta-\alpha)$$

A work in this pretext is very limited as it requires huge set of data to fit the curves; as a result an insubstantial work is reflected in the scientific community. To untangle this complexity, a model-free approach is suggested as it is intuitive that with a very limited data, the curve fitting is possible for obtaining reliable and consistent kinetic information for both isothermal and non-isothermal data. A more relevant information can be cited in (Vyazovkin and Wight 1999), and a model fitting approach to kinetic analysis of pure and crude glycerol is investigated where importantly activation energy of decomposition is also calculated. One of the important characteristics of this model is its activation energy and pre-exponential factor which can be calculated without histology of kinetic model.

Flynn-Wall-Ozawa Method (FWOM)

The method is based on the general form of kinetic formulae and is applicable to general types of reactions governed by a single activation energy. The rate equation developed is given as

$$\ln\left(\frac{dC}{dt}\right) - \ln\left(\frac{dC}{dA\theta}\right) = lnA - \frac{\Delta E}{RT}$$

The robustness of the FWO method is its flexibility to be used not only for kinetic curves but also for many other properties such as viscosity, density, and electro-conductivity that depends on the degree of conversion substance in these reactions. This method is found to be apt for single-stage first-order reaction. Interesting insights in brief can be reflected in (Mamleev et al. 2004) that emphasize on the cure kinetics for single and multi-stage curing process. Works on the applicability of these models can be referred from literature on castor oil pyrolysis, and it was found that the activation energy calculated from this model is meeting the experimental DTG curves. In contrast to this, a similar work is performed and proved that the method is suitable to derive the activation energy during curing, and the variation with the other experimental models is due to iso-conversional kinetic methods.

Kamal Model

With the aid of the proposed kinetic model, it is possible to obtain integral heats of reaction and rates of heat generation at different temperatures during a scanning experiment. The heat balance equation is given by

$$c_p(Q_R, T)\frac{dT}{dt} = Q_s(Q_{Ro}, T_0, T, S) - \dot{Q}_R(Q_R, T)$$

The isothermal DSC and rheological (viscosity-time) data is used to establish the above model, a work in this context can be found from (Sourour and Kamal 1976), and it is assumed that equation obeys homogenous reaction kinetics. It was found that activation energies are in good agreement with the experimental data. This method is suitable to incorporate effects of diffusion into above kinetic expression using a diffusion factor, and it was found that gel conversion is independent of cure temperature. It is also amenable and adoptable to TTT calibration. More suitable works in this context can be cited from the literature; Hosseinpour et al. (2016) investigated cure kinetics of an epoxy resin and others with aliphatic epoxy resin using Kamal method but without inclusion of diffusion factor, though considerable well-established results have been reported.

Kissinger Method

Curves of reaction rates vs temperature for constant heating rates constructed by analytical methods are used to demonstrate the effect of varying orders of reaction which in mathematical form is given as

$$\frac{E}{RT_m{}^2} = \frac{A}{\beta} e^{-\frac{E}{RTm}}$$

Work pertaining to this model can be found in (Chen et al. 1993) to obtain the peak maxima theoretically from thermogravimetric curves, and it was perceived that "the degree of reaction at the peak maxima under various heating rates is the same." The advantage of this method is that it doesn't require the reaction mechanism but just needs only to locate peak maximum temperature, which also serves a disadvantage for this model as it is difficult to predict the peak maxima for real reactions. Few works pertaining to these models can be cited to calculate the cure kinetics and activation energy of a carbon-fiber reinforced epoxy resin from silk and rice husks, and Paluvai et al. (2015) explained the thermal stability of a sisal fiber reinforced unsaturated polyester epoxy nanocomposites using Kissinger method. There is a new form of equation referred to as generalized Kissinger equation which is the most widely used form for predicting cure kinetic parameters.

The above models are the most widely used models in the scientific community due to their capabilities of reflecting the experimental curing behavior in a greater attention. Only few literature has been referred to realize the important parameters that the equations mostly depend on, which were discussed in the current context. With this intuition, we shall further discuss on shear and extension viscosity of the natural fiber epoxy composites.

Shear and Extension Viscosity of Natural Fiber Epoxy Composites

Shear viscosity and extensional viscosity are one of the foremost important rheological properties of polymer composites. They give material flow behavior under application of extension stress. There is an ample work on natural fiber epoxy

composites available in the literature, and (Jana and Prieto 2002) is one such work that defies the complexities involved in determining these two properties. The measurement of shear viscosity is basically carried out on Rheometers using a twin-cone configuration. The author added wood as a constituent material to the epoxy and found that as the composition was increased, the shear viscosity was drastically increased say from $7x10^4$Pa s to $3x10^6$Pa s. A notable insight similar to work of (Jana and Prieto 2002), a work from the same composite, added the effect of viscosity a little wider inferring that viscosity increase in the wood-epoxy system was due mainly to catalytic effects of wood particles; alongside increase in the viscosity has attributed to the vitrification of continuous polyphenylene ether (PPE). In another interesting work from (Wood et al. 2011), who investigated the influence of lignin on the mechanical properties of hemp/epoxy composites and found that there is enhancement in the mechanical properties, as the composition of lignin increased to 2.5% w/w, there is a significant drop in mechanical properties due to increase in viscosity resulting in the poor mixing.

Few reported works on natural fiber/epoxy composites can be cited in the literature such as rheological behaviors on hemp fibers and viscoelastic behavior on banana fiber, and a comprehensive review in this context for natural fibers that interceded epoxy systems was thoroughly emphasized in (Mittal et al. 2016). An investigation toward the thermal anisotropy of jute-based natural fiber epoxy composite was emphasized in (Cichocki and Thomason 2002) wherein the examination of fibrous microstructure as shown in Fig. 11 suggests the optical bright field micrographs of jute fiber; the hallow regions formed on the surface are infiltrated with epoxy indicating that a low-viscosity, low surface tension fluid in Archimedes principle likewise infiltration phenomena would have been reported.

The clear visibility of infiltrations in the fiber suggests that composites produced from low-viscosity thermosets have advantage of determining appropriate fiber volume fraction by the definition of composite, whereas when the composites are prepared from high-viscosity thermoplastics, it would be difficult to identify the epoxy infiltrates and hence intricate the analysis of fiber volume fraction.

In an investigation from (Mun et al. 2020), a decent information has been retrieved on the accountability of wettability on apparent viscosity of uncured liquid composites and subsequent curing process of the basalt fiber/epoxy composite. An interesting intuition to note is that composite treated with plasma reveals higher viscosity than other physiochemical modifications, indicating that epoxy is acting as a lubricant to inject ductility which is supported by the curing curves at escalating temperatures. The variation of viscosity against the temperature is shown in Fig. 12.

Chemorheology of Epoxy/Fiber Composites

Chemorheology is a subject to study deformation properties of reactive polymer systems (Halley 2012) and majorly includes specific heat, thermal conductivity, and compressibility. The essential key elements of chemorheology are:

1. Fundamental chemorheology
2. Chemo-viscosity profile
3. Gelation and vitrification
4. Properties and modeling

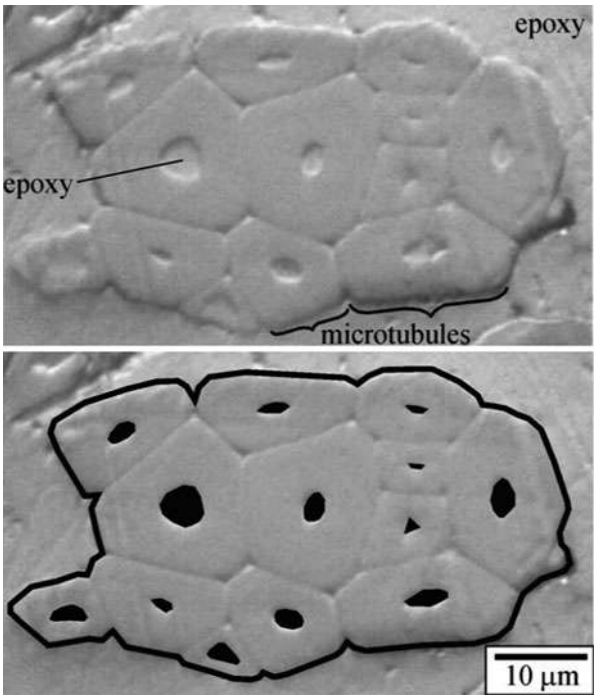

Fig. 11 Microtubes and infiltrations in the fiber. (Reused with permission from Cichocki and Thomason (2002))

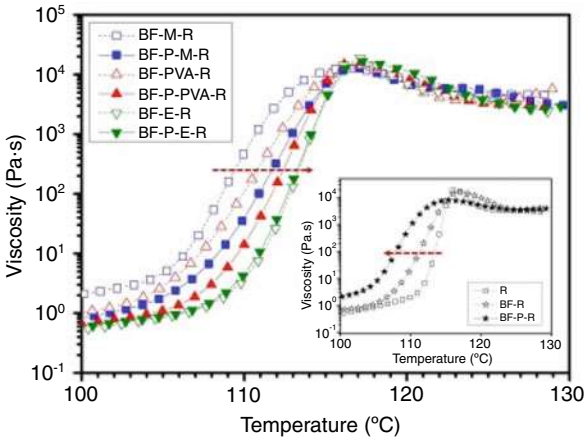

Fig. 12 Variation of viscosity against temperature. (Reused with permission from (Mun et al. 2020))

The fundamental chemorheological behavior deals with wall slip behavior, linear viscoelastic behavior, and existence of yield stress. A detailed emphasis on the same can be inferred from (Halley and George 2009) which discuses the understanding of shear rate effects, cure effects, and combined effects. To study these combined effects on chemorheological behavior of composite system, we have few models that are retrieved from (Domínguez and Madsen 2014) as shown in the Table 2.

Chemorheological modeling depends on the type of the processing, such as casting, potting, encapsulation, sealing and foaming, thermoset and reactive extrusion, molding, and high energy processing. An interesting work from (Domínguez and Madsen 2014) investigated the chemorheological properties such as activation energy of flow, and curing of polyfurfuryl alcohol resin system is discussed. The paper has estimated the viscosity at various temperatures to see the behavior of cure at elevated temperatures that helps to control the flow activation energy and has proper curing phenomena. Due to the advent of technology and techniques, the process optimization immediately received ample attention due to intricate process that chemorheological studies possess. In this context a work from (Lionetto et al. 2017) has studied the impact of adding binder powders into fiber reinforcements to observe the nature of the curing behavior. However interestingly it is observed that proper composition of binder inclusion to the fiber will establish an appropriate stoichiometric for resin hardener. This enabled the authors to optimize the curing parameters with a decent justification. To measure the practicability of the chemo studies, an interesting work is available in the literature (Sangregorio et al. 2019) on studying the cross-linking reactions in humin. The studies attributed to minimize the cycle time and internal stress generated alongside to minimize these stresses too. This way, rheology helps to enhance the process development and improve the

Table 2 List of chemorheology models

Model	Expression	System
Power law	$\eta = \eta_0 \exp\left[\frac{1}{\frac{T_g}{B}+\frac{\alpha}{B}\left(T-T_g\right)}\right] M_w$ $M_w = f(\alpha)$ $T_g = T_g(\alpha)$ $\eta_0 = A\gamma^{n-1}$	Epoxy resin/ silica
Power law/conversion/WLF	$\eta = A_1\gamma^{A_2\left[\frac{a_g}{a_g-\alpha}\right]^{A_3+A_4\alpha}} \exp\left[\frac{c_1\left(T-T_g\right)}{c_2+T-T_g}\right]$	Epoxy resin
(Williams-Landel-Ferry) WLF/Arrhenius	$log\eta* = ln\eta*(T,\omega) + k_\alpha \int exp\,\frac{\Delta E_k}{RT}\,dt$	Filled epoxy resin
Power law/Arrhenius/ molecular	$\eta = A\gamma^B \exp\left(\frac{c}{T}\right)\left[\frac{a_g}{a_g-\alpha}\right]^{D+E\alpha}$	Epoxy resin
Carreau	$\frac{\eta-\eta_a}{\eta_0-\eta_a} = \left[1+\left(\frac{\eta_0\gamma}{\tau*}\right)^2\right]^{\frac{n-1}{2}}$	Epoxy resin
Moldflow	$ln\eta = A_1 + A_2 ln\gamma + A_3 T + A_4\, ln\,\gamma^2 + A_5 \ln(\gamma T) + A_6 T^2 + (A_7 + A_8 X)\ln\left(\frac{a_g}{a_g - a}\right)$	Epoxy resin

performance of the final desired product. There is a need to study on chemorheological studies as natural fiber composites are mostly significant in high strength applications; as a result, not much emphasis and attention are provided to study the viscoelastic nature of these composites.

Molecular Dynamics (MD) Simulations for Rheological Studies

Due to the advent of technology, experimental complexities, cost-effectiveness, and reduction in time favored the entire material science community. The state-of-the-art understanding of the material behavior and travel through the micro-level, nano-level, to atomic level to establish a structure-property relation has been focused over the decades. However, they pose a few constraints; the degree of accuracy received a huge attention in the community. Out of the most widely available packages is the Large-scale Atomic/Molecular Massively Parallel Simulator (LAMMPS), an open source software designated to model the molecular dynamics of almost any kind of problem if a suitable mathematical model is chosen. The post-processing software OVITO visualizes the simulated results by providing the spectra of data. Relevant to the current context, very limited works are cited in the literature, i.e., to study the thermo-mechanical properties of the composite system.

A work from (Li et al. 2012) investigated the thermo-mechanical properties of the epoxy thermoset polymers using MD simulations and compared with the DSC investigations. It was found that T_g as a function of degree of conversion has shown 95% of confidence, and also the values refer to 545 K for MD simulations and 525 K for DSC investigations. In a prologue of MD simulations, from the author's experience, it is methodology inheritance that the molecular properties of any material system must be known in priority. For an instance, most commonly used properties are cohesive energy, chain stiffness, and grafting density. With the same inheritance as discussed by the author, a work from (Karuth et al. 2021) has evaluated the T_g of amorphous polymers using the cheminformatics and MD simulations together. Another work on the same context from (Morita et al. 2006; Yang et al. 2016; Park et al. 2021) mostly demonstrated the amenability of the MD simulations to study the rheological properties. But there is still lacuna in the context of natural fiber/epoxy composites due to the hydrophilic nature, and it poses sub-glass transitions which makes MD simulations difficult to configure the dynamic characteristic of the curing behavior. Still there is a considerable amount of research in progress to evaluate the storage and loss modulus and damping of the composite system. As the scale of MD simulations is at the atomic level, the order of the elastic modulus behavior prediction is hierarchal.

Closing Remarks

Natural fiber epoxy composites received significant attention in the aerospace, automotive, and biomedical industries. Recent developments in the composite materials found new class of materials such as natural fibers which have replaced

the classic metals and ceramics because of their ease of availability and easy processing. However making them amenable to applications has involved complexity in processing; hence the current chapter has provided a brief insight on the applications, processing, and characterization of epoxy resin-based natural fiber composites. Since most of the literature is available in the scientific community on the processing and applications of the fiber composites, a detailed attention on rheological properties has been emphasized in greater detail. The following observations are concisely earmarked for the readers:

1. It is observed that to obtain the desired properties, it is important to have a proper cure kinetics and mechanisms of the chosen composite.
2. The curing parameters such as curing temperature, viscosity, and rate of heat are crucial parameters which decide the thermal stability of the composite. Variation of these parameters helps to enhance the thermal stability hence mapping to thermal degradation respectively.
3. Glass transition temperature is one of the most crucial mechanisms in the curing process, which actually during characterization reflects a peak exotherm. This transition temperature is the zone where brittle materials tried to behave like a rubber and started flowing like a viscoelastic material.
4. Shear and extensional viscosity parameters have critical influence on the curing which decides the mechanical properties such as storage, loss modulus, impact strength, and strength to weight ratio.
5. Chemorheological studies on various natural fiber epoxy composites have been discussed, and it was identified that they also possess rheological properties, and the rheological studies also allow us to assist in optimizing the curing parameters.

References

F. Al-Sagheer, S. Muslim, Thermal and mechanical properties of chitosan/SiO2 hybrid composites. J. Nanomater. **2010** (2010)

M. Asim, M. Jawaid, M. Nasir, N. Saba, Effect of fiber loadings and treatment on dynamic mechanical, thermal and flammability properties of pineapple leaf fiber and kenaf phenolic composites. J. Renew. Mater. **6**(4), 383–393 (2018)

J. Banerjee, S. Kummara, A.S. Panwar, K. Mukhopadhyay, A.K. Saxena, A.R. Bhattacharyya, Influence of carbon nanotube type and novel modification on dispersion, melt-rheology and electrical conductivity of polypropylene/carbon nanotube composites. Polym. Compos. **42**(1), 236–252 (2021)

M. Barczewski, K. Sałasińska, J. Szulc, Application of sunflower husk, hazelnut shell and walnut shell as waste agricultural fillers for epoxy-based composites: A study into mechanical behavior related to structural and rheological properties. Polym. Test. **75**, 1–11 (2019)

S. Behl, A.D. Farahani, G. Rajan, A. Ellakwa, P. Farrar, P. Thordarson, B.G. Prusty, Evaluation of rheological behaviour of flowable dental composites reinforced with low aspect ratio micro-sized glass fibres. Dent. Mater. **37**(1), 131–142 (2021)

J.P. Bell, Flow orientation of short fiber composites. J. Compos. Mater. **3**(2), 244–253 (1969)

F.C. Campbell, A.R. Mallow, C.E. Browning, Porosity in carbon fiber composites an overview of causes. J. Adv. Mater. **26**(4), 18–33 (1995)

D. Chen, X. Gao, D. Dollimore, A generalized form of the Kissinger equation. Thermochim. Acta **215**, 109–117 (1993)

F.R. Cichocki Jr., J.L. Thomason, Thermoelastic anisotropy of a natural fiber. Compos. Sci. Technol. **62**(5), 669–678 (2002)

R.B. Da Cruz, E.P.L. Junior, S.N. Monteiro, L.H.L. Louro, Giant bamboo fiber reinforced epoxy composite in multilayered ballistic armor. Mater. Res. **18**(Suppl 2), 70–75 (2015). https://doi.org/10.1590/1516-1439.347514

F.S. Da Luz, S.N. Monteiro, E.S. Lima, É.P. Lima, Ballistic application of coir fiber reinforced epoxy composite in multilayered armor. Mater. Res. **20**, 23–28 (2017). https://doi.org/10.1590/1980-5373-MR-2016-0951

D. Dai, M. Fan, Wood fibres as reinforcements in natural fibre composites: Structure, properties, processing and applications, in *Natural Fibre Composites*, (Woodhead Publishing, 2014), pp. 3–65

N.V. David, M.J.J. Roslan, M.Q. Amri, I.J. Ryan, R. Sundram, V50 ballistic performance of unidirectional woven basalt fiber laminated composites. ASME Int. Mech. Eng. Congr. Expo. Proc. **9**, 1–5 (2017). https://doi.org/10.1115/IMECE2017-70903

M.M. Davoodi, S.M. Sapuan, D. Ahmad, A. Ali, A. Khalina, M. Jonoobi, Mechanical properties of hybrid kenaf/glass reinforced epoxy composite for passenger car bumper beam. Mater. Des. **31**(10), 4927–4932 (2010). https://doi.org/10.1016/j.matdes.2010.05.021

C. Deo, S.K. Acharya, Effect of moisture absorption on mechanical properties of chopped natural fiber reinforced epoxy composite. J. Reinf. Plast. Compos. **29**(16), 2513–2521 (2010). https://doi.org/10.1177/0731684409353352

L. Di Landro, G. Janszen, Composites with hemp reinforcement and bio-based epoxy matrix. Compos. Part B **67**, 220–226 (2014)

P.R.V. Doddi, R. Chanamala, S.P. Dora, Effect of fiber orientation on dynamic mechanical properties of PALF hybridized with basalt reinforced epoxy composites. Mater. Res. Exp. **7**(1), 015329 (2020)

J.C. Domínguez, B. Madsen, Chemorheological study of a polyfurfuryl alcohol resin system – Pre-gel curing stage. Ind. Crop. Prod. **52**, 321–328 (2014)

S. Etienne, C. Becker, D. Ruch, B. Grignard, G. Cartigny, C. Detrembleur, C. Calberg, R. Jérôme, Effects of incorporation of modified silica nanoparticles on the mechanical and thermal properties of PMMA. J. Therm. Anal. Calorim. **87**(1), 101–104 (2007)

P. Fernanda, Methods Used in the Study of the Physical Properties of Fats, in *Structure-Function Analysis of Edible Fats*, (AOCS Press, 2018), pp. 313–385

V. Fiore, G. Di Bella, A. Valenza, The effect of alkaline treatment on mechanical properties of kenaf fibers and their epoxy composites. Compos. Part B **68**, 14–21 (2015)

M.H. Gabr, M. Abd Elrahman, K. Okubo, T. Fujii, Effect of microfibrillated cellulose on mechanical properties of plain-woven CFRP reinforced epoxy. Compos. Struct. **92**(9), 1999–2006 (2010)

A.K. Guduru, V.N.B.P. Sodisetty, V.P.S. Katari, Design and Analysis of Natural Fibre Reinforced Epoxy Composites for Automobile Hood, SAE Technical Pap., no. October, pp. 2019–2020, (2019). https://doi.org/10.4271/2019-28-0086

P.J. Halley, Rheology of thermosets: The use of chemorheology to characterise and model thermoset flow behaviour, in *Thermosets*, (Woodhead Publishing, 2012), pp. 92–117

P. Halley, G. George, *Chemorheology of Polymers: From Fundamental Principles to Reactive Processing* (Cambridge University Press, 2009)

Y.K. Hamidi, M.A. Yalcinkaya, G.E. Guloglu, M. Pishvar, M. Amirkhosravi, M.C. Altan, Silk as a natural reinforcement: Processing and properties of silk/epoxy composite laminates. Materials **11**(11), 2135 (2018)

Hosseinpour, A., Nazockdast, H., Behzad, T., SalimiJazi, H.R., Investigation of the cure kinetics of an epoxy resin by advanced isoconversional and model-fitting methods, in *AIP Conference Proceedings*, vol. 1713, no. 1 (AIP Publishing LLC, 2016), p. 110004

A. Ivanič, G. Kravanja, W. Kidess, R. Rudolf, S. Lubej, The influences of moisture on the mechanical, morphological and thermogravimetric properties of mineral wool made from basalt glass fibers. Materials **13**(10), 2392 (2020)

A. Jabbar, J. Militký, J. Wiener, M. Karahan, Static and dynamic mechanical properties of novel treated jute/green epoxy composites. Text. Res. J. **86**(9), 960–974 (2016)
M. Jacob, B. Francis, S. Thomas, K.T. Varughese, Dynamical mechanical analysis of sisal/oil palm hybrid fiber-reinforced natural rubber composites. Polym. Compos. **27**(6), 671–680 (2006)
S.C. Jana, A. Prieto, On the development of natural fiber composites of high-temperature thermoplastic polymers. J. Appl. Polym. Sci. **86**(9), 2159–2167 (2002)
M. Jawaid, H.A. Khalil, Effect of layering pattern on the dynamic mechanical properties and thermal degradation of oil palm-jute fibers reinforced epoxy hybrid composite. Bioresources **6**(3), 2309–2322 (2011)
A. Karuth, A. Alesadi, W. Xia, B. Rasulev, Predicting glass transition of amorphous polymers by application of cheminformatics and molecular dynamics simulations. Polymer **218**, 123495 (2021)
H. Koushyar, S. Alavi-Soltani, B. Minaie, M. Violette, Effects of variation in autoclave pressure, temperature, and vacuum-application time on porosity and mechanical properties of a carbon fiber/epoxy composite. J. Compos. Mater. **46**(16), 1985–2004 (2012)
S.-M. Lai, F.-C. Yeh, Y. Wang, H.-C. Chan, H.-F. Shen, Comparative study of maleated polyolefins as compatibilizers for polyethylene/wood flour composites. J. Appl. Polym. Sci. **87**(3), 487–496 (2003). https://doi.org/10.1002/app.11419
C. Li, G.A. Medvedev, E.W. Lee, J. Kim, J.M. Caruthers, A. Strachan, Molecular dynamics simulations and experimental studies of the thermomechanical response of an epoxy thermoset polymer. Polymer **53**(19), 4222–4230 (2012)
F. Lionetto, A. Moscatello, A. Maffezzoli, Effect of binder powders added to carbon fiber reinforcements on the chemoreology of an epoxy resin for composites. Compos. Part B **112**, 243–250 (2017)
V. Mamleev, S. Bourbigot, M. Bras, J. Lefebvre, Three model-free methods for calculation of activation energy in TG. J. Therm. Anal. Calorim. **78**(3), 1009–1027 (2004)
E. Marsyahyo, Jamasri, H.S.B. Rochardjo, Soekrisno, Preliminary investigation on bulletproof panels made from ramie fiber reinforced composites for NIJ Level II, IIA, and IV. J. Ind. Text. **39**(1), 13–26 (2009). https://doi.org/10.1177/1528083708098913
A.L. Martínez-Hernández, C. Velasco-Santos, M. De-Icaza, V.M. Castano, Dynamical–mechanical and thermal analysis of polymeric composites reinforced with keratin biofibers from chicken feathers. Compos. Part B **38**(3), 405–410 (2007)
T.K. Mishra, A. Kumar, V. Verma, K.N. Pandey, V. Kumar, PEEK composites reinforced with zirconia nanofiller. Compos. Sci. Technol. **72**(13), 1627–1631 (2012)
M. Mittal, R. Chaudhary, Effect of fiber content on thermal behavior and viscoelastic properties of PALF/Epoxy and COIR/Epoxy composites. Mater. Res. Exp. **5**(12), 125305 (2018)
V. Mittal, R. Saini, S. Sinha, Natural fiber-mediated epoxy composites–a review. Compos. Part B **99**, 425–435 (2016)
S.N. Monteiro et al., Natural Curaua fiber-reinforced composites in multilayered ballistic armor. Metall. Mater. Trans. A Phys. Metall. Mater. Sci. **46**(10), 4567–4577 (2015). https://doi.org/10.1007/s11661-015-3032-z
S. Montserrat, J. Málek, A kinetic analysis of the curing reaction of an epoxy resin. Thermochim. Acta **228**, 47–60 (1993)
H. Morita, K. Tanaka, T. Kajiyama, T. Nishi, M. Doi, Study of the glass transition temperature of polymer surface by coarse-grained molecular dynamics simulation. Macromolecules **39**(18), 6233–6237 (2006)
S.Y. Mosavian, R. Ebrahimi-Kahrizsangi, M.M. Khah, Z. Hamidi, A. Rafiei, M. Behzadi, Effect of mechanical activation on the kinetics of silica carbothermal reduction in non-isothermal conditions. SILICON **10**(2), 387–394 (2018)
S.Y. Mun, J. Ha, S. Lee, Y. Ju, H.M. Lim, D. Lee, Prediction of enhanced interfacial bonding strength for basalt fiber/epoxy composites by micromechanical and thermomechanical analyses. Compos. Part A Appl. Sci. Manuf., 106208 (2020)

B.A. Muralidhar, Study of flax hybrid preforms reinforced epoxy composites. Mater. Des. **1980–2015**(52), 835–840 (2013)

N. Murugu Nachippan, M. Alphonse, V. Bupesh Raja, S. Shasidhar, G. Varun Teja, R. Harinath Reddy, Experimental investigation of hemp fiber hybrid composite material for automotive application, Mater. Today Proc., no. xxxx, (2020). https://doi.org/10.1016/j.matpr.2020.10.798

L.F.C. Nascimento, L.I.F. Holanda, L.H.L. Louro, S.N. Monteiro, A.V. Gomes, É.P. Lima Júnior, Evaluation of ballistic armor behavior with epoxy composite reinforced with Malva fibers. Miner. Met. Mater. Ser. **Part F7**, 647–655 (2017a). https://doi.org/10.1007/978-3-319-51382-9_71

L.F.C. Nascimento, L.I.F. Holanda, L.H.L. Louro, S.N. Monteiro, A.V. Gomes, É.P. Lima, Natural Mallow fiber-reinforced epoxy composite for ballistic armor against class III-A ammunition. Metall. Mater. Trans. A Phys. Metall. Mater. Sci. **48**(10), 4425–4431 (2017b). https://doi.org/10.1007/s11661-017-4264-x

S. Nayak, S.k. Khuntia, Development and study of properties of Moringa oleifera fruit fibers/polyethylene terephthalate composites for packaging applications. Compos. Commun. **15**, 113–119 (2019)

R.R. Niranjan, S. Junaid Kokan, R. Sathya Narayanan, S. Rajesh, V.M. Manickavasagam, B.V. Ramnath, Fabrication and testing of abaca fibre reinforced epoxy composites for automotive applications. Adv. Mater. Res. **718–720**, 63–68 (2013). https://doi.org/10.4028/www.scientific.net/AMR.718-720.63

S. Ojha, G. Raghavendra, S.K. Acharya, A comparative investigation of bio waste filler (wood apple-coconut) reinforced polymer composites. Polym. Compos. **35**(1), 180–185 (2014). https://doi.org/10.1002/pc.22648

F. Pallikari-Viras, X. Li, T.A. King, Thermal analysis of PMMA/gel silica glass composites. J. Sol-Gel Sci. Technol. **7**(3), 203–209 (1996)

N.R. Paluvai, S. Mohanty, S.K. Nayak, Studies on thermal degradation and flame retardant behavior of the sisal fiber reinforced unsaturated polyester toughened epoxy nanocomposites. J. Appl. Polym. Sci. **132**(24) (2015)

J.K. Pandey, V. Nagarajan, A.K. Mohanty, M. Misra, Commercial potential and competitiveness of natural fiber composites. Biocomposites, 1–15 (2015). https://doi.org/10.1016/B978-1-78242-373-7.00001-9

S.J. Park, M.K. Seo, Element and Processing, in *Interface Science and Technology*, vol. 18, (Elsevier, 2011), pp. 431–499

S. Park, J. Moon, B. Kim, M. Cho, Multi-scale coarse-grained molecular dynamics simulation to investigate the thermo-mechanical behavior of shape-memory polyurethane copolymers. Polymer **213**, 123228 (2021)

P.M. Pereira, J.C. Oliveira, Measurement of glass transition in native wheat flour by dynamic mechanical thermal analysis (DMTA). Int. J. Food Sci. Technol. **35**(2), 183–192 (2000)

S.V.N.B. Prasad, G.A. Kumar, K.V.P. Sai, B. Nagarjuna, Design and optimization of natural fibre reinforced epoxy composites for automobile application. Int. Conf. Mater. Manuf. Mach **2128**, 020016 (2019). https://doi.org/10.1063/1.5117928

R. Ramasubbu, S. Madasamy, Fabrication of automobile component using hybrid natural fiber reinforced polymer composite. J. Nat. Fibers **00**(00), 1–11 (2020). https://doi.org/10.1080/15440478.2020.1761927

L.A. Rohen, F.M. Margem, S.N. Monteiro, C.M.F. Vieira, B.M. De Araujo, E.S. Lima, Ballistic efficiency of an individual epoxy composite reinforced with sisal fibers in multilayered armor. Mater. Res. **18**(Suppl 2), 55–62 (2015). https://doi.org/10.1590/1516-1439.346314

S. Rwawiire, B. Tomkova, J. Militky, A. Jabbar, B.M. Kale, Development of a biocomposite based on green epoxy polymer and natural cellulose fabric (bark cloth) for automotive instrument panel applications. Compos. Part B Eng. **81**, 149–157 (2015). https://doi.org/10.1016/j.compositesb.2015.06.021

D.N. Saheb, J.P. Jog, Natural fiber polymer composites: A review. Adv. Polym. Technol. **18**(4), 351–363 (1999). https://doi.org/10.1002/(SICI)1098-2329(199924)18:4<351::AID-ADV6>3.0.CO;2-X

A. Sangregorio, N. Guigo, E.D. Jong, N. Sbirrazzuoli, Kinetics and chemorheological analysis of cross-linking reactions in humins. Polymers **11**(11), 1804 (2019)

N. Sgriccia, M.C. Hawley, Thermal, morphological, and electrical characterization of microwave processed natural fiber composites. Compos. Sci. Technol. **67**(9), 1986–1991 (2007)

Y.F. Shih, Mechanical and thermal properties of waste water bamboo husk fiber reinforced epoxy composites. Mater. Sci. Eng. A **445**, 289–295 (2007)

N. Shotton-Gale, D. Harris, S.D. Pandita, M.A. Paget, J.A. Allen, G.F. Fernando, Clean and environmentally friendly wet-filament winding, in *Management, Recycling and Reuse of Waste Composites*, (Woodhead Publishing, 2010), pp. 331–368

G.D. Shrigandhi, B.S. Kothavale, Biodegradable composites for filament winding process. Mater. Today Proc. **42**, 2762–2768 (2021)

S. Sourour, M.R. Kamal, Differential scanning calorimetry of epoxy cure: Isothermal cure kinetics. Thermochim. Acta **14**(1–2), 41–59 (1976)

A.T. Souza, R.F. Pereira Junio, L.D.M. Neuba, V.S. Candido, A.C.R. da Silva, A.R.G. de Azevedo, S.N. Monteiro, L.F.C. Nascimento, Caranan fiber from Mauritiella armata palm tree as novel reinforcement for epoxy composites. Polymers **12**(9), 2037 (2020)

J. Summerscales, N.P.J. Dissanayake, A.S. Virk, W. Hall, A review of bast fibres and their composites. Part 1 – Fibres as reinforcements. Compos. Part A Appl. Sci. Manuf. **41**(10), 1329–1335 (2010). https://doi.org/10.1016/J.COMPOSITESA.2010.06.001

N. Venkateshwaran, A.E. Perumal, D. Arun Sundaranayagam, Fiber surface treatment and its effect on mechanical and visco-elastic behaviour of banana/epoxy composite. Mater. Des. **47**, 151–159 (2013)

L. Vlaev, S. Turmanova, A. Dimitrova, Kinetics and thermodynamics of water adsorption onto rice husks ash filled polypropene composites during soaking. J. Polym. Res. **16**(2), 151–164 (2009). https://doi.org/10.1007/s10965-008-9213-3

S. Vyazovkin, C.A. Wight, Model-free and model-fitting approaches to kinetic analysis of isothermal and nonisothermal data. Thermochim. Acta **340**, 53–68 (1999)

B.M. Wood, S.R. Coles, S. Maggs, J. Meredith, K. Kirwan, Use of lignin as a compatibiliser in hemp/epoxy composites. Compos. Sci. Technol. **71**(16), 1804–1810 (2011)

D. Wu, Y. Sun, L. Wu, M. Zhang, Linear viscoelastic properties and crystallization behavior of multi-walled carbon nanotube/polypropylene composites. J. Appl. Polym. Sci. **108**(3), 1506–1513 (2008)

M.A. Yahya, Z. Al-Qodah, C.W.Z. Ngah, Agricultural bio-waste materials as potential sustainable precursors used for activated carbon production: A review. Renew. Sust. Energ. Rev. **46**, 218–235 (2015). https://doi.org/10.1016/j.rser.2015.02.051

Q. Yang, X. Chen, Z. He, F. Lan, H. Liu, The glass transition temperature measurements of polyethylene: Determined by using molecular dynamic method. RSC Adv. **6**(15), 12053–12060 (2016)

T. Yuan, J. Zeng, B. Wang, Z. Cheng, K. Chen, Lignin containing cellulose nanofibers (LCNFs): Lignin content-morphology-rheology relationships. Carbohydr. Polym. **254**, 117441 (2021)

Thermal Stability and Flame Retardancy of Epoxy/Natural Fiber Composites

25

Chanchira Jubsilp, Phattarin Mora, and Sarawut Rimdusit

Contents

C. Jubsilp · P. Mora
Department of Chemical Engineering, Faculty of Engineering, Srinakharinwirot University, Nakhon Nayok, Thailand
e-mail: chanchira@g.swu.ac.th; phattarin@g.swu.ac.th

S. Rimdusit (✉)
Department of Chemical Engineering, Faculty of Engineering, Chulalongkorn University, Bangkok, Thailand
e-mail: sarawut.r@chula.ac.th

S. Mavinkere Rangappa et al. (eds.), *Handbook of Epoxy/Fiber Composites*,
https://doi.org/10.1007/978-981-19-3603-6_26

Abstract

Natural fiber polymer composites (NFPCs) are materials of high-strength natural fiber-reinforced polymer matrices. With their eco-friendly nature and sustainability, NFPCs are getting more attention in academy and industrials to utilize natural fibers for potential applications, such as construction, automobile, marine, aerospace, and other applications. The mechanical characteristics and failure behaviors of NFPCs have been studied to compare with those of synthetic fiber-based composites. However, to replace the metal- or ceramic-based materials in the applications, an improvement of thermal stabilities, flame resistance, and dimensional stability at high temperature, which may extend their potential multidirectional applications, has also been presented.

With such context, this chapter provides the natural fiber-reinforced epoxy composites that showed high temperature stability and good flame retardancy and their applications. The effect of types and contents of natural fibers, modified surface fibers, and the addition of flame retardant on glass transition temperature, thermal degradation temperature, and flame retardancy of the composites have been investigated. Moreover, the important characteristics, such as physical and mechanical properties including strength under tensile, flexure, and impact loads, as well as water resistance, were also described.

Keywords

Thermosetting polymer · Copolymers · Biobased epoxy · Thermal property · Mechanical property · Friction

Introduction

Polymer composites reinforced with natural fibers, i.e., plant fibers including cotton (from seed hairs), flax and hemp (from stem fibers), sisal (from leaf fibers), and coconut (from husk fibers), are emerging very rapidly to substitute the metal- or ceramic-based materials and growing to replace synthetic fiber composite materials, i.e., glass fiber-reinforced composites in various applications, including building, construction, automotive, furniture, and packing (Mittal et al. 2016; Bachtiar et al. 2019). Between 2019 and 2024, the global market size of composites is rising from 90.6 to 131.6 billion US dollars with 7.7% compound annual growth rate (CAGR), and the highest CAGR belonged to the natural fiber composites (Research and Markets 2020). The requirement for lightweight and environmentally sustainable composites resulted in the growth of this composite's market. Furthermore, natural fibers showed superior advantages over synthetic fibers, such as renewable resources, biodegradability, inexpensiveness, less damage to processing equipment, and significant mechanical properties. Within the natural fiber composites market, it seems like that the automotive industrial remains the largest segment with value and volume. The growth of this segment may be due to the major driving forces such as increasing concerns for passenger safety and improvement of fuel economy. In addition, unique properties of NFPCs can capitalize to be an innovation and new product development

due to be eco-friendly materials, which are related to circular economy focusing on using renewable resources for manufacturing sectors. Moreover, for market expansion, some of the innovative composite products could be in attaining higher strength and stiffness, greater thermal stability, and better fire retardancy.

Epoxy resins are classified as thermosetting polymers and widely used as a matrix resin for natural fiber composites. An improvement of composite's properties due to good interaction between cellulose molecules of natural fibers and hydroxyl groups of the resin has been reported (Glaris et al. 2014; O'Brien and Hartman 1971). In addition, epoxy resins show good strength and toughness, low water absorption, good electrical insulator, and nonvolatile products. Epoxy resins were polymerized at room temperature or higher room temperature using hardeners without pressure and little or no shrinkage epoxy products after curing was obtained. However, epoxy resins show inherently low flame resistance since its nature is an organic substance that resulted in the limitation of their development and application (Ahamad and Alshehri 2013). Therefore, an integrity of structure of natural fiber/epoxy composites during and after ignition would be considered (Dodds et al. 2000). To improve flame-resistant properties, the addition of halogenated and nonhalogenated flame retardants has been studied (Chang et al. 2013; Levchik and Weil 2004). The enhancement of the flame retardancy by addition of flame retardants into polymers can have two actions as follows: (1) condensed phase and (2) gas phase. Coating and charring actions are condensed phase of flame retardants. Char formation would help to reduce diffusing of gaseous products to pyrolysis surface and to protect polymeric surfaces from heat and oxygen (in air), while mechanisms of hydrogen and hydroxyl radical scavengers provide combustion reactions for gas phase actions. The addition of halogenated flame retardants into polymers can improve the polymer's flame retardancy; whatever, these flame retardants produce environmental problems by releasing toxic products during combustion. Therefore, non-halogenated flame retardants such as phosphorus-containing compounds which are a great big increasing market share of flame retardants, are alternative to replace halogenated flame retardants. The phosphorus flame retardants do not generate any toxic gas and they can exhibit both condensed phase and/or gas phase fire retardant modes of action.

Therefore, this chapter reviews research and commercial sections of plant fiber/epoxy and wood flour/epoxy composites such as *Phormium tenax*, hemp, kenaf, flax, banana, bamboo, sisal, and wood flour from parawood. The effects of fiber contents, surface treatment techniques, coupling agents, and flame-retardant additives on required properties, i.e., thermal stability and flame retardancy have been presented. Potential applications for plant fiber/epoxy composites are also discussed.

Novel Thermosetting Polymer Based on Epoxy

Aliphatic, cycloaliphatic, or aromatic backbones containing epoxy resins with a three-membered ring structure can be called epoxides, oxiranes, or ethoxylines. The resins can react with other resins and polymers, imparting versatility to the resins. Insoluble and inflexible epoxy thermosets were obtained by addition of hardeners, i.e., anhydrides, amines, and amides. To simplify processing and modify

cured epoxy properties, fillers, diluents, plasticizers, and accelerators may be included in the compositions. In addition, to improve epoxy resins weakness, epoxy resins are tailored by different resins/polymers and reinforced with fillers/fibers to provide the desired additional property including fire resistance. On the market, there are basically two epoxy types, i.e., non-glycidyl epoxies and glycidyl epoxies, and various types of epoxies depend on molecular weight, epoxy equivalent weight (EEW), and viscosity, such as diglycidyl ether of bisphenol A (DGEBA), diglycidyl ether of bisphenol F (DGBEF), epoxy novolac, aliphatic epoxy resins, and glycidyl amine epoxy resins. Among the available petroleum-based epoxy resins in current market, DGEBA of 75% is used, and a global epoxy resin demand by sector is as follows: 50% coatings, 18% composites, 13% constructions, 8% electronics, 6% adhesives, 2% electrical, and 3% other (Vom Saal and Hughes 2005). In the year 2026, a predicted valuation of the total epoxy resin markets will achieve about USD 11.28 billion due to the growing demand of paints, coatings, and epoxy-based composites (Market Study Report, LLC 2020).

Chemistry of Preparation and Curing

Epoxy resins are prepared by condensation of epichlorohydrin with bisphenol A. In synthesis method, epichlorohydrin is excessively used, to leave epoxy groups on each end of low-molecular-weight polymer, and a viscous liquid or a brittle high-melting solid epoxy depends on the molecular weight. The formation of DGEBA prepared by using epichlorohydrin and bisphenol A is shown in Scheme 1.

For polymerization of epoxy, epoxide groups react with active hydrogen atoms of hardeners to produce copolymers. Epoxy resins are polymerized by acid anhydrides, urea, phenol-formaldehyde, polyamines, polyamides, and polysulfide through coupling or condensation reactions. The opening of epoxide ring in polymerization was obtained by using amine, giving a β-hydroxyamino linkage as can be seen in Scheme 2.

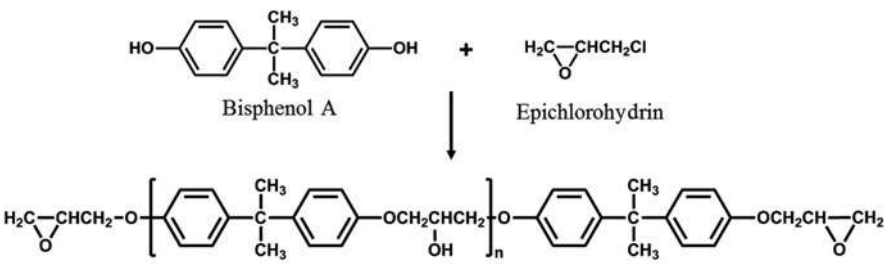

Scheme 1 Epichlorohydrin/bisphenol A-based epoxy (DGEBA) (Lee and Neville 1967)

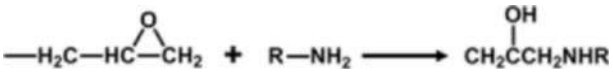

Scheme 2 Polymerization of epoxy resin (Lee and Neville 1967)

Properties and Applications

Epoxy resin acting as a matrix has been extensively used in fiber-reinforced composites due to extended use of the composites in industries, and the composites reached the requirements for high mechanical property with an outstanding adhesive property. In addition, epoxy resins can be cured in a wide temperature range, low shrinkage, and low moisture absorption; however, compared with phenolic resin, the epoxy resins are rather flammable and have thermal stability. Recently, bio-based epoxy resins are getting attention due to the reducing petroleum oil stocks and serious eco-friendly concerns. The economic and environmental values of the conversion of biomass to polymers or composites have been considered. For example, biobased epoxy resins were produced from renewable feedstocks such as vegetable oils (Liu et al. 2012; Park et al. 2004). Furthermore, bio-based epoxy resins have often possessed similar properties to petroleum-based ones. The various types of petroleum- and bio-based epoxy resins are respectively listed in Tables 1 and 2.

Table 1 Chemical structures of petroleum-based epoxy resins

Chemical structure	Chemical structure
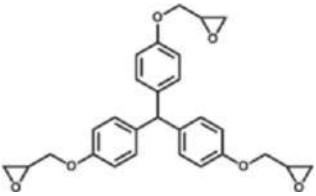 Trifunctional epoxy (Shieh et al. 1997)	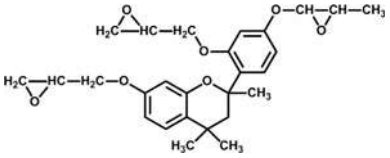 THBPBTH epoxy (Cheng 2009)
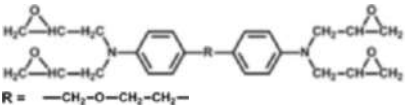 Tetraglycidyl diaminodiphenylmethane (TGDDM) (Mustaţa and Bicu 2000)	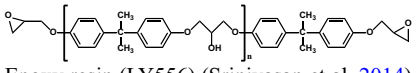 Epoxy resin (LY556) (Srinivasan et al. 2014)
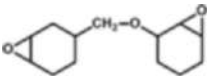 3,4-epoxycyclohexylmethyl-2′,3-epoxycyclohexyl ether (Xie and Wang 2001)	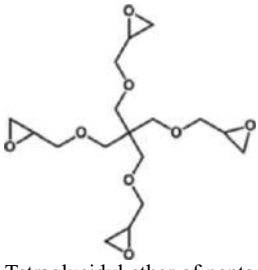 Tetraglycidyl ether of pentaerythritol (Szolnoki et al. 2015)
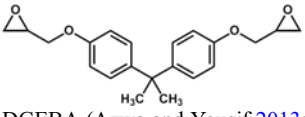 DGEBA (Azwa and Yousif 2013; Jubsilp et al. 2008)	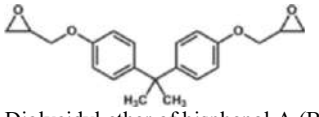 Diglycidyl ether of bisphenol A (Birkner et al. 2019)

Table 2 Chemical structures of bio-based epoxy resins

Chemical structure	Chemical structure
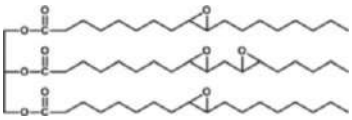 Epoxidized soybean oil (ESO) (Shibata et al. 2011)	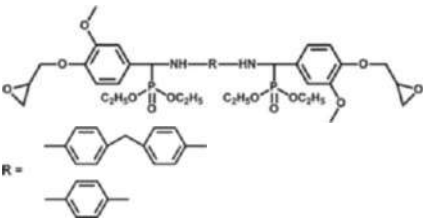 Phosphorus-containing bio-based epoxy (Wang et al. 2017)
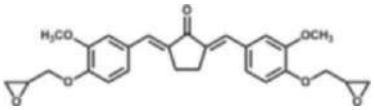 Vanillin-based epoxy (DGEDVCP) (Shibata and Ohkita 2017)	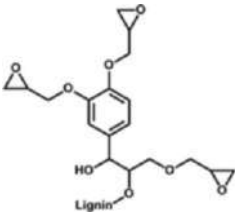 Diglycidyl ether deprotected lignin (DEDL) (Zhao and Abu-Omar 2017)
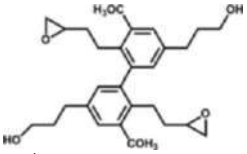 5,5′-Diglycidyl ether (Van de Pas and Torr 2017)	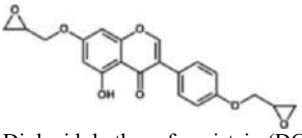 Diglycidyl ether of genistein (DGEG) (Dai et al. 2019)
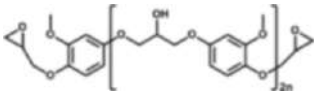 Vanillin-based epoxy (Nikafshar et al. 2017)	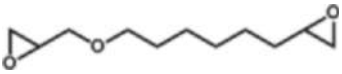 SR GreenPoxy 56 (Senthilkumar et al. 2021)

Thermal Stability and Flame Retardancy of Petroleum-Based Epoxies and Their Copolymers

Petroleum-based epoxy resin (DGEBA) shows exceptional performances that are suitable to use in surface coating, laminates, electronic/electrical industries, automotive, ship, building, and spacecraft (Kumar et al. 2018). However, in a heated environment, the application of epoxy resins is restricted due to only 19.8% for limiting oxygen index (LOI) (Cheng et al. 2020). To extend application choices of epoxy resins, improving thermal stability of epoxy resins is necessary. The two methods for epoxy resin modification to obtain better flame-retardant properties are as follows: (1) adding flame retardants into the substrate and (2) introducing inorganic flame-retardant elements to molecular chains. It was found that the second method displays more advantages because of the uniform dispersion with good

Table 3 Flame retardancy for STCA-cured epoxy and SCA-cured epoxy at various STCA and SCA contents (Cheng et al. 2020)

Sample (wt%)	LOI (%)	UL-94 rating	Dripping
Epoxy/SCA (50)	22.5	NR	Yes
Epoxy/SCA (52.4)	25.3	V-2	No
Epoxy/SCA (54.5)	27.2	V-1	No
Epoxy/SCA (56.5)	29.6	V-1	No
Epoxy/SCA (58.3)	31.4	V-0	No
Epoxy/SCA (60)	31.2	V-0	No
Epoxy/STCA (50)	23.6	V-2	No
Epoxy/STCA (52.4)	28.4	V-1	No
Epoxy/STCA (54.5)	31.2	V-1	No
Epoxy/STCA (56.5)	33.8	V-1	No
Epoxy/STCA (58.3)	33.4	V-0	No
Epoxy/STCA (60)	33.3	V-0	No

epoxy/flame-retardant adhesive. Recently, nitrogen, silicon, phosphorus, boron, titanium, and zirconium-containing halogen-free flame retardants have been prepared to replace a halogenated compound for epoxy resins due to focusing on environmental and human health. Flame retardancy and thermal stability of epoxy THPE triglycidyl ether (THPE-TE) cured with silicon/titanium flame-retardant elements-contained amino curing agent (STCA) to compare with THPE-TE cured by silicon-contained amino curing agent (SCA) have been reported by Cheng et al. (2020) as tabulated in Table 3.

It was found that STCA- and SCA-cured epoxy THPE-TE were generally employed by LOI and UL-94 vertical burning measurements. LOI value was gradually enhanced with an increased content of curing agent, i.e., LOI value = 31.4% (adding of 58.3 wt% SCA) and 33.8% (adding of 56.5 wt% STCA). UL-94 rating was also found to improve from V-2 to V-0. It is possible that STCA based on silicon/titanium showed a synergistic effect for epoxy compared with SCA. In addition, the STCA showed more effective flame retardancy property than the SCA for the epoxy resin. To measure thermal and combustion performances of SCA- and STCA-cured epoxy, the cured epoxy, i.e., epoxy/SCA (58.3 wt%) and epoxy/SCTA (56.5 wt%), was provided by cone calorimetry and thermogravimetric analysis, respectively. Their performances were also compared with pure epoxy as reported in Table 4. The epoxy/STCA showed higher degradation temperature, difficulty in ignition, lower smoke, and lesser toxic gases than the epoxy/SCA. These behaviors indicated that the Si–O–Ti formation of the STCA was found to enhance char shield after combustion, which could help stop the residual char from further rupturing.

The improvement of thermal stabilities and flame retardancy by blending of conventional epoxies with other polymers, such as phenolic-urea oligomers (Raj et al. 2012), phenolic resins (Jubsilp et al. 2008; Rimdusit and Ishida 2000a, b), and benzoxazine resins (Kimura et al. 1998; Rimdusit et al. 2005), was also reported. Raj et al. (2012) have studied thermal stabilities of epoxy blended with four phenolic-urea oligomers based on phenol (PU), m-cresol (CU), resorcinol (RU), and

Table 4 Thermal stability and combustion performance of epoxy/SCA (58.3 wt%) and epoxy/SCTA (56.5 wt%) compared with pure epoxy (Cheng et al. 2020)

Sample	Pure epoxy	Epoxy/SCA (58.3 wt%)	Epoxy/SCTA (56.5 wt%)
Degradation temperature (T_{d10}, °C)	250	310	390
Time to ignition (TTI, s)	28	40	45
Heat release rate (HRR)	362	288	218
CO $production_{avg.}$ (kg/kg)	0.13	0.10	0.07
CO_2 $production_{avg.}$ (kg/kg)	1.41	1.15	0.98

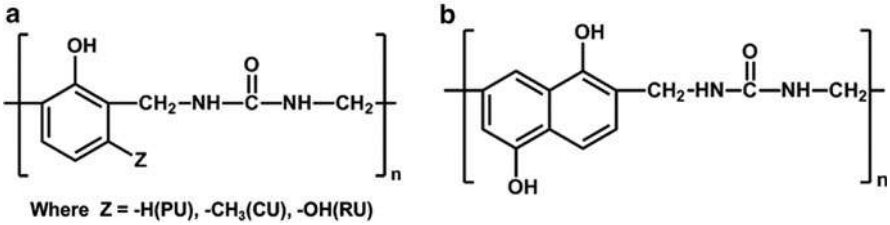

Scheme 3 Phenolic oligomer structures (**a**) PU, CU, and RU, (**b**) NU. (Reprinted with permission from Raj et al. (2012))

1,5-dihydroxy naphthalene (NU). The chemical structures of four phenolic resins are presented in Scheme 3.

Each of cured phenolic-urea oligomers is PU, CU, RU, and NU, while EPU, ECU, ERU, and ENU were labeled for the four cured blends between epoxy resin and phenolic-urea. To measure thermal stability, thermogravimetric analysis (TGA) was provided in this work. The TGA data of both cured four oligomer systems are concluded in Table 5.

It was found that the addition of phenolic-urea oligomer as curing agent into epoxy resin tended to increase degradation temperature and char yield as can be seen the T_{d10} value and char yield, respectively, compared to cured phenolic-urea oligomers. This behavior indicated that hydrogen bonds were formed from the existence of phenolic groups. In addition, to compare with diamines cured epoxy resin, the blending of epoxy with phenolic-urea oligomer showed the improved mechanical properties and higher thermal stability. Therefore, the epoxy-based matrix can be used for composites reinforced with fibers for engineering applications.

As abovementioned, epoxy resins were used for polymer composites reinforced with fibers, since they displayed high mechanical characteristics, high thermal stability, and low moisture absorption. However, hardeners of epoxy resins, i.e., anhydrides and amines, showed some problems, i.e., high toxicity and low storage stability. Then, in composite industries, the polymeric matrix, having user-friendly, easy to process, and more stability in storage, is still developed. Polybenzoxazine, a new phenolic type hardener/curing agent for epoxy, has been presented (Jubsilp et al.

Table 5 Thermal stability of phenolic-urea oligomers and epoxy-phenolic-urea blends. (Reprinted with permission from Raj et al. (2012))

Sample	T_{d0} (°C)	T_{d10} (°C)	Char yield at 800 °C (%)
Phenolic-urea oligomer			
PU	23	275	0.8
CU	28	238	1.3
RU	28	190	0.6
NU	28	55	1.0
Epoxy-phenolic-urea blends cured at the ratio (1:1)			
EPU	32	241	2.3
ECU	31	253	7.2
ERU	32	279	4.7
ENU	32	293	8.9

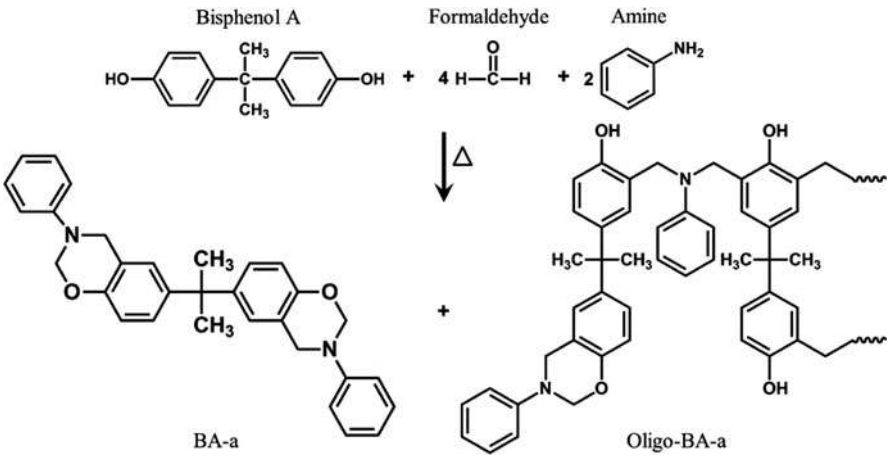

Scheme 4 Preparation and polymerization of bifunctional BA-a resin. (Reprinted with permission from Takeichi et al. (2011))

2010; Kimura et al. 1998; Rimdusit and Ishida 2000a, b). In polymeric composites, polybenzoxazine matrix was recommended to substitute phenolic and epoxy resins due to no generated gas in polymerization. The composite materials based on the resin showed sufficient heat resistance (high glass transition temperature) and strength than phenolic resin or epoxy resin (Kurihara et al. 2012). The conventional benzoxazine resin, i.e., BA-a, can be prepared from bisphenol A, formaldehyde, and aniline by patented solventless method (Ishida 1996) as shown in Scheme 4.

Benzoxazine resins can polymerize by ring-opening without any additional catalyst or curing agents and no by-products after curing. Polybenzoxazines also have low melt viscosity before curing. After curing, they showed high thermal properties, good mechanical properties, and low water absorption when compared

Table 6 Properties of common thermosetting matrix materials. (Reprinted with permission from Ishida (2011))

Property	Epoxy	Phenolic	BA-a benzoxazine	BA-m benzoxazine
Glass transition temperature (°C)	165	170	170	180
Curing shrinkage (%)	1–5	4.5	2.9/0	
Tensile strength (MPa)	59	48	64	44
Tensile modulus (GPa)	2.7	3.8	5.2	4.3
Flexural strength (MPa)	119	80–135	126	103
Flexural modulus (GPa)	2.9	2–4	4.5	3.8
Water absorption at 24 h (% at R.T.)	0.12	0.23	0.11	0.17

to phenolic and epoxy resins as can be seen in Table 6, thus making polybenzoxazines much interested in automotive, electronic packaging, and aerospace industrials. Importantly, benzoxazine resins are able to blend with various other substances to modify flame resistance and mechanical and thermal behaviors, such as blending with epoxy resins (Grishchuk 2011), polyurethanes (Rimdusit et al. 2005), polyimides (Takeichi et al. 2005), and dianhydrides (Jubsilp et al. 2012).

Kimura et al. (1998) have developed DGEBA-based epoxy resin with good thermal stability at 120–150 °C and able to mold by injection. They have compared epoxy resin cured by benzoxazine resin (BA-a) and phenolic novolac (BisA-N) with 2Et4MZ catalyst. They reported that the epoxy cured with BA-a showed greater heat resistance, moisture resistance, and mechanical properties than the epoxy resin cured with BisA-N/2Et4MZ. The T_g value at maxima loss tangent peak of dynamic mechanical analyzer (DMA) of the epoxy/BA-a (T_g = 175 °C) showed higher than that of the epoxy/BisA-N/2Et4MZ (T_g = 149 °C). In addition, Rimdusit and Ishida (2000a, b) have also reported the synergism in T_g and T_d of epoxy (E)/benzoxazine (B)/phenolic (P) resin-based ternary systems. The thermal property, thermal stability, and LOI value of the ternary systems are listed in Table 7.

The epoxy and benzoxazine resin contents significantly resulted in T_g of EBPs, while the improvement of thermal stability was observed with increasing epoxy resin content. These characteristics resulted from increased cross-link density. The char yield of the EBPs increased when compared to epoxy resin. This behavior is due to the higher char yield of polybenzoxazine and phenolic novolac than the epoxy resin. In case of LOI value, representing the minimum level of oxygen in the atmosphere, the higher LOI value shows the higher nonflammability. LOI values of the polymers can be estimated by Van Krevelen and Hoftyzer equation (Van Krevelen and Hoftyzer 1976), which is LOI = 17.5 + 0.4 CR (CR is char yield value). Self-extinguishing polymers are classified by LOI values more than 26.

Jubsilp et al. (2008) have studied the thermal stability and dynamic viscosity of epoxy (E)/benzoxazine (B)/phenolic resin (P) copolymer system at various epoxy contents. T_{d5} values under nitrogen atmosphere of each EBP composition are plotted in Fig. 1.

The T_{d5} of EBP copolymers clearly increased with an increased epoxy content (EBP181, EBP271, EBP361, EBP451, and EBP541), i.e., 357 °C for EBP181 to

Table 7 Thermal stabilities of EBP ternary systems. (Reprinted with permission from Rimdusit and Ishida (2000a))

EBP composition (wt%)	DMA T_g's	T_{d10} (°C)	Char yield at 800 °C (%)	LOI
EBP 181	170	368	32.5	30.5
EBP 271	176	371	31.5	30.1
EBP 361	178	375	31.0	29.9
EBP 451	180	378	30.0	25.5
EBP 541	168	381	25.8	27.8
EBP 631	154	382	21.4	26.1
EBP 111	130	375	38	32.7
EBP 211	145	380	33	30.7
EBP 311	150	400	25	27.5

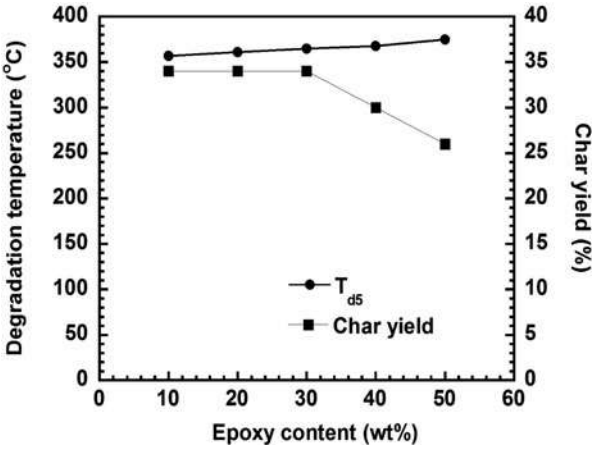

Fig. 1 Degradation and char yield of ternary system of epoxy (E), benzoxazine (B) and phenolic resin (P) at various mass compositions. (Reprinted with permission from Jubsilp et al. (2008))

373 °C for EBP541, while the T_{d5} of the polybenzoxazine equals to 332 °C (Rimdusit et al. 2006). The improvement of the T_{d5} of the EBP by increasing epoxy content was due to the cross-linking formation between the oxazine ring of polybenzoxazine and epoxy's hydroxyl group. The optimum phenolic novolac resin content can catalyze the benzoxazine resin and react with the epoxy resin to obtain an absolute networking. In addition, the char yield of the EBP copolymers reported at 800 °C increased with an increase of benzoxazine content, i.e., from 26% for EBP541 to 34% for EBP181. In addition, the liquefying temperature of the EBP system can be reduced by adding epoxy resin into the benzoxazine resin. This behavior has allowed to easily add high filler content into the EBP composites. In Fig. 2, when epoxy content increased in EBP mixtures, the liquefying temperatures of the mixtures systematically decreased. It was found that 75 °C for liquefying temperature belonged to EBP541, while EBP181 showed 92 °C for liquefying temperature. Furthermore, the gel point of the EBP mixtures decreased with increased benzoxazine resin content in EBPs. The lowest gel temperature of 162 °C belonged to the EBP181, while the gel temperatures of

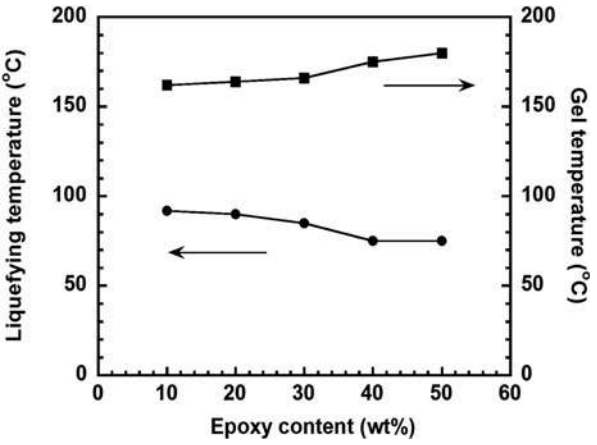

Fig. 2 Liquefying temperature and gel temperature of EBP mixtures. (Reprinted with permission from Jubsilp et al. (2008))

Table 8 Thermal behaviors and mechanical property of epoxy and epoxy/benzoxazine cured with various types of diamines. (Reprinted with permission from Grishchuk (2011))

Sample	T_g from DMA	E′ at R.T. (GPa)	T_{d2} (°C)	Char yield (%)
EP/DETA-Ref	130	2.69	327	9.0
EP/(DETA/DDM)-Ref	155	2.69	338	14.0
EP/DDM-Ref	174	2.63	362	17.5
EP/DETA:BOX (75:25)	134	3.25	317	14.0
EP/(DETA/DDM):BOX (75:25)	151	3.56	309	25.0
EP/DDM:BOX (75:25)	164	3.72	335	22.3

EBP271, EBP361, EBP451, and EBP541 were measured to be 164 °C, 166 °C, 175 °C, and 180 °C, respectively.

Thermal behaviors and mechanical property of benzoxazine (BOX)-modified DGEBA/amine to compare with the properties of reference epoxies were investigated (Grishchuk 2011). The amine hardeners at stoichiometric amounts added in epoxy were diethylenetriamine (DETA), 4,4′-diaminodiphenylmethane (DDM), and DETA/DDM at a 1/1 ratio. From Table 8, the incorporation of BOX into epoxy resin can help significantly enhance the storage modulus (E′) and char yield value compared to the diamine-cured epoxy polymer.

Thermal Stability and Flame Retardancy of Bio-Based Epoxy and Their Copolymers

Bio-based polymers synthesized from sucrose, lignin, and vegetable oils have currently been paying attention. In consequence, polymeric industrials are to find bio-based alternatives. In the case of DGEBA, the resin is prepared from

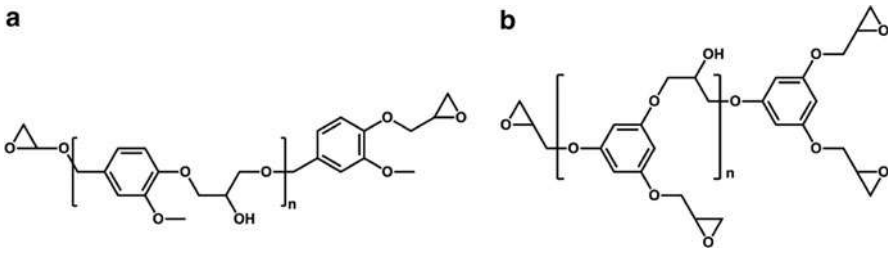

Scheme 5 (**a**) DGEVA and (**b**) PHTE (Specific Polymers 2021)

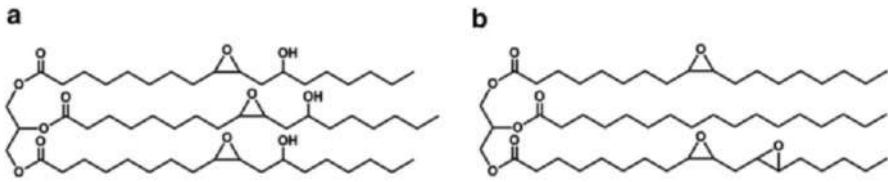

Scheme 6 Epoxidation of unsaturated vegetable oils: (**a**) epoxidized castor oil (ECO), (**b**) epoxidized rapeseed oil/St John's wort oil (Specific Polymers 2021)

bisphenol A, which is a reprotoxic substance; therefore, it is possible that this type of epoxy resin is under close monitoring and might be restricted in some applications, resulting in the bio-sourcing of epoxy receiving a great deal of attention. For example, bio-based epoxy resins have been developed and commercialized by Specific Polymers (2021). In Scheme 5, vanillin alcohol diglycidyl ether (DGEVA) and phloroglucinol triglycidyl ether (PHTE), aromatic resin bearing multifunctional glycidyl ether moieties, were based on the chemical modification of vanillin alcohol extracted from lignin or phloroglucinol extracted from algae.

In addition, epoxidation of unsaturated vegetable oils, i.e., epoxidized castor oil (Scheme 6a) and epoxidized rapeseed oil/St John's wort oil (Scheme 6b), was commercialized by Specific Polymers. They were synthesized in a wide range of epoxidized vegetable oils displaying an epoxy content from 2.5 to 7.0 mEq/g.

Furthermore, thermal properties of epoxy polymers based on epoxidized vegetable oils (EVOs) cured with disulfide-based aromatic dicarboxylic acid (DCA) were examined (Mauro et al. 2020). The thermal properties of 11 newly EVO cured with DCA are tabulated in Table 9. The higher functionality of EVO resulted in the higher reactivity and final properties. The epoxy polymers showed T_gs determined form tan δ peak in a ranging from 34 °C to 111 °C and T_{d5}s in a ranging of 265–285 °C. In addition, the solvent resistance and chemical recycling of the epoxy polymers have been investigated. The bio-based carbon content of epoxy polymers was from 58% to 79%, which can be used in coating or composite materials for automotive sectors.

The property comparison of bio-based epoxy to petroleum-based epoxy was presented by Liu et al. (2012). The bio-based epoxy prepared from a rosin-based epoxy

Table 9 Thermal properties of 11 newly epoxidized vegetable oil cured with DCA (Mauro et al. 2020)

VOs feedstock	EVOs	Epoxy content (mEq/g)	T_g (°C)	T_{d5} (°C)
Karanja oil	EKRNO	2.77	34	285
Castor oil	ECO	2.85	52	275
St John's wort oil	ESJWO	2.97	33	290
Peanut oil	EPO	3.35	35	285
Rapeseed oil	ERPO	3.99	51	285
Soybean oil	ESO	4.20	52	271
Rosehip seed oil	ERHO	4.70	60	275
Safflower oil	ESFO	4.93	68	271
Grapeseed oil	EGRO	4.94	67	265
Camelina oil	ECMO	5.29	85	265
Linseed oil	ELO	5.61	91	271
Hemp oil	EHO	6.09	76	265
Perilla oil	EPLO	6.77	111	265

Table 10 Thermal stability and mechanical properties of rosin-based epoxy and DEGBA. (Reprinted with permission from Liu et al. (2012))

Sample	T_g (°C)	T_d (°C)	σ_f (GPa)	E_f (MPa)
Rosin-based epoxy	164	328 (at 5% weight loss)	2.2	70
DGEBA	174 (Grishchuk 2011)	319 (at 2% weight loss) (Jin and Park 2008)	3.0 (Liu et al. 2010)	80 (Liu et al. 2010)

resin and a rosin-based hardener showed outstanding thermal stability and mechanical properties via the T_g, T_d, flexural strength (σ_f), and modulus (E_f) of cured epoxies. The results listed in Table 10 showed the T_g and T_d of the rosin-based epoxy of 164 °C and 328 °C, respectively. The σ_f and E_f of the rosin-based epoxy, i.e., 70 MPa and 2.2 GPa, respectively, were obtained. The results indicated the possibility to synthesize bio-based epoxy resin with high-performance and inspired researchers to explore more and more renewable alternatives to petroleum-based epoxy resin.

Moreover, the enhancement of thermal property and thermal stability of bio-based epoxy by blending with another bio-based polymer has been reported. Hombunma et al. (2020) have prepared bio-polymer blends from vanillin/furfurylamine-based benzoxazine (V-fa) and epoxidized castor oil (ECO). From Table 11, the thermal and mechanical properties of the ECO could be enhanced by blending with the V-fa as a result of the higher T_g, T_d, and char yield of the V-fa than those of the ECO.

Table 11 Thermal and mechanical properties of ECO/V-fa copolymers. (Reprinted with permission from Hombunma et al. (2020))

Sample (wt%)	T_g (°C)	T_{d10} (°C)	Char yield at 800 °C (%)	E′ from DMA at −100 °C (GPa)
ECO/V-fa (50/50)	100	343	34	1.59
ECO/V-fa (40/60)	110	345	35	1.73
ECO/V-fa (30/70)	130	346	48	1.86
ECO/V-fa (20/80)	158	357	55	2.27
V-fa	270	392	66	–

Natural Fiber-Reinforced Epoxy and Their Copolymers

Natural Fiber and Fabric-Reinforced Epoxy Resin

Reinforcement of fiber in polymers is a good-looking way to modify polymers. Fibers in various forms are as follows: short fiber, continuous fiber, and fabric. Currently, in the areas of engineering and research technology, requests of NFPCs which are a potential substitute for polymer composites reinforced with synthetic fibers, i.e., glass and carbon fibers, have increased dramatically.

De Rosa et al. (2010) have studied the thermal stability and mechanical property (tension and flexure modes) of *Phormium tenax* fiber-reinforced petroleum-based epoxy (SP Systems Ampreg 26) composites. The authors showed the chemical compositions of plant fibers as presented in Table 12. In comparison to other commercial plant fibers, *Phormium tenax* fibers have a rather low content of cellulose and high hemicellulose content. Chemical compositions of the fibers play a key role in the fiber toughness. The increased toughness with rising hemicellulose and lignin contents have been mentioned (Rajaei et al. 2018).

In this work, reinforcing fiber is a short fiber (20 mm length), and 20 wt% quasi-unidirectional fiber-reinforced epoxy composite was prepared. The epoxy composites showed higher modulus and strength than those of epoxy due to interface adhesion of fiber and matrix. In Fig. 3, degradation characteristics of *Phormium tenax* fiber showed two main stages. The first stage in a range of 200–305 °C (weight loss approximately 20%) is thermal depolymerization of hemicellulose and pectin, as well as the cleavage of glycosidic linkages of cellulose. The second stage found at 305–370 °C (weight loss approximately 45%) is attributed to the cellulose degradation. The residual weight of fibers was 15.7 wt% at 700 °C, while T_d and residual weight at various temperatures of the composite were higher than epoxy and fibers.

Table 12 Chemical content of natural fiber divided by categories. (Reprinted with permission from De Rosa et al. (2010))

Fiber	Cellulose (wt%)	Hemicellulose (wt%)	Lignin (wt%)
Bast fiber			
Kenaf	31–57	21.5	8–19
Jute	61–71.5	12.0–20.4	11.8–13
Flax	64.1–71.9	16.7–20.6	2.0–2.2
Hemp	70.2–74.4	17.9–22.4	3.7–5.7
Leaf fiber			
Phormium tenax	45.1–71.0	30.1	11.2
Banana	63–64	10–19	5
Sisal	65.8–78	8–14	10–14
Seed fiber			
Cotton	82.7–90	5.7	

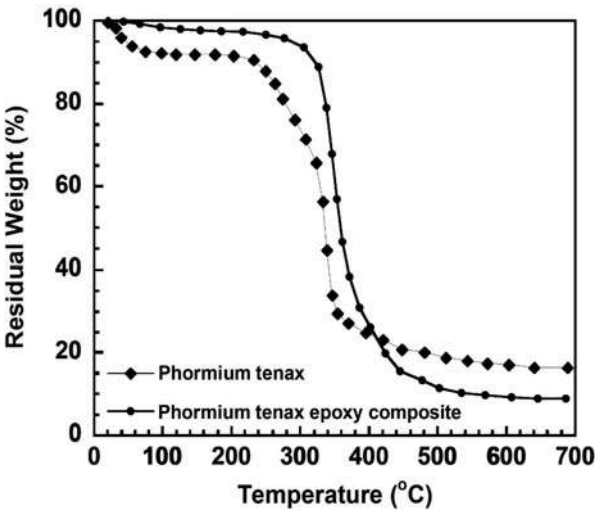

Fig. 3 TGA curves of *Phormium tenax* fibers and *Phormium tenax* epoxy composites. (Reprinted with permission from De Rosa et al. (2010))

This study suggested that the incorporation of natural fiber into epoxy composite could enhance in both mechanical property and thermal stability, depending on fiber components and compositions.

Generally, cellulose, hemicellulose, and lignin are a key chemical composition of natural fibers. The differences in the chemical compositions of natural fibers result in flammability. The higher cellulose content causes a higher flammability, whereas the higher lignin content leads to the greater char formation with lower degradation temperature. Azwa and Yousif (2013) have studied thermal degradation of short kenaf fiber-reinforced petroleum-based liquid epoxy (DER331) composites by using untreated kenaf fibers and alkaline-treated kenaf fibers. From thermogravimetric analysis (TGA), it was found that untreated kenaf fiber showed two obvious

Table 13 Mechanical and thermal properties of composites. (Reprinted with permission from Srinivasan et al. (2014))

Composites	Impact strength (J)	Flexural strength (MPa)	Degradation temperature (°C)	Char yield (%)	LOI
Flax/banana hybrid composite	16	13.54	365	18.42	25
Flax composite	11	11.59	372	9.69	21
Banana composite	12	9.76	374	1.27	18

peaks: (1) the first peek at 260 °C corresponds to hemicellulose degradation, and (2) the second peak (346 °C) corresponds to cellulose degradation. The addition of kenaf fibers into the epoxy can slightly improve the char formation and thermal stability of epoxy, while an alkalization causes to reduce these behaviors for the epoxy composite. This study also confirms that reinforcing epoxy resin with natural fiber, having high thermal stability (low hemicellulose content, high lignin content), is a potential way to develop the thermal stability of the polymer composites.

Hybrid composites have been developed to be engineering materials to replace the traditional ones. Two or more reinforcing fibers combined in polymeric matrix can improve the composite properties. Srinivasan et al. (2014) developed 40 vol% of banana and flax fiber (hybrid fibers)-reinforced epoxy resin (LY556) by using HY951 hardener. The structural buildup is a sandwich structure having hybrid flax fiber/banana fiber/flax fiber layers as a core material and glass fiber layer (GFRP) as a shell material. The strength of the hybrid composites under impact, flexure, and tensile modes is improved. The thermal stability and flame resistance of the flax/banana hybrid with GFRP composite are better than single flax fiber with GFRP and single banana fiber with GFRP composites, and the results are listed in Table 13. The results also revealed that the hybrid composite has better mechanical and thermal properties than the composite reinforced with single fiberglass.

Improved Flame Retardancy of Natural Fiber and Fabric-Reinforced Epoxy Composites and Their Copolymers

Petroleum-based epoxies are normally highly flammable and combustible. To improve the flame resistance of epoxy resins, fire retardants or copolymerization with other thermosetting polymers is incorporated. The flame retardancy of epoxy composites has been improved by adding of halogen flame retardants; however, due to toxicity and corrosive gases released from these flame retardants after ignition, they may be banned in some applications. Then, non-halogen flame retardants were developed and used for NFPCs based on epoxy.

Khalili et al. (2019) investigated the effects of flame retardants, i.e., zinc borate (ZB), ammonium polyphosphate (APP)/ZB, and alumina trihydrate (ATH)/ZB on flammability and thermal and mechanical properties of empty fruit bunch (EFB) fiber-filled DGEBA composites. The epoxy composite-filled ZB (5, 10, 15 wt%),

Table 14 Degradation temperature (T_{d50}) and vertical Bunsen burner test (for 12 s) of EFB-reinforced epoxy composites filled with fire-retardant hybrids. (Reprinted with permission from Khalili et al. (2019))

Composites	T_{d50} (°C)	Residual mass at 600 °C (%)	Drip flame time (s)	Burn length (mm)
EFB-reinforced DGEBA (control)	386	16	54.5	Complete burn
EFB-reinforced DGEBA/ZB15	405	35	0 (no drip)	Complete burn
EFB-reinforced DGEBA/APP5ZB10	401	34	0 (no drip)	Complete burn
EFB-reinforced DGEBA/APP10ZB5	398	32	0 (no drip)	Less than 3 mm
EFB-reinforced DGEBA/ATH10ZB5	398	31	0 (no drip)	Complete burn

APP/ZB (15 wt%), and ATH/ZB (15 wt%) were prepared. From Table 14, the adding of flame retardants can help enhance the thermal stability of the EFB-reinforced DGEBA composites. The DGEBA/EFB/ZB composite revealed a higher thermal stability than DGEBA/EFB/ATH and DGEBA/EFB/APP composites, since the ZB showed more enhancing flame retardancy than APP and ATH. In addition, flammability behaviors of the composites are also recorded in Table 14. The synergy and self-extinguishing the flame with 0 s flame time, 0 s drip flame time, and burn length less than 3 mm were obtained by adding APP of 10 wt% and ZB of 5 wt%.

To replace metallic structural units by polymer composites, the low flame resistance of the composites is one of the main limitations for automotive and aerospace industries that currently require renewable and/or biodegradable structural polymer composites. The natural fabric as reinforcing fiber with lower weight, lesser density, and lower costs accompanied with the renewability and biodegradability compared with synthetic fibers (carbon, glass, or aramid fibers) in bioepoxies was introduced. Szolnoki et al. (2015) have developed hemp fabric/epoxy composites with a 30% fiber content. The composites were prepared and introduced with phosphorus-based curing agent (TEDAP) into reinforcing fibers. From the results of thermal stability and flame retardancy as presented in Table 15, the addition of TEDAP into hemp fabric/epoxy composite was found to enhance LOI and flame resistance (UL-94 rating) compared to those of hemp fiber/epoxy composite without TEDAP. Furthermore, when treated fabrics (SiTHF-treated NF) were applied with epoxy/TEDAP matrix, the flame resistance with UL-94 V-0 rating was obtained.

Boccarusso et al. (2016) have studied composite system reinforced with natural fibers for aeronautic applications that required flame resistance. In this work, hemp-reinforced epoxy (I-SX10) biocomposites by adding ammonium polyphosphate (APP) as flame retardant were prepared by infusion technique. The fire and mechanical properties of the obtained biocomposites with various APP contents were provided by cone calorimeter, vertical burning, dynamic mechanical analyzer, and universal testing machine. The results in Table 16 showed that the flame properties

Table 15 Thermal stability and flame retardance of natural hemp fabric-reinforced epoxy composites. (Reprinted with permission from Szolnoki et al. (2015))

Property	Epoxy polymer	Epoxy/ phosphorus (2.5%)	Hemp fabric/ epoxy composite	Hemp fabric/ phosphorus (1.75%)/ epoxy composite	Thermotex- and sol-gel-treated hemp fabric (SiTHF: 1.47% Si)/phosphorus (2.14%)/epoxy composite
Degradation temperature at 5% weight loss	–	–	–	278.0	239.5
Char yield (%)	–	–	–	29.6	45.7
LOI	23.0	29.0	22.0	32	32
UL-94	HB	V-0	HB	V-1	V-0

Table 16 Flammability of hemp fabric/epoxy biocomposites. (Reprinted with permission from Boccarusso et al. (2016))

Sample	APP-unfilled biocomposite	16.32 wt% APP-filled biocomposite
Flame time (t_f) (s)	250.4	1.3
Drip time (t_d) (s)	1.0	0.0
Burn length (L_b) (mm)	260.2	5.0
Status of the test	Failed 	Passed 

of the APP-added biocomposite were improved when compared with the biocomposite without APP, while no effect on their mechanical characteristics and on the process feasibility was observed. Therefore, it was suggested that the adding of flame retardant enhanced the flame resistance of epoxy composites without sacrificing mechanical properties.

The effective method, copolymerization with other resins or polymers especially thermosetting polymers to improve epoxy properties, was mentioned above. BEP mixtures based on benzoxazine, epoxy, and phenolic novolac can provide suitable properties, especially in the highly filled systems. Highly filled BEP wood composites by using wood flour (parawood) as reinforcement were developed by Jubsilp et al. (2008). The modulus and char yield of the wood composites were enhanced with an increase of benzoxazine fraction in the BEP. This characteristic was due to the good compatibility between the wood flour and the BEP copolymers. The results

revealed that the addition of 70 wt% wood flour showed an increase in the modulus, i.e., 8.3 GPa for the BEP811 composite, whereas that of the BEP811 copolymer was found to be 5.9 GPa. In addition, the BEP wood composite also showed the relatively high flexural strength (70 MPa). Moreover, it was found that the addition of wood flour into the BEP copolymers could enhance the thermal stability of the wood composites. Figure 4 shows the degradation temperature and char yield of the wood composites. The degradation temperatures of the wood composites showed an increase with increasing epoxy resin content, i.e., from 273 °C for BEP811 composite to 280 °C for BEP451 composite, while the addition of benzoxazine resin was found to improve the char yield of the wood composites.

The char yield increment of the wood composites with increasing benzoxazine resin content implied that the wood composite showed a substantial effect on boosting flame retardance as char formation, a proactive difficulty to mass and heat transfer; in consequence, more oxygen is required for combustion. It is possible that ether linkage formation between a hydroxyl group of polybenzoxazine and an epoxide-enhanced cross-link density results in improved char formation. The chemical reaction between polybenzoxazine and epoxy is presented in Scheme 7.

Birkner et al. (2019) have compared the thermal stability and mechanical property of basalt fiber-reinforced bisphenol A-based epoxide (BADGE) cured with a novel amine hardener (APSI) to basalt fiber-reinforced BADGE cured with diamine hardener (IPDA). The basalt fiber-reinforced BADGE/APSI composite showed more flame resistance with a higher solid residue after oxidation. Furthermore, the BADGE/APSI and BADGE/IPDA reinforced with basalt fiber showed the storage modulus of an approximately sixfold increase, and the storage modulus of the basalt fiber/BADGE/APSI composite showed higher than that of the basalt fiber/BADGE/IPDA composite. Good interaction formation (covalent bonds) is possible between the free NH groups of epoxy matrix and some functional groups of sizing at the basalt fiber surface (Table 17).

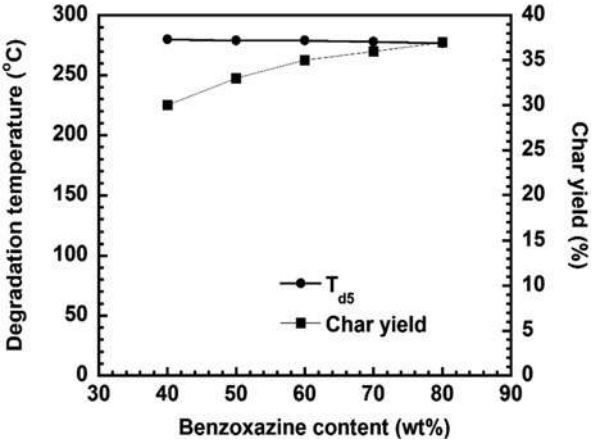

Fig. 4 Thermal stability of wood-substituted BEP composites at various benzoxazine contents. (Reprinted with permission from Jubsilp et al. (2008))

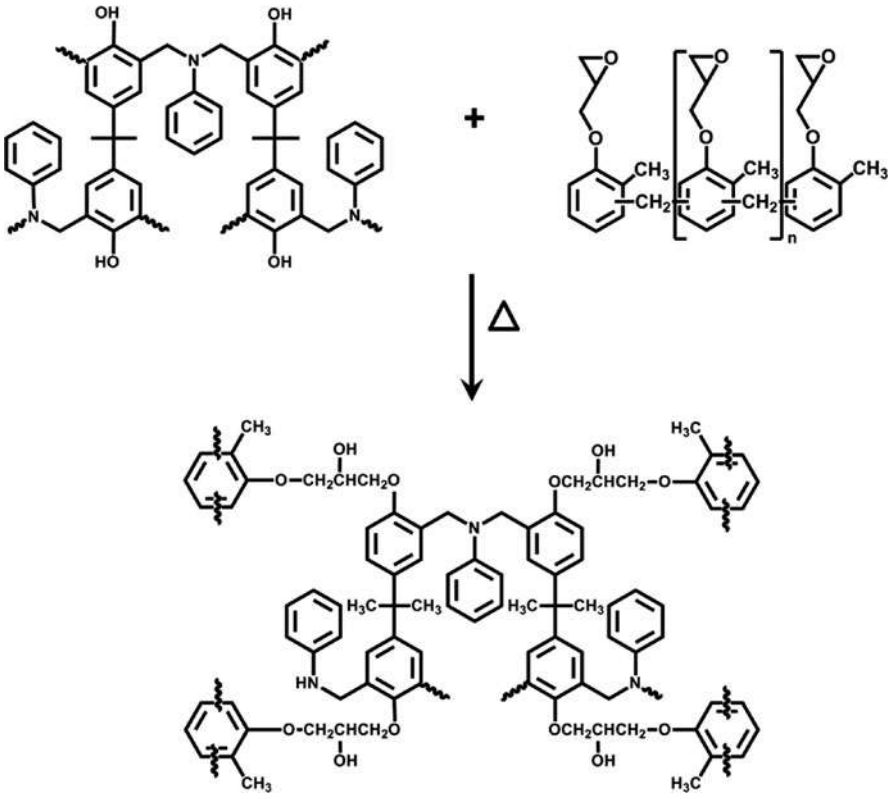

Scheme 7 Curing reaction of epoxy novolac resin with hydroxyl groups in polybenzoxazine. (Reprinted with permission from Jubsilp et al. (2010))

Table 17 Thermal properties of epoxy polymer and its composite (Birkner et al. 2019)

Sample	T_{d5} (°C)	Solid residue (%)	Storage modulus at 23 °C (GPa)	T_g (°C)
BADGE/IPDA (1:1 molar)	292	0	2.49	76
Basalt fiber-reinforced BADGE/IPDA (1:1 molar) composite	319	67	16.69	
BADGE/APSI (1:2 molar)	184	20	1.81	30.9
Basalt fiber-reinforced BADGE/APSI (1:2 molar) composite	330	73	17.21	

Bio-Based Epoxy and Their Copolymer Composites Reinforced with Natural Fiber

Development of bio-based epoxies is gaining increased attention to replace petroleum-based ones due to their environmental advantages. To improve their flame resistance, the blending of flame retardants in bio-based epoxies has been reported.

Dai et al. (2019) studied the flammability behaviors of a bioepoxy resin (DGEG) cured with 4,4-diaminodiphenylmethane (DDM). Only carbon, hydrogen, and oxygen element-containing DGEG/DDM was obtained. The DGEG/DDM showed 6.3 kJ/g for total heat release, 33.1% of LOI, and V-0 rating in UL94 test (as can see in Fig. 5). The DGEG/DDM displayed higher T_g (223 °C) when compared to DER332 epoxy cured with DDM, i.e., 175 °C. In addition, the increment 12% of storage modulus (25 °C), 19% of tensile strength, 33% of flexural strength, and 183% of residual char at 800 °C was observed. It can be seen that a new approach to synthesize high-performing flame-retardant epoxy resins can take the unique structure advantages of renewable compounds.

The addition of flame retardants for NFPCs was found to improve flame resistance, reduce visible smoke, and restrict produced product volume of the composites (Fatima and Mohanty 2011). Biocomposites based on bio-based polymer and biofiber (natural fiber) were prepared to protect the natural environment and save petroleum resources. Shibata et al. (2011) have successfully developed tannic acid-cured epoxidized soybean oil (ESO/TA) at 210 °C for 2 h at a ratio of epoxy/hydroxyl (l.0/1.4). The tensile strength (15.1 MPa), tensile modulus (458 MPa), and T_g (58 °C) for the cured ESO/TA were obtained. They also prepared ESO/TA/microfibrillated cellulose (MFC) biocomposites at various MFC contents in a range of 5–11 wt%. The MFC-reinforced ESO/TA biocomposites at 9 wt% MFC showed the highest T_g (61 °C) and tensile strength (26.3 MPa) as can be seen in Fig. 6. The tensile modulus of the biocomposites increased with an increase MFC content, up to 1.33 GPa at 11 wt% MFC. The T_{d5} of the biocomposites tended to reduce with an increase of MFC content, and the values were higher than that of dried MFC (315 °C).

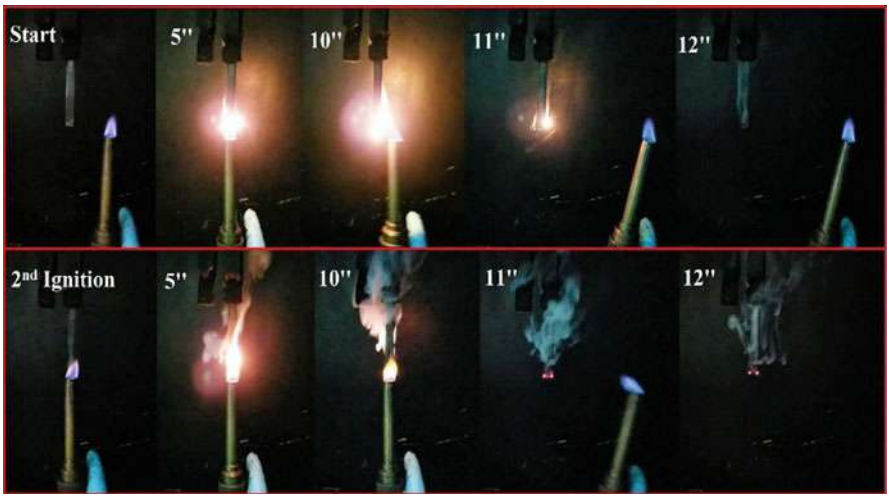

Fig. 5 UL-94 test for DGEG/DDM. (Reprinted with permission from Dai et al. (2019))

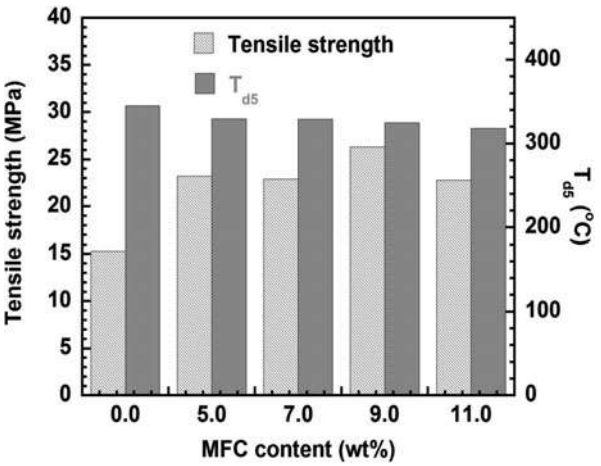

Fig. 6 Tensile strength and T_{d5} of ESO/TA/MFC biocomposites at various MFC contents (Shibata et al. 2011)

Table 18 Properties of bamboo/kenaf fibers/epoxy composites. (Reprinted with permission from Chee et al. (2019))

	Degradation temperature (at maximum rate of mass loss) (°C)			Complex modulus, E* (MPa)		
Composites	Before	After accelerated weathering	After soil burial	Before	After accelerated weathering	After soil burial
Pure epoxy	382.9	375.6	377.0	2844	3612	2728
B:K:30:70	371.0	329.8	377.0	3610	3949	2036
B:K:50:50	372.8	337.2	378.2	3944	4446	2236
B:K:70:30	379.9	351.1	383.5	3678	4146	2270

Chee et al. (2019) have evaluated the degradation temperature and complex modulus under environmental effects, i.e., exposing to accelerated weathering and soil burial of epoxy composites filled with 40 wt% bamboo fiber (B)/kenaf fiber (K). The different mass ratios of B to K, i.e., 30:70, 50:50, and 70:30, were prepared. From Table 18, it was found that the bamboo fiber showed more effect on degradation temperature and complex modulus of the composites after accelerated weathering and soil burial. The higher bamboo fiber content in the composites showed higher degradation temperature and complex modulus. Moreover, it was observed that the soil burial has led to more pronounced degradation, as compared to accelerated weathering. To balance of resistance to environmental effects, the epoxy composite reinforced with bamboo and kenaf fiber at 50:50 was suggested to be a potential biocomposite for structural applications.

Yorseng et al. (2020) have measured performances under accelerated weathering conditions of kenaf/sisal fibers/bio-based epoxy composites to compare with bio-based epoxy without kenaf/sisal fibers. The tensile properties, impact strength, morphology, degradation temperature, and water absorption of the composites

before and after weathering test were investigated. The results showed that those properties before and after weathering of the kenaf/sisal fiber-reinforced bio-based epoxy composites were moderately high in comparison to bio-based epoxy. Therefore, the bio-based epoxy composites are promising polymer composites for semi-structural applications.

Senthilkumar et al. (2021) have prepared fiber mats/epoxy biocomposites by layering sequence of sisal fiber mat (SSSS), hemp fiber mat (HHHH), and sisal/hemp mats (HSSH and HSHS). The accelerated weathering conditions related to approximately 1 year of the outdoor conditions were established for the bio-based epoxy and their composites. After weathered biocomposites, mechanical properties and thermal stability were measured and compared to the unweathered ones. The declined tensile strength of 7% and 13% and decreased flexural strength of 25% and 26% for the weathered HSSH and HSHS, respectively, were observed. In addition, thermal stability in term of degradation temperature at 5% weight loss (T_{d5}) and char yield of the unweathered and weathered biocomposites was reported. The T_{d5}s of the unweathered and weathered biocomposites were quite similar, while the char yield of the weathered biocomposites showed lower than that of unweathered ones. In Fig. 7, it was found that the impact strength of all unweathered and weathered biocomposites was similar. The impact strength of all unweathered biocomposites was approximately in the range of 13–19 kJ/m^2, while that of all weathered composites showed an approximate of 16–19 kJ/m^2. It can be summarized that this composite is optional for the outdoor structural applications with good impact strength.

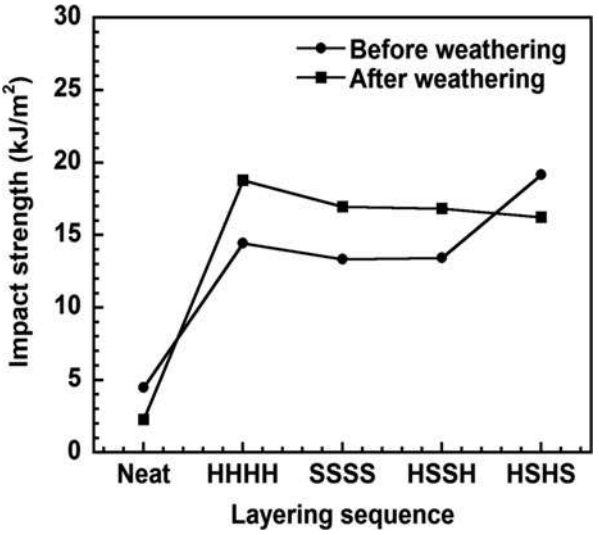

Fig. 7 Impact strength of sisal/hemp-reinforced epoxy biocomposites at different layering sequences before and after weathering (Senthilkumar et al. 2021)

Potential Applications Required Thermal Stability and Flame Retardancy of Natural Fiber-Reinforced Polymer Based on Epoxy and Their Copolymers

As aforementioned, in various applications using NFPCs, i.e., structural materials, transportation, and others as shown in Fig. 8, the flame retardancy requirement is fundamental. Therefore, the development of NFPCs shows a good flame resistance to fulfill safety measures.

Structural Materials

NFPCs have proved that they can be used as structural units, i.e., floors, decks, facades, and roofs, since natural fiber reinforcement can help enhance mechanical properties, i.e., high strength and structure (Pickering et al. 2016). However, in applications that has a fire risk, the composites with good flame resistance would be required. Venkateshwaran et al. (2013) have studied the effect of alkali (NaOH) treatment (conc. of 0.5–20%) on mechanical characteristics of banana/epoxy composites. The 1% NaOH-treated banana fiber/epoxy composites showed better properties

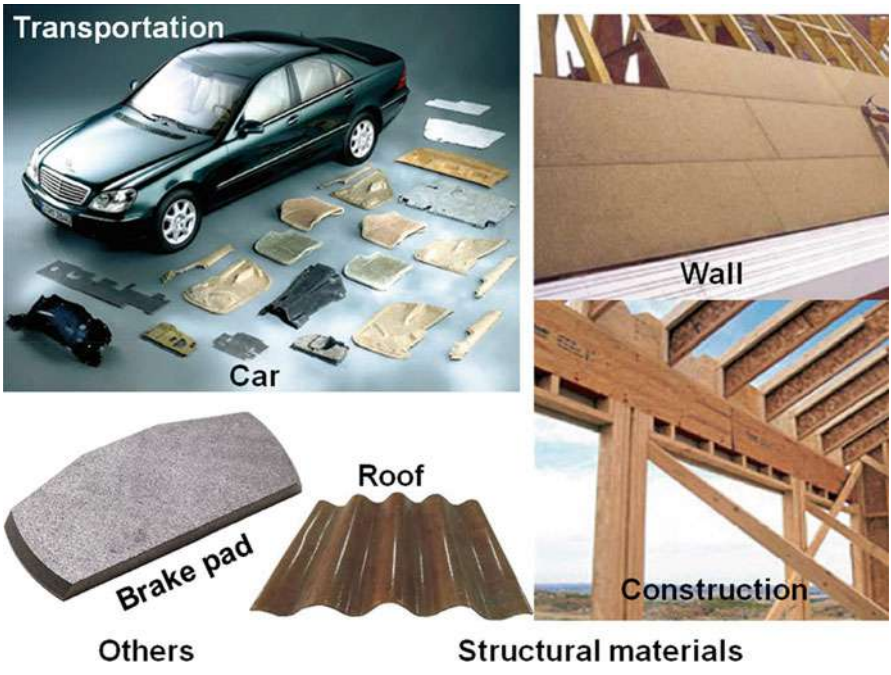

Fig. 8 NFPC applications (ICP Wind 2016–2020; Pollitt 2011; Suhaily et al. 2013)

when compared to other treated and untreated fiber/epoxy composites. The optimal alkali content on the reinforcing fiber surfaces may be a reason in getting better mechanical behaviors of the obtained composite. However, the excess alkali contents may damage the fiber surface, leading to decreased mechanical properties.

Transportation

NFPCs modified by flame retardants have been used in automotive and aerospace industries, especially for enhancing the interiors. However, the candidate materials for transportations have enormously strict rules and regulations, such as for aircraft interiors, they have to measure smoke density, burning, and releasing of heat after burning as recommended by the Code of Federal Regulation (CFR).

Flammability of the flax fabric/epoxy composite was measured and compared to that of glass fabric/polymeric composite (Rajaei et al. 2018). The flax fabric/epoxy composite showed poorer flame resistance. In comparison with the glass fabric/epoxy composite, a more rigorous burning of flax fabric/epoxy composite was observed from the 60 s under vertical burning. By adding intumescent flame retardant, the flax fabric/epoxy composite showed quite similar fire performance to the glass fabric/epoxy composite modified by intumescent flame retardant. The flax fabric-intumescent fire-retardant composite and glass fabric-intumescent fire-retardant composite took 14 and 15 s, respectively, to extinguish. This characteristic indicated that both composites were able to pass the CFR vertical burning. The peak of heat release rates of flax-intumescent fire-retardant composite was 269.4 kW/m^2, which was similar to that of the glass fabric-intumescent fire-retardant composite, i.e., 269.2 kW/m^2. The reason for the significant reduction in flammability of the flax fabric/epoxy composite was attributed to intumescent char formation. Moreover, the reaction between lignin component in flax fabric and intumescent fire retardant can help the enhancement of effective char formation.

Others

NFPCs are finding use in numerous applications: electrical and electronic industries, machinery, aerospace, sport, automobile, and construction industry, since they showed light weight, high strength, relatively low manufacturing cost, resistance to fatigue, and non-corrosive materials.

Tribo-composites of kenaf fiber/epoxy for bearing applications have been presented by Chin and Yousif (2009). The wear performance of the epoxy composites was enhanced by 85% when kenaf fibers were reinforced in the composite. To compare with polymer composites filled with jute, sugarcane, oil palm, and glass fibers from previous works, it was found that specific wear rates and friction coefficients of the kenaf fiber/epoxy composites, i.e., 0.15×10^{-5}–2.0×10^{-5} mm^3/Nm and 0.52–0.68,

respectively, showed better performance as the results of specific wear rates and friction coefficients of polymer composites from previous works were in a range of 0.1×10^{-5}–$10{,}000 \times 10^{-5}$ mm^3/N m and 0.02–1.0, respectively. Moreover, sisal fiber/phenolic composites for brake pad application were also investigated (Xin et al. 2007). The optimum friction and wear of sisal/phenolic brake pad composites belonged to the composite reinforced with approximately 43% sisal fiber content. In comparison with asbestos and mineral/steel fiber-based brake pads, sisal fiber/phenolic composites showed that the friction coefficient is good for fitting with low wave rate at different friction temperatures. Therefore, it is possible that the sisal fiber has the potential to replace asbestos for brake pad composites.

Some researchers from industrial (Force Technology 2014) showed a city bicycle frame prepared from flax fiber/bio-based epoxy composite. The composite was prepared to present that it can be structural materials. The selection of flax fiber was due to its high stiffness, low density, and excellent vibration damping. In addition, hybrid flax fiber/carbon fiber-reinforced bioepoxy composite showed good performances. Since carbon fibers improved mechanical property, while flex fibers enhanced damping property. For structural application as a city bicycle frame, a hybrid laminate consisting of flax fabric combined with glass fabric was also recommended.

Conclusions

NFPCs provided advantages to be useful in industrial applications, i.e., automotives, buildings, and constructions, due to relative light weight, low cost, biodegradability, low carbon footprint, and environmentally friendly materials when compared to synthetic fiber-reinforced composites. In addition, a positive effect on thermal stability, mechanical characteristics, and flame retardancy of polymers was obtained by adding natural fibers as reinforcement for polymer composites. This work summarizes the properties of the polymer matrices, i.e., petroleum- and bio-based epoxy resin, their copolymers, and natural fiber-reinforced epoxy composites: thermal property, mechanical behavior, and flame retardancy. The applications of the composites in structural, automobile, and brake pad were also discussed. The effects of chemical treatment of natural fiber and incorporation of flame-retardant elements in the composites on flammability were also addressed.

Acknowledgments The authors are grateful to the funding and support of the following: Basic Research Fund (Blue Sky) of the National Research Council of Thailand; the 90th Anniversary of Chulalongkorn University Scholarship; the Ratchadaphiseksomphot Endowment Fund of Chulalongkorn University; the National Nanotechnology Center (NANOTEC); the NSTDA; the Ministry of Science and Technology, Thailand; the Office of National Higher Education Science Research and Innovation Policy Council (NXPO); Program Management Unit Competitiveness (PMU C) (grant number C16F630128); and the Thailand Science Research and Innovation Fund (grant number 032/2564).

References

T. Ahamad, S. Alshehri, Thermal degradation and evolved gas analysis of epoxy (DGEBA)/novolac resin blends (ENB) during pyrolysis and combustion. J. Therm. Anal. Calorim. **111**(1), 445–451 (2013)

Z.N. Azwa, B.F. Yousif, Characteristics of kenaf fibre/epoxy composites subjected to thermal degradation. Polym. Degrad. Stab. **98**(12), 2752–2759 (2013)

E.V. Bachtiar, K. Kurkowiak, L. Yan, B. Kasal, T. Kolb, Thermal stability, fire performance, and mechanical properties of natural fibre fabric-reinforced polymer composites with different fire retardants. Polymers **11**, 699 (2019)

M. Birkner, S. Spange, K. Koschek, Basalt fiber reinforced polymers with improved thermal and mechanical properties by combination of twin polymerization with epoxide chemistry. Polym. Compos. **40**(8), 3115–3121 (2019)

L. Boccarusso, L. Carrino, M. Durante, A. Formisano, A. Langella, F. Memola Capece Minutolo, Hemp fabric/epoxy composites manufactured by infusion process: improvement of fire properties promoted by ammonium polyphosphate. Compos. Part B Eng. **89**, 117–126 (2016)

L.N. Chang, M. Jaafar, W.S. Chow, Thermal behavior and flammability of epoxy/glass fiber composites containing clay and decabromodiphenyl oxide. J. Therm. Anal. Calorim. **112**, 1157–1164 (2013)

S.S. Chee, M. Jawaid, M.T.H. Sultan, O.Y. Alothman, L.C. Abdullah, Accelerated weathering and soil burial effects on colour, biodegradability and thermal properties of bamboo/kenaf/epoxy hybrid composites. Polym. Test. **79**, 106054 (2019). https://doi.org/10.1016/j.polymertesting.2019.106054

J. Cheng, Curing behavior and thermal properties of trifunctional epoxy resin cured by 4, 4′-diaminodiphenyl sulfone. Express Polym. Lett. **3**, 501–509 (2009)

Z. Cheng, M. Fang, X. Chen, Y. Zhang, Y. Wang, H. Li, J. Qian, Thermal stability and flame retardancy of a cured trifunctional epoxy resin with the synergistic effects of silicon/titanium. ACS Omega **5**(8), 4200–4212 (2020)

C.W. Chin, B.F. Yousif, Potential of kenaf fibres as reinforcement for tribological applications. Wear **267**(9), 1550–1557 (2009)

J. Dai, N. Teng, J. Liu, J. Feng, J. Zhu, X. Liu, Synthesis of bio-based fire-resistant epoxy without addition of flame retardant elements. Compos. Part B Eng. **179**, 107523 (2019). https://doi.org/10.1016/j.compositesb.2019.107523

I.M. De Rosa, C. Santulli, F. Sarasini, Mechanical and thermal characterization of epoxy composites reinforced with random and quasi-unidirectional untreated *Phormium tenax* leaf fibers. Mater. Des. **31**(5), 2397–2405 (2010)

N. Dodds, A.G. Gibson, D. Dewhurst, J.M. Davies, Fire behaviour of composite laminates. Compos. A: Appl. Sci. Manuf. **31**(7), 689–702 (2000)

S. Fatima, A.R. Mohanty, Acoustical and fire-retardant properties of jute composite materials. Appl. Acoust. **72**(2), 108–114 (2011)

Force Technology, Learnings from designing and producing composite components with natural fibres (2014), https://forcetechnology.com. Accessed 28 Jan 2021

P. Glaris, J.-F. Coulon, M. Dorget, F. Poncin-Epaillard, Fluorinated epoxy resin as a low adhesive mould for composite material. Compos. Part B Eng. **63**, 94–100 (2014)

S. Grishchuk, Structure, thermal and fracture mechanical properties of benzoxazine-modified amine-cured DGEBA epoxy resins. Express Polym. Lett. **5**, 273–282 (2011)

P. Hombunma, T. Parnklang, P. Mora, C. Jubsilp, S. Rimdusit, Shape memory polymers from bio-based benzoxazine/epoxidized natural oil copolymers. Smart Mater. Struct. **29**(1), 015036 (2020). https://doi.org/10.1088/1361-665x/ab49e5

ICP Wind, ICP organic brake pad BSFG 300 series – replaces SVENDBORG 478-1486-802 (2016–2020), https://www.icpwind.com. Accessed 28 Jan 2021

H. Ishida, Process for preparation of benzoxazine compounds in solventless systems. US 5,543,516, 1996

H. Ishida, Overview and historical background of polybenzoxazine research, in *Handbook of Benzoxazine Resins*, ed. by H. Ishida, T. Agag, (Elsevier, Amsterdam, 2011), pp. 3–81
F.-L. Jin, S.-J. Park, Thermomechanical behavior of epoxy resins modified with epoxidized vegetable oils. Polym. Int. **57**, 577–583 (2008)
C. Jubsilp, T. Takeichi, S. Hiziroglu, S. Rimdusit, High performance wood composites based on benzoxazine-epoxy alloys. Bioresour. Technol. **99**(18), 8880–8886 (2008)
C. Jubsilp, K. Punson, T. Takeichi, S. Rimdusit, Curing kinetics of benzoxazine–epoxy copolymer investigated by non-isothermal differential scanning calorimetry. Polym. Degrad. Stab. **95**(6), 918–924 (2010)
C. Jubsilp, B. Ramsiri, S. Rimdusit, Effects of aromatic carboxylic dianhydrides on thermomechanical properties of polybenzoxazine-dianhydride copolymers. Polym. Eng. Sci. **52**(8), 1640–1648 (2012)
P. Khalili, X. Liu, K.Y. Tshai, C. Rudd, X. Yi, I. Kong, Development of fire retardancy of natural fiber composite encouraged by a synergy between zinc borate and ammonium polyphosphate. Compos. Part B Eng. **159**, 165–172 (2019)
H. Kimura, A. Matsumoto, K. Hasegawa, K. Ohtsuka, A. Fukuda, Epoxy resin cured by bisphenol A based benzoxazine. J. Appl. Polym. Sci. **68**(12), 1903–1910 (1998)
S. Kumar, S. Krishnan, S. Mohanty, S.K. Nayak, Synthesis and characterization of petroleum and biobased epoxy resins: a review. Polym. Int. **67**(7), 815–839 (2018)
S. Kurihara, H. Idei, Y. Aoyagi, M. Kuroe, Binder resin for friction material, binder resin composition for friction material, composite material for friction material containing the same, friction material and production method thereof. U.S. Patent 8,227,390 B2, 2012
H. Lee, K. Neville, *Handbook of Epoxy Resins* (McGraw-Hill, New York, 1967)
S.V. Levchik, E.D. Weil, Thermal decomposition, combustion and flame-retardancy of epoxy resins – a review of the recent literature. Polym. Int. **53**(12), 1901–1929 (2004)
F. Liu, Z. Wang, Y. Wang, B. Zhang, Copolymer networks from carboxyl-containing polyaryletherketone and diglycidyl ether of bisphenol-A: preparation and properties. J. Polym. Sci. B Polym. Phys. **48**, 2424–2431 (2010)
X.Q. Liu, W. Huang, Y.H. Jiang, J. Zhu, C.Z. Zhang, Preparation of a bio-based epoxy with comparable properties to those of petroleum-based counterparts. Express Polym. Lett. **6**(4), 293–298 (2012)
Market Study Report, LLC, The new research report on "global epoxy resin market" offers crucial insights pertaining to the key growth catalysts alongside the vast historical data of this business vertical. The document also intends to provide critical information regarding the current trends as well as other potential scenarios which are impacting the growth matrix of this industry over 2020–2026 (2020), https://www.globenewswire.com. Accessed 28 Jan 2020
C.D. Mauro, S. Malburet, A. Genua, A. Graillot, A. Mija, Sustainable series of new epoxidized vegetable oil-based thermosets with chemical recycling properties. Biomacromolecules **21**, 3923–3935 (2020)
V. Mittal, R. Saini, S. Sinha, Natural fiber-mediated epoxy composites-a review. Compos. Part B Eng. **99**, 425–435 (2016)
F. Mustaţa, I. Bicu, Multifunctional epoxy resins: synthesis and characterization. J. Appl. Polym. Sci. **77**, 2430–2436 (2000)
S. Nikafshar, O. Zabihi, S. Hamidi, Y. Moradi, S. Barzegar, M. Ahmadi, M. Naebe, A renewable bio-based epoxy resin with improved mechanical performance that can compete with DGEBA. RSC Adv. **7**, 8694–8701 (2017)
R.N. O'Brien, K. Hartman, Air infrared spectroscopy study of the epoxy-cellulose interface. J. Polym. Sci. Part C: Polym. Symp. **34**(1), 293–301 (1971)
S.-J. Park, F.-L. Jin, J.-R. Lee, Synthesis and thermal properties of epoxidized vegetable oil. Macromol. Rapid Commun. **25**, 724–727 (2004)
K.L. Pickering, M.G.A. Efendy, T.M. Le, A review of recent developments in natural fibre composites and their mechanical performance. Compos. A: Appl. Sci. Manuf. **83**, 98–112 (2016)

E. Pollitt, Automotive composites (2011), www.globalhemp.com. Accessed 28 Jan 2021
M.M. Raj, L.M. Raj, P.N. Dave, Glass fiber reinforced composites of phenolic–urea–epoxy resin blends. J. Saudi Chem. Soc. **16**, 241–246 (2012)
M. Rajaei, N.K. Kim, D. Bhattacharyya, Effects of heat-induced damage on impact performance of epoxy laminates with glass and flax fibres. Compos. Struct. **185**, 515–523 (2018)
Research and Markets, Composites market by fiber type (glass fiber composites, carbon fiber composites, natural fiber composites), resin type (thermoset composites, thermoplastic composites), manufacturing process, end-use industry and region – global forecast to 2025 (2020), https://www.researchandmarkets.com. Accessed 28 Jan 2021
S. Rimdusit, H. Ishida, Development of new class of electronic packaging materials based on ternary systems of benzoxazine, epoxy, and phenolic resins. Polymer **41**, 7941–7949 (2000a)
S. Rimdusit, H. Ishida, Synergism and multiple mechanical relaxations observed in ternary systems based on benzoxazine, epoxy, and phenolic resins. J. Polym. Sci. Part B: Polym. Phys. **38**, 1687–1698 (2000b)
S. Rimdusit, S. Pirstpindvong, W. Tanthapanichakoon, S. Damrongsakkul, Toughening of polybenzoxazine by alloying with urethane prepolymer and flexible epoxy: a comparative study. Polym. Eng. Sci. **45**, 288–296 (2005)
S. Rimdusit, W. Tanthapanichakoon, C. Jubsilp, High performance wood composites from highly filled polybenzoxazine. J. Appl. Polym. Sci. **99**, 1240–1253 (2006)
K. Senthilkumar, T. Ungtrakul, M. Chandrasekar, T. Senthil Muthu Kumar, N. Rajini, S. Siengchin, et al., Performance of sisal/hemp bio-based epoxy composites under accelerated weathering. J. Polym. Environ. **29**, 624–636 (2021)
M. Shibata, T. Ohkita, Fully biobased epoxy resin systems composed of a vanillin-derived epoxy resin and renewable phenolic hardeners. Eur. Polym. J. **92**, 165–173 (2017)
M. Shibata, N. Teramoto, K. Makino, Preparation and properties of biocomposites composed of epoxidized soybean oil, tannic acid, and microfibrillated cellulose. J. Appl. Polym. Sci. **120**, 273–278 (2011)
J.Y. Shieh, T.H. Ho, C.S. Wang, Synthesis and modification of trifunctional epoxy resins with polydimethylsiloxane for microelectronic encapsulation. Angew. Makromol. Chem. **245**, 125–137 (1997)
Specific Polymers, Bio-based epoxy resins (2021), https://ecoxy.eu. Accessed 28 Jan 2021
V.S. Srinivasan, S. Rajendra Boopathy, D. Sangeetha, B. Vijaya Ramnath, Evaluation of mechanical and thermal properties of banana–flax based natural fibre composite. Mater. Des. **60**, 620–627 (2014)
S. Suhaily, H.P.S. Abdul Khalil, W.O. Wan Nadirah, M. Jawaid, Bamboo based biocomposites, material, design and applications, in *Material Science: Advanced Topic*, ed. by Y. Mastai, (IntechOpen, London, 2013), pp. 489–517
B. Szolnoki, K. Bocz, P.L. Sóti, B. Bodzay, E. Zimonyi, A. Toldy, et al., Development of natural fibre reinforced flame retarded epoxy resin composites. Polym. Degrad. Stab. **119**, 68–76 (2015)
T. Takeichi, Y. Guo, S. Rimdusit, Performance improvement of polybenzoxazine by alloying with polyimide: effect of preparation method on the properties. Polymer **46**, 4909–4916 (2005)
T. Takeichi, T. Kawauchi, T. Agag, Polybenzoxazine/polyimide alloys, in *Handbook of Benzoxazine Resins*, ed. by H. Ishida, T. Agag, (Elsevier, Amsterdam, 2011), pp. 378–387
D.J. Van de Pas, K.M. Torr, Biobased epoxy resins from deconstructed native softwood lignin. Biomacromolecules **18**, 2640–2648 (2017)
D.W. Van Krevelen, P.J. Hoftyzer, *Properties of Polymer* (Elsevier, New York, 1976)
N. Venkateshwaran, A. Elaya Perumal, D. Arunsundaranayagam, Fiber surface treatment and its effect on mechanical and visco-elastic behaviour of banana/epoxy composite. Mater. Des. **47**, 151–159 (2013)
F.S. Vom Saal, C. Hughes, An extensive new literature concerning low-dose effects of bisphenol A shows the need for a new risk assessment. Environ. Health Perspect. **113**, 926–933 (2005)

S. Wang, S. Ma, C. Xu, Y. Liu, J. Dai, Z. Wang, X. Liu, J. Chen, X. Shen, J. Wei, J. Zhu, Vanillin-derived high-performance flame retardant epoxy resins: facile synthesis and properties. Macromolecules **50**, 1892–1901 (2017)

M. Xie, Z. Wang, Synthesis and properties of a novel cycloaliphatic epoxide. Macromol. Rapid Commun. **22**, 620–623 (2001)

X. Xin, C.G. Xu, L.F. Qing, Friction properties of sisal fibre reinforced resin brake composites. Wear **262**, 736–741 (2007)

K. Yorseng, S.M. Rangappa, H. Pulikkalparambil, S. Siengchin, J. Parameswaranpillai, Accelerated weathering studies of kenaf/sisal fiber fabric reinforced fully biobased hybrid bioepoxy composites for semi-structural applications: morphology, thermo-mechanical, water absorption behavior and surface hydrophobicity. Constr. Build. Mater. **235**, 117464 (2020)

S. Zhao, M.M. Abu-Omar, Synthesis of renewable thermoset polymers through successive lignin modification using lignin-derived phenols. ACS Sustain. Chem. Eng. **5**, 5059–5066 (2017)

Morphology and Mechanical Properties of Epoxy/Natural Fiber Composites

26

Poornima Vijayan P., Jesiya Susan George, Suraj P. R., and Sabu Thomas

Contents

P. Vijayan P. (✉)
Sree Narayana College for Women (Affiliated to University of Kerala), Kollam, Kerala, India
e-mail: drpoornimavijayanp@sncwkollam.org

J. S. George
School of Chemical Sciences, Mahatma Gandhi University, Kottayam, Kerala, India

International and Inter University Centre for Nanoscience and Nanotechnology (IIUCNN), School of Energy Materials, Mahatma Gandhi University, Kottayam, Kerala, India

S. P. R.
School of Chemical Sciences, Mahatma Gandhi University, Kottayam, Kerala, India

S. Thomas
International and Inter University Centre for Nanoscience and Nanotechnology (IIUCNN), School of Energy Materials, Mahatma Gandhi University, Kottayam, Kerala, India
e-mail: sabuthomas@mgu.ac.in

S. Mavinkere Rangappa et al. (eds.), *Handbook of Epoxy/Fiber Composites*,
https://doi.org/10.1007/978-981-19-3603-6_27

Abstract

Due to the growing interest toward sustainability, natural fiber-reinforced epoxy composites have gained considerable interest among researchers in the current era. The rapid developments on the production and applications of the natural fiber-reinforced epoxy composites validated excellent properties over synthetic fiber composites with reduced environmental impacts. These environment-friendly materials have potential applications in the various engineering and automobile sectors, and hence, considerable approaches have been made to improve their final performance. In recent years, several modifications have been introduced in the natural fiber/epoxy composites, increasing their performance. The current chapter covers the latest research efforts to improve the tensile, impact, flexural, and fracture toughness performance of natural fiber-reinforced epoxy composites. The failure mechanisms that operate in natural fiber-reinforced epoxy composites have also been discussed in detail. Further, the simultaneous incorporation of two or more different types of natural fibers into epoxy matrix and the incorporation of nanofillers into epoxy/natural fiber composites have been put forward as methods to further improve the mechanical performance of epoxy/natural fiber composites.

Keywords

Natural fiber composites · Epoxy · Mechanical properties

Introduction

Polymer composites are an established class of materials, in which particles or fibers are used as reinforcing fillers in the polymer matrix. The matrix surrounds and supports the reinforcing filler by maintaining their relative positions. Both thermoplastic and thermosetting polymers are commonly used as matrix phase in polymer composites. Various reinforcing fillers are embedded and arranged in a specific internal configuration to obtain the desired properties, which can be tailored for several applications (Harish et al. 2008; Sood and Dwivedi 2018). A properly designed polymer composite can integrate the properties of both the filler and the matrix, thereby achieving unique combination of mechanical performance like strength, stiffness, and toughness. Hence, it helps to fabricate a new material which cannot be achieved with any of the individual constituent material.

Fiber-Reinforced Polymer Composites

Fibers are strong and tough, but they are not very stiff owing to the shortness in diameter. Adding the fibers into the matrix ties the fibers together to form a composite structure, hence the stress can be transferred from one fiber to another

by sharing the load. Generally incorporating fibers enhances the modulus of the matrix material. Several factors such as orientation, distribution, and concentration of the fiber have significant influence on the strength and final properties of the fiber-reinforced composites (Mittal et al. 2016). Continuous fiber/long fiber composites and discontinuous/short fiber composites are the two major classes of fibrous composites. Long fiber composites have better strength and stiffness but are more difficult to process with polymer matrices. While, short fibers is generally used to fabricate composites with intricate internal shapes. Therefore, short fiber composites are usually prepared with thermoplastic polymer matrices and long fiber composites are prepared with epoxy or polyester thermosetting resin matrices (Om et al. 2016; Joshi et al. 2004). Carbon fiber-reinforced polymers (CFRP) are well known for the fabrication of lightweight high-performance composite structures. However, the urge to achieve sustainable development goals made plastic engineers/researchers to redirect their research to replace CFRPs with natural fiber-reinforced polymer composites (NFPC).

Natural Fiber-Reinforced Epoxy Composites

The widespread use of epoxy thermosets in automobile, aviation, marine, electrical, and construction industries demands sustainable light-weight derivatives (A.v et al. 2021; Vijayan P et al. 2018). Natural fibers exhibit many excellent properties such as low density, lower cost, renewability, and recyclability as well as good specific strength and high specific modulus. Incorporation of natural fibers is the most attractive way to modify the epoxy resin. Epoxy/natural fiber composite exhibited a unique combination of versatility, high performance, and processing advantages at comparatively cheaper rates on comparison with thermoplastics (John and Thomas 2008).

Natural fibers including plant fibers and animal fibers such as ramie fibers (Djafar et al. 2021), coir fibers (Romli et al. 2012), wool (Bharath et al. 2019), silk (Craven et al. 2000), chicken feather (Vijayan et al. 2021), etc. are frequently used as reinforcing fillers in epoxy resin. Plant fibers are generally isolated from various parts of plants like stem, seed, and leaf. These fibers give superior strength to the composites when incorporated in a polymer matrix (Saba et al. 2015). The massive availability of natural fibers, low cost, and ease of fabrication gained more interest in researchers to fabricate natural fiber-reinforced composites. Furthermore, the ecological benefit of biodegradability and safety during handling make them attractive fillers (Sumesh et al. 2020; Sathishkumar et al. 2020; Ramasubbu and Madasamy 2020). This chapter discusses the major researches that have been conducted in the area of epoxy/natural fiber composites.

Generally, for polymer composites, natural fibers are used in either of the following three different forms based on their aspect ratio. The first utilization of natural fiber as filler (powder form) in polymer is to enhance the desired properties of composite compared with the initial pure or virgin resin. In the second case, short

fibers are randomly arranged in a designed volume percentage. In the third case, natural continuous fibers are used for the fabrication of polymer composites.

Owing to the attractive specific strength and stiffness, mechanical behavior of natural fiber-reinforced polymer composites is of great interest to researchers in various fields of science and engineering. Traditional continuum mechanics, purely based on isotropy, homogeneity, and continuity of the solids, are not applicable in the case of heterogeneous composites, because microscopic particles and fibers within the composite are responsible for the overall properties of the composites. Thus, a detailed analysis on the micromechanics was employed to examine the property performance of the material and material structure, relatively in a finer scale (typically microscale), which helps to understand how mechanics is related to the microstructure of the materials. In this chapter, the influence of morphology on mechanical properties and their correlation in the natural fiber-reinforced epoxy composites was demonstrated in detail.

Mechanical Properties of Epoxy/Natural Fiber Composites

Among all other inherent properties of polymers, determination of mechanical properties is quite important, since virtually all service conditions and majority of end use of the fabricated composites involve mechanical loading. In general, selection of material for a particular application is based on mechanical properties such as tensile strength, tensile modulus, elongation, and impact strength. Important mechanical properties of the fiber-reinforced composites such as tensile strength, flexural strength, impact strength, and fracture toughness were discussed in detail with examples (Karthi et al. 2020). Through this chapter, a thorough understanding of mechanical properties of natural fiber-reinforced epoxy composites was presented. The following discussion on the mechanical performance is correlated with failure mechanism via a careful microscopic investigation of mechanically fractured surfaces of epoxy/natural fiber composites.

Tensile Properties of Natural Fiber-Reinforced Epoxy Composites

Stress–strain tests are considered as short-term tests, in which the mechanical loading is applied for a relatively short period of time. Stress–strain tests of plastics are mainly conducted to determine the rigidity and strength of plastics on time. Tensile elongation and tensile modulus measurements are the most important indications of strength in a material. Tensile measurement is the ability of a material to withstand force that tends to pull it apart and to determine to what extent the material stretches before breaking. Similarly, tensile modulus is an indication of the relative stiffness of the material and can be calculated from the stress–strain graph. According to American Society for Testing and Materials (ASTM D 638), samples must be conditioned at standard temperatures since tensile properties of the plastics change with very minute variations in the temperature; it is recommended that tests

be conducted in a temperature of 23 ± 2 °C and 50 ± 5% RH (relative humidity) (Shah 2007). Most of the epoxy/natural fiber composites have been reported to have superior tensile properties.

Yang et al. (2017) reported enhanced tensile toughness epoxy/silk composites. Total 30 and 60 volume percentage of silk fibers were incorporated into epoxy matrix and ensured a well embedded composite. Silk fabric is plain woven with two yarns of aligned orthogonally as shown in Fig. 1a. As a result of applied high-vacuum pressure during the fabrication process, matrix was permeated in between several gaps and voids in the fiber, hence the interfacial bonding was improved. The morphological analysis of the fractured surface exhibits a scale like morphology.

Typical stress strain behavior of neat epoxy and silk fiber-reinforced composites are given in Fig. 1. Owing to the high crosslink density, epoxy matrix are highly brittle and they exhibit catastrophic failure with a 3% failure strain in the tensile test. Different from neat epoxy matrix, silk-filled composites exhibited a macroscopic yielding. The silk fiber-reinforced epoxy resin exhibited a ductile failure with a 9% failure strain, far larger than pure epoxy matrix.

Hydrophilic and hydrophobic nature of natural fibers and polymers, respectively, result in the poor fiber matrix in the natural fiber-reinforced composites. The chemical treatment of natural fibers is reported to modify the fiber surface, which in turn enhances the fiber-matrix interaction. In such an attempt, Krishna and Kanny (2016) modified the kenaf fibers with a mixture of amino acids, glutamic acid, and lysine. Amino acid treatment helps in the removal of waxy coating and several impurities from the fiber surface with in turn makes the surface rougher and several

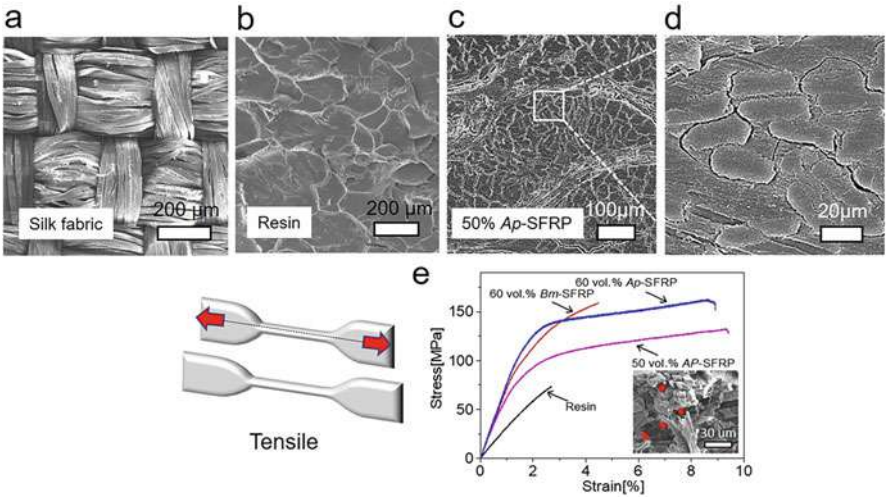

Fig. 1 Scanning Electron Microscopic images of the (**a**) the plain woven *Ap* silk fabric, (**b**) epoxy resin, (**c**) silk fiber-reinforced composites (SFRP), and (**d**) an enlarged view of the region in (**e**) uniaxial tensile mode and stress-strain curve (portion of the figure) (Yang et al. 2017). (Reproduced with thanks from Springer Nature, open access article distributed under the terms of the Creative Commons CC BY license)

fibers are split into fine ones. This could increase the ability of fibers to interlock with the epoxy matrix. Untreated fiber-reinforced composites exhibited tensile strength lower than the neat epoxy resin; this means that if the fibers are randomly dispersed in the epoxy matrix, they act as stress concentrators which in turn result in the premature failure of the composites. They observed that the treatment of fibers enhances the tensile properties of the composites. Especially lysine-treated fibers showed better tensile strength and modulus than the untreated and glutamic acid-treated fibers as shown in Fig. 2. Untreated kenaf fiber-reinforced composite resulted in broken fibers, crack propagations through the matrix, and debonding of the fiber and matrix happened at the interface (Fig. 2a). However, a kind of debonding happened at the interface of the glutamic acid-treated kenaf fiber epoxy composites. But in the case of lysine-treated kenaf fiber composites, a firmly packed interfacial bonding between fiber and matrix resulted in the enhanced toughness of the composites.

Figure 3 represents the fractured surface morphology of the alkali-treated jute fiber/epoxy composites as reported by Wang et al. (2019a). SEM images of the fractured surface of epoxy–fiber provide direct proof of improvement in fiber matrix interface. As shown in Fig. 3a, there was no cohesion between the fibers and the matrix, even despite a small amount of epoxy resin at the interface region. The failure mechanism for this composite was fiber–matrix debonding and depicts a lack of interaction between the jute fibers and the epoxy. However, after the treatment of the fibers, adhesion at the interface between the jute fiber and the epoxy is improved

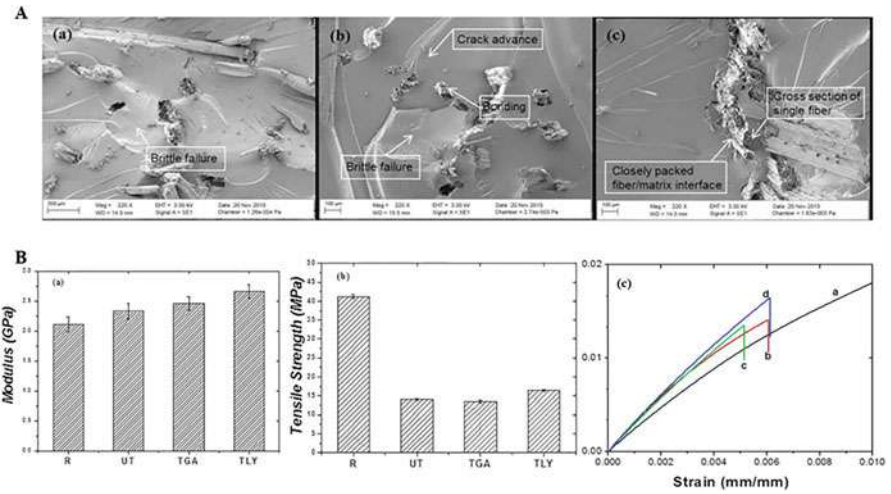

Fig. 2 (**A**) (**a**–**c**) SEM micrographs of the fracture surfaces of: (**a**) untreated kenaf fiber epoxy resin (UT), (**b**) glutamic acid-treated kenaf fiber/epoxy composites (TGA), and (**c**) lysine-treated kenaf fiber/epoxy composites; (TLY) (**B**) Stress strain curves of: (**a**) neat epoxy (R), (**b**) UT, (**c**) glutamic acid-treated kenaf fiber/epoxy composites, and (**d**) lysine-treated kenaf fiber/epoxy composite (Krishna and Kanny 2016). (Reproduced with thanks from Elsevier, License Number 5196551050223)

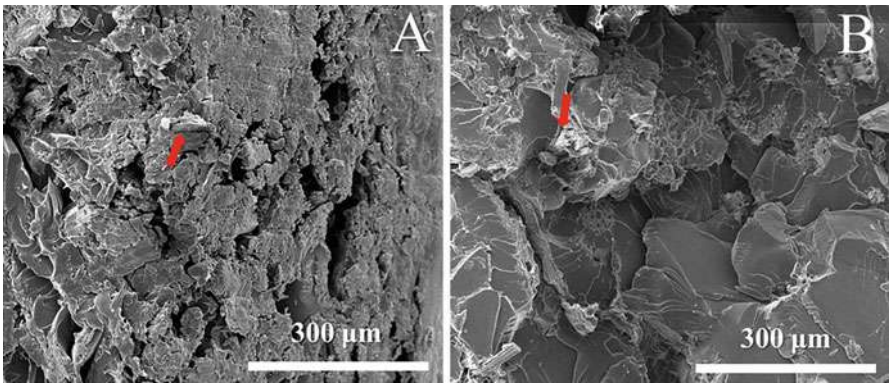

Fig. 3 Scanning electron micrograph of the fractured surface morphology of (**a**) untreated jute/epoxy composite and (**b**) treated jute/epoxy composite (Wang et al. 2019a). (Open access article distributed under the terms and conditions of the Creative Commons Attribution (CC BY) license)

as shown in Fig. 3b. This can be visible by the disappearance of boundary gaps between the epoxy and fiber surface (arrow). The improvement was explained by a strong interfacial interaction after the treatment of jute fiber.

Tensile Properties of Epoxy/Hybrid Natural Fiber Composites

It is a popular method to simultaneously incorporate two or more different types of natural fibers into polymer matrix for further property enhancement. Jawaid et al. (2015) found tensile properties of the epoxy/oil palm (EFB) composites increased by adding jute fibers into it. Bilayer hybrid composites are fabricated by simple hand layup technique. Weight ratio of oil palm fiber and jute were 4:1, 1:1, and 1:4, respectively. In all the cases, tensile strength and modulus increase with increasing the jute fiber loading. The incorporation of jute fibers into EFB composite enhances the load-bearing capability of the hybrid composites resulting in an improved stiffness. This is because of the enhanced tensile properties of the jute fibers (400–800 MPa) compared to low strength palm fibers (248 MPa). Scanning Electron Microscopic (SEM) images of the palm/epoxy composites (Fig. 4a) illustrate the poor adhesion between the fibers and matrix; hence, the fibers start to pull out and several cracks in the epoxy result in the weak interfacial interaction between epoxy and oil palm fibers which in turn results in the failure of the epoxy/oil palm fiber at a low load, whereas epoxy/jute exhibits better adhesion (Fig. 4) owing to the multi-cellular nature of jute fiber. In 1:1 and 4:1 hybrid composite, fiber/matrix debonding and fiber pullout are the major failure mechanisms. Hybrid composites with high loading of jute fiber (1:4) exhibited excellent mechanical properties among all; their scanning electron microscopic images clearly depict the strong interfacial interaction between jute fiber and epoxy matrix resulting in the effective stress transfer from matrix to fiber.

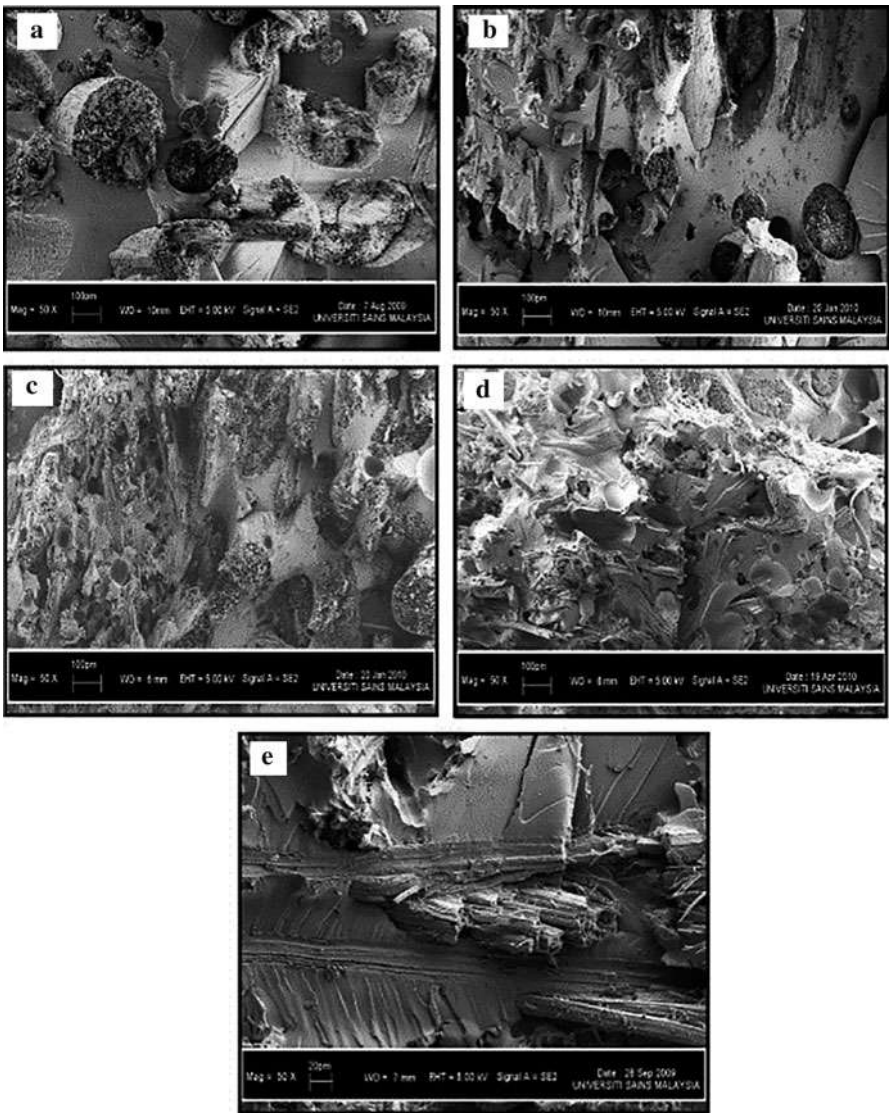

Fig. 4 SEM images of the tensile fractured surfaces of (**a**) EFB composite, (**b**) oil palm EFB: jute (4:1) hybrid composite, (**c**) oil palm EFB: jute (1:1) hybrid composite, (**d**) oil palm EFB: jute (1:4) hybrid composite, and (**e**) epoxy/jute composite (Jawaid et al. 2015). (Reproduced with thanks from Elsevier, License number 5196570884802)

Similarly, Bhoopalam et al. (2013) investigated the effect of jute and banana fibers on the mechanical properties of epoxy resin. They found that the addition of 50/50 of jute and banana fibers increases the mechanical properties. When the ratio of jute and banana fibers increases from 100/0, 75/25, to 50/50, mechanical properties also increase; however, further addition of banana fibers (25/75 and 0/100)

reduces the mechanical properties. Chaudhary et al. (2017) fabricated jute/hemp/flax epoxy composites; they found that the failure was due to fiber breakage and fiber pullout owing to the interaction between matrix and fiber. It was observed that bast and leaf fibers-reinforced composites exhibited better values of tensile strength as compared to other types of fiber-reinforced epoxy composites due to the enrichment of cellulose content and better bonding between natural fiber and matrix.

Tensile Properties of Nanostructure/Natural Fiber-Reinforced Epoxy Composites

In the past two decades, the material scientists have been extensively studied the role of nanofillers in the performance of the polymer matrix. Several scientists have applied the concept of nanocomposites to natural fiber-reinforced epoxy matrix too. Prasad et al. (2021) evaluated the tensile strength of nano titanium dioxide-coated flax fiber epoxy composites. They found that the treatment of silane-coupling agent and its grafting with the nano-TiO_2 help to achieve enhanced interfacial adhesion between the flax fiber and epoxy, which results in the improvement of mechanical properties. Tensile strength of unmodified flax fiber composite was 68 MPa, which increased to 78 MPa after modification with nano-TiO_2. Fibers can act as load-carrying agents; moreover, the TiO_2 coating on the flax fiber helps to resist moisture absorption of the composite . The increment in the tensile modulus symbolizes the increased stiffness by nano-coating on the flax fiber. Figure 5 represents the tensile strength and the morphology of the tensile-fractured surfaces. Fiber pullout was the major fracture mechanism in the unmodified fiber/epoxy composite, which clearly represents the poor fiber matrix-interfacial interaction. However, the surface-modified fiber composites exhibited minimal fiber pullout mechanism during

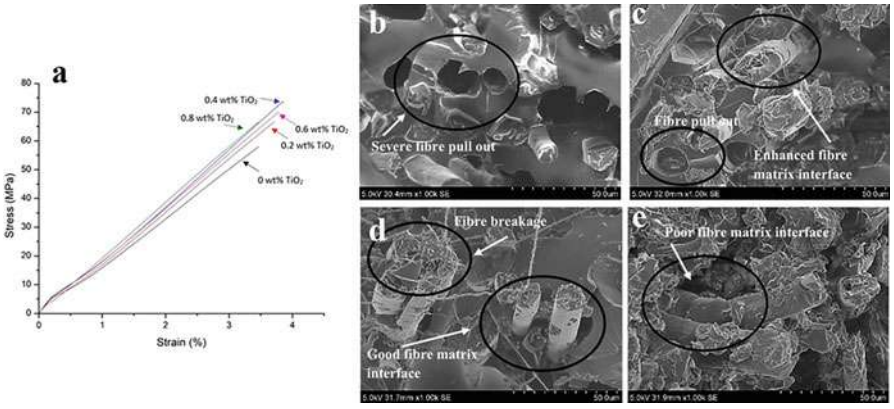

Fig. 5 (**a**) Stress-strain curve of the fiber-modified composites and SEM images of tensile-fractured surface of (**b**) 0, (**c**) 0.2, (**d**) 0.4, and (**e**) 0.6 wt% nano titanium dioxide-coated flax fiber composites (Prasad et al. 2021). (Reproduced with thanks from Elsevier, License number 5196870124245)

fracture owing to the enhanced fiber matrix bonding. Nanoparticle coating over fiber surface improves the surface roughness, which provides additional slots for mechanical interlocking in addition to the chemical bond formation. Moreover, presence of nanostructures around the fiber surface helps to deviate the path of crack also.

In another report, Mohan and Kanny (2011) reinforced epoxies with nanoclay and sisal fiber. The addition of nanoclay significantly modified the stress-strain behavior of the composites. They found that the modulus increases with the addition of nanoclay but the strength and strain values diminish after 3 wt% of clay. The increase in the elastic modulus of composites with organoclays was due to the exfoliation/intercalation of nanoclay in the epoxy matrix which immobilizes the polymer chains under loading. It is also observed from the stress–strain curves that the addition of nanoclay in epoxy resin changes the failure patterns from brittle to ductile failure, since this nanoclay acts as a crack arrestor during loading by inducing deformation mechanisms such as crack pinning and debonding.

Flexural Properties of Natural Fiber-Reinforced Epoxy Composites

Flexural strength is defined as the ability of a material to withstand the bending forces, applied perpendicular to the longitudinal axis. The stress applied in the flexural test is generally a combination of compressive and tensile stress epoxy. Polymeric materials generally break easily under the application of flexural load; the specimen is deflected until a rupture occurs in the outer fibers. Flexural test has several advantages over tensile test, including easiness in the specimen preparation, specimen alignment for test, and the application of small strain helps to detect the actual deformations. Either three-point loading or four-point loading is utilized in the flexural test. Three-point loading consists of a center loading on a simple supported beam. In brief, a rectangular shaped sample is placed on two supports and is loaded by means of a loading nose between the supports. However, in four-point loading system, two load points are equally spaced from the adjacent support points, in which the distance between load points is one-third of the support span. In this method, the sample to be tested rests on two supports and is loaded at two points.

Flexural Strength of Epoxy/Natural Fiber Hybrid Composite

Mylsamy et al. (Mylsamy and Rajendran 2011) reported the flexural strength of alkali-treated agave fiber-reinforced epoxy composites; they found that the alkali-treated fiber-reinforced epoxy composites show 15% enhancement in the flexural strength than the untreated one. Moreover, the alkali treated composites exhibited more toughness and shrinkage. The enhanced interfacial interaction of the alkali-treated fibers was favorable for the increment in flexural strength. Higher the area of contact between the treated fiber surface, the matrix better improves the adhesion. Vijay and Singaravelu (2016) fabricated cyperus Pangorei and jute fiber hybrid epoxy composites by hand layup technique. Highest flexural load was shown by epoxy/cyperus pangorei fiber/jute fiber hybrid composites when compared to pure

epoxy/cyperus Pangorei fiber and epoxy/jute fiber composites. The stiffer cyperus pangorei fibers, which are present at the outer layer of the composite, have high load-bearing capacity by lignin constituents and high surface roughness. Hence, cyperus fibers take the load at the surface, followed by transferring the load to jute fibers. They have found less fiber pullout in epoxy/cyperus pangorei fiber/jute fiber hybrid composites due to better bonding of cyperus fibers with the epoxy matrix. Fiore et al. (Fiore et al. 2015) treated kenaf fiber with NaOH and found that epoxy/treated kenaf fiber composites showed improved flexural moduli than neat epoxy. Alkali treatment of the fibers imparts more positive impact on flexural strength also. Owing to the improvement of the fibers–matrix compatibility, the alkali treatment highly influences flexural strength than flexural modulus.

Flexural Strength of Epoxy/Natural and Synthetic Fiber Hybrid Composites

Ramnath et al. (2013) examined the mechanical properties of glass fiber-reinforced epoxy (GFRP) composites with abaca and jute fibers. The hybrid composites were arranged in such a way that jute fiber was at the center flanked by abaca fiber on both sides; glass fiber was used to laminate the composite on the bottom and top, which helps to attain a surface finish and improves the strength. Abaca–jute hybrid composite showed better properties than the abaca fiber composites in tensile studies, but interestingly abaca fiber-reinforced composites exhibited superior flexural properties than the hybrid composite. The maximum flexural strength of the abaca fiber was owing to its uniform distribution of high-strength abaca fibers within the matrix. In addition to that, a better adhesion between abaca fiber and epoxy matrix was observed. Table 1 tabulated the flexural properties of glass fiber-reinforced epoxy composites (GFRP) with abaca and jute fiber.

Impact Strength of Natural Fiber-Reinforced Epoxy Composites

Impact properties of the polymers are closely related to the overall toughness of the material. Toughness of a polymer is defined as its ability to absorb the applied energy. Area under the stress-strain curve provides the toughness of the material. In general, toughness is measured in terms of impact energy. Higher the impact energy,

Table 1 Flexural properties of glass fiber-reinforced epoxy composites (GFRP) with abaca and jute fiber (Ramnath et al. 2013)

Sample	Flexural break load (kN)	Maximum displacement (mm)	Flexural strength (MPa)	Flexural modulus (MPa)
GFRP + abaca	1.55	4.6	12.5	1380
GFRP + jute	1.23	4.2	11.9	1216
GFRP + abaca + jute	1.49	4.3	12.1	1452

higher the toughness. Term impact resistance is used to define the ability of a material to resist breaking under a shock loading. The molecular flexibility plays a major role to determine the relative toughness of the material, e.g., in the case of brittle polymer polystyrene, the molecular segments are unable to disentangle and respond to the sudden application of a load, hence it undergoes a catastrophic brittle failure. However, in the case of flexible polymers like plasticized vinyls, exhibited high-impact behavior is due to the availability of large flexible segments of molecules to uncoil and respond to mechanical stress applied (Shah 2007; Wang et al. 2019b).

Cross-linked epoxy resins exhibited brittle fracture due to high crosslink density, which restricts their applications in the field which need high-impact strength. So far, various approaches have been explored by the research community by adding nanofillers, thermoplastics, and soft rubbers. An alternative way to improve the impact energy is to incorporate fibrous fillers into the epoxy resin, which act as stress-transfer agents. When a polymer is subjected to an impact loading, the fracture occurs in a characteristic fashion. Crack initiation energy is defined as the energy required to initiate a crack on the polymer surface by impact loading; if the applied load exceeds the crack initiate on energy, the crack starts to propagate. Finally, complete failure of the specimen occurs when the applied load surpasses crack propagation energy. Most importantly, systematic investigation of fiber-reinforced composites' impact resistance is a challenge since the impact strength is not only dependent on the material parameters, but also dependent on both test parameters, conditions and sample design. Most of the existing reports suggest that the incorporation of various fibers and fillers can cause a significant reduction in the crack initiation energy while, at the same time, addition of fiber reinforcements significantly enhances crack propagation resistance too. For instance, Nguyen and Nguyen (2021) reported the improved impact strength of banana fiber-reinforced epoxies by adding 20 wt% of fibers. They have noticed that the fiber pullout was the characteristic fracture mechanism. But Balaji et al. (2020) also investigated the effect of short banana fibers (20 mm) and found that the addition of 15 wt% banana fibers improved tensile, flexural, and impact properties. Impact strength of banana-reinforced composite was twice the impact strength of neat epoxy, due to the enhanced interfacial adhesion between fiber and the matrix. Alkali modification of natural fiber is a promising way to increase the interfacial adhesion between fiber and epoxy matrix. Venkateshwaran et al. (2013) investigated the effect of alkali treatment of short banana fibers on the mechanical strength of epoxy composites. They modified the fiber surface with different percentages of alkaline solution (0.5, 1.0, 2.0, 5.0, 15, and 20%). Impact strength of the treated composite was higher than that of untreated composite. They found that the percentage of NaOH has effect on the mechanical performance, and with 1 wt% of NaOH-treated fiber, an enhanced mechanical property was recorded. As the concentration of NaOH increases, the degree of damages in the fiber increases which in turn reduces the overall mechanical properties of the fiber-reinforced composites.

Impact Strength of Epoxy/Hybrid Natural Fiber Composites

According to the investigation of Jawaid et al. (2010) on oil palm empty fruit bunches (EFB) and jute fiber-reinforced hybrid epoxy sandwich composites (in which fibers are arranged in the following fashion EFB/jute/EFB and jute/EFB/jute), EFB/jute/EFB (66.7 J/m) exhibited higher impact strength than jute/EFB/jute composites (57 J/m). Moreover, they found that the sandwich-designed hybrid composites showed less impact strength compared to pure EFB composites (92.7 J/m). In another work, Jawaid et al. (2011) reported the enhanced impact strength of epoxy/empty fruit fiber bunches and jute fiber laminate with the help of 2-hydroxy ethyl acrylate-coupling agent. The impact strength was found to be 15 kJ/m^2 and 6.42 kJ/m^2, respectively, for EFB/jute/EFB and jute/EFB/jute epoxy laminates. The incorporation of the coupling agent results in the increment of 30% and 15% (a maximum impact strength was exhibited by laminates with EFB) as face and jute as core (EFB/jute/EFB) with coupling agent. In laminated composites without coupling agent, debonding of the fiber happened from the matrix due to poor interfacial adhesion between the fiber and matrix. However, upon addition of coupling agent, the fractured surfaces (B) of the laminates have several matrix elements over the fiber surface which depicts the enhanced interfacial adhesion between fiber and matrix. Similar findings were reported by Jafrey et al. (Jafrey et al. 2019) using jute/bamboo hybrid fibers.

Karthikeyan and Balamurugan (2012) studied the effect of fiber length and alkali treatment on the impact strength of epoxy/coir composites. The resistance to impact loading was increased with increase in the fiber length (30 mm). They also reported an increment in the impact strength for the alkali-treated coir fibers. Treatment of fiber with alkali makes the fiber surface more rough and results in better mechanical interlocking with a gradual increase in the number of reaction sites. Morphological analysis of the fracture surface depicted the existence of a strong fiber matrix interface due to the absence of fiber pullout mechanism, consequently increased impact strength too. Indeed, higher concentration of the alkali reduces the fiber strength also.

Anand et al. (2018) investigated the improvements in the impact strength of treated jute/kenaf fiber epoxy composites. Arrangement of fiber mats in alternating directions and these hybrid composites exhibited better impact strength than other compositions; this is because when the crack propagates through the hybrid composite, it passes through the epoxy matrix and then through the fibers. As it reaches the end of the fiber in a particular direction, suddenly it moves to the next fiber layer present in a different direction. This change in layers due to its alternating arrangement absorbs more energy by providing more surface area of fracture than a composite with fiber orientation in one direction. On the fracture morphology of impact-fractured surface of the composite, fiber fractures are due to the impact loading, and no trace of fatigue failure is observed in the composites.

Fracture Toughness of Epoxy/Natural Fiber Composites

Fracture toughness is a fundamental materials property, indicating the strain energy–absorbing ability of a material prior to its fracture. Fracture toughness is closely related to the amount of energy needed to create fracture surfaces. Higher the value of fracture toughness, higher the materials resistance to crack propagation. Generally, in fiber-reinforced polymers, fracture toughness could be influenced by applied stress, matrix crack, mode of fracture fiber bridging, fiber breakage, fiber debonding, and fiber-frictional pullout.

Ductile fracture absorbs more energy, whereas brittle fractures absorb less energy and are characterized by fractures with flat surface. Stress intensification factor (K) and strain energy release rate (G) are the two parameters used for the determination of fracture resistance. Release of energy during the crack propagation is a materials intrinsic property, which is not influenced by the size of the part. According to ASTM, stress intensity factor, K, can be written as follows,

$$K_I = \sigma\sqrt{\pi a} f(\mathrm{g}) \tag{1}$$

Where "a" is the initial crack length of the specimen, "$f(g)$" is a dimensionless factor depending on the specimen geometry and loading condition, and K_I is the Mode I critical stress intensity factor. The underlying principle behind the fracture mechanics is when the stress intensity factor at the crack tip reaches a critical value KC, unstable fracture occurs. Higher the fracture toughness value, a higher value of the stress intensity is required for crack propagation; hence the material has a greater resistance to brittle fracture. The critical stress intensity factor is determined using relatively simple laboratory specimen, the limiting value being $K_{IC}/K_{IIC}/K_{IIIC}$. Generally, three modes of loading are employed for measuring the fracture toughness; they are Mode I (tensile mode), Mode II (sliding or shear mode), and Mode III (tearing mode) and are schematically represented in Fig. 6.

In fiber-reinforced polymer composites, during tearing, matrix absorbs the energy while the fibers break by brittle failure. In some cases, pulling out of fibers from the matrix can also be found in some reports. Factors that contribute toughness to the

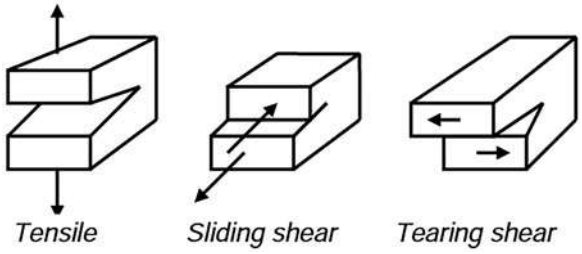

Fig. 6 Crack-opening modes in fracture toughness mode I (tensile), mode II (sliding shear), and mode III (tearing shear) (Prasad et al. 2011). (Open accesses licensed under Creative Commons Attribution 4.0 International License)

fiber-reinforced composites are the following: debonding between polymer matrix and fibers, the cracks deflection due to tilting or twisting movement around the fiber.

Pullout of fibers from the matrix follows a pullout mechanism and dissipates energy by friction. The pulled fibers may bridge both the crack surfaces and help to absorb the applied stress, which retards the crack propagation. Interlaminar fracture is another crucial concern in fiber-reinforced polymer composites. Interlaminar fracture reduces the stiffness of a system to a great extent, gradually leading to failure of the system during its service.

Mode of loading has a pronounced effect on the critical strain energy release rate (Gc) at which the delamination actually begins to extend; the value of Gc varies with the modes chosen for testing. Double Cantilever Beam (DCB) test is recommended to measure the Mode I fracture toughness GIC of the fiber-reinforced polymer composites according to ASTM D 5528 (Prasad et al. 2011; Chittimenu et al. 2021). K_{IC} is the factor of growing-resistance of a crack and hence the increase in KIC means that it is hard to form and the propagation of cracks.

Das and Biswas (2016) reported an increase in the fracture toughness of epoxy/coir fiber composites with increase of fiber length (3 to 9 mm) with a 15 wt% of fiber. The experimental K_{IC} value increases with the increase in coir fiber content and reveals an increased ability of the material to resist fracture as well as crack propagation. They have observed the delamination of the fibers from the resin surface due to the poor interfacial adhesion; also surfaces of the pulled-out fibers are very clean. They reported: As the fiber content increases, instead of getting good dispersion, severe agglomeration of fibers takes place; hence the resin cannot wet the fibers due to difficulty of the resin to reach in-between the two adjacent fibers. Yeo et al. (2017) modified the cellulose fibers with 3-glycidoxysialnae which were used to reinforce epoxy resin. The fracture toughness analysis of the silane-modified cellulose epoxy composites showed enhancement in the K_{IC} and G_{IC}. The modification on the cellulose fiber improved the fracture toughness of the epoxy material by 262.5%. The high values of K_{IC} and G_{IC} reflected the enhancement in the interfacial adhesion between epoxy matrix and cellulosic fibers in the salinized cellulose/epoxy composites. The fracture toughness in bamboo fiber-reinforced epoxy composite has been studied by Khan et al. (2017). The toughening mechanism operated in bamboo fiber-reinforced epoxy composite has been revealed by the careful analysis of SEM images of fracture surface. They have observed matrix cracking (Fig. 7b), fiber pullout (Fig. 7c), fiber breakage, and debonding (Fig. 7d and e) as the major failure mechanisms in bamboo fiber-reinforced epoxy composites. They have found pronounced effect of fiber length on fracture toughness. It was reported that fracture toughness increased with increase in fiber length (Fig. 7a). In such composites with randomly distributed fibers, as the stress is transferred from epoxy matrix to the deeply embedded fibers, the fiber breakage takes place instead of debonding or pullout. At the same time, fibers, which are not deeply embedded in the epoxy matrix, undergo the debonding phenomenon.

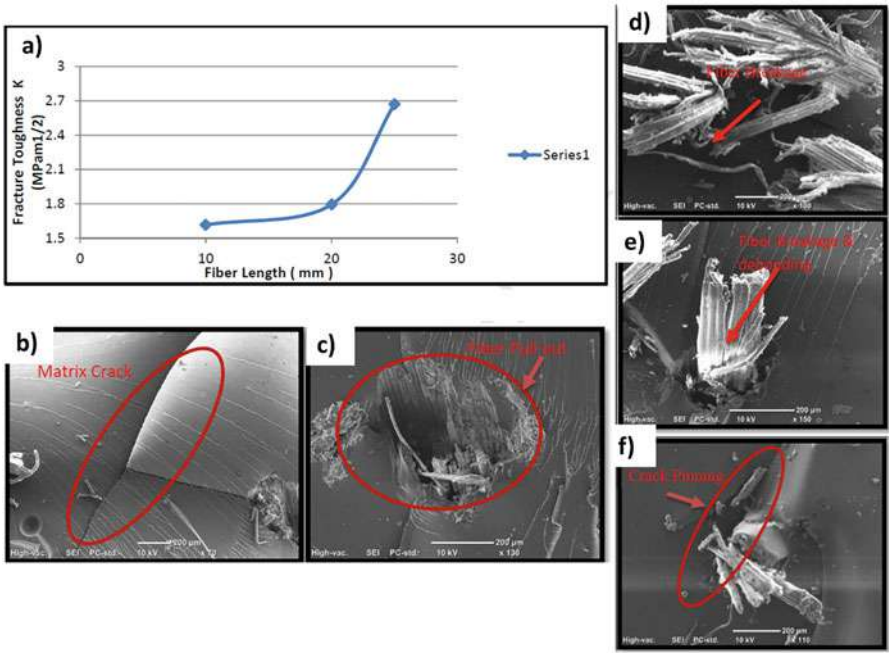

Fig. 7 Fracture toughness of bamboo-reinforced epoxy composites with different fiber length (Khan et al. 2017). (Reproduced with thanks from Elsevier, License number 5196880178225)

Fracture Toughness of Epoxy/Hybrid Natural Fibers Composites

Jabbar et al. (2017) modified jute fibers with cellulose nanofibrils which are used to reinforce epoxy resin. Fracture toughness of the prepared coatings was measured using single end notched bend (SENB) specimens. KQ (provisional fracture toughness) versus displacement curves (Fig. 8a) represents the crack growth behavior of the hybrid composites. The fracture mode was brittle for composite with zero cellulose content, showing slip-stick behavior. However, as the content of cellulose (over jute fiber) increases from 0 to 10%, the fracture mode changed from brittle to ductile failure; similarly, K_{Ic} values increased from 2.64 MPa.m$^{1/2}$ for composite having no cellulose fiber content to 3.20 MPa.m$^{1/2}$, 3.21 MPa.m$^{1/2}$, and 3.49 MPa.m$^{1/2}$, respectively, for composite having 3%, 5%, and 10% of cellulose fiber. They observed a linear increment in the fracture toughness value with cellulose coating over jute fiber.

Liu and Hughes (2008a) used a vacuum infusion process to prepare epoxy/flax fiber composites. They observed that the woven textile resulted in an increment of fracture toughness by 2–4 times K_{IC} over that of the unreinforced epoxy composites. The addition of flax fabric shows an improvement in the fracture toughness than the neat resin. This improvement is due to the increase in the fiber volume fraction and

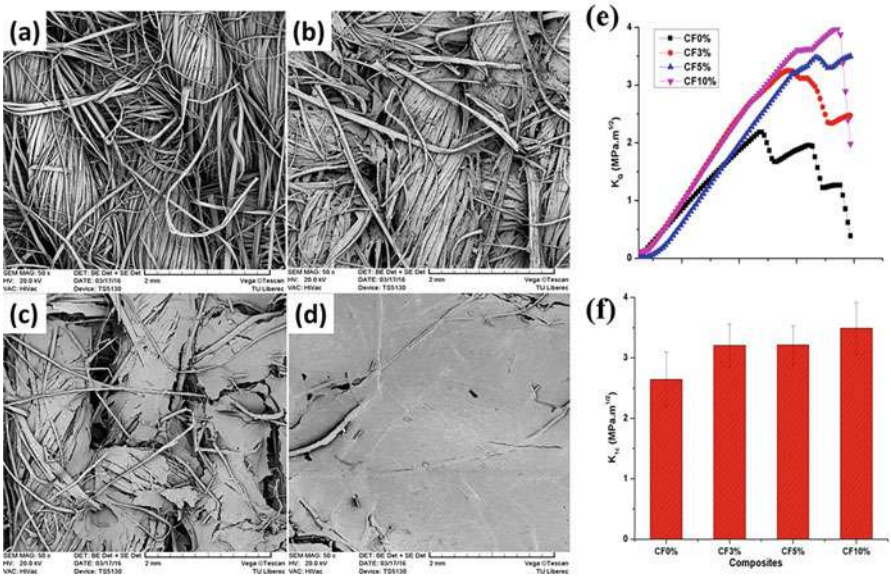

Fig. 8 (**a**–**d**) Morphology of the jute fibers coated with 0,2,5 and 10 wt% of nanocellulose (c) KQ versus displacement curves and (b) fracture toughness (K_{IC}) of uncoated and nanocellulose-coated jute/green epoxy composites (Jabbar et al. 2017). (Reproduced with thanks from Elsevier, License number 5196880515245)

better packing of the fibers, rather than due to the woven nature of the fabric. Similarly, Bensadoun et al. (Bensadoun et al. 2016) studied the effect of fiber arrangement on the interlaminar fracture toughness of flax fiber/epoxy composites and found that the woven fibers have more fracture toughness values when compared to unidirectionally arranged fiber composites. Prasad et al. (2019) reported the mode I and mode II fracture toughness of epoxy/flax/TiO_2 composites. Epoxy resin containing uniformly dispersed titanium dioxide particles exhibited relatively high-fractured surface area may contribute to an improved interlaminar fracture toughness value.

However, the existence of several resin lumps around the fiber assists to deviate the crack propagation. So, the crack is unable to proceed toward the fiber/matrix interface region. Hence an urgency of additional energy is needed for the propagation of crack in the matrix-modified composite samples due to the crack deviation phenomenon.

Moreover, better dispersion of the nanoparticle in epoxy matrix, resulting in the improvement of fiber matrix adhesion, helps to improve the mechanical interlocking between the crack interfaces. Also, at higher loading of nano TiO_2, also feeble penetration of nanoparticles into the fiber layers happened as shown in Fig. 9, and chances of agglomeration between or around the fiber matrix interface are also high, which in turn reduces the reduction of interlaminar fracture toughness in the composites.

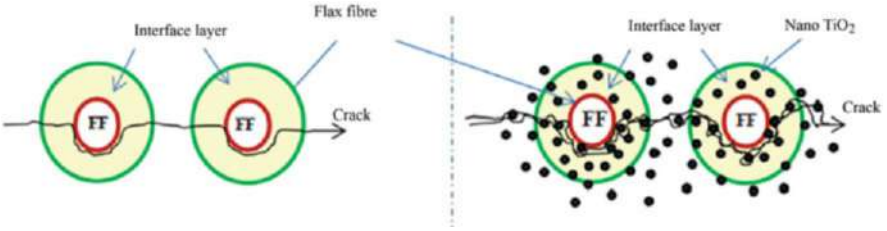

Fig. 9 Mechanism of crack propagation deviation in epoxy/flax/TiO_2 composites (Prasad et al. 2019). (Reproduced with thanks from Elsevier, License number 5196900595871)

Fracture energy absorption during crack propagation in fiber-reinforced materials follows one of the mechanisms such as matrix cracking, fiber/matrix interface debonding, fiber rupture, or fiber pullout. Madhusudhana et al. (2018) reported an increased fracture toughness of the epoxy reinforced with coconut shell powder in comparison with kolam powder and saw dust; additionally, they also observed fracture toughness value dependency on thickness.

On comparing the literature reports of natural fiber-reinforced polymer composites, fracture toughness is mainly influenced by the properties of the fiber chosen for reinforcing, its weight fraction instead of their microstructural arrangement in the matrix. In addition to this, couple of reports suggest that fracture toughness can be improved with higher loadings of the long fibers. Low loadings of natural fiber-reinforced composites have more matrix rich regions, hence the fiber loading is inadequate for load transfer from the host matrix; consequently, low loadings of natural fiber composites exhibit lower-fracture toughness values. Long fibers are more responsible for energy absorption during crack propagation due to debonding and pullout of the fibers. Long fibers dissipate more impact energy through the debonding fracture mechanism which occurs at the fiber matrix interface. This can be further explained by the fiber pullout from the matrix during loading which in turn dissipates energy as friction and thereby participates to fracture toughness. On the other hand, fibers with low strength will rupture instantaneously on loading prior to the pullout of the fiber, consequently resulting in lower fracture toughness value (Khan et al. 2017; Al-Maharma and Sendur 2018; Liu and Hughes 2008b; Wong et al. 2010; Eichhorn and Young 2004).

Conclusion

The fabrication of natural fiber-reinforced epoxy composites has emerged as a greener method to replace conventional synthetic fiber-reinforced epoxy composites. The epoxy thermoset matrices have been modified with several natural fibers such as sisal fiber, coir fiber, flax fiber, jute fiber, bamboo fiber, kenaf fiber, and many more. Natural fiber-reinforced epoxy composites have been widely evaluated for their mechanical performance to find their suitability for composite applications in automobile, aerospace, construction, marine, etc. Tensile, flexural,

impact, and fracture toughness of natural fiber-reinforced epoxy composites has been explored and was found superior in mechanical performance. Fiber parameters such as orientation, fiber length, surface treatment, weight fraction, etc. are found to inevitably affect the mechanical performance of epoxy/natural fiber composites. The in-depth analysis of mechanical failure has been reported by many investigators using scanning electron microscopic observation of failure surface. While the epoxy matrix is subjected to brittle failure, the natural fiber-reinforced epoxy composites mostly have a ductile fracture. Several mechanisms including fiber pullout, fiber breakage, and fiber debonding were reported as major fracture mechanism in epoxy/natural fiber composites. The use of hybrid natural fibers and chemical treatment of fiber surfaces highly influence the failure mechanism and have positive impact on mechanical properties of epoxy/natural fiber composites. In latest add-ons to natural fiber-reinforced epoxy composites, introduced nanofillers strengthen the matrix-fiber interface by providing mechanical interlocking in addition to the chemical bond. The natural fiber-reinforced epoxy composites are the future of composite industry which would have a huge impact on developing a sustainable society.

Acknowledgments We would like to thank Department of Science and Technology, India (DST), through Innovation of Science Pursuit for Inspire Research program (INSPIRE-IF190284) and Defence Research and Development Organisation (DRDO), Naval Research Board, India (NRB-429/MAT/18-19), for financial support.

References

A.B. A.V, P. Vijayan P, S. Thomas, J. Parameswaranpillai, D. Puglia, S. Siengchin, A. L, A. Manohar, Fabrication of water-resistant epoxy nanocomposite with improved dynamic mechanical properties and balanced thermal and dimensional stability: study on dual role of graphene oxide nanosheets and barium oxide microparticles. Colloids Surf. A Physicochem. Eng. Asp. **617**, 126405 (2021). https://doi.org/10.1016/j.colsurfa.2021.126405

A.Y. Al-Maharma, P. Sendur, Review of the main factors controlling the fracture toughness and impact strength properties of natural composites. Mater. Res. Express **6**, 022001 (2018). https://doi.org/10.1088/2053-1591/aaec28

P. Anand, D. Rajesh, M.S. Kumar, I.S. Raj, Investigations on the performances of treated jute/Kenaf hybrid natural fiber reinforced epoxy composite. J. Nat. Fibers (2018). https://doi.org/10.1007/s10965-018-1494-6

A. Balaji, R. Purushothaman, R. Udhayasankar, S. Vijayaraj, B. Karthikeyan, Study on mechanical, thermal and morphological properties of banana fiber – reinforced epoxy composites. J. Bio-Tribo-Corros. **60**, 2–10 (2020). https://doi.org/10.1007/s40735-020-00357-8

F. Bensadoun, I. Verpoest, A.W. Van Vuure, Interlaminar fracture toughness of flax-epoxy composites. J. Reinf. Plast. Compos. **36**, 21–36 (2016). https://doi.org/10.1177/0731684416672925

K.N. Bharath, G.B. Manjunatha, K. Santhosh, 5 – Failure analysis and the optimal toughness design of sheep–wool reinforced epoxy composites, in *Failure Analysis in Biocomposites, Fibre-Reinforced Composites and Hybrid Composites*, ed. by M. Jawaid, M. Thariq, N. Saba, (Woodhead Publishing, 2019), pp. 97–107. https://doi.org/10.1016/B978-0-08-102293-1.00005-X

M. Boopalan, M. Niranjanaa, M.J. Umapathy, Study on the mechanical properties and thermal properties of jute and banana fiber reinforced epoxy hybrid composites. Compos. Part B Eng. **51**, 54–57 (2013)

V. Chaudhary, P.K. Bajpai, S. Maheshwari, Studies on mechanical and morphological characterization of developed jute/hemp/flax reinforced hybrid composites for structural applications. J. Nat. Fibers **00**, 1–18 (2017). https://doi.org/10.1080/15440478.2017.1320260

H. Chittimenu, M. Pasupureddy, C. Muthukumar, S. Krishnasamy, S.M.K. Thiagamani, S. Siengchin, Fracture toughness of the natural fiber-reinforced composites: a review, in *Mechanical and Dynamic Properties of Biocomposites*, ed. by S. Krishnasamy, R. Nagarajan, S. M. K. Thiagamani, S. Siengchin, (Wiley-VCH GmbH, 2021), pp. 293–304

J.P. Craven, R. Cripps, C. Viney, Evaluating the silk/epoxy interface by means of the microbond test. Compos. A: Appl. Sci. Manuf. **31**, 653–660 (2000). https://doi.org/10.1016/S1359-835X(00)00042-7

G. Das, S. Biswas, Effect of fiber parameters on physical, mechanical and water absorption behaviour of coir fiber – epoxy composites. J. Reinf. Plast., 1–10 (2016). https://doi.org/10.1177/0731684415626594

Z. Djafar, I. Renreng, M. Jannah, Tensile and bending strength analysis of ramie fiber and woven ramie reinforced epoxy composite. J. Nat. Fibers **18**, 2315–2326 (2021). https://doi.org/10.1080/15440478.2020.1726242

S.J. Eichhorn, R.J. Young, Composite micromechanics of hemp fibres and epoxy resin microdroplets. Compos. Sci. Technol. **64**, 767–772 (2004). https://doi.org/10.1016/j.compscitech.2003.08.002

V. Fiore, G. Di Bella, A. Valenza, The effect of alkaline treatment on mechanical properties of kenaf fibers and their epoxy composites. Composites Part B: Engineering **68**, 14–21 (2015). ISSN 1359-8368

S. Harish, D.P. Michael, A. Bensely, D.M. Lal, A. Rajadurai, Mechanical property evaluation of natural fiber coir composite. Mater. Charact. **60**, 44–49 (2008). https://doi.org/10.1016/j.matchar.2008.07.001

A. Jabbar, J. Militky, J. Wiener, B. Madhukar, U. Ali, S. Rwawiire, Nanocellulose coated woven jute/green epoxy composites: characterization of mechanical and dynamic mechanical behavior. Compos. Struct. **161**, 340–349 (2017). https://doi.org/10.1016/j.compstruct.2016.11.062

D.D. Jafrey, G.S. Krishnan, P. Velmurugan, Investigation on the characteristics of bamboo/jute reinforced hybrid epoxy polymer composites. Mater. Res. Express **6**, 105346 (2019) https://ui.adsabs.harvard.edu/link_gateway/2019MRE.....6j5346J/10.1088/2053-1591/ab3ae7

M. Jawaid, H.P.S.A. Khali, A.A. Bakar, Mechanical performance of oil palm empty fruit bunches/jute fibres reinforced epoxy hybrid composites. Mater. Sci. Eng. **527**, 7944–7949 (2010). https://doi.org/10.1016/j.msea.2010.09.005

M. Jawaid, A.H. Bhat, A.A. Bakar, Impact properties of natural fiber hybrid reinforced epoxy composites. Adv. Mater. Res. **264**, 688–693 (2011). https://doi.org/10.4028/www.scientific.net/AMR.264-265.688

M. Jawaid, H.P.S.A. Khalil, A. Hassan, R. Dungani, A. Hadiyane, Effect of jute fibre loading on tensile and dynamic mechanical properties of oil palm epoxy composites. Compos. Part B **45**, 619–624 (2015). https://doi.org/10.1016/j.compositesb.2012.04.068

M.J. John, S. Thomas, Biofibres and biocomposites. Carbohydr. Polym. **71**, 343–364 (2008). https://doi.org/10.1016/j.carbpol.2007.05.040

S.V. Joshi, L.T. Drzal, A.K. Mohanty, S. Arora, Are natural fiber composites environmentally superior to glass fiber reinforced composites? Compos. Part A Appl. **35**, 371–376 (2004). https://doi.org/10.1016/j.compositesa.2003.09.016

N. Karthi, K. Kumaresan, S. Sathish, S. Gokulkumar, L. Prabhu, N. Vigneshkumar, An overview: natural fiber reinforced hybrid composites, chemical treatments and application areas. Mater. Today: Proc. **27**, 2828–2834 (2020). https://doi.org/10.1016/j.matpr.2020.01.011

A. Karthikeyan, K. Balamurugan, Effect of alkali treatment and fiber length on impact behavior of coir fiber reinforced epoxy composites. J. Sci. Ind. Res. **71**, 627–631 (2012)

Z. Khan, B.F. Yousif, M. Islam, Fracture behaviour of bamboo fiber reinforced epoxy composites. Compos. Part B **116**, 186–199 (2017). https://doi.org/10.1016/j.compositesb.2017.02.015

K.V. Krishna, K. Kanny, The effect of treatment on kenaf fiber using green approach and their reinforced epoxy composites. Compos. Part B Eng. **104**, 111–117 (2016). https://doi.org/10.1016/j.compositesb.2016.08.010

Q. Liu, M. Hughes, The fracture behaviour and toughness of woven flax fibre reinforced epoxy composites. Compos. Part A Appl. **39**, 1644–1652 (2008a). https://doi.org/10.1016/j.compositesa.2008.07.008

Q. Liu, M. Hughes, The fracture behaviour and toughness of woven flax fibre reinforced epoxy composites. Compos. A: Appl. Sci. Manuf. **39**, 1644–1652 (2008b). https://doi.org/10.1016/j.compositesa.2008.07.008

H.K. Madhusudhana, K. Ruhi, R.L. Anand, C.S. Venkatesha, Experimental study on fracture toughness of natural fibres reinforced hybrid composites. IOP Conf. Ser.: Mater. Sci. Eng. **376**, 012088 (2018). https://doi.org/10.1088/1757-899X/376/1/012088

V. Mittal, R. Saini, S. Sinha, Natural fiber-mediated epoxy composites – a review. Compos. Part B Eng. **99**, 425–435 (2016)

T.P. Mohan, K. Kanny, Water barrier properties of nanoclay filled sisal fibre reinforced epoxy composites. Compos. Part A Appl. Sci. **42**, 385–393 (2011). https://doi.org/10.1016/j.compositesa.2010.12.010

K. Mylsamy, I. Rajendran, The mechanical properties, deformation and thermomechanical properties of alkali treated and untreated Agave continuous fibre reinforced epoxy composites. Mater. Des. **32**, 3076–3084 (2011). https://doi.org/10.1016/j.matdes.2010.12.051

T.A. Nguyen, T.H. Nguyen, Banana fiber-reinforced epoxy composites: mechanical properties and fire retardancy. Int. J. Chem. Eng. **2021** (2021). https://doi.org/10.1155/2021/1973644

H. Om, M.K. Gupta, R.K. Srivastava, H. Singh, Study on the mechanical properties of epoxy composite using short sisal fibre study on the mechanical properties of epoxy composite using short sisal fibre. Mater. Today: Proc. **2**, 1347–1355 (2016). https://doi.org/10.1016/j.matpr.2015.07.053

M.S.S. Prasad, C.S. Venkatesha, T. Jayaraju, Experimental methods of determining fracture toughness of fiber reinforced polymer composites under various loading conditions. J. Miner. Mater. Charact. Eng. **10**, 1263–1275 (2011)

V. Prasad, K. Sekar, S. Varghese, M.A. Joseph, Enhancing Mode I and Mode II interlaminar fracture toughness of flax fibre reinforced epoxy composites with nano TiO2. Compos. Part A Appl. Sci. **124**, 105505 (2019). https://doi.org/10.1016/j.compositesa.2019.105505

V. Prasad, K. Sekar, M.A. Joseph, Mechanical and water absorption properties of nano TiO2 coated flax fibre epoxy composites. Constr. Build. Mater. **284**, 122803 (2021). https://doi.org/10.1016/j.conbuildmat.2021.122803

R. Ramasubbu, S. Madasamy, Fabrication of automobile component using hybrid natural fiber reinforced polymer composite fabrication of automobile component using hybrid natural fiber. J. Nat. Fibers **00**, 1–11 (2020). https://doi.org/10.1080/15440478.2020.1761927

B.V. Ramnath, S.J. Kokan, R.N. Raja, R. Sathyanarayanan, C. Elanchezhian, A.R. Prasad, V.M. Manickavasagam, Evaluation of mechanical properties of abaca – jute – glass fibre reinforced epoxy composite. Mater. Des. **51**, 357–366 (2013). https://doi.org/10.1016/j.matdes.2013.03.102

F.I. Romli, A.N. Alias, A.S.M. Rafie, D.L.A.A. Majid, Factorial study on the tensile strength of a coir fiber-reinforced epoxy composite. AASRI Procedia **3**, 242–247 (2012). https://doi.org/10.1016/j.aasri.2012.11.040

N. Saba, M. Jawaid, O.Y. Alothman, Recent advances in epoxy resin, natural fiber-reinforced epoxy composites and their applications. J. Reinf. Plast. Compos. **35**, 447–470 (2015). https://doi.org/10.1177/0731684415618459

G.K. Sathishkumar, M. Ibrahim, M.M. Akheel, G. Rajkumar, B. Gopinath, R. Karpagam, P. Karthik, M.M. Charles, G. Gautham, G.G. Shankar, Synthesis and mechanical properties of

natural fiber reinforced epoxy/polyester/polypropylene composites: a review. J. Nat. Fibers, 1–24 (2020). https://doi.org/10.1080/15440478.2020.1848723

V. Shah, *Handbook of Plastics Testing and Failure Analysis*, 3rd edn. (Wiley-VCH GmbH, 2007)

M. Sood, G. Dwivedi, Effect of fiber treatment on flexural properties of natural fiber reinforced composites: a review. Egypt. J. Pet. **27**, 775–783 (2018). https://doi.org/10.1016/j.ejpe.2017.11.005

K.R. Sumesh, K. Kanthavel, V. Kavimani, Peanut oil cake-derived cellulose fiber: extraction, application of mechanical and thermal properties in pineapple/flax natural fiber composites. Int. J. Biol. Macromol. **150**, 775–785 (2020). https://doi.org/10.1016/j.ijbiomac.2020.02.118

N. Venkateshwaran, A.E. Perumal, D. Arunsundaranayagam, Fiber surface treatment and its effect on mechanical and visco-elastic behaviour of banana/epoxy composite. Mater. Des. **47**, 151–159 (2013). https://doi.org/10.1016/j.matdes.2012.12.001

R. Vijay, D.L. Singaravelu, Experimental investigation on mechanical properties of Cyperus pangorei fibres -jute fibres based natural fibre composites. Int. J. Polym. Anal. **5341**, 617–627 (2016). https://doi.org/10.1080/1023666X.2016.1192354

P. Vijayan P, A. Tanvir, M. Mrlik, M. Urbanek, M. Al-Maadeed, TiO2/Halloysite hybrid filler reinforced epoxy nanocomposites. Polym. Compos. **39**, E2426–E2435 (2018). https://doi.org/10.1002/pc.24731

P.P. Vijayan, A.V.A. Bhanu, S.R. Archana, A. Babu, S. Siengchin, J. Parameswaranpillai, Development of chicken feather fiber filled epoxy protective coating for metals. Mater. Today: Proc. **41**, 468–472 (2021). https://doi.org/10.1016/j.matpr.2020.05.229

H. Wang, H. Memon, E.A.M. Hassan, S. Miah, A. Ali, Effect of jute fiber modification on mechanical properties of jute fiber composite. Materials **12**, 1–11 (2019a). https://doi.org/10.3390/ma12081226

S. Wang, J. Zhu, Y. Rao, B. Li, S. Zhao, H. Bai, J. Cui, Polydopamine modified graphene oxide-TiO2 nanofiller for reinforcing physical properties and anticorrosion performance of waterborne epoxy coatings. Appl. Sci. (Switzerland) **9** (2019b). https://doi.org/10.3390/app9183760

K.J. Wong, S. Zahi, K.O. Low, C.C. Lim, Fracture characterisation of short bamboo fibre reinforced polyester composites. Mater. Des. **31**, 4147–4154 (2010). https://doi.org/10.1016/j.matdes.2010.04.029

K. Yang, S. Wu, J. Guan, Z. Shao, R.O. Ritchie, Enhancing the mechanical toughness of epoxy-resin composites using natural silk reinforcements. Sci. Rep., 1–9 (2017). https://doi.org/10.1038/s41598-017-11919-1

J. Yeo, O.Y. Kim, S. Hwang, The effect of chemical surface treatment on the fracture toughness of micro fibrillated cellulose reinforced epoxy composites. J. Ind. Eng. Chem. **45**, 301–306 (2017). https://doi.org/10.1016/j.jiec.2016.09.039

Water Sorption and Solvent Sorption of Epoxy/Natural Fiber Composites

27

M. Somaiah Chowdary, Gujjala Raghavendra, Shakuntala Ojha, and M. S. R. Niranjan Kumar

Contents

M. S. Chowdary
Department of Mechanical Engineering, National Institute of Technology Warangal, Warangal, Telangana, India

Department of Mechanical Engineering, Prasad V. Potluri Siddhartha Institute of Technology, Kanuru, Andhra Pradesh, India

G. Raghavendra (✉)
Department of Mechanical Engineering, National Institute of Technology, Warangal, India
e-mail: raghavendra.gujjala@nitw.ac.in

S. Ojha
Department of Mechanical Engineering, Kakatiya Institute of Technology and Science, Warangal, Telangana, India

M. S. R. N. Kumar
Department of Mechanical Engineering, Prasad V. Potluri Siddhartha Institute of Technology, Kanuru, Andhra Pradesh, India

S. Mavinkere Rangappa et al. (eds.), *Handbook of Epoxy/Fiber Composites*,
https://doi.org/10.1007/978-981-19-3603-6_28

Abstract

Natural fiber composites are gaining significant importance as a reinforcement in polymers due to their sustainability, accessibility, enhanced mechanical properties, strength-to-weight ratio, and low cost. In applications, wherever water immersion is necessary, there will be degradation of mechanical, thermal, and wear properties, since one of the disadvantages of the natural fiber-reinforced epoxy composites is that they are hydrophilic. This chapter deals with various factors like the treatment of fiber, aging time, fiber content, and hybridization of fiber in the composite, which influence water sorption and solvent sorption of epoxy/natural fiber composites.

Keywords

Water Sorption · Natural Fibers · Epoxy · Solvent Sorption

Introduction

Over the most recent decades, there has been keen user alertness of novel products from renewable sources. Environmental marketing, new guidelines on reutilizing, societal impact, and improvements in moral standards have driven customers to purchase environmentally friendly goods. So in this decade, composite materials emerged as a new, exciting form of material that provides a new class of advantages for this modern technology. Polymers are desirable engineering materials due to their unique properties, such as high specific strength and corrosion resistance, in addition to their variety and design versatility. By adding suitable fillers/fibers to polymers, they can be made more effective. Our interest in these composite materials is natural fiber-reinforced epoxy composites (NFRECs). The most used fibers as reinforcements are generally synthetic fibers. Due to increasing awareness among the consumers, researchers get inclined toward natural fiber reinforcement. Also, natural fibers are low in cost compared to synthetic fibers since they are readily available in nature and very few processing techniques are required for final reinforcement as fiber (Raghavendra et al. 2013; Saba and Jawaid 2017; Khan et al. 2018). There are six primary forms of natural fiber. They are graded as follows: fibers of bast (jute, flax, hemp, ramie, and kenaf), fibers of a leaf (abaca, sisal, and pineapple), fibers of seed (coir, cotton), fibers of core (kenaf, hemp, and jute), fibers of grass and reed (wheat, maize, and rice), and fibers of all other varieties (wood and roots) (Thakur et al. 2014). Some of the natural fibers as reinforcements can be seen in Table 1. Plants that generate natural fibers are graded as primary and secondary, depending on their use. Primary plants are grown as a by-product of their fiber content, while secondary plants are plants where the fibers are produced as a by-product. Examples of primary crops include jute, cotton, kenaf, and sisal. Examples of secondary crops include pineapple, oil palm, and coir. Table 1 presents the primary fibers used

Table 1 Natural fibers and botanical name, origin, and their availability in the world (Mohammed et al. 2015; Ahmad et al. 2015; Satyanarayana et al. 2007)

Fiber source	Botanical name	Origin	World production (10^3 ton)
Bamboo	*Bambusa*	Grass	30,000
Sugarcane bagasse	–		75,000
Jute	*Corchorus capsularis*	Bast	2300
Kenaf	*Hibiscus cannabinus*	Bast	970
Flax	*Linum usitatissimum*	Bast	830
Grass	–		700
Sisal	*Agave siciliana*	Leaf	375
Hemp	*Cannabis sativa*	Stem	214
Coir	*Cocos nucifera*	Fruit	100
Ramie	*Boehmeria nivea*	Stem	100
Abaca	Musa textile	Leaf	70

commercially in composites, which are now available and produced all over the world (Mohammed et al. 2015).

The natural fiber reinforcement can be separated according to length, scale, and orientation which can be in the form of a particle or a fiber. Depending on its length-to-diameter ratio, the fiber itself is continuous or discontinuous (i.e., chopped). The fiber-reinforced phase structure is generally known as woven or nonwoven. Woven fabric is defined by continuous interlacing, in a regular pattern, of perpendicular yarns. Yarns are structures that consist of multiple fibers that are interlocked (Peças et al. 2018). NFRECs, which are environmentally friendly, are being developed to meet the requirement of various automotive, aerospace, sports equipment, marine and civil, etc. (Peças et al. 2018; Holbery and Houston 2006; Shakuntala et al. 2014; Outline 2015; Lotfi et al. 2019) NFRECs have gained importance because of added advantages such as superior mechanical properties, durability, high corrosion resistance, and low cost (Bouhfid et al. 2018; Amir et al. 2018; Ngo 2018; Gujjala et al. 2014) compared to traditional metals. But in applications where there is contact or immersion in water or solvents like kerosene, saline water, methanol, etc., water and solvent absorption occurs, leading to degradation of properties such as mechanical, thermal, and tribological properties (Saharudin et al. 2016). The natural fiber consists of hemicellulose, cellulose, lignin, pectin, wax, substances soluble in water, and fat (Sanjay et al. 2018; Ojha et al. 2014; Fuqua et al. 2016; Ali et al. 2016). Cellulose is considered the fiber structure's mainframe element, which imparts fiber stiffness, strength, and structural durability. However, cellulose and hemicellulose are the main components of natural fiber, which consume the most significant amount of humidity. Lignin provides efficient hemicellulose/cellulose protection alongside extreme environmental conditions such as moisture and temperature.

The fibers entrap water from the atmosphere through hydroxyl groups found in the fiber. Three main water sorption mechanisms in NFRECs have been established: the diffusion, capillary, and transfer of water particles (Dhakal et al. 2007;

Al-Maharma and Al-Huniti 2019). Diffusion is an unsystematic procedure in which the water passages from high absorption regions to low absorption. The behavior of diffusion in epoxy composites follows the Fickian and non-Fickian models of absorption. On the other hand, the capillary carrying process occurs in the holes at the interface of the fiber/epoxy. The intake of water is problematic since it can tip to matrix cracking, dimensional volatility, and more inferior mechanical properties of polymer composites reinforced with fiber. The specific water increases with excessive water absorption, whereas free water decreases (Azwa et al. 2013). Water-soluble materials initiate to escape from fiber and eventually result in ultimate debonding among matrix and fiber. Figure 1 shows the diffusion process of water molecules into the natural composite structure mentioned above. Natural fibers are hydrophilic, which absorb the water molecules. Due to absorption, the natural fiber starts swelling, which creates an evident change in the composites' dimensions and affects the interface bonding between the fiber and the matrix. The fiber's swelling leads to the breaking of interface bonding with the matrix; if the matrix is brittle, some microcracks are also formed due to the fiber's swelling, which is shown in Fig. 1a. After reaching the fiber's maximum swelling, the fiber starts contracting and returning to the standard dimensions. Still, the matrix that is deformed due to swelling remains unchanged in dimensions. Those gaps will be filled with water molecules, which later start slowly separating the water-soluble matter from the fiber, shown in Fig. 1b, c. When the composites are clearly dried and taken away from the moisture environment, the water molecules clearly evaporate and clear debonding and separation of fiber and matrix are observed which decrease the mechanical and tribological properties of the composite.

Water absorption content is less in epoxy and synthetic reinforced composites compared to NFRECs (Sgriccia et al. 2008). H. Alamri et al. (Alamri and Low 2012) examined the mechanical properties and water absorption properties of recycled cellulose fiber-reinforced epoxy composites. They have concluded that cellulose fiber-reinforced epoxy composites absorb more water compared to pure epoxy

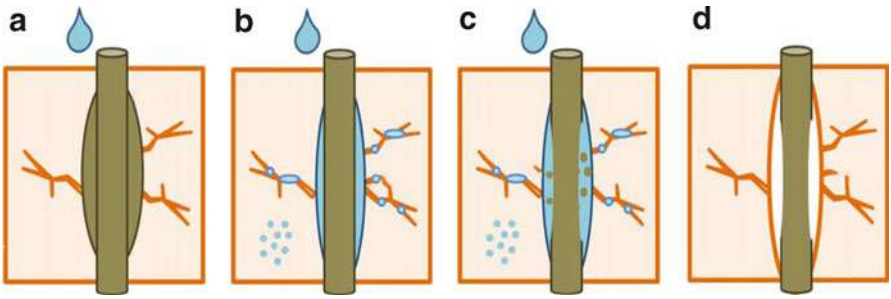

Fig. 1 Deprivation of interfacial bond due to water sorption: (**a**) evolution of microcracks in epoxy due to expansion of swollen fiber, (**b**) distribution of water molecules in the widespread matrix along with the fiber/epoxy interface, (**c**) escape of water-soluble fiber mechanisms, (**d**) final matrix-fiber debonding happens. (Reprinted with permission from (Azwa et al. 2013))

composites. As fiber content increases, water uptake and diffusion coefficient are growing, which shows the hydrophilic nature of the natural fiber-reinforced composites. Even cellulose fibers comprise the lumen, a hollow region that allows more water to be observed, indicating the capillarity effect and water absorption behavior are Fickian.

Z. Leman et al. (2008) studied the effects of environments on the fiber surface properties of sugar palm fiber-reinforced epoxy composites. To detect and quantify organic contamination and the population of microorganisms in both seawater and freshwater, a biochemical oxygen demand (BOD) test was conducted. They concluded that there are more microorganisms in marine water than in freshwater. This large microorganism population can help to degrade pectin and hemicellulose more efficiently, resulting in a more robust surface and matrix adhesion of the fiber. Using the DO meter, the pH values of seawater and freshwater were also calculated. The more significant the pH value, the faster will be the deterioration of hemicelluloses. Its salinity was another reason which caused further degradation by seawater. Work on water absorption and solvent absorption activity has been carried out several times. Water absorption is calculated using the formula (Gupta and Srivastava 2016a; Panchal et al. 2018; Prakash et al. 2017)

$$W\% = \frac{W_2 - W_1}{W_1} \times 100 \tag{1}$$

where W_1 = weight of the sample before soaked in water and W_2 = weight of the sample after soaked in water, and sorption coefficients are calculated by using the formula (Gupta and Srivastava 2016a; Panchal et al. 2018; Prakash et al. 2017).

$$S = \frac{M_S}{Mt} \tag{2}$$

where Ms = percentage of water uptake at saturation time and M_t = percentage of water uptake at a specific time. The diffusion coefficient (mm^2/s), which is a kinetic parameter, is calculated using the formula (Gupta and Srivastava 2016a).

$$D = \pi\left(\frac{t^2 m^2}{16 Ms^2}\right) \tag{3}$$

where m = slope of the linear portion of the sorption curve and t = sample initial thickness in mm.

Different factors have been identified as responsible for the degradation of properties in the composite, such as fiber treatment, aging period, fiber content, and hybridization of fibers affecting water absorption and solvent absorption. Methods are also studied to reduce the fibers' hydrophilic aspect and improve fiber surface bond to the surrounding matrix. Therefore, the purpose of this chapter is to summarize and discuss water sorption and solvent sorption behavior of NFRECs and factors influencing water absorption behaviors of NFRECs.

Water Sorption of Natural Fiber-Reinforced Epoxy Composites (NFRECs)

Natural Fiber-Reinforced Composites

Natural fibers such as jute, sisal, hemp, coconut, kenaf, bamboo, flax, etc., which exist generally in nature, are used as reinforcement in epoxy-based composites (Ferreira et al. 2019). The wide range of applications of NFRECs is increasing rapidly in a variety of engineering fields. Various forms of natural fiber-reinforced epoxy composite have been given great standing in several automotive applications. Many automotive companies use natural fiber as reinforcement in epoxy-based composites. In addition to the automobile industry, the standards for natural fiber composites have also been used in building and construction, sports, and aerospace (Mohammed et al. 2015). One of the disadvantages of NFRECs is they are prone to high water sorption. Natural fiber consists of cellulose, hemicellulose, lignin, pectin, wax, water-soluble compounds, and fat (Ojha et al. 2016). Cellulose is known to be the primary building block of the fiber system. It gives the fiber rigidity, strength, and structural firmness. Nevertheless, cellulose and hemicellulose are the key components of natural fiber that absorb water's maximum volume. Lignin provides active protection for hemicellulose/cellulose besides adverse climatic conditions such as moisture and temperature (Thakur and Thakur 2014). Figure 2 shows the abovementioned natural fiber and its constituents and constituents that absorb water.

Water Sorption Behavior of Natural Fiber-Reinforced Composites

The water absorption is very much apparent if natural fiber-reinforced composites are exposed to liquid media (Sood and Dwivedi 2018). R. Masoodi et al. (Masoodi and Pillai 2012) studied the water absorption of epoxy and bio-epoxy weaved jute fiber-reinforced composites with 1–2 fiber layers. Bio-based epoxy composites showed more water sorption than epoxy composites due to hydroxyl groups existing in bio-epoxies (Masoodi and Pillai 2012). The two-layered jute fiber showed

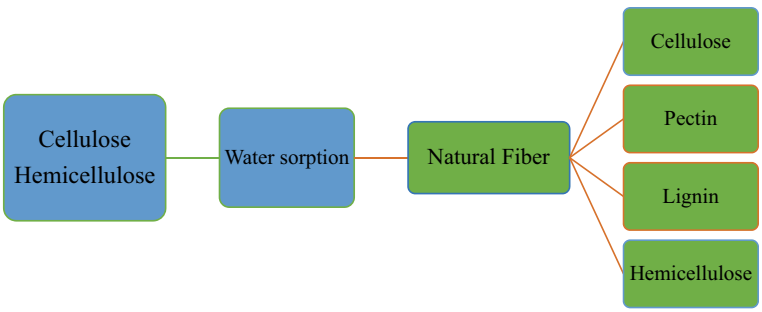

Fig. 2 The components of natural fiber and components that absorb water

maximum water absorption and swelling in both composites, which indicate that the fiber content is increasing, moisture absorption is increasing (Alamri and Low 2012), and a similar result is observed (Gupta and Srivastava 2016a). Both specimens displayed a high swelling rate at the start of the moistening test, but the swelling rate reduced asymptotically over the period.

Anu Gupta et al. (Gupta 2014) studied water absorption properties of bamboo fiber-reinforced epoxy composites and concluded that water absorption rises with fiber content since bamboo fiber is hydrophilic and epoxy is hydrophobic. The cellulose's high content in bamboo fiber contributes to more water entering the interface through the microcracks caused by the fibers' swelling. This swelling stress additionally contributes to composite failure. Samples are submerged in the water for around 60 days. Initially, sorption (%) is linear at the start and then decelerates and approaches saturation after an extended period (where U1 = epoxy +10 wt.% of fiber and for U2, U3, and U4 following weight % increase of fiber up to 40 wt.%) following the Fickian diffusion cycle.

U. Huner et al. (Huner 2015) have determined the water absorption behavior of hemp fiber-reinforced epoxy composites and found that with an increase in fiber content, there is a high level of moisture absorption of natural fiber-reinforced epoxy composites. The reasoning may be that the flax fibers contain plenty of polar hydroxide clusters resulting in a high moisture absorption level, and this phenomenon can be seen in Fig. 3. An additional result of rising the water absorption rate of composites is the nature of flax fiber; voids within composites lead to microchannel development. Here, two temperatures are maintained (25 °C and 90 °C) of which samples immersed in 25 °C tend to absorb more water amounts than 90 °C.

G. Das et al. (Das and Biswas 2016) have reported the water absorption properties of coir fiber-reinforced epoxy composites for different fiber lengths

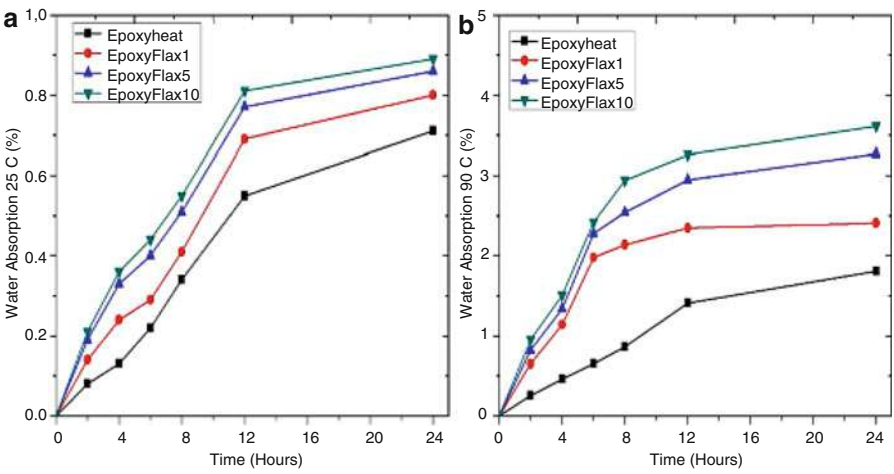

Fig. 3 Water absorption of hemp fiber-reinforced epoxy composites at (**a**) 25 °C and (**b**) 90 °C (Huner 2015). (Reprinted with permission from (Huner 2015))

and wt.% of fiber. In all cases, in the beginning, the water absorption cycle is severe and flattened off over a certain amount of time until it reaches equilibrium. The rate of water absorption is typically significantly impacted by the density and void quality of the composite. The longer the fiber, the higher the intake of water. Water absorption levels are also observed to increase with high fiber content. Composites with a coir fiber content of 20 wt.% display a higher rate of water absorption compared to 5 wt.% of fiber. This may be due to the coir fibers which produce different polar hydroxide groups, resulting in increased absorption of natural fiber-based polymer composites.

A. Devadas et al. (2018) studied the water absorption properties of kenaf fiber-reinforced epoxy composites and reported that pure epoxy composites exhibited minor water absorption. In contrast, samples with 5% kenaf fiber have the least water absorption among other reinforcements. And 20% reinforcement showed maximum water absorption. This is due to the hydrophilic nature of the NFRECs.

J. Gassan et al. (Gassan and Bledzki 1999) studied the effect of moisture absorption on jute fiber-reinforced epoxy composites. The impact of water absorption on epoxy resins containing untreated and silane-treated jute fibers has been discussed in this study. Silane treatment of fibers resulted in improved tensile and flexural strength and improved up to 30%.

L. Yan et al. (Yan and Chouw 2015) analyzed flax fiber-reinforced epoxy composites under the influence of three environmental conditions, i.e., seawater, water, and 5% NaOH solution and concluded that the weight gain behavior of the flax fabric/epoxy composites was similar in the three aging conditions, i.e., a large increase was observed in the initial 2 months of immersion and only slightly increased until the stage of saturation. All three aging solutions have resulted in significant deterioration of the tensile and flexural properties of the composites. The largest reduction is the specimen immersed in NaOH solution, followed by the smallest decline in seawater and the sample immersed in water.

It can be outlined that NFRECs are sensitive to humidity and exposure to moisture will cause them to lose their functionality in time. This factor must be considered when making a composite that can be used in a high humidity atmosphere. One of them is selecting the appropriate fiber to confirm it has the real properties for increased moisture resistance. Comparing high temperature and low temperature, the amount of sorbed water at a higher temperature was smaller, and the sorption equilibrium at the higher temperature was reached much faster. Polymers are augmented with fibers to produce a composite that is tougher and less likely to crack.

Nevertheless, natural fiber reinforcement in an epoxy material makes it more vulnerable to moisture absorption. When the proportion of fibers in wt.% increases, so does the rate of absorption of moisture. For NFRECs to be used outdoors, fiber content should only be confined only to achieve its necessary strength. This minimizes the absorption of moisture and increases composite durability.

Deprivation of Mechanical Properties Due to Water Sorption and Solvent Sorption

When deciding the application of NFRECs, the mechanical characteristics remain very important. And the decline of mechanical properties when exposed to liquid media is apparent. Fibers are hydrophilic, and polymers are hydrophobic (Zamri et al. 2012; Moudood et al. 2018). G Raghavendra et al. (Raghavendra et al. 2015) inspected the water sorption properties of jute fiber-reinforced epoxy composites under different environments and their effect on mechanical properties. Samples are with three distinctions by varying the number of layers, i.e., 1, 2, 3 layers. With jute reinforcement in epoxy, there is an increase in mechanical properties, both bending and tensile, for all layers, with three-layered jute fiber showing the best value. When samples are immersed in various environments, such as saline, mineral water, or subzero temperatures, deprivation of properties and solvent absorption occur in all of them. The saturation absorption time was observed after an 8-day immersion. Compared to all the environments, saline environment showed the least degradation of properties with 35% degradation of tensile properties while mineral water by 25% and the subzero environment by 17.5%. This is due to increase of voids in the fiber content. SEM images of tensile specimens that are immersed in different environments can be seen in Fig. 4. We can observe fiber pullout and swelling, which is the reason for degraded properties under different environments.

MO. Prakash et al. (2018) determined the mechanical properties of arhar fiber-reinforced epoxy composites under different environments for 9 days. Three different wt.% of the fiber is chosen, i.e., 5, 10, and 15, for the fabrication of the specimens. As the fiber content increases, the moisture absorption also increases because of the fiber's hydrophilic nature. Mechanical properties were found to be ideal at 10 wt.% of fiber loading. When the samples were immersed in different environments, saline water environment had the maximum degradation of mechanical properties where there is a 43% reduction in strength than normal specimens. Less effect is found for water and subzero immersions. Fig. 5 shows the tensile strength of epoxy and arhar fiber with different wt.% in different environments.

E. Muñoz et al. (Muñoz and García-Manrique 2015) reported the effects of water absorption on flax fiber-reinforced bio-epoxy composites. Immersion of flax fiber-reinforced bio-epoxy composites in the water at room temperature was used to investigate the water absorption effect on mechanical properties. Because of the higher cellulose content, water absorption increases as the fiber weight fraction increases. At room temperature, composites exhibit Fickian water absorption behavior. The findings suggest that water absorption causes flax fibers in the composite material to swell, positively affecting mechanical properties. The tensile strength of all water-immersed specimens studied is greater than that of dry samples due to stronger interfacial bonding between the fiber and the matrix. As the water absorption content increases, so do the flexural properties. Because water absorption has no negative effect on the mechanical properties of these flax fiber composites, they have the potential to be used in outdoor applications.

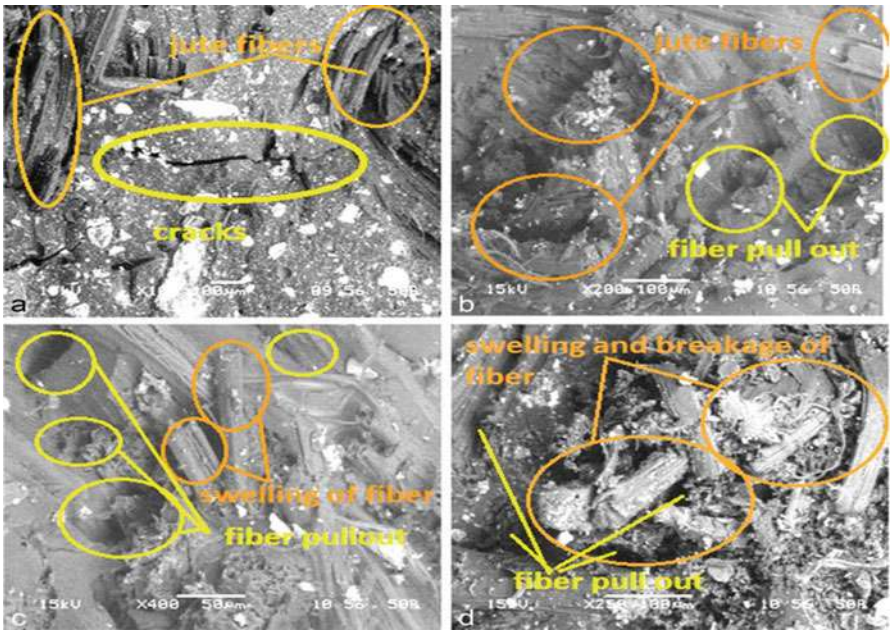

Fig. 4 SEM images of tensile-tested specimens in different environments: (**a**) natural, (**b**) subzero, (**c**) mineral water, (**d**) saline water (Raghavendra et al. 2015). (Reprinted with permission from (Raghavendra et al. 2015))

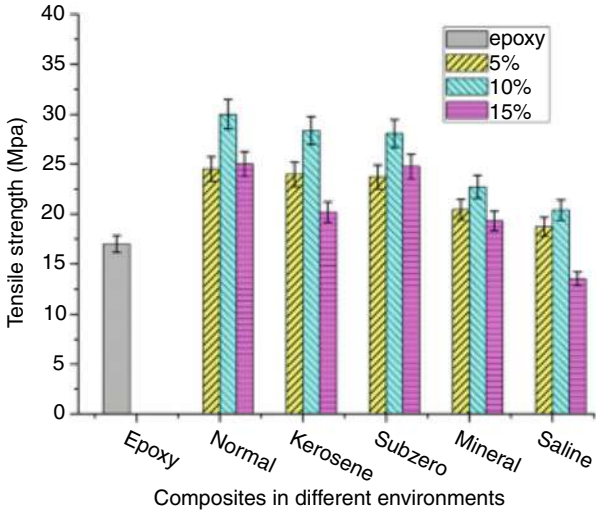

Fig. 5 The tensile strength of arhar fiber-reinforced epoxy composites in different environments (Prakash et al. 2018). (Reprinted with permission from (Prakash et al. 2018))

Chittaranjan Deo et al. (Deo and Acharya 2010) studied the moisture absorption behavior on the mechanical properties of *Lantana camara* fiber-reinforced epoxy composites. Samples were prepared by five different wt.% (10, 20, 30, 40), and samples were placed in three other solvents, i.e., steam, saline, and subzero temperatures. Tensile and flexural strength improved as fiber content was increased. At 30 wt.% fiber content, the highest values were achieved. Because of the increased voids and cellulose content, moisture uptake increases with fiber loading. The composite's moisture absorption was higher in a steam environment than in saline water or subzero temperature environment. The composites followed Fick's law projections under all environmental conditions. Mechanical properties (tensile and flexural) were found to be reduced in all cases. Moisture percolates through the matrix until it reaches the interphase region and reinforcement. Dissolution of the polymer matrix, debonding of the fiber-matrix interphase, and fiber degradation during moisture aging can reduce the composite's mechanical properties.

Deprivation of Wear Properties Due to Water Sorption and Solvent Sorption

Wear is unnecessary damage to a solid's surface owing to its relative motion, which involves the total material loss from the contact area. It is a natural reaction of a substance, which can be either mechanical or chemical (Boggarapu et al. 2020). Wear and friction are the principal causes of material failure and damage to equipment (Sumithra and Sidda Reddy 2018; Milosevic et al. 2020). M.O. Prakash et al. (2017) examined the influence of different environments on the degradation of tribological properties of arhar fiber-reinforced epoxy composites under various environments such as mineral water, saline water, subzero environment, and kerosene and in dry conditions. The uptake of moisture is more during the initial period; as time passed, humidity absorption decreased and became saturated. The behavior of moisture absorption is due to the natural fiber's hydrophilic nature in the composites. As the fiber content increases, free OH groups are seen increasing, which tends to absorb more moisture content. Since the composite samples take in the moisture content, the composite sample weight increases. More absorption is found in mineral water because mineral water is very high in diffusivity and less absorption in subzero conditions. After all, the moisture content is less in the subzero environment. Maximum erosion is observed for saline water immersion which can be seen in Fig. 6.

Factors Influencing Water Sorption and Solvent Sorption of Epoxy/Natural Fiber

Various factors are responsible for the degradation of properties of underwater sorption and solvent sorption of NFRECs such as the treatment of fiber, fiber content, hybridization, and aging time in the composite.

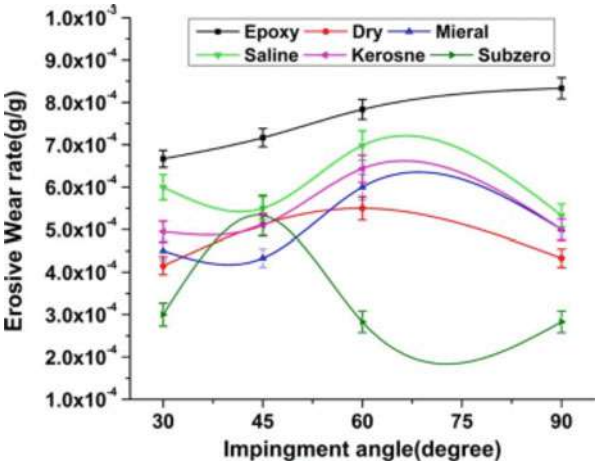

Fig. 6 Erosion wear behavior of 10 wt.% samples in different environmental conditions (Prakash et al. 2017). (Reprinted with permission from (Prakash et al. 2017))

Effect of Fiber Treatment and Aging Time on Water Sorption and Solvent Sorption

The proper interfacial bond between fiber-matrix shows an active part in defining the composites' properties. The adequate bonding between the fiber and the matrix is a basic necessity for high strength in the resulting composite (Hamid et al. 2012). But the hydrophilic natural fibers will affect the fiber-matrix reaction. Thus, treatment is needed to improve interfacial bonding efficiency, increasing the composite properties (Li et al. 2007; Wang et al. 2007). V. Mittal et al. (Mittal and Sinha 2017) studied the mechanical properties and water absorption of alkali-treated wheat straw fiber (WSF)-reinforced epoxy composites. Epoxy is reinforced with WSF with five different wt.% (5, 10, 15, 20, 25). Also, fibers are treated with (1, 3, 5 wt.%) alkali, out of which 5 wt. % fiber with 3% alkali-treated composition showed improved tensile and flexural properties related to other treated and fiber wt.% combinations. Figure 7 shows the amount of water absorbed in untreated and specific amounts of alkali-treated WSF-epoxy composites. WSF-reinforced composites have been observed to have a higher absorption of water than pure epoxy resin. It may be because more water is absorbed by lignocellulose materials, which are present in the fiber. Instead, it was observed that the alkali-treated WSF/epoxy composite reduced water absorption, as presented in Fig. 7. The 5% NaOH-treated WSF composite showed optimum at 5% alkali-treated WSF fiber which had 3.5% of absorbed water whereas the untreated WSF composite had 5% absorbed water after 10 days. From this, we can say that alkali treatment declines the water absorption characteristics of composites.

A study by B.M. Reddy et al. (2018) showed that alkali-treated *Cordia dichotoma* fiber reinforced with epoxy has the least water absorption than untreated fiber when reinforced with epoxy. All the samples are treated with 5% NaOH (alkali treatment) with different wt.% and untreated fiber with the same wt.% are considered for the experimentation. Out of which 10 wt.% sample with alkali treatment showed the

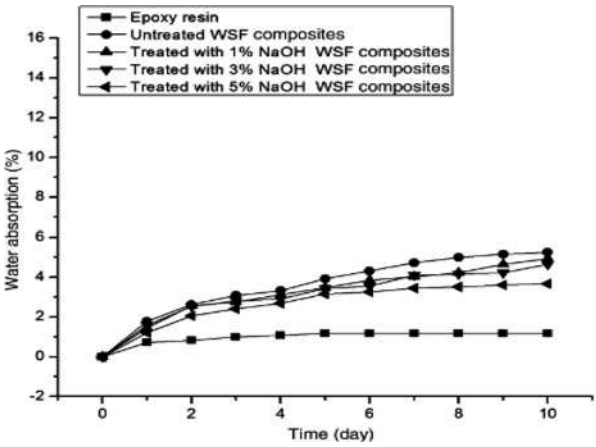

Fig. 7 Water absorption of WSF composites both treated and untreated (Mittal and Sinha 2017). (Reprinted with permission from (Mittal and Sinha 2017))

least water absorption properties, this was due to alkali-treated fiber is less hydrophilic as several hydrophilic hydroxyl groups reduce by reacting with 5% NaOH which leads to prohibiting of water from the substrate of the composite. The amount of water sorption followed Fickian behavior. All of the composites show a sharp increase in the water uptake at the start (up to 72 h) and reach saturation later, a point wherein no water is absorbed after 192 h. Table 2 shows the various fiber treatments of different natural fiber-reinforced epoxy composites and their effect on improving water absorptions and multiple properties of the NFRECs. From the study, it can be concluded that the treatment of fiber reduced water absorption to a greater extent. As fiber treatment with any chemical agents reduced the fiber's hydrophilic nature, it reduced the water absorption.

Effect of Fiber Content on Water Sorption and Solvent Sorption

It is worth noticing that the water absorption rate of composites increases by increasing fiber wt.%. In particular, the size and shape of the reinforcement considerably affect the absorption of composites by water. G. Rajeshkumar et al. (Rajeshkumar et al. 2016) studied the water absorption behaviors of *Phoenix* sp. fiber-reinforced epoxy composites. Dissimilar particle sizes and various lengths are chosen for the experimentation with different fiber vol.% under other environmental conditions. All the composites displayed an increase in water sorption when there was an increase in fiber size and length and fiber volume content. Fiber content with 50% and fiber length 30 mm showed the maximum water sorption and fiber content with 10%, and fiber length 10 mm showed the least water sorption. Comparing with size and length, 300 μm fiber particle size absorbed the least water absorption to fiber length. The effect of the reinforcement material on the composites' water absorption behavior may be due to the improved number of free OH groups on the lignocellulosic fiber surface,

Table 2 The various effects of fiber treatments on water sorption

Reference	Composite	Treatment (%)	Immersion time and temperature	Findings
(Venkateshwaran et al. 2013)	Banana/ epoxy	Alkali (0–20% NaOH)	30 min	1% is the optimum treatment since the least moisture absorption is found 15% lesser intake compared to untreated fiber
(Kushwaha and Kumar 2010)	Bamboo/ epoxy	5% NaOH followed by five different saline treatments	30 min at room temperature	5% NaOH and (aminopropyl) triethoxysilane-treated bamboo epoxy composite showed minimum water absorption compared to other saline treatments
(Anbukarasi and Kalaiselvam 2015)	*Luffa*/ epoxy	2% NaOH	1 h at room temperature	Water absorption was reduced by 13.8% compared to the untreated fiber
(Mittal and Sinha 2015)	Bagasse/ epoxy	1% NaOH followed by 1% acrylic solution	1 h at ambient temp	Water absorption was seen reduced in treated fiber, and 5 wt.% treated fiber showed the least water absorption
(Suckley et al. 2017)	Bagasse/ epoxy	1,3,5,7% NaOH	18 h	3% NaOH-treated bagasse fiber exhibited the least water absorption while untreated fiber exhibited maximum water absorption
(Goud and Rao 2011)	*Roystonea regia*/ Epoxy	5% NaOH	2 h	After 120 h of immersion in distilled water, the absorption of untreated fiber composites was 2.34 times greater than that of alkali-treated fiber composites. This is because, after alkali injection, the wettability of the resin rises, which decreases air-filled voids, leading to a decreased water-absorbing propensity

coming into contact with the free water molecules that appear to form hydrogen bonds with them, leading to swelling phenomena.

K. Velusamy et al. (Velusamy et al. 2018) reported *Calotropis gigantea* fiber-reinforced epoxy composites' water absorption behavior. The experiments were

performed at various temperatures such as 10, 40, and 70 °C with varying fiber length of 30 mm and volume fractions of 0, 5, 10, 15, 20, 25, and 30% for a duration of 15 days. The water absorption rate is noted to have risen with the surge in the number of days of immersion, irrespective of the proportion of the fiber length. Owing to the epoxy resin's hydrophobic nature, the neat epoxy displayed a very low water absorption rate for all days. Given the hydrophilic nature of *Calotropis gigantea* fibers, *Calotropis gigantea* fibers' introduction improved composites' water absorption rate. Further hydrophilicity is seen to increase the composites, which are reinforced by a volume of 30%. A similar water absorption pattern is witnessed at all temperature levels, but the water absorption rate increases with the water temperature rise. The increase in temperature promotes diffusivity, which results in the formation of microcracks on the fiber and matrix interface area (Velusamy et al. 2018). The surge in water absorption rate would decline the composites' mechanical properties. Due to the lower hydrophilic nature, the composites with the smaller length and lesser volume fraction of fiber display the slightest water absorption rate. The higher immersion temperature had increased the rate of water absorption.

Effect of Hybridization on Water Absorption and Solvent Absorption

Hybridization occurs by reinforcing natural fibers/natural fibers, natural fibers/synthetic fibers, synthetic fibers/synthetic fibers, natural fibers/fillers, synthetic fibers/fillers, natural fibers/synthetic fibers/with polymer (Singh and Mukhopadhyay 2020). And our interest is to study the effect of hybridization of NFRECs' water absorption properties. M.K. Gupta et al. (Gupta and Srivastava 2016b) determined the water absorption behavior of hybrid sisal/jute fiber-reinforced epoxy composites. Hybrid composite with contents of jute 50% and sisal 50% exhibited improved water absorption resistance compared to other normal and hybrid composites. This is due to improved interfacial bonding between matrix and fibers. The hybrid composite with jute and sisal 50:50 showed 50% less water absorption while treated jute and treated sisal 50:50 showed 72% less water absorption compared to jute fiber-reinforced composites. The composite with 50:50 jute and sisal showed the lowest water absorption coefficient. From this, it can be understood that the hybridization of composites shows a better response to water absorption properties compared to normal composites.

S. Bhaskara et al. (2016) have studied the water absorption properties of hybrid jute and banana fiber-reinforced epoxy composites. Due to voids and high porosity on the surface, the water absorption potential increases as fiber loading increases. The absorption of water has been maintained at approximately 216 h, and no major changes in composite hybrid samples weight were observed after this period. The maximum water absorption percentage is for the composite made of 30 wt.% of banana and 10 wt.% of jute fiber. The hybrid composite of 30 wt.% jute and 10 wt.% banana fiber showed the lowest water absorption compared to other samples. Jute fiber has an improved aspect ratio, lowest sorption, permeability, and diffusion ratio than banana fiber, resulting in poorer water absorption ability as a higher weight ratio for a composite made of jute fiber. The highest percentage of water absorption is the maximum for the samples

having high banana fiber content. The cause can be due to the banana fibers having a high degree of polar hydroxide absorption compared to jute fiber.

Daniel D Jafrey et al. (2019) examined the water absorption properties of bamboo- and jute-reinforced hybrid epoxy composites. They prepared samples with different stacking sequences and immersed them in water for about 16 days. As the number of days increases, the water absorption characteristics are increased. Water absorption properties were grown for 14 days, and composites became saturated afterward. Jute-bamboo-jute-reinforced hybrid composite showed the maximum water absorption due to voids and pores, which resulted in greater water absorption. The composite manufactured with bamboo-jute-bamboo showed a lower moisture absorption because the matrix and fiber have a strong bond. Table 3 shows the hybridization of several natural fibers on water sorption and solvent absorption.

Table 3 The hybridization of natural fiber on water sorption and solvent absorption

Reference	Fiber 1	Fiber 2	Findings
(Boopalan et al. 2013)	Jute	Banana	Water absorption properties were studied at the immersion of the sample at 23 °C. Hybrid composite with a weight ratio of 50:50 showed the least water absorption compared to other composites
(Venkateshwaran et al. 2011)	Banana	Sisal	Water absorption properties were studied at room temperature and found that the hybrid samples showed the least water absorption. There is an 18% decrease in water uptake compared to banana-reinforced composites
(Maslinda et al. 2017)	Kenaf	Jute hemp	The water absorption pattern of these composites was found to follow the behavior of the non-Fickian model. Moreover, their hybridization, woven kenaf's water-resistant properties, jute, and hemp fiber have been enhanced
(Venkateshwaran and Elayaperumal 2012)	Woven jute	Woven banana	Banana fiber composites have the lowest moisture absorption percentage for various types of composite tested. Due to jute fiber's sensitivity to moisture, the jute/banana/jute layering series has the highest moisture absorption percentage since jute fiber contains the highest coefficients of sorption, diffusion, and permeability
(Saw et al. 2012)	Jute	Coir	Composite samples are prepared with individually treated and untreated fiber, and samples were immersed at 25 °C and 50 °C temperature for a period of 120 h. Hybridized composites with a fiber ratio of 50:50 with treatment showed the least water absorption at 25 °C
(Sathish et al. 2017)	Flax	Bamboo	Hybrid composites with 30% flax and 10% bamboo showed the least water absorption than other normal and hybrid specimens. Interestingly with higher bamboo content, water absorption is more

Conclusions

Reinforcement with natural fiber with a particular loading greatly enhances its properties for epoxy composites. But immersion of samples in water leads to water sorption and further leads to its degradation of properties. Various factors are responsible for the degradation of properties of underwater sorption and solvent sorption of NFRECs such as the treatment of fiber, fiber content, hybridization, and aging time in the composite. These effects are studied in this chapter, and various conclusions can be drawn from this study which is discussed below.

1. Since water acts as a plasticizer, degradation of properties takes place upon immersion of samples in water.
2. The process of absorption in NFRECs follows the Fickian and non-Fickian models of absorption.
3. Fiber treatment shows a significant role in decreasing water absorption and solvent absorption. As treatment of fiber with any chemical agents reduced fiber's hydrophilic nature, it reduced water absorption.
4. Water uptake content increases with exposure time, but it becomes saturated at one point in time, and when the temperature has seen increasing water absorption rate increases for NFRECs.
5. Fiber content is also the factor that influences water sorption. When fiber content increases, water absorption increases. It can be attributed to the increased number of free OH groups on the lignocellulosic fiber surface that tend to form hydrogen bonds with them as they come into contact with the free water molecules, leading to swelling phenomena.
6. The hybridization of composites shows a better response to water absorption properties than normal composites due to improved interfacial bond among fiber and matrix.

References

F. Ahmad, H.S. Choi, M.K. Park, A review: natural fiber composites selection in view of mechanical, light weight, and economic properties. Macromol. Mater. Eng. **300**, 10–24 (2015). https://doi.org/10.1002/mame.201400089

H. Alamri, I.M. Low, Mechanical properties and water absorption behaviour of recycled cellulose fibre reinforced epoxy composites. Polym. Test. **31**, 620–628 (2012). https://doi.org/10.1016/j.polymertesting.2012.04.002

A. Ali, K. Shaker, Y. Nawab, M. Jabbar, T. Hussain, J. Militky, V. Baheti, Hydrophobic treatment of natural fibers and their composites – a review. J. Ind. Text. **47**, 2153–2183 (2016). https://doi.org/10.1177/1528083716654468

A. Al-Maharma, N. Al-Huniti, Critical review of the parameters affecting the effectiveness of moisture absorption treatments used for natural composites. J. Compos. Sci. **3**, 27 (2019). https://doi.org/10.3390/jcs3010027

S.M.M. Amir, M.T.H. Sultan, M. Jawaid, A.H. Ariffin, S. Mohd, K.A.M. Salleh, M.R. Ishak, A.U. Md Shah, Nondestructive testing method for Kevlar and natural fiber and their hybrid composites, in *Durability and Life Prediction in Biocomposites, Fibre-Reinforced Composites*

and Hybrid Composites, (Woodhead Publishing, 2018), pp. 367–388. https://doi.org/10.1016/B978-0-08-102290-0.00016-7

K. Anbukarasi, S. Kalaiselvam, Study of effect of fibre volume and dimension on mechanical, thermal, and water absorption behaviour of luffa reinforced epoxy composites. Mater. Des. **66**, 321–330 (2015). https://doi.org/10.1016/j.matdes.2014.10.078

Z.N. Azwa, B.F. Yousif, A.C. Manalo, W. Karunasena, A review on the degradability of polymeric composites based on natural fibres. Mater. Des. **47**, 424–442 (2013). https://doi.org/10.1016/j.matdes.2012.11.025

S. Bhaskara, R. Devireddy, S. Biswas, Physical and thermal properties of unidirectional banana – jute hybrid fiber-reinforced epoxy composites. J. Reinf. Plast. Compos. (2016). https://doi.org/10.1177/0731684416642877

V. Boggarapu, R. Gujjala, S. Ojha, A critical review on erosion wear characteristics of polymer matrix composites. Mater. Res. Express. **7** (2020). https://doi.org/10.1088/2053-1591/ab6e7b

M. Boopalan, M. Niranjanaa, M.J. Umapathy, Study on the mechanical properties and thermal properties of jute and banana fiber reinforced epoxy hybrid composites. Compos. Part B Eng. **51**, 54–57 (2013). https://doi.org/10.1016/j.compositesb.2013.02.033

N. Bouhfid, M. Raji, R. Boujmal, H. Essabir, M.O. Bensalah, R. Bouhfid, A.K. Qaiss, Numerical modeling of hybrid composite materials, in *Modelling of Damage Processes in Biocomposites, Fibre-Reinforced Composites and Hybrid Composites*, (Elsevier Science & Technology, 2018). https://doi.org/10.1016/B978-0-08-102289-4.00005-9

G. Das, S. Biswas, Effect of fiber parameters on physical, mechanical and water absorption behaviour of coir fiber-epoxy composites. J. Reinf. Plast. Compos. **35**, 628–637 (2016). https://doi.org/10.1177/0731684415626594

C. Deo, S.K. Acharya, Effect of moisture absorption on mechanical properties of chopped natural fiber reinforced epoxy composite. J. Reinf. Plast. Compos. (2010). https://doi.org/10.1177/0731684409353352

A. Devadas, U. Nirmal, J. Hossen, T. Mcnally, Investigation into mechanical & tribological performance of kenaf fibre particle reinforced composite. Cogent Eng. **5**, 1–23 (2018). https://doi.org/10.1080/23311916.2018.1479210

H.N. Dhakal, Z.Y. Zhang, M.O.W. Richardson, Effect of water absorption on the mechanical properties of hemp fibre reinforced unsaturated polyester composites. Compos. Sci. Technol. **67**, 1674–1683 (2007). https://doi.org/10.1016/j.compscitech.2006.06.019

D.P. Ferreira, J. Cruz, R. Fangueiro, *Surface Modification of Natural Fibers in Polymer Composites* (Elsevier, 2019). https://doi.org/10.1016/B978-0-08-102177-4.00001-X

M.A. Fuqua, S. Huo, C.A. Ulven, Natural fiber reinforced composites. Polym. Rev. **52**, 259 (2016). https://doi.org/10.1080/15583724.2012.705409

J. Gassan, A.K. Bledzki, Effect of cyclic moisture absorption desorption on the mechanical properties of silanized jute-epoxy composites. Polym. Compos. **20**, 604–611 (1999). https://doi.org/10.1002/pc.10383

G. Goud, R.N. Rao, The effect of alkali treatment on dielectric properties of Roystonea regia/epoxy composites. Int. J. Polym. Anal. Charact. **16**, 239–250 (2011). https://doi.org/10.1080/1023666X.2011.570039

R. Gujjala, S. Ojha, S.K. Acharya, S.K. Pal, Mechanical properties of woven jute-glass hybrid-reinforced epoxy composite. J. Compos. Mater. **48**, 3445–3455 (2014). https://doi.org/10.1177/0021998313501924

A. Gupta, Synthesis, chemical resistance, and water absorption of bamboo fiber reinforced epoxy composites. Polym. Compos. (2014). https://doi.org/10.1002/pc.23164

M.K. Gupta, R.K. Srivastava, Properties of sisal fibre reinforced epoxy composite. Indian J. Fibre Text. Res. **41**, 235–241 (2016a)

M.K. Gupta, R.K. Srivastava, Mechanical, thermal and water absorption properties of hybrid sisal/jute fiber reinforced polymer composite. Indian J. Eng. Mater. Sci. **23**, 231–238 (2016b)

M.R.Y. Hamid, M.H. Ab Ghani, S. Ahmad, Effect of antioxidants and fire retardants as mineral fillers on the physical and mechanical properties of high loading hybrid biocomposites

reinforced with rice husks and sawdust. Ind. Crop. Prod. **40**, 96–102 (2012). https://doi.org/10.1016/j.indcrop.2012.02.019

J. Holbery, D. Houston, Natural-fiber-reinforced polymer composites in automotive applications. JOM –WARRENDALE **58**, 80–86 (2006)

U. Huner, Effect of water absorption on the mechanical properties \of flax fiber reinforced epoxy composites. Adv. Sci. Technol. Res. J. **9**, 1–6 (2015). https://doi.org/10.12913/22998624/2357

D.D. Jafrey, G. SaiKrishnan, P. Velmurugan, Investigation on the characteristics of bamboo/jute reinforced hybrid epoxy polymer composites. Mater. Res. Express. (2019). https://doi.org/10.1088/2053-1591/ab3ae7

M.Z.R. Khan, S.K. Srivastava, M.K. Gupta, Tensile and flexural properties of natural fiber reinforced polymer composites: a review. J. Reinf. Plast. Compos. (2018). https://doi.org/10.1177/0731684418799528

P.K. Kushwaha, R. Kumar, Studies on water absorption of bamboo-epoxy composites: effect of silane treatment of mercerized bamboo. J. Appl. Polym. Sci. **115**, 1846–1852 (2010). https://doi.org/10.1002/app

Z. Leman, S.M. Sapuan, M. Azwan, M.M.H.M. Ahmad, M.A. Maleque, The effect of environmental treatments on fiber surface properties and tensile strength of sugar palm fiber-reinforced epoxy composites. Polym. Plast. Technol. Eng. **47**, 606–612 (2008). https://doi.org/10.1080/03602550802059451

X. Li, Æ.L.G. Tabil, Æ.S. Panigrahi, Chemical treatments of natural fiber for use in natural fiber-reinforced composites: a review. J. Polym. Environ. **15**, 25–33 (2007). https://doi.org/10.1007/s10924-006-0042-3

A. Lotfi, H. Li, D.V. Dao, G. Prusty, Natural fiber–reinforced composites: a review on material, manufacturing, and machinability. J. Thermoplast. Compos. Mater. (2019). https://doi.org/10.1177/0892705719844546

A.B. Maslinda, M.S.A. Majid, M.J.M. Ridzuan, M. Afendi, A.G. Gibson, Effect of water absorption on the mechanical properties of hybrid interwoven cellulosic-cellulosic fibre reinforced epoxy composites. Compos. Struct. **167**, 227–237 (2017). https://doi.org/10.1016/j.compstruct.2017.02.023

R. Masoodi, K.M. Pillai, A study on moisture absorption and swelling in bio-based jute-epoxy composites. J. Reinf. Plast. Compos. **31**, 285–294 (2012). https://doi.org/10.1177/0731684411434654

M. Milosevic, P. Valášek, A. Ruggiero, Tribology of natural fibers composite materials: an overview. Lubricants **8**, 42 (2020). https://doi.org/10.3390/lubricants8040042

V. Mittal, S. Sinha, Effect of chemical treatment on the mechanical and water absorption properties of bagasse fiber-reinforced epoxy composites. J. Polym. Eng. **35**, 545–550 (2015). https://doi.org/10.1515/polyeng-2014-0270

V. Mittal, S. Sinha, Study the effect of fiber loading and alkali treatment on the mechanical and water absorption properties of wheat straw fiber-reinforced epoxy composites. Sci. Eng. Compos. Mater. **24**, 731–738 (2017). https://doi.org/10.1515/secm-2015-0441

L. Mohammed, M.N.M. Ansari, G. Pua, M. Jawaid, M.S. Islam, A review on natural fiber reinforced polymer composite and its applications. Int. J. Polym. Sci. **2015** (2015). https://doi.org/10.1155/2015/243947

A. Moudood, A. Rahman, A. Ochsner, M. Islam, G. Francucci, Flax fiber and its composites: an overview of water and moisture absorption impact on their performance. J. Reinf. Plast. Compos. (2018). https://doi.org/10.1177/0731684418818893

E. Muñoz, J.A. García-Manrique, Water absorption behaviour and its effect on the mechanical properties of flax fibre reinforced bioepoxy composites. Int. J. Polym. Sci. **2015**, 16–18 (2015). https://doi.org/10.1155/2015/390275

T.-D. Ngo, Natural fibers for sustainable bio-composites, in *Natural and Artificial Fiber-Reinforced Composites as Renewable Sources*, (IntechOpen, 2018). https://doi.org/10.5772/intechopen.71012

S. Ojha, G. Raghavendra, S.K. Acharya, A comparative investigation of bio waste filler (wood apple-coconut) reinforced. Polym. Compos. (2014). https://doi.org/10.1002/pc.22648
S. Ojha, G. Raghavendra, S.K. Acharya, Utilization of waste carbon as reinforcement in thermoset composites, in *Spherical and Fibrous Filler Composites*, (Wiley-VCH, 2016), pp. 203–229. https://doi.org/10.1002/9783527670222.ch8
C. Outline, Composites. (2015). https://doi.org/10.1016/B978-1-4557-3195-4.00002-3
M. Panchal, G. Raghavendra, M.O. Prakash, S. Ojha, P.S. Chandra Bose, Moisture absorption behavior of treated and untreated eggshell particulate epoxy composites. Silicon **10**, 859–867 (2018). https://doi.org/10.1007/s12633-016-9541-6
P. Peças, H. Carvalho, H. Salman, M. Leite, Natural fibre composites and their applications: a review. J. Compos. Sci. **2**, 66 (2018). https://doi.org/10.3390/jcs2040066
M.O. Prakash, G. Raghavendra, M. Panchal, S. Ojha, B.A. Reddy, Effects of environmental exposure on tribological properties of Arhar particulate/epoxy composites. Polym. Compos. **39**, 3102–3109 (2017). https://doi.org/10.1002/pc.24316
M.O. Prakash, G. Raghavendra, M. Panchal, S. Ojha, P.S. Chandra Bose, Influence of distinct environment on the mechanical characteristics of Arhar fiber polymer composites. Silicon **10**, 825–830 (2018). https://doi.org/10.1007/s12633-016-9536-3
G. Raghavendra, S. Ojha, S.K. Acharya, Jute fiber reinforced epoxy composites and comparison with the glass and neat epoxy composites. J. Compos. Mater. (2013). https://doi.org/10.1177/0021998313499955
G. Raghavendra, K.A. Kumar, M.H. Kumar, S. Ojha, Moisture absorption behavior and its effect on the mechanical properties of jute-reinforced epoxy composite. Polym. Polym. Compos. **16**, 101–113 (2015). https://doi.org/10.1002/pc.23610
G. Rajeshkumar, V. Hariharan, V. Fiore, T. Scalici, Synergistic effect of fiber content and length on mechanical and water absorption behaviors of Phoenix sp. fiber-reinforced epoxy composites. J. Ind. Text. **47**, 211–232 (2016). https://doi.org/10.1177/1528083716639063
B.M. Reddy, Y.V.M. Reddy, B.C.M. Reddy, Effect of alkali treatment on mechanical, water absorption and chemical resistance properties of Cordia-Dichotoma fiber reinforced epoxy composites. Int. J. Appl. Eng. Res. **13**, 3709–3715 (2018)
N. Saba, M. Jawaid, *3. Epoxy Resin Based Hybrid Polymer Composites* (Elsevier, 2017). https://doi.org/10.1016/B978-0-08-100787-7.00003-2
M.S. Saharudin, R. Atif, I. Shyha, F. Inam, The degradation of mechanical properties in polymer nano-composites exposed to liquid media – a review. RSC Adv. **6**, 1076–1089 (2016). https://doi.org/10.1039/c5ra22620a
M.R. Sanjay, P. Madhu, M. Jawaid, P. Senthamaraikannan, S. Senthil, S. Pradeep, *Characterization and Properties of Natural Fiber Polymer Composites: A Comprehensive Review* (Elsevier B.V, 2018). https://doi.org/10.1016/j.jclepro.2017.10.101
S. Sathish, K. Kumaresan, L. Prabhu, N. Vigneshkumar, Experimental investigation on volume fraction of mechanical and physical properties of flax and bamboo fibers reinforced hybrid epoxy composites. Polym. Polym. Compos. **25**, 229–236 (2017). https://doi.org/10.1177/096739111702500309
K.G. Satyanarayana, J.L. Guimara, F. Wypych, Studies on lignocellulosic fibers of Brazil. Part I: Source, production, morphology, properties and applications. Composites Part A **38**, 1694–1709 (2007). https://doi.org/10.1016/j.compositesa.2007.02.006
S.K. Saw, G. Sarkhel, A. Choudhury, Preparation and characterization of chemically modified jute – coir hybrid fiber reinforced epoxy novolac composites. J. Appl. Polym. Sci. (2012). https://doi.org/10.1002/app.36610
N. Sgriccia, M.C. Hawley, M. Misra, Characterization of natural fiber surfaces and natural fiber composites. Composites Part A **39**, 1632–1637 (2008). https://doi.org/10.1016/j.compositesa.2008.07.007
O. Shakuntala, G. Raghavendra, A. Samir Kumar, Effect of filler loading on mechanical and tribological properties of wood apple shell reinforced epoxy composite. Adv. Mater. Sci. Eng. (2014). https://doi.org/10.1155/2014/538651

V.K. Singh, S. Mukhopadhyay, Hybrid biocomposites. Indian J. Fibre Text. Res. **45**, 224–246 (2020)

M. Sood, G. Dwivedi, Effect of fiber treatment on flexural properties of natural fiber reinforced composites: a review. Egypt. J. Pet. **27**, 775–783 (2018). https://doi.org/10.1016/j.ejpe.2017.11.005

S. Suckley, P. Deenuch, N. Disjareon, S. Phongtamrug, Effects of alkali treatment and fiber content on the properties of bagasse fiber-reinforced epoxy composites. Key Eng. Mater. **757**, 40–45 (2017). https://doi.org/10.4028/www.scientific.net/KEM.757.40

H. Sumithra, B. Sidda Reddy, A review on tribological behaviour of natural reinforced composites. J. Reinf. Plast. Compos. **37**, 349–353 (2018). https://doi.org/10.1177/0731684417747742

V.K. Thakur, M.K. Thakur, Processing and characterization of natural cellulose fibers/thermoset polymer composites. Carbohydr. Polym. **109**, 102–117 (2014). https://doi.org/10.1016/j.carbpol.2014.03.039

V.K. Thakur, M.K. Thakur, R.K. Gupta, Review: raw natural fiber – based polymer composites. Int. J. Polym. Anal. Charact. **19**, 256–271 (2014). https://doi.org/10.1080/1023666X.2014.880016

K. Velusamy, P. Navaneethakrishnan, G. Rajeshkumar, The influence of fiber content and length on mechanical and water absorption properties of Calotropis Gigantea fiber reinforced epoxy composites. J. Ind. Text. **48**, 1274–1290 (2018). https://doi.org/10.1177/1528083718763778

N. Venkateshwaran, A. Elayaperumal, Mechanical and water absorption properties of woven jute/banana hybrid composites. Fibers Polym. **13**, 907–914 (2012). https://doi.org/10.1007/s12221-012-0907-0

N. Venkateshwaran, A. Elaya Perumal, A. Alavudeen, M. Thiruchitrambalam, Mechanical and water absorption behaviour of banana/sisal reinforced hybrid composites. Mater. Des. **32**, 4017–4021 (2011). https://doi.org/10.1016/j.matdes.2011.03.002

N. Venkateshwaran, A. Elaya Perumal, D. Arunsundaranayagam, Fiber surface treatment and its effect on mechanical and visco-elastic behaviour of banana/epoxy composite. Mater. Des. **47**, 151–159 (2013). https://doi.org/10.1016/j.matdes.2012.12.001

B. Wang, S. Panigrahi, L. Tabil, W. Crerar, Pre-treatment of flax fibers for use in rotationally molded biocomposites. J. Reinf. Plast. Compos. **26**, 447–463 (2007). https://doi.org/10.1177/0731684406072526

L. Yan, N. Chouw, Effect of water, seawater and alkaline solution ageing on mechanical properties of flax fabric/epoxy composites used for civil engineering applications. Constr. Build. Mater. **99**, 118–127 (2015). https://doi.org/10.1016/j.conbuildmat.2015.09.025

M.H. Zamri, H.M. Akil, A.A. Bakar, Z.A.M. Ishak, L.W. Cheng, Effect of water absorption on pultruded jute/glass fiber-reinforced unsaturated polyester hybrid composites. J. Compos. Mater. **46**, 51–61 (2012). https://doi.org/10.1177/0021998311410488

Damage Sensing in Natural Fiber/Epoxy Composites

28

Vijaya Chalivendra

Contents

Abstract

There has been a greater interest in natural fiber-reinforced composites in the recent past due to their abundance and reduced carbon footprint. Although these composites do not exhibit superior mechanical properties when compared to synthetic counterparts such as glass/carbon and Kevlar® laminated composites, their use can be made attractive by making them multifunctional. In this chapter, an experimental investigation of multifunctional jute/epoxy composites under quasi-static shear, fracture, and flexural loading conditions was presented. These composites were embedded with multiwall carbon nanotubes (CNTs) in the matrix and reinforced with short carbon fibers between the laminates using electro-flocking process. A combination of ultrasonication and shear mixing was used to disperse CNTs in the matrix, and vacuum infusion process was employed to fabricate the natural fiber-laminated composites. Damage sensing in these composites was made through

V. Chalivendra (✉)
Department of Mechanical Engineering, University of Massachusetts, Dartmouth, MA, USA
e-mail: vchalivendra@umassd.edu

S. Mavinkere Rangappa et al. (eds.), *Handbook of Epoxy/Fiber Composites*,
https://doi.org/10.1007/978-981-19-3603-6_48

piezo-resistance measurements that were made using novel four-circumferential measurement system under above loading conditions.

Keywords

Natural fiber composites · Carbon nanotubes · Damage sensing · Interlaminar shear · Fracture, Curved beam

Introduction

Natural fiber composites have gained lot of interest due to their light weight, low cost, renewability, and biodegradability. They have been used in automobile industry with parts such as headliners, seat backs, dashboards, package trays, door panels, dashboards, and interior parts (Holbery and Houston 2006; Pecas et al. 2018). In addition to these, they have been used in structural load bearing applications such as foot bridge in Eindhoven, Netherlands (Smits 2016). Although these composites are being used in real-life applications, plant-based natural fiber composites are hydrophilic because they are made of cellulose. The plant-based natural fibers need chemical treatment to make them hydrophobic so that they can last long for outdoor applications, especially to avoid dimensional instability and microbial attack. To address this issue, researchers came up with chemical treatments of jute fibers (Seki 2009; Sarikanat 2010; Pinto et al. 2014). The jute fibers were first had alkaline (NaOH) treatment to open the jute yarn and remove some part of lignin and hemicellulose. After this treatment, they were subjected to saline treatments to make them hydrophobic. In some cases, saline-treated composites demonstrated improvement in both mechanical and flexural properties (Seki 2009; Sarikanat 2010; Pinto et al. 2014).

There has been extensive literature available on mechanical and fracture studies of various kinds of natural fiber composites. In this chapter, few selective studies of jute/epoxy composites are discussed due to relevance to their damage-sensing studies (Mir et al 2010; Sarikanat 2010) investigated mechanical properties of jute/epoxy composites at different temperature conditions. They employed full-field digital image correlation technique (DIC) to obtain the nonuniform deformation related to change in local volume in the jute fibers when the mechanical loads are applied. When the temperature of composite was raised to 180 °C, they noticed a 50% loss in mechanical strength. Hossain et al. (Hossain et al. 2013) investigated the effect of various fiber stacking sequence on tensile and flexure properties of jute/epoxy composites of 25% volume fraction of jute. For composites with 0/0/0/0 and 0/+45°/−45°/0 stacking sequence, longitudinal tensile strength was higher than that of the transverse direction. However, for 0/90°/90°/0 laminate, tensile strength was almost same for both directions. Prasob and Sasikumar (Prasob and Sasikumar 2018) studied the presence of ZnO and TiO_2 nanoparticles in woven jute/epoxy composites at room and subzero temperatures. They investigated the effect of various weight percentages of these nanoparticles on static

mechanical and impact properties. Overall, their findings showed that the addition of fillers improved the mechanical properties. Regarding fracture studies, Pinto et al. (Pinto et al. 2013) performed quasi-static fracture characterization on jute/epoxy composites when they are reinforced with micro-sized nylon fibers along the thickness direction between the jute laminates. The addition of z-direction reinforcement improved the mode-I fracture toughness by 80% compared to those without nylon fibers between the laminates due to crack bridging. Recently, Balcioğlu (Balcioğlu 2020) reported the fracture behavior of silicon carbide (SiC) microparticle-filled jute-/epoxy-laminated composites. In his study, the effect of the particles having three different sizes of three different volume fractions on fracture toughness is investigated. The fracture toughness of SiC-filled jute-/epoxy-laminated composites demonstrated higher values than that of pure jute/epoxy composites. Moreover, the filler percentage and granule size have varying impact on the fracture toughness values.

Structural health monitoring of composite structures has been of recent interest with advent of use of carbon-based nano materials. There were several studies reported in the literature on use of carbon nanotubes (CNTs) in laminated composites to detect damage via piezo-resistance measurements (Sherman et al. 2019a,b; O'Donnell et al. 2019, 2020a,b). The electrical conductive network of CNTs changes or breaks during the deformation and micro-crack formation in these composites. These network changes are later correlated with various damage mechanisms such as matrix cracking and interlaminar delamination. Recently the author's group conducted experimental studies to investigate the damage sensing in jute-/epoxy-laminated composites by embedding CNTs in matrix and reinforcing submicron-sized carbon fibers between the laminates using electro-flocking technology. This chapter discusses damage sensing using electrical measurements obtained from the changes in three-dimensional conductive network generated from CNTs and carbon fibers under quasi-static shear, fracture, and flexural loading conditions. The outline of this chapter is as follows: (a) materials and fabrication of composites, (b) electrical measurement technique, (c) electrical resistivity of composites under no load conditions, (d) interlaminar shear strength and damage sensing under shear loading conditions, (e) fracture initiation toughness and damage sensing under fracture loading conditions, (f) damage sensing of curved composites under flexure loading, and (g) conclusions.

Three-Dimensional Conductive Natural Fiber Composites

The polymer matrix used in this study is bisphenol-A EpoThin epoxy resin system. This was supplied by Buehler, IL, USA. Jute yarn was used to prepare unidirectional and cross-ply laminates. It was donated by Stuart C. Hurlbert & Co. Inc., MA, USA. PAN-based carbon fibers (CFs) of 150 μm long (Asbury Graphite Mills, Inc., NJ, USA) and 350 μm long (E&L Enterprises, Inc., LA, USA) were used for through-thickness reinforcement between the jute laminates. The carbon content and mass density and of these two CFs are 99% and 1.8 g/cc, respectively. Multiwall carbon

nanotubes (MWCNTs) of different weight percentages were considered in composites different loading conditions. The MWCNTs (supplied by Cheap Tubes Inc., VT, USA) have length of 1–12 μm, diameter of 13–18 nm, and the purity of more than 99%. The silver paint used to paint circumferential probes was purchased from SPI® Supplies, PA, USA.

Since jute is hydrophilic, it was treated using first alkaline treatment and followed by trimethoxysilane solution (APTMS) treatment. During the alkali treatment, 5% aqueous NaOH solution was used, and the jute fibers were drenched in the solution for 120 min. These fibers were later washed with distilled water before they were drenched for 60 min in a 2% aqueous acetic acid solution. To check the neutrality of the treated fibers, the phenolphthalein solution was then used. Finally, the fibers were washed sufficiently with distilled water again and then dried for 24 h in the oven at 80 °C. Upon completion of the alkaline treatment, these treated jute fibers were immersed in a solution of 5% APTMS in methanol for 60 min, and they were then dried at 100 °C. The details of the jute fiber treatment methods are discussed in this published article (Yang et al. 2019a).

First, required amounts of epoxy resin (Buehler Epothin 20–8140-128), hardener (Buehler Epothin 20–8142-064), and multiwall carbon nanotubes (MWCNTs) were taken into a container and then mixed using a hand-stirrer for 5 min. Since CNTs have high surface energy, they tend to agglomerate when they are mixed in polymer matrix. Hence, in our study, the CNTs were dispersed by using a combination of shear mixing and ultrasonication. Shear mixing provides macroscopic mixing, whereas ultrasonication performs nanoscale dispersion of CNTs. Since ultrasonication generates heat in the mix, the whole mix of CNTs with epoxy was placed in an ice bath. The ice bath prevents degradation of epoxy and keeps the mix at room temperature. The settings and the duration of shear mixer and ultrasonicator are provided in the published article (Yang et al. 2019a). Upon shear mixing and ultrasonication, a vacuum chamber was employed to get rid of the entrapped air bubbles which were formed during the above mixing process.

Carbon fibers having two different lengths (150 μm and 350 μm) are reinforced on the jute laminates using University of Massachusetts Dartmouth's electro-flocking technology (Kim et al. 2011). In this technique, the measured amount of carbon fibers was placed on bottom electrode plate evenly. The jute fabric applied with a layer of above CNT-embedded epoxy mix was attached to the top electrode plate. Upon application of high voltage difference (40–60 kV) between these two electrodes, the carbon fibers move upward and embed into the jute layer. The carbon fibers of four different flock densities (500, 1000, 1500, 2000 fibers/mm^2) were reinforced in this study. This process was repeated to produce the required number of flocked jute fabrics. These fabrics were stacked, and then standard vacuum infusion was employed to infuse CNT-embedded epoxy mix into the stack of laminates. Composites of two different stacking sequence (0-0-0-0) and (0-90-0-90) were considered in this study. The details of the vacuum infusion were well discussed in this Reference (Pinto et al. 2014). The laminated composites were cured for 24 hours at a constant compressive load of 4 tons to press out additional resin in the composite. The compressive loading is employed to enhance the volume fraction of jute fibers in the composite. Test

specimens of required configurations were cut from these sheets, and minimum eight specimens were tested for each composite type.

Electrical Measurement System

Novel four-circumferential probe measurement system was employed to measure the electrical response of the composite under various loading conditions. Figure 1 shows the electrical probe measurement system with specimen having four-circumferential probes. A DC current source (Keithley Instruments, Model 66220) was employed to supply constant current through the outer probes, which is essential during the entire duration of the experiment. A pair of electrometers (Keithley Instruments, Model 6514) was used to record the voltage from the inner probes. Finally, a digital multimeter (Keithley Instruments, Model 2000 DMM) was then utilized to record the voltage difference between two electrometers. The electrometers have very high impedance, and they avert the seepage of current into the multimeter. The measured voltage from the multimeter was later used to determine the electrical resistance of the inner section of the specimen using the Ohm's law. LabVIEW data acquisition was employed to capture the voltage measurements.

A double-notch test specimen (shown in Fig. 2) using ASTM D3846 standard was used for damage sensing under shear loading conditions. These two notches were made to half of the sample's thickness, which are 3.2 mm away from the center of the test specimen. Under far-field tensile loading, an in-plane shear deformation is created between these two notches causing interlaminar shear failure between the laminates. Four-circumferential ring probes (FCRP) are put on the surface of the specimen using highly conductive silver paint. The constant current was sent via outer probes, and change in voltage due to damage was measured from the inner probes. The details of the instrumentation and data acquisition are similar to Fig. 1.

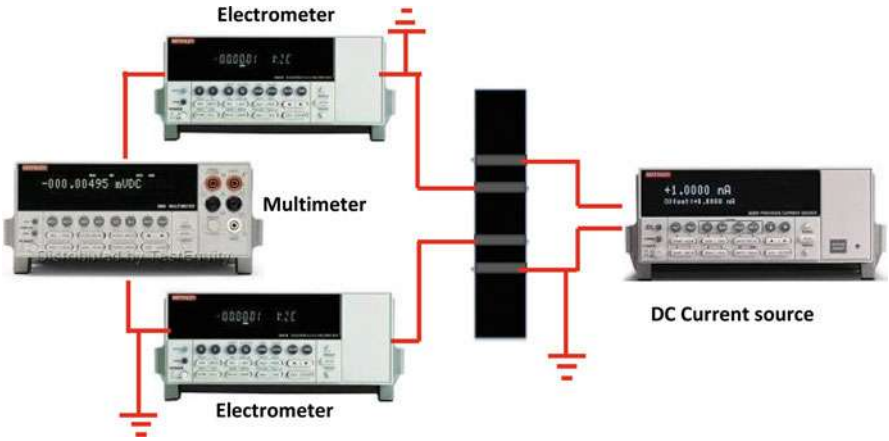

Fig. 1 Electrical measurement system using four-circumferential probes measurement system

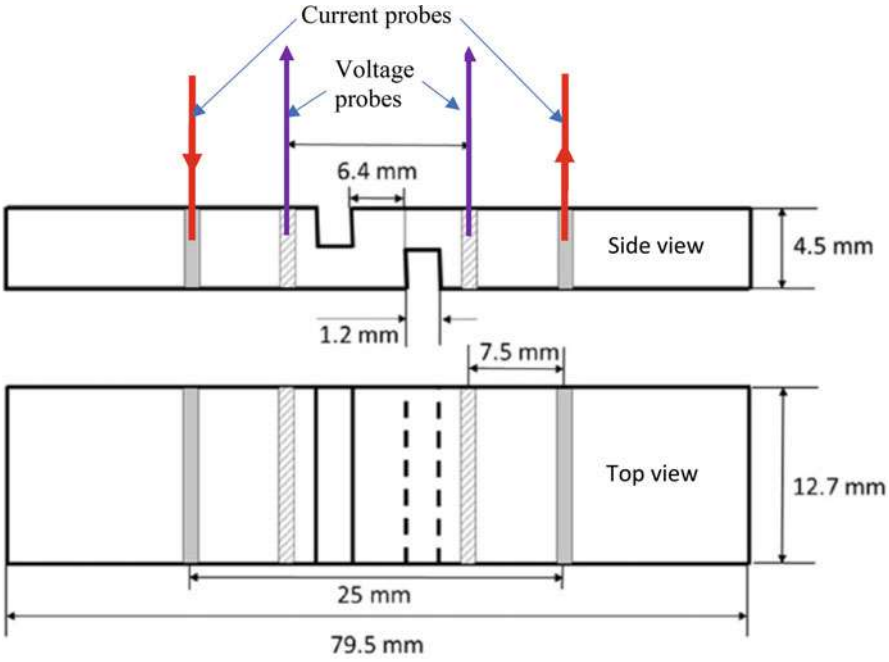

Fig. 2 Electrical and shear characterization of composites with double-notch specimen

The crosshead displacement and load values were used to determine the shear strain and shear stress (Yang et al. 2018). The shear stress-strain values were later correlated with the electrical resistance change.

A double-cantilever beam (DCB) specimen configuration (shown in Fig. 3(a)) based on ASTM D5528 is considered for damage monitoring under mode-I fracture loading conditions. To determine the change in electrical resistance, a modified and novel four-probe system as shown in Fig. 3(b) was used, where the constant current was supplied through-thickness from top to bottom of the specimen (Yang et al. 2019b). Voltage probes were positioned circumferentially around the laminates both above and below the crack line. Once again, the measurement system shown in Fig. 1 was used to capture the electrical resistance change during the crack initiation and for entire crack propagation.

A 90° curved beam test specimen as shown in Fig. 4 is employed for understanding damage sensing in curved composites under flexural loading. To generate an initial crack, a nonadhesive thin Teflon film of 15 mm width was placed on the midplane of the composite while fabrication (Yang et al. 2020). Using ASTM-D6415 standard, the test specimens were cut to the desired dimensions. The specimen dimensions include a width of 25 mm, a fillet radius of 6.25 mm, and leg length of 100 mm. The constant current probes and voltage probes are their positions for measuring changing electric response shown in Fig. 4.

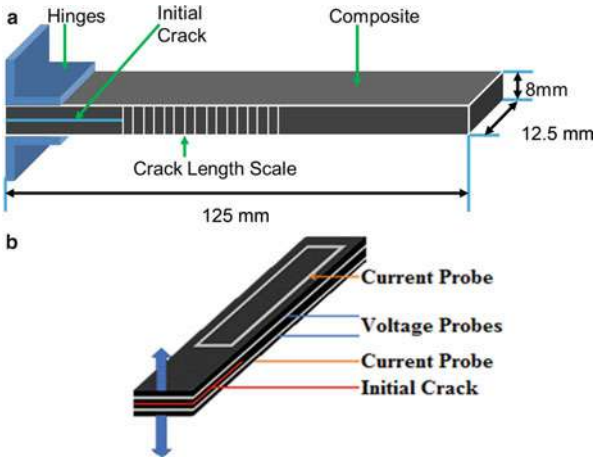

Fig. 3 Double-cantilever beam specimen configuration for electrical and fracture characterization of composites

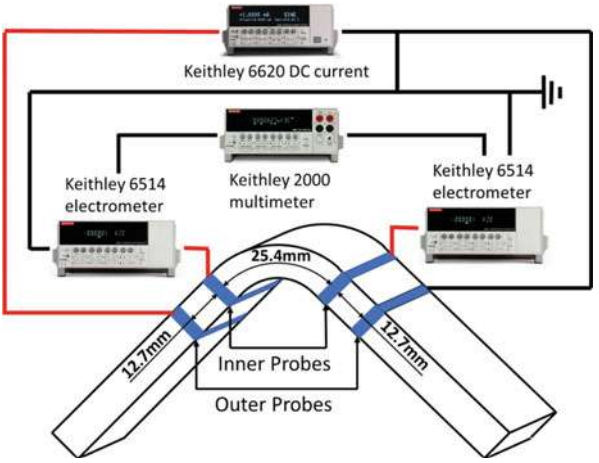

Fig. 4 Curved beam specimen configuration for electrical and flexure characterization of composites (Yang et al. 2020). (Reproduced by permission from Elsevier)

Electrical Resistivity Measurements Under No Load Conditions

The electrical resistivity values under no load conditions for all composite types of two different amounts of CNTs (0.1 and 0.25 wt.%), two different carbon fiber lengths (150 μm and 350 μm), four different carbon fiber densities (500, 1000. 1500, 2000 fibers/mm^2), and two different jute laminates (0-0-0-0 and 0-90-0-90) are shown in Fig. 5. Overall, there is slight increase in resistivity in the composites when amount of CNTs decreased from 0.1%wt. to 0.025%wt. However, for the composite with (0-0-0-0) jute orientation, 350 μm carbon fiber length, and 500 fiber/mm^2 fiber density,

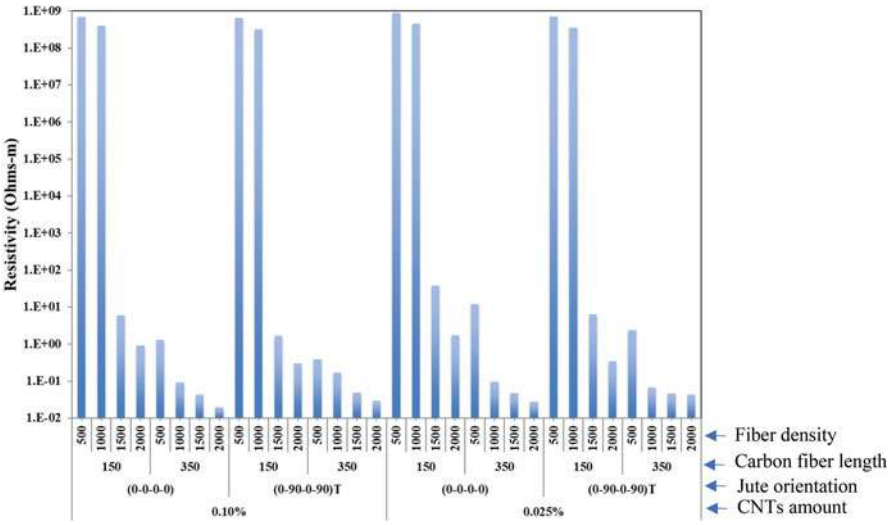

Fig. 5 Electrical resistivity of jute/epoxy composites of various configurations (Yang et al. 2019a). (Reproduced by permission from John & Wiley & Sons, Inc.)

the increase in resistivity is about 850%. It is quite evident that the carbon fiber length has major effect on electrical resistivity values. The composites made with carbon fiber length of 350 μm showed great decrease in resistivity values when compared to those of 150 μm. The carbon fiber length of 350 μm can penetrate into the jute laminates and also make better connections with the CNTs in the jute yarns (which were filled with CNT-embedded epoxy due their opened structure during the treatment process). For composites made with 0.025% CNTs, (0-90-0-90) jute orientation and carbon fiber density of 1000 fiber/mm^2, the resistivity of 150 μm carbon fiber length is almost 10^9 times to that of 350 μm.

In addition to carbon fiber length, the carbon fiber density played a major impact on the resistivity. The impact is more pronounced for composites made of carbon fiber length of 150 μm. For example, for a composite of jute fiber orientation of (0-0-0-0) and CNTs amount of 0.1%wt., the resistivity decreased exponentially from 5×10^8 ohms-m to 5 ohms-m when the fiber density increased from 1000 to 1500 fibers/mm^2. For composites of 350 μm carbon length, the decrease in resistivity is not as drastic as that of 150 μm. For example, the decrease is only of the order of two for composites made with jute orientation of (0-0-0-0), 0.025 %wt. of CNTs when the fiber density increased from 500 to 1000 fibers/mm^2.

The effect of jute orientation has marginal effect on the change in resistivity values. There is no change in resistivity values for the composites of lower carbon fiber densities of 500 and 1000 fibers/mm^2. However, the resistivity change can be noticed for composites of higher carbon fiber densities (1500 and 2000 fibers/mm^2).

For a composite type of 150 μm carbon fiber length, 1500 fiber/mm^2 fiber density, and 0.025%wt. CNTs, the resistivity value decreased by about 500% for jute orientation of (0-90-0-90) compared to that of (0-0-0-0) orientation. At the

intersection of (0-90-0-90) jute yarns, the carbon fibers have more spacing to penetrate compared to (0-0-0-0). The penetrated carbon fibers make more electrical connections with CNTs that lies between the laminates and also with carbon fibers of neighboring laminates.

Mechanical Response and Damage Sensing in Composites Under Shear Loading Conditions

Table 1 provides the interlaminar shear strength of composites of different amounts of CNTs wt.%, two different carbon fiber lengths, four different carbon fiber densities, and two jute orientations. It is evident from the top of the table that composites of no carbon fibers and orientation of jute play a significant role on the interlaminar shear strength. The shear strength of unidirectional orientation is five times to that of cross-ply orientation. During the process of fabrication of these composites, combination of vacuum infusion and compression molding allowed the jute yarns to interpenetrate for unidirectional composites. This exits the extra amount of epoxy that exists between the laminates and induces strong bond between the laminates.

Addition of carbon fibers along through-thickness direction improved the shear strength considerably. In the case of unidirectional composite of carbon fiber length of 350 μm, fiber density of 1000 fibers/mm^2, and 0.025% of CNTs, the highest value of shear strength is observed, and this value is about 50% more than that of composite with no carbon fibers. Other factors such as CNTs wt.%, carbon fiber density, and carbon fiber lengths did not make significant impact on the shear strength. An increasing trend of shear strength from zero fiber density to 1000 fibers/mm^2 is noticed; however, with additional amount of carbon fiber density to 2000 fibers/mm^2, shear strength decreased marginally for all composite types.

To investigate the effect of amount of CNTs weight percentage on the damage sensing, a comparison of electrical response along with shear stress-strain response for two different CNTs wt.%, namely, 0.025 and 0.1, is shown in Fig. 6. For this comparison, cross-ply (0-90-0-90) composites of carbon fiber length of 350 μm and fiber density of 1000 fibers/mm^2 are considered. The electrical-shear response is divided into three zones. There is no change in electrical resistance in the zone-I because the carbon nanotubes make new connections under shear loading conditions before seeing noticeable damage occurs in the composite (Yang et al. 2018). In addition, the duration of zone-I is small in composites with lower weight percentage of 0.025. It is because with less amount CNTs, lesser new connections can be made. During zone-II, there is a steady increase in resistance for both composite cases. Since the bonding between carbon fibers and epoxy is poor, there exists delamination between them causing the disconnection of electrical network. At later stage, the debonding induces micro-cracking with increase in shear deformation, which will increase the resistance of the composite. The amount of resistance increase is almost three times higher in composites of 0.025% CNTs compared to that of 0.1%. With

Table 1 Interlaminar shear strength (C, cross-ply; U, unidirectional; NCF, no carbon fibers)

Carbon fiber density	Carbon fiber length	Jute orientation	CNTs wt. %	Shear strength (MPa)
		C	NCF	5.6
		U	NCF	27.8
500	150	C	0.025	8.2
			0.1	6.8
		U	0.025	33.9
			0.1	30.5
	350	C	0.025	11.5
			0.1	10.0
		U	0.025	37.6
			0.1	35.0
1000	150	C	0.025	10.1
			0.1	9.5
		U	0.025	36.5
			0.1	34.1
	350	C	0.025	13.8
			0.1	11.9
		U	0.025	41.7
			0.1	39.8
1500	150	C	0.025	8.2
			0.1	7.7
		U	0.025	34.9
			0.1	32.1
	350	C	0.025	12.4
			0.1	10.9
		U	0.025	39.3
			0.1	37.6
2000	150	C	0.025	8.2
			0.1	7.7
		U	0.025	34.5
			0.1	31.9
	350	C	0.025	11.3
			0.1	10.1
		U	0.025	39.9
			0.1	37.7

less CNTs concentration, it is expected to have much higher disruption in electrical network for the same amount of shear deformation at the end of zone-II.

In zone-III, the composites of 0.025% CNTs did not show significant increase in resistance as that of 0.1%. The amount of increase of resistance in 0.025% CNTs is only by 65%, whereas it is about 500%. This is because the electrical network is predominantly broken in zone-II in the composite of 0.025% compared to 0.1%. In the composite of 0.1% CNTs, the initial conductive network is very rich; there is a

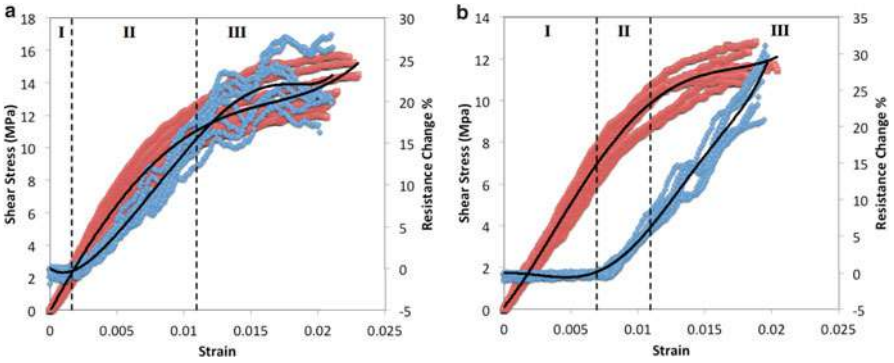

Fig. 6 Electrical and shear stress-strain response of composites with CNTs wt.% of (**a**) 0.025 and (**b**) 0.1 (Yang et al. 2018). (Reproduced by permission from IOP Publishing)

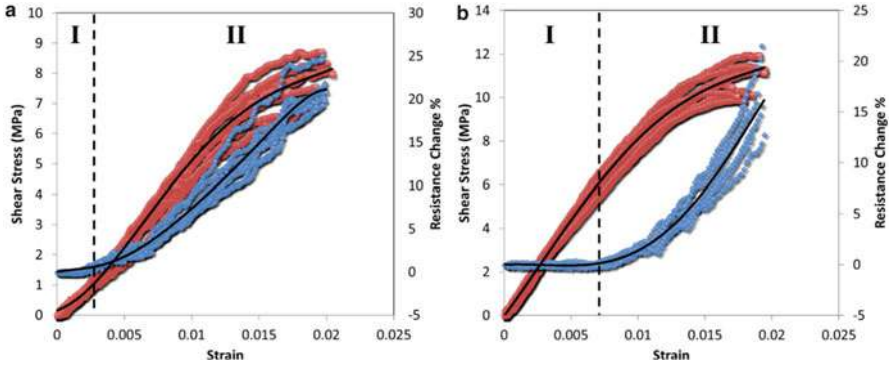

Fig. 7 Electrical and shear response of composites with carbon fiber length of (**a**) 150 μm and (**b**) 350 μm (Yang et al. 2018). (Reproduced by permission from IOP Publishing)

great scope to break the network with further increase in shear deformation in zone-III. This provides a design option for engineers to choose a composite system that can provide different sensitivities of electrical response at different stages of shear deformation.

Figure 7 shows the electrical and shear stress-strain response as a function of carbon fiber length for a cross-ply composite having 0.1% of CNTs and carbon fiber density of 1500 fibers/mm^2. The electrical response is divided into two zones, where the zone-I is attributed to no change in electrical resistance as discussed above. The length of zone-I is longer for composites made of carbon fiber length of 350 μm because these composites have superior conductive network where the carbon fibers can penetrate into neighboring jute laminates. Moreover, the cross-ply layup also provides better open spacing for the penetration of longer carbon fibers. Zone-II is almost similar for both composite types at constant carbon fiber density; however, the peak resistance change at break is slightly higher for composites shorter carbon fiber length compared to those of longer carbon fiber lengths.

Fracture Initiation Toughness

Fracture toughness values of unidirectional composites of two different carbon fibers and four different fiber densities are shown in Table 2. Composites having carbon fibers showed improvement in fracture toughness compared to that no carbon fibers. Composite of carbon fiber length of 350 μm and fiber density of 2000 fibers/mm^2 demonstrated the highest fracture toughness value compared to that of no carbon fibers. This value is about 75% higher than that of composite with no carbon fibers. For composite of similar carbon fiber length (e.g.,350 μm), fiber density shows significant improvement on the fracture toughness when it is increased from 500 to 1000 fibers/mm^2. Carbon fibers bridge the crack initiation and require more energy to pull out and break them. On the other hand, with further increase in fiber density from 1000 to 2000 fibers/mm^2, a marginal increase in fracture toughness is noticed.

Electrical Response and Damage Sensing in Composites Under Fracture Loading Conditions

Through-thickness electrical response of jute/epoxy composites of carbon fiber density of 1000 fibers/mm^2 of two different carbon fiber lengths of 150 μm and 350 μm under fracture loading conditions is shown in Fig. 8. The electrical response is divided into three zones based on crack dynamics. For both carbon fiber lengths, the zone-I is defined until the initiation of the pre-crack in the DCB specimen configuration shown in Fig. 3. The percentage change in electrical resistance associated with micro-crack formation and damage initiation at the fracture process zone is only 7.5% in the composite of carbon fiber length of 150 μm; however, it is only 2.5% in the case of composite with carbon fiber length of 350 μm. The composite with carbon fiber length of 350 μm has rich conductive network due to penetration of long carbon fibers into the jute laminates as discussed in the section "Electrical Resistivity Measurements Under No Load Conditions." Although the damage zone might be similar in both composite types, with rich conductive network, the percentage change in resistance is lower for composites with carbon fiber length of 350 μm. Both zone-II and zone-III are associated with crack propagation between

Table 2 Fracture initiation toughness (NCF: no carbon fibers)

Carbon Fiber length	Carbon Fiber density	G_{IC} (kJ/m^2)
NCF		1.61
150	500	2.07
	1000	2.12
	1500	2.59
	2000	2.69
350	500	2.19
	1000	2.62
	1500	2.63
	2000	2.81

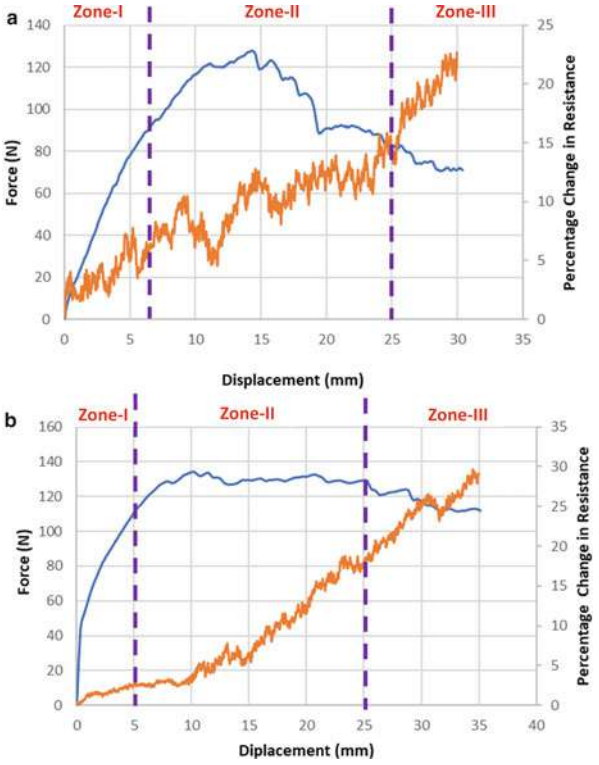

Fig. 8 Electrical and fracture response of composites having carbon fibers of 1000 fibers/mm^2 and fiber length of (**a**) 150 μm and (**b**) 350 μm

the jute laminates in the composite. For a crack opening displacement of 25 mm, the load values are steady for composite of 350 μm carbon fiber length compared to its counterpart. This is due to fact that long fibers effectively bridge the crack growth compared to shorter fibers. The percentage change in resistance of composites of carbon fiber length of 350 μm is about 17.5% compared to 15% of composite with carbon fiber length of 150 μm. In contrary to zone-I, the propagating crack breaks conductive network more in composites of longer carbon fibers with damage mechanisms such as fiber debonding and pullouts. These mechanisms disconnect the conductive network of longer fibers with CNTs and carbon fibers of neighboring laminates. These phenomena continue in zone-III in both composite types; however, the composites of longer carbon fiber lengths showed higher overall percentage resistance change of 28% compared to 22% of that of shorter fibers.

Figure 9 shows the electrical response of composites of carbon fiber density of 2000 fibers/mm^2 for two different carbon fiber lengths of 150 μm and 350 μm. Once again, the electrical response associated with damage evolution under fracture loading is divided into three different zones. The end of the zone-I represents the crack initiation point for both composite types. The composites having carbon fiber length of 150 μm demonstrated higher percentage change in resistance of 30% compared to only 10% change in resistance for that of 350 μm. This is again due

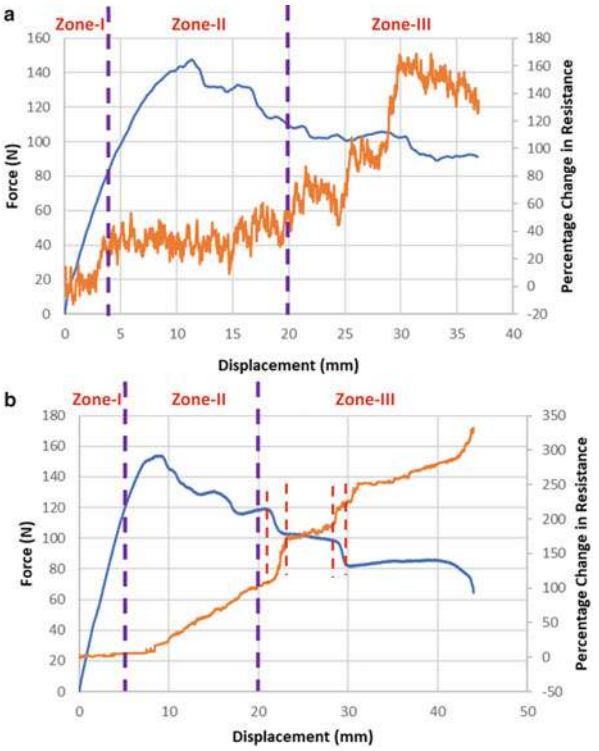

Fig. 9 Electrical and fracture response of composites having carbon fibers of 2000 fibers/mm^2 and fiber length of (**a**) 150 μm and (**b**) 350 μm

to the presence of strong electrically conductive network present in the composites of longer fibers. The damage in fracture process zone is significantly more in composites of shorted carbon fiber length because they cannot penetrate through the laminates. Composites of longer fibers can bridge the crack front and can still maintain good conductive network.

In zone-II, at fiber density of 2000 fibers/mm^2, the composites having longer fibers demonstrate about 90% increase in resistance, whereas the composites with shorter carbon fiber length showed only 10% increase in resistance. Although in both composite types, the propagating crack breaks the conductive network, the presence of damage is much higher in composites of longer fibers due to fiber pullouts and breaking. For zone-III, the composites of 350 μm longer carbon fibers demonstrate stick-slip mechanism during the crack propagation due to fiber bridging. This phenomenon can be noticed, where for each drop in load, there is corresponding increase in resistance as shown with dotted lines in Fig. 9(b). During these two intervals, the crack is arrested for a while with almost no change in resistance. This is not the case for composites of short carbon fiber length, where the changes in electrical resistance are sporadic and do not show stick-slip mechanism due to lack of penetration of fibers into neighboring laminates.

Electrical Response and Damage Monitoring of Curved Beams Under Flexure Loading Conditions

The electrical and flexure response of composites of carbon fiber density of 1500 fibers/mm^2 with two different carbon fiber lengths of (a) 150 μm and (b) 350 μm is shown in Fig. 10. The electrical response is divided into two zones. As discussed in the section "Electrical Measurement System," this specimen configuration has an initial crack. The zone-I is associated with the crack initiation for both composite types. Before the crack initiation, no delamination or visible structural damage was observed. During this zone, the percentage change in resistance increases steadily. This increase is due to the damage around the fracture process zones of both the crack-tips and the separation of CNTs in the tension zone of bent specimen. Since this is a curved beam, the maximum tensile stress below the neutral surface is slightly higher than the compressive stress. The net effect of this tensile stress

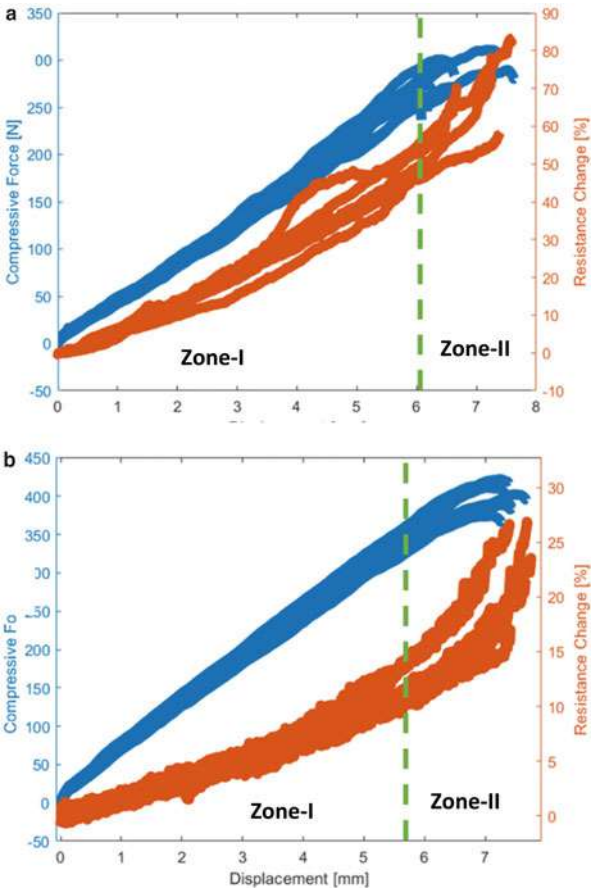

Fig. 10 Electrical and flexure response of composites having carbon fibers of 1500 fibers/mm^2 and fiber length of (**a**) 150 μm and (**b**) 350 μm (Yang et al. 2020)

increases the distance between CNTs, between the carbon fibers, and also between the CNTs and carbon fibers. In addition, the tensile stress also breaks the interface between carbon fibers and epoxy. The separated carbon fibers cause the increase in resistance by disconnecting with neighboring CNTs and carbon fibers. The percentage change in resistance at the instant of crack initiation for composite of carbon fiber length of 150 μm is five times higher than that of carbon fiber length of 350 μm. For the same fiber density of 1500 fibers/mm^2, longer fibers generate a superior conductive network with both neighboring CNTs and with carbon fibers than the shorter fibers. Although the extent of damage might be similar in these composite types, the weaker conductive networks in composites of shorter carbon fiber length undergo higher resistance change as demonstrated in the figure. In zone-II, at higher fiber density of 1500 fibers/mm^2, the carbon fibers were effective in bridging the crack growth. Hence the additional cracks were formed in the tensile zone underneath the neutral surface. The final or peak percentage resistance change of composite of 150 μm was about three times to that of 350 μm. This is again due to better initial network of composite of longer fibers, where presence of propagating cracks did not change network as much as that of shorter carbon fibers.

Conclusions

This chapter summarizes the recent studies on fabrication and experimental investigation on damage sensing of three-dimensional conductive jute-/epoxy-laminated composites under various loading conditions. These composites are multifunctional, where the through-thickness reinforcement of carbon fibers can help to detect the damage along with CNTs through piezo-resistivity but also improve both interlaminar shear strength and fracture toughness of the composites by bridging the crack growth. The experimental results provide valid information for industrial users to choose the right amounts of CNTs and carbon fibers in the composites. The results also serve as necessary validation data for developing and investigating damage sensing using numerical and analytical models, which are very few in the current literature. Most importantly, by enhancing multifunctionality of the natural fiber composites, they become quite attractive in automobile, aerospace, and construction industries.

Acknowledgments The authors acknowledge the financial support of the National Science Foundation (NSF) under grant number CMMI-1563040.

References

H.E. Balcioğlu, Fracture behaviors of SiC particle filled and jute fiber reinforced natural composites. J. Nat. Fibers (2020). https://doi.org/10.1080/15440478.2020.1811186

J. Holbery, D. Houston, Natural-fiber-reinforced polymer composites in automotive applications. JOM **58**, 80–86 (2006). https://doi.org/10.1007/s11837-006-0234-2

M.R. Hossain, M.A. Islam, A.V. Vuurea, I. Verpoest, Tensile behavior of environment friendly jute epoxy laminated composite. Procedia Eng **56**, 782–788 (2013). https://doi.org/10.1016/j.proeng.2013.03.196

Y.K. Kim, A.F. Lewis, J.M. Rice US Patent 7981495 (2011)

A. Mir, R. Zitoune, F. Collombet, Study of mechanical and thermomechanical properties of jute/epoxy composite laminate. J. Reinf. Plast. Compos. **29**(11), 1669–1680 (2010). https://doi.org/10.1177/0731684409341672

J. O'Donnell, V. Chalivendra, A. Hall, M. Haile, L. Nataraj, M. Coatney, Y. Kim, Electro-mechanical studies of multi-functional glass fiber/epoxy reinforced composites. J. Reinf. Plast. Compos. **38**(11), 506–520 (2019). https://doi.org/10.1177/0731684419832796

J. O'Donnell, V. Chalivendra, A. Hall, Y. Kim, Damage monitoring in multi-functional glass fiber composites under mode-I fracture loading. J. Compos. Mater. (2020a). https://doi.org/10.1177/0021998320939637

J. O'Donnell, V. Chalivendra, A. Hall, Y. Kim, Damage monitoring in multi-functional glass fiber composites under mode-I fracture loading. J. Compos. Mater. (2020b). https://doi.org/10.1177/0021998320939637

P. Pecas, H. Carvalho, H. Salman, M. Leite, Natural fibre composites and their applications: A review. J. Compos. Sci. **2**, 66 (2018). https://doi.org/10.3390/jcs2040066

M. Pinto, V.B. Chalivendra, Y.K. Kim, A.M. Lewis, Effect of surface treatment and Z-axis reinforcement on the Interlaminar fracture of jute/epoxy laminated composites. Eng. Fract. Mech. **114**, 104–114 (2013). https://doi.org/10.1016/j.engfracmech.2013.10.015

M. Pinto, V.B. Chalivendra, Y.K. Kim, A.M. Lewis, Evaluation of surface treatment and fabrication methods for jute fiber/epoxy laminar composites. Polym. Compos. **35**(2), 310–317 (2014). https://doi.org/10.1002/pc.22663

P.A. Prasob, M. Sasikumar, Static and dynamic behavior of jute/epoxy composites with ZnO and TiO2 fillers at different temperature conditions. Polym. Test. **69**, 52–62 (2018). https://doi.org/10.1016/j.polymertesting.2018.04.040

M. Sarikanat, The influence of oligomeric siloxane concentration on the mechanical behaviors of alkalized jute/modified epoxy composites. J. Reinf. Plast. Compos. **29**(6), 807–817 (2010). https://doi.org/10.1177/0731684408100700

Y. Seki, Innovative multifunctional siloxane treatment of jute fiber surface and its effect on the mechanical properties of jute/thermoset composites. Mater. Sci. Eng. A **508**, 247–252 (2009). https://doi.org/10.1016/j.msea.2009.01.043

R. Sherman, V. Chalivendra, A. Hall, M. Haile, L. Nataraj, M. Coatney, Y. Kim, Electro-mechanical characterization of three-dimensionally conductive graphite/epoxy composites under tensile and shear loading. Compos. Commun. **15**, 30–33 (2019a). https://doi.org/10.1016/j.coco.2019.05.010

R. Sherman, V. Chalivendra, A. Hall, M. Haile, L. Nataraj, M. Coatney, Y. Kim, Characterization of electro-mechanical response in novel carbon fiber composite materials. J. Compos. Mater. **53**(19), 2675–2686 (2019b). https://doi.org/10.1177/0021998319839113

J. Smits, Fiber-reinforced polymer bridge design in the Netherlands: Architectural challenges toward innovative, sustainable, and durable bridges. Engineering **2**, 518–527 (2016). https://doi.org/10.1016/J.ENG.2016.04.004

S. Yang, V.B. Chalivendra, Y. Kim, Damage sensing in multi-functional hybrid natural fiber composites under shear loading. Smart Mater. Struct. **27**, 115034 (2018). https://doi.org/10.1088/1361-665X/aae7f2

S. Yang, V.B. Chalivendra, E. Benjamin, Y. Kim, Electrical response of novel carbon nanotubes embedded and carbon fiber Z-axis reinforced jute/epoxy laminated composites. Polym. Compos. **50**, E1189–E1198 (2019a). https://doi.org/10.1002/pc.24935

S. Yang, V.B. Chalivendra, Y. Kim, Electro-fracture studies of natural fiber composites. J. Nat. Fibers (2019b). https://doi.org/10.1080/15440478.2019.1685425

S. Yang, C. Meninno, V.B. Chalivendra, Y. Kim, Electro-bending behavior of curved natural fiber laminated composites. Compos. Struct. **238**, 112004 (2020). https://doi.org/10.1016/j.compstruct.2020.112004

Modeling and Simulation of Epoxy/Natural Fiber Composites

29

Chunhong Wang, Chao Lu, Lijian Wang, Qi Zuo, Anik Das, Kushairi Mohd Salleh, and Sarani Zakaria

Contents

Abstract

The research on epoxy/natural fiber composites and their modeling and simulation methods developed in recent years is summarized. Natural fiber reinforced composites (NFRC), also known as a biological composite material due to their proportion, are abundant with natural ingredients, coupled with the most essential environmental factors, such as biodegradability, renewability, and recyclability. Epoxy/natural fiber composites are known for their low cost, light weight, and relatively high specific strength and renowned for its durability. Therefore, epoxy/

C. Wang · C. Lu · L. Wang · Q. Zuo · A. Das
School of Textile Science and Engineering, Tiangong University, Tianjin, China

Key Laboratory of Advanced Textile Composite Materials, Tiangong University, Tianjin, China

K. M. Salleh (✉) · S. Zakaria (✉)
Bioresources and Biorefinery Laboratory, Department of Applied Physics, Faculty of Science and Technology, Universiti Kebangsaan Malaysia, UKM, Bangi, Selangor, Malaysia
e-mail: kushairisalleh@ukm.edu.my; szakaria@ukm.edu.my

S. Mavinkere Rangappa et al. (eds.), *Handbook of Epoxy/Fiber Composites*,
https://doi.org/10.1007/978-981-19-3603-6_30

natural fiber composites provide a sustainable and resilient alternative to the existing synthetic fiber composites. Researchers are studying the properties of NFRC materials in depth to consider their reliability to be used in, but not limited to, aircraft, automobiles, ships, sports equipment, and composite materials for other engineering fields. The modeling and simulation of epoxy/natural fiber composites are an effective means to improve the design and overall performance of the products. The progress of modeling and simulation of epoxy/natural fiber composites on mechanical properties, moisture absorption, and thermal conductivity in recent years is comprehensively summarized from various aspects/types of analysis, types of natural fiber composites, types of the model employed, simulation platforms, and parameters and research results. The main application theories and methods in this field are extensively outlined to feed the readers with the research findings in this field and provide some guidance and idea for related research. The modeling and simulation technique of epoxy/natural fiber composites is an effective way to optimize the structure design and overall performance of the products.

Keywords

Epoxy · Natural fiber composites · Modeling · Simulation

Introduction

Climate warming has become an indisputable fact, and its impact on the precious but limited resources of our planet is equally indisputable. In recent years, catchwords like carbon footprint and "greenhouse gases" are of main concern worldwide due to environmental problems that increased seriously. The amount of carbon set free into the air formed on fuel utilization contributes a lot to the carbon footprint. Carbon footprints are principally classified into two sections, that is, primary and secondary footprints. The primary footprint relates to the carbon release directly through fuel burning to generate energy accumulation for electricity, heating, transportation, etc. The carbon emission caused by the life cycle of products and sustainability makes up the secondary footprints (Herd 2011). Therefore, the reduced amount of energy required for production and less count on the carbon-emitting fuels can reduce carbon footprint.

The report entitled *China's Emergence as a Market Economy: Achievements and Challenges* pointed out that China, the USA, and India are the three major countries contributing to polluting the atmosphere (Herd 2011). It was reported that an astonishing 50,000 MJ (approximately 3 ton CO_2 emissions) net replacing 30% glass fiber reinforcement with 65% hemp fiber in the life cycle of the composite materials could save thermoplastic in 1 ton (Pervaiz and Sain 2003). More encouragingly, plant fibers absorb more CO_2 during the growing phase than they release during product processing since they are carbon-positive materials.

For a long time in the past, synthetic fiber reinforced composites like glass fiber and carbon fiber reinforced composites had been applied on automotive, rail transit,

aerospace, and defense applications on a large scale. This is mainly used due to the relatively high mechanical properties, including tensile/flexural strength and stiffness, good fatigue properties, and durability. Nevertheless, the indelible environmental impact of using synthetic-based composites cannot be ignored and has a growing concern in recent years. Synthetic fiber is highly dependent on petroleum resources, which will cause pollution to the environment in the production process; this kind of composite material is not easy to degrade after being discarded, which brings great harm to the ecological environment. At the same time, glass fiber is also harmful to the human skin and the respiratory tract. Gradually realizing the greening of composite materials, that is, gradually replacing synthetic fiber reinforced composites with natural fiber reinforced composites, is the most excellent solution to environmental and resource problems caused by the large-scale use of synthetic fibers.

As a consequence, with the improvement of people's understanding and acceptance of environmental protection materials, it is necessary to use natural fibers as alternative reinforcement materials of composites. There are abundant natural fiber resources on the earth, and they are biodegradable and recyclable. Making full use of natural plant fibers, exerting their unique functional characteristics, and developing new application fields are the development and utilization of plant fibers and plant wastes and a major hotspot and breakthrough point in material research today. The use of renewable biomass resources to develop environmentally friendly green composite materials has become one of the hotspots of attention and research in countries worldwide. Natural fiber composite materials have several advantages: low price, low density, specific strength, excellent corrosion resistance, degradability, recyclability, and renewable. Good biodegradability and renewable are its most prominent characteristics, which are incomparable with other inorganic fiber materials. Compared with the four traditional materials (steel, cement, plastic, and wood), plant fiber has a more comprehensive range of rich sources and types, providing a broader development platform for plant fiber composites and plays a significant role in the construction industry and other fields. Natural fiber, as an alternative material, with commensurate mechanical and physical properties as traditional synthetic fiber, is attracting more and more attention and investigation in the field of engineering material. Therefore, with the deepening of the concept of sustainable development of raw materials, as a leading environment-friendly material, plant fiber composites will be the key field of international high-tech new materials research in the new era and play an increasingly vital role in the field of new composite materials.

Nowadays, bio-composite materials made from natural fibers and resin are being consumed on a large scale both in the commercial and domestic sectors due to their low density. Compared with the conventional materials, the innate specific tensile strength and stiffness make the natural fiber reinforced composites (NFRC) exploited for various applications, such as automotive interior, architectural decoration, and packaging industries. It is reported that natural fiber reinforced composites took over an extensive account of over 11% of the global fiber reinforced composites market in 2019 and are substantially rising in recent years (JEC 2020).

Epoxy resin has outstanding physical, mechanical, and electrical insulation properties, excellent adhesion with various materials, and flexible application, which are much better than other thermosetting plastics. Therefore, it can be used in coatings, composite materials, casting materials, adhesives, molding materials, injection molding materials, and extensive applications. Epoxy resins and their fiber reinforced composite products are polymer composites preferred in many applications such as automotive, rail transit, aerospace, military, and building because of their excellent mechanical strength, good corrosion resistance, good electrical insulation, and less volatile substance release. The production of epoxy composites with natural fibers is one of the major areas of interest (Datta and Woch 2014).

With the increasing popularity of natural fiber composite materials, researchers have investigated the mechanical, thermal, stiffness, vibration, and tribological properties of natural fiber composite materials through experiments. However, experimental research has brought the inevitable: time-consuming, high cost, natural error, machine error, and human error. At present, most biological composites turn the research focus of natural fiber composites to computational methods to simulate the mechanical and thermal properties of NFRC accurately. The remarkable growth of computational techniques has sped up the progress of modeling and simulation of composite materials under various complex service environments. Various available software have been used to model and simulate composite materials, saving on the consumption of time, raw materials, and labor. Furthermore, geometric optimization-based computational techniques play a significant role in the advancement of structural strength. It is critical to evaluate a newly developed material's mechanical strength before putting them into the practical application parts where various application requirements are raised. The shell model, solid continuum shell model, and solid-solid model were developed by researchers for the simulation of the specimens. Successfully, simulation and prediction of natural fiber reinforced epoxy composites are obtained despite the fact of the complex physical and chemical micro-structures of natural fiber, which indicate that the modeling and simulation based on computational techniques could be used for the prediction of the mechanical properties (including tensile, flexural, and impact behavior). Resin infiltration stage, moisture absorption, thermal, and acoustic properties can also be simulated by means of numerical simulation (Alhijazi et al. 2020).

The current work has gathered the published documents from 2002 to 2021 regarding epoxy/natural fiber composites and simulation from the Web of Science (Fig. 1). It shows a trend in the development of the research area of modeling and simulation of epoxy/natural fiber composites. Modeling and simulation of epoxy/natural fiber composites began in 2002. They were conducted by 0 to 4 researchers per year until 2012, and this topic has attracted attention from many researchers. The number of published articles was increased and reached a peak of 20 papers in 2019. Figure 2 shows that India is the most enthusiastic in contributing research to modeling and simulating epoxy/natural fiber composites. Meanwhile, the USA and China rank second and third, respectively.

The growing utilization of natural fiber reinforced composites calls for effective structural design and development of material to give full play to the advantages of

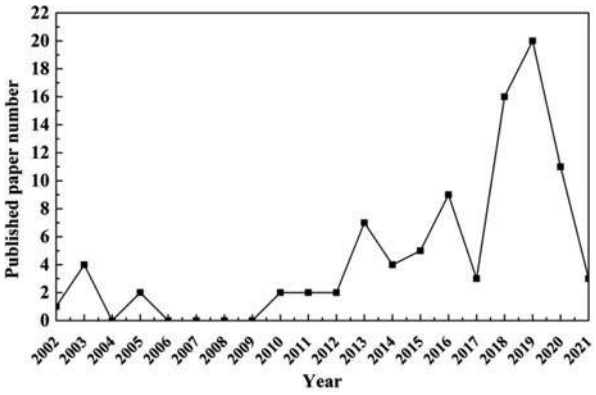

Fig. 1 Statistic from WOS database in published documents per year. Search keywords: (Topic= "natur* fib* composit*" and "simulation" and "epoxy") (22/2/2021)

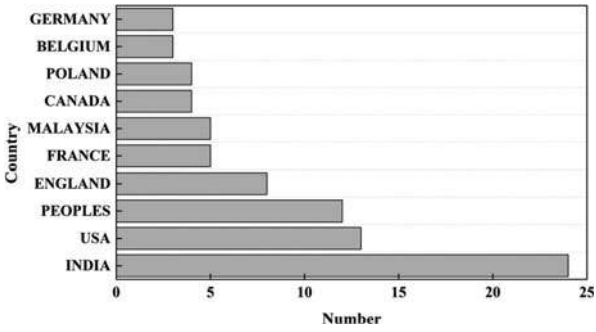

Fig. 2 Statistic from WOS database in published documents by country. Search keywords: (Topic= "natur* fib* composit*" and "simulation" and "epoxy") (22/2/2021)

raw materials and avoid defects as much as possible. The optimum performance could be therefore achieved. There is no dispute that it will cost a lot if all aspects of properties are evaluated experimentally. In minimizing waste of resources, computational techniques are developed by scientists and engineers to simulate the thermal, physical, and mechanical properties of the newly developed materials. The findings in the experiment could be verified more efficiently as well (Chandramohan and Presin 2017).

Analytical and numerical methods are applied in the modeling and design of natural fiber reinforced composites along with the development of diverse methods, approaches, and models. Modeling and simulation methods used to evaluate the characteristics of natural fiber reinforced composites presented high efficacy. Thus, the thermal, physical, or mechanical properties of natural fibers and their reinforced composites could be ideally predicted. The precise solutions of simple geometrical bodies made of natural fiber reinforced composite materials, such as columns, beams, plates, and shells, can be easily obtained through the analysis of analytical models. For some complex geometric structures, shapes, and load distributions, accurate solutions are challenging to obtain, and only approximate solutions can be obtained, not accurate solutions. Among all approximate methods, the finite

element method is popular in the engineering field because it can solve the model with any shape, material, boundary condition, and load.

This chapter focuses on the research on modeling and simulation of natural fiber reinforced composites of epoxy/natural fiber composites aspiring to highlight the key available approaches/techniques that can be implemented to investigate their properties analytically and numerically. Information from the published studies has been collected and compared, including fiber type, model type, simulation parameters, analysis type and platform, and accuracy of the model/method.

Modeling and Simulation Strategies for Natural Fiber Composites

Analytical Models

The specific properties of composite materials can be predicted by mathematical computation when the characteristics of matrix and reinforcement are experimentally obtained. In general, the elastic modulus, shear modulus, volume fraction, and Poisson's ratio of fiber and matrix in the composites are the necessary parameters in the fundamental micromechanics theories. Other parameters, such as orthographic properties, fiber orientation, density, aspect ratio, and viscoelastic behavior, are also required explicitly in some models. The prediction of composites made from woven fabrics reinforcement is usually much more complicated than reinforced with continuous/random fiber distribution. The rule of mixtures (ROM) is the easiest existing method to predict the elastic property of the fiber reinforced composites among a variety of theoretical models. However, the ROMs are only applicable to the continuous and unidirectional fiber. Other methods like Halpin and Tsai equations are also used to predict composites' elastic properties. Cox's model is the most frequently used analytical model to evaluate the impact of short fibers on the strength and modulus of composites (Shinde et al. 2017).

The interface damage analysis of fiber reinforced polymer composites is usually separated into three stages. First, complete bonding is performed on the fiber/matrix interface, and then friction contact is performed on the fiber/matrix interface to simulate its mechanical properties. Finally, the spring element is used to define the interface according to the constitutive relationship.

In many instances, flax and hemp are the two kinds of natural fibers preferred in the analytical research of natural fiber reinforced composites. Meanwhile, various analytical theories involving analysis of mechanical, thermal, and acoustic properties of natural fiber reinforced composites are developed. For instance, ROM; Puck failure theories; Halpin, Tsai-Wu, Tsai-Hill, Nairn Shear-lag, Mendels et al. stress transfer; fatigue-life (S-N) curves; and Hirsch are the choices for the analysis of stiffness, elastic modulus, strength, and fatigue-life response. Johnson-Champoux-Allard is suitable for the evaluation of natural fiber reinforced composites' sound absorption. The basic information of research methods adopted by researchers is listed in Table 1.

Table 1 Analytical methods utilized to study natural fiber reinforced composites

Fiber type	Matrix	Analytical	Objective of the study	Platform	Ref.
Hemp	HDPE	Fatigue-life (S-N) curves	Fatigue-life response	Not mentioned	(Fotouh et al. 2014)
Manila hemp	Polylactic acid	Square arrayed pipe filament	Transverse thermal conductivity	Not mentioned	(Ke et al. 2012)
Flax	Epoxy	Tsai-Hill, Tsai-Wu, Ashin, and Puck failure theories	Stiffness, strength, and interaction	MATLAB	(Koh and Madsen 2018)
Flax laminates	Epoxy	Mesoscale damage theory	Mechanical response, stiffness degradation, and inelasticity	Not mentioned	(Chemisky et al. 2017)
B & jute	Recycled high-density polyethylene/ polypropylene	Variable-order creep model	Creep behavior	MATLAB	(Xiang et al. 2020)

Fiber reinforced composites have been extensively employed in aerospace and other fields. Most aircraft have a certain life requirement, which means that their structure needs to bear a long period of cyclic load. In the early days, most of the composite materials used in aircraft were non-main load-bearing structures, the working stress was not high, and the fatigue problem of composites structure was not prominent. With the gradual application of composite materials to the main load-bearing structure, the requirement of structural weight reduction is higher and higher, which makes the fatigue problem of composites structure constantly appear. Over the years, a lot of research work has been done on the fatigue properties of composite materials, and many different models have been developed, trying to simulate the fatigue behavior of composite materials and predict fatigue life. With the development of composite fatigue theory, a large number of fatigue models have been proposed to predict life and damage. At present, composite fatigue models can be divided into three categories: fatigue life model, phenomenological model, and progressive damage model (Brod et al. 2019).

Most fatigue models are built based on a specific material, specific ply sequence, and specific load form; the performance of models strongly depends on a large number of test data because the existing theory analysis model is not mature enough. In many cases, the composites' structure design often needs to use a larger safety factor to ensure structural safety. With the high cost of the test to verify results in the composites' weight advantage, it is difficult to give full play. Therefore, it is of great significance to improve the fatigue life prediction and damage analysis methods for the practical application of composites structures (Bergmann and Prinz 2010).

The fatigue life model extracts the fatigue life information of the structure from the S-N curve or the equal life curve of the existing structure. The result given is the

number of fatigue failure cycles of the specimen under a certain load. Most of the existing fatigue life prediction models use traditional mathematical models or numerical methods to construct formulas or draw CLD curves. Some models have low test costs and simple calculations, but the error between prediction results and test data is significant. Other models with relatively accurate prediction results need a large number of test S-N curves as support materials. Their models contain various parameters that need to be optimized or empirically estimated (Bergmann and Prinz 2010).

The phenomenological fatigue model of composite materials describes the damage caused by fatigue through the attenuation of a specific material or structural parameter. The residual strength model and residual stiffness model are two mainstream fatigue phenomenological models. The fatigue life of composites can be predicted by introducing strength degradation or stiffness degradation to consider the actual damage state of materials. The main shortcomings of the current phenomenological model are as follows: it cannot completely and accurately describe the whole strength/stiffness attenuation process; it is only suitable for specific materials and limited range of load levels; there are many parameters to be determined by test; it is only suitable for the uniaxial load (Brod et al. 2019).

Compared with the other two models, the progressive damage model can predict fatigue life and use appropriate failure criteria and damage variables to degrade material properties to realize the function of predicting damage propagation and residual mechanical properties. According to the actual demand, the progressive damage model has been developed to analyze macro-damage, micro-damage, and delamination damage (Khaldi et al. 2016).

Since the end of the 1980s, models for predicting fatigue damage propagation have been proposed. Due to the lack of powerful computer technology, the early progressive damage model is only an empirical formula used to describe the fatigue damage evolution process of materials. With the development of computer and finite element modeling technology, progressive damage models with more powerful functions and broader application scope have been proposed one after another (Bergmann and Prinz 2010). The fatigue life model is the first developed fatigue model (Xiaoquan and Xiaoyuan 2020). Because there is no need to understand the physical mechanism of damage, the fatigue life model is the simplest of the three types of models widely used in the life estimation of engineering structures. However, these models usually need to be calibrated for specific cases, so their application scope is limited. In contrast, the phenomenological model can more clearly characterize the cumulative characteristics of structural fatigue damage with the help of residual strength/stiffness and can be established by simple mathematical methods. Therefore, this kind of model is broadly applied in predicting fatigue life and residual mechanical properties in engineering practice. The progressive damage model can predict the fatigue life and residual mechanical properties of structures and classify and quantitatively describe the fatigue damage, which cannot be realized by the fatigue life model and phenomenological model. However, the complexity and high cost of progressive damage models are often not accepted by engineering

practice. They are frequently used in the research field of structural damage mechanism analysis (Alhijazi et al. 2020).

The development of the composites fatigue model is inseparable from the progress of test technology and basic theory. Most of the existing composites fatigue models have been proven to be accurate by experiments. The future fatigue models will focus on reducing the implementation cost and improving versatility. Applying fatigue models to complex conditions (such as random load spectrum, hydrothermal environment) and complex structures is the primary goal of composites fatigue model research (Xiaoquan and Xiaoyuan 2020).

Finite Element Analysis

Finite element analysis is a kind of analysis method based on computer software, degenerating the 3D model into a finite amount of microscopic elements to solve engineering problems. The mesh shapes can be chosen depending on the structure of the objects. Furthermore, the analysis results can be calculated at the mesh nodes. The results are dynamically displayed on the computer, making it possible to observe the change of internal structure. Through the finite element analysis, researchers can simulate the complex virtual experiment in the user interface environment and view the experimental results. Finite element analysis can be repeated iterations to optimize the results and improve the accuracy, which can effectively shorten the product development cycle and improve the service life of the product. Therefore, it is economical and practical to use the finite element method for numerical simulation. In addition, the fiber matrix interaction can be analyzed by changing the combination mode and volume fraction of fiber matrix. For these reasons, numerical simulation is sometimes a better choice than an experiment, especially when the combination of various fibers and matrix and the effect of different fiber volume fraction on the properties of composites are explored. Nevertheless, this does not mean that the experimental research can be entirely abandoned because the premise of finite element analysis is to grasp the properties and parameters of materials correctly, and only through experimental verification can the accuracy of finite element analysis results be judged.

The literature review indicated that a similar result with the experimental test could be obtained through the FEA, where implied FEA model can be utilized to analyze natural fiber composites efficaciously under the circumstances of fiber positioning in composites symmetry and regularity (Alhijazi et al. 2020). All kinds of materials' shapes, properties, boundary conditions, and loading modes can be defined in FEA. Hence, the FEA is becoming a universal technique in academia and engineering problem-solving. As mentioned above, FEA is operated in software virtually, the data visualization can be achieved, and researchers can read and analyze easily. The conduction of iterations contributes to the accurate and optimized results that originate output from the software and therefore reduce the time cost of product development and enhance the lifetime of the products. The finite element

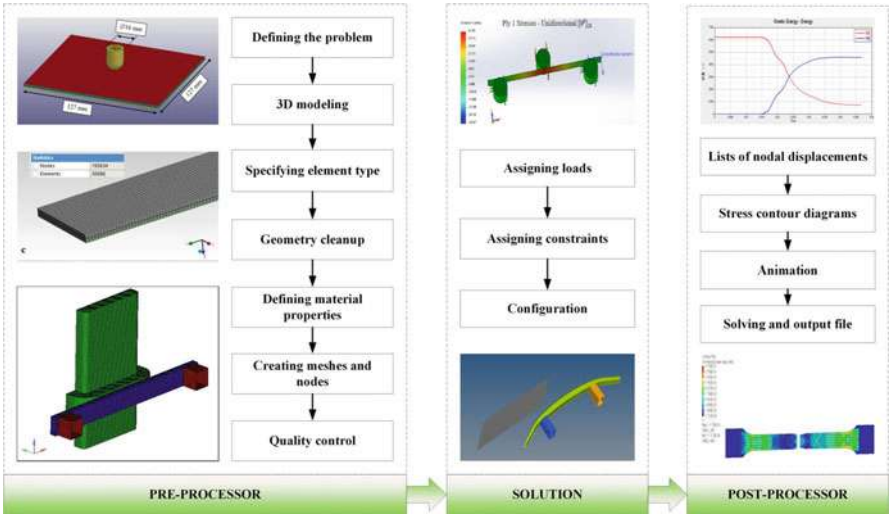

Fig. 3 Overview of FEA steps. (From Sy et al. (2019), Kumar et al. (2018), Davoodi et al. (2011), and Rahman (2017) with permission)

analysis mainly includes three parts, pre-processing, solution, and post-processing (Naveen et al. 2019). The overview of FEA steps is presented in Fig. 3.

Pre-Processing

The main work of pre-processing is to build one-dimensional, two-dimensional, or three-dimensional models of the research object; assign appropriate material models, elements, meshes, and material properties to different parts of the model; and impose appropriate structural or thermal boundary conditions and loads on the model according to the application requirements, such as thermal load, structural load, electrical load, or magnetic load. The commercial software that can do this job includes AutoCAD, SOLIDWORKS, CATIA, Creo, Solid Edge, ANSYS, LS-PrePost, OptiStruct, and COMSOL. For the design of complex geometry such as car body, train body, and aircraft fuselage, special software must be used to mesh the complex geometry to capture the real-time response of materials to the applied load. HyperMesh is a commonly used mesh generation software in the finite element field.

Defining the Problem

Defining the problem is the first step in any finite element analysis. The problems to be solved in the finite element analysis of composite materials include structural analysis, fluid analysis, thermal analysis, heat transfer analysis, buckling analysis, electromagnetic analysis, electrical analysis, and multiple physical analysis (coupled field). The analysis type is corresponding to the nature of the load. In addition, if two fields act on the analysis object at the same time, the coupled field analysis must be preinstalled in FEA software.

Part Modeling

After defining the analysis problem and selecting the analysis type that matches the actual situation, modeling the parts of the analysis object is the next step. In reality, structural components usually contain too many complex structural details, which is unfavorable for the rapid establishment of the model, so simplifying the structure without affecting the analysis results can be considered. Simplifying the three-dimensional shape of the structure to a two-dimensional shape can reduce the calculation time and simplify the calculation.

Material Modeling

Unlike metal materials, natural fiber reinforced composite materials have the characteristics of anisotropy, so the orthotropic material model is needed. The orthotropic material model assumes the elastic modulus in X, Y, and Z directions.

Material Properties

The NFRC material characteristics obtained through the experimental test must be input into the finite element model as material parameters. This is usually a prerequisite for effective finite element analysis of the material: unidirectional elastic modulus, ultimate tensile strength, Poisson's ratio, in-plane shear strength, and shear modulus.

Meshing

The type and size of the mesh determine the accuracy and speed of the finite element model. Firstly, the finite element model of natural fiber composite is discretized with coarse mesh, and then the mesh is refined according to the experimental results. When the mesh size reaches the optimal, further reducing the mesh size does not significantly improve the accuracy of the results but increases the calculation time.

Solution

Load, stiffness matrix, node displacement, element stress, element strain, and other parameters are stored in the finite element software in matrix form. After the mesh is successfully divided, the element stiffness matrix, the overall stiffness matrix, and the overall force vector will be generated at the back end of the analysis software.

Typical finite element solvers include ANSYS and LS-DYNA. The time of the finite element solution relies on the number of elements and nodes, which are directly affected by the size and quality of the mesh. Only after the finite element model is solved can the finite element results be estimated effectively, that is, displacement, temperature, pressure, or velocity.

Boundary Conditions

For accurately solving the finite element model, it is required to introduce appropriate boundary conditions, i.e., structural boundary conditions and thermal boundary conditions, and all the boundary conditions need to be applied to the nodes.

Loading

The natural fiber composites in the real environment may be subjected to a structural load, thermal load, pressure load, bending load, or fatigue load. Therefore, it is essential to apply the load corresponding to the real environment to the established model in the finite element analysis software. The load must be applied along with the node. When the above work is completed, the finite element analysis can be carried out.

Solving

The solution database file in the FEA solver is then used for the solution once all pre-processing has been completed.

Post-Processing

The calculation results of displacement, temperature, pressure/velocity, stress, and strain can be displayed in the finite element analysis software. The finite element post-processor can also generate data tables, graphics, and animation according to the demand. The response of the designed structural components under various loading conditions can be easily obtained, so the raw materials and time costs for sample preparation and experimental testing can be reduced.

Extraction of Results

After successfully solving the finite element model by the post-processor, the extracted results, such as displacement, stress, strain, pressure, temperature, and velocity, should be carried out to enable a virtual simulation of the actual NFRC product.

Outcome of Finite Element Analysis Results

The finite element analysis results show the design defects of structural components and predict the stress concentration or excessive deformation of structural components in service, which will provide sufficient suggestions for design improvement or further experiments in natural fiber composites.

A variety of analysis methods can be employed to predict composite materials' properties, including various analyses such as multi-physics, electrical, buckling, electromagnetic, heat transfer, fluid, thermal, structural, and acoustic. Nevertheless, as for the natural fiber reinforced composites, mechanical properties are most evaluated by this FEA method. Only a few researchers tried to solve moisture absorption and thermal problems by using FEA (Jain et al. 2019). Even though the model could be analyzed from one dimension to three dimensions, 3D models are preferable to obtain accurate results, particularly when loads are applied in the out-of-plane direction (Chen et al. 2019). The 3D mold is easy to prepare since it can be molded in advance and imported through the software before analysis. Different raw material properties are defined in modeling and simulation depending on the type of analysis. Poisson's ratio, Young's modulus, breaking elongation, shear strength, and density are essential parameters for studying mechanical properties. Meanwhile, thermal conductivity values of fibers and matrix are required for the thermal

behavior analysis, and orthotropic mechanical characteristics are required when minding estimating the sound absorption coefficient (Dragonetti et al. 2020).

It is a matter of convention that it is hard to determine the exact orthotropic properties of newly developed natural fiber reinforced composites. As a result, researchers are more inclined to consider their materials as isotropic, far different from the orthotropic materials. Thus, the assignment of Young's modulus and Poisson's ratio becomes easier (Hao et al. 2020).

It is undeniable that FEA is becoming a useful tool in engineering, and many FEA software has been developed and sold in the market. In addition, MATLAB is also the right-hand assistant of finite element modeling and optimization, which is widely used. Some analysis theories are gradually developed and become an important part of NFRC theoretical analysis.

Modeling and Simulation Analysis of Natural Fiber Composite Processing and Properties

In the production of structural bio-based composites, liquid composite molding (LCM) of plant fiber composites has attracted much attention. A deep understanding of the resin impregnation process and flow behavior in plant fiber reinforcements is crucial to manufacturing quality composites. As the primary goal of any LCM process is to make sure complete mold filling, successful LCM execution requires, in particular, understanding, managing, and optimizing the mold filling stage. Not surprisingly, in order to optimize the LCM operation, computational mold filling simulations are commonly used as a cost-efficient and time-saving instrument (Pantaloni et al. 2020).

Natural fibers, especially plant fibers, have identical morphologies and compaction behavior that influence their permeability. Plant fiber reinforcements bear higher permeability than synthetic fiber reinforcements comparatively. Assessment of in-plane permeability of plant fiber reinforcements has been done considering primary use of mineral oil (non-polar) or glycerin solution (polar) as the test fluid, although to control the process better (e.g., maintaining constant viscosity and temperature) where viscosity is compared to thermosetting resins. Throughout the assessment, various samples can be used, such as woven fabrics and non-woven mats. Very few studies have tested permeability, particularly at elevated temperatures of plant fiber reinforcements with catalyzed thermosetting resins. Those who run the studies have effectively exploited fill times shorter than the resin pot life. Plant fibers generally contain rough surfaces rich in functional groups (hydroxyls), which have an affinity with conventional LCM resins, such as epoxy, polyester, vinyl ester, and phenolic.

Flow Simulation of Natural Fiber Composites

A primary objective in LCM is controlled and complete filling of the mold with adequate wetting of fibers. Because of micro-void formation and poor interfacial

adhesion, poor mechanical properties result from poor fiber wetting and occur through uncontrolled and incomplete filling that result in the formation of defects (e.g., dry spots), poor part quality, even part scrapping, and waste of content. Optimization of mold fill time is vital in controlling mold filling while abstaining from fluid pressure build-up. The microscopic and macroscopic flow of the liquid resin through gaps is significant to study within yarns and tows and the porous preform, respectively. The complex mold filling process is influenced by various factors, including permeability, the pressure differential in the mold cavity, resin injection rate, resin viscosity (as a function of time), and the inlet and outlet positions gates. Permeability studies and the law of Darcy, which can be obtained by averaging methods from the Navier-Stokes equation, are also used to model the dynamic viscous flow of resin in porous media.

Dual-Scale Flow and Capillarity

As a preform is generally made of yarns, a dual-scale flow is typically involved in its impregnation. Resin flow between yarns (inter-yarn) is referred to as macro-flow, while micro-flow is referred to as resin flow through the yarns (intra-yarn). Inertial forces can be ignored as resin flows at low Reynolds numbers. The viscous flow of the resin dominates the macro-flow, while the micro-flow is guided by the capillary pressure produced within the tows. It is essential to study capillary effects, not least because they play an important role in the void formation process in LCM. As Fig. 4 shows, capillary flow dominates at low-flow velocities (and high fiber volume fractions), leading to inter-yarn voids. In contrast, viscous flow dominates at high-flow velocities (low fiber volume fractions), resulting in intra-yarn voids. The dual-scale flow is described as follows since impregnation in composites also leads to non-wetting dynamic angles. The resin impregnates transversally in the yarns as the inter-yarn flow front progresses. The inter-yarn flow rate is minimized as the resin fills the yarn. The resin flow front is impossible to completely saturate and fill the yarns if the inter-yarn flow rate is higher than the intra-yarn flow rate, resulting in the presence of intra-yarn voids. Usually, this is the case of Ksat/Kunsat >1. On the other hand, if the intra-yarn flow rate is higher than the inter-yarn flow rate, the yarn will be saturated with resin, while the inter-yarn regions will remain unfilled. In the inter-yarn regions, this can result in notable porosity. This is the Kunsat/Ksat >1. For

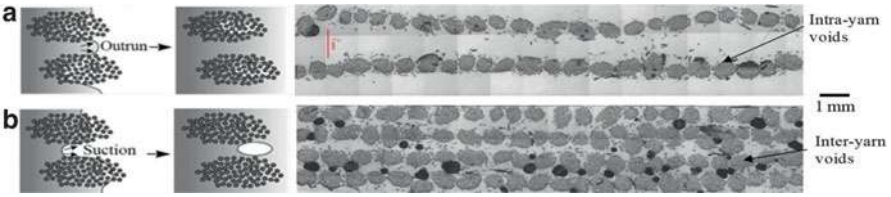

Fig. 4 Voids can be created by the complex dual-scale flow of resin in fibrous preforms. (From Shah et al. (2012) with permission)

plant fiber composites, both effects have shown (Fig. 4) fiber volume fraction function. An ideal flow velocity (viz. capillary number) exists where the capillary effect is optimum, resulting in equivalent flow rates in the inter- and intra-yarn regions and, therefore, no (or minimal) creation of voids (Shah et al. 2012).

Macro-scale flow refers to the resin advance between yarns or tows (i.e., inter-yarn flow), while micro-scale flow refers to the resin penetration into the yarn (i.e., intra-yarn flow). Notice that on the two scales, permeability is also distinct. For example, (a) the yarn is not properly impregnated for low fiber content due to low yarn permeability but high overall permeability, and thus intra-yarn voids can form, while (b) for high fiber content, although the yarn and overall permeability are similar, capillary flow dominates in the yarn, and thus inter-yarn voids are created. Images replicated by author D.U.S. showing unidirectional fabrics of jute and flax impregnated in atmospheric conditions by epoxy and polyester resins (Pantaloni et al. 2020; Shah et al. 2012).

Maximum permeability tests have so far been carried out on natural fiber reinforcements on the weighting of a valid 1D Darcy's rule. By using the traditional model, the mold filling of natural fiber reinforcements has been successfully simulated by some researchers, including Kong et al. (2014). To predict fill times (and choose an effective or an adequate injection pressure) and ensure complete impregnation, they conducted a resin flow study on the upper and lower sections of a flax-vinyl ester agricultural chemical storage tank.

The software named Nastran was chosen to analyze the chemical storage tank base on the finite element method. The maximum compressive stress, tensile stress, and buckling load factor results are obtained after FEA, indicating that the structural design is reasonable and safe. The designed natural fiber reinforced resin-based chemical storage tank is considered to be of high quality and stable. As shown in Fig. 5a, the container's stress contour is presented clearly by the FEA analysis. The resin flow analysis of VARTM manufacturing method was conducted after the structural design and evaluation. This step confirmed the manufacturing possibility using VARTM, checked resin flow filling time, and confirmed no dry-patch. RTM-Worx FEM flow simulation solver was used to do the resin flow process

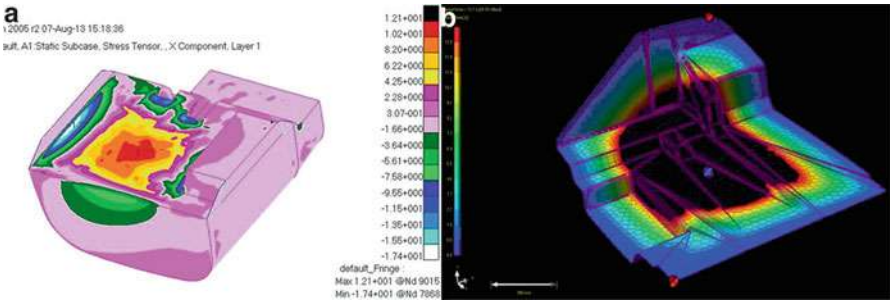

Fig. 5 Stress contour (**a**) and flow simulation (**b**) of the chemical tank by FEA. (From Kong et al. (2014) with permission)

analysis. Since the permeability coefficient data is important for resin flow analysis, the design and manufacture of a permeability test rig and the subsequent test should be performed before the resin flow simulation. Figure 5b shows the simulation of the tank portion.

The parameter of permeability is essential in the LCM process of composites to better understand the resin filling stage. Compared with synthetic/chemical fiber, the natural fiber reinforcement made from flax, hemp, jute, and sisal fibers show much higher permeability innately. However, wood fiber reinforcements are proven to have less permeability than the bast fibers. The permeability of natural fiber reinforcements tends to increase with the increase of the porosity. The modified Carman-Kozeny equation is able to mold this kind of porous material. For the yarn reinforcements, the yarn thickness and twist are the main factors that influence the permeability. Good permeability of yarn can be obtained by increasing the yarn diameter, choosing long fiber for yarn manufacturing, and decreasing the twist of the yarn. Fluid absorption and swelling are demonstrated to be the main mechanisms in natural fiber preforms. Saturated permeability tends to be higher than unsaturated permeability for natural preforms, but the difference disappears with increasing porosity (decreasing fiber volume fraction) (Pantaloni et al. 2020).

Flow Process Design

The first step should be a primary design of the flow process. In accordance with the injection port's design concept and the vent for the VARTM process, to facilitate the injection of the resin, the injection port should be designed at the center or one edge of the mold. The vent should be designed at the edge of the mold, while the injection port is located in the middle of the mold and vice versa. In short, to prevent the formation of a dry spot, the vent should have the longest distance to the injection port. Du and co-researchers screened out the optimization injection scheme by comparing six different injection schemes (Du et al. 2013). What is different is the number and positions of the injections and vents.

The various filling times of the six schemes under the same simulation conditions show a great gap between each other. The fastest filling speed is five times the slowest. By comparing the different schemes, a conclusion can be drawn that the more the model had injection ports, the shorter the filling times will be achieved. This is because the resin will pass a far distance to impregnate the fiber reinforcement well; thus, fewer injections are set. The injection position will also influence resin infiltration's uniformity into the reinforcement on a large scale because of the bubble formation. The addition of the vent will also help in the release of the bubbles during the VARTM process.

The injection position will influence the resin confluence timing and join each other, thus influencing the forming of voids or dry spots and causing intense stress and cracks. The optimization position setting of injections becomes particularly important. The vent will affect the rid of the bubbles; thus, the vents should be located at the intersectional areas of resins to remove the bubbles efficiently. The top

corners were easy to store the bubbles when 90% of the mold filling process was done, then triggering the weak resin field. So, the vent should be mounted in the upper corners as well.

VARTM is a method of composite fabrication where the resin flow stage is very significant. The resin flowing phase of composites such as the automotive bumper beam could be well simulated using the virtual flow program RTM-Worx. Usually, there will be several injection ports and vents throughout the optimization system. The simulation results will lead to a realistic process, save resources, and indirectly promote the composites' efficiency. As the complexity or size of the component increases or advanced fiber preforms exhibiting low permeability are introduced, mold filling under vacuum pressure becomes more difficult. This leads to dry spots needing part repair or scrap. Hence, to improve the yield and performance of the process, resin flow control becomes essential.

Bender and co-researchers demonstrated an experimental setup of the VARTM method for flow rate control (Bender et al. 2006). To change the pressure difference between the injections and vent position, the flow rate controller evacuates the infusion bucket and applies pressure control. Meanwhile, to change the injection bucket's pressure and the flow rate of the VARTM operation, a fuzzy logic controller was implemented. By virtual flow simulation (LIMS), the system was optimized offline, and the physical limits of such a system were determined. For a broad range of permeability and viscosity values, the flow rate controller effectively controls the constant flow rate.

Mechanical Property Simulation of Natural Fiber Composites

Nowadays, researchers increasingly attempt modeling and simulation to analyze the experimental phenomenon as a fast and low-cost tool. Simulation platforms, for example, ANSYS, ABAQUS, MATLAB, LS-DYNA, Nastran/Patran, Siemens PLM NX 10.0, and NISA, have been significantly used for this kind of analytical work. Further, analytical techniques, for example, experimental modal analysis, Newton-Raphson non-linear, ROM, Maximum strain and Tsai-Wu, Weibull distribution, J-Integral, Chamis model, Nielsen Elastic model, and Halpin-Tsai model, are also extensively used in the mechanical property simulation of natural fiber composites.

Compared to glass and carbon fiber reinforced composites, the numerical modeling and simulation of natural fiber composites are scarcely reported in the past. The initial FEA steps consist of creating the model geometry followed by assigning the characteristics of the material. Unlike the glass and carbon composites, specific failure criteria should be considered in the modeling and simulation of natural fiber composites as it defines the failure initiation and propagation.

As we all know, natural fiber has a complex microstructure, and its properties mainly depend on its plant species, climate, and planting conditions. Finite element analysis can effectively assess the effects of reinforcement type, volume fraction, aspect ratio, and fiber orientation on natural fiber composites' mechanical and

thermal properties. As a general rule, cellulose, hemicellulose, lignin, and pectin are the main components of natural fiber, which, together with the microstructure of the fiber, determine the mechanical properties of natural fiber. Because of the complexity of natural fiber structure in different length scales, the homogenization method can be used to signify the relationship between microstructure and macrostructure behavior. The representative volume element method is a multi-scale finite element model based on homogenization, reflecting the characteristics of natural fiber and NFRC in the uniform microstructure.

Most conventional materials, such as metals and glass, can be analyzed under the assumption that they are isotropic and homogeneous. In the analysis of anisotropic materials, the coordinate transformation is usually used. The material properties measured in the material coordinate system can be easily converted to the problem coordinate system, thus eliminating the anisotropy problem. In principle, the inhomogeneity can be addressed by direct numerical simulation of a composite structure containing all the microstructure details using finite element analysis. But this requires extremely fine-grained meshing, resulting in millions of degrees of freedom. In fact, the meshing of most real composite structures generates trillions of degrees of freedom. It is not always possible to use hardware and software to perform such as large finite element analysis. Through the proper modification of the model, the effective homogeneous material can be used to replace the heterogeneous composite material to achieve almost the same accuracy as the direct numerical simulation, and many orders of magnitude will reduce the cost. The process of replacing the original non-uniform multiphase model with a uniform model is called homogenization. Homogenization is performed on a representative block of the original non-uniform material, which is a tiny point compared with the entire structure. Homogenization can be used in the construction model to derive the full set of effective material properties of the three-dimensional structure. It can also be used to simulate the overall material response under simple loading conditions. Since a tiny microstructure representative block is used for homogenization purposes, the mechanics involved are called mesomechanics. The homogenization model is fictitious, but it is equivalent to the original non-uniform material. This homogenization can be achieved through atomic simulations or experiments.

Particularly worth mentioning is that the natural fiber shows a different manner compared to synthetic fibers in the tensile property evaluation. Synthetic fibers' failure criteria are usually applied in natural fiber composite analysis due to the lack of specific failure criteria of natural fiber. As a result, this strategy will help predict ultimate tensile strength at the expense of ignoring other characteristics like a non-linear tensile response (Lee et al. 2017). Researchers used numerical modeling and simulation to evaluate the tensile behavior much more than other mechanical properties of natural fiber, where the tensile strength and stress/strain properties of natural fiber were analyzed. There is limited FEA research on the natural fiber reinforced epoxy composites. Thus, the composites with thermoplastic resin matrix are chosen as FEA objects, such as vinyl ester, PE, and PP. Figure 6 shows an agave NFRC beam under bending load. In the interaction module, the general contact (standard) between the bracket, the loading head, and the parts is defined. The

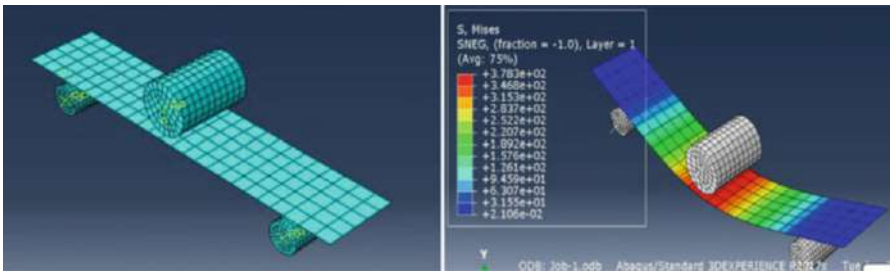

Fig. 6 Carbon/jute fabric reinforced epoxy hybrid composites. (From Ali et al. (2019) with permission)

friction coefficient is 0.15 in the tangent direction, and it is hard mechanical contact in the normal direction. In the bending test simulation, the reference point of 3 mm radius support column is constrained as an external force, while the reference point of the upper column (loading head) is displaced by displacement load.

Other modeling and simulation researches are introduced briefly in the following section, and all the experimental and numerical result data show satisfactory agreement. Characteristics of failure modes and strength of natural fiber composites were analyzed experimentally and numerically in works done by Kumar et al. (2018). CATIA was used as the software to build the 3D model and numerically simulated it in ANSYS Workbench 16.2 under the given boundary conditions. In the aerospace industry, reasonable prediction of tensile and bending strength of natural fiber specimens is very important to reduce the number of expensive tests in the design stage. Patil studied the effects of alkali-treated sweet lime and lemon reinforced epoxy composites (Patil et al. 2018). It was concluded that the experimental result was well-matched with the simulated result that was obtained from the ANSYS workbench 16.2, with the errors ranging from 2 to 15%.

Meanwhile, Goudar and co-researchers developed a multi-scale finite element model using the Digimat-FE software and successfully simulated and predicted the tensile strength of natural fiber reinforced epoxy composites (Goudar et al. 2020). It is suggested that the Digimat-FE is also suitable for the field of natural fiber reinforced epoxy composites with a comparable predicted result with the experimental data. Charpy impact, flexural, and tensile tests were operated accordingly. The 3D models were usually built-in software, assuming that the fibers were distributed in the composites unidirectionally. Meanwhile, Gupta and co-researchers carried out the mechanical tests through the FEA. The analytical relation between fiber volume ratio and the mechanical properties was acquired based on a data-driven decision method (Gupta et al. 2020). The high degree of matching between the simulation analysis results and the experimental results in the above cases means that at this stage, effective simulation of various mechanical properties of natural fiber composite materials can be achieved by means of finite element analysis.

Hybrid composite analysis also found a way by using modeling and simulation techniques. Banana/coir reinforced hybrid composites were modeled and simulated by the researches. The comparable result can be obtained from the FEA with the

experimental result. FEA suggested that it is possible to decrease stress concentration by increasing fiber percentage and slight experimental variation. However, the porosity, anisotropy, and interphase properties were neglected. In another study, glass-flax hybrid composites were prepared by hand lay-up method, and FEA simulated the mechanical properties on ANSYS except for the experimental impact, flexural, and tensile test (Ramesh and Sudharsan 2017). FEA is considered dependable for hybrid composites since the experimental result shows satisfactory agreement with the FEA results.

Apart from the tensile, flexural, and impact analysis, FEA was also applied to simulate the compression behavior of natural fiber composites. For example, a series of quasi-static compression on cotton fiber reinforced epoxy composite tubes were carried out (Mahdi et al. 2003). The agreement of numerical and experimental results is limited, which indicated that the finite element analysis buckling is not the optimal method for tube compression analysis. More accurate simulation results for the post-buckling response and crush failure can be obtained from the more detailed non-linear analysis.

The low-velocity impact performance of composites was extensively operated experimentally in many researcher's work to understand the failure mode of the laminated composites. This kind of work is bound to waste much time, money, and other resources. Therefore, the FEA was gradually applied in impact analysis and demonstrated to be effective for predicting damage response of glass fiber and carbon fiber composites as well as the natural fiber composites.

Low-velocity impact testing was carried out numerically in previous work (Menna et al. 2011). They conducted a numerical simulation of low-velocity impact tests on glass/epoxy laminates using LS DYNA. The lamination was modeled with 3D elements combined with orthotropic failure criteria. The simulation shows satisfactory agreement between experimental and numerical results. Similar work is done by Berk and coworkers, where the effect of low-velocity impact on the glass fiber and carbon fiber reinforced resin composites was performed by the environment, and FEA and LS DYNA were used for the numerical simulation (Berk et al. 2016). As a result, a gratifying agreement between the experimental and numerical results was obtained as well. Gupta and co-researchers also carried out the low-velocity impact test on glass fiber reinforced composites (Gupta et al. 2018). The numerical model contributes to predicting the delamination size, shape, and orientation, and good agreement was ultimately obtained.

In order to further explore the possibility of FEA on natural fiber reinforced composites, few numerical simulation studies on natural fiber reinforced composites' impact behavior were operated by the researchers. Riccio and coworkers used the ABAQUS to simulate the impact response of flax-based honeycomb cores composites (Riccio et al. 2018). An 8-node continuous shell element was used to model the composite materials. A cohesive element was used to model the interface between the honeycomb components to simulate the separation phenomenon inside the core. In general, the numerical results are in good agreement with the experimental results.

Sy et al. (2019) used commercial software LS DYNA to perform low-speed impact tests and numerical analysis on unidirectional and cross-laminated flax/epoxy laminated plates. Figure 7 shows the established 3D model in isometric and side view. In terms of the front and rear surface damage of the laminate, a good correlation was again obtained between the experimental results and the numerical results, as Fig. 8 shows. The Von Mises stress peak along the 0° direction of the unidirectional laminated plate consists of the matrix crack in the experimental laminated plate. It was also found that the peak stress of cross-shaped Von Mises on the laminated plate was in good agreement with the cross-shaped matrix crack on the actual specimen. In addition, the front butterfly-shaped delamination is closely related to the shape of the front von Mises stress peak in the LS-DYNA results.

Ravandi and co-researchers established a three-dimensional finite element model of low-velocity impact of flax fiber non-woven laminates and FC4 hybrid laminates. They studied the material behavior and damage mechanism under two different

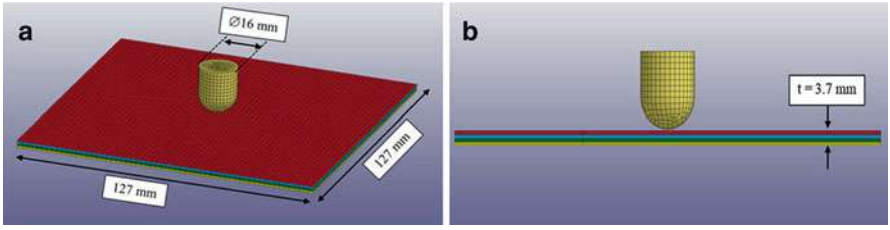

Fig. 7 LS-DYNA flax/epoxy composite impact assembly model: (**a**) isometric view; (**b**) side view. (From (Sy et al. 2019) with permission)

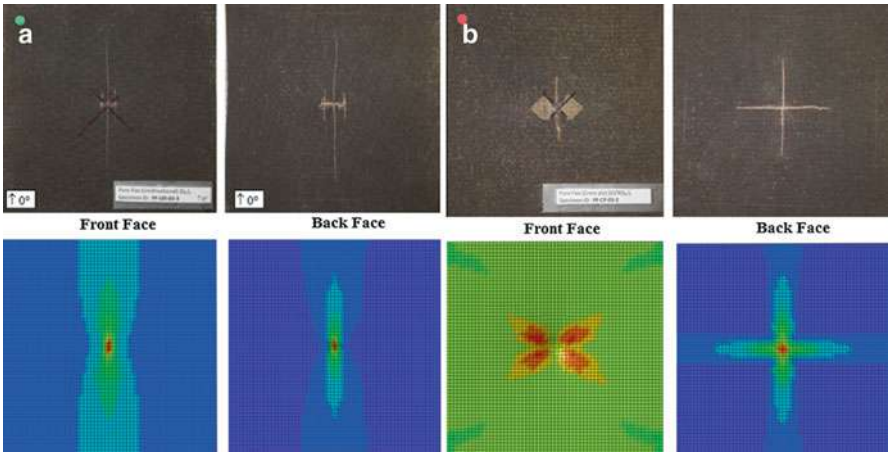

Fig. 8 Experimental and numerical cross-ply laminate conditions impact: (**a**) post E = 8 J; (**b**) post E = 20. (From (Sy et al. 2019) with permission)

impact energies (Ravandi et al. 2018). The finite element analysis results show that the energy dissipation of in-plane matrix damage in both hybrid and non-hybrid laminates is significantly higher than in laminates, indicating that interlamination is not the critical failure mode for composite materials. In hybrid composites, the contribution of matrix damage results in the total absorbed energy increases because the addition of carbon fiber improves the damage resistance of the composites. In addition, it was found that the energy dissipation of the carbon fiber cord was much higher than that of the linen cord. The effects of fiber reinforced type, hybrid material, fiber type, structure, and core fiber orientation on the impact damage resistance of composites structures were studied experimentally.

Further mechanical properties are likely to be simulated by FEA at a significantly lower cost than experimental tests. For instance, Davoodi and coworkers used CATIA and ABAQUS platforms to numerically analyze the impact properties of kenaf/glass/epoxy composites automobile bumpers (Davoodi et al. 2011). Eight bumper beam concepts with the same material model were simulated under the standard conditions of the low impact test. The results show that the reasonable choice of concept has an important influence on the structural strength, and the composite is a constant. Figure 9 shows the displacement curve of the automobile beam after the impact load is applied. FEA results showed that kenaf/glass fiber hybrid material reinforced epoxy composites could be used in small car bumper

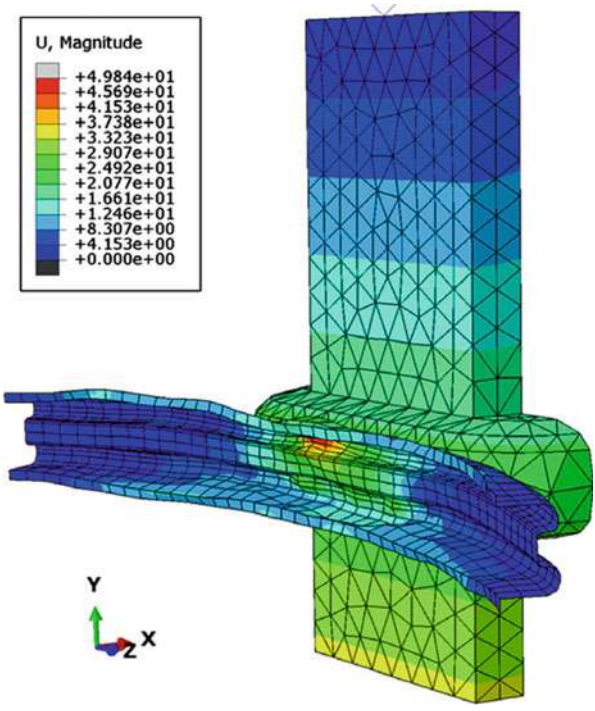

Fig. 9 Displacement profile of double-hat profile after impact. (From Glouia et al. (2019) with permission)

beams. Under normal circumstances, the difference between the experimental and FEA results is caused without considering the material properties. It is worth mentioning that natural fibers are orthotropic, and NFRC also contains pores, discontinuities, and porosity (Glouia et al. 2019).

Failure Simulation of Natural Fiber Reinforced Polymer Composites

For half a century, the failure theory of composite materials has been the focus of attention. Researchers have put forward dozens of theories, but so far, none of them can successfully predict all the failure behaviors of composites that we can observe. In the vast majority of literature, researchers seek and verify the effectiveness of numerical analysis by comparing the numerical prediction data with the experimental test data and rarely reveal their shortcomings. After a long time, the accuracy of a theoretical prediction can reach less than 10%, the accuracy of a theoretical prediction can be even less than 5%, and the failure mode is completely consistent with the experimental results. Hence, an illusion of the failure theory of composite materials has developed to a very mature stage. Is this really the case? The conclusion is not optimistic. The strength theory of composite materials is still in the stage of vigorous development. There are many aspects of advanced numerical calculation methods to be verified and improved, and there is still a certain distance from the mature engineering application.

The stress state of a single ply is generally one or a combination of the following states: (1) the tensile stress along the fiber direction corresponds to the failure mode of fiber fracture or fiber pullout; (2) the compressive stress along the fiber direction corresponds to the local instability and kink of the fiber; (3) stretching in the direction perpendicular to the fiber, corresponding to the breaking of the matrix; (4) the compressive stress along the direction perpendicular to the fiber corresponds to the shear failure of the matrix; (5) shear stress, corresponding to macroscopic shear failure. It is undeniable that only when various failure modes are considered in the analysis of composite materials can the performance be evaluated accurately.

Moisture Absorption and Thermal Property Simulation of Natural Fiber Composites

Composite materials are often in a humid environment during transportation, storage, and use. In this environment, composite materials will absorb moisture, which causes changes in the quality of the sample and changes in performance. The presence of water will have two effects on the composite material: first, water as a plasticizer plasticizes the resin matrix, causing expansion, and lowering the glass transition temperature; second, water hydrolyzes the resin structure, interface structure, and desorption. Therefore, long-term exposure to the material in a humid environment will reduce the performance of the material itself.

This change in the mechanical properties of composite materials is closely related to the stability of fibers, resins, and interfaces to water. At high temperatures, due to the different coefficients of thermal expansion between the fiber and the resin matrix, thermal stress is generated at the interface, the resin matrix is swelled by hot water, swelling stress is generated at the interface, and the diffusion and penetration of water molecules through the interface will cause the interface to fall off. Sticky, thereby accelerating the deterioration of composite materials. The diffusion of water in the composite material, a part of the water enters the polymer material structure, the solvation of water causes the resin matrix to swell, and the chain relaxes. At the same time, water will diffuse along with the interface between the fiber and the matrix. For composite materials, the bonding strength of the interface between the matrix and the reinforcement is destroyed, which reduces the integrity of the fiber and the matrix. The surface treatment of the fiber improves the interface bonding force between the fiber and the matrix, which is beneficial to enhance the moisture and heat resistance of the composite material, causes the interface to debond, and leads to the decrease of the mechanical properties of the composite.

So far, the simulation of various NFRC characteristics on natural fiber is still limited, namely, thermal, aerodynamic, acoustical, vibration, and hygroscopicity. The research on hygrothermal properties of composites plays an important role in aerospace, shipbuilding, etc. In 1968, American research institutions published a report on the effect of moisture on the mechanical properties of carbon fiber reinforced composites. Since the mid-1970s, there have been numerous literature reports on the hygrothermal properties of synthetic fiber composites. The fibers in synthetic fiber (such as glass fiber and carbon fiber) composites are generally non-hygroscopic. Theoretically, the wet diffusivity of composites can be predicted by the wet diffusivity of the resin matrix and the percentage of fiber. However, natural fibers are different from synthetic fibers. All-natural fibers are hydrophilic, which is the main disadvantage of natural fibers. Natural fibers tend to absorb water, so their mechanical properties will degrade over time. The degradation of the mechanical properties of these natural fiber composites in humid environments limits their potential applications. Natural fiber composite materials are widely used in various fields of composite materials, which is the starting point of current research, so they must be protected from moisture.

Temperature and humidity have significant effects on the mechanical properties of natural fiber reinforced composites, especially the long-term mechanical properties. The high water absorption of natural fiber, as Table 2 shows, is incompatible

Table 2 Saturated moisture absorption of different natural fibers at 65% RH

Fiber	Saturated moisture absorption (%)
Flax fiber	7
Hemp fiber	7
Abaca fiber	7
Tequila fiber	8
Sisal fiber	7

with a hydrophobic polymer, resulting in the performance degradation of natural fiber composites.

The heat resistance of fiber reinforced resin-based composites is usually characterized by its glass transition temperature, and dynamic thermomechanical analysis tests can determine its value. The bending vibration of the material measures the modulus and loss factor during the constant temperature heating process. The temperature change curve and the temperature corresponding to the maximum loss on the curve is the glass transition temperature. During the damp-heat aging process, certain molecular motion units in the resin matrix are inhibited or activated, and these changes can be reflected in changes in the glass transition temperature. The glass transition temperature is mainly affected by the resin matrix. The research results show that most resin-based composite materials' glass transition temperature decreases with the extension of the damp and heat time, and the initial decline is relatively rapid. As the moisture absorption of the composite material becomes saturated, the glass transition temperature also tends to a constant value.

The reasons for the changes in the heat resistance of composite materials due to damp-heat aging mainly include two aspects: temperature-induced resin post-curing (chemical changes) and composite materials' swelling and plasticizing physical changes. The post-curing of the resin increases the cross-link density of the composite material, which will cause the glass transition temperature to increase. The moisture absorption of the composite material will cause the water molecules and some polar groups in the matrix to destroy the cross-linking points formed by the interaction of the original polar groups in the matrix. In addition, the water molecules are small in volume and easy to permeate and diffuse, which makes the matrix have a plasticizing effect, provides greater free volume for segment movement, and reduces the glass transition temperature of the material – the effects of post-curing and moisture absorption on the glass transition temperature conflict with each other. In a certain period, which factor plays a major role depends on the material system and curing process. The material system cured at room temperature is more sensitive to post-curing. The post-curing speed is faster under damp and heat conditions, and the material system cured at high temperature (the curing temperature is higher than the damp heat test temperature) is less sensitive to post-curing. The moisture absorption rate of different material systems is also different. The system with more polar hydrophilic groups absorbs moisture quickly, and the system with polycondensation and solidification is prone to produce more micropores and absorb moisture faster. In a material system that absorbs moisture quickly, the decrease in glass transition temperature caused by moisture absorption can offset the increase in glass transition temperature caused by post-curing. Therefore, under two opposite factors, the changing trend of the heat resistance of different composite materials is not entirely the same.

After the fiber reinforced resin-based composite material absorbs moisture, its mechanical properties will change with the moisture absorption rate. Different mechanical properties (tension, compression, bending, shear, etc.) have different influencing factors, and the material parameters that control them are also different. Therefore, the influence of the humid and hot environment on the different mechanical properties of

composite materials depends on the material parameters that control the properties. Humid and hot environments affect the situation. The effect of the hot and humid environment on the mechanical properties of composite materials is mainly realized by different degrees of damage to the resin matrix and the bonding interface between reinforcing fibers and resin.

The results show that the axial tensile properties of unidirectional composites are mainly controlled by the reinforcing fibers, and most of the reinforcing fibers hardly change during the hygrothermal aging process, so the axial tensile properties of the composites do not affect by the hygrothermal environment. The transverse, compressive, flexural, and shear properties of quasi-isotropic laminates and unidirectional composites are mainly controlled by the resin matrix and the interfacial bond strength between the matrix and the fiber, so these properties decrease with the increase of the damage degree of the matrix and the interface between the matrix and the fiber. The higher the temperature and the higher the humidity, the greater the decline of these mechanical properties. When the equilibrium moisture absorption rate is reached, it will drop to the lowest point. The higher the equilibrium moisture absorption rate, the lower the retention rate of these mechanical properties. The more serious the damage of the composites by hygrothermal aging is.

When the influence of hygrothermal aging on the mechanical properties of fiber reinforced resin matrix composites is mainly through the resin matrix and matrix/fiber interface, the specific mechanism includes the following aspects: the resin matrix is plasticized and softened by absorbing water, resulting in a considerable decrease in modulus, and its supporting effect and ability to transmit loads are weakened; the resin matrix absorbs water to produce micro-cracks and crack propagation, resulting in a decrease in the strength of the matrix; the matrix resin and the reinforcing fiber absorb moisture and expand, but the coefficient of thermal expansion is inconsistent. The matrix cracks extend to the fiber and break the chemical bond of the matrix resin/fiber bonding interface, causing the resin/fiber interface to break and debond. The hot and humid environment affects the mechanical properties of fiber reinforced resin composites and affects the failure mode. The specific failure mode depends on the strength of the matrix and the fiber/resin interface strength. If the latter is greater than the former, the matrix is destroyed first; if the latter is smaller than the former, interface failure occurs. Most of the dry environment damage at room temperature is the mixed damage of the matrix and the interface, and the damage in the interface under the high temperature and high humidity environment is mostly.

Some investigators have studied the hygroscopic behavior of natural fiber composites in a hot and humid environment. Doan and coworkers studied the moisture absorption properties of jute fiber reinforced polypropylene composites (Doan et al. 2007). They discovered that the diffusion process of water in jute fiber reinforced polypropylene composites in accordance with Fick's law. With the increase of fiber content, the moisture absorption increased, and the moisture absorption of modified polypropylene composites decreased compared with unmodified polypropylene composites. Dhakal and coworkers studied the moisture absorption behavior of hemp fiber reinforced unsaturated polyester composites in room temperature water

bath and boiling point water bath (Dhakal et al. 2007). The results show that the water absorption increases with the increase of fiber volume fraction due to increased porosity and cellulose content. They also noted that the water absorption process of these composites conforms to Fick's law at room temperature but not at high temperature. Meanwhile, Espert and coworkers studied the hygroscopic behavior of natural fiber composites at different temperatures (Espert et al. 2004). It was discovered that the hygroscopic process in line with Fick's second law, and the diffusion coefficient is related to temperature.

The mechanical properties of natural fiber reinforced composites decrease after moisture absorption. Some researchers have indicated the effect of moisture absorption on the mechanical properties of natural fiber reinforced composites. Duigou and coworkers pointed out the effect of moisture content on flax fiber reinforced epoxy composites' properties (Duigou et al. 2013). They learned that the interfacial shear strength decreased with the increase of immersion time, decreased rapidly 15 min before immersion, and stabilized. Espert and co-researchers studied the hygroscopic behavior of natural fiber composites at different temperatures, observing the samples' morphological changes before and after contact with water by using a scanning electron microscope, and found the destructive effect of water on the fiber structure (Espert et al. 2004). Similarly, in their research, Yan and coworkers studied the hydrothermal aging mechanism of unidirectional flax fiber reinforced epoxy composites (Yan and Bing 2016). It was noticed that the different expansion between the matrix and fiber resulted in the change of mechanical properties of the composites. Meanwhile, Takemura (2009) studied the effect of water absorption on hemp fiber reinforced composites' mechanical properties. They discovered that the water absorption rate increased with the increase of water absorption time. The water absorption rate reached at equilibrium stage within 30 days, and the duration had nothing to do with the fiber volume fraction. After 182 days in water, the strength reduced by 70%, and after drying, the strength recovered by 57%. After water absorption, the strength of resin and fiber declined by 62% and 13%, respectively. The decrease of composite strength was due to the influence of the matrix.

There are only a few studies that involved the FEA in investigating natural fiber reinforced composite hygrothermal properties. For instance, Jain and co-researchers studied the mass diffusion of agave/epoxy NFRC under several environmental conditions. The average length of the fiber is 2.8 m, and the diameter is between 100 and 150 m (Jain et al. 2019). In addition, the fibers mentioned above are considered to be homogeneous and isotropic. The water concentration distribution of agave NFRC treated by sodium hydroxide and washed with water at 75 °C was observed. It was indicated that the hygroabsorbability of the composite materials increased with the increase of time. The finite element analysis results are in good agreement with the experimental results (Vats et al. 2020).

Based on the law of minimum thermal resistance and the law of equivalent specific thermal conductivity, a meso-mechanical model of effective thermal conductivity of short fiber hybrid composites is established (Devireddy and Biswas 2016). The thermal conductivity of composite materials in finding the effective thermal conductivity of a short hybrid fiber reinforced polymer was numerically

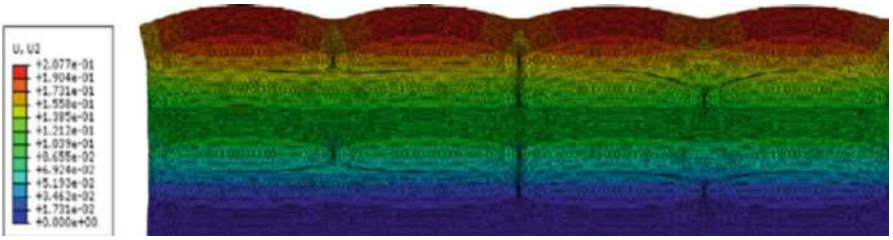

Fig. 10 Swelling of the flax-epoxy specimens at saturation with different fiber expansion coefficient. (From Chilali et al. (2018) with permission)

calculated using the steady-state thermal conductivity. Experimental results and analytical methods are used to verify the proposed model and numerical results. The effective thermal conductivity predicted by the model and the finite element method is in good agreement with the experimental values within the acceptable ranges of 0 ~ 6.5% and 0 ~ 11%, respectively.

Since the experimental study of water diffusion in natural fiber-based composites is a long process, numerical analysis was conducted. Numerical simulation of moisture diffusion helps predict the moisture increase of composite materials over time. Once the results are verified at the sample level, they can extend to the component level to obtain a clear image of the increase in moisture of the entire product made of composite materials. This can be used to guide the optimal design of new natural fiber-based composite materials.

In order to simulate the hydro-elastic behavior of twill linen fabric reinforced epoxy composites, Chilali and co-researchers estimated the water diffusion coefficient and hygroscopic expansion parameters of flax fibers (Chilali et al. 2018). The dimensional changes of the flax epoxy resin samples before and after the aging treatment are obtained through experiments. The transverse expansion rate is about 6.45%, and the warp and weft changes are almost insignificant. Finite element simulations reveal a high mechanical stress concentration at the fiber-matrix interface caused by the differential swelling between the flax fabric and the epoxy resin. Figure 10 depicts the transverse displacement distribution of the flax-epoxy composites at saturation. When the natural fiber is combined with the polymer matrix, the accessibility of the plant fiber to water is significantly reduced, thereby limiting the expansion of the plant fiber. Therefore, the expansion coefficient of the fiber in the resin is very different from the expansion coefficient of the plant fiber alone in water.

Conclusion

This chapter provides a comprehensive summary of recent studies on modeling and simulation of epoxy/natural fiber composites behavior. The resin infiltration process, tensile, flexural, impact, compression, moisture absorption, and thermal properties

are concerned. In terms of numerical calculation and analysis, most studies pay attention to the mechanical properties of composites, such as tensile, bending, and impact. However, few studies are focusing on their hygroscopic, thermal, and acoustic properties. Flax and hemp are the most considered fibers in the modeling and simulation of NFRC regardless of the theoretical analysis or FEA. ANSYS is the most used finite element analysis platform in NFRC modeling and simulation, including solid element and shell element.

Acknowledgments Thanks to the Ministry of Higher Education (MOHE) of Malaysia via research grant LRGS/1/2019/UKM-UKM/5/1, National Natural Science Foundation of China (Project 11,802,205), and Tianjin Research Innovation Project for Postgraduate Students (Project: 2020YJSB063).

References

M. Alhijazi, Q. Zeeshan, Z. Qin, B. Safaei, M. Asmael, Nanotechnol. Rev. **9**, 853 (2020)
A. Ali, M.A. Nasir, M.Y. Khalid, S. Nauman, K. Shaker, S. Khushnood, K. Altaf, M. Zeeshan, A. Hussain, J. Mech. Sci. Technol. **33**(9), 1–10 (2019)
D. Bender, J. Schuster, D. Heider, Compos. Sci. Technol. **66**, 2265 (2006)
H.W. Bergmann, R. Prinz, Int. J. Numer. Methods Eng. **27**, 323 (2010)
B. Berk, R. Karakuzu, B.M. Icten, V. Arikan, Y. Arman, C. Atas, A. Goren, J. Compos. Mater. **50**(25), 3551–3559 (2016)
M. Brod, G. Just, A. Dean, E. Jansen, I. Koch, R. Rolfes, M. Gude, Thin-Walled Struct. **139**, 219 (2019)
D. Chandramohan, A. Presin, Data Br. **13**, 460 (2017)
Y. Chemisky, F. Meraghni, H. Bougherara, Compos. Part B Eng. **119**, 168–183 (2017)
X. Chen, M.H. Fu, L. Hu, Smart Mater. Struct. **28**(8), 085004 (2019)
A. Chilali, M. Assarar, W. Zouari, H. Kebir, R. Ayad, Compos. Struct. **206**, 177 (2018)
J. Datta, M. Woch, Polym. Bull. **71**, 3035 (2014)
M.M. Davoodi, S.M. Sapuan, D. Ahmad, A. Aidy, A. Khalina, M. Jonoobi, Mater. Des. **32**, 4857 (2011)
S. Devireddy, S. Biswas, Proc. Inst. Mech. Eng. Part L J. Mater. Des. Appl. **1464420716656883 35**(15), 1157–1172 (2016)
H.N. Dhakal, Z.Y. Zhang, M. Richardson, Compos. Sci. Technol. **67**, 1674 (2007)
T. Doan, H. Brodowsky, E. Mader, Compos. Sci. Technol. **67**, 2707 (2007)
R. Dragonetti, M. Napolitano, L. Boccarusso, M. Durante, Appl. Acoust. **167** 107379 (2020)
R.K. Du, F.F. Wang, X.H. Chen, Y.F. Zhang, G.Z. Zhao, Y.Q. Liu, Adv. Mater. Res. **753–755**, 236 (2013)
A.L. Duigou, P. Davies, C. Baley, Compos. Part A Appl. Sci. Manuf. **48**, 121 (2013)
A. Espert, F. Vilaplana, S. Karlsson, Compos. Part A Appl. Sci. Manuf. **35**, 1267 (2004)
A. Fotouh, J.D. Wolodko, M.G. Lipsett, Compos. Part B Eng. **62**, 175 (2014)
Y. Glouia, Y. Chaabouni, A.E. Oudiani, I. Maatoug, S. Msahli, Int. J. Adv. Manuf. Technol. **103**(9–12) 4671–4680 (2019)
S. Goudar, R.K. Jain, D. Das, Polym. Compos. **41**, 505–521 (2020)
A.K. Gupta, R. Velmurugan, M. Joshi, Int. J. Crashworthiness **23**, 87 (2018)
U.S. Gupta, M. Dhamarikar, A. Dharkar, S. Tiwari, R. Namdeo, Adv. Compos. Hybrid Mater. **3**(4), 530–540 (2020)
X. Hao, H. Zhou, B. Mu, L. Chen, R. Ou, Compos. Part B Eng. **185**, 107778 (2020)
R. Herd, V. Koen, P. van den Noord, OECD Secretary General (2011). https://www.oecd.org/economy/surveys/publicationsdocuments/reports/11/

D. Jain, I. Kamboj, T.K. Bera, A.S. Kang, R.K. Singla, Int. J. Heat Mass Transf. **130**, 431 (2019)
JEC, *JEC Observer: Overview of the Global Composites Market 2019–2024* (JEC Group, Paris, 2020)
L. Ke, H. Takagi, R. Osugi, Z. Yang, Compos. Sci. Technol. **72**, 633 (2012)
M. Khaldi, A. Vivet, A. Bourmaud, Z. Sereir, B. Kada, J. Appl. Polym. Sci. **133**(31), 43760 (2016)
R. Koh, B. Madsen, Mech. Mater. **124**, 26–32 (2018)
C. Kong, H. Park, H. Lee, J. Lee, Int. J. Mater. Mech. Manuf. **2**, 256 (2014)
G.R. Kumar, R. Vijayanandh, M.S. Kumar, S.S. Kumar, in *2nd International Conference on Condensed Matter & Applied Physics.*, ed by M.S. Shekhawat, S. Bhardwaj, B. Suthar (2018). AIP Conference Proceedings, Bikaner, INDIA
Lee, Heow, Pueh, Kureemun, Umeyr, Tran, Le, Quan, Ngoc, Zhong, Int. J. Appl. Mech. **9**, 1750045 (2017)
E. Mahdi, A. Hamouda, B.B. Sahari, Y.A. Khalid, Appl. Compos. Mater. **10**(2), 67–84 (2003)
C. Menna, D. Asprone, G. Caprino, V. Lopresto, A. Prota, Int. J. Impact Eng. **38**, 677 (2011)
J. Naveen, M. Jawaid, A. Vasanthanathan, M. Chandrasekar, Model. Damage Process. Biocomposites, Fibre-Reinforced Compos. Hybrid Compos **6**, 39–44 (2019)
D. Pantaloni, A. Bourmaud, C. Baley, M.J. Clifford, M.H. Ramage, D.U. Shah, Materials (Basel). **13**(21), 4811 (2020)
A.Y. Patil, N.U. Hrishikesh, G.D. Basavaraj, G.R. Chalageri, K.G. Kodancha, Mater. Today-Proceedings **5**, 7532 (2018)
M. Pervaiz, M.M. Sain, Resour. Conserv. Recycl. **39**, 325 (2003)
M.Z. Rahman. Mechanical Performance of Natural / Natural Fiber Reinforced Hybrid Composite Materials Using Finite Element Method Based Micromechanics and Experiments. (2017). UTAH STATE UNIVERSITY, Logan, Utah
M. Ramesh, P. Sudharsan, Silicon **10**(3), 47–757 (2017)
M. Ravandi, U. Kureemun, M. Banu, W. Teo, L. Tong, T. Tay, H. Lee, J. Compos. Mater. **53**(12), 1717–1734 (2018)
A. Riccio, A. Raimondo, S. Saputo, A. Sellitto, M. Battaglia, G. Petrone, Compos. Struct. **202**, 909 (2018)
D.U. Shah, P.J. Schubel, P. Licence, M.J. Clifford, Compos. Sci. Technol. **72**, 1909 (2012)
S.S. Shinde, A.V. Salve, S. Kulkarni, Mater. Today Proc. **4**, 1683 (2017)
B.L. Sy, Z. Fawaz, H. Bougherara, Compos. Part A Appl. Sci. Manuf. **126**, 105582 (2019)
K. Takemura, Key Eng. Mater. **417–418**, 161 (2009)
S. Vats, T.K. Bera, D. Jain, Arab. J. Sci. Eng. **45**, 1207 (2020)
G. Xiang, D. Yin, R. Meng, S. Lu, J. Appl. Polym. Sci. **137**(24) 48796 (2020)
C. Xiaoquan, D.U. Xiaoyuan, J. Beijing Univ. Aeronaut. Astronaut. **47**(7), 1311–1322 (2020)
L. Yan, X. Bing, Polym. Degrad. Stab. **126**, 144 (2016)

Recycling and Biodegradation Studies of Epoxy/Natural Fiber Composites

30

G. Rajeshkumar, S. Arvindh Seshadri, and T. K. Gowtham Keerthi

Contents

Abstract

In the recent years, the natural fiber-reinforced epoxy composites are widely used for various structural applications owing to their high strength-to-weight and stiffness-to-weight ratios, high corrosion resistance, and low cost. Recent modifications in the waste management regulations, as well as environmental awareness among the society, necessitate the establishment of recycling routes for epoxy-based natural fiber composite materials, if they are to remain competitive. Furthermore, the biodegradable property of these composites also plays a vital role in the waste management, because day by day the usage of composites is being increased, and the adoption of recycling methods alone does not satisfy the

G. Rajeshkumar (✉) · S. A. Seshadri · T. K. G. Keerthi
Department of Mechanical Engineering, PSG Institute of Technology and Applied Research, Coimbatore, Tamil Nadu, India
e-mail: rajesh@psgitech.ac.in

S. Mavinkere Rangappa et al. (eds.), *Handbook of Epoxy/Fiber Composites*,
https://doi.org/10.1007/978-981-19-3603-6_49

requirements. In this context, this chapter briefly presents an overview of the recycling methods available to recycle and biodegradation behavior of the epoxy-based natural fiber composites.

Keywords

Natural fibers · Biodegradation · Recycling · Epoxy

Introduction

Recently, the usage of natural fiber-based composites (NFCs) for various industrial applications have been increased due to the environmental consciousness (Rajeshkumar et al. 2021b; Rajeshkumar 2021). These types of composites have high strength-to-weight ratio and high corrosion resistance, are low cost, and are biodegradable (Rajeshkumar et al. 2021f; Ravikumar et al. 2020). The properties of the NFCs are influenced by the binding capability among the constituents, type of materials, and manufacturing process used for fabrication (Karthi et al. 2021; Nagarjun et al. 2020; Nagarjun et al. 2021). The fully biodegradable composites are not highly suitable for outdoor applications; therefore, partial biodegradable composites fabricated by reinforcing the natural fibers into the synthetic resins are preferred for such applications. For most of the partial biodegradable composites, epoxy matrix have been used due to its unique properties such as high mechanical strength, low viscosity, excellent dimensional stability, resistance to moisture absorption, etc. (Mittal and Chaudhary 2019).

The biodegradable composites support to reduce the landfill sites all over the world. However, the production of biodegradable resins with good properties is costlier than the synthetic resins, and its use is restricted to some specific applications. The biodegradability of composites is dependent on the constituents used and their chemical structure. Biodegradation is caused by biological activity, primarily the enzymatic behavior of microorganisms and can be assessed over time using standard tests. In the case of epoxy-based composites, the weight loss due to degradation will be minimum, and a literature reported that the weight loss of pure epoxy was ranging between 0.3 and 0.5% (Chee et al. 2019). On the other hand, the recycling of composites also supports to maintain the healthy environment. However, the recycling of the epoxy is a very challenging task, because it is a cross-linked polymer and is highly impossible to remold by the application of heat (Pickering 2006). In the recent years, high priority is given to the waste management, which promotes the usage of different methods such as mechanical comminution and thermal process for recycling the thermoset resins. In this chapter, the previous works which reported the methods available to recycle and biodegradation behavior of the natural fiber/epoxy composites are highlighted.

Natural Fibers

Natural fibers are the fibers which are obtained from plants, minerals, and animals (Fig. 1). Fibers are hair-like material that has continuous filaments or elongated pieces. They can be used as reinforcement for making composites and are also used in a wide range of applications (Sumesh et al. 2021; Rajeshkumar et al. 2021c).

Natural fibers are having advantages like low cost, easy availability, recyclable, and biodegradable and are used in applications like aerospace, automotive, marine, building and construction, etc. (Rajeshkumar et al. 2021a, e). Some of the disadvantages are hydrophilicity, low strength, and low durability (Rajeshkumar et al. 2021d). Most of the researches are going on to overcome these disadvantages. Natural fibers have three main structural components, namely, cellulose, hemicellulose, and lignin. Plant fiber comprises of primary cell at the outer side, three secondary walls at the interior side, and lumen at the center. The fiber quality depends on the harvest phase (fiber thickness and adhesion between the fiber), growth of the plant (location of the crop and climatic conditions), and supply phase (method of transportation). Therefore, to obtain the best quality of fibers, the above conditions should be optimized (Sanjay et al. 2019; Ramakrishnan et al. 2021). A natural fiber at microlevel consists of fibers and matrices. The fibers are made by cellulose, and matrices are made by lignin and hemicellulose. During the growth of cell, fiber is made up of primary cell which is covered by the secondary cell. The secondary cell is made up of three layers in which the middle layer determines the property of the fiber (Vinayagamoorthy 2017).

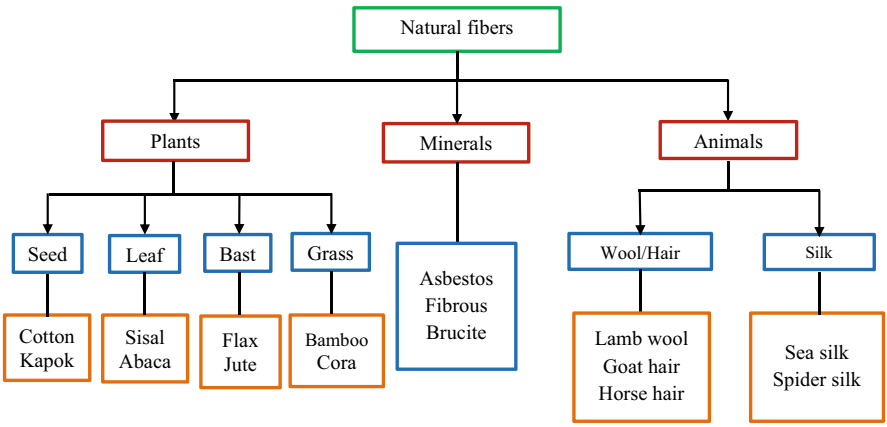

Fig. 1 Classifications of natural fibers

Epoxy Resin

Epoxy resin were discovered in 1909 by Prilezhaev (Jin et al. 2015). Epoxy is a thermosetting polymer obtained from the monomer that contains at least one or more epoxide groups. They can be cross-linked or homopolymerized into a 3D curative. The epoxy resins which are employed in commercial applications are oligomers of diglycidyl ether of bisphenol A (DGEBA). The two major classes of epoxies are non-glycidyl and glycidyl epoxies. Glycidyl epoxy resins can be divided into glycidylamine, glycidyl-ester, and glycidyl-ether. Epoxies are now mixed with a variety of curing agents/hardener, such as anhydrides, amines, and amides. Among these, amine-based hardeners are most commonly used. When compared to polyester or vinyl ester, epoxy necessitates the usage of larger amount of curing agents. The commonly adopted resin to hardener ratio is 1:1 or 2:1. The pros and cons of the epoxy resins can be tailored by the chemical structure of the resin and hardener (Saba et al. 2016). Epoxy resins have found various applications (Fig. 2) due to their extraordinary mechanical properties, good adhesion strength, and high electrical resistance (Rajeshkumar et al. 2021c; Jin et al. 2015). Epoxy which is a thermoset does not melt, unlike thermoplastics. Hence, it cannot be reprocessed once the network is formed. Epoxy resin can be used to produce parts with complex shapes as the monomers have low viscosity, which enables easy shaping and fixing after the monomers have cured (González et al. 2012).

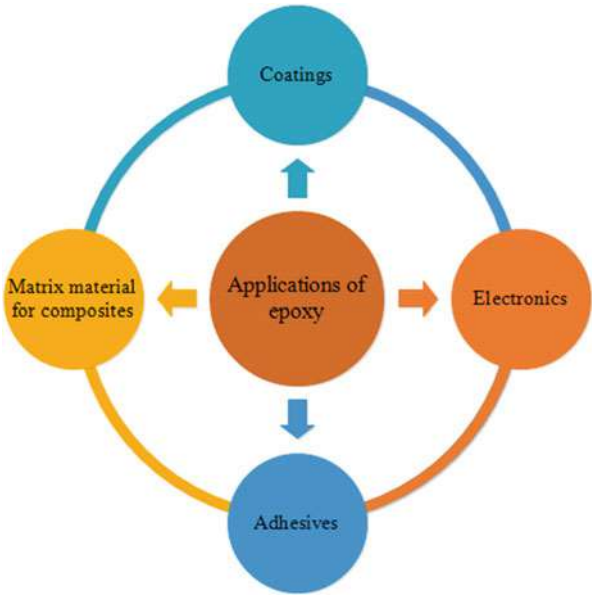

Fig. 2 Applications of epoxy

Recycling of Epoxy/Natural Fiber Composites

In the past three decades, the world has witnessed a significant change in the usage of materials in various commercial and domestic applications. There has been a tremendous increase in the usage of polymer matrix composites materials (specifically epoxy-based composite materials). Additionally, epoxy-based natural fiber composites have also found widespread application in the last few years. These trends raise a few important questions related to the end-of-life disposal of the components made from epoxy-based natural fiber composites. Therefore, it has become an indispensable task to recycle epoxy-based natural fiber composites. However, it is an arduous task to replace epoxy-based composites, and the cost connected with recycling is much greater than disposal in landfills (Pickering 2006).

In order to solve the issues of recycling epoxy/natural fiber composites, researchers have studied different methods to recycle epoxy and their composites. These can be classified into three major types: mechanical, chemical, and thermal, (Fig. 3). Among these, mechanical and thermal methods are the most common; however, chemical methods are also gaining attention in the recent past (Yang et al. 2012; Cestari et al. 2019).

Mechanical Recycling

The principle behind the mechanical recycling process is as follows: The size of the composites is reduced using a mechanical force or by grinding. This method is practically a more feasible option than other recycling processes. However, it is important to note that the energy required to break down the composite materials

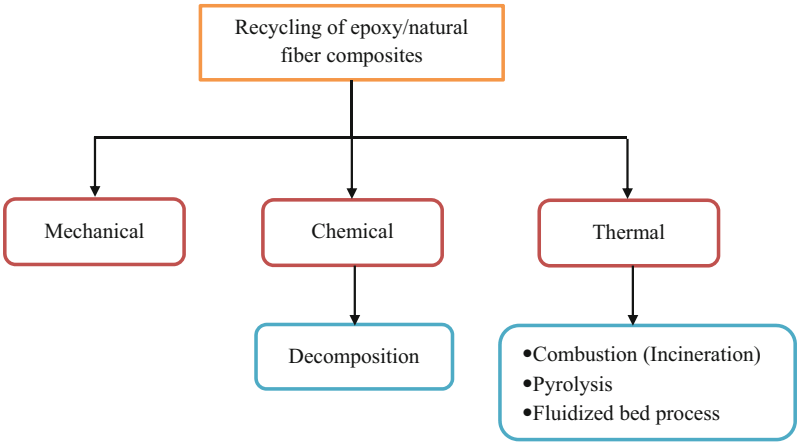

Fig. 3 Methods to recycle epoxy/natural fiber composites

Table 1 Different types of grinding machines and their mechanism (Inoh et al. 1994)

Type of grinding machine		Grinding mechanism
Ball mill	Air classifier	–
	Rolling vibration and epicyclic mill	Compression and impact
Roll mill	Roller	Compression between rollers
Jet mill	Air impact	Attrition among particles
	Impact board	Impact
High-speed hammer mill	Screen classifier	Impact between hammer and particles
Others	Mortar, stone mill	Attrition

mechanically is significantly high, which makes it a less economically attractive method. The first step in mechanical grinding is to break the composite into smaller particles. This is followed by the breakdown of the smaller particles using advanced equipment (Asmatulu et al. 2014). The different types of grinding machines and their mechanism are listed in Table 1.

Perrin et al. (2006) put forward another method consisting of two steps to recycle epoxy-based composites. In the initial step, the composite is transformed into fine powder with the help of mechanical grinding. This is followed by the shredding and the partial dissolution of filler material in an acidic solution. A major difficulty in recycling epoxy-based natural fiber composites is separation of the fiber from the epoxy resin.

Chemical Recycling

The recycling of epoxy resins is a difficult process because of their complex cross-linked structure. Chemical recycling is a more effective method in breaking and reversing the chemical structure of epoxy into its original constituents. This method can be utilized to degrade epoxy-based products and their composites. However, as there are fibers present in epoxy-based composites, it is a complicated and tedious task to recycle them. Chemical recycling can be classified into various classes based on the technique and chemicals utilized (Morales Ibarra 2018). This is illustrated in Fig. 4.

A significant amount of research was performed by Dang et al. (2002, 2005), on the recycling of epoxy and their composites using chemical methods. The decomposition of epoxy was carried out with the help of nitric acid, following which the products were repolymerized using a suitable curing agent. The cured epoxy resin exhibited low resistance to nitric acid. This characteristic can be effectively utilized to recycle epoxy-based products.

Another process by which the chemical structure of epoxy can be broken down is by solvolysis (Asmatulu et al. 2014). In this process, solvents and heat are used to break the chemical structure. Different solvents, such as alcohols (Piñero-Hernanz

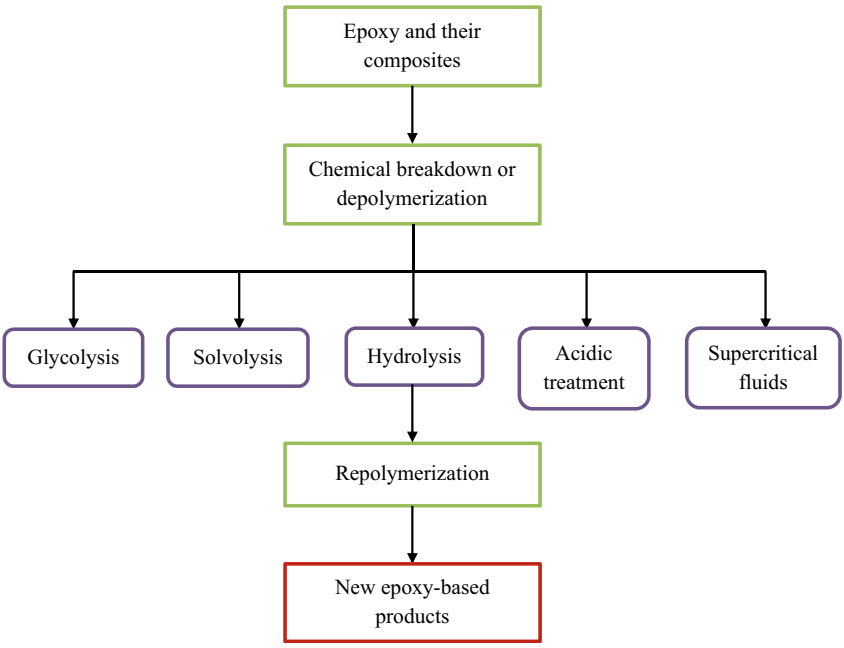

Fig. 4 Classification of chemical recycling process

et al. 2008), acetone at super critical condition, etc., are used. Super critical ammonia has been used to decompose the structure of epoxy (Mormann and Frank 2006).

There have also been other interesting works which deal with the use of acids to decompose the structure of epoxy (Jyothi V. Sunny 2016). Enzymes can also be utilized to degrade epoxy-based products. Another method is to create molecules with cleavable epoxide groups (Buchwalter and Kosbar 1996) and produce biodegradable epoxy resins (Datta and Włoch 2014).

On the whole, chemical recycling is an interesting option to recycle epoxy-based natural fiber composites as it allows for the repolymerization of residue for new products (Morales Ibarra 2018).

Thermal Recycling

Energy Recovery Using Combustion

In this method, the composites are combusted to recover the energy in the form of heat. The energy is majorly recovered from the epoxy resin, which is of smaller proportion in the composite compared to fillers and fibers. The fillers and fibers are combustible and make up the largest portion of the composites. The calorific value of epoxy resins is in the order of 30,000 kJ.kg. The inorganic substances that are obtained from the combustion process is used as additives in the cement industry (Asokan et al. 2009).

Pyrolysis

In pyrolysis, epoxy/natural fiber composites are heated to extremely high temperature in absence of oxygen, to break it down to smaller particles. The organic part of the composites which is broken down in the form of oils and gases are used as fuels. Pyrolysis can be used to break down the polymer network along with energy recovery, which can then be used as feedstock in chemical processing (Jyothi V. Sunny 2016).

Pyrolysis has become a standard method to recycle polymer-based products, and it can be done in various types of reactors (Blazsó 2009; Yun et al. 2014). Several composite manufacturers have also adopted pyrolysis to recycle polymer-based composite materials.

Biodegradation Studies of Natural Fiber/Epoxy Composites

In biodegradation tests, the composites are buried in the soil, where they are exposed to moisture and microbial attack. The microbial attack on the polymer (epoxy) causes degradation of molecules which results in the formation of pores and microcracks on the matrix surface. The water molecules can enter through these gaps and reach the hydrophilic natural fibers. The fiber swells as it absorbs more water, causing more stress at the interfacial site, and this leads to microcrack formation. These microcracks in the composites act as an entry point to water content, thus causing fungal growth around the swollen fiber, which ultimately reduces the properties of the natural fiber/epoxy composites. The biodegradation process occurs in natural fiber-based polymeric composites as depicted in Fig. 5.

Jute/Epoxy Composites with Wood Dust Fillers

Jute fiber-based epoxy composites were prepared, and their biodegradation behavior was studied by Dinesh et al. (Dinesh et al. 2020). In addition to the jute fibers, wood dust fillers (rosewood and padauk) were also added to the epoxy to produce hybrid composites (Table 2).

Biodegradation test was done by using bacterial suspension of the composites (of size $50 \times 50 \times 3$ mm^3). The test was carried out for 48 days, and the weight of the samples was noted at regular intervals of time.

The results indicated that the weight of the composites increased initially for 27 days, after which it started to reduce. W2 composite was found to be less biodegradable because of its low water absorption capacity. The composites W1 and W3 possessed greater biodegradability, when compared to W2 composite, as they exhibited good moisture absorption capacity. The maximum biodegradability was achieved in the case of W4 composite due to the poor wettability present between matrix and fiber.

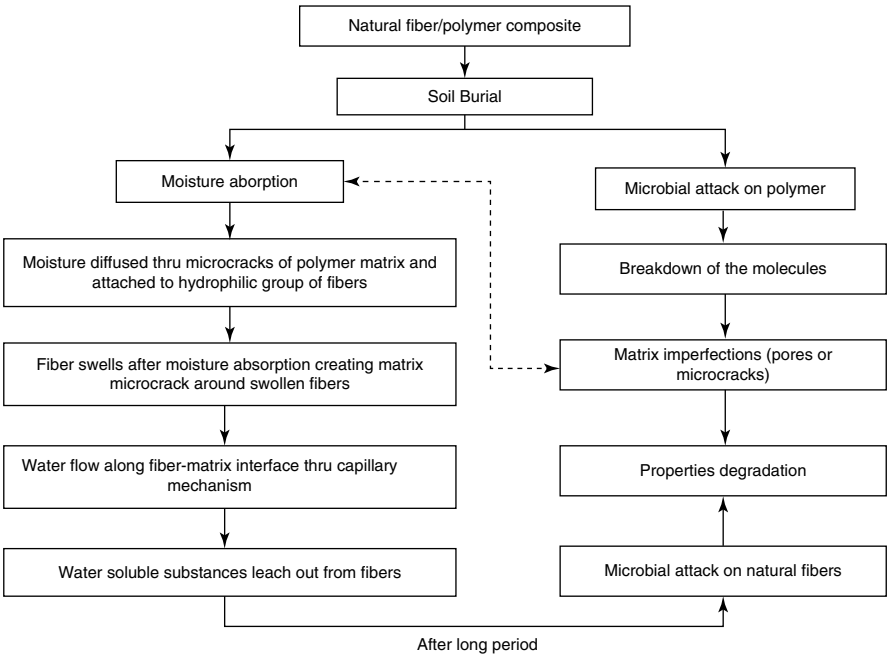

Fig. 5 Process of biodegradation of natural fiber-based polymer composites. (Reproduced with permission from Elsevier, license number: 5056411316624) (Chee et al. 2019)

Table 2 Formulation of composites/hybrid composites

Designation	Wood filler (wt.%)		Jute fiber (wt.%)	Epoxy (wt.%)
	Rosewood	Padauk		
W1	10	–	50	40
W2	–	5	50	40
W3	5	5	50	40
W4	–	–	50	50

Bamboo/Kenaf/Epoxy Hybrid Composites

The matrix material was epoxy (bisphenol A), while amine was utilized as the hardener. The resin-to-hardener ratio was fixed at 2:1. The reinforcements that were used were kenaf and bamboo mats that had a density of 0.8 kg/m^2 and 0.6 kg/m^2, respectively (Chee et al. 2019). The respective chemical compositions of the fibers used are enlisted in Table 3. Bamboo/kenaf composites with different compositions (Table 4) were manufactured

Soil burial test was conducted to determine the biodegradable nature of the composite specimens. The specimens were divided into the rectangular plates of

Table 3 Chemical composition of bamboo and kenaf fibers

Natural fiber	Cellulose (wt.%)	Hemicellulose (wt.%)	Lignin (wt.%)
Bamboo	72.6	11.1	9.5
Kenaf	65.7	17.8	6.0

Table 4 Composition of bamboo/kenaf/epoxy hybrid composites

Specimen	Epoxy content (wt.%)	Bamboo content (wt. %)	Kenaf content (wt.%)
Epoxy	100	0	0
Epoxy/bamboo	60	40	0
Epoxy/kenaf	60	0	40
Epoxy/bamboo/kenaf (30/70)	60	12	28
Epoxy/bamboo/kenaf (50/50)	60	20	20
Epoxy/bamboo/kenaf (70/30)	60	28	12

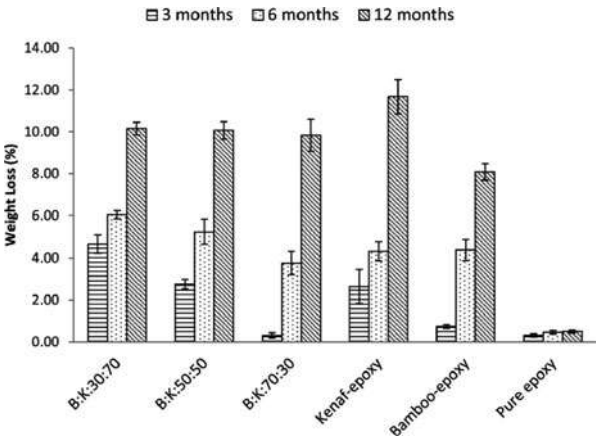

Fig. 6 Biodegradation or weight loss (%) of bamboo/kenaf/epoxy hybrid composites. (Reproduced with permission from Elsevier, license number: 5056411316624) (Chee et al. 2019)

dimensions 10 cm × 4 cm. The biodegradation study was conducted for a time period of 3, 6, and 12 months. The specimens were kept in a polybag, and two holes were provided for water and air circulation. They were then buried at a depth of 10 cm from the surface. When the time arrived for testing, the samples were removed and rinsed with deionized water. This was followed by drying the samples in an oven at 70 °C for one day and storing them in a desiccator. Subsequently, the weight loss was calculated (Fig. 6). When the samples are underground, biodegradation occurs due to moisture and the enzymatic action by microorganisms, causing the sample to lose its weight. When the burial time increases, weight loss of the material also increases significantly. High percentage of kenaf fiber led to high weight loss after

3 and 6 months. Among hybrid composites, epoxy/bamboo/kenaf (30/70) had maximum degradability. The weight loss of the specimen after 3, 6, and 12 months were 4.66%, 6.05%, and 10.15%, respectively. Epoxy/bamboo/kenaf (70/30) had the lowest biodegradable capacity with a weight loss of 0.31% and 3.76% after 3 and 6 months, and it had been increased to 9.83% after 12 months. On the other hand, pure epoxy had minimum biodegradability with a weight loss of 0.3 to 0.5% during the testing period. It has been said that hemicellulose is the fiber component that plays a vital role in biodegradation and moisture component.

Pineapple Leaf/Coir/Epoxy Hybrid Composites

Epoxy resin of grade LY 556 and hardener [TETA (triethylenetetramine)] was used. The ratio of resin to the harder were taken as 2:1 (Mittal and Chaudhary 2019). Coir and pineapple fibers were used as reinforcements, whose chemical compositions are listed in Table 5. The composites were alkali treated with NaOH solution, and experiment was conducted with both alkali-treated composites and untreated composites. There were 23 different biocomposites samples, including alkali treated and untreated, developed during the experiment.

Composites reinforced with raw and alkali-treated fibers were buried under the soil for 110 days, and their weight loss (%) was recorded. The specimen was taken out after every 10 days from the soil, and it was rinsed with deionized water and dried at 70 °C for one day. The weight loss of an epoxy thermoset was found to increase when it was mixed with PALF-coir fiber. On comparing with all the other composites, pure PALF-epoxy composite exhibited the highest percentage of biodegradability. When the percentage of coir was increased, it was noted that the weight loss in the composites declined. The coir fiber consists of high lignin content (40–45%), which resists the attack of bacteria and microorganisms. Due to this, pure coir composites exhibited least biodegradability. Alkali-treated biocomposites had higher biodegradability than untreated ones. However, certain NaOH-treated composites were found to possess lower biodegradation capability compared to the untreated composites. This was attributed to the removal of hydroxyl and other polar functional groups.

Emu/Epoxy Composites

The matrix employed was epoxy, and emu fiber was utilized as the reinforcement material (V. Chandrasekhar et al. 2015). The composites were produced with

Table 5 Chemical compositions of coir and pineapple fibers

Natural fiber	Cellulose (wt.%)	Hemicellulose (wt.%)	Lignin (wt.%)
Coir	32–43	0.15–0.25	40–45
Pineapple leaf (PALF)	70–82	18.8	5–12.7

different percentage of the fiber (1 wt.% to 5 wt.%). The composites were then buried under the earth for experimental purpose. The biodegradation test was conducted at Hyderabad, and it was divided into two segments.

In the first segment, the test was performed by exposing the composites to the atmosphere. The weight loss of composite reinforced with 5 wt.% of fibers was noticed to be 0.82% after one month. At the end of the second month, the weight loss rose to 1.36%, following which it remained unaltered. Similarly, the weight loss for other percentages of fiber was shown in graph. The authors also observed that the weight loss of the composites increased with the increase in fiber weight fraction.

In the second segment, the composites were buried under the soil at a depth of 0.3 m. The composite reinforced with 5 wt.% of fiber exhibited a weight loss of around 1.4% after the first month. This value reached to approximately 1.8% at the end of the second month, after which no change was observed in the weight loss.

Conclusions and Future Perspective

The natural fiber-based composites are widely in automobile, aerospace, construction, and sporting applications. In particular, the automobile industries are showing concern about recyclability of its parts. However, the recycling issues are more complex due to knowledge limitations, engineering challenges, lack in selection and development of materials, and composite life cycle studies. On the other hand, the epoxy-based natural fiber composites are considered as the partial biodegradable composites, since the epoxy polymers are non-biodegradable ones. Therefore, at present, the epoxy-based natural fiber is very poor in terms of recycling and biodegradation. A scientific or technological breakthrough is highly expected to reuse such composites; hence, a lot of scope is there for the researchers to satisfy the above requirements.

References

E. Asmatulu, J. Twomey, M. Overcash, Recycling of fiber-reinforced composites and direct structural composite recycling concept. J. Compos. Mater. **48**, 593–608 (2014). https://doi.org/10.1177/0021998313476325

P. Asokan, M. Osmani, A.D.F. Price, Assessing the recycling potential of glass fibre reinforced plastic waste in concrete and cement composites. J. Clean. Prod. **17**, 821–829 (2009). https://doi.org/10.1016/j.jclepro.2008.12.004

M. Blazsó, Pyrolysis for recycling waste composites. Manag. Recycl. Reuse Waste Compos. **102–121** (2009). https://doi.org/10.1533/9781845697662.2.102

S.L. Buchwalter, L.L. Kosbar, Cleavable epoxy resins: Design for disassembly of a thermoset. J. Polym. Sci. Part A Polym. Chem. **34**, 249–260 (1996). https://doi.org/10.1002/(SICI)1099-0518(19960130)34:2<249::AID-POLA11>3.0.CO;2-Q

S.P. Cestari, D.F. da Silva Freitas, D.C. Rodrigues, L.C. Mendes, Recycling processes and issues in natural fiber-reinforced polymer composites, in *Green Composites for Automotive Applications*, ed. by G. Koronis, A. Silva, (Elsevier, 2019), pp. 285–299

V. Chandrasekhar, V. Dr, D. Pandurangadu, T. Subba Rao, Biodegradation of emu feather fiber reinforced epoxy composites. Int. J. Eng. Res. **V4**, 609–613 (2015). https://doi.org/10.17577/ijertv4is060768

S.S. Chee, M. Jawaid, M.T.H. Sultan, et al., Accelerated weathering and soil burial effects on colour, biodegradability and thermal properties of bamboo/kenaf/epoxy hybrid composites. Polym. Test. **79**, 106054 (2019). https://doi.org/10.1016/j.polymertesting.2019.106054

W. Dang, M. Kubouchi, S. Yamamoto, et al., An approach to chemical recycling of epoxy resin cured with amine using nitric acid. Polymer (Guildf) **43**, 2953–2958 (2002). https://doi.org/10.1016/S0032-3861(02)00100-3

W. Dang, M. Kubouchi, H. Sembokuya, K. Tsuda, Chemical recycling of glass fiber reinforced epoxy resin cured with amine using nitric acid. Polymer (Guildf) **46**, 1905–1912 (2005). https://doi.org/10.1016/j.polymer.2004.12.035

J. Datta, M. Włoch, Selected biotrends in development of epoxy resins and their composites. Polym. Bull. **71**, 3035–3049 (2014). https://doi.org/10.1007/s00289-014-1229-8

S. Dinesh, P. Kumaran, S. Mohanamurugan, et al., Influence of wood dust fillers on the mechanical, thermal, water absorption and biodegradation characteristics of jute fiber epoxy composites. J. Polym. Res. **27** (2020). https://doi.org/10.1007/s10965-019-1975-2

M.G. González, J.C. Cabanelas, J. Baselga, Applications of FTIR on epoxy resins-identification, monitoring the curing process, phase separation and water uptake, in *Infrared Spectroscopy-Materials Science, Engineering and Technology*, ed. by T. M. Theophanides, (InTech, 2012), pp. 261–284

T. Inoh, T. Yokoi, K. Sekiyama, et al., SMC recycling technology. J. Thermoplast. Compos. Mater. **7**, 42–55 (1994)

F.L. Jin, X. Li, S.J. Park, Synthesis and application of epoxy resins: A review. J. Ind. Eng. Chem. **29**, 1–11 (2015). https://doi.org/10.1016/j.jiec.2015.03.026

N. Karthi, K. Kumaresan, G. Rajeshkumar, et al., Tribological and thermo-mechanical performance of chemically modified Musa acuminata/Corchorus capsularis reinforced hybrid composites. J. Nat. Fibers **00**, 1–14 (2021). https://doi.org/10.1080/15440478.2020.1870614

M. Mittal, R. Chaudhary, Biodegradability and mechanical properties of pineapple leaf/coir Fiber reinforced hybrid epoxy composites. Mater. Res. Express **6** (2019). https://doi.org/10.1088/2053-1591/aaf8d6

R. Morales Ibarra, Recycling of thermosets and their composites, in *Thermosets: Structure, Properties, and Applications: Second Edition*, ed. by Q. Guo, 2nd edn., (Elsevier Ltd, 2018), pp. 639–666

W. Mormann, P. Frank, (Supercritical) ammonia for recycling of thermoset polymers. Macromol. Symp. **242**, 165–173 (2006). https://doi.org/10.1002/masy.200651024

J. Nagarjun, J. Kanchana, G. Rajesh Kumar, Improvement of mechanical properties of coir/epoxy composites through hybridization with sisal and palmyra palm fibers. J. Nat. Fibers **0478** (2020). https://doi.org/10.1080/15440478.2020.1745126

J. Nagarjun, J. Kanchana, G. RajeshKumar, et al., Enhancement of mechanical behavior of PLA matrix using tamarind and date seed micro fillers. J. Nat. Fibers **00**, 1–13 (2021). https://doi.org/10.1080/15440478.2020.1870616

D. Perrin, C. Guillermain, A. Bergeret, et al., SMC composites waste management as reinforcing fillers in polypropylene by combination of mechanical and chemical recycling processes. J. Mater. Sci. **41**, 3593–3602 (2006). https://doi.org/10.1007/s10853-005-5563-y

S.J. Pickering, Recycling technologies for thermoset composite materials-current status. Compos. Part A Appl. Sci. Manuf. **37**, 1206–1215 (2006). https://doi.org/10.1016/j.compositesa.2005.05.030

R. Piñero-Hernanz, J. García-Serna, C. Dodds, et al., Chemical recycling of carbon fibre composites using alcohols under subcritical and supercritical conditions. J. Supercrit. Fluids **46**, 83–92 (2008). https://doi.org/10.1016/j.supflu.2008.02.008

G. Rajeshkumar, Cellulose fiber from date palm petioles as potential reinforcement for polymer composites: Physicochemical and structural properties. Polym. Compos., 1–11 (2021). https://doi.org/10.1002/pc.26106

G. Rajeshkumar, S. Arvindh Seshadri, G.L. Devnani, et al., Environment friendly, renewable and sustainable poly lactic acid (PLA) based natural fiber reinforced composites – A comprehensive review. J. Clean. Prod. **310**, 127483 (2021a). https://doi.org/10.1016/j.jclepro.2021.127483

G. Rajeshkumar, G.L. Devnani, J.P. Maran, et al., Characterization of novel natural cellulosic fibers from purple bauhinia for potential reinforcement in polymer composites. Cellulose **28**, 5373–5385 (2021b). https://doi.org/10.1007/s10570-021-03919-2

G. Rajeshkumar, V. Hariharan, S. Indran, et al., Influence of sodium hydroxide (NaOH) treatment on mechanical properties and morphological behaviour of Phoenix sp. fiber/epoxy composites. J. Polym. Environ. **29**, 765–774 (2021c). https://doi.org/10.1007/s10924-020-01921-6

G. Rajeshkumar, A. Seshadri, K.R. Sumesh, K.C. Nagaraja, Influence of Phoenix sp. fiber content on the viscoelastic properties of polymer composites, in *Materials, Design, and Manufacturing for Sustainable Environment*, ed. by S. Mohan, S. Shankar, G. Rajeshkumar, (Springer, Singapore, 2021d), pp. 131–139

G. Rajeshkumar, S.A. Seshadri, M.B. Mohammed, et al., Eco-friendly wood fibre composites with high bonding strength and water resistance, in *Eco-Friendly Adhesives for Wood and Natural Fiber Composites*, ed. by M. Jawaid, T. A. Khan, M. Nasir, M. Asim, (Springer, Singapore, 2021e), pp. 105–122

G. Rajeshkumar, S.A. Seshadri, S. Ramakrishnan, et al., A comprehensive review on natural fiber/nano-clay reinforced hybrid polymeric composites: Materials and technologies. Polym. Compos. **42**(8), 3687–3701 (2021f)

S. Ramakrishnan, K. Krishnamurthy, G. Rajeshkumar, M. Asim, Dynamic mechanical properties and free vibration characteristics of surface modified jute fiber/nano-clay reinforced epoxy composites. J. Polym. Environ. **29**, 1076–1088 (2021). https://doi.org/10.1007/s10924-020-01945-y

P. Ravikumar, A.R. Suresh, G. Rajeshkumar, An investigation into the tribological properties of bidirectional jute/carbon fiber reinforced polyester hybrid composites. J. Nat. Fibers **0478** (2020). https://doi.org/10.1080/15440478.2020.1764444

N. Saba, M. Jawaid, O.Y. Alothman, et al., Recent advances in epoxy resin, natural fiber-reinforced epoxy composites and their applications. J. Reinf. Plast. Compos. **35**, 447–470 (2016). https://doi.org/10.1177/0731684415618459

M.R. Sanjay, S. Siengchin, J. Parameswaranpillai, et al., A comprehensive review of techniques for natural fibers as reinforcement in composites: Preparation, processing and characterization. Carbohydr. Polym. **207**, 108–121 (2019). https://doi.org/10.1016/j.carbpol.2018.11.083

K.R. Sumesh, V. Kavimani, G. Rajeshkumar, et al., Effect of banana, pineapple and coir fly ash filled with hybrid fiber epoxy based composites for mechanical and morphological study. J. Mater. Cycles Waste Manag. (2021). https://doi.org/10.1007/s10163-021-01196-6

J.V. Sunny, Recycling of polymer belnds and composites (epoxy blends). Recycl. Polym. Methods Charact. Appl., 209–222 (2016)

R. Vinayagamoorthy, A review on the polymeric laminates reinforced with natural fibers. J. Reinf. Plast. Compos. **36**, 1577–1589 (2017). https://doi.org/10.1177/0731684417718385

Y. Yang, R. Boom, B. Irion, et al., Recycling of composite materials. Chem. Eng. Process. Process Intensif. **51**, 53–68 (2012). https://doi.org/10.1016/j.cep.2011.09.007

Y.M. Yun, M.W. Seo, G.H. Koo, et al., Pyrolysis characteristics of GFRP (Glass Fiber Reinforced Plastic) under non-isothermal conditions. Fuel **137**, 321–327 (2014). https://doi.org/10.1016/j.fuel.2014.08.001

Applications and Drawbacks of Epoxy/Natural Fiber Composites

31

Akarsh Verma, Naman Jain, and Radha Raman Mishra

Contents

Abstract

Epoxy is a thermosetting polymer and due to its versatile characteristic it is made useful as matrix material in fabrication of polymer composite. Wide diversity of epoxy composites make its application in different industries such as coating, insulator, electric components, adhesives, sound acquisition, automobile, packaging, construction material, etc. The major application of epoxy composites is in the area of thermal insulation such as electric switch board, decorative article coating, tiles, and other civil constructions works. Another important property of epoxy composite is of good electric insulator as compared to metal matrix composites. But there are also some limitations such as low impact strength,

A. Verma (✉)
Department of Mechanical Engineering, University of Petroleum and Energy Studies, Dehradun, India

N. Jain
Department of Mechanical Engineering, Meerut Institute of Engineering and Technology, Meerut, India

R. R. Mishra
Department of Mechanical Engineering, Birla Institute of Technology and Science, Pilani, India
e-mail: rraman.mishra@pilani.bits-pilani.ac.in

S. Mavinkere Rangappa et al. (eds.), *Handbook of Epoxy/Fiber Composites*,
https://doi.org/10.1007/978-981-19-3603-6_32

nonbiodegradability, delamination, brittleness, and fracture toughness behavior, which limit its applications. To overcome these limitations, certain measures have been taken by different researchers such as incorporation of natural fibers, modification in chemical structure, particle reinforcement, etc.. Natural fibers come out as one of the prominent sources of reinforcement material for polymer composites due to their high strength and modulus of the fibers, fiber dispersion, fiber-matrix adhesion, and increase in toughness of the matrix. In this chapter overview of natural fibers with their advantages and disadvantages as reinforcement material in polymer composites has been provided. Studies of thermosetting polymer mainly epoxy resin including its thermal, mechanical, and chemical properties also have been done. Comparison of thermosetting resin with thermoplastic resin and curing stages of epoxy composites is discussed. Application of epoxy composites reinforced with natural fiber as thermal and electrical insulator is done in detail.

Keywords

Epoxy resin · Natural fibers · Composites · Applications · Drawbacks

Introduction

Both thermosets and thermoplastic polymers are widely employed as matrix component for the composites materials. Thermoplastic polymers are linear/branched organic long chains formed by combining together the same repeated structure called monomers. There are weak secondary bonds between these long chains of molecules, which provide mechanical stiffness and strength. As a matter of the fact that the chemical bonds (between the molecules) can be easily broken, thermoplastic materials can be easily remelted. On the other hand, thermosetting polymers are composed of three dimensionally networked molecules or rigid and long cross-linked chains; therefore, once polymerized, these types of polymers cannot be softened by heating. Usually there are several performance dissimilarities between the thermosetting and thermoplastic matrices. The highly cross-linked structure of thermosets polymers composites provides potential for higher service temperatures and modulus of elasticity as compared with the thermoplastics. But thermoplastics polymer composites often have very high ductility and impact strength as compared to the thermosets polymer composites.

Among the numerous issues that persuade processability are the processing requirements such as the pressure, time and temperature, and matrix viscosity. Low viscosity eases the impregnation of the reinforcement phase, where each reinforcement (in the form of fiber) should be ideally enclosed by the matrix phase (without any kind of voids). Melt viscosity of the fully polymerized thermoplastics is higher than the thermosets matrices. Due to highly viscous nature of thermoplastics, high pressure is essential to get the identical degree of material flow as with the thermosets case, but in various cases this difference is not so much. Major

Table 1 Outline of disadvantages and advantages of thermoplastic and thermoset polymers

Property	Thermoplastic	Thermoset
Young's modulus	Medium	High
Recyclability	Good	Limited
Toughness	High	Medium
Processing temperature	High	Low
Viscosity	High	Low
Processing pressure	High	Low
Health concern	Less	More
Cycle time	Short	Long
Service temperature	High	High
Shelf life	Long	Short

advantages of thermoplastics polymer is that they only need to be melted, shaped, and then ultimately cooled to attain dimensional stability at one go. On the other hand, one of the disadvantages of thermosets polymer is that it takes several days to achieve about 90% cross-link. Another disadvantage of thermosets is that they make chemical reaction involving toxic substance and chemical reactions which are unpleasant to work. In disparity, the structure (molecular) of fully polymerized thermoplastics composes them chemically inert if processed rightly, signifying that no harmful substances need to be thought of. Table 1 reviews the disadvantages and advantages associated with thermoplastic and thermoset polymeric materials.

Natural Fiber

Fibers are hair-like materials which are discrete elongated pieces or continuous filaments. They are majorly of two types: synthetic fiber and natural fiber. Fibers obtained from the vegetables, animals, or minerals sources are known as natural fibers. Some of them can be spun into the filaments form, threads, or ropes. They can be utilized as reinforcement phase inside the composites materials domain. Organic natural fibers can be derived from either the animal or plant sources. The chief chemical structures are based on the proteins for animal fibers and cellulose for the plant fibers. Cellulose-based fibers are of most attention for composites as they are relatively stronger, easy to extract, low cost, and stiffer than their animal counterparts. Mallick (1993) (Mallick 1993) characterized the fibers on the basis of their aspect ratio. The distribution of fiber dimensions in a sample can be characterized by taking ratio of the length and diameter of the individual fibers and assuming a cylindrical geometry. Natural occurring fibers have maximum density of about 1.5 grams/cc. On the other hand, some natural fibers such as wood fibers have hollow and have low densities in their original form and can be densified through processing techniques (Saxena et al. 2008). Some other parameters which play important roles in the characterization of fiber reinforcement composites are the volume fraction of fibers, strength and modulus of the fibers, fiber-matrix adhesion, fiber dispersion, and toughness of the matrix phase. Chemically natural fibers are composted of

lignocellulosic, i.e., helically wound cellulose microfibrils binded by the lignin matrix and hemicellulose. The chemical composition, i.e., percentage of cellulose, hemi-cellulose, lignin, etc. of natural fibers varies depending upon the fiber type (Young 1986; Mohanty et al. 2001; Zafeiropoulos et al. 2002). Henceforth, based on work of Bledzki et al. (Bledzki et al. 1996), all natural fibers are hydrophilic in nature (can absorb water) and their moisture regain can reach up to approximately 3–13%. Properties of the natural fibers such as mechanical properties, crystallinity, bonding to the matrix, and fiber variability should be well thought-out when picking the appropriate cellulose fibers for use in the composites domain. Mechanical properties are more significant when choosing a cellulose fiber to give the preeminent reinforcement in a composite domain. Lilholt and Bjerre (Lilholt and Bjerre 1997) in the year 1997 compared the properties different novel natural fibers used for fabrication of composites material.

Advantages of the Natural Fibers

- Production with low cost and investment when compared to high-performance fibers which make natural fibers prominent material for developing countries.
- Thermal recycling of natural fiber is also possible whereas a glass fiber causes environment issue during combustion.
- Many researchers reported that natural fiber–based composites have higher specific strength and stiffness and the low specific weight as compared to synthetic fiber glass.
- They provide better acoustic, thermal, and electrical insulation properties, particularly as switch boards, construction material part, and automotive interior, due to the presence of void/lumen in fiber domain.
- These natural fibers do not cause any lung diseases or allergies if breathed in or came into contact with.

Disadvantages of Natural Fibers

- The price of fibers can fluctuate by harvest (Mohanty et al. 2002).
- Lower durability due to high environmental degradation (Joshi et al. 2004).
- Hydrophilic nature of natural fibers results in moisture absorption which causes swelling of fibers.
- Lower strength, stiffness, and particularly impact strength as compared with other reinforced composites (Marsh 2003).

Other factors such as the age of plant, growing environment, species, quality of soil, humidity, and temperature influence the qualities of natural fibers. There are different fields where natural fiber can be engaged: automobile, nonstructural composites, structural composites, geotextiles, moulded products, filters, sorbents, packaging, and in combinations with other materials (Fowler et al. 2006; Ashori 2008).

Dweib et al. (Dweib et al. 2004; Dweib et al. 2006) reported that many components of automobiles are already produced with biodegradable composites; mainly used matrix was polyester or polypropylene and fibers like hemp, flax, and sisal. The aim of use of natural fiber is weight reduction, low price, and marketing rather than technical demands. The present applications of the natural fiber are in the field of biodegradable composites to produce high strength, impact, and energy absorption composites, such as bicycle helmets and car fenders (Saheb and Jog 1999; Aminabhavi et al. 1990; Rout et al. 2001) and targeting the markets for biodegradable, cheaper, and biocompatible materials, such as structural elements and packaging (Varma et al. 1986). Taylor in 2002 (Taylor 2002) reported many applications of wood powder–based composites such as carpeting on the consoles, doors, trunk liners, headlines, and seat backs. These composites have 50% polypropylene and 50% wood flour with other additives for appearance and performance enhancements. Taylor (2002) (Taylor 2002) also reported that other uses of wood fiber–based composites are picnic tables, industrial flooring, deck surface boards, etc.

Epoxy Resin

Epoxy is thermosetting resin (polymerizable in nature) that exhibits excellent corrosion resistance, less shrinkage, high tensile strength, low creep, high modulus, etc. and hence broadly used. The chief shortcoming of epoxy resin is that it takes long curing time, possesses brittle nature, and its decrement of properties in the existence of water/moisture environment (Saadati et al. 2005). Increasing demands of light weight material for industrial and commercial application result in fabrication and characterization of polymer-based composites. To fulfill the current demands of society thermosetting resin–based composites come out to be more promising materials having application in different areas such as automobile, packaging, coating, furniture, construction, etc. Versatile characteristics of epoxy thermoset resin–based composites are its wide diversity which made it suitable for coating, packaging, insulator, automobile, construction, etc. applications. Epoxy monomer structure consists of three-member ring formed between two carbon atoms and an oxygen atom. Carbon atoms of ring are electrophilic in nature due to dissimilar electronegativity of oxygen and carbon atom. This atomic arrangement results in highly reactive nature of epoxy to undergo ring opening reaction in the presence of nucleophiles.

Now a days researchers shifted their interest toward multifunctioning epoxy resin. Due to dynamic nature of the market, digitalization and automation of production lines in manufacturing companies, as well as demands of smart material with multifunctional performance are increasing. Requirement of smart materials with multifunctional performance also causes breakthrough in plastic/polymer/composite industry. As major market of polymer industry is ruled by epoxy resin, therefore researchers modify the epoxy resin through chemical treatment, or tailor the properties by blending and reinforcement. Some of the major areas where research is been going on are recyclability issue or biodegradability, brittleness, curing process,

high temperature stability, electrical conductivity, etc. To improve toughness of epoxy composites, carbon nanotubes, nano-titanium dioxide, grapheme, nano-silica or nano-silica rubber, and polysiloxane rubber have been used by different researchers (Domun et al. 2015; Zha et al. 2017; Pinto et al. 2015; Liu et al. 2016; Kamar and Drzal 2016; Carolan et al. 2016; Dong et al. 2014; Naebe et al. 2014). Other works also reported that toughness or mechanical properties as well as glass transition temperature of epoxy plastic also can be improved with the help of hyperbranched polymers (Miao et al. 2015). Another disadvantage of epoxy product is that after cross-linking, size and shape changeability takes place in the thermoplastic materials. Covalent adaptable networking concept is then employed by the researchers to tailor the epoxy product to make it thermoplastic in nature. This concept has been facilitated by vitrimer polymers having cross-linked polymer network which thermally activated in such a way that overall network connectivity and cross-linked density is been maintained. Studies also show the double relaxation behavior when vitrimers epoxy was been cured by fatty acid (Snijkers et al. 2017). Another limitation of epoxy polymer–based composites is slow curing process which limits its application in certain fields. Some researchers used catalyst to decrease the curing time even at higher temperature but result in decrement in shell life. Latent curing catalysts/agents such as thios or imidazoles at ambient temperature and at higher temperature phenols or anhydrides are been employed to reduce curing time. Polybenzoxazines (Zhang et al. 2017), 2-(2-hydroxyphenyl) imidazoles (Kudo et al. 2015), triazabicylodecene tetraphenylborate (Konuray et al. 2017), etc. have been used by researchers to enhance the curing process of epoxy resin. With depletion of fossil fuel, the increasing demand of recyclability of plastic product becomes one of the challenges in front of researchers. Various chemical processes, self-healing properties, and biodegradability of the thermoset epoxy polymer have been studied (Ma and Webster 2018; Zou et al. 2017; Scheiner et al. 2016; Urdl et al. 2017). Transesterification reaction in case of epoxy vitrimers enables recyclability, stress relief thermoforming, and self-healing properties. Epoxy composites have their application as structure material, transportation, biomedical implements, aerospace, automobile, etc. These applications field demands self-healing nature of resin with intact thermomechanical properties. Both intrinsic and extrinsic approaches have been employed by the researchers for overcome the early-stage crakes. To overcome the fracture or damage by impact extrinsic self-healing polymers have been used. But benefits of intrinsic self-healing polymer are more and mostly preferred over extrinsic polymers.

Applications of the Epoxy Resin Composites

Curing phases of epoxy resin can be classified into three different phases:

(i) First phase is known as open time/wet layup time; this phase occurs just after the mixing of epoxy and hardener. In this phase mixture remains in liquid stage, i.e., suitable to mould or coating.

(ii) Second phase is gel phase (initial cure epoxy); this phase comes when the cross-linking just initiated and mixture goes into gel phase, i.e., into hard rubber stage. At this phase epoxy surface may still be bonded to or recoated without special preparation but this ability starts diminishing as the time of curing increases.
(iii) Third phase is solid phase where chemical cross-linking reaction is almost completed (about 90%). The mixture that is finally mould into solid state gets some mechanical strength and further be utilized for end product such as insulator, electric board switches, tiles, construction material, etc.

Moderate tensile strength and good impact strength of epoxy-based composites make it more suitable for construction purposes such as tile and floor coating (Pegoretti et al. 1996). Moreover, epoxy composites cannot be reshaped or remould under heat and pressure, therefore make promising material for electric switches/boards (Raquez et al. 2010; Yousefi et al. 1997). Packaging and furniture application of epoxy composites may be attributed to water intake resistance, high cross-linked structure, and resistance to chemical and better thermal stability (Guilleminot et al. 2008; Gourichon et al. 2008). Sekhar et al. (2015) (Sekhar et al. 2015a) did the TGA/DSC analysis on the emu feather–reinforced epoxy composite by varying 1–5% weight of fibers and also varying the lengths from 1–5 cm. Glass transition temperature (Tg) of fiber-reinforced composites was found to be lowered as compared to neat composites. Tg followed inverse relation with the length of the fiber upto 3 cm and then increased upto 5 cm. Addition of fibers had shifted to higher temperature as compared to neat epoxy with having degradation temperature of about 345.5 °C. The addition of emu feather fibers improved the thermal stability. Sekhar et al. (2015) (Sekhar et al. 2015b) explored the chemical resistance characteristic of epoxy (Araldite LY-556) and emu bird feather composites. Fibers were chemically treated with different medium such as acids, alkalis, solvents, etc. before adding to the matrix. Comparatively pure epoxy showed escalated resistance to chemicals. When fibers were treated with acid and base medium weight gain of composites occurred whereas weight loss was observed when treated with solvents like benzene, toluene, and C-tetra chloride. Ozen et al. (2013) (Ozen et al. 2013) fabricated the chicken feather fiber (CFF) and G-fibers hybrid composites with epoxy as matrix phase. Major focus of the fabricated composites is mechanical properties. Reinforcing 10% CFF fiber showed highest tensile strength. Other than that immaculate epoxy showed higher thermal conductivity than CFF reinforced composite. Young's modulus decreases with increase in fiber content and maximum impact strength was obtained at 20% CFF. Mishra (2012) (Mishra 2012) fabricated the rubber-bust epoxy composites to study the dry sliding wear behavior. Lowest wear rate was obtained at 10% rubber dust.

Thermal Insulator

One of the selection criteria for polymer during fabrication of polymer composites is its thermal characteristic. The major areas of application where thermal insulation characteristic of polymer composites required are electric switch board, decorative

article coating, tiles, and other civil constructions works. To measure the thermal conductivity the temperature of two parallel surfaces (T_1 – T_2) is measured at constant heat flux (Q). Equation 1 can be used to calculate the thermal conductivity of the sample mathematically:

$$Q = kA\frac{T_1 - T_2}{t} \tag{1}$$

where t is the thickness of sample and A is cross-section area.

Shalwan et al. (Shalwan et al. 2017) in 2017 studied the insulation characteristic of epoxy composites reinforced with sisal fiber. To measure the thermal conductivity of fabricated epoxy/sisal fiber sample (as per the ASTM D5930–17 standard) three drills from surface to center had been done at interval of 20 mm. To insulate the sample from surrounding M-flex insulation pipe was used. Six thermocouples were used to measure the temperature, placed at each hole of the slab. From one end heat is supplied at 1 kW rate and temperature readings were noted every minute. Temperature stability was reached after 20 minutes. Results show that temperature drop almost become constant after 50 mm. Insulation rate increases from 200 to 400% with increase in sisal fiber content from 20 to 40%. This effect can be correlated with natural fiber structure, i.e., presence of void (Chung 2000; Ramamurthy et al. 2009). But due to alkali treatment of sisal fiber, outer layer was removed and void content decreases which reduces the insulation rate. Wang et al. (Wang et al. 2017) studied the insulation characteristic of epoxy coating with sepiolite/hollow glass microspheres as binary fillers. Mixture of sepiolite (10 vol. %)/hollow glass microspheres (HGM at different content) and epoxy were coated on anodized AZ31B Mg alloy plates. Best results were obtained at 45% of HGM and about 200 °C temperature difference. Thermal conductivity coefficient was also determined with the help of finite element method using ANSYS software. Hassan et al. (Hassan et al. 2020) estimated the thermal properties of epoxy composite reinforced with natural fiber waste obtained from cotton, sugarcane, and coconut. Thermal properties such as diffusivity, linear coefficient of thermal expansion, resistance, and conductivity of the prepared samples were tested. Result shows that with increase in fiber content conductivity of epoxy composites decreases. Moreover, lowest thermal conductivity is shown by coconut fiber–reinforced composites. Lower value of conductivity is correlated to the presence of air void in natural fiber structure. Thermal diffusivity of composites improves due to fiber reinforcement. Sugarcane fiber–reinforced composites show more diffusivity as compared with cotton and coconut fibers due to higher content of lignin and hemicelluloses. Coefficient of thermal expansion (CTE) of cotton fiber–reinforced composite was highest as compared to sugarcane and coconut fiber. This result is correlated with the chemical composition of above three fibers. Cotton fiber contains more cellulose having linear structure as compared with hemicelluloses and lignin, therefore extends more on heat gain. With increase in CTE fiber content decreases. Nanda and Satapathy (Nanda and Satapathy 2020) studied the thermal behavior of short human hair (SHF)/epoxy composites with 10 wt% of solid glass microspheres

(SGM). ASTM E1530–06 standard has been adopted to calculate the thermal conductivity of material. Thermal conductivity of composites having SGM is lower as compared to the epoxy/SHF composites. Moreover, with increase in SHF content thermal conductivity of composites decreases; this may be correlated to lower thermal conductivity of SHF as compared to neat epoxy. There is about 21.76% reduction of thermal conductivity of SHF/epoxy composite at 20 wt% of SHF. It is the ability of the material to get polarized under the external applied electric field. To measure the dielectric constant of the composite material parallel-plate capacitor setup is used where fabricated sample is treated as dielectric material between the two electrode plates.

Dielectric Material

One of the imperative properties of epoxy composite is good electric insulator properties as compared to metal matrix composites. Application of natural fiber–reinforced composites further enhances electric insulation to the epoxy composites. Mathematically dielectric constant of material is calculated by the given formula in Eq. 2:

$$D_k = \frac{Ct}{\varepsilon_o A} \tag{2}$$

where C is the capacitance, t is thickness of sample, ϵ_o is vacuum dielectric constant, and A is the sample area.

Agrawal and Satapathy (Agrawal and Satapathy 2015) studied the effect of short hair fiber (SHF) on dielectric behavior of epoxy composites. With increase in frequency and weight percentage of SHF the dielectric constant of the fabricated composites decreases. This result may be correlated to low dielectric constant and SHF as well as increase in void volume of composites (Kumar et al. 2013). On the other hand, with increase in frequency molecule vibration increases result in improper orientation of dipoles. Dhal and Mishra (Dhal and Mishra 2013) investigated the electric properties by calculating dielectric properties of epoxy composites reinforced with brown grass flower broom (BGFB). Dielectric constant and loss decreases with increase in frequency and become almost constant at higher values of frequency. Variation in dielectric constant and loss with respect to weight content is very ambiguous, at low frequency dielectric constant and loss at 20 wt.% is very high as compared with 10 wt.% and neat composites. This may be correlated to three major factors that are porosity content of composites, material properties, and interracial bonding. Jayamani et al. (Jayamani et al. 2014) investigated the dissipation factor, dielectric properties, and loss factor of epoxy composites reinforced with pineapple leaf fiber (PLF). They also evaluated the effect of frequency, fiber loading, and surface modification of fiber on the abovementioned properties of epoxy/PLF composites. Dielectric constant was evaluated with the help of HP 16451 dielectric test mixture at various weight contents, i.e., 5, 10, 15, and 20 wt%. Alkali treatment of PLF is been done prior reinforcement to epoxy hardener mixture. Both fiber loading and alkali treatment affect dielectric properties of the fabricated composites.

With increase in frequencies dielectric constant decreases and then become constant. Fiber-reinforced composites show higher value of dielectric constant as compared with neat epoxy. Polarizations such as electronic, interracial, dipole, and atomic is the major factor affecting the dielectric constant. Reinforcement of PLF in epoxy composites results in higher interfacial polarization due to heterogeneity at low frequency, and variation in conductivities of the fibers and matrix. Addition of fiber results in interracial and orientation polarization which increases the dielectric constant. Moreover, dielectric constant decreases with increase in frequency which may be credited to the space polarization. Dielectric constant of the epoxy depends upon the polarity of the polymer chain other than that crystallization, temperature, branching, and applied voltage frequency which also play the important role (Izdebska and Thomas 2015). Raw natural PLF fiber contains moisture which has high dipole characteristic which results in overall improvement of dielectric constant of composite. Alkali treatment results in removal of hemicelluloses and constituent of xylene and substantial portion of uronic acid that further improves crystallinity and reduction in the sorption capacity of the PLF (Izdebska and Thomas 2015). One of the applications for natural fiber/epoxy composite is reported by Zhan et al. (Zhan et al. 2011) as printed circuit boards. They have used chicken feather fiber (CFF) as the natural fiber for reinforced material. The results show that CFF-epoxy composite has higher electric resistance as compared with E-glass.

Applications and Drawbacks of Natural Fiber/Epoxy Composites

Various applications of epoxy resin–based natural fibers composites materials include adhesives, skis and snow boards, circuit boards, aerospace components, hockey sticks, boats and ships, insulator rods, pressure vessels, rocket housings, hard tissue and dentist applications, skate boards, aircraft parts, prepreg and autoclave, bicycle frames, vacuum infusion, arrow shafts, wind turbine blades, pipes, packaging, and recreational equipments (Saba et al. 2016).

Major drawbacks of this class of composites are their expensive nature, excessive shrinkage, less resiliency, large variation in properties, and unavailability of components to manufacture them. Instead of having wide range of applications major disadvantages of thermoset polymer composites (like epoxy) are biodegradability and recyclability. Nonbiodegradable nature of epoxy is due to the presence of cross-linked network. During hardening process it reacts irreversibly with the hardener resulting thermoset in nature which cannot be reuse/reshape. The only process left to overcome the plastic pollution is to (a) either burn it under extreme precaution to neutralize the effect of toxic gasses obtained after burning or (b) by land filling the plastic waste. Both cases result in environment issues which is one of the major disadvantages of epoxy-based composites. From past decades researchers/industrialists use epoxy resin in various fields without proper investigation of their biodegradable nature. Shortfall in landfilling areas and nonbiodegradable nature of epoxy becomes one of the major sources of land and water pollutions in the developing

countries. Concerning above issue many developed and developing countries have banned the use of nonbiodegradable plastic use, which results in shifting of researcher's interest toward biodegradable plastics. Epoxy is oil-based resin that comes under petroleum products which is the main reason for pollution. One can expose to the epoxy in different mays such as dermal (contact through skin), inhalation (through vapor), orally (through mouth), etc. Virgin epoxy is nontoxic in nature but on the other hand when mixed with curing agents may damage. Now a days many researchers also found fungal and bacterial microflora which have been extracted from the surface epoxy–based old art works, which gives hope toward the degradation of epoxy composites. In some work, seawater inculcated with bacteria is also been used for degradation of epoxy.

Another area where epoxy composites limit their application is due the hydrophobic nature. Very low water absorption behavior of epoxy composites may be taken as positive side but also have negative impact in some applications such as packaging films for chemicals, detergents, semi-cooked product, membrane, biomedical field, etc. Different researchers working on epoxy composites have also reported the water absorption/uptake test in their work. Reports show that about 10–20% water absorption of fabricated epoxy-based composites and water uptake mainly depends upon the void content. Moreover, if the epoxy-based composites consist of natural fiber as a filer/reinforcement material than with increase in natural fiber content water absorption of composites also increases.

Authors Contribution in this Respective Field

All the authors have contributed a lot in fabricating and characterizing various types of composites (Verma et al. 2018a; Verma et al. 2021a; Verma et al. 2019a; Verma and Singh 2019). We have also extensively worked with natural fibers and polymer composites (both synthetic and natural resins). The applications for which we design the composites were coatings, high toughness, automobile parts, lightweight structures, and vibration isolators (Verma et al. 2019b; Verma et al. 2017; Verma et al. 2018b; Jain et al. 2019; Verma et al. 2019c; Bharath et al. 2020; Verma et al. 2021b; Singh et al. 2020; Verma et al. 2020; Rastogi et al. 2020; Marichelvam et al. 2021; Bharath et al. 2021).

Acknowledgments "Academic and Monetary support from the University of Petroleum and Energy Studies, Dehradun, India (SEED Grant) is gratefully appreciated."

Competing Interests "The authors declare that they have no known competing financial interests or personal relationships that could have appeared to influence the work reported in this chapter."

Animal Research (Ethics) "This chapter does not contain any studies with human participants or animals performed by the authors."

Consent to Publish (Ethics) "The authors give the consent to publish this work."

References

A. Agrawal, A. Satapathy, Effect of Al2O3 addition on thermo-electrical properties of polymer composites: An experimental investigation. Polym. Compos. **36**(1), 102–112 (2015)

T.M. Aminabhavi, R.H. Balundgi, P.E. Cassidy, A review on biodegradable plastics. Polym.-Plast. Technol. Eng. **29**(3), 235–262 (1990)

A. Ashori, Wood–plastic composites as promising green-composites for automotive industries! Bioresour. Technol. **99**(11), 4661–4667 (2008)

K.N. Bharath, P. Madhu, T.G. Gowda, A. Verma, M.R. Sanjay, S. Siengchin, A novel approach for development of printed circuit board from biofiber based composites. Polym. Compos. **41**(11), 4550–4558 (2020)

K.N. Bharath, P. Madhu, T.Y. Gowda, A. Verma, M.R. Sanjay, S. Siengchin, Mechanical and chemical properties evaluation of sheep wool fiber–reinforced vinylester and polyester composites. Mater. Perform. Charact. **10**(1), 99–109 (2021)

A.K. Bledzki, S. Reihmane, J. Gassan, Properties and modification methods for vegetable fibers for natural fiber composites. J. Appl. Polym. Sci. **59**(8), 1329–1336 (1996)

D. Carolan, A. Ivankovic, A.J. Kinloch, S. Sprenger, A.C. Taylor, Toughening of epoxy-based hybrid nanocomposites. Polym. (United Kingdom) **97**, 179–190 (2016). https://doi.org/10.1016/j.polymer.2016.05.007

D.D.L. Chung, Cement reinforced with short carbon fibers: A multifunctional material. Compos. Part B **31**(6–7), 511–526 (2000)

J.P. Dhal, S.C. Mishra, Processing and properties of natural fiber reinforced polymer composites. J. Mater. (2013). https://doi.org/10.1155/2013/297213

N. Domun, H. Hadavinia, T. Zhang, T. Sainsbury, G.H. Liaghat, S. Vahid, Improving the fracture toughness and the strength of epoxy using nanomaterials – A review of the current status. Nanoscale **7**, 10294–10329 (2015). https://doi.org/10.1039/C5NR01354B

W. Dong, H.C. Liu, S.J. Park, F.L. Jin, Fracture toughness improvement of epoxy resins with short carbon fibers. J. Ind. Eng. Chem. **20**, 1220–1222 (2014). https://doi.org/10.1016/j.jiec.2013.06.053

M.A. Dweib, B. Hu, A. O'donnell, H.W. Shenton, R.P. Wool, All natural composite sandwich beams for structural applications. Compos. Struct. **63**(2), 147–157 (2004)

M.A. Dweib, B. Hu, H.W. Shenton Iii, R.P. Wool, Bio-based composite roof structure: Manufacturing and processing issues. Compos. Struct. **74**(4), 379–388 (2006)

P.A. Fowler, J.M. Hughes, R.M. Elias, Biocomposites: Technology, environmental credentials and market forces. J. Sci. Food Agric. **86**(12), 1781–1789 (2006)

B. Gourichon, M. Deléglise, C. Binetruy, P. Krawczak, Dynamic void content prediction during radial injection in liquid composite molding. Compos. A: Appl. Sci. Manuf. **39**(1), 46–55 (2008)

J. Guilleminot, S. Comas-Cardona, D. Kondo, C. Binetruy, P. Krawczak, Multiscale modelling of the composite reinforced foam core of a 3D sandwich structure. Compos. Sci. Technol. **68**(7–8), 1777–1786 (2008)

T. Hassan, H. Jamshaid, R. Mishra, M.Q. Khan, M. Petru, J. Novak, R. Choteborsky, M. Hromasova, Acoustic, mechanical and thermal properties of green composites reinforced with natural fibers waste. Polymers **12**(3), 654 (2020)

J. Izdebska, S. Thomas, *Printing on Polymers: Fundamentals and Applications* (William Andrew, 2015)

N. Jain, A. Verma, V.K. Singh, Dynamic mechanical analysis and creep-recovery behaviour of polyvinyl alcohol based cross-linked biocomposite reinforced with basalt fiber. Mater. Res. Expr. **6**(10), 105373 (2019)

E. Jayamani, S. Hamdan, M.R. Rahman, M.K.B. Bakri, Comparative study of dielectric properties of hybrid natural fiber composites. Procedia Eng. **97**, 536–544 (2014)

S.V. Joshi, L.T. Drzal, A.K. Mohanty, S. Arora, Are natural fiber composites environmentally superior to glass fiber reinforced composites? Compos. A: Appl. Sci. Manuf. **35**(3), 371–376 (2004)

N.T. Kamar, L.T. Drzal, Micron and nanostructured rubber toughened epoxy: A direct comparison of mechanical, thermomechanical and fracture properties. Polym. (United Kingdom) **92**, 114–124 (2016). https://doi.org/10.1016/j.polymer.2016.03.084

A.O. Konuray, X. Fernandez-Francos, X. Ramis, Latent curing of epoxy-thiol thermosets. Polym. (United Kingdom) **116**, 191–203 (2017). https://doi.org/10.1016/j.polymer.2017.03.064

K. Kudo, M. Furutani, K. Arimitsu, Imidazole derivatives with an intramolecular hydrogen bond as thermal latent curing agents for thermosetting resins. ACS Macro Lett. **4**, 1085–1088 (2015). https://doi.org/10.1021/acsmacrolett.5b00601

V. Kumar, N.K. Sharma, R. Kumar, Dielectric, mechanical, and thermal properties of bamboo–polylactic acid bionanocomposites. J. Reinf. Plast. Compos. **32**(1), 42–51 (2013)

H. Lilholt, A.B. Bjerre, Composites based on jute-fibres and polypropylene matrix, their fabrication and characterization, in *Proceedings of the 18th Riso International Symposium on Materials Science: Polymeric Composites – Expanding the Limits*, (Riso National Laboratory, Roskilde, pp. 411–423 (1997)

S. Liu, X. Fan, C. He, Improving the fracture toughness of epoxy with nanosilica-rubber core-shell nanoparticles. Compos. Sci. Technol. **125**, 132–140 (2016). https://doi.org/10.1016/j.compscitech.2016.01.009

S. Ma, D.C. Webster, Degradable thermosets based on labile bonds or linkages: A review. Prog. Polym. Sci. **76**, 65–110 (2018). https://doi.org/10.1016/j.progpolymsci.2017.07.008

P.K. Mallick, *Fiber Reinforced Composites: Materials, Manufacturing and Design*, 2nd edn. (CRC Press (Revised and Expanded), Boca Raton, 1993)

M.K. Marichelvam, P. Manimaran, A. Verma, M.R. Sanjay, S. Siengchin, K. Kandakodeeswaran, M. Geetha, A novel palm sheath and sugarcane bagasse fiber based hybrid composites for automotive applications: An experimental approach. Polym. Compos. **42**(1), 512–521 (2021)

G. Marsh, Next step for automotive materials. Mater. Today **4**(6), 36–43 (2003)

X. Miao, Y. Meng, X. Li, A novel all-purpose epoxy-terminated hyperbranched polyether sulphone toughener for an epoxy/amine system. Polym. (United Kingdom) **60**, 88–95 (2015). https://doi.org/10.1016/j.polymer.2015.01.034

A. Mishra, Dry sliding wear behavior of epoxy-rubber dust composites. Int. J. Mech. Aerospace Indust. Mechatron. Manufact. Eng. **6**(7), 1218–1223 (2012)

A.K. Mohanty, M. Misra, L.T. Drzal, Surface modifications of natural fibers and performance of the resulting biocomposites: An overview. Compos. Inter. **8**(5), 313–343 (2001)

A.K. Mohanty, L.T. Drzal, M. Misra, Engineered natural fiber reinforced polypropylene composites: Influence of surface modifications and novel powder impregnation processing. J. Adhes. Sci. Technol. **16**(8), 999–1015 (2002)

M. Naebe, J. Wang, A. Amini, H. Khayyam, N. Hameed, L.H. Li, Y. Chen, B. Fox, Mechanical property and structure of covalent functionalised graphene/epoxy nanocomposites. Sci. Rep. **4**, 1–7 (2014). https://doi.org/10.1038/srep04375

B.P. Nanda, A. Satapathy, Thermal, acoustic, and dielectric behavior of epoxy-based hybrid composites using short hair fiber. J. Braz. Soc. Mech. Sci. Eng. **42**, 1–12 (2020)

M.S. Ozen, M. Yuksek, M. Uzun, E. Sancak, İ. Usta, O. Atak, Press forming of chicken feather fibre (CFF) reinforced bio-composites: Effects of CFF on mechanical and thermal properties. Nano Studies. **7**, 161–168 (2013)

A. Pegoretti, M.L. Accorsi, A.T. Dibenedetto, Fracture toughness of the fibre-matrix interface in glass-epoxy composites. J. Mater. Sci. **31**(23), 6145–6153 (1996)

D. Pinto, L. Bernardo, A. Amaro, S. Lopes, Mechanical properties of epoxy nanocomposites using titanium dioxide as reinforcement – A review. J. Nano. Res. **95**, 506–524 (2015). https://doi.org/10.4028/www.scientific.net/JNanoR.30.9

K. Ramamurthy, E.K. Nambiar, G.I.S. Ranjani, A classification of studies on properties of foam concrete. Cem. Concr. Compos. **31**(6), 388–396 (2009)

J.M. Raquez, M. Deléglise, M.F. Lacrampe, P. Krawczak, Thermosetting (bio) materials derived from renewable resources: A critical review. Prog. Polym. Sci. **35**(4), 487–509 (2010)

S. Rastogi, A. Verma, V.K. Singh, Experimental response of nonwoven waste cellulose fabric–reinforced epoxy composites for high toughness and coating applications. Mater. Perform. Charact. **9**(1), 151–172 (2020)
J. Rout, M. Misra, S.S. Tripathy, S.K. Nayak, A.K. Mohanty, The influence of fibre treatment on the performance of coir-polyester composites. Compos. Sci. Technol. **61**(9), 1303–1310 (2001)
P. Saadati, H. Baharvand, A. Rahimi, J. Morshedian, Effect of modified liquid rubber on increasing toughness of epoxy resins. Iranian Polym. J. **14**, 637–646 (2005)
N. Saba, M. Jawaid, O.Y. Alothman, M.T. Paridah, A. Hassan, Recent advances in epoxy resin, natural fiber-reinforced epoxy composites and their applications. J. Reinf. Plast. Compos. **35**(6), 447–470 (2016)
D.N. Saheb, J.P. Jog, Natural fiber polymer composites: A review. Adv. Polym. Technol.: J. Polym. Proc. Ins. **18**(4), 351–363 (1999)
M. Saxena, R.K. Morchhale, P. Asokan, B.K. Prasad, Plant fiber—Industrial waste reinforced polymer composites as a potential wood substitute material. J. Compos. Mater. **42**(4), 367–384 (2008)
M. Scheiner, T.J. Dickens, O. Okoli, Progress towards self-healing polymers for composite structural applications. Polym. (United Kingdom) **83**, 260–282 (2016). https://doi.org/10.1016/j.polymer.2015.11.008
V.C. Sekhar, V. Pandurangadu, T.S. Rao, Chemical analysis of emu feather fiber reinforced epoxy composite. Int. J. Eng. Res. Appl. **5**, 67–72 (2015a)
V.C. Sekhar, V. Pandurangadu, T.S. Rao, Evaluation of mechanical properties of emu feather fiber reinforced epoxy composites. Int. J. Emerg. Technol. Adv. Eng. **5**(6), 386–391 (2015b)
A. Shalwan, M. Alajmi, A. Alajmi, Insulation characteristics of sisal fibre/epoxy composites. Int. J. Poly. Sci. (2017)
K. Singh, N. Jain, A. Verma, V.K. Singh, S. Chauhan, Functionalized graphite–reinforced cross-linked poly (vinyl alcohol) nanocomposites for vibration isolator application: Morphology, mechanical, and thermal assessment. Mater. Perform. Charact. **9**(1), 215–230 (2020)
F. Snijkers, R. Pasquino, A. Maffezzoli, Curing and viscoelasticity of vitrimers. Soft Matter **13**, 258–268 (2017). https://doi.org/10.1039/C6SM00707D
A. Taylor, Case study on fibres in composite materials, eg. Hemp in automotive applications. 4th meeting of government-industry forum on non-food uses of crops, GIFNFC 4/4 fibres in composite materials, DTI Conference Centre, London (2002)
K. Urdl, A. Kandelbauer, W. Kern, U. Muller, M. Thebault, E. Zikulnig-Rusch, Selfhealing of densely crosslinked thermoset polymers – A critical review. Prog. Org. Coat. **104**, 232–249 (2017). https://doi.org/10.1016/j.porgcoat.2016.11.010
D.S. Varma, M. Varma, I.K. Varma, Coir fibers. 3. Effect of resin treatment on properties of fibers and composites. Ind. Eng. Chem. Prod. Res. Dev. **25**(2), 282–289 (1986)
A. Verma, V.K. Singh, Mechanical, microstructural and thermal characterization of epoxy-based human hair–reinforced composites. J. Test. Eval. **47**(2), 1193–1215 (2019)
A. Verma, A. Gaur, V.K. Singh, Mechanical properties and microstructure of starch and sisal fiber biocomposite modified with epoxy resin. Mater. Perfor. Charact. **6**(1), 500–520 (2017)
A. Verma, A. Parashar, M. Packirisamy, Atomistic modeling of graphene/hexagonal boron nitride polymer nanocomposites: A review. Wiley Interdiscip. Rev.: Comput. Mol. Sci. **8**(3), e1346 (2018a)
A. Verma, P. Negi, V.K. Singh, Physical and thermal characterization of chicken feather fiber and crumb rubber reformed epoxy resin hybrid composite. Adv. Civil Eng. Mater. **7**(1), 538–557 (2018b)
A. Verma, R. Kumar, A. Parashar, Enhanced thermal transport across a bi-crystalline graphene–polymer interface: An atomistic approach. Phys. Chem. Chem. Phys. **21**(11), 6229–6237 (2019a)
A. Verma, P. Negi, V.K. Singh, Experimental analysis on carbon residuum transformed epoxy resin: Chicken feather fiber hybrid composite. Polym. Compos. **40**(7), 2690–2699 (2019b)

A. Verma, C. Singh, V.K. Singh, N. Jain, Fabrication and characterization of chitosan-coated sisal fiber–Phytagel modified soy protein-based green composite. J. Compos. Mater. **53**(18), 2481–2504 (2019c)

A. Verma, K. Baurai, M.R. Sanjay, S. Siengchin, Mechanical, microstructural, and thermal characterization insights of pyrolyzed carbon black from waste tires reinforced epoxy nanocomposites for coating application. Polym. Compos. **41**(1), 338–349 (2020)

A. Verma, W. Zhang, A.C. Van Duin, ReaxFF reactive molecular dynamics simulations to study the interfacial dynamics between defective h-BN nanosheets and water nanodroplets. Phys. Chem. Chem. Phys. **23**(18), 10822–10834 (2021a)

A. Verma, N. Jain, S.M. Rangappa, S. Siengchin, M. Jawaid, Natural fibers based bio-phenolic composites, in *Phenolic Polymers Based Composite Materials*, (Springer, Singapore, 2021b), pp. 153–168

J. Wang, Y. Tian, J. Zhang, Thermal insulating epoxy composite coatings containing sepiolite/hollow glass microspheres as binary fillers: Morphology, simulation and application. Sci. Eng. Compos. Mater. **24**(3), 379–386 (2017)

R.A. Young, Structure, swelling and bonding of cellulose fibers, in *Cellulose: Structure, Modification and Hydrolysis*, (Wiley, New York, 1986), pp. 91–128

A. Yousefi, P.G. Lafleur, R. Gauvin, Kinetic studies of thermoset cure reactions: A review. Polym. Compos. **18**(2), 157–168 (1997)

N.E. Zafeiropoulos, D.R. Williams, C.A. Baillie, F.L. Matthews, Engineering and characterisation of the interface in flax fibre/polypropylene composite materials. Part I. Development and investigation of surface treatments. Compos. A: Appl. Sci. Manuf. **33**(8), 1083–1093 (2002)

R. Zha, M. Chen, T. Shi, R. Nadimicherla, T. Jiang, Z. Zhang, M. Zhang, Double dimensionally ordered nanostructures: Toward a multifunctional reinforcing nanohybrid for epoxy resin. RSC Adv. **7**, 1177–1190 (2017). https://doi.org/10.1039/C6RA26365H

M. Zhan, R.P. Wool, J.Q. Xiao, Electrical properties of chicken feather fiber reinforced epoxy composites. Compos. A: Appl. Sci. Manuf. **42**(3), 229–233 (2011)

S. Zhang, P. Yang, Y. Bai, T. Zhou, R. Zhu, Y. Gu, Polybenzoxazines: Thermal responsiveness of hydrogen bonds and application as latent curing agents for thermosetting resins. ACS Omega **2**, 1529–1534 (2017). https://doi.org/10.1021/acsomega.7b00075

W. Zou, J. Dong, Y. Luo, Q. Zhao, T. Xie, Dynamic covalent polymer networks: From old chemistry to modern day innovations. Adv. Mater. **29**, 1606100 (2017). https://doi.org/10.1002/adma.201606100

Part III

Epoxy/Synthetic/Natural fiber Hybrid Composites

Introduction to Epoxy/Synthetic/Natural Fibre Composites

32

Lin Feng Ng

Contents

Abstract

Composite materials have shown various outstanding characteristics over metallic alloys. These lightweight materials have been subjected to a continuous evolution over the past decades. Today, composite materials have been broadly applied in several industrial applications such as aerospace and automotive components. In order to reach a balance point between the mechanical properties and environmental concerns, the idea of incorporating two or more types of fibres within a single matrix has been ignited to r1educe the reliance on synthetic fibres. As a result, embedding two or more types of fibres in the polymer matrix has led to the development of advanced hybrid composites. It is well-known that hybrid composites encompass several attractive features compared to non-hybrid

L. Feng Ng (✉)
Centre for Advanced Composite Materials (CACM), School of Mechanical Engineering, Faculty of Engineering, Universiti Teknologi Malaysia, Johor Bahru, Johor, Malaysia
e-mail: linfeng@utm.my

S. Mavinkere Rangappa et al. (eds.), *Handbook of Epoxy/Fiber Composites*,
https://doi.org/10.1007/978-981-19-3603-6_33

composite materials. This chapter intends to provide a comprehensive overview of the synthetic/natural fibre-reinforced epoxy hybrid composites. In particular, the background of the hybrid composites and their constituents are briefly discussed. Moreover, the future trend of hybrid composites is also clearly demonstrated.

Keywords

Hybrid composites · Natural fibres · Synthetic fibres · Epoxy matrix

Introduction

Fibre-reinforced composites are those heterogeneous materials consisting of at least two different constituents which are bonded to each other. Each of the constituents in the composite materials has its unique mechanical and chemical properties. The coalescence of two different materials has resulted in the development of new materials with improved functional properties over each individual constituent. Composite materials can be developed using numerous techniques, such as autoclave, hand lay-up, wet lay-up, vacuum-assisted resin transfer moulding, pultrusion, extrusion, bladder moulding, compression moulding, etc. In composite materials, the matrix has roles in transferring the applied load to the surrounding fibres and maintaining the geometrical shape of the materials. In contrast, the fibres embedded in the polymer matrix act as a load-carrying component, leading to the improved mechanical performance of the materials. There are several types of composite materials; however, fibre-reinforced composites are among the most widely explored composite materials recently. Today, composite materials have been widely employed in various industrial and outdoor applications such as automotive and marine structures, sports equipment, space transport, construction, medicine and electrical components (Scholz et al. 2011; Pickering et al. 2016; Naebe et al. 2016; Yan et al. 2016; Habibi et al. 2018).

It is undoubtedly that composite materials have been subjected to permanent interest among industries and research communities owing to their various excellent characteristics over other materials. In comparison with metal alloys, composite materials are relatively insensitive to fatigue loading, allow more freedom of tailoring the mechanical properties in a judicious way and possess high specific mechanical properties and corrosion resistance, which make them an attractive and alternative material to supersede metal alloys in various industrial fields. Truthfully, the fracture of the structural components is commonly due to fatigue failure. Fatigue failure is sudden, fast and catastrophic. Thus, it may jeopardise the safety of the people. Due to the high fatigue resistance of composite materials, they have attracted the attention of the aerospace industries to employ such materials. Apart from the high fatigue resistance, lightweight and high specific mechanical properties are particularly attractive, since these characteristics can reduce energy consumption

(Ng et al. 2020). It was found that the fibre-reinforced composites are 30–40% lighter than steel of equal strength (Zhang et al. 2012).

Composite materials can be based on synthetic or natural fibres embedded in the polymer matrix. The addition of reinforcing materials in the composites is shown to have some benefits over those monolithic polymer materials. Hence, the majority of the composite materials in the market have been dominated by synthetic fibres such as glass, aramid and carbon fibres primarily due to their high mechanical strength. Even though most of the composite materials are based on synthetic fibres, the contemporary trend has been shifted from the synthetic to natural fibres owing to the increasing environmental awareness and concerns. Synthetic fibre-reinforced thermoset composites are not biodegradable under the normal environmental condition, and they cannot be recycled or reprocessed. This condition eventually results in a large amount of waste production and accumulation. Therefore, a massive effort has been made to explore the feasibility and potential of natural fibres as alternative resources for composite materials to replace synthetic fibres. In an effort to explore the potential of natural fibre-based composite materials, several obstacles such as relatively low mechanical strength and high moisture sensitivity of such materials have arisen. These obstacles have retarded the use of natural fibres in certain load-critical applications. In this regard, the idea of combining different types of fibre in the polymer matrix has been stimulated. Hybrid composites consisting of two or more types of fibre within a single polymer matrix have led to the improvement from the perspective of environmental concerns and mechanical properties. In fact, hybrid composites can be divided into several categories, which are synthetic/synthetic, synthetic/natural and natural/natural hybrid composites (Feng et al. 2020a). However, hybrid composites based on synthetic/natural fibres are especially promising and the most widely explored materials, because such materials are speculated to achieve the goal of developing a sustainable material with high mechanical properties without compromising the environmental friendliness. To expand the possible applications involving natural fibre-reinforced composites, synthetic/natural fibre-reinforced composites as potential hybrid materials have successfully gained the interest of researchers around the world. To date, numerous research studies have been conducted to explore the mechanical properties of synthetic/natural fibre-reinforced epoxy hybrid composites (Kureemun et al. 2018; Sanjay and Yogesha 2018; Safri et al. 2018; Mostafa 2019; Calabrese et al. 2020).

Hybrid Composites

The primary purpose of developing hybrid composites is to improve the overall performance of the materials. When compared to the conventional isotropic materials such as metals, the mechanical properties of hybrid composites can be designed and tailored following the requirements of particular applications. Moreover, the overall performance of the materials can be optimised by hybridising more fibres in the polymer matrix. It had been shown that the shortcomings of one fibre could be

compensated with the advantages of another fibre in the hybrid composites, therefore improving the overall performance of the materials. As reported by Pandya et al. (2011), it is possible to combine the benefits of two fibres while eliminating the less desirable properties. As a result, the properties of hybrid composites could surpass their respective non-hybrid composites. Another reason for achieving the improved mechanical performance of hybrid composites is the diameter of two different fibres. Multiple types of fibres having similar lengths but different fibre diameters provide additional advantages to the hybrid composites. The addition of the fibre with a smaller diameter increases the fibre aspect ratio, which is the ratio of length to diameter, increasing the effective interfacial region. Thus, the stress transfer efficiency in the hybrid composites could be enhanced. Furthermore, the stress can be bridged by the surrounding high elongation fibre after the breakage of low elongation fibre, giving better stress transfer between fibre and matrix (Sreekala et al. 2002). Another benefit of combining two types of fibre with different levels of elongation is the energy absorbing capacity can be increased, and hence the impact strength of the hybrid composites is improved. Subramaniam et al. (2019) performed an indentation test on woven kenaf/glass-reinforced hybrid composite-metal laminates. The mass of the hybrid composites was normalised since the glass and kenaf fabrics have different areal densities. They noticed that the energy absorption of hybrid composite-metal laminates with glass fibres as the outermost skin layers was higher than that of non-hybrid glass fibre-based composite-metal laminates. The outermost glass fibres are able to evenly distribute the applied stress, whereas the middle kenaf fabrics limit the crack propagation.

In the era of industrialisation, the requirements such as high mechanical strength and stiffness, excellent durability and high impact strength are taken into consideration during the material selection process. Meanwhile, low-cost, lightweight and sustainability have also become critical and vital criteria to be considered in order to develop materials that can deliver the optimal desirable properties. To achieve this goal, synthetic/natural fibre-reinforced hybrid composites with several attractive features have been developed. Synthetic/natural fibre-reinforced hybrid composites can be considered as promising materials having high mechanical strength and lightweight characteristics. Concurrently, the incorporation of natural fibre in the hybrid composites can improve the environmental friendliness of the materials. When looking into the research studies focusing on synthetic/natural fibre-reinforced hybrid composites, the majority of the research works aim at reducing the dependence on the synthetic fibres. Synthetic fibres may lead to disposal issues which cause environmental damages, since they are not biodegradable. These disadvantages of synthetic fibres are regarded as the driving factors that expedite the substitution of synthetic fibres with natural fibres. Nevertheless, the substitution of non-hybrid synthetic fibre-based composites with non-hybrid natural fibre-reinforced composites is not realistic due to the several hurdles of natural fibres such as low mechanical strength, high moisture sensitivity and non-uniformity.

Among the various types of synthetic fibre that have been utilised for the hybridisation with natural fibres, glass fibre is the most widely explored synthetic fibre for both the non-hybrid or hybrid composites. The low cost, along with the high mechanical strength, allows glass fibre to be the successor over other synthetic fibres. Cicero et al. (2002) revealed that the improvement in the mechanical properties of hybrid composites is mainly due to the partial incorporation of glass fibre. The improvement in the overall performance of the hybrid composite materials is known as positive hybrid effect. The properties of the hybrid composites are not certainly following the rule of mixture through the direct consideration of properties of each individual constituent. Thus, there may have a positive or negative deviation from the properties estimated using the rule of mixture. The positive hybrid effect can be explained by the crack on the weaker fibre which is bridged by the surrounding stronger fibre, thus improving the mechanical properties of the composite materials. It is estimated that the optimum positive hybrid effect can be acquired when the two hybridising fibres are strain compatible, since the strength of the hybrid composites is also governed by the failure strain of each fibre in the materials (Sreekala et al. 2002).

Theoretically, it is possible to estimate the properties of hybrid composites consisting of different types of reinforcements using the rule of hybrid mixtures, as shown in Eq. 1.

$$P_h = P_{f1}V_{f1} + P_{f2}V_{f2} \tag{1}$$

where P_h is the properties of the hybrid composites to be determined; P_{f1} and P_{f2} indicate the properties of the first and second fibre, respectively; V_{f1} and V_{f2} refer to the volume fraction of each respective fibre in the hybrid composites. It should be mentioned that the total volume fraction of V_{f1} and V_{f2} is equal to 1.

Synthetic Fibre

As mentioned in the previous section, there are several types of synthetic fibres, which include carbon, glass and aramid fibres. Most of the synthetic fibres are manufactured from coal minerals, petroleum and natural gas. Synthetic fibres have been widely explored in innumerable research studies for the past few decades. Synthetic fibre-based composites are lighter than metal alloys, and they possess high strength-to-weight ratio, allowing them as an excellent candidate for various engineering applications. Despite the several attractive advantages offered by synthetic fibres, previous studies have reported the severe drawbacks of synthetic fibres towards the environment and human health. Furthermore, the manufacturing process of synthetic fibres consumes an enormous amount of energy compared to natural fibres. Figure 1 depicts the three widely used synthetic fibres, namely, glass, aramid and carbon fibres.

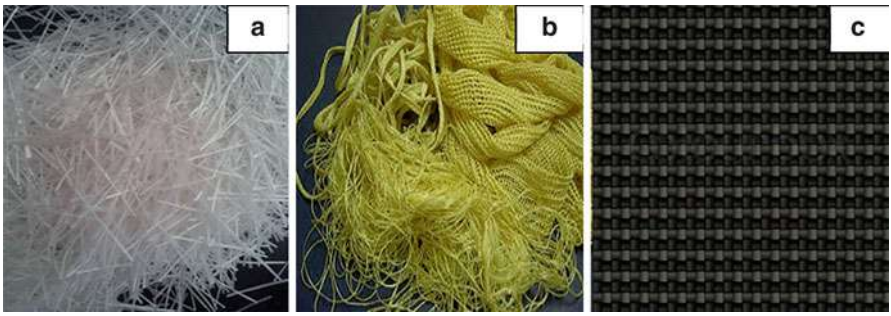

Fig. 1 Typical synthetic fibres: (**a**) glass, (**b**) aramid and (**c**) carbon. (Reprinted with permission from Saba and Jawaid 2017). Copyright 2021, Elsevier

Glass Fibre

In the market, it has been estimated that approximately 90% of the global composite materials are dominated by glass fibre as reinforcement (Shah et al. 2013; Thomason et al. 2014). The balance in high mechanical strength and low cost of glass fibre compared to carbon and aramid fibres has led to its widespread usage around the world. The high mechanical strength of glass fibre is attributed to the silica network structure. Moreover, glass fibre-reinforced composites show a very high energy-absorbing capacity. Ma et al. (2020) reported that the glass fibre-reinforced epoxy composites possessed the highest energy absorption compared to aramid and carbon fibre-reinforced composites. When the mass of the materials was taken into consideration, it was found that glass fibre-reinforced composites had comparable specific energy absorption to the aramid fibre-reinforced composites. Besides, glass fibre also has high thermal stability and excellent moisture resistance. These characteristics allow glass fibre to have stable functional properties and excellent dimensional stability during its service life. Glass fibre is produced from several constituents, including silica, soda, clay, limestone, boric acid and several types of metallic oxides. These constituents are subjected to the heating process involving melting and blending at a temperature of around 1400 °C, and subsequently, the fine filaments of glass fibre are produced.

In general, several grades of glass fibre can be produced by altering the chemical composition to a certain extent. The chemical composition of glass fibre with different grades is shown in Table 1. As can be seen in Table 1, the main constituent of glass fibre is silica, which is followed by other oxides. The purpose of producing different grades of glass fibre is to tailor the mechanical properties to meet the requirements for certain applications. Among several grades of glass fibre, S- and E-glass are the most commonly used fibre in a wide variety engineering applications. E-glass is the most inexpensive glass fibre since its production cost is the lowest among all grades of glass fibre. E-glass fibre is commonly produced for those of engineering applications, where high strength and electrical resistivity are required. In contrast, S-glass possesses the highest tensile strength among all grades of glass

Table 1 Chemical composition of glass fibre with different grades (Derradji et al. 2018). Copyright 2021, Elsevier

GF-type oxide	A-glass (%)	C-glass (%)	E-glass (%)	S-2-glass (%)
SiO_2	63–72	64–68	52–56	64–66
Al_2O_3	0–6	3–5	12–16	24–25
B_2O_3	0–6	4–6	5–10	–
CaO	6–10	11–15	16–25	0–0.2
MgO	0–4	2–4	0–5	9.5–10
BaO	–	0–1	–	–
$Na_2O + K_2O$	14–16	7–10	0–2	0–0.2
TiO_2	0–0.6	–	0–1.5	–
Fe_2O_3	0–0.5	0–0.8	0–0.8	0–0.1
F_2	0–0.4	–	0–1	–

Table 2 Compiled properties of some glass fibres (Gowayed 2013). Copyright 2021, Elsevier

Grade of glass fibre	Density (g/cm^3)	Tensile strength (MPa)	Tensile modulus (GPa)	Strain at break (mm/mm)
E-glass	2.55	3450	72	1.8–3.2
S-glass	2.50	3500	87	4
C-glass	2.49	3300	69	–

fibre, which is particularly developed for military applications. Meanwhile, other grades of glass fibre are also produced for certain other applications. For instance, A-glass, which is the first original type of glass fibre, is primarily used in those applications where high durability, strength and electric resistivity are required. Table 2 depicts the compiled physical and tensile properties of glass fibres with certain grades. It is shown that S-glass exhibits superior tensile properties over E-glass and C-glass, especially the tensile modulus and strain at break, implying that the toughness of S-glass is greater than both E-glass and C-glass. The main shortcomings of glass fibre are high density, non-biodegradable and high abrasion during handling.

The exploration of glass fibre-reinforced composites had been initiated in the last few decades. Glass fibre-reinforced composites exhibit high mechanical strength and low-cost characteristics, which have eventually gained great interest from industries and researchers worldwide. However, the negative impacts on the environment such as non-biodegradable characteristic and high energy consumption of glass fibre have restricted its applications and continuous exploration in the industries and research fields. An effort has been made towards the development of synthetic/natural hybrid composites to substitute non-hybrid glass fibre-reinforced composites. Owing to the advantages provided by glass fibres, the use of glass fibre as reinforcement has been extended to hybrid composite materials. Composite materials consisting of natural and glass fibres have been widely explored recently to develop a sustainable and promising material that can achieve the balance in environmental friendliness and

mechanical properties. In addition to the balance properties, the incorporation of glass fibre in the hybrid composite materials is able to reduce the moisture sensitivity, therefore preventing the environmental decay of the materials during their service life.

Carbon Fibre

Carbon fibre is regarded as another type of synthetic fibre that consists of at least 92% of carbon as the composition. Carbon fibre was first developed in the 1850s, which encompasses the highest mechanical strength in comparison with glass and aramid fibres. This type of synthetic fibre has high resistance against photo-degradation and alkaline substances. Due to its low density, high mechanical strength, excellent electrical and thermal properties, carbon fibre is commonly employed in engineering applications, such as military, aircraft and construction, where high mechanical strength and modulus are required. Nevertheless, carbon fibre is more expensive than both aramid and glass fibre, and the brittle characteristic of such fibre eventually results in weak fatigue resistance. Expanding the use of carbon fibre in large-scale applications is possible only if carbon fibre can be manufactured at a low processing cost without compromising its mechanical properties.

In general, there are two precursors for the manufacturing process of carbon fibre, which are known as polyacrylonitrile (PAN) and pitch-based precursors, as shown in Fig. 2. When comparing the cost of these two manufacturing techniques, the carbon fibre produced from the PAN-based precursors has high mechanical strength, but it is very expensive, mainly due to the high manufacturing cost. In contrast, the carbon fibre manufactured from the pitch-based precursors is relatively inexpensive; however, its mechanical strength is lower than those of carbon fibre derived from PAN-based precursors. Although it has relatively low tensile strength, pitch-based carbon fibre exhibits higher tensile modulus and strain-to-failure over PAN-based carbon fibre. Thus, pitch-based carbon fibre is more attractive because it encompasses high mechanical strength and strain-to-failure while having a low-cost characteristic. The tensile properties of PAN- and pitch-based carbon fibre with several designations are summarised in Table 3.

Despite there are two precursors for making carbon fibre, approximately 90% of carbon fibre is obtained from the PAN-based precursor, while the remaining 10% is derived from pitch-based precursor (Tanzi et al. 2019). In fact, the manufacturing process of PAN-based carbon fibre consists of several major stages. The process is initiated by wet spinning the PAN polymer solution to obtain the PAN-precursor filaments. The next step involves the stabilisation of PAN-precursor filaments through the heat treatment at a temperature between 200 °C to 300 °C for a specific duration of time. Then, the carbonisation of the filaments takes place at a temperature up to 1500 °C to eliminate those non-carbon atoms, such as oxygen and nitrogen atoms. The graphitisation is the final and the last step of producing PAN-based carbon fibre. In graphitisation, the carbon filaments are heated up to a range of

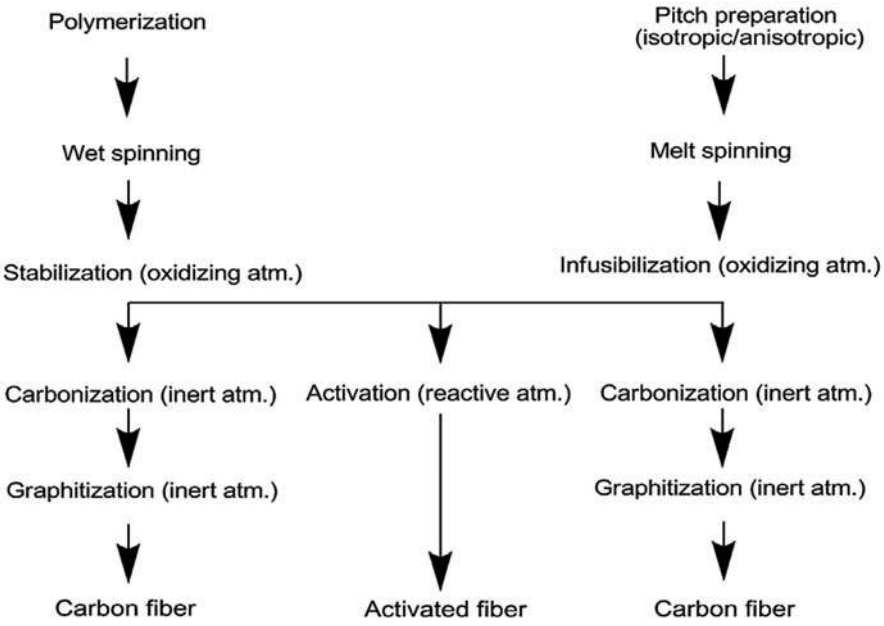

Fig. 2 Basic steps of deriving carbon fibre from PAN- and pitch-based precursors. (Reprinted with permission from Chung 1994). Copyright 2021, Elsevier

Table 3 Tensile properties of carbon fibres (Derradji et al. 2018). Copyright 2021, Elsevier

Precursor	Designation	Tensile strength (MPa)	Tensile modulus (GPa)	Elongation at break (%)
PAN-based	T-300	3530	230	1.5
	T-400H	4410	250	1.8
	T-800H	5590	294	1.9
	T-1000	7060	294	2.4
Pitch-based	P-25	1400	160	0.9
	P-75S	2100	520	0.4
	P-120S	2200	827	0.27
	E-35	2800	241	1.03
	E-75	3100	516	0.56

temperatures between 2000 °C to 3000 °C to promote the growth of graphitic crystals. It was reported that the graphitisation for a short period of 7 s already has a significant enhancement in the graphitic crystal structure (Greene et al. 2002). However, the cost of graphitisation is expensive as it requires maintaining a high temperature for a certain period, and thus the duration of the process is often minimised to reduce the cost.

The steps in the manufacturing process of pitch-based carbon fibre are akin to the PAN-based carbon fibre. Only the initial stages of the manufacturing process of pitch-based and PAN-based carbon fibre are different. The cost of pitch-based carbon fibre is lower than that of PAN-based carbon fibre as the pitch precursor is a by-product obtained from petroleum refining or coal coking. As earlier mentioned, the tensile modulus of pitch-based carbon fibre is higher than that of PAN-based carbon fibre. This is because pitch-based carbon fibre is more graphitisable than PAN-based carbon fibre. The manufacturing process of pitch-based carbon fibre initiates by melt spinning to obtain pitch precursor filaments. After that, the filaments are subjected to a heating process at a temperature around 200 °C to 300 °C for stabilisation and infusibilisation. After infusibilisation, the processing steps of pitch-based carbon fibre are similar to PAN-based carbon fibre. It is worth noting that the increase in temperature during carbonisation generally increases both tensile strength and modulus of pitch-based carbon fibre. However, any further increase in temperature over the critical limit could undermine the tensile strength but still increase the tensile modulus as the microstructure of carbon is altered to be more graphitic.

Carbon fibre has indeed shown outstanding mechanical strength over glass and aramid fibres. The high strength to weight ratio characteristic of carbon fibre is especially promising in the transportation sectors, which can tremendously decrease energy consumption without compromising safety performance. Carbon fibre-reinforced composites are always considered as competing materials to metallic alloys in engineering applications. The only inhibitor of using carbon fibre-based composites for engineering applications is the high cost compared to glass and aramid fibres. Optimising the manufacturing process of carbon fibre could be an alternative way to reduce the cost of carbon fibre. Since the processing cost has a significant impact on the cost of carbon fibre, it is expected that the reduction in the processing cost could expand the use of carbon fibre for large-scale applications.

Aramid Fibre

Aramid fibre has been a well-known organic fibre consisting of aromatic polyamides. The molecular structure of aramid fibre is formed by long-chain repeating units of monomers. The decomposition temperature of aramid fibre is very high, which can be above 500 °C. It is manufactured by spinning the solid-state fibre from the liquid chemical solution. Aramid fibre is also commonly known as Kevlar, a trade name of aramid fibre, which was firstly developed in the 1960s by Du Pont. Similar to glass fibre, aramid fibre can be categorised into several groups, which are Kevlar 149, Kevlar 29 and Kevlar 49. The different grades of Kevlar fibre are due to the fact that the changes in the process condition alter the crystallinity level, producing higher modulus aramid fibre. For example, Kevlar 149 has an ultra-high modulus, whereas Kevlar 49 and Kevlar 29 exhibit an intermediate and high modulus characteristics, respectively. However, Kevlar 29 and Kevlar 49 are among the most widely used reinforcing materials in both engineering applications and research studies. The compiled properties of Kevlar fibre with different grades are summarised in Table 4.

Table 4 Compiled properties of Kevlar fibre (Gowayed 2013). Copyright 2021, Elsevier

Grade of Kevlar	Density (g/cm^3)	Tensile strength (MPa)	Tensile modulus (GPa)	Strain at break (mm/mm)
Kevlar 29	1.44	2920	70.5	3.6
Kevlar 49	1.45	3600–4100	130	2.8
Kevlar 149	1.47	3400	185	2.0

Aramid fibre is considered a high-performance reinforcing material due to its several superior characteristics, such as low-density, high-strength and outstanding impact properties. However, aramid fibre has comparatively poor bending strength and shear properties, which are considered as the shortcomings of such fibre. Among the superior characteristics of aramid fibre, the impact resistance of this fibre is particularly outstanding, and thus it is often used in those military applications involving high-velocity impact. Examples of the applications are ballistic protective applications, protective apparel, aircraft body parts and helmets. Besides, aramid fibre also has a very low density, which is even lower than both carbon and glass fibres, and therefore, it is a very competent reinforcing material for military applications. Because of its low-density characteristic, aramid fibre has excellent specific properties. When looking into its mechanical strength, the tensile strength of aramid fibre falls between those of carbon and glass fibres.

Although aramid fibre has shown remarkable impact and lightweight properties, it is very sensitive to ultraviolet light, inferring that this fibre is susceptible to photodegradation when exposed to ultraviolet light. The colour of fabrics made of aramid fibre often changes, and the strength of the aramid fibre significantly deteriorates with the presence of ultraviolet light, which could eventually accelerate the failure of the whole structure. Several researchers have proven that thermal and light irradiations result in apparent damage and detrimental effect on the tensile strength of aramid fibre (Said et al. 2006; Liu et al. 2008; Abu Obaid et al. 2011). An initiative has been taken to improve the photoresistance of aramid fibre to extend its service life in outdoor applications. The addition of photo-stabilisers is an alternative method, which is generally implemented to improve the photostability of aramid fibre. Unfortunately, there is a difficulty to incorporate photo-stabilisers on the aramid fibre since the aramid fibre has weak compatibility with most of the photo-stabilisers, such as titanium dioxide and zinc oxide. This obstacle has become a challenging issue for researchers to enhance the resistance of aramid fibre to ultraviolet light. To overcome the obstacle of incorporating photo-stabiliser with the aramid fibre, an idea of using oxide-based coatings through the sol-gel technique has arisen.

In fact, the sol-gel technique, which provides a platform for the photo-stabiliser and aramid fibre, offers various benefits, such as low processing cost, low pressure required, short duration and less damage to the substrate materials. In addition, photoresistance coating films with a large area can be formed easily as the sol-gel technique is a liquid-phase process. In the sol-gel approach, the process is related to the hydrolysis and condensation of metal alkoxide compounds, which can be described as the chemical Eqs. (2), (3) and (4) (Assink and Kay 1988).

$$M(OR)_x + H_2O \rightarrow M(OR)_{x-1}OH + ROH \quad (2)$$

$$2\,M(OR)_{x-1}OH \rightarrow (OR)_{x-1}M - O - M(OR)_{x-1} + H_2O \quad (3)$$

$$M(OR)_{x-1}OH + ROH \rightarrow (OR)_{x-1}M - OR + H_2O \quad (4)$$

where M is the metal ion (Ti, Zn, Si, Al, etc.) and R is the alkyl group (methyl, butyl, ethyl, etc.). The chemical reactions, as described in Eqs. (2), (3) and (4), form an oxide backbone in the solution. The sol-gel solution becomes rigid once it is subjected to heating or exposed to the environment. With the use of photo-stabiliser through sol-gel technique, a transparent and strong adhesive coating film containing ultraviolet light stabiliser can be applied, and therefore the aramid fibre is sheathed by the protective layer, which has a high resistance to the light irradiation. Apart from providing light irradiation resistance, sol-gel technology is also used to provide shelter against moisture uptake.

Aramid fibre is hydrophilic in nature due to the presence of hydrogen bonding in its aromatic ring, and therefore it tends to absorb moisture from the surrounding. When aramid fibre is exposed to the environment with high temperature and humidity, this fibre is susceptible to hydrolytic degradation. Due to the polar nature of aramid fibre, it is necessary to combine with moisture-resistant materials such as sol-gel or hydrophobic polymer matrix during its service life. As a high-performance fibre, the polar nature of aramid fibre is actually considered beneficial as this characteristic enhances the wettability of the fibre. This characteristic allows such fibre to be chemically more reactive than polyethene fibre, which is another type of high-performance fibre, commonly used in ballistic applications.

Kevlar fibre has been broadly employed in military applications due to its excellent energy absorbing capacity. Kevlar battle jacket was first introduced by the US army in 1983. In addition to body armour, this fibre with the coalescence of ceramic is being used in combat helmets. This fibre is very effective in absorbing energy during an impact event. The excellent impact resistance of Kevlar fibre is attributed to its high tenacity, high modulus and low density. In comparison with other ballistic fibres, the tenacity, specific strength and modulus of Kevlar are significantly higher than silk and nylon-66. Furthermore, the Kevlar fibre is shown to have higher strength than steel when their weights are normalised. This makes Kevlar fibre an alternative ballistic material to replace steel in military applications. Traditionally, multiple layers of Kevlar fibre are used for the bullet-resistant body armour since more layers of Kevlar fibre provide additional protection.

Natural Fibre

Nowadays, natural fibres have been subjected to permanent interest among research communities due to their environmental friendliness. The ever-growing issue associated with waste accumulation has invigorated the demand for more environmental-friendly materials. Natural fibres have been widely explored as reinforcing materials

Table 5 Advantages and disadvantages of natural fibres

Advantages	Disadvantages
Low energy consumption	High moisture sensitivity
Less abrasive to tooling	Low mechanical strength
Biodegradable	High batch-to-batch variation
Renewable	Incompatibility with hydrophobic polymer matrix
Low cost	
Carbon dioxide neutral	
Highly abundant	
Lightweight	
High specific properties	
High energy recovery through incineration	

to replace synthetic fibres, particularly glass fibre. Natural fibres display various virtues over glass fibre. The advantages offered by natural fibres include low density, high specific mechanical properties, less energy consumption, less abrasion, biodegradable, high abundance and low cost. These advantages make natural fibres prime reinforcing materials in the replacement of glass fibre for composites. The advantages and disadvantages of natural fibres are summarised in Table 5.

Natural fibres are very attractive in automotive sectors owing to their green characteristic and lightweight behaviour. The non-renewable and limited petroleum resources have stimulated the demand for lightweight materials for the vehicle components in order to reduce the overall weight and petroleum consumption of the vehicles. Since the density of natural fibres is lower than that of glass fibre, the incorporation of natural fibres as the reinforcing materials for vehicle components could tremendously reduce the overall weight. It is anticipated that the reduction of vehicle weight up to 10% results in a drop in fuel consumption by approximately 7% (Lyu and Choi 2015). Besides that, the incorporation of lightweight natural fibres could indirectly reduce carbon dioxide emissions. In this case, it had been shown that reducing the weight of the vehicle by 50% could lead to a drop in carbon dioxide emission by 3.07 million tons (Nurul Hidayah et al. 2019). Therefore, it could be seen that the incorporation of natural fibres is indeed beneficial to the automotive sectors and the environment. Currently, natural fibres are employed in automotive industries for non-structural components such as dashboards, seatbacks and interior door panels (Ng et al. 2020).

The mechanical properties of natural fibres mainly depend on their chemical contents and structures. It is undeniable that the degree of polymerisation, cellulose content and microfibrillar angle also play a vital role in determining the mechanical strength of natural fibres. Generally, the mechanical strength of natural fibres increases with the increase in cellulose content. In addition, the low microfibrillar angle, which is parallel to the loading direction, tends to provide higher mechanical strength to the natural fibres. Conversely, the high microfibrillar angle leads to the higher ductility of the natural fibres. These properties undoubtedly have a decisive effect on the mechanical properties of natural fibre-reinforced composites. Since the

chemical contents and structures have major impacts on the mechanical properties of natural fibres, different types of natural fibres, such as pineapple leaf fibre, kenaf, flax, jute, oil palm, etc., have their own distinctive mechanical properties. Besides that, other factors, such as the harvesting period, extraction methods and growth environment, also affect the mechanical strength of natural fibres. In the case of natural fibre-reinforced composites, the mechanical properties are governed by various factors such as fibre-matrix compatibility, fibre composition and fibre orientations.

Generally, natural fibres can be classified into three categories, which are animal fibres, plant fibres and mineral fibres. However, plant fibres are the most extensively used natural fibres in composite fields, most probably because they are highly abundant while having the ability to reduce ecological risk. When looking into types of plant fibres, they can be further divided into several groups based on their origins, such as bast, leaf, seed and fruit fibres. Table 6 shows examples of natural fibres based on their origins. Plant fibres from different origins have their unique mechanical properties. Generally, bast fibres encompass relatively high mechanical properties compared to leaf, seed and fruit fibres, whereas leaf fibres possess higher ductility than bast fibres.

As depicted in Fig. 3, plant fibre structure comprises lumen, primary cell wall and secondary cell wall. Each layer consists of cellulose embedded in the matrix of hemicellulose-lignin. The chemical constituents of plant fibres include cellulose, hemicellulose, lignin, pectin and wax. Cellulose is a highly crystalline structure that provides mechanical strength to plant fibres. Theoretically, the cellulose fibrils possess stiffness, which can be 30 times higher than hemicellulose and lignin (Lai et al. 2008). Hemicellulose consists of highly branched polysaccharides, including glucose, mannose, galactose, xylose, etc. (Azwa et al. 2013). It forms cross-linking with cellulose through the covalent and non-covalent bonds, forming the structural component of the plant fibres. Despite the fact that the cellulose and hemicellulose are not bonded mainly through the strong covalent bond, they are still very difficult to separate. It has been revealed that the moisture content of hemicellulose is high, which is approximately 2.6 times greater than lignin (Bledzki and Gassan 1999). A lower amount of hemicellulose content is desirable because the high hemicellulose content prominently influences thermal stability and increases the moisture uptake capacity of the plant fibres.

Lignin is water-insoluble, three-dimensional and long-chain natural polymers which consist of phenylpropane units linked by ether bonds. Lignin occupies the spaces between cellulose, hemicellulose and pectin in the fibre structures. In other words, lignin acts as an adhesive for the plant cell wall, which enhances the stiffness

Table 6 Examples of natural fibres based on their origins

Origin	Plant fibre
Bast	Kenaf, flax, hemp, jute, ramie, roselle, banana
Leaf	Pineapple, abaca, agave, sisal, curaua, cantala
Seed	Cotton, kapok, loofah, milkweed
Fruit	Oil palm and coir

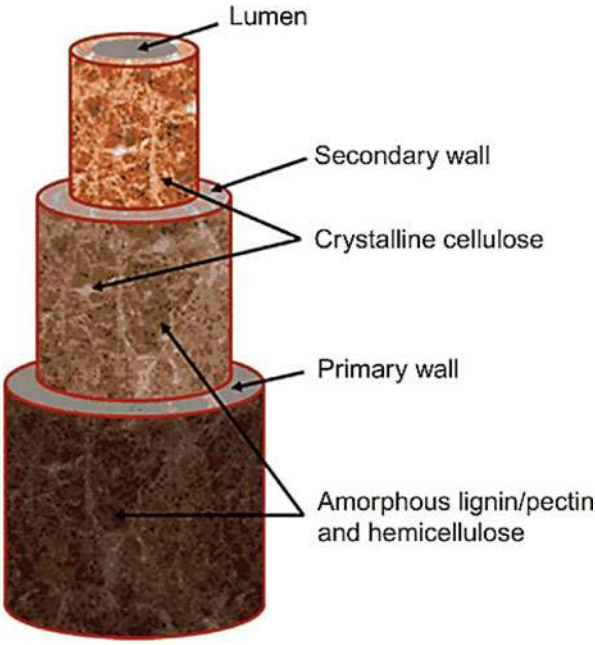

Fig. 3 Plant fibre structure. (Reprinted with permission from Bhattacharyya et al. 2015). Copyright 2021, Elsevier

and rigidity of the plant fibres. It has been proven that lignin has a softening and melting temperatures at around 90 °C and 170 °C, respectively (Gurunathan et al. 2015). The lignin content indeed has a significant effect on the moisture uptake of plant fibre. In general, plant fibres with high lignin content tend to have lower moisture sensitivity. The lignin acts as a barrier against the water molecules from penetrating into the fibres. The primary function of pectin in fibre structure is for binding. It binds the filaments into bundles and attaches them to the stem. Nonetheless, both lignin and pectin are considered as weaker polymers when compared to cellulose, and they are generally removed before the fibres are embedded with the polymer matrix. After removing the lignin, pectin and some other impurities from the fibre, more reactive groups of cellulose can be exposed, which may react with the polymer matrix, thereby improving the mechanical properties of the composite materials. Moreover, the elimination of the lignin, pectin and impurities gives the flexibility to the microfibrils to rearrange themselves towards the loading direction, leading to higher fibre strength when subjected to tension. Meanwhile, fibre surface roughness is also increased after partial removal of the unnecessary chemical contents. Subsequently, the fibre aspect ratio and mechanical interlocking between fibre and matrix can be greatly improved. All these factors contribute to the enhancement in the mechanical strength of natural fibre-based composites.

Although chemical composition has a decisive effect on the mechanical properties of plant fibres, it is undeniable that other factors, such as plant growth condition, harvesting period, fibre extraction method and supply stage, also have a great

Table 7 Factors affecting fibre quality at various phases (Dittenber and Gangarao 2012). Copyright 2021, Elsevier

Phase	Factor affecting fibre quality
Plant growth condition	Plant species Crop cultivation Plant location Fibre origin Environmental condition
Harvesting period	Plant maturity
Fibre extraction method	Decortication process Type of retting method
Supply stage	Transportation condition Storage condition Fibre age

influence on the mechanical properties of plant fibres. Table 7 shows the factors affecting the mechanical properties of plant fibres. The previous literature study had shown that the strength could be reduced by 15% if the fibre is harvested 5 days after the optimum harvesting time (Pickering et al. 2007). Liu et al. (2015) had reported similar findings in which the mechanical strength of plant fibres deteriorated after the optimum harvesting time due to the reduction in cellulose deposition, leading to the detrimental effect on the fibre properties. In addition to the harvesting time, Bos et al. (2002) concluded that the flax fibre extracted manually exhibited 20% higher strength than flax fibre extracted mechanically.

Although natural fibres have shown innumerable virtues in terms of ecological and mechanical performance, the intrinsic hydrophilic behaviours, poor fibre-matrix compatibility, non-uniformity and low mechanical properties are always the main challenges that restrict the use of natural fibres in several load-critical applications. One way to enhance fibre-matrix compatibility and reduce the hydrophilic behaviour of natural fibres is through chemical modification. Chemical modification of natural fibres could promote strong fibre-matrix adhesion and reduce the hydrophilicity of natural fibres, thereby achieving the exemplary mechanical properties of natural fibre-based composites. Among the chemical modification methods, alkali and silane treatments are the most commonly applied techniques to tackle the shortcomings of natural fibres. Alkali treatment alters the fibre surface structure, partially eliminates a certain amount of unnecessary chemical constituents of natural fibres and exposes more reactive groups of cellulose. As a result, the mechanical interlocking between fibre and matrix is tremendously enhanced, leading to the optimum mechanical properties. In addition to the natural fibre-based composites, alkali treatment can also positively affect the mechanical strength of natural fibres. Bharath et al. (2020) concluded that the alkali treatment improved the crystallinity and mechanical properties of *Moringa oleifera* fibre as a potential reinforcement for composite materials. In contrast, silane treatment acts as a coupling agent which provides a bridge at the fibre-matrix interface. The silane is a bi-functional molecule, which could simultaneously interact with fibres and the polymer matrix, consequently improving the interfacial adhesion. Generally, the moisture uptake of natural fibre-based composites is found to be higher than synthetic fibre-based composites owing to the intrinsic

hydrophilic behaviour of natural fibres. The degradation of the composites resulting from the moisture uptake might initiate micro-crack which negatively affects the composite performance (Yorseng et al. 2020). On this token, it is worth mentioning that the chemical treatments are able to reduce the moisture uptake of the natural fibres, so the long-term performance of the composites can be enhanced.

Even though the implementation in chemical treatments leads to the increase in mechanical properties, the chemical concentration at a massive level should be avoided as it could weaken the mechanical properties of the natural fibre-based composites. Asumani et al. (2012) identified the effect of alkali and silane treatments on the mechanical properties of kenaf fibre-reinforced polypropylene composites. Positive findings have been found, in which the alkali treatment up to a concentration of 6 wt% improved the mechanical properties of the composites. However, the mechanical properties were enhanced to a greater extent with the combination of alkali and silane treatments. It is interesting to note that the specific mechanical properties of alkali/silane-treated kenaf-based composites were comparable to the glass fibre-reinforced composites. Fiore et al. (2015) revealed similar results, where the 6 wt% alkali treatment enhanced the mechanical properties of kenaf fibre-reinforced epoxy composites, which is mainly due to the improvement in the interfacial adhesion. Sathish Kumar et al. (2020) concluded that 6% NaOH concentration, processing temperature of 30 °C, 8 h of processing time and a fibre-solution weight ratio of 1:15 offered the optimum tensile properties to the kenaf fibre-reinforced composites.

In addition to the alkali and silane treatments, physical methods such as corona and plasma treatments can be applied to natural fibres as well to improve the fibre-matrix bonding without altering the chemical composition of natural fibres. Although the chemical modification endows exemplary mechanical properties to the natural fibre-based composites, their mechanical strength is still lower than synthetic fibre-based composites. Hence, adopting natural fibres alone in composite materials could not achieve the desirable characteristics for certain engineering applications. In this case, the incorporation of natural fibre alone in composite materials is not realistic due to their several drawbacks. Therefore, hybridisation is considered as a relatively new concept to tackle the shortcomings of non-hybrid natural fibre-reinforced composites. The hybridisation of synthetic fibre and natural fibre in composite materials could improve the mechanical strength of the composite materials. Meanwhile, the moisture sensitivity of the hybrid composite materials could be drastically reduced.

Epoxy Matrix

The polymer matrix is one of the main constituents of composite materials. The rigidity and shape of the composite materials are maintained through the presence of the polymer matrix. Besides that, the polymer matrix protects the fibres from environmental decay. The polymer matrix can be classified into two main groups, which are thermoplastic and thermoset polymer matrices. The difference between

thermoplastic and thermoset are that thermoset is not recyclable and heat softened, whereas thermoplastic can be melted, reshaped and recycled. The typical thermoplastic polymer matrices include polypropylene, polyurethane, polyamides, polyethene and so on, while thermoset polymer matrices include epoxy, unsaturated polyester and phenol-formaldehyde. Although the recyclability of thermoplastic is attractive, the thermoset has better mechanical properties, thermal stability, chemical resistance and durability. Another main advantage of thermoset is its relatively low processing temperature compared to thermoplastic. High processing temperature is generally required for thermoplastic-based composites. Conversely, the thermoset-based polymer can be easily processed at low temperature without resulting in fibre degradation. The low processing temperature is favourable for natural fibre-based composites as natural fibres are susceptible to thermal degradation at elevated temperatures. Among the thermoset matrix, epoxy has been one of the most widely used polymer matrices in composite materials owing to its several benefits such as good adhesion with fibres and excellent mechanical strength. Natural fibres are often incompatible with non-polar polymers such as polypropylene and polyethene. The fibre-matrix incompatibility results in insufficient fibre wetting, which subsequently leads to the retardation of stress transfer from the matrix to the reinforcing fibre. However, the incompatibility is not an issue when using a polar thermoset matrix. Rassmann et al. (2011) revealed that epoxy-based composites had higher strength than polyester- and vinyl ester-based composites. The failure behaviour of epoxy-based composites was essentially due to fibre fracture, indicating a good fibre-matrix adhesion.

Epoxy belongs to the thermoset polymer, which is extensively used to develop composite materials, particularly synthetic fibre-based composites. The characteristics such as excellent adhesion with most of the reinforcements, good corrosion resistance and superior mechanical and thermal properties make epoxy the prior choice as the polymer matrix for composite materials. These properties can be further enhanced by the assimilation of the additives. The epoxy matrix is a non-recyclable polymer, inferring that the curing process is irreversible. Once the epoxy matrix is cured, it cannot be reformed and reprocessed. The polymer chain of the epoxy matrix is held by strong covalent bonds which become highly cross-linked after processing, and thus it cannot be reprocessed after the curing. The other weaknesses of the epoxy matrix are that they are susceptible to thermal degradation at high temperatures and tend to have high water absorption. Moisture uptake has been one of the factors that affects the environmental durability of the polymers, altering their physical and mechanical properties. Moisture uptake of epoxy has been shown to have deleterious effects on the epoxy properties at elevated temperatures (Karad et al. 2005). It was shown that the moisture absorption of epoxy could also lead to plasticisation, which may occur through several mechanisms depending on the interaction of water molecules and the polymer. The plasticisation eventually depresses the glass transition temperature of the polymer. As a consequence, the moisture negatively influences the final performance of the products, particularly for their long-term service life. However, the moisture absorption of different types of epoxy may differ by a factor of 3 to 10, depending on the types of curing agents

(Akay et al. 1997). The moisture absorption of epoxy is attributed to the affinity of the highly polar functional groups which could react with the water molecules.

The changes in the moisture content of epoxy matrix or epoxy-based composite materials could induce swelling that causes the residual stress in the composite materials, which has a negative impact on the fracture behaviour of the composite materials. Hence, the problem related to the high moisture absorption of the epoxy matrix should not be neglected. Due to the wide applications of epoxy in several sectors such as aerospace and automotive, intensive research works have been conducted to reduce its moisture absorption in order to improve its environmental durability and long-term performance. One of the efficient techniques to reduce the moisture absorption of the epoxy matrix is the addition of multiwalled carbon nanotubes (MWCNTs). It has been experimentally proven that the addition of merely 0.3 wt% MWCNTs was able to reduce the moisture absorption of epoxy by approximately three times compared to neat epoxy polymer, implying that the hygrothermal resistance of the epoxy was considerably improved (Starkova et al. 2013). The addition of filler materials hinders the intermolecular movement of the polymer, creating a more compact structure of the material which lessens the free volume content and space available for water diffusion. Thus, the level of moisture uptake of the epoxy is apparently dropped. Another technique to reduce the high moisture uptake of the epoxy matrix is through the co-reaction of cyanate esters and epoxy, which modifies the branch density of the network and the chemical composition. By blending the cyanate esters and epoxy, the moisture sensitivity, dielectric loss and viscosity are significantly reduced (Karad et al. 2005). With the reduction of moisture sensitivity, epoxy having high mechanical strength and good compatibility with reinforcing materials can be an excellent polymer matrix for composite materials. Owing to the several benefits of epoxy, it is currently being used as matrix materials for commercial synthetic fibre-reinforced composite materials.

Bio-Based Epoxy Polymer

As mentioned earlier, epoxy resin is one of the most extensively used thermoset polymer matrices in the composite field. The majority of the epoxy resins in composite materials are derived from petroleum. This petroleum-based epoxy resin has gained broad interest in industries and research areas because of its low-cost characteristic and high mechanical properties. The condensation process of bisphenol A (BPA) and epichlorohydrin is the primary reaction to produce epoxy resin, which accounts for approximately 75% of the total epoxy production in the world. However, the fluctuation of petroleum prices and the depletion of petroleum resources have spurred the initiation to reduce the use of epoxy and substitute it with alternative materials. Moreover, another driving factor in reducing the use of petroleum-based epoxy resin is associated with severe environmental concerns. The hydrolysis of epoxy functional groups in the water could bioaccumulate, and they are considered moderately toxic to aquatic organisms (Sogancioglu et al. 2020).

In addition, the production of petroleum-based epoxy resin and the incineration of composite materials cause the emission of greenhouse gases and pollution.

On the other hand, the hardeners or curing agents are the crucial components to react with epoxy resin during the curing process. These curing agents are also primarily synthesised from petroleum, and most of the hardeners are considered toxic before the curing process (Baroncini et al. 2016). Because of the non-recyclable and non-biodegradable behaviours of epoxy as well as the toxicity of the curing agents, bio-based materials have been gaining popularity throughout the years. Thermoplastic polymers have received significant attention recently due to their recyclability. Unlike thermoset polymers, thermoplastic polymers can be easily remoulded and reshaped by applying heat until the melting temperature of the materials. Nevertheless, some of the conventional thermoplastics such as polypropylene, polyethene and polystyrene are also non-biodegradable, which entails the increasing waste accumulation on the earth. Typically, the mechanical properties of thermoplastic polymers are lower than epoxy.

Today, a continuous effort has been dedicated to the exploration of biocomposite materials in order to reduce the negative impacts on the environment. Truthfully, biocomposite materials should consist of reinforcements and polymer matrices, which are renewable, environmentally friendly and bio-degradable. More importantly, the bio-composites should have no toxicity, inferring that these materials must have no harmful effects on animals and human beings. In fact, epoxy resin can also be synthesised from several types of natural oils such as linseed, sunflower, palm oil and soybean. Other natural green resources, such as sugars, polysaccharides, lignin, lipids, proteins and other monomers, can also be used to yield bio-based thermoset polymers. These bio-based polymers do not reveal any toxicity during production and service life, making them have a high potential to be used in large-scale applications. Moreover, the new bio-epoxy based composites often show comparable properties to the traditional epoxy-based composites. Scarponi et al. (2016) revealed that the flexural and impact properties of hemp fibre-reinforced bio-epoxy composites were similar to the contemporary epoxy-based composites. Nikafshar et al. (2017) reported very promising results in which the bio-based epoxy polymer with the addition of 2 wt% inorganic accelerator showed slightly higher tensile and impact strength than petroleum-based epoxy polymer.

However, plant oils are particularly attractive due to their versatility, less expensive, highly available, renewable and biodegradable. Plant oils are composed of unsaturated triglycerides, which are formed by linking the three fatty acids to glycerol through the ester bond. Among the various types of plant oils, soybean oil is regarded as the semi-drying plant oil, which has received great attention nowadays because of its low cost, high availability and renewable characteristics. Similar to other plant oils, triglycerides, as the building blocks, are the main constituent of soybean oil. Soybean oil is possible to be subjected to epoxidation to form epoxidised soybean oil (ESO). The epoxidation of soybean oil is performed by reacting the non-conjugated C=C double bonds of the oil with the concentrated hydrogen peroxide and either acetic or formic acids. The mineral acid acts as the catalyst during epoxidation. After the epoxidation, the C=C double bonds are

converted to epoxy groups, which are non-toxic and highly reactive. Currently, ESO is primarily utilised as the plasticiser for polyvinyl chloride (PVC), chlorinated rubber and polyvinyl alcohol (PVA) emulsions. Meanwhile, it has been subjected to continuous growth as a bio-epoxy resin for the composite materials, mainly attributed to its green characteristics. In addition to the plasticiser and matrix material, ESO can also be used as gels and oleochemical carbonates. The epoxidation is not restricted to soybean oil; other bio-based plant oils can also be epoxidised to develop bio-epoxy.

In spite of the optimistic features of epoxidised plant oils, these bio-based epoxy polymers cannot attain the high mechanical properties as obtained in those petroleum-based epoxy polymers. Due to the low functionality and the lack of rigid aromatic and cycloaliphatic structures in the plant oils, the mechanical strength and stiffness of the bio-based epoxy polymers are lower than petroleum-based epoxy. Moreover, the glass transition temperature (T_g) of plant oil-based epoxy is lower than conventional epoxy, which inevitably limits their applications worldwide. Therefore, plant oil-based epoxy as the polymer matrix for composite materials still remains a challenging issue. However, blending the epoxidised plant oils with the petroleum-based epoxy is considered an alternative way to reach satisfactory results. The mixture of epoxidised plant oils with the petroleum-based epoxy with different relative ratios has significant influences on the mechanical and thermal properties. In this context, the mixture consisting of bio-based and commercial epoxy has undoubtedly shown some favourable results in terms of mechanical properties. Niedermann et al. (2017) concluded that the jute fibre-reinforced composites based on 25 wt% ESO-containing epoxy polymer showed comparable mechanical properties to those based on commercial epoxy polymer. Although the mechanical strength and stiffness of epoxy-based on plant oils are lower than the conventional epoxy polymers, the addition of plant oil-based epoxy improves the toughness and processability of the resulting polymers owing to the high flexibility of the network structures of the plant oils. These findings demonstrated that the bio-based epoxy could partially replace the commercial epoxy without apparently deteriorating the mechanical properties.

Besides plant oils, another alternative material that is suitable to replace petroleum-based epoxy is bio-based epoxy based on lignin. Lignin is the promising and second most plentiful natural polymer after cellulose. Its aromatic backbone structures and the highly cross-linked phenolic network could resolve the demerits of low mechanical strength and stiffness as observed in those plant oil-based epoxy. Cellulose, hemicellulose and lignin are the three main chemical constituents of the plant cell walls. In the pulp and paper industry, lignin is found in a large quantity as the by-product, which is separated from the cellulose after the kraft process. It is estimated that the annual global production of lignin is around 50 million tons, and a large amount of lignin is subjected to incineration to generate energy while the remaining amount of lignin is used in chemical conversion to yield lignosulfonates (Demuner et al. 2019). The high volume of lignin produced during the kraft process presents an opportunity to develop bio-based epoxy using lignin. The main obstacles in developing lignin-based epoxy polymer are the high polydispersity, poor solubility and heterogeneity of lignin. On the other hand, anhydrides and amines are among

the most widely used curing agents or hardeners for epoxy resins. It was found that the anhydrides-type curing agent offers the highest mechanical strength and stiffness to the epoxy polymers, but this curing agent is prone to hydrolytic degradation. It should be emphasised that the curing agents can also be derived from the bio-renewable and inexpensive natural resources to replace those petroleum-based curing agents. Some examples of bio-based curing agents are plant oil-based polyamine, terpene maleic anhydride, maleopimaric acid, etc. Several literature studies have reported that the incorporation of bio-based curing agents improved the T_g and had comparable mechanical properties to the conventional epoxy materials (Wang et al. 2011; Chang et al. 2015; François et al. 2017).

Void Content in Composite Materials

Composite materials have been used in large-scale engineering applications, particularly in the transportation sectors. In the aerospace sectors, composite materials are employed for the primary and secondary structures. Therefore, the quality of the composite materials should be carefully scrutinised and optimised to ensure excellent safety performance. If the damages from the manufacturing defects are underestimated or neglected, the composite structure may fail catastrophically during its service life. Voids are one of the most common manufacturing defects in composite materials. Other manufacturing defects include resin-rich or resin-poor region and fibre-matrix debonding. However, voids have been widely studied because they have adverse effects on a wide range of composite properties. The formation of voids during the manufacturing process leads to the reduction in the strength and stiffness of the composite materials. The intention of incorporating fibres in composite materials is to reduce the reliance on plastics and improve mechanical properties. The loads are transferred from the polymer matrix to the fibre through the interfacial shear, thereby improving the load-carrying capacity of the composite materials. Nevertheless, the presence of voids in the composite laminates might retard the load transfer efficiency, resulting in the reduction in mechanical properties. Furthermore, the void contents may act as the stress concentration points, resulting in the crack initiation which eventually causes the premature failure of the composite materials.

Generally, the void formation occurs during the composite manufacturing process where the air is entrapped in the composite materials, leading to the formation of unoccupied pores which reduce the overall fibre volume fraction. In fact, the chemical reaction of polymerisation, volume changes due to the shrinkage of resin during curing and void nucleation from the volatile substances are the driving factors, that result in the presence of air during the composite manufacturing process (Lebel et al. 2019). However, the air entrapment is often because of the inhomogeneous fibre architecture, which causes the resin flow through the fibre preform with non-uniform permeability. The non-uniform permeability eventually leads to the variability of the resin to flow velocity, which is exacerbated by the capillary effect of the resin flow. When incorporating the natural fibres in the composite materials, the

formation of voids is most probably due to the moisture content of the fibres, especially when involving the heating process during the composite fabrication. The moisture evaporates when heating, resulting in an increase in void content. Apart from the entrapped air, the high viscosity of the resin impedes the fibre impregnation and results in void development as the resin is difficult to fill the spaces between the fibres. Typically, the voids can be in micro or macro levels, depending on the velocity of the resin flow. When the velocity of the resin flow is high, the viscous forces are dominant over the capillary forces, which promote the formation of micro-voids. In contrast, macro-voids are formed when the capillary forces are dominant over the viscous forces at low resin velocity. There are some techniques that can be applied to minimise and purge the void contents in the composite materials. Vacuum bagging is a commonly applied technique that utilises the vacuum system to remove the voids.

In fact, the manufacturing techniques and processing parameters have decisive effects on void formation. The autoclave process is the most successful manufacturing method to produce composite materials with minimum or zero void content. The autoclave is widely used in aerospace industries to manufacture composite materials, primarily for the primary structures. The composite preforms are stacked and vacuum bagged in the autoclave, which are followed by several process cycles, including heating, pressurisation and cooling. The vacuum and pressure in the autoclave aid in removing entrapped air or other volatile substances in the composites. Overall, the composites with low void content can be easily obtained through the autoclave process, but the processing cost will be very high. Due to the high processing cost of the autoclave, other alternative out-of-autoclave methods such as resin transfer moulding, resin infusion technique and vacuum-assisted resin transfer moulding with lower processing cost have been developed. Nonetheless, these out-of-autoclave methods are unable to produce the void-free composite materials as obtained from the autoclave. Thus, a manufacturing method that can produce composite materials with high quality at a low processing cost is required. Recently, a new approach has been established in which the void-free composite materials can be produced without an autoclave process (Lee et al. 2020). This approach utilises thin film of carbon nanotubes (CNTs) to generate heat by applying electric current to the film, allowing the composite materials to cure and consolidate. Besides, the CNTs sandwiched between the two materials could reduce the void content by enhancing the resin flow through the capillary pressure. In addition to producing high-quality composites, it has been reported that this approach can be performed at a low processing cost compared to the autoclave process.

Out-of-autoclave techniques are often used to prepare composites for certain industrial applications at minimised manufacturing costs. Producing a void-free composite is not necessary for certain industrial applications. Generally, the void content should be below 1% for the primary structural applications in aerospace industries, while void content of 5% is acceptable for other non-load critical applications. However, it should be emphasised that the void content should be controlled at an acceptable range to maintain the quality of the composite materials. In order to eliminate the voids, processing parameters, including the temperature and pressure,

should be carefully controlled. Liquid composite moulding (LCM) is an alternative technique used to produce composite materials at a low processing cost. However, it is difficult to control the temperature and pressure in LCM, leading to a higher amount of voids in the composites. The temperature plays an essential role in determining the viscosity of the resin, thus controlling the resin flow towards the reinforcements. It has been shown that the increase of curing temperature reduces the viscosity of the resin, making the voids be easily squeezed out. In addition, increasing the curing temperature allows the resin to fill the voids in the composites, decreasing the void contents. Similar to the temperature, the increase of cure pressure could restrict the void growth, hence reducing the void content (Li et al. 2015). Nevertheless, the excessive external pressure causes the geometrical inconsistency of the composites as the resin flow is increased, and it will be drawn out from the composites (Chang et al. 2017). If the temperature and pressure are adequately controlled, the voids and water vapour could be squeezed out from the composites, producing composites with low porosity and high performance. Therefore, experimental investigations on the optimised processing parameters are of the utmost importance.

Potential Applications of Hybrid Composites

Inconsistency of fuel cost and the depletion of non-renewable energy resources motivate the researchers to search for high-performance and lightweight materials for transportation sectors. In this case, glass fibre-reinforced composites have displayed some unique properties, which could fulfil the requirements for automotive and aerospace applications. Nevertheless, the extensive use of synthetic fibre-based materials has resulted in an ecological issue such as waste accumulation, since synthetic fibre is generally non-biodegradable. Therefore, the current effort has been given towards the feasibility of replacing synthetic with natural fibres. The combination of synthetic and natural fibres in polymer matrix is expected to display a synergistic effect which cannot be realised by those non-hybrid composites. The majority of the failure in aircraft components are due to repetitive fatigue loading, and fatigue failure has become the primary concern in aircraft industries. In this context, one of the benefits provided by natural fibres is their low fatigue sensitivity, indicating that their fatigue strength degradation rate is lower than glass fibres. Thus, the combination of synthetic and natural fibres in the hybrid composites is expected that can provide good fatigue strength with low fatigue sensitivity to the materials. Besides that, natural fibres possess a lower density than glass fibre, implying that the total weight of the structures could be reduced with the partial substitution of glass fibre with natural fibres. Once the overall weight of the automotive or aircraft components is reduced, the energy efficiency of the automobile can be significantly improved.

In addition to automotive and aircraft applications, hybrid composites have shown some beneficial characteristics to military applications. The military applications are mainly dominated by the Kevlar fibre due to its extraordinary impact

resistance, high chemical resistance and lightweight characteristic. There is no doubt that Kevlar fibre has a very high potential in military applications. The primary obstruction of these Kevlar fibre-based composites is the high cost. In order to reduce the cost of the products, it is recommended that the Kevlar fibre in the composites could be partially substituted by natural fibres. By proper designing the hybrid composites, the hybrid composites could have comparable impact properties to the non-hybrid synthetic fibre-based composites. Ismail et al. (2018) studied the low-velocity impact response of woven kenaf/Kevlar fibre-reinforced epoxy composites. The findings showed that the hybrid composite laminates exhibited comparable energy absorption to those non-hybrid Kevlar-reinforced composites. Furthermore, Yahaya et al. (2015) performed a Charpy impact test on the woven kenaf/Kevlar-reinforced epoxy composites. The results presented superior impact properties of hybrid kenaf/Kevlar-reinforced composites in which the hybrid composites possessed higher energy absorption than non-hybrid Kevlar- and kenaf-reinforced composites. However, it was found that the impact toughness of non-hybrid Kevlar-based composites was slightly higher than hybrid composites. Overall, it was identified that the fibre stacking sequence in the composite laminates indeed has a significant effect on the mechanical properties. Hybrid composites with the placement of high strength synthetic fibre as the outermost skin layers have comparable mechanical strength to the non-hybrid composites since the outermost skin layers are the main component in sustaining the load, particularly out-of-plane loading. By designing hybrid composites practically and judiciously, hybrid composites undoubtedly have a high potential to supersede non-hybrid synthetic fibre-based composites in a broad range of engineering applications.

Future Direction of Hybrid Composite Materials

Hybrid composites composing of multiple types of fibres embedded within a single matrix have drawn the attention of researchers, scientists and engineers. However, it is expected that the hybridisation concept can also be extended to the hybrid sandwich structure, namely, fibre metal laminates (FMLs), which is regarded as a relatively new material in the composite field. The sandwich structure of FMLs consists of both metallic layers and composite materials. In fact, FMLs, as depicted in Fig. 4, are formed through the coalescence of metallic materials and polymer composites by means of adhesive agents incorporated at the metal-composite interfaces. FMLs are commonly based on synthetic fibre-reinforced epoxy composites and aluminium alloys with different grades. The commercially available FMLs are glass laminate aluminium-reinforced epoxy (GLARE), aramid-reinforced epoxy aluminium laminate (ARALL) and carbon fibre-reinforced epoxy aluminium laminate (CARALL). These three main types of FMLs are based on non-hybrid synthetic fibre-reinforced epoxy composites.

FMLs are the contemporary substrates to be used as fuselage materials in aerospace industries. The initial intention of developing FMLs is to tackle the shortcoming of poor fatigue resistance of metal alloys in aerospace sectors (Feng

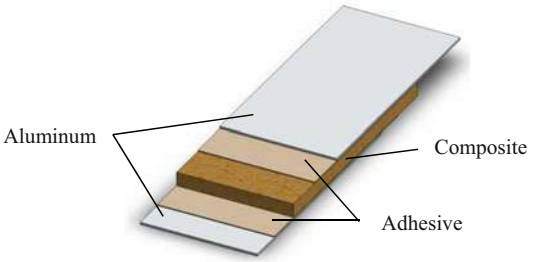

Fig. 4 FMLs with 2/1 stacking sequence

and Malingam 2019). The rapid fatigue crack growth rate of metal alloys could lead to catastrophic and sudden failures which are extremely dangerous. Therefore, the combination of polymer composites with metal alloys has been shown to have lower fatigue crack growth rate than metal alloys alone. The previous literature studies attested that FMLs have very low fatigue crack growth rate compared to metallic materials (Homan 2006; Alderliesten 2019). Initially, it was observed that the adhesively bonded aluminium layers had better fatigue crack growth resistance than metal alloys. Subsequently, polymer composites were added to the structure to develop the sandwich concept of FMLs, which may further improve fatigue crack resistance of the materials. Although the initial purpose of developing FMLs was to improve the fatigue crack resistance of the metallic structures, other benefits such as excellent damage tolerance, corrosion resistance and burn-through resistance were soon evident. These properties have made FMLs one of the promising materials in composite fields.

The superior fatigue crack resistance of the FMLs over metal alloys is attributed to their fibre bridging mechanism. During the fatigue loading, the fatigue crack initiates at the metallic layers instead of polymer composite as the high modulus metallic layers tend to sustain more loads compared to polymer composites. However, a certain amount of the load is transferred from the metallic layers to the fibre in composite materials, which, in turn, restrain and restrict the fatigue crack opening. In this phenomenon, the fibre is elongated by the crack opening, but the level of fibre elongation is limited owing to the stiffness of the fibre. The fibre remains intact and bridges the crack during the fatigue crack growth, which indirectly reduces the stress intensity, hence enhancing the fatigue crack resistance. The fatigue life of metal alloys is actually dominated mainly by the crack initiation phase as the crack propagation rate of metal alloys is extremely high, whereas the fatigue life of FMLs is mostly conquered by the crack propagation phase. In addition to improved fatigue life, the low fatigue crack growth rate increases the inspection interval for the fatigue failure of the materials, thereby preventing catastrophic failure which could endanger human life. However, the efficiency of the fibre bridging mechanism is highly dependent on the adhesion level between metal alloys and composites. It had been shown that the surface treatment could lead to a rough surface of metal alloys, thereby improving the adhesion level and mechanical properties of the adhesive-bonded materials (Ng et al. 2019).

Owing to the innumerable benefits of FMLs over metal alloys, these composite sandwich materials have been widely explored to extend their applications from the aerospace to automotive sectors. Due to the increasing ecological concern and environmental awareness, an initiative has been taken to incorporate natural fibres to replace synthetic fibres in FMLs. Several research studies have been performed to explore the possibility of incorporating natural fibres in FMLs. Vieira et al. (2017) had performed an investigation on the FMLs based on sisal fibre-reinforced epoxy composites. They concluded that FMLs possessed better mechanical performance than their respective composite materials. Feng et al. (2020b) revealed similar findings in which the pineapple fibre-based FMLs had higher mechanical properties than their respective composite materials. In terms of the specific mechanical properties, FMLs still showed outstanding specific mechanical properties over their respective composites.

When referring to the literature studies, the outstanding characteristics of hybrid composites and FMLs were evident. In order to further improve the mechanical and physical properties while resolving the disadvantages of each individual material, the hybridisation concept can be applied to FMLs. By applying the hybridisation concept on FMLs, the advantages inherited from the hybrid composites and FMLs can be combined, thus developing cost-effective, environmental-friendly and sustainable composite materials. Recently, several research studies have been performed to explore FMLs based on natural/synthetic fibre-reinforced composites, and positive findings were revealed. Mohammed et al. (2018) studied the mechanical properties of FMLs based on flax, kenaf and carbon fibre-reinforced composites. The results demonstrated FMLs based on flax/carbon-reinforced hybrid composites had higher mechanical properties than FMLs based on kenaf/carbon-reinforced hybrid composites. Abd El-Baky et al. (2020) investigated the mechanical properties of FMLs comprising of jute/glass fibre-reinforced hybrid composites. They concluded that the mechanical properties of FMLs were significantly improved through the hybridisation of glass and jute fibre compared to those based on non-hybrid jute fibre-reinforced composites.

Apart from the tensile and flexural properties, the fatigue properties of FMLs can be enhanced through hybridisation. It had been mentioned that FMLs possess excellent fatigue crack resistance due to the fibre bridging mechanism, which restrains and restricts the fatigue crack propagation rate. The incorporation of natural and synthetic fibres could further enhance the fatigue properties of FMLs owing to high modulus of synthetic fibres and low fatigue sensitivity of natural fibres. Fatigue failure of the materials usually is associated with modulus degradation during the fatigue loading, and thus high modulus could lead to better fatigue performance of the materials. On the other hand, the stiffening effect is generally observed in natural fibres in which the modulus of the materials increases at the initial stage of fatigue loading. This phenomenon is because of the realignment of the microfibrillar angle towards the loading direction, which increases the modulus of the materials. Ng et al. (2017) had concluded that FMLs based on hybrid composites apparently improved the fatigue strength and reduced the fatigue sensitivity of the materials. Feng et al. (2019) had also performed a fatigue life assessment on FMLs based on kenaf/glass

fibre-reinforced hybrid composites. They showed that FMLs based on hybrid composites had the highest endurance strength and lowest fatigue sensitivity coefficient compared to those FMLs based on non-hybrid synthetic and natural fibre-reinforced composites. In addition, the combination of metal alloys and composite materials can significantly reduce the water absorption and diffusion coefficient, because the addition of metal alloys acts as a barrier against the moisture penetration into the materials.

Conclusion

The hybridisation concept has gained wide acceptance among researchers and scientists owing to their unique properties, which cannot be achieved by single fibre-reinforced composites. The hybridisation of synthetic and natural fibres in composite materials can enhance the mechanical properties while reducing water absorption. Using non-hybrid natural fibre-reinforced composites to replace synthetic fibre-based composites is not realistic since the mechanical strength of natural fibres is prominently weaker than synthetic fibres. Furthermore, the intrinsic high moisture sensitivity of natural fibres eventually results in the penetration of water molecules into the composites, particularly epoxy-based composites. As a consequence, the high moisture content leads to the strength degradation of composite materials, which deteriorates the overall performance during their service life. Batch-to-batch variation in the mechanical and physical properties is another factor that restricts the applications of natural fibre-based composites.

Towards the bio-based composites, the commercial petroleum based-epoxy polymers should be superseded by bio-based epoxy polymers synthesised from renewable and environmental-friendly materials such as plant oils. Mixing bio-based with commercial epoxy at an optimum ratio has been identified to have high mechanical properties while having high processability. Apart from plant oils, lignin is another promising natural resource to synthesise bio-based epoxy. The aromatic backbone structures and highly cross-linked phenolic network of lignin could resolve the drawbacks of low strength and stiffness of plant oil-based epoxy. Besides, lignin is regarded as the by-product in the pulp and paper industries. Following the waste-to-wealth concept, lignin indeed shows a very high potential to synthesise bio-based epoxy in the replacement of commercial epoxy polymers.

Voids are always a challenging issue in the composite field as voids have detrimental effects on the mechanical properties of composites. The occurrence of voids in the composite materials is due to the air entrapment which decreases the overall fibre volume fraction. However, the voids can be eliminated by properly controlling the processing temperature and pressure during the manufacturing process. Increasing the temperature and pressure during the composite manufacturing process facilitates the removal and collapse of the voids, producing composite materials with low void content. In this context, the autoclave is the most successful manufacturing method that can produce composite materials with zero or very low void content, typically less than 1%. Recently, a new manufacturing method has been established in which high-quality composite materials can be manufactured

without using an autoclave. Therefore, composite materials with low void content can be manufactured at a low processing cost.

Due to the several limitations of natural fibres, the idea of hybridising different types of fibres in composite materials has been raised. Composite materials based on both natural and synthetic fibres have shown a great prospect to be used in engineering applications in order to reduce the dependency on non-hybrid synthetic fibre-reinforced composites. Improved mechanical properties and damage tolerance, reduction in fatigue sensitivity and moisture uptake, as well as the reduction in the negative impact on the environment are the driving factors that make hybrid composites becoming the promising materials to be utilised in engineering applications. Because of the presence of natural fibres in the hybrid composites, chemical treatments can be applied to improve the fibre-matrix interfacial bonding in order to obtain the exemplary mechanical properties of hybrid composites. A further enhancement is possible by applying the hybridisation concept into FMLs. It is expected that hybridising synthetic and natural fibres into FMLs can definitely develop a cost-effective material with excellent mechanical properties and damage tolerance while reducing the negative impact on the environment.

References

M.A. Abd El-Baky, A.E. Alshorbagy, A.M. Alsaeedy, M. Megahed, Fabrication of cost effective fiber metal laminates based on jute and glass fabrics for enhanced mechanical properties. J. Nat. Fibers (2020). https://doi.org/10.1080/15440478.2020.1739594

A. Abu Obaid, J.M. Deitzel, J.W. Gillespie, J.Q. Zheng, The effects of environmental conditioning on tensile properties of high performance aramid fibers at near-ambient temperatures. J. Compos. Mater. **45**, 1217–1231 (2011). https://doi.org/10.1177/0021998310381436

M. Akay, S.K.A. Mun, A. Stanley, Influence of moisture on the thermal and mechanical properties of autoclaved and oven-cured Kevlar-49/epoxy laminates. Compos. Sci. Technol. **57**, 565–571 (1997). https://doi.org/10.1016/S0266-3538(97)00017-1

R. Alderliesten, Fatigue in fibre metal laminates: The interplay between fatigue in metals and fatigue in composites. Fatigue Fract. Eng. Mater. Struct. **42**, 2414–2421 (2019). https://doi.org/10.1111/ffe.12995

R.A. Assink, B.D. Kay, Sol-gel kinetics I. Functional group kinetics. J. Non-Cryst. Solids **99**, 359–370 (1988). https://doi.org/10.1016/0022-3093(88)90441-3

O.M.L. Asumani, R.G. Reid, R. Paskaramoorthy, The effects of alkali–silane treatment on the tensile and flexural properties of short fibre non-woven kenaf reinforced polypropylene composites. Compos. Part A Appl. Sci. Manuf. **43**, 1431–1440 (2012). https://doi.org/10.1016/j.compositesa.2012.04.007

Z.N. Azwa, B.F. Yousif, A.C. Manalo, W. Karunasena, A review on the degradability of polymeric composites based on natural fibres. Mater. **Des**. **47**, 424–442 (2013). https://doi.org/10.1016/j.matdes.2012.11.025

E.A. Baroncini, S. Kumar Yadav, G.R. Palmese, J.F. Stanzione, Recent advances in bio-based epoxy resins and bio-based epoxy curing agents. J. Appl. Polym. Sci. **133**, 44103 (2016). https://doi.org/10.1002/app.44103

K.N. Bharath, P. Madhu, T.G.Y. Gowda, M.R. Sanjay, V. Kushvaha, S. Siengchin, Alkaline effect on characterization of discarded waste of *moringa oleifera* fiber as a potential eco-friendly reinforcement for biocomposites. J. Polym. Environ. **28**, 2823–2836 (2020). https://doi.org/10.1007/s10924-020-01818-4

D. Bhattacharyya, A. Subasinghe, N.K. Kim, in *Multifunctionality of Polymer Composites. Challenges and New Solutions, ed. by* K. Friedrich, U. Breuer (William Andrew, Norwich, 2015), p. 102

A.K. Bledzki, J. Gassan, Composites reinforced with cellulose based fibres. Prog. Polym. Sci. **24**, 221–274 (1999). https://doi.org/10.1016/S0079-6700(98)00018-5

H.L. Bos, M.J.A. Van Den Oever, O.C.J.J. Peters, Tensile and compressive properties of flax fibres for natural fibre reinforced composites. J. Mater. Sci. **37**, 1683–1692 (2002). https://doi.org/10.1023/A:1014925621252

L. Calabrese, V. Fiore, P. Bruzzaniti, T. Scalici, A. Valenza, Pinned hybrid glass-flax composite laminates aged in salt-fog environment: Mechanical durability. Polymers (Basel). **12**, 40 (2020). https://doi.org/10.3390/polym12010040

R. Chang, J. Qin, J. Gao, Fully biobased epoxy from isosorbide diglycidylether cured by biobased curing agents with enhanced properties. J. Polym. Res. **21**, 52 (2015). https://doi.org/10.1007/s10965-015-0692-8

T. Chang, L. Zhan, W. Tan, S. Li, Void content and interfacial properties of composite laminates under different autoclave cure pressure. Compos. Interfaces **24**, 529–540 (2017). https://doi.org/10.1080/09276440.2016.1237113

D.D.L. Chung, *Carbon Fiber Composites, 1st edn.* (Butterworth-Heineman, Boston, 1994), pp. 3–11

J.A. Cicero, J.R. Dorgan, S.F. Dec, D.M. Knauss, Phosphite stabilization effects on two-step melt-spun fibers of polylactide. Polym. Degrad. Stab. **78**, 95–105 (2002). https://doi.org/10.1016/S0141-3910(02)00123-4

I.F. Demuner, J.L. Colodette, A.J. Demuner, C.M. Jardim, Biorefinery review: Wide-reaching products through kraft lignin. Bioresources **14**, 7543–7581 (2019). https://doi.org/10.15376/biores.14.3.Demuner

M. Derradji, J. Wang, W. Liu, *Phthalonitrile Resins and Composites: Properties and Applications,* 1st edn. (William Andrew, Norwich, 2018), pp. 241–294

D.B. Dittenber, H.V.S. Gangarao, Critical review of recent publications on use of natural composites in infrastructure. Compos. Part A Appl. Sci. Manuf. **43**, 1419–1429 (2012). https://doi.org/10.1016/j.compositesa.2011.11.019

N.L. Feng, S. Dhar Malingam, in *Mechanical and Physical Testing Biocomposites, Fibre-Reinforced Composites and Hybrid Composites*, ed. by M. Jawaid, M. Thariq, N. Saba, (Woodhead Publishing, Cambridge, 2019), p. 307

N.L. Feng, S. DharMalingam, K.A. Zakaria, M.Z. Selamat, Investigation on the fatigue life characteristic of kenaf/glass woven-ply reinforced metal sandwich materials. J. Sandw. Struct. Mater. **21**, 2440–2455 (2019). https://doi.org/10.1177/1099636217729910

N.L. Feng, S.D. Malingam, R. Jenal, Z. Mustafa, S. Subramonian, A review of the tensile and fatigue responses of cellulosic fibre-reinforced polymer composites. Mech. Adv. Mater. Struct. **27**, 645–660 (2020a). https://doi.org/10.1080/15376494.2018.1489086

N.L. Feng, S.D. Malingam, N.M. Ishak, K. Subramaniam, Novel sandwich structure of composite-metal laminates based on cellulosic woven pineapple leaf fibre. J. Sandw. Struct. Mater. **23**, 3450–3465 (2020b). https://doi.org/10.1177/1099636220931479

V. Fiore, G. Di Bella, A. Valenza, The effect of alkaline treatment on mechanical properties of kenaf fibers and their epoxy composites. Compos. Part B Eng. **68**, 14–21 (2015). https://doi.org/10.1016/j.compositesb.2014.08.025

C. François, S. Pourchet, G. Boni, S. Rautiainen, J. Samec, L. Fournier, C. Robert, C.M. Thomas, S. Fontaine, Y. Gaillard, V. Placet, L. Plasseraud, Design and synthesis of biobased epoxy thermosets from biorenewable resources. Comptes Rendus Chim. **20**, 1006–1016 (2017). https://doi.org/10.1016/j.crci.2017.10.005

Y. Gowayed, in *Developments in Fiber-Reinforced Polymer Composites in Civil Engineering, ed. by N. Uddin* (Woodhead Publishing, Cambridge, 2013), p. 3

M.L. Greene, R.W. Schwartz, J.W. Treleaven, Short residence time graphitization of mesophase pitch-based carbon fibers. Carbon **40**, 1217–1226 (2002). https://doi.org/10.1016/S0008-6223(01)00301-3

T. Gurunathan, S. Mohanty, S.K. Nayak, A review of the recent developments in biocomposites based on natural fibres and their application perspectives. Compos. Part A Appl. Sci. Manuf. **77**, 1–25 (2015). https://doi.org/10.1016/j.compositesa.2015.06.007

M. Habibi, L. Laperrière, H.M. Hassanabadi, Influence of low-velocity impact on residual tensile properties of nonwoven flax/epoxy composite. Compos. Struct. **186**, 175–182 (2018). https://doi.org/10.1016/j.compstruct.2017.12.024

J.J. Homan, Fatigue initiation in fibre metal laminates. Int. J. Fatigue **28**, 366–374 (2006). https://doi.org/10.1016/j.ijfatigue.2005.07.030

M.F. Ismail, M.T.H. Sultan, A. Hamdan, A.U.M. Shah, A study on the low velocity impact response of hybrid Kenaf-Kevlar composite laminates through drop test rig technique. Bioresources **13**, 3045–3060 (2018). https://doi.org/10.15376/biores.13.2.3045-3060

S.K. Karad, D. Attwood, F.R. Jones, Moisture absorption by cyanate ester modified epoxy resin matrices. Part V: effect of resin structure. Compos. Part A Appl. Sci. Manuf. **36**, 764–771 (2005). https://doi.org/10.1016/j.compositesa.2004.10.022

U. Kureemun, M. Ravandi, L.Q.N. Tran, W.S. Teo, T.E. Tay, H.P. Lee, Effects of hybridization and hybrid fibre dispersion on the mechanical properties of woven flax-carbon epoxy at low carbon fibre volume fractions. Compos. Part B Eng. **134**, 28–38 (2018). https://doi.org/10.1016/j.compositesb.2017.09.035

W.L. Lai, M. Mariatti, J.S. Mohamad, The properties of woven kenaf and betel palm (areca catechu) reinforced unsaturated polyester composites. Polym.-Plast. Technol. Eng. **47**, 1193–1199 (2008). https://doi.org/10.1080/03602550802392035

F. LeBel, É. Ruiz, F. Trochu, Void content analysis and processing issues to minimize defects in liquid composite molding. Polym. Compos. **40**, 109–120 (2019). https://doi.org/10.1002/pc.24609

J. Lee, S.S. Kessler, B.L. Wardle, Void-free layered polymeric architectures via capillary-action of nanoporous films. Adv. Mater. Interfaces **7**, 1901427 (2020). https://doi.org/10.1002/admi.201901427

Y. Li, Q. Li, H. Ma, The voids formation mechanisms and their effects on the mechanical properties of flax fiber reinforced epoxy composites. Compos. Part A Appl. Sci. Manuf. **72**, 40–48 (2015). https://doi.org/10.1016/j.compositesa.2015.01.029

X. Liu, W. Yu, P. Xu, Improving the photo-stability of high performance aramid fibers by sol-gel treatment. Fibers Polym. **9**, 455–460 (2008). https://doi.org/10.1007/s12221-008-0073-6

M. Liu, D. Fernando, G. Daniel, B. Madsen, A.S. Meyer, M.T. Ale, A. Thygesen, Effect of harvest time and field retting duration on the chemical composition, morphology and mechanical properties of hemp fibers. Ind. Crop. Prod. **69**, 29–39 (2015). https://doi.org/10.1016/j.indcrop.2015.02.010

M.Y. Lyu, T.G. Choi, Research trends in polymer materials for use in lightweight vehicles. Int. J. Precis. Eng. Manuf. **16**, 213–220 (2015). https://doi.org/10.1007/s12541-015-0029-x

Q. Ma, M.R.M. Rejab, S. Kang, M.S. Idris, M.A.A.M. Zin, The energy-absorbing characteristics of single spherical-roof contoured-core (SRCC) cell with composite materials. Int. J. Automot. Mech. Eng. **17**, 8265–8273 (2020). https://doi.org/10.15282/ijame.17.4.2020.04.0624

I. Mohammed, A.R.A. Talib, M.T. Hameed Sultan, M. Jawaid, A.H. Ariffin, S. Saadon, Mechanical properties of fibre-metal laminates made of natural/synthetic fibre composites. Bioresources **13**, 2022–2034 (2018). https://doi.org/10.15376/biores.13.1.2022-2034

N.H. Mostafa, Tensile and fatigue properties of Jute-Glass hybrid fibre reinforced epoxy composites. Mater. Res. Express **6**, 085102 (2019). https://doi.org/10.1088/2053-1591/ab21f9

M. Naebe, M.M. Abolhasani, H. Khayyam, A. Amini, B. Fox, Crack damage in polymers and composites: A review. Polym. Rev. **56**, 31–69 (2016). https://doi.org/10.1080/15583724.2015.1078352

L.F. Ng, D. Sivakumar, K.A. Zakaria, M.Z. Selamat, Fatigue performance of hybrid fibre metal laminate structure. Int. Rev. Mech. Eng. **11**, 61–68 (2017). https://doi.org/10.15866/ireme.v11i1.10532

L.F. Ng, D. Sivakumar, X.J. Woo, S. Kathiravan, I. Siva, The effects of bonding temperature and surface roughness on the shear strength of bonded aluminium laminates using polypropylene based adhesive. J. Adv. Manuf. Technol. **13**, 113–127 (2019)

L.F. Ng, S. Dhar Malingam, M.Z. Selamat, Z. Mustafa, O. Bapokutty, A comparison study on the mechanical properties of composites based on kenaf and pineapple leaf fibres. Polym. Bull. **77**, 1449–1463 (2020). https://doi.org/10.1007/s00289-019-02812-0

P. Niedermann, G. Szebényi, A. Toldy, Effect of epoxidized soybean oil on mechanical properties of woven jute fabric reinforced aromatic and aliphatic epoxy resin composites. Polym. Compos. **38**, 884–892 (2017). https://doi.org/10.1002/pc.23650

S. Nikafshar, O. Zabihi, S. Hamidi, Y. Moradi, S. Barzegar, M. Ahmadi, M. Naebe, A renewable bio-based epoxy resin with improved mechanical performance that can compete with DGEBA. RSC Adv. **7**, 8694–8701 (2017). https://doi.org/10.1039/C6RA27283E

I. Nurul Hidayah, D. Nuur Syuhada, H.P.S. Abdul Khalil, Z.A.M. Ishak, M. Mariatti, Enhanced performance of lightweight kenaf-based hierarchical composite laminates with embedded carbon nanotubes. Mater. Des. **171**, 107710 (2019). https://doi.org/10.1016/j.matdes.2019.107710

K.S. Pandya, C. Veerraju, N.K. Naik, Hybrid composites made of carbon and glass woven fabrics under quasi-static loading. Mater. Des. **32**, 4094–4099 (2011). https://doi.org/10.1016/j.matdes.2011.03.003

K.L. Pickering, G.W. Beckermann, S.N. Alam, N.J. Foreman, Optimising industrial hemp fibre for composites. Compos. Part A Appl. Sci. Manuf. **38**, 461–468 (2007). https://doi.org/10.1016/j.compositesa.2006.02.020

K.L. Pickering, M.G.A. Efendy, T.M. Le, A review of recent developments in natural fibre composites and their mechanical performance. Compos. Part A Appl. Sci. Manuf. **83**, 98–112 (2016). https://doi.org/10.1016/j.compositesa.2015.08.038

S. Rassmann, R. Paskaramoorthy, R.G. Reid, Effect of resin system on the mechanical properties and water absorption of kenaf fibre reinforced laminates. Mater. Des. **32**, 1399–1406 (2011). https://doi.org/10.1016/j.matdes.2010.09.006

N. Saba, M. Jawaid, in *Hybrid Polymer Composite Materials Properties and Characterisation, ed. by V.K. Thakur, M.K. Thakur, A. Pappu* (Woodhead Publishing, Cambridge, 2017), p. 57

S.N.A. Safri, M.T.H. Sultan, M. Jawaid, K. Jayakrishna, Impact behaviour of hybrid composites for structural applications: A review. Compos. Part B Eng. **133**, 112–121 (2018). https://doi.org/10.1016/j.compositesb.2017.09.008

M.A. Said, B. Dingwall, A. Gupta, A.M. Seyam, G. Mock, T. Theyson, Investigation of ultra violet (UV) resistance for high strength fibers. Adv. Sp. Res. **37**, 2052–2058 (2006). https://doi.org/10.1016/j.asr.2005.04.098

M.R. Sanjay, B. Yogesha, Studies on hybridization effect of jute/kenaf/E-glass woven fabric epoxy composites for potential applications: Effect of laminate stacking sequences J. Ind. Text. **47**, 1830–1848 (2018). https://doi.org/10.1177/1528083717710713

R. Sathish Kumar, N. Muralidharan, R. Sathyamurthy, Optimization of alkali treatment process parameters for kenaf fiber: Experiments design. J. Nat. Fibers (2020). https://doi.org/10.1080/15440478.2020.1856276

C. Scarponi, F. Sarasini, J. Tirillò, L. Lampani, T. Valente, P. Gaudenzi, Low-velocity impact behaviour of hemp fibre reinforced bio-based epoxy laminates. Compos. Part B Eng. **91**, 162–168 (2016). https://doi.org/10.1016/j.compositesb.2016.01.048

M.S. Scholz, J.P. Blanchfield, L.D. Bloom, B.H. Coburn, M. Elkington, J.D. Fuller, M.E. Gilbert, S.A. Muflahi, M.F. Pernice, S.I. Rae, J.A. Trevarthen, S.C. White, P.M. Weaver, I.P. Bond, The use of composite materials in modern orthopaedic medicine and prosthetic devices: A review. Compos. Sci. Technol. **71**, 1791–1803 (2011). https://doi.org/10.1016/j.compscitech.2011.08.017

D.U. Shah, P.J. Schubel, M.J. Clifford, P. Licence, Fatigue life evaluation of aligned plant fibre composites through S–N curves and constant-life diagrams. Compos. Sci. Technol. **74**, 139–149 (2013). https://doi.org/10.1016/j.compscitech.2012.10.015

M. Sogancioglu, E. Yel, G. Ahmetli, Behaviour of waste polypropylene pyrolysis char-based epoxy composite materials. Environ. Sci. Pollut. Res. **27**, 3871–3884 (2020). https://doi.org/10.1007/s11356-019-07028-3

M.S. Sreekala, J. George, M.G. Kumaran, S. Thomas, The mechanical performance of hybrid phenol-formaldehyde-based composites reinforced with glass and oil palm fibres. Compos. Sci. Technol. **62**, 339–353 (2002). https://doi.org/10.1016/S0266-3538(01)00219-6

O. Starkova, S. Chandrasekaran, L.A.S.A. Prado, F. Tölle, R. Mülhaupt, K. Schulte, Hydrothermally resistant thermally reduced graphene oxide and multi-wall carbon nanotube based epoxy nanocomposites. Polym. Degrad. Stab. **98**, 519–526 (2013). https://doi.org/10.1016/j.polymdegradstab.2012.12.005

K. Subramaniam, S. Dhar Malingam, N.L. Feng, O. Bapokutty, The effects of stacking configuration on the response of tensile and quasi-static penetration to woven kenaf/glass hybrid composite metal laminate. Polym. Compos. **40**, 568–577 (2019). https://doi.org/10.1002/pc.24691

M.C. Tanzi, S. Farè, G. Candiani, Foundations of Biomaterials Engineering, 1st edn. (Academic Press, USA, 2019), pp. 137–196

J.L. Thomason, L. Yang, R. Meier, The properties of glass fibres after conditioning at composite recycling temperatures. Compos. Part A Appl. Sci. Manuf. **61**, 201–208 (2014). https://doi.org/10.1016/j.compositesa.2014.03.001

L.M.G. Vieira, J.C. dos Santos, T.H. Panzera, J.C.C. Rubio, F. Scarpa, Novel fibre metal laminate sandwich composite structure with sisal woven core. Ind. Crop. Prod. **99**, 189–195 (2017). https://doi.org/10.1016/j.indcrop.2017.02.008

H. Wang, H. Wang, G. Zhou, Synthesis of rosin-based imidoamine-type curing agents and curing behavior with epoxy resin. Polym. Int. **60**, 557–563 (2011). https://doi.org/10.1002/pi.2978

R. Yahaya, S.M. Sapuan, M. Jawaid, Z. Leman, E.S. Zainudin, Effect of layering sequence and chemical treatment on the mechanical properties of woven kenaf–aramid hybrid laminated composites. Mater. Des. **67**, 173–179 (2015). https://doi.org/10.1016/j.matdes.2014.11.024

L. Yan, B. Kasal, L. Huang, A review of recent research on the use of cellulosic fibres, their fibre fabric reinforced cementitious, geo-polymer and polymer composites in civil engineering. Compos. Part B Eng. **92**, 94–132 (2016). https://doi.org/10.1016/j.compositesb.2016.02.002

K. Yorseng, S.M. Rangappa, J. Parameswaranpillai, S. Siengchin, Influence of accelerated weathering on the mechanical, fracture morphology, thermal stability, contact angle, and water absorption properties of natural fiber fabric-based epoxy hybrid composites. Polymers (Basel). **12**, 2254 (2020). https://doi.org/10.3390/polym12102254

J. Zhang, K. Chaisombat, S. He, C.H. Wang, Hybrid composite laminates reinforced with glass/carbon woven fabrics for lightweight load bearing structures. Mater. Des. **36**, 75–80 (2012). https://doi.org/10.1016/j.matdes.2011.11.006

Thermal Analysis of Hybrid Epoxy/Synthetic/Natural Fiber Composites

33

Mariana D. Banea, Jorge S. S. Neto, and Daniel K. K. Cavalcanti

Contents

Abstract

Hybrid epoxy/synthetic/natural fiber composites can be found in applications in many industrial sectors, such as automotive, construction, marine industry, and sports, among others. The natural fibers are mainly used due to eco-friendliness and lower weight and cost, while the synthetic reinforcements (e.g., glass, carbon and Kevlar fibers) provide higher strength, increased fiber/matrix interfacial strength and lower water absorption. Thermal stability of hybrid epoxy/synthetic/natural fiber composites is an important aspect to be considered, since the processing temperature plays a critical role in the fabrication process of the composites. At higher temperatures, the natural fiber components (i.e., cellulose, hemicellulose, and lignin) start to degrade and the key properties (mechanical and thermal) of the composite change. The incorporation of synthetic fibers in natural fiber-reinforced composites have the potential to increase their thermal stability. Different methods are used in the literature to determine the thermal properties of composite materials and also help to understand and determine the suitability of composites for a certain application. Thermogravimetric analysis (TGA), differential scanning calorimetry (DSC), thermomechanical analysis (TMA), and

M. D. Banea (✉) · J. S. S. Neto · D. K. K. Cavalcanti
Federal Center of Technological Education of Rio de Janeiro (CEFET/RJ), Rio de Janeiro, Brazil
e-mail: doina.banea@cefet-rj.br

S. Mavinkere Rangappa et al. (eds.), *Handbook of Epoxy/Fiber Composites*,
https://doi.org/10.1007/978-981-19-3603-6_50

differential mechanical thermal analysis (DMA) are used to investigate the thermal stability of composites. The percentage of weight loss, degradation temperature, T_g, thermal expansion coefficient (CTE), and viscoelastic properties (storage modulus, loss modulus, and the damping factor) are the most common thermal properties determined by these methods. This chapter presents an overview of the main techniques used for thermal analysis of hybrid epoxy/synthetic/natural fiber composites. The main factors that affect the thermal properties of the composite materials (fiber and matrix type; the presence of additive fillers, fiber content, and fiber orientation; the chemical treatment of the fibers; manufacturing process; and type of loading) are briefly discussed.

Keywords

Natural fibers · Hybrid epoxy/synthetic/natural fiber composites · Thermal analysis · Thermogravimetric analysis (TGA) · Differential scanning calorimetry (DSC) · Thermomechanical analysis (TMA) · Differential mechanical thermal analysis (DMA)

Introduction

The aeronautics and automotive industries are constantly looking for the development of lighter and more resistant materials in order to improve the efficiency and reliability of their systems (Banea and da Silva 2009). However, other required characteristics of composite materials such as renewability and low environmental impact and cost are increasingly being considered. Consequently, there has been an increasing growth in research and innovation in the natural fiber-reinforced composite (NFRC) materials, mainly due to the advantages of these materials compared to synthetic fiber-reinforced composites, such as low environmental impact and low cost which support their potential across a wide range of applications (Wambua et al. 2003; Budhe et al. 2019; Banea et al. 2021). However, one of the drawbacks is that the NFRCs present relatively low mechanical properties. One method to increase their mechanical performance in order to extend their applications is hybridization. Thus, hybrid composites, which contain one or more types of reinforcement, are gaining growing research interest (Swolfs et al. 2014; de Araujo Alves Lima et al. 2020; Cavalcanti et al. 2019). Hybrid composites consist of a combination of two or more fibers, which can be arranged in a random, layer-by-layer, or in-yarn manner, in a polymer matrix. The possible combinations of fibers in hybrid composites consist of synthetic/synthetic, natural/synthetic, and natural/natural fiber types. For instance, using natural fibers brings several advantages, such as the abovementioned eco-friendliness and lower weight and cost, while the synthetic fibers present higher strength, increased fiber/matrix interfacial strength, and lower water absorption.

It is well-known that the mechanical properties (e.g., tensile, flexural, and impact) of composite materials depend on the fiber properties, the interfacial adhesion strength

between fiber/matrix, and the matrix's properties (Pickering et al. 2016). Therefore, choosing the correct fiber/matrix combination is fundamental to obtain good mechanical and thermal properties of composite materials (Cavalcanti et al. 2021).

Different combinations of fiber types (natural or synthetic) can be used to improve the performance of hybrid composites. In general, the natural fibers can be divided into three main groups regarding their origin: mineral, animal, and cellulose/lignocellulose. The cellulose/lignocellulose fibers are the most suitable natural fibers to be used in hybrid composites due to their relatively low price and higher mechanical properties compared to the other natural fiber types (mineral and animal). Further, the cellulosic fibers can also be subdivided into different categories corresponding to the plant part that originated them. The most common natural fibers used to produce hybrid synthetic/natural fiber composites are as follows: jute, sisal, ramie, hemp, kenaf, banana, curauá, pineapple, abaca, bamboo, flax, and palm (Chandrasekar et al. 2017; Li et al. 2020). All these fibers are mainly made of cellulose (α-cellulose), hemicellulose, and lignin. They also present small quantities of waxes in their outer part. However, the chemical composition and cell structure of natural fibers are quite complicated (de Araujo Alves Lima et al. 2020). Each fiber is essentially a composite in which rigid cellulose microfibrils are embedded in a soft lignin and hemicellulose matrix. Moreover, the microfibrils are helically wound along the fiber axis to form hollow cells. For instance, the curauá, jute, and sisal morphology are different with distinct lumen diameters (4, 6, and 8 μm, respectively) and cell wall thickness (Li et al. 2020). Besides, they also present different percentages of lignin, cellulose, and hemicellulose in their configuration. It is worth to mention that the amount of cellulose and lignin in the natural fibers depends on the environmental conditions during the plant cultivation, soil properties, irrigation, and extraction techniques (i.e., automatic harvesting or manual extractions) (Li et al. 2020). These characteristics change the natural fibers' morphology and, consequently, their mechanical and thermal properties. The natural fibers have relatively low degradation temperatures (e.g., approx. 200 °C), and for this reason, they cannot be used beyond a certain temperature limit during the manufacture of composites (Araújo et al. 2008). It was shown in the literature that the cellulose content of the natural fibers causes flammability and the lignin content causes char. Consequently, the higher the cellulose and lignin content in a natural fiber is, the higher the flammability and char production is and the lower the degradation temperature of the composite is (Araújo et al. 2008). One method used to increase the stability of natural fiber-reinforced composites at elevated temperatures is to use chemical treatments along with fire-retardant materials (Banea et al. 2021).

On the other hand, glass, carbon, and aramid fibers are the synthetic fibers, which are used in hybrid synthetic/natural fiber composites mainly because of their high stiffness and strength properties. However, the main drawbacks of using these fibers in hybrid natural/synthetic composites are related to their poor biodegradability, initial processing costs, recyclability, energy consumption, machine abrasion, some health hazards, etc.

The most common matrices used to produce hybrid synthetic/natural fiber composites are the polymeric matrices due to lightweight, less abrasiveness, and significant relationship between cost and mechanical properties. Another important aspect

is that the polymeric matrices can be processed at low temperatures, which is a critical factor for natural fibers. The polymeric matrices can be divided into two main groups: thermoplastic and thermosetting. Thermoplastic matrices are made by different polymers that can be softened, melted, and, also, recycled by the application of heat. However, the continuous reprocessing of these polymers can deteriorate their mechanical and thermal properties. On the other hand, the thermoset matrices can hardly be recycled or change their shape once the polymerization is concluded. However, the use of thermoset matrices for the fabrication of hybrid natural fiber composites ensures higher strength and moisture resistance.

Epoxy and unsaturated polyester resins are the main thermoset resins used to manufacture hybrid natural/synthetic composites. The main advantages of epoxy resins are as follows: generally high thermal and mechanical properties, high water and chemical resistance, controllable viscosity, low cure-shrinkage, easy cure coupled with high T_g, and excellent adhesion properties. In addition, no volatile agents are formed during the curing process, which is an important advantage as compared to phenolic, polyester, and vinyl ester resins. Finally, the shrinkage associated with epoxy resins is lower compared to polyesters. However, one disadvantage is that epoxy resins are relatively brittle, which is detrimental to the interlaminar properties between the matrix and the fiber reinforcement. It is known that epoxy resin cures from liquid to solid through a catalytic chemical reaction and they form extremely strong bonds that cannot be easily reversed or reformed, and for this reason, the performance of this matrix material is superior to other matrices. However, for the same reason, their recycling remains challenging, which is a major drawback nowadays as increasing industrial sectors (e.g., automotive sector) have regulations regarding the sustainability.

Hybrid epoxy/synthetic/natural fiber composites can be found in applications in many industrial sectors, such as automotive, construction, marine industry, and sports, among others. Moreover, the most promising applications of epoxy hybrid polymer composites are in automotive industry. In general, they are used in nonstructural car body parts, such as the following: door panels, package trays, hat racks, instrument panels, internal engine covers, sun visors, boot liners, and oil-air filters. However, they are moving ahead to be used in more structurally demanding parts, such as seat backs, exterior underfloor paneling, as well as anti-roll bars (Pickering et al. 2016; Ravishankar et al. 2019; de Queiroz et al. 2020). They can also be used in construction and building applications, like bricks, door panels, roofing sheets, furniture panels, etc. Hybrid natural/synthetic polymer composites are also used in railway coach interiors and in aircraft industries to make interior parts, among others.

In this context, the thermal stability of hybrid epoxy/synthetic/natural fiber composites is an important aspect to be considered, since the processing temperature plays a crucial role in the composite fabrication process. The composites should be thermally stable as heat from mechanical energy can reduce the loading capacity. Different methods are used in the literature to determine the thermal properties of composite materials and also help to understand and determine the suitability of the composites for a certain application. This chapter presents an overview of the main techniques used for thermal analysis of hybrid epoxy/synthetic/natural fiber

composites. The main factors that affect the thermal properties of the composite materials (fiber and matrix type; the presence of additives fillers, fiber content, and fiber orientation; the chemical treatment of the fibers; manufacturing process; and type of loading) are briefly discussed.

Thermal Properties of Hybrid Epoxy/Synthetic/Natural Fiber Composites

The main techniques used for thermal analysis of hybrid epoxy/synthetic/natural fiber composites are as follows: thermogravimetric analysis (TGA), differential scanning calorimetry (DSC), thermomechanical analysis (TMA), and dynamic mechanical analysis (DMA). The main thermal properties of the composites provided by these techniques are as follows: the crystallization temperature (T_c), melting temperature (T_m), glass transition temperature (T_g), thermal expansion coefficient (CTE), viscoelastic behavior, and thermal stability. It was shown in the literature that several factors can affect the thermal properties of the composite materials, such as the following: fiber and matrix type, manufacturing process, and type of loading (Saba and Jawaid 2018; Saba et al. 2016; Kumar et al. 2020). In addition, the fiber orientation and volume and chemical treatment of the fibers will also impact the thermal properties of the composites.

Figure 1 summarizes the main methods used in the literature to determine the thermal properties of composite materials (the scheme shows which technique is the most indicated to determine a specific property, where the blue color represents the recommended method and the black represents the alternative method).

Thermogravimetric Analysis (TGA)

TGA consists on measuring the weight of a material sample, in an atmosphere of nitrogen, helium, air, or other gases, as a function of increasing temperature or isothermally as a function of time (Krishnasamy et al. 2019; Asim et al. 2019). Typical thermogravimetric parameters consist of moisture, volatile substances, loss on ignition, or ash. Different temperatures and measurement times are applied in accordance with the matrix type of the composite sample (Lin 2016; Asim et al. 2019, 2020; Krishnasamy et al. 2019).

Figure 2 shows a typical TGA graph with the main parameters provided by this method: m_s (starting mass), m_f (end mass), point A (degradation start), point B (degradation end), point C (degradation middle point), temperature points (T_a, T_b, and T_c), and time points (t_a, t_b, and t_c) (Krishnasamy et al. 2019; Asim et al. 2020). The thermal data obtained from the TGA curve depends on several factors, such as the following: sample mass and shape, atmosphere, flow rate, heating rate, and the treatment applied (Asim et al. 2020).

The thermogravimetric behavior of hybrid synthetic/natural composites depends on composite constituents (fibers and matrix). For example, similar natural fibers such as jute, sisal, wood, and cotton have similar TG/DTG curves and thermal

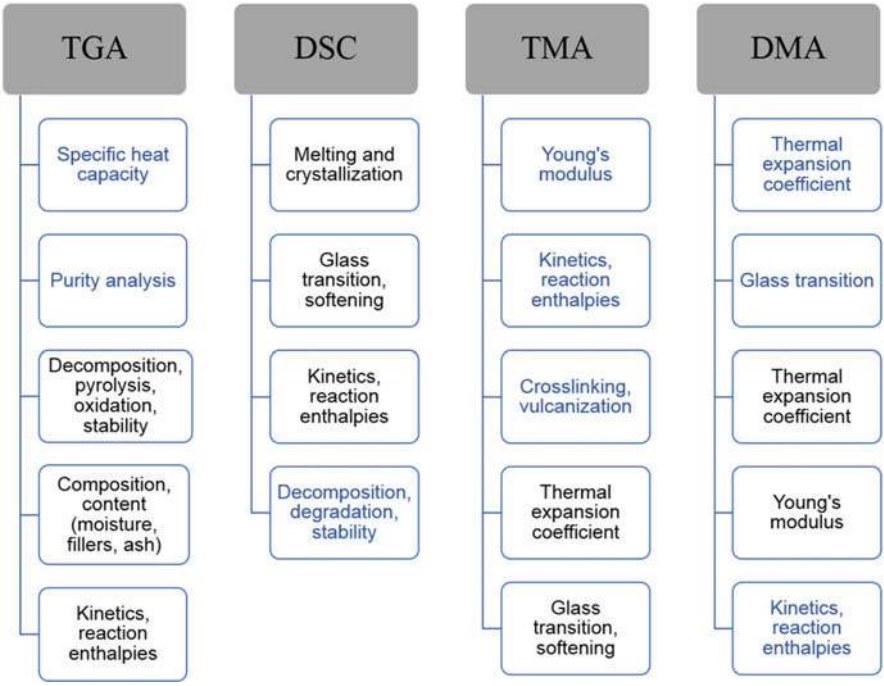

Fig. 1 Schematic of the principal methods used to determine the thermal properties of composite materials (where the blue color represents the recommended method and the black represents the alternative method to determine a specific property). (Authors source)

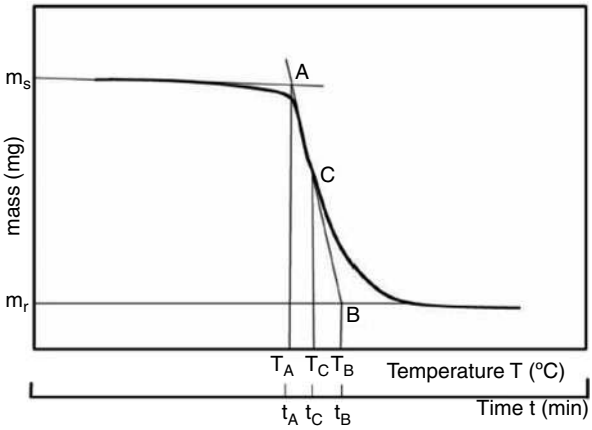

Fig. 2 A schematic illustration of a typical TGA curve where m_s is the starting mass, m_f represents the end mass, point A (degradation start), point B (degradation end), point C (degradation middle point), temperature points (T_a, T_b, and T_c), and time points (t_a, t_b, and t_c). (Author source)

decomposition pattern. The derivative thermogravimetric test (DTG) shows the maximum rate of peak thermal decomposition, and fiber constituents are indicated by peaks in each degradation range.

Lignocellulose fibers (i.e., jute, flax, wood, sisal, ramie, curauá, and others) present the three stages of degradation: The first stage is related to water loss by natural fiber (60–100 °C). The second stage is related to the loss of the main constituents of the fibers – hemicellulose, cellulose, and lignin (200–500 °C). Finally, the last stage of degradation is the formation of active coal as a form of residue (Guo et al. 2019; Członka et al. 2020; Jawaid et al. 2013a; El Boustani et al. 2017; Dalla Libera Junior et al. 2020).

Several authors used the thermogravimetric analysis to determine the thermal properties of hybrid epoxy/synthetic/natural composites (Chee et al. 2019a; Naveen et al. 2019; Pereira et al. 2020; Braga and Magalhaes Jr 2015; Aisyah et al. 2019; Arshad et al. 2021). For example, Naveen et al. (2019) studied the effect of hybridization on the mechanical and thermal properties of epoxy-based Kevlar fiber (K) and *Cocos nucifera* sheath (CNS) composites. The following percentages were investigated: 100 K/0 CNS (S1), 75 K/25 CNS (S2), 50 K/50 CNS (S3), 25 K/75 CNS (S4), and 0 K/100 CNS (S5). The composite fabrication method used was the hand-layup technique followed by hot pressing. It was shown that the TGA curve presents three different degrading regions: The initial degradation (100–200 °C) is related to the evaporation of water particles found on the fiber surface and dehydration of the secondary alcoholic groups. The second stage of degradation occurs between 150 °C and 500 °C with the decomposition of lignocellulosic materials. The authors state that the following constituents are found in these ranges: hemicellulose, 150–350 °C; lignin, 250–500 °C; and cellulose, 275–500 °C. Finally, the third stage occurs above 500 °C with the total decomposition of the composite and formation of char residue. The authors concluded that the 75 K/25 CNS hybrid composite presented the highest thermal stability when compared to the 50 K/50 CNS, 25 K/75 CNS, and 0 K/100 CNS composites. The 75 K/25 CNS hybrid composite presented values of 369 °C for the T_{onset}, 581 °C for the T_{end}, and 14.67% char residue, respectively.

Braga et al. (Braga and Magalhaes 2015) investigated the influence that the wt% of glass fiber had on the mechanical and thermal properties of the jute/glass fiber epoxy-based composites. The studied percentages were as follows: 69% of epoxy resin – 31% of jute fiber and 0% of glass fiber (E69-J31-V0), 68% of epoxy resin – 25% of jute fiber and 7% of glass fiber (E68-J25-V7), and 64% of epoxy resin – 18% of jute fiber and 19% of glass fiber (E64-J18-V19). They found that an increased weight percentage of the glass fiber had a positive effect in the thermal properties of the composite. The TGA showed that the final thermal degradation occurred between 200 °C and 450 °C. Approximately, 70% of degradation was observed due to degradation of the jute fibers, and the residual amount of the total mass was 6.48%. For the E68-J25-V7 composite samples, the TGA curve showed 1.52% of the weight loss. The final weight loss (approximately 68.97%) was found for temperatures between 200 °C and 450 °C, and the residual amount was 17.5% of the original mass. A mass loss of 1.27% at 100 °C was observed for the E68-J18-V19 composite, while for the E69-J31-V0 composite, the mass loss was of 1.97%. However, for the E68-J18-V19 composite, the mass loss was 24.19%, showing that the presence of glass fiber in the composite contributed to the reduction in material volatility, as can be seen in Fig. 3.

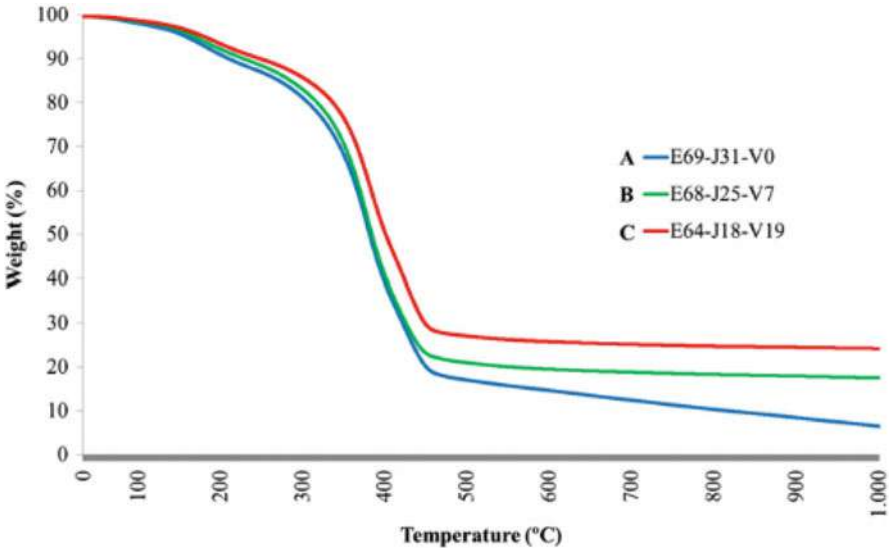

Fig. 3 Combined TGA graph of different composite materials (A – 69% epoxy resin–31% jute fiber–0% glass fiber (E69-J31-V0); B – 68% epoxy resin–25% jute fiber–7% of glass fiber (E68-J25-V7); and C – 64% epoxy resin–18% jute fiber–19% glass fiber (E64-J18-V19)). (With permission of Springer from Braga and Magalhaes (2015))

Aisyah et al. (2019) analyzed the effects that the hybridization had on the thermal properties of hybrid (carbon + kenaf) composite. The hybrid fabrics used two types of weave designs: a 5 × 5 satin kenaf and a 6 × 6 plain kenaf. The composites were designated as the following: carbon + plain kenaf fabric + carbon fiber (CP5), carbon + plain kenaf fabric + carbon fiber (CP6), carbon + satin kenaf fabric + carbon fiber (CS5), and carbon + satin kenaf fabric + carbon fiber (CS6). They found that the hybrid composite with the 6 × 6 design was the most thermally stable composite when compared to the other studied hybrid composites. However, the pure carbon fiber-reinforced composites still presented the highest thermal stability when compared to all studied composites.

Pereira et al. (2020) investigated the mechanical and thermal properties of epoxy/hybrid composites manufactured by hand-layup technique followed by compression molding. The following configurations were studied: sisal (S), sisal + ramie (S + R), sisal + curauá (S + C), and sisal + glass fibers (S + G). TGA was used to measure the mass loss of composites as a function of temperature. Figure 4 shows the composite thermal degradation as a function of hybridization. The thermal stability of the composites is related to the onset of a massive weight loss, and this was clearly observed as a sharp downward inclination in the TG curve, which can be seen at 240–420 °C in Fig. 4a. The DTG curves for the epoxy sisal-based hybrid composites are presented in Fig. 4b. It was found that the major degradation peaks were at 337 °C and are almost the same for pure sisal and the studied hybrid composites.

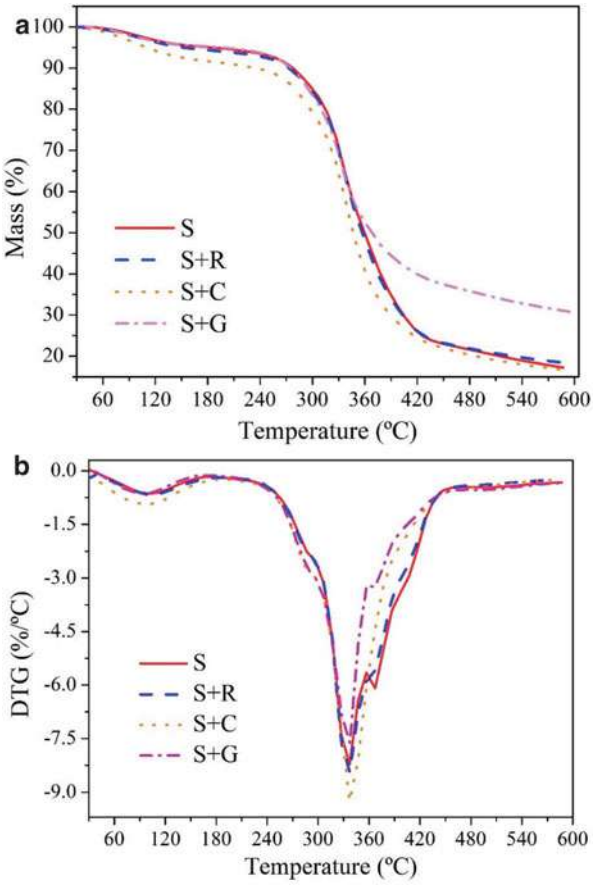

Fig. 4 Thermal analysis curves for different hybrid composites (*S* sisal, *S* + *R* sisal + ramie, *S* + *C* sisal + curauá, *S* + *G* sisal + glass fiber): (**a**) TGA and (**b**) DTG. (Reproduced with permission from authors of Pereira et al. (2020))

Sisal + glass fiber composites presented lower speed of mass loss compared to the other samples.

Arshad et al. (2021) studied the effect of addition of titanium carbide (TiC) nanoparticles in composites reinforced with coconut and basalt fibers in epoxy and bio-epoxy matrices. The configurations being studied were pure bio-epoxy (BE33), 10 wt% of coir fiber + basalt (CBBE33), 5 wt% of coir fiber + basalt + 5 wt% of TiC (CBABE33), pure epoxy (SE), 10 wt% of coir fiber + basalt (CSE), and 5 wt% of coir fiber + basalt + 5 wt% of TiC (CBASE). The results showed that the presence of TiC in composites based on epoxy and bio-epoxy increased the thermal stability of the composites. The authors report that the composite CBABE33 and CBASE obtained a residual mass of 33.7% and 28.2%, respectively.

Sumesh et al. (Sumesh and Kanthavel 2019) investigated the effect of the aluminum oxide nanoparticle (Al_2O_3) on sisal/coir, sisal/banana, and banana/coir hybrid composites. The mechanical and thermal properties of the composites were analyzed.

The weight percentages of studied aluminum oxide (Al_2O_3) were 0, 1, 2, and 3. The authors reported that the presence of aluminum oxide (Al_2O_3) increased the onset of thermal degradation of the composite. For the sisal/coir composite modified with 3% nano alumina, the T_{onset} value was 127.77 °C, compared to the T_{onset} of the unmodified composites which was 121.66 °C. For the sisal/banana composite, the best case was found for the 1% of nanoparticles (T_{onset} of 146.38 °C when compared to the unmodified specimens which had a T_{onset} of 133.17 °C). Finally, for the banana/coir composite, the best case was 3% of nanoparticles with a T_{onset} of 152.97 °C compared to T_{onset} of 103.9 °C found for the unmodified samples.

Jesuarockiam et al. (2019) studied the thermal properties of hybrid Kevlar/*Cocos nucifera* sheath (CNS) modified with graphene nanoplatelets (GNP). The following cases were investigated: 100 K/0 CNS, 75 K/25 CNS, 50 K/50 CNS, 25 K/75 CNS, and 0 K/100 CNS with a variation in the percentage of incorporated GNP of 0.25%, 0.5%, and 0.75%. The composites were manufactured via hand-layup technique followed by hot pressing. The GNP was added to the epoxy resin and mixed using the ultra-sonication technique. They found that the 75 K/25 CNS + 0.75 wt% GNP presented similar thermal stability to the pure Kevlar composite. Furthermore, the authors report that the presence of the GNP nanoparticles increased the thermal stability of all studied configurations.

Ridzuan et al. (2016) investigated the effect of the alkalinization treatment on the thermal and mechanical properties of the hybrid *Pennisetum purpureum*/glass fiber composite. The hybrid composites were fabricated through the vacuum infusion process. The composites studied were: *P. purpureum*/glass untreated, 5% of alkali purpureum/glass and 10% of alkali purpureum/glass. It was found that the hybrid composites subjected to the 5% alkaline treatment presented a T_{onset} and T_{end} higher than the other studied cases. The DTG results showed three degradation stages in the form of peaks (see Fig. 5). The authors report that the first peak is related to the water

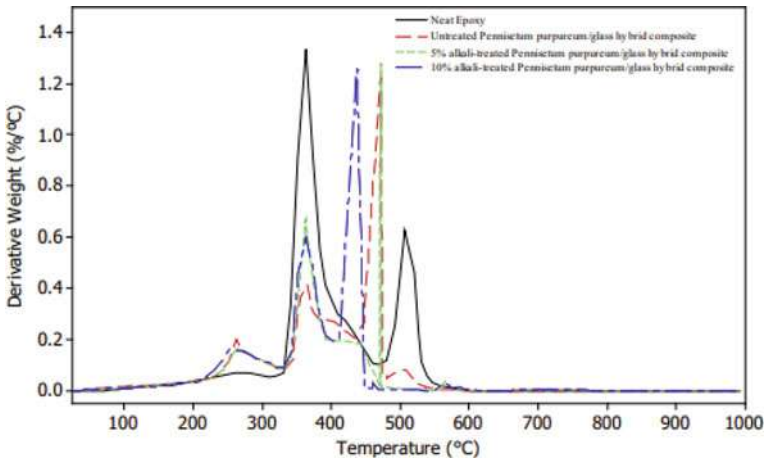

Fig. 5 Derivative thermogravimetric (DTG) analysis curves obtained for *Pennisetum purpureum*/glass-reinforced hybrid composites. (Reproduced with permission from Ridzuan et al. (2016))

molecules found in the fiber constituents (hemicellulose). The hybrid composite's second and third peak presented lower values than the resin's peak.

Zin et al. (2019) used TGA to investigate the thermal properties of hybrid composites of banana, pineapple, and glass fiber-reinforced epoxy matrix with different fiber volume fractions (30%, 40%, 50% in weight). The studied cases were as follows: glass-banana-PALF (GBP), 30% glass-banana (GB30), 40% glass-banana (GB40), 50% glass-banana (GB50), 30% glass-PALF (GP30), 40% glass-PALF (GP40), and 50% glass-PALF (GP50). The banana/glass composite with 40 wt% presented a T_{onset} of 349.12 °C, while the composite with 30 and 50 wt% reached a value of 327.29 °C and 328.03 °C, respectively. The PALF/glass composite with 40 wt% had a T_{onset} value of 341.14 °C, while the composite with 30 and 50 wt% presented a T_{onset} value of 319.46 °C and 313.78 °C, respectively. GBP composite reached a value of 336.96 °C of initial degradation. GB40 and GP40 presented the best performance when compared to the other hybrid composites.

Dhakal et al. (2013) analyzed the effect of carbon fiber hybridization on the thermal stability of flax composites using the thermogravimetric analysis (TGA). The compression molding technique was used to manufacture the composites. The studied configurations were the following: 6 ply flax fiber cross-ply orientation – (Flax CP), ply unidirectional carbon fiber + 2 ply flax fiber – (Flax CP – Carbon), 6 ply unidirectional carbon fiber – (Carbon), 6 ply unidirectional flax fiber – (Flax UD), and 2 ply unidirectional carbon fiber + 2 ply flax fiber – (Flax UD – Carbon). They found that the carbon fiber hybridization can significantly influence the thermal stability of flax composites. The carbon fiber hybridization on flax composites decreased the rates of weight losses, and the residual char yield of the carbon hybridized composites was higher than that of flax composites without carbon fiber hybridization.

Safri et al. investigated the impact that the benzoylation chemical treatment had on the mechanical and thermal properties of a hybrid glass fiber (GF)/sugar palm (SPF)-reinforced composite (Safri et al. 2020). The following fiber percentages were used – 30%, 50%, and 70% – and the following hybrid cases were studied: epoxy/glass fiber (EP 90%/GF 10%), epoxy/sugar palm fiber untreated (EP 90%/SPF 10%), (EP 90%/10% SPF/3% GF) untreated, (EP 90%/5% SPF/5% GF) untreated, (EP 90%/3% SPF/7% GF) untreated, epoxy/sugar palm benzol treated (EP 90%/SPF 10%), (EP 90%/SPF 7%/GF 3%) benzoyl treated, (EP 90%/SPF 5%/GF 5%) benzoyl treated, and (EP 90%/SPF 3%/GF 7%) benzoyl treated. It was found that the EP/SPF 3%/GF 7% benzoyl treated composite presented an increase in thermal properties, with an increase in T_{onset} and final degradation temperature. Furthermore, the authors report that the chemical treatment increased the interfacial adhesion between fiber and matrix. Mazlan et al. (2020) analyzed the effect that the inclusion of clay in the thermal properties of a hybrid kenaf/glass fiber composite has. They found that the TKG 1% composite presented the highest thermal stability between the studied cases.

Sathiyamoorthy and Senthilkumar (2020) studied the effect that the hybridization had on a jute/carbon fiber-reinforced composite. They found that the T_{onset} was 165 °C for the hybrid composite, while for the jute composite, a value of 153 °C was found. The authors report that mass loss occurred three times: the first mass loss

occurred at 30–126 °C due to water evaporation, the second mass loss was at 153–306 °C with the degradation of the hemicellulose and lignin constituents, and finally the last mass lost occurred at 306–390 °C due to cellulose degradation. Table 1 summarizes the results from several recent studies on the effect of hybridization on the thermal properties of hybrid synthetic/natural composites.

Differential Scanning Calorimetry (DSC)

The DSC measures the temperature and heat flux associated with material transitions as a function of temperature and time. This technique provides qualitative and quantitative information on physical and chemical changes involving endothermic (heat absorption) and exothermic (heat released) processes. The exothermic and endothermic peaks and magnitudes indicate the thermal phase transformation of the composites (Saw and Datta 2009; Aji et al. 2011). Thermal data extracted from this analysis are the following: the glass-transition temperature (T_g), crystallization temperature (T_c), fusion temperature (T_m), enthalpy variation, and heat capacity as can be seen in Fig. 6 (Chandrasekar et al. 2017).

The T_g is an important material property when considering the composites for a particular end-use application. T_g is the temperature band in which a thermoset polymer changes from a rigid to a more flexible or rubbery state. It is well-known that the "normal" state of most thermoset polymers at room temperature is rigid (amorphous solid). Below the T_g, the molecular chains of the thermoset resins do not present enough energy to let them move around (the molecules are frozen in place as a rigid structure because of the short chain length, molecular groups separating off the chain and interlocking with each other). Moreover, when the polymer resin is heated, the molecules of the polymer resin gain energy, and they can start to move around. The amorphous rigid structure of the thermoset polymer resin is transformed to a flexible structure (rubbery state), when a certain heat energy is attained and the polymer molecules are allowed to move freely around each other. This transition point is termed the glass transition temperature. Another polymer might need to have strong physical properties when it is being used at an elevated temperature. To conclude, the service temperature of polymer resins (e.g., epoxy) should be always below the glass transition temperature. If the composites are used above their T_g, they will quickly lose their mechanical properties (strength and stiffness), and they will continue to maintain some mechanical properties until the temperature reaches T_m.

In general, the epoxy resins have good mechanical properties below 100 °C, and some more heat-resistant types/kinds can be used up to 200 °C. It is well-known that the T_g of epoxy resins can be affected by the curing process and also the hardener used. Typically, a higher cure temperature provides a higher T_g of the composite.

The T_c is associated with the energy gain to form organized polymeric chains (Lin 2016) and is found in a temperature range above that of the T_g but lower than the T_m. Finally, the T_m is when the crystalline polymers lose their bonds and turn into a liquid. This process is called endothermic transition (Lin 2016). In general, T_m for a

Table 1 Effect of hybridization on the thermal properties of hybrid composites obtained from TGA

Composite	Main parameters used in the analysis	Effect of hybridization on the thermal properties	Ref.
Cocos nucifera sheath (CNS)/ Kevlar	The temperature was ramped from 30 °C to 900 °C with a heating rate of 10 °C/min The measurements were performed in a dynamic nitrogen atmosphere (50 mL/min). Samples of approx. 20 mg were used The equipment used was Mettler Toledo TGA	The 75% G/25% CNS hybrid presented the highest thermal stability when compared to the other hybrid composites	Naveen et al. (2019)
Sisal/glass	The temperature was ramped from 30 °C to 600 °C with a heating rate of 10 °C/min, under a nitrogen atmosphere Samples of approx. 20 mg The equipment used was NETZSCH TG 209 F3 Tarsus	The hybridization increased the thermal stability when compared to the pure sisal	Pereira et al. (2020)
Jute/glass	The temperature was ramped from 35 °C to 1000 °C with a heating rate of 20 °C/min, under a nitrogen atmosphere. Samples of approx. 10 mg were used. The equipment used was TA Instruments	The increase in fiber glass content wt% increased the thermal stability of hybrid jute/glass composites	Braga and Magalhaes (2015)
Kenaf/carbon	The temperature was ramped from 25 °C to 800 °C with a heating rate of 10 °C/min, under a nitrogen atmosphere at a flow rate of 50 mL/min. Samples of approx. 8–10 mg. The equipment used was TGA Q500 TA Instruments	The hybridization produced higher thermal stability with the increase in fiber content when compared to other hybrid composites	Aisyah et al. (2019)
Kenaf/glass/clay	The temperature was ramped from 30 °C to 700 °C with a heating rate of 10 °C/min, under a nitrogen atmosphere at a flow rate of 50 mL/min.	The chemical treatment and hybridization both increased the thermal stability	Mazlan et al. (2020)

(continued)

Table 1 (continued)

Composite	Main parameters used in the analysis	Effect of hybridization on the thermal properties	Ref.
	The equipment used was the TA Instruments Q500 TGA		
Cocos nucifera sheath (CNS)/ Kevlar/graphene nanoplatelets (GNP)	The temperature was ramped from 30 °C to 900 °C with a heating rate of 10 °C/min, under a nitrogen atmosphere at a flow rate of 50 mL/min. Samples of around 20 mg. The equipment used was Mettler Toledo TGA	The 75% G/25% CNS/0.75 wt% of GNP hybrid obtained the highest thermal stability values when compared to the pure Kevlar composite	Jesuarockiam et al. (2019)
Pennisetum purpureum/glass	The temperature was ramped from 30 °C to 1000°C with a heating rate of 10 °C/min, under a nitrogen atmosphere at a flow rate of 20 mL/min. Samples of 10–15 mg. The equipment used was Mettler Toledo TGA	The increased alkaline treatment of the fiber decreased the quantity of residue from the hybrid composite	Ridzuan et al. (2016)
Banana/PALF/ glass	The temperature was ramped from 30 °C to 600 °C with a heating rate of 10 °C/min, under a nitrogen atmosphere at a flow rate of 20 mL/min. Samples of around 4.9–8.9 mg. The equipment used was the TA Instruments Q500 TGA	The group with fiber percentage of 40 for both banana-glass and PALF-glass hybrid composite presented the best thermal stability, within the studied composites	Zin et al. (2019)
Sugar palm/glass	The temperature was ramped from 25 °C to 900 °C with a heating rate of 10 °C/min, under a nitrogen atmosphere. The equipment used was TA Instruments Q500 TGA	The benzoyl treatment and the hybridization increased the thermal properties of the studied hybrid composites	Safri et al. (2020)
Flax/carbon	The temperature was ramped from room temperature to 550 °C under a nitrogen atmosphere. Samples of around 5–8 mg. The heating rate of 20 °C/min was used. The equipment used was TA TGA Q50 V	The hybridization reduced the studied composites thermal degradation rate	Dhakal et al. (2013)

(continued)

Table 1 (continued)

Composite	Main parameters used in the analysis	Effect of hybridization on the thermal properties	Ref.
Jute/carbon	The temperature was ramped from 20 °C to 800 °C with a heating rate of 20 °C/min, under a nitrogen atmosphere. Samples of approx. 5–6 mg were tested with the TA Instruments SDT Q600 Model equipment	The hybridization of the composites presented good thermal stability at high temperatures	Sathiyamoorthy and Senthilkumar (2020)
Coir/basalt/ titanium carbide (TiC)	The temperature was ramped from 30 °C to 600 °C with a heating rate of 15 °C/min, under a nitrogen atmosphere. Samples were tested with the Mettler Toledo Model equipment	The presence of titanium carbide (TiC) increases the thermal stability of the composite	Arshad et al. (2021)
Sisal/coir/ banana/oxide of aluminum (Al_2O_3)	The temperature was ramped from 50 °C to 600 °C with a heating rate of 30 °C/min, under a nitrogen atmosphere	The presence of oxide of aluminum (Al_2O_3) increased the T_{onset}	Sumesh and Kanthavel (2019)

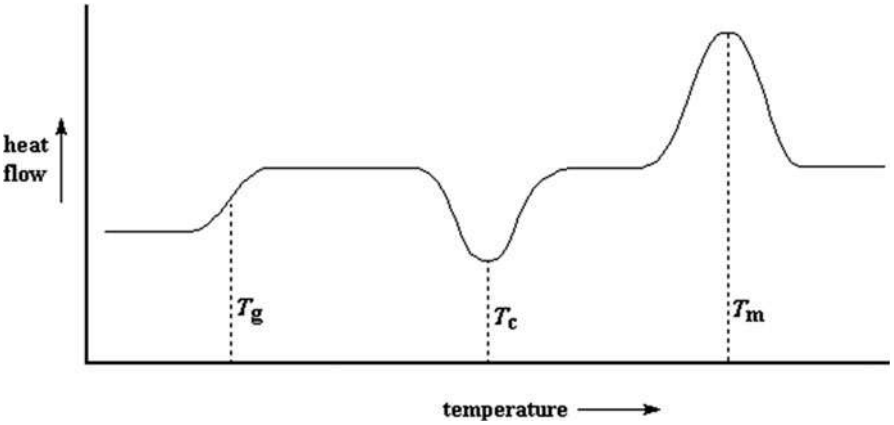

Fig. 6 Schematic illustration of a typical DSC curve where T_g represents the glass-transition temperature, T_c is the crystallization temperature, and T_m is the fusion temperature. (Author source)

thermoset polymer is higher than its T_g (see Fig. 6). At a temperature above T_g but below T_m, the polymer resin is in the rubbery state, and the material can exhibit large deformation under relatively low load.

There are several factors that can affect the data collected by the DSC analysis, such as the sample size and shape, heat ramp, and type of atmosphere. Several

authors used the DSC technique to study the effect of hybridization on the T_g and the peaks (endothermic and exothermic) of hybrid epoxy/synthetic/natural composites (Gupta 2018; Aisyah et al. 2019; Pereira et al. 2020; Safri et al. 2020; Naveen et al. 2019).

Pereira et al. (2020) used DSC to investigate the influence of the hybridization on the thermal properties of pure sisal and epoxy hybrid composites. Figure 7 shows an example of DSC curves for the studied composites (S – sisal; S + R – sisal + ramie; S + C – sisal + curauá; S + G – sisal + glass fiber). It can be seen that two events predominate, endothermic and exothermic around 100 °C and 375 °C, respectively. Sisal + curauá was the sample that absorbed the most heat in the endothermic event and the one that least released heat in the exothermic event.

Aisyah et al. (2019) also used the DSC method to investigate the influence that the hybridization technique had on the thermal properties of a kenaf/carbon composite. They found that the incorporation of the carbon fiber had a positive impact in thermal degradation characteristics of the hybrid composites as they increased their decomposition temperature.

Jesuarockiam et al. (2019) investigated the thermal properties of the hybrid Kevlar/*Cocos nucifera* sheath (CNS) modified with graphene nanoplatelets (GNP) by using the DSC analysis. The main properties analyzed were glass transition (T_g) curing temperature and decomposition temperature. They found that the T_g of the pure epoxy composites was between 60 °C and 70 °C. With the inclusion of GNP in 0.25 and 0.5 wt%, the T_g measured was 70 °C and 80 °C, respectively. However, the authors reported that the composite with 0.75 wt% of GNP did not present any significant improvement in glass transition properties. The authors also state that the endothermic transition occurs between 380 °C and 600 °C for the composites with Kevlar, *Cocos nucifera*, GNP, and epoxy. However, the 100% *Cocos nucifera* presents thermal decomposition between 350 °C and 400 °C.

Safri et al. (2020) studied the influence of benzoyl treated sugar palm/glass fiber hybrid and pure sugar palm composite on the mechanical and thermal

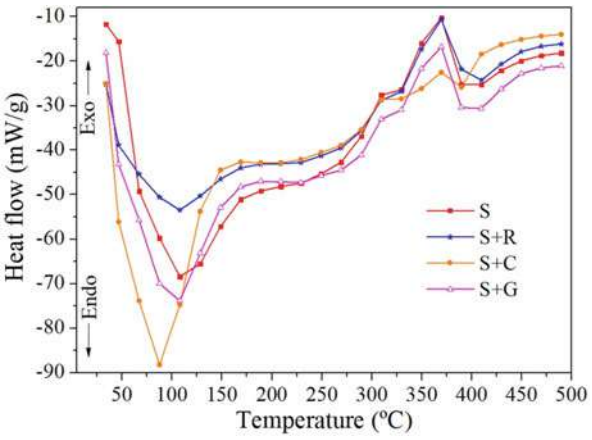

Fig. 7 DSC curves of epoxy sisal-based composites as a function of hybridization (*S* sisal, *S* + *R* sisal + ramie, *S* + *C* sisal + curauá, *S* + *G* sisal + glass fiber). (Reproduced with permission from authors of Pereira et al. (2020))

properties. They found that the addition of glass fiber and chemical treatment increased the peak T_m and T_g of the hybrid composite. On the other hand, the chemical treatment increased the T_m for pure sugar composite when compared to the untreated composite. However, the authors report that T_g did not present significant change.

Prasad et al. (2018) investigated the effect of the addition of nano TiO_2 in composites reinforced by flax fibers. The mechanical, thermal, and water absorption properties were analyzed. The percentages of TiO_2 were 0, 0.5, 0.7, and 0.9. The authors reported that the addition of nano TiO_2 increased the glass transition (T_g) of composite. The T_g value found for 0.7% of TiO_2 modified composites was approx. 70 °C, while for 0%, it was 65 °C.

Sumesh et al. (2019) studied the effect of biosynthesized alumina nano powder (BSANP-C) in composite banana/coir, sisal/coir, and sisal/banana. The mechanical and thermal properties were analyzed. The studied configurations were banana + coir (HBC), sisal + coir (HSC), and sisal + banana (HSB). The variation of the alumina nanoparticle was 0, 1, 2, 3, and 5 wt%. They found that the HBC composite obtained an increase in the endothermic peak of 114 °C with the 3 wt% of nano alumina when compared to the 105.71 °C of pure HBC. Furthermore, HSC and HSB composites with addition of 3 wt% showed values of 112.67 °C and 118.66 °C, respectively when compared to composites without nano alumina which showed 108.16 °C and 90.54 °C, respectively. The authors mention that the presence of nano alumina increased the thermal stability of the composite.

Table 2 summarizes the results from several recent studies on the effect of hybridization on the thermal properties of hybrid composites obtained from the DSC analysis.

Thermomechanical Analysis (TMA)

TMA detects the changes in sample height as a function of temperature and measures expansion coefficients and softening temperatures. This technique is complementary to the DSC, TGA, and DMA techniques (Saba and Jawaid 2018). TMA utilizes different sample geometries using specialized probes for compression, flexure (bending), and tension (see Fig. 8).

The principal information generated by these tests are the following: crystallization and melting temperature, glass transition (T_g), reaction enthalpies, softening temperature, Young's modulus, and thermal expansion coefficient (CTE) (Saba and Jawaid 2018; Nijman et al. 2016; James 2017). CTE is a material property which indicates the extent to which a material expands upon heating (Lin 2016; Saba and Jawaid 2018). The strength of the interatomic bonding will have a direct impact in the material's CTE, as a stronger interatomic bonding will result in less dimensional variation. Polymers, in general, have high CTE due to their relatively weak secondary intermolecular bonds. Therefore, higher cross-linking will reduce the CTE (Saba and Jawaid 2018; Lin 2016). The expansion test is the most used as stated by James (James 2017). The probe is kept in contact with the specimen's surface and will

Table 2 Effect of hybridization on the thermal properties of hybrid composites obtained by DSC analysis

Composite	Main parameters used in the DSC analysis	Effect of hybridization on the thermal properties	Ref.
Sisal/glass	The temperature was ramped from 30 °C to 500 °C with a heating rate of 20 °C/min, under a nitrogen atmosphere at a flow rate of 50 mL/min. Samples of around 20 mg. The equipment used was NETZSCH DSC 200F3 Maia	The natural/synthetic hybrid composite presented the lowest endothermic peak when compared to the other hybrid composites studied	Pereira et al. (2020)
Kenaf/carbon	The temperature was ramped from 25 °C to 350 °C with a heating rate of 10 °C/min, under a nitrogen atmosphere. Samples of 3–4 mg were tested. The equipment used was TA Instruments DSC Q20	The hybridization technique improved the thermal properties of the composites by increasing the decomposition temperature	Aisyah et al. (2019)
Sugar palm/glass	The temperature was ramped from 25 °C to 450 °C with a heating rate of 10 °C/min, under an inert atmosphere. Samples of around 5–6 mg. The equipment used was TA Instruments DSC Q20	The benzoyl treatment increased the T_g and T_m of the studied hybrid composites	Safri et al. (2020)
Cocos nucifera sheath (CNS)/ Kevlar/graphene nanoplatelets (GNP)	The temperature was ramped from 25 °C to 900 °C with a heating rate of 10 °C/min, under a nitrogen atmosphere. Samples of around 20 mg. The equipment used was DSC analyzer (Mettler Toledo)	The addition of GNP improved both the thermal resistance and stability of the hybrid composites	Jesuarockiam et al. (2019)
Cocos nucifera sheath (CNS)/ Kevlar	The temperature was ramped from 30 °C to 900 °C with a heating rate of 10 °C/min, under a nitrogen atmosphere samples of approx. 20 mg. The equipment used was DSC (Mettler Toledo)	The DSC results found were similar to the TGA. The 75% G/25% CNS hybrid composites presented lower endothermal peaks when compared to the other studied hybrid composites	Naveen et al. (2019)
Jute + TiO_2	The temperature was ramped from 0 °C to 100 °C with a heating rate of 10 °C/min, under a	The presence of TiO_2 increased the T_g of the composites	Prasad et al. (2018)

(continued)

Table 2 (continued)

Composite	Main parameters used in the DSC analysis	Effect of hybridization on the thermal properties	Ref.
	nitrogen atmosphere at 50 mL/min. The equipment used was the TA Instruments Q20 DSC		
Sisal/coir/ banana + nano alumina	The temperature was ramped from 50 °C to 300 °C with a heating rate of 30 °C/min, under an inert atmosphere	The presence of nano alumina increased the thermal stability of the composites	Sumesh et al. (2019)

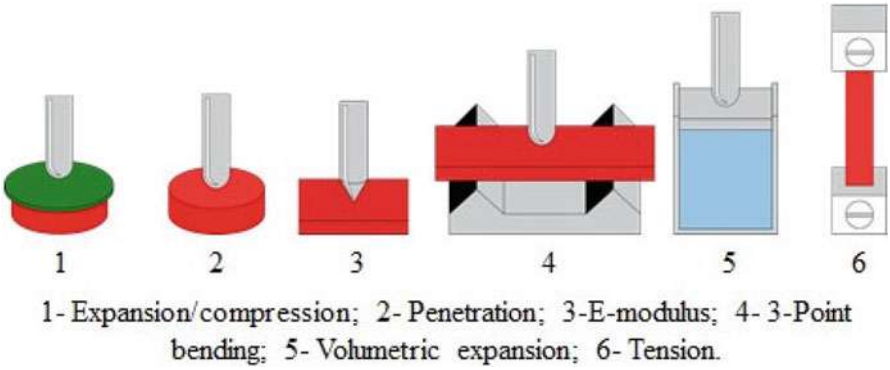

Fig. 8 TMA sample geometries used for testing. (Author source)

move with its expansion or retraction, as can be seen in Fig. 8, item 1. The tensile test is used to investigate the expansion and retraction behavior of films and fibers.

Several authors (James 2017; Saba and Jawaid 2018) report that the TMA technique is more accurate in determining the T_g temperature of the polymeric materials when compared to the DSC techniques.

Dynamic Mechanical Analysis (DMA)

Dynamic mechanical analysis (DMA) determines the following data: storage modulus (E'), loss modulus (E''), damping factor ($tan\ \delta = E''/E'$), and glass transition temperature (T_g) (Chandrasekar et al. 2017). The storage modulus (E') is associated with the energy storage of the elastic characteristics of the material (Lu and Oza 2013; Neto et al. 2019; Saba et al. 2016). It decreases with increase in temperature and is associated with "stiffness" of the composite sample (Lu and Oza 2013; Saba et al. 2016). The loss modulus (E'') is associated with the energy dissipation promoted by the viscous part of the composite sample. This dissipation is related to the internal molecular friction of the molecular chains due to the following factors:

morphological transformation and relaxation, morphology, and system heterogeneity (Saba et al. 2016; Asim et al. 2019). The damping factor is defined by dividing the storage and loss modulus ($tan\ \delta = E''/E'$) and is associated with the internal mobility of the polymeric molecular chains, showing the influence of the fiber/matrix interactions (Saba et al. 2016; Neto et al. 2019; Jawaid et al. 2013b). A high $tan\ \delta$ value shows that the system is dissipating more energy than it is storing due to fiber/matrix interaction quality, while a low $tan\ \delta$ value shows that the polymeric chain has lower mobility, showing a good fiber/matrix interfacial interaction. The measurements of the complex modulus are typically made as temperature is increased at a constant heating rate in order to determine T_g using the DMA technique.

In the DMA, the samples can be tested in different configurations (e.g., dual cantilever, single cantilever, three-point bending, torsion, shear, tension, and compression). The choice of the fixture will depend on the material used and the desired result. However, the most used configuration for composite materials is the three-point bending configuration, as it removes the combined loading induced by a single or double cantilever mode and produces measurable strains in moderately stiff materials.

An example of a typical set of curves obtained from DMA tests showing the relationship between storage modulus (E'), loss modulus (E''), and $tan\ \delta$ as a function of temperature can be seen in Fig. 9. From a DMA curve, the T_g is found from either the first inflection point of the storage modulus curve, the peak of the loss modulus curve, or the peak of the tan delta curve. It should be noted that the value of T_g depends on the method used, especially for highly cross-linked thermosets, which have a broad transition range.

It was also shown that depending on the methodology used, the value of T_g obtained by using the DMA method can vary by up to 25 °C. It was recommended in the literature that the most conservative method is to take the T_g as the first inflection

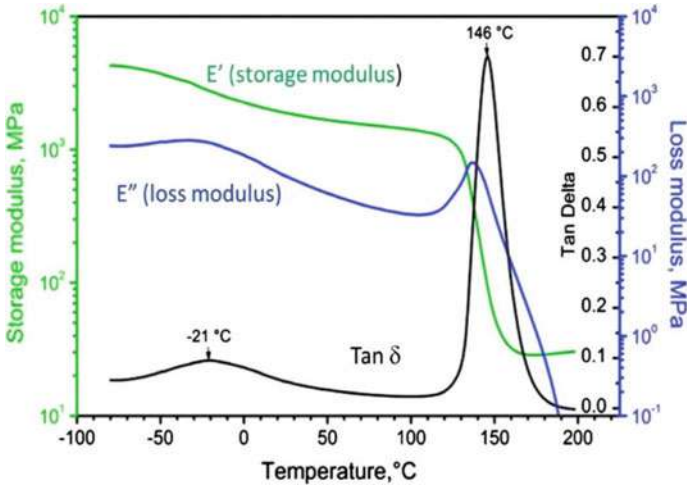

Fig. 9 Relationship between E', E'', and $tan\ \delta$ vs. temperature in the DMA test. (Reproduced with permission from Saba et al. (2016))

point, or the onset of the drop in modulus, while the least conservative method is the *tan δ* peak (Akay 1993).

Saba et al. (2016) related that the cross-linking effects are visible in the DMA test, as can be seen in Fig. 10. Within the glassy region, both the loss and storage moduli may not vary as a function of cross-linking. Highly cross-linked polymers, such as epoxy, present higher modulus due to their restricted structure and high rigidity, while the lightly cross-linked polymers present a less restrictive structure and lower loss modulus. This is reinforced by Nurul Hidayah et al. (2019), as the composites presented a steady reduction of E' in both glass and rubbery phases due to the increase in polymer chain movement. This movement is facilitated by an increase in temperature, which generates a loosening effect between the polymeric chains, resulting in the rubbery plateau region. The storage modulus (E') presents three phases: rigid, glass transition, and rubbery phase (see Fig. 10). In the first phase, the material is tightly packed and stiff in nature because of the rigid polymeric chain (Nurazzi et al. 2020). The E' decreases above the T_g due to the increase in mobility of polymeric chain in the second phase. Polymeric chain movement decreases the fiber/matrix adhesion as well as the stiffness. Finally, in the third phase (the rubbery plateau region), the materials' mobility increases due to the higher temperature, and there is no significant change in the storage modulus (Nurazzi et al. 2020).

The thermal properties of the composites obtained from DMA depends on the physical or structural arrangement of phases, such as interface, morphology, and the nature of composite constituents. It was shown in the literature that the presence of additives fillers, fiber content, fiber orientation, the chemical treatment of the fibers, and the mode of testing rules the dynamic mechanical properties of a composite material (Saba et al. 2016; Ashok et al. 2019).

Several researchers used the DMA tests to study the influence of hybridization on the thermal properties of the hybrid composites (Neto et al. 2019; Fiore and Calabrese 2019; Chee et al. 2019b; Gupta 2018; Mazlan et al. 2020; Selver et al.

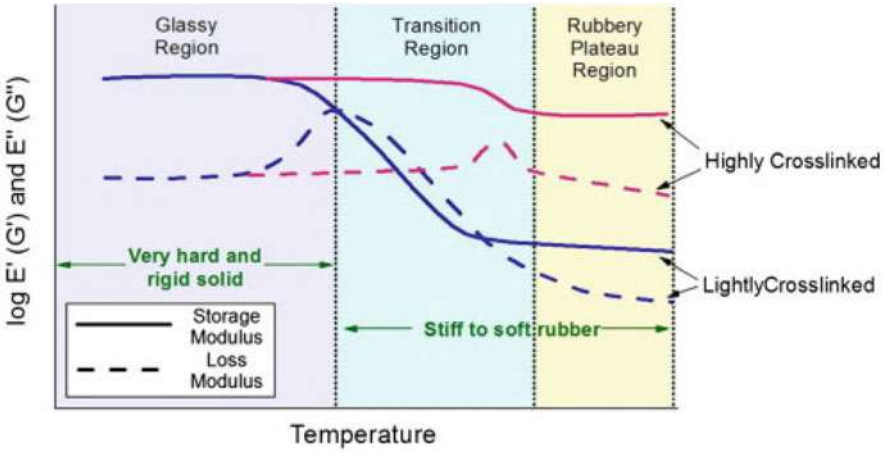

Fig. 10 The effect of cross-linking in the storage and loss modulus for each region of the DMA test. (Reproduced with permission from Saba et al. (2016))

2018). Selver et al. (2018) studied the effect that the hybridization technique had on the thermomechanical properties of hybrid synthetic/natural composites (i.e., glass-glass (GG), jute-jute (JJ), flax-flax (FF), glass-jute (GJ), jute-glass (JG), glass-flax (GF), and flax-glass (FG)). They found that the hybridization of the synthetic fibers with the natural fibers had a positive effect in the storage modulus (E') of the composites when compared to the pure natural composites (JJ and FF). Furthermore, it was reported that the T_g of the pure natural composites are marginally higher than the one found for the glass fiber composite.

Gouda et al. (2020) also used DMA to analyze the effect of the micro filler of bamboo and graphene nanoplatelets (GNPs) on the thermomechanical properties of epoxy-based composites. The bamboo micro filler was treated by mercerization with 6 wt% of sodium hydroxide (NaOH) for 8 h at 48 °C. Then, they were washed and dried in a muffle furnace at 60 °C for 6 h. The composites studied were as follows: micro filler bamboo (GB0), micro filler bamboo + 0.1 wt% of graphene nanoplatelets (GB2.5 wt%), micro filler bamboo + 0.1 wt% of graphene nanoplatelets (GB 5 wt%), micro filler bamboo + 0.1 wt% of graphene nanoplatelets (GB 7.5 wt%), micro filler bamboo + 0.1 wt% of graphene nanoplatelets (GB 10 wt%), and micro filler bamboo + 0.1 wt% of graphene nanoplatelets (12.5 wt%). The authors mention that the nanofiller percentage of GNPs has remained constant. They found that the storage modulus increased for GB 5 wt% and GB 7.5 wt% when compared to GB 0. However, GB 10 wt% and GB 12.5% showed a decrease in the module compared to GB 0. The best case in terms of thermal properties found by the authors was for the GB 7.5 wt% specimens.

Raghu and Goud (2020) studied the effect of hybridization on the mechanical and thermal properties of composites reinforced by *Calotropis procera*/glass fiber. The weight percentage variation of fiber in the composite was 5, 10, 15, and 20. The studied cases were 100% epoxy resin (sample 1), 20Wt% *Calotropis procera* fiber (sample 2), 15wt% *Calotropis procera* fiber + 5% glass fiber (sample 3), 10wt% *Calotropis procera* fiber + 10% glass fiber (sample 4), 5wt% *Calotropis procera* fiber + 15% glass fiber (sample 5), and 20wt% glass fiber (sample 6). They found that the increase of glass fiber content increased the storage modulus and the T_g of the composites investigated.

Zin et al. (2019) used the dynamic mechanical analysis (DMA) to analyze the thermal stability of hybrid composites of banana, PALF fiber, and woven glass epoxy composite by varying fiber weight fractions (0.3–0.5 Vf). They found that the PALF hybrid composites had a higher T_g than banana hybrid composites in all fiber content composition. This indicated that PALF has higher thermal stability than banana fiber. Finally, the DMA showed a shift in the T_g for banana-glass hybrid composite, from 30 to 40 wt%, indicating optimum condition that contributed to molecular structure stability of the composite.

Naveen et al. (2019) investigated the effect of adding different wt% of *Cocos nucifera* sheath (CNS) on the dynamic mechanical and thermal properties of Kevlar/epoxy composites for structural applications at elevated temperature. They found that the 25% CNS/75% K presented a storage modulus higher than the pure Kevlar composites (see Fig. 11). This was explained by the combination of the dense fabric architecture of the CNS and higher modulus of Kevlar fabric However, increasing

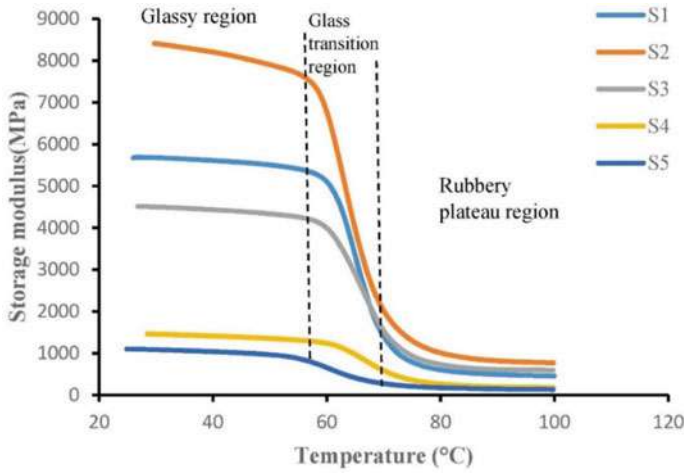

Fig. 11 Effect of *Cocos nucifera* sheath (CNS) loading on the storage modulus of Kevlar/epoxy laminates. The composites are designated as the following: S1 – 100% Kevlar/epoxy composites; S2 – 75% Kevlar/25% CNS; S3 – 50% Kevlar/50% CNS; S4 – 25% Kevlar/75% CNS; S5 – 100% CNS-based laminates. (Reproduced with permission from Naveen et al. (2019))

the CNS content loosens the polymeric chain structure of the composites and reduces the stiffness. The *tan δ* values of the Kevlar composites presented the lowest values when compared to the other studied composites. Moreover, the hybrid composites presented higher values of T_g compared to the pure natural composites, showing good fiber/matrix interfacial interaction.

Mazlan et al. (2020) also used the DMA technique to investigate the thermal properties of a kenaf-glass fiber hybrid composite modified with clay nanoparticles (1% and 5%). The following cases were studied: pure kenaf (UK/EP), kenaf-glass + 1% clay (UKG 1%), kenaf-glass + 5% clay (UKG 5%), kenaf treated pure (TK/EP), kenaf-glass treated + 1% clay (TKG 1%), and kenaf-glass treated + 5% clay (TKG 5%). The composites were chemically treated with NaOH for 4 h as to improve fiber/matrix interfacial adhesion. They found that TKG 1% composite provided the highest storage modulus at room temperature with 136.74% higher than UKG 1% composite due to the polymer chain diffusion between well-dispersed clay structures. TKG 1% also achieved the highest loss modulus, which indicates the strongest internal friction among other composites. However, the authors report that the inclusion of the clay in the composites had a negative effect on T_g, where the TKG1% composite exhibited the lowest T_g (72 °C compared to 89.97 °C found for UK/EP). This was explained by the fact that the elimination of hemicellulose due to fiber treatment lowered the stiffness of natural fiber.

Nurul Hidayah et al. (2019) analyzed the effect that the addition of multiwalled carbon nanotubes (MWCNTs) has in the thermomechanical properties of a kenaf-glass and kenaf-carbon fiber hybrid composites. The composites were manufactured by the hand-layup technique and vacuum bagging. The studied cases were glass-kenaf-glass (GKKG), carbon-kenaf-carbon (CKKC), ink/MWCNT/GKKG, and ink/MWCNT/CKKC. They found that the incorporation of MWCNT increased the

storage modulus properties of the GKKG composite. However, for the CKKC, the incorporation of the MWCNT decreased the composites storage modulus properties. The authors state that this loss in storage modulus properties is related to the nanotube agglomeration within the composites. Ridzuan et al. (2016) examined the impact that chemical treatment had on the thermal properties of the *Pennisetum purpureum*/glass-reinforced epoxy hybrid composites. They found that the chemical treatments improved the composite's storage modulus properties when compared to the untreated composites. Furthermore, it was found that the 5% alkaline treatment increased the $T_{g,}$ while the composite with 10% alkaline treatment presented a reduction in T_g when compared to the untreated composites. Safri et al. (2019) analyzed the effect that the chemical treatments had on the viscoelastic properties of the glass fiber (GF)-sugar palm (SPF) hybrid composite. Epoxy/glass fiber (EP 90%/GF 10%), epoxy/sugar palm fiber untreated (EP 90%/SPF 10%), (EP 90%/10% SPF/3% GF) untreated, (EP 90%/5% SPF/5% GF) untreated, (EP 90%/3% SPF/7% GF) untreated, epoxy/sugar palm benzol treated (EP 90%/SPF 10%), (EP 90%/SPF 7%/GF 3%) benzoyl treated, (EP 90%/SPF 5%/GF 5%) benzoyl treated, (EP 90%/SPF 3%/GF 7%) benzoyl treated cases were studied. Figure 12 presents the dynamic mechanical properties of all composites studied. The authors showed that the dynamic mechanical properties of the sugar palm composites increased after the benzoylation treatment. The sugar palm/glass fiber composites made of EP/30 TSPF/70 GF presented the best performance in terms of the dynamic mechanical properties (higher loss modulus, higher storage modulus, tan δ) compared to other sugar palm/glass fiber composite formulations. All composites that underwent chemical treatment and hybridization presented an increase in T_g. The loss modulus of the untreated composite (EP 90%/3% SPF/7% GF) had a value of 295.84 MPa compared to the 193.4 MPa value of treated composite (EP 90%/SPF 3%/GF 7%). The authors state that the decrease in loss modulus causes storage modulus to increase. Further, the *tan δ* showed that all composites that underwent hybridization presented a damping factor higher than those found in non-hybrid composites. The authors state that the reason is the fact that the glass fiber addition in the natural composites improves the stress-transfer between the fiber and matrix. They concluded that the positive shift in the T_g value after the glass fiber addition into the sugar palm composites and after the benzoylation treatment on the sugar palm fiber proves the good interfacial reaction between the fiber and matrix.

Jesuarockiam et al. (2019) studied the effect of graphene nanoplatelets (GNP) on the hybrid Kevlar (K)/*Cocos nucifera* sheath (CNS) composite. The viscoelastic properties were analyzed by the dynamic mechanical analysis (DMA). The results showed that the percentages of 0.25 wt% and 0.5 wt% of GNP increased the storage modulus of the composite. However, the weight percentage of 0.75 did not show a significant increase in all cases. The loss modulus of composites modified with 0.25 and 0.5 wt% of GNP also showed an increase. However, the specimens modified with 0.75 wt% of GNP do not present any significant gain. The hybridization of the composites by addition of GNP increased the T_g of the composites. The T_g value found for the 25 K/75 CNS + 0.5 wt% GNP was 71.21 °C, while for the 100% CNS composite was 62.22 °C and for the 100% K composite was 66.60 °C.

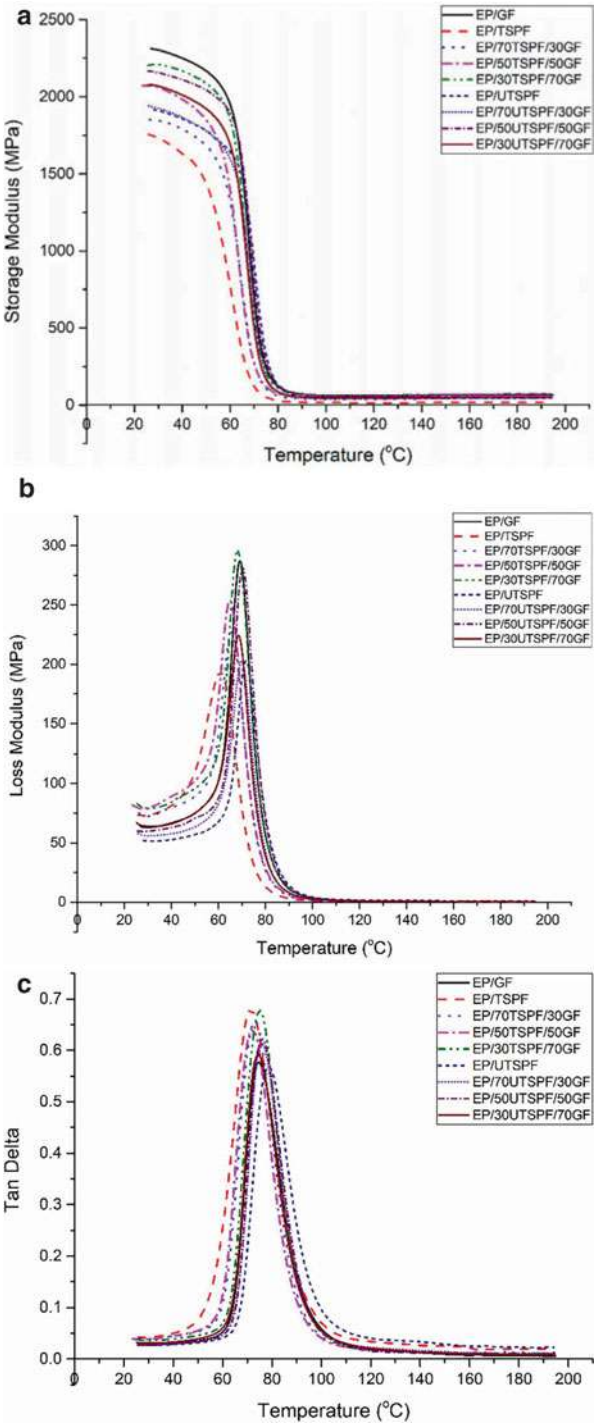

Fig. 12 The dynamic mechanical properties of all composites: (**a**) storage modulus; (**b**) loss modulus; (**c**) tan delta (epoxy/glass fiber (EP 90%/GF 10%), epoxy/sugar palm fiber untreated (EP 90%/SPF 10%), (EP 90%/10% SPF/3% GF) untreated, (EP 90%/5% SPF/5% GF) untreated, (EP 90%/3% SPF/7% GF) untreated, epoxy/sugar palm benzoyl treated (EP 90%/SPF 10%), (EP 90%/SPF 7%/GF 3%) benzoyl treated, (EP 90%/SPF 5%/GF 5%) benzoyl treated, (EP 90%/SPF 3%/GF 7%) benzoyl treated). (Reproduced with permission from Safri et al. (2019))

Table 3 Effect of hybridization on the thermal properties of hybrid composites obtained from DMA analysis

Composite	Main parameters used in the analysis	Effect of hybridization on the thermal properties	Ref.
Flax/glass and jute/glass	**Single cantilever beam test** with a frequency of 1 Hz and an oscillation amplitude of 150 μm The equipment used TAQ800 The temperature was ramped from 35 °C to 200 °C with a heating rate of 2 °C/min. Rectangular specimens (28 × 7 mm) were used	Natural fiber composite presented better damping characteristics compared to glass fiber composites. *tan δ* of jute and flax composites was 13% and 16% higher compared to glass fiber composites	Selver et al. (2018)
Cocos nucifera sheath (CNS)/Kevlar	**Three-point bending test** with a frequency of 1 Hz and a controlled sinusoidal. Equipment used was TA 800. The temperature was ramped from room to 200 °C with a heating rate of 10 °C/min. Rectangular specimens of 60 × 12.5 × 3 mm^3	Hybridization with 25% CNS/75% K presented superior storage modulus value when compared to the pure Kevlar composite	Naveen et al. (2019)
Kenaf/glass/clay	**Dual cantilever beam test** with a frequency of 10 Hz and an oscillation amplitude of 15 μm The equipment used was DMA Q800 TA The temperature was ramped from 30 °C to 150 °C with a heating rate of 5 °C/min. Rectangular specimens of 60 × 12 × 3.2 mm^3	The treatment of the hybrid composite reinforced with 1 wt% nanoclay increased the storage modulus by 136% but had the lowest T_g value (72 ° C) when compared to the untreated hybrid composite with 1 wt% nanoclay (76 °C)	Mazlan et al. (2020)
Cocos nucifera sheath (CNS)/Kevlar/graphene nanoplatelets (GNP)	**Three-point bending test** with a frequency of 1 Hz and a controlled sinusoidal. Equipment used: TA 800. The temperature ramp used was from room temperature to 200 °C with a heating rate of 10 °C/min Rectangular specimens'	For the 50% CNS/50% K and 0.75 wt% of GNP composites, similar storage and loss moduli were observed when compared to the pure Kevlar composite. The 50% CNS/50% K and 0.75 wt% of GNP case presented a T_g of 69.89 °C, while for the	Jesuarockiam et al. (2019)

(continued)

Table 3 (continued)

Composite	Main parameters used in the analysis	Effect of hybridization on the thermal properties	Ref.
	size was $60 \times 12.5 \times 3$ mm^3	pure Kevlar this value was 66.6 °C	
Pennisetum purpureum/glass	**Dual cantilever test** with a frequency of 1 Hz. Equipment used: Pyris Diamond DMA. The temperature was ramped from 30 °C to 150 °C with a heating rate of 3 °C/min. Rectangular specimens of $20 \times 10 \times 2.3$ mm^3	The 5% alkaline treatment of hybrid composite increased the thermal properties (storage modulus and T_g) when compared to other cases, while the composite with 10% alkaline treatment presented a reduction in T_g when compared to the untreated composites	Ridzuan et al. (2016)
Banana/PALF/glass	**Three-point bending test** with a frequency of 1 Hz. The temperature was ramped from 0 °C to 160 °C with a heating rate of 3 °C/min	The 30 wt% banana-glass fiber hybrid composite presented the highest T_g when compared to other studied cases	Zin et al. (2019)
Kenaf-carbon/glass-kenaf + MWCNT	**Three-point bending test** with oscillatory sine-wave stress with 1 Hz frequency and amplitude of 10 μm. Equipment used: Mettler Toledo DMA 861. The temperature was ramped from room temperature at 150 °C with a heating rate of 5 °C/min. Rectangular specimens of 50×10 mm in size	The addition of MWCNT in hybrid composites produced a significant increase of E' (glassy region) for the kenaf-glass composite, when compared to the unfilled case, while a decreasing trend was observed for the kenaf-carbon case composite. The T_g increased for the MWCNT + kenaf-glass composite as a function of filler content	Nurul Hidayah et al. (2019)
Sugar palm/glass	**Dual cantilever test** with an oscillatory frequency of 1 Hz. Equipment used: DMA Instrument Q800 V20.24 Build 43 module DMA multifrequency. The temperature was ramped from 25 °C to 150 °C	The hybridization and benzoyl treatment increased the storage and loss modulus of the composites	Safri et al. (2019)

(continued)

Table 3 (continued)

Composite	Main parameters used in the analysis	Effect of hybridization on the thermal properties	Ref.
	with a heating rate of 5 °C/min		
E-glass or N-glass chopped strand mats (CSMs) and jute (J) fabrics and four different hybrid composites	The temperature was ramped from 30 °C to 180 °C. A frequency of 1 Hz and rectangular specimens of 60 × 12 × 2 and 4 mm were used	Glass fiber composites presented a higher storage modulus (E') compared to jute fiber-reinforced composites. The E' values of glass-jute fiber hybrid composites was between those of glass and jute composites The incorporation of the jute fiber lowered the damping factor of the jute/glass fiber-reinforced epoxy composite	Ghosh et al. (1997)
Bamboo + graphene nanoplatelets (GNPs)	**Dual cantilever test** with an oscillatory frequency of 1 Hz and load 150 N was used for this analysis. The temperature was ramped from room temperature to 200 °C with a heating rate of 5 °C/min dimensions of specimens: 63.5 × 12.7 × 3 mm	The increase of the bamboo micro filler up to 7.5 wt% increased the storage modulus.	Gouda et al. (2020)

Table 3 summarizes several recent studies on the effect of hybridization on the thermal properties of hybrid composites obtained through DMA analysis.

Conclusions

This chapter presents an overview of the main techniques used for thermal analysis of hybrid epoxy/synthetic/natural fiber composites. The main methods used to determine the thermal properties of composite materials and the suitability of hybrid composites for a certain application (thermogravimetric analysis (TGA), differential scanning calorimetry (DSC), thermomechanical analysis (TMA), and differential mechanical thermal analysis (DMA)) are presented. The percentage of weight loss, degradation temperature, T_g, thermal expansion coefficient (CTE), and viscoelastic

properties (storage modulus, loss modulus, and the damping factor) are the most common thermal properties determined by these techniques.

It was shown that different factors affect the thermal properties of the composites (i.e., fiber and matrix type; the presence of additives fillers, fiber content, and fiber orientation; the chemical treatment of the fibers; manufacture process; and type of loading). Using natural fibers with low lignin content leads to better thermal performance of composites. By removing of lignin through fiber treatment, improved thermal resistance of composites can be obtained. Another method to improve the thermal stability of the natural/synthetic hybrid fiber composites explored in the literature is using coupling agents for the natural fibers. Further improvements in thermal stability of hybrid composites can be obtained by using filler materials in the matrix or for grafting the fibers. Finally, the incorporation of synthetic fibers in natural fiber-reinforced composites increases their thermal stability.

References

H. Aisyah, M. Paridah, S. Sapuan, A. Khalina, O. Berkalp, S. Lee, C. Lee, N. Nurazzi, N. Ramli, M. Wahab, Thermal properties of woven kenaf/carbon fibre-reinforced epoxy hybrid composite panels. Int. J. Polym. Sci. **8**, 5258621 (2019)

I. Aji, E. Zainudin, A. Khalina, S. Sapuan, M. Khairul, Thermal property determination of hybridized kenaf/PALF reinforced HDPE composite by thermogravimetric analysis. J. Therm. Anal. Calorim. **109**(2), 893–900 (2011)

M. Akay, Aspects of dynamic mechanical analysis in polymeric composites. Compos. Sci. Technol. **47**(4), 419–423 (1993)

J.R. Araújo, W.R. Waldman, M.A. De Paoli, Thermal properties of high density polyethylene composites with natural fibres: coupling agent effect. Polym. Degrad. Stab. **93**(10), 1770–1775 (2008). https://doi.org/10.1016/j.polymdegradstab.2008.07.021

M.N. Arshad, H. Mohit, M.R. Sanjay, S. Siengchin, A. Khan, M.M. Alotaibi, A.M. Asiri, M.A. Rub, Effect of coir fiber and TiC nanoparticles on basalt fiber reinforced epoxy hybrid composites: physico-mechanical characteristics. Cellulose (2021). https://doi.org/10.1007/s10570-021-03752-7

R. Ashok, C. Srinivasa, B. Basavaraju, Dynamic mechanical properties of natural fiber composites – a review. Adv. Compos. Hybrid Mater. **2**, 1–22 (2019)

M. Asim, M. Jawaid, M.T. Paridah, N. Saba, M. Nasir, R.M. Shahroze, Dynamic and thermo-mechanical properties of hybridized kenaf/PALF reinforced phenolic composites. Polym. Compos. **40**(10), 3814–3822 (2019)

M. Asim, M.T. Paridah, M. Chandrasekar, R.M. Shahroze, M. Jawaid, M. Nasir, R. Siakeng, Thermal stability of natural fibers and their polymer composites. Cellulose **174**, 175 (2020)

M. Banea, L.F. da Silva, Adhesively bonded joints in composite materials: an overview. Proc. Inst. Mech. Eng. L J. Mater. Des. Appl. **223**(1), 1–18 (2009)

M.D. Banea, J.S.S. Neto, D.K.K. Cavalcanti, Recent trends in surface modification of natural fibres for their use in green composites, in *Green Composites*, ed. by S. Thomas, P. Balakrishnan, (Springer, Singapore, 2021), pp. 329–350. https://doi.org/10.1007/978-981-15-9643-8_12

R. Braga, P. Magalhaes Jr., Analysis of the mechanical and thermal properties of jute and glass fiber as reinforcement epoxy hybrid composites. Mater. Sci. Eng. C **56**, 269–273 (2015)

S. Budhe, S. de Barros, M.D. Banea, Theoretical assessment of the elastic modulus of natural fiber-based intra-ply hybrid composites. J. Braz. Soc. Mech. Sci. Eng. **41**(6) (2019). https://doi.org/10.1007/s40430-019-1766-z

D.K.K. Cavalcanti, M.D. Banea, J.S.S. Neto, R.A.A. Lima, L.F.M. da Silva, R.J.C. Carbas, Mechanical characterization of intralaminar natural fibre-reinforced hybrid composites. Compos. Part B Eng. **175**, 107149 (2019). https://doi.org/10.1016/j.compositesb.2019.107149

D.K.K. Cavalcanti, M.D. Banea, J.S.S. Neto, R.A.A. Lima, Comparative analysis of the mechanical and thermal properties of polyester and epoxy natural fibre-reinforced hybrid composites. J. Compos. Mater. **55**(12), 1683–1692 (2021). https://doi.org/10.1177/0021998320976811

M. Chandrasekar, M. Ishak, S. Sapuan, Z. Leman, M. Jawaid, A review on the characterisation of natural fibres and their composites after alkali treatment and water absorption. Plast. Rubber Compos. **46**(3), 119–136 (2017)

S.S. Chee, M. Jawaid, M. Sultan, O.Y. Alothman, L.C. Abdullah, Evaluation of the hybridization effect on the thermal and thermo-oxidative stability of bamboo/kenaf/epoxy hybrid composites. J. Therm. Anal. Calorim. **137**(1), 55–63 (2019a)

S.S. Chee, M. Jawaid, M. Sultan, O.Y. Alothman, L.C. Abdullah, Thermomechanical and dynamic mechanical properties of bamboo/woven kenaf mat reinforced epoxy hybrid composites. Compos. Part B Eng. **163**, 165–174 (2019b)

S. Członka, A. Strąkowska, A. Kairytė, Effect of walnut shells and silanized walnut shells on the mechanical and thermal properties of rigid polyurethane foams. Polym. Test. **87**, 106534 (2020)

V. Dalla Libera Junior, R.M. Leão, V. Franco Steier, S.M. da Luz, Influence of cure agent, treatment and fibre content on the thermal behaviour of a curaua/epoxy prepreg. Plast. Rubber Compos. **49**(5), 214–221 (2020)

R. de Araujo Alves Lima, D. Kawasaki Cavalcanti, J. de Souza e Silva Neto, H. Meneses da Costa, M.D. Banea, Effect of surface treatments on interfacial properties of natural intralaminar hybrid composites. Polym. Compos. **41**(1), 314–325 (2020). https://doi.org/10.1002/pc.25371

H.F.M. de Queiroz, M.D. Banea, D.K.K. Cavalcanti, Experimental analysis of adhesively bonded joints in synthetic- and natural fibre-reinforced polymer composites. J. Compos. Mater. **54**(9), 1245–1255 (2020). https://doi.org/10.1177/0021998319876979

H.N. Dhakal, Z.Y. Zhang, R. Guthrie, J. MacMullen, N. Bennett, Development of flax/carbon fibre hybrid composites for enhanced properties. Carbohydr. Polym. **96**(1), 1–8 (2013). https://doi.org/10.1016/j.carbpol.2013.03.074

M. El Boustani, G. Lebrun, F. Brouillette, A. Belfkira, Effect of a solvent-free acetylation treatment on reinforcements permeability and tensile behaviour of flax/epoxy and flax/wood fibre/epoxy composites. Can. J. Chem. Eng. **95**(6), 1082–1092 (2017)

V. Fiore, L. Calabrese, Effect of stacking sequence and sodium bicarbonate treatment on quasi-static and dynamic mechanical properties of flax/jute epoxy-based composites. Materials **12**(9), 1363 (2019)

P. Ghosh, N.R. Bose, B.C. Mitra, S. Das, Dynamic mechanical analysis of FRP composites based on different fiber reinforcements and epoxy resin as the matrix material. J. Appl. Polym. Sci. **64**(12), 2467–2472 (1997). https://doi.org/10.1002/(SICI)1097-4628(19970620)64:12<2467::AID-APP21>3.0.CO;2-X

K. Gouda, S. Bhowmik, B. Das, Synergetic effect of micro-bamboo filler and graphene nano-platelets on thermomechanical properties of epoxy-based hybrid composite. JOM **72**(12), 4466–4476 (2020). https://doi.org/10.1007/s11837-020-04125-4

Y. Guo, S. Zhu, Y. Chen, D. Li, Thermal properties of wood-plastic composites with different compositions. Materials **12**(6), 881 (2019)

M. Gupta, Thermal and dynamic mechanical analysis of hybrid jute/sisal fibre reinforced epoxy composite. Proc. Inst. Mech. Eng. L J. Mater. Des. Appl. **232**(9), 743–748 (2018)

J. James, Thermomechanical analysis and its applications, in *Thermal and Rheological Measurement Techniques for Nanomaterials Characterization*, (Elsevier, Cambridge, MA, 2017), pp. 159–171

M. Jawaid, H.A. Khalil, A.A. Bakar, A. Hassan, R. Dungani, Effect of jute fibre loading on the mechanical and thermal properties of oil palm–epoxy composites. J. Compos. Mater. **47**(13), 1633–1641 (2013a)

M. Jawaid, H.A. Khalil, A. Hassan, R. Dungani, A. Hadiyane, Effect of jute fibre loading on tensile and dynamic mechanical properties of oil palm epoxy composites. Compos. Part B Eng. **45**(1), 619–624 (2013b)

N. Jesuarockiam, M. Jawaid, E.S. Zainudin, M. Thariq Hameed Sultan, R. Yahaya, Enhanced thermal and dynamic mechanical properties of synthetic/natural hybrid composites with graphene nanoplateletes. Polymers **11**(7), 1085 (2019)

S. Krishnasamy, S.M.K. Thiagamani, C.M. Kumar, R. Nagarajan, R. Shahroze, S. Siengchin, S.O. Ismail, M.P. Indira Devi, Recent advances in thermal properties of hybrid cellulosic fiber reinforced polymer composites. Int. J. Biol. Macromol. **141**, 1–13 (2019)

T.S.M. Kumar, K. Senthilkumar, M. Chandrasekar, S. Subramaniam, S.M. Rangappa, S. Siengchin, N. Rajini, Influence of fillers on the thermal and mechanical properties of biocomposites: an overview, in *Biofibers and Biopolymers for Biocomposites*, (Springer, Berlin, 2020), pp. 111–133

M. Li, Y. Pu, V.M. Thomas, C.G. Yoo, S. Ozcan, Y. Deng, K. Nelson, A.J. Ragauskas, Recent advancements of plant-based natural fiber–reinforced composites and their applications. Compos. Part B Eng. **200**, 108254 (2020). https://doi.org/10.1016/j.compositesb.2020.108254

S.-Y. Lin, An overview of advanced hyphenated techniques for simultaneous analysis and characterization of polymeric materials. Crit. Rev. Solid State Mater. Sci. **41**(6), 482–530 (2016)

N. Lu, S. Oza, A comparative study of the mechanical properties of hemp fiber with virgin and recycled high density polyethylene matrix. Compos. Part B Eng. **45**(1), 1651–1656 (2013)

N. Mazlan, T. Chai Hua, M.T.H. Sultan, K. Abdan, Thermogravimetric and dynamic mechanical analysis of woven glass/kenaf/epoxy hybrid nanocomposite filled with clay. Adv. Mater. Process. Technol. **7**, 1–14 (2020)

J. Naveen, M. Jawaid, E. Zainudin, M.T. Sultan, R. Yahaya, M.A. Majid, Thermal degradation and viscoelastic properties of Kevlar/*Cocos nucifera* sheath reinforced epoxy hybrid composites. Compos. Struct. **219**, 194–202 (2019)

J. Neto, R. Lima, D. Cavalcanti, J. Souza, R. Aguiar, M. Banea, Effect of chemical treatment on the thermal properties of hybrid natural fiber-reinforced composites. J. Appl. Polym. Sci. **136**(10), 47154 (2019). https://doi.org/10.1002/app.47154

M. Nijman, N. Fedelich, A. Hammer, E. Hempel, N. Jing, R. Riesen, J. Schawe, M. Schubnell, C. Wrana, *Thermal Analysis in Practice: Tips and Hints* (Mettler-Toledo GmbH, Cham, 2016)

N.M. Nurazzi, A. Khalina, S.M. Sapuan, R.A. Ilyas, S.A. Rafiqah, Z.M. Hanafee, Thermal properties of treated sugar palm yarn/glass fiber reinforced unsaturated polyester hybrid composites. J. Mater. Res. Technol. **9**(2), 1606–1618 (2020). https://doi.org/10.1016/j.jmrt.2019.11.086

I. Nurul Hidayah, D. Nuur Syuhada, H.P.S. Abdul Khalil, Z.A.M. Ishak, M. Mariatti, Enhanced performance of lightweight kenaf-based hierarchical composite laminates with embedded carbon nanotubes. Mater. Des. **171**, 107710 (2019). https://doi.org/10.1016/j.matdes.2019.107710

A.L. Pereira, M.D. Banea, J.S. Neto, D.K. Cavalcanti, Mechanical and thermal characterization of natural intralaminar hybrid composites based on sisal. Polymers **12**(4), 866 (2020)

K.L. Pickering, M.A. Efendy, T.M. Le, A review of recent developments in natural fibre composites and their mechanical performance. Compos. A: Appl. Sci. Manuf. **83**, 98–112 (2016)

V. Prasad, M.A. Joseph, K. Sekar, Investigation of mechanical, thermal and water absorption properties of flax fibre reinforced epoxy composite with nano TiO_2 addition. Compos. A: Appl. Sci. Manuf. **115**, 360–370 (2018). https://doi.org/10.1016/j.compositesa.2018.09.031

M.J. Raghu, G. Goud, Development of *Calotropis procera*–glass fibers reinforced epoxy hybrid composites: dynamic mechanical properties. J. Nat. Fibers **10**, 1–8 (2020). https://doi.org/10.1080/15440478.2020.1745119

B. Ravishankar, S.K. Nayak, M.A. Kader, Hybrid composites for automotive applications – a review. J. Reinf. Plast. Compos. **38**(18), 835–845 (2019). https://doi.org/10.1177/0731684419849708

M. Ridzuan, M.A. Majid, M. Afendi, M. Mazlee, A. Gibson, Thermal behaviour and dynamic mechanical analysis of *Pennisetum purpureum*/glass-reinforced epoxy hybrid composites. Compos. Struct. **152**, 850–859 (2016)

N. Saba, M. Jawaid, A review on thermomechanical properties of polymers and fibers reinforced polymer composites. J. Ind. Eng. Chem. **67**, 1–11 (2018)

N. Saba, M. Jawaid, O.Y. Alothman, M. Paridah, A review on dynamic mechanical properties of natural fibre reinforced polymer composites. Constr. Build. Mater. **106**, 149–159 (2016)

S.N.A. Safri, M.T.H. Sultan, M. Jawaid, M.S. Abdul Majid, Analysis of dynamic mechanical, low-velocity impact and compression after impact behaviour of benzoyl treated sugar palm/glass/epoxy composites. Compos. Struct. **226**, 111308 (2019). https://doi.org/10.1016/j.compstruct.2019.111308

S.N.A. Safri, M.T.H. Sultan, A.U.M. Shah, Characterization of benzoyl treated sugar palm/glass fibre hybrid composites. J. Mater. Res. Technol. **9**(5), 11563–11573 (2020). https://doi.org/10.1016/j.jmrt.2020.08.057

M. Sathiyamoorthy, S. Senthilkumar, Mechanical, thermal, and water absorption behaviour of jute/carbon reinforced hybrid composites. Sadhana **45**(1), 278 (2020). https://doi.org/10.1007/s12046-020-01514-y

S.K. Saw, C. Datta, Thermo mechanical properties of jute/bagasse hybrid fibre reinforced epoxy thermoset composites. Bioresources **4**(4), 1455–1475 (2009)

E. Selver, N. Ucar, T. Gulmez, Effect of stacking sequence on tensile, flexural and thermo-mechanical properties of hybrid flax/glass and jute/glass thermoset composites. J. Ind. Text. **48**(2), 494–520 (2018)

K.R. Sumesh, K. Kanthavel, Green synthesis of aluminium oxide nanoparticles and its applications in mechanical and thermal stability of hybrid natural composites. J. Polym. Environ. **27**(10), 2189–2200 (2019). https://doi.org/10.1007/s10924-019-01506-y

K.R. Sumesh, K. Kanthavel, A. Ajithram, P. Nandhini, Bioalumina nano powder extraction and its applications for sisal, coir and banana hybrid fiber composites: mechanical and thermal properties. J. Polym. Environ. **27**(9), 2068–2077 (2019). https://doi.org/10.1007/s10924-019-01496-x

Y. Swolfs, L. Gorbatikh, I. Verpoest, Fibre hybridisation in polymer composites: a review. Compos. A: Appl. Sci. Manuf. **67**, 181–200 (2014). https://doi.org/10.1016/j.compositesa.2014.08.027

P. Wambua, J. Ivens, I. Verpoest, Natural fibres: can they replace glass in fibre reinforced plastics? Compos. Sci. Technol. **63**(9), 1259–1264 (2003). https://doi.org/10.1016/S0266-3538(03)00096-4

M.H. Zin, K. Abdan, M.N. Norizan, The effect of different fiber loading on flexural and thermal properties of banana/pineapple leaf (PALF)/glass hybrid composite, in *Structural Health Monitoring of Biocomposites, Fibre-Reinforced Composites and Hybrid Composites*, ed. by M. Jawaid, M. Thariq, N. Saba, (Woodhead Publishing, Sawston, 2019), pp. 1–17. https://doi.org/10.1016/B978-0-08-102291-7.00001-0

Microscopic Analysis of Hybrid Synthetic/Vegetable Fiber-Reinforced Epoxy Composites

34

A Systematic Review

Francisco M. Monticeli, Roberta M. Neves, José Humberto S. Almeida Jr., and Heitor Luiz Ornaghi Jr.

Contents

Abstract

Hybridization of synthetic with natural fibers has been increasingly studied over the last decades given the potential to partially replace glass fibers with natural ones aiming at meeting both design requirements and environmental concerns. Despite some drawbacks about natural fibers, such as high moisture absorption and low mechanical properties, the combination with synthetic fibers is a suitable route to overcome these drawbacks. Usually, hybrid fiber-reinforced composites need to meet mechanical constraints, and consequently the microstructure of the composite must be taken care of to generate structures with proper mechanical performance. This chapter presents a systematic review on hybrid synthetic/vegetable composites reinforced epoxy composites focusing on research papers published from 2016 to 2020. A total of 531 papers were initially found, but after

F. M. Monticeli
Department of Materials and Technology, Fatigue and Aeronautic Materials Research Group, School of Engineering, Sao Paulo State University (UNESP), Guaratingueta, SP, Brazil

R. M. Neves · H. L. Ornaghi Jr. (✉)
Postgraduate Program in Mining, Metallurgical and Materials Engineering, Federal University of Rio Grande do Sul (UFRGS), Porto Alegre/RS, Brazil

J. H. S. Almeida Jr.
Advanced Composites Research Group, School of Mechanical and Aerospace Engineering, Queen's University Belfast, Belfast, UK

S. Mavinkere Rangappa et al. (eds.), *Handbook of Epoxy/Fiber Composites*,
https://doi.org/10.1007/978-981-19-3603-6_38

the exclusion criteria following the PRISMA protocol, 32 articles remained and were included in this review. The presented results focus on the type of microscopy method and analysis of the composites. In brief, this study aims to help to identify the main gaps in the literature related to the proposed topic.

Keywords

Systematic review · Hybrid composites · Void · Microscopy

Introduction

Fiber hybridization in polymeric composite materials is being increasingly utilized to take the best characteristics of each fiber, that is, the good mechanical properties and low variability of synthetic fibers with the low cost and environmental appealing of natural ones. Some vegetable fibers even have similar properties when compared to laminates with only synthetic fibers (Romanzini et al. 2012, 2013; Almeida et al. 2012; Venkatasudhahar et al. 2020; Acharya et al. 2019; Ornaghi et al. 2010). The aforementioned characteristics allow the use of hybrid composites in medium to low mechanical performance applications, such as in automobile, civil, and sporting goods (Monte Vidal et al. 2020; Monticeli et al. 2019, 2020; Reis et al. 2020).

Mechanical and thermal properties are directly influenced by processing characteristics, such as void formation, fibers distribution, fiber volume fraction, and morphology (Monticeli et al. 2019, 2020; Lundström et al. 1993; Grunenfelder and Nutt 2010; Devalve and Pitchumani 2013). The determination of these characteristics (quantitatively or qualitatively) is usually elucidated by microscopy analysis that includes SEM (scanning electron microscopy), TEM (transmission electron microscopy), OM (optical microscopy), X-ray μCT (micro-computed tomography), and CVM (color video microscope) (Romanzini et al. 2012; Garcea et al. 2018; Paciornik and ḋAlmeida 2010).

In this context, this work aims at compiling studies on the most used microscopy analysis and methods related to synthetic/vegetable hybrid composites of the last five years using three different search databases. For that, a systematic review is performed followed Preferred Reporting Items for Systematic Reviews and Meta-analyses (PRISMA) guidelines.

Systematic Review

A systematic review is described as "explicit and reproducible methods to systematically search, critically appraise, and synthesize on a specific issue. It synthesizes the results of multiple primary studies related to each other by using strategies that reduce biases and random errors" (Ganeshkumar and Gopalakrishnan 2013). Since it follows a methodical protocol, future research about a specific topic is guided due to inclusion of past and current studies. The PRISMA can be found in detail in Ref (Shamseer et al. 2015).

Briefly, a systematic review answers a focused question based on a severe and rigorous scientific search allowing the anticipation of potential problems and indicating gaps in knowledge that can be explored by researchers. Although it is very common in medicine-related studies, it is very scarce in engineering-related fields. This is mainly due to the need to perform controlled clinical issues where a discerning and severe study is necessary because the reproduction and veracity of collected data must be strictly reproduced.

In this line, the aim of this systematic review is to compile data between 2016 and 2020 on composites with epoxy resin as matrix and synthetic plus natural fiber as reinforcements. The focus is on microscopy methods and analyses. Other important factors such as stacking sequence, type of synthetic/vegetable fibers used, epoxy type + hardener, abs chemical treatment (when applied) are mentioned.

Systematic Review Methodology

The papers were selected using the Scopus (www.scopus.com), Web of Science (www.webofknowledge.com), and SciFinder (https://sso.cas.org/) online databases. The search terms were: ([epoxy] AND [hybrid] AND [composites] AND [fiber] AND [microscopy]). The results are limited to English language articles published between 2016 and 2020. The identified articles have their titles and abstracts independently assessed by two reviewers (Neves, R.M., and Monticeli, F.M.) to identify their allocation in the systematic review.

From all obtained documents using the selected keywords, it was excluded reviews, conference papers, and notes. Furthermore, the following exclusion criteria are applied: epoxy resin is not a matrix; the composite is not hybrid; epoxy hybrid composite without vegetal fiber; epoxy hybrid composite without synthetic fiber; epoxy hybrid synthetic/vegetal composite without microscopy; add another material.

In the end, 32 studies of interest left. It is valid to mention that only microscopies (SEM, MET, OM, X-ray μCT, and CVM) are discussed in this study.

Data Collection and Analysis

A schematic flowchart representing a step-by-step process in presented in Fig. 1. The number of identified, included, and excluded (along with the reason) studies are indicated. The search with Scopus, Web of Science, and Scifinder online databases identified a total of 531 studies. From those, after excluding some papers which do not reach the initial criteria (as epoxy matrix, for example), a total of 200 papers remained. All excluded papers are described in detail in the flowchart.

After this step, 168 papers are excluded due to duplicity from different databases. Then, 32 papers underwent full-text analysis and are included here.

Figure 2 shows the systematic review results for the last 5 years (2016–2020), analytically presented in Table 1. It is worth noting an increasing use of microscopy analysis methods to analyze the phases, defects, and fracture mechanisms in

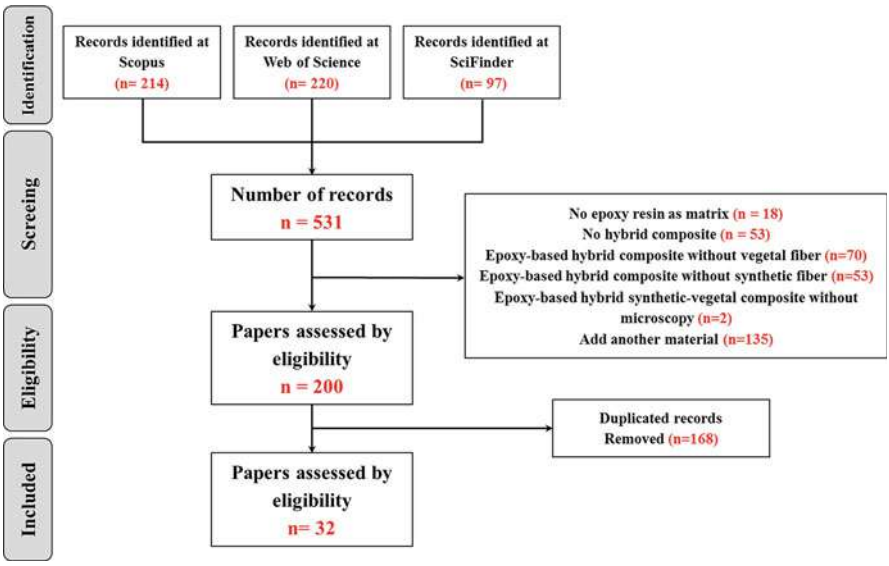

Fig. 1 Systematic review flowchart in accordance with PRISMA protocol

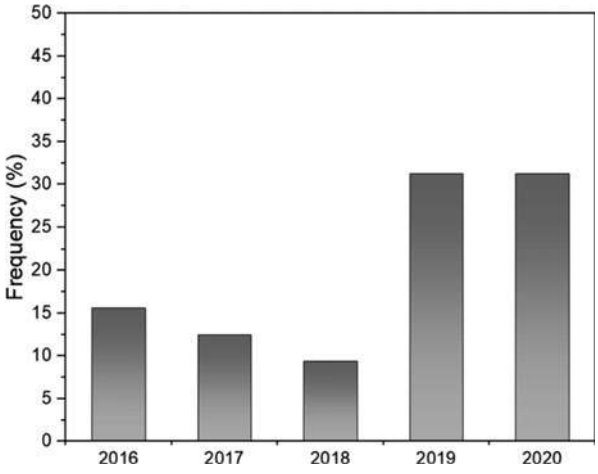

Fig. 2 Number of published papers on microscopy analysis of hybrid composites over the last 5 years

synthetic/natural hybrid thermoset composites. This trend is associated with the greater possibility of applying composites with natural fiber reinforcement in different applications (Saidane et al. 2017; Al-Hajaj et al. 2018; Giridharan 2019).

The hybrid composites present a range of possibilities in the stacking sequence, generating several possibilities in terms of combinations of fibers at different layers, for instance natural/natural fiber composite, synthetic/synthetic fiber composite, and hybrid interface laminate. The use of different layers results in a change in the final

Table 1 Microscopy analysis of synthetic/natural fiber hybrid composite

Ref.	Epoxy/ Hardener type	Synthetic fiber type	Vegetal fiber Type	Stacking sequence	Chemical treatment	Microscopy method	Microscopy analysis
(Fiore et al. 2017)	Bio-based Super Sap 100 // Hardener Super Sap 1000 (100:48)	(B) Unidirectional basalt fabric	(J) Jute plain weave bidirectional 0°/90°	**i.** J_8 **ii.** B/J/B/J_4/B/J/B **iii.** $B_2/J_6/B_2$	n.d.	Scanning electron microscopy (SEM) Gold coating	*Fractography*: **i.** jagged surfaces, **ii.** wide basalt-jute interface cracks, **iii.** less basalt-jute interface cracks
(Yahaya et al. 2016)	DER 331 // Amine harder (2:1)	(Ke) plain weave Kevlar	(K) Kenaf fibers mats	**i.** Kwoven/Ke, **ii.** Kunid/Ke, **iii.** Kmats/Ke	n.d.	Scanning electron microscopy (SEM) palladium coating	*Fractography*: weak fiber/matrix interface with voids and cracks
(Ridzuan et al. 2016b)	Epoxy Amite 100 series hardener (3:1)	(G) woven E-glass fibers	(P) *P. purpureum* grass fiber	Stacking sequence: **i.** 0.3P, **ii.** 0.24P/0.06G **iii.** 0.18P/0.12G **iv.** 0.12P/0.18G **v.** 0.3G All with 70% epoxy resin and interleaved sequence	n.d.	Field emission scanning electron microscopy (FESEM) platinum coating 3–5 kV	*Fractography*: Matrix cracking, debonding of fiber/matrix interface, voids, fiber pull-out, fiber splitting, fiber fracture, effect of water molecules

(continued)

Table 1 (continued)

Ref.	Epoxy/ Hardener type	Synthetic fiber type	Vegetal fiber Type	Stacking sequence	Chemical treatment	Microscopy method	Microscopy analysis
(Jeyasekaran et al. 2016)	LY556 // hardener HY951 (10:1)	(G) unidirectional glass fiber	(Ba) uUnidirectional Banana fiber	Interleaved	n.d.	Scanning electron microscopy (SEM) 5 kV	*Fractography*: G – fiber fracture, matrix fracture, matrix dislocation and debonding, fiber pull-out, matrix crack, matrix agglomeration. Hybrid – B fracture zone, glass fiber pull-out, matrix agglomeration, matrix fracture, dislocation of fiber and matrix, glass fiber fracture, debonding, matrix crack
(Ridzuan et al. 2016a)	Epoxy Amite 100 series hardener (3:1)	(G) woven E-glass fibers	(P) *P. purpureum* grass fiber	Interleaved (test temperature): **i.** untreated (25–80 °C) **ii.** 5% Alkaline (25–80 °C) **iii.** 10%	Alkali Treatment (5–10%)	Field emission scanning electron microscopy (FESEM) platinum coating 3–5 kV	*Fractography*: **i.** (25 °C) rough surface morphology, long fiber pull-out; (40 °C) voids, fiber pull-out; (60 °C) debonding of

				Alkaline (25–80 °C)			fiber/matrix interface; (80 °C) softening of the epoxy matrix. **ii.** (25 °C) fiber/ matrix interfacial debonding, pull out mechanisms, or matrix cracking, fibrillation of fibers; (40 °C) more fiber pull-out; (60 °C) fiber/matrix interfacial debonding; (80 °C) softening of the matrix. **iii.** (40 °C) voids, fiber pull out, fiber breakage, fiber splitting, fiber/matrix interface debonding, fiber damage, and nonuniform matrix surface texture, excess delignification of

(continued)

Table 1 (continued)

Ref.	Epoxy/ Hardener type	Synthetic fiber type	Vegetal fiber Type	Stacking sequence	Chemical treatment	Microscopy method	Microscopy analysis
							the fiber; (60 °C) fiber/matrix debonding; (80 °C) delamination of glass fibers
(Behera et al. 2019)	LY-556 // hardener HY-951 (10:1)	(Ke) The Kevlar K-29 fiber	(L) Luffa fiber	Unidirectional: **i.** L, **ii.** L/Ke, **iii.** Ke Random: **iv.** L, **v.** L/Ke, **vi.** Ke all with 90% epoxy resin and 10% of fiber	1, 3, 5, 7, 9 wt. % of NaOH solution	Scanning electron microscope (SEM)	*Fractography*: **i.** fiber failure; **ii.** fiber debonding and matrix-fiber debonding; **iii/vi.** voids and cracks in fiber/matrix interface
(Saidane et al. 2017)	SR 1500 // hardener SD 2503 (100:33)	(G) twill glass fiber fabric	(F) Twill weave flax fabric	**i.** F, **ii.** [G/F4]s, **iii.** [G2/F3]s, **iv.** [G3/F2]s, **v.** [G4/F]s, **vi.** G	n.d.	Scanning electron microscope (SEM) 30 kV	*Fractography*: **i/vi**. matrix cracking, fiber/matrix debonding, fiber and matrix failure; **ii/iii/iv/v.** matrix cracking, fiber/matrix debonding, fiber and matrix

							failure, delamination
(Ramesh et al. 2017)	LY 556 // Hardener HY 951 (10:1)	(C) unidirectional carbon fibers mat	(BA) Banana fibers	Interleaved **i.** C, **ii.** 0.8C/0.2Ba **iii.** 0.6C/0.4Ba **iv.** 0.4C/0.6Ba **v.** 0.2C/0.8Ba **vi.** Ba	NaOH solution	Scanning electron microscope (SEM) gold coating 2 kV	*Fractography*: Internal cracks, fractured surfaces and internal structure, banana fibers and fiber fracture, broken banana fibers, water absorbed matrix layer, fiber swelling
(Ridzuan et al. 2017)	Epoxy Amite 100 series (3:1)	(G) woven E-glass fibers	(P) *Pennisetum purpureum* grasses fiber	Stacking sequence: **i.** 0.24P/0.06G **ii.** 0.18P/ 0.12G **ii.** 0.12P/0.18G **iv.** 0.3G All with 70% epoxy resin and interleaved sequence	Alkali Treatment (5–10%)	Field- emission scanning electron microscopy (FESEM) gold coating 3 kV	*Fractography*: Untreated – voids, fiber pull-out, debonding of fiber/matrix interface, matrix cracking, fiber breakage, fiber splitting, lumens and a porous structure; 5% treated – epoxy matrix smooth surface, compressive cellular structure breakage, no signs of fiber debonding, pull-

(continued)

Table 1 (continued)

Ref.	Epoxy/ Hardener type	Synthetic fiber type	Vegetal fiber Type	Stacking sequence	Chemical treatment	Microscopy method	Microscopy analysis
							out mechanisms, or matrix cracking, fibrillation; 10% treated – voids, fiber pull-out, debonding, fiber breakage, and high levels of matrix cracking, fiber splitting, concentration of the alkaline solution, weakened and damaged fibers
(Dhakal et al. 2018)	M56 epoxy	(C) unidirectional carbon fiber prepregs	(F) Unidirectional flax fiber	**i.** C, **ii.** F, **iii.** C/F	n.d.	Color video microscope (CVM) Scanning electron microscope (SEM) 15 kV Optical microscope (OM) X-ray	*OM/SEM Fractography*: micro-machining, sharing, abrasion and erosion actions, fracture clearly/sharply, straight, smoothly and perpendicularly; **ii.** combined

						micro-computed tomography (X-ray μCT)	scooping (or sweeping) and ploughing actions, ductile shear and cutting/ deformation wear phenomena, striations; **ii.** high fractured or broken fibers and fiber-uncut or pull-out; **iii.** missing fiber segment and matrix fall-out, inter-laminar delamination and drilled hole walls *X-ray μCT Fractography*: peel-up delamination of the plies at the hole entry, push-out delamination, high shock wave and built-up drilling, scattered and small voids

(continued)

Table 1 (continued)

Ref.	Epoxy/ Hardener type	Synthetic fiber type	Vegetal fiber Type	Stacking sequence	Chemical treatment	Microscopy method	Microscopy analysis
							CVM Roughness: **i.** 3.34, **ii.** 7.21, **iii.** 5.99
(Al-Hajaj et al. 2018)	Araldite LY 1564 // Aradur 22.962 (40:3)	(C) carbon fiber	(F) Flax fiber	i. $[0/90_{C2}/0_{F12}/0/90_{C2}]$ ii. $[0/90_{C2}/\pm45_{F6S}/0/90_{C2}]$	n.d.	Optical microscopy (OM) Scanning electron microscopy (SEM)	*SEM Fractography*: **i/ii.** Carbon and flax fiber pullout and breakage, edge delamination between adjacent fiber/ matrix layers (cohesive failure) *OM fractography*: **i/ii.** Fiber pull-out and breakage, matrix failure, flax fiber/epoxy shear failure, delamination between layers, and debonding at fiber/matrix interfaces,

							delamination, fiber breakage; **i.** interlaminar crack, fiber buckling, C/epoxy layers crack growth in a zigzag pattern, F/epoxy layers longitudinal cracks; **ii.** delamination, fiber buckling, C/epoxy layers crack growth in a zigzag pattern, F/epoxy layers 45° angle crack *OM phase content (%)*: **i.** void 2.97, fiber 42.90, C 11.98, F 30.86, matrix 54.13; **ii.** void 2.19, fiber 45.90, C 11.79, F 34.10, matrix 51.92
(Giridharan and Jenarthanan 2019)	Grade AW106	(G) plain weave glass fiber mat	(Co) Cotton fibers	Interleaved	n.d.	Scanning electron microscopy (SEM) 5 kV	*Fractography*: Short fractured fibers projecting out of the matrix and no pull-out failure

(continued)

Table 1 (continued)

Ref.	Epoxy/ Hardener type	Synthetic fiber type	Vegetal fiber Type	Stacking sequence	Chemical treatment	Microscopy method	Microscopy analysis
(Alves et al. 2019)	Epikote Resin MGS RIM135 // Hardeners RIMH137 and RIMH134	(G) Biaxial ±45° non-woven fiberglass fabric	(J) Woven Jute fabric 0/90°	**i.** G_5 **ii.** $G/J_2/G$ $(\pm 45)_s$ **iii.** $G/J_2/G$ $(0/90)_s$ **iv.** $G/J_2/G$ $(\pm 45/0/90)_s$	Glass fiber surface treatment commercially named SE1500	Optical microscopy (OM)	*Fractography*: Resin-rich region, crack between Jute layers; **i.** delamination between hybrid layers, resin-rich; **ii.** glass fractured fiber, inter fiber fracture, splitting; **iii.** Cracking in jute layers
(Borukati et al. 2019)	LY -556 // HY -951	(C) carbon fiber	(ST) *Sansevieria trifasciata* Fiber	**i.** C **ii.** 0.9C/0.1ST **iii.** 0.8C/0.2ST **iv.** 0.7C/0.3ST **v.** 0.6C/0.4ST	5% NaOH	Scanning electron microscopy (SEM)	*Fractography*: resin microspores/ cracks, deboning and delamination of fiber
(Chapman and Dhakal 2019)	Hex Ply M56	(C) Unidirectional carbon fiber	(F) Unidirectional flax fiber	**i.** F_8 **ii.** C_8 **iii.** $C_2/F_4/C_2$	n.d.	Scanning electron microscopy (SEM) gold/palladium coating 15 kV	*Fractography*: **i.** extensive fiber breakage and disorder, play matrix cracking and debonding, fiber bending

							and debonding around a kink band of the flax fibers structure, twisted and flattened fiber, debonding and shear slippage; **ii.** uniform breakage, fiber breakage, severe delamination pattern; **iii.** wide area of damage through the fibers, degree of fibrillation, cracking, tearing and delamination, carbon and flax fibers in a chaotic site, explosive event, fiber pull-out
(Amir et al. 2019)	HL002TA // Hardener HL002TB	(Ke) woven Kevlar fabric	(EFB) eEmpty fruit bunch fiber mats	**i.** Ke/EFB/Ke **ii.** EFB/Ke/ EFB	n.d.	Scanning electron microscopy (SEM)	*Fractography*: EFB – brittle fracture, K – ductile fracture fiber pull-out, voids, fiber bending
(Dhakal and Sain 2020)	Hex Ply M56	(C) Unidirectional carbon fiber	(F) Unidirectional flax fiber		n.d.	Environmental scanning	*Fractography*: **i.** kink bands

(continued)

Table 1 (continued)

Ref.	Epoxy/ Hardener type	Synthetic fiber type	Vegetal fiber Type	Stacking sequence	Chemical treatment	Microscopy method	Microscopy analysis
				i. F_8 **ii.** C_8 **iii.** $C_2/F_4/C_2$		electron microscopy (E-SEM)	owing to fiber bending and buckling, delamination, lumen of flax fiber was elongated; **ii.** fiber pull-out, brittle fashion of broken fibers. **iii.** damage at matrices, and at the fiber/matrix interfaces, delamination between the plies micro-cracks can be initiated at the interfaces and promote accelerated crack propagation
(Cavalcanti et al. 2019)	AR260 // hardener AH260 (100:26)	(G) Glass fiber	(J) Jute fiber	Interleaved 0.6 J/0.4G	(NaOH) Alkaline treatment + Silane treatment Glycidoxypropyltrimethoxysilane (2%)	Scanning electron microscopy (SEM) platinum	*Fractography*: bundle structure fibers, pull-out fiber, voids, fiber

						coating 20 kV	bending and breakage
(Yusuff et al. 2019)	Epoxy resin	(C) Carbon fiber	(K) Kenaf fiber	Interleaved **i.** 40:60 **ii.** 60:40 fiber-matrix ratio	n.d.	Scanning electron microscopy (SEM) 8 kV	C – the gap between warp and weft yarns was very small and tight; K – gap between warp and weft yarns not too tight; *Fractography*: **i.** less matrix cracking, microcrack, fiber pull-out; **ii.** fiber pull-out, voids, more fiber breakage, delamination, planar distortion
(Saidane et al. 2019)	SR 1500 // hardener SD 2503 (100:33)	(G) Twill weave glass fiber	(F) Twill weave flax fabric	**i.** F_5 **ii.** $(G/F)_6$ **iii.** G_{10}	n.d.	Scanning electron microscopy (SEM)	*Fractography*: **i.** large fiber bridging, rough fiber surfaces, fiber/matrix debonding, fiber and bundle failure and matrix cracking; **ii.** fewer rough surface (less fiber bridging), fiber/matrix

(continued)

Table 1 (continued)

Ref.	Epoxy/ Hardener type	Synthetic fiber type	Vegetal fiber Type	Stacking sequence	Chemical treatment	Microscopy method	Microscopy analysis
							debonding; **iii.** intermediate fiber bridging, torn out fibers, several fiber failures, stretched fiber, bundle fiber
(Giridharan 2019)	Grade AW-106 // Hardener HV 953 U	(G) Plain weave mat of E-glass fabrics	(R) Ramie fiber	Interleaved	n.d.	Scanning electron microscopy (SEM)	*Fractography*: short fractured fibers projecting out of the matrix, no pullout failure
(Meenakshi and Krishnamoorthy 2019)	LY 556 // hardener HY-951 (10:1)	(G) Biaxial glass fiber	(F) Biaxial flax and (S) biaxial sisal fibers	Untreated: **i.** G/F/G **ii.** G/S/G **iii.** S/G/F Treated: **iv.** G/F/G **v.** G/S/G **vi.** S/G/F	Alkali treatment 10% NaOH	Scanning electron microscopy (SEM)	*Fractography*: Untreated – fiber pull-out, voids and incomplete impregnation; Treated – no fiber pull-out, appropriate impregnation, uniformity on the fractured surface
(Margabandu and Subramaniam 2020)	LY556 // HY951 (10:1)	(C) Twill weave carbon fabric	(J) Plain weave jute fabric	**i.** J_4 **ii.** C_4	Sodium hydroxide (NaOH)	Scanning electron	*Fractography*: **i.** fiber pull-out and voids;

				iii. J/C_2/J **iv.** C/J_2/C		microscopy (SEM)	**ii.** delamination in the middle C plies; **iii.** surface crake at the bottom ply; **iv.** cavities, fibers fractures, J fiber pull-out
(J R and Goud 2020)	L-12 // hardener K-6	(G) Glass fibers	(Cap) chopped *Calotropis procera* plant	**i.** epoxy resin **ii.** 0.2Cap **iii.** 0.15Cap/0.05G **iv.** 0.1Cap/0.1G **v.** 0.05Cap/0.15G **vi.** 0.2 G ii-vi. 80% of epoxy resin	Alkali treatment 5% NaOH	Scanning electron microscopy (SEM)	*Fractography*: bending of fibers, broken fibers, matrix cracking, and the cavity formation due to the fiber pullout, worn out fibers, debonding and breaking of *Calotropis procera* fibers, pull-out of glass fibers
(Karimzadeh et al. 2020)	Epoxy resin (1006)	(G) Glass fibers	(Pi) Pineapple Leaf Fiber	**i.** Pi/G/Pi/G **ii.** Pi/G_2/Pi **iii.** G/Pi_2/G **iv.** Pi_4	n.d.	Scanning electron microscopy (SEM) gold coating 15 kV	*Fractography*: **i/ii/iii.** microcrack, surfaces flaws, fiber splitting, glass fiber pull-out, Pi fiber pull-out; **iv.** microcrack, fiber debonding

(continued)

Table 1 (continued)

Ref.	Epoxy/ Hardener type	Synthetic fiber type	Vegetal fiber Type	Stacking sequence	Chemical treatment	Microscopy method	Microscopy analysis
(Acharya et al. 2019)	Araldite LY556 // HY951 hardener (10:1)	(G) E-glass mat	(J) Woven jute mat fiber	**i.** $G/J_8/G$ **ii.** $(G/J/G/J/G)_s$ **iii.** $(J/G/J/G/J)_s$	n.d.	Scanning electron microscopy (SEM) 10 kV	*Fractography*: small wear debris is scattered on the surface; **i.** surface cracks, broken fiber; **ii.** bare fiber, less wear debris; **iii.** lot of wear debris
(Khalid et al. 2020)	epotec yd 128 // hardener epotec TH 8279 (100:33)	(C) Plain woven carbon fabric	(J) Plain-woven jute fabric	**i.** C_5 **ii.** $C_2/J/C_2$ **iii.** C/J/C/J/C **iv.** $C/J_3/C$	n.d.	Scanning electron microscopy (SEM) 5 kV	*Fractography*: Pull-out jute fiber, delamination, matrix fails in form of matrix fragmentation, voids, matrix failure
(Seghini et al. 2020)	PRIME 27 // PRIME 20 slow hardener (100:28)	(B) Basalt woven fabric	(F) Biotex twill flax fabric	(0/90): **i.** B **ii.** F **iii.** Hybrid (±45): **iv.** B	n.d.	Scanning electron microscopy (SEM)	*Fractography*: **i/iv.** Matrix failure (brittle failure), basalt fiber and flax yarn pull-out, fiber failure

				v. F **vi.** Hybrid			(transverse failure) and fiber or yarn debonding; **ii/v.** voids, matrix cracking, debonding, fiber pull-out; **iv/vi.** both fiber pull-out, debonding
(Venkatasudhahar et al. 2020)	LY556 // HY951	(C) Carbon fiber fabric	(J) Jute fiber fabric, (Ba) banana fiber fabric	**i.** $C/J_3/C$ **ii.** $C/Ba_3/C$ **iii.** C/J/Ba/J/C **iv.** C/Ba/J/Ba/C **v.** Ba_5 **vi.** J_5	Alkaline treatment NaOH	Scanning electron microscopy (SEM) gold coating	*Fractography*: Untreated – cavities, cleavage fracture, cone fracture Treated – micro voids, cleavage fracture
(Pereira et al. 2020)	AR260 // AH260 (100:26)	(G) Glass fiber	(S) Sisal, (R) ramie and (Cu) curaua fabric fibers	Interleaved: **i.** S/R **ii.** S/Cu **iii.** S/G	n.d.	Scanning electron microscopy (SEM) gold coating 20 kV	*Fractography*: Fiber pull-out, crack in matrix, fragile fracture, cavity, voids, debonding
(Abd El-baky et al. 2020)	Kemapoxy 150 RGL (2:1)	(G) Plain weave E-glass (B) twill basalt fiber fabric	(F) Woven flax fiber	**i.** F_6 **ii.** B_6 **iii.** G_6 **iv.** $(G/F_2)_s$ **v.** $(G/B_2)_s$ **vi.** $(G/F/B)_s$ **vii.** $(G/B/F)_s$	n.d.	Scanning electron microscopy (SEM) gold coating 20 kV	*Fractography*: **i.** Kinking band and micro-buckling, A crack propagated across the specimen, fiber

(continued)

Table 1 (continued)

Ref.	Epoxy/ Hardener type	Synthetic fiber type	Vegetal fiber Type	Stacking sequence	Chemical treatment	Microscopy method	Microscopy analysis
				viii. G/B/F/B/ F/G **ix.** $(B/G/F)_s$ **x.** $(B/F/G)_s$ **xi.** $(F/B/G)_s$			breakage, voids; **ii.** width in the tensile side, matrix cracking, voids, matrix dislocation; **iii.** A crack propagated across the specimen width, fiber breakage, matrix fretting, voids, matrix dislocation; **iv-xi.** A crack propagated across the specimen width, delamination, A crack propagated

							across the specimen width, fiber breakage, matrix cracking, voids, kinking band, fiber pull-out, fiber/matrix debonding
(Shenoy Heckadka et al. 2020)	PF50	(Ut) uUltrahigh-molecular-weight polyethylene	(F) Flax and (J) jute fibers bidirectionally woven mats	i. $(Ut_2/F/J)_s$ ii. $(Ut_2/J/F)_s$ iii. $(J_2/Ut/F)_s$ iv. $(J_2/F/Ut)_s$ v. $(F_2/J/Ut)_s$ vi. $(F_2/Ut/J)_s$	10% NaOH treatment	Scanning electron microscopy (SEM) gold coating 10–15 kV	*Fractography*: Fiber breakage, fiber shearing, jute debris, fiber splitting, voids, delamination, crack propagation

material properties since the synergy between the reinforcements affect the impregnation quality and defect formation (Al-Hajaj et al. 2018). Failure mechanisms can also change upon different hybridization strategies (Abd El-baky et al. 2020).

Figure 3 presents the stacking sequence frequency identified in all studies. Most studies were neglected using non-hybrid composites (only with synthetic or natural fiber) in their analyzes, limiting an effective improvement analysis of impregnation and the failure mechanisms (Amir et al. 2019; Ridzuan et al. 2016a; Yahaya et al. 2016). The most used type of hybrid is interleaved stacking sequence, as this increases the number of hybrid interfaces in the material, which with a positive synergy could significantly increase the mechanical performance (Shenoy Heckadka et al. 2020). Two types of stacking are also presented. Hybrid 1 represents synthetic fibers on both surfaces and natural fibers at the middle, while Hybrid 2 is the opposite. In general, synthetic reinforcements have higher stiffness and strength, while natural fibers have the advantages of environmental issue – energy economy through weight reduction and recyclability (Acharya et al. 2019; Abd El-baky et al. 2020; Seghini et al. 2020).

Most studies use hand lay-up method as the preferred processing method, as shown in Fig. 4. This method is fast and non-expensive; however, infusion methods (vacuum infusion and resin transfer molding (RTM)) are more suitable toward decreasing defects through impregnation with greater processing control, mainly in the regions of natural fibers, which present more porous surfaces (Alves et al. 2019; Ridzuan et al. 2016b; Dhakal and Sain 2020). Compression molding processing also shows a low frequency of use (Dhakal and Sain 2020; Chapman and Dhakal 2019).

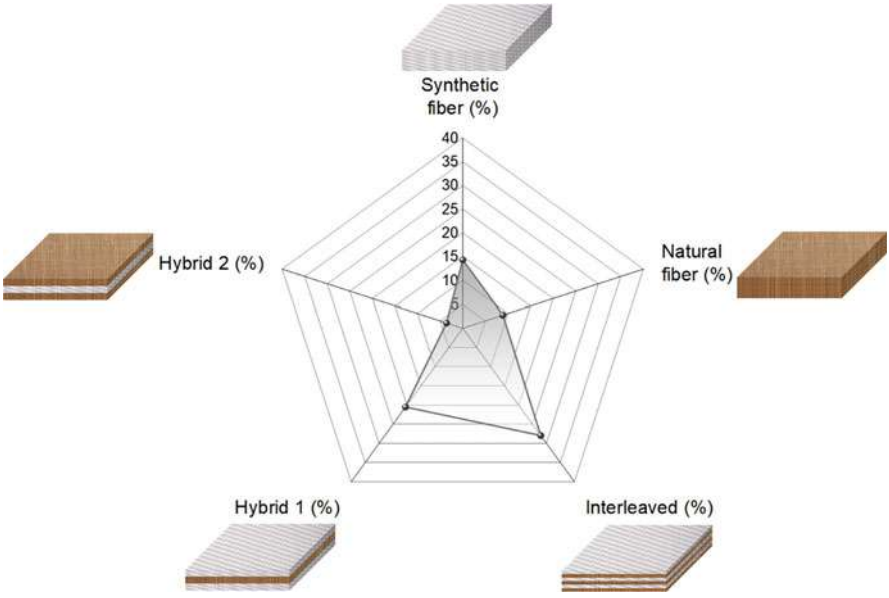

Fig. 3 Stacking sequence frequency of hybrid and non-hybrid composites

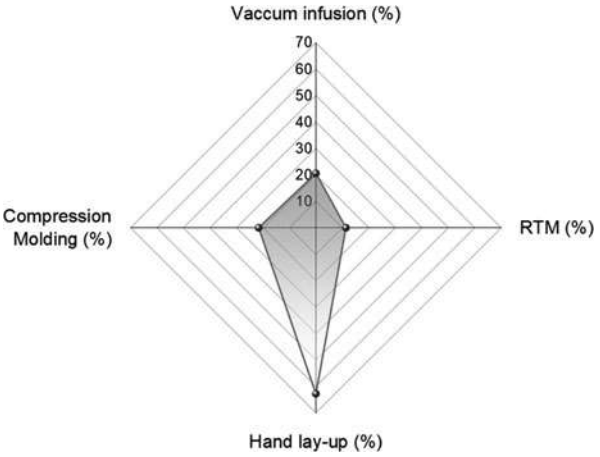

Fig. 4 Processing methods frequency

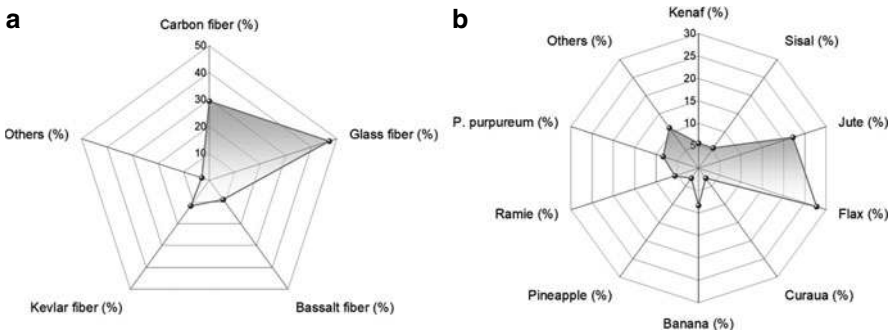

Fig. 5 Reinforcements frequency used for hybrid composites: (**a**) synthetic fibers and (**b**) natural fiber

Figure 5 presents the reinforcements frequency used. There is a greater range for natural reinforcements (Fig. 5b) than synthetic reinforcements (Fig. 5a). The most used synthetic reinforcement is glass fiber due to its synergy with natural fibers and epoxy resin and keeping the cost of the material lower than carbon and fibers (Monticeli et al. 2020; Giridharan and Jenarthanan 2019). There is a wider range for natural fibers, considering that studies in the literature continually demonstrate the possibility of using a new source for natural fiber (Siva et al. 2020). Nevertheless, flax and jute are the most used fibers in hybrid composites. On the other hand, carbon and fibers could be used to decrease surface roughness (Dhakal et al. 2018), provide more uniform rupture breakage (Chapman and Dhakal 2019), and reduce void content (Amir et al. 2019; Seghini et al. 2020) of such hybrid composites.

The frequencies of microscopic analysis methods used follow this sequence: SEM (86%), OM (8%), X-Ray μCT (3%), and CVM (3%). Figure 6 illustrates that microscopy techniques are mainly used for fractography analysis to identify the

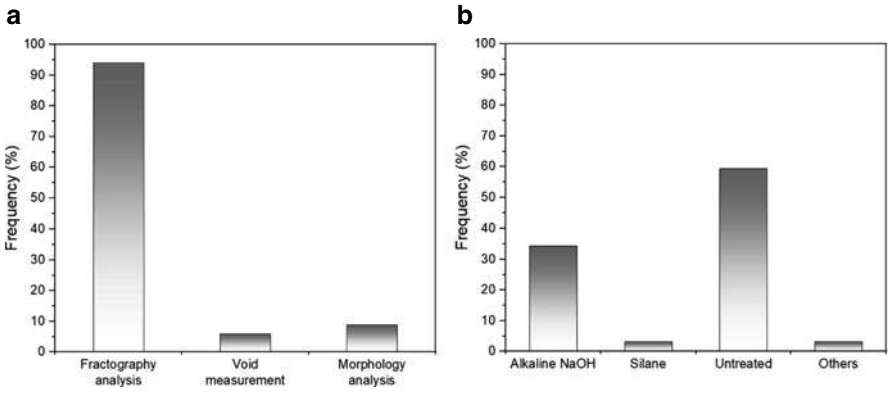

Fig. 6 (**a**) Microscopy analysis frequency and (**b**) chemical treatments frequency applied to the reinforcements

fracture mechanisms. According to Al Hajaj et al. (2018), microscopy analysis is a reliable procedure to measure void content, morphology, and position, as well as phase content (reinforcement thickness, fiber angle, fiber/matrix fraction). The quantitative microscopy analysis expands property and processing analyses with a high degree of reliability. Such microscopic analyses are very useful to voids and defects measurement, quantification of phase volume (Bodaghi et al. 2016; Hamidi et al. 2005), development of physical model to measure the strain energy release ratio through microscopy fracture measurement (Daneshjoo et al. 2018; Wong et al. 2014). For that purpose, X-Ray μCT has been increasingly used due to the higher precision and three-dimensional analysis without the need to cut or polish samples, which can change or create more defects (Dhakal et al. 2018).

Chemical treatments directly affect the surface adhesion of natural fibers and epoxy resins. About 60% of the works do not apply any surface treatment, a factor that results in increased void content, fiber pull-out fracture mechanisms, and interfacial resistance decay (Ridzuan et al. 2016a; Meenakshi and Krishnamoorthy 2019). The alkaline treatment with NaOH solution is the most used method (mainly 5%), in which it solves problems related to low interfacial adhesion between fiber and matrix at low cost (Ramesh et al. 2017; Borukati et al. 2019). However, 10% of NaOH solution shows overestimated treatment values, in which it generates agglomeration and reduction of mechanical properties, evidenced through fracture mechanisms (Ridzuan et al. 2016a, 2017). Other treatments can also enhance mechanical properties and reduce void content; however, there are few studies (<6%) for a deeper assessment of the failure mechanisms generated by other chemical treatments in natural fibers in hybrid composites.

Figure 7 shows all combinations between natural and synthetic reinforcements with epoxy resin found in this work. This scheme provides the possibility to find the lack in the literature of combinations of synthetic/natural fibers for microscopic analysis of fracture and phase content in hybrid composites.

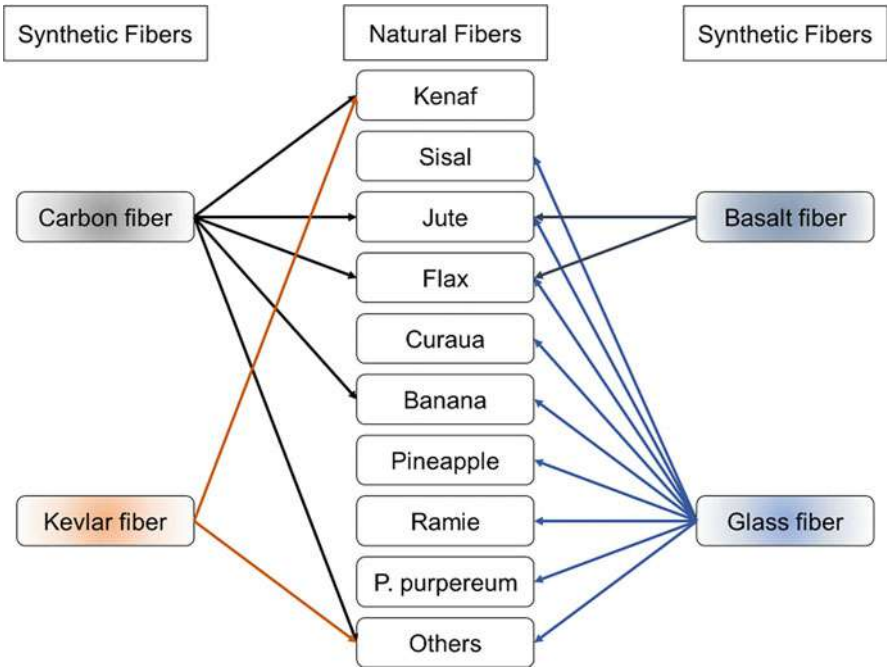

Fig. 7 Synthetic and natural fiber combination scheme

Future perspectives

Based on the present systematic review, the main prospects show a huge potential related to non-mechanical properties, since most of the studies focuses on mechanical and thermal properties. New technologies and design tools contribute to extend the potential of hybrid composite materials. Swolfs et al. (2019) point out recent trends in hybridization as three main areas: i) pseudo-ductile and ductile fiber-hybrids to solve the problem of ductility because advanced composites are usually brittle, ii) functional properties, in which many orders of magnitudes are differed instead the typically one to two orders of magnitude, and iii) environmental impact, toward developing more sustainable hybrid composites.

Conclusions

This chapter summarized recent progress regarding microscopy methods and analyses for hybrid synthetic/vegetable fiber-reinforced composites. The types of reinforcement, architectures, and combinations of fibers were presented. All papers listed in this systematic review and presented in Table 1 clearly indicated the main characteristics and findings that can be explored in microscopy techniques to

characterize a particular property of the composite. The decision of the type of the fiber, as well as their combination, impacts not only on cos-related and environmental-related issues but on the void formation and consequently on the final properties of the hybrid laminate

Acknowledgments The authors would like to thank the following granting foundations. FM Monticeli (FAPESP); RM Neves (CAPES); JHS Almeida Jr. (CAPES); and HL Ornaghi Jr. (CNPq Process number 151438/2020-0).

References

M.A. Abd El-baky, M.A. Attia, M.M. Abdelhaleem, M.A. Hassan, Mechanical characterization of hybrid composites based on flax, basalt and glass fibers. J. Compos. Mater. **54**(27), 4185–4205 (2020)

S.K. Acharya, T. Bera, V. Prakash, S. Pradhan, Effect of stacking sequence on the tribological behaviour of jute-glass hybrid epoxy composite. Mater. Today Proc. [Internet] **28**, 936–939 (2019). https://doi.org/10.1016/j.matpr.2019.12.328

Z. Al-Hajaj, R. Zdero, H. Bougherara, Mechanical, morphological, and water absorption properties of a new hybrid composite material made from 4 harness satin woven carbon fibers and flax fibers in an epoxy matrix. Compos. Part A Appl. Sci. Manuf. [Internet] **115**, 46–56 (2018). https://doi.org/10.1016/j.compositesa.2018.09.015

J.H.S. Almeida, H.L. Ornaghi, S.C. Amico, F.D.R. Amado, Study of hybrid intralaminate curaua/glass composites. Mater. Des. **42**, 111–117 (2012)

J.L.C. Alves, K.S. Prado, J.M.F. de Paiva, Compressive and interlaminar shear strength properties of biaxial fiberglass laminates hybridized with jute fiber produced by vacuum infusion. J. Nat. Fibers [Internet] **00**(00), 1–16 (2019). https://doi.org/10.1080/15440478.2019.1697996

S.M.M. Amir, M.T.H. Sultan, M. Jawaid, S.N.A. Safri, A.U.M. Shah, M.R. Yusof, et al., Effects of layering sequence and gamma radiation on mechanical properties and morphology of Kevlar/oil palm EFB/epoxy hybrid composites. J. Mater. Res. Technol. [Internet] **8**(6), 5362–5373 (2019). https://doi.org/10.1016/j.jmrt.2019.09.003

A. Behera, J. Dehury, M.M. Thaware, A comparative study on laminated and randomly oriented Luffa-Kevlar reinforced hybrid composites. J. Nat. Fibers [Internet] **16**(2), 237–244 (2019). https://doi.org/10.1080/15440478.2017.1414653

M. Bodaghi, C. Cristóvão, R. Gomes, N.C. Correia, Experimental characterization of voids in high fiber volume fraction composites processed by high injection pressure RTM. Compos. Part A Appl. Sci. Manuf. **82**, 88–99 (2016)

S.R. Borukati, B.D. Prasad, A. Ramesh, Development and characterization of natural fiber /carbon fiber reinforced hybrid composite material. Mater. Today Proc. [Internet] **18**, 5394–5399 (2019). https://doi.org/10.1016/j.matpr.2019.07.567

D.K.K. Cavalcanti, M.D. Banea, J.S.S. Neto, R.A.A. Lima, L.F.M. da Silva, R.J.C. Carbas, Mechanical characterization of intralaminar natural fiber-reinforced hybrid composites. Compos. Part B Eng. [Internet] **175**, 107149 (2019). https://doi.org/10.1016/j.compositesb.2019.107149

M. Chapman, H.N. Dhakal, Effects of hybridisation on the low velocity falling weight impact and flexural properties of flax-carbon/epoxy hybrid composites. Fibers **7**(11), 95 (2019)

Z. Daneshjoo, M.M. Shokrieh, M. Fakoor, A micromechanical model for prediction of mixed mode I/II delamination of laminated composites considering fiber bridging effects. Theor. Appl. Fract. Mech. [Internet] **2018**(94), 46–56 (2018). https://doi.org/10.1016/j.tafmec.2017.12.002

C. Devalve, R. Pitchumani, Simulation of void formation in liquid composite molding processes. Compos. Part A Appl. Sci. Manuf. [Internet] **51**, 22–32 (2013). https://doi.org/10.1016/j.compositesa.2013.03.016

H.N. Dhakal, M. Sain, Enhancement of mechanical properties of flax-epoxy composite with carbon fiber hybridisation for lightweight applications. Materials (Basel) **13**(1), 109 (2020)

H.N. Dhakal, S.O. Ismail, S.O. Ojo, M. Paggi, J.R. Smith, Abrasive water jet drilling of advanced sustainable bio-fiber-reinforced polymer/hybrid composites: a comprehensive analysis of machining-induced damage responses. Int. J. Adv. Manuf. Technol. **99**(9–12), 2833–2847 (2018)

V. Fiore, T. Scalici, D. Badagliacco, D. Enea, G. Alaimo, A. Valenza, Aging resistance of bio-epoxy jute-basalt hybrid composites as novel multilayer structures for cladding. Compos. Struct. [Internet] **160**, 1319–1328 (2017). https://doi.org/10.1016/j.compstruct.2016.11.025

P. Ganeshkumar, S. Gopalakrishnan, Systematic reviews and meta-analysis: understanding the best evidence in primary healthcare. J. Fam. Med. Prim. Care **2**(1), 9 (2013)

S.C. Garcea, Y. Wang, P.J. Withers, X-ray computed tomography of polymer composites. Compos. Sci. Technol. [Internet] **156**, 305–319 (2018). https://doi.org/10.1016/j.compscitech.2017.10.023

R. Giridharan, Preparation and property evaluation of glass/ramie fibers reinforced epoxy hybrid composites. Compos. Part B Eng. [Internet] **167**, 342–345 (2019). https://doi.org/10.1016/j.compositesb.2018.12.049

R. Giridharan, M.P. Jenarthanan, Preparation and characterisation of glass and cotton fibers reinforced epoxy hybrid composites. Pigment Resin Technol. **48**(4), 272–276 (2019)

L.K. Grunenfelder, S.R. Nutt, Void formation in composite prepregs – effect of dissolved moisture. Compos. Sci. Technol. [Internet] **70**(16), 2304–2309 (2010). https://doi.org/10.1016/j.compscitech.2010.09.009

Y.K. Hamidi, L. Aktas, M.C. Altan, Three-dimensional features of void morphology in resin transfer molded composites. Compos. Sci. Technol. **65**(7–8), 1306–1320 (2005)

M. J R, G. Goud, Development of Calotropis procera-glass fibers reinforced epoxy hybrid composites: dynamic mechanical properties. J. Nat. Fibers [Internet] **00**(00), 1–8 (2020). https://doi.org/10.1080/15440478.2020.1745119

A.S. Jeyasekaran, K.P. Kumar, S. Rajarajan, Numerical and experimental analysis on tensile properties of banana and glass fibers reinforced epoxy composites. Sadhana – Acad. Proc. Eng. Sci. **41**(11), 1357–1367 (2016)

A. Karimzadeh, M.Y. Yahya, M.N. Abdullah, K.J. Wong, Effect of stacking sequence on mechanical properties and moisture absorption characteristic of hybrid PALF/glass fiber composites. Fibers Polym. **21**(7), 1583–1593 (2020)

M.Y. Khalid, M.A. Nasir, A. Ali, A. Al Rashid, M.R. Khan, Experimental and numerical characterization of tensile property of jute/carbon fabric reinforced epoxy hybrid composites. SN Appl. Sci. [Internet] **2**(4) (2020). https://doi.org/10.1007/s42452-020-2403-2

T.S. Lundström, B.R. Gebart, C.Y. Lundemo, Void formation in RTM. J. Reinf. Plast. Compos. **12**(12), 1339–1349 (1993)

S. Margabandu, S. Subramaniam, An experimental investigation of thrust force, delamination and surface roughness in drilling of jute/carbon hybrid composites. World J. Eng. **17**(5), 661–674 (2020)

C.M. Meenakshi, A. Krishnamoorthy, Study on the effect of surface modification on the mechanical and thermal behaviour of flax, sisal and glass fiber-reinforced epoxy hybrid composites. J. Renew. Mater. **7**(2), 153–169 (2019)

D.C.S. Monte Vidal, H.L. Ornaghi, F.G. Ornaghi, F.M. Monticeli, H.J.C. Voorwald, M.O.H. Cioffi, Effect of different stacking sequences on hybrid carbon/glass/epoxy composites laminate: thermal, dynamic mechanical and long-term behavior. J. Compos. Mater. **54**(6), 731–743 (2020)

F.M. Monticeli, H.L. Ornaghi, H.J.C. Woorwald, M.O.H. Cioffi, Three-dimensional porosity characterization in carbon/glass fiber epoxy hybrid composites. Compos. Part A Appl. Sci. Manuf. **125**, 105555 (2019)

F.M. Monticeli, J.H.S. Almeida, R.M. Neves, F.G. Ornaghi, H.L. Ornaghi, On the 3D void formation of hybrid carbon/glass fiber composite laminates: a statistical approach. Compos. Part A Appl. Sci. Manuf. [Internet] **137**, 106036 (2020). https://doi.org/10.1016/j.compositesa.2020.106036

H.L. Ornaghi, A.S. Bolner, R. Fiorio, A.J. Zattera, S.C. Amico, Mechanical and dynamic mechanical analysis of hybrid composites molded by resin transfer molding. J. Appl. Polym. Sci. **118**, 887–896 (2010)

S. Paciornik, J. ́dAlmeida, Digital microscopy and image analysis applied to composite materials characterization. Rev. Mater. **15**(2), 183–191 (2010)

A.L. Pereira, M.D. Banea, J.S.S. Neto, D.K.K. Cavalcanti, Mechanical and thermal characterization of natural intralaminar hybrid composites based on sisal. Polymers (Basel) **12**(4), 866 (2020)

M. Ramesh, R. Logesh, M. Manikandan, N.S. Kumar, D.V. Pratap, Mechanical and water intake properties of banana-carbon hybrid fiber reinforced polymer composites. Mater. Res. **20**(2), 365–376 (2017)

A.K. Reis, F.M. Monticelli, R.M. Neves, L. Felipe, D.P. Santos, Creep behavior of polyetherimide semipreg and epoxy prepreg composites: structure vs. property relationship. J. Compos. Mater. **54**, 4121 (2020)

M.J.M. Ridzuan, M.S.A. Majid, M. Afendi, M.N. Mazlee, A.G. Gibson, Thermal behaviour and dynamic mechanical analysis of Pennisetum purpureum/glass-reinforced epoxy hybrid composites. Compos. Struct. [Internet] **152**, 850–859 (2016a). https://doi.org/10.1016/j.compstruct.2016.06.026

M.J.M. Ridzuan, M.S. Abdul Majid, M. Afendi, K. Azduwin, N.A.M. Amin, J.M. Zahri, et al., Moisture absorption and mechanical degradation of hybrid Pennisetum purpureum/glass-epoxy composites. Compos. Struct. [Internet] **141**, 110–116 (2016b). https://doi.org/10.1016/j.compstruct.2016.01.030

M.J.M. Ridzuan, M.S. Abdul Majid, S.M. Hafis, K. Azduwin, The effects of alkali treatment on the mechanical and morphological properties of Pennisetum purpureum/glass-reinforced epoxy hybrid composites. Plast. Rubber Compos. **46**(10), 421–430 (2017)

D. Romanzini, H.L.J. Ornaghi, S.C. Amico, A.J. Zattera, Preparation and characterization of ramie-glass fiber reinforced polymer matrix hybrid composites. Mater. Res. **15**(3), 415–420 (2012)

D. Romanzini, A. Lavoratti, H.L. Ornaghi, S.C. Amico, A.J. Zattera, Influence of fiber content on the mechanical and dynamic mechanical properties of glass/ramie polymer composites. Mater. Des. [Internet] **47**, 9–15 (2013). https://doi.org/10.1016/j.matdes.2012.12.029

E.H. Saidane, D. Scida, M. Assarar, R. Ayad, Damage mechanisms assessment of hybrid flax-glass fiber composites using acoustic emission. Compos. Struct. [Internet] **174**, 1–11 (2017). https://doi.org/10.1016/j.compstruct.2017.04.044

E.H. Saidane, D. Scida, M.J. Pac, R. Ayad, Mode-I interlaminar fracture toughness of flax, glass and hybrid flax-glass fiber woven composites: Failure mechanism evaluation using acoustic emission analysis. Polym. Test [Internet] **75**, 246–253 (2019). https://doi.org/10.1016/j.polymertesting.2019.02.022

M.C. Seghini, F. Touchard, F. Sarasini, L. Chocinski-Arnault, M.R. Ricciardi, V. Antonucci, et al., Fatigue behaviour of flax-basalt/epoxy hybrid composites in comparison with non-hybrid composites. Int. J. Fatigue [Internet] **139**, 105800 (2020). https://doi.org/10.1016/j.ijfatigue.2020.105800

L. Shamseer, D. Moher, M. Clarke, D. Ghersi, A. Liberati, M. Petticrew, et al., Preferred reporting items for systematic review and meta-analysis protocols (prisma-p) 2015: elaboration and explanation. BMJ [Internet] **349**, 1–25 (2015). https://doi.org/10.1136/bmj.g7647

S. Shenoy Heckadka, R. Pai Ballambat, V. Kini Manjeshwar, M. Kumar, P. Hegde, A. Kamath, Influence of stack sequence on the mechanical characteristics of hybrid composites analyzed using cone beam computed tomography and scanning electron microscopy. Polym. Compos. **41**, 5059–5071 (2020)

R. Siva, T.N. Valarmathi, K. Palanikumar, A.V. Samrot, Study on a novel natural cellulosic fiber from Kigelia africana fruit: characterization and analysis. Carbohydr. Polym. [Internet] **244**, 116494 (2020). https://doi.org/10.1016/j.carbpol.2020.116494

Y. Swolfs, I. Verpoest, L. Gorbatikh, Recent advances in fiber-hybrid composites: materials selection, opportunities and applications. Int. Mater. Rev. [Internet] **64**(4), 181–215 (2019). https://doi.org/10.1080/09506608.2018.1467365

M. Venkatasudhahar, P. Kishorekumar, R.N. Dilip, Influence of stacking sequence and fiber treatment on mechanical properties of carbon-jute-banana reinforced epoxy hybrid composites. Int. J. Polym. Anal. Charact. [Internet] **25**(4), 238–251 (2020). https://doi.org/10.1080/1023666X.2020.1781481

A. Wong, L.H. Mark, M.M. Hasan, C.B. Park, The synergy of supercritical CO2and supercritical N2in foaming of polystyrene for cell nucleation. J. Supercrit. Fluids [Internet] **90**, 35–43 (2014). https://doi.org/10.1016/j.supflu.2014.03.001

R. Yahaya, S.M. Sapuan, M. Jawaid, Z. Leman, E.S. Zainudin, Effect of fiber orientations on the mechanical properties of kenaf–aramid hybrid composites for spall-liner application. Def. Technol. [Internet] **12**(1), 52–58 (2016). https://doi.org/10.1016/j.dt.2015.08.005

M.I. Yusuff, N. Sarifuddin, Z. Ahmad, Mechanical properties of woven carbon fiber/kenaf fabric reinforced epoxy matrix hybrid composites. Malays. J. Microsc. **15**(1), 10–16 (2019)

Morphology and Mechanical Properties of Epoxy/Synthetic/Natural Fiber Composites

35

Bejoy Francis

Contents

Abstract

Epoxy resin is a widely used matrix materials for making composite materials. Natural as well as synthetic fibers are extensively used in composites. The use of synthetic fibers can be reduced by using natural fibers along with synthetic fibers. Natural fibers like hemp, flax, kenaf, jute, etc. have been used in conjunction with synthetic fibers like glass, Kevlar, and carbon. The ultimate properties are depen-

B. Francis (✉)
Department of Chemistry, St. Berchmans College, Kottayam, Kerala, India
e-mail: bejoy@sbcollege.ac.in

S. Mavinkere Rangappa et al. (eds.), *Handbook of Epoxy/Fiber Composites*,
https://doi.org/10.1007/978-981-19-3603-6_39

dent of many parameters. The type of fibers, ratio of natural to synthetic fiber, the weaving and stacking pattern, fiber ply arrangement, etc. are some of the important factors governing the properties of the hybrid composites. This chapter outlines the mechanical properties and morphology of various natural/synthetic hybrid fiber composites with epoxy resin as the matrix material.

Keywords

Epoxy resin · Hybrid composite · Natural fiber · Synthetic fiber

Introduction

Composite materials offer a combination of materials with diverse properties, shape, size, etc. to another unit having properties better than its components. Composite materials have high specific strength, good creep and fatigue resistance, good corrosion resistance, etc. depending on the constituents. Among the various composite materials fiber-reinforced polymers are extremely useful. They are used for automotive and marine applications, aerospace industry, aircraft industry, making sports goods, etc. Synthetic fibers are used to reinforce polymers in demanding applications. But much concern had arisen about the environmental impact of these materials. Developing ecofriendly materials or making the materials more ecofriendly is the need of the hour.

Good specific strength and modulus, low cost, easy availability, good acoustic property, as well as nonabrasive and biodegradability are characteristic features of natural fibers. Their drawbacks are high moisture absorption, low wettability, and low thermal stability during processing and poor adhesion with the matrix (Sivakumar et al. 2018; Latif et al. 2014; Ashik and Sharma 2015; Asumani et al. 2012). In order to reduce the use of synthetic fibers, natural fibers can be used in conjunction with synthetic fibers for many applications. This type of hybridization yield materials with comparable physical properties with that of synthetic fiber composites. Hybrid composites can be fabricated in different ways: (i) layer-by-layer arrangement of different fibers, (ii) yarn-by-yarn arrangement in which different types of fibers are present in one layer, and (iii) mixing different types of fibers in a single yarn (Swolfs et al. 2014).

The research on hybrid composites is wide and different combinations of natural and synthetic fibers have been fabricated and the properties were investigated. Thermosetting resins have been widely used as matrices in composite materials. Epoxy resin being a versatile thermosetting resin is one of the important matrices used for fabricating composites because of their ease of fabrication and excellent properties. This chapter deals with the mechanical and morphological properties of natural/synthetic hybrid fiber composites with epoxy resin as matrix. Glass, aramid, and carbon fibers were the common synthetic fibers used to hybridize with various natural fibers. The properties of hybrid composites of a specific synthetic fiber with various natural fibers are described in this chapter.

Glass Fiber/Natural Fiber Hybrid Composites

Glass fiber is a commercially very important fiber. It has been used to hybridize with many natural fibers. The following section describes the mechanical properties of various glass/natural fiber hybrid systems.

Glass/Flax Hybrid Composites

Hybridization of woven flax with woven glass fiber improved the tensile properties compared to flax only epoxy composites (Saidane et al. 2016). The mechanical failure of the hybrid composites is characterized by brittle failure. Hybridization with glass enhanced the tensile properties of flax composites. The percentage elongation was also found to increase on hybridization due to higher percentage elongation at failure of glass fiber (2–4.8%) compared to that of flax fiber (1.2–1.6%). The increase in properties is dependent on the percentage of glass fiber in the composite. Aging and water absorption could affect the ultimate properties of composites. Upon aging at 55 °C for 38 days in water, the tensile properties decreased in the hybrid composites, although hybridization decreased water uptake. The swelling of flax fibers generated shear stress along the glass/flax interfaces leading to delamination. Also aging at 55 °C caused residual shrinkage stress due to the large difference and the opposite values between the coefficient of thermal expansion of flax and glass fibers (flax fibers: $-1 \times 10^{-6}\,^{\circ}\mathrm{C}^{-1}$ versus glass fibers: $5 \times 10^{-6}\,^{\circ}\mathrm{C}^{-1}$) (Le Duigou et al. 2010). The specific tensile strength of unaged samples was close to the rule of mixtures given by equation

$$P_{\mathrm{Hybrid}} = P_1 V_1 + P_2 V_2$$

where P_{Hybrid} is the property to be studied of the hybrid composite, P_1 and P_2 the corresponding properties of the nonhybrid composites 1 and 2, and V_1 and V_2 the volume fractions of the reinforcements in hybrid composites, while respecting the relationship $V_1 + V_2 = 1$. But aging resulted in a negative hybrid effect as shown in Fig. 1.

The stacking sequence has strong influence on the mechanical properties of hybrid composites. Recent investigation on hybrid composites by Wang et al. (2020) revealed the importance of stacking pattern. The stacking pattern with F2G4F2 pattern, i.e., four layers of glass is arranged between two layers of flax, has maximum tensile properties among the various systems studied. The values were less than that predicted by rule of mixtures due to the displacement resulting from the clearance in the testing machine joints, the specimen slippage from the grippers, and shear deformation in the adhesive material between specimen and tabs. However, the tensile properties are very close to each other when the ratio of the hybrid fibers are kept constant. A different load transfer mechanism is responsible for this type of behavior. On the application of load to a sandwich-type arrangement with high strength material in the core, the load moved to the strong core layer (Attia et al. 2017).

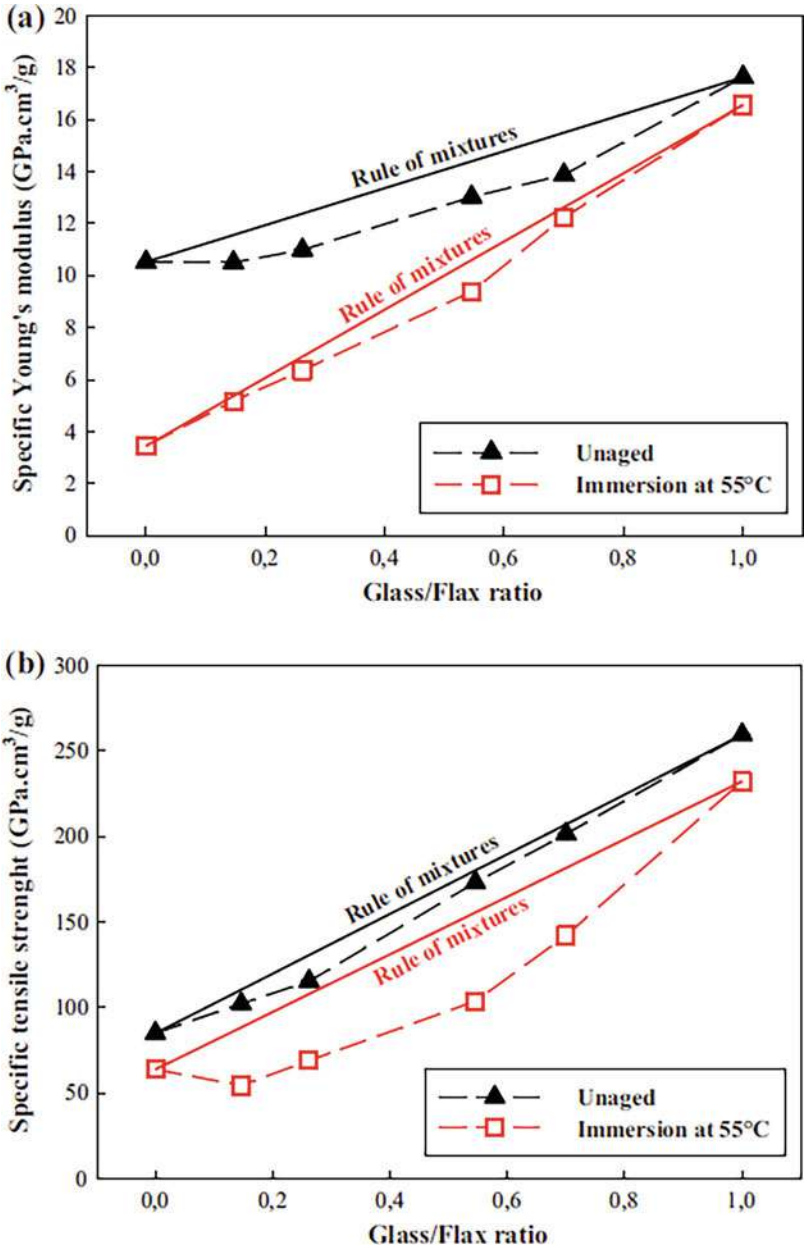

Fig. 1 Hybrid effect for tensile properties as function of glass/flax ratio; (**a**) specific Young's modulus, (**b**) specific tensile strength (Saidane et al. 2016). (Reproduced with permission from Elsevier, License No.: 517870055876)

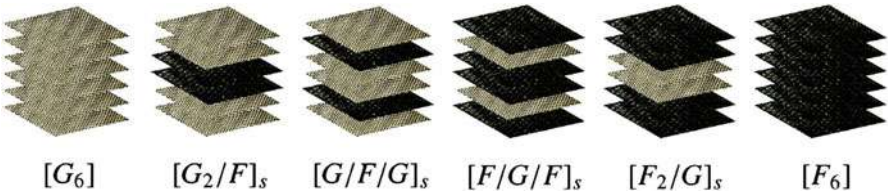

Fig. 2 Stacking sequence of laminates (Cihan et al. 2019). (Reproduced with permission from Elsevier, License No.: 5171870399083)

In contrast to tensile properties, flexural properties are dependent on the layup pattern when the hybrid ratio is kept same. The H6 arrangement (G2F4G2), i.e., four layers of flax is arranged between two layers of glass, showed the best properties among the various systems. The flexural properties are dependent on the outer layer since the load is initially distributed on the compression side and then on the tensile side. If flax or glass fiber is arranged in dispersed pattern like H3 (FGFGFGFG), the delamination is increased as a result of reduced interface bonding. Hence the improvement in properties is less in such cases. The failure modes during bending failure have been identified using scanning electron microscopy. The fracture morphology on compression side of glass fiber showed glass fiber stripping and delamination from the epoxy resin matrix. On the tensile side, fiber fracture and delamination were seen. The flax fiber on compression side shows buckling and compression folds and on tensile side fiber pullout was observed.

Another stacking pattern and the tensile strength of samples against E glass content are shown in Figs. 2 and 3, respectively (Cihan et al. 2019). Variation in tensile properties is observed upon hybridization. Hybrid composites have better tensile properties than flax only composites but lower properties compared to glass only composites. The tensile properties of flax composites increased with the introduction of glass fiber and the same decreased by introduction of flax fibers into glass fiber composites as seen from Fig. 3. In the case of hybrid composites maximum tensile properties are obtained when the two glass layers are placed side by side rather than separated by flax layers.

In hybrids, different levels of delamination are observed other than fiber pullout and brittle fiber failure. The interfacial bonding is the key factor determining the ultimate properties. Flax fiber/epoxy interface is weak since flax is hydrophilic in nature. The weak interface decreased the interfacial stress transfer. In hybrid composites, the incompatibility with matrix causes debonding of flax layers and delamination cracks were found between flax and glass plies on visual inspection.

Acoustic emission studies is a useful technique to study the failure modes in composites. The damage mechanism during tensile testing for aged and unaged composites was investigated by Saidane et al. (2017). The damage mechanisms were arrived at from acoustic emission and microscopic analysis. In unaged hybrid and

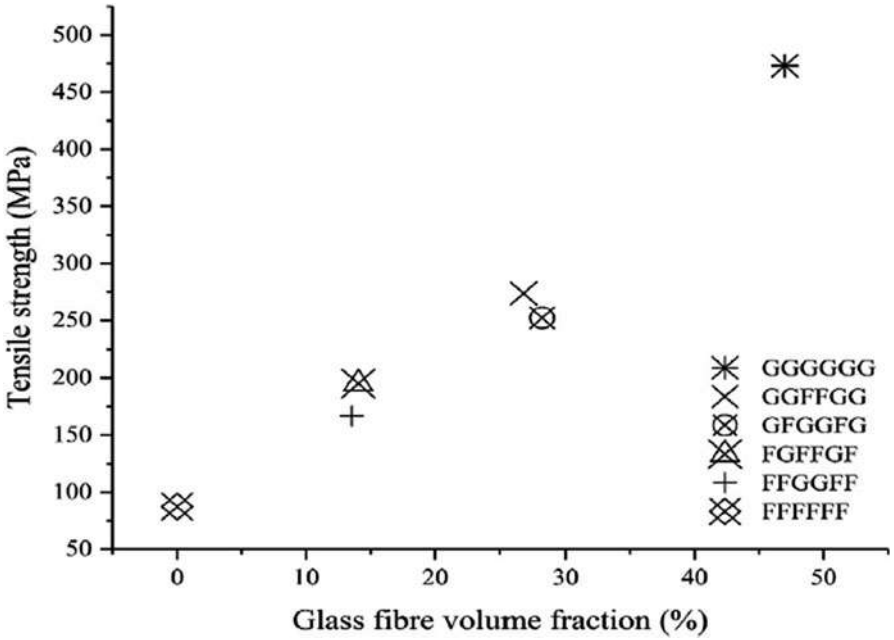

Fig. 3 Effect of E-glass fiber volume fraction on tensile strength (Cihan et al. 2019). (Reproduced with permission from Elsevier, License No.: 5171870399083)

unaged and aged (water immersion at 55 °C) nonhybrid composites, the failure occurred through matrix cracking, fiber/matrix debonding, and fiber failure. In water-aged hybrid composites, delamination between flax and glass fiber layers was observed in addition to the three failure modes mentioned above. Also, multivariable analysis revealed that the major contributing factor to composite damage was fiber failure and it increased with aging due to the degradation of the fiber/matrix interface. In a similar manner the failure mechanism of mode I interlaminar fracture toughness was evaluated (Saidane et al. 2019). The hybrid composite exhibited interlaminar fracture toughness greater than glass fiber composite but less than that of flax fiber composite. The combination of two fibers led to crack path deviation. The initial toughness is governed by glass fiber and at higher load it is taken over by flax fiber. Figure 4 displays the evolution versus time and crosshead displacement of the cumulative number of hits of each class, combined with double cantilever beam load.

Three regions are found from the graphs. The first region corresponds to failure free domain and second and third regions correspond to the initiation and propagation of delamination. Four damage mechanisms, namely matrix cracking, fiber/matrix debonding, delamination, and fiber failure were identified in the case of hybrid and flax fiber composite whereas only the first three are observed in glass fiber composites from acoustic emission studies. The scanning electron micrographs in Fig. 5 provided further evidences for these mechanisms.

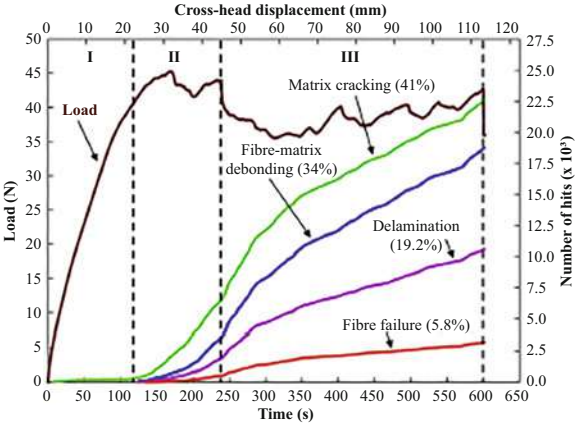

(a)

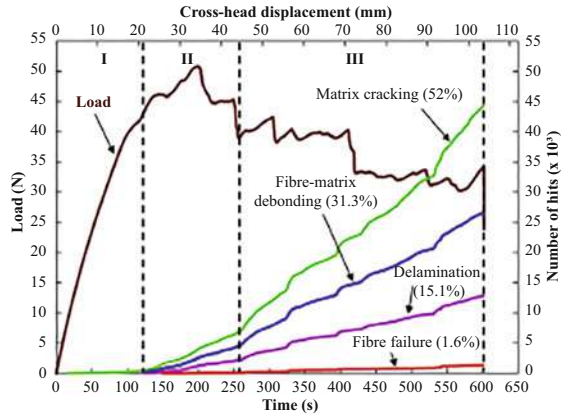

(b)

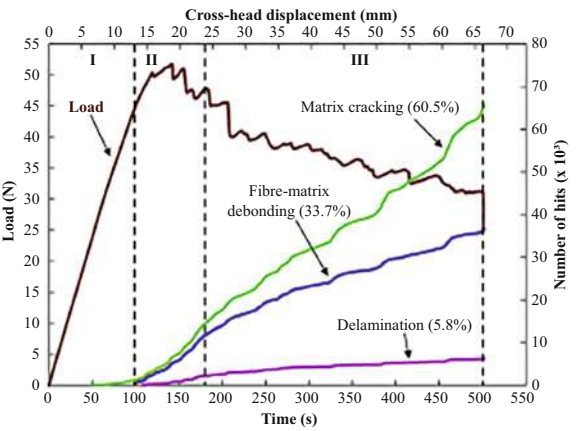

(c)

Fig. 4 Load and cumulative number of hits of the AE signals versus time and crosshead displacement from DCB tests for (**a**) FFRE, (**b**) HFRE, and (**c**) GFRE specimens (Saidane et al. 2019). (Reproduced with permission from Elsevier, License No.: 5171871331044)

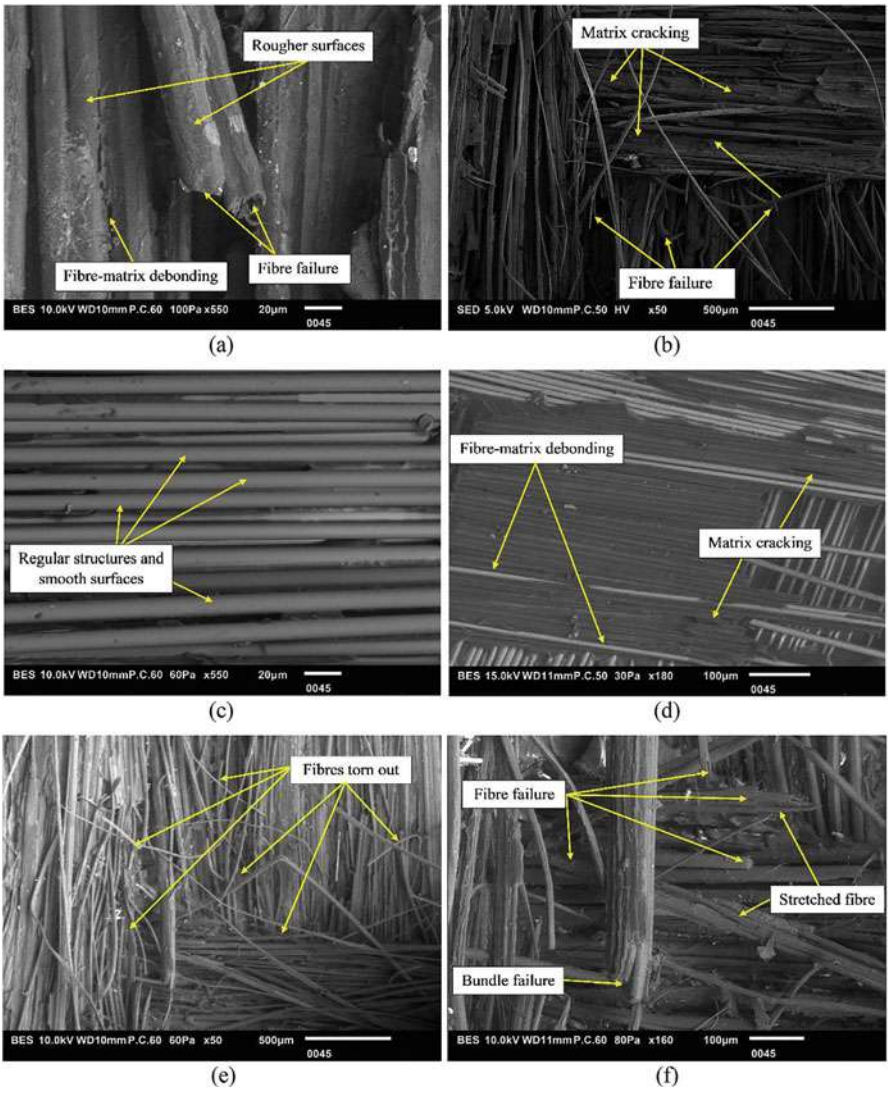

Fig. 5 SEM images of fracture surfaces of (**a**) and (**b**) FFRE, (**c**) and (**d**) GFRE, (**e**) and (**f**) HFRE (Saidane et al. 2019). (Reproduced with permission from Elsevier, License No.: 5171871331044)

Fiore et al. (2018) studied the bearing behavior of pin-loaded hybrid glass/flax laminates. The incorporation of outer glass layers improved the mechanical performance of the flax composite. The parameters that influenced the mechanical performance were the fiber characteristics, diameter of pin (D), composite width (W), and hole position from free edge of the laminate (E). They identified four failure models, namely shear out, net tension, cleavage, and bearing in the laminates. Bearing fracture becomes the main fracture mechanism for high values of W/D and E/D

ratios, net tension region is defined for high E/D and low W/D values, and the shear out region is identified from low E/D and high W/D ratios in the failure map chart. Premature failure mechanisms like shear out and net tension are catastrophic in nature and resulted in collapse of the samples immediately after the initiation of damage. Figure 6 shows the evolution of fracture by varying E/D and W/D geometric ratios as a function of the glass fiber content. It was concluded from the figure that placing exterior glass skins in a pure flax laminate (i.e., glass/flax laminate) allowed significant extension of the bearing region. The minimum values of E/D and W/D ratios for attaining full laminate strength deduced from the graph was 2.4 and 3.1, respectively.

Aging of the above composites in salt spray fog environmental conditions decreased the mechanical performance (Calabrese et al. 2020). It also affected the failure mechanism. Aging favored catastrophic failure mechanisms like shear out and net tension.

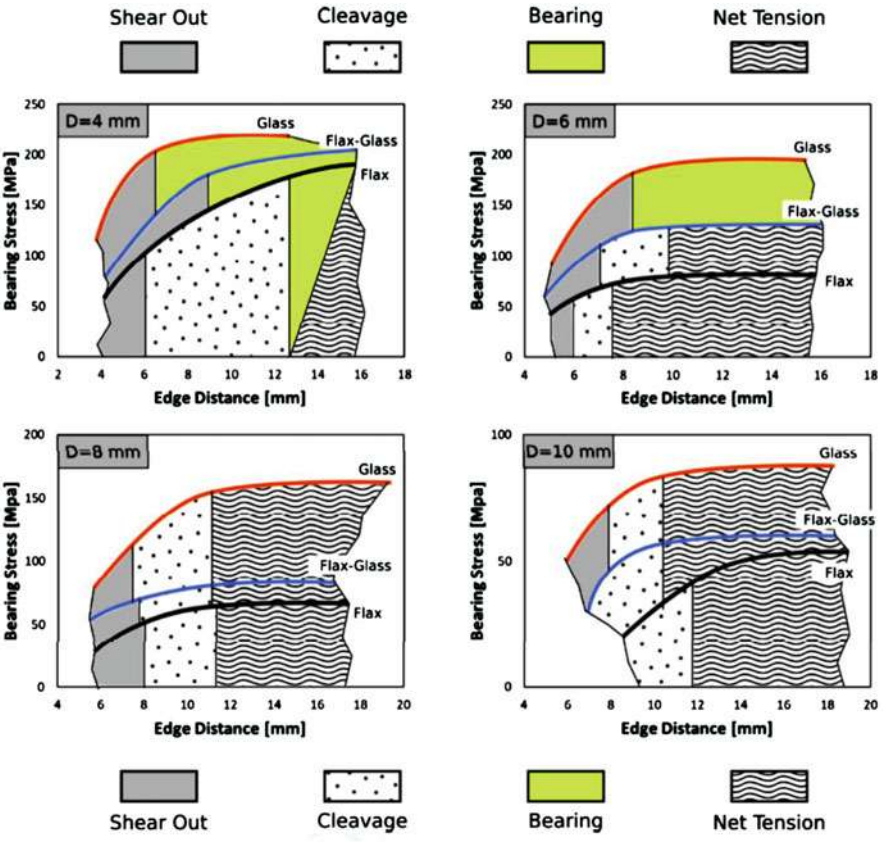

Fig. 6 Failure maps of different types of composites (Fiore et al. 2018). (Reproduced with permission from Elsevier, License No.: 5171880086215)

Glass/Jute Hybrid Composites

One of the first investigations of the hybridization of jute fiber with glass was done by Gujjala et al. (2014). Equal weight percent of woven jute and glass mat were used in the hybrid composites. The hybridization of jute fiber with the stronger and stiffer glass increased the properties of jute fiber composites. As reported earlier in other hybrid composites, maximum increase in tensile strength (66%) was obtained when glass fiber was used as the outer layer. The hybrid composites retained 90% of the flexural properties of the glass/epoxy composites. However, the stacking sequence was alternate glass and jute layers in this case. The morphological features of the tensile fracture surfaces revealed glass fiber stretching and another is jute fiber breakage without any stretching and bending of glass fiber. The flexural surfaces showed bending of glass fiber and brittleness of jute fiber.

Table 1 depicts the mechanical properties of various glass/jute hybrid composites. Here either a layer of jute or glass is used in the hybrid composites (Braga and Magalhaes Jr 2015). As expected, the mechanical properties increased with increase in glass fiber content when compared to jute fiber composites. The increase in flexural strength is less compared to tensile properties. In these studies, maximum properties are obtained in composites with glass fiber as outer layer (Nagaraj et al. 2020). If the properties are compared with glass fiber composites instead of jute fiber composites, the hybrid composites have lower properties than the glass fiber composites. Flexural strength is an exception as reported by Magarajan et al. (2018). About 65% increase in flexural strength is seen in hybrid composites due to the weave architecture of the fibers.

Similar increase in mechanical properties with increase in glass content in hybrid composites is observed by Rafiquzzaman et al. (2016). The hybrid with 40% overall fiber and 30% glass fiber showed maximum impact strength. The main fracture mechanisms were found to be longitudinal splits, matrix cracking, and delamination from scanning electron microscopic studies of the fracture surfaces.

The compressive strength of the hybrids was higher than that of jute only composites and it increased first with number of layers of glass mats and then decreased (Samanta et al. 2015). The mechanical properties increased with the addition of shear thickening fluid to hybrid composite at various compositions. The reason for this trend is not yet identified (Abhishek et al. 2017).

Table 1 Mechanical properties of composite materials (Braga and Magalhaes Jr 2015)

Composite	Density (g/cm^3)	Tensile strength (MPa)	Flexural strength (MPa)	Flexural modulus (MPa)	Impact (J)
E69-J31-V0	0.95	29.52	28.18	1249.92	3.44
E69-J31-V0	1.03	49.80	28.74	1189.18	3.53
E64-J18-V19	1.14	56.68	28.81	1830.68	5.49

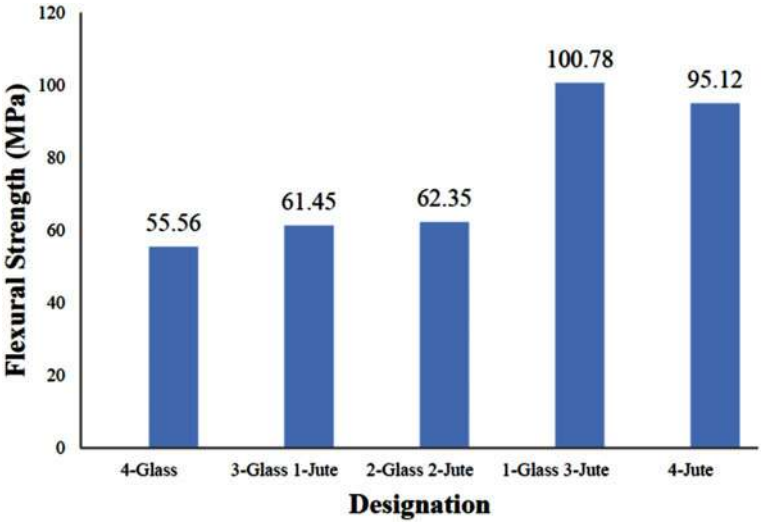

Fig. 7 Flexural strength of composite samples (Bajpai et al. 2018). (Reproduced with permission from Elsevier, License No.: 5171890162204)

The wear rate of jute and glass epoxy composites are less than that of pure epoxy laminates. The wear rate increased with increase in applied load. Hybridizing jute and glass fibers enhanced the wear properties of the single fiber composites and better properties were observed in hybrids with higher jute content (Jha et al. 2018).

The hybridization configuration, layer-by-layer or yarn-by-yarn hybridization, can affect the properties of the composites. In the studied composites, the tensile properties of hybrids are intermediate between glass only and jute only composites. The tensile properties were higher for yarn-by-yarn hybridization and flexural properties for layer-by-layer hybridization with glass fiber as the outer layers (Ouarhim et al. 2020). Bajpai et al. (2018) developed jute/glass hybrid composites for making industrial safety helmets. The flexural strength and impact strength are shown in Figs. 7 and 8, respectively. Comparing the properties of ABS and hybrid composites, the composite with three layers of glass and one layer of jute has better properties.

Glass/Kenaf Hybrid Composite

Nonwoven kenaf and glass fiber mat were hybridized in various stacking sequence to fabricate epoxy hybrid composites. The tensile properties are shown in Fig. 9. The maximum tensile strength among the hybrid composites is shown by glass/kenaf/glass system. This particular sample had low void, good interfacial adhesion and good wetting. The outer glass layers absorbed large part of the applied stress (Vinoth et al. 2020).

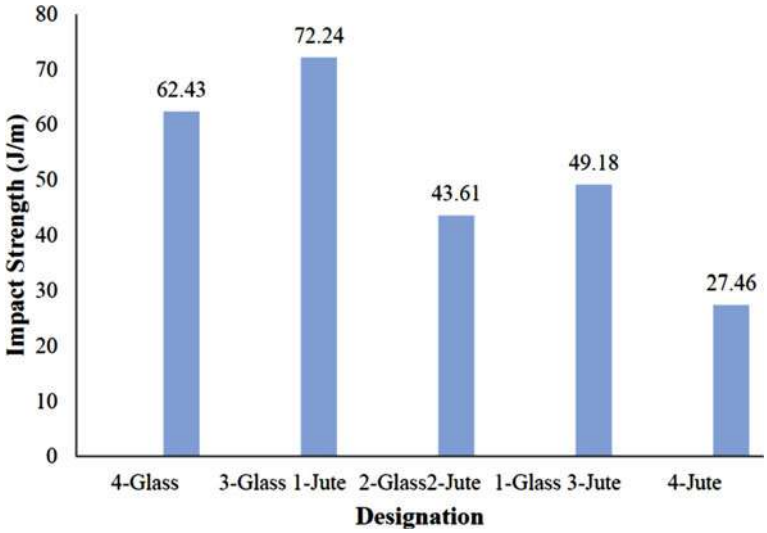

Fig. 8 Impact strength of composite samples (Bajpai et al. 2018). (Reproduced with permission from Elsevier, License No.: 5171890162204)

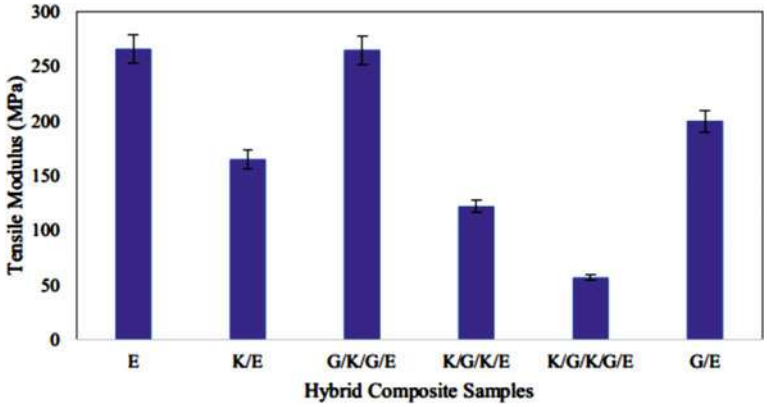

Fig. 9 Tensile strength of E, K/E, G/K/G/E, K/G/K/E, K/G/K/G/E, and G/E hybrid composites (E – epoxy, K – kenaf, G – glass) (Vinoth et al. 2020). (Reproduced with permission from Elsevier, License No.: 5171890394416)

The composite structures may suffer damage especially internal delamination upon low velocity impact and this damage usually go unnoticed. These damages cause reduction in strength and then failure which may be catastrophic. Compression after impact tests will help to quantify such damages. The samples were subjected to low velocity impact first for studying internal delamination. A schematic diagram of the fabricated hybrid system is shown in Fig. 10. This arrangement has glass to kenaf

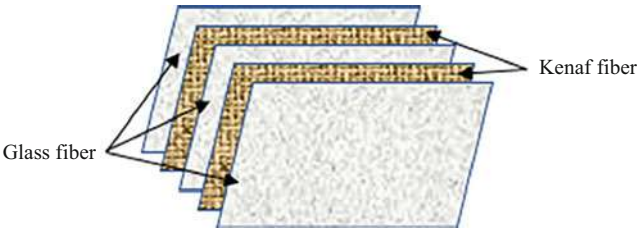

Fig. 10 Stacking sequence of the hybrid composites with glass fiber at the outermost layer (Ismaila et al. 2019). (Reproduced with permission from Elsevier, License No.: 5171890614092)

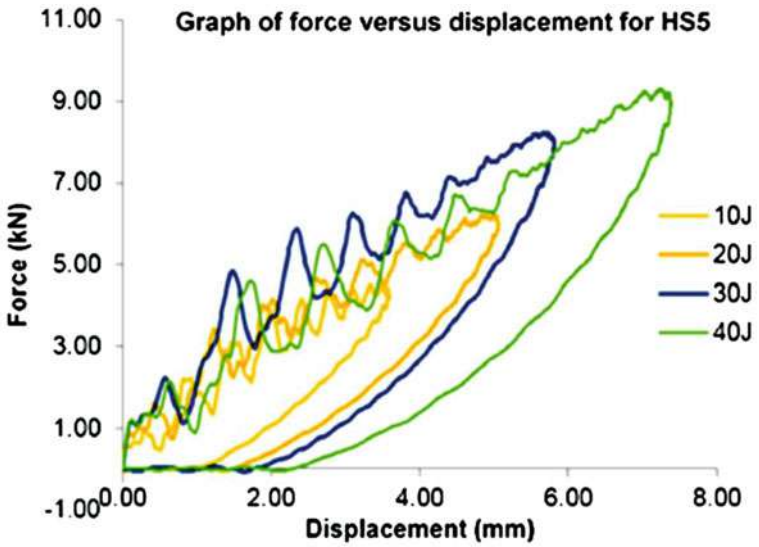

Fig. 11 Force displacement curves for hybrid sample at different energy levels (Ismaila et al. 2019). (Reproduced with permission from Elsevier, License No.: 5171890614092)

ratio of 75:25. The force displacement curves of a hybrid system is given in Fig. 11 (Ismaila et al. 2019).

The closed loops in the figure revealed no penetration of the sample by the striker and the striker rebounded. This hybrid composite could withstand energy up to 40 J. The damage area increased with increase in impact energy. For example, damage area increased from 235.03 mm^2 to 2885.94 mm^2 on increasing the impact energy from 10–40 J. The compressive load force and displacement of the specimens are shown in Fig. 12.

The compressive force decreased and displacement increased as the impact energy of the samples increased. The damage became visible using naked eye after testing. It means that the damage caused by impact test to the inner layers was transferred to the outer layers due to delamination.

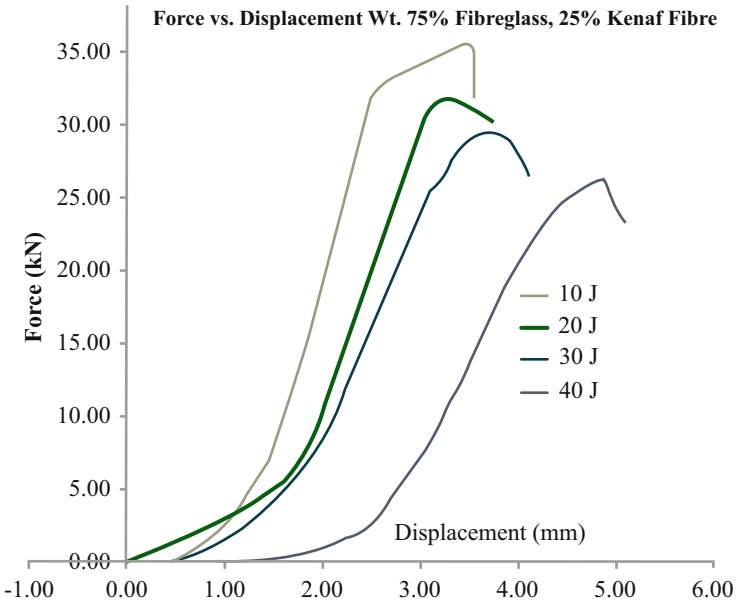

Fig. 12 Compressive force-displacement curves from the compression after impact testing (Ismaila et al. 2019). (Reproduced with permission from Elsevier, License No.: 5171890614092)

The structural performance of filament wound kenaf glass hybrid tube was investigated by Supian et al. (2020). An increase in properties was observed in hybrid composites. The hybrid tubes failed by delamination, buckling, splitting, and splaying due to microfracture nucleated with small intralaminar crack.

Glass/Sisal Hybrid Composite

Few systematic studies were reported on hybrid composites of glass and sisal. Treated sisal fiber was used to prepare the hybrid composites. Maximum mechanical properties are obtained when the sisal content was 4% and glass fiber was kept as the outer layer (Rana et al. 2017). Karthick et al. (2020) investigated the properties of hybrid composites with sodium hydrate–treated sisal and glass fiber hybrid systems. The stacking pattern was GSSSG (G – glass, S – sisal). Surface-treated sisal fiber–based hybrid systems gave better properties than untreated fiber systems.

Glass/Sugarcane Hybrid Composite

Sugar cane fibers in hybrid systems are used after surface treatment to improve the interfacial adhesion between fiber and epoxy matrix. The short fiber hybrid composites have better mechanical properties than sugarcane fiber only composites

Table 2 Flexural and compressive properties of pure GF, pure TSPF, pure UTSPF, and SPF/GF/epoxy hybrid composites (various fiber-fiber ratios) (Safri et al. 2018)

Composite specimens	Flexural strength (MPa)	Composite yield Strength (MPa)	Flexural modulus (MPa)	Compressive modulus (MPa)
GF (100%)	54.3	63.4	3793.5	1593.0
TSPF (100%)	36.6	51.5	1945.9	1481.6
TSPF/GF (70%:30%)	42.4	60.6	3029.0	1585.1
TSPF/GF (50%:50%)	50.0	60.0	3252.4	1579.3
TSPF/GF (30%:70%)	56.9	62.8	3579.7	1655.5
UTSPF (100%)	38.8	45.9	2339.1	1352.9
UTSPF/GF (70%:30%)	38.8	49.0	2702.9	1382.1
UTSPF/GF (50%:50%)	47.2	53.6	3166.3	1482.0
UTSPF/GF (30%:70%)	51.3	55.0	3197.8	1477.1

(Kumar et al. 2017). Jawaid and coworkers (Safri et al. 2018, 2019) conducted detailed study of sugarcane/glass hybrid systems. The sugarcane to glass ratio was varied keeping the overall fiber content constant. About 10–15 cm long fibers were mixed and used to fabricate the composites. Surface treatment was necessary for achieving good mechanical properties. Surface treatment of sugarcane fiber was done using benzoyl chloride. The flexural and compressive properties of the composites are given in Table 2. The surface-treated fibers showed good mechanical properties than the untreated fiber composites. This is due to the improved interfacial adhesion between the fiber and matrix due to the removal of some lignin from the fiber surface. Addition of glass fiber has a positive effect on the properties of the composites. Maximum properties are shown in the case of treated sugarcane fiber to glass ratio is 30:70.

The force-time graph of the treated hybrid composite is shown in Fig. 13. The presence of sample failure due to loss of stiffness is observed in the graph. The peak force increased with increase in impact energy.

Closed force-displacement curves similar to Fig. 11 were obtained in hybrid composites. Similar pattern was observed at all impact energies with linear elastic behavior up to damage initiation point. It was also observed that although the samples were damaged by the impactor, it was not penetrated by the impactor. Ultrasonic C-scan of the damaged area showed continuously distributed matrix cracking around the impacted area. In the present system the damaged area is not circular because long fibers were used to fabricate the composites. The damaged area

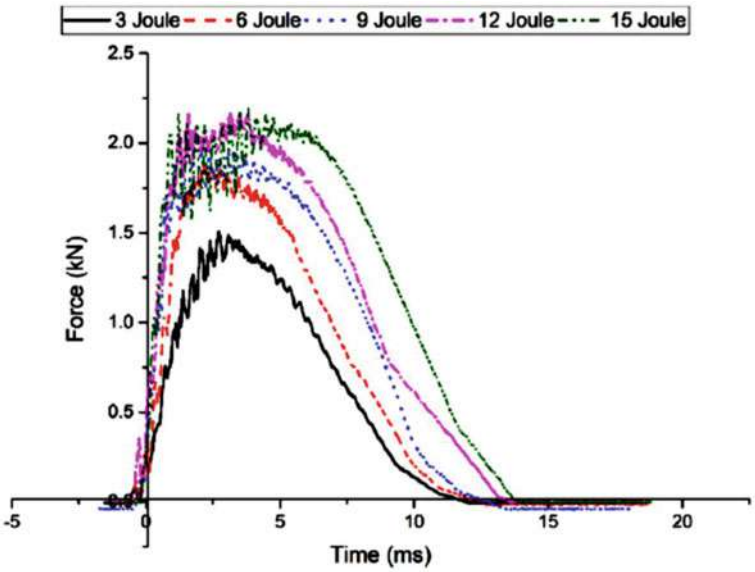

Fig. 13 Force-time curves for EP/30TSPF/70GF composite (Safri et al. 2018). (Reproduced with permission from Elsevier, License No.: 5171901508145)

increases with increase in impact energy. Compression after impact studies showed that compressive strength decreased with increase in impact energy or otherwise in samples with large damage area.

Glass/Other Natural Fiber Hybrid Composites

The effect of hybridization of glass with several other natural fibers other than those discussed so far was also investigated. Alkali treatment, moisture absorption, and elevated temperature decreased the impact properties of *Pennisetum purpureum* fiber/glass fiber/epoxy hybrid composites (Ridzuan et al. 2018). Mechanical properties increased on hybridization with glass fiber in the case of palm fiber (Raju and Balakrishnan 2020) and *Bauhinia racemosa* fibers (Saravanan et al. 2019). Hybridization of ramie fiber and glass fiber improved the tensile, flexural, and impact properties than ramie only or glass only composites. Hybrids with 30% fiber showed maximum properties (Giridharan 2019). Alkali-treated ruffia fiber/glass hybrid systems have better mechanical properties than the untreated ruffia fiber/glass hybrid systems. In both cases ruffia fiber was kept as the core and glass as the skin. The increase in property is due to the better interfacial adhesion and to the pores in treated fiber which were penetrated by the resin and brought about mechanical interlocking (Ouarhim et al. 2018). The effect of testing temperature of composites was studied by Cerbu et al. (2020). Upon heating the samples, the tensile strength and modulus of elasticity decreased. Microcracks were developed at the interface between fiber and

matrix as a consequence of the different expansion coefficients of the epoxy resin and the reinforcing fibers. As a result, residual thermal stresses were developed at the interface. These microcracks weakened the matrix fiber interface and decreased the tensile properties (Mittal and Chaudhary 2018).

Aramid Fiber/Natural Fiber Hybrid Composites

Aramid fibers are important high strength synthetic fiber used in many structural applications. Though not used as much as glass, aramid fibers are also used to hybridize with natural fibers.

Kevlar/Kenaf Hybrid Composites

Hand layup process was used to prepare the composites. Kevlar fibers were used to hybridize with unidirectional (UD), woven, and mat kenaf fiber. The mechanical properties were found to change as a result of hybridization. The layering pattern, kenaf to aramid ratio, chemical treatment, etc. influenced the properties of the composites. In general, the mechanical properties are enhanced by hybridizing with aramid fibers (Ramasamy et al. 2021).

Yahaya et al. (2014) in their studies varied kenaf:Kevlar ratio in the composites keeping the overall fiber content to about 30%. The tensile and flexural properties, impact strength, and interlaminar shear strength (ILSS) varied with respect to fiber ratio in the composites. The increase in Kevlar fiber content had a positive effect on the mechanical properties except ILSS where interfacial properties are the determining factor. The tensile properties of the composites increase with increase in Kevlar content in the hybrid. The void content in the hybrids increased with increase in kenaf content. The presence of voids and lower interfacial adhesion between kenaf and epoxy had a detrimental effect on ILSS.

The layering pattern had some impact on the mechanical properties of the hybrid composites (Yahaya et al. 2015a). For example, composites with four layers have better mechanical properties compared to three-layer composites. Tensile strength increased from 99.4 MPa to 123 MPa. Also the tensile and flexural properties are better when aramid was kept as the outer layer because it absorbed the stress and distributed over the entire composite. Hence the inner kenaf layer experienced less stress. The stress-strain behavior of the composites was nonlinear as shown in Fig. 14. The beginning of a nonlinearity shows the breakage of kenaf fiber.

In the case of flexural studies, better properties were exhibited when the high strength Kevlar layer was kept as the outside layer. The treatment of kenaf with sodium hydroxide removed the natural and artificial impurities from the fiber surface resulting in the improvement of fiber matrix adhesion and reduction in voids present in the composites. Scanning electron microscopy revealed fiber pullout, fiber/matrix incompatibility, and matrix cracking and voids in the kenaf/aramid/kenaf sample resulting in poor properties.

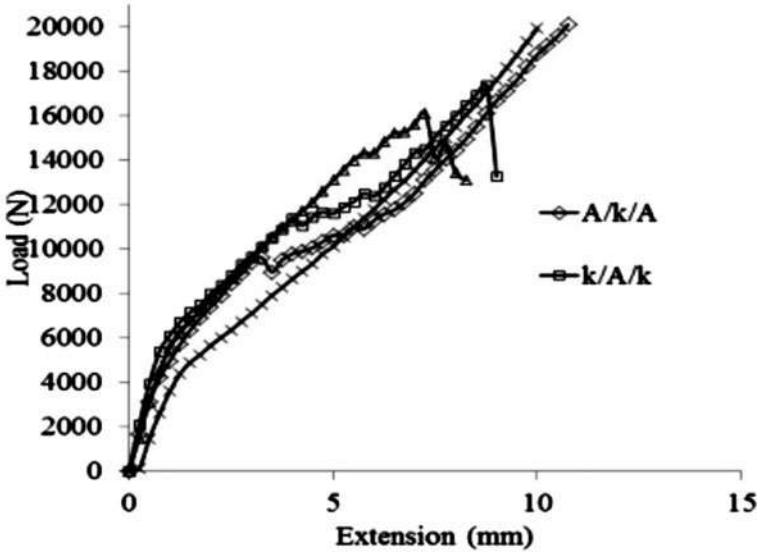

Fig. 14 Load-extension curve for hybrid composites (Yahaya et al. 2015a). (Reproduced with permission from Elsevier, License No.: 5171910453510)

Yahaya et al. (2015b) found that fiber orientation was also important in determining the mechanical properties. Unidirectional kenaf hybridized with Kevlar fiber gave better tensile properties than woven and mat hybrid systems. In the case of UD composites, the fracture of fiber involves fiber/matrix debonding, fiber pullout, and stress distribution due to fiber fracture and multiple fibers (Peijs et al. 1994). The composite contains many fibers and the breaking strain and modulus of individual fibers contributed to the total tensile strength (Jawaid et al. 2013; Abdul Khalil et al. 2007). When woven fabric was used, the weaving points acted as energy concentrators which ultimately reduced the strength of the composite (Kun and Liang 2010).

The morphological analysis using scanning electron microscopy gave more insight into the tensile performance of the composites. The UD kenaf fiber showed good interlayer bonding and low matrix cracking or debonding; woven composites showed weak kenaf/matrix bonding, matrix crack, and fiber breakage; and kenaf mat composite showed poor interfacial bonding and low or adequate amount of matrix.

Yahaya et al. (2016) later in their studies found that the woven kenaf gave better mechanical properties than UD composites. The difference in behavior is due to the difference in the type of woven kenaf fiber used. In this study they used table looms weaved kenaf fabric instead of hand-weaved fiber in the previous study.

Kevlar/Flax Hybrid Composites

A detailed study of the mechanical properties of flax/Kevlar hybrid composites revealed a 10% difference in failure strength between warp and weft samples

(Audibert et al. 2018). The difference in tension between warp and weft yarns during weaving is reflected in the composites. The results obtained from progressive load-unload test (CRP) gave insight into the material damage evolution. The decrease in tensile stress was delayed in the hybrid composite compared to flax fiber composite. The beginning of damage was due to flax fiber pullout, which was compensated by the aramid fiber in the hybrid composite.

Hybridization with Kevlar slowed the composite failure compared to flax fiber composite because of the load transfer to Kevlar fibers. Unlike the carbon or glass composite, hysteresis behavior was seen in hybrid composite. CRP testing revealed that this phenomenon was due to multiple fiber pullout which can be seen from the scanning electron micrographs in Figs. 15 and 16. The effect of viscous strain induced by the fibers is less compared to elastic and plastic strain.

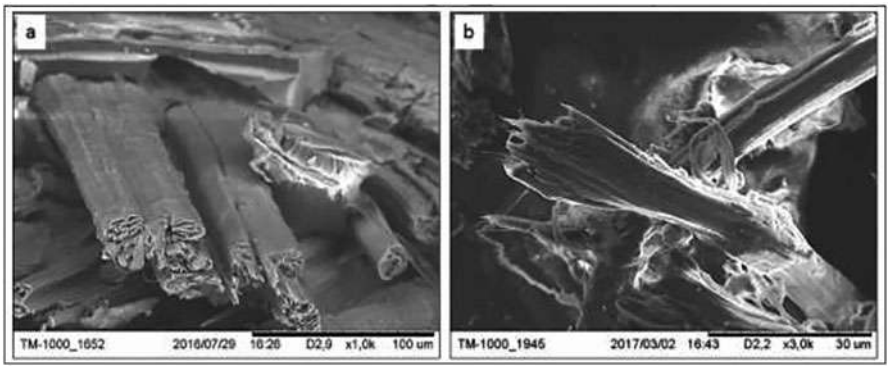

Fig. 15 Scanning electron micrographs of flax fiber failure after tensile test on Kevlar/flax composite: (**a**) Flax fiber pullout; (**b**) Flax fiber failure (Audibert et al. 2018). (Reproduced with permission from Elsevier, License No.: 5174531389432)

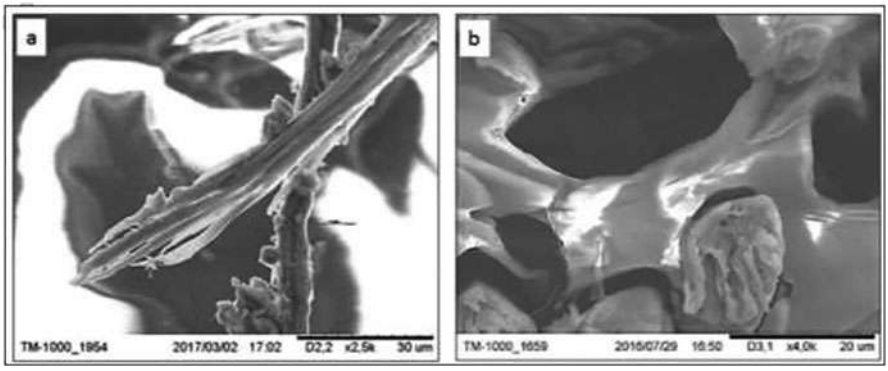

Fig. 16 Scanning electron micrographs of Kevlar fiber failure after tensile test on Kevlar/flax composite: (**a**) Kevlar fiber splitting; (**b**) Kevlar fiber pullout (Audibert et al. 2018). (Reproduced with permission from Elsevier, License No.: 5174531389432)

The comparison between the damage evolution of the hybrid composite in the out-of-fiber direction was similar to that of flax composite and the nature of the fiber had no influence on the damage mechanism in the composite. The elastic, plastic, and damage properties have contributions from the properties of the matrix and the fiber interface. However, the hysteresis was greater in the out-of-fiber direction than that in the fiber direction. It had contribution from the shearing of the polymer matrix that introduced a viscous behavior in out-of-fiber direction (Ahci and Talreja 2006).

Three regions can be observed in the flexural stress-strain graph shown in Fig. 17. In the first part, the material exhibited a linear behavior with 10 GPa flexural modulus. A second zone appeared from a strain of 0.8% until 2.8%, which is characterized by irreversible strain and loss of stiffness. Finally, the end of the curve is characterized by the final failure driven by tensile fiber breakage.

The change in mechanical properties of composite with flax layers sandwiched between Kevlar layers are summarized in the Table 3 (Sarwar et al. 2020). The hybridization with Kevlar fibers improved the mechanical properties of flax epoxy composites.

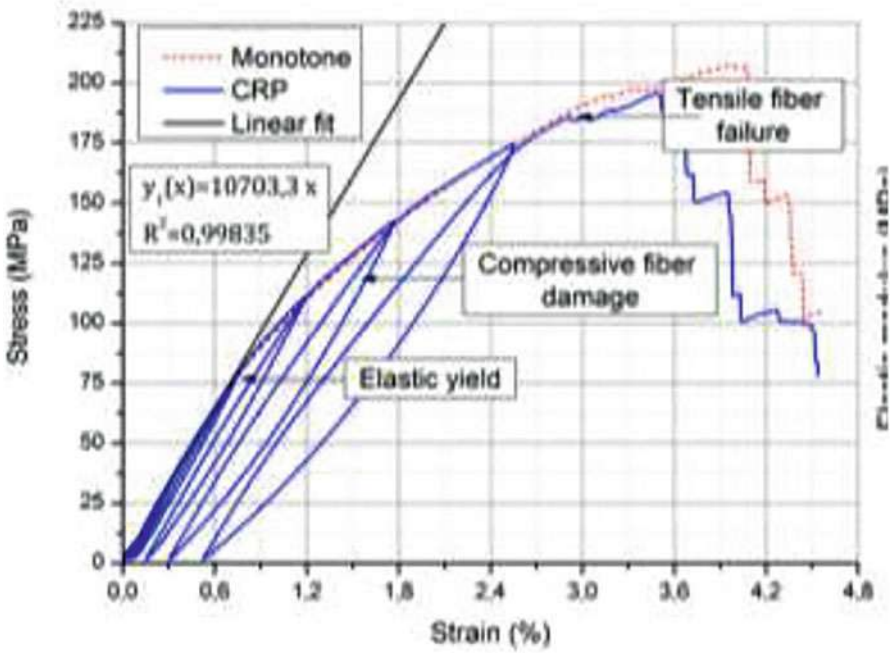

Fig. 17 Stress-strain curve of a Kevlar/flax composite subjected to three-point bending with a strain rate of 1 mm/min (Audibert et al. 2018). (Reproduced with permission from Elsevier, License No.: 5174531389432)

Table 3 Percent change in mechanical properties with respect to Kevlar/epoxy and flax/epoxy composites. (+) indicates improvement, and(−) indicates reduction (Sarwar et al. 2020)

Property	Percent change w.r.t pure Kevlar/epoxy (KE)			Percent change w.r.t pure flax/epoxy (FE)		
	UD [W_{K2}/0_{F6}]s	CP [W_{K2}/$(0/90)_{F3}$] s	AP [W_{K2}/$\pm45_{F3}$]s	UD [W_{K2}/0_{F6}]s	CP [W_{K2}/$(0/90)_{F3}$] s	AP [W_{K2}/$\pm45_{F3}$]s
E_T (GPa)	−20.95	−44.95	−60.36	−3.09	27.98	137.85
σ_{UT} (MPa)	−36.92	−54.04	−62.14	17.08	56.96	171.22
E_C (GPa)	−10.01	−54.90	−63.85	12.40	−1.84	127.79
σ_{UC} (MPa)	11.15	−17.02	−20.28	−8.72	−10.06	−3.76
E_B (GPa)	−9.18	−10.35	−30.01	−11.54	–	–
σ_{UB} (MPa)	−18.75	−25.67	−34.24	2.19	–	–
G (GPa)	−39.32	−47.99	−5.88	−5.31	–	–
τ_U (MPa)	−25.94	−47.28	−51.11	395.82	–	–

Reproduced with permission from Elsevier, License No.: 5172031019614

Fig. 18 Micrographs of tensile fracture (Maharana et al. 2020). (Reproduced with permission from Elsevier, License No.: 5172020355798)

Kevlar/Jute Hybrid Composites

The composites with four different fiber orientations (0^0, 30°, 45°, and 60°) and three different fiber loading (30%, 40%, and 50%) were fabricated and the properties were investigated (Maharana et al. 2020). The Kevlar content was maintained 20% in all the composites. The tensile strength was maximum for 40% fiber and 30° orientation, but flexural strength was maximum for 50% fiber and 45° orientation. The properties were dependent on void content and it increased with increase in fiber content. Fiber pullout and matrix cracking was observed in the micrographs shown in Fig. 18.

The falling weight impact tests of jute/Kevlar hybrid laminates showed that the dynamic reaction of the composites depends upon the flexible properties of the fiber material (Bhanupratap 2020). Crack initiation and penetration were observed in the composites. But the extent of penetration was dependent on the type of composite.

Kevlar/Other Natural Fiber Hybrid Composites

In hybrid composites made of Kevlar and oil palm, better properties were achieved when Kevlar was placed as the outside layer (Sultana et al. 2019). The Kevlar/oil palm/Kevlar stacking pattern yielded better tensile properties because woven Kevlar was used as the skin of the laminate. Irradiation with γ rays had a positive effect on the tensile strength. The tensile strength decreased with increase in γ ray dose (Machnowski et al. 2012). The flexural properties increased as a result of irradiation and maximum was observed with 50 kGy dose. Irradiation with gamma rays affected the fiber polymers structure and noncellulosic impurities present in the natural fiber. Cross-linking and chain scission occurred as a result of irradiation. But chain scission decreased the tensile properties at higher doses. The increase in properties was due to cross-linking which enhanced the interfacial adhesion between the fiber and matrix.

Tensile strength improved in the case of kenaf/aramid and impact strength increased in neem/aramid hybrid composites (Rajesh et al. 2019). Cocos nucifera is a naturally woven dense fiber with different fiber diameters and higher lignin content. Higher lignin content of the *Cocos nucifera* sheath improved the bending resistance of it. Tensile strength decreased when Kevlar is hybridized with *Cocos nucifera* fiber (Naveen et al. 2019). However, the flexural properties shown in Fig. 19 revealed that the composite with 75% Kevlar showed better properties than the pure Kevlar and pure *Cocos nucifera* composites. Comparable impact properties were also shown by the abovementioned hybrid system. This is attributed to the peculiar architecture of *Cocos nucifera* which enhanced its bending properties and also to the woven Kevlar fiber. Low cellulose content of the *Cocos nucifera* sheath produce a rough fiber surface and it formed hydrogen bond with the adjacent cellulose and hydrophobic polymer matrix. Also, lignin acts as a cementing material.

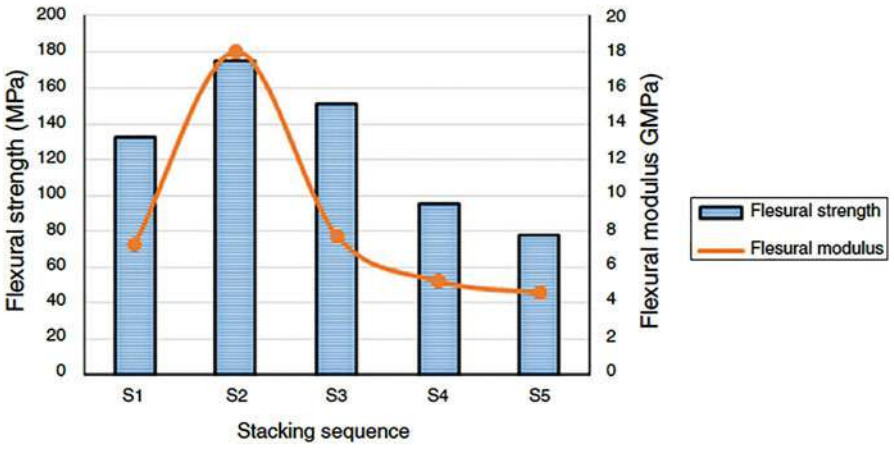

Fig. 19 Flexural strength and modulus of the laminated hybrid composites (Naveen et al. 2019). (Reproduced with permission from Elsevier, License No.: 5172020621273)

All these factors played a role in increasing the tensile and flexural properties of this particular composition.

Carbon Fiber/Natural Fiber Hybrid Composites

Relatively less work is carried out on the hybridization of natural fiber and carbon fiber. Carbon is expensive and is usually used for high-end applications. Natural fibers are not suitable for majority of such applications. However, some natural fibers were hybridized with carbon fiber. The following section details the mechanical properties of carbon fiber/natural fiber hybrid composites.

Carbon/Flax Hybrid Composites

Hybridization of flax fiber with carbon enhanced the tensile properties of flax/epoxy composites. The major change was found in the modulus of the composites. The hybrids have higher tensile modulus than carbon only and flax only composites (Dhakal and Sain 2020). Fiber plies orientation and the interactions between fiber plies and the interfacial adhesion between the reinforcing fibers and the matrix were the important parameters determining the tensile properties of the composites. The hybrid systems showed less brittle failure mechanism. Studies by Kureemun et al. (2018) gave more insight into the hybrid composites.

The stress-strain behavior of the nonhybrid and hybrid systems is shown in Fig. 20. Significant difference in stress-strain behavior is seen between carbon and flax epoxy composites. Carbon composite was much more linear than flax epoxy composites. The hybrid systems have less nonlinear behavior compared to flax/epoxy systems and it was dependent on the carbon fiber content and stacking pattern. The deviation from linearity was less in the case of composites with blocked carbon plies. The stacking pattern of the fibers have some influence on the stiffness of the hybrid systems. Carbon/flax alternative arrangement gave less stiffness compared to blocked (carbon fibers are placed side by side) carbon/flax hybrid systems as seen from Fig. 20. Carbon fibers deformed more in response to stress when they are interspersed with single flax plies than when they are stacked together. The flax plies are more compliant than carbon plies because of the presence of large resin-rich zones and lower density. The blocking of carbon plies resulted in nesting phenomena. Nesting gave rise to small resin pockets and improved interlaminar shear strength and stiffness. The nesting phenomenon is shown in Fig. 21.

The thin carbon plies (compared to flax plies) conformed to the curvature of the adjacent flax plies upon consolidation. The large crimp mismatch between carbon and flax developed considerable distortion to the carbon plies and resulted in stiffness reduction.

Brittle fracture of carbon and flax fibers was the main failure mechanism in the hybrid systems. Carbon fibers failed first followed by flax fibers. Also, cracks were formed at the carbon/flax interface due to the failure of carbon plies. The flexural

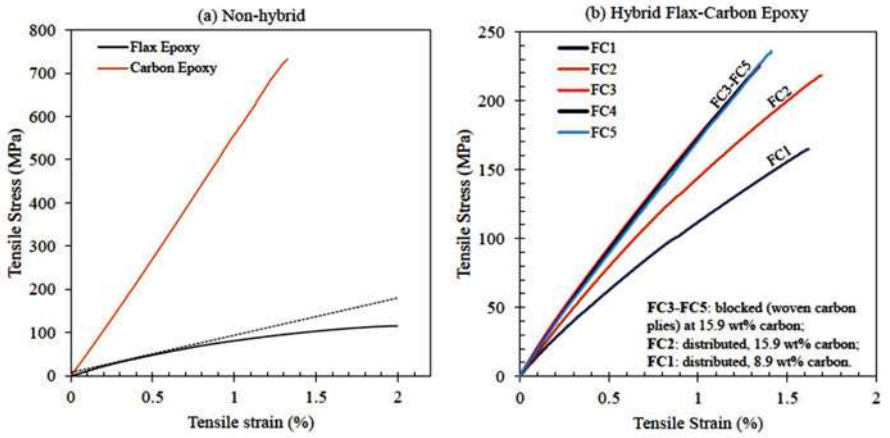

Fig. 20 Stress-strain characteristics of (**a**) nonhybrid flax and (**b**) hybrid laminates under tension (Kureemun et al. 2018). (Reproduced with permission from Elsevier, License No.: 5172020855997)

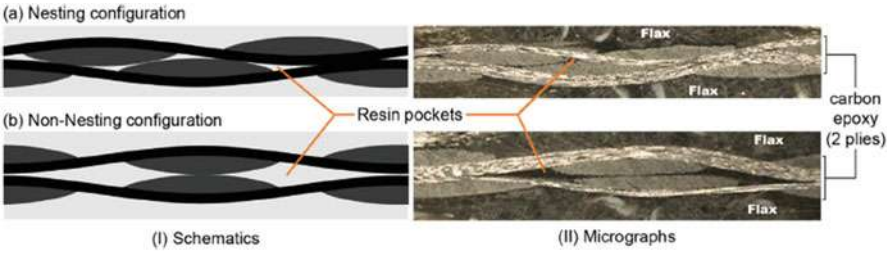

Fig. 21 (I) Schematic diagram illustrating interlayer (**a**) nesting and (**b**) non-nesting configurations in woven carbon epoxy plies. (II) Micrographs of two carbon epoxy plies sandwiched between flax in hybrid laminates (Kureemun et al. 2018). (Reproduced with permission from Elsevier, License No.: 5172020855997)

strength and modulus increased on hybridization with carbon fiber (Dhakal et al. 2013). Fiber tearing and breakage and delamination were the failure mechanisms in the hybrid systems. Lee et al. (2020) observed the dependence of position of carbon fiber on the flexural properties of hybrid systems. Maximum flexural properties are shown when carbon was placed as the outer layer and flax as the core. The flexural properties were less when carbon fiber was present only on one side of the laminate.

Sarasini et al. (2016) reported pine tree damage pattern and reversed pine tree damage pattern on the hybrid composited after low energy impact test. Stiff and thick composites showed pine tree pattern and flexible thin composites showed reversed pine tree pattern. Flax fibers being more compliant prevented the propagation of damage to the core. Flax/carbon/flax stacking pattern gave good properties. A carbon fiber content of 8% was reported to enhance the strength and stiffness by

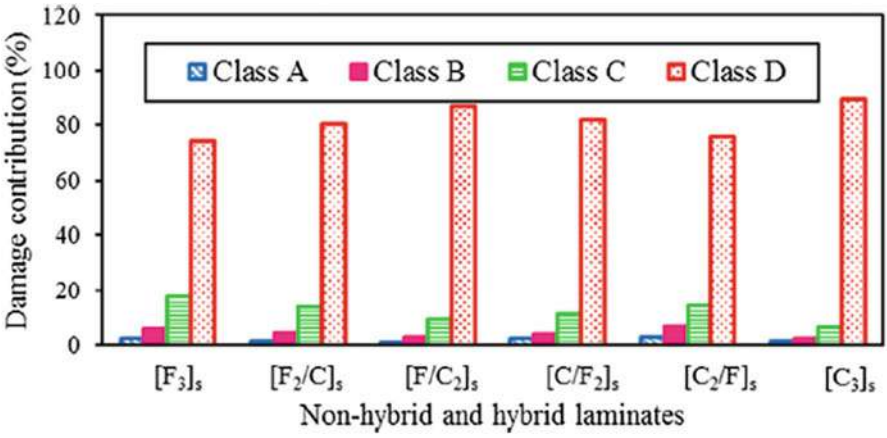

Fig. 22 Damage mechanism contribution in the hybrid composites (Ameur et al. 2019). (Reproduced with permission from Elsevier, License No.: 5172021438908)

50%. Results from flexural property investigation after impact test showed the damage tolerance behavior of hybrid composites. These composites retained the flexural strength and stiffness to a satisfactory level, especially the flax/carbon/flax hybrid system.

Hybrid systems with woven carbon fiber and cross-ply flax fibers with carbon at the outer surface have better penetration resistance (Al-Hajaj et al. 2019). These composites prevented and minimized matrix crack initiation and crack propagation through the plate thickness by absorbing impact energy through fiber bridging at crossover points at which the warp yarn and weft yarn physically intersected. The crossover points acted as stress distributors and prevented damage.

Acoustic emission studies of the hybrid systems were helpful in identifying the damage mechanism as discussed earlier for other systems. Matrix cracking, fiber/matrix debonding, delamination, and fiber pullout and fiber breakage were found to occur in the hybrid composites (Ameur et al. 2019). The relative contribution of each mechanism to the total failure is shown in Fig. 22. The most significant energy mechanism is the fiber breakage followed by the contribution of delamination, then matrix cracking, and lastly the contribution of fiber/matrix debonding.

Carbon/Hemp Hybrid Composites

Hybridization of hemp with carbon fiber improved the damping properties of carbon only composites (De Fazio et al. 2021). The hybrid composites showed more ductile behavior than carbon fiber composites upon low velocity impact testing. The damage extension was also low in hybrid composites due to the damping properties of hemp fibers. During impact testing, the hemp layers improved the damping properties and the delamination was localized at the hemp/carbon interface to a large extent.

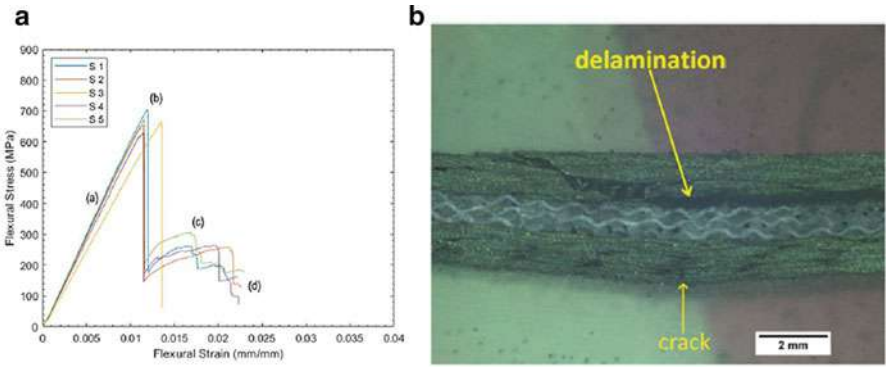

Fig. 23 Flexural stress-strain curves (**a**) and a representative cross-section (**b**) of a symmetric hybrid sample (configuration S) at the end of the bending test (Pinto et al. 2020). (Reproduced with permission from Elsevier, License No.: 5172030538692)

A detailed study of hemp hybridized with carbon fiber was carried out by Pinto et al. (2020). The flexural stress-strain behavior of symmetric hybrid sample in which the hemp layers are stacked together close to the neutral axis is shown in Fig. 23. The laminate responded elastically up to the critical value of 665 MPa with the same modulus as that of CFRP. The damage started to propagate in the upper portion of the laminate which is seen as a drop in the stress-strain curve. The crack propagated up to the carbon/hemp interface and it bends at this point creating a plateau around 200 MPa and finally the crack propagated thorough the bottom layer causing complete failure. This type of stacking generated a combination of different failure mechanisms and damage propagation mechanisms. The elastic portion of the curve was not affected by the presence of hemp layers. When the hemp layers were placed on the tensile portion of the laminate, the flexural properties decreased because the hemp layers experienced large stress.

Carbon/Jute Hybrid Composites

The effect of stacking pattern in jute/carbon hybrid composites on the mechanical properties was investigated by Sujon et al. (2020). The ratio of carbon to jute was constant in the composites. The unidirectional composite laminates exhibited maximum tensile strength compared to angle ply and cross-ply laminates since the force was parallel to the aligned long fibers. Maximum tensile strength was exhibited when jute ply was placed as the surface layer and the tensile strength increased with hybridization when compared to jute/epoxy composites. Maximum flexural strength was shown by unidirectional composites with carbon fiber as the surface layers. Compared to angle ply and cross-ply laminates, the stress was uniformly and effectively transferred within the matrix unidirectional fibers. Resin transfer molded carbon/jute hybrid composites exhibited better tensile properties than jute only composites (Ashworth et al. 2016). The pressure changes during processing affected

the properties. An increase in pressure decreased the tensile properties (98.4 MPa at 4 bar, 92.4 MPa at 8 bar) due to the damage of jute fibers at higher pressures.

Conclusion

Hybridization of natural fiber with synthetic fibers is a useful and effective method to improve the performance of natural fiber composites with epoxy resin as matrix. A good number of natural fibers were hybridized with synthetic fibers like glass, Kevlar, and carbon. Among the various synthetic fibers, hybrid systems with glass fiber were the most investigated because of its wide commercial applications. Although hybridization can be done in many ways, layer-by-layer arrangement was followed in most systems. Woven fibers were used in majority of the systems. The mechanical properties of the hybrid system were better than that of natural fiber only composites and in some cases even better than the synthetic fiber only composites. The important factors determining the ultimate properties were the natural fiber to synthetic fiber ratio, stacking sequence, total fiber content, and fiber treatment. The choice of the component fibers was also important in determining the properties. A very detailed analysis of the properties was done in several hybrid systems, but it is lacking in many of the reported systems. Further investigation is needed to correlate various parameters with the ultimate properties.

Reference

H.P.S. Abdul Khalil, S. Hanida, C.W. Kang, N.A. Nik Fuaad, Agro-hybrid composite: The effects on mechanical and physical properties of oil palm fiber (efb)/glass hybrid reinforced polyester composites. J. Reinf. Plast. Compos. **26**, 203–218 (2007). https://doi.org/10.1177/0731684407070027

M.R. Abhishek, P.M. Suresh, S.H.S. Murthy, Evaluation of mechanical properties of jute/E-glass epoxy hybrid composites by varying fiber loading with and without shear thickening fluid. Mater. Today: Proc. **4**, 10858–10862 (2017). https://doi.org/10.1016/j.matpr.2017.08.039

E. Ahci, R. Talreja, Characterization of viscoelasticity and damage in high temperature polymer matrix composites. Compos. Sci. Technol. **66**, 2506–2519 (2006). https://doi.org/10.1016/j.compscitech.2006.02.012

Z. Al-Hajaj, B.L. Sy, H. Bougherara, R. Zdero, Impact properties of a new hybrid composite material made from woven carbon fibres plus flax fibres in an epoxy matrix. Compos. Struct. **208**, 346–356 (2019). https://doi.org/10.1016/j.compstruct.2018.10.033

M.B. Ameur, A. El Mahi, J.L. Rebiere, I. Gimenez, M. Beyaoui, M. Abdennadher, M. Haddar, Investigation and identification of damage mechanisms of unidirectional carbon/flax hybrid composites using acoustic emission. Eng. Fract. Mech. **216**, 106511 (2019). https://doi.org/10.1016/j.engfracmech.2019.106511

K.P. Ashik, R.S. Sharma, A review on mechanical properties of natural fiber reinforced hybrid polymer composites. J. Miner. Mater. Charact. Eng. **3**, 420–426 (2015). https://doi.org/10.4236/jmmce.2015.35044

S. Ashworth, J. Rongong, P. Wilson, J. Meredith, Mechanical and damping properties of resin transfer moulded jute-carbon hybrid composites. Compos. B **105**, 60–66 (2016). https://doi.org/10.1016/j.compositesb.2016.08.019

O.M.L. Asumani, R.G. Reid, R. Paskaramoorthy, The effects of alkali–silane treatment on the tensile and flexural properties of short fibre non-woven kenaf reinforced polypropylene composites. Compos. Part A Appl. Sci. Manuf. **43**, 1431–1440 (2012). https://doi.org/10.1016/j.compositesa.2012.04.007

M.A. Attia, M.A.A. El-baky, A.E. Alshorbagy, Mechanical performance of intraply and inter-intraply hybrid composites based on e-glass and polypropylene unidirectional fibers. J. Compos. Mater. **51**, 381–394 (2017). https://doi.org/10.1177/0021998316644972

C. Audibert, A.S. Andreani, E. Lainé, J.C. Grandidier, Mechanical characterization and damage mechanism of a new flax-Kevlar hybrid/epoxy composite. Compos. Struct. **195**, 126–135 (2018). https://doi.org/10.1016/j.compstruct.2018.04.061

P.K. Bajpai, K. Ram, L.K. Gahlot, V.K. Jha, Fabrication of glass/jute/epoxy composite based industrial safety helmet. Mater. Today: Proc. **5**, 8699–8706 (2018). https://doi.org/10.1016/j.matpr.2017.12.296

R. Bhanupratap, Impact damage resistance of Jute/Kevlar hybrid composite laminates subjected to varying heights: An experimental approach. Mater. Today: Proc. **39**, 1396–1401 (2020). https://doi.org/10.1016/j.matpr.2020.04.873

R.A. Braga, P.A.A. Magalhaes Jr., Analysis of the mechanical and thermal properties of jute and glass fiber as reinforcement epoxy hybrid composites. Mater. Sci. Eng. C **56**, 269–273 (2015). https://doi.org/10.1016/j.msec.2015.06.031

L. Calabrese, V. Fiore, P. Bruzzaniti, T. Scalici, A. Valenza, Pinned hybrid glass-flax composite laminates aged in salt-fog environment: Mechanical durability. Polymers **12**, 40 (2020). https://doi.org/10.3390/polym12010040

C. Cerbu, H. Wang, M.F. Botis, Z. Huang, C. Plescan, Temperature effects on the mechanical properties of hybrid composites reinforced with vegetable and glass fibers. Mech. Mater. **149**, 103538 (2020). https://doi.org/10.1016/j.mechmat.2020.103538

M. Cihan, A.J. Sobey, J.I.R. Blake, Mechanical and dynamic performance of woven flax/E-glass hybrid composites. Compos. Sci. Technol. **172**, 36–42 (2019). https://doi.org/10.1016/j.compscitech.2018.12.030

D. De Fazio, S. Cuomo, L. Boccarusso, F. Pinto, M. Durante, M. Meo, Design and characterization of hybrid hemp/carbon laminates with improved impact resistance. Mater. Today: Proc. **34**, 194–201 (2021). https://doi.org/10.1016/j.matpr.2020.02.732

H.N. Dhakal, M. Sain, Enhancement of mechanical properties of flax-epoxy composite with carbon fibre hybridisation for lightweight applications. Materials **13**, 109 (2020). https://doi.org/10.3390/ma13010109

H.N. Dhakal, Z.Y. Zhang, R. Guthrie, J. MacMullen, N. Bennett, Development of flax/carbon fibre hybrid composites for enhanced properties. Carbohydr. Polym. **96**, 1–8 (2013). https://doi.org/10.1016/j.carbpol.2013.03.074

V. Fiore, L. Calabrese, T. Scalici, P. Bruzzaniti, A. Valenza, Bearing strength and failure behavior of pinned hybrid glass-flax composite laminates. Polym. Test. **69**, 310–319 (2018). https://doi.org/10.1016/j.polymertesting.2018.04.041

R. Giridharan, Preparation and property evaluation of glass/ramie fibers reinforced epoxy hybrid composites. Compos. Part B Eng. **167**, 342–345 (2019). https://doi.org/10.1016/j.compositesb.2018.12.049

R. Gujjala, S. Ojha, S.K. Acharya, S.K. Pal, Mechanical properties of woven jute–glass hybrid-reinforced epoxy composite. J. Compos. Mater. **48**, 3445–3455 (2014). https://doi.org/10.1177/0021998313501924

M.F. Ismaila, T.H. Mohamed, M.T.H. Sultana, A. Hamdana, A.U.M. Shaha, M. Jawaid, Low velocity impact behaviour and post-impact characteristics of kenaf/glass hybrid composites with various weight ratios. J. Mater. Res. Technol. **8**, 2662–2673 (2019). https://doi.org/10.1016/j.jmrt.2019.04.005

M. Jawaid, H.P.S. Abdul Khalil, A. Hassan, R. Dungani, A. Hadiyane, Effect of jute fibre loading on tensile and dynamic mechanical properties of oil palm epoxy composites. Compos. Part B Eng. **45**, 619–624 (2013). https://doi.org/10.1016/j.compositesb.2012.04.068

K. Jha, B.B. Samantaray, P. Tamrakar, A study on erosion and mechanical behavior of jute/E-glass hybrid composite. Mater. Today: Proc. **5**, 5601–5607 (2018). https://doi.org/10.1016/j.matpr.2017.12.151

P. Karthick, A.A.E. Andrews, G. Srinath, N. Tejesh, K.A. Reddy, V.N.U. Rao, Persuade of sodium hydrate and potassium permanganate treated sisal/textile-grade glass fibers hybrid composite. Mater. Today: Proc. **33**, 2818–2821 (2020). https://doi.org/10.1016/j.matpr.2020.02.702

G.H. Kumar, H. Babuvishwanath, R. Purohit, P. Sahu, R.S. Rana, Investigations on mechanical properties of glass and sugarcane fiber polymer matrix composites. Mater. Today: Proc. **4**, 5408–5420 (2017). https://doi.org/10.1016/j.matpr.2017.05.052

C.C. Kun, C.Y. Liang, Ballistic-proof effects of various woven constructions. Fibers Text. East. Eur. **18**, 63–67 (2010)

U. Kureemun, M. Ravandi, L.Q.N. Tran, W.S. Teo, T.E. Tay, H.P. Lee, Effects of hybridization and hybrid fibre dispersion on the mechanical properties of woven flax-carbon epoxy at low carbon fibre volume fractions. Compos. Part B **134**, 28–38 (2018). https://doi.org/10.1016/j.compositesb.2017.09.035

S.S. Latif, S. Nahar, M. Hasan, Fabrication and electrical characterization of bamboo fiber-reinforced polypropylene composite. J. Reinf. Plast. Compos. **34**, 187–195 (2014). https://doi.org/10.1177/0731684414565941

A. Le Duigou, P. Davies, C. Baley, Interfacial bonding of flax fiber/poly(L-lactide) bio-composites. Compos. Sci. Technol. **70**, 231–239 (2010). https://doi.org/10.1016/j.compscitech.2009.10.009

H.P. Lee, U. Kureemun, M. Ravandi, W.S. Teo, Performance of interlaminar flax-carbon hybrids under bending. Procedia. Manufact. **43**, 658–665 (2020)

W. Machnowski, B. Gutarowski, J. Perkowski, H. Wrzosek, Effects of gamma radiation on the mechanical properties of and susceptibility to biodegradation of natural fibers. Text. Res. J. **83**, 44–55 (2012). https://doi.org/10.1177/0040517512449045

U. Magarajan, S.D. Kumar, D. Arvind, N. Kannan, P. Hemanandan, A comparative study on the static mechanical properties of glass fiber vs glass-jute fiber polymer. Compos. Mater. Today: Proc. **5**, 6711–6716 (2018). https://doi.org/10.1016/j.matpr.2017.11.328

S.M. Maharana, P. Samal, J. Dehury, P.P. Mohanty, Effect of fiber content and orientation on mechanical properties of epoxy composites reinforced with jute and kevlar. Mater. Today: Proc. **26**, 273–277 (2020). https://doi.org/10.1016/j.matpr.2019.11.239

M. Mittal, R. Chaudhary, Development of PALF/glass and coir/glass fiber reinforced hybrid epoxy composites. J. Mater. Sci. Surf. Eng. **6**, 851–861 (2018) https://doi.org/10.jmsse/2348-8956/6-5.1

C. Nagaraj, D. Mishra, J.D.P. Reddy, Estimation of tensile properties of fabricated multi layered natural jute fiber reinforced E-glass composite material. Mater. Today: Proc. **27**, 1443–1448 (2020). https://doi.org/10.1016/j.matpr.2020.02.864

J. Naveen, M. Jawaid, E.S. Zainudina, M.T.H. Sultan, R. Yahaya, Mechanical and moisture diffusion behaviour of hybrid kevlar/cocos nucifera sheath reinforced epoxy composites. J. Mater. Res. Technol. **8**, 1308–1318 (2019). https://doi.org/10.1016/j.jmrt.2018.07.023

W. Ouarhim, H. Essabir, M.O. Bensalah, N. Zari, R. Bouhfid, A.E.K. Qaiss, Structural laminated hybrid composites based on raffia and glass fibers: Effect of alkali treatment, mechanical and thermal properties. Compos. Part B Eng. **154**, 128–137 (2018). https://doi.org/10.1016/j.compositesb.2018.08.004

W. Ouarhim, H. Essabir, M.O. Bensalah, D. Rodrigue, R. Bouhfid, A.E. Qaiss, Hybrid composites and intra-ply hybrid composites based on jute and glass fibers: A comparative study on moisture absorption and mechanical properties. Mater. Today Commun. **22**, 100861 (2020). https://doi.org/10.1016/j.mtcomm.2019.100861

T. Peijs, E.A.M. Smets, L.E. Govaert, Strain rate and temperature effects on energy absorption of polyethylene fibres and composites. Appl. Compos. Mater. **1**, 35–54 (1994). https://doi.org/10.1007/BF00567210

F. Pinto, L. Boccarusso, D. De Fazio, S. Cuomo, M. Durante, M. Meo, Carbon/hemp bio-hybrid composites: Effects of the stacking sequence on flexural, damping and impact properties. Compos. Struct. **242**, 112148 (2020). https://doi.org/10.1016/j.compstruct.2020.112148

M. Rafiquzzaman, M.M. Islam, M.H. Rahman, M.S. Talukdar, M.N. Hasan, Mechanical property evaluation of glass–jute fiber reinforced polymer composites. Polym. Adv. Technol. **27**, 1308–1316 (2016). https://doi.org/10.1002/pat.3798

S. Rajesh, B. Vijayaramnath, C. Elanchezhian, S. Vivek, M.H. Prasadh, M. Kesavan, Experimental investigation of tensile and impact behavior of aramid-natural fiber composite. Mater. Today: Proc. **16**(2019), 699–705 (2019). https://doi.org/10.1016/j.matpr.2019.05.148

K. Raju, M. Balakrishnan, Evaluation of mechanical properties of palm fiber/glass fiber and epoxy combined hybrid composite laminates. Mater. Today: Proc. **21**, 52–55 (2020). https://doi.org/10.1016/j.matpr.2019.05.359

M. Ramasamy, A.R. Daniel, M. Nithya, S.S. Kumar, R. Pugazhenthi, Characterization of natural – Synthetic fiber reinforced epoxy based composite – Hybridization of kenaf fiber and kevlar fiber. Mater. Today: Proc. **37**, 1699–1705 (2021). https://doi.org/10.1016/j.matpr.2020.07.243

R.S. Rana, A. Ashish Kumre, S. Rana, R. Purohit, Characterization of properties of epoxy sisal/glass fiber reinforced hybrid composite. Mater. Today: Proc. **4**, 5445–5451 (2017). https://doi.org/10.1016/j.matpr.2017.05.056

M.J.M. Ridzuan, M.S. Abdul Majid, A. Khasri, K.S. Basaruddin, A.G. Gibson, Effect of moisture exposure and elevated temperatures on impact response of Pennisetum purpureum/glass reinforced epoxy (PGRE) hybrid composites. Compos. Part B Eng. **160**, 84–93 (2018). https://doi.org/10.1016/j.compositesb.2018.10.029

S.N.A. Safri, M.T.H. Sultan, N. Saba, M. Jawaid, Effect of benzoyl treatment on flexural and compressive properties of sugar palm/glass fibers/epoxy hybrid composites. Polym. Test. **71**, 362–369 (2018). https://doi.org/10.1016/j.polymertesting.2018.09.017

S.N.A. Safri, M.T.H. Sultan, M. Jawaid, M.S.A. Majid, Analysis of dynamic mechanical, low-velocity impact and compression after impact behaviour of benzoyl treated sugar palm/glass/epoxy composites. Compos. Struct. **226**, 111308 (2019). https://doi.org/10.1016/j.compstruct.2019.111308

E.H. Saidane, D. Scida, M. Assarar, H. Sabhi, R. Ayad, Hybridisation effect on diffusion kinetic and tensile mechanical behaviour of epoxy based flax–glass composites. Compos. Part A **87**, 153–160 (2016). https://doi.org/10.1016/j.compositesa.2016.04.023

E.H. Saidane, D. Scida, M. Assarar, R. Ayad, Damage mechanisms assessment of hybrid flax-glass fiber composites using acoustic emission. Compos. Struct. **174**, 1–11 (2017). https://doi.org/10.1016/j.compstruct.2017.04.044

E.H. Saidane, D. Scida, M.J. Paca, R. Ayadb, Mode-I interlaminar fracture toughness of flax, glass and hybrid flax-glass fiber woven composites: Failure mechanism evaluation using acoustic emission analysis. Polym. Test. **75**, 246–253 (2019). https://doi.org/10.1016/j.polymertesting.2019.02.022

S. Samanta, M. Muralidhar, T.J. Singh, S. Sarkar, Characterization of mechanical properties of hybrid bamboo/GFRP and jute/GFRP composites. Mater. Today: Proc. **2**, 1398–1405 (2015). https://doi.org/10.1016/j.matpr.2015.07.059

F. Sarasini, J. Tirillo, S. D'Altilia, T. Valente, C. Santulli, F. Touchard, L.C. Arnault, D. Mellier, L. Lampani, P. Gaudenzi, Damage tolerance of carbon/flax hybrid composites subjected to low velocity impact. Compos. B **91**, 144–153 (2016). https://doi.org/10.1016/j.compositesb.2016.01.050

G. Saravanan, G.B. Bhaskar, E. Kaviyarasan, B. Naveen, S. Prabakaran, S. Rajesh, Experimental investigation of mechanical behavior of bauhinia racemosa – Based glass fiber reinforced composite. Mater. Today: Proc. **16**, 758–765 (2019). https://doi.org/10.1016/j.matpr.2019.05.156

A. Sarwar, Z. Mahboob, R. Zdero, H. Bougherara, Mechanical characterization of a new Kevlar/Flax/epoxy hybrid composite in a sandwich structure. Polym. Test. **90**, 106680 (2020). https://doi.org/10.1016/j.polymertesting.2020.106680

D. Sivakumar, L.F. Ng, N.F.M. Zalani, M.Z. Selamat, A.F.A. Ghani, S.H.S.M. Fadzullah, Influence of kenaf fabric on the tensile performance of environmentally sustainable fibre metal laminates. Alex. Eng. J. **57**, 4003–4008 (2018). https://doi.org/10.1016/j.aej.2018.02.010

M.A.S. Sujon, M.A. Habib, M.Z. Abedin, Experimental investigation of the mechanical and water absorption properties on fiber stacking sequence and orientation of jute/carbon epoxy hybrid composites. J. Mater. Res. Technol. **9**, 10970–10981 (2020). https://doi.org/10.1016/j.jmrt.2020.07.079

M.T.H. Sultana, M. Jawaid, S.N.A. Safri, A.U.M. Shah, M.R. Yusof, J. Naveen, S. Mohd, K.A.-M. Salleh, N. Saba, Effects of layering sequence and gamma radiation on mechanical properties and morphology of Kevlar/oil palm EFB/epoxy hybrid composites. J. Mater. Res. Technol. **8**, 5362–5373 (2019). https://doi.org/10.1016/j.jmrt.2019.09.003

A.B.M. Supian, S.M. Sapuan, M.Y.M. Zuhri, E.S. Zainudin, H.H. Ya, Crashworthiness performance of hybrid kenaf/glass fiber reinforced epoxy tube on winding orientation effect under quasi-static compression load. Def. Technol. **16**, 1051–1061 (2020). https://doi.org/10.1016/j.dt.2019.11.012

Y. Swolfs, L. Gorbatikh, I. Verpoest, Fiber hybridisation in polymer composites: A review. Compos. Part A Appl. Sci. Manuf. **67**, 181–200 (2014). https://doi.org/10.1016/j.compositesa.2014.08.027

K. Vinoth, M.N.M. Ansari, S. Begum, Z. Yahya, A. Atiqah, Effect of fiber loading on tensile strength of kenaf/glass fiber epoxy hybrid composite for insulator application. Mater. Today: Proc. **29**, 123–126 (2020). https://doi.org/10.1016/j.matpr.2020.05.684

H. Wang, L. Yang, H. Wu, Study on mechanical and thermomechanical properties of flax/glass fiber hybrid-reinforced epoxy composites. Polym. Compos. **42**, 714–723 (2020). https://doi.org/10.1002/pc.25860

R. Yahaya, S.M. Sapuan, M. Jawaid, Z. Leman, E.S. Zainudin, Mechanical performance of woven kenaf-Kevlar hybrid composites. J. Reinf. Plast. Compos. **33**, 2242–2254 (2014). https://doi.org/10.1177/0731684414559864

R. Yahaya, S.M. Sapuan, M. Jawaid, Z. Leman, E.S. Zainudin, Effect of layering sequence and chemical treatment on the mechanical properties of woven kenaf-aramid hybrid laminated composites. Mater. Des. **67**, 173–179 (2015a). https://doi.org/10.1016/j.matdes.2014.11.024

R. Yahaya, S.M. Sapuan, M. Jawaid, Z. Leman, E.S. Zainudin, Effects of kenaf contents and fiber orientation on physical, mechanical, and morphological properties of hybrid laminated composites for vehicle spall liners. Polym. Compos. **36**, 1469–14786 (2015b). https://doi.org/10.1002/pc.23053

R. Yahaya, S.M. Sapuan, M. Jawaid, Z. Leman, E.S. Zainudin, Effect of fiber orientations on the mechanical properties of kenaf–aramid hybrid composites for spall-liner application. Defe. Technol. **12**, 52–58 (2016). https://doi.org/10.1016/j.dt.2015.08.005

Water Sorption and Solvent Sorption Techniques of Epoxy/Synthetic/Natural Fiber Composites

36

Mariana D. Banea and Sandip Budhe

Contents

Abstract

This chapter presents the main characteristics of water and solvent sorption and its effects on the behavior of epoxy/natural/synthetic fiber-reinforced polymer composites. Various models which were proposed in the literature to describe the kinetics of moisture sorption into polymers and their composites are briefly discussed. Basic Fickian diffusion models and more elaborate models that account for anomalous (i.e., non-Fickian) moisture absorption often exhibited by the thermoset resins are covered. It was shown that several factors affect the way in which hybrid epoxy/synthetic/natural composites absorb water (i.e., temperature, fiber volume fraction, type of fiber (permeable or impermeable), area of exposed surfaces, degree of cross-linking, degree of crystallinity of the epoxy matrix, etc.). Consequently, the accurate determination of diffusivity and

M. D. Banea (✉)
Federal Center of Technological Education of Rio de Janeiro (CEFET/RJ), Rio de Janeiro, Brazil

S. Budhe
Department of Mechanical Engineering, National Institute of Technology, Calicut, Kerala, India

S. Mavinkere Rangappa et al. (eds.), *Handbook of Epoxy/Fiber Composites*,
https://doi.org/10.1007/978-981-19-3603-6_40

moisture uptake in a composite is a fundamental step in the accurate prediction of moisture-induced degradation. In general, the presence of natural fibers in the composite increases the moisture absorption. Thus, it is recommended that the amount of natural fiber in a composite is restricted to its optimum fiber/matrix ratio in order to attain maximum strength and limit its moisture predisposition. One effective way to reduce the water absorption is the hybridization of natural fiber composites with synthetic fibers (glass, Kevlar, or carbon), enabling a proper balance in performance and cost.

Keywords

Diffusion · Water sorption · Natural fiber · Synthetic fiber · Hybrid composites · Diffusion mechanisms

Introduction

There is an increasing interest in natural fiber-reinforced composites (NFRCs) by the industry, due to their biodegradable characteristics to produce sustainable products. The use of natural fibers presents important advantages, such as biodegradability, low density, good acoustic isolation, and low cost, when compared to their synthetic fiber counterparts. However, their main disadvantages are the variability in fiber quality and absorption of humidity due to the hydrophilic characteristic of the fiber, which leads to low interfacial adhesion between the fiber and the hydrophobic matrix and, consequently, relatively low mechanical properties (Pickering et al. 2016; Budhe et al. 2019; Cavalcanti et al. 2021). Different techniques have been used by researchers to surpass these shortcomings, such as chemical treatments of the fibers and the hybridization techniques (Cavalcanti et al. 2019; Lima et al. 2020). The hybridization technique is the use of one or more type of fiber (natural or synthetic) within the polymeric matrix and can be done either intralaminar or interlaminar (within the same layer or in different layers, respectively) (Neto et al. 2019).

Hybrid epoxy/synthetic/natural fiber composites can be found in applications in many industrial sectors, such as automotive, construction, marine industry, and sports, among others. Moreover, the most promising applications of epoxy hybrid polymer composites are in automotive industry (e.g., door panels, package trays, hat racks, instrument panels, internal engine covers, sun visors, boot liners, oil air filters). More recently, they are moving ahead to more structurally demanding parts such as seat backs, exterior underfloor paneling, as well as anti-roll bars (de Queiroz et al. 2020). They are also used in railway coach interiors and in aircraft industries to make interior parts, among others. However, these composites are usually exposed to a range of aggressive environments (e.g., extreme temperature cycles, ultraviolet (UV) radiation, moisture, alkaline/salt environments, etc.).

Moisture absorption is one of the main disadvantages experienced with natural fiber-reinforced composites. It has been shown to increase with increased fiber content and temperature as well as being influenced by fiber treatment/coupling

agent and also fiber arrangement. Consequently, the accurate determination of diffusivity and moisture uptake in a polymer composite is a fundamental step in the accurate prediction of moisture-induced degradation. The effect of water and solvent sorption on the durability of epoxy/natural/synthetic fiber-reinforced polymer composites is an important aspect to be considered since it plays a key role in the composites' durability and service life. Composite materials are exposed to wet or humid environments, resulting in considerable moisture absorption during their service life. The absorbed moisture alters the physical and mechanical properties of the composites and significantly compromises their performance. This chapter presents the main characteristics of water and solvent sorption and its effects on the behavior of epoxy/natural/synthetic fiber-reinforced polymer composites.

Mechanics of Water Sorption of Polymer Composites

The kinetics of moisture absorption into polymers and their composites was described in the literature by several models. The Fickian diffusion model is one of the most widely used. However, more elaborate methods that take into account the anomalous (i.e., non-Fickian) moisture absorption which is usually exhibited by the thermoset resins were also developed. In a simple case of one-dimensional Fickian diffusion, diffusivity (D) and maximum moisture absorption of the composite are sufficient to describe the absorption kinetics. However, for more complex absorption behaviors such as non-Fickian models (i.e., a two-phase model), additional absorption parameters are needed, so that the experimentally observed absorption behavior can be replicated. It should be noted that the need to use non-Fickian models derives from the experimentally observed absorption phenomena during the thermogravimetric experiments of several thermosetting polymers and composites (Bond 2005). The water sorption and desorption by a composite material are usually measured by the weight gain and weight loss, and the sorption behavior is characterized by different mechanisms. The phenomenon of moisture and fluid ingress or uptake is most often governed by a thermodynamic driving force, osmosis, reverse osmosis, or diffusion (Chiang et al. 1996).

The diffusion mechanism model is well characterized for the absorption of moisture. Diffusion is the result of random molecular movement in mass, and its math governing equation is similar to that of a heat conduction process. This diffusion factor was recognized by Fick in 1855, and he gave a material diffusion equation which is similar to the heat conduction (Fick 1855). Shen and Springer (Shen and Springer 1976), based on Fick's law, studied the absorption and desorption of water in composite materials and presented expressions for the moisture distribution and moisture content as a function of time for one-dimensional composite materials. In this model, a square array of fiber is idealized, and the flow of heat or water is considered as following straight line paths, which is overly simplistic. In spite of the fact that the data presented by them agreed with their model, composite diffusivity values reported by the wider literature are much higher than

their theoretical predictions. This is to be expected given the simplified nature of the theory. As the model assumes straight line paths, the water cannot flow around the fibers; this will generate disagreement with experimental observations. There are a number of other models in the available literature that were applied in water diffusivity in composite materials such as Rayleigh's equation, Shirrel and Halpin, the Halpin-Tsai equation, and Woo and Piggott. All these models have in common an analogy with thermal/electrical conductivity. However, diffusivity is related to both the rate of diffusion and the equilibrium uptake; therefore, a direct analogy is not appropriate. Kondo and Taki have pointed out the mistake in the analogy. Shear modulus corresponds to the product of diffusivity and equilibrium concentration instead of diffusivity alone. This is due to the fact that the relative moisture concentration corresponds to temperature in the thermal analogy. By using relative concentration, Fick's law takes the familiar form used today (Bao and Yee 2002a, b).

Fick's first law in one dimension states that the particle flux J (number per unit area per unit time) in a steady state is proportional to the concentration gradient dC/dx. The proportionality constant D is called diffusion coefficient, which is always assumed to be a constant.

$$J = -D.\frac{dC}{dx} \tag{1}$$

Moisture diffusion in composites is a kind of mass diffusion and follows Fick's law (Gao and Zhou 2019).

By considering Fick's first law and the flux through two arbitrary points in the material, it is possible to derive Fick's second law.

Fick's second law (Fick 1855) refers to the accumulation or depletion of concentration, C, over time when steady-state conditions are not achieved. This can be determined from the spatial derivative of the flux:

$$\frac{\partial C}{\partial t} = -\frac{\partial J}{\partial t} = D.\left[\frac{(\partial^2 C)}{(\partial x^2)}\right] \tag{2}$$

The time-dependent concentration distribution along the thickness direction can be obtained by solving the differential Eq. (2) with the method of separation of variables.

The time-dependent concentration distribution along the thickness direction can be obtained as (see Fig. 1):

$$C(x,t) = C_0\left(1 - \frac{4}{\pi}\sum_{k=1}^{\infty}\frac{1}{2k-1}\,sin\,\frac{(2k-1)\pi}{h}x.e^{-\frac{(2k-1)^2\pi^2 Dt}{h^2}}\right) \tag{3}$$

$C(x,\ t)$ is the moisture concentration at a point and x is its distance from the central plane at a given time t.

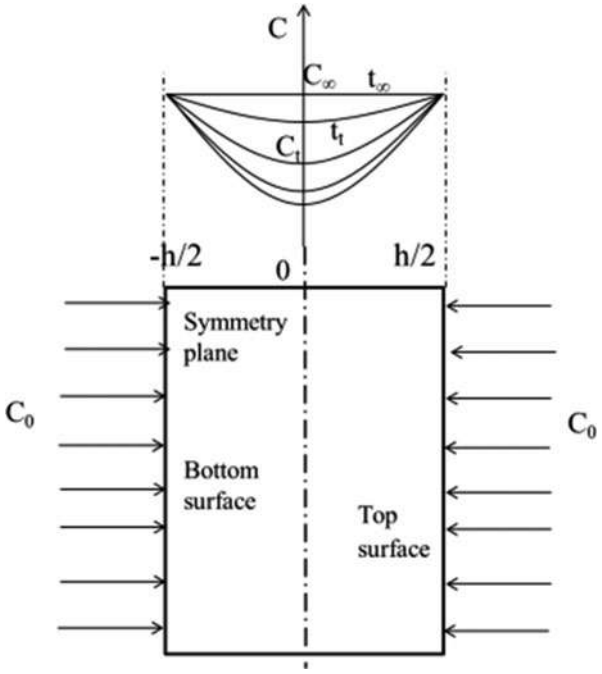

Fig. 1 Schematics of boundary condition and moisture concentration distribution versus time of one-dimensional moisture diffusion (author source)

Further, by integrating the concentration $C(x, t)$ in the thickness, i.e., x, direction, the weight gain of one-dimensional moisture diffusion process is as follows:

$$W(t) = C_0 h\left(1 - \frac{8}{\pi^2}\sum_{k=1}^{\infty}\frac{1}{(2k-1)^2}.e^{-\frac{(2k-1)^2\pi^2 Dt}{h^2}}\right) \tag{4}$$

Therefore, if the water absorption behavior follows the Fickian diffusion law, then the diffusion coefficient can be determined from the initial slope of moisture uptake w(t) versus square root of time.

The above equation was simplified by Shen and Springer (Shen and Springer 1976) who state that there are two cases: in the first one, where M_t/M_m is lower than 0.6, the curve is correlated by:

$$\frac{M_t}{M_\infty} = 4\sqrt{\frac{Dt}{\pi h^2}} \tag{5}$$

and in the second case, where M_t/M_m is higher than 0.6:

$$\frac{M_t}{M_\infty} = 1 - \exp\left[-7.3\left(\frac{Dt}{h^2}\right)^{0.75}\right] \tag{6}$$

The diffusion coefficient D can be deducted from Eq. 7:

$$D = \pi\left(\frac{kh}{4M_{\infty}}\right)^2 \tag{7}$$

Further, a correction factor was used to take into account the length and width of the specimens. Thus, the corrected diffusion coefficient can be obtained from Eq. 8:

$$D_c = D\left(1 + \frac{h}{L} + \frac{h}{w}\right)^{-2} \tag{8}$$

It was shown in the literature that the moisture uptake of epoxy matrix composites can be well described by Fick's law. However, some studies have found that in the case of long-term measurements, it often no longer follows Fick's law, especially for conditions of high temperature and high humidity (Gurtin and Yatomi 1979; Bond 2005). The moisture curve behavior changes with the temperature, and at high temperature, Fick's law doesn't follow the trend of moisture curve. For unidirectional glass fiber-reinforced composites (UD-GFRP) and unidirectional carbon fiber-reinforced composites (UD-CFRP), in the initial stages, water uptake agrees well with Fick's laws, but in later periods, they diverge greatly from Fick's model, especially at higher temperature (Gao and Zhou 2019).

Fick's law perfectly fits for the moisture curve of the composite material until any damage such as crack, surface loss, any void, etc. occurs. This damage is generally observed for long-time immersion or at higher temperature and higher humidity, and that is the reason why Fick's law does not fit after the initial linear curve of moisture absorption. It was observed that the moisture weight gains continue to increase after the saturation points predicted by Fick's law. This behavior is known as two-stage water uptake phenomenon and is mainly noticeable when the composite samples are subjected to high temperatures and also for long-term measurements. Loos and Springer reported that, at lower temperatures, the water absorption phenomenon is well predicted by Fick's law; however, at higher temperatures, the moisture absorption follows a non-Fickian behavior (Loos and Springer 1981). Figure 2 shows the schematic diagram of single-phase and double-phase absorption model. The plausible explanation for dual-phase absorption model is mainly due to the micro-cracks developed on the surface and inside the materials and the high-temperature environment (Zhou and Lucas 1995).

Two-stage moisture absorption phenomenon by the composite material is well defined by the Langmuir equation (model), and it is found to be in agreement with the experimental moisture curve as shown in Fig. 2. In this model, both free water and bound water absorption by the composite are accounted for, which also helps to fit the curve after the damage mechanism (Gao and Zhou 2019).

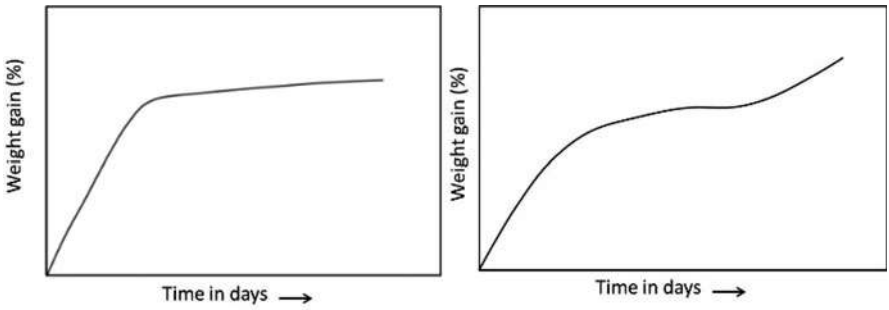

Fig. 2 (**a**) A schematic diagram of a single-phase absorption model. (**b**) A schematic diagram of a dual-phase absorption model. (author source)

The Langmuir equation can be written as follows:

$$D\frac{\partial^2 C}{\partial x^2} = \frac{\partial C}{\partial t} + \frac{\partial c}{\partial t} \tag{9}$$

$$\frac{\partial C}{\partial t} = \beta C - \alpha c \tag{10}$$

where C is the free water concentration, C_∞ is the saturated value of C, c is the bound water concentration, and c_∞ is its saturation concentration. α and β are two constants that represent the probabilities of water releasing and bonding in the composites with respect to unit time.

The moisture absorption is considered as saturated in the second uptake stage when the rates of free and bound water reach equilibrium.

The concentrations of free water and bound water over time can be obtained by solving Eq. (9):

$$C(x,t) = C_\infty\left(1 - \frac{4}{\pi}\sum_{k=1}^{\infty}\frac{1}{2k-1}\,sin\,\frac{(2k-1)\pi}{h}x.e^{-\frac{(2k-1)^2\pi^2 Dt}{h^2}}\right) \tag{11}$$

$$c(x,t) = \frac{\beta}{\alpha}c_\infty\left(1 - \frac{4}{\pi}\sum_{k=1}^{\infty}\frac{1}{2k-1}\,sin\,\frac{(2k-1)\pi}{h}x.e^{-\alpha t}\right) \tag{12}$$

It can be seen that Eq. (11) is the same as Eq. (3).

Further, by integrating the sum of the two water concentrations along the composite thickness (h), the moisture absorption gain is:

$$G(t) = \int_0^h (C(x,t) + c(x,t))dx \tag{13}$$

$$G(t) = G_{so}\left[\frac{\alpha}{\alpha+\beta}\left(1 - \frac{8}{\pi^2}\sum_{n=1}^{\infty}\frac{1}{n^2}e^{\frac{-n^2\pi^2 Dt}{h^2}}\right) + \frac{\beta}{\alpha+\beta}(1 - e^{-\alpha t})\right] \quad (14)$$

The detailed stepwise mathematical description and solution could be found in the references (Gurtin and Yatomi 1979; Bond 2005).

Zhou and Lucas examined the effect of water on graphite/epoxy composites at different temperatures. From the experimental results, cracks, peeling, voids, and surface dissolution of the graphite/epoxy composite laminate were observed after long-time immersion in distilled water (Zhou and Lucas 1995). Figure 3 shows the schematic diagram of typical weight change profiles of graphite/epoxy composites under different water environment conditions. In Fig. 3a, the moisture absorption by the composite is fully agreed till the saturation point (this is the ideal case). In Fig. 3b, in the initial region, Fick's law is obeyed, and subsequently the experimental data deviates from the Fickian behavior. This has occurred due to cracking which

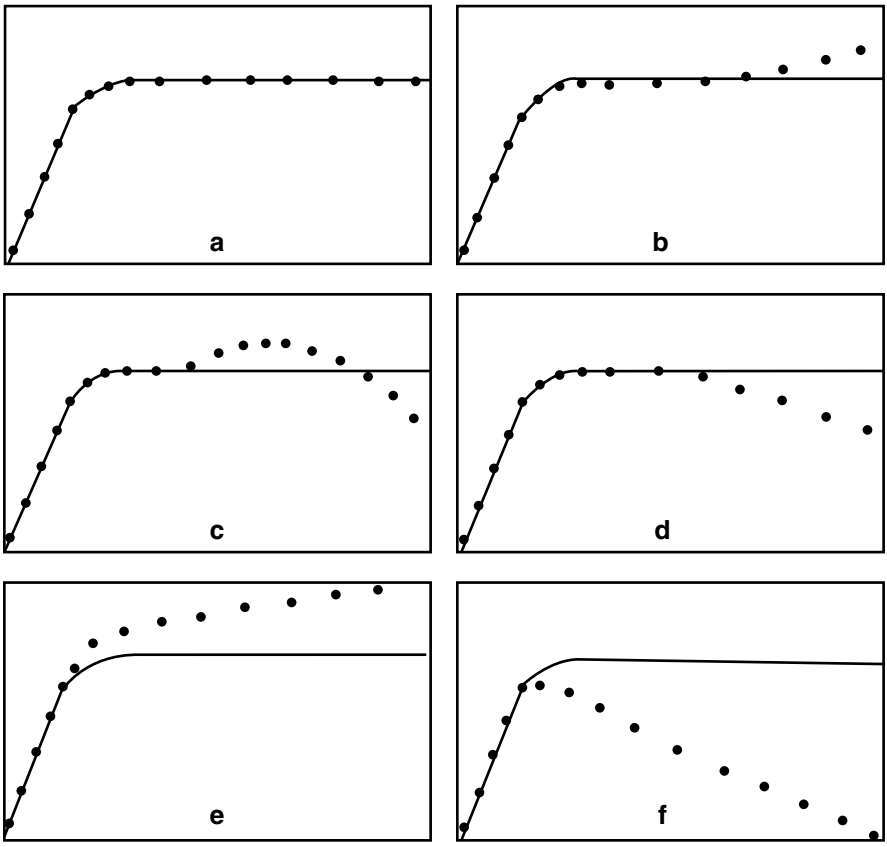

Fig. 3 The schematic diagram of typical weight change profiles of graphite/epoxy composites under water environment. (Reproduced with permission from Zhou and Lucas (1995))

further resulted in an increased moisture absorption. In Fig. 3c, initially no cracks exist, and later, cracks develop, which resulted in the dissolution and peeling of the resin matrix. There are two ways in which the profile from Fig. 3d is possible. First, there are no cracks and peeling at the initial stage. Second, no cracks develop, and the absorption curve obeys Fick's law until surface mass loss occurs (this is the case of neat resins). In Fig. 3e, cracks develop quickly, and the weight increase is higher than that of Fick's law behavior (in this case no mass loss occurs). Finally, the last case is when surface peeling is the dominant mechanism and weight loss occurs rapidly (Fig. 3f).

Moisture concentration-dependent diffusion and dual diffusivity are the two models which assess the moisture diffusion behavior for hybrid composite materials (Huo et al. 2014).

Numerical investigations via finite element analysis (FEA) have been carried out in the literature regarding the water uptake behavior of natural fiber composites. Initially, experimentally deduced diffusion coefficients are calculated, and then they are used as inputs for the numerical model. Fick's law-based codes are available commercially in software such as Abaqus. With the diffusion coefficient assumed to be constant, the model is used to find the concentration, C. It has been shown in the literature that the model presents a good fit with the experimental results (Jain et al. 2019a, b).

Most prediction models are determined based on a cell model. The Springer and Tsai model is conceived of a simple straight line path; Rayleigh's equation derived the electrical conductivity of a medium with cylindrical obstacles in a rectangular organization without consideration for a diffusion path. Furthermore, Rayleigh's is quite similar to Halpin-Tsai when the fiber diffusivity coefficient is null. Regardless of the model, only the fiber volume fraction is considered; however, the effects of fiber arrangement are significant in moisture diffusion. This is because tortuosity in diffusion path is a function of fiber volume fraction, arrangement, and clustering. The FEA technique has good accuracy in simulating water diffusion based on Fick's law via the representative elementary volume (REV) for low fiber volume fractions ($v_f = 0.3$). However, when higher volume fractions are considered (i.e., $v_f > 0.65$), it does not work. This has been attributed to the contact of the fibers which alters the moisture diffusion path significantly. This has been remedied by the calculation of a new diffusion coefficient evaluated by the inverse method for the case of a more realistic fiber distribution (Pan et al. 2019; Joliff et al. 2014).

Main Characteristics of Water and Solvent Sorption of Fiber-Reinforced Composites

It was shown in the literature that most of the moisture is absorbed by the epoxy resin, followed by the interphase between fiber-matrix region and least by the fiber in the composite material. The natural fibers are more prone to moisture absorption compared to the synthetic fiber in composite materials, as the natural fibers are hydrophilic in nature, while the synthetic fibers absorb much less moisture, as they

are hydrophobic in nature. In the following section, the moisture absorption behavior of each component of composite materials is briefly discussed.

Water and Solvent Sorption by the Epoxy Resin

Researchers developed two important mechanisms that generally describe the nature of water sorption in epoxy resins: the first one termed by some researchers as Type I bound water is the free volume process, which assumes that water diffuses into the epoxy resin and resides in the free volume of the material. It was stated in the literature that this corresponds to a water molecule which forms a single hydrogen bond with the epoxy resin network and hence it owns a lower activation energy and is easily removed from the resin (Zhou and Lucas 1999a, b). The second approach (termed as a Type II bound) is the interaction concept that states that the water molecules couple strongly with some hydrophilic functional groups such as hydroxyl or amine in epoxy resin. This Type II bound water possesses higher activation energy and is more complicated to remove from the epoxy resin. The amount of Type II bound water depends on the exposure temperature and also the time period of water exposure, which results in a greater amount of Type II bound water (Zhou and Lucas 1999a, b).

Apicella et al. investigated the water absorption phenomenon in a glassy epoxy resin and reported that three absorption modes are responsible for the final moisture content in the composite. First, dissolution of water in the polymer resin network occurs, followed by the moisture absorption onto the surface of vacuoles which define the excess free volume of the glassy structure of the epoxy resin and finally the hydrogen bonding between polymer hydrophilic groups and water occurs (Apicella et al. 1984). It was also reported that the water molecules can interact by forming hydrogen bonds with hydrophilic groups in epoxy resin, while other water molecules are retained in free volume of the material. Contrary to this, Woo and Piggott states that the water molecules were not bound to polar groups or to hydrogen bonding sites in epoxy resin (Woo and Piggott 1987). Clustering of water molecules in the polymer was reported rather than complete molecular separation.

In most of the cases, the moisture absorption by the epoxy resin follows Fick's law curve using the diffusion mechanism, but that is not always sufficient, as it depends on several parameters. Most of the moisture behavior of epoxy resin is either a single-phase model or a double-phase model that depends on multiple parameters, such as type of hardener, curing condition and temperature, type of resin, temperature and humidity condition, exposure duration, etc. (Zhou and Lucas 1999a, b).

Bonniau and Bunsell noticed that single phase and double phase depended on the use of hardener to cure the epoxy (Bonniau and Bunsell 1984). For instance, single-phase water absorption was observed when diamine hardeners are used to cure epoxy resin, while a two-phase absorption was seen when the same epoxy resin is cured with a dicyandiamide hardener. Figure 4 shows an example of the water

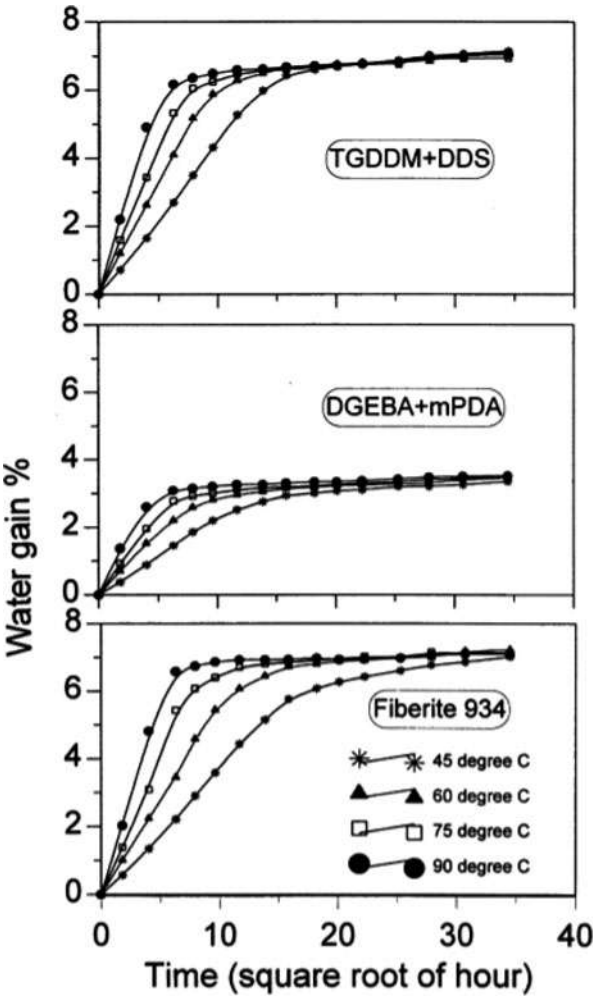

Fig. 4 Water absorption profiles of the three-epoxy system at different temperatures for 1530 h. (Reproduced with permission from Zhou and Lucas (1999a))

sorption profiles of three epoxy resin systems cured with different hardeners. It is observed that one of the epoxy systems absorbs quite low moisture (3.35 wt %) content compared to the others (6.95 and 6.80 wt %), due to resin chemistry (Zhou and Lucas 1999a). These results show that the hardeners play an important role in deciding the single-phase or double-phase moisture absorption. A careful selection of the hardener is very important in order to assure the cure at low temperature and also follow single-phase absorption phenomenon. In addition to that, blends with other filler materials can enhance the epoxy material properties such as moisture absorption and mechanical, thermal, and physical properties.

The most widely used technique to improve the overall mechanical and physical properties of the composite materials is to remove the moisture from the composites.

However, desorption from high moisture saturation tended to leave small residual moisture content, which could only be removed by heating at high-enough temperature as blistering may occur (Zhou and Lucas 1999a). Several researchers have reported that some of the absorbed water could not be removed from the composite material unless a higher desorption temperature was used (Zhou and Lucas 1999a; Marsh et al. 1988). It was reported that the absorbed water could not be fully removed from the material during desorption at lower temperatures and that temperatures higher than the glass transition temperature (T_g) of the composite need to be applied to remove the residual water (Marsh et al. 1988). However, it was shown in the literature that small percentage of moisture in the composite had not a major impact on their mechanical performance.

Moisture weight gain by the epoxy polymer during the absorption cycles depends on many parameters, most significantly the temperature and humidity conditions. It is known that the higher the moisture equilibrium content, the higher the swelling stress in the materials and the higher the possibility that micro-cracking and hydrolysis will occur (Gao and Zhou 2019).

A comprehensive awareness of the processes that govern the bonding of water molecules to epoxy resins is crucial to an in-depth understanding of hygrothermal effects. Despite significant research efforts aimed at investigating these effects, water diffusion modes and the relevant mechanisms in epoxy resins are not yet fully understood.

The water sorption effects in epoxy resins are relatively complex as the epoxy resin diffusion kinetics depends on several parameters such as the chemical composition of the resin, the curing temperature, and/or the curing agent nature.

Water and Solvent Sorption by the Interface of Fiber and Matrix/Resin

The interface between fiber and matrix is one of the critical parameters as it absorbs more moisture and subsequently affects the composite performance. For example, Joliff et al. reported that the water diffusion coefficient is approximately five times higher in the interphase area than in the matrix and this experimental study is in good agreement with the analytical and finite element models (Joliff et al. 2014). Most of the moisture absorption occurs in the gaps at the fiber-matrix interface space using the capillary transport mechanism. There are many possibilities to produce the gap/crack between the fiber and matrix interface, and Fig. 5 shows the possibilities to produce crack/gap (Azwa et al. 2013). One is from the fabrication process of the composites, where the impregnation of the fibers with the matrix was inadequate. This can help to absorb moisture using the capillary mechanism and pass through and toward the interphase between the fiber and matrix (Fig. 5a). The transport of water molecules through the micro-cracks that can appear in the matrix is especially relevant as results in fiber swelling and occurs mainly in natural fiber-reinforced composites as the fiber absorbs more moisture (Fig. 5b). In some of the composites under the solvent water-soluble substance, leaching takes place, which reduces the

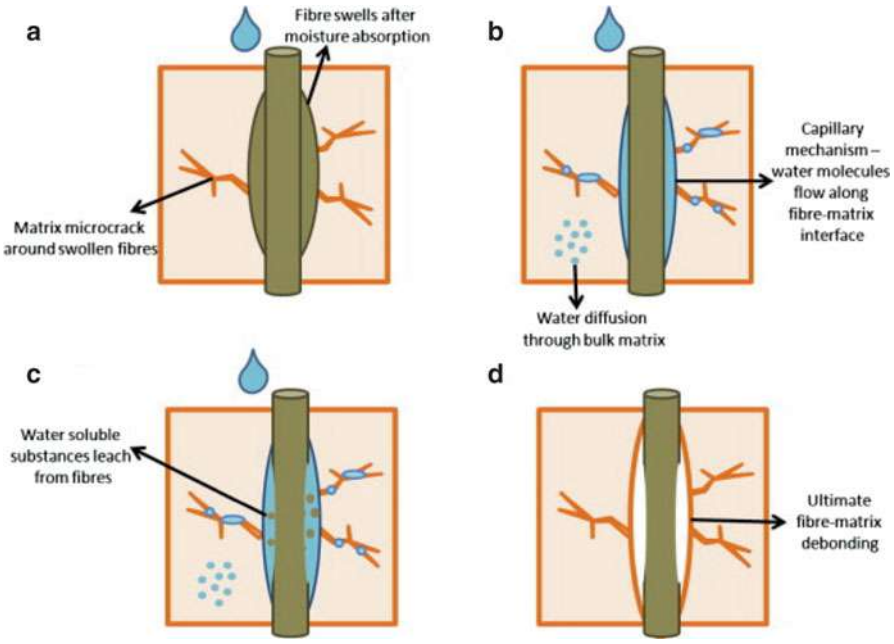

Fig. 5 Effect of water on fiber-matrix interface: (**a**) micro-crack formation owing to fiber swelling; (**b**) water molecules diffuse in the bulk matrix and flow along the fiber-matrix interface; (**c**) water-soluble substance leaching; and (**d**) debonding of fiber-matrix interface. (Reproduced with permission from Azwa et al. (2013))

total weight of the composite even by the absorption of water (Fig. 5c), and for such cases, the Fickian curve doesn't follow the moisture absorption behavior (Azwa et al. 2013). Further, the quantity of water absorbed by the epoxy resin is different than that absorbed by the fibers. These result in a significant difference in water-induced volumetric expansion as well as different thermal coefficient expansion between the epoxy matrix and the fibers and thus lead to the development of localized stress and strain fields in fiber-reinforced composites (Vadadi et al. 2003; Azwa et al. 2013). The micro-crack that appears in a brittle epoxy matrix is due to the swelling of the fiber and mismatch in thermal and moisture expansion of fiber and matrix (Fig. 5d).

Water and Solvent Sorption by the Fibers

The fiber component of polymer composite materials absorbs less moisture/solvent, especially when synthetic fibers (e.g., glass, carbon, etc.) are compared to natural fibers. Natural fibers contain large quantities of cellulose which helps to absorb more moisture. Figure 6 shows that there is a significant difference in the moisture absorption content by the different fiber composite materials (Barjasteh and Nutt 2012). It implies that each fiber has its own capacity to absorb certain levels of

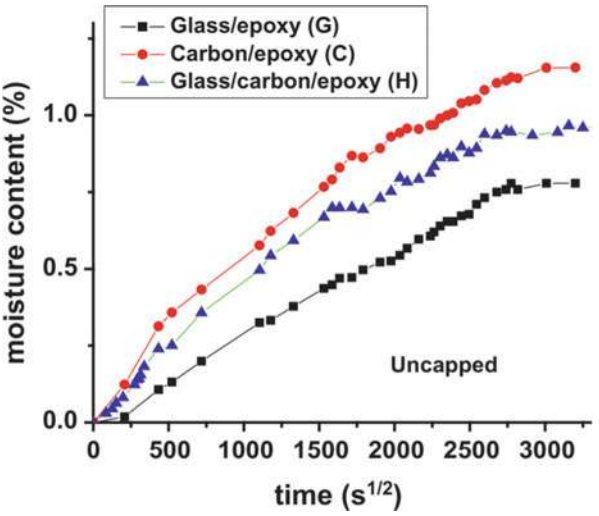

Fig. 6 Percent weight change versus the square root of time for uncapped unidirectional glass/carbon/epoxy (H), carbon/epoxy (C), and glass/epoxy (G) composite rods exposed to 60 C and 85% humidity chamber. (Reproduced with permission from Barjasteh and Nutt (2012))

Table 1 Average moisture and cellulose content of natural fibers

Natural fiber	Moisture (%)	Cellulose (%)	Reference
Jute	9.93	63.24	Giridhar et al. 1986
Sisal	6.20	78	Giridhar et al. 1986
Flax	10	64–72	Munoz and Garcia-Manrique 2015
Kenaf	6–20	45–57	Mochane et al. 2019
Hemp	10.8	74.4	Dhakal et al. 2007
Ramie	12–17	69–91	Mochane et al. 2019
Abaca	9.62–14	53–63	Mochane et al. 2019
Rice husk	9.91	38–45	Mochane et al. 2019
Bamboo	9	26–43	Mochane et al. 2019
Banana	10–11	63–83	Mochane et al. 2019
Coir	10	41.7	Mochane et al. 2019

moisture. On a similar note, it would be advisable to use the hybrid composite material which can balance the moisture content level with achieving the desired mechanical performance.

The natural fibers generally absorb more moisture due to large contents of cellulose. The average moisture content by different natural fibers is listed in Table 1, and the variation of moisture absorption is quite dependent on the cellulose content in the natural fiber. It was shown in the literature that moisture absorption in natural fiber composite materials can be reduced through fiber modifications (i.e., alkalization) and using of coupling agents (Banea et al. 2021). Fiber treatments are crucial to enhance strength and moisture durability of natural fiber composite materials mainly by promoting improved fiber/matrix interface. Also, water-resistant coating can be applied on the composite surface to avoid contact between moisture

and fiber. However, in some cases, the bonding strength is reduced (Xie et al. 2010). Thus, it is required to make a compromise/optimization between the silane and other coating to prevent moisture in such way that the strength of the composite would not be compromised.

As the natural fibers are predisposed to moisture attack, it is expected that the durability of natural fiber composites will decrease with increased fiber content. Consequently, the amount of fiber in a composite shall be limited to its optimum fiber/matrix ratio in order to achieve maximum strength capacity and limit its moisture susceptibility. This balance may be found via natural/natural fiber hybridization. For instance, Maslinda et al. investigated the moisture uptake behavior and mechanical effects in interwoven cellulosic composites. Epoxy polymer infusion technique was used to fabricate kenaf/jute and kenaf/hemp composites. Fiber content was kept at approx. 30% by weight. Both neat and hybrid composites were fabricated (i.e., KK, JJ, HH, KJ, KH). It was reported that the kenaf neat case absorbed more water than its jute and hemp composite counterparts. The natural/natural composites presented significantly lower moisture uptake when compared to the neat cases. The kenaf/jute reportedly absorbed 46% less water than the neat cases. Furthermore, for the kenaf/hemp hybrid composite, the moisture uptake reduction was 64% and 58% when compared to the neat kenaf and hemp composites, respectively (Maslinda et al. 2017).

Yorseng et al. investigated the effect of accelerated weathering and water absorption on the properties of kenaf and sisal neat and hybrid epoxy composites. The weathering took place in a UV chamber where the specimens were exposed to repeated radiation cycles for 555.55 h. The hand lay-up technique was used, and three layers of material were applied. The stacking sequence was varied as follows: KKK, KSK, SKS, and SSS. Immersion time was up to 120 days. It was reported that the neat epoxy resin absorbed approx. 2%, while all the natural fiber composites absorbed upward of 3%. After UV weathering, the water absorption increased by roughly 1% for all cases; this was linked to the formation of micro-cracks and fiber degradation due to the radiation (Yorseng et al. 2020).

Tabrej et al. investigated the effect of stacking sequence of kenaf/jute hybrid epoxy composites in water uptake behavior and thickness swelling. Kenaf and jute mats were applied at 30% fiber weight along with hand lay-up technique. The stacking sequences were K/J/K and J/K/J. Distilled water was used and the immersion time was up to 50 days. It was observed that the K/J/K presented higher water uptake than the J/K/J case, approx. 15% and 11%, respectively. The thickness swelling behavior was similar for both cases (approx. 9% for J/K/J and 10% for K/J/K) (Tabrej et al. 2019).

Furthermore, Chilali et al. demonstrated that the phenomenon of water absorption (absorption kinetics) of flax/epoxy composites is dependent on a number of factors such as specimen aspect ratio, thickness, and fiber orientation. It was shown that the saturation process was principally governed by the thickness direction and diffusion occurs mainly via this direction for an aspect ratio (l/h) greater than 60. Regarding the thickness, it was shown that diffusion kinetics decreases with an increase in thickness. An increase in water absorption speed of approx. 50% was reported

increasing specimen thickness from 3 mm to 10 mm. It was demonstrated that the maximum water uptake decreased in an almost linear fashion with the thickness and this was linked with a decrease in water diffusion rate. Moreover, the effect of the fiber orientation was also studied. It was observed that the diffusion rate and saturation weight increased as a function of fiber orientation, for example, an increase of approx. 48% in water diffusion rate for the 45° sample compared to the 0° one, as well as an increase in approx. 45% in saturation weight (Chilali et al. 2017).

Moisture diffusion in fiber-reinforced polymer composites has been reported to follow different mechanisms. Generally, the fiber swells as it absorbs water, which ultimately leads to fiber/matrix interface debonding. However, if there are preferential moisture absorption directions, for example, if synthetic (hydrophobic) fiber fabrics are on the outside of a natural/synthetic composite, the moisture diffusion modes will vary. Three main moisture diffusion modes have been reported: through the thickness direction, through the fiber direction, and through 3D water diffusion (Chilali et al. 2017). The first mode is characterized by water molecule diffusion inside micro-cavities, porosities, and defects as well as capillarity through micro-cracks existing in the matrix. Water molecules then arrive at the fiber-matrix interface and subsequently begin to infiltrate the hydrophilic components of the natural fiber as well as filling fabrication voids. The second mode is characterized by water molecule diffusivity by capillarity through micro-cracks present in the fiber-matrix interface and lumen parts that are not completely covered by the resin. This mode has been reported to generate higher fiber swelling as well as moisture content at saturation. Finally, the third mode is governed by the thinner dimension (generally thickness). When this dimension is the thickness, water molecules diffuse mostly by the first mode but also along the warp and weft directions due to edge effects. When the thinner dimension is either length or width, the primary mode is the second mode followed by edge effect influences in the thickness direction. In general, moisture diffusion in a composite depends on a variety of parameters such as fiber volume fraction, voids, temperature, fiber orientation and stacking sequence, fiber nature, presence of fillers, fiber surface treatments, and immersion time. Higher immersion times, natural fiber volume fraction, and voids as well as temperature will increase composite moisture uptake (Maslinda et al. 2017). On the other hand, fiber stacking sequence and orientation (i.e., hydrophobic fiber fabrics on the outer layers, as well as 0° orientation of the natural fiber), higher volume of hydrophobic filler materials, and chemical fiber surface treatments lower the water uptake of the composites (Prasad et al. 2018; Cheng et al. 2020; Manteghi et al. 2017).

Moisture Absorption Behavior of Epoxy/Natural/Synthetic Fiber-Reinforced Polymer Composites

Epoxy natural/synthetic hybrid composites with the combinations of glass, Kevlar, and carbon as synthetic fibers and flax, hemp, banana, kenaf, jute, sisal, and many others as a natural fiber were studied by several researchers (Braga et al. 2015;

Saidane et al. 2016; Al-Hajaj et al. 2018; Calabrese et al. 2019; Sujon et al. 2020). The glass fiber is the most used synthetic fiber in combination with other natural fibers for the hybrid composites. The main reasons for this are the good capability of glass fibers to resist various weathering conditions and that they are economically feasible and have low moisture absorption capability and high dimensional stability.

Braga and Magalhaes 2015, studied the water absorption regarding hybrid jute and glass fiber-reinforced epoxy composites. The fabricated composites were laminated with different weight ratios: 69/31/0 (E69-J31-V0), 68/25/7 (E68-J25-V7), and 64/18/19 (E64-J18-V19). They found that higher water absorption was linked with an increase with natural fiber content, while the opposite trend was observed for synthetic fiber content. The E69-J31-V0 presented a moisture uptake of 15.8%, while E68-J25-V7 and E64-J18-V19 cases 13.7% and 11.7%.

Al-Hajaj et al. 2018, studied hybrid epoxy/natural/synthetic composite fabricated from two distinct configurations of four harness satin woven carbon fibers and flax fibers in an epoxy matrix (Type A configuration: ($[0\text{-}90_{C2}/0_{F12}/0\text{-}90_{C2}]$) of four harness satin woven carbon fibers (i.e., fiber bundle alternating in a 3:1 under weave with orientation at 0° and 90°) plus "unidirectional" flax fibers and Type B configuration (i.e., $[0\text{-}90_{C2}/\pm45_{F6S}/0\text{-}90_{C2}]$) of four harness satin woven carbon and ±45° alternating flax fibers). Figure 7 shows the water absorption analysis graph for the two types of hybrid composites investigated. It can be seen that the water absorption decreased when Type A is compared with B composite (the water absorption in percentage by weight for Type A was 4.84 compared to Type B which was 8.32%). Also, the diffusion coefficient of Type A was lower

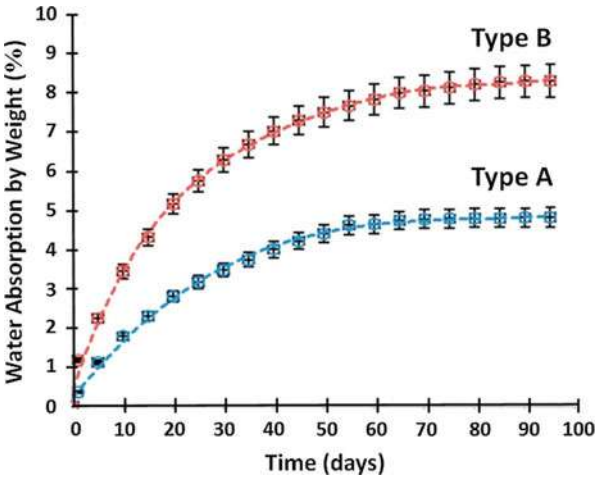

Fig. 7 Water absorption analysis graph for hybrid composites made of carbon fibers and flax fibers in an epoxy matrix. Type A configuration: ($[0\text{-}90_{C2}/0_{F12}/0\text{-}90_{C2}]$) of four harness satin woven carbon fibers (i.e., fiber bundle alternating in a 3:1 under weave with orientation at 0° and 90°) plus "unidirectional" flax fibers and Type B configuration (i.e., $[0\text{-}90_{C2}/\pm45_{F6S}/0\text{-}90_{C2}]$) of four harness satin woven carbon and ±45° alternating flax fibers). (Reproduced with permission from Al-Hajaj et al. 2018)

(3.65 × 10–13) compared to Type B (6.36 × 10–13 m^2/s). It was concluded that by shielding the inner natural fiber core with an external synthetic fiber layer, the water absorption was maintained to 4.8–8.3%.

Sujon et al. 2020 investigated the effect of fiber orientation and stacking sequence on the water absorption of jute/carbon epoxy hybrid composites. Four different stacking sequences and three different fiber orientations were studied. Fig. 8 shows an example of representative water absorption curves of hybrid composites as a function of fiber orientation (i.e., unidirectional, angle-ply, and cross-ply) (Sujon et al. 2020). It was found that the natural core of six layers of jute fiber enveloped by two layers of carbon fiber on both sides (C2J6C2) presented the lowest amount of water absorption rate (3.8%), while the most significant water absorption rates were found for the angle-ply (S5) 6.16% and cross-ply (S9) 5.9% cases, respectively. The

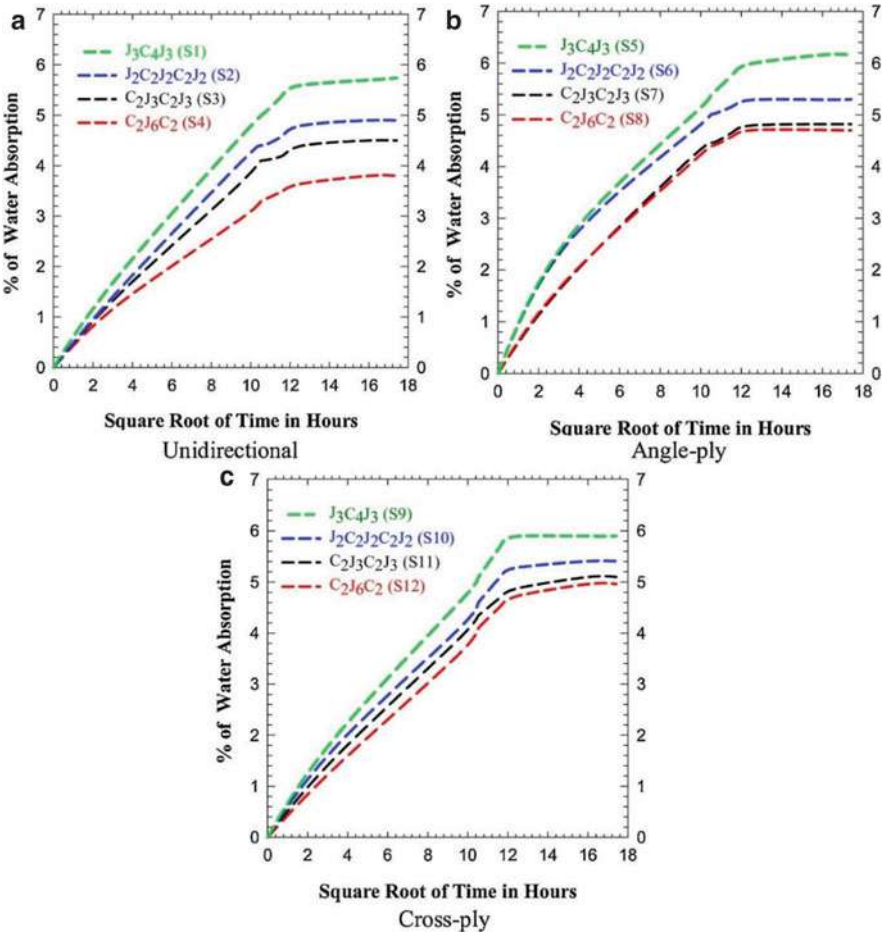

Fig. 8 Water absorption curve: (**a**) unidirectional, (**b**) angle-ply, and (**c**) cross-ply hybrid composites. (Reproduced with permission from Sujon et al. (2020))

authors concluded that by using different fiber orientations in the hybrid composites, only a small variation in the moisture uptake was observed.

El-Baky and Attia investigated the water absorption effect on the in-plane shear properties of jute-glass-carbon-reinforced composites. Bidirectional plain weave jute fabrics were used along with chopped glass mats and twill weave carbon fabrics as reinforcement fibers. The hand lay-up process was used to manufacture the composites, and the stacking sequence was varied. Both distilled water and seawater were used. Nine different stacking sequences were studied, including the neat jute (J6), glass (G6), and interplay hybrids such as GJG (GJJJJG) and JGJ (JGGGGJ) among others. Immersion time was up to 60 days. As expected, the highest water uptake was for the neat jute case and the lowest for the hybrid synthetic case (CGC). The natural/synthetic hybridization presented significant water uptake decrease. The application of synthetic layers on the outer layers of the natural/synthetic composite yielded moisture uptake decreases of approx. 5% and 7% when the GJG and CJC cases are compared to the J6 case, respectively. The behavior for distilled and seawater was similar (El-Baky and Attia 2019).

Akil et al. studied the effect of water absorption on the mechanical behavior of pultruded jute/glass fiber-reinforced polyester composites. Jute fibers (J), glass roving (G), and chopped strand mat (C) were used along with a protection surface veil for a specific configuration (S) made of polyester fibers. Unidirectional jute/glass fiber thermoset composites were fabricated via a pultrusion machine. The following stacking sequences were studied: JJ, GJJG, CGJJGC, and SGJJGS. The water absorption behavior was significantly improved by the hybridization technique. The neat jute case presented a water absorption at saturation of 47.65%, while the GJJG case presented a saturation content of 13.31%, representing one of the most significant decreases in moisture uptake as a function of synthetic hybridization in the available literature. A further decrease of approx. 5% was observed for the chopped mat case, while a slight increase of 9% was found for the polyester fiber surface case, when compared to the GJJG case, respectively (Akil et al. 2014).

In summary, the hybridization technique of natural fiber composites with either synthetic or other natural fibers that present lower water absorption capabilities is a proficient alternative in order to reduce moisture ingress within the fabricated composites. Particularly, synthetic fibers may be set up in such a way that a more random closely packed structure is formed, further hindering water molecule diffusion within the composite. This helps to prevent the contact of the water molecules with the hydrophilic groups present in the natural fibers as well as composite fabrication voids.

In addition to hybridization, other solutions to control the hydrophilicity of natural fibers were studied in the literature, such as fiber treatments (i.e., alkalization, acetylation, bleaching, grafting, or coating) (Banea et al. 2021). Other methods employed to improve fiber/matrix interfacial adhesion consist in the application of binding solutions including silanes, maleated polypropylene (MAPP), and titanates (Mokhothu and John 2017).

Another way to decrease the effect of water absorption in composites is to incorporate synthetic fillers which can fill the voids and better distribute the internal

stresses in the composites (Alamri and Low 2012; Prasad et al. 2018). For example, the inclusion of metal oxide particles within the structure of natural fiber composites improves their humidity absorption and swelling properties due to the increased capability of hydrophobic metal oxides to bond with hydrophobic polymers. Several researchers have investigated the effects of the incorporation of TiO_2 nanofiller and glass powder in the polymer matrix with the objective of delaying the effect of water absorption on composites (Pinto et al. 2015; Prasad et al. 2018). Prasad et al. 2018, analyzed the influence of TiO_2 nanofiller on the durability behavior of flax epoxy composites. It was found that the addition of nano-TiO_2 in the matrix lowers the water absorption tendency. The diffusion coefficient was decreased by 31.66% for nano-TiO_2-modified flax fiber composite when compared to the unmodified case.

Recently, Nath et al. investigated the effect of moisture absorption on the mechanical properties of jute epoxy composites reinforced with cenosphere fillers. Plain weave jute fabrics were used along with an epoxy resin and micro-cenosphere filler. The hand lay-up fabrication method was used with the aid of a wooden mold. The number of jute mats was varied, i.e., 2, 3, 4, and 5, as well as the weight percentage of filler material, i.e., 0, 5, and 10%. As expected, inverse trends of moisture uptake were found by the increase of natural fiber loading and mineral filler loading. In other words, the higher the weight percent of naturel fiber, the higher the moisture uptake at equilibrium. In contrast, the lowest moisture uptake was recorded for the highest mineral filler loading, i.e., the 10% case. The water uptake behavior was non-Fickian for all cases (Nath et al. 2019).

Prasob and Sasikumar investigated the effect of ZnO and TiO_2 fillers in the dynamic behavior of jute/epoxy composites at different temperatures. Bidirectional plain weave jute fabrics were used as reinforcement along with an epoxy resin. Both fillers were nanoscale. The fillers were initially microscale and were decreased in scale by the ball milling technique. The filler weight fractions studied were 2, 4, and 6%. The fillers were stirred with the neat resin prior to application on the jute fabrics. Hand lay-up method was used. A significant water absorption decrease as a function of filler loading was observed. The lowest moisture uptake reported was for the 6 wt % ZnO case, presenting a water uptake decrease of 214% when compared to the unfilled case. The behavior was non-Fickian (Prasob and Sasikumar 2018).

Swain et al. studied the influence of fiber surface treatments on the durability properties of aluminum oxide-filled jute/epoxy composites. Commercially available jute bidirectional fabrics along with micro-aluminum oxide and epoxy resin were used. The fibers were treated with alkali and benzoyl solutions in separate groups. The filler was manually mixed into the neat resin, and the hand lay-up technique was used. Filler and fiber loading were varied, i.e., 5 and 10 wt. % of filler and 10, 20, 30, and 40 wt. % of fiber. Chemical treatment and filler loading presented significant effects in diminishing the moisture uptake at saturation. For the untreated cases with 5% filler loading, an increase in fiber loading promoted an increase in moisture uptake quasi-linearly. On the other hand, at lowest fiber loading (10%), for the 5% filler content, both chemical treatments presented the same water uptake. For the highest fiber loading (40%), the benzoyl treatment presented lower moisture uptake compared to the alkali treatment. For the 10% filler content cases, the untreated fiber

composites presented identical water uptake trends compared to the 5% content cases. However, for the alkali treated fibers and 10% filler content, the 40% fiber loading case presented the highest moisture uptake, but all the other cases presented essentially identical trends (Swain and Biswas 2017).

Furthermore, the role of these fillers, when they are applied alongside other treatments such as chemical and physical, is significant as they perform many tasks at the interface. For example, they enhance the mechanical interaction via the increase of surface roughness of the natural fibers and generate improvements in the water barrier properties of natural composites by providing additional indirect paths that decrease the water absorption into the composite structure. Consequently, a general decrease in the water penetration is achieved, as well as the removal of air gaps and voids that result from the poor hydrophilic fiber/hydrophobic matrix compatibility by modifying them with fillers (Mohan and Kanny 2011; Alamri and Low 2012).

Table 2 presents a summary of some recent studies on the water absorption behavior of hybrid composites.

Effect of Water Sorption on the Mechanical Properties of Epoxy/Natural/Synthetic Fiber-Reinforced Polymer Composites

The water and solvent sorption alter the physical and mechanical properties of the composites and significantly compromise their performance. In most of the cases, a negative impact on the mechanical properties of composite materials by increasing the quantity of water/solvent sorption was found. However, some researchers found positive influence for the composite having lower percentage of moisture content. The degree of degradation that takes place in a fiber-reinforced polymer composite is directly related to the amount of moisture that is absorbed by the fiber and the epoxy resin.

Mechanical properties of epoxy/synthetic/natural fiber composites were evaluated in the literature through experimental studies, with different combination of materials and exposure conditions (Venkateshwaran et al. 2011; Maslinda et al. 2017). It was shown that the main causes for strength reduction with the moisture absorption are weakening of bonding between the fiber and matrix, swelling of fibers especially for natural fiber, softening of matrix, crack produced in matrix, local strain due to different coefficients of expansion of fiber and matrix, etc. (Ray 2006; Ridzuan et al. 2016; Chaudhary et al. 2020). Consequently, the degradation level depends on the exposure time, exposure condition, type of matrix, and type of natural and synthetic fiber used, among others.

The hybrid composites show some positive influence of moisture on the mechanical properties, especially for natural-natural and natural-synthetic hybrid composites (Muñoz and García-Manrique 2015; Maslinda et al. 2017). The impacts of moisture on the natural-epoxy composite material and synthetic-epoxy composite material are quite different as both the natural and synthetic fibers absorb different quantities of moisture level. Very little moisture is absorbed by the synthetic fiber

Table 2 Water absorption behavior of hybrid epoxy composites

Composite	Details of the process	Water absorption	Ref.
Jute/banana	Commercially available jute fabric was used as well as manually woven banana fabrics (BF) Hand lay-up fabrication technique	The different fibers present different water absorption behaviors. BF composites absorb the least amount of water. The stacking sequence was also observed to be important in the water absorption, with the BJB case presenting lower water absorption than the JBJ case	Venkateshwaran and Perumal 2012
H/J/epoxy H/F/epoxy H/J/F/epoxy	Woven bidirectional mats of hemp, jute, and flax were used. Epoxy resin was used along with the hand lay-up compression fabrication technique	The fibers present different moisture uptake behaviors. The flax/epoxy case absorbed the smallest amount of moisture (1.8%). The addition of jute and hemp increased the water absorption by up to 3% for the jute/hemp/flax case	Chaudhary et al. 2020
Date palm leaf (DPL)/ glass	Short DPL fibers were treated with NaOH (1%) and washed with distilled water. Short E-glass fibers were used. Epoxy resin was mixed with the fibers, and the hand lay-up technique was used along with dead weight compression molding	Composite water absorption was significantly affected as a function of DPL fiber content Most significant water uptake was reported for the 30 wt % DPL case	Swain et al. 2020
Jute/glass	Jute and glass fiber fabrics were used along with the hand lay-up technique. Open mold room temperature curing. Epoxy resin, jute, and glass fiber weight ratios were varied	The smallest amount of water uptake at saturation was reported for the hybrid composite with a 64/18/19 (resin/jute/glass) ratio (11.7% after 1172 h immersion in water)	Braga et al. 2015
Flax/glass	Glass and flax fiber plates were fabricated via the compression molding technique. Four layers of glass (2 on each side) and a core of 12 layers of flax were used. The glass layers were unidirectional, while for the flax core, both a unidirectional plate and a ± 45-degree orientation plate were fabricated	The orientation of the flax fiber core had a significant effect in the water absorption behavior. The unidirectional flax/glass/ epoxy composite presented a lower moisture uptake (4.6%) after 40 days compared to the ±45-degree orientation case (6%)	Manteghi et al. 2017

(continued)

Table 2 (continued)

Composite	Details of the process	Water absorption	Ref.
Sugar palm fiber (SPF)/ glass	Long washed and dried SPF along with long E-glass fibers were used. Epoxy resin was used with the hand lay-up technique. Resin and fiber volume fraction was varied, and both benzoyl treated and untreated SPF composites were fabricated	The benzoyl treated SPF composites presented more moisture uptake than the untreated case. It was linked to lignin and polysaccharide degradation due to the treatment. The glass fiber hybridization significantly decreased the water uptake	Safri et al. 2020
Kenaf/PET fiber	Manually interwoven kenaf/ PET fabric. Composite fabrication via vacuum infusion. Weight percentage composition of epoxy, kenaf, and PET: 70/15/15 and 60/20/20	Maximum water absorption was observed for the 70/15/ 15 case (approx. 4%)	Dan-Mallam et al. 2015
Flax/TiO_2	Flax plain weave bidirectional fabric was used along with nano-titanium dioxide. Hand lay-up compression mold fabrication technique was used. The following filler weight percentages were studied: 0.5, 0.7, and 0.9	The addition of the nanofiller significantly decreased the water absorption. The diffusion coefficient was diminished by approx. 32%. Water absorption behavior was plateau-like for the 0.7 and 0.9%wt cases	Prasad et al. 2018
RCF/n-SiC	Recycled cellulose fiber (RCF) and nano-silicon carbide (n-SiC) materials were used Hand lay-up close mold room temperature cure process Nanofiller weight percentages studied: 1, 3, and 5%	Decrease in water absorption for higher nanofiller fractions was observed. The 5% n-SiC case presented the lowest water absorption compared to the unfilled case (approx. 47%)	Alamri and Low 2012
Sisal/ micro−/ nanoclay	VARIM composite fabrication technique was used. Nano- and microclay were mixed to the resin via a magnetic stirrer. Filler weight percentages used were 1, 3, and 5 for nanoclay and only 5% for microclay	The water absorption continually and significantly decreases as a function of nanoclay fraction. The 5% case presented a threefold decrease compared to the unfilled case The equilibrium water content was higher for the macroscale filled case; however, the diffusivity did not vary as a function of filler scale	Mohan et al. 2011

(continued)

Table 2 (continued)

Composite	Details of the process	Water absorption	Ref.
Luffa/coir/SiO_2 nanospheres	Epoxy matrix was used along SiO_2 nanospheres and luffa and coir fibers. The luffa fiber was macroscale reinforcement, while the coir was pulverized via milling into micro-sized fillers. The silica nanospheres were fabricated via the Stöber process. The individual reinforcement fraction was varied, but the total was kept at 40%. The fillers were homogenized via ultrasonication, and the fabrication process was dead weight closed molding	The water absorption characteristics of the composite were significantly affected by fiber and nanofiller reinforcement. The neat luffa/epoxy composite exhibited the highest water absorption (~8%). Decreasing luffa content and increasing coir led to a decrease in water uptake (approx. 3% for the L20-C20/E case). The SiO_2 nanospheres presented a highly significant water uptake decrease (0.14%)	Anbukarasi et al. 2019

(carbon, glass fiber, etc.) as it is hydrophobic in nature, while the natural fiber absorbs a large quantity of moisture as it is hydrophilic in nature.

Most of the researchers and scientists are in favor of the use of natural fiber composite materials over the synthetic composites as the natural fiber is easily available, cheap, light in weight, and most importantly environmentally friendly as it is biodegradable. However, the lower mechanical strength and large moisture absorption during the service period hamper their performance, which restricts the use in secondary application areas only. Most of the mechanical properties of moisture saturated natural composite materials are reduced when compared to the dry composite materials. The performance reduction is more severe with increasing the immersion time, as more water is absorbed. Matrix cracking, delamination, and voids increase the penetration of water and fiber swelling and weakening of the interface between the fiber and matrix are the possible causes for the poor performance (Wang et al. 2006). During the moisture absorption, the natural fiber-reinforced composites absorbed more water and swelling takes place and this swelling of the fiber changes the dimension of the composite and micro-cracks start to nucleate on the matrix (Maslinda et al. 2017). On the other hand, very few researchers found the positive effect of water absorption on the mechanical performance of the composite materials. Munoz et al. found that water-immersed (768 h in water) specimens presented higher tensile strength compared to the dry samples. This behavior was linked to the swelling of the fibers as a result of the water absorption in high percentages. Another explanation was that the cavities between the fiber and the matrix that may form during manufacturing process due to a poor impregnation or the shrinkage of the resin during cure were filled up and all this can eventually lead to an improvement of the mechanical properties (Muñoz and García-Manrique 2015). Similar results were found by Dhakal et al., where increments in

the strength after a period of water immersion compared to the specimens without water absorption were also observed (Dhakal et al. 2007). The authors also state that this behavior might be due to the filling up of the gaps between fiber and the matrix, as a result of the swelling of the fiber.

Lignin acts to protect the fibers from moisture degradation owing to its hydrophobic features, and, in theory, fiber-reinforced composites containing higher lignin content as a filler should present increased resistance to moisture absorption. Consequently, the selection of natural fiber of hybridization should be the one with the higher lignin content which makes barrier for the water. For composites that are exposed to humidity for long periods, a brittle epoxy resin may experience microcracking due to the swelling tendency of the fibers. As a consequence, the interface is continuously attacked due to the preferential path of the water molecules via capillary cracks, which will ultimately result in debonding the fiber from the matrix.

The poor interfacial adhesion is one of the prime causes for the degradation of composite even in hybrid composite materials. Structural defects such as delamination, matrix cracking, and voids increase the ability of hybrid composites to absorb moisture and decrease the strength of the moisture-saturated composite due to the degradation of the interface between the matrix and fiber (Maslinda et al. 2017). The most significant parameters responsible for the structural failure in hybrid composites are the content of porosity and air voids.

Calabrese et al. 2019 investigated the effect of glass fiber hybridization on the durability characteristics of flax fiber-reinforced epoxy composites and glass/flax hybrid composites. They found that the glass fibers had a significant role on the water absorption behavior in the composites. The water absorption for the flax fiber-reinforced composites was 12 times higher than the glass fiber-reinforced composites.

Ramesh et al. 2016 found that the sisal/jute/glass epoxy composites present better tensile strength, flexural strength, impact strength, and water absorption characteristics than single natural fiber for either sisal or jute fiber reinforced with glass fiber composites (Ramesh et al. 2016). The hybridization method was shown to improve the in-plane shear properties of both dry and saturated composites.

Shrivastava et al. studied the effect of moisture absorption on the performance of coconut-glass fiber epoxy hybrid composites. It was found that increasing the coconut coir fiber content in the composite specimen increases the water absorption (Shrivastava et al. 2017). Through proper fiber selection in the hybrid composites and design, a balance between moisture absorption, strength, cost, and performance of hybrid composites could be achieved through hybridization. Therefore, the higher the content of synthetic hydrophobic fiber in a hybrid natural composite, the lower the content and absorption speed of moisture will be.

Saidane et al. 2016 also found that the hybridization of flax-epoxy composites with glass fiber sensibly diminished the moisture uptake and diffusion coefficient. The flax-glass fiber hybrid composites presented improvements of the tensile properties under hygrothermal environment at relatively low temperatures but had a deleterious effect on tensile properties at high temperatures.

The diffusion of water molecules into the structure of a hybrid composite is responsible for different types of failures taking place mainly due to natural fiber swelling, which lead to swelling-related stresses and composite failure. Other significant effects are also present owing to the moisture absorption such as the decrease of the fiber/matrix interfacial bond strength, diminishing of the natural fiber stiffness, stress corrosion of synthetic fibers, as well as the plasticization of the polymer matrix (Akil et al. 2014). Water absorption also initiate the delamination between the glass and flax fiber layers, which will ultimately lead to an overall reduction in the maximum tensile strength of the saturated composite (Saidane et al. 2016). On the other hand, it has also been reported that the ductility of the hybrid composites increases in certain cases due to the penetration of water molecules within composite defects such as cracks and cavities (Ghani et al. 2012).

Conclusion

This chapter reviewed the state of knowledge regarding the main characteristics of water and solvent sorption and its effects on the behavior of epoxy/natural/synthetic fiber-reinforced polymer composites. During their service life, composite materials are exposed to different environments (e.g., wet or humid), which results in substantial water uptake. The absorbed humidity changes the physical, thermal, and mechanical properties of composites and consequently compromises their performance. It was shown that moisture absorption increases with increased fiber content and temperature. Also, it is influenced by fiber treatment/coupling agent and fiber arrangement. In general, the presence of natural fibers in the composite increases the moisture absorption of the composite. The water absorption produces swelling of natural fiber-reinforced composites and decreases their mechanical properties, with the exception of impact properties which are usually found to increase.

There are various models available in the literature to describe the kinetics of water sorption into epoxy resins and their hybrid composites. These models vary from simple Fickian models to more elaborate methodologies that account for anomalous (i.e., non-Fickian) moisture sorption. However, for the sorption models that account for non-Fickian effects, the dependence of the model parameters on the material micro- or nanostructure has not been completely investigated. Usually, these coefficients are obtained as curve fitting parameters to reproduce experimentally the moisture absorption curves. Thus, there is little or no fundamental physical insight into what these parameters represent and how their values change as the polymer resin or composite microstructure changes. It should be stressed that these parameters should be associated to the composite constituents and the volume fraction of the reinforcements in addition to the type of the resin.

Hybridization of composites received popularity due to the improved performance of the resulting composite materials, and the biggest benefit is to overcome the limitation that hurdles the applicability of natural fiber-reinforced composites in structural applications. Hybridization of natural fiber composites with conventional synthetic fiber is a big step from an economical viewpoint. However, the quality of

the natural fibers such as percentage of cellulose, lignin, and other components, which depend on the growth conditions and maturity, still brings inconsistency in the resulting properties of hybrid composites such as moisture absorption, mechanical and physical performance, etc. Without a doubt, research on the treatments and control over the quality of natural fibers can revolutionize their commercialization and practical applications. In addition, using a second reinforcement such as fillers in either micro- or nano-size can improve the composites' durability. Finally, with improvements in durability studies on hybrid synthetic/natural composites, there is a huge potential for these materials to succeed in commercial markets in the future.

Chemical diffusion between composites and solvents is a less investigated subject in the available literature, and this topic needs to be studied in the future.

References

H.M. Akil, C. Santulli, F. Sarasini, J. Tirillò, T. Valente, Environmental effects on the mechanical behaviour of pultruded jute/glass fiber-reinforced polyester hybrid composites. Compos. Sci. Technol. **94**, 62–70 (2014)

H. Alamri, I.M. Low, Effect of water absorption on the mechanical properties of n-SiC filled recycled cellulose fiber reinforced epoxy eco-nanocomposites. Polym. Test. **31**(6), 810–818 (2012). https://doi.org/10.1016/j.polymertesting.2012.06.001

Z. Al-Hajaj, R. Zdero, H. Bougherara, Mechanical, morphological, and water absorption properties of a new hybrid composite material made from 4 harness satin woven carbon fibers and flax fibers in an epoxy matrix. Compos. A: Appl. Sci. Manuf. **115**, 46–56 (2018) https://doi.org/10.1016/j.compositesa.2018.09.015

K. Anbukarasi, S.I. Hussain, A.A. Roseline, S. Kalaiselvam, Effect of SiO2 nanospheres on mechanical, thermal and water absorption behaviours of luffa-coir/epoxy hybrid composites. Mater. Res. Express **6**, 125618 (2019)

A. Apicella, R. Tessieri, C. de Cataldis, Sorption modes of water in glassy epoxies. J. Membr. Sci. **18**, 211–225 (1984). https://doi.org/10.1016/S0376-7388(00)85035-8

Z. Azwa, B. Yousif, A. Manalo, W. Karunasena, A review on the degradability of polymeric composites based on natural fibers. Mater. Design **47**, 424–442 (2013)

M.D. Banea, J.S.S. Neto, D.K.K. Cavalcanti, in *Recent Trends in Surface Modification of Natural Fibers for Their Use in Green Composites*, Green Composites, ed. by S. Thomas, P. Balakrishnan, (Springer Singapore, Singapore, 2021), pp. 329–350. https://doi.org/10.1007/978-981-15-9643-8_12

L.R. Bao, A.F. Yee, Moisture diffusion and hygrothermal aging in bismaleimide matrix carbon fiber composites: Part I-Uni-weave composites. Compos. Sci. Technol. **62**, 2099–2110 (2002a)

L.R. Bao, A.F. Yee, Moisture diffusion and hygrothermal aging in bismaleimide matrix carbon fiber composites: Part II-woven and hybrid composites. Compos. Sci. Technol. **62**, 2111–2119 (2002b)

E. Barjasteh, S.R. Nutt, Moisture absorption of unidirectional hybrid composites. Compos. A: Appl. Sci. Manuf. **43**, 158–164 (2012)

D.A. Bond, Moisture diffusion in a fiber-reinforced composite: Part I – Non-Fickian transport and the effect of fiber spatial distribution. J. Compos. Mater. **39**(23), 2113–2141 (2005)

P. Bonniau, A.R. Bunsell, A comparative study of water absorption theories applied to glass epoxy composites in Springer GS Chapter 18, in *Environmental Effects on Composite Materials*, vol. 2, (Technomic Publishers, Lancaster, 1984)

R.A. Braga, P.A.A. Magalhaes Jr., Analysis of the mechanical and thermal properties of jute and glass fiber as reinforcement epoxy hybrid composites. Mater. Sci. Eng. C **56**, 269–273 (2015)

S. Budhe, S. de Barros, M.D. Banea, Theoretical assessment of the elastic modulus of natural fiber-based intra-ply hybrid composites. J. Braz. Soc. Mech. Sci. Eng. **41**(6), 263 (2019) https://doi.org/10.1007/s40430-019-1766-z

L. Calabrese, V. Fiore, T. Scalici, A. Valenza, Experimental assessment of the improved properties during aging of flax/glass hybrid composite laminates for marine applications. J. Appl. Polym. Sci. **136**(14), 47203 (2019) https://doi.org/10.1002/app.47203

D.K.K. Cavalcanti, M.D. Banea, J.S.S. Neto, R.A.A. Lima, Comparative analysis of the mechanical and thermal properties of polyester and epoxy natural fiber-reinforced hybrid composites. J. Compos. Mater. **55**, 1683–1692 (2021). https://doi.org/10.1177/0021998320976811

D.K.K. Cavalcanti, M.D. Banea, J.S.S. Neto, R.A.A. Lima, L.F.M. da Silva, R.J.C. Carbas, Mechanical characterization of intralaminar natural fiber-reinforced hybrid composites. Compos. Part B **175**, 107149 (2019). https://doi.org/10.1016/j.compositesb.2019.107149

V. Chaudhary, P.K. Bajpai, S. Maheshwari, Effect of moisture absorption on the mechanical performance of natural fiber reinforced woven hybrid bio-composites. J. Nat. Fibers **17**, 84–100 (2020)

M. Cheng, Z. Zhong, U. Kureemun, D. Cao, H. Hu, H.P. Lee, S. Li, Environmental durability of carbon/flax fiber hybrid composites. Compos. Struct. **234**, 111719 (2020)

A. Chilali, M. Assarar, W. Zouari, H. Kebir, R. Ayad, Effect of geometric dimensions and fibre orientation on 3D moisture diffusion in flax fibre reinforced thermoplastic and thermosetting composites. Compos. Part A **95**, 75–86 (2017)

Y.M. Chiang, P. Dunbar, W. Birnie, D. Kingery, *Physical Ceramics: Principles for Ceramic Science and Engineering* (Wiley, New York, 1996) ISBN: 978-0-471-59873

Y. Dan-Mallam, H.T. Wei, M.S. Abdul Majid, Mechanical characterization and water absorption behaviour of interwoven kenaf/PET fiber reinforced epoxy hybrid composite. Int. J. Polym. Sci. **4**, 1–13 (2015)

H.F.M. de Queiroz, M.D. Banea, D.K.K. Cavalcanti, Experimental analysis of adhesively bonded joints in synthetic- and natural fiber-reinforced polymer composites. J. Compos. Mater. **54**(9), 1245–1255 (2020). https://doi.org/10.1177/0021998319876979

H.N. Dhakal, Z.Y. Zhang, M.O.W. Richardson, Effect of water absorption on the mechanical properties of hemp fiber reinforced unsaturated polyester composites. Compos. Sci. Technol. **67**(7–8), 1674–1683 (2007)

A. El-baky, M.A. Attia, Water absorption effect on the in-plane shear properties of jute–glass–carbon-reinforced composites using Iosipescu test. J. Compos. Mater. **53**, 3033–33045 (2019)

A. Fick, Ueber diffusion. Ann. Phys. **170**, 59–86 (1855) https://doi.org/10.1002/andp.18551700105

C. Gao, C. Zhou, Moisture absorption and cyclic absorption–desorption characters of fiber-reinforced epoxy composites. J. Mater. Sci. **54**, 8289–8301 (2019)

M. Ghani, Z. Salleh, K.M. Hyie, M. Berhan, Y. Taib, M. Bakri, Mechanical properties of kenaf/fiberglass polyester hybrid composite. Procedia Eng. **41**, 1654–1659 (2012)

J. Giridhar, Kishore, R.M.V.G. Rao, Moisture absorption characteristics of natural fiber composites. J. Reinf. Plast. Compos. **5**(2), 141–150 (1986). https://doi.org/10.1177/073168448600500205

M.E. Gurtin, C. Yatomi, On a model for two phase diffusion in composite materials. J. Compos. Mater. **13**(2), 126–130 (1979)

Z. Huo, V. Bheemreddy, K. Chandrashekhar, R.A. Brack, Modelling of concentration-dependent moisture diffusion in hybrid fiber-reinforced polymer composites. J. Compos. Mater., 1–10 (2014)

D. Jain, S. Harpreet, T.K. Bera, R. Jain, Comparison of different hydrophobic treatments for the durability improvement of Palmyra natural fiber composites under hydrothermal ageing environments. J. Nat. Fibers **17**, 1668–1682 (2019a)

D. Jain, I. Kamboj, T.K. Bera, A.S. Kang, R.K. Singla, Experimental and numerical investigations on the effect of alkaline hornification on the hydrothermal ageing of agave natural fiber composites. Int. J. Heat Mass Transf. **130**, 431–439 (2019b)

Y. Joliff, W. Rekik, L. Belec, J.F. Chailan, Study of the moisture/stress effects on glass fiber/epoxy composite and the impact of the interphase area. Compos. Struct. **108**, 876–885 (2014)
R. Lima, D. Cavalcanti, J. de Souza, H. da Costa, M.D. Banea, Effect of surface treatments on interfacial properties of natural intralaminar hybrid composites. Polym. Compos. **41**(1), 314–325 (2020). https://doi.org/10.1002/pc.25371
A.C. Loos, G.S. Springer, Moisture absorption of polyester-E glass composites, in *Environmental Effects on Composite Materials*, ed. by G. S. Springer, (Technomic Publishing Co. Inc., Westport, 1981), pp. 51–62
S. Manteghi, Z. Mahboob, Z. Fawaz, H. Bougherara, Investigation of the mechanical properties and failure modes of hybrid natural fiber composites for potential bone fracture fixation plates. J. Mech. Behav. Biomed. Mater. **65**, 306–316 (2017)
L.L. Marsh, R. Lasky, D.P. Seraphim, G.S. Springer, in *Environmental Effects on Composite Materials, 3*, ed. by G. S. Springer, (Technomic Publishing Co, Westport, 1988), p. 51
M.S. Maslinda, A. Majid, M.J.M. Ridzuan, M. Afendi, A.G. Gibson, Effect of water absorption on the mechanical properties of hybrid interwoven cellulosic-cellulosic fiber reinforced epoxy composites. Compos. Struct. **167**, 227–237 (2017)
M.J. Mochane, T.C. Mokhena, T.H. Mokhothu, A. Mtibe, E.R. Sadiku, S.S. Ray, I.D. Ibrahim, O.O. Daramola, Recent progress on natural fiber hybrid composites for advanced applications: A review. eXPRESS. Polym. Lett. **13**(2), 159–198 (2019)
T.P. Mohan, K. Kanny, Water barrier properties of nanoclay filled sisal fiber reinforced epoxy composites. Compos. A: Appl. Sci. Manuf. **42**(4), 385–393 (2011)
T.H. Mokhothu, M.J. John, Bio-based coatings for reducing water sorption in natural fiber reinforced composites. Sci. Rep. **7**, 133351–133358 (2017) https://doi.org/10.1038/s41598-017-13859-2
E. Muñoz, J.A. García-Manrique, Water absorption behaviour and its effect on the mechanical properties of flax fiber reinforced bioepoxy composites. Int. J. Polym. Sci. **6**, 1–10 (2015)
S. Nath, H. Jena, S.D. Priyanka, Analysis of mechanical properties of jute epoxy composite with cenosphere filler. SILICON **11**, 645–671 (2019)
J. Neto, R. Lima, D. Cavalcanti, J. Souza, R. Aguiar, M. Banea, Effect of chemical treatment on the thermal properties of hybrid natural fiber-reinforced composites. J. Appl. Polym. Sci. **136**(10), 47154 (2019)
Y. Pan, G. Xian, H. Li, Numerical modeling of moisture diffusion in an unidirectional fiber-reinforced polymer composite. Polym. Compos. **40**, 401–413 (2019)
K.L. Pickering, M.A. Efendy, T.M. Le, A review of recent developments in natural fiber composites and their mechanical performance. Compos. A: Appl. Sci. Manuf. **83**, 98–112 (2016)
D. Pinto, L. Bernardo, A. Amaro, S. Lopes, Mechanical properties of epoxy nanocomposites using titanium dioxide as reinforcement–a review. Constr. Build. Mater. **95**, 506–524 (2015)
V. Prasad, M.A. Joseph, K. Sekar, Investigation of mechanical, thermal and water absorption properties of flax fiber reinforced epoxy composite with nano TiO2 addition. Compos. A: Appl. Sci. Manuf. **115**, 360–370 (2018)
P.A. Prasob, M. Sasikumar, Static and dynamic behavior of jute/epoxy composites with ZnO and TiO2 fillers at different temperature conditions. Polym. Test. **69**, 52–62 (2018)
M. Ramesh, K. Palanikumar, H.K. Reddy, Evaluation of mechanical and interfacial properties of sisal/jute/glass hybrid fiber reinforced polymer composites. Trans. Indian Inst. Metals **69**, 1851–1859 (2016)
B.C. Ray, Temperature effect during humid ageing on interfaces of glass and carbon fibers reinforced epoxy composites. J. Colloid Interface Sci. **298**, 111–117 (2006)
M.J.M. Ridzuan, M.S. Abdul Majid, M. Afendi, K. Azduwin, N.A.M. Amin, J.M. Zahri, A.G. Gibson, Moisture absorption and mechanical degradation of hybrid Pennisetum purpureum/glass–epoxy composites. Compos. Struct. **141**, 110–116 (2016)
S.N.A. Safri, M.T.H. Sultan, A.U.M. Shah, Characterization of benzoyl treated sugar palm/glass fiber hybrid composites. J. Mater. Res. Technol. **9**, 11563–11573 (2020)

E.H. Saidane, D. Scida, M. Assarar, H. Sabhi, R. Ayad, Hybridisation effect on diffusion kinetic and tensile mechanical behaviour of epoxy based flax–glass composites. Compos. A: Appl. Sci. Manuf. **87**, 153–160 (2016)

C.H. Shen, G.S. Springer, Moisture absorption and desorption of composite materials. J. Compos. Mater. **10**(1), 2–20 (1976)

R. Shrivastava, A. Telang, R.S. Rana, R. Purohit, Mechanical properties of coir/ Glass fiber epoxy resin hybrid composite 5th international conference of materials processing and characterization (ICMPC 2016). Mater. Today Proc. **4**, 3477–3483 (2017)

A.S. Sujon, M.A. Habib, M.Z. Abedin, Experimental investigation of the mechanical and water absorption properties on fiber stacking sequence and orientation of jute/carbon epoxy hybrid composites. J. Mater. Res. Technol. **9**(5), 10970–10981 (2020)

P.T.R. Swain, S.N. Das, P.K. Patnaik, A. Purohit, The influence of moisture absorption on the mechanical and thermal properties of chemically treated DPL reinforced hybrid composite. Mater. Sci. Forum **978**, 316–322 (2020)

P.T.R. Swain, S. Biswas, Influence of fiber surface treatments on physico-mechanical behaviour of jute/epoxy composites impregnated with aluminium oxide filler. J. Compos. Mater. **51**(21), 3909–3922 (2017)

K. Tabrej, M.T.H. Sultan, M. Jawaid, Physical performance of kenaf/jute mat reinforced epoxy hybrid composites. Int. J. Recent Technol. Eng. **8**, 448–452 (2019)

N. Venkateshwaran, A.E. Perumal, A. Alavudeen, M. Thiruchitrambalam, Mechanical and water absorption behaviour of banana/sisal reinforced hybrid composites. Mater. Des. **32**, 4017–4021 (2011)

N. Venkateshwaran, E. Perumal, Mechanical and water absorption properties of woven jute/banana hybrid composites. Fibers Polym. **13**, 907–914 (2012)

W. Wang, M. Sain, P. Cooper, Study of moisture absorption in natural fiber plastic composites. Compos. Sci. Technol. **66**, 379–386 (2006)

M. Woo, M.J. Piggott, Water absorption of resins and composites I: Epoxy homopolymers and copolymers. Compos. Technol. Res. **9**, 101 (1987)

Y. Xie, C.A. Hill, Z. Xiao, H. Militz, C. Mai, Silane coupling agents used for natural fiber/polymer composites: A review. Compos. Part A Appl. Sci. Manuf. **41**, 806–819 (2010)

K. Yorseng, S.M. Rangappa, J. Parameswaranpillai, S. Siengchin, Influence of accelerated weathering on the mechanical, fracture morphology, thermal stability, contact angle, and water absorption properties of natural fiber fabric-based epoxy hybrid composites. Polymers **12**(10), 2254 (2020)

J. Zhou, J.P. Lucas, The effects of a water environment on anomalous absorption behavior in graphite/epoxy composites. Compos. Sci. Technol. **53**, 57–64 (1995)

J. Zhou, J.P. Lucas, Hygrothermal effects of epoxy resin. Part I: The nature of water in epoxy. Polymer **40**, 5505–5512 (1999a)

J. Zhou, J.P. Lucas, Hygrothermal effects of epoxy resin. Part II: Variations of glass transition temperature. Polymer 40, 5513–5522 (1999b)

Miscellaneous Study on Epoxy/Synthetic/Natural Fiber Hybrid Composites

37

Lin Feng Ng

Contents

Abstract

The contemporary trend has attested that fiber-reinforced composites have been utilized to replace steel and other metal alloys in a broad range of engineering applications, particularly in the transportation sectors to improve energy efficiency without compromising safety performance. The intensive research works toward the excellent mechanical performance of composite materials without compromising the environmental friendliness have stimulated the growth of hybrid composites. The hybrid composites refer to the materials which are composed of multiple types of synthetic or natural fibers within a single polymer matrix. Over the years, it has been proven that hybrid composites have shown innumerable benefits over non-hybrid composite materials in terms of mechanical performance and ecological concerns. Nevertheless, the challenging issues which

L. F. Ng (✉)
Centre for Advanced Composite Materials (CACM), School of Mechanical Engineering, Faculty of Engineering, Universiti Teknologi Malaysia, Johor Bahru, Johor, Malaysia
e-mail: linfeng@utm.my

S. Mavinkere Rangappa et al. (eds.), *Handbook of Epoxy/Fiber Composites*,
https://doi.org/10.1007/978-981-19-3603-6_41

affect the miscellaneous properties of hybrid composite materials still exist and have not been fully resolved. This chapter aims at providing brief overview of the factors influencing the miscellaneous properties of composite materials. Furthermore, the miscellaneous properties of various types of hybrid composites are briefly discussed and demonstrated.

Keywords

Hybrid composites · Natural fibers · Synthetic fibers · Epoxy · Miscellaneous properties

Introduction

Throughout the years, fiber-reinforced composites (FRPs) are considered well-known materials to be used in various engineering applications. In fact, the development of FRPs is to reduce the dependence on the plastics by partially incorporating fibers in the polymer matrix (Ng et al. 2020). Surprisingly, it was found that the presence of fibers in FRPs could increase mechanical and physical properties in comparison with neat polymers. In addition, FRPs also have shown some benefits such as high corrosion resistance, outstanding fatigue resistance, and great strength-to-weight ratio compared to metal alloys (Feng et al. 2020a). Thus they have been broadly used to replace metal alloys. In comparison with metal alloys, the high specific mechanical properties are particularly promising as the lightweight characteristic of FRPs results in a reduction in energy consumption without significantly increasing the safety risk. For example, the fuel consumption can be reduced by approximately 0.7 l/100 km with a reduction in the vehicle mass by 100 kg (Alkbir et al. 2016; Almansour et al. 2017). Currently, FRPs have been employed for the automotive and marine structural components, aerospace transport, and sports equipment (Habibi et al. 2018). In the transportation sectors, the use of FRPs to replace metal alloys for the interior components of the vehicle can drastically reduce the energy consumption owing to the lightweight characteristic of FRPs. The demand for lightweight FRPs in aircraft structures is continuously growing, mainly driven by the high specific properties and excellent durability.

Apart from high specific properties, FRPs have shown excellent fatigue resistance compared to metal alloys. FRPs are relatively insensitive to fatigue loading and thus prolong their service life. Fatigue crack growth can occur under certain loading conditions, which eventually leads to the catastrophic failure of the entire structure. During the fatigue loadings, the crack of metal alloys is generally initiated after a certain number of cycles, and it continuously propagates until failure. In contrast, the fatigue failure of the FRPs is commonly associated with the initiation of microscopic crack which gradually propagates until fracture. Therefore, the use of materials with high fatigue resistance for structural applications is necessary as it can avoid the catastrophic failure of the components, which can

endanger human life. However, there are some aspects such as fiber and matrix properties, fiber orientations, and fiber contents that can considerably affect the fatigue properties of FRPs.

In the global market, the majority of FRPs are dominated by synthetic fibers due to the high mechanical strength of such fibers. The most widely used synthetic fibers in FRPs include carbon, glass, and aramid fibers. Among the synthetic fibers, glass fiber has received the most attention among research communities because it is inexpensive and possesses high mechanical strength. Nonetheless, the extensive use of glass fiber has led to an enormous disaster on the environment and human health. The non-biodegradable characteristic of glass fiber ends up in the accumulation of the waste products on the earth. However, the stricter environmental regulations and arising ecological awareness have ignited the trend of shifting the use of synthetic fibers to natural fibers in FRPs. The natural fibers have been considered as an alternative natural resource to tackle the main demerits of synthetic fibers.

Intensive research works have been performed to determine the advantages and usability of FRPs in several engineering applications. Even though FRPs have evident innumerable virtues over metal alloys, FRPs have been found to have poor resistance toward impact loadings. FRPs are often fragile and very sensitive to impact loading, which subsequently reduces their potential as promising lightweight materials. Strength loss and premature failure of the FRPs may occur when the materials are subjected to repetitive impact loadings. Most of the FRPs are exposed to impact loadings such as bird strikes or runway debris during their service life, particularly in transportation sectors. Thus, the FRPs should be designed and developed by considering the damage mechanism and impact loadings. Today, the continuous evolution of the FRPs in the field of composite materials had led to the growth of hybridization concept by embedding multiple types of reinforcement in the polymer matrix.

Generally, the mechanical properties of FRPs are identified through various experimental tests. However, the mechanical properties of the FRPs can also be predicted by implementing Halpin-Tsai and rule of mixture (ROM). In comparison with Halpin-Tsai, ROM, as shown in Eq. (1), is more often employed as it is relatively simple and gives acceptable prediction value compared to experimental findings. The theoretical prediction using ROM is not restricted to mechanical properties, but it can also be applied to predict the physical and thermal properties of composite materials. Behzad and Sain (2007) employed ROM to predict the thermal properties of unidirectional hemp fiber-reinforced composites. The predicted thermal properties obtained from ROM model showed a strong correlation with the experimental findings. Noryani et al. (2019) applied the ROM model and statistical analysis to identify the density and tensile properties of coir, kenaf, and cotton fiber-reinforced composites. They concluded that the statistical model was well incorporated with the ROM model to predict the physical and tensile properties of the composites for automotive applications.

$$P_c = P_f V_f + P_m(1 - V_f) \tag{1}$$

where P_c is the properties of composites, P_f is the fiber properties, P_m is the matrix properties, and V_f is the fiber volume fraction.

When using ROM to predict mechanical properties of composite materials, there are four important assumptions (Rangaraj and Bhaduri 1994): (1) the fibers are evenly distributed in the composites, (2) perfect fiber-matrix interfacial adhesion, (3) no void content in the composites, and (4) both fibers and matrix behave as perfectly linear elastic materials. ROM is actually established as mathematical expression to evaluate the axial properties of unidirectional fiber-reinforced composites (Cordin et al. 2018; Antin et al. 2019). It had been proven that the estimation of tensile properties of natural fiber-reinforced composites using ROM model is only in good agreement at low fiber composition. The prediction starts to deviate from the actual experimental findings when the fiber content in the composites is high. Joseph et al. (2003a) compared the experimental results with the theoretical prediction of mechanical properties of short sisal fiber-reinforced composites. In accordance with the results, the gap between the experimental results and ROM theoretical prediction augmented with the increase of fiber content, mainly attributed to the occurrence of fiber agglomeration as a result of high fiber content, causing the deviation of the theoretical prediction from the experimental results. This phenomenon is not limited to short fiber-reinforced composites, but long and woven fiber-reinforced composites as well. Thereafter, the evolution of this model had been realized through the modified ROM as shown in Eq. (2) to improve the accuracy of ROM (Cullen et al. 2013; Virk et al. 2017):

$$P_c = \kappa \eta_d \eta_l \eta_0 P_f V_f + P_m (1 - V_f) \tag{2}$$

where κ is the fiber area connection factor for non-circular fibers, η_d is the fiber diameter distribution factor, η_l is the fiber length distribution factor, and η_0 is the fiber orientation factor.

Hybrid Composites

Hybrid composites are the relatively new composite materials which have gained increasing attention from researchers around the world. The intention of developing hybrid composites is to resolve the shortcomings of non-hybrid composites, achieving the balance in environmental friendliness and material properties. The contemporary trend in the field of composite materials has shifted from the use of synthetic fibers to natural fibers, mainly due to ecological issues. Natural fibers have indeed demonstrated a lot of benefits compared to synthetic fibers. Low density, low cost, less energy consumption, highly abundant, high specific properties, and biodegradability are among the virtues provided by natural fibers. Furthermore, FRPs reinforced by natural fibers have been found to have high electrical resistance, excellent thermal and acoustic insulating properties, and high fracture toughness (Venkateshwaran et al. 2012). All these properties allow natural fibers to be extensively used to supersede synthetic fibers in FRPs. The demand for natural fiber-based

FRPs is continuously arising, and the use of such materials has been extended to automotive industries.

Meanwhile, natural fibers also have some disadvantages that retard the applications of natural fibers to a greater extent. Natural fibers are known to have high moisture sensitivity, low mechanical strength, high batch-to-batch variation, low thermal stability, and poor compatibility to hydrophobic polymer matrices. The previous literature studies have made experimental investigations to scrutinize the potential of incorporating natural fibers in FRPs. The findings revealed that natural fiber-based FRPs possessed good stiffness, but the mechanical strength of natural fiber-based FRPs could not reach the same level as glass fiber-reinforced composites (Oksman et al. 2003). Therefore, using natural fibers to replace synthetic fibers in FRPs fully is not realistic due to the presence of several limitations.

To resolve the limitations of natural fiber-based FRPs, an idea of incorporating various types of fibers in the single polymer matrix has been raised. Hybrid composites refer to the amalgamation of two or more types of fibers in the polymer matrix. Typically, synthetic/synthetic, synthetic/natural, and natural/natural fiber-based hybrid composites are the three categories of fiber-reinforced hybrid composites. However, hybrid composites based on the synthetic/natural fibers are the most popular and widely explored materials in recent research studies. This is because the synthetic/natural fiber-based hybrid composites can reach the goals of reducing the dependence on synthetic fibers while resolving the limitations of natural fibers. The balance in the mechanical properties and environmental friendliness can be reached through this hybridization concept. It is anticipated that the combination of two different types of fiber in composite materials could result in the synergetic effect.

Hybrid composites made of two types of fibers having different diameters and mechanical strengths provide various advantages over single fiber-reinforced composite. Due to the different diameters of fibers in the hybrid composites, the aspect ratio (length-to-diameter ratio) can be greatly improved, leading to enhanced stress transfer efficiency. It is expected that the weaknesses of one fiber can be offset by the advantages of another fiber in hybrid composites, providing an alternative way to achieve the balance properties. Moreover, the additional advantage is that the mechanical properties of the hybrid composites can be designed and tailored more practically under certain applications. With the incorporation of natural fibers in the hybrid composites, the mass of the structure can be further reduced compared to metal alloys and non-hybrid synthetic fiber-based composites as the density of natural fibers is remarkably lower than glass fiber. The lightweight property is especially desired in the transportation sectors to improve energy efficiency. Owing to the advantages of glass fiber, the majority of the research studies focus on the hybridization of natural fibers and glass fiber in hybrid composites (Velmurugan and Manikandan 2007; Jarukumjorn and Suppakarn 2009; Ng et al. 2017a; Feng et al. 2019). The combination of natural fibers with glass fibers can definitely improve the mechanical strength and reduce the moisture sensitivity in comparison with non-hybrid natural fiber-based composites.

In engineering applications, materials are commonly subjected to repetitive cyclic loadings which can result in catastrophic failure although the cyclic stress is

generally lower than their mechanical strength. Indeed, fatigue failure is associated with the continuous decrease of the stiffness, which subsequently leads to the fracture of the materials (Lee and Barr 2004). Since stiffness is an important property to resist fatigue loading, the addition of high modulus synthetic fibers in the composites is envisaged to improve the fatigue properties. Liang et al. (2012) found that the glass fiber-reinforced epoxy composites had greater fatigue strength than flax fiber-reinforced epoxy composites. Shahzad (2011) reported that the hybridization of glass fiber with hemp fiber in the composites improved the fatigue strength compared to non-hybrid hemp fiber-based composites. Still, no improvement in fatigue sensitivity was noticed. It is the addition of glass fiber that could undoubtedly improve the fatigue strength; however, the presence of natural fiber in the hybrid composite is necessary as well to reduce the fatigue sensitivity of the materials. Natural fibers had been shown to be relatively insensitive to fatigue loading compared to synthetic fibers. Natural fibers could show a stiffening effect which is the increase of modulus at the early stage of repetitive cyclic loads. The reason for the stiffening effect is most probably attributed to the rearrangement of the microfibrils toward the loading direction. Furthermore, natural fibers have the ability to peel off the damaged cell wall and continuously transfer the load to other undamaged layers (Silva et al. 2009). All these characteristics make natural fibers encompass relatively lower fatigue sensitivity than synthetic fibers. Asgarinia et al. (2015) studied the fatigue properties of woven flax/glass fiber-reinforced epoxy hybrid composites. The introduction of glass fiber is undoubtedly beneficial to the fatigue strength of the hybrid composite laminates. In comparison with non-hybrid glass fiber-based composites, hybrid composite laminates had shown a more stable stiffness during fatigue loading. Ng et al. (2017b) obtained a similar result where the kenaf/glass fiber-reinforced hybrid composite-metal laminates showed lower fatigue sensitivity than glass fiber-based composite-metal laminates. This result infers that the fatigue strength degradation rate of hybrid composites was lower than glass fiber-based composite.

In fact, the miscellaneous properties of hybrid composites are highly dependent on several decisive aspects such as types of fiber, fiber orientations, fiber length, fiber compatibility, fiber composition, and also fiber-matrix adhesion level, which are very similar to non-hybrid composites. It had been identified that hybrid composites show higher mechanical performance when incorporating two fibers which have high strain compatibility. It is undeniable that the types of fiber also have a decisive effect in determining the mechanical properties of hybrid composites. The mechanical properties of natural fibers primarily depend on the chemical composition in which high cellulose content endows natural fibers with a greater mechanical strength since cellulose is the main constituent that is responsible for the mechanical strength of the natural fibers. Besides, the microfibrillar angle of natural fibers also has a substantial effect on the mechanical properties of natural fibers. Natural fibers with low microfibrillar angle have higher mechanical strength. Conversely, those fibers with high microfibrillar angle show greater ductility.

Theoretically, the mechanical properties of hybrid composites can be determined by applying rule of hybrid mixture (RoHM). In addition to mechanical properties,

RoHM can be utilized to predict the thermal properties of hybrid composites as well. Devireddy and Biswas (2016) had demonstrated that the thermal properties of hybrid composites can be determined using RoHM, and the results were in good agreement with the experimental data. The positive or negative hybrid effect generally refers to the deviation from the properties of hybrid composites. When glass fiber is incorporated into the natural fiber-based composites, improvement in the mechanical strength is noticed, this phenomenon is known as the positive hybrid effect. It is expected that the hybridization concept can develop cost-effective composite materials for various industrial applications. More importantly, the development of hybrid composites is believed to prominently reduce the negative impact on the environment.

Factors Influencing Miscellaneous Properties of Composites

Natural fibers have been subjected to permanent interest among research communities due to their promising and sustainable advantages over synthetic fibers. These advantages offered by natural fibers lead to the continuous exploration of natural fibers either in non-hybrid or hybrid composite materials. Hence, it is vital to determine and identify the factors that could have a prominent influence on the miscellaneous properties of composites, especially when incorporating natural fibers in the composite materials. After identifying the factors affecting the miscellaneous properties of natural fiber-based composites, more comprehensive research studies can be performed to further improve the mechanical performance of the materials.

Fiber Selection

Fiber selection is undoubtedly one of the decisive factors that determine the mechanical properties of composites. Each of the natural fibers has varying mechanical properties due to the difference in their chemical compositions. Generally, higher mechanical strength is achieved with natural fibers having high cellulose content and low microfibrillar angle, which is commonly noticed in those bast fibers such as flax, kenaf, jute, ramie, and hemp. This is most probably due to the need for a higher structural requirement to support the stalk of the plant. Table 1 summarizes the chemical composition of natural fibers. Table 2 records the compiled properties of natural fibers.

In addition to chemical composition, the mechanical properties of natural fibers are also affected by the growing conditions such as extraction methods, harvesting time, and storage conditions. For instance, the strength of natural fibers drops by 15% after 5 days from the optimum harvesting time (Pickering et al. 2007). Moreover, those natural fibers extracted manually have 20% higher strength than that of fibers extracted mechanically (Bos et al. 2002). It is also noted that different types of natural fibers have varying diameters, indicating that the aspect ratio of the natural fiber might be different. A high fiber aspect ratio is generally favorable to the

Table 1 Chemical composition of natural fibers (Faruk et al. 2012)

Fiber	Cellulose (wt%)	Hemicellulose (wt%)	Lignin (wt%)	Waxes (wt%)
Bagasse	55.2	16.8	25.3	–
Bamboo	26–43	30	21–31	–
Flax	71	18.6–20.6	2.2	1.5
Kenaf	72	20.3	9	–
Jute	61–71	14–20	12–13	0.5
Hemp	68	15	10	0.8
Ramie	68.6–76.2	13–16	0.6–0.7	0.3
Abaca	56–63	20–25	7–9	3
Sisal	65	12	9.9	2
Coir	32–43	0.15–0.25	40–45	–
Oil palm	65	–	29	–
Pineapple	81	–	12.7	–
Curaua	73.6	9.9	7.5	–
Wheat straw	38–45	15–31	12–20	–
Rice husk	35–45	19–25	20	14–17
Rice straw	41–57	33	8–19	8–38

Table 2 Compiled properties of natural fibers (Faruk et al. 2012)

Fiber	Tensile strength (MPa)	Tensile modulus (GPa)	Elongation at break (%)	Density (g/cm^3)
Bagasse	290	17	–	1.25
Bamboo	140–230	11–17	–	0.6–1.1
Flax	345–1035	27.6	2.7–3.2	1.5
Kenaf	930	53	1.6	–
Jute	393–773	26.5	1.5–1.8	1.3
Hemp	690	70	1.6	1.48
Ramie	560	24.5	2.5	1.5
Abaca	400	12	3–10	1.5
Sisal	511–635	9.4–22	2.0–2.5	1.5
Coir	175	4–6	30	1.2
Oil palm	248	3.2	25	0.7–1.55
Pineapple	400–627	1.44	14.5	0.8–1.6
Curaua	500–1150	11.8	3.7–4.3	1.4

mechanical strength of FRPs as it can improve the load-transferring efficiency from the matrix to the fiber through the interfacial shear mechanism. During tensile loading, the tensile stress increases along the fiber length; thus, the length of the fibers needs to be long enough to withstand the maximum applied load. Radzi et al. (2017) have demonstrated that the increase in fiber length improved the mechanical properties and thermal stability of roselle reinforced polyurethane composites.

The tip of the fiber generally acts as the stress concentration points which induce the crack initiation in the composite materials. Due to this reason, the short fiber-

reinforced composites with low fiber content could have lower mechanical strength than the neat polymer. Hence, the fiber length should be greater than the critical fiber length (L_c) in order to have a maximum reinforcing effect in the composite materials. The L_c can be expressed as in Eq. (3):

$$\frac{L_c}{d} = \frac{\sigma_f}{2\tau_i} \tag{3}$$

where d is the fiber diameter, σ_f is the tensile strength of fiber, and τ_i is the interfacial shear strength.

From Eq. (3), it can be seen that L_c is highly dependent on the interfacial shear strength, indicating that it is possible to reduce the critical fiber length by enhancing the interfacial shear strength. Although increasing the fiber length leads to the enhancement in the load-bearing capacity of the fiber, agglomeration of the fibers and poor fiber dispersion might occur when the fiber length is too long. This is mainly due to the formation of hydrogen bonding between the fibers.

Since the presence of fibers in FRPs had been identified to increase the mechanical properties, the effects of fiber composition on the miscellaneous properties of FRPs have been widely investigated. Throughout the years, it has been proven that the increase of fiber composition in FRPs indeed improves the mechanical and thermal properties. The addition of the fibers in FRPs increases the load-bearing capacity of the materials. Radzi et al. (2017) reported that the mechanical properties of roselle fiber-reinforced polyurethane composites increased tremendously with the increase of fiber composition in the composites. The highest mechanical properties and thermal stability of the composites were noticed when increasing the fiber content to 40 wt%. Akhtar et al. (2016) performed an experimental study on the mechanical properties of kenaf fiber-based composites with varying fiber loadings. They concluded that the composites had the maximum mechanical properties when increasing the fiber content to 40 wt%. However, the findings obtained in a recent study by Prakash et al. (2020) showed a different trend where the highest mechanical properties were obtained by increasing the fiber content up to 30 wt% in the *Syngonanthus nitens* fiber-reinforced composites. The mechanical properties dropped when the fiber composition was above 30 wt%. Nayak et al. (2010) obtained a similar result in which the incorporation of banana fiber at the fiber content of 30 wt% in the composite materials resulted in optimum mechanical properties. It can be seen that the optimum mechanical and thermal properties of composites can be obtained when the fiber composition is in the range of 30–40 wt%. Nevertheless, the mechanical properties of the composites drop once the fiber composition exceeds the critical limits. The drop in the mechanical properties of composites is attributed to the insufficient polymer matrix to bind with the reinforcement, resulting in the inefficiency of load transfer, and thus the mechanical properties of the composites drop. Although increasing the fiber content in FRPs leads to the improvement in miscellaneous properties, the moisture uptake increases with the increase of fiber content. This can eventually undermine the long-term service performance of FRPs as the moisture uptake can lead to the decay of the materials.

Besides physical, mechanical, and thermal properties, it had been shown that the fiber content and fiber type have a decisive effect on the tribological behavior of composite as well. A research study had been conducted by Gehlen et al. (2020) on the tribological behavior of randomly distributed sisal/glass fiber-reinforced composites with varying fiber contents. An increase in the coefficient of friction was noticed when increasing the fiber content in the hybrid composites. When comparing the wear resistance of sisal to that of glass fiber-based composites, the highest wear resistance was observed in those sisal fiber-based composites, whereas the glass fiber-based composites demonstrated the lowest wear resistance due to the abrasive effect of glass fiber. The introduction of sisal fiber in the hybrid composites improved the wear resistance as sisal fiber limits the mobility of glass fiber in the composites. Aslan et al. (2018) also revealed that the increase of the sisal fiber content in both the sisal/glass and sisal/carbon-reinforced hybrid composites increased the coefficient of friction. The addition of randomly aligned natural fibers in the composite materials increases the discontinuous phases which led to the increment in the coefficient of friction. However, it should be emphasized that the coefficient of friction and wear performances of composites are highly affected by the fiber orientation. The coefficient of friction of composites increases when the fiber orientation is normal to the sliding direction. Yousif and Chin (2012) identified the influence of fiber orientation on the tribological properties of kenaf fiber-reinforced epoxy composites. When comparing to composites with parallel orientation, the composites with fiber orientation, which was normal to the sliding direction, exhibited higher wear resistance and coefficient of friction.

Fiber Alignment

On further looking into the fiber orientation, the FRPs with fiber alignment more parallel to the loading direction tend to have higher mechanical properties. The optimum mechanical strength can be achieved by aligning all the fiber parallel to the loading direction. Nevertheless, such composites will have poor mechanical strength when subjected to transverse loading. The unidirectional fiber-reinforced composites are considered an anisotropic material because their properties may vary with different loading directions. Conversely, randomly aligned fiber-reinforced composites are considered isotropic, inferring that such materials have similar mechanical strength in all directions. In comparison with unidirectional fiber-reinforced composites, composites based on randomly aligned fiber tend to have lower mechanical strength. However, unidirectional composites can be designed in a more isotropic manner by using multiple plies of continuous fiber with different fiber orientations such as 0°, 90°, and $\pm 45^\circ$ to sustain the applied load in different directions.

In order to develop composite materials which are isotropic and have relatively high mechanical strength, woven fibers have been employed as reinforcement in composite materials. Woven fibers allow more freedom to tailor the mechanical properties by altering the fiber orientations. Truthfully, the development of woven fiber-reinforced composites is to mimic the isotropic properties of conventional metal

alloys. In recent years, woven fabrics have gained their popularity in the research communities owing to their several attractive features such as good dimensional stability and excellent mechanical properties. Although woven fabrics have shown various excellent properties, their mechanical properties are governed by several factors such as yarn and matrix properties, fabric count, and weaving pattern (Yang and Zeng 2018). The typical examples of the weave pattern of woven fabrics include plain, twill, basket, and satin. The woven fabrics are formed through the interlacement of warp and weft yarns, resulting in high mechanical interlocking which retards the crack propagation and thus providing high damage tolerance and resistance against out-of-plane loadings to the composite materials. When comparing to continuous fiber, the deformation behavior of woven fabric is relatively complex as it involves several damage mechanisms such as in-plane redistribution, reorientation, crimp interchange, yarn stretching and un-crimping, yarn slipping, and scissoring effect (Mishra et al. 2017). Figure 1 demonstrates typical forms of fiber in composite materials.

Intensive research studies have been conducted to determine the mechanical properties of composites with different fiber orientations. The mechanical properties of woven fabric-reinforced composites at different fiber orientations are particularly attractive to the researchers. Cordin et al. (2018) analyzed the tensile properties of cellulose-type lyocell reinforced polypropylene composites with different fiber orientations. Five different fiber orientations, as illustrated in Fig. 2, were fixed in this research study. In accordance with the findings obtained, composites with fiber

Fig. 1 Fiber types: (**a**) random chopped fiber, (**b**) long fiber (**c**), plain weave woven fiber

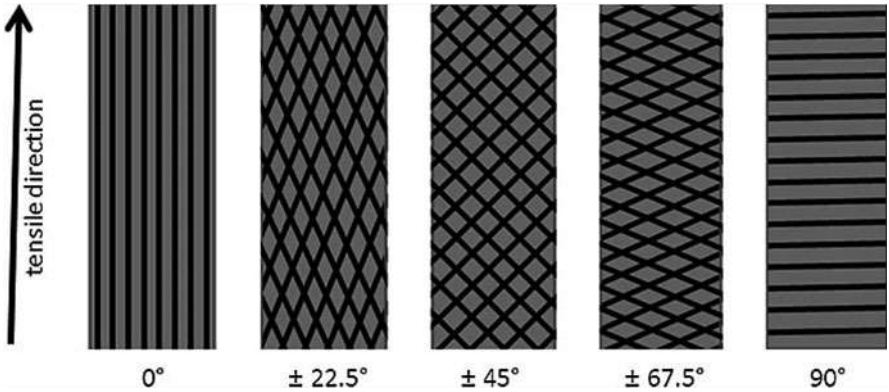

Fig. 2 Schematic diagram of composites with varying fiber orientations (Cordin et al. 2018)

orientation of 0° encompassed the highest tensile strength and modulus in comparison with other fiber orientations. Increasing the fiber angle deteriorated the tensile properties of composites. This shows that minimal alteration in the fiber angle could weaken the tensile properties of the composites. It was attested that the tensile properties of composites with the fiber orientation of ±45° were even lower than pure polypropylene. However, composites with fiber orientation of ±45° displayed the highest elongation because the composites are dominated by the matrix properties. Any increase or decrease of fiber angle reduced the elongation of the composites. Ng et al. (2017a) demonstrated similar results in which the tensile strength of woven kenaf fiber-reinforced composite-metal laminates was the highest when the fiber orientation was fixed at 0°/90°. Furthermore, the highest elongation was found in those composite-metal laminates with a fiber orientation of ±45°. Another research study was conducted by Sharba et al. (2016) to determine the tensile, compressive, and flexural properties of kenaf/glass fiber-based hybrid composites with varying kenaf alignments. The unidirectional kenaf-based hybrid composites were found to have the highest tensile and compressive strength, whereas woven kenaf reinforced composites encompassed the highest flexural strength.

Interfacial Bonding

It is well-known that the incorporation of reinforcement in the composite materials could improve the mechanical properties and thermal stability. However, an excellent fiber-matrix interfacial bonding is required to achieve the exemplary mechanical strength of the composite materials, particularly natural fiber-reinforced composites. Apart from mechanical strength, the wear resistance and thermal properties of composite materials are improved as well with excellent fiber-matrix adhesion. Feng et al. (2020b) demonstrated that the NaOH and silane treatments enhanced the interfacial bonding of kenaf and pineapple leaf fiber-reinforced composites, thus augmenting the mechanical properties of the materials. The improvement in the

mechanical properties of chemically treated composite materials is due to the greater fiber-matrix bonding which improves the stress transfer efficiency between the fiber and matrix. Neto et al. (2019) showed that chemical treatments could improve the thermal stability of the natural fiber-based hybrid composites. It can be seen that the thermal degradation temperature of composites is increased after chemical treatments. This phenomenon is most probably because of the increase in the molecular weight as a result of the enhanced cross-linking between the epoxy and the fiber (Nayak and Mohanty 2010). Goriparthi et al. (2012) had identified that the chemically treated jute fiber-based composites had higher wear resistance than that of untreated composites. Several factors could influence the wear resistance of composite materials. Stiffness, toughness, hardness, and fiber-matrix adhesion are those factors that determine the wear resistance of FRPs. In comparison with untreated composites, the relatively high stiffness and interfacial bonding of chemically treated composites avoid a high level of weight loss, indicating greater wear resistance of the materials. From the literature studies, it is obvious that a strong interfacial adhesion is necessary for composite materials to have long-term durability performance. Today, there has been a growing interest in employing natural fibers to supersede synthetic fibers in composite materials. Hence, it is particularly vital to enhance the interfacial bonding between natural fibers and polymer matrix.

In the FRPs, the interfacial area is an important site for the stress transfer between the polymer matrix and the fiber; thus, a remarkable interfacial bonding is required to achieve the maximum reinforcing effect. In this context, natural fibers have very limited compatibility with hydrophobic polymer matrix owing to their intrinsic hydrophilic behavior. Apart from the poor interfacial bonding, the hydrophilic behavior of natural fibers could also result in the high moisture uptake which negatively affects their long-term performance. Since the past decades, an attempt had been given to alter the hydrophilic behavior of natural fibers through chemical modification. This method tends to endow the composites with high fiber-matrix adhesion level in order to achieve the exemplary mechanical strength. Alkali treatment is among the most extensively used fiber treatments to improve the fiber-matrix interfacial adhesion (Sheshmani et al. 2012). This treatment alters the fiber surface structure by eliminating a certain amount of chemical constituents such as lignin, wax, pectin, hemicellulose, and impurities while exposing more cellulose on the fiber surface for bonding with the polymer matrix. Figure 3 illustrates the structure of

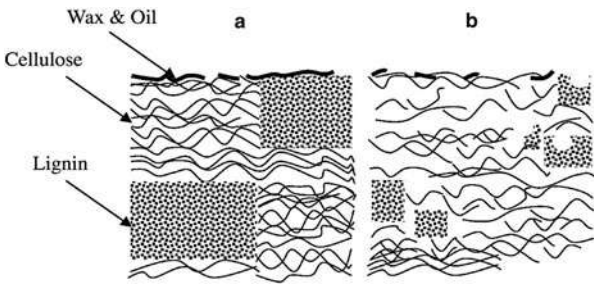

Fig. 3 Structure of natural fibers: (**a**) untreated, (**b**) alkali-treated (Mwaikambo and Ansell 2002)

untreated and alkali-treated natural fibers. The fiber surface becomes rougher after the alkali treatment. As a consequence, the mechanical interlocking between the fiber and matrix is greatly improved. The mechanical properties of the composites are then enhanced. Apart from the improved mechanical interlocking, alkali treatment also results in acetylation of the hydroxyl groups on the fiber surface, which decreases the moisture absorption of the fibers and thus enhances the compatibility of the fibers with the matrix. Several literature studies have also reported that alkali treatment can increase the fiber strength (Joseph et al. 2003b; Hossain et al. 2013; Asim et al. 2016). Due to the removal of a certain amount of unnecessary chemical contents, it allows more flexibility of the microfibrils to rearrange themselves toward the loading direction during stretching, thus increasing the mechanical strength of natural fibers. Nonetheless, it is worth mentioning that the alkali concentration above a critical level could lead to excessive delignification of the fibers, resulting in the damage of fiber structure, thus deteriorating the mechanical strength of fibers and composites.

Silane treatment is another approach to enhance the bonding level of natural fibers and polymer matrix by providing a bridge across the interface. Silane is a bi-functional molecule which could simultaneously interact with fiber and matrix, forming siloxane bridge at the interface. Silane treatment involves several stages, namely, hydrolysis, self-condensation, adsorption, and chemical grafting (Xie et al. 2010). Figure 4 depicts the several stages in the silane treatment. During the hydrolysis, the alkoxy groups of silane are hydrolyzed with the presence of water to form the more reactive silanol groups which may then interact with hydroxyl groups on cellulosic fibers and functional groups of the polymer matrix. In order to have complete hydrolysis of silane, the addition of water during the treatment is essential. A certain amount of silane molecules condense themselves to form a macromolecular network. However, the condensation of silane molecules should be minimized to ensure the maximum interaction between the silane molecules and functional groups of fibers and matrix. After the formation of reactive silanol groups, these silanol groups are being absorbed by the hydroxyl groups of fibers via the hydrogen bonds. Under the heating condition, these hydrogen bonds can be converted into strong covalent bonds. Since there are pores on the fiber surface, the silanol monomers are able to penetrate into the pores and develop a strong mechanical interlocking with the fibers, thus enhancing the fiber-matrix interfacial adhesion (Kabir et al. 2012).

Acetylation is also a recognized chemical treatment which introduces acetyl functional groups to interact with hydroxyl groups of organic compounds. This process can be catalyzed by soaking the fibers in the acetic acid and subsequently treated with acetic anhydride for a period of 1–3 h at elevated temperature. Acetylation improves the adhesion level between fiber and matrix by making the fiber surface rougher which offers better mechanical interlocking with the matrix. Besides, acetylation also reduces the hydrophilic behavior of natural fibers through the esterification. The hydroxyl groups of the fibers react with the acetyl groups, reducing the hydrophilicity of the fibers. The moisture uptake of the fibers is considerably reduced because hydroxyl groups have been replaced with acetyl

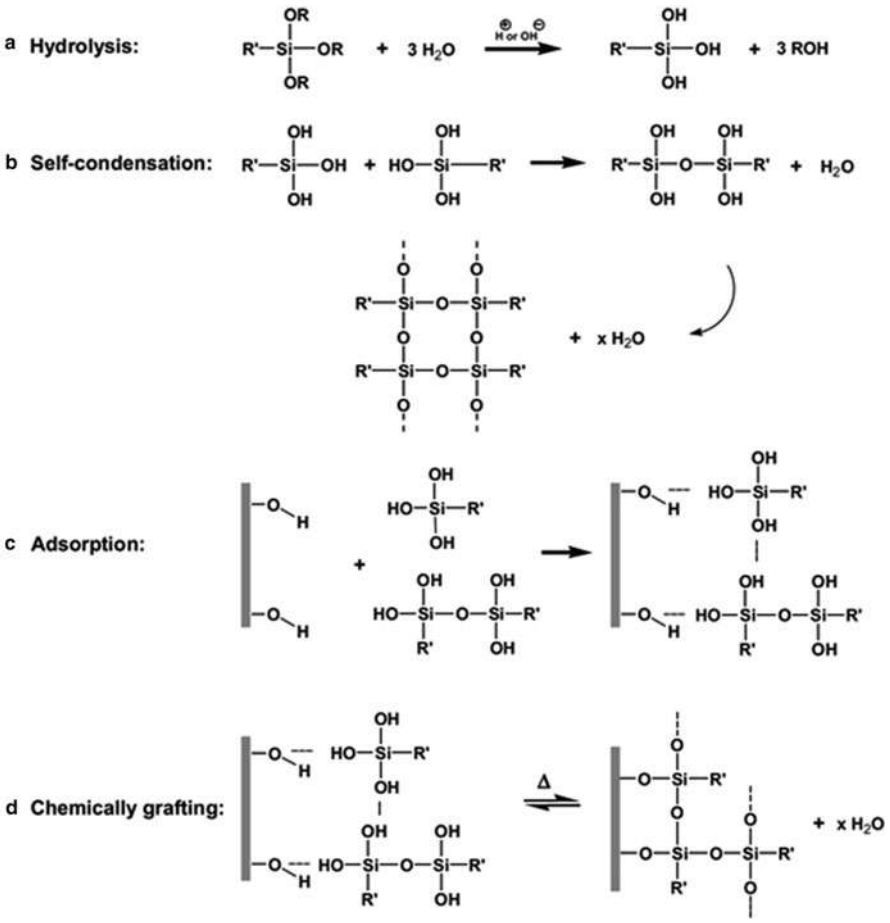

Fig. 4 Several stages in silane treatment (Xie et al. 2010)

groups after the treatment. Hence, the dimensional stability of the natural fiber-based composites can be enhanced. It should be noted that the acetylation leads to the deleterious effect on the mechanical properties once the chemical concentration exceeds the critical level. This detrimental effect is because of the cellulose degradation and fiber cracking with the presence of a catalyst (Bledzki et al. 2008). The reaction of acetic anhydride and natural fibers during the treatment is represented in Eq. (4):

$$\begin{aligned} &\text{Fiber} - \text{OH} + \text{CH}_3 - \text{C}(=\text{O}) - \text{O} - \text{C}(=\text{O}) - \text{CH3} \\ &\quad \rightarrow \text{Fiber} - \text{OCOCH}_3 + \text{CH}_3\text{COOH} \end{aligned} \tag{4}$$

Bledzki et al. (2008) performed an experimental investigation on the effect of acetylation on the mechanical, thermal, and water absorption properties of flax fiber-

reinforced polypropylene composites. They reported that the acetylated flax fiber displayed 50% lower moisture absorption than untreated flax fiber. Moreover, approximately 25% improvement in the mechanical properties was found in those acetylated flax fiber-reinforced composites. However, the acetylated composites showed lower Charpy impact strength than untreated composites. This is most probably due to the strong fiber-matrix adhesion which increases the brittleness of the composites, resulting in a reduction in the toughness. In comparison with untreated flax fiber-based composites, acetylated flax fiber-based composites had higher thermal stability. Wang and Petrů (2019) identified the effect of different types of chemical treatment on the dynamic mechanical behavior of flax fiber-reinforced epoxy composites. They concluded that acetylation offered the highest damping performance compared to alkali, silane, and alkali-silane treatments. In addition, acetylated flax fiber composites had the lowest moisture uptake compared to other chemical treated composites.

Another alternative method such as benzoylation can be applied on natural fibers as well to improve their interfacial adhesion. Benzoylation is performed using benzoyl chloride to improve the interfacial adhesion and reduce the hydrophilic behavior, resulting in the exemplary mechanical strength of the composites. Apart from the mechanical strength, the thermal stability of the fibers is enhanced as well after benzoylation. However, alkali treatment is usually required before the benzoylation treatment. Alkali pretreatment aims at reducing the unnecessary chemical constituents of natural fibers and exposing more reactive hydroxyl groups of the cellulose on the fiber surface for benzoylation. Paul et al. (2008) stated that the alkali treatment leads to the partial elimination of hydroxyl groups and the fiber becomes more reactive for benzoylation treatment. During benzoylation treatment, the hydroxyl groups are substituted by the benzoyl groups (C_6H_5CO) attaching on the cellulose backbone. Subsequently, the moisture sensitivity of the natural fibers is reduced, and the interfacial bonding with the matrix is enhanced. Swain and Biswas (2017) discovered the influence of benzoylation treatment on the physico-mechanical and water absorption behaviors of bi-directional flax fiber-reinforced epoxy composites. The findings showed that the combination of alkali and benzoylation treatment offered the greatest mechanical properties and lowest void content to the flax fiber-based composites compared to those of untreated and alkali-treated composites. In addition, the moisture absorption of the chemical treated composites was significantly dropped. Another research study was conducted by Kalia et al. (2011) on the thermal stability, morphology, and crystallinity of sisal fiber. They found out that the combination of benzoylation treatment and methyl acrylate grafting could enhance the thermal stability and crystallinity of sisal fibers. Moreover, the fiber surface becomes rougher after the benzoylation treatment and grafting of methyl acrylate. Although chemical treatments improve the fiber-matrix interfacial adhesion, thermal stability, and moisture resistance of the natural fiber-based composites, the extent of improvement depends on the types of chemical treatment. Mathew et al. (2004) identified the tensile and thermal properties of short isora fiber-reinforced composites after subjected to fiber treatments. Alkali, acetylation, benzoylation, toluene di-isocyanate, and silane treatments were applied to the

isora fiber. They reported that the alkali-treated isora fiber-based composites possessed the highest thermal stability. However, silane-treated composites had the highest tensile strength compared to other chemically treated composites. Innumerable literature studies have proven that the chemical treatments inevitably lead to the exemplary mechanical, thermal, and morphological properties of natural fiber-based composites. This phenomenon can be regarded as an indicator that the chemical treatments are greatly indispensable when natural fibers are employed as reinforcement in composite materials.

Miscellaneous Properties of Epoxy/Synthetic/Natural Fiber Hybrid Composites

In recent years, the extensive use of inorganic fibers has deteriorated the environment at an intimidating pace. Waste production and accumulation have been a challenging issue due to the non-biodegradable characteristic of the materials. The arising ecological and environmental alertness has stimulated the idea of adopting natural fibers for the replacement of non-organic fibers. Throughout the years, the composite materials employed in engineering applications have been dominated by synthetic fibers such as carbon, glass, and aramid fibers. Thus, it is vital to reduce the dependence on synthetic fibers.

In spite of the innumerable environmental-friendly characteristics shown by natural fibers, they have various shortcomings compared to synthetic fibers. High moisture uptake and low mechanical strength of natural fibers are among the main drawbacks that retard their use in engineering applications, particularly when high strength characteristic is required. Owing to the drawbacks of natural fibers, the replacement of synthetic fibers with natural fibers in composite materials is not possible. Therefore, the concept of hybridization would be an alternative approach to achieve the balance between the environmental friendliness and mechanical properties of composite materials. Hybridization involves the utilization of at least two different types of fiber embedded within a single matrix. Generally, there are three groups of fiber-reinforced hybrid composites, namely, synthetic/synthetic, synthetic/natural, and natural/natural. However, hybrid composites based on synthetic/natural fibers are the most widely studied materials because such materials have shown great potential to achieve the goal of developing green and high mechanical strength materials.

Mechanical Properties of Epoxy/Synthetic/Natural Fiber Hybrid Composites

The mechanical properties of hybrid composites based on synthetic and natural fibers embedded in the epoxy matrix have been widely studied by researchers nowadays. In composite materials, glass fiber is the most extensively used synthetic fiber due to its low cost and high strength characteristics. Therefore, it was found that the majority of the works focus on the glass fiber-based hybrid composites. In

addition to the factors affecting the miscellaneous properties of composite materials as briefly shown in the previous section, it had been identified that fiber stacking sequence also has a decisive effect on the mechanical properties of woven fiber-reinforced hybrid composites.

Braga and Magalhaes (2015) analyzed the mechanical properties of woven jute/glass fiber-reinforced epoxy hybrid composites. They concluded that higher mechanical properties were observed in those hybrid composites with high glass fiber content. Yahaya et al. (2015) incorporated woven Kevlar fiber in the kenaf fiber-reinforced epoxy hybrid composites to determine their mechanical properties. However, they revealed similar results where the addition of Kevlar fiber improved the mechanical properties of the hybrid composites, especially when Kevlar fiber was located at the outermost layers of the composite laminates. Jusoh et al. (2016) studied the mechanical properties of hybrid composites based on woven glass, basalt, flax, and jute fibers embedded in the epoxy matrix. Glass fiber was hybridized with three types of natural fibers, respectively. The stacking sequences were separated into two major groups, namely, sandwich-like and intercalation. The results showed the tensile properties of the hybrid composites with intercalated stacking sequences dropped slightly in comparison with sandwich-like stacking sequences. A similar trend was noticed in the flexural properties of hybrid composites in which those hybrid composites with sandwich-like stacking sequences showed higher flexural properties, particularly when glass fibers were incorporated as the outermost skin layers. When comparing the mechanical properties of hybrid composites with different types of natural fiber, basalt-based hybrid composites had the highest mechanical properties compared to flax and jute fiber-based hybrid composites. Latha et al. (2016) experimentally investigated the mechanical properties of woven bamboo/glass fiber-reinforced epoxy composites with varying stacking sequences. They obtained similar results in which the hybrid composites exhibited higher mechanical strength when the glass fiber was placed as the outermost skin layers. Latha and Rao (2018) made a further exploration of the effect of ceramic filler on the mechanical properties of woven bamboo/glass fiber-reinforced epoxy composites. They revealed that the incorporation of zirconia and titania increased the mechanical strength of the hybrid composites. As expected, the addition of high-strength glass fiber led to a positive hybrid effect. Arpitha et al. (2017) investigated the effect of hybridization on the mechanical properties of woven sisal/glass fiber-reinforced epoxy hybrid composites. They concluded that the increase of glass fiber layers in the composite laminates improved the mechanical properties, indicating the positive hybrid effect on the mechanical properties of the hybrid composites. Selver et al. (2018) performed a similar study on the mechanical properties of flax/glass and jute/glass fiber-reinforced epoxy hybrid composites with varying stacking sequences. They revealed that the flax/glass fiber-reinforced hybrid composites had higher mechanical properties than those of jute/glass fiber-reinforced hybrid composites. This is probably due to the intrinsic high mechanical strength of flax compared to jute fibers. Furthermore, it was found that the partial incorporation of glass fiber in the composite laminates

led to the positive hybrid effect where the mechanical properties were significantly improved compared to those of non-hybrid jute and flax-based composite laminates. Sanjay and Yogesha (2018) did an investigation on the mechanical properties of woven jute/kenaf/glass fiber-reinforced epoxy hybrid composites with different stacking sequences. They obtained similar results in which the positive hybrid effect was found by incorporating glass fiber in the respective jute and kenaf fiber-based composite laminates. The positive hybrid effect is particularly significant when hybridizing two types of natural fibers with glass fibers. On average, kenaf/glass fiber-based hybrid composite demonstrated higher mechanical properties compared to jute/glass fiber-based hybrid composite due to the greater mechanical strength of kenaf fiber. The literature studies as mentioned above demonstrated that the stacking sequences undoubtedly have a decisive effect on the mechanical properties of woven synthetic/natural fiber-reinforced epoxy hybrid composites. The majority of the works revealed that the placement of high-strength synthetic fiber as the outermost skin layers in hybrid composite laminates is the most promising stacking sequence. The outermost fiber layers could sustain a higher amount of load, particularly when subjected to out-of-plane loading.

Apart from woven fabric, the mechanical properties of unidirectional and random fiber-reinforced hybrid composites are also widely studied. Rout and Satapathy (2012) analyzed the influence of rice husk content on the mechanical properties of rice husk/glass fiber-based hybrid composites. It was concluded that the increase of rice husk filler improved the tensile modulus and energy absorption but impaired the tensile and flexural strength of the hybrid composites. Ridzuan et al. (2016) identified the effect of moisture absorption on the mechanical properties of unidirectional *Pennisetum purpureum*/woven glass fiber-reinforced epoxy hybrid composites. The mechanical strength of both non-hybrid and hybrid composites degraded after water absorption. On average, the addition of glass fiber increased the mechanical strength of the hybrid composites. Sarasini et al. (2016) conducted a low-velocity impact test to determine the damage tolerance of unidirectional flax/carbon fiber-reinforced epoxy hybrid composite laminates. Five different applied energies ranging from 5 J to 30 J were fixed, and the flexural properties of the composite laminates were identified as well. Figure 5 displays the load-displacement curves of flax/carbon fiber-based composites. As can be seen in Fig. 5, the penetration only occurred in non-hybrid flax fiber-based composites at the energy level of 30 J. Overall, the energy absorption capacity of flax fiber was better than carbon fiber due to the presence of an extended plateau. However, the post-impact flexural properties of carbon fiber-based composite laminates were superior to those of flax fiber-based composite laminates. Therefore, the hybridization of carbon and flax fibers in the composite laminates can reach the balance in the energy-absorbing capacity and post-impact flexural properties. Yahaya et al. (2016) performed mechanical characterization on the kenaf/aramid fiber-reinforced epoxy composites. Woven aramid fiber was hybridized with kenaf fiber which was in the form of woven fabric, unidirectional, and mat. Interestingly, woven kenaf/aramid fiber-based hybrid

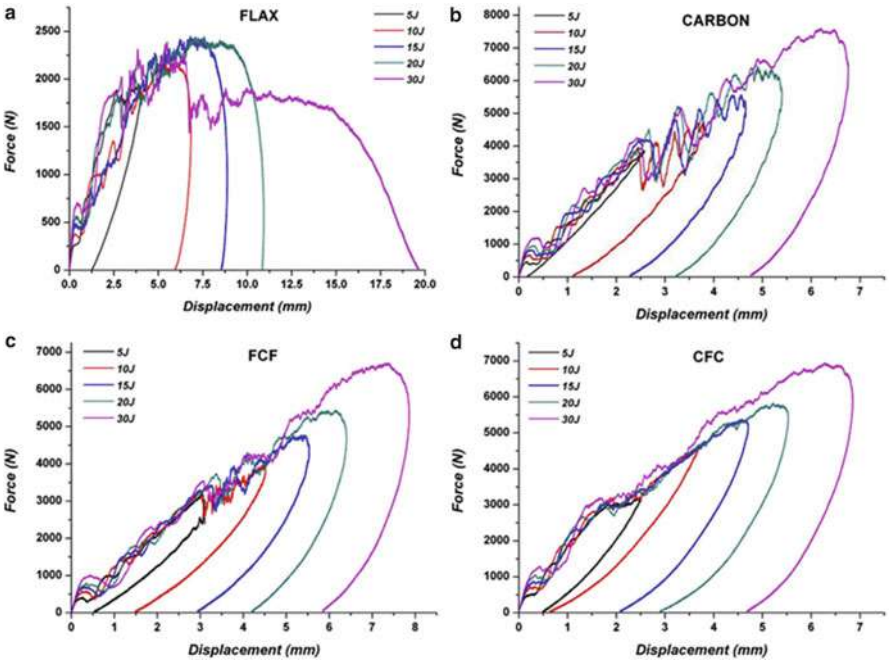

Fig. 5 Load-displacement curves of flax/carbon fiber-based composites (Sarasini et al. 2016)

composites demonstrated the greatest tensile and impact strengths. In contrast, non-woven kenaf mat/aramid fiber-based hybrid composites presented the lowest tensile and impact strengths. Nonetheless, unidirectional kenaf/aramid fiber-reinforced epoxy composites showed the highest flexural strength instead of woven kenaf/aramid fiber-reinforced epoxy composites. The results imply that the mechanical properties of hybrid composites are indeed affected by the fiber alignment. Ramesh et al. (2017) determined the mechanical properties of unidirectional banana/carbon fiber-reinforced epoxy hybrid composites with varying relative fiber ratios. An improvement in the mechanical properties was observed when incorporating carbon fiber in the composites. Safri et al. (2019) analyze the impact properties of sugar palm/glass fiber-reinforced epoxy hybrid composites. The hybrid composites were composed of 7% of glass fiber and 3% of benzoyl-treated sugar palm fiber. They concluded that the hybrid composites could not effectively withstand the impact loading above 15 J. Sujon et al. (2020) identified the mechanical properties of jute/carbon fiber-reinforced epoxy hybrid composites with varying fiber stacking sequences and orientations. The findings showed that the unidirectional jute/carbon fiber-based composites had superior mechanical properties compared to angle-ply and cross-ply composites. The highest tensile strength was found in those hybrid composites with carbon fabrics as the core layers. However, the highest flexural and impact strength were both found in those hybrid composites with carbon fiber as the outermost skin layers.

Thermal Properties of Epoxy/Synthetic/Natural Fiber Hybrid Composites

The thermal properties of natural fiber-based composites are considered as one of their major limitations in engineering applications. The degradation of fiber components such as cellulose, hemicellulose, and lignin occurs at a high temperature, resulting in the deterioration in their overall performance (Asim et al. 2020). Hence, it is necessary to study the thermal properties of composite materials, especially non-hybrid and hybrid natural fiber-based composites in order to understand the thermal effect on the materials. Thermogravimetric analysis (TGA) is regarded as one of the basic evaluations of the thermal stability of the materials. TGA is performed on composite materials by determining their mass with respect to the temperature and time. Dynamic mechanical analysis (DMA) is another effective tool to determine the viscoelastic properties of the composite materials such as the storage and loss modulus as well as tan δ versus temperature.

Braga and Magalhaes (2015) evaluated the thermal properties of woven jute/glass fiber-reinforced hybrid composites through TGA. The TGA results of both non-hybrid and hybrid composites are illustrated in Fig. 6. The mass loss was noticed in non-hybrid and hybrid composites along with the increase of temperature. Nonetheless, the overall mass loss dropped with the partial incorporation of glass fiber in the composites. Selver et al. (2018) did an experimental investigation on the thermal properties of woven flax/jute/glass fiber-reinforced epoxy composite laminates through TGA and DMA. It was shown that the decomposition temperature of jute and flax fibers is similar to each other. When comparing non-hybrid flax and jute

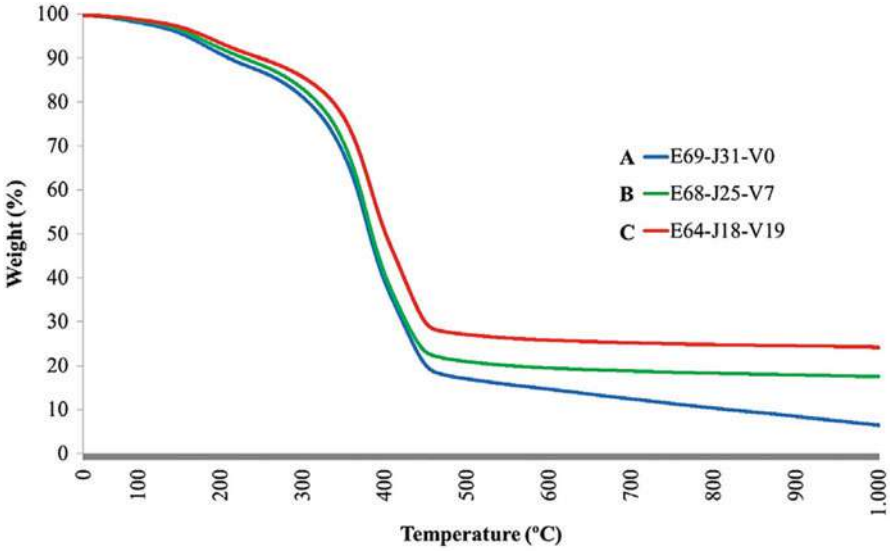

Fig. 6 TGA curves of jute/glass fiber-based hybrid composites (Braga and Magalhaes 2015)

fiber-based composites, the storage and loss modulus were found to be higher in those hybrid composites particularly when the glass fiber was located in the outermost layers of hybrid composites. Nevertheless, the tan δ was found to be higher when incorporating flax and jute fibers in the composites in comparison with non-hybrid glass fiber-based composites. The results implied that the damping behavior of hybrid composites was greater than non-hybrid glass fiber-based composites.

Safri et al. (2019) analyze the effect of benzoyl treatment on the dynamic mechanical properties of sugar palm/glass fiber-reinforced epoxy hybrid composites with varying relative fiber ratios. According to the results, the glass transition temperatures of the composites are close to each other. Moreover, the storage modulus of the composites increased with the increase of glass fiber content. The increment in the storage modulus of hybrid composites can be explained by the high modulus of glass fiber which increased the storage modulus. It is interesting to note that the benzoyl-treated hybrid composites showed the highest loss modulus. In contrast, the lowest loss modulus was noticed in those benzoyl-treated non-hybrid sugar palm reinforced epoxy composites. In terms of tan δ, the addition of glass fiber increased the damping factor of the hybrid composites. On average, benzoyl-treated hybrid composites had shown a better damping factor than that of untreated hybrid composites. The hybrid composites with relative fiber ratios of 30:70 (sugar palm-glass) demonstrated comparable dynamic mechanical properties to the non-hybrid glass fiber-based composites, indicating the potential of substituting glass fiber with sugar palm fiber in the composites. A recent thermogravimetric and dynamic mechanical analysis was conducted by Mazlan et al. (2020) on the woven kenaf/glass-reinforced epoxy composites filled with clay. They found out that the addition of clay increased the degradation temperature of the hybrid composites. Furthermore, alkali treatment on kenaf fiber and the incorporation of glass fiber were identified as the two driving factors toward the enhanced thermal stability of the composites. From the viewpoint of dynamic mechanical properties, the highest storage and loss modulus were found in those chemically treated hybrid composites with the addition of 1% clay. The addition of clay limits the mobility of the epoxy matrix and thus increases the modulus of the composites. Overall, the addition of glass fiber in the hybrid composites was beneficial to the thermal and dynamic mechanical properties as glass fiber encompasses relatively high thermal resistance and stiffness.

Water Absorption of Epoxy/Synthetic/Natural Fiber Hybrid Composites

It is commonly known that the moisture uptake of natural fibers is a challenging issue to be resolved in order to extend their use in a wide variety of applications. Chemical treatments have been identified that could reduce the hydrophilicity of natural fibers. However, hybridization is regarded as another straightforward technique to lessen the moisture sensitivity of natural fiber-based composites. Innumerable research studies have been carried out to identify the moisture absorption of synthetic/natural fiber-reinforced epoxy hybrid composites.

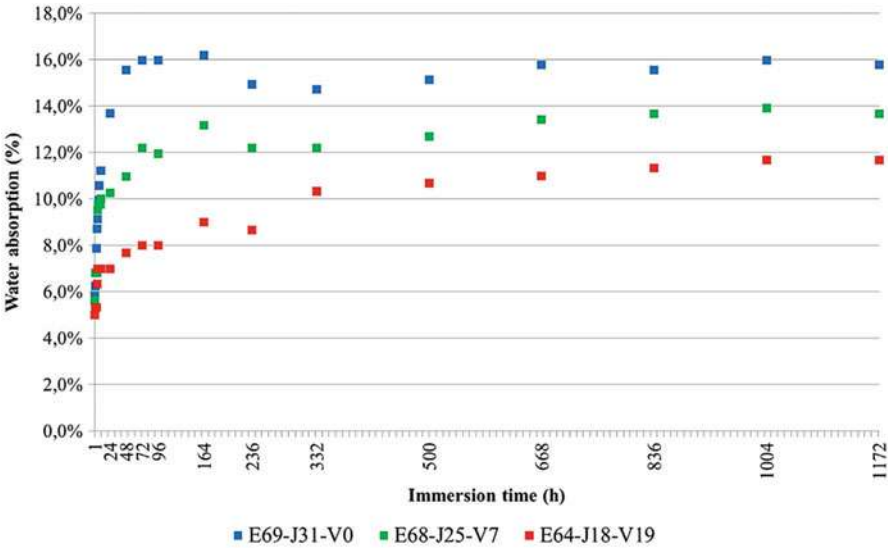

Fig. 7 Water absorption of jute/glass fiber-based hybrid composites (Braga and Magalhaes 2015)

Braga and Magalhaes (2015) analyzed the effect of hybridization on the moisture uptake of woven jute/glass fiber-reinforced hybrid composites. The findings, as depicted in Fig. 7, showed a sharp increase in the moisture uptake of the composite laminates regardless of the fiber types. On average, the hybridization of jute with glass fibers reduced the moisture uptake of the hybrid composite laminates. Ridzuan et al. (2016) determined the moisture absorption of unidirectional *Pennisetum purpureum*/woven glass fiber-reinforced epoxy hybrid composites. The moisture absorption of hybrid composites was compared to that of non-hybrid *Pennisetum purpureum* fiber-based composites. The findings showed that the moisture absorption of non-hybrid and hybrid composites increased with the increase of immersion time. In comparison with hybrid composites, non-hybrid *Pennisetum purpureum* fiber-based composites showed the highest moisture absorption. However, the moisture absorption of hybrid composites reduced with the increase of glass fiber content. The presence of glass fiber acts as the barrier against the moisture uptake, and it could also avoid direct contact between the moisture and the *Pennisetum purpureum* fiber. Yahaya et al. (2016) determined the moisture uptake behavior of kenaf/Kevlar fiber-reinforced epoxy hybrid composites with varying kenaf fiber orientations. They revealed that hybrid composites based on non-woven kenaf mat had the highest moisture uptake. In contrast, the moisture uptake of hybrid composites based on woven and unidirectional kenaf fiber was very similar. This could be attributed to the higher void content of non-woven kenaf mat relative to woven and unidirectional kenaf fiber-based hybrid composites. However, a different behavior was observed from the thickness swelling of hybrid composites. The highest thickness swelling was found in those hybrid composites with unidirectional kenaf fiber, which was followed by woven and non-woven kenaf mat.

Ramesh et al. (2017) evaluated the water uptake of unidirectional banana/carbon fiber-reinforced epoxy hybrid composites. From the results, it was observed that the water uptake of non-hybrid banana fiber-based composites was higher than hybrid composites. As expected, the increase of carbon fiber content reduced the ability of the composites to absorb water. This can be ascribed to the intrinsic hydrophobic behavior of carbon fiber. Sujon et al. (2020) studied the water absorption of woven jute/carbon fiber-reinforced epoxy hybrid composites with varying fiber stacking sequences and orientations. All the composites had a total number of ten fiber layers in which six layers were jute fiber and the other four layers were carbon fiber. On average, it was seen that the hybrid composites with jute fiber as the outermost skin layers had the highest water absorption. Conversely, the lowest water absorption was found in those hybrid composites with carbon fiber as the outermost skin layers. Due to the presence of carbon fiber which acts as a barrier against the water absorption, the placement of carbon fiber as the skin layers could be an alternative way to prevent the penetration of water molecules. When comparing the water absorption of hybrid composites with different fiber orientations, hybrid composites based on unidirectional fibers had the lowest amount of water uptake. The highest water absorption was identified in those hybrid composites with angle-ply fiber orientation. The water absorption of cross-ply hybrid composites was in between unidirectional and angle-ply hybrid composites.

Tribological Properties of Epoxy/Synthetic/Natural Fiber Hybrid Composites

Tribology often involves the principles of friction, wear, and lubrication of the materials. In practice, it deals with the interface between two or more components in relative motion. This relative motion between two components may result in friction and wear at the interface. Tribological properties of the materials have been widely studied because engineering structural components are always related to tribology. Polymer composites have gained widespread usage in various engineering applications to replace metal; thus, more attention should be given to the tribological properties of composite materials. Generally, the addition of fiber in the polymer matrix could enhance the wear resistance of the composite materials. Meanwhile, the coefficient of friction of the materials will be increased with the addition of fiber due to the increase of the discontinuous phase in the composite materials. Although friction and wear are commonly linked to each other in the sense that the frictional force might lead to the wear of the materials, the increase of frictional force does not always increase the wear loss. The coefficient of friction of polymer composites is adjustable, inferring that this property can be increased or decreased by using fillers. For example, the addition of fillers such as graphite, molybdenum sulfide, and hexagonal boron nitride aims at reducing the coefficient of friction of the composite materials. When considering the growing interest in the use of natural fiber in the hybrid composites, the exploration of the tribological properties of natural fiber-based hybrid composites is indispensable.

Patel et al. (2011) made a comparison between the wear resistance of non-hybrid woven jute and hybrid jute/glass fiber-reinforced epoxy composites. It can be seen that the hybridization of jute and glass fiber enhanced the wear resistance of the hybrid composites in comparison with non-hybrid jute-based composites. Among the hybrid composites, the wear resistance was the highest when the jute fiber was placed in the outermost skin layers of hybrid composites. These results presented that the fiber stacking sequence indeed has a significant effect on the wear resistance of hybrid composites. Biswas and Xess (2012) determined the erosive wear behavior of short bamboo/glass fiber-reinforced epoxy hybrid composites with varying total fiber contents. The relative fiber ratio of bamboo to glass was fixed at 1:1. The findings showed that a total fiber content of 15 wt% offered the lowest erosion rate to the hybrid composites, whereas the highest erosion rate was found in neat epoxy. On average, increasing the total fiber content up to 30 wt% and 45 wt% increased the erosion rate of the hybrid composites. Rout and Satapathy (2012) studied the wear resistance of rice husk/glass fiber-reinforced composites with varying rice husk contents. The results showed that the addition of rice husk particulate in the hybrid composites significantly improved the wear resistance. Latha et al. (2016) explored the tribological properties of woven bamboo/glass fiber-reinforced epoxy composites with different stacking sequences. The addition of bamboo fiber showed a positive effect on the tribological properties in which the presence of bamboo fiber improved the wear resistance of the hybrid composites compared to non-hybrid glass fiber-based composites. The wear resistance of hybrid composites was especially promising when the bamboo fiber was placed in the outermost layers of composites. At low impingement angle, non-hybrid bamboo fiber-based composites exhibited the highest wear resistance. However, the wear resistance of non-hybrid bamboo fiber-based composites reduced with an increase of the impingement angle. At the impingement angle of 90°, the highest wear resistance was found in those hybrid composites with the bamboo fiber as the outermost skin layers. Latha and Rao (2018) further explored the effect of ceramic filler on the tribological properties of woven bamboo/glass fiber-reinforced epoxy composites. They found that the addition of 6 wt% zirconia (ZrO_2) filler enhanced the wear resistance of the hybrid composites. The wear resistance of the composites dropped with a further increase of ZrO_2 above 6 wt%. This may be due to the poor interaction between the filler and epoxy at high ZrO_2 content. Overall, the wear rate is augmented with the increase of impact velocity. Table 3 summarizes the literature studies of synthetic/natural fiber-reinforced epoxy hybrid composites.

Conclusion

Synthetic/natural fiber-reinforced hybrid composites have shown distinctive properties that can be employed in nonstructural and structural applications to reduce the reliance on synthetic fibers. The utilization of natural fibers allows the hybrid composites becoming more economical and environmental friendly. This chapter provides an overview of the factors affecting the miscellaneous properties of

Table 3 Summary of the literature studies of synthetic/natural fiber reinforced epoxy hybrid composites

Reinforcement		Miscellaneous properties	Parameter	References
Natural	Synthetic			
Kenaf	Kevlar	Mechanical properties	Stacking sequence	Yahaya et al. (2015)
Basalt/flax/jute	Glass	Mechanical properties	Stacking sequence; fiber types	Jusoh et al. (2016)
Sisal	Glass	Mechanical properties	Stacking sequence	Arpitha et al. (2017)
Kenaf/jute	Glass	Mechanical properties	Stacking sequence; fiber types	Sanjay and Yogesha (2018)
Flax	Carbon	Low-velocity impact	Stacking sequence	Sarasini et al. (2016)
Jute	Glass	Mechanical properties; thermal properties; water absorption	Relative fiber content	Braga and Magalhaes (2015)
Flax/jute	Glass	Mechanical and thermal properties	Stacking sequence; fiber types	Selver et al. (2018)
Sugar palm	Glass	Low-velocity impact; thermal properties	Energy level; benzoyl treatment; relative fiber ratio	Safri et al. (2019)
Kenaf	Glass	Thermal properties	Clay content; hybridization	Mazlan et al. (2020)
Pennisetum purpureum	Glass	Mechanical properties; water absorption	Moisture degradation; relative fiber ratio	Ridzuan et al. (2016)
Kenaf	Kevlar	Mechanical properties; water absorption	Fiber alignment	Yahaya et al. (2016)
Banana	Carbon	Mechanical properties; water absorption	Relative fiber ratio	Ramesh et al. (2017)
Jute	Carbon	Mechanical properties; water absorption	Stacking sequence; fiber orientation	Sujon et al. (2020)
Bamboo	Glass	Mechanical properties; tribological properties	Stacking sequence	Latha et al. (2016)
Bamboo	Glass	Mechanical properties; tribological properties	Ceramic filler content; stacking sequence	Latha and Rao (2018)
Rice husk	Glass	Mechanical properties; tribological properties	Rice husk content	Rout and Satapathy (2012)
Jute	Glass	Tribological properties	Stacking sequence	Patel et al. (2011)
Bamboo	Glass	Tribological properties	Total fiber content	Biswas and Xess (2012)

non-hybrid and hybrid composite materials. The miscellaneous properties of hybrid composites are highly dependent on the fiber properties such as fiber alignment, fiber orientation, and fiber size. Apart from that, the fiber stacking sequence has been found to have a significant effect on the mechanical, tribological, and water absorption properties of woven synthetic/natural fiber-reinforced composites. The incorporation of synthetic fiber as the outermost skin layers in the hybrid composites had been identified to have high potential in resisting the mechanical loads, particularly when subjected to out-of-plane loading. Since the outermost skin layers are the main components sustaining the applied load, the placement of high strength synthetic fiber as the outermost skin layers could be an alternative arrangement in hybrid composites. Several literature studies have demonstrated that the hybrid composites with high strength synthetic fibers as the outermost skin layers exhibited comparable mechanical properties to non-hybrid synthetic fiber-reinforced composites. In the viewpoint of water absorption, hybridization of natural with synthetic fibers also showed a beneficial characteristic as the hydrophobic synthetic fiber acts as a barrier against the moisture uptake of the hybrid composites. It should be emphasized that the placement of synthetic fibers as the outermost skin layers showed a reduction in the moisture uptake to a greater extent. However, the greatest wear resistance of the hybrid composites was obtained when the natural fibers are placed as the outermost skin layers. This might be attributed to the higher wear resistance of natural fibers than synthetic fibers. In addition to mechanical, tribological, and water absorption properties, hybridization of natural with synthetic fibers also showed improvement in the thermal properties compared to those of non-hybrid natural fiber-based composites. The addition of synthetic fiber in the hybrid composite improved the storage and loss modulus as well as the damping factor. In accordance with the literature studies as mentioned above, it is anticipated that the hybridization of natural with synthetic fibers could develop a cost-effective composite material with a more favorable balance between the material properties and environmental friendliness.

References

M.N. Akhtar, A.B. Sulong, M.K.F. Radzi, N.F. Ismail, M.R. Raza, N. Muhamad, M.A. Khan, Prog. Nat. Sci. Mater. Int. **26**, 657 (2016)

M.F.M. Alkbir, S.M. Sapuan, A.A. Nuraini, M.R. Ishak, Compos. Struct. **148**, 59 (2016)

F.A. Almansour, H.N. Dhakal, Z.Y. Zhang, Compos. Struct. **168**, 813 (2017)

K.N. Antin, A. Laukkanen, T. Andersson, D. Smyl, P. Vilaça, Materials (Basel) **12** (2019)

G.R. Arpitha, M.R. Sanjay, P. Senthamaraikannan, C. Barile, B. Yogesha, Exp. Tech. **41**, 577 (2017)

S. Asgarinia, C. Viriyasuthee, S. Phillips, M. Dubé, J. Baets, A. Van Vuure, I. Verpoest, L. Lessard, J. Reinf. Plast. Compos. **34**, 857 (2015)

M. Asim, M. Jawaid, K. Abdan, M.R. Ishak, J. Bionic Eng. **13**, 426 (2016)

M. Asim, M.T. Paridah, M. Chandrasekar, R.M. Shahroze, M. Jawaid, M. Nasir, R. Siakeng, Iran. Polym. J. **29**, 625 (2020)
M. Aslan, M. Tufan, T. Küçükömeroğlu, Compos. Part B Eng. **140**, 241 (2018)
T. Behzad, M. Sain, Polym. Eng. Sci. **47**, 977 (2007)
S. Biswas, P.A. Xess, Int. J. Mech. Ind. Eng. **1**, 79 (2012)
A.K. Bledzki, A.A. Mamun, M. Lucka-Gabor, V.S. Gutowski, Express Polym Lett **2**, 413 (2008)
H.L. Bos, M.J.A. Van Den Oever, O.C.J.J. Peters, J. Mater. Sci. **37**, 1683 (2002)
R.A. Braga, P.A.A. Magalhaes, Mater. Sci. Eng. C **56**, 269 (2015)
M. Cordin, T. Bechtold, T. Pham, Cellulose **25**, 7197 (2018)
R.K. Cullen, M.M. Singh, J. Summerscales, J. Compos. **2013**, 1 (2013)
S.B.R. Devireddy, S. Biswas, J. Reinf. Plast. Compos. **35**, 1157 (2016)
O. Faruk, A.K. Bledzki, H.P. Fink, M. Sain, Prog. Polym. Sci. **37**, 1552 (2012)
N.L. Feng, S. DharMalingam, K.A. Zakaria, M.Z. Selamat, J. Sandw. Struct. Mater. **21**, 2440 (2019)
N.L. Feng, S.D. Malingam, C.W. Ping, N. Razali, Polym. Compos. **41**, 1255 (2020a)
N.L. Feng, S.D. Malingam, N. Razali, S. Subramonian, J. Bionic Eng. **17**, 380 (2020b)
G.S. Gehlen, P.D. Neis, L.Y. de Barros, J.C. Poletto, M. Ebeling, N.F. Ferreira, S.C. Amico, C.C. Angrizani, Polym. Compos. **41**, 112 (2020)
B.K. Goriparthi, K.N.S. Suman, N. Mohan Rao, Compos. Part A Appl. Sci. Manuf. **43**, 1800–1808 (2012)
M. Habibi, L. Laperrière, H.M. Hassanabadi, Compos. Struct. **186**, 175 (2018)
S.I. Hossain, M. Hasan, M.N. Hasan, A. Hassan, Adv. Mater. Sci. Eng. **2013**, 1 (2013)
K. Jarukumjorn, N. Suppakarn, Compos. Part B Eng. **40**, 623 (2009)
P.V. Joseph, G. Mathew, K. Joseph, S. Thomas, P. Pradeep, J. Appl. Polym. Sci. **88**, 602 (2003a)
P.V. Joseph, K. Joseph, S. Thomas, C.K.S. Pillai, V.S. Prasad, G. Groeninckx, M. Sarkissova, Compos. Part A Appl. Sci. Manuf. **34**, 253 (2003b)
M.S.M. Jusoh, C. Santulli, M.Y.M. Yahya, N.S. Hussein, H.A.I. Ahmad, Mater. Sci. Eng. with Adv. Res. **1**, 19 (2016)
M.M. Kabir, H. Wang, K.T. Lau, F. Cardona, Compos. Part B Eng. **43**, 2883 (2012)
S. Kalia, V.K. Kaushik, R.K. Sharma, J. Nat. Fibers **8**, 27 (2011)
P.S. Latha, M.V. Rao, Silicon **10**, 1543 (2018)
P.S. Latha, M.V. Rao, V.V.K. Kumar, G. Raghavendra, S. Ojha, R. Inala, J. Ind. Text. **46**, 3 (2016)
M.K. Lee, B.I.G. Barr, Cem. Concr. Compos. **26**, 299 (2004)
S. Liang, P.B. Gning, L. Guillaumat, Compos. Sci. Technol. **72**, 535 (2012)
L. Mathew, K.U. Joseph, R. Joseph, Prog. Rubber Plast. Recycl. Technol. **20**, 337 (2004)
N. Mazlan, T. Chai Hua, M.T.H. Sultan, K. Abdan, Thermogravimetric and dynamic mechanical analysis of woven glass/kenaf/epoxy hybrid nanocomposite filled with clay. Adv. Mater. Process. Technol. (2020). https://doi.org/10.1080/2374068X.2020.1755114
R. Mishra, H. Jamshaid, J. Militky, Fibers Polym. **18**, 1369 (2017)
L.Y. Mwaikambo, M.P. Ansell, J. Appl. Polym. Sci. **84**, 2222 (2002)
S.K. Nayak, S. Mohanty, J. Reinf. Plast. Compos. **29**, 1551 (2010)
S.K. Nayak, S. Mohanty, S.K. Samal, Polym. Compos. **31**, 1247 (2010)
J.S.S. Neto, R.A.A. Lima, D.K.K. Cavalcanti, J.P.B. Souza, R.A.A. Aguiar, M.D. Banea, J. Appl. Polym. Sci. **136**, 47154 (2019)
L.F. Ng, D. Sivakumar, K.A. Zakaria, O. Bapokutty, Pertanika J. Sci. Technol. **25**, 1 (2017a)
L.F. Ng, D.M. Sivakumar, K.A. Zakaria, M.Z. Bin Selamat, Int. Rev. Mech. Eng. **11**, 61 (2017b)
L.F. Ng, S. Dhar Malingam, M.Z. Selamat, Z. Mustafa, O. Bapokutty, Polym. Bull. **77**, 1449 (2020)
M. Noryani, S.M. Sapuan, M.T. Mastura, M.Y.M. Zuhri, E.S. Zainudin, J. Renew. Mater. **7**, 1165 (2019)
K. Oksman, M. Skrifvars, J.F. Selin, Compos. Sci. Technol. **63**, 1317 (2003)
B. Patel, S. Acharya, D. Mishra, Int. J. Eng. Sci. Technol. **3**, 213 (2011)
S.A. Paul, A. Boudenne, L. Ibos, Y. Candau, K. Joseph, S. Thomas, Compos. Part A Appl. Sci. Manuf. **39**, 1582 (2008)

K.L. Pickering, G.W. Beckermann, S.N. Alam, N.J. Foreman, Compos. Part A Appl. Sci. Manuf. **38**, 461 (2007)
V. Prakash, T. Bera, S. Pradhan, S.K. Acharya, J. Indian Acad. Wood Sci. **17**, 73 (2020)
A.M. Radzi, S.M. Sapuan, M. Jawaid, M.R. Mansor, Fibers Polym. **18**, 1353 (2017)
M. Ramesh, R. Logesh, M. Manikandan, N.S. Kumar, D.V. Pratap, Mater. Res. **20**, 365 (2017)
S.S. Rangaraj, S.B. Bhaduri, J. Mater. Sci. **29**, 2795 (1994)
M.J.M. Ridzuan, M.S. Abdul Majid, M. Afendi, K. Azduwin, N.A.M. Amin, J.M. Zahri, A.G. Gibson, Compos. Struct. **141**, 110 (2016)
A.K. Rout, A. Satapathy, Mater. Des. **41**, 131 (2012)
S.N.A. Safri, M.T.H. Sultan, M. Jawaid, M.S. Abdul Majid, Compos. Struct. **226**, 111308 (2019)
M.R. Sanjay, B. Yogesha, J. Ind. Text. **47**, 1830 (2018)
F. Sarasini, J. Tirillò, S. D'Altilia, T. Valente, C. Santulli, F. Touchard, L. Chocinski-Arnault, D. Mellier, L. Lampani, P. Gaudenzi, Compos. Part B Eng. **91**, 144 (2016)
E. Selver, N. Ucar, T. Gulmez, J. Ind. Text. **48**, 494 (2018)
A. Shahzad, J. Reinf. Plast. Compos. **30**, 1389 (2011)
M.J. Sharba, Z. Leman, M.T.H. Sultan, M.R. Ishak, M.A. Azmah Hanim, Bioresources **11**, 1448 (2016)
S. Sheshmani, A. Ashori, F. Farhani, J. Appl. Polym. Sci. **123**, 1563 (2012)
F.A. Silva, N. Chawla, R.D. de Toledo Filho, Mater. Sci. Eng. A **516**, 90 (2009)
M.A.S. Sujon, M.A. Habib, M.Z. Abedin, J. Mater. Res. Technol. **9**, 10970 (2020)
P.T.R. Swain, S. Biswas, J. Compos. Mater. **51**, 3909 (2017)
R. Velmurugan, V. Manikandan, Compos. Part A Appl. Sci. Manuf. **38**, 2216 (2007)
N. Venkateshwaran, A. Elayaperumal, G.K. Sathiya, Compos. Part B Eng. **43**, 793 (2012)
A.S. Virk, W. Hall, J. Summerscales, Mater. Sci. Technol. **28**, 864 (2017)
X. Wang, M. Petrů, Materials (Basel) **12** (2019)
Y. Xie, C.A.S. Hill, Z. Xiao, H. Militz, C. Mai, Compos. Part A Appl. Sci. Manuf. **41**, 806 (2010)
R. Yahaya, S.M. Sapuan, M. Jawaid, Z. Leman, E.S. Zainudin, Mater. Des. **67**, 173 (2015)
R. Yahaya, S.M. Sapuan, M. Jawaid, Z. Leman, E.S. Zainudin, Def. Technol. **12**, 52 (2016)
Y. Yang, P. Zeng, Compos. Struct. **201**, 434 (2018)
B.F. Yousif, C.W. Chin, Surf. Rev. Lett. **19**, 1250050 (2012)

Modeling and Simulation of Failure in Fiber-Reinforced Polymer Composites

38

Wenjin Xing and Youhong Tang

Contents

Abstract

This chapter provides an overview of widely used computational approaches to fracture and their application in the failure modeling and simulation of fiber-reinforced polymer composite materials and structures. Cohesive elements, eXtended finite element method (XFEM) as discrete crack approaches, and

W. Xing (✉) · Y. Tang (✉)
Institute for NanoScale Science and Technology, College of Science and Engineering, Flinders University, Adelaide, SA, Australia
e-mail: wenjin.xing@flinders.edu.au; youhong.tang@flinders.edu.au

S. Mavinkere Rangappa et al. (eds.), *Handbook of Epoxy/Fiber Composites*,
https://doi.org/10.1007/978-981-19-3603-6_42

phase field models as a continuous crack approach are described in detail. Emphasis is placed on the mathematical formulation and numerical implementation aspects of these computational fracture approaches. Proper microscopic boundary conditions in the context of multiscale modeling are reported. The covered computational fracture approaches are used to investigate the failure responses of fiber-reinforced polymer composites subjected to monotonic loading, with failure resolution at different characteristic length scales. The investigations confirm the potential and power of the continuous and discontinuous crack approaches in predicting the complex failure mechanisms in composite structures.

Keywords

Failure modeling · Computational fracture approaches · Multiscale · Fiber-reinforced polymer composites · Simulation

Introduction

Due to unique and attractive physical properties, fiber-reinforced polymer (FRP) composites have found widespread applications in sectors such as aerospace, automotive, sporting, and construction. The distributed fibers can be made by either synthetic (e.g., carbon, glass, aramid) or natural (e.g., flax, jute, wood) materials. The former group has relatively outstanding and stable mechanical properties, whereas the latter group is typically low-cost, nonabrasive, and biodegradable (Saheb and Jog 1999). The polymers as holding matrices can be classified into thermosets and thermoplastics. The selection of candidate fibers and matrix relies on specific application purposes and surrounding details during service.

To reduce the overall weight of machines or devices, FRP composite structures and components are considered and deployed, most of the time for load-carrying, so their strength and toughness are of great interest. Compared to most conventional engineering materials such as glass and steel, the failure process of FRP composites is much more complicated, since they exhibit an inherent heterogeneity with distinct internal interfaces. Therefore, the reliable and accurate failure prediction of FRP composite structures under diverse loading conditions encounters a grand challenge for researchers and engineers. Although nondestructive damage detection techniques can be used for evaluating the current health state of structures, the collapse moment is very difficult to foresee without involving any modeling and simulation procedure, given limited experimentation (Talreja and Singh 2012).

Computational Fracture Approaches

Fracture as a major form of material failure involves crack initiation and propagation. Cracks have two separated surfaces and break the continuity of an intact material.

Since fracture can severely deteriorate the service performance of composite structures and pose a potential threat to economy and safety, its modeling and simulation via computational approaches is of critical importance. Computational fracture approaches can be classified into two general groups of continuous crack approaches and discrete crack approaches (Rabczuk 2013). These approaches are most often implemented in the broad framework of finite element methods (FEMs). Popular continuous crack approaches include gradient models, nonlocal models, viscous models, or phase field approaches, just to name a few. They all smear the crack over a certain width without representing the discrete crack topology, and involving a tracking algorithm. Concerning the global response, such continuous crack approaches usually work as well as discrete crack approaches. However, the computational cost is typically much higher, as a sufficiently fine discretization is required for the resolution of the crack width. For example, interface thickness for FRP composites varies from a few hundred nanometers to several micrometers, indicating a comparably small length scale parameter in a continuous crack model, and a tiny mesh size on the interface.

On the contrary, the discrete crack approaches represent the discrete crack geometry, as well as imitating the realistic displacement separation. Representative computational approaches for discrete fracture are remeshing techniques, element deletion, cohesive elements, embedded finite elements, extended finite elements, and particles methods. While adopting discrete crack approaches, a common assumption is that the surrounding material of the crack keeps intact, without considering any softening. The discrete crack approaches necessitate two key ingredients: the incorporation of the crack kinematics, and description of fracture criteria for crack initiation and propagation. Some discrete crack approaches, such as cohesive elements and remeshing techniques, have to align the crack along element boundaries; however, others like embedded finite elements and extended finite elements enable mesh-independent crack propagation by exploiting the concept of partition of unity.

Multiscale Nature

Due to the hierarchical and heterogeneous nature of FRP composite materials, the experimental or numerical studies of fracture in composite structures rely on the length scale of observation. FRP composite materials exhibit different failure mechanisms and processes across length scales. At the macroscale, the composite material can be considered as homogeneous yet anisotropic media for which there is no considerable account for fibers, matrix, and in-between interfaces. The effective mechanical properties can be obtained by either experimentally conducting mechanical testing, or numerically performing homogenization techniques. The macroscopic fracture process can be simulated with these effective properties including several key fracture parameters such as material strength and fracture energy in each direction, and at the interply interface (Orifici et al. 2008; Liu and Zheng 2010). Currently, there have been various failure theories to predict the damage initiation, such as Hashin (Hashin 1980), Tsai-Hill (Tsai 1965), and Tsai-Wu (Tsai and Wu 1971). Most failure criteria are interactive criteria, taking account for interactions between the stress or strain components.

At the mesoscale of a laminate, each ply is individually distinguished and homogenized to an orthotropic material in which the fiber direction is implicitly indicated in the ply properties (Van der Meer 2012).

At the microscopic scale where fiber cross-sections can be clearly seen, multiple failure events take place that simultaneously interact with each other. Therefore, it is essential to apply micromechanical models embedded with continuous or discrete crack approaches to characterize the complex failure process (González and LLorca 2007; Totry et al. 2010). To achieve this objective, a representative volume element (RVE) of the microstructure is first constructed mostly based on the geometrical features (e.g., shape, spatial distribution, alignment, volume fraction, and interface thickness) and their statistics obtained from the captured morphology of the composite material. Second, the material properties for each constituent are assigned, followed by other standard FEM operations, such as meshing, prescribing load conditions, and computing. After extraction according to homogenization theories, the homogenized properties can be deployed to the macroscale for use in phenomenological constitutive models. At the same time, the damage profile or crack path can be clearly observed on the RVE under excessive loading. The sequence and extent of damage events can provide valuable insights to the entire failure process, and also help with the design of reliable and durable composite structures (LLorca et al. 2011).

In this chapter, we focus on the popular failure/fracture modeling approaches and their application in the FRP composite structures. The remainder of this chapter is structured as follows. In section "Discontinuous Crack Approaches," we outline two discrete crack approaches: cohesive elements and eXtended finite element method (XFEM), by starting with stating a cohesive crack problem. Considering that cohesive elements are widely used in practice, relevant critical aspects such as mixed-mode cohesive laws and drawbacks associated with (intrinsic) cohesive elements are mentioned. In section "Continuous Crack Approaches," a continuous crack approach is discussed that is phase field model, given the fact that phase field models are receiving increasing attention and interest over the last few years. In section "Boundary Conditions on RVE," potential choices for boundary conditions on RVEs are reported for prescribing macroscopic constraints on the micromechanical model. In section "Numerical Illustrations," a set of numerical illustrations is presented to demonstrate the efficacy of the mentioned computational approaches. Simulation examples for real-world composite structures using FEM yet without considering failure processes are provided in section "Practical Applications," followed by conclusions in the end.

Discontinuous Crack Approaches

Cohesive Crack Problem

Before introducing different numerical approaches to fracture, the mathematical boundary value problem should be first set up. Let us consider a cracked body denoted by Ω, as shown in Fig. 1. The crack and its virtual extension divide the whole domain into two nonoverlapping subdomains Ω^+ and Ω^-. The crack is assumed to include a traction-free portion and a cohesive zone. The nonlinear

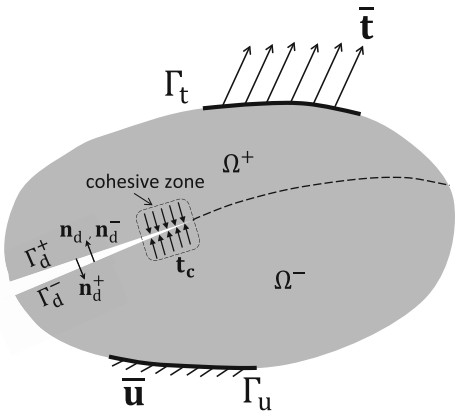

Fig. 1 A two-dimensional fracture problem. The cohesive crack behavior is characterized by the cohesive zone model in the wake of the fictitious crack

material behavior due to various progressive damage mechanisms, including microcracking, is idealized to be restricted to the cohesive zone, while the remaining bulk is assumed linear elastic.

The governing equations comprise the balance of linear momentum, the essential and natural boundary conditions, and the traction continuity across the crack surfaces

$$\nabla \cdot \boldsymbol{\sigma} + \mathbf{b} = \mathbf{0} \quad \text{in } \Omega \tag{1a}$$

$$\boldsymbol{\sigma} \cdot \mathbf{n} = \bar{\mathbf{t}} \quad \text{on } \Gamma_t \tag{1b}$$

$$\mathbf{u} = \bar{\mathbf{u}} \quad \text{on } \Gamma_u \tag{1c}$$

$$-\boldsymbol{\sigma} \cdot \mathbf{n}_d^+ = \boldsymbol{\sigma} \cdot \mathbf{n}_d^- = \mathbf{t}_c \quad \text{on } \Gamma_d \tag{1d}$$

where $\mathbf{t}_c$ is the cohesive traction vector across the crack Γ_d with the unit normal vector $\mathbf{n}_d$ $\left(\mathbf{n}_d = \mathbf{n}_d^- = -\mathbf{n}_d^+\right)$.

Using the principle of virtual work, the weak form corresponding to the strong form of the cohesive crack problem Eq. (1) is derived as

$$\int_\Omega \boldsymbol{\sigma} : \varepsilon(\delta\mathbf{v})\, d\Omega + \int_{\Gamma_d} \mathbf{t}_c \cdot \delta\mathbf{v}\, d\Gamma_d = \int_\Omega \mathbf{b} \cdot \delta\mathbf{v}\, d\Omega + \int_{\Gamma_t} \bar{\mathbf{t}} \cdot \delta\mathbf{v}\, d\Gamma \quad \forall \delta\mathbf{v} \in \mathcal{V} \tag{2}$$

where $\mathcal{V}$ is the functional space of admissible virtual displacements. The operator $[\![\cdot]\!]$ represents the jump of a variable across the crack surfaces. For example, $[\![\mathbf{u}]\!]$ denotes the displacement jump of the crack. The cohesive traction $\mathbf{t}_c$ is an explicit function of the displacement jump $[\![\mathbf{u}]\!]$, determined by a defined cohesive law.

There are two classes of cohesive law models namely (a) initially elastic cohesive laws (*intrinsic model*) and (b) initially? rigid cohesive laws (*extrinsic model*)

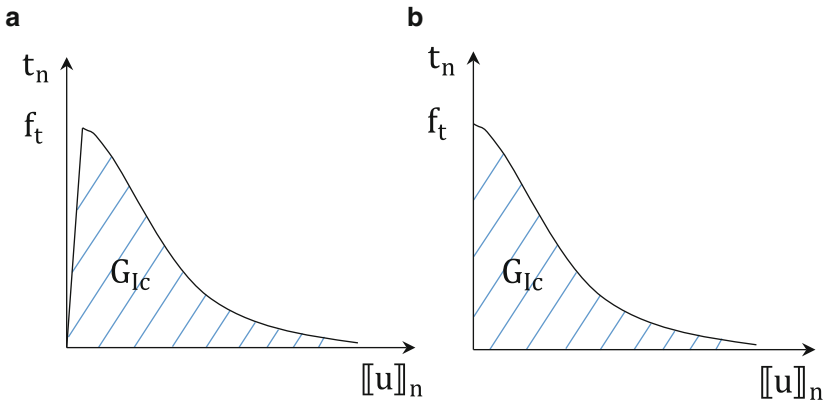

Fig. 2 Schematic of two types of traction-separation laws

(Needleman 1987; Camacho and Ortiz 1996; Kubair and Geubelle 2003). Two typical representatives of those traction-separation law models are illustrated in Fig. 2. It should be mentioned that the initiation criterion is inherently considered in the intrinsic model, whereas in the extrinsic model a separate initiation criterion is essential for starting the fracture process.

The cohesive zone model can be represented by cohesive elements, XFEM, or meshless methods. In the following, we will discuss the cohesive elements and XFEM method.

Cohesive Elements

Cohesive elements (or called interface elements) are extensively utilized to address interface problems, such as composite delamination and interface debonding. At the same time, cohesive elements are also used when capturing complex fracture mechanisms such as crack branching and crack coalescence, where they are explicitly inserted *a priori* along any potential cracking path in the continuum. In this section, the four-node 1*D* linear cohesive elements with initially elastic cohesive laws (see Fig. 2a) are described. Cohesive elements are inserted before the simulation starts and the cohesive law consists of an initial elastic branch with a rather high artificial stiffness.

Kinematics of Cohesive Elements

The bulk is discretized by continuum elements and the crack is discretized by cohesive elements which are one dimension less than the continuum elements, see Fig. 3. Each cohesive element has two characteristic faces, the upper and lower faces, used to model the difference in the displacements at the attached sides of the continuum elements.

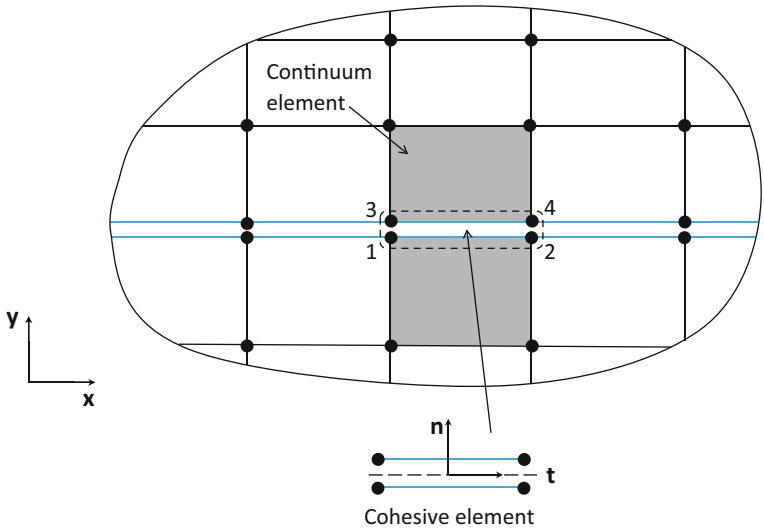

Fig. 3 1D linear cohesive elements are embedded between continuum elements to model the crack. Global coordinates and local coordinates are denoted by (x, y) and $(\mathbf{t}, \mathbf{n})$, respectively. The nodes for the typical cohesive element are ordered 1, 2, 3, 4

With the nodal displacements given for a four-node cohesive element, the global displacements of the upper face (marked by sign +) and lower face (marked by sign –) of the cohesive element are interpolated as

$$\begin{aligned} \mathbf{u}^{+} &= N_1 \mathbf{u}_3 + N_2 \mathbf{u}_4 \\ \mathbf{u}^{+} &= N_1 \mathbf{u}_1 + N_2 \mathbf{u}_2, \end{aligned} \tag{3}$$

where N_1, N_2 are the shape functions of the two-node line elements, and ($\mathbf{u}_3$, $\mathbf{u}_4$) and ($\mathbf{u}_1$, $\mathbf{u}_2$) are the upper-face and the lower-face global nodal displacements, respectively.

The global displacement jump (separation) for the typical crack segment represented by the cohesive element under consideration is then expressed as

$$\mathbf{u} = \mathbf{u}^{+} - \mathbf{u}^{-} = \mathbf{N}_{\text{int}} \begin{bmatrix} \mathbf{u}_3 - \mathbf{u}_1 \\ \mathbf{u}_4 - \mathbf{u}_2 \end{bmatrix}, \tag{4}$$

with $\mathbf{N}_{\text{int}}$ being the shape function matrix of the cohesive element,

$$\mathbf{N}_{\text{int}} = \begin{bmatrix} N_1 & 0 & N_2 & 0 \\ 0 & N_1 & 0 & N_2 \end{bmatrix}, \tag{5}$$

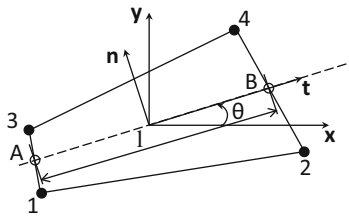

Fig. 4 Definition of the local axes (**t**, **n**), midplane *AB*, and rotation angle θ in a cohesive element

where the subscript "int" has been added to distinguish from that of the continuum elements. Eq. (4) can be modified by introducing a separation-displacement relation matrix $\mathbf{L}_s$

$$\mathbf{L}_s = \begin{bmatrix} -1 & 0 & 0 & 0 & 1 & 0 & 0 & 0 \\ 0 & -1 & 0 & 0 & 0 & 1 & 0 & 0 \\ 0 & 0 & -1 & 0 & 0 & 0 & 1 & 0 \\ 0 & 0 & 0 & -1 & 0 & 0 & 0 & 1 \end{bmatrix}, \tag{6}$$

such that

$$\mathbf{u} = \mathrm{N}_{\mathrm{int}} \mathbf{L}_s [\mathbf{u}_1, \mathbf{u}_2, \mathbf{u}_3, \mathbf{u}_4]^T. \tag{7}$$

To diminish the effect of rigid rotations of cohesive elements, the global coordinate system (**x**, **y**) should be transformed to a local coordinate system (**t**, **n**) aligned with the midplane of the cohesive element, see Fig. 4. The midplane *AB* connecting midside points of the cohesive element defines the local tangential direction **t**. The normal (thickness) axis direction **n** is then obtained as the cross product of the out-of-plane and tangent directions.

To change between the local and global displacements, an orthogonal rotational matrix **Q** is introduced

$$\mathbf{Q} = \begin{bmatrix} \cos\theta & \sin\theta \\ -\sin\theta & \cos\theta \end{bmatrix}, \tag{8}$$

where θ is the rotation angle with respect to the global axes and defined as (see Fig. 4)

$$\begin{aligned} \theta &= \arccos\left(\frac{x_B - x_A}{l}\right) \\ l &= \sqrt{(x_B - x_A)^2 + (y_B - y_A)^2}. \end{aligned} \tag{9}$$

Accordingly, the local separation $[\![\mathbf{u}]\!]^l$ is obtained by the application of the transformation matrix onto the global separation $[\![\mathbf{u}]\!]$

$$\mathbf{u}^l = \mathbf{Q}\mathbf{u} \tag{10}$$

Once the local separation is defined, the local cohesive traction field $\mathbf{t}_c^l$ can be derived through the traction-separation law that describes the crack behavior. The rate form of the cohesive crack constitutive equation can be symbolized as

$$\dot{\mathbf{t}}_c^l = \mathbf{T}\dot{\mathbf{u}}^l, \tag{11}$$

where $\mathbf{T}$ is the cohesive (material) tangent matrix whose precise form relies on the adopted traction-separation law. The global cohesive traction field $\mathbf{t}_c$ is transformed from the local cohesive traction field $\mathbf{t}_c^l$ using the transformation matrix $\mathbf{Q}$

$$\dot{\mathbf{t}}_c = \mathbf{Q}^T\dot{\mathbf{t}}_c^l = \mathbf{Q}^T\mathbf{T}\mathbf{Q}\dot{\mathbf{u}} = \mathbf{Q}^T\mathbf{T}\mathbf{Q}\mathbf{N}_{\text{int}}\mathbf{L}_s\mathbf{L}_e\mathbf{U}. \tag{12}$$

where use of Eqs. (7, 10, 11) was made in sequence in the above derivation, and $\mathbf{L}_e$ is the so-called element location matrix depending on node numbers.

Cohesive Elements Formulation

With the (discretized) approximations for the displacement jumps at hand and for the displacements within the continuum elements, considering their variational forms, Eq. (2) can be discretized as

$$\mathbf{f}_{\text{int}} + \mathbf{f}_{\text{coh}} = \mathbf{f}_{\text{ext}} \tag{13}$$

with

$$\begin{aligned}
\mathbf{f}_{\text{int}} &= \sum_{e=1}^{n_{\text{bulk}}} \mathbf{L}_e^T \int_{\Omega_e} \mathbf{B}_e^T \boldsymbol{\sigma}_e \, d\Omega \\
\mathbf{f}_{\text{coh}} &= \sum_{e=1}^{n_{\text{int}}} \mathbf{L}_e^T \mathbf{L}_s^T \int_{\Gamma_d} \mathbf{N}_{\text{int}}^T \mathbf{t}_c \, d\Gamma \\
\mathbf{f}_{\text{ext}} &= \sum_{e=1}^{n_{\text{bulk}}} \mathbf{L}_e^T \left(\int_{\Omega_e} \mathbf{N}_e^T \mathbf{b}_e \, d\Omega + \int_{\Gamma_e} \mathbf{N}_e^T \bar{\mathbf{t}}_e \, d\Gamma \right),
\end{aligned} \tag{14}$$

where the internal force vector $\mathbf{f}_{\text{int}}$ and external force vector $\mathbf{f}_{\text{ext}}$ are computed from contributions of n_{bulk} continuum elements, whereas $\mathbf{f}_{\text{int}}$ is assembled from n_{int} cohesive elements.

The linearization of the (global) cohesive force vector in Eq. (14) results in the cohesive tangent stiffness matrix. For a cohesive element, the cohesive tangent stiffness matrix is written as

$$\mathbf{K}_e^{\text{int}} = \mathbf{L}_s^T \int_{\Gamma_d} \mathbf{N}_{\text{int}}^T \mathbf{Q}^T \mathbf{T} \mathbf{Q} \mathbf{N}_{\text{int}} \mathbf{L}_s \, d\Gamma, \tag{15}$$

which is an 8×8 matrix for four-node linear cohesive elements, and it is then assembled to the appropriate locations by the element location matrix $\mathbf{L}_e$. The tangent stiffness matrix remains unaltered.

Nguyen (2014) presented an automatic preprocessing procedure for inserting cohesive elements into places where possible crack initiation and propagation are permitted to occur. This increases the flexibility for using cohesive elements in the whole domain for simulation.

Remark 1. *An alternative implementation of the cohesive zone concept allocates discrete point-wise spring elements at FE node pairs on the intended crack surface or interface* (Xie and Waas 2006; Xie et al. 2006). *It makes use of a discrete cohesive zone model that engages a force-separation relation. Tractions distributed on the interface are explicitly lumped to point-wise spring elements instead of their surface contribution being accounted for through performing numerical integration as in the cohesive elements just described.*

Mixed-Mode Cohesive Laws

When describing progressive separation processes in materials, a variety of cohesive (traction-separation) laws can be considered. These cohesive laws generally have distinct shapes for quasi-brittle and ductile materials, depending on the intrinsic nature of materials. Since mixed-mode loading scenarios are frequently encountered in engineering practice, a mixed-mode cohesive law formulation is necessary. In the literature, two main categories of cohesive law formulations exist, namely potential-based formulations (Needleman 1987; Tvergaard and Hutchinson 1993; Ortiz and Pandolfi 1999; Park et al. 2009) and non-potential-based formulations (Xie and Waas 2006; Camanho et al. 2003; Geubelle and Baylor 1998; Turon et al. 2006).

In the first family of formulations, a potential function is first constructed, perhaps using a one-dimensional generalized relationship between the equivalent traction and separation as in Ortiz and Pandolfi (1999). Normal and tangential cohesive laws are merely the derivatives of this potential function with respect to the corresponding normal and tangential separations.

In the second family of formulations, normal and tangential cohesive laws under mixed-mode conditions are not required to be related through a potential function. Their interaction may be governed through extra criteria such as the well-known power law criterion for crack growth (Xie and Waas 2006). In a distinct setting in which each traction component is a function of both normal and tangential separations, a single effective law and a constant scaling factor have been used to treat mixed-mode crack propagation in Geubelle and Baylor (1998). It is noteworthy that some of the non-potential-based implementations encounter a critical issue that nonzero tractions on the crack surface can be found in the final failure state (Nguyen and Waas 2016). To address this issue, an incremental mixed-mode evolution law was developed in Joseph et al. (2018) where the energy remaining to be dissipated is estimated at each load increment following an assumption that the ratio of energy

remaining to be dissipated for the individual modes is proportional to the ratio of energy dissipated by the individual modes so far. Nguyen and Waas (2016) examined different cohesive formulations and proposed a novel mixed-mode cohesive formulation where the mode-II cohesive law is scaled to the mode-I cohesive law, and an effective separation is defined for the scaled law. In this way, physically realistic and numerically stable results were obtained.

In the following, a mixed-mode cohesive formulation following the work by Turon et al. (2006) is described in the two-dimensional setting, where an equivalent displacement jump $[\![u]\!]_{eq}$ is defined as

$$u_{eq} = \sqrt{\langle u_n \rangle^2 + u_s^2}, \tag{16}$$

with $[\![u]\!]_n$ and $[\![u]\!]_s$ being the normal and shear (tangential) components of displacement jump in the local coordinate system, respectively. For a bilinear shape of the softening law, two essential equivalent displacement jump parameters need to be determined at which damage is considered to be initiated and completed. These two equivalent displacement jump parameters are not unique and recognized to depend on the relation between the normal and shear components at the interface. This relation may be captured by the following mode-mixity parameter β (Turon et al. 2006)

$$\beta = \frac{|\, u_s \,|}{\langle u_n \rangle + |\, u_s \,|}, \tag{17}$$

For the detailed treatment of damage initiation criterion, damage evolution law, and tangent stiffness matrix, interested readers refer to Turon et al. (2006).

Drawbacks of Intrinsic Cohesive Elements

1. **Artificial Compliance**

Cohesive elements with an intrinsic cohesive law are not very effective when used for modeling bulk cracking. One major reason is that cohesive elements have to be *a priori* present along all the shared edges of the continuum elements, leading to artificial compliance at the same time. To keep the unnecessary opening to a minimum in the elastic regime, sufficiently high artificial stiffness has to be considered. This may lead to an issue of spurious traction oscillations, as discussed in the literature (Schellekens and De Borst 1993). A widely used strategy to mitigate oscillations is by means of reduced Lobatto integration (Schellekens and De Borst 1993; Simone 2004). Svenning (2016) attributed traction oscillations to the violation of the inf-sup condition and suggested a weak penalty formulation for the intrinsic cohesive elements. Based on a traction approximation that fulfils the inf-sup condition, oscillation free response is expected without the need to modify cohesive zone laws or introduce additional unknowns.

2. **Small Element Sizes**

To fully resolve the cohesive tractions with accuracy and seek the stable post-peak response at each load increment, the size of cohesive elements has to be sufficiently small compared to the characteristic length l_{cz} of the cohesive zone model (Camacho and Ortiz 1996; Falk et al. 2001; Turon et al. 2007). Note that the length l_{cz} is defined as the distance from the crack tip to the point of maximum cohesive traction. The number of elements N_e^{cz} used in the cohesive zone can be defined as

$$N_e^{cz} = \frac{l_{cz}}{l_e}, \tag{18}$$

where l_e is the typical element size in the propagation direction of cracks. Note that l_{cz} can have varied definitions in the literature (Dugdale 1960; Hillerborg et al. 1976).

Small values of cohesive element size would typically result in considerable computational burden, since the size of the cohesive zone of materials is normally small compared to the whole structure. Falk et al. (2001) used N_e^{cz} between two and five elements in the cohesive zone in their simulations. Turon et al. (2007) proposed to adjust the maximum interfacial strength in the computations with coarse meshes. By reducing the maximum interfacial strength, the cohesive zone length l_{cz} can be enlarged such that the cohesive zone is able to comprise more elements. Zander et al. (2017) proposed a multilevel *hp*-adaptivity approach for cohesive fracture where the computational burden was significantly reduced while allowing for an accurate resolution of the cohesive zone.

3. **Convergence Issues**

Alfano and Crisfield (2003) proposed a local arc-length method combined with line-search techniques to alleviate convergence issues when using cohesive elements in their delamination analysis. A poor convergence rate or even divergence can be manifested by local elastic snapbacks on the global load-displacement diagram under displacement loading control (Gao and Bower 2004; Zander et al. 2017). The standard Newton-Raphson method cannot capture such snapbacks as the convergence radius is no longer existent. Another interpretation of the convergence problem is the appearance of several zero or negative eigenvalues in stiffness matrices of damaging elements, thereby resulting in the ill-conditioning of the global discrete system (Liu and Zheng 2010). To make the solution procedure more robust, Chaboche et al. (2001) and Gao and Bower (2004) proposed viscous regularization techniques. Yu et al. (2016) applied such techniques to the numerical study of hydrogen embrittlement under constant displacement condition.

From the energy point of view, the surplus energy released during creation of new free surfaces can appear in other forms, such as kinetic energy or viscous energy. The cohesive traction during separation is adjusted by the rate of separation and the

additional energy dissipation by viscosity is thereby dependent on the rate of separation. For small enough step increments, a positive definite tangent stiffness for the cohesive constitutive model can be expected, which should result in reasonable numerical convergence.

Following the viscous regularization technique by Gao and Bower (2004), a small viscous term is added to the cohesive traction-separation relation. This technique is quite straightforward in practical applications. Let us take a one-dimensional cohesive law in terms of traction t and separation δ for example. The modified traction t_μ can be expressed as

$$t_\mu(\delta) = t(\delta) + \eta \cdot \frac{t_f \delta}{\delta_f}, \tag{19}$$

where η stands for the viscosity parameter; t_f and δ_f are the maximum cohesive strength and the separation corresponding to total failure. In this manner, the dependence of cohesive traction on the rate of separation is explicitly considered. Another alternative is to introduce a viscous constant through controlling the evolution rate of damage variable (Abaqus 2012), by which the increase in damage is slowed down.

Caution should be exercised in choosing the appropriate viscosity parameter, since too high damping may significantly affect the accuracy of solutions, while for low values, convergence may not be attained (Zander et al. 2017). Obtaining an optimal value for the viscosity parameter is a manual process that requires trial and error until the change in response is insignificant.

The Extended Finite Element Method

The eXtended finite element method (XFEM) is a widespread numerical technique for modeling discontinuous and moving interfaces. It is based on the concept of a *partition of unity* and can be viewed as a special case of the partition of unity method (PUM) (Babuška and Melenk 1997). In the literature, a quite similar method to the XFEM is known as the generalized finite element method (GFEM) (Strouboulis et al. 2001).

For any arbitrary field function $f(\mathbf{x})$, the following equality always holds

$$\sum_{i=1}^{n} \varphi_i(\mathbf{x}) f(\mathbf{x}) = f(\mathbf{x}), \quad \text{if} \quad \sum_{i=1}^{n} \varphi_i(\mathbf{x}) = 1. \tag{20}$$

In this case, functions $\varphi_i(\mathbf{x})$ are said to form a partition of unity.

A typical example is the standard finite element method where the shape functions form a partition of unity. The underlying idea of the PUM is that the standard finite element approximation space is enriched by products of the partition-of-unity functions and deliberately selected functions. These selected functions are the so-called *enrichments* and are usually constructed on the basis of *a priori* knowledge

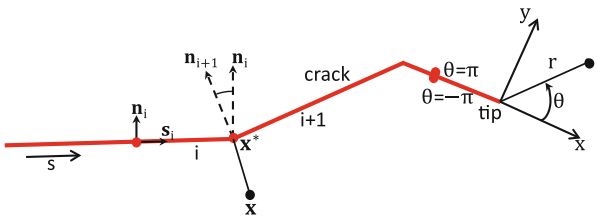

Fig. 5 A crack with kinks to approximate a smooth curved crack with a local polar coordinate system at the crack tip. **x*** is the closest point to **x** on the crack

of the solution of the original physical problem. In this manner, the crucial characteristics of the problem are captured by the enriched approximation, which would otherwise be difficult or even impossible by the piecewise polynomial approximation in the standard FEM.

One remarkable feature of the PUM is the local compact support of the enriched functions, which is achieved by multiplying the enrichment functions with the standard nodal shape functions that take place of $\varphi_i(\mathbf{x})$ in Eq. (20); thus the resulting global stiffness matrix remains sparse. The enrichment functions can be recovered exactly within regions of interest due to the property of partition of unity of the standard shape functions. To avoid linear dependency, the enriched functions should not come from the span of the partition of unity functions.

Whenever particular characteristics are required, additional degrees of freedom are added to the nodes within the enriched regions. Therefore, the mesh topology can be preserved without the need to update for conforming to the interface geometry. This property is quite powerful especially for evolving internal interfaces (e.g., cracks) (Moës et al. 1999; Chessa et al. 2002; Sukumar et al. 2003). In the following, a curved crack that has been approximated with piecewise straight crack segments will be discussed.

The dominant features of the solution to a brittle fracture problem are that the crack is discontinuous in displacements (i.e., crack opening) and the stresses and strains are singular at the crack tip. To capture the highly nonlinear displacement field and the singularity at the crack tip, the branch functions obtained from the exact near-tip asymptotic displacement field are taken as the enrichment functions (Dolbow et al. 2001)

$$B_\alpha(r,\theta) \equiv \left\{ \sqrt{r}\,\sin\frac{\theta}{2}, \sqrt{r}\,\cos\frac{\theta}{2}, \sqrt{r}\,\sin\frac{\theta}{2}\,\sin\theta, \sqrt{r}\,\cos\frac{\theta}{2}\,\sin\theta \right\}, \tag{21}$$

where (r, θ) are the local polar coordinates defined at the crack tip; see Fig. 5. The local polar coordinates r and θ can be evaluated from the local Cartesian coordinates x and y

$$r(x,y) = \sqrt{x^2+y^2}, \quad \theta(x,y) = \operatorname{sgn}(y)\,\arccos\frac{x}{\sqrt{x^2+y^2}}. \tag{22}$$

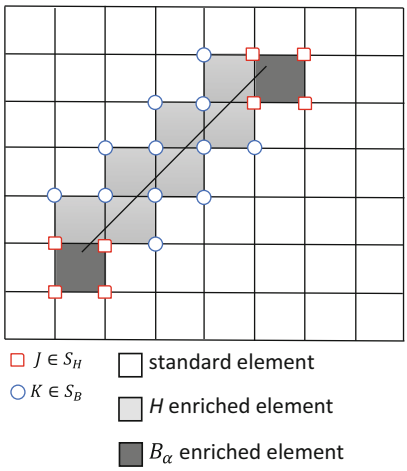

Fig. 6 A typical FE mesh with a crack. The circled nodes are enriched with the Heaviside function, and the squared nodes are enriched with near-tip asymptotic fields

From the above equation, the range of θ is $[-\pi, \pi]$, where $-\pi$ and π correspond to points on the bottom surface and top surface of the crack segment on which the crack tip is located. It is realized that the first function $\sqrt{r}\sin\frac{\theta}{2}$ in Eq. (21) is discontinuous across the crack segment with the crack tip while the remaining three functions are continuous.

The nodes whose support is entirely bisected by the crack, see Fig. 6, are enriched with the Heaviside (step) function $H(\mathbf{x})$ shifted on the crack path. Simply, the crack is often explicitly described by a polyline that can be parametrized by the crack length s, as in Fig. 5. The Heaviside function reads

$$H(\mathbf{x}) = \begin{cases} 1 & \text{for}(\mathbf{x} - \mathbf{x}^*) \cdot \mathbf{n}_i > 0, \\ 0 & \text{for}(\mathbf{x} - \mathbf{x}^*) \cdot \mathbf{n}_i < 0, \end{cases} \tag{23}$$

where $\mathbf{x}^*$ is the closest point on the i-th crack segment to the point $\mathbf{x}$ and $\mathbf{n}_i$ is the unit normal to the current crack segment through the point $\mathbf{x}^*$ such that $\mathbf{s}_i \times \mathbf{n}_i = \mathbf{e}_z$ with $\mathbf{e}_z$ is the unit vector normal to and pointing out of the page. $\mathbf{s}_i$ is the tangential unit vector parallel to the i-th crack segment where $\mathbf{x}^*$ locates. In the case where no unique normal but a cone of normals is defined at $\mathbf{x}^*$, $H(\mathbf{x}) = 1$ if the vector $(\mathbf{x} - \mathbf{x}^*)$ belongs to the cone of normals at $\mathbf{x}^*$ and otherwise 0. By using the Heaviside function, the character of displacement discontinuity along the entire crack is captured exactly where it needs to be identified.

In summary, the approximate displacement field for the body with a linear elastic crack by exploiting the PUM is

$$\mathbf{u}(\mathbf{x}) = \sum_{I \in S} N_I(\mathbf{x})\mathbf{a}_I + \sum_{J \in S_H} N_J(\mathbf{x})H(\mathbf{x})\mathbf{b}_J + \sum_{K \in S_B} N_K(\mathbf{x}) \sum_{\alpha=1}^{4} B_\alpha(\mathbf{x})\mathbf{b}_K^\alpha, \tag{24}$$

where nodes in set S_H are such that their support is split by the crack and nodes in S_B belong to the elements that contain a crack tip. The nodes in these two different sets are enriched with the Heaviside function $H(\mathbf{x})$ in Eq. (23) and the branch functions $B_\alpha(\mathbf{x})$ in Eq. (21), respectively. The number of enriched degrees of freedom per node is equal to the number of terms in the enriched basis multiplied by the spatial dimension.

Following the Bubnov-Galerkin procedure, the discrete equation $\mathbf{Kd} = \mathbf{f}$ is obtained corresponding to the weak form of the XFEM formulation. Special care is needed for the integration of the weak form since the enrichment functions are discontinuous or even singular within the elements. The standard approach for the numerical integration in the XFEM is to split the crack intersected elements into integration subcells (normally triangles) (Khoei 2014). In practice, this is performed according to the geometrical data of the element nodes, intersection points of the crack path with element edges, and the crack tip.

Cohesive Crack with XFEM

To deal with cohesive cracks with the XFEM formulation, we follow the work presented by Wells and Sluys (2001). To allow displacement discontinuities within continuum elements, the Heaviside function defined in Eq. (23) is used. The approximated displacement field can be represented as

$$\mathbf{u} = \mathbf{Na} + H_{\Gamma_d}\mathbf{Nb}, \tag{25}$$

where $\mathbf{N}$ is the matrix of the standard finite element shape functions; the subscript Γ_d has been added to H to indicate that the Heaviside function is centered along the discontinuity Γ_d; the vector $\mathbf{a}$ contains the regular degrees of freedom and the vector $\mathbf{b}$ contains the enriched degrees of freedom. The displacement jump at the discontinuity can be interpolated as

$$\mathbf{u} = \mathbf{Nb}. \tag{26}$$

By taking the symmetric gradient of Eq. (25), the strain field in enriched elements can be expressed as

$$\varepsilon = \mathbf{Ba} + H_{\Gamma_d}\mathbf{Bb} + \left(\delta_{\Gamma_d}\overline{\overline{\mathbf{n}}}\right)\mathbf{Nb}, \tag{27}$$

where δ_{Γ_d} is the Dirac delta distribution as a result of differentiation of the discontinuous Heaviside function; the matrix $\overline{\overline{\mathbf{n}}}$ (not explicitly given here) contains the normal components to the discontinuity.

Inserting the strain expression from Eq. (27) into the weak form of the balance of linear momentum without considering the body forces leads to

$$\int_\Omega \nabla^s\delta\widehat{\mathbf{v}} : \boldsymbol{\sigma}\, d\Omega + \int_\Omega H_{\Gamma_d}\nabla^s\delta\mathbf{v} : \boldsymbol{\sigma}\, d\Omega + \int_{\Gamma_d} \mathbf{t}_c \cdot \delta\mathbf{v}\, d\Gamma_d = \int_{\Gamma_t} \bar{\mathbf{t}} \cdot \delta\widehat{\mathbf{v}}\, d\Gamma, \tag{28}$$

where $\delta\widehat{\mathbf{v}}$ and $\delta\,[\![\mathbf{v}]\!]$ are separate admissible displacement variations; $\mathbf{t}_c$ are the cohesive tractions acting on the discontinuity. The integration property of the Dirac delta distribution and Cauchy's stress theorem were used in the derivation of the third term in Eq. (28). Note that the external force contribution, that is the right-hand side of Eq. (28), does not involve $\delta\,[\![\mathbf{v}]\!]$ related terms in order to simplify in practice the application of traction and displacement boundary conditions.

After deriving the variational formulation as Eq. (28), the next step is to derive the discrete FE equations. The variations $\delta\widehat{\mathbf{v}}$ and $\delta\,[\![\mathbf{v}]\!]$ can be expressed in terms of variations $\delta\mathbf{a}$ and $\delta\mathbf{b}$ of nodal degrees of freedom $\mathbf{a}$ and $\mathbf{b}$ in Eq. (25)

$$\delta\widehat{\mathbf{v}} = \mathbf{N}\delta\mathbf{a}, \quad \delta\mathbf{v} = \mathbf{N}\delta\mathbf{b}. \tag{29}$$

Accordingly, the corresponding gradients of the variations $\delta\widehat{\mathbf{v}}$ and $\delta\,[\![\mathbf{v}]\!]$ are

$$\nabla^s\delta\widehat{\mathbf{v}} = \mathbf{B}\delta\mathbf{a}, \nabla^s\delta\mathbf{v} = \mathbf{B}\delta\mathbf{b}. \tag{30}$$

Inserting these variations into the variational formulation Eq. (28) and taking variations in turn $\delta\widehat{\mathbf{v}}$ and $\delta\,[\![\mathbf{v}]\!]$ while fixing the other result in

$$\int_\Omega \mathbf{B}^T\boldsymbol{\sigma}\,d\Omega = \int_{\Gamma_t} \mathbf{N}^T\bar{\mathbf{t}}\,d\Gamma, \tag{31a}$$

$$\int_{\Omega^+} H_{\Gamma_d}\mathbf{B}^T\boldsymbol{\sigma}\,d\Omega + \int_{\Gamma_d} \mathbf{N}^T\mathbf{t}_c\,d\Gamma_d = \mathbf{0}. \tag{31b}$$

Note that the integration domain of the first integral in Eq. (31b) is Ω^+ (Fig. 1), for which $\delta\,[\![\mathbf{v}]\!]$ is nonzero. From Eq. (31), the equivalent internal nodal forces relating to the regular degrees of freedom $\mathbf{a}$ and to the enriched degrees of freedom $\mathbf{b}$ are written as

$$\mathbf{f}_a^{\text{int}} = \int_\Omega \mathbf{B}^T\boldsymbol{\sigma}\,d\Omega, \tag{32a}$$

$$\mathbf{f}_b^{\text{int}} = \int_{\Omega^+} H_{\Gamma_d}\mathbf{B}^T\boldsymbol{\sigma}\,d\Omega + \int_{\Gamma_d} \mathbf{N}^T\mathbf{t}_c\,d\Gamma_d. \tag{32b}$$

As can be seen from Eq. (32), the internal force vector $\mathbf{f}_a^{\text{int}}$ is of the usual form for finite elements, and the internal force vector $\mathbf{f}_b^{\text{int}}$ must be zero as indicated by Eq. (31b), which imposes traction continuity in a weak sense.

The global stiffness matrix can be obtained as by linearizing Eq. (32)

$$\mathbf{K}_{\text{xfem}} = \begin{bmatrix} \mathbf{K}_{aa} & \mathbf{K}_{ab} \\ \mathbf{K}_{ba} & \mathbf{K}_{bb} \end{bmatrix}, \tag{33}$$

where the constituting components are

$$\begin{aligned}\mathbf{K}_{aa} &= \int_{\Omega} \mathbf{B}^T \mathbf{D} \mathbf{B}\, d\Omega, \\ \mathbf{K}_{ab} &= \mathbf{K}_{ba} = \int_{\Omega^+} H_{\Gamma_d} \mathbf{B}^T \mathbf{D} \mathbf{B}\, d\Omega, \\ \mathbf{K}_{bb} &= \int_{\Omega^+} H_{\Gamma_d} \mathbf{B}^T \mathbf{D} \mathbf{B}\, d\Omega + \int_{\Gamma_d} \mathbf{N}^T \mathbf{Q}^T \mathbf{T} \mathbf{Q} \mathbf{N}\, d\Gamma_d,\end{aligned} \tag{34}$$

where the generic rate form of the bulk constitutive model $\dot{\boldsymbol{\sigma}} = \mathbf{D} : \dot{\varepsilon}$ and the generic rate form of the cohesive constitutive model posed in Eq. (11) have been taken into account. The integration of the discontinuity term in Eq. (31b) over the discontinuity is straightforward. In the case of a two-dimensional implementation, the discontinuity, represented by a set of connected straight line segments, can be integrated using a one-dimensional integration scheme. The implementation of the cohesive XFEM in an existing FE code needs extra modifications in order to find the elements affected by the cracks and to modify the element stiffness matrices of these enriched elements.

In the numerical implementation, when Dirichlet boundary conditions are applied at the enriched nodes, the shifted basis enrichment scheme is suggested such that the enrichment term vanishes at the nodes and thus the blending elements problem is avoided (Zi and Belytschko 2003).

One should notice that in Eq. (25), there is no enrichment term for the crack tip equivalent to the last term in Eq. (24). In this case, the crack tip has to be located on the element edge in order to ensure that the crack tip keeps closed, leading to a fully cracked element.

The initiation or propagation of the discontinuity is governed by a fracture criterion. One commonly adopted criterion is the criterion of maximum principal tensile stress (Wells and Sluys 2001). If the maximum principal tensile stress at any integration point in the element ahead of the crack exceeds the tensile strength of materials, a new discontinuity is introduced or the existing discontinuity is extended with a predefined length. After reaching equilibrium at each time step, we need to check whether or not the fracture criterion is violated at any integration point. If so, we extend the current discontinuity and then recompute the time step for the equilibrium of the system; otherwise we commit the solution and enter the next time step. The reason for the recomputation of the time step is that the just converged nonlinear solution no longer corresponds to an equilibrium state for the modified topology of extending cracks under the same load level.

Due to jumps in the approximated stresses, it may happen that existing crack tips do not extend, but rather new cracks initiate one or two elements away from these tips. In fact, it is often the case that only one main crack will propagate and recently initiated cracks will close. However, the opening and closure of several cracks at the same time can adversely affect the convergence. To this end, new cracks are only permitted to initiate outside a neighborhood of the existing crack tip. This

neighborhood can be defined as a circle centered at the crack tip of radius equal to three to five times element characteristic length. This often provides reasonable results in practice, since new cracks at very small distances cause little extra energy dissipation.

Continuous Crack Approaches

Phase Field Model

In recent years, the phase field model for fracture mechanics is of increasing interest, which bypasses certain limitations of linear elastic fracture mechanics theory of Griffith (Francfort and Marigo 1998). Although the original Griffith's theory can describe crack propagation adequately, it is insufficient to account for complex crack phenomena such as crack initiation, branching, and coalescence.

The phase field model applies a scalar field to smear out the crack surface over the domain as shown in Fig. 7. The phase field model involves a minimization of the regularized form of the Griffith energy, Π, in an elastic body with evolving cracks (Miehe et al. 2010b). To describe damage, a crack phase-field function $d(\mathbf{x})$ is introduced. Its value varies between 0 and 1, representing the unbroken and fully broken material, respectively. Without accounting for body forces and surface tractions, this regularized form can be expressed as

$$\Pi(\mathbf{u}, d) = \int_{\Omega} [g(d)\Psi_{+}(\varepsilon) + \Psi_{-}(\varepsilon)]\, d\Omega + G_c \int_{\Omega} \gamma\, d\Omega, \tag{35}$$

where $g(d)$ denotes a degradation function that captures the effect of damage in the diffuse zone on the elastic strain energy and material stiffness. A common choice for $g(d)$ is a parabolic degradation function: $g(d) = (1 - d)^2 + k$ with k being a small number ensuring the numerical stability of the solution (Miehe et al. 2010b). The strain energy density Ψ in the first term is decomposed into two components of positive and negative to differentiate between tensional and compressive effects on

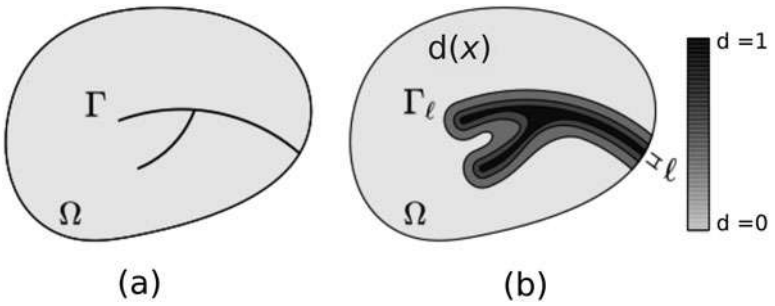

Fig. 7 Diffusive approximation of a discrete sharp crack (**a**) by a phase field $d(\mathbf{x})$ (**b**)

the crack behavior (Amor et al. 2009). The second term in this equation is the regularized form of the fracture energy and corresponds to a representation of diffusive crack topology. A so-called crack density functional γ appears in the second term when transforming the surface integral to the volume integral. As a function of a length-scale parameter l and the phase field d, this crack density functional regularizes the crack topology. The introduced length scale parameter l controls the diffusing profile of the transition zone in the smeared crack, spreading from the intact state to the fully damaged state. One common form of crack density functional (quadratic form) is expressed as follows

$$\gamma = \frac{d^2}{2l} + \frac{l}{2}|\nabla d|^2. \tag{36}$$

There are different schemes for the decomposition of the strain energy density in Eq. (35), in order to maintain resistance in compression and during crack closure. Two notable schemes are the spectral tension-compression decomposition (Miehe et al. 2010a) and the volumetric-deviatoric split (Amor et al. 2009). For example, in the volumetric-deviatoric split, the positive and negative parts of the strain energy are

$$\begin{aligned} \Psi_+(\varepsilon) &= \frac{\lambda}{2}\langle tr[\varepsilon]\rangle_+^2 + \mu tr\left[\varepsilon_+^2\right] \\ \Psi_-(\varepsilon) &= \frac{\lambda}{2}\langle tr[\varepsilon]\rangle_-^2 + \mu tr\left[\varepsilon_-^2\right], \end{aligned} \tag{37}$$

where λ and μ are Lame's constants; ε_+ and ε_- are the positive and negative parts of the strain tensor. To guarantee the irreversibility of the fracture process, a history field needs to be defined, which describes the maximum of the positive strain energy density occurred

$$\mathcal{H}^{n+1} = \max\left(\mathcal{H}^n, \Psi_+^{n+1}\right). \tag{38}$$

The weak form can be readily obtained by taking the stationary of the Lagrangian functional $\delta\Pi(\mathbf{u}, d) = 0$. After application of the Gauss divergence theorem and considering that the weak form must hold for any arbitrary admissible variations, we reach the balance equations

$$\begin{aligned} \nabla \cdot \boldsymbol{\sigma} + \mathbf{b} &= 0 \\ G_e\left(\frac{1}{l}d - l\Delta d\right) &= 2(1-d)\mathcal{H}, \end{aligned} \tag{39}$$

where $\mathbf{b}$ denotes the body force, and Δd refers to the Laplacian of the phase field.

FE Discretization

The two primary fields, namely the displacement and phase fields, and their gradients can be discretized as

$$\begin{aligned} \mathbf{u} &= \mathbf{N}_u(\mathbf{x})\mathbf{u}_u, \quad \nabla\mathbf{u} = \mathbf{B}_u(\mathbf{x})\mathbf{u}_u \\ d(\mathbf{x}) &= \mathbf{N}_d(\mathbf{x})\mathbf{d}_d, \quad \nabla d(\mathbf{x}) = \mathbf{B}_d(\mathbf{x})\mathbf{d}_d \end{aligned} \tag{40}$$

where $\mathbf{u}_u$ and $\mathbf{d}_d$ are the nodal displacement and phase field vectors, respectively. $\mathbf{N}_u$ and $\mathbf{N}_d$ are the operators containing shape functions associated with the displacement and phase field approximations. $\mathbf{B}_u$ and $\mathbf{B}_d$ are the operators containing the partial derivatives of the shape functions with respect to the spatial coordinates. The same discretization is employed for the variations of the two primary fields and their gradients.

To calculate the solution at each time increment, the following algebraic equation system is solved in an iterative manner

$$\begin{bmatrix} \mathbf{r}^u \\ \mathbf{r}^d \end{bmatrix} = 0, \tag{41}$$

with

$$\begin{aligned} \mathbf{r}^u &= \mathbf{f}^{\text{ext}} - \int_\Omega \mathbf{B}_u^T \boldsymbol{\sigma}\, d\Omega = 0 \\ \mathbf{r}^d &= \int_\Omega -G_c\left(l\mathbf{B}_d^T\nabla d + \frac{1}{l}\mathbf{N}_d d\right) + 2(1-d)\mathbf{N}_d\mathcal{H}\, d\Omega. \end{aligned} \tag{42}$$

In the simulation with the phase field model, the used element size h for discretization is likely to affect the convergence of the numerical results to those corresponding to the real discrete crack. Miehe et al. (2010b) recommended that the requirement $h \leq l/2$ must be met.

The phase field model produces a multi-field finite element problem. The global solution is composed of two fields, whose respective solutions can be obtained using either a monolithic or an alternate minimization (or staggered) solution scheme. However, the monolithic solution scheme is numerically unstable for the deformation-fracture coupled problem. To that end, the staggered solution scheme is much preferred in the literature, where two independent minimization procedures take place (Molnár and Gravouil 2017; Wu and Huang 2020).

Boundary Conditions on RVE

Multiscale modeling is important for estimating effective properties, and capturing complex multiscale failure processes in FRP composite materials and structures. To transfer useful information across two scales, a fundamental requirement is energetic consistency. The Hill-Mandel condition (Hill 1963), also termed as the macro-homogeneity condition, states that the local stress power at a macroscopic material point should be equal to the average of the stress power at the microscale

$$\boldsymbol{\sigma}_{\text{M}} : \dot{\varepsilon}_{\text{M}} = \langle \boldsymbol{\sigma}_m : \dot{\varepsilon}_m \rangle. \tag{43}$$

After elaborate algebraic manipulations, the Hill-Mandel condition can be transformed to an equivalent expression

$$\left\langle \widetilde{\boldsymbol{\sigma}}_m : \dot{\widetilde{\varepsilon}}_m \right\rangle = \frac{1}{\mid \Omega_m \mid} \int_{\Gamma_m} \widetilde{\mathbf{t}}_m \cdot \dot{\widetilde{\mathbf{u}}}_m d\Gamma_m = 0, \tag{44}$$

in which the displacement fluctuation vector $\widetilde{\mathbf{u}}_m$ and boundary traction fluctuation vector $\widetilde{\mathbf{t}}_m = \widetilde{\boldsymbol{\sigma}}_m \cdot \mathbf{n}_m$ at the microscale have been introduced.

There are two obvious ways to fulfil the requirement that the average in Eq. (44) vanishes, either setting the displacement or traction fluctuation field on the boundary to zero. The first yields the so-called linear displacement boundary conditions and the latter leads to the so-called uniform traction boundary conditions in the literature. Because the analysis of RVE models under consideration is displacement driven, in the sequel we only focus on the kinematical types of boundary conditions (BCs).

Linear Displacement BCs

As the name indicates, the displacement of the RVE boundary is linear and given by

$$\mathbf{u}_m = \varepsilon_{\mathrm{M}} \cdot \mathbf{X}_m \quad \forall \mathbf{X}_m \in \Gamma_m. \tag{45}$$

It is easy to verify that the linear displacement boundary conditions satisfy the average strain assumption, therefore we omit the proof details here. Due to $\widetilde{\mathbf{u}}_m = \mathbf{0}$ on the boundary, it is concluded from Eq. (44) that the Hill-Mandel condition holds true. Note that in this case, since the RVE problem is deformation driven, the average stress assumption needs to be derived from the Hill-Mandel condition. The numerical implementation of this type of BCs is quite straightforward such that it is not provided here.

Minimal Kinematic BCs

Considering Eq. (44), another way to satisfy the Hill-Mandel condition is to prescribe the boundary tractions by means of

$$\mathbf{t}_m = \boldsymbol{\sigma}_{\mathrm{M}} \cdot n_m, \tag{46}$$

which defines uniform tractions on the boundary of RVE. Since the use of Eq. (46) is not consistent with the deformation-driven FE analysis, as an equivalent to Eq. (46), the minimal kinematic BCs state

$$\varepsilon_{\mathrm{M}} = \frac{1}{\mid \Omega_m \mid} \int_{\Gamma_m} \mathbf{u}_m \bigotimes^s \mathbf{n}_m \, d\Gamma_m. \tag{47}$$

In the numerical context, Eq. (47) can be treated with a Lagrange multiplier method where the stress components $\boldsymbol{\sigma}_{\mathrm{M}}$ act as the Lagrangian multipliers, as mentioned in Miehe et al. (2002).

Periodic BCs

When the RVE has a periodicity in microstructure, periodic BCs are a natural choice. Periodic BCs postulate that the displacement fluctuation field across the RVE boundary is periodic along the periodic directions of the microstructure.

Let us consider a two-dimensional square periodic RVE with bottom-left corner (0, 0) and top-right corner (L_m, L_m) as shown in Fig. 8, where the boundary Γ_m has been decomposed into two parts Γ_m^- and Γ_m^+ such that $\Gamma_m = \Gamma_m^- \cup \Gamma_m^+$ and $\Gamma_m^- \cap \Gamma_m^+ = \emptyset$. In the periodic BCs, except the corner vertex 3, each point $\mathbf{X}_m^+$ on the boundary Γ_m^+ is mapped to its unique corresponding point $\mathbf{X}_m^-$ on the boundary Γ_m^- according to the mapping φ_{per}

$$\begin{aligned} \mathbf{X}_m^- &= \varphi_{\mathrm{per}}\left(\mathbf{X}_m^+\right), \\ \varphi_{\mathrm{per}} : \left(L_m, Y_p\right) &\rightarrow \left(0, Y_p\right) \text{ or } \left(X_p, L_m\right) \rightarrow \left(X_p, 0\right), \end{aligned} \tag{48}$$

where X_p and Y_p refer to X-axis and Y-axis coordinate values of arbitrary point p, respectively. Note the corner vertex 3 has two pairing points (corners), vertex 2 and vertex 4. With these preliminaries, the periodic BCs are defined as

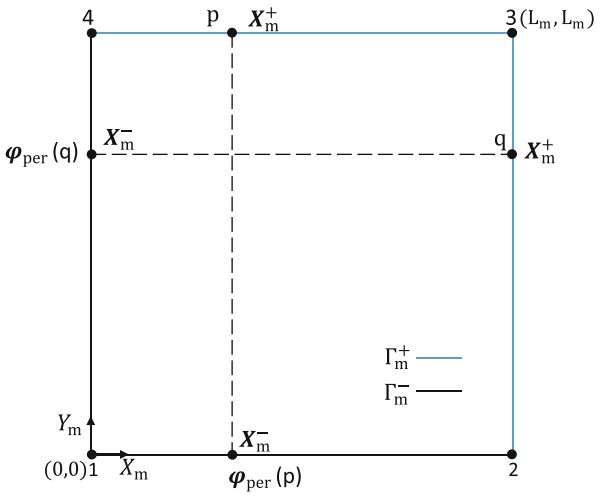

Fig. 8 Schematic representation of a periodic RVE with mapped boundaries; Corner vertices are labelled 1, 2, 3, 4

$$\mathbf{u}\Gamma_m = \mathbf{u}_m^+ - \mathbf{u}_m^- = \varepsilon_{\mathrm{M}} \cdot \left(\mathbf{X}_m^+ - \mathbf{X}_m^-\right), \mathbf{t}_m^+ = -\mathbf{t}_m^-, \tag{49}$$

where use of the notation $()^+ = ()|_{\mathbf{X}^+}$ with $\mathbf{X}^+ \in \Gamma_m^+$ and $()^- = ()|_{\mathbf{X}^-}$ with $\mathbf{X}^- \in \Gamma_m^-$ has been made. The second sub-equation in Eq. (49) implies the anti-periodicity character of boundary tractions.

For the sake of completeness, let us check the equality between the (given) macroscale strain and the averaged microscale strain,

$$\begin{aligned}\langle \varepsilon_m \rangle &= \frac{1}{|\,\Omega_m\,|}\left(\int_{\Gamma_m^+} \mathbf{u}_m^+ \otimes^s \mathbf{n}_m^+ \, d\Gamma_m + \int_{\Gamma_m^-} \mathbf{u}_m^- \otimes^s \mathbf{n}_m^- \, d\Gamma_m\right) \\ &= \frac{1}{|\,\Omega_m\,|}\int_{\Gamma_m^+} (\mathbf{u}_m^+ - \mathbf{u}_m^-) \otimes^s \mathbf{n}_m^+ \, d\Gamma_m \\ &= \frac{1}{|\,\Omega_m\,|}\varepsilon_{\mathrm{M}} . \int_{\Gamma_m^+} (\mathbf{X}_m^+ - \mathbf{X}_m^-) \otimes^s \mathbf{n}_m^+ \, d\Gamma_m \\ &= \varepsilon_{\mathrm{M}},\end{aligned} \tag{50}$$

wherein the fact that $\mathbf{n}_m^+ = -\mathbf{n}_m^-$ has been used twice. It is not difficult to observe the satisfaction of the Hill-Mandel condition from the fact that the expression Eq. (44) vanishes, due to the point-wise periodicity of the boundary displacement fluctuations and point-wise anti-periodicity of boundary traction fluctuations.

Hybrid BCs

The hybrid BCs proposed in Hirschberger et al. (2008, 2009) and adopted in Verhoosel et al. (2010) and Nguyen et al. (2011) are a combination of linear displacement BCs and periodic BCs, as shown in Fig. 9. Along the tangential direction of a material interface or crack, periodic fluctuations are assumed. Macroscopic deformations, such as macroscale interface opening $[\![\mathbf{u}]\!]_{\mathrm{M}}$, are enforced by linear displacement BCs acting on the RVE edges that are not across the interface or crack.

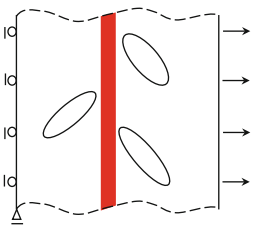

Fig. 9 Schematic representation of hybrid BCs for the tensile failure mode, in which periodic constraints are applied on the top and bottom edges and linear displacement constraints on the left and right edges. The red thick line represents a strain localization band, and the ellipses denote heterogeneities

Numerical Illustrations

Herein, we demonstrate three representative numerical examples by utilizing the computational approaches covered in the previous sections, including an open hole tensile test, single-edge notched bending test, and micromechanical test. Table 1 summarizes the details of these numerical tests.

Open Hole Tensile Test

Different failure mechanisms include interlaminar delamination, fiber fracture, and intralaminar matrix cracking. Sometimes called transverse cracks, these matrix cracks are usually transverse to the loading direction. Open hole laminate specimens consisting of 9 individual plies made of carbon fiber/epoxy resin composites, with dimensions of $200 \times 30 \times 2.7\,\text{mm}^3$ (length × width × thickness), were fabricated in the work by Vigueras et al. (2015). The stacking sequence was $[90°/+45°/-45°/90^0/0°]_s$. In their numerical failure modeling, the XFEM with extrinsic cohesive laws was adopted for capturing the ply failure, and cohesive elements were used for modeling delamination between neighboring plies. The cohesive parameters were obtained from a real double-cantilever beam test for the interlaminar intrinsic cohesive law, and a micro-meso computational model for the intralaminar extrinsic cohesive law. The constitutive law for the bulk intact material was characterized by a linear elastic transversely isotropic material model. The matrix cracking profile evolution at each ply of varying fiber orientation, and the delamination development between adjacent plies were carefully examined, with a direct or quantitative comparison against observations from X-ray computed tomography micrographs. The crack densities and their variations in different plies were different, depending on the fiber orientation and constraints from the adjacent plies. Meanwhile, the delamination shape, location,

Table 1 Modeling and simulation of failure in FRP composites

Numerical test	Characteristic scale	Approaches	Loading conditions	Failure modes
Open hole tensile	Meso/ply scale	XFEM + cohesive elements	Uniaxial tension	Matrix cracking, delamination
Single-edge notched bending	Macro- and microscales	Phase field model + cohesive elements	Bending	Matrix cracking, fiber/matrix debonding
Micromechanical	Microscale	XFEM + cohesive surface contact	Biaxial transverse loadings via periodic BCs	Matrix cracking

and magnitude varied at different interfaces. For example, the delamination at the edges was less extensive than around the hole in the interfaces close to the middle symmetric plane. The interactions between matrix cracks and delamination were well predicted by this discrete crack modeling approach, since this approach is capable to capture high stresses at the tip of transverse cracks. Figure 10 shows the details of matrix cracking and delamination in the open hole composite laminate under tension.

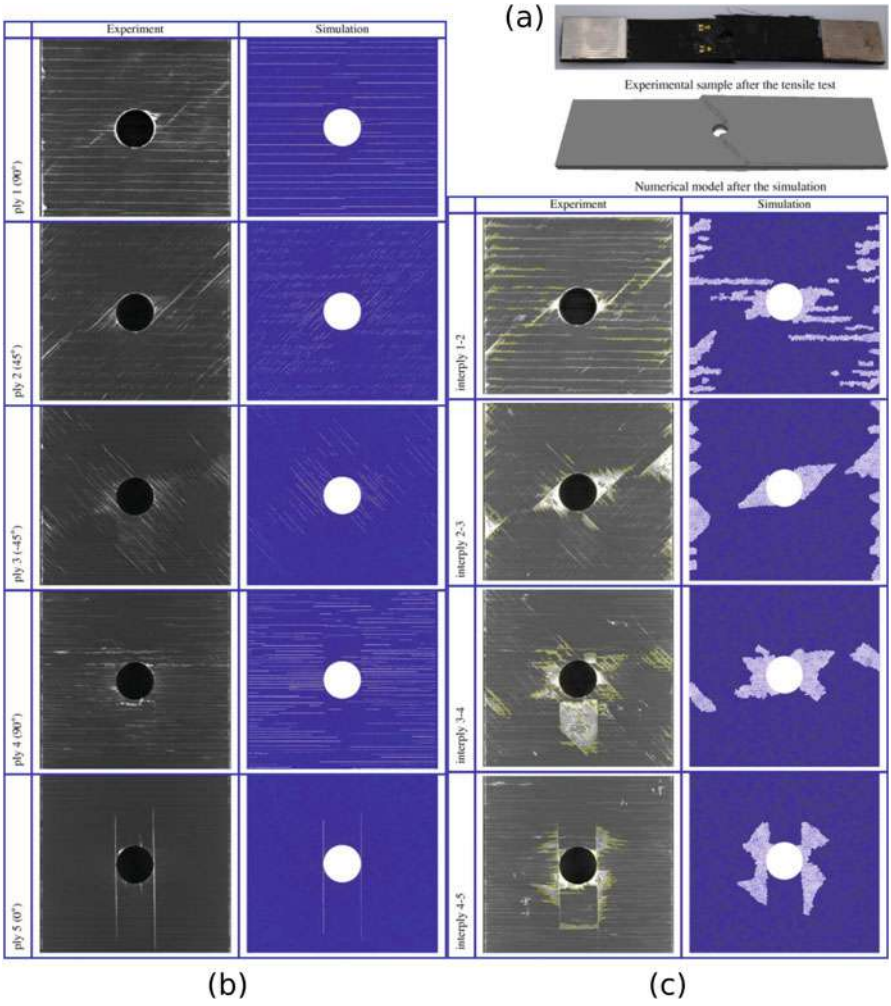

Fig. 10 (**a**) Final fracture profiles of the experimental sample and numerical model after tensile testing. (**b**) Matrix cracks for plies 1, 2, 3, 4 and 5 at 90% failure load. (**c**) Delamination at 90% failure load. (Adapted with permission from Vigueras et al. 2015. © 2015, Elsevier Ltd.)

Single-Edge Notched Bending Test

To reveal the interactions between the microstructural details and the fracture process in fiber-reinforced polymer composites, Tan and Martínez-Pañeda (2020) presented a coupled PF-CZM framework, where the phase field (PF) model and the cohesive zone model (CZM) were employed to simulate the matrix cracking, and fiber-matrix interface debonding, respectively. To capture the interactions, an embedded cell model resolving the composite microstructure was linked with the remaining material domain characterized by homogenized anisotropic elastic constitutive laws. The studied mechanical problem was a single-notched beam under three-point bending, as displayed in Fig. 11a. Inside the embedded cell with a fiber volume fraction of 54%, the glass fiber diameter varied between 13 μm and 17 μm.

As shown in Fig. 11b, the numerical model can accurately capture the experimentally measured response of the bending beam including the pre-critical and

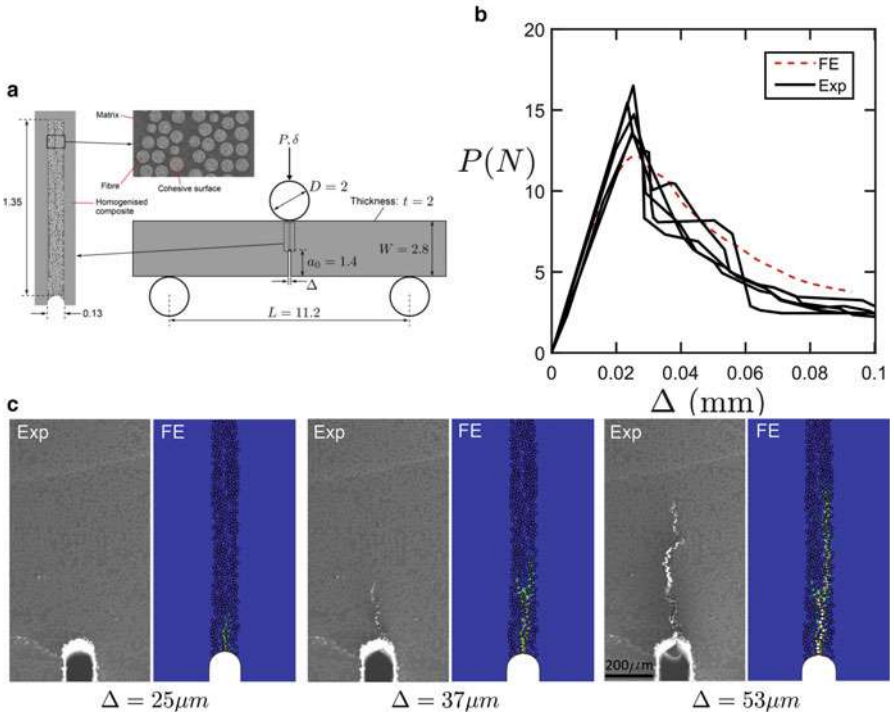

Fig. 11 (**a**) Schematic representation of single-edge notched bending testing. All dimensions are in mm. (**b**) Comparison of experimental and numerical load-CMOD curves. (**c**) Progressive crack propagation at low magnification. (Adapted with permission from Tan and Martínez-Pañeda 2020. © 2020, Elsevier Ltd.)

post-critical regimes in terms of the load-CMOD (crack mouth opening displacement) relation, $P - \Delta$. Moreover, the numerical model adequately reproduces the microscopic deformation and progressive failure process as observed by a sequence of scanning electron micrographs (Fig. 11c). In brief, the failure process starts with interface debonding between the fibers and matrix at high stress sites, which yields voided regions that continuously grow under loading. The final continuous crack is formed by the coalescence of the interfacial voids and the matrix cracks between voids.

Micromechanical Test

Micromechanical modeling is necessary to capture complex failure modes and their interactions in composite structures. To study the effects of variability in the microstructure of unidirectional composites on transverse properties, Bhuiyan et al. (2020) performed a series of FEM simulations based on generated synthetic microstructures following real microstructural statistics. The XFEM and cohesive surface approaches were employed to predict failure initiation strengths of the stochastic microstructures, based on which stochastic failure envelopes were depicted for two biaxial loadings in the transverse plane. Their simulation results revealed the significance of matching the statistics of synthetic microstructure with a real microstructure. In this way, the large scatters in the mechanical properties of composite structures could be predicted by means of considering morphological variations. Figure 12 shows failure profiles in a synthetic microstructure, at different ratios of biaxial transverse tensile loading, and two stochastic failure envelopes, obtained through microscopic modeling with prescribed periodic BCs.

Practical Applications

The last section illustrates the failure modeling and simulation at the specimen scale. However, their practical application still requires huge effort, given the factors including but not limited to large dimensions of industrial structures, complex geometries, strong nonlinearities upon material failure, and limited high-performance computing resources. Here, we present three real-world usage examples of FEM in FRP composite structures, which were only focused on simple mechanical analysis without modeling failure. Despite ignoring failure processes, these examples justify the significance of modeling and simulation that can reduce enormous costs associated with manufacturing prototypes and carrying out mechanical tests in the area of composite materials.

In sport sector, FRP composite structures are increasingly used due to their high strength but low weight. Tryggvason et al. (2020) applied a transient FEM model to

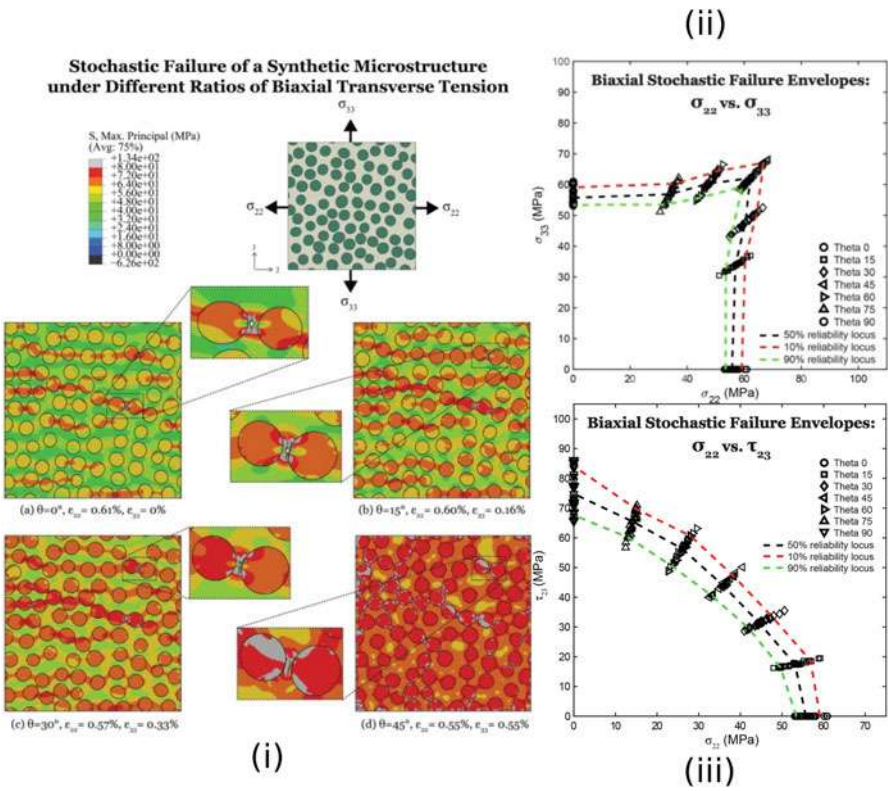

Fig. 12 (i) Failure initiation and evolution in a synthetic microstructure, at different ratios of biaxial transverse tensile loading. (ii) and (iii) $\sigma_{22} - \sigma_{33}$ and $\sigma_{22} - \tau_{23}$ stochastic failure envelopes showing the variability in strengths due to morphological variation in synthetic microstructures. (Adapted with permission from Bhuiyan et al. 2020. c 2020, Elsevier Ltd.)

simulate mechanical reactions to external loads for a prosthetic foot, and to analyze its functional characteristics (Fig. 13I). In aerospace sector, reducing component and assembly weights has been a forefront focus of engineers. Gad-el Hak (2019) simulated composite turbine blades to compare their mechanical performance with that of the stainless steel ones (Fig. 13II). They also showed that fiber orientation has a significant effect on the deformation of the rotor blades. In automotive sector, crashworthiness analysis is inevitable before a new vehicle comes into the market. Impact simulation is important for safety studies in possible collisions. Abdel-Nasser (2013) simulated the vehicle-lighting columns impact (Fig. 13III) and found that the lighting column made of the FRP composite material can more effectively decelerate the vehicle and absorb greater impact energy, thus decreasing the injury risk of vehicle occupants.

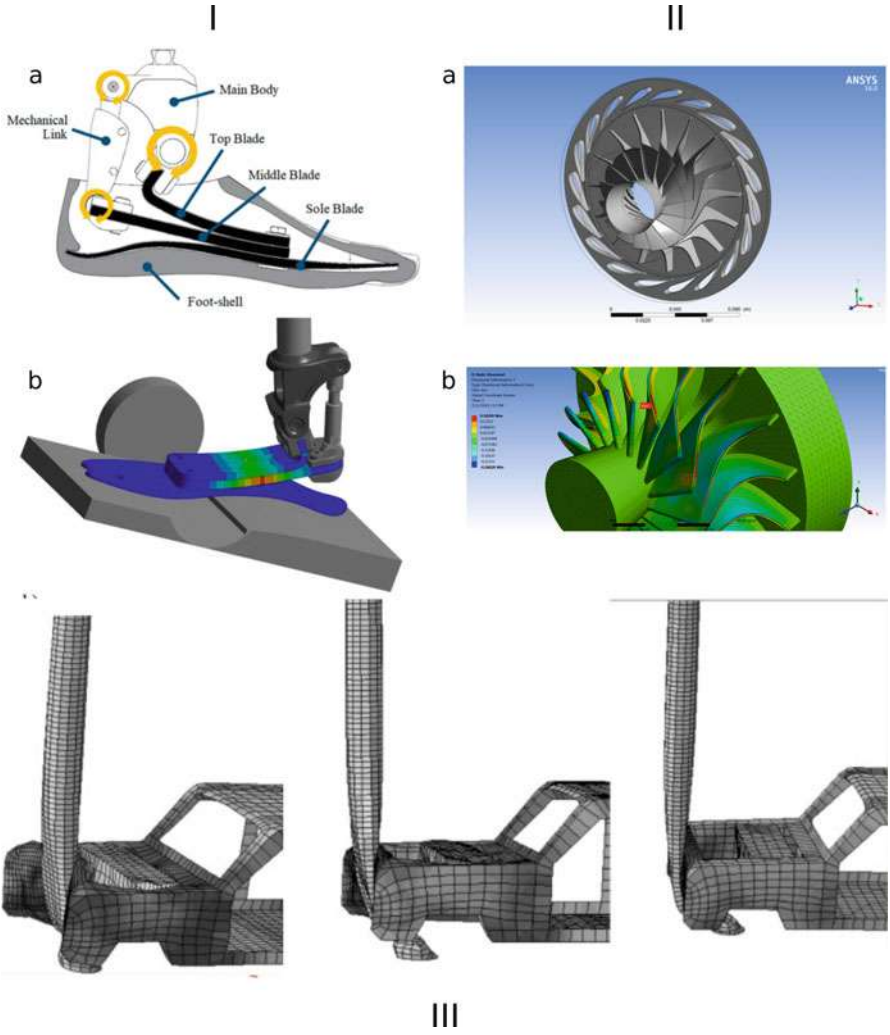

Fig. 13 Three usage examples of FEM in FRP composite structures in different sectors: (I) sport, (II) aerospace, and (III) automotive. Panel (I): (a) Schematic of a prosthetic foot with FRP composite leaf springs colored black; (b) Simulation result showing strain energy at 0.45 s. Adapted under Creative Common License (Tryggvason et al. 2020). Panel (II): (a) Three-dimensional geometrical model of a radial inflow turbine; (b) Directional deformation along the z direction for the composite rotor with a fiber orientation of 40°. Adapted under Creative Common License (Gad-el Hak, 2019). Panel (III) Deformation history of the lighting column in collision made of the FRP composite material. Adapted under Creative Common License (Abdel-Nasser 2013).

Conclusions

In summary, we have described the multiscale nature of FRP composites and outlined the finite element formulation and implementation details for several computational fracture approaches, which are useful to numerically study and predict the failure or collapse of FRP composite structures. Numerical examples were provided to confirm the potential and power of these approaches. Practical applications of FEM in analyzing complex and large real-world FRP composite structures were demonstrated without accounting for any failure.

The discussed computational fracture approaches have been little employed for real-world composite structures. However, this is not the only difficulty. Even for laboratory-level small specimens, high-fidelity modeling, and simulation over the whole collapse period for FRP composite structures in three dimensions that incorporates two or more length scales remains extremely challenging. To this end, the state-of-art computational fracture models need to undergo further significant developments in terms of efficiency, robustness, accuracy, and applicability. Moreover, they can be combined with other advanced numerical techniques, such as parallel computing and model order reduction in order to largely reduce simulation time, computation complexity, or computation expense.

References

Abaqus, *Abaqus 6.12 Theory Manual* (Dassault Systèmes Simulia Corp., Providence, 2012)

Y.A. Abdel-Nasser, Frontal crash simulation of vehicles against lighting columns using fem. Alex. Eng. J. **52**(3), 295–299 (2013)

G. Alfano, M. Crisfield, Solution strategies for the delamination analysis based on a combination of local-control arc-length and line searches. Int. J. Numer. Methods Eng. **58**(7), 999–1048 (2003)

H. Amor, J.-J. Marigo, C. Maurini, Regularized formulation of the variational brittle fracture with unilateral contact: Numerical experiments. J. Mech. Phys. Solids **57**(8), 1209–1229 (2009)

I. Babuška, J.M. Melenk, The partition of unity method. Int. J. Numer. Methods Eng. **40**(4), 727–758 (1997)

F.H. Bhuiyan, S.H.R. Sanei, R.S. Fertig III, Predicting variability in transverse effective elastic moduli and failure initiation strengths in UD composite microstructures due to randomness in fiber location and morphology. Compos. Struct., 111887 (2020)

G.T. Camacho, M. Ortiz, Computational modelling of impact damage in brittle materials. Int. J. Solids Struct. **33**(20–22), 2899–2938 (1996)

P.P. Camanho, C.G. Davila, M. De Moura, Numerical simulation of mixed-mode progressive delamination in composite materials. J. Compos. Mater. **37**(16), 1415–1438 (2003)

J.L. Chaboche, F. Feyel, Y. Monerie, Interface debonding models: A viscous regularization with a limited rate dependency. Int. J. Solids Struct. **38**(18), 3127–3160 (2001)

J. Chessa, P. Smolinski, T. Belytschko, The extended finite element method (XFEM) for solidification problems. Int. J. Numer. Methods Eng. **53**(8), 1959–1977 (2002)

J. Dolbow, N. Moës, T. Belytschko, An extended finite element method for modeling crack growth with frictional contact. Comput. Methods Appl. Mech. Eng. **190**(51-52), 6825–6846 (2001)

D.S. Dugdale, Yielding of steel sheets containing slits. J. Mech. Phys. Solids **8**(2), 100–104 (1960)

M.L. Falk, A. Needleman, J.R. Rice, A critical evaluation of cohesive zone models of dynamic fractur. Le Journal de Physique IV **11**(PR5), Pr5–43 (2001)

G.A. Francfort, J.-J. Marigo, Revisiting brittle fracture as an energy minimization problem. J. Mech. Phys. Solids **46**(8), 1319–1342 (1998)
I. Gad-el Hak, Fluid-structure interaction for biomimetic design of an innovative lightweight turboexpander. Biomimetics **4**(1), 27 (2019)
Y. Gao, A. Bower, A simple technique for avoiding convergence problems in finite element simulations of crack nucleation and growth on cohesive interfaces. Model. Simul. Mater. Sci. Eng. **12**(3), 453 (2004)
P.H. Geubelle, J.S. Baylor, Impact-induced delamination of composites: A 2d simulation. Compos. Part B **29**(5), 589–602 (1998)
C. González, J. LLorca, Mechanical behavior of unidirectional fiber-reinforced polymers under transverse compression: Microscopic mechanisms and modeling. Compos. Sci. Technol. **67**(13), 2795–2806 (2007)
Z. Hashin, Failure criteria for unidirectional fiber composites. J. Appl. Mech. **47**, 329 (1980)
R. Hill, Elastic properties of reinforced solids: Some theoretical principles. J. Mech. Phys. Solids **11**(5), 357–372 (1963)
A. Hillerborg, M. Modéer, P.-E. Petersson, Analysis of crack formation and crack growth in concrete by means of fracture mechanics and finite elements. Cem. Concr. Res. **6**(6), 773–781 (1976)
C.B. Hirschberger, N. Sukumar, P. Steinmann, Computational homogenization of material layers with micromorphic mesostructure. Philos. Mag. **88**(30–32), 3603–3631 (2008)
C. Hirschberger, S. Ricker, P. Steinmann, N. Sukumar, Computational multiscale modelling of heterogeneous material layers. Eng. Fract. Mech. **76**(6), 793–812 (2009)
A.P. Joseph, P. Davidson, A.M. Waas, Open hole and filled hole progressive damage and failure analysis of composite laminates with a countersunk hole. Compos. Struct. **203**, 523–538 (2018)
A.R. Khoei, *Extended Finite Element Method: Theory and Applications* (Wiley, 2014)
D.V. Kubair, P.H. Geubelle, Comparative analysis of extrinsic and intrinsic cohesive models of dynamic fracture. Int. J. Solids Struct. **40**(15), 3853–3868 (2003)
P. Liu, J. Zheng, Recent developments on damage modeling and finite element analysis for composite laminates: A review. Mater. Des. **31**(8), 3825–3834 (2010)
J. LLorca, C. González, J.M. Molina-Aldareguía, J. Segurado, R. Seltzer, F. Sket, M. Rodríguez, S. Sádaba, R. Muñoz, L.P. Canal, Multiscale modeling of composite materials: A roadmap towards virtual testing. Adv. Mater. **23**(44), 5130–5147 (2011)
C. Miehe, J. Schröder, M. Becker, Computational homogenization analysis in finite elasticity: Material and structural instabilities on the micro-and macro-scales of periodic composites and their interaction. Comput. Methods Appl. Mech. Eng. **191**(44), 4971–5005 (2002)
C. Miehe, M. Hofacker, F. Welschinger, A phase field model for rate-independent crack propagation: Robust algorithmic implementation based on operator splits. Comput. Methods Appl. Mech. Eng. **199**(45–48), 2765–2778 (2010a)
C. Miehe, F. Welschinger, M. Hofacker, Thermodynamically consistent phase-field models of fracture: Variational principles and multi-field FE implementations. Int. J. Numer. Methods Eng. **83**(10), 1273–1311 (2010b)
N. Moës, J. Dolbow, T. Belytschko, A finite element method for crack growth without remeshing. Int. J. Numer. Methods Eng. **46**(1), 131–150 (1999)
G. Molnár, A. Gravouil, 2d and 3d Abaqus implementation of a robust staggered phase-field solution for modeling brittle fracture. Finite Elem. Anal. Des. **130**, 27–38 (2017)
A. Needleman, A continuum model for void nucleation by inclusion debonding. J. Appl. Mech. **54**, 525 (1987)
V.P. Nguyen, An open source program to generate zero-thickness cohesive interface elements. Adv. Eng. Softw. **74**, 27–39 (2014)
N. Nguyen, A.M. Waas, A novel mixed-mode cohesive formulation for crack growth analysis. Compos. Struct. **156**, 253–262 (2016)
V.P. Nguyen, O. Lloberas-Valls, M. Stroeven, L.J. Sluys, Homogenization-based multiscale crack modelling: From micro-diffusive damage to macro-cracks. Comput. Methods Appl. Mech. Eng. **200**(9–12), 1220–1236 (2011)

A.C. Orifici, I. Herszberg, R.S. Thomson, Review of methodologies for composite material modelling incorporating failure. Compos. Struct. **86**(1–3), 194–210 (2008)
M. Ortiz, A. Pandolfi, Finite-deformation irreversible cohesive elements for three-dimensional crack-propagation analysis. Int. J. Numer. Methods Eng. **44**(9), 1267–1282 (1999)
K. Park, G.H. Paulino, J.R. Roesler, A unified potential-based cohesive model of mixed-mode fracture. J. Mech. Phys. Solids **57**(6), 891–908 (2009)
T. Rabczuk, Computational methods for fracture in brittle and quasi-brittle solids: State-of-the-art review and future perspectives. ISRN Appl. Math. **2013** (2013)
D.N. Saheb, J.P. Jog, Natural fiber polymer composites: A review. Adv. Polym. Technol. J. Polym. Process. Instit. **18**(4), 351–363 (1999)
J. Schellekens, R. De Borst, On the numerical integration of interface elements. Int. J. Numer. Methods Eng. **36**(1), 43–66 (1993)
A. Simone, Partition of unity-based discontinuous elements for interface phenomena: Computational issues. Commun. Numer. Methods Eng. **20**(6), 465–478 (2004)
T. Strouboulis, K. Copps, I. Babuska, The generalized finite element method. Comput. Methods Appl. Mech. Eng. **190**(32–33), 4081–4193 (2001)
N. Sukumar, D.L. Chopp, B. Moran, Extended finite element method and fast marching method for three-dimensional fatigue crack propagation. Eng. Fract. Mech. **70**(1), 29–48 (2003)
E. Svenning, A weak penalty formulation remedying traction oscillations in interface elements. Comput. Methods Appl. Mech. Eng. **310**, 460–474 (2016)
R. Talreja, C.V. Singh, *Damage and Failure of Composite Materials* (Cambridge University Press, 2012)
W. Tan, E. Martinez-Paneda, Phase field predictions of microscopic fracture and R-curve behaviour of fibre-reinforced composites. Compos. Sci. Technol. **202**, 108539 (2020)
E. Totry, J.M. Molina-Aldareguia, C. Gonzalez, J. LLorca, Effect of fiber, matrix and interface properties on the in-plane shear deformation of carbon-fiber reinforced composites. Compos. Sci. Technol. **70**(6), 970–980 (2010)
H. Tryggvason, F. Starker, C. Lecomte, F. Jonsdottir, Use of dynamic FEA for design modification and energy analysis of a variable stiffness prosthetic foot. Appl. Sci. **10**(2), 650 (2020)
S.W. Tsai, *Strength Characteristics of Composite Materials. Technical Report* (Philco Corp, Newport Beach, 1965)
S.W. Tsai, E.M. Wu, A general theory of strength for anisotropic materials. J. Compos. Mater. **5**(1), 58–80 (1971)
A. Turon, P.P. Camanho, J. Costa, C. Davila, A damage model for the simulation of delamination in advanced composites under variable-mode loading. Mech. Mater. **38**(11), 1072–1089 (2006)
A. Turon, C.G. Davila, P.P. Camanho, J. Costa, An engineering solution for mesh size effects in the simulation of delamination using cohesive zone models. Eng. Fract. Mech. **74**(10), 1665–1682 (2007)
V. Tvergaard, J.W. Hutchinson, The influence of plasticity on mixed mode interface toughness. J. Mech. Phys. Solids **41**(6), 1119–1135 (1993)
F.P. Van der Meer, Mesolevel modeling of failure in composite laminates: Constitutive, kinematic and algorithmic aspects. Arch. Comput. Methods Eng. **19**(3), 381–425 (2012)
C.V. Verhoosel, J.J. Remmers, M.A. Gutierrez, R. De Borst, Computational homogenization for adhesive and cohesive failure in quasi-brittle solids. Int. J. Numer. Methods Eng. **83**(8–9), 1155–1179 (2010)
G. Vigueras, F. Sket, C. Samaniego, L. Wu, L. Noels, D. Tjahjanto, E. Casoni, G. Houzeaux, A. Makradi, J.M. Molina-Aldareguia, et al., An XFEM/CZM implementation for massively parallel simulations of composites fracture. Compos. Struct. **125**, 542–557 (2015)
G.N. Wells, L. Sluys, A new method for modelling cohesive cracks using finite elements. Int. J. Numer. Methods Eng. **50**(12), 2667–2682 (2001)
J.-Y. Wu, Y. Huang, Comprehensive implementations of phase-field damage models in Abaqus. Theor. Appl. Fract. Mech. **106**, 102440 (2020)
D. Xie, A.M. Waas, Discrete cohesive zone model for mixed-mode fracture using finite element analysis. Eng. Fract. Mech. **73**(13), 1783–1796 (2006)

D. Xie, A.G. Salvi, C. Sun, A.M. Waas, A. Caliskan, Discrete cohesive zone model to simulate static fracture in 2D triaxially braided carbon fiber composites. J. Compos. Mater. **40**(22), 2025–2046 (2006)
H. Yu, J.S. Olsen, V. Olden, A. Alvaro, J. He, Z. Zhang, Viscous regularization for cohesive zone modeling under constant displacement: An application to hydrogen embrittlement simulation. Eng. Fract. Mech. **166**, 23–42 (2016)
N. Zander, M. Ruess, T. Bog, S. Kollmannsberger, E. Rank, Multi-level hp-adaptivity for cohesive fracture modeling. Int. J. Numer. Methods Eng. **109**(13), 1723–1755 (2017)
G. Zi, T. Belytschko, New crack-tip elements for XFEM and applications to cohesive cracks. Int. J. Numer. Methods Eng. **57**(15), 2221–2240 (2003)

Advances in Epoxy/Synthetic/Natural Fiber Composites

39

Jyotishkumar Parameswaranpillai, Jineesh Ayippadath Gopi, Murthy Chavali, C. D. Midhun Dominic, Sabarish Radoor, Aswathy Jayakumar, Suchart Siengchin, Sanjay Mavinkere Rangappa, Senthilkumar Krishnasamy, Nishar Hameed, and Sabu Thomas

Contents

J. Parameswaranpillai (✉) · J. A. Gopi · M. Chavali
Division of Chemistry, Department of Science, Faculty of Science & Technology, Alliance University, Bengaluru, Karnataka, India
e-mail: jyotishkumar.p@alliance.edu.in; jineesh.ag@alliance.edu.in; siva.chavali@alliance.edu.in

C. D. Midhun Dominic
Department of Chemistry, Sacred Heart College (Autonomous), Kochi, Kerala, India
e-mail: midhundominic@shcollege.ac.in

S. Radoor · A. Jayakumar
Department of Mechanical and Process Engineering, King Mongkut's University of Technology North Bangkok, The Sirindhorn International Thai-German Graduate School of Engineering (TGGS), Bangsue, Bangkok, Thailand

S. Siengchin · S. M. Rangappa
Department of Materials and Production Engineering, The Sirindhorn International Thai German Graduate School of Engineering (TGGS), King Mongkut's University of Technology North Bangkok (KMUTNB), Bangsue, Bangkok, Thailand
e-mail: suchart.s.pe@tggs-bangkok.org

S. Krishnasamy
Department of Mechanical Engineering, Francis Xavier Engineering College, Tirunelveli, Tamilnadu, India

N. Hameed
School of Engineering, Swinburne University of Technology, Hawthorn, VIC, Australia
e-mail: nisharhameed@swin.edu.au

S. Thomas
International and Inter University Centre for Nanoscience and Nanotechnology (IIUCNN), School of Energy Materials, Mahatma Gandhi University, Kottayam, Kerala, India
e-mail: sabuthomas@mgu.ac.in

S. Mavinkere Rangappa et al. (eds.), *Handbook of Epoxy/Fiber Composites*,
https://doi.org/10.1007/978-981-19-3603-6_52

Abstract

Nowadays, polymer-based composites are used in several applications because of their promising characteristics. Polymers, such as epoxies, polyesters, phenolics, polyimides, etc. have been used in aerospace, marine, electrical, food packaging, cosmetic, medical, and high-temperature applications. Among these polymers, epoxies are widely being used in the composite industry due to their higher specific strength, low cost, and good thermo-mechanical properties. Properties of epoxies can be modified with the incorporation of natural and synthetic fibers. The deformation behavior of epoxy composites under different loading conditions is studied by different researchers and the deformation behavior of composites depends upon factors such as the type of fibers, length of fibers, loading of fibers, orientation of fibers, chemical treatment of fibers, processing technique, and hybrid network of fibers. The hybrid fiber system comprising more than one fiber is an efficient method to further enhance the performance of the epoxy composites. This chapter gives an overview of the mechanical, thermal, and aging properties of epoxy-fiber hybrid composites.

Keywords

Epoxy matrix composites · Fibers · Hybrid · Mechanical · Thermal · Aging

Introduction to Epoxy Resins

Epoxy resins are essential thermosetting polymers that find applications in almost all industries, including coatings, adhesives, automotive, aerospace, and civil engineering. Epoxy polymers were invented in the year 1930 (May 2018). The presence of one or more epoxide groups identifies the epoxy resin. The epoxies can be classified based on the number of epoxide groups present in the epoxy resin. Non-glycidyl and glycidyl epoxides are two classes of epoxies. Glycidyl epoxies include glycidyl amine, glycidyl ester, and glycidyl ether. Diglycidyl ether of bisphenol A-based epoxy resin is the most commercially used epoxy resins (Parameswaranpillai et al. 2017a; George et al. 2014; Hameed et al. 2018). Versatile aliphatic epoxy resins, novolac, glycidyl amine were also established in the epoxy market. Recently bioepoxy resins from plant products have received wide acceptance. These kinds of resins would be helpful to reduce the use of harmful bisphenol-A (Wang et al. 2021a; Pulikkalparambil et al. 2021).

The epoxy resins are low-molecular-weight linear monomers, which undergo a curing reaction upon mixing with curing agents/hardeners. Amines, anhydrides, acids, bases, phenols, etc., have been used as curing agents. Among these, amines are the most widely used hardeners. The mechanisms of the curing reactions are studied by many researchers (Ehlers et al. 2007; Ivankovic et al. 2003; Morancho et al. 2020; Liu et al. 2009; Ochi et al. 1995). During curing, physical changes would

happen to lead to an increase in the viscosity of the epoxy, followed by gelation and vitrification. After the curing, the resin would be completely converted to a hard solid (Jyotishkumar et al. 2011a). The curing of epoxy resins can be studied by differential scanning calorimetry (DSC) (Roşu et al. 2002), Fourier transform infrared (FTIR) spectroscopy (Smith et al. 1984), rheological measurements (Roller 1986), and pressure-volume-temperature measurements (Ramos et al. 2005). The mechanical properties such as fracture toughness (Park et al. 2000), tensile properties (Sastra et al. 2006), flexural properties (Yousif et al. 2012), interlaminar shear strength (ILSS) (Banerjee et al. 2021) of the cured epoxy system can be measured using the universal testing machine. The viscoelastic properties of the cured epoxy can be measured using dynamic mechanical analysis (Anand et al. 2021). The thermal stability can be measured using thermogravimetric analysis (TGA) and DSC (Konnola et al. 2016; Wei et al. 1993). The thermal expansion can be measured using a thermomechanical analyzer (Jyotishkumar et al. 2011b). The volume shrinkage can be measured using PVT measurements (Jyotishkumar et al. 2011a). Microscopy techniques such as atomic force microscopy (AFM), scanning electron microscopy (SEM), transition electron microscopy (TEM), optical microscopy, and confocal microscopy are used to study the morphology of epoxy polymers and their composites (Navarchian et al. 2019; Madeshwaran et al. 2018; Stratigaki et al. 2022). One of the drawbacks of the cured epoxy resin was its high brittleness which limits its application. Therefore, modifications of epoxy resins are significant in terms of their applications in various fields. One of the easiest ways to improve the toughness of epoxy systems can be the incorporation of a second component. The liquid functionalized rubber (Thomas et al. 2008), thermoplastic (Hodgkin et al. 1998), block copolymers (Parameswaranpillai et al. 2017b), nanofillers (Ma et al. 2021; Parameswaranpillai et al. 2013), fibers (Kumar et al. 2021), etc., were used as the second phase to enhance the characteristic properties of epoxy.

The applications of epoxy resins and epoxy composites are compiled from different kinds of literature (Jin et al. 2015; Wazalwar et al. 2021; Mangalgiri 1999) and shown in Fig. 1.

Natural Fiber and Synthetic Fiber-Reinforced Epoxy Composites

Epoxy-based synthetic and natural composites are an emerging area in engineering composites. The advantages of the epoxy composites are their long life, lightweight, easy processing, and low cost. Synthetic fibers are man-made fibers with beneficial properties such as stiffness and high tensile strength (TS) which makes them suitable reinforcements for epoxy composites. Synthetic fibers such as carbon fibers, glass fibers, aramid fibers, carbon nanotubes, graphene, carbon nanofibers, etc., have been used for the fabrication of epoxy composites. Rafique et al. (2016) reviewed recent advances in carbon nanotube-filled epoxy composites as high-performance materials with special reference to the fabrication of the composites. Synthesis and properties such as barrier, thermal, and mechanical properties of petroleum and renewable-based epoxy polymers and their composites were reviewed by Paluvai et al. (2014) and also suggested methods for improving the properties. Hydrothermal aging

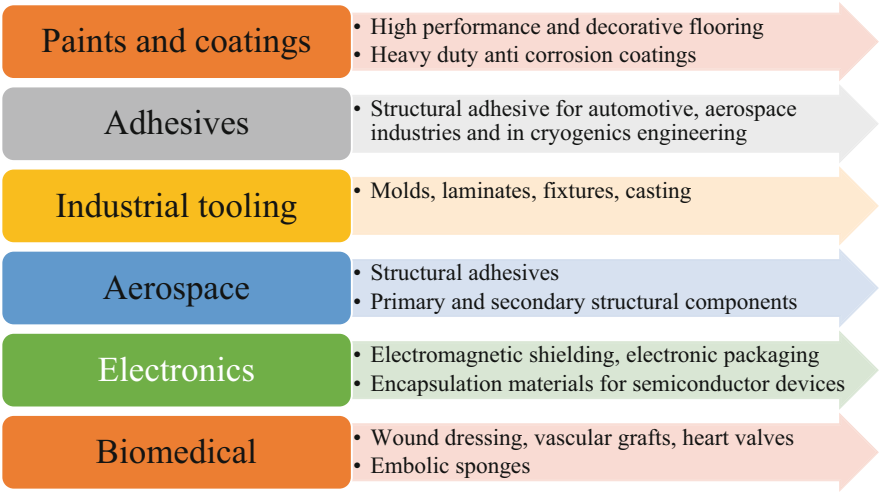

Fig. 1 Applications of epoxy resins and composites

resistance is crucial for aeronautic structures and carbon fiber is the choice for automobile and aerospace applications, due to its high strength, modulus, corrosion resistance, and hydrothermal aging resistance (Cysne Barbosa et al. 2017). Guermazi et al. (2014) observed good hydrothermal aging resistance for carbon/epoxy composites compared to glass/epoxy and hybrid epoxy composites. Obradović et al. (2021) studied the effect of water/moisture absorption (72 h) on the tensile and impact behavior of epoxy/Kolon fiber composites reinforced by SiC nanofiber. The parameters such as tensile elongation, tensile energy absorption, of epoxy/Kolon fiber were improved with the reinforcement with SiC nanofibers.

In recent years, natural fibers have been preferred over synthetic fibers because of their good strength and stiffness, sustainability, eco-friendliness, easy processing, biodegradability, lower carbon footprint, and low cost. Also, synthetic fibers have a minimum possibility for recyclability. Some of the widely used natural fibers for the composite industry are ramie, hemp, kenaf, jute, sisal, bamboo, banana, sugar palm, and oil palm fibers (Vinod et al. 2020). Mittal et al. (2016) compiled the literature which discusses the effect of different natural fibers, their loading, geometry, size of the fiber, chemical functionalization of natural fibers, and coupling agents for the better interaction between polymer matrix and natural fibers. The reinforcing effects of various natural fibers on the mechanical properties of epoxies are compiled by researchers and these studies have shown the applicability of these epoxy composites in different engineering applications (Parbin et al. 2019; Sathishkumar et al. 2020). Though the natural fibers have many advantages, these fibers are hydrophilic, which results in the intake of water that results in the composite's swelling, leading to poor performance. Thus, water absorption is a significant drawback of natural fiber-reinforced composites and limits the durability of composites. To improve the interfacial interaction between the polymers and fillers, methods such as chemical

treatment, hybrid filler system, the introduction of coupling agents, etc., onto the natural fiber have been used extensively. However, the use of chemicals for the treatment of natural fiber is not environmentally friendly. Hence, a hybrid fiber system comprising of natural fiber and synthetic fiber is an alternate technique to enhance the performance of the composites (Mochane et al. 2019). The synergistic effect from the individual fibers contributes to the performance of the hybrid composites. Many studies reported synergic improvement in the properties of epoxy with the incorporation of both synthetic and natural fibers. The hybrid composites with natural fiber and synthetic fibers have many added advantages, such as improved thermo-mechanical performance and reduced moisture absorption. Also, one can make the composites greener by introducing natural fiber in synthetic fiber-reinforced composites. Several methods such as (i) hand layup, (ii) vacuum infusion process, (iii) autoclave, (iv) filament winding, (v) compression molding, and (v) pultrusion are used in the manufacturing of epoxy composites. The resin transfer molding, vacuum infusion process, and autoclave are widely employed in the automotive sector. Some literature related to epoxy–natural fiber-natural fiber hybrid composites are listed in Table 1.

A significant number of studies were performed on epoxy natural fiber/synthetic fiber hybrid composites. Glass fibers, Kevlar, and carbon fibers along with natural fibers were widely used to prepare epoxy hybrid composites with improved properties. Table 2 lists literature related to natural fiber/synthetic fiber epoxy composites.

Also, a significant number of studies have been reported on the improvement on tensile, compressive, flexural and impact properties of epoxy polymers by using two or more synthetic fibers (Selmy et al. 2012; Kalantari et al. 2016; Dong 2016; Hashim et al. 2019; Guo et al. 2022; Monticeli et al. 2022; Alsaadi et al. 2018; Ravindran et al. 2018; Wang et al. 2021b).

Mechanical and Thermal Properties of Hybrid Epoxy Matrix Composites

The hybrid composites possess a higher load-bearing capacity compared to the composites containing single fiber. The mechanical properties of hybrid fiber composites depend on the nature and properties of matrix and fibers, dispersion and distribution of fibers, loading of fibers, the orientation of the fibers, hybrid fiber networks, interaction between the matrix and fibers, etc. Prediction of mechanical properties can be performed with the help of theoretical models such as Voigt, Reuss, Hirsch, and Tsai–Pagano (Mochane et al. 2019). Satheeshkumar et al. (2014) reviewed advances in the field of polymer hybrid fiber composite with special reference to TS, FS, dynamic mechanical properties, tribological properties, and water absorption characteristics of the hybrid fibers-polymer composites.

Yahaya et al. (2016) studied the hybridization effect of kenaf and Kevlar fiber in epoxy composites and found that the hybrid network improved the impact properties. An epoxy hybrid composite with 40 wt.% fiber content with an equal

Table 1 Epoxy–natural fiber/natural fiber hybrid composites

S. No.	Epoxy resin	Natural fiber 1	Natural fiber 2	Major characteristics	Reference
1	Liquid epoxy resin (DER-331) and modified cyclo aliphatic amine as a hardener	Bamboo fiber	Kenaf fiber	The incorporation of fibers in the epoxy polymers reduced the oxidation onset temperature compared to the pure epoxy due to the presence of OH groups in natural fibers. Hybrid composite with higher kenaf fiber content showed better thermo-oxidative stability among hybrid composites.	Chee et al. (2018)
2	Epoxy resin-based on bisphenol-A (DER-331) and modified cyclo aliphatic amine as a hardener	Bamboo fiber	Kenaf fiber	A positive hybridization effect in dimensional stability and viscoelastic properties were observed.	Chee et al. (2019)
3	Epoxy resin-based on bisphenol-A (LY 556) corresponding hardener (HY 951)	Short banana fiber	Jute fiber	The incorporation of fibers decreased the thermal diffusivity of the epoxy composites and thus possess better thermal insulating properties.	Devireddy and Biswas (2016)
4	Epoxy resin (DGEBP-A) and curing agent (poly amido phenol)	Jute fiber	Banana fiber	Composite with 50 wt% jute and banana fiber (1:1) content provides higher TS, higher thermal resistance, and less water absorption compared to composite with only jute fibers.	Boopalan et al. (2013)
5	Bioepoxy	Jute fiber	Hemp fiber	Jute fiber as a core layer and hemp fiber as a skin layer provided higher TS	Vinod et al. (2022)

(continued)

Table 1 (continued)

S. No.	Epoxy resin	Natural fiber 1	Natural fiber 2	Major characteristics	Reference
				and flexural strength (FS). But the ILSS was reduced for the composite.	
6	Medium-viscosity, unmodified epoxy resin based on bisphenol-A araldite LY556 and hardener HY- 917	Gourd sponge	Coir fiber	In the hybrid composites, TS and impact strength (IS) were highest with increasing coir content and FS was highest with increasing gourd sponge content.	Mehra et al. (2021)
7	Epoxy resin-based on bisphenol-A (LY556) and hardener (LY953) in the 4:1 ratio	Banana fiber	Sisal fiber and sawdust	Provided higher TS, compressive, FS, and IS.	Kumari et al. (2022)
8	Epoxy resin LY556 and hardener HY951	Areca fiber	Kenaf fiber	The composite with all kenaf fiber mats (5 layers) showed the highest modulus and glass transition temperature (T_g).	Sathyaseelan et al. (2021)
9	Epoxy resin-based on bisphenol-A (LY 556 resin) with hardener	Nettle fiber	Bauhinia vahlii fiber	The hybrid composite possesses improved mechanical and sliding wear properties which make it a candidate for applications where both tribological resistance and strength are required.	Kumar et al. (2020)

amount of bamboo fiber and kenaf fiber showed better dimensional stability and dynamic mechanical properties compared to single fiber composites (Chee et al. 2019). Goud et al. (Goud and Rao 2012) prepared *Roystonea* regia/glass fiber epoxy hybrid composites and observed that the TS, tensile modulus (TM), FS, and impact strength (IS) increased with an increase in the glass fiber loading. This was due to the inherent strength of glass fibers. SEM studies showed very good dispersion of both fibers in the epoxy matrix. The prepared hybrid composites showed the combined properties of mechanical strength, lower density, and

Table 2 Epoxy – natural fiber/synthetic fiber hybrid composites

S. No.	Epoxy resin	Natural fiber	Synthetic fiber	Major Characteristics	Reference
1	Evopreg EPC300-F150U epoxy prepregs	Flax fiber	Glass fiber	The hybrid composite with alternate flax and glass layers reported the best fatigue resistance.	Barouni et al. (2022)
2	Epoxy resin (LY 1564) and hardener (Aradur 22,962)	Flax	Carbon fiber	The hybrid composite with woven carbon fiber and cross-ply flax fiber provided better impact properties compared to woven carbon fiber and unidirectional flax fibers hybrid composites.	Al-Hajaj et al. (2019)
3	Epoxy resin (AW-106) and hardener (HV 953 U)	Ramie fibers	Glass fibers	The composite of 10 wt.% ramie fiber and 20 wt.% glass fibers showed higher TS and this composite was more eco-friendly compared to epoxy-full glass fiber composite.	Giridharan (2019)
4	Araldite® LY 1564 low viscosity epoxy with Aradur® 22,962 hardener polyamine	Flax fibers	Woven carbon fibers	Epoxy hybrid composite with 2 outer layers of 4 harness satin woven carbon fibers +12 layers of unidirectional flax fibers as inner-core showed higher mechanical strength compared to hybrid composite with 2 outer layers of 4 harness satin woven carbon fibers +12 layers of alternating obliquely-angled flax fibers.	Al-Hajaj et al. (2018)
5	SR 1710/SD 7820 (Sicomin) epoxy system	Flax fiber	Kevlar fiber	Hybrid composite with Kevlar fibers and flax fibers	Audibert et al. (2018)

(continued)

Table 2 (continued)

S. No.	Epoxy resin	Natural fiber	Synthetic fiber	Major Characteristics	Reference
				showed intermediate mechanical properties compared to composites with only Kevlar and composite only flax composites.	
6	Low viscosity epoxy resin (araldite LY1564) with hardener (Aradur3486)	Flax fibers	Silk fibers	The incorporation of flax fibers in epoxy-silk composite increased TS, FS, and IS.	Wu et al. (2019)
7	Epoxy resin and epoxy hardener used were Zeepoxy HL002 TA/B	Sugar palm fiber	Glass fiber	Hybrid composites of benzoyl chloride treated sugar palm fiber and glass fiber hybrid composites showed higher FS and compressive strength compared to untreated hybrid composites. Also, the incorporation of glass fiber increased the compressive and FS of the epoxy hybrid composites.	Safri et al. (2018)
8	Epoxy resin YD535LV and hardener TH7255	Coir fiber	Carbon fiber	Compared to untreated coir/ carbon fiber composite, alkaline treated coir/carbon fiber showed better mechanical properties. An improvement in the interfacial bonding between the alkaline treated coir and epoxy matrix is observed in the SEM micrographs.	Singh et al. (2020)
9	Epoxy resin araldite LY 556 and hardener HY 991	Sisal fiber	Glass fiber	Composites using hybrid sisal-glass fiber-reinforced polymer showed better impact properties compared	Sriranga et al. (2021)

(continued)

Table 2 (continued)

S. No.	Epoxy resin	Natural fiber	Synthetic fiber	Major Characteristics	Reference
				to single fiber composites.	
10	EpoxAmite 100 series resin with a hardener	*Pennisetum purpureum* fibers	Glass fiber	Alkaline treated *Pennisetum purpureum* fiber and glass fiber hybrid composite showed better initial degradation temperature, high storage modulus at room temperature, TS, and FS.	Ridzuan et al. (2016)

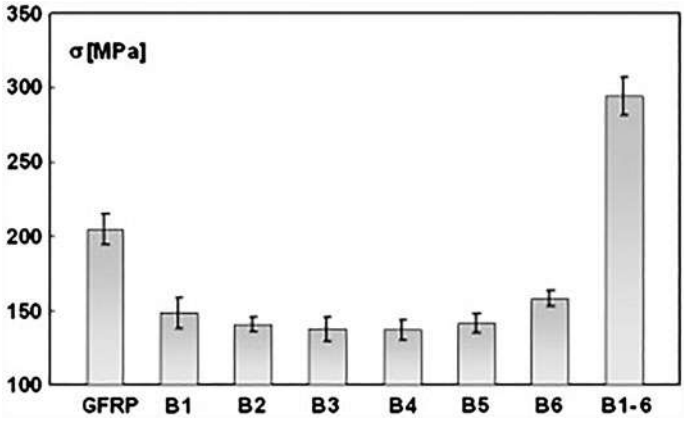

Fig. 2 The FS of GFRP and hybrid composites (Fiore et al. 2011). (Reproduced with thanks from Elsevier, License Number: 5261050752485)

eco-friendliness. Jawaid et al. (2013) fabricated epoxy-hybrid composites by using jute and oil palm fibers with different hybrid fiber ratios. The increase in the loading of jute fiber increases the TS and TM. An oil palm fiber and jute fiber ratio of 1:4 provided the highest TS of 37.9 MPa and TM of 3.31 GPa at total fiber loading of 40 wt%.

Fiore et al. (2011) studied the three-point bending and tensile properties of glass mat/epoxy composite (GFRP), and hybrid epoxy composites containing glass mat and unidirectional basalt fabric fabricated by vacuum bagging. The six-layered E-glass mat was used in GFRP. In hybrid composites (B1-B5), one layer of E-glass mat was replaced by unidirectional basalt fabric, and in B1–6 hybrid composite, basalt fabrics were used as the exterior layers (B1–6). The flexural results shown in Fig. 2 indicated that the hybrid composites with basalt as the exterior layers

possess higher FS. The researchers used finite element analysis to evaluate the performance of the composites numerically and compared the results with experimental values. It was observed that the stress was uniformly distributed in hybrid composites when the basalt fiber was positioned as exterior layers. The study further confirmed that the hybrid composites with basalt as the exterior layers (B1–6) are excellent materials for manufacturing complex structures like ship hulls.

In recent work, Fiore and Calabrese (2019) studied the epoxy composites with flax and/or jute plain weave fabrics and tested them for quasi-static and viscoelastic properties. The composites fabricated are untreated flax fiber-reinforced composites, sodium bicarbonate treated flax fiber-reinforced composites, jute fiber-reinforced composites, treated jute fiber-reinforced composites, flax-hybrid (F/J/F/J/F), treated flax hybrid (F/J/F/J/F), jute-hybrid (J/F/J/F/J), and treated jute hybrid (J/F/J/F/J) composites. Five layers of the woven fabrics were used for neat flax and jute fabric reinforced composites. The effect of the hybrid fiber system on the flexural properties of untreated and treated composites is given in Fig. 3. The jute reinforced composites showed a brittle behavior with high flexural strength (FS) of 88.8 MPa, modulus of 4.78 GPa, and strain 2.77%. On the other hand, the flax reinforced composites showed an elastoplastic behavior with less strength of 73.7 MPa, modulus 3.85 GPa, and strain 5%. The high stiffness of the jute fiber led to the high modulus of the composites. On the other hand, the low strain was due to the reinforcement of jute fiber with epoxy matrix. The bicarbonate treatment led to an increase in FS of the flax composites with a reduction in % strain. Compared to untreated jute reinforced composites, treated jute composite showed only marginal variations.

Pathak et al. (2016) synthesized graphene oxide (GO) and introduced GO in carbon fiber/−epoxy composites to fabricate high-performance hybrid composites. The incorporation of 0.3 wt% GO content improved the FS, flexural modulus (FM), and ILSS. The researchers confirmed that the hydrogen bonding between GO and carbon fiber (Fig. 4) and GO and matrix resulted in good interfacial adhesion between the filler and polymer, causing possible interlocking between GO and matrix due to the rough surface of graphene. Thus, the researchers claim that the performance of carbon fiber epoxy composites can be enhanced by hybridizing with GO nanoparticles.

Guo et al. (2009) studied the wear resistance of hybrid nano-SiO_2 and carbon fiber modified epoxy composites. The nano-SiO_2 was grafted with styrene and maleic anhydride before mixing it with epoxy resin and curing agent for effective covalent bonding between the filler and matrix. Later the pre-cured epoxy mixture was mixed with short carbon fibers. The hybrid composites showed higher wear and friction resistance compared to single filler composites. The positive synergistic effect of the hybrid composites was due to the increased surface hardness, self-lubrication, and formation of transfer film. The composite's best tribological performance was observed with 4 wt.% and 6 wt.% nano-SiO_2 and carbon fiber, respectively. Many studies reported a significant increase in mechanical and thermal properties by incorporating nanofillers in natural fiber reinforced epoxy

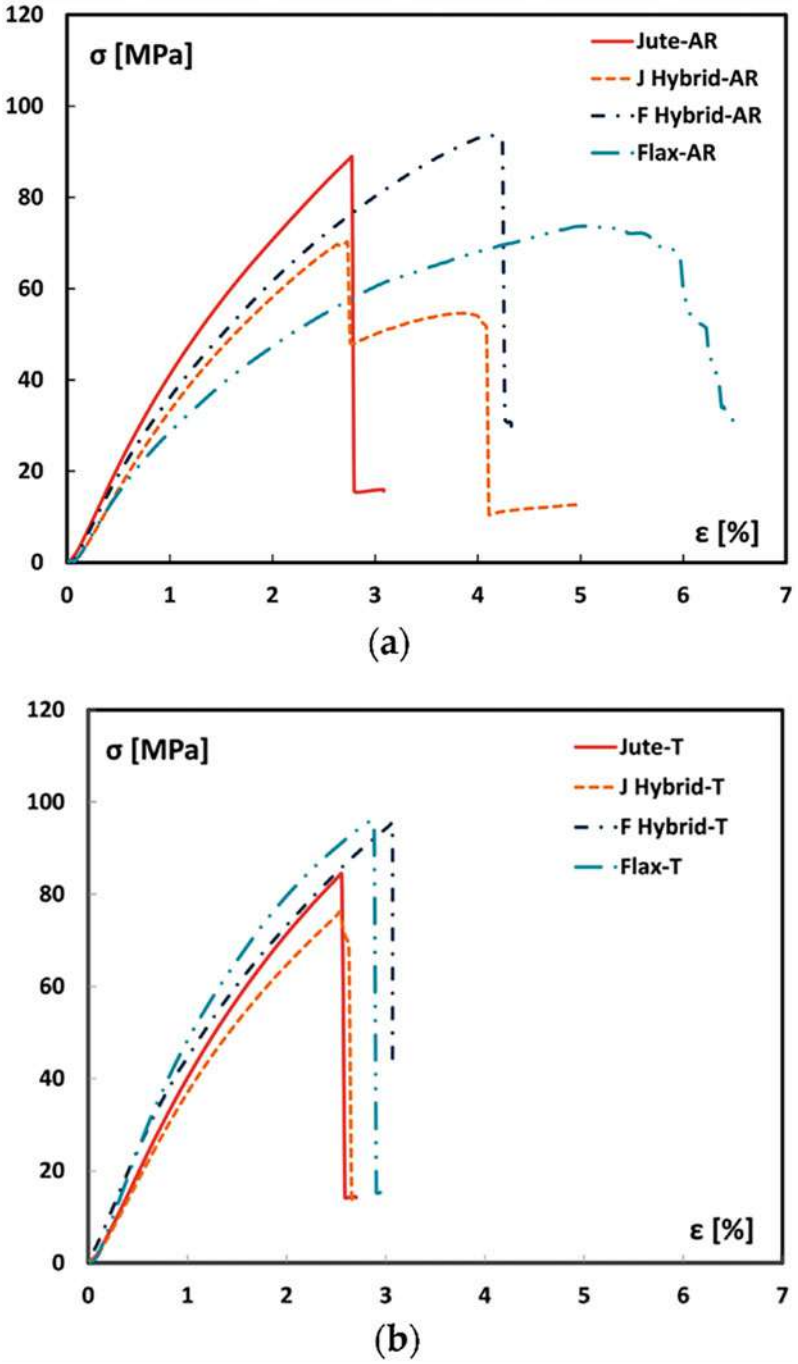

Fig. 3 Flexural stress-strain curve of untreated and treated hybrid composites (Fiore and Calabrese 2019)

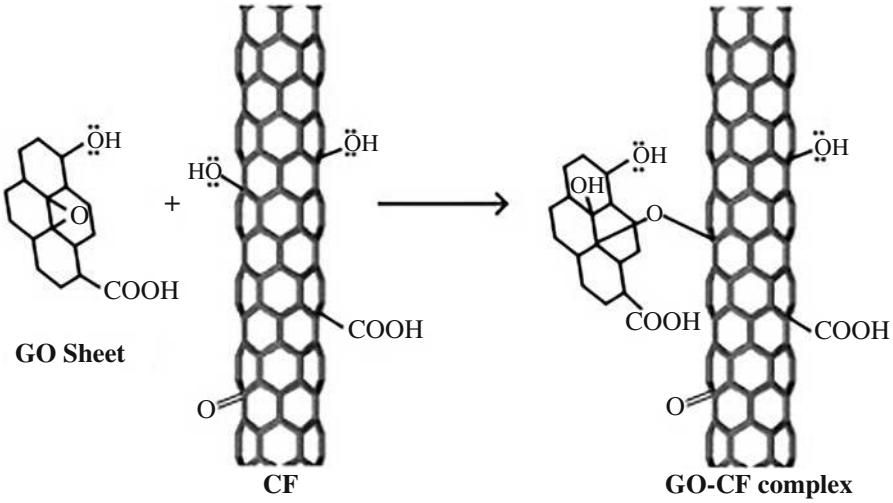

Fig. 4 Hydrogen bonding between GO and carbon fiber (Pathak et al. 2016). (Reproduced with thanks from Elsevier, License Number:5261060091537)

composites. Arshad et al. (2021) reported improvement in strength, hardness, and thermal stability with incorporating TiC in coir and basalt reinforced synthetic and bioepoxy composites due to the increased interfacial bonding between the filler and the polymer due to their nano size.

Despite the excellent mechanical properties and low density, polymer-natural fiber composites showed low-temperature resistance. At high temperatures, accelerated oxygen-induced aging could take place which led to the deterioration of properties as well as a reduction in weight for the composites. These are disadvantages of natural fiber-based composites and limit their application in the field of automotive, construction, and aerospace industries (Chee et al. 2019). To enhance the thermal stability of natural fiber-based composites, surface treatment of fibers and the hybridization of fibers can be efficiently used. Surface treatments such as alkaline treatment and silanization can enhance the thermal stability of the natural fiber. Neto et al. (2019) studied the effect of alkaline treatment of jute, sisal, and ramie fibers and reported higher thermal stability for treated hybrid composites compared to the untreated natural fiber incorporated epoxy composites. The morphology studies using SEM revealed that the alkaline treatment modifies the surface of the natural fiber which led to better interfacial adhesion between fillers and epoxy matrix which eventually led to higher thermal stability. Boopalan et al. (2013) studied the thermal properties of a hybrid fiber system of jute and banana fiber in the epoxy matrix. Hybrid composite with an equal content of jute and banana fiber showed the highest heat deflection temperature compared to the composites with only jute or banana fiber in it. The thermal stability of a natural fiber-filled epoxy composite can be improved by the addition of a thermally stable synthetic fiber such as carbon fiber (Singh et al. 2020).

Aging Effects on Epoxy Matrix and Epoxy/Fiber-Reinforced Composites

The performance and durability of epoxy-based composites depend on the operational conditions. For instance, (i) temperature, (ii) rain, (iii) humidity, (iv) ultraviolet (UV) radiation, and (v) operational stress may deteriorate the epoxy-based structural component and performance. Studies have shown that the composites exposed to the external environment may undergo moisture absorption, photooxidative, and thermo-oxidative degradation. The aging of the composites is caused by physical and chemical changes. The physical aging of the composites involves structural changes, while the chemical changes involve crosslinking or chain scission due to the heat generated during the operational conditions (Tsotsis et al. 1999). The physical and chemical aging caused the embrittlement of the composites (Cysne Barbosa et al. 2017). The embrittlement of the polymer composite was because of the chain scission that dominates over the crosslinking while aging. The temperature of the working environment has a significant influence on the long-term performance of the composites. This is because the rate of chain scission of the polymer chains was more at elevated temperatures, especially above the glass transition temperature (T_g). The changes in mechanical properties during operation have caused concerns over the long-term performance of these composites. Therefore, careful evaluation of the performance of these composites under different operational conditions is required. This is because the structural components made of epoxy-based composites should withstand various operating conditions.

For advanced applications, the structural composite components should have good aging resistance. However, several studies have reported crack and structural failure as a result of aging in operational environmental conditions. Thus, many studies are focused on fatigue and damage tolerance of the composite industry (Shahzad 2011; Gassan 2002). For long service life, damage tolerance and good aging resistance are required for advanced applications, whereby designing of the structural components is essential. Computer programming and stimulation can be effectively utilized to design composites successfully. Thus, the information on epoxy-based composites' durability, service life, and performance under various environmental conditions are preferred to study. The decomposition or degradation of the structural components based on epoxy-based composites can be evaluated using FTIR, Nuclear Magnetic Resonance (NMR), mechanical studies, ILSS, compressive strength, SEM of accelerated environmental studies, damping studies, etc. In accelerated environmental studies, the sample is exposed to controlled conditions of temperature, moisture, and UV radiations for a specific period equivalent to a few years in normal environmental conditions so as have a detailed understanding of the aging of the epoxy composites (Senthilkumar et al. 2020). From the research studies discussed above, it can be concluded that the composite performance was related to the type of fiber, the matrix, polymer/fibers interface, mechanical stress, weathering exposure time, environmental condition, humidity, water absorption, fatigue, and coating. The durability of fiber, matrix, and polymer/fiber interface is also essential for composite applications. The mechanical stress, fatigue, and water uptake may

cause stress within the polymer composite resulting in strength reduction, fiber-matrix debonding, plasticization, swelling of fibers and matrix, and generation of microcracks in the matrix. The plasticization and swelling are reversible, which means the effect of plasticization and swelling cannot be removed upon drying the samples. However, microcracking and debonding is irreversible (Schutte 1994). The structure of polymer also influences the long-term performance of the composites. If hydrophilic groups are present in the polymers, water molecules can interact with the polymer matrix and easily diffuse into the matrix. In the case of epoxy composites, even after complete curing, one can find free hydroxyl groups. Therefore, water may diffuse into the epoxy matrix. The cyclic loads may cause more damage than static loads in both dry and wet conditions as well as the damage could be more in the wet condition rather than in dry conditions. Therefore, the influence of mechanical stress/fatigue in automobile, aerospace, and satellite structural component cannot be neglected. An overview of the aging properties of fiber-reinforced polymers was reviewed by Mayandi et al. (2020).

On exposure to a different environment such as moisture and heat, the thermal stability of natural fiber decreases and this leads to fiber swelling as well as cracking. The thermal stability of natural fiber mainly depends on its chemical structure and composition. For example, higher lignin content leads to better thermal stability and higher cellulose content leads to lower thermal stability (Wang et al. 2005; Mariam et al. 2019; Dittenber and Gangarao 2012). Compared to natural fibers, synthetic fibers generally show resistance toward thermal and hydrothermal aging. Hydrothermal aging on different fiber-reinforced epoxy composites have been studied by different researchers (Wang et al. 2018; Dewimille and Bunsell 1982; Bockenheimer et al. 2004).

To achieve excellent mechanical and hydrothermal resistance, flax, and carbon fibers can be used as the reinforcing fibers in epoxy composites. This can be achieved by preparing the composites with a flax fiber layer in the interior of the composites and carbon fiber layers on the outside of the composites. An enhancement in the toughness can be achieved by the flax fabric and an enhancement in the hydrothermal resistance and strength can be achieved by the outer carbon fiber fabric. Hybrid composite with carbon fiber on the surface showed a drastic decrease of 1/16th in the diffusion rate of water compared to the composites alternating layer of flax and carbon fibers (Wang et al. 2020). Muralidharan et al. (2022) prepared epoxy composites of carbon fiber and Kevlar fiber. Hydrothermal aging studies have been done by performing tensile studies on the samples which are immersed in seawater at different temperatures such as 20 °C, 40 °C, and 60 °C. Studies showed that hybrid composites can be selected for various suitable structural/engineering applications, especially in the manufacturing of wind/tidal turbines.

Oguz et al. (2020) analyzed the effect of the sequence of stacking of aramid fiber and glass fiber layers in an epoxy matrix on the hydrothermal aging. The stacking sequences of fabrics influenced the water gain of the composites and found that the stacking sequence of glass-aramid-glass showed less water absorption compared to aramid-glass-aramid stacking. Studies also showed that an increase in temperature reduced the properties of the composites to a higher extent. The immersion of

samples in distilled water also led to a decrease in the flexural properties. The SEM analysis results indicated that the temperature led to delamination and fiber/matrix crack and it is more visible in the glass fiber/matrix interface. The moisture absorption of the polymer composites during their operational condition may cause deteriorating effects in polymers, such as plastination, drop-in T_g, decrease in mechanical strength, and reduction in the elastic modulus (Pandian et al. 2014). It has been reported that the moisture may react with epoxy resin structure and, hence, significantly affect the aging process (Dao et al. 2006). The UV radiation caused photooxidative degradation. The photooxidative degradation is due to the generation of free radicals in the polymer matrix caused by the chain scission resulting in the generation of cracks within the matrix, and ultimately, the mechanical properties will be reduced (Yousif and Haddad 2013). It should be noted that if the composites were not coated, then the composite's surface may degrade due to photo and thermo-oxidative degradation. Hence, the fibers present in the epoxy matrix may expose to water, increasing moisture absorption. Thus, the combination of moisture absorption, thermal and UV degradation had a significant effect on the thermomechanical properties of the composites.

In an interesting work, Dao et al. (2006) studied the accelerated thermal aging of the aerospace structural components based on epoxy composites. The composites were subjected to thermal aging at four temperatures 70, 120, 170, and 200 °C for 7500 h. The researchers used FTIR to study the chemistry behind thermo-oxidative aging. The FTIR spectra of unaged samples, aged samples, and during the aging process were tested. The thermal aging at 70 °C is comparable with the surface temperature of the aircraft. The spectral changes are the least at low temperatures (70 °C and 120 °C) of thermal aging. However, at 170 °C of thermal aging, the oxidation of the border group of aliphatic groups of epoxy chains was observed from the FTIR spectra. Thus, at high service temperatures, the thermo-oxidative attack may result in a chain break down of the main chain and result in the loss of resin from the composite surface, resulting in surface embrittlement. Fiore et al. (2017) studied the aging resistance of jute/basalt fiber reinforced bioepoxy composites. Three different stacking sequences, such as hybrid, sandwich, and intercalated, have been used to fabricate the composite. The fabricated composites were subjected to aging studies for 14, 28, 56, and 84 days. The samples before and after aging were characterized for DSC and mechanical properties. The DSC of the unaged samples showed the presence of an uncured fraction of the epoxy system; this was understandable from the exothermic DSC peak. However, the exothermic peak height was reduced for the aged samples, suggesting the post-curing of the composites during the aging process. The FS and FM of the aged composites were reduced, while the elongation at break was increased. The drop in strength during aging is due to the degradation of the composites. The IS had increased; this result showed plasticization of the composites during the aging process caused by water exposition. On the other hand, the viscoelastic properties showed a significant increase in T_g and a drop in the tan delta peak height after the aging process due to post-curing. Hashim et al. (2020) studied the effect of accelerating weathering on the moisture absorption, swelling, and mechanical properties of the epoxy/basalt single fiber composites and

hybrid epoxy/basalt/nanosilica and/or graphene nanoplatelets composites. The concentration of the GnP used was 0.1%, and nanosilica was 5 wt.%. For the comparison, epoxy/glass single fiber composites and hybrid composites were prepared. The composites after aging showed color fading, void formation, fiber splitting, and resin flaking due to the degradation. The water absorption and swelling of the single fiber composites are reduced by incorporating nanofillers. The aged samples showed higher water absorption and swell more. However, the hydrophobic nanofiller in hybrid composites prevents the entering of water into the composites, and hence these composites swell less and absorb less water. The hybrid composites showed higher tensile and flexural properties. The mechanical properties are reduced after aging due to the fiber and matrix degradation, which causes a reduction in the interfacial adhesion between the fiber and epoxy matrix. The reduction in mechanical properties is marginal in the case of hybrid composites after the aging test. Thus, the study concludes that the nanofiller enhanced the properties of the composites and protected them from degradation. Hofer Jr. et al. (1978) observed good tensile fatigue resistance for the hybrid composites comprising graphite and glass in the ratio of 2:1 in the epoxy matrix. The glass single fiber in the epoxy matrix undergoes rapid degradation with cyclic mechanical stress.

Chang et al. (Chang and Chow 2010) fabricated glass fiber/epoxy/OMMT hybrid nanocomposites and studied the effect of accelerated weathering on the flexural and fracture toughness of the composites. The epoxy composites were fabricated with three layers of glass fiber. The concentration of OMMT used was 0, 1, 2, 3, and 4 wt. %. The XRD results confirmed the exfoliation of OMMT in epoxy glass fiber composites up to 3 wt.% OMMT. The FS, FM, and fracture toughness of the glass fiber composite were improved with the incorporation of the OMMT, and the maximum properties were observed at 2 wt.% OMMT followed by a decrease at higher loading. The FS of the glass fiber single composites and hybrid composites were retained even after the accelerating weathering test. However, the fracture toughness is reduced approximately 20% irrespective of the composites. The drop in fracture toughness was due to the notch sensitivity of the composites, which act as crack initiators. The effect of seawater aging on the flexural and impact properties of glass/aramid/epoxy hybrid composites was tested by Oğuz et al. (2021). The test was carried out at two different temperatures at 258 °C and 708 °C for 1000 h. The water gain is highest at higher temperatures. The FS and IS were both reduced with hydrothermal aging. The FS of the composites is higher for the redried composites than for the wet samples. The debonding of the fiber/matrix interface and the generation of cracks increase with water aging temperature. Barbosa et al. (Cysne Barbosa et al. 2017) studied the long-term durability of carbon fiber reinforced epoxy composites. The ILSS and viscoelastic properties showed only marginal changes in properties. However, increased crack density, fiber rupture, and fiber buckling were observed in the fracture surface of the aged samples.

Natural fibers reinforced epoxy composites have gained attention in the composite industry. However, the performance of these composites in a humid atmosphere is a concern. Calabrese et al. (2019) studied the effect of the Salt-Fog Environment on the mechanical properties of pinned hybrid glass/flax epoxy composites. The

samples were coded as GFA, GFB, and GBC for 0, 30, and 60 aging days, respectively. The bearing test results of composite samples with 4 mm hole diameter, 12 mm edge distance, and 15 mm width showed good bearing stress of ca. 200 MPa for the unaged composite. The bearing stress decreased gradually with aging time. This is because flax fiber will absorb water resulting in the weakening of interfacial adhesion between the fiber and polymer and thus resulting in the weakening of the stress of the composites. On the other hand, composites with 8 mm hole diameter, 9 mm edge distance, and 15 mm width showed a different trend. The bearing stress of the composites was not affected with aging; however, the modulus was reduced while the elongation at break was increased. This result revealed the softening of the composites because of the presence of hydrophilic natural fiber. Based on the findings, the authors developed a schematic of the failure mechanism of the composites with different hole diameters with respect to edge distance, as shown in Fig. 5.

In an interesting work by Fiore et al. (2020), untreated and sodium bicarbonate treated flax, jute, and flax/jute hybrid (F hybrid (F/J/F/J/F) and J hybrid (J/F/J/F/J))

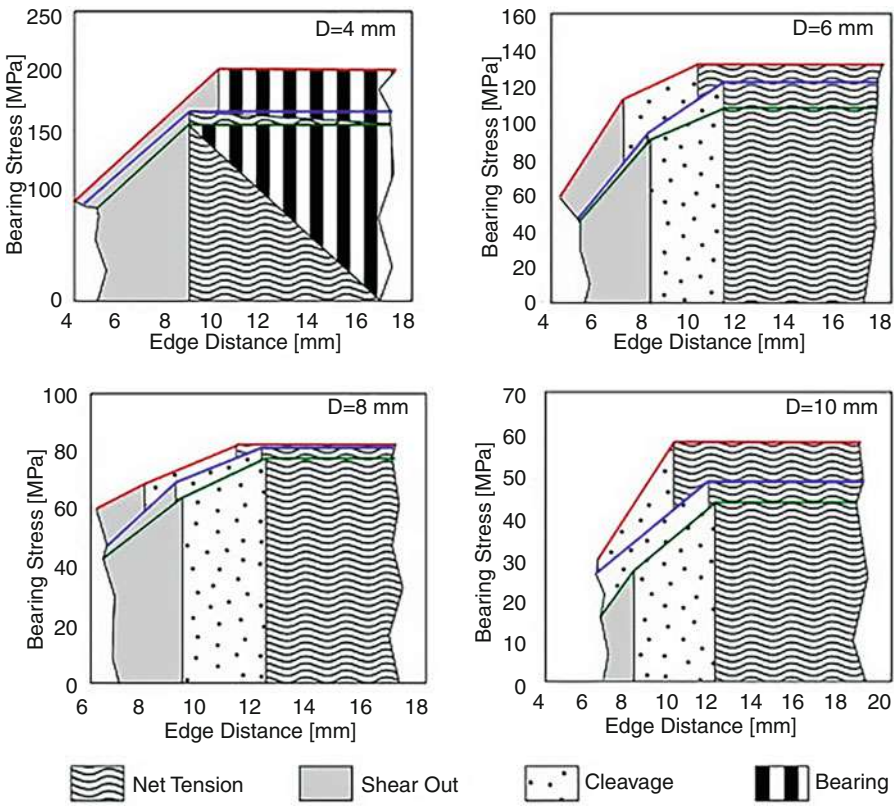

Fig. 5 Schematic of failure mechanism of the composites with different hole diameter with respect to edge distance (Calabrese et al. 2019)

fiber reinforced epoxy composites were exposed to Salt-Fog Spray Environment for up to 2 months and were characterized for dynamic mechanical analysis. The treated flax and F hybrid (F/J/F/J/F) composites maintained the storage modulus and their tan delta peak height even after the aging studies and were least affected. But the treatment caused a drop in storage modulus and an increase in tan delta peak height for the treated jute and J hybrid (J/F/J/F/J) composites due to the weakening of the jute/epoxy interface. This study showed that the sodium bicarbonate treatment was not favorable for the surface treatment of jute in jute reinforced epoxy composites. Ali et al. (2010) studied the accelerated aging of Arenga pinnata fiber-reinforced epoxy composites (APFREC) and reported some surprising results. The researchers observed that the TS and elongation at break were improved after the accelerated aging test. On the other hand, the modulus and IS values of composites reduced marginally after aging. The researchers concluded that the increase in strength and elongation could be due to the structural changes of the composites caused during accelerated thermal aging. Wang et al. (Wang and Petrů 2019) fabricated flax fabric reinforced epoxy composite and studied hydrothermal aging stability of the composites. Before fabricating the composites, the flax fabric was treated with alkali, saline, acetylation, and alkali-salinization. The fabricated composite samples were soaked in distilled water at 60°C and were taken out on 4th, 9th, and 16th day for the DMA analysis. After the surface treatment, the storage modulus and T_g were increased. The acetylated composites showed the best resistance against hydrothermal aging. Jawaid et al. (2016) studied the effect of UV accelerated environmental aging of pure oil palm empty fruit bunch (OPEFB) reinforced composites, pure jute fibers reinforced composites and hybrid composites. The hybrid composites with different layering patterns (OPEFB/jute/OPEFB and Jute/OPEFB/jute) were fabricated. The results reported a drop in the tensile properties of both hybrid and pure composites with aging due to lignin and fiber-matrix interfacial bonding degradation.

Narendar et al. (2014) fabricated neat epoxy, nylon fiber/epoxy composite, coir pith/epoxy composite, and hybrid nylon fiber/epoxy/coir pith composites. The TS, FS, IS, hardness, and flammability of the composites were measured. The hybrid composites with three layers of nylon and NaOH treated coir pith give the best mechanical properties and showed good resistance against flammability. Both nylon fabric and treated coir pith form a hydrogen bond with epoxy resin. The effect of aging of the composites in water for 31 days at 30 °C was investigated. The aged coir pith modified composites showed the lowest retention of the IS; this was due to the absorption of water during the aging test, resulting in the degradation of the matrix-fiber bonding. Thus, this composite is not suitable for a moist environment. However, the NaOH treated coir pith epoxy composite, and hybrid composite showed good retention in IS. Recently, Narendra et al. (2018) treated coir pith with various chemical reagents such as NaOH, CH_3-COOH, H_2SO_4, $CH_2 = CHCOOH$, NaOCl, and dicumyl peroxide, and were used as a modifier for epoxy resin along with nylon fibers. A series of composites have been prepared. The TGA studies showed higher thermal stability for the treated composites. Further, the samples were subjected to thermal aging in a thermal oven for 74 h and 10 min at 70 °C, equivalent to 70 days

of aging in the natural environment. The aged samples were then characterized for IS. The epoxy composite reinforced with untreated coir pith showed poor IS retention, and a drop in IS of 38.72% was observed. The chemically treated composites showed better IS retention. However, the best properties for the hybrid epoxy composites were observed with nylon fiber/treated coir pith. The increasing number of nylon layers improved the thermal stability, heat distortion temperature, and IS retention properties.

Future prospects

Most of the composites are used for external applications and are subjected to repeated vibrations and shocks that might result in crack formation or fracture that may eventually fail the composite component. Self-healing fiber composites is a novel area where the fiber composite is filled with microcapsules or micro containers filled with self-healing agents. However, more work on these areas is required for the practical application of self-healing composites in all environmental conditions. Another area of concern is the moisture absorption of polymer composites, especially with natural fibers. Coming to recycling epoxy composites, it is challenging to recycle thermosets. One method of recycling is grounding. Here the epoxy composites afterlife use can be grounded to make it into fine powder. These powders can be used for the fabrication of composites. More studies should be carried out on the use of machine learning tools such as artificial intelligence, for the prediction of the performance of the epoxy composites. The modelling of hybrid fiber-filled epoxy composites may reduce the time and money in optimizing the processing conditions to achieve superior epoxy hybrid fiber composites. The machining of epoxy-fiber hybrid composites needs to be analyzed which is essential for end-use applications. In the future, the toolbox for the selection of suitable fiber systems and the processing conditions need to be developed for tailor-made properties required for certain applications. LCA (Life cycle assessment) of epoxy-hybrid fiber composites are essential as it is a key environmental management factor for the industry and public sector. In future, studies should also be focused on the preparation of epoxy-fiber composites using the additive manufacturing technique, such as three-dimensional printing. This allowed the manufacturing of composites, with high precision and complexity. Studies on the development of additive manufacturing techniques to prepare epoxy hybrid fiber composites which is essential for the manufacturing of defect-free complex-shaped products from especially natural fiber-based epoxy composites.

Conclusions

This book chapter discussed recent works of literature on epoxy-matrix hybrid composites and analyzed their various properties and applications. Though the epoxy matrix has many advantages compared to other thermoset matrices, curing

and aging characteristics play a significant role in industries. Modification of epoxy matrix could help to enhance its properties such as (i) fire resistance, (ii) wear, (iii) brittleness, etc.

Using natural fibers with epoxy matrix provides many advantages compared to epoxy matrix-synthetic fiber-reinforced composites such as lower density, less cost, biodegradability, etc. But there are concerns related to the aging, and moisture absorption of natural fiber-filled epoxy composites. The performance of epoxy composites can be enhanced using hybrid fiber systems. Furthermore, the deformation behavior of epoxy matrix hybrid composites was discussed along with the aging characteristics of various epoxy-fiber hybrid composites. The significance of recycling epoxy matrix composites was also taken into consideration. Recent research works show that there is a huge potential for epoxy-natural fiber hybrid composites to be used in various applications.

References

Z. Al-Hajaj, R. Zdero, H. Bougherara, Mechanical, morphological, and water absorption properties of a new hybrid composite material made from 4 harness satin woven carbon fibres and flax fibres in an epoxy matrix. Compos. Part A Appl. Sci. Manuf. **115**, 46–56 (2018). https://doi.org/10.1016/J.COMPOSITESA.2018.09.015

Z. Al-Hajaj, B.L. Sy, H. Bougherara, R. Zdero, Impact properties of a new hybrid composite material made from woven carbon fibres plus flax fibres in an epoxy matrix. Compos. Struct. **208**, 346–356 (2019). https://doi.org/10.1016/J.COMPSTRUCT.2018.10.033

A. Ali, A.B. Sanuddin, S. Ezzeddin, The effect of aging on Arenga pinnata fiber-reinforced epoxy composite. Mater. Des. **31**, 3550–3554 (2010). https://doi.org/10.1016/J.MATDES.2010.01.043

M. Alsaadi, M. Bulut, A. Erkliğ, A. Jabbar, Nano-silica inclusion effects on mechanical and dynamic behavior of fiber reinforced carbon/Kevlar with epoxy resin hybrid composites. Compos. Part B Eng. **152**, 169–179 (2018). https://doi.org/10.1016/J.COMPOSITESB.2018.07.015

A. Anand, S.K. Ghosh, A.O. Fulmali, R.K. Prusty, Enhanced barrier, mechanical and viscoelastic properties of graphene oxide embedded glass fibre/epoxy composite for marine applications. Constr. Build. Mater. **268**, 121784 (2021). https://doi.org/10.1016/J.CONBUILDMAT.2020.121784

M.N. Arshad, H. Mohit, M.R. Sanjay, S. Siengchin, A. Khan, M.M. Alotaibi, A.M. Asiri, M.A. Rub, Effect of coir fiber and TiC nanoparticles on basalt fiber reinforced epoxy hybrid composites: Physico–mechanical characteristics. Cellulose **28**, 451–3471 (2021). https://doi.org/10.1007/S10570-021-03752-7

C. Audibert, A.S. Andreani, É. Lainé, J.C. Grandidier, Mechanical characterization and damage mechanism of a new flax-Kevlar hybrid/epoxy composite. Compos. Struct. **195**, 126–135 (2018). https://doi.org/10.1016/J.COMPSTRUCT.2018.04.061

P. Banerjee, S. Kumar, S. Bose, Thermoreversible bonds and graphene oxide additives enhance the flexural and Interlaminar shear strength of self-healing epoxy/carbon fiber laminates. ACS Appl. Nano Mater. **4**, 6821–6831 (2021). https://doi.org/10.1021/ACSANM.1C00888/SUPPL_FILE/AN1C00888_SI_001.PDF

A. Barouni, C. Lupton, C. Jiang, A. Saifullah, K. Giasin, Z. Zhang, H.N. Dhakal, Investigation into the fatigue properties of flax fibre epoxy composites and hybrid composites based on flax and glass fibres. Compos. Struct. **281**, 115046 (2022). https://doi.org/10.1016/J.COMPSTRUCT.2021.115046

C. Bockenheimer, D. Fata, W. Possart, New aspects of aging in epoxy networks. II. Hydrothermal aging. J. Appl. Polym. Sci. **91**, 369–377 (2004). https://doi.org/10.1002/APP.13093

M. Boopalan, M. Niranjanaa, M.J. Umapathy, Study on the mechanical properties and thermal properties of jute and banana fiber reinforced epoxy hybrid composites. Compos. Part B Eng. **51**, 54–57 (2013). https://doi.org/10.1016/J.COMPOSITESB.2013.02.033

L. Calabrese, V. Fiore, P. Bruzzaniti, T. Scalici, A. Valenza, Pinned hybrid glass-flax composite laminates aged in salt-fog environment: Mechanical durability. Polymers **12**, 40 (2019). https://doi.org/10.3390/POLYM12010040

L.N. Chang, W.S. Chow, Accelerated weathering on glass fiber/epoxy/Organo-montmorillonite nanocomposites. J. Compos. Mater. **44**, 1421–1434 (2010). https://doi.org/10.1177/0021998309360944

S.S. Chee, M. Jawaid, M.T.H. Sultan, O.Y. Alothman, L.C. Abdullah, Evaluation of the hybridization effect on the thermal and thermo-oxidative stability of bamboo/kenaf/epoxy hybrid composites. J. Therm. Anal. Calorim. **137**, 55–63 (2018). https://doi.org/10.1007/S10973-018-7918-Z

S.S. Chee, M. Jawaid, M.T.H. Sultan, O.Y. Alothman, L.C. Abdullah, Thermomechanical and dynamic mechanical properties of bamboo/woven kenaf mat reinforced epoxy hybrid composites. Compos. Part B Eng. **163**, 165–174 (2019). https://doi.org/10.1016/J.COMPOSITESB.2018.11.039

A.P. Cysne Barbosa, A.P. Ana, E.S.S. Guerra, F.K. Arakaki, M. Tosatto, M.C. Maria, J.D. José, Accelerated aging effects on carbon fiber/epoxy composites. Compos. Part B Eng. **110**, 298–306 (2017). https://doi.org/10.1016/J.COMPOSITESB.2016.11.004

B. Dao, J. Hodgkin, J. Krstina, J. Mardel, W. Tian, Accelerated aging versus realistic aging in aerospace composite materials. II. Chemistry of thermal aging in a structural composite. J. Appl. Polym. Sci. **102**, 3221–3232 (2006). https://doi.org/10.1002/APP.24573

S.B.R. Devireddy, S. Biswas, Thermo-physical properties of short banana–jute fiber-reinforced epoxy-based hybrid composites. Proc. Inst. Mech. Eng. L. **232**, 939–951 (2016). https://doi.org/10.1177/1464420716656883

B. Dewimille, A.R. Bunsell, The modelling of hydrothermal aging in glass fibre reinforced epoxy composites. J. Phys. D. Appl. Phys. **15**, 2079 (1982). https://doi.org/10.1088/0022-3727/15/10/026

D.B. Dittenber, H.V.S. Gangarao, Critical review of recent publications on use of natural composites in infrastructure. Compos. Part A Appl. Sci. Manuf. **43**, 1419–1429 (2012). https://doi.org/10.1016/J.COMPOSITESA.2011.11.019

C. Dong, Uncertainties in flexural strength of carbon/glass fibre reinforced hybrid epoxy composites. Compos. Part B Eng. **98**, 176–181 (2016). https://doi.org/10.1016/J.COMPOSITESB.2016.05.035

J.E. Ehlers, N.G. Rondan, L.K. Huynh, H. Pham, M. Marks, T.N. Truong, Theoretical study on mechanisms of the epoxy−amine curing reaction. Macromolecules **40**, 4370–4377 (2007). https://doi.org/10.1021/MA070423M

V. Fiore, L. Calabrese, Effect of stacking sequence and sodium bicarbonate treatment on quasi-static and dynamic mechanical properties of flax/jute epoxy-based composites. Materials **12**, 1363 (2019). https://doi.org/10.3390/MA12091363

V. Fiore, G. Di Bella, A. Valenza, Glass–basalt/epoxy hybrid composites for marine applications. Mater. Des. **32**, 2091–2099 (2011). https://doi.org/10.1016/J.MATDES.2010.11.043

V. Fiore, T. Scalici, D. Badagliacco, D. Enea, G. Alaimo, A. Valenza, Aging resistance of bio-epoxy jute-basalt hybrid composites as novel multilayer structures for cladding. Compos. Struct. **160**, 1319–1328 (2017). https://doi.org/10.1016/J.COMPSTRUCT.2016.11.025

V. Fiore, C. Sanfilippo, L. Calabrese, Dynamic mechanical behavior analysis of flax/jute fiber-reinforced composites under salt-fog spray environment. Polymers **12**, 716 (2020). https://doi.org/10.3390/POLYM12030716

J. Gassan, A study of fibre and interface parameters affecting the fatigue behaviour of natural fibre composites. Compos. Part A Appl. Sci. Manuf. **33**, 369–374 (2002). https://doi.org/10.1016/S1359-835X(01)00116-6

S.M. George, D. Puglia, J.M. Kenny, J. Parameswaranpillai, S. Thomas, Reaction-induced phase separation and thermomechanical properties in epoxidized styrene- block -butadiene- block

-styrene triblock copolymer modified epoxy/DDM system. Ind. Eng. Chem. Res. **53**, 6941–6950 (2014). https://doi.org/10.1021/IE404124B/SUPPL_FILE/IE404124B_SI_001.PDF

R. Giridharan, Preparation and property evaluation of Glass/Ramie fibers reinforced epoxy hybrid composites. Compos. Part B Eng. **167**, 342–345 (2019). https://doi.org/10.1016/J.COMPOSITESB.2018.12.049

G. Goud, R.N. Rao, Mechanical and electrical performance of Roystonea regia/glass fibre reinforced epoxy hybrid composites. Bull. Mater. Sci. **35**, 595–599 (2012). https://doi.org/10.1007/S12034-012-0324-4

N. Guermazi, N. Haddar, K. Elleuch, H.F. Ayedi, Investigations on the fabrication and the characterization of glass/epoxy, carbon/epoxy and hybrid composites used in the reinforcement and the repair of aeronautic structures. Mater. Des. **56**, 714–724 (2014). https://doi.org/10.1016/J.MATDES.2013.11.043

Q.B. Guo, M.Z. Rong, G.L. Jia, K.T. Lau, M.Q. Zhang, Sliding wear performance of nano-SiO2/short carbon fiber/epoxy hybrid composites. Wear **266**, 658–665 (2009). https://doi.org/10.1016/J.WEAR.2008.08.005

R. Guo, G. Xian, F. Li, C. Li, B. Hong, Hygrothermal resistance of pultruded carbon, glass and carbon/glass hybrid fiber reinforced epoxy composites. Constr. Build. Mater. **315**, 125710 (2022). https://doi.org/10.1016/J.CONBUILDMAT.2021.125710

N. Hameed, L.F. Dumée, F.M. Allioux, M. Reghat, J.S. Church, M. Naebe, K. Magniez, J. Parameswaranpillai, B.L. Fox, Graphene based room temperature flexible nanocomposites from permanently cross-linked networks. Sci. Rep. **8**, 2803 (2018). https://doi.org/10.1038/s41598-018-21114-5

N. Hashim, D.L.A. Majid, E.S. Mahdi, R. Zahari, N. Yidris, Effect of fiber loading directions on the low cycle fatigue of intraply carbon-Kevlar reinforced epoxy hybrid composites. Compos. Struct. **212**, 476–483 (2019). https://doi.org/10.1016/J.COMPSTRUCT.2019.01.036

U.R. Hashim, A. Jumahat, M. Jawaid, R. Dungani, S. Alamery, Effects of accelerated weathering on degradation behavior of basalt fiber reinforced polymer nanocomposites. Polymers **12**, 2621 (2020). https://doi.org/10.3390/POLYM12112621

J.H. Hodgkin, G.P. Simon, R.J. Varley, Thermoplastic toughening of epoxy resins: A critical review. Polym. Adv. Technol. **9**, 3–10 (1998). https://doi.org/10.1002/(SICI)1099-1581(199801)9:1<3::AID-PAT727>3.0.CO;2-I

K.E. Hofer, M. Stander, L.C. Bennett, Degradation and enhancement of the fatigue behavior of glass/graphite/epoxy hybrid composites after accelerated aging. Polym. Eng. Sci. **18**, 120–127 (1978). https://doi.org/10.1002/PEN.760180210

M. Ivankovic, L. Incarnato, J.M. Kenny, L. Nicolais, Curing kinetics and chemorheology of epoxy/anhydride system. J. Appl. Polym. Sci. **90**, 3012–3019 (2003). https://doi.org/10.1002/APP.12976

M. Jawaid, H.P.S. Abdul Khalil, A. Hassan, R. Dungani, A. Hadiyane, Effect of jute fibre loading on tensile and dynamic mechanical properties of oil palm epoxy composites. Compos. Part B Eng. **45**, 619–624 (2013). https://doi.org/10.1016/J.COMPOSITESB.2012.04.068

M. Jawaid, N. Saba, O. Alothman, M.T. Paridah, Effect of accelerated environmental aging on tensile properties of oil palm/jute hybrid composites. AIP Conf. Proc. **1787**, 040007 (2016). https://doi.org/10.1063/1.4968086

F.L. Jin, X. Li, S.J. Park, Synthesis and application of epoxy resins: A review. J. Ind. Eng. Chem. **29**, 1–11 (2015). https://doi.org/10.1016/J.JIEC.2015.03.026

P. Jyotishkumar, J. Pionteck, C. Özdilek, P. Moldenaers, U. Cvelbar, M. Mozetic, S. Thomas, Rheology and pressure–volume–temperature behavior of the thermoplastic poly(acrylonitrile-butadiene-styrene)-modified epoxy-DDS system during reaction induced phase separation. Soft Matter **7**, 7248–7256 (2011a). https://doi.org/10.1039/C1SM05718A

P.J. Jyotishkumar, J. Pionteck, R. Hässler, S.M. George, U. Cvelbar, S. Thomas, Studies on stress relaxation and thermomechanical properties of poly(acrylonitrile-butadiene-styrene) modified epoxy-amine systems. Ind. Eng. Chem. Res. **50**, 4432–4440 (2011b). https://doi.org/10.1021/IE1016915

M. Kalantari, C. Dong, I.J. Davies, Multi-objective analysis for optimal and robust design of unidirectional glass/carbon fibre reinforced hybrid epoxy composites under flexural loading. Compos. Part B Eng. **84**, 130–139 (2016). https://doi.org/10.1016/J.COMPOSITESB.2015.08.050

R. Konnola, J. Parameswaranpillai, K. Joseph, Mechanical, thermal, and viscoelastic response of novel in situ CTBN/POSS/epoxy hybrid composite system. Polym. Compos. **37**, 2109–2120 (2016). https://doi.org/10.1002/PC.23390

S. Kumar, K.K.S. Mer, B. Gangil, V.K. Patel, Synergistic effect of hybrid Himalayan nettle/Bauhinia-vahlii fibers on physico-mechanical and sliding wear properties of epoxy composites. Def. Technol. **16**, 762–776 (2020). https://doi.org/10.1016/J.DT.2019.08.006

S. Kumar, A. Malek, R. Babu, S. Mathur, Ballistic efficiency of multilayered armor system reinforced with jute-Kevlar epoxy composite against high-energy steel Core Projectile. J. Mater. Eng. Perform. **30**, 8447–8464 (2021). https://doi.org/10.1007/S11665-021-06057-9

N. Kumari, M. Paswan, K. Prasad, Effect of sawdust addition on the mechanical and water absorption properties of banana-sisal/epoxy natural fiber composites. Mater. Today Proc. **49**, 1719–1722 (2022). https://doi.org/10.1016/J.MATPR.2021.07.489

H. Liu, K. Xu, H. Ai, L. Zhang, M. Chen, Preparation and characterization of phosphorus-containing Mannich-type bases as curing agents for epoxy resin. Polym. Adv. Technol. **20**, 753–758 (2009). https://doi.org/10.1002/PAT.1319

H. Ma, M.A. Aravand, B.G. Falzon, Synergistic enhancement of fracture toughness in multiphase epoxy matrices modified by thermoplastic and carbon nanotubes. Compos. Sci. Technol. **201**, 108523 (2021). https://doi.org/10.1016/J.COMPSCITECH.2020.108523

S.R. Madeshwaran, R. Jayaganthan, R. Velmurugan, N.K. Gupta, A.V. Manzhirov, Mechanical and thermal properties of MoS_2 reinforced epoxy nanocomposites. J. Phys. Conf. Ser. **991**, 012054 (2018). https://doi.org/10.1088/1742-6596/991/1/012054

P.D. Mangalgiri, Composite materials for aerospace applications. Bull. Mater. Sci. **22**, 657–664 (1999). https://doi.org/10.1007/BF02749982

M. Mariam, M. Afendi, M.S. Abdul Majid, M.J.M. Ridzuan, A.I. Azmi, M.T.H. Sultan, Influence of hydrothermal ageing on the mechanical properties of an adhesively bonded joint with different adherends. Compos. Part B Eng. **165**, 572–585 (2019). https://doi.org/10.1016/J.COMPOSITESB.2019.02.032

C. May, *Epoxy Resins: Chemistry and Technology*, 2nd edn. (Routledge, New York, 2018)

K. Mayandi, N. Rajini, N. Ayrilmis, M.P. Indira Devi, S. Siengchin, F. Mohammad, H.A. Al-Lohedan, An overview of endurance and ageing performance under various environmental conditions of hybrid polymer composites. J. Mater. Res. Technol. **9**, 15962–15988 (2020). https://doi.org/10.1016/J.JMRT.2020.11.031

A.K. Mehra, R. Saini, A. Kumar, The effect of fibre contents on mechanical and moisture absorption properties of gourd sponge/coir fibre reinforced epoxy hybrid composites. Compos. Commun. **25**, 100732 (2021). https://doi.org/10.1016/J.COCO.2021.100732

V. Mittal, R. Saini, S. Sinha, Natural fiber-mediated epoxy composites – A review. Compos. Part B Eng. **99**, 425–435 (2016). https://doi.org/10.1016/J.COMPOSITESB.2016.06.051

M.J. Mochane, T.C. Mokhena, T.H. Mokhothu, A. Mtibe, E.R. Sadiku, S.S. Ray, I.D. Ibrahim, O.O. Daramola, Recent progress on natural fiber hybrid composites for advanced applications: A review. Express Polym Lett **13**, 159–198 (2019). https://doi.org/10.3144/EXPRESSPOLYMLETT.2019.15

F.M. Monticeli, H.J.C. Voorwald, M.O.H. Cioffi, The influence of carbon-glass/epoxy hybrid composite under mode I fatigue loading: Hybrid fiber bridging zone model. Compos. Struct. **286**, 115274 (2022). https://doi.org/10.1016/J.COMPSTRUCT.2022.115274

J.M. Morancho, X. Ramis, X. Fernández-Francos, O. Konuray, J.M. Salla, Serra, Dual curing of an epoxy resin with dicarboxylic acids. J. Therm. Anal. Calorim. **142**, 607–615 (2020). https://doi.org/10.1007/S10973-020-09523-Z

M. Muralidharan, T.P. Sathishkumar, N. Rajini, P. Navaneethakrishnan, S. Arun Kumar, S.O. Ismail, K. Senthilkumar, S. Siengchin, Evaluation of tensile strength retention and service life prediction of hydrothermal aged balanced orthotropic carbon/glass and Kevlar/glass fabric reinforced polymer hybrid composites. J. Appl. Polym. Sci. **139**, 51602 (2022). https://doi.org/10.1002/APP.51602

R. Narendar, K. Priya Dasan, M. Nair, Development of coir pith/nylon fabric/epoxy hybrid composites: Mechanical and ageing studies. Mater. Des. **54**, 644–651 (2014). https://doi.org/10.1016/J.MATDES.2013.08.080

R. Narendar, K. Priya Dasan, K. Rajendran, Coir pith/nylon/epoxy hybrid composites and their thermal properties: Thermogravimetric analysis, thermal ageing, and heat deflection temperature. J. Vinyl Addit. Technol. **24**, 297–303 (2018). https://doi.org/10.1002/VNL.21594

A.H. Navarchian, N. Najafipoor, F. Ahangaran, Surface-modified poly(methyl methacrylate) microcapsules containing linseed oil for application in self-healing epoxy-based coatings. Prog. Org. Coatings **132**, 288–297 (2019). https://doi.org/10.1016/J.PORGCOAT.2019.03.029

J.S.S. Neto, R.A.A. Lima, D.K.K. Cavalcanti, J.P.B. Souza, R.A.A. Aguiar, M.D. Banea, Effect of chemical treatment on the thermal properties of hybrid natural fiber-reinforced composites. J. Appl. Polym. Sci. **136**, 47154 (2019). https://doi.org/10.1002/APP.47154

V. Obradović, D. Simić, P. Sejkot, K.V. Machalická, M. Vokáč, Moisture absorption characteristics and effects on mechanical properties of Kolon/epoxy composites. Curr. Appl. Phys. **26**, 16–23 (2021). https://doi.org/10.1016/J.CAP.2021.03.015

M. Ochi, N. Tsuyuno, K. Sakaga, Y. Nakanishi, Y. Murata, Effect of network structure on thermal and mechanical properties of biphenol-type epoxy resins cured with phenols. J. Appl. Polym. Sci. **56**, 1161–1167 (1995). https://doi.org/10.1002/APP.1995.070560916

Z.A. Oguz, A. Erklig, Ö.Y. Bozkurt, Degradation of hybrid aramid/glass/epoxy composites hydrothermally aged in distilled water. J. Compos. Mater. **55**, 2043–2060 (2020). https://doi.org/10.1177/0021998320984237

Z.A. Oguz, A. Erklig, Y. Bozkurt, Effects of hydrothermal seawater aging on the mechanical properties and water absorption of glass/aramid/epoxy hybrid composites. Int. Polym. Process. **36**, 79–93 (2021). https://doi.org/10.1515/IPP-2020-3963/MACHINEREADABLECITATION/RIS

N.R. Paluvai, S. Mohanty, S.K. Nayak, Synthesis and modifications of epoxy resins and their composites: A review. Polym Plast Technol Eng. **53**, 1723–1758 (2014). https://doi.org/10.1080/03602559.2014.919658

A. Pandian, M. Vairavan, W.J. Jebbas Thangaiah, M. Uthayakumar, Effect of moisture absorption behavior on mechanical properties of basalt fibre reinforced polymer matrix composites. J. Compos. **2014**, 1–8 (2014). https://doi.org/10.1155/2014/587980

J. Parameswaranpillai, A. George, J. Pionteck, S. Thomas, Investigation of cure reaction, rheology, volume shrinkage and thermomechanical properties of Nano-TiO_2 filled epoxy/DDS composites. J. Polym. **2013**, 1–17 (2013). https://doi.org/10.1155/2013/183463

J. Parameswaranpillai, N. Hameed, J. Pionteck, E. M. Woo (eds.), *Handbook of epoxy blends* (Springer Nature, 2017a), pp. 1–1121. https://doi.org/10.1007/978-3-319-40043-3

J. Parameswaranpillai, S.P. Ramanan, S. Jose, S. Siengchin, A. Magueresse, A. Janke, J. Pionteck, Shape memory properties of epoxy/PPO-PEO-PPO triblock copolymer blends with tunable thermal transitions and mechanical characteristics. Ind. Eng. Chem. Res. **56**, 14069–14077 (2017b). https://doi.org/10.1021/ACS.IECR.7B03676/SUPPL_FILE/IE7B03676_SI_001.PDF

S. Parbin, N.K. Waghmare, S.K. Singh, S. Khan, Mechanical properties of natural fiber reinforced epoxy composites: A review. Procedia Comput. Sci. **152**, 375–379 (2019). https://doi.org/10.1016/J.PROCS.2019.05.003

S.J. Park, M.H. Kim, J.R. Lee, S. Choi, Effect of fiber–polymer interactions on fracture toughness behavior of carbon fiber-reinforced epoxy matrix composites. J. Colloid Interface Sci. **228**, 287–291 (2000). https://doi.org/10.1006/JCIS.2000.6953

A.K. Pathak, M. Borah, A. Gupta, T. Yokozeki, S.R. Dhakate, Improved mechanical properties of carbon fiber/graphene oxide-epoxy hybrid composites. Compos. Sci. Technol. **135**, 28–38 (2016). https://doi.org/10.1016/J.COMPSCITECH.2016.09.007

H. Pulikkalparambil, J. Parameswaranpillai, S. Siengchin, J. Pionteck, UV light triggered self-healing of green epoxy coatings. Constr. Build. Mater. **305**, 124725 (2021). https://doi.org/10.1016/J.CONBUILDMAT.2021.124725

I. Rafique, A. Kausar, Z. Anwar, B. Muhammad, Exploration of epoxy resins, hardening systems, and epoxy/carbon nanotube composite designed for high performance materials: A review. Polym Plast Technol Eng. **55**, 312–333 (2016). https://doi.org/10.1080/03602559.2015.1070874

J.A. Ramos, N. Pagani, C.C. Riccardi, J. Borrajo, S.N. Goyanes, I. Mondragon, Cure kinetics and shrinkage model for epoxy-amine systems. Polymer **46**, 3323–3328 (2005). https://doi.org/10.1016/J.POLYMER.2005.02.069

A.R. Ravindran, R.B. Ladani, S. Wu, A.J. Kinloch, C.H. Wang, A.P. Mouritz, Multi-scale toughening of epoxy composites via electric field alignment of carbon nanofibres and short carbon fibres. Compos. Sci. Technol. **167**, 115–125 (2018). https://doi.org/10.1016/J.COMPSCITECH.2018.07.034

M.J.M. Ridzuan, M.S.A. Majid, M. Afendi, M.N. Mazlee, A.G. Gibson, Thermal behaviour and dynamic mechanical analysis of Pennisetum purpureum/glass-reinforced epoxy hybrid composites. Compos. Struct. **152**, 850–859 (2016). https://doi.org/10.1016/J.COMPSTRUCT.2016.06.026

M.B. Roller, Rheology of curing thermosets: A review. Polym. Eng. Sci. **26**, 432–440 (1986). https://doi.org/10.1002/PEN.760260610

D. Roşu, C.N. Caşcaval, F. Musta, C. Ciobanu, Cure kinetics of epoxy resins studied by non-isothermal DSC data. Thermochim. Acta **383**, 119–127 (2002). https://doi.org/10.1016/S0040-6031(01)00672-4

S.N.A. Safri, M.T.H. Sultan, N. Saba, M. Jawaid, Effect of benzoyl treatment on flexural and compressive properties of sugar palm/glass fibres/epoxy hybrid composites. Polym. Test. **71**, 362–369 (2018). https://doi.org/10.1016/J.POLYMERTESTING.2018.09.017

H.Y. Sastra, J.P. Siregar, S.M. Sapuan, M.M. Hamdan, Tensile properties of Arenga pinnata fiber-reinforced epoxy composites. Polym. Plast. Technol. Eng. **45**, 149–155 (2006). https://doi.org/10.1080/03602550500374038

T.P. Sathishkumar, J. Naveen, S. Satheeshkumar, Hybrid fiber reinforced polymer composites – A review. J. Reinf. Plast. Compos. **33**, 454–471 (2014). https://doi.org/10.1177/0731684413516393

G.K. Sathishkumar, M. Ibrahim, M. Mohamed Akheel, G. Rajkumar, B. Gopinath, R. Karpagam, P. Karthik, M. Martin Charles, G. Gautham, G. Gowri Shankar, Synthesis and mechanical properties of natural fiber reinforced epoxy/polyester/polypropylene composites: A review. J. Nat. Fibers (2020). https://doi.org/10.1080/15440478.2020.1848723

P. Sathyaseelan, P. Sellamuthu, L. Palanimuthu, Dynamic mechanical analysis of areca/kenaf fiber reinforced epoxy hybrid composites fabricated in different stacking sequences. Mater. Today Proc. **39**, 1202–1205 (2021). https://doi.org/10.1016/J.MATPR.2020.03.590

C.L. Schutte, Environmental durability of glass-fiber composites. Mater. Sci. Eng. R Reports. **13**, 265–323 (1994). https://doi.org/10.1016/0927-796X(94)90002-7

A.I. Selmy, A.R. Elsesi, N.A. Azab, M.A. Abd El-Baky, In-plane shear properties of unidirectional glass fiber (U)/random glass fiber (R)/epoxy hybrid and non-hybrid composites. Compos. Part B Eng. **43**, 431–438 (2012). https://doi.org/10.1016/J.COMPOSITESB.2011.06.001

K. Senthilkumar, S. Subramaniam, T. Ungtrakul, T.S.M. Kumar, M. Chandrasekar, N. Rajini, S. Siengchin, J. Parameswaranpillai, Dual cantilever creep and recovery behavior of sisal/hemp fibre reinforced hybrid biocomposites: Effects of layering sequence, accelerated weathering and temperature. J. Ind. Text. (2020). https://doi.org/10.1177/1528083720961416

A. Shahzad, Comparison of tensile properties and impact damage tolerance of hemp and glass fiber composites. J. Reinf. Plast. Compos. **30**, 1877–1893 (2011). https://doi.org/10.1177/0731684411431123

Y. Singh, J. Singh, S. Sharma, T.D. Lam, D.N. Nguyen, Fabrication and characterization of coir/carbon-fiber reinforced epoxy based hybrid composite for helmet shells and sports-good applications: Influence of fiber surface modifications on the mechanical, thermal and morphological properties. J. Mater. Res. Technol. **9**, 15593–15603 (2020). https://doi.org/10.1016/J.JMRT.2020.11.023

R.E. Smith, F.N. Larsen, C.L. Long, Epoxy resin cure. II. FTIR analysis. J. Appl. Polym. Sci. **29**, 3713–3726 (1984). https://doi.org/10.1002/APP.1984.070291207

B.K. Sriranga, L.J. Kirthan, G. Ananda, The mechanical properties of hybrid laminates composites on epoxy resin with natural jute fiber and S-glass fibers. Mater. Today Proc. **46**, 8927–8933 (2021). https://doi.org/10.1016/J.MATPR.2021.05.363

M. Stratigaki, C. Baumann, R. Göstl, Confocal microscopy visualizes particle–crack interactions in epoxy composites with optical force probe-cross-linked rubber particles. Macromolecules **55**, 1060–1066 (2022). https://doi.org/10.1021/ACS.MACROMOL.1C02366

R. Thomas, D. Yumei, H. Yuelong, Y. Le, P. Moldenaers, Y. Weimin, T. Czigany, S. Thomas, Miscibility, morphology, thermal, and mechanical properties of a DGEBA based epoxy resin toughened with a liquid rubber. Polymer **49**, 278–294 (2008). https://doi.org/10.1016/J.POLYMER.2007.11.030

T.K. Tsotsis, S. Keller, J. Bardis, J. Bish, Preliminary evaluation of the use of elevated pressure to accelerate thermo-oxidative aging in composites. Polym. Degrad. Stab. **64**, 207–212 (1999). https://doi.org/10.1016/S0141-3910(98)00190-6

A. Vinod, M.R. Sanjay, S. Suchart, P. Jyotishkumar, Renewable and sustainable biobased materials: An assessment on biofibers, biofilms, biopolymers and biocomposites. J. Clean. Prod. **258**, 120978 (2020). https://doi.org/10.1016/J.JCLEPRO.2020.120978

A. Vinod, J. Tengsuthiwat, Y. Gowda, R. Vijay, M.R. Sanjay, S. Siengchin, H.N. Dhakal, Jute/Hemp bio-epoxy hybrid bio-composites: Influence of stacking sequence on adhesion of fiber-matrix. Int. J. Adhes. Adhes. **113**, 103050 (2022). https://doi.org/10.1016/J.IJADHADH.2021.103050

X. Wang, M. Petrů, Effect of Hygrothermal aging and surface treatment on the dynamic mechanical behavior of flax fiber reinforced composites. Materials **12**, 2376 (2019). https://doi.org/10.3390/MA12152376

W. Wang, M. Sain, P.A. Cooper, Hygrothermal weathering of rice hull/HDPE composites under extreme climatic conditions. Polym. Degrad. Stab. **90**, 540–545 (2005). https://doi.org/10.1016/J.POLYMDEGRADSTAB.2005.03.014

Z. Wang, G. Xian, X.L. Zhao, Effects of hydrothermal aging on carbon fibre/epoxy composites with different interfacial bonding strength. Constr. Build. Mater. **161**, 634–648 (2018). https://doi.org/10.1016/J.CONBUILDMAT.2017.11.171

A. Wang, X. Wang, G. Xian, Mechanical, low-velocity impact, and hydrothermal aging properties of flax/carbon hybrid composite plates. Polym. Test. **90**, 106759 (2020). https://doi.org/10.1016/J.POLYMERTESTING.2020.106759

Z. Wang, P. Gnanasekar, S.S. Nair, S. Yi, N. Yan, Curing behavior and thermomechanical performance of bioepoxy resin synthesized from Vanillyl alcohol: Effects of the curing agent. Polymers **13**, 2891 (2021a). https://doi.org/10.3390/POLYM13172891

Y. Wang, W. Zhu, B. Wan, Z. Meng, B. Han, Hygrothermal ageing behavior and mechanism of carbon nanofibers modified flax fiber-reinforced epoxy laminates. Compos. Part A Appl. Sci. Manuf. **140**, 106142 (2021b). https://doi.org/10.1016/J.COMPOSITESA.2020.106142

R. Wazalwar, M. Sahu, A.M. Raichur, Mechanical properties of aerospace epoxy composites reinforced with 2D nano-fillers: Current status and road to industrialization. Nanoscale Adv. **3**, 2741–2776 (2021). https://doi.org/10.1039/D1NA00050K

J. Wei, M.C. Hawley, J.D. Delong, M. Demeuse, Comparison of microwave and thermal cure of epoxy resins. Polym. Eng. Sci. **33**, 1132–1140 (1993). https://doi.org/10.1002/PEN.760331706

C. Wu, K. Yang, Y. Gu, J. Xu, R.O. Ritchie, J. Guan, Mechanical properties and impact performance of silk-epoxy resin composites modulated by flax fibres. Compos. Part A Appl. Sci. Manuf. **117**, 357–368 (2019). https://doi.org/10.1016/J.COMPOSITESA.2018.12.003

R. Yahaya, S.M. Sapuan, M. Jawaid, Z. Leman, E.S. Zainudin, Effect of fibre orientations on the mechanical properties of kenaf–aramid hybrid composites for spall-liner application. Def. Technol. **12**, 52–58 (2016). https://doi.org/10.1016/J.DT.2015.08.005

E. Yousif, R. Haddad, Photodegradation and photostabilization of polymers, especially polystyrene: Review. Springerplus **2**, 1–32 (2013). https://doi.org/10.1186/2193-1801-2-398/FIGURES/49

B.F. Yousif, A. Shalwan, C.W. Chin, K.C. Ming, Flexural properties of treated and untreated kenaf/epoxy composites. Mater. Des. **40**, 378–385 (2012). https://doi.org/10.1016/J.MATDES.2012.04.017

Applications and Drawbacks of Epoxy/Synthetic/Natural Fiber Hybrid Composites

40

E. A. Franco-Urquiza

Contents

E. A. Franco-Urquiza (✉)
National Council for Science and Technology (CONACYT–CIDESI), National Center for Aeronautic Technologies (CENTA), Querétaro, Mexico
e-mail: edgar.franco@cidesi.edu.mx

S. Mavinkere Rangappa et al. (eds.), *Handbook of Epoxy/Fiber Composites*,
https://doi.org/10.1007/978-981-19-3603-6_43

Abstract

This chapter presents the progress of hybrid natural/synthetic fiber composites. Only epoxy-based composites were considered. Hybrid natural/synthetic fiber composites meet design requirements, combine the fibers' characteristics, and are cheaper than conventional composites, primarily because of natural fiber. The mechanical properties, moisture absorption, fracture, and flame behavior are reviewed. Natural fibers are treated to increase their interaction with the epoxy resin matrix that results in the better mechanical performance of hybrid composites. The advances and main drawbacks of hybrid natural/synthetic fiber composites and the leading applications and expectations that these novel materials can provide to various industrial sectors to develop less expensive and environmentally friendly components are presented. There are several topics to be investigated, highlighting the particular objective of experimenting with these materials, solving the problems already detected, and innovating in a disruptive research methodology that allows a significant advance in the use of hybrid natural/synthetic fiber composites for engineering and technological applications.

Keywords

Epoxy · Synthetic fibers · Natural fibers · Hybrid composites

Introduction

Fiber-reinforced polymers (FRP) are composite materials that consist of a polymeric matrix and a reinforcing phase (large fibers). Sometimes fillers or additives are added to the resin during the manufacturing process to increase properties, expand functionality, and reduce the cost of composite materials. The fibers' primary function is to carry loads along their longitudinal direction, while the matrix holds the fibers together, transfers stresses between them, and protects them from mechanical or environmental damage. Furthermore, the deformation at the break of the matrix must be greater than the fibers it supports. Although fibers play a dominant role in determining composites' stiffness and strength, the matrix's selection determines the maximum service temperature. Matrix materials can be divided into thermosetting and thermoplastic polymers. Thermoplastics are high-molecular-weight linear or branched polymers that can be transformed several times because they are processable by melting, although this leads to degradation. Thermosetting materials have low viscosity and react (cure) to form a three-dimensional infusible network; hence, they cannot be reprocessed.

There are several commercial resins available that provide a wide range of applications according to the requested requirements. The most popular resin

matrices are epoxy, phenolic, polyester, and vinyl ester. Epoxy resins are more expensive and widely used in structural and high-tech applications because of the excellent mechanical properties and resistance to moisture compared to polyesters or vinyl resins. Phenolic and polyimide resins are used for dielectric and high-temperature applications, respectively.

Fibers are classified as natural or synthetic fibers. There is a broad diversity of fibers and matrices that provide a wide variety of properties in composites, although the results of only a few fiber-polymer combinations have been reported. According to the type of matrix and reinforcement (Callister 2001), the general classification of composites is presented in Fig. 1.

Thermoplastic fibers, like polyester, nylon, acrylic, or polypropylene fibers, offer a wide range of values of different mechanical properties. However, these thermoplastic fibers are most oriented to the textile industry and interior building products.

Synthetic fibers for structural applications are commonly used as reinforcement of composite materials for engineering parts and components. However, the manufacture of these synthetic fibers carries tremendous challenges, such as high energy consumption, environmental damage, high production cost, and the rate of depletion of the oil supply. These problems force the composites developers to find viable alternatives for the production of FRP systems. An alternative is to use natural fibers because they are a renewable resource, low density, high mechanical properties, and biodegradable (Mohanty et al. 2005; Pickering et al. 2016; Yan et al. 2014). However, natural fibers have some limitations since they are hygroscopic, and moisture weakens the reinforcement-matrix interface, reducing the composite's mechanical properties. Besides, natural fibers present a noticeable variation in their mechanical properties related to the crop and harvest quality, limiting their use in composites for structural or engineering applications.

The combination of synthetic and natural fibers allows increasing the structural capacities of composite materials, which benefit from both types of reinforcement. This combination is known as hybridization. The current chapter deals with hybrid composites, where the mechanical performance of epoxy composites reinforced with natural and synthetic fibers is presented in detail.

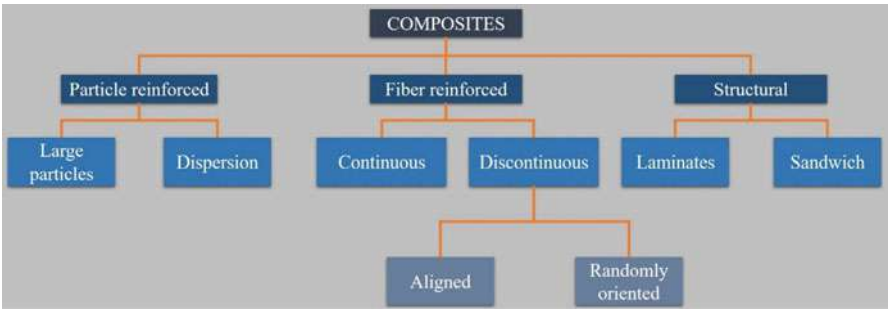

Fig. 1 A general classification of composite materials

High-Performance Fibers

High-performance fibers made of glass, carbon, and aramid represent a particular category of fibers used for structural engineering and high-tech applications. They have low density, high strength, high modulus, and exceptionally high-temperature resistance. Aerospace, ground transportation, biotechnology, computing, infrastructure, and communication systems are the most common industrial applications. The exceptional properties of the high-performance fibers can be designed during their manufacturing process.

Glass is the oldest high-performance fiber (GF) and is the reinforcement material mostly used in industry because of its mechanical performance, superior chemical resistivity, and insulation properties (Lima et al. 2019). Glass fiber-reinforced polymer (GFRP) composites are used in the construction field (36%), followed by the transport sector (34%), the electronics industry (14%), and sports (14%).

GFs are classified according to their properties into E glass, AR glass, R glass, and S glass. E glass is the most widely used fiber, because it requires non-expensive raw materials, with less than 1 wt.% of alkali oxides. The letter E refers to its principal use in electrical insulator applications. S glass has a higher strength than E glass as it contains a high amount of silica oxide, aluminum oxide, and magnesium oxide compared to E glass. Glass fibers are made by extruding molten glass through metal dies with tiny holes and then drawing the fibers into filaments with diameters in the range of 3–20 μm. Because the fibers' high abrasiveness can cause defects that degrade the fibers' properties, they are coated with a binder material that improves the glass surface's adhesion to the polymer resins.

Carbon fiber (CF) is a synthetic fiber composed primarily of carbon, as it is produced from a precursor polymer, commonly rayon, polyacrylonitrile (PAN), or a petroleum-derived resin. CFs produced from PAN are obtained by a three-step process: (1) stabilization, (2) carbonization, and (3) graphitization. Temperature plays a crucial role in obtaining high-strength carbon fiber (1500–2000 °C) or high modulus carbon fiber (2500–3000 °C) during graphitization. The space industry was the leading promoter to develop this resin because of the mechanical properties and lightness.

CFs are classified according to the mechanical properties as:

- Ultra-high modulus, UHM type (modulus >450 Gpa)
- High modulus, HM type (350–450 Gpa modulus)
- Intermediate modulus, IM type (200–350 Gpa modulus)
- Low modulus and high tensile strength, HT type (modulus <100 Gpa, tensile strength >3.0 Gpa)
- Super high strength, SHT type (tensile strength >4.5 Gpa)

The high cost of carbon fiber is the primary concern associated with its growth and prevents its use in large applications. However, as the acquisition cost decreases, this fiber's use expands to other technological fields, such as aeronautics, automotive, naval, and sporting goods (mainly bicycles).

According to the MarketsandMarkets report (consulted online in November 2020, https://www.marketsandmarkets.com/), the carbon fiber market is projected to grow to USD 13.3 billion by 2029, at a CAGR of 11.0%. The market is growing due to the increasing demand from technology sectors such as aerospace, defense, automotive, infrastructure, and wind power. However, the main growth restriction is the cost of carbon fiber. In the automotive sector, this fiber is used only in high-end racing cars and sports cars, although today, this fiber is currently used in the 3D printing of parts and components. The advantage of this technique is that the carbon fiber's content and orientation are controllable, which facilitates the optimization process. Carbon fiber 3D printing also allows high precision in manufacturing parts for multiple sectors, having the aerospace and automotive industries as end users. This technology and its many variants are expected to revolutionize carbon fiber parts and components' manufacturing process, offering several market opportunities for the coming years.

Aramid fibers are polyamides formed by the reaction of an amino group with a carboxyl group. The presence of aromatic rings in the aramid fibers' structure provides high impact resistance and thermal stability. Aramid fibers are prepared by spinning and extrusion processes. They are classified as high modulus fibers, although they exhibit ductile break rather than the brittle break that characterizes carbon fibers. Aramid fibers are potentially used in aerospace and military applications, primarily for ballistic purposes. Two of the commercially known aramid fibers are Kevlar, a high-strength fiber, and Nomex, a heat-resistant fiber.

Natural Fibers

Nowadays, the needs for environmentally friendly industrial products are in strong growth due to ecological concern, attention to the environment, and new international rules and regulations. Extensive studies on natural fibers (Ahmad et al. 2015; Biagiotti et al. 2004; Gholampour and Ozbakkaloglu 2020; Mohanty et al. 2005; Shireesha and Nandipati 2019; Thyavihalli Girijappa et al. 2019) show their potential as useful reinforcement for composite materials. Natural fibers also provide a healthier manufacturing process for workers than synthetic fibers. Besides, natural fibers offer good thermal properties, low cost, low density, and excellent acoustic performance. These advantages make natural fibers attract attention and are widely used in automotive, packaging, and construction. However, natural fibers are far from being used in nonstructural applications due to their relatively low mechanical performance. Natural fibers are classified according to their origin in vegetable or animal fibers (Mochane et al. 2019). All plant fibers are made of cellulose, while animal fibers are made of proteins (wool, silk, and hair). Unlike vegetable fibers, animal fibers are not used as reinforcements in composite materials.

Plant fibers are classified according to their usefulness in primary (plant fibers) and secondary (extraction of by-products). In addition, plant fibers are categorized based on the area of the plant from which they are extracted (Mochane et al. 2019):

- Stem fibers
- Leaf fibers
- Fruit fibers
- Seed fiber
- Stalk fiber

The plant fibers mainly used as reinforcements in composite materials are jute, hemp, flax, and sisal. The general classification of plant fibers is presented in Fig. 2.

Plant fibers are lignocellulose made up of cellulose, hemicellulose, lignin, low-molecular-weight compounds soluble in water (pectin), and wax substances. Cellulose is the major component (about 50%), followed by lignin (about 20%) and hemicellulose (about 15%) (Gholampour and Ozbakkaloglu 2020; Gurunathan et al. 2015; Mohanty et al. 2005; Shireesha and Nandipati 2019). Figure 3 shows the schematic representation of cellulose microfibrils' cellular structure, which depends on the plant's specific type and is responsible for the fiber's mechanical properties (Silva et al. 2009). As shown in Fig. 3, the elemental fibers present hierarchical microstructures formed by a central channel called the lumen (responsible for the transport of water and nutrients during the life of the plant) and by the cell wall that surrounds the lumen that is formed by several layers, commonly referred to as secondary cell walls, primary cell walls, and middle lamella. Each fiber cell wall contains primary and secondary walls of microfibrils. The cell wall of elemental fiber is composed of semicrystalline cellulose microfibrils oriented in an amorphous hemicellulose-lignin matrix (Silva et al. 2009).

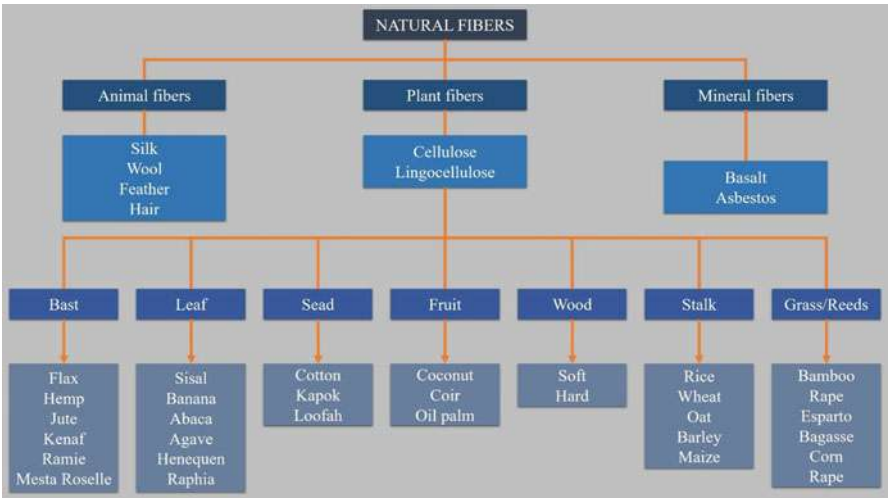

Fig. 2 A general classification of natural fibers

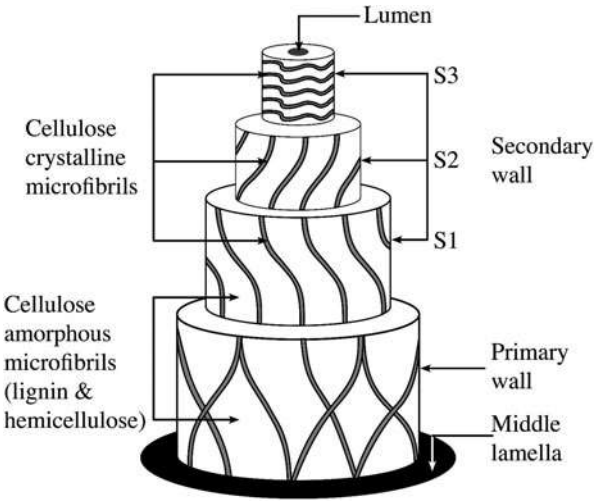

Fig. 3 Schematic representation of the microstructure of plant fibers. (Adapted with permission from Silva et al. (2009))

Hybrid Composites

Hybrid composite materials are multifunctional materials that meet multiple requirements in advanced structural parts. Hybrid composites can refer to a mixture of two reinforced matrices or a matrix reinforced by at least two different reinforcements. For the latter case, epoxy resins are reinforced with fibers of distinct nature to combine their individual properties to cover the engineering requirements for structural applications. The properties of hybrid composites depend on several factors like the proportion of the different types of fibers, the length and orientation of the fibers, the configuration of the fiber fabrics, the fiber-fiber and fiber-matrix interactions, and the stacking sequences of fiber layers (Assarar et al. 2015; Flynn et al. 2016; Lima et al. 2019; Megahed et al. 2020; Nisini et al. 2017; Puttegowda et al. 2018; Ramesh et al. 2015; Winkelmann et al. 2020).

As previously mentioned, natural fibers have the advantages of low density, high strength, and high stiffness are renewable and low cost. However, these fibers have disadvantages that include lower durability and low impact resistance than synthetic fibers. The hygroscopic nature of natural fibers reduces the mechanical performance of hybrid composites because water molecules weaken the interfacial adhesion between constituents (do Nascimento Santos et al. 2017; Flynn et al. 2016; Naveen et al. 2018; Thyavihalli Girijappa et al. 2019).

Industrial sectors like automotive, aircraft interior structures, building, and other structural industries require synthetic fibers. However, the most significant restraint of synthetic fibers is that they require a large amount of energy during their production process and are not recyclable, hindering environmental protection protocols and sustainable development.

The combination of synthetic fibers with plant fibers represents an excellent alternative for use in composite materials. Hybridization of synthetic fibers with plant fibers balances reasonable costs and combines optimal mechanical properties compared to simple synthetic fiber materials (Al-Hajaj et al. 2018; Puttegowda et al. 2018; Rajesh Jesudoss Hynes et al. 2020; Ravishankar et al. 2019; Safri et al. 2018).

The mechanical performance and thermal properties of natural/synthetic fibers hybrid composites are reported in the literature (Flynn et al. 2016; Kureemun et al. 2018; Winkelmann et al. 2020). Some works (Lima et al. 2019; Mochane et al. 2019; Ramesh et al. 2015) underline the humidity strongly influences the natural/synthetic fiber composites' mechanical properties. Plant fibers are hydrophilic due to their porous structure and can absorb large amounts of water. Hybridization offers an efficient method of combining fibers with different properties for superior properties and cost reduction benefits. The objective is to combine the interweave synthetic and natural fibers or vary the stacking sequence of single layers to optimize the cost-effectiveness of the composite laminate properties.

Hybrid Bast Fiber Composites

Many plant fibers can be used as reinforcement in FRP composites. However, fibers from the bast plant family are commonly reported in the literature. Table 1 presents the mechanical properties of the hybrid epoxy/synthetic/natural composites obtained from the literature. It is necessary to underline that there is a wide range of research opportunities in the field of hybrid composite materials. Most of these variables are constituents, volume fraction, fill content, fabric configurations, layer orientation, thickness, and moisture. All these variables modify the mechanical properties of hybrid composites.

Kenaf Fiber

Kenaf fiber is widely used to reinforce composite materials due to the excellent mechanical properties that this fiber offers. Kenaf (Hibiscus cannabinus) fiber is endemic to Asia, and it consists of 70% cellulose, 19% hemicellulose, and 3% lignin. Interestingly, this fiber overgrows in 3 months, contributing to sustainability as a natural resource (Yusuff et al. 2020). It is relevant to underline the kenaf fiber obtained from the bast region has better mechanical strength than the core zone, and up to 40% of the bast region can be transformed into fibers, which makes them economically comparable to other plants. Even though kenaf fibers exhibit high strength and stiffness, they are nonabrasive, have low density, and are profitable (Yan et al. 2014; Yusuff et al. 2020). The kenaf plant's short growth cycle combined with the low water requirement makes it more suitable for composites and other applications. The excellent mechanical properties and the low density of kenaf fibers make them possible to replace part of the fiberglass to reduce composites' weight and cost.

Table 1 Mechanical properties of the hybrid epoxy/synthetic/natural composites

Material	Tension		Flexural		Moisture	
Bast fibers	E (GPa)	σ_y (MPa)	E (GPa)	σ_f (MPa)	%	References
Kenaf fiber	21–60	350–600			11	Yusuff et al. (2020) and Ren et al. (2019)
Kenaf/ carbon fibers	7.5–9	104–127	16–18	185–224	6	Bakar et al. (2013) and Sapiai et al. (2014)
Kenaf/ glass fibers	5.6	65	5.8	116	8	Sapiai et al. (2015)
Kenaf/ aramid fibers	3.3–6	140	2–8	60–100	8	Yahaya et al. (2016)
Flax fiber	60–80	800–1500			7–10	Mochane et al. (2019) and Yan et al. (2014)
Flax/ carbon fibers	25–37	338–413			5–8	Al-Hajaj et al. (2018)
Flax/ glass fibers	40	410			6	Zhang et al. (2013)
Flax/ aramid fibers	16	172	10	200		Audibert et al. (2018)
Hemp fiber	30	550–900				Mwaikambo and Ansell (2002) and Shahzad (2011)
Hemp/ carbon fibers	8.9	103	1.8	105	6	Ramesh et al. (2019)
Hemp/ glass fibers		38			7–9	Bhoopathi et al. (2014)
Hemp/ aramid fibers	8.3	124	1.5	104		Jani et al. (2019) and Suresha et al. (2018)
Jute fiber	13–26.5	393–800			12	Ravishankar et al. (2019) and Ashraf et al. (2019)
Jute/ carbon fibers	2.3	95			2.3	Wang et al. (2011)
Jute/ glass fibers	3.1–4.3	12–165	5.8	102	7.6	Aquino et al. (2007)
Jute/ aramid fibers	1.7–3.9	60–160				Bhanupratap and Chittappa (2017)

The study of hybrid kenaf/carbon fiber and kenaf/glass fiber composites is widely reported in the literature (Al-Hajaj et al. 2018; Rajesh Jesudoss Hynes et al. 2020) Generally, a chemical treatment is carried out to improve the kenaf fiber's adhesion with the epoxy resin and increase the hybrid composites' mechanical performance. This treatment consists of modifying the kenaf fibers in an alkaline solution, mainly sodium hydroxide (NaOH), to remove lignin, pectin, waxy substances, and surface impurities on the fiber cell wall (Mwaikambo and Ansell 2002). Alkali treatment promotes the natural fibers-polymer resins interaction and favors the tensile, flexural strength, and stiffness of plant fibers reinforced epoxy composites. In contrast, the synthetic fibers (mainly glass) are treated with a silane coupling agent to improve their mechanical performance. The modification of the kenaf fiber surface employing chemical treatment with alkali at different NaOH concentrations can influence the hybrid composites' mechanical resistance, since it can provide an excellent interfacial bond between the fibers and the epoxy resin (Franco-Urquiza and Rentería-Rodríguez 2020; Ren et al. 2019).

The chemical alkali treatment consists of immersing the kenaf fiber in a NaOH solution for a few hours. Subsequently, the treated kenaf fiber is subjected to a drying process for 1 h at approximately 100 °C in a high-temperature coil. The presence of any impurity alters the adhesion properties between the fibers and the matrix resin (Hassan et al. 2018).

Therefore, the removal of impurities leads to better adhesion between the fibers and the polymer matrix, contributing to increased mechanical performance. However, kenaf fibers' surface can be damaged if they are treated under a high concentration of the alkaline solution, reducing hybrid composites' mechanical performance (Yan and Chouw 2015).

FRP composites are formed by stacking layers of fibers oriented in different directions to obtain quasi-isotropic laminates. The stacking sequence of individual fiber layers (fabrics or unidirectional layers) influences the mechanical properties of hybrid kenaf/glass fiber composites and is of particular interest to the scientific community. The fibers' arrangement also represents a significant impact on the final properties of hybrid composites, although the measurable results vary considerably due to the absence of a standardized extraction fibers method that promotes hybrid composites' excellent mechanical performances.

Another factor that affects the mechanical performance of hybrid kenaf/glass fiber composites is the laminate thickness, which is crucial in the manufacture of hybrid composites to meet design requirements (Banakar 2012).

Kenaf/Carbon Fibers

The weave patterns, stacking sequence, and orientation of unidirectional fibers are known to control, in part, the mechanical properties of composites. In this sense, the investigations carried out (Aisyah et al. 2018) conclude that the structure, the resistance, and the number of stacked layers significantly affect the hybrid composites' properties. For example, plain weave fabrics show better adhesion compared to

satin fabrics. The authors performed an extensive study and observed the hybrid kenaf/carbon fiber composites failed due to a combination of intense fiber extraction, fiber breakage, interlayer delamination, and voids. These failure modes occurred more evidently in the satin fabric specimen. The authors also detected an evident crack across the hybrid fabrics and epoxy interface post-delamination (Fig. 4), indicating that the fiber pullout phenomenon is present in the system (Fig. 4b, c), and the impact properties are strongly affected by the structure of the woven fabric and the properties of the resin.

In the case of stacking unidirectional fibers, the effects of different orientations of kenaf and carbon fibers on the hybrid composites' mechanical performance (Sapiai et al. 2014) have been evaluated. The general results conclude that the highest tensile and compressive strength is obtained in the longitudinal direction compared to the transverse direction. The properties are higher in the fibers' longitudinal direction because they depend on the fibers' tensile strength. Meanwhile, in the transverse direction, they depend on the shear properties of the polymer matrix. Observations by scanning electron microscopy (SEM) reveal that the most common failure modes in hybrid composites are low fiber adhesion, lack of compaction between constituents, and manufacturing voids (Aisyah et al. 2018). Therefore, it is assumed that

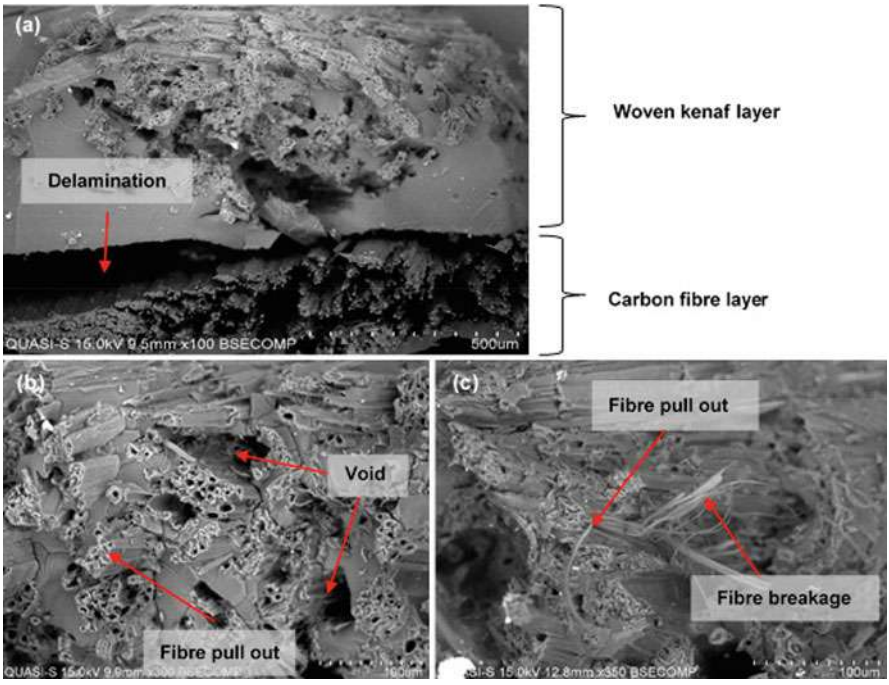

Fig. 4 SEM micrographs on the fracture surface impact: (**a**) delamination between kenaf and carbon layers, (**b** and **c**) fiber pullout breakage, and voids detected at higher magnifications. (Reproduced with permission from Aisyah et al. (2018))

modifying the fibers, increasing the fiber content, and reducing voids increase the tensile properties.

Hybrid kenaf/carbon fiber composites have been studied to evaluate the influence of both the treatment and the fiber volume content on the hybrid composites' mechanical and thermal properties. The flexural strength of hybrid kenaf/carbon fibers composites increases as the fiber content up to a limiting capacity, where the mechanical properties decrease dramatically. Similar behavior was observed for the impact resistance (Aisyah et al. 2018; Hassan et al. 2018; Rajesh Jesudoss Hynes et al. 2020). On the other hand, the thermomechanical analysis showed the untreated kenaf fibers exhibit a higher modulus of storage, loss modulus, and damping factor than composites with treated fibers. In this case, the hybrid composites with treated kenaf fibers lead to the deterioration of the composite properties due to an incompatibility between the carbon and kenaf fibers that promotes the separation of the reinforcement and matrix phases, which is appreciated when the test is carried out at elevated temperatures (Cicala et al. 2018; Mochane et al. 2019).

The mechanical properties of hybrid composites depend on the kind of reinforcements and the fiber/matrix interactions. Bakar et al. (2013) studied the impact properties of hybrid kenaf/carbon fiber composites. In this work, the fibers were impregnated manually, with a fiber content of 20 wt.% to evaluate the effect of reinforcement in various kenaf/carbon ratios on impact properties. Interesting was the modification of the epoxy resin by adding liquid epoxidized natural rubber to improve its toughness. In addition to the epoxy resin, the fibers were treated to improve the interaction between the constituents. Thus, carbon fibers were subjected to gamma radiation, while kenaf fibers were treated with alkaline solutions. The authors observed that the epoxy resin modification favors the flexural strength and the fracture toughness of the manufactured hybrid composites. Increasing the carbon fiber content and its modification contribute to improving hybrid kenaf/carbon fiber composites' impact properties. The modification of the kenaf fibers seems to improve the hybrid composites' flexural properties without appreciating a significant variation in fracture toughness.

Kenaf/Glass Fibers

The automotive sector uses kenaf fibers for car interior parts to reduce the vehicle's weight and minimize fuel consumption, thus reducing harmful gases (Mochane et al. 2019; Puttegowda et al. 2018; Ravishankar et al. 2019; Yusuff et al. 2020). The low- and high-speed impact analysis is of considerable interest because hybrid kenaf/glass fiber composites are used for automobiles' exterior parts. Ismail et al. (2019) performed low-speed impact tests on epoxy/kenaf/glass fibers hybrid composites by varying the fiber content. They observed that the hybrid composite showed the best properties with 75% fiberglass and 25% kenaf. They also analyzed the damaged area through dye penetration tests, observing that the less damaged samples showed higher resistance to compression, which was performed after the impact test.

Kenaf/Aramid Fibers

Aramid fiber exhibits excellent tensile strength with superior impact properties. Aramid fiber is employed as a secondary reinforcement to improve hybrid kenaf/aramid fiber composites' impact properties. One way to evaluate the impact properties is to vary the layers' orientation and the Kevlar fiber content. According to some reports (Bakar et al. 2013), the highest impact strength was obtained with a sequence of two-layer Kevlar/kenaf/two-layer Kevlar and combined orientations (0/90), and the hybrid composite with 22/78 kenaf/Kevlar ratio presented the better mechanical properties because of the excellent interaction between fibers and matrix. By increasing the kenaf fiber content, the strength tends to reduce because of the low resistance of kenaf fiber to deformation. Another study (Bakar et al. 2013) related the influence of kenaf fibers' fabric configuration on hybrid kenaf/aramid fiber composites' mechanical properties. The authors evaluated three different configurations: plain weave, unidirectional (UD), and nonwoven. The results showed that plain weave exhibits relevant Young's modulus and strength compared to UD and nonwoven. The UD configuration gives the highest value in flexural strength; meanwhile, the lowest flexural strength was obtained in nonwoven kenaf fiber.

Flax Fiber

Flax fiber is one of the most widely studied natural fibers within the bast family. People in the pre-Hispanic era used flax fibers to make various types of ropes, assemble work tools, weave sacks and baskets. Flax (*Linum usitatissimum*) is typically grown in regions with temperate climates. However, flax is also grown in southern Europe, Argentina, India, China, and Canada. The intrinsic properties of flax fiber, such as high strength and stiffness and low elongation at break, are of particular interest in composite materials research because these properties are a consequence of several factors, such as the plant's origin, the growing conditions, and the plant's age. Some authors (Yan et al. 2014) stated that the mechanical properties of flax fibers depended on the stem area they are obtained. Flax fibers extracted from the lower part of the stem have the worst mechanical properties, while fibers located in the middle of the stem show the best mechanical performance. Despite the multiple advantages offered by flax fiber, it is relevant to underline that these fibers are usually expensive due to the cultivation process and the conditions required during the storage of the fibers, since the flax plant is susceptible to a wide variety of fungal diseases, pests, and rusts.

The extraction process also influences the mechanical properties of the flax fiber (Torres et al. 2020; Torres-Arellano et al. 2020). It is common to extract flax fibers through manual or mechanical processes. Manually extracted fibers have mechanical properties superior to those extracted mechanically because mechanical extraction processes induce damage to the fibers due to a twisting effect, which reduces their tensile strength. However, the mechanical evaluation of these fibers indicates that the fibers extracted manually have a high degree of dispersion in the results compared to

the fibers extracted mechanically, which could be due to the homogeneity of defects produced by a mechanized system versus a manual process that involves multiple nonmeasurable factors during the process of obtaining the fibers. On the other side, the fibers separated by enzymatic treatment present less damage than fibers obtained by mechanical processes. Zeng et al. (2015) used a flax fiber extraction method that consisted of pretreating the fibers with ammonia and compared the results with a mechanical extraction process, finding that the flax's tensile and flexural properties fibers increased due to treatment.

Flax/Carbon Fibers

Hybrid flax/carbon fiber composites combine the excellent mechanical properties of carbon fibers and the outstanding impact absorption properties of flax fiber, which is why they are used in the automotive sector. The use of hybrid flax/carbon fiber composites in structural applications for the automotive sector requires tests representing real events such as a car accident. The dart drop impact test is performed to obtain information on the energy absorption capacity of hybrid composites. This test also allows the analysis of the morphology and propagation of the damage to reveal the materials' appropriate uses for structural applications.

Flax fiber composites have a low energy absorption capacity compared to composites made from carbon fibers. The reason is that the impact resistance of flax fibers is much lower than carbon fibers, although carbon presents a fragile behavior that makes it challenging to approve safety issues in automotive catastrophes. Replacing part of the carbon fibers with flax fibers allows the hybrid composite to combine both fibers' characteristics. Some studies demonstrated that hybrid flax/carbon composites enhance the impact properties of the epoxy composites. The energy impact absorption increased considerably by combining carbon fiber fabrics with unidirectional flax fibers (Flynn et al. 2016; Mahboob et al. 2017). Furthermore, the partial substitution of carbon fibers by flax fibers does not compromise the hybrid composite's impact resistance. Conversely, substituting bidirectional flax fiber fabrics for unidirectional carbon fiber layers results in a substantial improvement in flexural modulus and strength of hybrid composites compared to the flax fiber-reinforced epoxy composites.

Madina Shamsuyeva et al. (2019) demonstrated the feasibility of combining synthetic and natural fibers to enhance the isotropic mechanical performance by analyzing epoxy resin composites' flexural properties reinforced with flax and hybrid fabrics of flax/carbon and flax/glass fibers. The authors indicated the possibility of fabricating hybrid composites up to 50 wt.% of carbon or glass fibers leads to a significant improvement in the biocomposites' flexural strength and modulus. Furthermore, they conducted extensive research to understand the infiltration and elimination of voids. Figure 5 shows composites with a different void content. The flax composite with plain weaved textile with the lowest thickness shows nearly no voids. The flax composites with twill weaved and satin weaved fabrics have many large voids and some voids, respectively, although these voids are significantly smaller than the twill weaved composite. In the case of hybrid textiles, the void

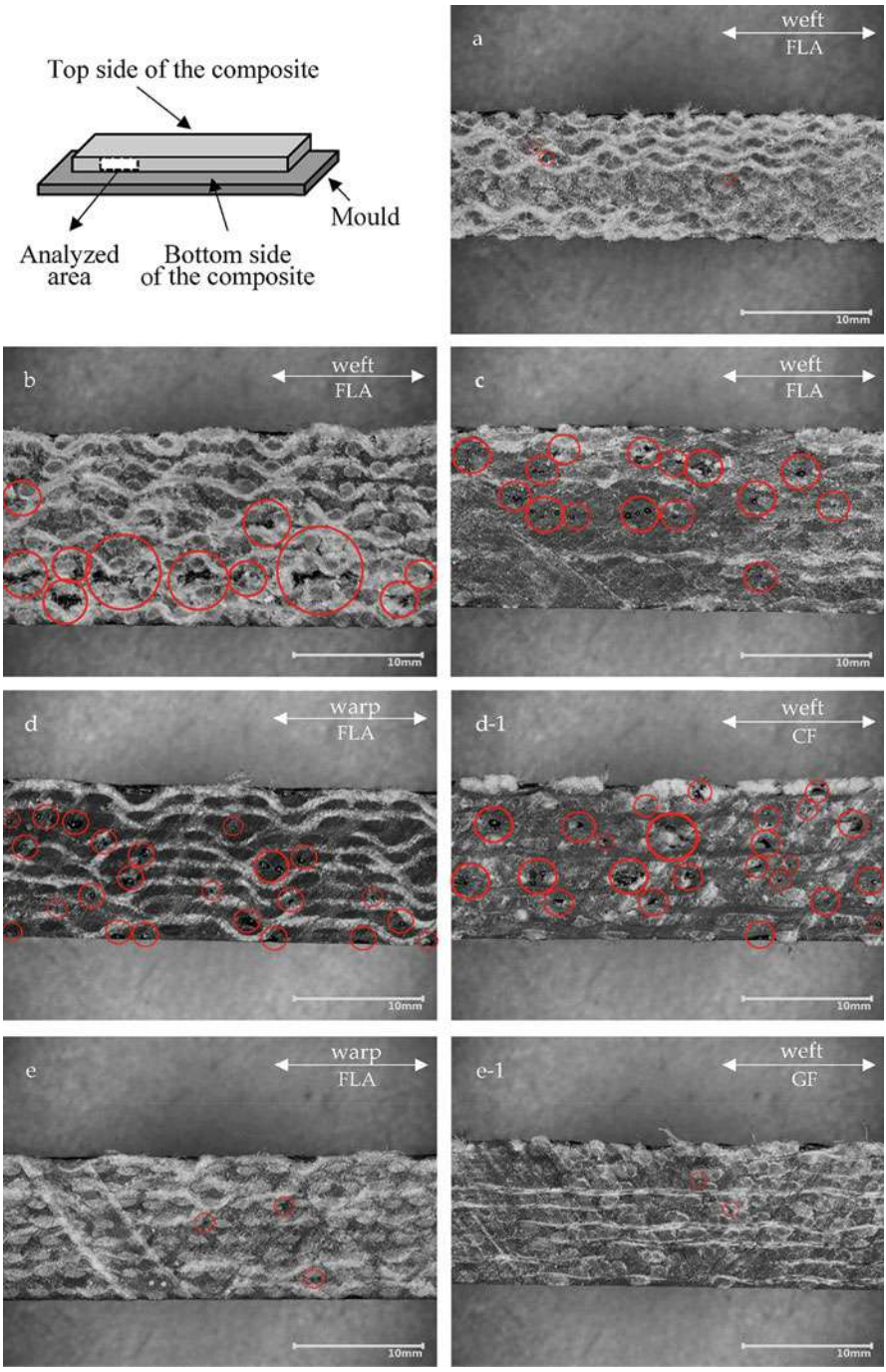

Fig. 5 Digital observation of the cross sections of the flax composites: (**a**) plain, (**b**) twill, (**c**) satin weaved textiles, and hybrid textiles composing of (**d**) flax/carbon warp, (**d1**) flax/carbon weft, (**e**) flax/glass warp, (**e1**) flax/glass weft. (Reproduced with permission from Shamsuyeva et al. (2019))

content in the composite with flax/carbon textile is significantly higher than in the case of the composite with flax/glass textile. The authors point out this behavior further explains the lower density of the flax/carbon composite than the flax/glass composite. The authors conclude the source of the voids in hybrid composites should point to two main reasons: manufacturing defects or incomplete infiltration. However, the manufacturing process was the same for all composites, and no visual defects were observed. Therefore, the higher void content in the hybrid flax/carbon composite should be attributed to incomplete infiltration.

Avoiding water absorption is essential in composites for structural applications, as it can cause delaminations and fatigue cracks (Dhakal et al. 2013). Hybrid flax/carbon composites containing bidirectional and unidirectional layers of carbon and flax fibers are tested to compare their mechanical performance and moisture absorption. Composites with unidirectional layers showed better mechanical properties than composites with woven fibers. In addition, flax fibers improve the toughness of the hybrid composites by hindering the crack propagation, and carbon fibers favor the thermal stability, water absorption, strength, and stiffness of the hybrid composites (Dhakal et al. 2013).

Sarasini et al. (2016) evaluated the hybrid flax/carbon fiber composites' post-impact bending behavior and concluded that hybridization improves tolerance to damage, maintaining stiffness and resistance to bending. Other studies highlight flax fiber's properties to increase the damping coefficient in hybrid carbon fiber composites compared to carbon fiber composites but at the expense of elastic modulus and strength (Le Guen et al. 2016).

Flax/Glass Fibers

Fiberglass has superior tensile strength and ductility mechanical properties to flax fibers. However, flax fibers have higher stiffness, and their density is almost half that of E-glass fiber. The tensile properties of hybrid flax/glass fiber composites are evaluated, considering the stacking sequence of unidirectional fibers, which positively influence the tensile strength and break, but not the elastic modulus. On the other hand, the fracture toughness and interlaminar shear strength of the hybrid composites were even higher than the fiberglass-reinforced composites due to the excellent interface performance associated with the twisted flax yarn structure, the rough flax fiber surface, and the fiber bridges between the flax and glass layers (Zhang et al. 2013).

Saidane et al.(2017) reported higher values of Young's modulus and strength for hybrid flax/glass fiber composites. The water absorption was measured in hybrid composites immersed in a tank with water at 55 °C. They used a scanning electron microscope to identify damage mechanisms, evaluating the damage mechanism by the number of hits and acoustic energy. The results obtained concluded that if the number of impacts does not generate significant fiber failures, its contribution to the failure is relevant in the accumulated acoustic emission energy. Calabrese et al. (2019) compared the mechanical properties and robustness of hybrid flax/glass

composites with individual glass and flax fibers reinforced epoxy composites for marine applications. The composites were tested in a salt fog chamber for 60 days, finding the hybrid composites have better elastic modulus, strength, and higher aging resistance compared to individual composites.

Flax/Aramid Fibers

Kevlar comes in different types of fibers and filaments with their individual properties and performance criteria. Kevlar 29 and Kevlar 49 are the most commonly used grades. Kevlar 49 has higher tensile strength and stiffness than Kevlar 29, while both maintain the same density. Kevlar 29 comes in a tighter weave, and thus the fabrics are built for ballistic protection. Kevlar 29 is predominantly used in protective body armor, armor helmets, ballistic panels, ropes, and cables. Meanwhile, Kevlar 49 is suited for high-performance composite applications such as boats, aircraft, and sporting equipment.

Hybrid flax/Kevlar fiber composites are also used in sandwich structures, where the response to damage caused by multiple loading and unloading sequences is analyzed, with maximum loads progressively increasing until failure occurs. Flax/Kevlar hybridization provides significant damage reduction; hence, the damage is not always proportional to load or inelastic strain accumulation.

Ahmed Sarwar et al. (2020) mentioned the gap of scientific publications on epoxy's mechanical properties reinforced by hybrid flax/Kevlar fibers. Based on this observation, they evaluated the properties of hybrid flax/Kevlar fiber composites under a sandwich-type configuration. The sandwich consisted of 12 layers of flax under three different configurations (0, 0/90, and $\neq 45^{\circ}$) that acted as the structure's core. The outer faces were fabricated by using two layers of Kevlar (plain weave). The mechanical characterization consisted of tensile, compression, flexural, and hardness tests. The water absorption was also evaluated. The results demonstrated the hybridization system improved the mechanical performance of flax composites in the different configuration tests. However, the moisture absorption increased considerably as a consequence of the flax content. Combining the strength of flax fibers and the low compressive strength of Kevlar fibers leads to different failure mechanisms in hybrid composites. Therefore, it is necessary to identify the failure mechanisms that occur during the test to correlate their effects on hybrid composites' mechanical behavior (Audibert et al. 2018). Compressive properties are underestimated due to buckling. Therefore, it is convenient to evaluate the compression behavior through a three-point bending test. The test results were compared with the single flax and Kevlar composites. The hybrid composite exhibited a marked non-linear anisotropic behavior caused by the Kevlar fibers' plastic deformation, promoting the separation of the flax fibers and reduced stiffness. On the other hand, the hybrid composite revealed similar compression values as the single Kevlar composite but lowered tensile performance. The hybrid composite showed intermediate mechanical properties between the single linen and aramid composites.

Hemp Fiber

Hemp (*Cannabis sativa*) is a plant native to central Asia cultivated for more than 10,000 years. Unlike flax fiber, the environmental conditions required for growing hemp plants allow them to grow in different parts of the world. According to the Food and Agriculture Organization of the United Nations (FAO), almost half of the world's industrial hemp supply is grown in China, with the rest grown in Chile, France, North Korea, and Spain.

Hemp fiber has a low production cost and a high cellulose content that favors its mechanical performance. The high strength and rigidity of hemp fibers make them a reinforcing material in composite materials. In recent years, an exponential increase in the use of hemp for various applications has been observed (Shahzad 2011). However, hemp fiber composites are oriented to nonstructural applications due to the high variability in mechanical properties and the susceptibility to moisture. The components of hemp fibers are cellulose, hemicellulose, lignin, and pectin, although the main disadvantage is the irregularity in their composition attributed to the lack of homogeneity in the physical characteristics of the hemp plant (Shahzad 2011).

The hemp fibers' diameters vary significantly depending on the climatic conditions and the soil nutrients during the cultivation, which influences the constituents' content and the plant's development. Morvan et al. (2003) demonstrated that the hemp fibers' diameter is more significant in the halfway part of the stem than in the lower or upper zones, pointing out that the diameter is much smaller during the flowering stage than in the ripening stage. This variability in diameter is expected to impart dispersion to the mechanical properties of the hemp fibers.

Hemp/Carbon Fibers

The hybridization of carbon and hemp fiber composites allows their use in structural applications. Thus, it is necessary to integrate the ductility of hemp fibers with the stiffness of carbon fibers, allowing different energy dissipation mechanisms according to the arrangement of the layers of carbon fibers and hemp fibers. However, there are just a few scientific articles that deal with studying the mechanical behavior of hybrid carbon/hemp fiber composites (Pinto et al. 2020; Yan et al. 2014). Most of these studies indicate the feasibility of combining hemp and carbon fabrics to improve hybrid composites' mechanical performance, depending on the stacking sequence. Some authors (Pinto et al. 2020) evaluated the possibility of exchanging three layers of carbon with hemp fabrics, considering the layers' relative position on the bending, interlaminar shear, and impact properties. The authors found that placing the layers in the sequence C/H/H/C improved flexural modulus, absorbed energy, and the extent of damage after impact.

Other authors (Scutaru and Baba 2014) characterized the impact behavior of hybrid hemp fiber composites, pointing out that the sequence of carbon/hemp/carbon/hemp layers absorbs a considerable amount of energy in the impact zone. The damage trace gradually diminishes due to the hemp fibers' excellent ductility

combined with the carbon fibers' stiffness that reduces delamination. This commitment present in hybrid hemp composites allows the automotive sector to consider them in areas susceptible to impact.

Ramesh et al. (2019) analyzed the mechanical properties of hybrid hemp/carbon fiber composites performing an alkaline treatment on the hemp fibers. The elastic behavior and the prediction of the composite materials' resistance were carried out employing finite element analysis, coinciding with the experimental results. Hemp fibers treated with alkali showed better mechanical performance than untreated fibers.

Hemp/Glass Fibers

Hybrid hemp/glass fiber composites are used primarily for semi-structural applications due to the properties of fiberglass. Although fiberglass is mostly used as reinforcement for polyester resins, it is possible to find some research articles that analyze hybrid hemp/glass fabrics used as reinforcements for epoxy resins (Cicala et al. 2018; Shahzad 2011). One of these works focused on the mechanical results of hybrid hemp/glass and hemp/carbon, with similar thickness and manufactured by hand layup technique. The mechanical properties of hybrid composites that contained carbon fibers were superior to the hybrid hemp/glass fiber composites; however, the mechanical performance was notoriously higher when comparing with single-fiber composites.

Throughout this book chapter, it has been mentioned that chemical modifications improve the weak interfacial interaction between the fiber and the polymer matrix. The chemical modification enables the activation of hydroxyl groups that effectively interlink with the polymer chains. Coupling agents have two functions: the first is to react with cellulose hydroxyl groups; the second one is to react with functional groups on the polymeric matrix. The alkaline treatment is one of the most used chemical treatments in natural fibers, since it increases the surface's roughness by eliminating most of the hemp lignin and hemicellulose. Alkali treatment improves hemp fibers' heat resistance due to removing waxy layers and other impurities from the surface (John and Venkata Naidu 2004; Naveen et al. 2018; Puttegowda et al. 2018; Ramesh et al. 2015; Wang et al. 2011). However, a prolonged period results in surface damage of the fibers and, consequently, a decrease in hybrid composites' hardness resistance.

Fiberglass is classified according to its applications. The epoxy hybrid composites of E-glass fiber and alkaline-treated hemp have been developed to know the mechanical performance of moisture absorption as a function of variable parameters, such as the alkaline treatment of the hemp fiber and the natural fiber content. The results obtained revealed that the NaOH treatment improved the mechanical properties of the hybrid composites. However, moisture absorption increased as the fiber volume fraction increased due to the high cellulose content, which decreases the hardness, tensile, and flexural properties of the hybrid composites (Puttegowda et al. 2018; Ramesh et al. 2015; Wang et al. 2011).

Hemp/Aramid Fibers

A common way to increase impact resistance in materials is to introduce a hard mineral filler such as sand, although it considerably increases the composite material's density. An alternative is to add short and modified hemp fibers without implying a considerable increase in the hybrid composite's density (aramid and hemp have similar densities values) but increasing its stiffness and energy absorption capacity.

Kevlar fiber-reinforced polymer composites are widely used as high-speed impact-resistant materials. However, similar to other FRP systems, these materials are sensitive to projectile impacts that produce delaminations. The use of hemp fiber could favor the impact behavior of Kevlar composites. Some works detail the use of natural reinforcements (palm and coconut shells) to improve resistance to fracture (Puttegowda et al. 2018) (Jani et al. 2019). The results revealed that the inclusion of an optimal amount of coconut shell in the epoxy resin improves the tensile strength of the hybrid composites, while the inclusion of palm shell increased the breaking stress. However, the unfilled hybrid hemp/Kevlar fiber composites present higher tensile strength and ductility than the Kevlar composites.

Jute Fiber

Jute fiber (*Corchorus capsularis*) belongs to the bast fiber family and is typically grown in tropical regions in Asia. Jute is grown in a humid atmosphere and can survive flooding. Jute fibers are inexpensive (jute is grown solely to extract its fibers), with broad availability and good thermal and insulation properties. Asia is the largest jute producer and contributes around 95% of the world's total jute production. The annual production of jute in the world remains around 3 million tons. The global jute bag market attained a value of USD 1.9 billion in 2020. The market is expected to reach USD 3.3 billion by 2026 while registering a CAGR of 9.4% during the forecast period of 2021–2026 (according to the report consulted online in November 2020 in https://www.expertmarketresearch.com/reports/jute-bag-market).

In general, jute plants (which can be 1–4 m long) are cut as close to the ground as possible and soaked in water to remove pectins and other waxy substances. Jute fiber structure and quality depend on factors like growth environment, weather conditions, cultivation, plant maturity, and extraction techniques. The fiber from the stem is extracted by hand, after which the fibers are washed and dried. A difficulty in the sanding procedure (retting procedure) is that the stem's thicker parts take longer to be removed than the thinner parts. Some authors extensively describe the process of harvesting and extraction of jute fibers (Puttegowda et al. 2018).

The textile industry mostly consumes jute fiber, and its primary demand is in the production of bags for packaging various agricultural products like rice, wheat, vegetables, corn, and coffee beans. Jute fabrics are also used as carpet backing. In the automotive sector, jute fiber can be used to manufacture nonstructural components such as door panels and trunk liners.

Jute/Carbon Fibers

In recent years, various studies have been conducted on hybrid jute-based composites. Hybridizing jute with synthetic fibers is a cost-effective and environmentally friendly alternative. Hybrid jute/carbon fiber composites involve high modulus and strength at low cost. Ashworth et al. (2016) evaluated this type of composites impregnated with epoxy resin and manufactured employing the resin transfer molding technique. They found the tensile modulus increases considerably for the hybrid composites compared to the single jute composites. Sezgin et al. (2016) prepared epoxy/jute/carbon hybrid composites using the vacuum infusion technique and evaluated the influence of different stacking sequences of jute and carbon layers on the damping properties. The results indicated that if the carbon fiber is placed on the composite's outer layers, higher storage modulus and loss values are obtained. Other studies highlight that hybrid jute and carbon fiber composites improve ductility and impact resistance compared to carbon composites (Ramana and Ramprasad 2017). However, one of the main drawbacks of jute fiber for use in polymeric composites is moisture absorption. Some research has focused on studying the water absorption in hybrid jute/carbon fiber composites, measuring the immersion time and the fiber content (Sezgin et al. 2016; Wang et al. 2011). The study revealed that moisture absorption increases with the natural fiber content, which influences hybrid composites' mechanical performance. Maximum impact resistance decreased with moisture content due to delamination and breakage of jute fibers.

Jute/Glass Fibers

Hybridization of jute fibers with glass fibers improves the hybrid composites' mechanical properties. Various authors (Ashraf et al. 2019) analyzed the mechanical behavior of epoxy resins reinforced with jute fiber and fiberglass, finding better mechanical properties when fiberglass is added to the jute composite. Additionally, Abdullah-Al-Kafi et al. (2005) found that hybrid composites' mechanical properties are further increased when natural fibers are treated with ultraviolet radiation. The surface treatments include physical, chemical, physicochemical, and mechanical surface modification methods, which effectively improve jute fibers' mechanical properties (Ashraf et al. 2019).

Selver et al. (Abdullah-Al-Kafi et al. 2005) studied the effect of stacking sequence on hybrid jute/fiberglass composites' mechanical performance. Natural fibers reduced composites' overall density and increased flexural strength when glass fibers are used as outer layers.

Ahmed et al. (2007) observed that Young's modulus increased with increasing fiberglass content, while Poisson's ratio decreased due to the differences in the transverse and longitudinal strains of single jute fiber composite compared to hybrid jute/fiberglass fiber composite. Other works (Ahmed et al. 2006) deal with fiberglass content in hybrid jute/glass fiber composites on the mechanical properties. The

results showed that the addition of only 16.5% by weight of fiberglass improved the mechanical properties substantially. Furthermore, the hybrid composites showed better resistance to humidity due to the presence of the glass fiber.

Jute fiber is hydrophilic, implying a significant impediment to getting higher mechanical properties in composites reinforced with this natural fiber. There are numerous works (Aquino et al. 2007) that treat the effects of humidity on different mechanical properties of hybrid jute/fiberglass composites, having the same general observation, in that the content of moisture decreases the mechanical properties of the hybrid composites because water disrupts fiber/matrix adhesion. Zamri et al. (2012) studied the effects of water absorption on the hybrid jute/fiberglass composite's mechanical properties.

The study consisted of immersing the hybrid composites in different water types: distilled water, seawater, and acid solution, all of them at room temperature. The authors observed that the composites absorb a more significant amount of distilled water, followed by the acidic solution and finally the seawater. In addition, the hybridization of jute fibers with glass fibers reduces the maximum moisture absorption and favors the mechanical properties of the composite.

Jute/Aramid Fibers

Epoxy resins reinforced with Kevlar and jute fibers lead to a remarkable improvement in mechanical properties compared to other materials (metallic) used to manufacture automobile bumpers. Many research topics are related to explore cheaper and lighter materials that meet and improve the energy absorption criteria in a crash event. Hybrid natural/synthetic fiber composites can be used for automotive applications because they are lightweight, high stiffness, and much more robust than existing bulk material. Further, hybrid composites also have good energy absorption characteristics as compared to metallic materials. Hybrid jute/Kevlar fiber composites are used to test jute fiber's effect on the impact resistance of Kevlar fiber-reinforced epoxy composites. Most of these hybrid composites are manufactured by employing the hand layup procedure. Some authors (Supian et al. 2018) tested the efficacy of hybrid jute/Kevlar composite in tube form using three layers of fibers. The tubes were tested under a compression test at a constant crush rate. The results showed that the jute fiber tubes were ineffective and failed dramatically. However, replacing a jute fiber layer with a Kevlar fiber layer led to improved mechanical performance. Another study consisted of preparing hybrid jute/Kevlar fiber composites to evaluate their structural behavior using Ansys software. The results were compared with those obtained by polycarbonate fiber-reinforced composites, because they are currently used in bumpers. Hybrid composites showed excellent mechanical behavior, and the stacking sequence of fiber layers has a significant effect on the strength. Therefore, hybrid composites can be used successfully for automotive bumper applications.

R. Bhanupratap et al. (Bhanupratap 2020) investigated the effect of Kevlar and jute fibers on mechanical-thermal behavior through dynamic mechanical analysis, finding an increase in the glass transition temperature when Kevlar fabrics were added and increased. Sunil Manohar Maharana et al. (2020) evaluated the morphology and properties of hybrid jute/Kevlar fiber composites by using 20 wt.% of Kevlar fiber. However, the content of jute fiber was varied. Both the tensile and flexural strengths reached their maximum value in jute fiber content of 40 wt.%, observing higher jute contents leads to a considerable reduction in mechanical properties. Some reports underline the tensile strength is greatly influenced by the different fiber proportions of Kevlar and jute fabrics. Also, proper transmission and distribution of stress applied by the epoxy resin results in the hybrid composite's increased strength. The tensile properties of the hybrid jute/Kevlar fiber composites increase with the Kevlar addition layer's increase because of the epoxy matrix's strong bond with the synthetic fiber.

The stacking sequence (altering the Kevlar layers' position) significantly affects jute fiber hybrid composites' flexural strength. However, for the case of the same weight fraction of Kevlar and jute fiber, the sequence of layers represents a low effect on the tensile properties, but any amount of Kevlar fiber higher than jute fiber leads to a remarkable increase in tensile and flexural strength and impact energy and reduces the weight of the sample. On the other hand, a higher amount of jute fiber entails a higher cost in manufacturing the hybrid composite, since it requires a higher volume fraction of epoxy resin.

Other Fibers Used for Hybrid Composites

Basalt Fibers

Basalt fiber is gaining attraction to hybrid natural/synthetic fiber composites. Basalt fibers are natural mineral fibers that originated from basalt rocks. This fiber is obtained from a complex production process in which the basalt rock is melted in a gas furnace at a temperature superior to 1500 °C, followed by a centrifugation process. In general, basalt fiber is considered an alternative to glass fiber reinforcement for FRP systems. They are about 5% denser than standard fiberglass but show higher tensile and compressive strength. Besides, basalt fiber is resistant to acids and has a high modulus of elasticity, with exceptional toughness. Basalt fiber is also used to manufacture fire-resistant textile materials for the aerospace and the automotive industry. As they are resistant to the alkaline environment (such as AR fiberglass), it is feasible to use them as concrete reinforcement. Basalt fibers are also healthier and environmentally friendly than glass fibers, as they are natural, inert, and classified as nontoxic and noncarcinogenic. Some research works (Saleem et al. 2020) report the hybridization of basalt fibers with other synthetic fibers (glass and carbon). However, just a few publications detail their use as hybrid reinforcement of epoxy resins (Dorigato and Pegoretti 2013; Sarasini et al. 2013).

Sisal Fibers

Sisal fiber (*Agave sisalana*) is one of the most used natural fibers since the agave plant's cultivation is diverse. Sisal fiber is extracted from the plant's leaves, and it is the most widely used plant fiber in FRP systems within the leaf family. A sisal plant can produce between 250 and 300 leaves, which contain around 1000 fibers (Lima et al. 2019). Although endemic to tropical regions in America, the sisal plant is currently cultivated in Asia's tropical zones. Every year almost 4.5 million tons of sisal fiber are produced worldwide. Tanzania, Brazil, and Mexico are the major producing countries. Sisal fiber is widely used in the manufacture of twine due to its strength, durability, stretchability, and resistance to saltwater deterioration. The sisal fiber length varies between 1 and 2 m (Lima et al. 2019). Some authors have conducted very exhaustive and detailed studies on sisal fibers'microstructure (Mukherjee and Satyanarayana 1986), underlying the sisal leaves contain three types of fibers: mechanical, ribbon, and xylem. In spite of sisal fiber being one of the most used natural fibers, its use in technological applications is still underused due to its low affinity with synthetic polymer resins and high hydrophilicity, which leads to a weak interface and high moisture absorption. However, a potential application is the manufacture of light roof panels with good fire resistance. Other relevant applications are in the sectors of aeronautics, automotive, and civil, among others.

Hybrid sisal/glass fiber composites have shown very relevant characteristics compared to other hybrid or single composites. The excellent properties of these hybrid composites depend on the fibers' combinations and the matrix selection. The mechanical properties of the hybrid sisal/glass fiber composites are influenced by the fibers' orientation, stacking sequence of layers, treatment of fibers, the addition of fillers, and the manufacturing process. The elastic modulus, tensile, flexural, and impact strength have better mechanical performance when fibers are oriented in the applied load's longitudinal direction than random or transversal orientation (Lima et al. 2019). Higher mechanical properties of hybrid sisal/glass fiber composites are obtained by increasing the glass fiber content.

Other properties like hardness, compression, shear, and tear strength are improved with the addition of glass fiber and modified sisal fibers. The hybrid sisal/glass fiber composites also showed high resistance to chemicals, except sodium carbonate and toluene (Lima et al. 2019). The addition of nanofillers, the increase of glass fiber content, and the use of surface treatments for sisal fibers decrease the water absorption capacity on hybrid composites.

Applications of Hybrid Natural/Synthetic Fiber Composites

Transportation

Nowadays, hybrid composite materials are manufactured and used in structural, semi-structural, and engineering applications. The multiple investigations carried out agree that hybrid composites of natural and synthetic fibers satisfy the need to

reduce operation, maintenance, and manufacturing costs. They also optimize performance requirements in terms of the range of applicability, resistance, and payload.

As presented in this chapter, the automotive sector looks for hybrid composites to manufacture door panels, dashboards, and frame profiles for automobiles. Natural fibers as a substitute for synthetic fibers for high-performance applications have been a relevant issue in the industry and academic community. Kenaf fibers have mechanical properties comparable to fiberglass and are being studied to evaluate their possible application in the automotive industry. Nanoparticles are introduced in the hybrid composites to increase the interaction between natural and synthetic fibers with the polymer matrix, providing a relevant mechanical performance/weight ratio (Puttegowda et al. 2018; Ravishankar et al. 2019; Sarker et al. 2019).

In brake systems, the use of hybrid kenaf/carbon fiber composites to manufacture the handbrake device inside the car cabin is of considerable interest due to moisture absorption. In the aerospace industry, hybrid composites of natural/synthetic fibers are positioned for the aircraft cabin interior applications and semi-structural panels. For the aerospace sector, hybrid composites must meet various requirements for their demanding industrial sector implementation. Three of the most relevant requirements are safety, weight, and flammability. For this, flame retardants are used to produce hybrid composites with high resistance to flame propagation. Hybrid composites are used in roof panels, interior wall panels, structural floors, and overhead storage compartments. Carbon fiber is commonly used for these applications, resulting in high costs. Therefore, investigations have been carried out to elucidate carbon fiber composites' possible substitution with hybrid natural/synthetic fiber composites. Some investigations employ the use of basalt fiber, combining it with sisal fibers. The combination of sisal and basalt fibers impregnated with epoxy resin promotes better performance than other fiber combinations, like glass fiber, due to the strong compatibility between sisal and basalt fibers. Besides, basalt-epoxy systems showed better affinity than fiberglass. The results open the window of opportunities for structural hybrid natural/synthetic composites in the aircraft cabin interiors field.

Energy Generation

The development of renewable energy sources has become one of the critical aspects of governments' energy policy and ministries of science and research because they contribute efficiently to reducing greenhouse gas emissions. The greater participation of renewable energies (solar and wind) in the energy balance reduces dependence on products and energy sources based on oil. In solar energy, hybrid natural/synthetic fiber composites can be used to build semi-structural bases, energy storage cabinets, and parabolic-trough collector components. The use of hybrid composites can also reduce the cost of tundish col. and the cost of tundish collectors. However, this application is currently made for polyester resins, and it is expected that the results with epoxy resin be published in a short time. In the case of wind energy, the main focus is on the performance of wind turbines. Hybrid natural/synthetic fiber composites are used to manufacture the blades and the wind rotor's protector, since

these elements allow optimizing the efficiency of power generation and, therefore, its price. Hybrid synthetic fiber composites (carbon/fiberglass) were the first to be used in the manufacture of wind blades, observing the 30% of carbon fiber content can be replaced with basalt fibers for the application of turbine blades. Because the blades of a wind turbine are a critical and expensive component of a wind turbine system, it is necessary to investigate the potential of sustainable plant fiber reinforcements as a substitute for conventional E-glass fibers in small wind turbine (SWT) blades.

A recent study (Corona et al. 2015) consisted of using three different fibers to evaluate the mechanical properties of hybrid composites and estimate their performance in experimental wind blades. The conventional synthetic candidates were carbon and glass fibers, while the natural reinforcement was flax fiber. A comparative analysis was performed with the experimental results and finite element dimensioned prototypes of wind blades. The three different configurations of reinforced composites were flax/epoxy, carbon/epoxy, and hybrid 50/50 flax-carbon/epoxy, finding that carbon composites have a very high performance of wind blades, which was attributed to the intrinsic characteristics of carbon fiber. However, the hybrid flax/carbon composites showed encouraging results. Therefore, it is highly recommended to test other natural fibers to optimize wind blade performance. Wind blades are large components, and it is necessary to consider their manufacturing and life cycle's environmental sustainability. In this way, an analysis of five different types of composites was performed: flax, carbon, glass, flax/carbon, and flax/glass. Contrary to expectations, the study showed that composite materials' environmental sustainability based on natural fibers is similar or even lower than synthetic composites. This observation is mainly due to the demand for the epoxy resin to impregnate natural fibers, which counteracts the environmental sustainability improvements obtained with natural fibers' application.

Composite Armor

Composite materials are attractive for armor applications due to their low specific gravity. In this sense, the composites are commonly used from vehicle bumpers, such as motorcycle helmets and bulletproof vests. Synthetic fibers (aramid, carbon, and glass) have been widely employed to reinforce epoxy resins to study their applicability in armor systems.

Aramid fibers are efficient reinforcements to stop different types of projectiles. In the case of bullets, they perform a rotational movement around their axis to maintain the stability of their trajectory so that when they impinge on the Kevlar fabric, it causes entanglement of the fibers around the bullet and facilitates its arrest. However, the Kevlar fabric is very ineffective against hard-core projectiles, which allows the aramid fibers to break due to shear. For this reason, some shielding systems tend to integrate an outer layer made up of high-strength metals (titanium or uranium). Aramid fiber composites are most commonly used for armor coatings due to their high mechanical performance and ductility. However, the costs for its production are considerably high. Hybrid natural/synthetic fibers have attained relevant interest in

ballistics, as the stacking sequence, layers orientation, and composite thickness directly influence ballistic resistance. Using different stacking sequences allows the ballistic behavior of hybrid compounds to be evaluated. The arrangement of Kevlar and nonwoven kenaf fiber layers was recently studied, using different sequences, placing the kenaf fiber in the inner, outer, and alternate layers. The hybrid composite with the kenaf fibers in the outer layers was found to have more excellent ballistic resistance than the other composites, and better results were obtained using randomly oriented kenaf fiber fabrics. Furthermore, the energy absorption increased with the increasing density of the composite surface. The results demonstrated the viability of employing natural fibers in combination with synthetic fibers for armoring systems.

Drawbacks Epoxy/Synthetic/Natural Fiber Hybrid Composites

A hybrid composite's mechanical properties depend on its constituents' intrinsic properties that combine during the manufacturing process to complement and enhance conventional composite materials' properties. Throughout this chapter, synthetic fibers' drawbacks, in terms of cost, preparation, health, environment, and natural fibers' benefits, have been expressed. Although natural fibers are obtained from renewable sources and are friendly to the environment compared to synthetic fibers, they also have certain disadvantages: the high dispersion of the fibers' quality and high variability in their mechanical properties. Natural fibers also have a high moisture absorption capacity and low thermal stability. High moisture absorption is the main drawback of natural fibers since it favors dimensional instability and weakens the interfacial bond between the polymeric matrix and the fiber, favoring the deterioration of the composite's mechanical properties. In order to overcome these drawbacks, natural fibers are treated to modify their surface and favor the fiber-polymer interaction. The treatments can be chemical (alkaline) or physical (plasma) mainly. At other times, an organic modifier is incorporated into the polymeric resin during the composites' manufacture. Any of the different treatments to which natural fibers are exposed can lead to contamination to the environment and increase the use of inorganic materials, which causes a continuous debate in the definition of green composites.

It can be said that the production of synthetic fibers involves considerable economic and environmental intensity. In the case of natural fibers, their harvest is labor-intensive, since in most cases, it is based on labor. In this sense, most natural plants are harvested manually, and the fibers are extracted with nonconventional machines that are easily operated without quality control. Therefore, the production and extraction of natural fibers imply enormous human resources, which also favors creating employment opportunities.

Thermosetting polymers have several advantages in producing structural components, as they have high rigidity and strength, with high resistance to temperature. However, the main drawback of synthetic thermosetting resins is their zero recyclability and lack of biodegradability. Furthermore, epoxy resins are toxic, polluting,

and carcinogenic because they contain bisphenol A diglycidyl ether. At present, different alternatives for epoxy resins based on vegetable oil and other organic materials are being developed. These resins are expected to contain more and more organic matter and to have the ability to achieve the excellent performance of synthetic resins. Today, biobased thermosetting resins contain a percentage of 30–54% organic content. In summary, epoxy resins are also capable of hybridization. The mechanical properties of hybrid fiber-reinforced epoxy resins are an exciting topic that is currently being studied.

Challenges and Opportunities for Hybrid Natural/Synthetic Fiber Composites

There are many expectations for using hybrid natural/synthetic fiber composites. However, many challenges must first be overcome for these materials before used in a more significant number of engineering applications. Future challenges could be divided into two routes to follow. The first is optimizing the improvements and challenges found to date in hybrid composites. In this first case, the homogeneity of natural fibers' properties, with total quality control of cultivation, extraction, and preparation, allows the industry to have greater confidence in this renewable material as a reinforcing resource in structural components. Avoiding the hydrophilicity of natural fibers implies an even more significant challenge given their characteristics. Finding alternatives to chemical modifiers' use reduces the manufacturing costs and favors recycling problems. There is also a pressing need to improve mechanical properties, such as stiffness and fracture resistance, particularly toughness, of hybrid composites.

The second is starting the disruptive study that encompasses other natural fiber families, different fabric styles, and finding solutions in the design, simulation, and prediction failures in hybrid composites. In this second case, it is clear that there is still much to explore in the hybrid natural/synthetic fiber composites field. A broad and vast field of study uses different families of plants that could be used as hybrid reinforcement in FRP systems. There is relevant progress in using plant fibers from the bast family as reinforcements, and some results using agave fibers belong to the leaf family. However, there is still a lot of research work to be pursued in the rest of the natural fibers available. In this sense, part of the research work performed in the fiber layers' arrangement and their intercalation has been presented here. However, there is much work to do about the diverse fabric configurations. The most studied configurations are the unidirectional fibers and plain weave, but there is low information on fabrics such as twill, satin, basket, leno, mock, etc. The use of two or more natural and synthetic reinforcements has not been studied in-depth and could address multifunctional situations. The influence of the various manufacturing techniques on the properties of hybrid composites begins to have greater relevance, which is attributed to the gain in knowledge of natural and synthetic fibers commonly used in the manufacture of hybrid composites. Studying and documenting the different

manufacturing processes' effects allow the greater scope of using hybrid composites in various engineering sectors.

Hybridization of two different fiber types has proven to be an adequate strategy for designing diverse materials suitable for many requirements. The grouping of individual characteristics to cover many applications in just one material offers potential prospects for advanced materials technologies.

New and innovative hybrid composites could be addressed to develop shielding systems against electromagnetic interference (EMI). Electromagnetic interference is a primary issue for the military, aerospace, and communications sectors. Electromagnetic signals alter electronic devices and damage internal components that can lead to several disasters. On the other hand, magnetic fields affect the immune system. Metals are often used as shielding materials. However, their high density and low corrosion resistance favor the search for alternative materials. A recent study showed the possibility of using magnetite in the kenaf fiber composites as an alternative to produce EMI shields (Mochane et al. 2019; Puttegowda et al. 2018). The hybrid composite absorbed less amount of water due to the interaction between magnetite and kenaf fibers.

Conclusions

Hybrid composites reinforced with natural and synthetic fiber have gained evident popularity in recent years, not only because of their mechanical behavior but also because natural fibers provide a competitive market for diverse and distinct uses.

The main properties of epoxy/synthetic/natural fiber hybrid composites depend on fiber volume content, stacking sequence, layers orientation, interfacial adhesion, manufacturing process, extraction methodology and cultivation (in plant fibers), and composite thickness. The synthetic/natural hybrid composites are fabricated with conventional techniques like manual impregnation, vacuum bag infusion, and compression. However, few results detail the use of more sophisticated techniques such as RTM or autoclaving. The types of fabrics are a vast field to investigate, as is the fiber layers' orientation and arrangement in hybrid composites. The combination of fabric types and their hybridization would result in a vast line of research. Hybridization of the fabrics can be intralaminated and interlaminated. In intralaminate, natural and synthetic fibers are weaved together into a single layer, while interlaminate is the arrangement of different layers of individual fibers. Synthetic fibers have higher properties than natural fibers, but it is possible to balance cost and performance through the quantity and correct fibers' selection.

The properties of the hybrid composites depend mainly on the fibers' compatibility and interaction and the polymer matrix. The interfacial adhesion increases when the natural fibers' surface is modified, favoring the interaction between the constituents and reducing the absorption of moisture. However, the modifications are not environmentally friendly because they involve chemical products.

The quality of natural fibers is an issue that requires the attention of the industries interested in marketing them. Much work remains to be done in the sense of

controlling plant growth under measurable and recordable conditions. In this way, the industry would have higher quality natural fibers and without much disparity in their properties.

Natural fibers offer an excellent opportunity for use in composite materials. However, just the stem fiber family has been used as an effective reinforcement of hybrid composites, followed by some research on leaf fibers. The rest of the families are waiting to be evaluated and studied, which offers a wide field of research in the field of composite materials.

References

Abdullah-Al-Kafi, M.Z. Abedin, M.D.H. Beg, K.L. Pickering, M.A. Khan, Study on the mechanical properties of jute/glass fiber-reinforced unsaturated polyester hybrid composites: effect of surface modification by ultraviolet radiation. J. Reinf. Plast. Compos. **25**(6), 575–588 (2005). https://doi.org/10.1177/0731684405056437

F. Ahmad, H.S. Choi, M.K. Park, A review: natural fiber composites selection in view of mechanical, light weight, and economic properties. Macromol. Mater. Eng. **300**(1), 10–24 (2015). https://doi.org/10.1002/mame.201400089

K.S. Ahmed, S. Vijayarangan, C. Rajput, Mechanical behavior of isothalic polyester-based untreated woven jute and glass fabric hybrid composites. J. Reinf. Plast. Compos. **25**(15), 1549–1569 (2006). https://doi.org/10.1177/0731684406066747

K.S. Ahmed, S. Vijayarangan, A.C.B. Naidu, Elastic properties, notched strength and fracture criterion in untreated woven jute–glass fabric reinforced polyester hybrid composites. Mater. Des. **28**(8), 2287–2294 (2007). https://doi.org/10.1016/j.matdes.2006.08.002

H.A. Aisyah, M.T. Paridah, A. Khalina, S.M. Sapuan, M.S. Wahab, O.B. Berkalp, C.H. Lee, S.H. Lee, Effects of fabric counts and weave designs on the properties of laminated woven kenaf/carbon fibre reinforced epoxy hybrid composites. Polymers **10**(12), 1320 (2018). https://doi.org/10.3390/polym10121320

Z. Al-Hajaj, R. Zdero, H. Bougherara, Mechanical, morphological, and water absorption properties of a new hybrid composite material made from 4 harness satin woven carbon fibres and flax fibres in an epoxy matrix. Compos. A: Appl. Sci. Manuf. **115**, 46–56 (2018). https://doi.org/10.1016/j.compositesa.2018.09.015

E.M.F. Aquino, L.P.S. Sarmento, W. Oliveira, R.V. Silva, Moisture effect on degradation of jute/glass hybrid composites. J. Reinf. Plast. Compos. **26**(2), 219–233 (2007). https://doi.org/10.1177/0731684407070030

M.A. Ashraf, M. Zwawi, M. Taqi Mehran, R. Kanthasamy, A. Bahadar, Jute based bio and hybrid composites and their applications. Fibers. **7**(9), 77 (2019). https://doi.org/10.3390/fib7090077

S. Ashworth, J. Rongong, P. Wilson, J. Meredith, Mechanical and damping properties of resin transfer moulded jute-carbon hybrid composites. Compos. Part B Eng. **105**, 60–66 (2016). https://doi.org/10.1016/j.compositesb.2016.08.019

M. Assarar, W. Zouari, H. Sabhi, R. Ayad, J.-M. Berthelot, Evaluation of the damping of hybrid carbon–flax reinforced composites. Compos. Struct. **132**, 148–154 (2015). https://doi.org/10.1016/j.compstruct.2015.05.016

C. Audibert, A.S. Andreani, É. Lainé, J.C. Grandidier, Mechanical characterization and damage mechanism of a new flax–Kevlar hybrid/epoxy composite. Compos. Struct. **195**, 126–135 (2018). https://doi.org/10.1016/j.compstruct.2018.04.061

M.A.A. Bakar, S. Ahmad, W. Kuntjoro, S. Kasolang, Effect of carbon fibre ratio to the impact properties of hybrid kenaf/carbon fibre reinforced epoxy composites. Appl. Mech. Mater. **393**, 136–139 (2013). https://doi.org/10.4028/www.scientific.net/AMM.393.136

P. Banakar, Preparation and characterization of the carbon fiber reinforced epoxy resin composites. IOSR J. Mech. Civ. Eng. **1**, 15–18 (2012)

R. Bhanupratap, Jute/Kevlar fibre reinforced epoxy composites: a dynamic mechanical study. Mater. Today Proc. **22**, 3145–3151 (2020). https://doi.org/10.1016/j.matpr.2020.03.451

R. Bhanupratap, H.C. Chittappa, Study of tensile behaviour by variation of Kevlar to the jute fibre epoxy hybrid composites. Int. J. Eng. Res. Technol. **6**(6), 32 (2017). https://doi.org/10.17577/IJERTV6IS060462

R. Bhoopathi, M. Ramesh, C. Deepa, Fabrication and property evaluation of banana-hemp-glass fiber reinforced composites. Procedia Eng. **97**, 2032–2041 (2014). https://doi.org/10.1016/j.proeng.2014.12.446

J. Biagiotti, D. Puglia, J.M. Kenny, A review on natural fibre-based composites – part I. J. Nat. Fibers **1**(2), 37–68 (2004). https://doi.org/10.1300/J395v01n02_04

L. Calabrese, V. Fiore, T. Scalici, A. Valenza, Experimental assessment of the improved properties during aging of flax/glass hybrid composite laminates for marine applications. J. Appl. Polym. Sci. **136**(14), 47203 (2019). https://doi.org/10.1002/app.47203

W.D. Callister Jr., *Fundamentals of Materiales Science and Engineering* (Wiley, Hoboken, 2001). https://doi.org/10.1007/978-981-10-2529-7_2

G. Cicala, E. Pergolizzi, F. Piscopo, D. Carbone, G. Recca, Hybrid composites manufactured by resin infusion with a fully recyclable bioepoxy resin. Compos. Part B Eng. **132**, 69–76 (2018). https://doi.org/10.1016/J.COMPOSITESB.2017.08.015

A. Corona, C. Markussen, M. Birkved, B. Madsen, Comparative environmental sustainability assessment of bio-based fibre reinforcement materials for wind turbine blades. Wind Eng. **39**(1), 53–64 (2015). https://doi.org/10.1260/0309-524X.39.1.53

H.N. Dhakal, Z.Y. Zhang, R. Guthrie, J. MacMullen, N. Bennett, Development of flax/carbon fibre hybrid composites for enhanced properties. Carbohydr. Polym. **96**(1), 1–8 (2013). https://doi.org/10.1016/j.carbpol.2013.03.074

M.J. do Nascimento Santos, J.M.P.Q. Delgado, A.G. Barbosa de Lima, Synthetic fiber-reinforced polymer composite manufactured by resin transfer molding technique: foundations and engineering applications. Diff. Found. **14**, 21–42 (2017). https://doi.org/10.4028/www.scientific.net/df.14.21

A. Dorigato, A. Pegoretti, Flexural and impact behaviour of carbon/basalt fibers hybrid laminates. J. Compos. Mater. **48**(9), 1121–1130 (2013). https://doi.org/10.1177/0021998313482158

J. Flynn, A. Amiri, C. Ulven, Hybridized carbon and flax fiber composites for tailored performance. Mater. Des. **102**, 21–29 (2016). https://doi.org/10.1016/j.matdes.2016.03.164

E. Franco-Urquiza, A. Rentería-Rodríguez, Effect of nanoparticles on the mechanical properties of kenaf fiber-reinforced bio-based epoxy resin. Text. Res. J. (2020). https://doi.org/10.1177/0040517520980459

A. Gholampour, T. Ozbakkaloglu, A review of natural fiber composites: properties, modification and processing techniques, characterization, applications. J. Mater. Sci. **55**(3), 829–892 (2020). https://doi.org/10.1007/s10853-019-03990-y

T. Gurunathan, S. Mohanty, S.K. Nayak, A review of the recent developments in biocomposites based on natural fibres and their application perspectives. Compos. A: Appl. Sci. Manuf. **77**, 1–25 (2015). https://doi.org/10.1016/j.compositesa.2015.06.007

A. Hassan, M.R.M. Isa, Z.A.M. Ishak, N.A. Ishak, N.A. Rahman, F.M. Salleh, Characterization of sodium hydroxide-treated kenaf fibres for biodegradable composite application. High Perform. Polym. **30**(8), 890–899 (2018). https://doi.org/10.1177/0954008318784997

M.F. Ismail, M.T.H. Sultan, A. Hamdan, A.U.M. Shah, M. Jawaid, Low velocity impact behaviour and post-impact characteristics of kenaf/glass hybrid composites with various weight ratios. J. Mater. Res. Technol. **8**(3), 2662–2673 (2019). https://doi.org/10.1016/j.jmrt.2019.04.005

S.P. Jani, A.S. Kumar, M.A. Khan, S. Sajith, A. Saravanan, Influence of natural filler on mechanical properties of hemp/Kevlar hybrid green composite and analysis of change in material behavior

using acoustic emission. J. Nat. Fibers **18**, 1–12 (2019). https://doi.org/10.1080/15440478.2019.1692321

K. John, S. Venkata Naidu, Sisal fiber/glass fiber hybrid composites: the impact and compressive properties. J. Reinf. Plast. Compos. **23**(12), 1253–1258 (2004). https://doi.org/10.1177/0731684404035270

U. Kureemun, M. Ravandi, L.Q.N. Tran, W.S. Teo, T.E. Tay, H.P. Lee, Effects of hybridization and hybrid fibre dispersion on the mechanical properties of woven flax-carbon epoxy at low carbon fibre volume fractions. Compos. Part B Eng. **134**, 28–38 (2018). https://doi.org/10.1016/j.compositesb.2017.09.035

M.J. Le Guen, R.H. Newman, A. Fernyhough, G.W. Emms, M.P. Staiger, The damping–modulus relationship in flax–carbon fibre hybrid composites. Compos. Part B Eng. **89**, 27–33 (2016). https://doi.org/10.1016/j.compositesb.2015.10.046

A.V.N.A. Lima, J.L. Cardoso, C.J.S. Lobo, Research on hybrid sisal/glass composites: a review. J. Reinf. Plast. Compos. **38**(17), 789–821 (2019). https://doi.org/10.1177/0731684419847272

S.M. Maharana, P. Samal, J. Dehury, P.P. Mohanty, Effect of fiber content and orientation on mechanical properties of epoxy composites reinforced with jute and Kevlar. Mater. Today Proc. **26**, 273–277 (2020). https://doi.org/10.1016/j.matpr.2019.11.239

Z. Mahboob, I. El Sawi, R. Zdero, Z. Fawaz, H. Bougherara, Tensile and compressive damaged response in flax fibre reinforced epoxy composites. Compos. A: Appl. Sci. Manuf. **92**, 118–133 (2017). https://doi.org/10.1016/j.compositesa.2016.11.007

M. Megahed, R.M. Abo-bakr, S.A. Mohamed, Optimization of hybrid natural laminated composite beams for a minimum weight and cost design. Compos. Struct. **239**, 111984 (2020). https://doi.org/10.1016/j.compstruct.2020.111984

M.J. Mochane, T.C. Mokhena, T.H. Mokhothu, A. Mtibe, E.R. Sadiku, S.S. Ray, I.D. Ibrahim, O.O. Daramola, Recent progress on natural fiber hybrid composites for advanced applications: a review. Express Polym. Lett. **13**(2), 159–198 (2019). https://doi.org/10.3144/expresspolymlett.2019.15

A. Mohanty, M. Misra, L. Drzal, S. Selke, B. Harte, G. Hinrichsen, Natural fibers, biopolymers, and biocomposites, in *Soy Protein-Based Plastics, Blends, and Composites*, vol. 1, (Taylor & Francis, Boca Raton, 2005), pp. 1–36. https://doi.org/10.1201/9780203508206

C. Morvan, C. Andème-Onzighi, R. Girault, D.S. Himmelsbach, A. Driouich, D.E. Akin, Building flax fibres: more than one brick in the walls. Plant Physiol. Biochem. **41**(11), 935–944 (2003). https://doi.org/10.1016/j.plaphy.2003.07.001

P.S. Mukherjee, K.G. Satyanarayana, Structure and properties of some vegetable fibres. J. Mater. Sci. **21**(1), 51–56 (1986). https://doi.org/10.1007/BF01144698

L.Y. Mwaikambo, M.P. Ansell, Chemical modification of hemp, sisal, jute, and kapok fibers by alkalization. J. Appl. Polym. Sci. **84**(12), 2222–2234 (2002). https://doi.org/10.1002/app.10460

J. Naveen, M. Jawaid, P. Amuthakkannan, M. Chandrasekar, Mechanical and physical properties of sisal and hybrid sisal fiber-reinforced polymer composites, in *Mechanical and Physical Testing of Biocomposites, Fibre-Reinforced Composites and Hybrid Composites*, (Elsevier, Amsterdam, 2018). https://doi.org/10.1016/B978-0-08-102292-4.00021-7

E. Nisini, C. Santulli, A. Liverani, Mechanical and impact characterization of hybrid composite laminates with carbon, basalt and flax fibres. Compos. Part B Eng. **127**, 92–99 (2017). https://doi.org/10.1016/j.compositesb.2016.06.071

K.L. Pickering, M.G.A. Efendy, T.M. Le, A review of recent developments in natural fibre composites and their mechanical performance. Compos. A: Appl. Sci. Manuf. **83**, 98–112 (2016). https://doi.org/10.1016/j.compositesa.2015.08.038

F. Pinto, L. Boccarusso, D. De Fazio, S. Cuomo, M. Durante, M. Meo, Carbon/hemp bio-hybrid composites: effects of the stacking sequence on flexural, damping and impact properties. Compos. Struct. **242**, 112148 (2020). https://doi.org/10.1016/j.compstruct.2020.112148

M. Puttegowda, S.M. Rangappa, M. Jawaid, P. Shivanna, Y. Basavegowda, N. Saba, Potential of natural/synthetic hybrid composites for aerospace applications, in *Sustainable Composites for*

Aerospace Applications, (Elsevier, Amsterdam, 2018). https://doi.org/10.1016/B978-0-08-102131-6.00021-9

N. Rajesh Jesudoss Hynes, R. Sankaranarayanan, J. Senthil Kumar, S. Mavinkere Rangappa, S. Siengchin, Mechanical behavior of synthetic/natural fibers in hybrid composites, in *Hybrid Fiber Composites*, (Wiley, Hoboken, 2020), pp. 129–146. https://doi.org/10.1002/9783527824571.ch8

M.V. Ramana, S. Ramprasad, Experimental investigation on jute/carbon fibre reinforced epoxy based hybrid composites. Mater. Today Proc. **4**(8), 8654–8664 (2017). https://doi.org/10.1016/j.matpr.2017.07.214

M. Ramesh, P. Sudharsan, K. Palanikumar, Processing and mechanical property evaluation of flax-glass fiber reinforced polymer composites. Appl. Mech. Mater. **766–767**, 144–149 (2015). https://doi.org/10.4028/www.scientific.net/amm.766-767.144

M. Ramesh, C. Deepa, G.R. Arpitha, V. Gopinath, Effect of hybridization on properties of hemp-carbon fibre-reinforced hybrid polymer composites using experimental and finite element analysis. World J. Eng. **16**(2), 248–259 (2019). https://doi.org/10.1108/WJE-04-2018-0125

B. Ravishankar, S.K. Nayak, M.A. Kader, Hybrid composites for automotive applications – a review. J. Reinf. Plast. Compos. **38**(18), 835–845 (2019). https://doi.org/10.1177/0731684419849708

Z. Ren, C. Wang, Q. Zuo, S.H. Siddique Yousfani, N.I.S. Anuar, S. Zakaria, X. Liu, Effect of alkali treatment on interfacial and mechanical properties of kenaf fibre reinforced epoxy unidirectional composites. Sains Malays. **48**(1), 173–181 (2019). https://doi.org/10.17576/jsm-2019-4801-20

S.N.A. Safri, M.T.H. Sultan, M. Jawaid, K. Jayakrishna, Impact behaviour of hybrid composites for structural applications: a review. Compos. Part B Eng. **133**, 112–121 (2018). https://doi.org/10.1016/j.compositesb.2017.09.008

E.H. Saidane, D. Scida, M. Assarar, R. Ayad, Damage mechanisms assessment of hybrid flax-glass fibre composites using acoustic emission. Compos. Struct. **174**, 1–11 (2017). https://doi.org/10.1016/j.compstruct.2017.04.044

A. Saleem, L. Medina, M. Skrifvars, Mechanical performance of hybrid bast and basalt fibers reinforced polymer composites. J. Polym. Res. **27**(3) (2020). https://doi.org/10.1007/s10965-020-2028-6

N. Sapiai, A. Jumahat, R.N. Hakim, Tensile and compressive properties of hybrid carbon fiber/kenaf polymer composite. Adv. Environ. Biol. **8**(8), 2655–2661 (2014)

N. Sapiai, A. Jumahat, J. Mahmud, Flexural and tensile properties of kenaf/glass fibres hybrid composites filled with carbon nanotubes. J. Teknol. **76**(3), 115–120 (2015). https://doi.org/10.11113/jt.v76.5524

F. Sarasini, J. Tirillò, M. Valente, T. Valente, S. Cioffi, S. Iannace, L. Sorrentino, Effect of basalt fiber hybridization on the impact behavior under low impact velocity of glass/basalt woven fabric/epoxy resin composites. Compos. A: Appl. Sci. Manuf. **47**, 109–123 (2013). https://doi.org/10.1016/j.compositesa.2012.11.021

F. Sarasini, J. Tirillò, S. D'Altilia, T. Valente, C. Santulli, F. Touchard, L. Chocinski-Arnault, D. Mellier, L. Lampani, P. Gaudenzi, Damage tolerance of carbon/flax hybrid composites subjected to low velocity impact. Compos. Part B Eng. **91**, 144–153 (2016). https://doi.org/10.1016/j.compositesb.2016.01.050

F. Sarker, P. Potluri, S. Afroj, V. Koncherry, K.S. Novoselov, N. Karim, Ultra-high performance of nano-engineered graphene-based natural jute fiber composites. ACS Appl. Mater. Interfaces **11**, 23 (2019)

A. Sarwar, Z. Mahboob, R. Zdero, H. Bougherara, Mechanical characterization of a new Kevlar/flax/epoxy hybrid composite in a sandwich structure. Polym. Test. **90**, 106680 (2020). https://doi.org/10.1016/j.polymertesting.2020.106680

M.L. Scutaru, M. Baba, Investigation of the mechanical properties of hybrid carbon-hemp laminated composites used as thermal insulation for different industrial applications. Adv. Mech. Eng. **6**, 829426 (2014). https://doi.org/10.1155/2014/829426

H. Sezgin, O.B. Berkalp, R. Mishra, J. Militky, Investigation of dynamic mechanical properties of jute/carbon reinforced composites. Composites **14**(12), 19 (2016)
A. Shahzad, Hemp fiber and its composites – a review. J. Compos. Mater. **46**(8), 973–986 (2011). https://doi.org/10.1177/0021998311413623
M. Shamsuyeva, J. Winkelmann, H.-J. Endres, Manufacture of hybrid natural/synthetic fiber woven textiles for use in technical biocomposites with maximum biobased content. J. Compos. Sci. **3**(2), 43 (2019). https://doi.org/10.3390/jcs3020043
Y. Shireesha, G. Nandipati, State of art review on natural fibers. Mater. Today Proc. **18**, 15–24 (2019). https://doi.org/10.1016/j.matpr.2019.06.272
R. Silva, S.K. Haraguchi, E.C. Muniz, A.F. Rubira, Aplicações de fibras lignocelulósicas na química de polímeros e em compósitos. Quim. Nova **32**, 661–671 (2009)
A.B..M. Supian, S.M. Sapuan, M.Y.M. Zuhri, E.S. Zainudin, H.H. Ya, Hybrid reinforced thermoset polymer composite in energy absorption tube application: a review. Def. Technol. **14**(4), 291–305 (2018). https://doi.org/10.1016/j.dt.2018.04.004
K.V. Suresha, H.K. Shivanand, A. Amith, H.N. Vidyasagar, Evaluation of mechanical properties of hybrid fiber (hemp, jute, kevlar) reinforced composites. AIP Conf. Proc. **1943**, 1–7 (2018). https://doi.org/10.1063/1.5029685
Y.G. Thyavihalli Girijappa, S. Mavinkere Rangappa, J. Parameswaranpillai, S. Siengchin, Natural fibers as sustainable and renewable resource for development of eco-friendly composites: a comprehensive review. Front. Mater. **6**, 226 (2019). https://doi.org/10.3389/fmats.2019.00226
M. Torres, V.R. Rodriguez, P.I. Alcantara, E. Franco-Urquiza, Mechanical properties and fracture behaviour of agave fibers bio-based epoxy laminates reinforced with zinc oxide. Journal of Industrial Textiles. (2020). https://doi.org/10.1177/1528083720965689
M. Torres-Arellano, V. Renteria-Rodríguez, E. Franco-Urquiza, Mechanical properties of natural-fiber-reinforced biobased epoxy resins manufactured by resin infusion process. Polymers. **12**(12), 2841 (2020). https://doi.org/10.3390/polym12122841
J. Wang, L. Zhao, X. Qin, Study on the mechanical properties of jute/carbon hybrid composites. Adv. Mater. Res. **331**, 110–114 (2011). https://doi.org/10.4028/www.scientific.net/AMR.331.110
J. Winkelmann, M. Shamsuyeva, H.-J. Endres, Hybrid fabrics for use in bio-based composites for technical applications. Mater. Today Proc. **31**, S263–S268 (2020). https://doi.org/10.1016/j.matpr.2019.12.097
R. Yahaya, S.M. Sapuan, M. Jawaid, Z. Leman, E.S. Zainudin, Effect of fibre orientations on the mechanical properties of kenaf–aramid hybrid composites for spall-liner application. Def. Technol. **12**(1), 52–58 (2016). https://doi.org/10.1016/j.dt.2015.08.005
L. Yan, N. Chouw, Effect of water, seawater and alkaline solution ageing on mechanical properties of flax fabric/epoxy composites used for civil engineering applications. Constr. Build. Mater. **99**, 118–127 (2015). https://doi.org/10.1016/j.conbuildmat.2015.09.025
L. Yan, N. Chouw, K. Jayaraman, Flax fibre and its composites – a review. Compos. Part B Eng. **56**, 296–317 (2014). https://doi.org/10.1016/j.compositesb.2013.08.014
I. Yusuff, N. Sarifuddin, A.M. Ali, A review on kenaf fiber hybrid composites: mechanical properties, potentials, and challenges in engineering applications. Prog. Rubber Plast. Recycl. Technol. (2020). https://doi.org/10.1177/1477760620953438
M.H. Zamri, H.M. Akil, A.A. Bakar, Z.A.M. Ishak, L.W. Cheng, Effect of water absorption on pultruded jute/glass fiber-reinforced unsaturated polyester hybrid composites. J. Compos. Mater. **46**(1), 51–61 (2012). https://doi.org/10.1177/0021998311410488
X. Zeng, S.J. Mooney, C.J. Sturrock, Assessing the effect of fibre extraction processes on the strength of flax fibre reinforcement. Compos. A: Appl. Sci. Manuf. **70**, 1–7 (2015). https://doi.org/10.1016/j.compositesa.2014.12.004
Y. Zhang, Y. Li, H. Ma, T. Yu, Tensile and interfacial properties of unidirectional flax/glass fiber reinforced hybrid composites. Compos. Sci. Technol. **88**, 172–177 (2013). https://doi.org/10.1016/j.compscitech.2013.08.037

Index

S. Mavinkere Rangappa et al. (eds.), *Handbook of Epoxy/Fiber Composites*,
https://doi.org/10.1007/978-981-19-3603-6